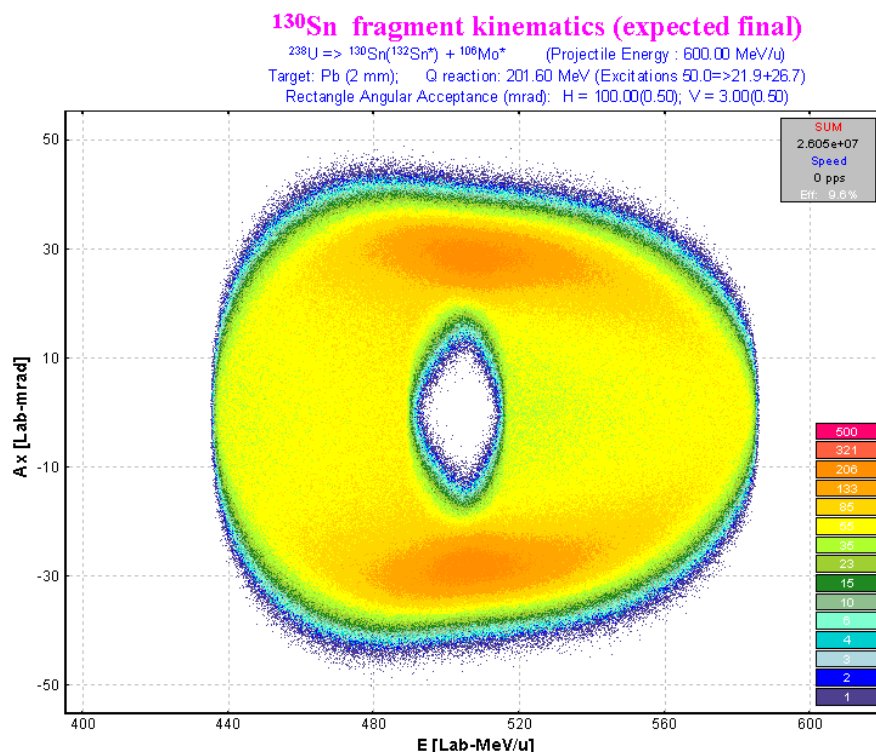




O.Tarasov<sup>1,2</sup>, D.Bazin<sup>1</sup>

<sup>1</sup> NSCL-Cyclotron Laboratory, Michigan State University, East Lansing, MI 48824-1321, USA

<sup>2</sup> Flerov Laboratory of Nuclear Reactions, JINR, 141980 Dubna, Moscow region, Russia




## Contents:

<b>1. VERSION 7.5: ABRASION-FISSION</b> .....	<b>15</b>
1.1. INTRODUCTION.....	15
1.2. DE-EXCITATION PROCESS.....	16
1.2.1. <i>The break-up channel in the evaporation cascade</i> .....	17
1.2.1.1. The limiting temperature as a function of mass number.....	17
1.2.2. <i>Dissipation effects in fission</i> .....	19
1.2.3. <i>Evaporation calculator modifications</i> .....	21
1.3. FISSION BARRIERS.....	23
1.3.1. <i>The Fission barrier dialog</i> .....	23
1.3.2. <i>ETFSI and experimental fission barriers</i> .....	24
1.3.3. <i>Calculation models (#0,1,2)</i> .....	24
1.3.3.1. Shell corrections.....	24
1.3.3.2. Odd-Even corrections.....	24
1.3.4. <i>Fission barrier plot</i> .....	26
1.3.5. <i>Influence of corrections for fission barriers on abrasion-fission cross-sections</i> .....	27
1.4. SECONDARY REACTIONS IN TARGET.....	28
1.4.1. <i>Reexamination of secondary reactions calculation procedure</i> .....	28
1.4.1.1. Dependence on the distribution dimension ( $NP_{\text{evap}}$ ).....	28
1.4.1.2. The "Secondary reactions" dialog modification.....	29
1.4.1.2.1. Secondary reactions analysis plots.....	29
1.4.1.3. Determination of the region of nuclei for secondary reactions calculations.....	30
1.4.1.4. Revision of optimal target thickness calculations for SR mode.....	31
1.4.2. <i>Calculation of secondary reaction contributions to fragments with zero primary production cross-section</i> .....	33
1.4.2.1. Secondary Reactions plots: SR coefficients & reduced cross-sections.....	34
1.4.3. <i>SR calculation speed</i> .....	35
1.4.3.1. Acceleration filters for secondary reactions calculations.....	36
1.4.3.1.1. Corner rectangle filter.....	36
1.4.3.1.2. Diagonal filter.....	38
1.4.3.1.3. Application of acceleration filters.....	39
1.5. ABRASION-FISSION.....	41
1.5.1. <i>Three excitation energy regions AF model</i> .....	41
1.5.1.1. Abrasion-Fission dialog.....	41
1.5.1.2. Fission excitation function.....	42
1.5.1.3. Calculation of final fission fragment production.....	44
1.5.1.3.1. Width of charge distribution.....	44
1.5.1.3.2. Modification of evaporation cascade subroutines.....	44
1.5.1.4. Additional settings.....	46
1.5.2. <i>Kinematics</i> .....	47
1.5.2.1. Production of $^{100}\text{Zr}$ .....	47
1.5.2.2. Angular acceptance.....	48
1.5.2.3. Thick target.....	49
1.5.3. <i>Abrasion-Fission plots</i> .....	50
1.5.3.1. New plot options.....	51
1.5.3.1.1. Final (after de-excitation) and initial cross-section plots.....	51
1.5.3.1.2. Excitation energy plot.....	52
1.5.4. <i>Abrasion-Fission settings discussions</i> .....	52
1.5.4.1. Excitation energy of fission fragment (TXE).....	52
1.5.4.2. Excitation energy region (EER) boundaries.....	55
1.5.4.3. Excitation energy per abraded nucleon for Abrasion-Ablation.....	58
1.5.4.4. Dissipation effects in fission.....	60
1.5.4.5. Break-up de-excitation channel.....	60
1.5.4.6. Fission barrier.....	61
1.5.4.7. Cross-section suppression coefficient.....	62
1.5.4.8. Restore previous AF settings.....	62
1.5.5. <i>Secondary reactions for Abrasion-Fission</i> .....	63
1.5.6. <i>Setting up LISE to calculate yield of AF products through the spectrometer</i> .....	65
1.5.6.1. Experiment settings.....	65
1.5.6.1.1. Spectrometer choice.....	65
1.5.6.1.2. Primary beam, target, selected fragment.....	65

1.5.6.2. Abrasion-Fission settings .....	66
1.5.6.3. Spectrometer tuning for the fragment of interest .....	66
1.5.6.4. Yield calculation.....	67
1.5.6.5. Optimum target.....	67
1.5.6.6. Secondary reactions.....	68
1.5.6.7. Cleaning .....	69
1.5.6.8. Charge states.....	70
1.5.6.9. Go to more exotic case of <sup>83</sup> Zn .....	71
1.5.6.10. Examples .....	71
1.5.7. <i>LISE's options modifications connected with the AF mechanism</i> .....	72
1.5.7.1. New transmission parameter "Sum of reactions" .....	72
1.5.7.2. User cross-section file .....	75
1.5.7.3. Transmission result file .....	75
1.5.8. <i>INC fission</i> .....	76
1.5.8.1. Recommended EER parameters for light targets in the LISE++ Abrasion-Fission model .....	80
1.5.8.1.1. Hydrogen target.....	80
1.5.8.1.2. Deuterium target.....	82
1.5.8.1.3. Targets with Z ≥ 2 .....	82
1.5.9. <i>Comparison with experimental data</i> .....	83
1.5.9.1. Total fission cross-sections of <sup>238</sup> U at relativistic energies .....	83
1.5.9.2. <sup>208</sup> Pb(1AGeV) + p,d.....	84
1.5.9.3. <sup>238</sup> U(1AGeV) + Pb.....	89
1.5.9.4. <sup>238</sup> U(750AMeV) + Be.....	91
1.5.9.5. <sup>238</sup> U(1AGeV) + p.....	92
1.6. NEW UTILITIES .....	95
1.6.1. <i>User cross-section analysis using Abrasion-Ablation model</i> .....	95
1.6.1.1. AA parameters corresponding to EPAX.....	97
1.6.2. <i>Optimum charge state combination</i> .....	100
1.6.3. <i>Charge state combination calculation for the optimal target thickness utility</i> .....	102
1.6.3.1. Target optimization options.....	103
1.6.3.2. Optimal target searching methods .....	104
1.6.4. <i>Rate &amp; transmission calculation batch mode</i> .....	104
1.6.5. <i>Target and wedge optimization</i> .....	106
1.6.5.1. Secondary Reactions contribution option .....	109
1.6.5.2. "Keep value" parameter .....	110
1.6.5.3. Target and wedge optimization for charge states .....	111
1.6.5.3.1. No charge states .....	111
1.6.5.3.2. Spectrometer tuned to only one charge state combination .....	112
1.6.5.3.3. Optimization of the charge state combination.....	113
1.6.5.3.4. Results.....	113
1.6.5.4. Wedge-shape and curved profile degraders properties.....	115
1.6.5.5. Setting discussions.....	118
1.6.5.5.1. Acceptance.....	118
1.6.5.5.2. Wedge selection slits.....	120
1.6.5.5.3. Isobars A=32 .....	120
1.7. MASSES. AME2003 .....	122
1.7.1. <i>New mass excess files in the LISE package</i> .....	123
1.7.2. <i>"Unknown" - new type of isotope designation for the table of nuclides</i> .....	123
1.7.2.1. Particle bound, quasi bound and unbound nuclei .....	123
1.7.2.2. How to load information from the user mass excess file in the navigation scheme .....	125
1.7.2.3. Modifications in the database plot.....	125
1.8. LISE++ BLOCK STRUCTURE DEVELOPMENT .....	126
1.8.1. <i>New material block: FaradayCup</i> .....	126
1.8.2. <i>Append blocks in the current open configuration from other LISE files</i> .....	126
1.9. DIFFERENT .....	127
1.9.1. <i>User cross-section file</i> .....	127
1.9.1.1. User cross-section file: reaction property .....	127
1.9.1.2. User file of reduced cross-sections .....	128
1.9.1.3. CS files in LISE++ package .....	128
1.9.2. <i>Curved profile degrader modifications</i> .....	129
1.9.3. <i>Logotypes and references</i> .....	131
1.9.4. <i>2D-plots: contours &amp; projections</i> .....	132

1.9.4.1. Contour dialog.....	132
1.9.4.1.1. Window and contour projections on an axis for 2D Cross-section plot.....	132
1.9.5. Fission channel for the fusion-evaporation excitation function plot.....	133
1.9.6. Abrasion-Ablation: fast mode for heavy projectiles.....	134
1.9.7. The "About" dialog modifications.....	134
1.9.8. PACE4: User's limits for Angular and Energy distributions of residues.....	134
1.9.9. Gas density dialog.....	135
1.9.10. Block labels for the transport envelope.....	135
1.9.11. Drift block.....	135
1.9.12. Compound targets for AA calculations, fusion-residues and fission reactions.....	136
1.9.13. Choice of horizontal axis for 2D-plots.....	136
1.9.14. Version numbers.....	136
1.9.15. LISE user statistics.....	136
1.10. USER REQUESTS AND BUGS REPORT.....	138
1.10.1. Corrections.....	138
1.10.2. User requests.....	139
1.11. NEXT STEPS DEVELOPMENT.....	140
1.11.1. First priority.....	140
Long-term.....	140
Short-term.....	140
1.11.2. Second priority task.....	140
1.11.3. Third priority task.....	140
ACKNOWLEDGEMENTS.....	141
<b>2. VERSION 7.1: COULOMB FISSION.....</b>	<b>142</b>
2.1. INTRODUCTION.....	142
2.2. FISSION FRAGMENT KINEMATICS AT INTERMEDIATE AND HIGH ENERGIES.....	143
2.2.1. Kinematical description.....	143
2.2.2. Monte Carlo simulation of fission fragment angular and energy transmissions.....	143
2.2.2.1. 2D fragment plot (Monte Carlo) – version 7.1.....	146
2.2.2.2. Using target thickness.....	147
2.2.2.2.1. MCmethod calculation speed.....	148
2.2.2.3. Excitation energies.....	149
2.2.2.4. Expected final fragment.....	149
2.2.2.5. Total kinetic energy of fission fragments.....	150
2.2.2.6. Fragment distribution to plot.....	150
2.2.2.7. Broadening due to particle emission.....	150
2.2.3. Fission kinematics used by the LISE "distribution" method (DistrMethod).....	151
2.2.3.1. Class "MatrixKinematics": fission kinematics by LISE "distribution" method.....	151
2.2.3.1.1. AX&AY matrices.....	151
2.2.3.1.2. "Base" and "Acquired" distributions.....	153
2.2.3.2. Fission kinematics debug distributions.....	153
2.2.4. Comparison of calculations using the Monte Carlo method and the "MatrixKinematics" class.....	157
2.2.5. Angular distribution cut by the momentum slits.....	159
2.2.5.1. Angular distribution cut by the momentum slits: option "Do not use".....	159
2.2.5.2. Angular distribution cut by the momentum slits: option "Use for MatrixKinematics class".....	161
2.2.5.3. Angular distribution cut by the momentum slits: option "Use for All distributions".....	162
2.3. COULOMB FISSION FRAGMENT PRODUCTION CROSS-SECTIONS.....	164
2.3.1. Electromagnetic fission cross-section.....	164
2.3.1.1. Electromagnetic excitation.....	164
2.3.1.1.1. Equivalent photon spectrum.....	165
2.3.1.1.2. Giant dipole resonance.....	165
2.3.1.1.3. Giant quadrupole resonance.....	165
2.3.1.2. Fission deexcitation channel.....	166
2.3.1.3. Dependences of average excitation energy and EM fission cross-section from beam energy.....	166
2.3.2. A semi-empirical model of the fission-fragment properties.....	167
2.3.2.1. Potential energy at the fission barrier.....	167
2.3.2.2. Pairing corrections.....	168
2.3.2.3. Post-scission nucleon emission.....	170
2.3.3. How it works in LISE++?.....	172
2.3.3.1. Fission cross-section matrix (FCSM).....	172

2.3.3.2. Fission fragment cross-section for transmission calculations .....	173
2.3.3.3. Suppression values for fission production cross-sections .....	174
2.3.3.4. Recalculation of fission fragment cross-sections .....	174
2.3.3.5. File of fission fragment cross-sections .....	174
2.3.3.6. Simulation of "abrasion-fission" (nuclear fission) .....	175
2.4. PLOTS FOR "COULOMB FISSION" MODE (MENU 1D-PLOT) .....	176
2.4.1. Cross-sections .....	176
2.4.1.1. "EM fission cross-section" option .....	176
2.4.1.2. "Differential cross-section" option .....	178
2.4.2. Total kinetic energy and post-scission nucleon emission plots .....	180
2.4.2.1. Calculation of conjugate final fragment .....	180
2.4.3. Kinetic energy plots .....	181
2.4.4. Plot of evaporated nucleon yields .....	183
2.5. SPECTROMETER SETTINGS IN THE CASE OF FISSION .....	187
2.5.1. Fission fragment momentum distribution and spectrometer settings .....	187
2.5.2. Secondary reactions in the target .....	190
2.5.3. Optimal thickness target calculations .....	191
2.6. COMPARISONS OF LISE CALCULATIONS WITH EXPERIMENTAL DATA AND THE MOCADI CODE .....	192
2.6.1. Kinematics calculation in the case of thick targets .....	192
2.6.2. Fission-fragment production cross-sections .....	195
2.6.3. TKE comparisons .....	196
2.7. OTHER .....	198
2.7.1. Projection on an axis in Monte Carlo plots .....	198
2.7.2. Equilibrium thickness calculation methods in the Production dialog .....	198
2.7.3. Navigation map: projectile & fragment .....	198
2.7.4. "Table of nuclides" background .....	198
2.7.5. New configuration files .....	199
2.7.6. Charge state suppression values .....	199
2.7.7. Rate Calculator .....	200
2.7.8. 2D-plot "Range-X" .....	202
2.8. BUG AND REMARK REPORT .....	204
2.9. NEXT STEPS DEVELOPMENT .....	204
Short-term plans for Coulomb fission .....	204
Long-term plans .....	204
ACKNOWLEDGEMENTS .....	205
<b>3. VERSION 6.5: ISOL METHOD .....</b>	<b>206</b>
3.1. ISOL METHOD .....	206
3.1.1. Mass separator "MASHA" .....	207
3.1.2. Charge states .....	209
3.2. OTHER .....	210
3.2.1. Electric dipole: separation plane .....	210
3.2.2. Wedge angle dialog .....	210
3.2.3. MSP-144 modification .....	210
ACKNOWLEDGEMENTS .....	210
<b>4. VERSION 6.4 .....</b>	<b>211</b>
4.1. LISE FOR "UNPRIVILEGED" USERS .....	211
4.1.1. The "\user\MyDocuments\LISE" directory .....	211
4.1.1.1. Using the folder "My Documents" for users with administrative privileges .....	211
4.1.2. "Charge", "Global", "PACE4" & "BI" for "unprivileged" users .....	212
4.2. USER'S MASS-EXCESS FILE .....	212
4.2.1. Use of mass models .....	212
4.2.2. UME file format .....	213
4.2.3. UME file editing .....	213
4.3. USER'S CROSS-SECTION FILE .....	214
4.3.1. Methods to keep user CS .....	215
4.3.2. User CS in plots .....	215
4.4. ABRASION-ABLATION REVISION .....	216

4.4.1. Evaporation cascade .....	216
4.4.2. Corrections of low energy region .....	219
4.4.2.1. Level density .....	219
4.4.2.2. Temperature .....	221
4.4.3. $\gamma$ -channel in evaporation cascade .....	221
4.4.4. Calculation of temperature in Evaporation calculator .....	222
4.4.5. "BarFac" - fission barrier coefficient .....	222
4.4.6. Excitation energy of prefragment .....	223
4.4.7. Comparison with experimental data .....	224
4.4.7.1. $^{58}\text{Ni}+\text{Be}$ .....	224
4.4.7.1.1. Step 1: Excitation energy .....	224
4.4.7.1.2. Step 2: Deduced effective Coulomb barrier .....	225
4.4.7.1.3. Step 3: Effect of pairing correlations .....	226
4.4.7.1.4. Step 4: Use of two excitation energy regions .....	227
4.4.7.1.5. Results .....	229
4.4.7.2. $^{40}\text{Ar} + \text{Be,C}$ .....	230
4.4.7.3. Other experimental data .....	231
4.4.8. Cross-section & minimum separation energy dependence .....	232
4.4.9. Three step Abrasion-Ablation model .....	233
4.5. OTHER .....	233
4.5.1. Drift block in the Beam analyzer dialog .....	233
4.5.2. New options for cross-section plot .....	234
4.5.3. Writing files from the "Statistics" windows .....	234
4.5.4. PACE4 modifications .....	235
4.5.4.1. Number of cascades .....	235
4.5.4.2. BarFac modifications .....	235
4.5.4.3. Cross-section file .....	235
4.5.5. Secondary reactions (in target) corrections .....	235
4.5.6. Configuration files .....	237
4.5.7. Bug report .....	237
ACKNOWLEDGEMENTS .....	237
<b>5. VERSION 6.3 .....</b>	<b>238</b>
5.1. CHARGE STATES CALCULATIONS .....	238
5.1.1. "GLOBAL" (charge states calculations) .....	238
5.1.1.1. "GLOBAL" for "Windows"  .....	239
5.1.1.2. Use of GLOBAL's calculations in LISE++ .....	240
5.1.1.3. "GLOBAL" in LISE.XLS .....	241
5.1.1.4. GLOBAL's new features .....	242
5.1.1.4.1. Options for final energy projectile .....	242
5.1.1.4.2. Optimization for a thick target .....	242
5.1.1.4.3. Calculations for a projectile with atomic number lower than 29 .....	243
5.1.2. Q-state calculations: optimization for speed .....	243
5.1.2.1. Tabulation of Q-states .....	244
5.1.2.2. Restrictions for improbable Q-states .....	244
5.1.3. Nonequilibrium charge state calculations .....	244
5.1.4. Excel: new sheet and functions with charge states .....	245
5.1.5. Equilibrium thickness plot .....	247
5.1.6. Physical Calculator Charge state values ( $\langle Q \rangle$ , $\Delta Q$ ) .....	247
5.2. MODIFICATION OF EVAPORATION CALCULATIONS .....	248
5.2.1. Level density calculations .....	248
5.2.1.1. Level density and temperature plots .....	248
5.2.2. Fission channel in evaporation cascade .....	249
5.2.3. Plot of decay channel probabilities .....	249
5.3. OTHER .....	251
5.3.1. New angular transmission method .....	251
5.3.2. Possibility to modify EPAX 2.15 .....	251
5.3.3. Monte Carlo plot saving and use by the "BI" code .....	252
5.3.4. New configurations .....	253

5.3.5. <i>Bug corrections</i> .....	253
5.4. COMPARISON BETWEEN LISE CALCULATIONS AND EXPERIMENTAL RESULTS .....	254
5.4.1. <i>Charge state distributions</i> .....	254
5.4.2. <i>Fragment parallel momentum distributions</i> .....	256
5.4.3. <i>LISE Abrasion-Ablation model</i> .....	257
5.5. STATUS OF THE CODE .....	258
5.5.1. <i>LISE tutorial</i> .....	258
5.5.2. <i>User statistics</i> .....	259
5.5.3. <i>Future perspectives for LISE++ (version 6.4)</i> .....	259
ACKNOWLEDGEMENTS.....	259
<b>6. VERSION 6.2 .....</b>	<b>260</b>
6.1. TRANSPORT ENVELOPE CALCULATION PACKAGE.....	260
6.2. CODE “CHARGE”.....	261
6.3. BRHO (ERHO) ANALYZER DIALOG.....	262
6.4. NEW OPTICAL BLOCKS.....	265
6.4.1. <i>Compensating dipole</i> .....	265
6.4.1.1. MARS spectrometer configuration.....	266
6.4.2. <i>Electrostatic dipole</i> .....	267
6.4.2.1. The kinematic separator “VASSILISSA” configuration .....	267
6.4.2.2. Tuning the spectrometer for fusion-evaporation residue .....	268
6.4.2.3. Choice of charge state of ion to set the spectrometer .....	269
6.4.2.4. Calculation of energy and angular distribution of fusion-evaporation residues .....	270
6.4.2.5. Suppression of the primary beam .....	270
6.4.2.6. Residue transmission calculation.....	274
6.4.3. <i>Gas-filled magnetic dipole</i> .....	275
6.4.3.1. Gas pressure optimization plot .....	276
6.4.3.2. The Dubna GFS configuration.....	278
6.5. NEW FEATURES AND CORRECTIONS .....	278
6.5.1. <i>Gas density calculations in the dialog "Material"</i> .....	278
6.5.2. <i>The “Beam” dialog: several possibilities to enter a beam energy</i> .....	279
6.5.3. <i>Spectrometer setting for the primary beam in the fusion mode</i> .....	279
6.5.4. <i>Angular straggling</i> .....	279
6.5.5. <i>Corrections and changes</i> .....	280
6.6. SUB-BARRIER FUSION CROSS-SECTION .....	281
6.7. THE CODE “BI” DEVELOPMENT .....	283
6.8. FUTURE PERSPECTIVES FOR LISE++ (VERSION 6.3).....	284
ACKNOWLEDGEMENTS.....	284
<b>7. VERSION 6.1 .....</b>	<b>285</b>
7.1. INTRODUCTION.....	286
7.1.1. <i>How to download LISE++</i> .....	286
7.1.2. <i>New file formats</i> .....	286
7.1.3. <i>Support of “classic” LISE files</i> .....	287
7.2. DESIGNING YOUR OWN SPECTROMETER .....	287
7.2.1. <i>Set-up dialog: new main feature</i> .....	288
7.2.2. <i>Scheme of spectrometer</i> .....	290
7.2.2.1. Settings of spectrometer scheme .....	291
7.3. DESCRIPTION OF BLOCKS AND THEIR PROPERTIES.....	291
7.3.1. <i>Optical block</i> .....	291
7.3.1.1. Optical block: properties and methods .....	292
7.3.1.1.1. Optical matrix of LISE++ block.....	292
7.3.1.1.2. Acceptances and slits .....	293
7.3.1.1.3. Momentum acceptance of spectrometer .....	295
7.3.1.2. Blocks from optical class.....	295
7.3.1.2.1. Drift block .....	295
7.3.1.2.2. Rotation beam block.....	296
7.3.2. <i>Dispersive block</i> .....	296
7.3.2.1. Properties and methods.....	296
7.3.2.1.1. Computational values (fields) .....	296

7.3.2.1.2. Calibration file .....	297
7.3.2.2. Dispersive block on the base of Magnetic dipole .....	298
7.3.2.3. Wien velocity filter .....	298
7.3.2.4. Compensating dipole after the Wien velocity filter .....	299
7.3.3. <i>Material blocks</i> .....	299
7.3.3.1. Material (detector) block: properties and methods .....	301
7.3.4. <i>Degrader in the dispersive focal plane</i> .....	302
7.3.4.1. Wedge angle calculation .....	303
7.3.4.2. Possible problems in wedge angle calculation .....	305
7.3.4.3. Curve profile degrader .....	306
7.3.4.4. Use of two wedges .....	307
7.3.4.5. Double acceptance effect .....	307
7.4. TRANSMISSION AND FRAGMENT OUTPUT CALCULATIONS .....	309
7.4.1. <i>Transmission calculation in a block</i> .....	309
7.4.1.1. Transmission statistics .....	310
7.4.2. <i>Charge states</i> .....	311
7.4.3. <i>Results file</i> .....	312
7.4.4. <i>Previous isotope area rectangle</i> .....	312
7.5. IMPROVED MASS FORMULA WITH SHELL CROSSING CORRECTIONS .....	312
7.5.1. <i>Shell crossing corrections</i> .....	316
7.5.2. <i>Use of LDM parameterizations in LISE++</i> .....	317
7.5.3. <i>LDM parameterizations and accuracy of cross-section calculations</i> .....	318
7.6. UPDATING AND NEW UTILITIES .....	319
7.6.1. <i>Emittance of beam</i> .....	319
7.6.2. <i>Preferences</i> .....	320
7.6.3. <i>Optimum target</i> .....	320
7.6.4. <i>Dialogs Goodies &amp; Physical calculator</i> .....	320
7.6.5. <i>Matrix calculator</i> .....	321
7.6.6. <i>Range optimizer – Gas cell utility</i> .....	322
7.6.7. <i>LISE for Excel</i> .....	324
6.7. <i>Cyrillic and Hex-style converter</i> .....	325
7.7. PLOTS .....	325
7.7.1. <i>Transmission plots</i> .....	325
7.7.2. <i>Two-dimensional plots</i> .....	327
7.7.3. <i>Debug distributions</i> .....	327
7.8. FUTURE DEVELOPMENTS OF LISE++ .....	329
ACKNOWLEDGEMENTS .....	329
<b>8. FUSION - VERSION 5.15 .....</b>	<b>331</b>
8.1. HOW TO CALCULATE FUSION RESIDUE TRANSMISSION (STEP BY STEP) .....	332
8.1.1. <i>Choosing Reaction type</i> .....	332
8.1.2. <i>Beam, Target, Residue settings</i> .....	332
8.1.3. <i>Options</i> .....	333
8.1.3.1. The “Preferences” dialog .....	333
8.1.3.2. The “Prefragment search and Evaporation options” dialog .....	333
8.1.4. <i>Residue excitation function</i> .....	333
8.1.5. <i>Setting of residue ion charge</i> .....	335
8.1.6. <i>Target thickness</i> .....	335
8.1.7. <i>Separation</i> .....	336
8.2. CHARACTERISTICS OF FUSION RESIDUE CALCULATIONS .....	337
8.2.1. <i>Kinematics distributions of fusion residues</i> .....	338
8.2.1.1. Momentum distribution .....	338
8.2.2. <i>Angular distributions</i> .....	338
8.2.3. <i>Fusion residue cross sections</i> .....	340
8.2.3.1. Comparison between LISE and PACE4 fusion residue cross sections .....	340
8.2.4. <i>Transmission of the primary beam</i> .....	342
8.3. OTHER TOPICS .....	344
8.3.1. <i>Two-dimensional plots for cross sections, transmission and database characteristics</i> .....	344
8.3.2. <i>Modification of evaporation calculation procedure</i> .....	344



8.3.3. <i>LISE.xls – stopping power functions</i> .....	345
Acknowledgement.....	345
<b>9. PACE4 - VERSION 5.13</b> .....	<b>346</b>
9.1. PACE4.....	347
9.1.1. <i>Introduction</i> .....	347
9.1.2. <i>Modifications</i> .....	347
9.1.3. <i>Visualization of PACE4 calculations</i> .....	349
9.1.4. <i>Comparisons of PACE4 and LISE AA-model calculations</i> .....	349
9.2. OPTION & CONFIGURATION FILES.....	352
9.2.1. <i>Structure of files</i> .....	352
9.2.1.1. Configuration file (LCF-extension).....	352
9.2.1.2. Option file (OPT-extension).....	352
9.2.1.3. Data file (LIZ-extension).....	353
9.2.2. <i>New features</i> .....	353
9.3. FILE CONVERTER FROM FORTRAN TO C.....	353
9.4. OTHER.....	355
9.4.1. <i>Modernization of the Abrasion-Ablation model</i> .....	355
9.4.2. <i>New NSCL ftp-address</i> .....	355
9.4.3. <i>New model for projectile fragmentation velocity</i> .....	356
9.4.4. <i>Changes in the Utilities menu</i> .....	356
9.4.5. <i>LISE code references</i> .....	356
9.4.6. <i>Future steps of the LISE code development</i> .....	356
<b>10. VERSION N°5.9-10</b> .....	<b>357</b>
10.0.1. <i>The Nuclear Spectrometry Handbook of J.Kantele - version 5.10</i> .....	357
10.0.1.1. About The Handbook .....	358
10.0.1.1.1. General description .....	358
10.0.1.1.2. Key Features .....	358
10.0.1.1.3. Contents: .....	358
10.0.1.2. List of programs .....	359
10.0.2. <i>MSP144 focal plane detector</i> .....	361
10.0.3. <i>Chemical properties of element</i> .....	361
10.0.4. <i>Units Converter – version 5.9</i> .....	361
<b>11. VERSION N°5.8</b> .....	<b>363</b>
11.1. AUTO MODE FOR THE ABRASION-ABLATION MODEL .....	363
11.2. ON-LINE LISE ANALYSIS OF EXPERIMENTAL PLOTS .....	364
11.3. CALCULATION OF THE WEDGE THICKNESS.....	366
<b>12. LISE &amp; EXCEL - VERSION 5.7</b> .....	<b>367</b>
<b>13. LISE &amp; INTERNET - VERSION 5.6</b> .....	<b>369</b>
13.1. ACCESS TO DATABASES.....	369
13.1.1. <i>Isomer database</i> .....	369
13.1.2. <i>TOI</i> .....	369
13.2. CHECK TO THE NEW VERSION .....	371
13.3. MAIL AND REGISTRATION FROM THE CODE .....	371
<b>14. VERSION N°5.5</b> .....	<b>372</b>
14.1. BRHO SCANNING PLOT.....	372
14.1.1. <i>Comparison of calculations with experimental data</i> .....	372
14.2. OPTIONS FILES.....	374
14.3. PRINT OF THE DIALOGS "PHYSICAL CALCULATOR" AND "GOODIES" .....	374
<b>15. ABRASION-ABLATION V.1.3 – VERSION 5.4</b> .....	<b>375</b>
<b>16. PREFRAGMENT EXCITATION ENERGY – VERSION 5.3</b> .....	<b>379</b>
<b>17. START CONFIGURATION – VERSION 5.2</b> .....	<b>381</b>
<b>18. TRANSFORMATION AMEV TO MEV/U – VERSION 5.1</b> .....	<b>382</b>
<b>19. VERSION 4.20</b> .....	<b>384</b>

19.1. ATIMA (ATOMIC INTERACTION WITH MATTER).....	384
19.2. STOPPING POWER. ENERGY LOSS. ....	386
19.3. RANGES.....	387
19.4. ENERGY-LOSS AND RANGES STRAGGLING .....	387
19.4.1. Angular straggling.....	388
19.5. MISCELLANEOUS.....	388
19.5.1. Range plot.....	388
19.5.2. Physical Calculator.....	389
Acknowledgement.....	390
<b>20. VERSION 4.18 .....</b>	<b>391</b>
20.1. INTRODUCTION.....	391
20.2. EVAPORATION CALCULATOR .....	392
20.2.1. Evaporation calculator plots.....	393
20.2.2. Evaporation settings.....	395
20.2.2.1. Tunneling for charge particles.....	395
20.2.2.2. Option to take into account unbound nuclei.....	396
20.3. GEOMETRICAL ABRASION-ABLATION MODEL .....	396
20.3.1. Abrasion-Ablation settings.....	397
20.3.1.1. LISE corrections.....	397
20.3.1.2. Excitation energy.....	398
Epilogue.....	400
<b>21. VERSION 4.17 .....</b>	<b>401</b>
21.1. SHORT REVIEW OF THE KINEMATICS CALCULATORS IN PREVIOUS VERSIONS OF THE CODE .....	401
21.2. KINEMATICS CALCULATOR .....	401
21.3. MISCELLANEOUS.....	403
21.3.1. Simultaneous and separate changes of horizontal slits.....	403
21.3.2. Stepping of dipole values.....	404
21.3.3. Dimension of Secondary reactions distributions.....	404
21.3.4. Accelerator Radio Frequency fraction for dE-TOF plot.....	405
21.3.5. Statistical characteristics of plot distributions .....	405
21.3.6. Bugs.....	405
21.3.6.1. Error in the list of recently used file.....	405
<b>22. VERSION 4.16 .....</b>	<b>407</b>
22.1. LISE WEB SITES .....	407
22.2. INSTALLATION .....	408
22.2.1. LISE installation for Windows NT or Windows 2000 without administrator privileges.....	408
22.2.2. Getting things in order in the LISE directory and LISE menu .....	409
<b>23. VERSIONS 4.14, 4.15 .....</b>	<b>410</b>
23.1. PLOT CALIBRATION UTILITIES – VERSION 4.15 .....	410
23.1.1. Calibration of physical parameters.....	411
23.1.2. Two-dimensional plots in the “calibration” mode.....	411
23.1.3. New options of plots .....	412
23.2. NSCL & THE LISE CODE - VERSION 4.14 .....	413
23.2.1. Calibration of A1900’s dipoles.....	413
23.2.2. Support of NSCL specters.....	413
23.2.3. Balls animation for Windows NT.....	413
23.2.4. Optimization of Monte-Carlo plots.....	414
<b>24. VERSIONS 4.10, 4.11, 4.12, 4.13 .....</b>	<b>415</b>
24.1. PREPRINT OF LISE PAPER .....	415
24.2. SCATTERING CALCULATOR – VERSION 4.13 .....	415
24.3. MASS-SEPARATOR MODE - VERSION 4.12.....	420
24.3.1. Cutout of the second dipole.....	420
24.3.2. New dE-X plot in the dispersive focal plane.....	421
24.3.3. New opportunity to select the velocity of reaction products.....	423
24.3.4. New image of the dialogue “Beam” .....	425

24.3.5. <i>It is still necessary to work on:</i> .....	425
24.4. THE AUTOMIZED SEARCH OF TWO-DIMENSIONAL PEAKS IN SPECTA AND DEFINITION OF THEIR CHARACTERISTICS (BI CODE) - VERSION 4.11 .....	426
24.5. PREFRAGMENT SEARCH - VERSION 4.10 .....	432
24.5.1. <i>Attempt to extrapolate cross-sections of exotic nuclei</i> .....	434
24.5.2. <i>Calculation of isotope characteristics with the semi empirical formula</i> .....	435
<b>25. VERSION 4.9 .....</b>	<b>437</b>
25.1. INTRODUCTION.....	437
25.2. LONGITUDINAL MOMENTUM DISTRIBUTION WIDTHS .....	438
25.2.1. <i>Systematic of momentum distributions from reactions with relativistic ions of D.J.Morrissey</i> .....	438
25.2.2. <i>Heavy ion projectile fragmentation: A reexamination by W.A.Friedman</i> .....	439
25.2.2.1. "Coulomb correction" of Friedman .....	440
25.2.3. <i>Simple parametrization of fragment reduced widths in heavy ion collisions (R.H.Tripathi et al.)</i> .....	440
25.2.4. <i>Role of intrinsic width in the fragment momentum distributions in heavy ion –collisions (R.H.Tripathi et al.)</i> .....	440
25.2.5. <i>Influence of projectile energy on the reduced width of longitudinal momentum distribution</i> .....	441
25.3. FRAGMENT VELOCITY .....	442
25.3.1. <i>Fragment velocity: removing 8 MeV per ablated nucleon</i> .....	443
25.3.2. <i>Fragment velocity on the basis of surface energy exceed</i> .....	443
25.4. NEW UNIVERSAL MODEL OF MOMENTUM DISTRIBUTION ON THE BASIS OF GAUSSIAN AND EXPONENT CONVOLUTION .....	445
<b>26. VERSION 4.8 .....</b>	<b>449</b>
26.1. REDUCTION OF A FRAGMENT OUTPUT DUE TO REACTIONS.....	449
26.1.1. <i>Reactions in a target (stripper)</i> .....	449
26.1.2. <i>Reactions in a wedge</i> .....	450
26.1.3. <i>Reactions in materials</i> .....	450
26.2. CALCULATION OF THE SECONDARY REACTIONS CONTRIBUTION IN A FRAGMENT OUTPUT .....	451
26.2.1. <i>Secondary reactions and Optimal target calculations subroutine</i> .....	453
26.3. OTHER.....	453
26.3.1. <i>New generator of random numbers</i> .....	453
26.3.2. <i>Creation of a file with results of secondary reactions contribution</i> .....	453
26.3.3. <i>Call of a web-homepage of the LISE program from dialogue ABOUT</i> .....	455
26.3.4. <i>Angles of an inclination of a target and a stripper</i> .....	455
26.3.5. <i>Calculation of optimal target thickness from an inclination of a target</i> .....	456
26.3.6. <i>File of transmission calculation results</i> .....	456
<b>27. VERSION 4.7 .....</b>	<b>457</b>
27.1. SECONDARY REACTIONS IN A TARGET .....	457
27.2. PLOTS.....	461
27.2.1. <i>Some distributions for cross section distribution plot</i> .....	461
27.2.2. <i>Possibility to plot transmitted fragments with given charge states</i> .....	461
27.2.3. <i>Transmission characteristics plot</i> .....	461
27.2.4. <i>Manual scale of axis</i> .....	462
27.3. MECHANISM OF REACTION.....	463
27.3.1. <i>Momentum distributions from reactions</i> .....	463
27.3.2. <i>Fragment velocity</i> .....	463
27.3.3. <i>Charge states distribution</i> .....	464
27.4. OTHER.....	464
27.4.1. <i>New configuration files</i> .....	464
27.4.2. <i>Total reaction cross section</i> .....	465
27.4.3. <i>Database half-lives</i> .....	465
27.4.4. <i>Corrections</i> .....	465
<b>28. VERSION 4.6 .....</b>	<b>466</b>
28.1. DEGRADER AFTER TARGET: CONTRIBUTION IN FRAGMENT DISTRIBUTIONS .....	466
28.2. CHARGE STATE DISTRIBUTION IN TRANSMISSION CALCULATION .....	468
28.3. DEVELOPMENT .....	468
28.3.1. <i>M5678-spectrometer's calibration</i> .....	468
28.3.2. <i>Energy Rest in Physical calculator</i> .....	468

28.3.3. TOF shift.....	468
28.3.4. Note of base configuration used for calculations.....	469
28.3.5. Bug.....	469
28.4. BRIEF DESCRIPTION OF PREVIOUS VERSION (4.5.5-4.5.8) CHANGES.....	469
version 4.5.8.....	469
version 4.5.7.....	470
version 4.5.6.....	470
version 4.5.5.....	470
<b>29. VERSIONS 4.2.1 - 4.5.....</b>	<b>472</b>
29.1. MONTE CARLO METHOD FOR TWO-DIMENSIONAL PLOTS (VERSION 4.5).....	473
29.1.1. Speed of Monte Carlo acquisition.....	474
29.1.2. Settings of Monte Carlo method for two-dimensional plots.....	475
29.1.2.1. Distribution compression for Monte Carlo plot.....	475
29.1.2.2. Pixel for one event for Monte Carlo plot.....	475
29.1.2.3. Resolutions and thickness defects.....	476
29.2. IN-BUILT CUBIC SPLINE PROCEDURE (VERSION 4.4).....	476
29.2.1. Transformation of distributions.....	476
29.2.2. Edge's effects.....	477
29.3. DEVELOPMENT.....	478
29.3.1. Different methods to draw one-dimensional plots.....	478
29.3.2. Dimension of distributions.....	478
29.3.3. New plots.....	479
29.3.4. Mode "auto" for the Wien filter and D6-dipole calculations.....	480
29.3.5. Note of base configuration used for calculations.....	480
29.3.6. Bugs.....	480
29.3.6.1. Energy loss calculation in thin material.....	480
29.3.6.2. Calculations with a primary beam in dialogues TOOLS and Physical calculator.....	480
29.4. BRIEF DESCRIPTION OF PREVIOUS VERSION (4.2.1-4.3.15) CHANGES.....	480
version 4.3.....	480
version 4.2.5.....	481
version 4.2.4.....	482
version 4.2.3.....	482
version 4.2.2.....	483
version 4.2.1.....	484
<b>30. VERSION 4.2.....</b>	<b>485</b>
30.1. NEW DIMENSION " kW " TO ENTER AN INTENSITY OF THE PRIMARY BEAM.....	485
30.2. NEW RESULT FILE - ENERGY, TOF, ENERGY LOSS IN MATERIALS.....	485
30.3. CONFIGURATION FILES.....	485
30.4. " UNBOUND " - NEW CHARACTERISTIC MODE TO PLOT IN THE NUCLIDE CHART.....	486
30.5. NEW COMMAND - TRANSMISSION CALCULATION OF NUCLEI CHOSEN BY PREVIOUS COMMAND AREA TRANSMISSION CALCULATION.....	486
30.6. NEW PLOT A/Q - Y (POSITION IN THE THE FINAL FOCAL POINT AFTER THE WIEN FILTER).....	487
30.7. CORRECTIONS.....	487
<i>B.Blank's modification of the cross section parametrization - 4 (EPAX 2.15) to treat more correctly pick-up reactions. ( )</i> .....	487
<i>revision of the nuclide table.....</i>	487
<i>changes MeV/A to AMeV.....</i>	487
<i>revision of half-lives in the nuclides database.....</i>	487
<i>correction of the charge distribution 1 (Leon et al. ) for high energy.....</i>	487
<i>bug in the animation subroutine.....</i>	487
30.8. VERSION 4.1.....	488
30.8.1. version 4.0.30 (16-02-00) Menu "Calculations" -> Reaction's characteristics.....	488
30.8.2. version 4.0.29 (11-02-00) Ion charge state distribution for low energy.....	488
30.8.3. version 4.0.25 (01-02-00).....	488
30.8.4. version 4.0.19 (22-01-00) Struggle with bugs.....	488
<b>31. VERSION 4.0.17.....</b>	<b>489</b>

31.1. WEDGE PROFILES .....	489
31.2. OPTIC AND DEGRADER .....	490
31.3. EXAMPLES OF CALCULATION WITH DEGRADER OF DIFFERENT PROFILES .....	491
31.3.1. <i>Wedge selections plots for different cases of degrader profile</i> .....	492
Figures 697, 698, 699, 700. ....	493
31.3.2. <i>Range distributions in the silicon detector for different cases of degrader profile</i> .....	494
<b>32. VERSION 4.0 .....</b>	<b>495</b>
32.1. VERSION 4.0.* .....	495
<i>version 4.0.14</i> .....	495
<i>version 4.0.10</i> .....	496
Global reconstruction of transmission calculation modules .....	496
<i>version 4.0.9</i> .....	496
<i>version 4.0.8</i> .....	496
<i>version 4.0.7</i> .....	498
<i>version 4.0.3</i> .....	498
32.2. VERSION 3.9.* .....	498
<i>version 3.9.5</i> .....	498
<i>version 3.9.4</i> .....	498
<i>version 3.9.2</i> .....	498
<i>version 3.9.1</i> .....	498
<i>version 3.5</i> .....	498
<b>33. VERSION 3.4 .....</b>	<b>500</b>
33.1. INTRODUCTION (BRIEF DESCRIPTION OF PREVIOUS SERIES) .....	500
33.2. DIPOLE “D6” AFTER THE WIEN FILTER .....	501
33.2.1. <i>Angle of platform</i> .....	501
33.3. IMAGE SHIFT.....	502
33.3.1. <i>Image size</i> .....	503
33.3.2. <i>Separation with the Dipole D6</i> .....	503
33.3.3. <i>The program “LISE” for the new spectrometer VAMOS</i> .....	505
33.4. NEW FEATURES OF THE VERSION 3.4 .....	506
33.4.1. <i>Physical calculator</i> .....	506
33.4.2. <i>Configuration file</i> .....	507
33.4.3. <i>Target Angle</i> .....	508
33.4.4. <i>List of recently used files</i> .....	508
33.4.5. <i>Calculation of Q-ground value for binary reaction</i> .....	509
33.4.6. <i>Chromatic mode (Dispersion <math>\neq</math> 0)</i> .....	509
33.5. DEVELOPMENT .....	512
33.5.1. <i>Results file</i> .....	512
33.5.2. <i>New parameterization</i> .....	512
33.5.3. <i>Trigonometric function of the in-built calculator</i> .....	513
33.5.4. <i>Three points interpolation for the energy loss and range subroutines</i> .....	513
33.6. PLOTS.....	514
33.6.1. <i>Image after Wedge &amp; D6 (one-dimensional plot) and dE - Y image (after wedge &amp; D6)</i> .....	514
33.6.2. <i>dE-dE plot</i> .....	515
33.6.3. <i>dE-X plot</i> .....	515
33.6.4. <i>Realistic image of peaks</i> .....	515
33.6.5. <i>Plot of Q-ground values</i> .....	516
33.6.6. <i>Gray and Color Palettes for two-dimensional plots</i> .....	516
33.7. BUGS.....	516
33.7.1. <i>The thickness dialog - density</i> .....	516
33.7.2. <i>The dialog “Calibrations”</i> .....	516
33.7.3. <i>Adaptation the code to the PC emulator on Mac</i> .....	516
33.7.4. <i>Negative dispersion</i> .....	516
33.7.5. <i>After reading of a LISE-file the program did not calculate magnetic field</i> .....	516
33.7.6. <i>Distributions</i> .....	516
<b>34. VERSION 2.2: LISE (DOS )REFERENCE MANUAL.....</b>	<b>517</b>

34.1. GENERAL DESCRIPTION .....	517
34.2. LIST OF FEATURES .....	517
34.2.1. <i>Simulation of experimental conditions</i> .....	517
34.2.2. <i>Calculations performed</i> .....	517
34.2.3. <i>Display</i> .....	518
34.2.4. <i>Files and results output</i> .....	518
34.2.5. <i>User-friendly features</i> .....	518
34.3. CALCULATIONS .....	519
34.3.1. <i>Reaction mechanism and cross sections</i> .....	519
34.3.2. <i>Beam optics</i> .....	519
34.3.3. <i>Acceptance and transmission calculations</i> .....	520
34.3.4. <i>Energy loss and range tables</i> .....	520
34.4. DETAILED OPERATING DESCRIPTION .....	521
34.4.1. <i>Mouse handling in menus</i> .....	521
34.4.2. <i>Keyboard entries</i> .....	521
34.4.3. <i>Description of each command following the menu structure</i> .....	521
34.5. TUTORIAL : A SAMPLE CALCULATION.....	530
34.6. COMPUTER CONSIDERATIONS.....	533
REFERENCES .....	535

# 1. Version 7.5: Abrasion-Fission

## 1.1. Introduction

Fission observed after the collision of Uranium projectiles with target nuclei is due to both electro-magnetic and to nuclear processes. At large impact parameters, the long-range Coulomb force dominates (Coulomb fission). The projectile is excited mostly to the region of giant resonance by exchange of virtual photons; the system then decays by neutron emission or by fission (see Fig.1).

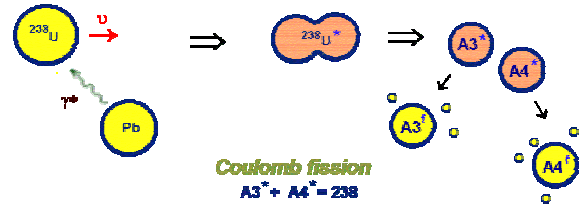


Fig.1. Coulomb fission scheme.

### Abrasion-Fission : fission of a heavy projectile after abrasion by a target heavier than Be

At smaller impact parameters, peripheral nuclear collisions take place, and the fissile projectile is left abraded and excited. After de-excitation by nucleon emission, it can undergo fission with a finite probability [Hes96] as well as of break-up. Three de-excitation channels should be taken into account after abrasion: fission (Fig.2), break-up (Fig.3), and evaporation of light particles (Fig.4).

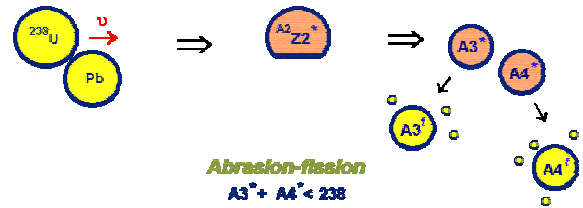


Fig.2. Abrasion-fission scheme.



Fig.3. Abrasion-Break-up scheme.



Fig.4. Abrasion-Evaporation scheme.

In the case of fission of an incident projectile in result of collisions with a light target nucleus (see Fig.5) we will be using the term “INC\* fission” in this documentation.

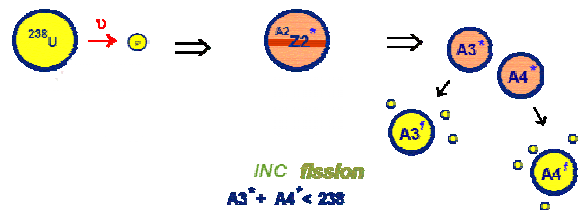


Fig.5. INC fission scheme.

### INC fission : fission of a heavy projectile on light targets (p,d,<sup>3</sup>He,α).

A new model based on the fast analytical calculation of ABRASION-FISSION fragment transmission through a fragment separator has been developed in the framework of the code LISE++.

Before discussing Abrasion-Fission it is necessary to explain a number of changes and new developments in the program that were included to provide all of the important components to analyze the Abrasion-Fission fragment production, such as dissipation effects in fission, break-up de-excitation channels, secondary reactions in the target, and a reexamination of fission barriers.

\* Intra-Nuclear Cascade

## 1.2. De-excitation process

The decay of highly excited nuclei takes place via various processes, which have great practical importance [Sch02] such as fission, spallation, fragmentation and others. The compound-nucleus mechanism dominating at low excitation energies changes into simultaneous decay into many fragments with increasing energy. In order to describe qualitatively the de-excitation process of highly excited nuclei there are three principal approaches pursued in the new version of the code. They are available through the “Evaporation options” dialog (in the case of fusion or fission reactions set in the code, see Fig.6) or from the “Prefragment search and Evaporation option” dialog (in the case of projectile fragmentation) (see Fig.7):

- Dissipative effects in fission (frames “A”),
- Break-up channel (frames “B”),
- Fission barrier reexamination (frame “C”).

These new features were implemented to achieve better agreement between LISE calculations and data from GSI experimental and theoretical approaches. In this chapter we will explain the nature of these new effects. The influence of these parameters on the models in the final Abrasion-Fission fragment production will be presented in chapter [1.5. Abrasion-Fission](#).

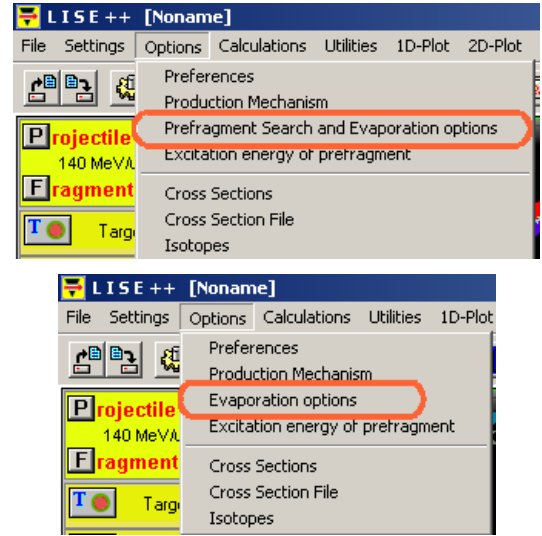


Fig.6. The “Options” menu

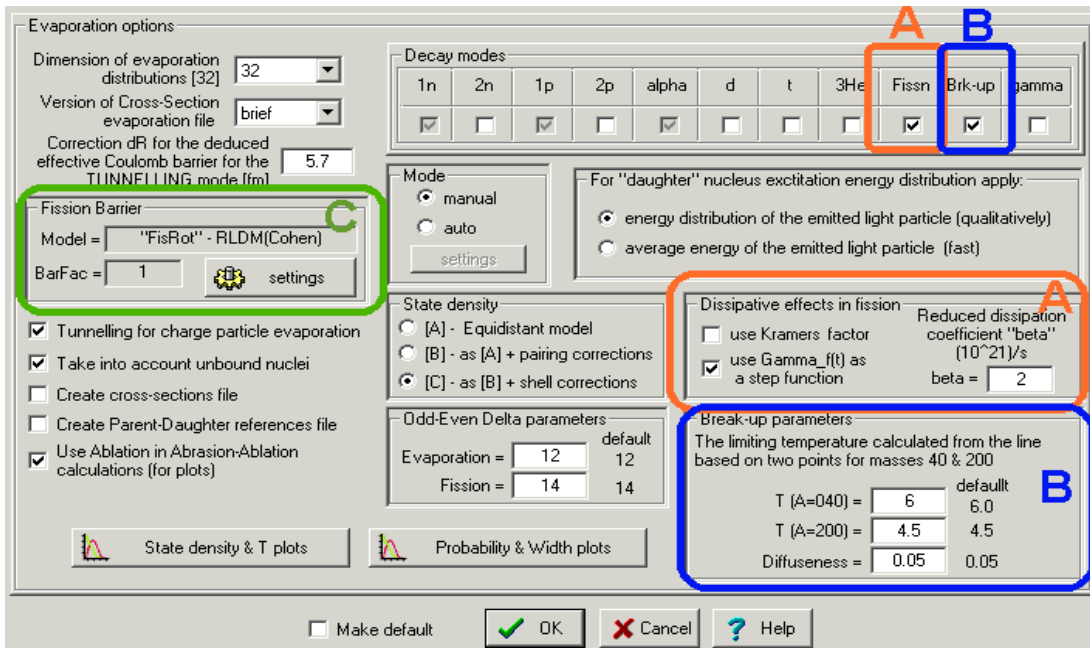


Fig.7. The “Evaporation option” dialog.



### 1.2.1. The break-up channel in the evaporation cascade

It is suggested that the “**break-up channel**” is a simultaneous decay of a highly excited nucleus into many fragments. **Abrasion-breakup** is break-up of the projectile residue after abrasion by a target when the nuclear temperature of the fragment exceeds the limiting temperature.

*The code doesn't calculate mass and element distributions of fragments after break-up\**! The principal aim of this version is calculation of Abrasion-Fission products. This is the reason why break-up events are excluded from the following calculations. Future plans are to make an analysis of the products from Abrasion-Breakup with sequential decay as was done for Abrasion-Evaporation and Abrasion-Fission channels in the current version of LISE++.

#### 1.2.1.1. The limiting temperature as a function of mass number

The limiting temperature is calculated as a function of the mass between  $A=40$  and  $A=200$  (see Fig.7, frame “B”). The default values are taken from the paper [De96] (see Fig.8). If you prefer the limiting temperature to be constant for all masses as in [Sch02] just set the same value for both masses in the dialog. To avoid a jump in the widths calculation of de-excitation channels, the break-up channel shape is represented by a Fermi distribution  $\rho(T) = 1 - 1/(1 + \exp[(T - T_{lim})/d])$ , where  $d$  is the diffuseness (default value is equal to 0.05), which can be modified in the “Evaporation options” dialog (see Fig.7, frame “B”).

By clicking the “Probability & Widths plots” button in the “Evaporation options” dialog it is possible to match the probabilities of different de-excitation channels as a function of excitation energy (see Fig.9).

**Note:** Comparison between Abrasion-Ablation calculations with the break-up option and experimental values of fragment production cross-sections in fragmentation of intermediate beams ( $Z=16-28$ ) indicates that the limiting temperature should be larger for fragments with masses less than 40 was predicted in [De96]. Consequently we propose increasing the limiting temperature for this case for low masses or turning off the break-up channel, since its contribution should be insignificant.

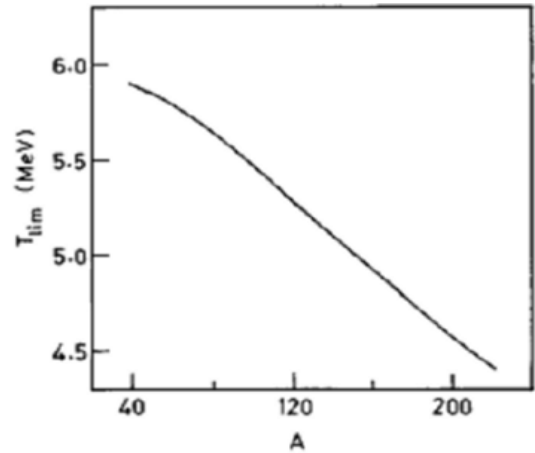


Fig.8. The limiting temperature  $T_{lim}$  as a function of mass number on the  $\beta$ -stability line [De96].

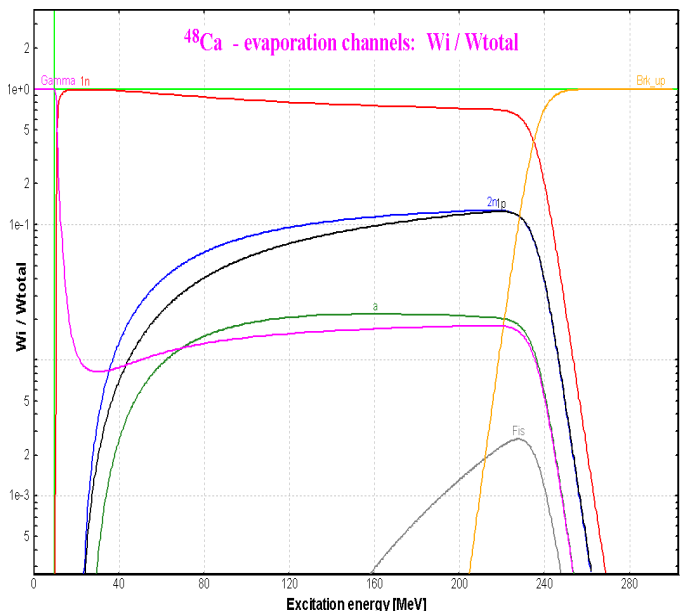
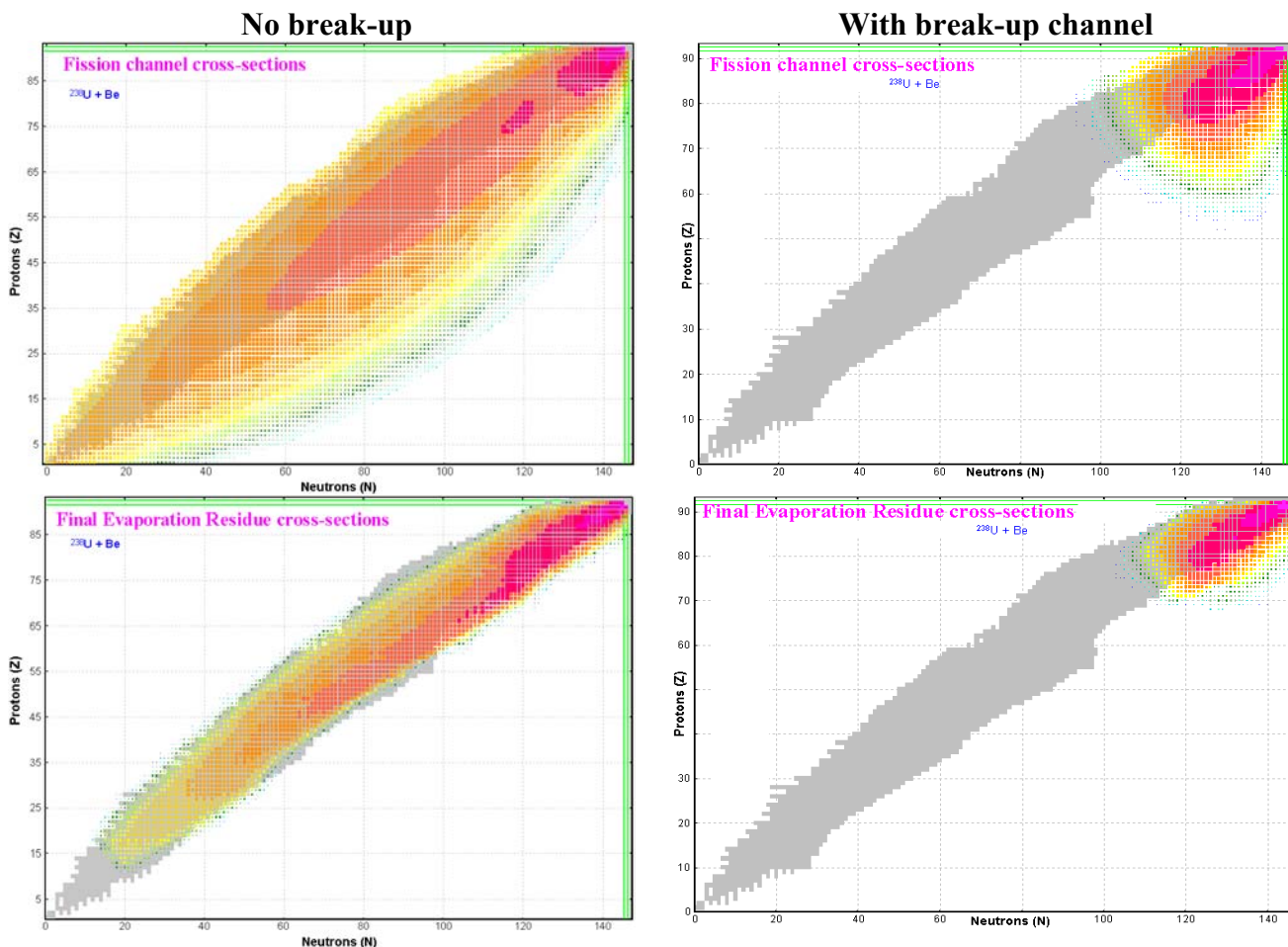


Fig.9.  $^{48}\text{Ca}$  de-excitation channel probabilities as a function of the excitation energy. The break-up is taken into account and begins to dominate at energies above 240 MeV.

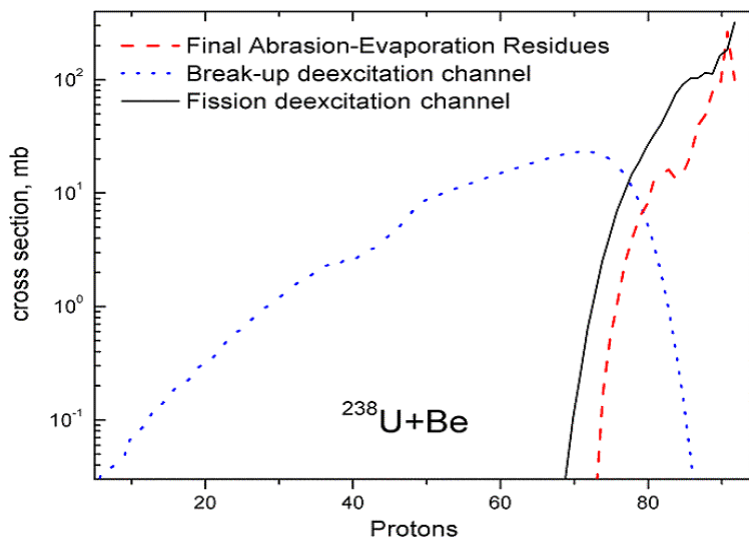
\*as it was done in [Sch02]. In order to simulate the production of residues in the fragmentation of  $^{238}\text{U}$  projectiles with LISE++ you have to turn off the break-up channel and use the “triangle” excitation function. See chapter 4.6 “Excitation energy of Prefragment” of the documentation for version 6.4 ([http://groups.nsl.msu.edu/lise/6\\_4/lise++\\_6\\_4.pdf](http://groups.nsl.msu.edu/lise/6_4/lise++_6_4.pdf)).

### 1.2.1.1.1. The crucial role of the break-up channel in heavy projectile fragmentation

The crucial role of break-up channel contributions in the fragment production in reactions with heavy projectiles at relativistic energies is demonstrated well in Fig.10 and Fig.11.



**Fig.10.** Fission channel cross-sections resulting from  $^{238}\text{U}(1\text{AGeV})$  abrasion by a Be target (top panel). The bottom pictures show the final evaporation residue cross-sections in the same reaction. Calculations shown on the left plots were done without the Break-up channel, whereas for the plots on the right side the break-up channel was taken into account.



**Fig.11.** Nuclear charge yields for different de-excitation channels after  $^{238}\text{U}(1\text{AGeV})$  abrasion on a Be-target.

**Notes:** Several cross-sections shown in Fig.10 are outside the LISE nuclide table due to fact that unbound nuclei are taken into account for the fission de-excitation channel. In the case of evaporation residues, only particle-bound nuclei can be produced. The code calculates separation energies from LISE LDM2 using AME2003 data, but the LISE nuclide table is based on old measurements and can be modified manually by the user.

### 1.2.2. Dissipation effects in fission

Dissipation is a fundamental process in nuclei that determines the time an excited nucleus needs to populate the available space and to reach equilibrium [Jur02]. The concept of dissipation was already introduced by Kramers [Kra40] more than sixty years ago, but the success of the transition-state model of Bohr and Wheeler [Boh39] prevented his idea from being established [Jur02, Jur03]. However, it was shown by different groups in the 80's that measured pre-scission neutron multiplicities were much larger than the predictions of the transition-state model. This discrepancy was interpreted as an indication that **the de-excitation process of a highly excited heavy nucleus is a dynamical process.**

Recently at GSI an analysis of dissipative effects in nuclear fission observed in the fragmentation of  $^{238}\text{U}$  projectiles was performed by A.Ingatyuk et al [Ign95], and new signatures of dissipation in fission induced by relativistic heavy-ion collisions were obtained by B.Jurado et al. [Jur02, Jur03]. Using results of these studies, the dissipation effects in fission were implemented in the LISE++ code.

In the quasi-stationary approximation Kramers obtained the following equation for the fission width:

$$\Gamma_f^K = K \cdot \Gamma_f^{BW} \quad /1/$$

where  $\Gamma_f^{BW}$  is the fission-decay width given by the transition-state model, and  $K$  is the factor:

$$K = \sqrt{1 + \gamma^2} - \gamma \quad /2/$$

with

$$\gamma = \beta/2\omega_0 \quad /3/$$

where  $\beta$  is the reduced dissipation coefficient, and  $\omega_0$  is the frequency of the harmonic-oscillator potential that osculates the fission barrier at the saddle point. LISE fixed this potential equal to  $\hbar\omega_0 = 1 \text{ MeV}$  for the fission width calculations.

The fission process requires a finite time. The dependence of this transient time  $\tau$  on the dissipation coefficient for the underdamped and the overdamped regions is the following:

$$\tau_{under} = \frac{1}{\beta} \ln \frac{10B_f}{T}, \quad \text{for } \beta > 2\omega \quad /4/$$

$$\tau_{over} = \frac{\beta}{2\omega^2} \ln \frac{10B_f}{T}, \quad \text{for } \beta < 2\omega \quad /5/$$

The transient times defined in following Equations /4,5/ are shown in Fig.12<sup>♦</sup> together with numerical solutions of the Fokker-Planck equation [Bha86].

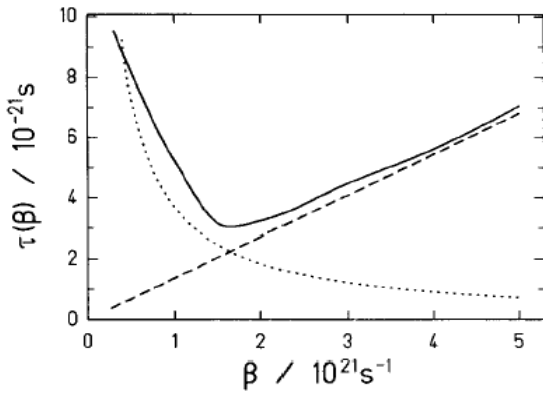
Taking into account the transient time, the ratio of the widths for fission and neutron emission can be written as

$$\frac{\Gamma_f(\beta)}{\Gamma_n + \Gamma_p + \Gamma_\alpha} = K(\beta) \cdot \frac{\Gamma_f^{BW}}{\Gamma_n + \Gamma_p + \Gamma_\alpha} \cdot \exp\left(-\frac{\tau(\beta)}{\tau_{v\pi}}\right) \quad /6/$$

where  $\tau_{v\pi} = \hbar/(\Gamma_n + \Gamma_p + \Gamma_\alpha)$  is the mean life-time against neutron, proton and alpha-particle emission.

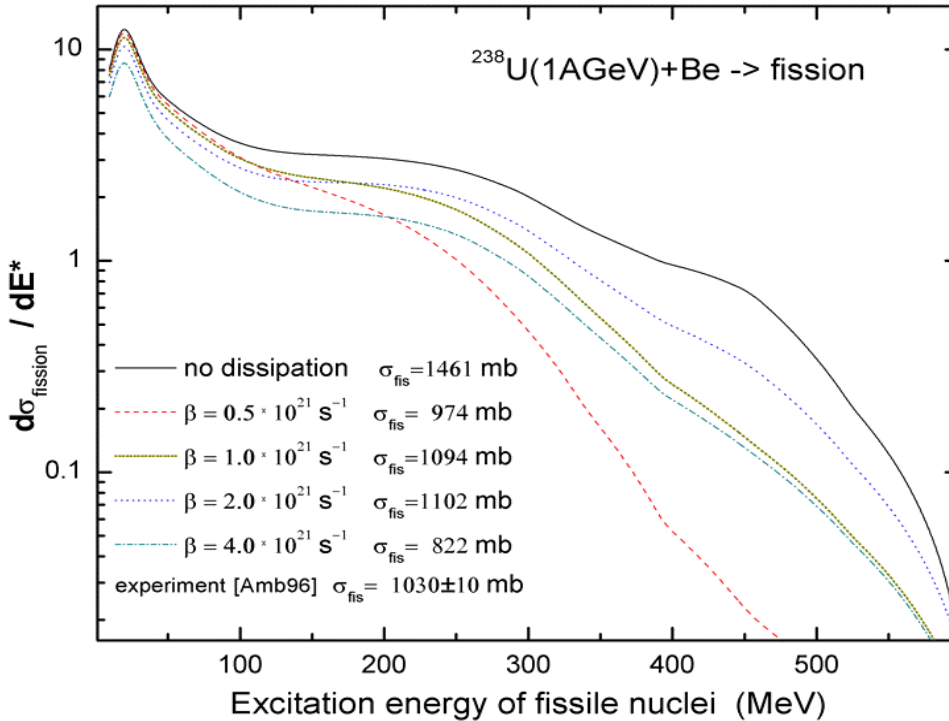
---

<sup>♦</sup> it was taken from [Ign95].



**Fig.12.** Calculated transient times  $\tau(\beta)$  for the overdamped and underdamped regimes (Eqs./4,5/ with  $B_f = 4$  MeV,  $T = 1$  MeV,  $\omega = 1.31 \cdot 10^{21} \text{ s}^{-1}$ ) [Bha86]. The dashed line corresponds to overdamped motion: the transient time increases with increasing viscosity. The dotted curve shows the case of underdamped motion, which leads to an increase in the transient time when the viscosity becomes very small and the energy is slowly dissipated into collective motion. The solid curve is calculated from a numerical solution of the Fokker-Planck equation.

The transient time is defined as  $\tau(\beta) = \max(\tau_{under}, \tau_{over})$  in LISE. The factor  $K$  is set to 1 in Equation /6/ to calculate the fission-width if “Use Kramers factor” is turned off in the “Evaporation options” dialog (see Fig.7, frame “A”). The user can modify the reduced dissipation coefficient  $\beta$  and turn on/off the dissipation effects for fission based on Equation /6/.



**Fig.13.** Fission summary excitation functions with different reduced dissipation coefficients and without dissipation effects for fissile nuclei produced in the reaction  $^{238}\text{U}(1\text{AGeV})+\text{Be}$ .

The following parameters for the Abrasion-Ablation model were used to produce these calculations:

Excitation energy:

Method #2

$Ex = 13.3 \text{ dA}$

$\sigma = 9.6 \text{ (dA)}^{0.5}$

Channels:

$p, n, 2n, \alpha, \text{fission, break-up}$

Break-up:

$T(40)=6.0, T(200)=4.5$

$NP = 16; SE: \text{DB0+Cal2};$

Kramers factor: YES

BarFac=1; Mode: auto

Fission summary excitation functions without dissipation effects and with different reduced dissipation coefficients for fissile nuclei produced in the reaction  $^{238}\text{U}(1\text{AGeV})+\text{Be}$  are shown in Fig.13 to demonstrate how total nuclear fission cross-section and the shape of the fission excitation functions can depend on the dissipation effects. A more detailed analysis of the dissipation effects in the fission summary excitation function and comparisons with experimental data will be presented in chapter “1.5.4.4. Dissipation effects in fission”.

### 1.2.3. Evaporation calculator modifications

Some modifications were made in the Evaporation calculator related to the introduction of a new decay channel (see Fig.14, frame “A”). The initial\* abrasion cross-section, the summed cross-sections of residues production, the cross-sections for fission and break-up de-excitation channels are given in frame “B” in Fig.14. The initial cross-section consists of residue (Abrasion-evaporation) cross-sections, fission and break-up channels.

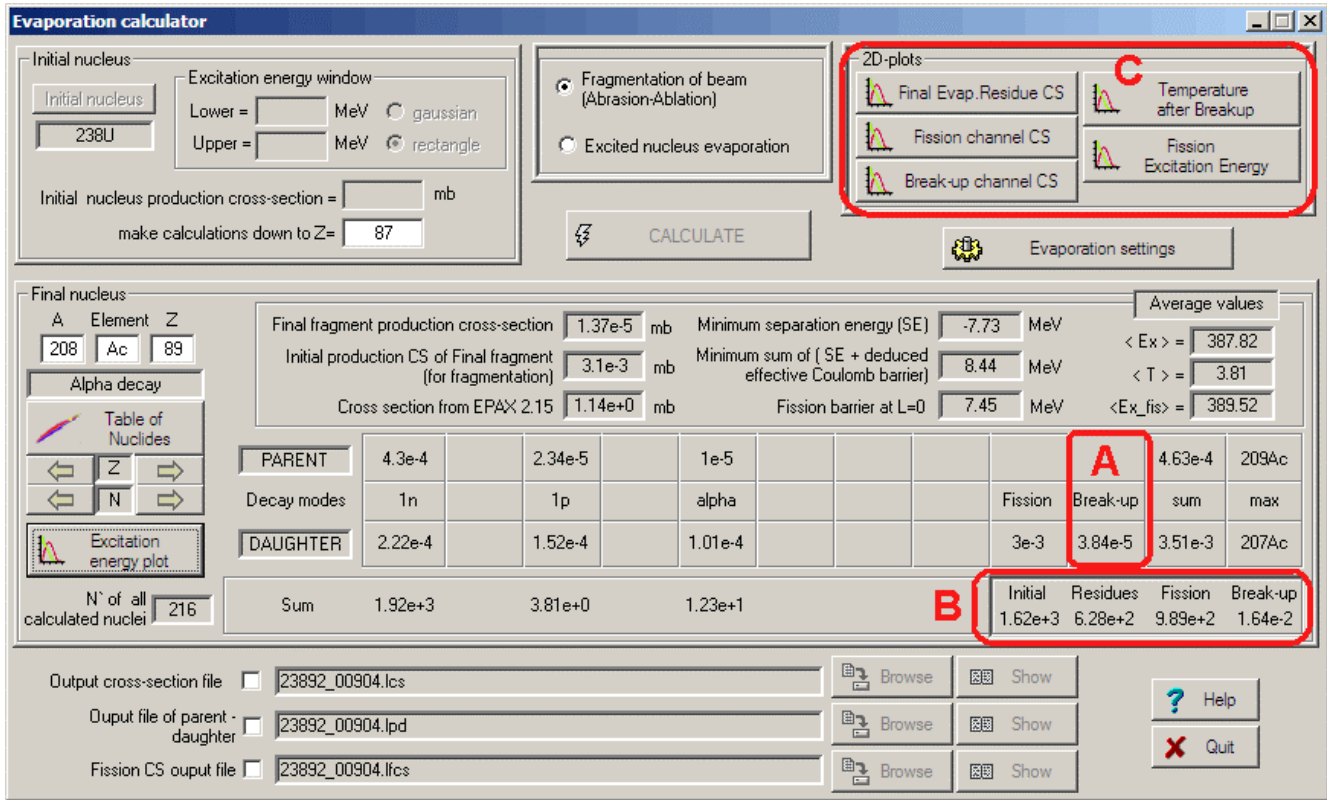


Fig.14. The Evaporation calculator. New modifications are marked by red rectangles.

The Evaporation calculator allows one to visualize the dynamics of the de-excitation of the nucleus, and the history of excitation. The input parent excitation channels for the  $^{208}\text{Ac}$  nucleus in  $^{238}\text{U}(1\text{AGeV})+\text{Be}$  are shown in Fig.15, the corresponding de-excitation channels in Fig.16. From Fig.15 it is possible to conclude that the more intense component of the excitation function corresponds to the initial abrasion (blue curve), but the main channel producing the final fragment  $^{208}\text{Ac}$  in the ground state (Abrasion-Evaporation) is the 1n-channel (low energy part of the excitation function between zero and the minimum separation energy marked by the green vertical line). The sum dominating de-excitation channel is fission, but it is easy to see from Fig.16 that the break-up channel begins to prevail at energies above 520 MeV. Parameters of these calculations are given in the break-up channel 2D-plot in Fig.17. Fission channel and final evaporation residue cross-section 2D-plots with and without break-up channel were already shown in Fig.10.

\* The sum of cross-sections from the initial nucleus down to an element Z (see Fig.14), down to which calculations were done.

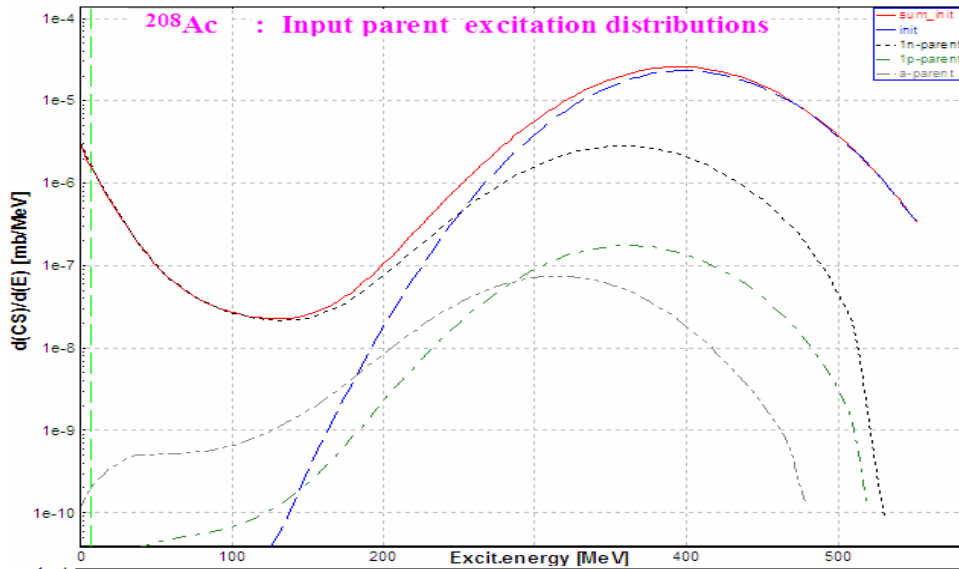


Fig.15. Input parent and initial abrasion contributions to the excitation function of  $^{208}\text{Ac}$  in the reaction  $^{238}\text{U}(1\text{AGeV})+\text{Be}$ .

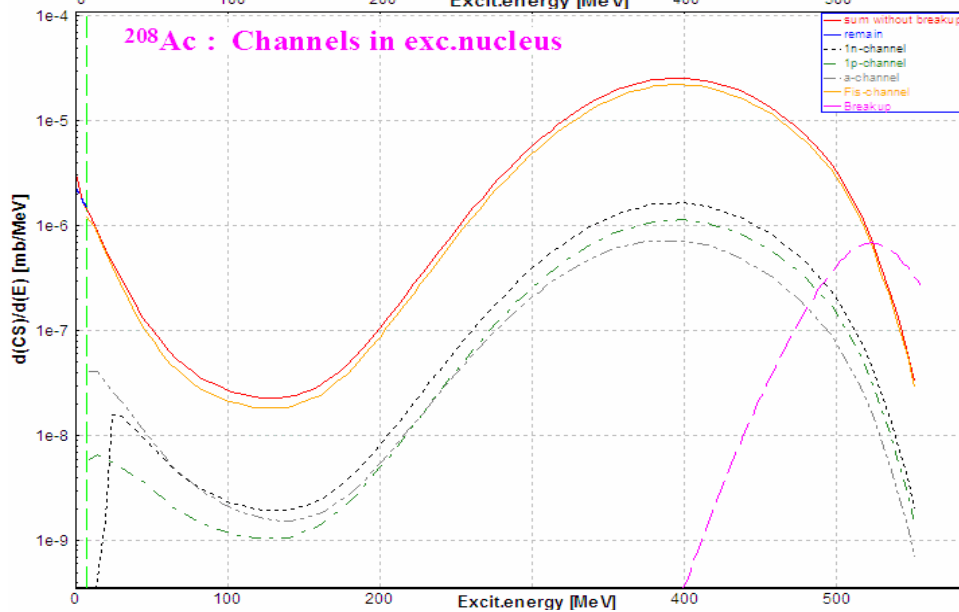


Fig.16. De-excitation channels of  $^{208}\text{Ac}$  in the reaction  $^{238}\text{U}(1\text{AGeV})+\text{Be}$ .

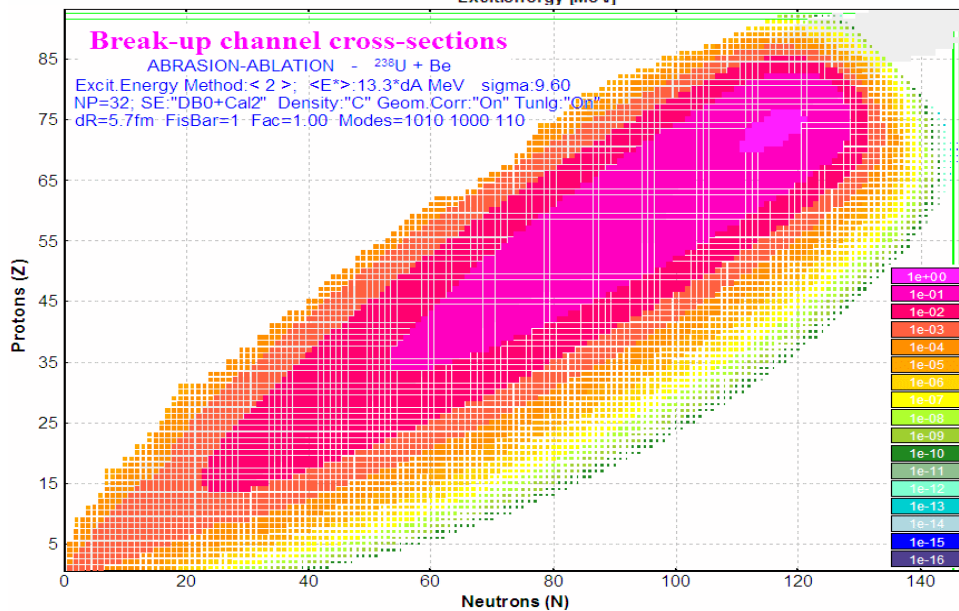


Fig.17. 2D-plot of break-up de-excitation channel cross-sections for  $^{238}\text{U}(1\text{AGeV})$  abrasion on a Be-target.

### 1.3. Fission barriers

The LISE code needs fission barriers for:

- Calculation of fission de-excitation channels for the estimation of the total cross-sections of Coulomb and Abrasion fission as well as abrasion-evaporation residues. For the next version, plans are to develop the model to calculate fusion-fission production cross-sections in the low excitation energy region where the fission barrier plays a crucial role<sup>♦</sup>.
- Calculation of decay widths in the post-scission nucleon emission procedure.

The Cohen-Plasil-Swiatecki rotating liquid drop fission barrier [Coh74] without shell and odd-even corrections was used in the previous version of LISE. A large fission yield was found close to the proton shell  $Z=82$  during the development of the Abrasion-Fission model in the LISE code. This high yield contradicted experimental data. It was explained by the small height of the fission barrier, which is expected to grow near shell closures. In this context it was a necessity to introduce shell corrections and odd-even effects. Other fission barrier models and the possibility to use experimental values for the fission barrier were implemented in the code.

#### 1.3.1. The Fission barrier dialog

The “Fission barrier” dialog (see Fig.18) can be reached by clicking on the “Settings” button of the “Fission barrier” frame in the “Evaporation option” dialog (see Fig.7, frame “C”).

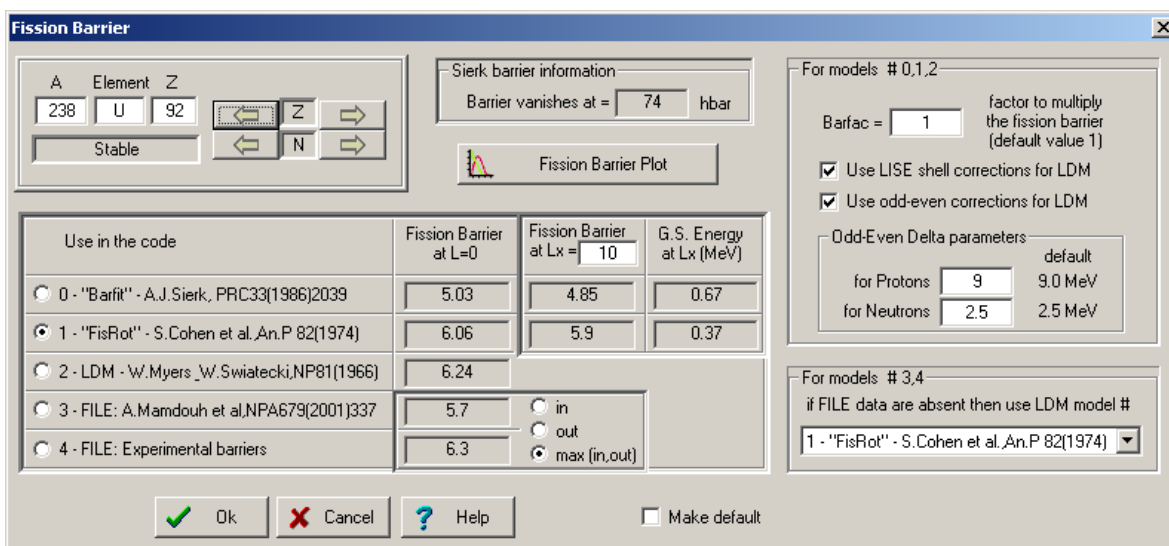


Fig.18. The “Fission barrier” dialog.

The user can choose from five options available in the code: three models (Sierk [Sie86], Cohen [Coh74], Myers[Mye66]) to calculate a fission barrier or extract it from files (Mamdout [Mam01] and experimental data [Smi93]). If the selected option is “take data from the file” (model #3,4) and interested data are absent in the corresponding data-file then the code uses one of three calculation models which is set in the dialog (right bottom frame in the Fission barrier dialog).

<sup>♦</sup> As well as to take into account an angular momentum of the compound nucleus for fission barrier calculation and subsequent fission fragment production cross-section calculations.

### 1.3.2. ETFSI and experimental fission barriers

The file “**fis-barrier-etfsi.dat**” in the directory “\bin” contains calculated fission barriers by the ETFSI<sup>♥</sup> method [Mam01]. The file “**fis-barrier-user.dat**” contains information about experimental fission barrier values extracted from the site <http://www.ndc.tokai.jaeri.go.jp/~fukahori/RIPL-2/>.

#### **File format:**

The separation between values can be by tab, comma, or space.

If one of the barriers (“Bin” or “Bout”) is absent then substitute any letter (We used “X”)

“#”-char in the beginning of line denotes comments.

The line contains four values:        Z ,    A ,    Bin ,    Bout

for example:                        90 ,    230 ,    6.1 ,    6.8

Using one of three buttons “In”, “Out”, “Max(in,out)” the user can define which kind of fission barrier will be used in the code for models #3 and #4.

### 1.3.3. Calculation models (#0,1,2)

The fission barrier used in the code is equal to the sum of the calculated value in the selected model at  $L=0$  plus shell and odd-even corrections:

$$B_{f\_final} = B_{f\_init}(at L=0) \cdot b + \Delta_{shell} + \Delta_{odd-even} , \quad /7/$$

where  $b$  (Barfac) is the factor to multiply the fission barrier. The default value is  $b=1$ . This factor can be changed by user in the Fission barrier dialog (right bottom frame in Fig.18).

#### 1.3.3.1. Shell corrections

For shell corrections the code takes the difference between LISE LDM#2 with shell corrections and LISE LDM#2 without shell corrections using the new compilation of Atomic Mass Evaluation 2003 (Chapter 1.7. Masses. AME2003). For details about shell corrections see chapter “5. Improved mass formula with shell crossing corrections” in the LISE v.6 documentation [http://groups.nslc.msu.edu/lise/6\\_1/lise++\\_6.pdf](http://groups.nslc.msu.edu/lise/6_1/lise++_6.pdf).

Fig.19 and Fig.20 show the fission barriers of Polonium isotopes ( $Z=84$ ) without and with shell corrections.

#### 1.3.3.2. Odd-Even corrections

Odd-even corrections are calculated in the following way:

$$\Delta_{odd-even} = ((N\%2) \cdot V_N + (Z\%2) \cdot V_Z) / \text{sqrt}(N+Z) , \quad /8/$$

where  $N$  is the number of neutrons in the nucleus,  $Z$  is the number of protons,  $V_N$  is the value for neutrons (from LISE fit<sup>▲</sup> is equal to 2.5 MeV),  $V_Z$  is the value for protons (from LISE fit is equal to 9.0 MeV).

Fig.21 and Fig.22 show fission barriers of Uranium isotopes ( $Z=92$ ) without and with odd-even corrections. The grey curve corresponds to experimental data.

---

<sup>♥</sup> Predictions of the fission barriers and saddle point deformations obtained within the Extended Thomas-Fermi plus Strutinsky Integral (ETFSI) method for 2301 nuclei with  $78 \leq Z \leq 120$  [Mam98, Mam01, Smi93]

<sup>▲</sup> Calculated fission barriers (Sierk and Choen) with shell corrections and ALL ( $Z=80-96$ ) experimental data (file “fis-barrier-user.dat”) were fitted to get factors for odd-even corrections.



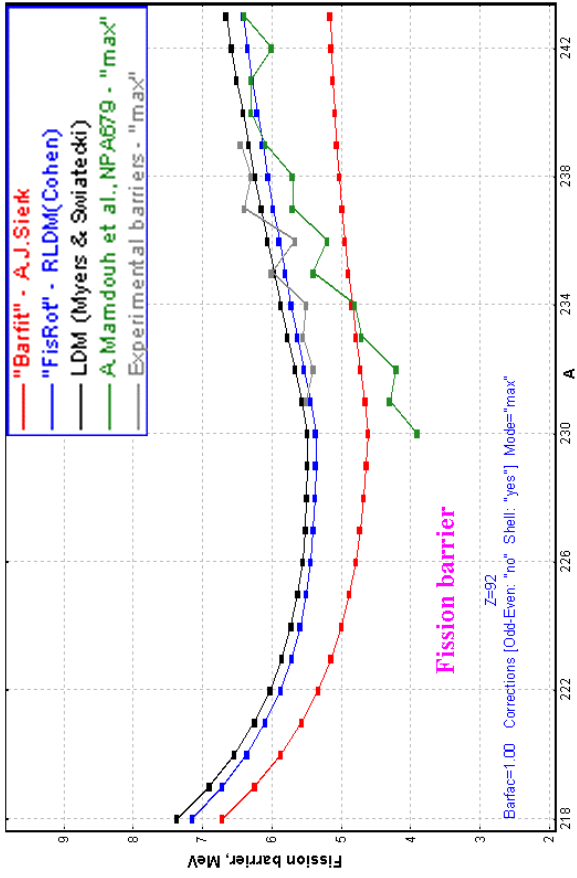


Fig.21. Fission barriers of Uranium isotopes calculated with shell and without odd-even corrections.

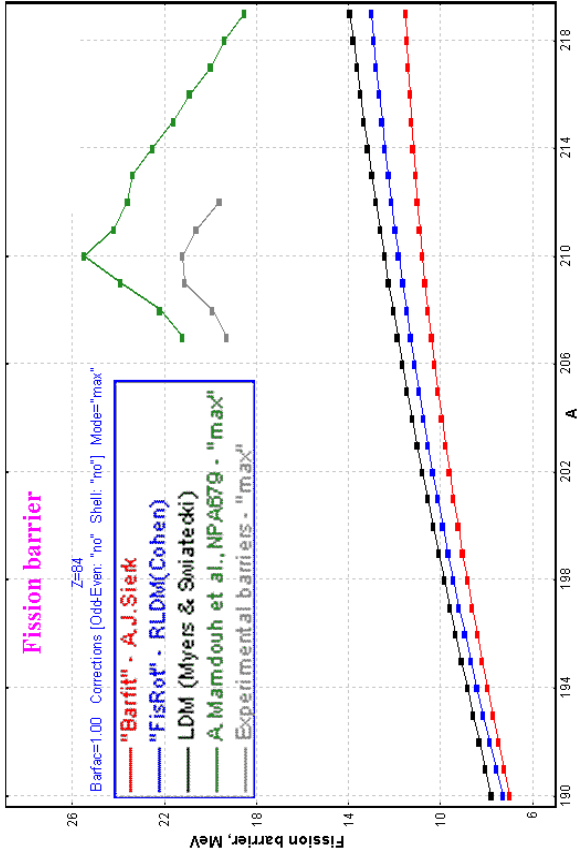


Fig.19. Fission barriers of Polonium isotopes calculated without shell and odd-even corrections.

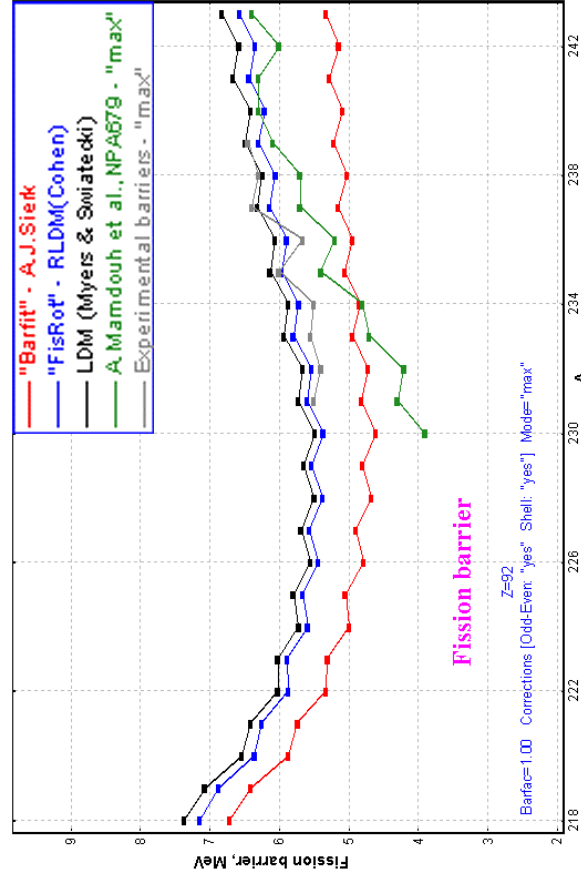


Fig.22. Fission barriers of Uranium isotopes calculated with shell and odd-even corrections.

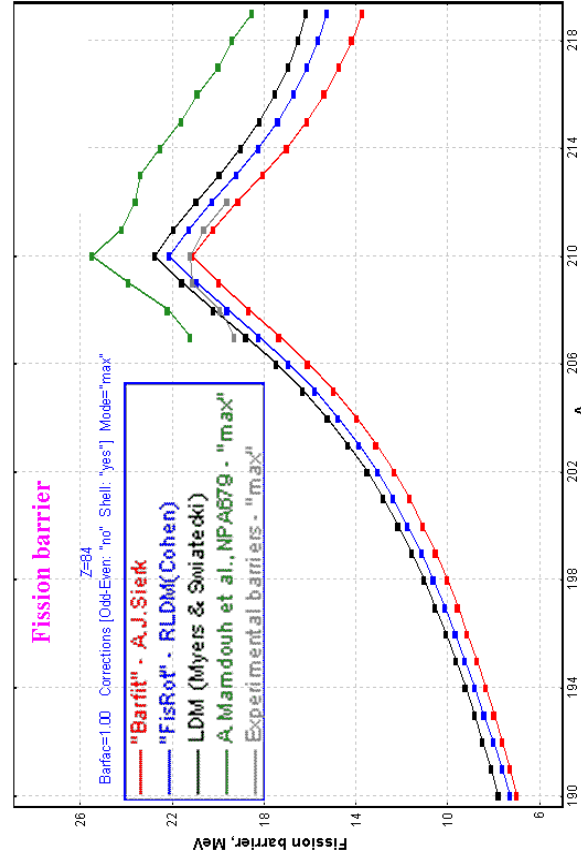


Fig.20. Fission barriers of Polonium isotopes calculated with shell and without odd-even corrections.

### 1.3.4. Fission barrier plot

Some LISE fission barrier plots have already been shown in the previous chapter. Use the “Fission barrier plot” button from the “Fission barrier” dialog (see Fig.18) to build the “Fission barrier plot” dialog (see Fig.23).

There are several opportunities to plot fission barrier values:

- One and two dimensional plots
- Differences between models
- ALL models together in one plot (see Fig.23). But it works only if
  - ❑ one-dimensional plot mode is selected
  - ❑ plot one data set is selected (**not** difference between data sets)
  - ❑  $X_{min} = X_{max}$

If one of these requirements is not met then the “All methods” string disappears in the dropdown list box.

An example of a 2D fission barrier plot is given in Fig.24 and an example of a plot of the difference between methods in Fig.25.

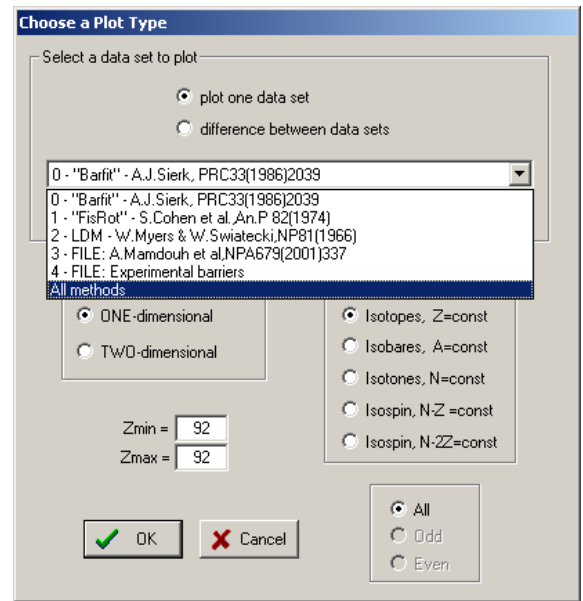


Fig.23. The “Fission barrier plot” dialog.

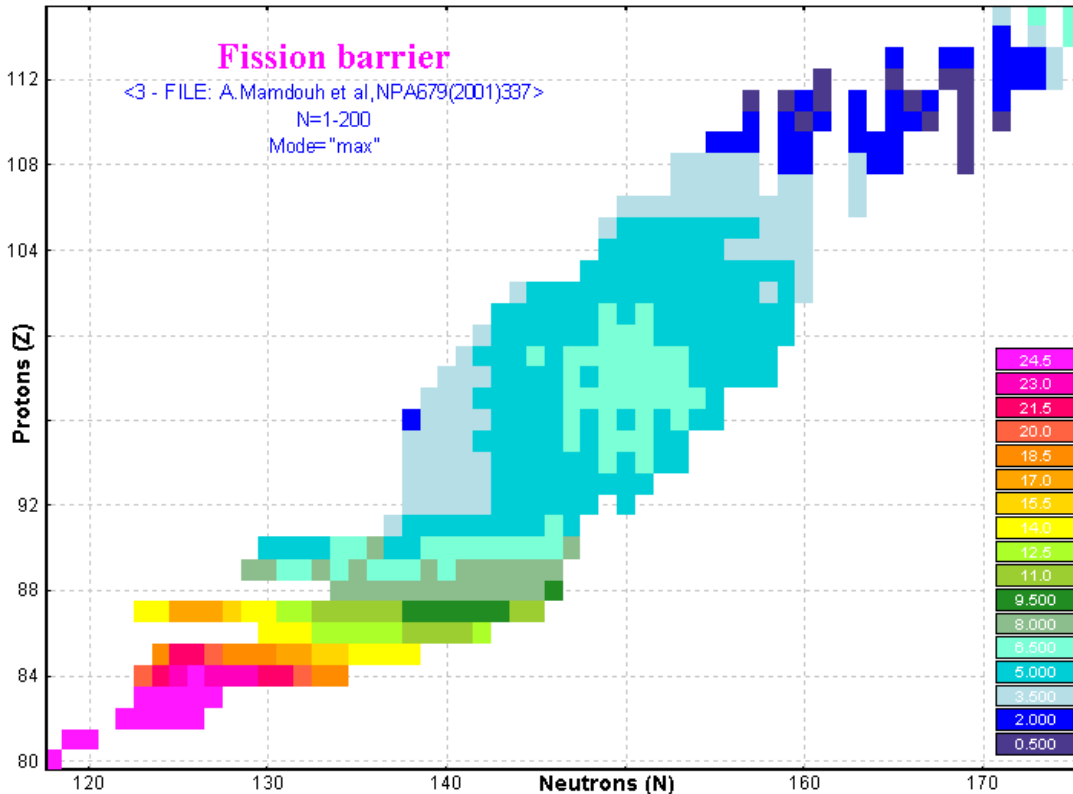
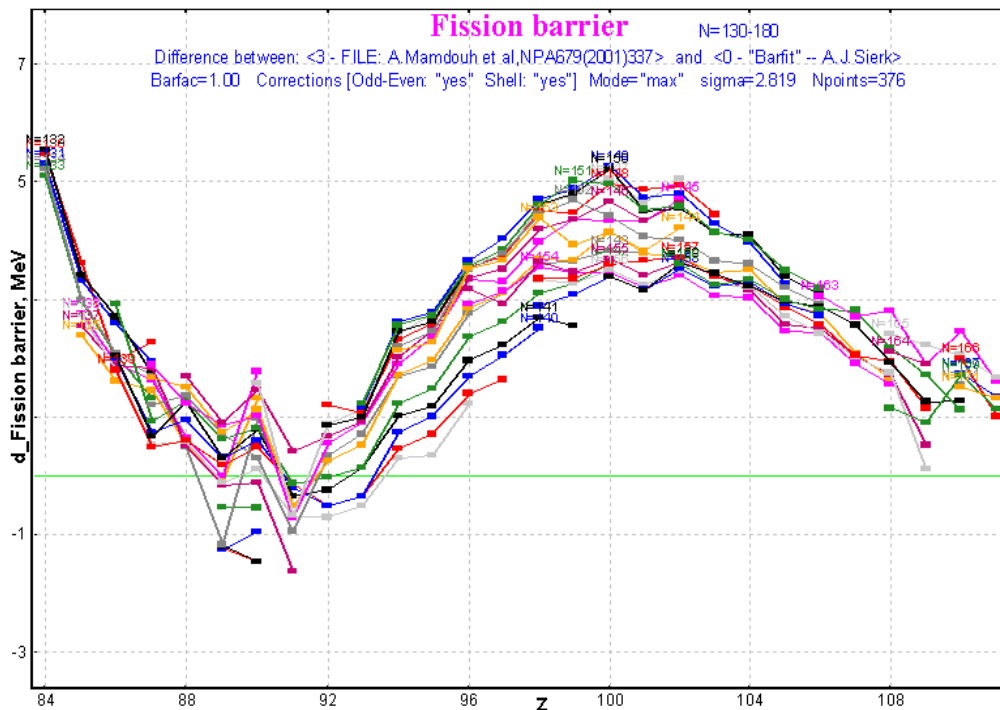


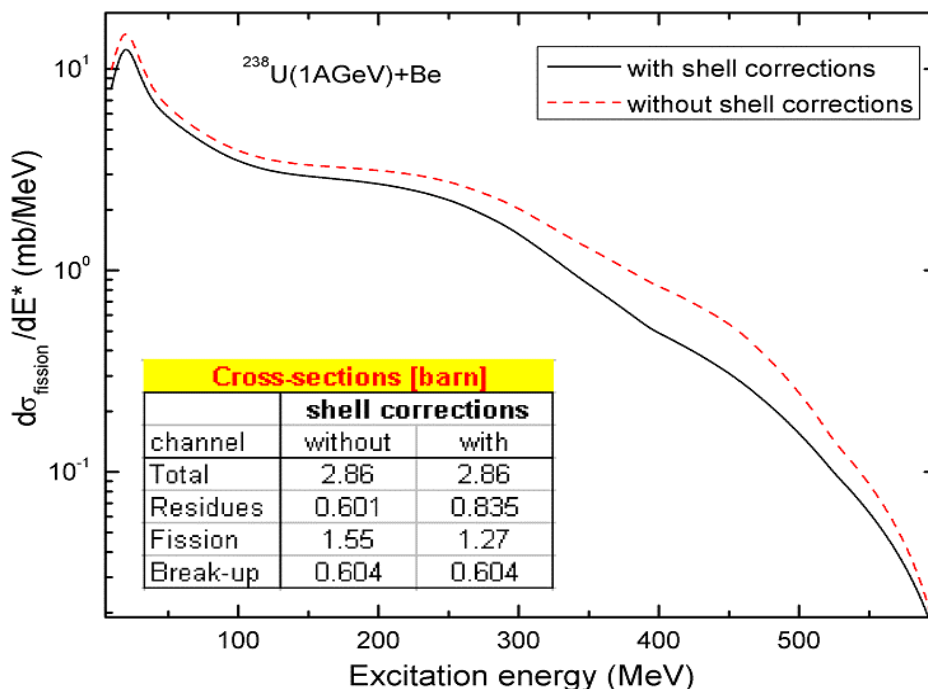
Fig.24. Example of the 2D fission barrier plot for the fission barrier model #3 (A.Mamdouh et al.)



**Fig.25.** Example of the fission barrier plot of the difference between models #3 (A.Mamdouh et al.) and #0 (A.Sierk).

### 1.3.5. Influence of corrections for fission barriers on abrasion-fission cross-sections

Fission summary excitation functions with and without shell corrections for fission barriers of fissile nuclei produced in the reaction  $^{238}\text{U}(1\text{AeV})+\text{Be}$  are shown in Fig.26. The insert on the figure shows channel cross-sections. It can be seen that shell corrections for fission barriers increase residue production by 40% and decrease the fission channel probability. Abrasion-ablation model parameters used were the same as shown in Fig.13 except Kramers' factor was turned off and the reduced dissipation coefficient  $\beta$  was set to  $1.5 \cdot 10^{21} \text{ s}^{-1}$ .



**Fig.26.** Fission summary excitation functions with/without shell corrections for fission barriers of fissile nuclei produced in the reaction  $^{238}\text{U}(1\text{AeV})+\text{Be}$ .

## 1.4. Secondary reactions in target

### 1.4.1. Reexamination of secondary reactions calculation procedure

The secondary reactions (SR) calculation procedure has undergone some cardinal changes due to the following causes:

- **The dependence on the dimension value** ( $NP_{evap}$ ) of SR distributions. The previous algorithm of calculations was valid, when the target ( $T$  - thickness) was divided into  $NP_{evap}$  slices, the condition  $T \cdot \sigma / NP_{evap} \rightarrow 0$  is true. In other words there should not be a difference at the end of the target between calculations if different values of  $NP_{evap}$  are used.
- **A zero primary fragment cross-section.** The code multiplied a coefficient by the primary fragment cross-section output to include a SR contribution:  $Y_{final} = Coef_{secondary} \cdot Y_{primary}$ .

This is correct for EPAX where a non-zero production cross-section exists for each nucleus if its neutron and proton numbers do not exceed the neutron and proton numbers of the primary beam correspondingly. But in the case of Abrasion-Ablation or fission induced reactions there are a lot of nuclei produced just due to secondary reactions with a zero primary production cross-section.

- **The new reaction mechanism: Abrasion-fission.** In this case the first-step reaction is assumed to always correspond to the reaction mechanism set in the code, but for the second and the following steps the projectile fragmentation mechanism is assumed, and just the EPAX parameterization is used to calculate secondary cross-sections to make it faster.
- **The calculation speed is a very important factor in the case of heavy projectiles like  $^{238}\text{U}$ .**

#### 1.4.1.1. Dependence on the distribution dimension ( $NP_{evap}$ )

To expedite the evaluation of the analytical formulas for two-step reactions, and in order to include all multi-step processes, the program LISE++ uses numerical integration. At each target slice  $dx$  the yield of each fragment  $i$  produced by secondary reactions (i.e. other than the direct one-step-fragmentation) is calculated using the formula:

$$dN_i = \sum_j^{\text{rhombus}} \sigma_{j \rightarrow i} N_j dx - \sigma_i N_i dx, \quad /9/$$

with initial conditions  $N_i = 0$  and  $N_P = 1$ , where  $P$  stands for the projectile and  $i$  for the fragments. The summation in Eq./9/ is limited to a rhombus domain which includes the projectile and the fragment, in order to exclude contributions from negligible secondary reactions. The contribution from secondary reactions is then added to the total yield of each fragment before the next iteration. The number of iterations can be varied and as already was said in the case of thick slices ( $dx = T / NP_{evap}$ ) this method is not correct.

The new procedure to calculate SR contributions constitutes an iteration method with a complicated analytical solution based on equations (5-11) of the LISE paper [Baz02].

After this reexamination of secondary reactions, it is recommended not to use large dimensions of SR distributions in the case of calculation of SR coefficients for all fragments (mode #1 in the “Secondary reactions in target“ dialog in Fig.28). The default value is 16 and the user can make sure himself there is not a

huge difference in SR coefficients with the use of  $NP_{evap} = 16$  or  $NP_{evap} = 128$ . In the mode #1 the code uses SR calculations just at the end of the target, but a large value of  $NP_{evap}$  is required for the optimal thickness target procedure where the code needs to get the SR coefficient at any point in the target. In this case the code automatically increases the  $NP_{evap}$  value up to 128 just temporarily.

### 1.4.1.2. The "Secondary reactions" dialog modification

In the new version all operations with secondary reactions were moved from the "Preferences" dialog to the "Secondary reactions in target" dialog (see Fig.28), which is available from the "Options" menu (see Fig.27). If you want to set SR calculations then use the checkbox in the upper part of the dialog.

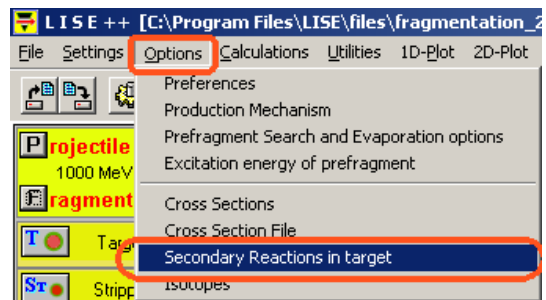


Fig.27. The "Options" menu.

Where are secondary reactions used in LISE?

#0 - Optimum target thickness calculations. The SR coefficient is needed just for the fragment of interest, but the coefficient should be calculated at different thickness values.

#1. Produce secondary reaction coefficients for all fragments transmitted through a spectrometer to calculate final rates of fragments. It is necessary to use SR coefficients only at the end of the target.

#2. Secondary reactions contribution analysis in the "Secondary Reactions" dialog. Use the corresponding button (see Fig.28).

Note: Don't forget to click the "Apply" button to accept changes for any calculations in this dialog. If the user clicks the "Ok" button, then he leaves the dialog and all changes done by him will be automatically accepted.

#### 1.4.1.2.1. Secondary reactions analysis plots

There are very convenient tools to analyze the dependence of the output of secondary reactions on target thickness (Fig.29), to get information on what intermediate fragments give the largest contribution of secondary reactions to the final output of the nucleus of interest (Fig.30), and to see if the filter was effectively chosen.

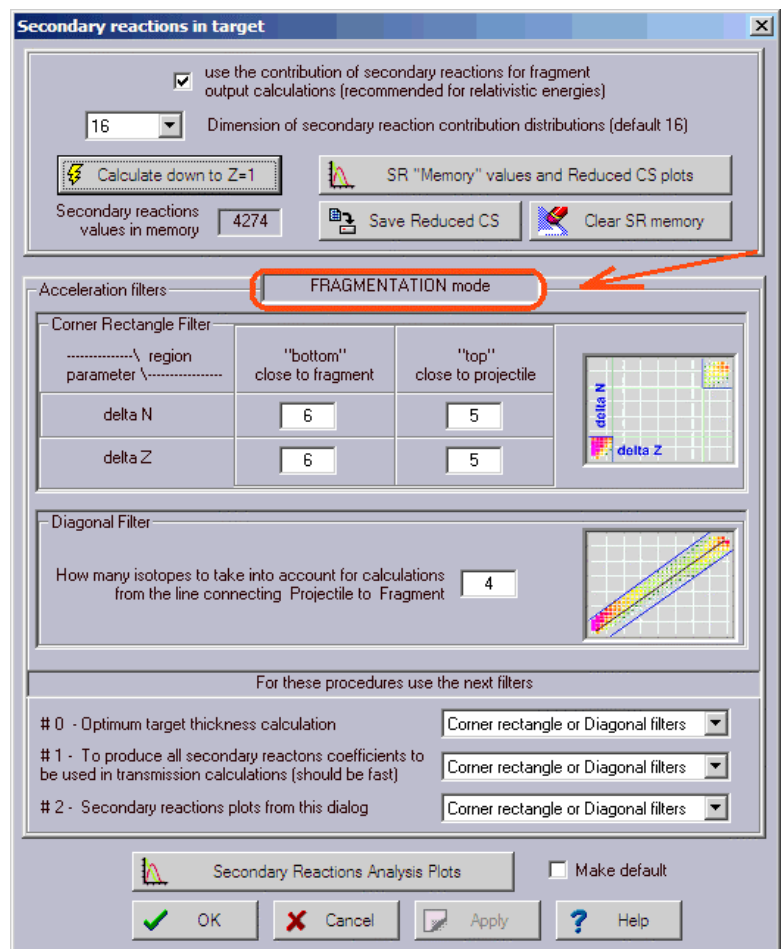
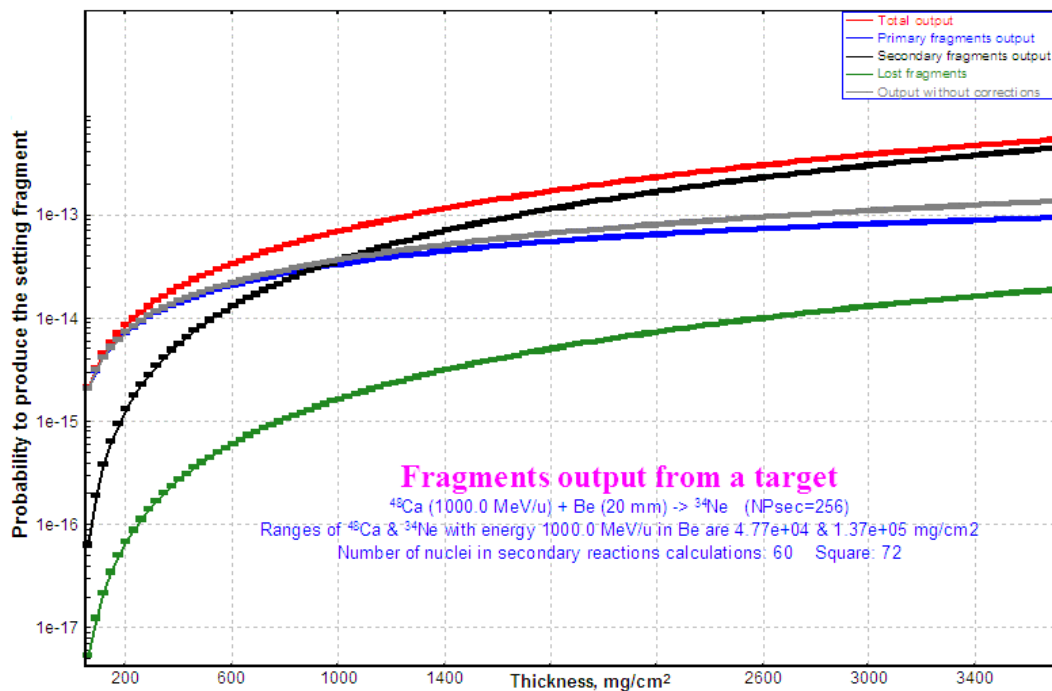


Fig.28. The "Secondary reactions in target" dialog.



**Fig.29.** Probability (per one particle of the primary beam) from Be-target thickness value to produce the  $^{34}\text{Ne}$  nucleus in the fragmentation of  $^{48}\text{Ca}$  beam, taking into account secondary reactions in the target. See Table 1 for definitions of curves.

**Table 1.** Definitions of curves in Fig.29.

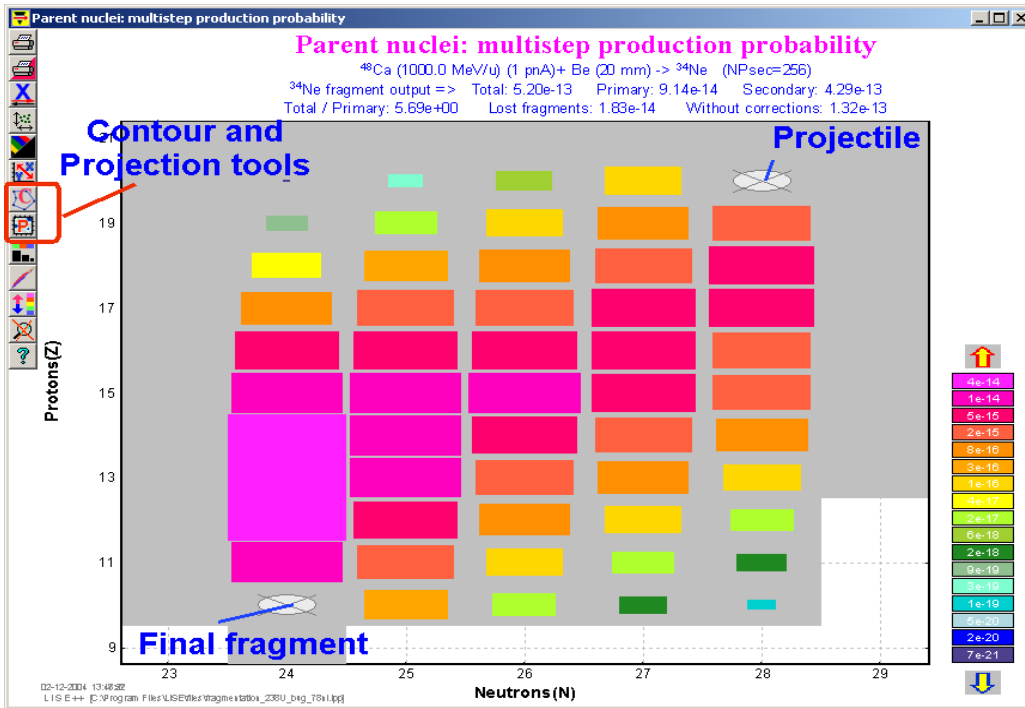
Value	Definition
Total output	Sum of primary output ( $^{48}\text{Ca} \rightarrow ^{34}\text{Ne}$ ) and secondary contributions ( $^{48}\text{Ca} \rightarrow ** \rightarrow ^{34}\text{Ne}$ ) taking into account the loss of fragments of interest and primary beam particles due to reactions with atoms of the target.
Primary fragment output	primary output ( $^{48}\text{Ca} \rightarrow ^{34}\text{Ne}$ ) taking into account losses of fragment of interest and primary beam particles due to reactions with atoms of the target.
Secondary output	secondary contributions ( $^{48}\text{Ca} \rightarrow ** \rightarrow ^{34}\text{Ne}$ ) taking into account the loss of fragment of interest and primary beam particles due to reactions with atoms of the target.
Lost fragments	Loss of $^{34}\text{Ne}$ fragments in a target slice (produced in primary reactions as well as in secondary reactions) due to reactions with target atoms.
Output without corrections	No secondary reactions, no reactions of produced $^{34}\text{Ne}$ fragments with the target. This is valid for very thin targets.

Fig.29 shows the probability to produce the fragment of interest ( $^{34}\text{Ne}$ ) per one particle of the primary  $^{48}\text{Ca}$  beam. It can be seen that at the Be-target thickness equal to  $1\text{g/cm}^2$ , the secondary reactions contribution begins to dominate over the primary fragment output.

Fig.30 shows the probability to produce the final fragment through intermediate nuclei. It is possible to see from the figure that isotones  $N=24$  ( $^{36}\text{Mg}$ ,  $^{37}\text{Al}$ ,  $^{38}\text{Si}$ ) are the most probable intermediate nuclei to produce  $^{34}\text{Ne}$  in secondary reactions.

#### 1.4.1.3. Determination of the region of nuclei for secondary reactions calculations

It is possible to load the procedure to calculate secondary reaction coefficients in two ways: from the SR dialog (the “Calculate down to  $Z=1$ ” button in Fig.28) and by clicking on the isotope of interest ( $Z_i, N_i$ ) with the right mouse button. In the previous version in the second case, the code calculated SR coeffi-



**Fig.30.** Two-dimensional plot of the probability to produce the  $^{34}\text{Ne}$  nucleus through intermediate nuclei from fragmentation of the  $^{48}\text{Ca}$  beam on a Be-target (20mm).

coefficients just for nuclei in a rectangle ( $Z_i, N_i, Z_p, N_p$ ) determined by the projectile ( $Z_p, N_p$ ) and the fragment clicked. But if the user clicked the next left isotope or the next lower isotone the code began to recalculate SR coefficients again, for the new rectangle ( $Z_i, N_i-1, Z_p, N_p$ ) for example.

In the new version if the user clicks on the isotope in the table of nuclides, with mode secondary reactions turned on, then the code asks the user to choose a range for nuclei (see Fig.31). There are three possibilities to define the user's region for calculations. After 5 seconds if the user did not choose something in this dialog then the dialog will be closed, selecting the mode "All nuclei".

The user can press the "Escape" key to break secondary reactions calculations.

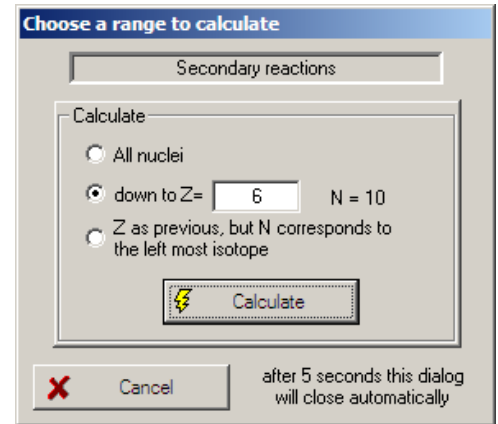
#### 1.4.1.4. Revision of optimal target thickness calculations for SR mode

There are two principal changes done in the new version:

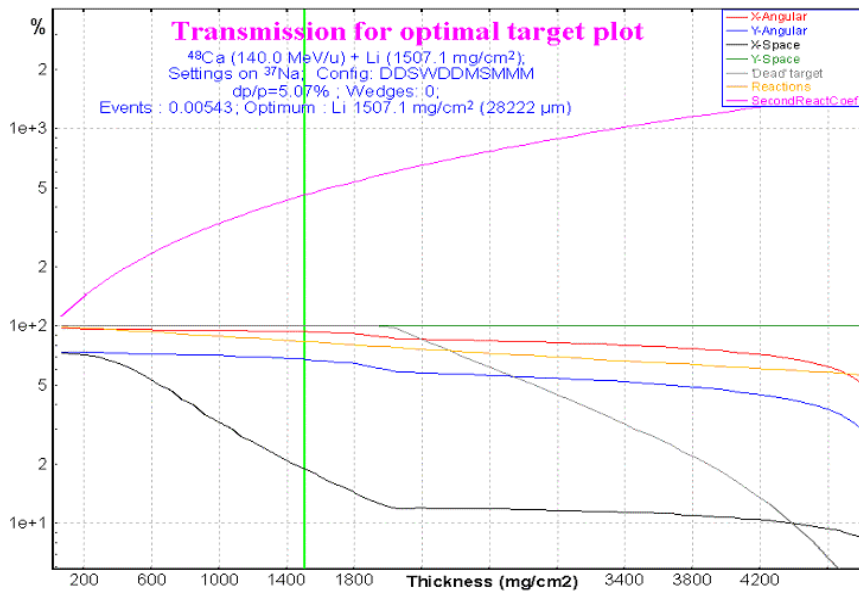
- Plot of the secondary reaction coefficient versus target thickness;
- Consideration of the situation when a fragment primary production cross-section is equal to zero.

The code plots the distribution (pink curve in Fig.32) of the SR coefficient from the target thickness in the "Transmission for optimal target plot" if SR mode is turned on. If a fragment primary production cross-section is equal to zero then the SR coefficient is always equal to 1.

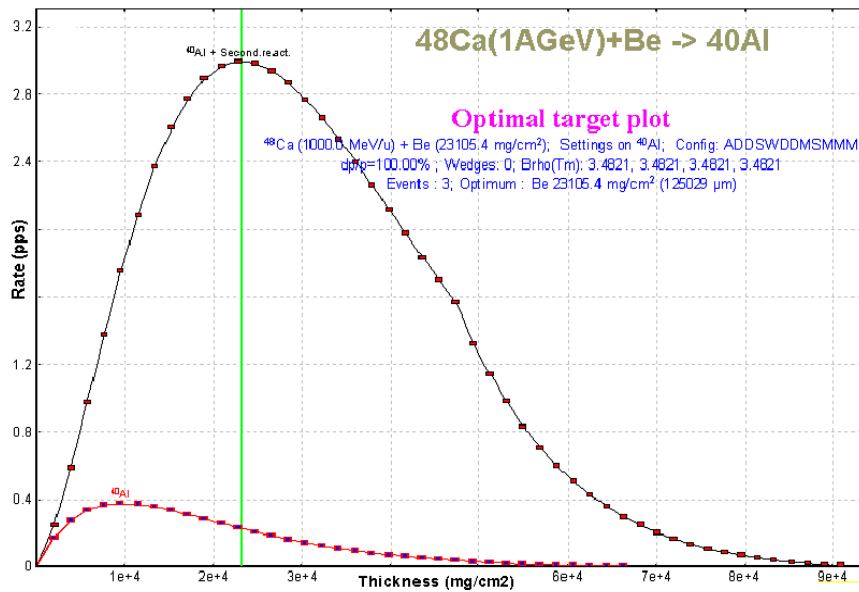
Fig.33 and Fig.34 show LISE++ calculation examples of optimal thickness target plots for cases with non-zero and with zero primary production cross-sections respectively.



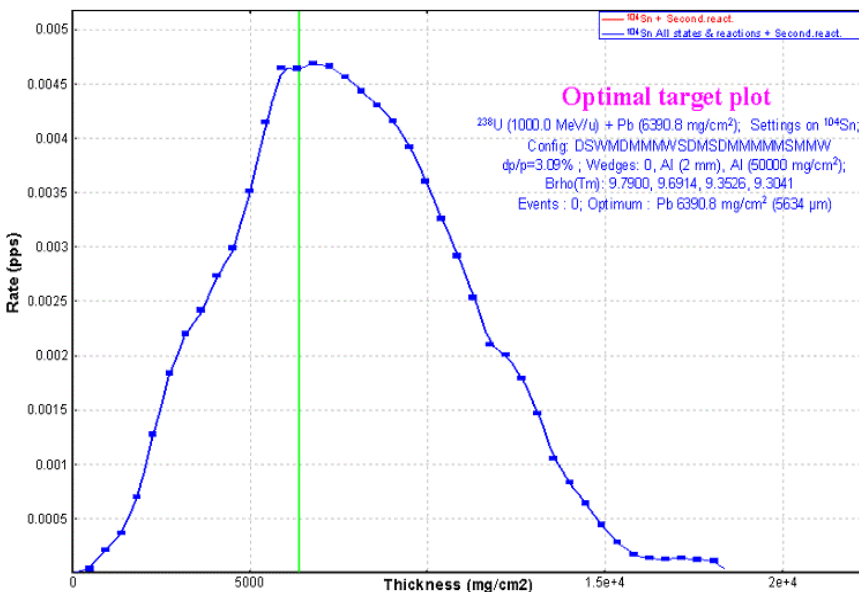
**Fig.31.** The "Choose a range for calculations" dialog in the "secondary reactions in target" mode.



**Fig.32.** Transmission coefficients versus target thickness for production of the  $^{37}\text{Na}$  nucleus in the reaction  $^{48}\text{Ca}(140\text{MeV}) + \text{Be}$  with the A1900 fragment separator. The secondary reaction coefficient (pink color) is always more or equal to 1.



**Fig.33.** Rates of  $^{40}\text{Al}$  fragments produced in fragmentation of the  $^{238}\text{U}(1\text{AGeV})$  for different  $\text{Be}$ -target thickness with SR contribution (black curve) and without SR contribution (red curve).



**Fig.34.** Rates of  $^{104}\text{Sn}$  fragments produced in induced fission of the  $^{238}\text{U}(1\text{AGeV})$  beam for different  $\text{Pb}$ -target thicknesses with SR contribution. The primary cross-section to produce  $^{104}\text{Sn}$  is equal to zero.



### 1.4.2. Calculation of secondary reaction contributions to fragments with zero primary production cross-section

As was already mentioned before, the code in the previous version used a coefficient multiplied with the primary fragment cross-section output to include a SR contribution:  $Y_{final} = Coef_{secondary} \cdot Y_{primary}$ . This means it was not possible to calculate the SR contribution to a nucleus' rate if the primary production cross-section was equal to 0.

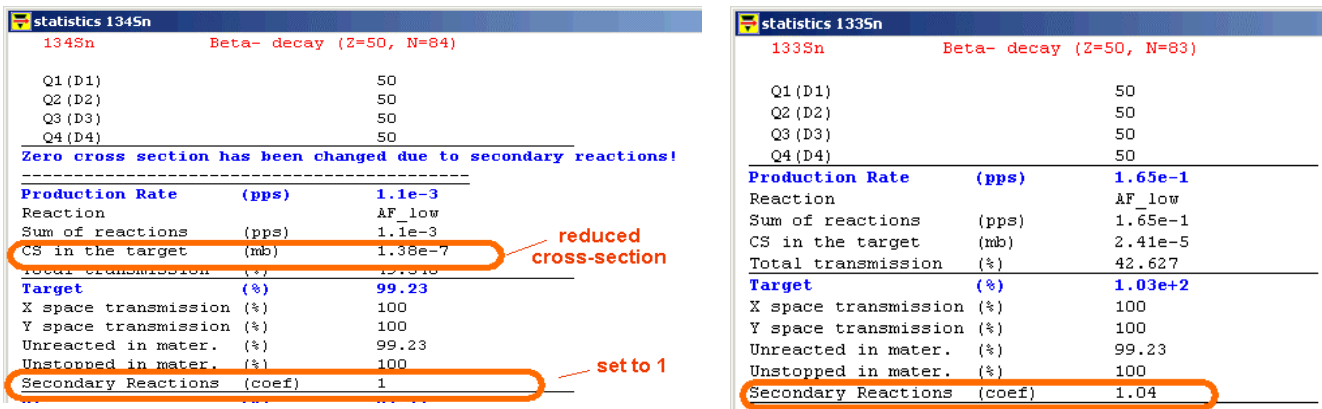
In order to use the SR contribution for nuclei with zero primary production cross-sections the following assumptions have been implemented in the code:

- ❑ If the primary production cross-section is equal to zero in the user cross-section file or in the calculations when the SR mode is turned on, then the code sets the primary production cross-section ( $\sigma_{primary}$ ) equal to 1e-99 mb.
- ❑ The code calculates the SR coefficient ( $\tau_{SR}$ ) relative to the new primary production cross-section ( $\sigma_{primary}^*$ ).
- ❑ The code calculates the reduced production cross-section of the fragment, which will be used for the next step in the calculations of the fragment rate.

$$\sigma_{reduced} = \sigma_{primary}^* \cdot \tau_{SR} \quad /10/$$

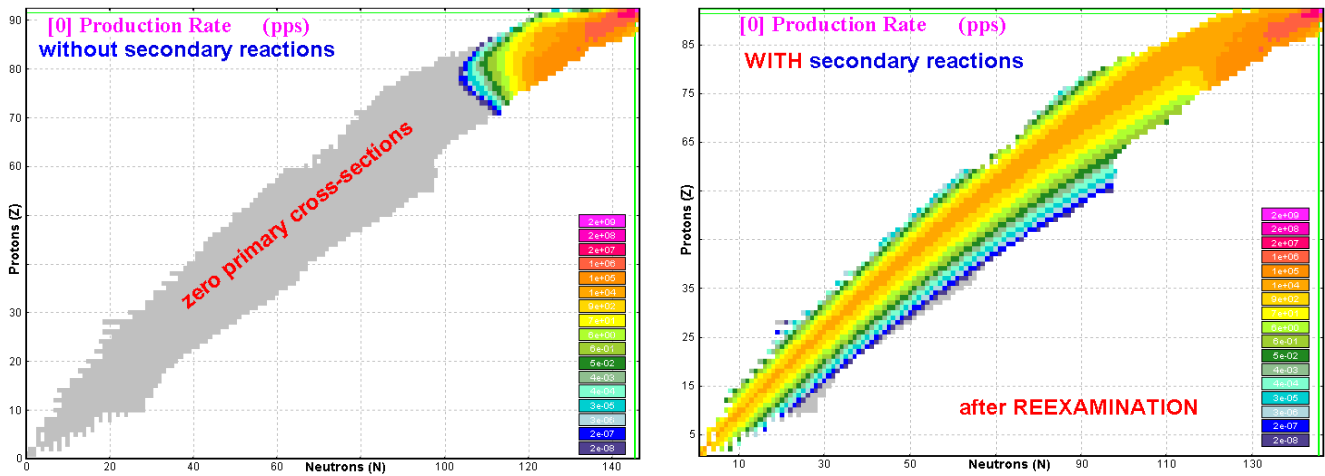
*Note:* A reduced cross-section is a function of the target thickness!

- ❑ Then LISE++ sets  $\tau_{SR}$  equal to 1. In this case, if you click on the isotope in the table of nuclides, you will get the statistics window with the message “Zero cross-section has been changed due to secondary reactions” (see left plot in Fig.35) and with the **reduced** cross-section value. In the case of fragments with non-zero primary cross-section the code shows the **primary** production cross-section value and the **un-modified** SR coefficient (see right plot in Fig.35).



**Fig.35.** Statistics windows for transmission of  $^{134}\text{Sn}$  and  $^{133}\text{Sn}$  fragments produced in induced fission of  $^{238}\text{U}$  (1AGeV) beam using a Be target (0.2 mm thickness).

Fig.36 shows the production rates of fragments produced in the abrasion-evaporation of a  $^{238}\text{U}$  (1 AGeV) beam just after the Be-target (10 mm). The left (right) plot shows production rates without(with) SR contributions. The calculations were done with the primary production cross-sections calculated by LISE's Abrasion-Ablation model taking into account fission and break-up de-excitation channels.

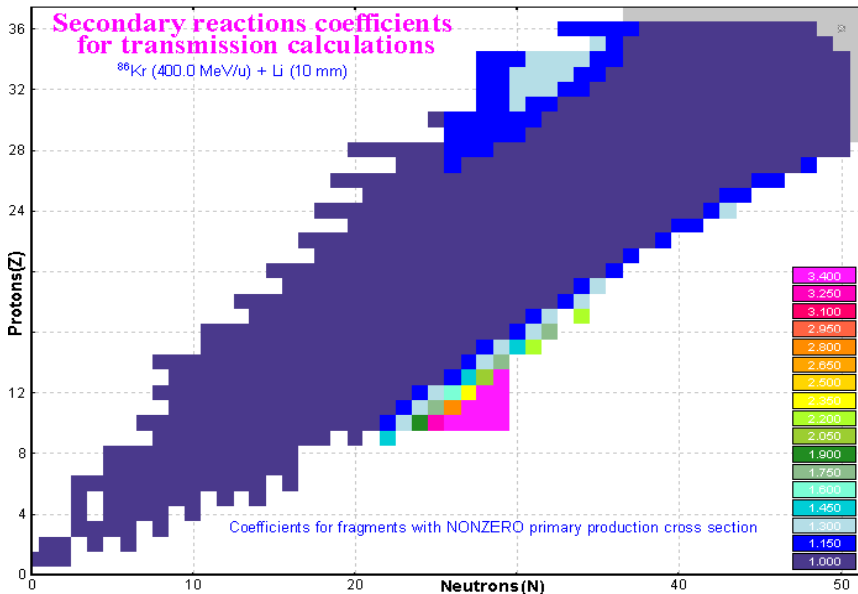


**Fig.36.** Production rates of fragments just after the 10 mm Be-target produced in Abrasion → Residues reaction with a  $^{238}\text{U}(1\text{AGeV})$  beam without (left) and with (right) SR contribution.

#### 1.4.2.1. Secondary Reactions plots: SR coefficients & reduced cross-sections

It is possible to visualize the results of the SR coefficients calculations using the “SR memory plot” button in the “Secondary reactions in target” dialog (see Fig.28).

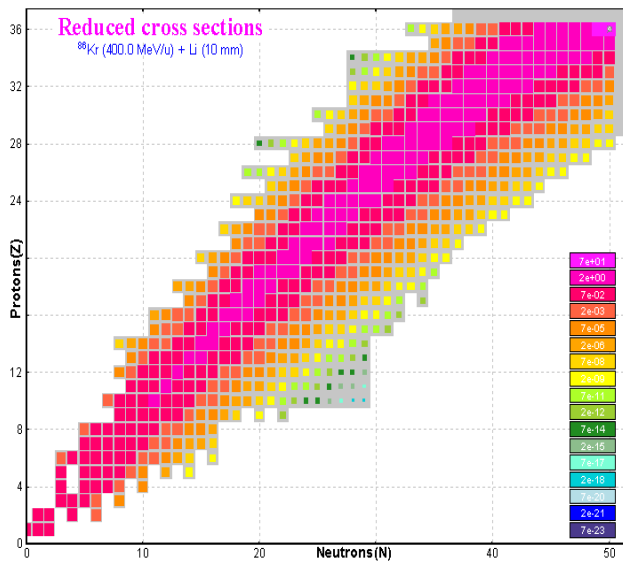
Fig.37 shows the SR coefficients for fragments with non-zero primary cross-sections produced in the fragmentation of a  $^{86}\text{Kr}(400\text{AMeV})$  beam on a Lithium target (10 mm). Primary cross-sections were calculated with the EPAX parameterization. From this plot it is visible for which nuclei it is possible to gain in final fragment output due to the contribution of secondary reactions.



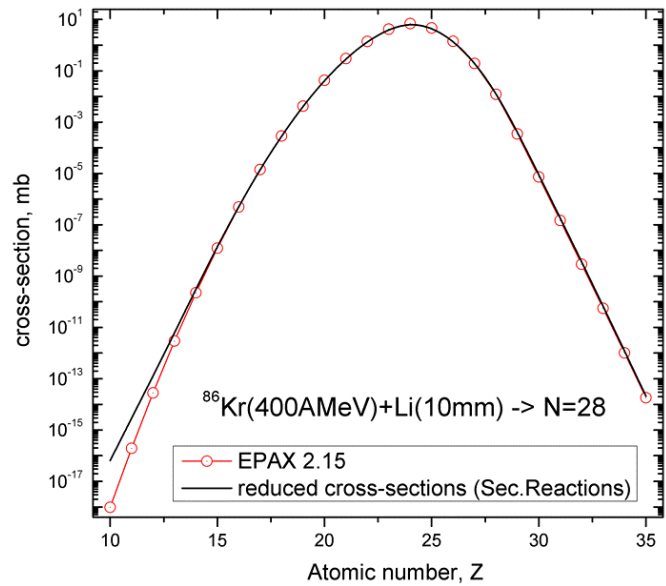
**Fig.37.** Secondary reactions coefficients for fragments produced in fragmentation (EPAX 2.15) of a  $^{86}\text{Kr}(400\text{AMeV})$  beam on a Lithium target (10 mm).

Reduced cross-sections can be saved (see Fig.28) in the user cross-section file with extension “cs2” and then the user can load them as “user” cross-sections through the “cross-section file dialog”.

Fig.38 shows the reduced cross-sections for fragments produced in the fragmentation (EPAX 2.15) of a  $^{86}\text{Kr}(400\text{AMeV})$  beam on a Lithium target (10 mm). Reduced cross-sections are calculated using Eq./10/ and provide very important information in the case of zero-primary cross-sections. Using this plot and the new tool of projection onto an axis for two-dimensional plots (see 1.9.4.1.1. Window and contour projections on an axis for 2D Cross-section plot) the user can extract data to a projection 1D-plot to compare with primary cross-sections as shown in Fig.39 for isotones with  $N=28$ .



**Fig.38.** Reduced cross-sections for fragments produced in the fragmentation (EPAX 2.15) of a  $^{86}\text{Kr}(400\text{AMeV})$  beam on a Lithium target (10 mm).



**Fig.39.** Reduced cross-sections (black curve) and EPAX calculations (red curve) for isotones with  $N=28$  produced in the fragmentation of a  $^{86}\text{Kr}(400\text{AMeV})$  beam on a Lithium target.

The SR calculation procedure in the case of Abrasion – Fission has several peculiarities which will be described later on in chapter 1.5.5. Secondary reactions for Abrasion-Fission.

### 1.4.3. SR calculation speed

SR calculation speed becomes a very important characteristic with increasing projectile mass. In the case of light projectiles ( $^{40}\text{Ar}$ ,  $^{48}\text{Ca}$ ), the elapsed time to calculate all SR coefficients is about several seconds, whereas for projectile fragmentation of a  $^{238}\text{U}$  beam ( $N_{\text{Pevap}}=16$ ) it increases to 224 seconds! To calculate all SR coefficients, the code takes from the table of nuclides the most left ( $N_{\text{min}}$ ), right ( $N_{\text{max}}$ ), top ( $Z_{\text{max}}$ ) and bottom ( $Z_{\text{min}}$ ) nuclei to create an initial rectangle of calculations. This means the rectangle is defined by the projectile and proton ( $0,1,N_{\text{beam}},Z_{\text{beam}}$ ) and the number of isotopes participating in SR calculations is equal to  $(N_{\text{beam}}+1) \cdot Z_{\text{beam}}$ . The code calculates final SR coefficients only for existing nuclei in the table of nuclides. As a result there are 2536 nuclei used to calculate SR coefficients for the projectile fragmentation of  $^{238}\text{U}$  beam and 194 nuclei for the  $^{40}\text{Ar}$  beam respectively.

One of the possibilities was already mentioned above in chapter 1.4.1.3., “Determination of the region of nuclei for secondary reactions calculations”, to avoid SR calculations for elements with low atomic number ( $Z$ ), if not needed by the user.

After reexamination of the SR calculations procedure (see chapter 1.4.1.1. Dependence on the distribution dimension ( $N_{\text{Pevap}}$ )) it is recommended to use smallest value of the SR distribution dimension, which is 16. The quality of the calculations does not undergo crucial changes when increasing the calculation speed. Table 2 demonstrates that an increase of the SR distribution dimension by a factor of 16 corresponds to an increase of the elapsed time by a factor of 17 and a decrease of in calculation quality of about 6 percent.

**Table 2.** Results of the  $^{78}\text{Ni}$  SR coefficient calculations produced in the fragmentation of a  $^{238}\text{U}(1\text{A GeV})$  beam on a Beryllium target ( $11\text{ g/cm}^2$ ) as a function of the SR distribution dimension. Calculations were done without acceleration filters using mode #2 (Secondary reactions contribution analysis). EPAX parameterization was used to calculate the primary production cross-sections.

Dimension, NPevap	Time elapsed, sec	$^{78}\text{Ni}$ SR coefficient	Total probability to produce $^{78}\text{Ni}$ per one particle of the beam
16	82	59.6	4.58e-17
32	170	61.5	5.10e-17
64	354	62.4	5.27e-17
128	715	62.8	5.46e-17
256	1380	63.0	5.52e-17

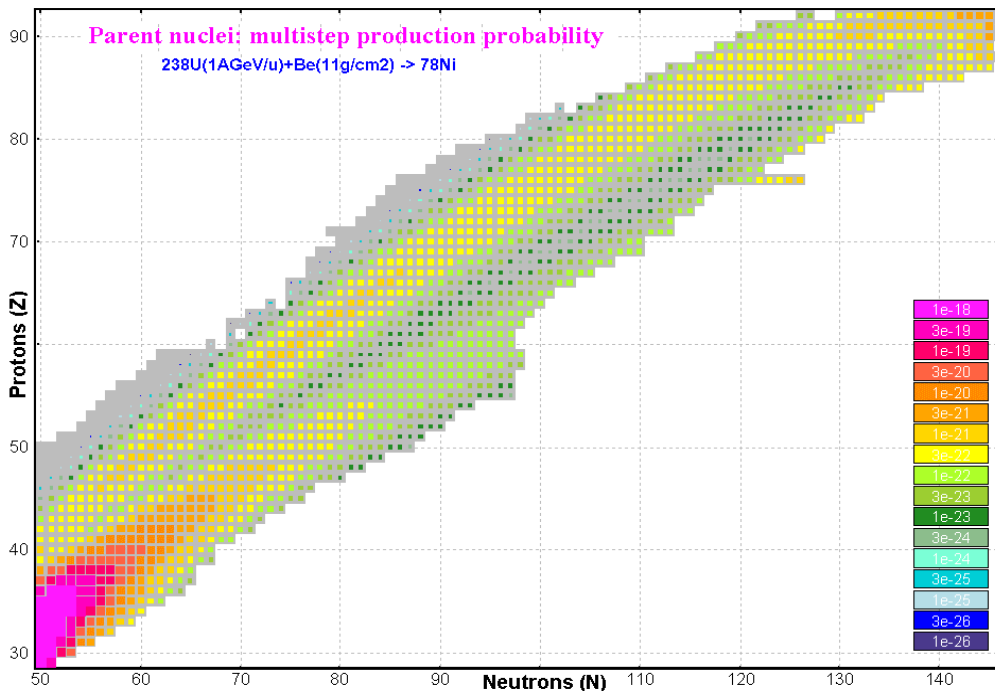
### 1.4.3.1. Acceleration filters for secondary reactions calculations

To significantly decrease SR calculation time in the case of heavy projectiles, the “acceleration filters” have been developed and incorporated into the code. The main idea of the acceleration filters is to decrease the number of intermediate parent nuclei. The filters exclude intermediate nuclei with small SR contribution to the final nucleus. There are two kinds of filters “corner rectangle” and “diagonal” based on methods to truncate regions.

**Note:** It is recommended for a new combination of beam & target to run the SR calculations procedure without filters to clarify from the “Parent nuclei: multi-step production probability” plot what kind of filters and parameters are needed.

#### 1.4.3.1.1. Corner rectangle filter

Results of the multi-step production probability of  $^{78}\text{Ni}$  fragment SR calculations produced in a fragmentation of a  $^{238}\text{U}(1\text{A GeV})$  beam on a Beryllium target ( $11\text{ g/cm}^2$ ) are shown in Fig.40. The EPAX parameterization has been used to calculate the primary production cross-sections.



**Fig.40.** The “Parent nuclei: multi-step production probability” plot for  $^{78}\text{Ni}$  fragments from the fragmentation of  $^{238}\text{U}(1\text{A GeV})$  on a Be target (thickness  $11\text{ g/cm}^2$ ). No filters were applied for calculation of this plot.

Projections of the 2D-plot in Fig.40 on the horizontal and the vertical axis are shown in Fig.41. Blue rectangles on both plots of Fig.41 indicate regions with insignificant production contribution to  $^{78}\text{Ni}$  final output. More intense parent nuclei are located close to the final fragment and projectile. In order to increase the SR calculations speed it is necessary to cut the regions with insignificant production contribution or in other words just to select regions close to the final fragment and the projectile. To exclude nuclei with small contributions, the rectangle filter has been incorporated into the code for SR calculations.

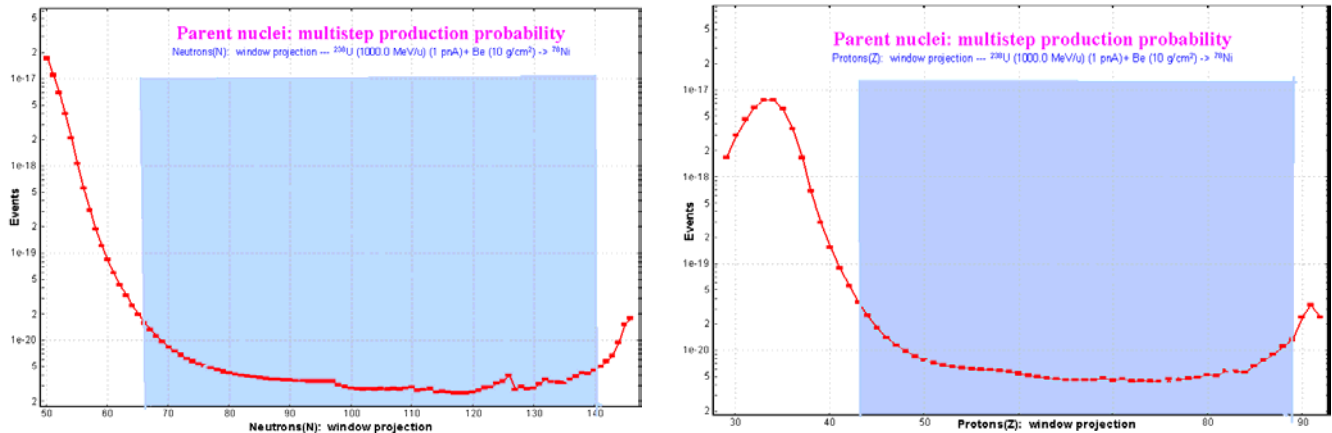


Fig.41. Projections of the 2D-plot in Fig.40 on horizontal (corresponds to neutrons) and vertical (corresponds to proton) axis.

The rectangle filter can be applied for all three modes using secondary reactions (see the “Secondary reactions in target” dialog in Fig.28). The rectangle filter has four parameters (two  $\delta N$  and two  $\delta Z$ ), which determine the sizes of two rectangles (top and bottom) to cut the necessary regions. How the filter works and what the parameters mean is easy to understand from Fig.42, which shows the same plot as Fig.40 but with the rectangle filter applied.

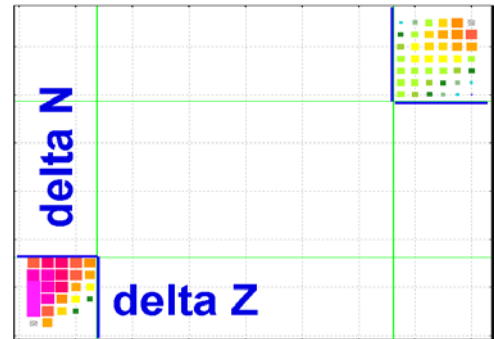


Fig.42. The same plot as Fig.40 but the rectangle filter has been applied.

Table 3 shows the elapsed time and SR coefficient values depending on the parameters of the rectangle filter to estimate the SR contribution for  $^{78}\text{Ni}$  fragments produced in the fragmentation of a  $^{238}\text{U}$  (1AGeV) beam on a Beryllium target ( $11 \text{ g/cm}^2$ ).

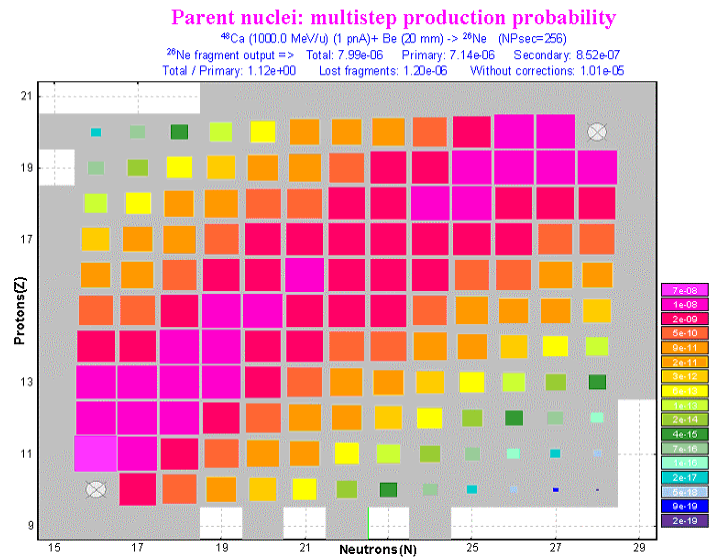
Table 3. Results of the  $^{78}\text{Ni}$  SR coefficient calculations produced in fragmentation of a  $^{238}\text{U}$  (1AGeV) beam on a Beryllium target ( $11 \text{ g/cm}^2$ ) depending on the parameters for the rectangle filter. Calculations were done for SR distribution dimension 16 (except the last row where  $NP_{\text{evap}}=128$ ) using mode #2 (Secondary reactions contribution analysis). The EPAX parameterization was used to calculate the primary production cross-sections.

Rectangle filter				Time elapsed (sec)	$^{78}\text{Ni}$ SR coefficient	Total probability to produce $^{78}\text{Ni}$ per one beam particle
bottom		top				
$\delta N$	$\delta Z$	$\delta N$	$\delta Z$			
No filter	No filter	No filter	No filter	84	59.6	4.58e-17
35	35	20	20	21.5	53.9	4.14e-17
25	25	10	10	6.5	50.9	3.91e-17
20	15	8	8	1.32	49.2	3.79e-17
15	12	4	4	< 0.3	47.7	3.67e-17
15	12	4	4	4.69 (NP=128)	48.3	4.19e-17

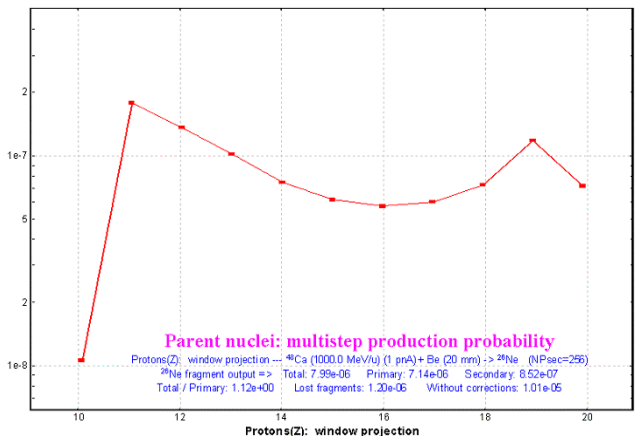
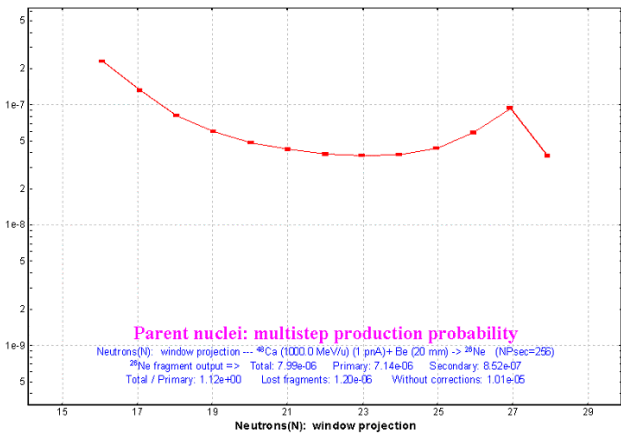
### 1.4.3.1.2. Diagonal filter

Results of multi-step production probabilities of  $^{26}\text{Ne}$  fragment SR calculations produced in the fragmentation of a  $^{48}\text{Ca}$  (1AGeV) beam on a Beryllium target (20 mm) are shown in Fig.43. The EPAX parameterization has been used to calculate the primary production cross-sections.

Projections of the 2D-plot in Fig.43 on horizontal and vertical axes are presented in Fig.44. It is possible to see that in this case the difference between the maximum values and values in the center ( $N=22$  and  $Z=16$ ) is less than one order of magnitude, whereas in the case of  $^{78}\text{Ni}$  fragment SR calculations produced in the fragmentation of a  $^{238}\text{U}$  (1AGeV) beam on a Beryllium target ( $11\text{ g/cm}^2$ ) shown in Fig.40 this difference is more than 4 orders of magnitude. More intense parent nuclei are located close to the line connecting the final fragment and the projectile. In order to increase the SR calculation speed in this case it is necessary to select a region close to this line. This line looks like the diagonal of a rectangle; this is the reason why the new filter has been named “diagonal”.



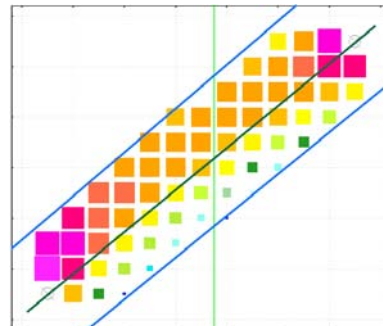
**Fig.43.** The “Parent nuclei: multi-step production probability” plot for  $^{26}\text{Ne}$  fragment in the fragmentation of a  $^{48}\text{Ca}$  (1AGeV) on Be target (thickness 10 mm). No filters were applied for this plot.



**Fig.44.** Projections of the 2D-plot in Fig.43 on horizontal (corresponds to neutrons) and vertical (corresponds to proton) axes.

The diagonal filter has just one parameter which is the “stripe width” of the cut. How the filter works and the parameter meaning is easy to understand from Fig.45, which shows the same plot as Fig.43 but with the diagonal filter applied.

Table 4 shows the elapsed time and SR coefficient values depending on the parameter of the diagonal filter to estimate the SR contribution for  $^{26}\text{Ne}$  fragments produced in the fragmentation of a  $^{48}\text{Ca}$  (1AGeV) beam on a Beryllium target (108 mm).

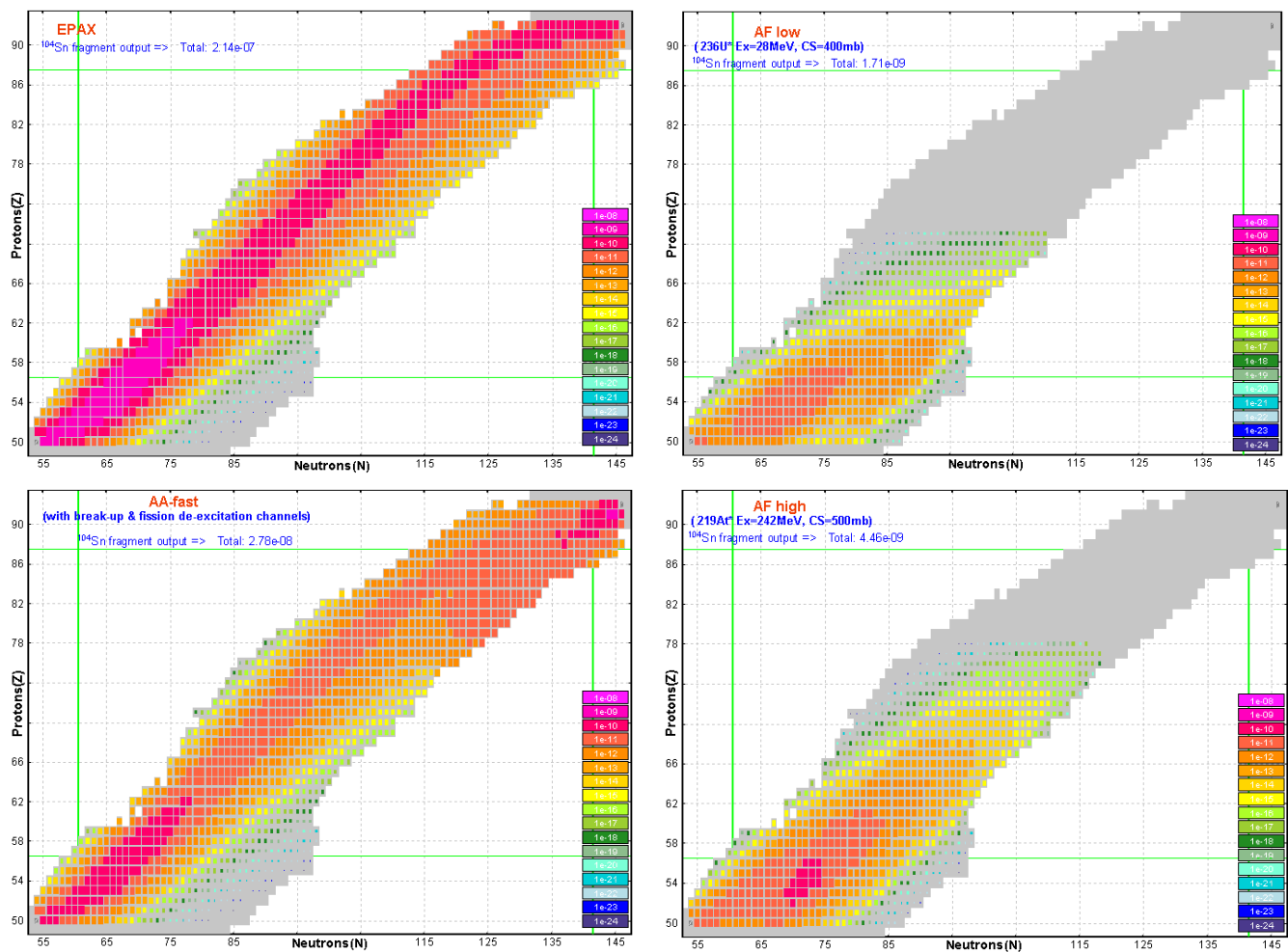


**Fig.45.** The same plot as Fig.43 but the **diagonal** filter has been applied. The “stripe width” parameter is equal to 3.

**Table 4.** Results of the  $^{26}\text{Ne}$  SR coefficient calculations for fragmentation of a  $^{48}\text{Ca}$  (1AGeV) beam on a Beryllium target (20 g/cm<sup>2</sup> or 108 mm) depending on the parameter of the diagonal filter. Calculations were done for SR distribution dimension equal to 512 using mode #2 (Secondary reactions contribution analysis). The EPAX parameterization was used to calculate the primary production cross-sections.

Diagonal filter: Stripe width	Time elapsed, sec	$^{26}\text{Ne}$ SR coefficient	Total probability to produce $^{26}\text{Ne}$ per particle of the beam
No filter	16.6	1.80	1.51e-5
8	15.7	1.80	1.51e-5
6	13.4	1.80	1.51e-5
5	10.9	1.80	1.51e-5
4	7.9	1.79	1.50e-5
3	5.2	1.72	1.44e-5
2	2.3	1.53	1.29e-5
1	< 0.5	1.21	1.02e-5

### 1.4.3.1.3. Application of acceleration filters



**Fig.46.** Multi-step production probabilities to produce  $^{104}\text{Sn}$  from the primary reaction  $^{238}\text{U}(1\text{AGeV}) + \text{Be}(11\text{g/cm}^2)$  using different reaction mechanisms. Left top: fragmentation (EPAX), Left bottom: fragmentation (Abrasion-Ablation, fast mode), Right top: Abrasion-Fission "low" ( $E_x=28\text{ MeV}$ ), Right bottom: Abrasion-Fission "high" ( $E_x=242\text{ MeV}$ ).

The selection of the filter type is determined by **the mode of SR calculation** (see Fig.28) and **the type of reaction mechanism** (see Fig.46). Based on this picture we can conclude:

- ❑ For fission reactions we do not need diagonal and top rectangle filter, but the bottom rectangle filter should have a large size;
- ❑ For fragmentation reaction we need the diagonal filter as well as both rectangle filters.

The code has two sets of filters: fragmentation and fission, and automatically uses the fragmentation set if the reaction mechanism is set to fragmentation. The fission filter set is used for all other reactions. If you want to edit the fission filter set you have to be sure that you are not working under fragmentation conditions. The current filter mode is shown in the middle of the “Secondary reactions” dialog (see Fig.28). Initially both these sets use acceleration filters and their default values are shown in Table 5.

Table 5. Initial values of filters sets.

Filter			Filters set	
			Fragmentation	Fission
Corner rectangle	bottom	dN	6	25
		dZ	6	20
	top	dN	5	0
		dZ	5	0
Diagonal	Parameter		4	-
Procedure mode			Combined (Corner+ Rectangle)	Rectangle
#0 - optimal target thickness				
#1 – to produce all secondary reactions coefficients to be used in transmission calculations				
#2 - secondary reaction plots from this dialog				

Fig.47 and Fig.48 demonstrate the use of different filter sets in the reaction  $^{238}\text{U}$  (1AGeV) + Be (1g/cm<sup>2</sup>) to produce  $^{202}\text{Pt}$  assuming the fragmentation mechanism, and the  $^{132}\text{Sn}$  isotope using AF reaction mechanism.

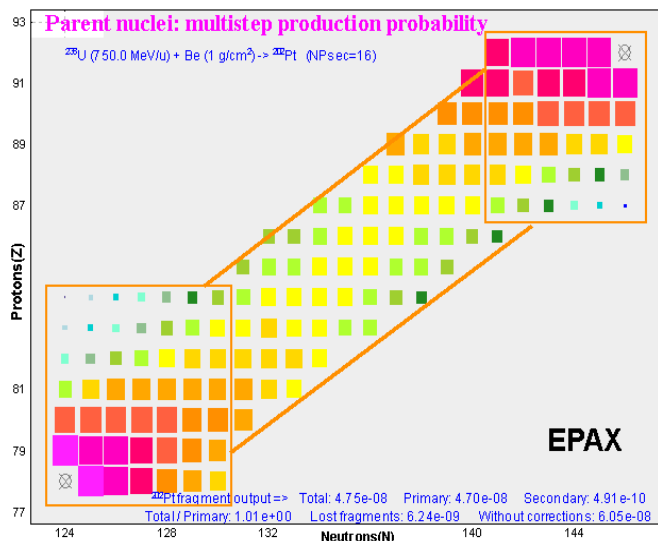


Fig.47. Multi-step production probabilities to produce  $^{202}\text{Pt}$  fragment from the primary reaction  $^{238}\text{U}$  (1AGeV) + Be (1g/cm<sup>2</sup>) [fragmentation] using the **fragmentation filters set** (see Table 5).

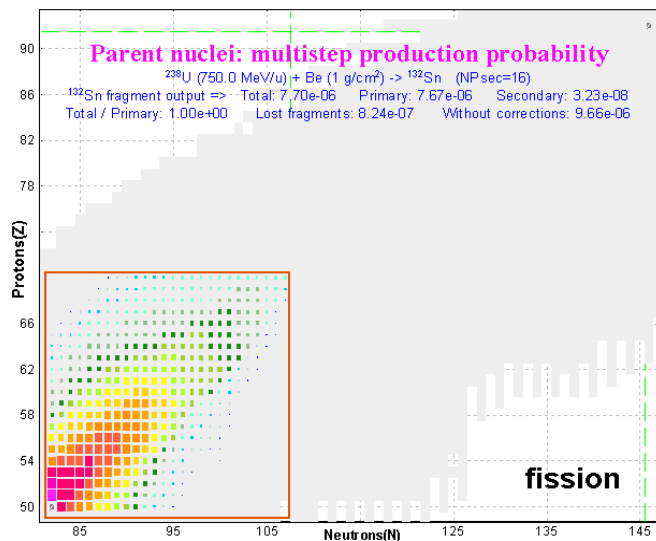


Fig.48. Multi-step production probabilities to produce  $^{132}\text{Sn}$  from the primary reaction  $^{238}\text{U}$  (1AGeV) + Be (1g/cm<sup>2</sup>) [Abrasion-Fission] using the **fission filters set** (see Table 5).



### 1.5. Abrasion-Fission

The basic complexity in the case of Abrasion-Fission is the fact that there are more than 1000 fissile nuclei (see right top plot in Fig.10.) after abrasion of a fast heavy projectile by a target compared to only one fissile nucleus in the case of Coulomb fission. To overcome this problem, a model with three-excitation energy regions has been recently developed in the framework of LISE for calculations of Abrasion-Fission fragment production.

#### 1.5.1. Three excitation energy regions AF model

The model suggests just three fissile nuclei for different excitation energy regions, which are calculated by using LISE++ Abrasion-Ablation model. The excitation region is determined by three parameters: excitation energy, cross-section, and fissile nucleus. A two-excitation energy region model has been proposed by M. Bernas et al. [Ber03]. For nuclear fission from  $^{238}\text{U}+p$  at 1AGeV they concluded that experimental results are compatible with two mean primary fissioning nuclei: for the asymmetric mode  $^{234}\text{U}$  and for the symmetric mode  $^{221}\text{Th}$ , with 6 post-scission neutrons added. We began also by developing a two-excitation-energy-region model for analytical fast calculation of AF products, but a drop in isotope cross-sections took place (see Fig.49). To eliminate this discrepancy the third (Middle) excitation energy region has been incorporated into the model. It certainly has complicated the program and takes more time for calculation.

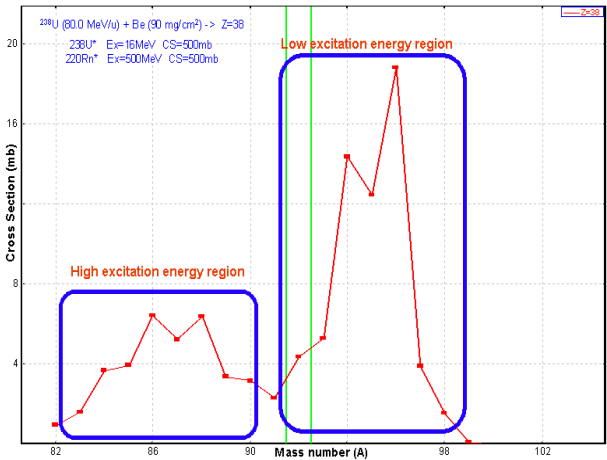


Fig.49. Mass distribution of Strontium fission fragments for  $^{238}\text{U}(80\text{A MeV})+\text{Be}$  calculated by the two-excitation energy region model.

#### 1.5.1.1. Abrasion-Fission dialog

The Abrasion-Fission dialog (see Fig.50) allows the modification of three EER model settings (see “1.5.6.2. Abrasion-Fission settings” for how to load this dialog alternatively). LISE initializes three excitation regions, regardless of target material and primary beam energy, in the following way for the  $^{238}\text{U}$  primary beam:

Excitation region	Fissile nucleus	Ex.energy, MeV	Cross section, mb
Low	$^{237}\text{U}$	25	300
Middle	$^{232}\text{Th}$	100	1000
High	$^{226}\text{Ra}$	250	800

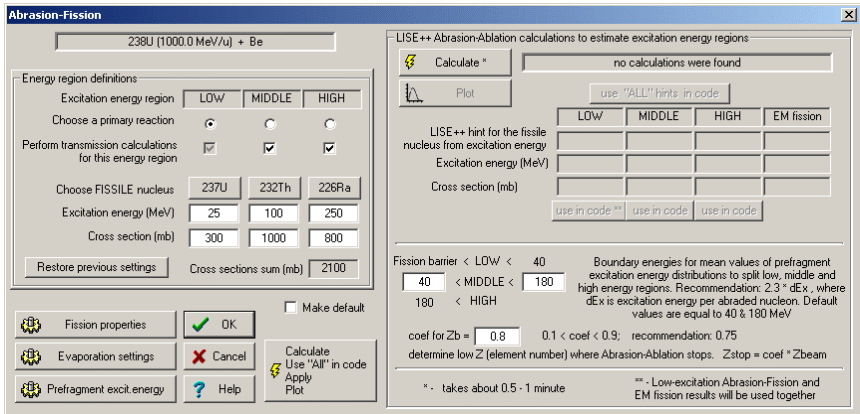


Fig.50. The “Abrasion-Fission” dialog. An initial state of the dialog is shown: no calculations were found.

You can define parameters of EERs manually or use hints from LISE Abrasion-Ablation calculations.

### 1.5.1.2. Fission excitation function

By clicking the “Calculate” button in the Abrasion-Fission dialog, you start Abrasion-Ablation calculations for nuclei from the projectile down to “coef\_for\_Zb”× Zb, where Zb is the atomic number of the projectile, and coef\_for\_Zb is the value defined in the dialog (default 0.75). There is no necessity to calculate cross-sections for more light elements because break-up channel dominates.

The code temporarily sets the following parameters to calculate the fission de-excitation function:

NPEvap:	16	Tunneling:	Yes
Mode (Auto/Manual):	Manual	State density:	[C] (pairing + shell corrections)
Daughter excitation energy distribution calculate:	qualitatively		
Take into account unbound nuclei:	Yes		
De-excitation channels:	n, 2n, p, α, fission, break-up		

After AA calculations, the code restores the previous parameters. Statistics parameters (mean value, standard deviation, and area) of the de-excitation fission function (see Fig.16) of each isotope are saved in the operating memory. Based on the boundaries of excitation regions and the mean values of de-excitation fission functions, the code sorts nuclei by regions. The next step is summing de-excitation fission functions by region and calculating the most probable fissile nucleus, assuming for simplicity that de-excitation fission functions have a Gaussian distribution.

It is necessary to remember about Coulomb fission! In the case of a heavy target and relativistic energy of primary beam, its contribution is very significant. Electro-magnetic fission and Low excitation energy AF will result if you click the “use in code” button for Low EER. LISE AA calculation results are shown in the AF dialog (Fig.51) and can be plotted.

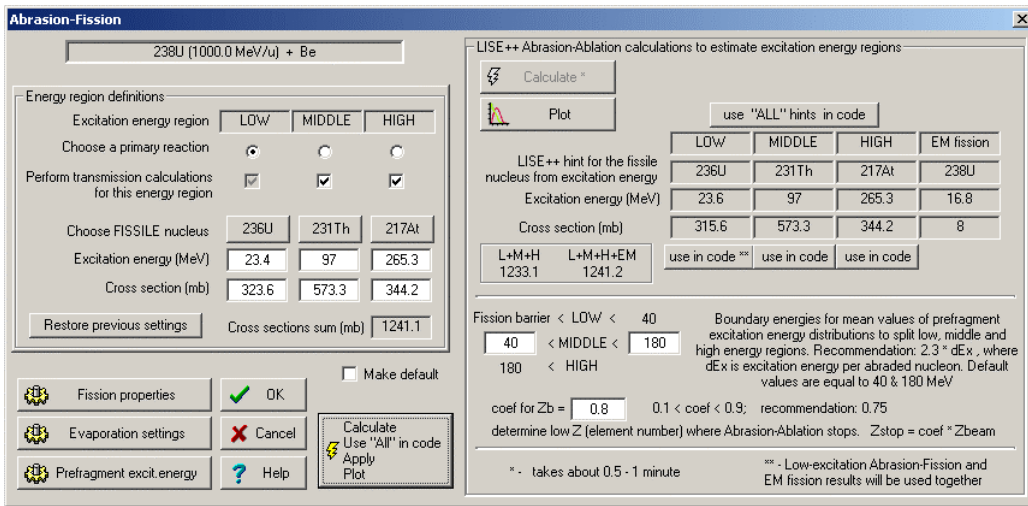
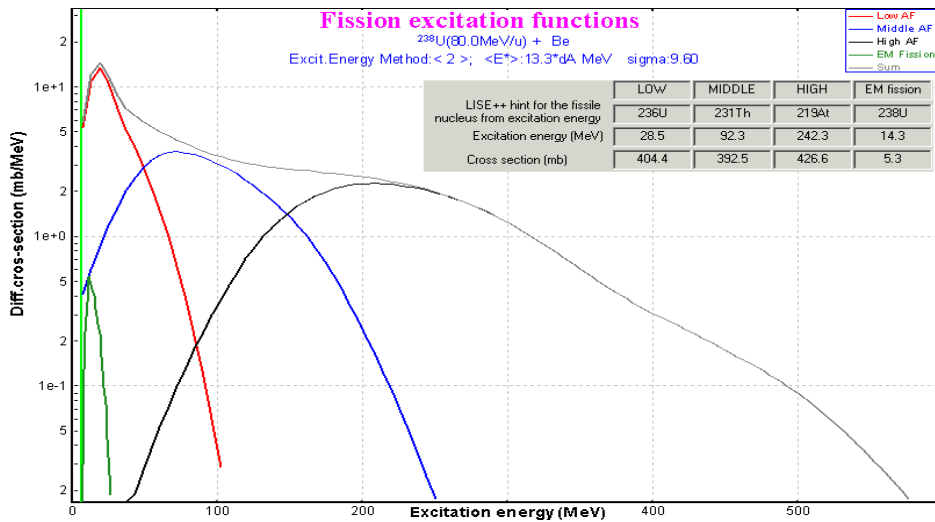
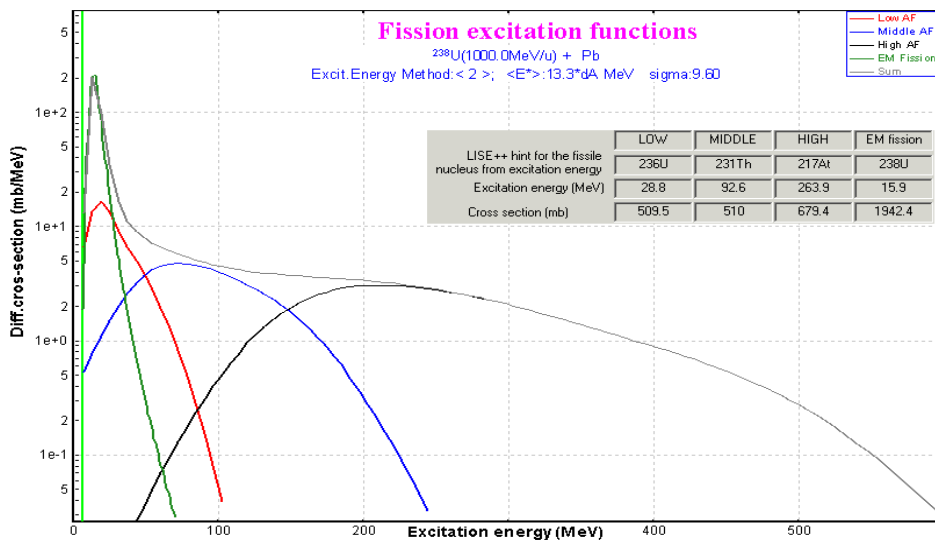


Fig.51. The “Abrasion-Fission” dialog after AF settings calculations.

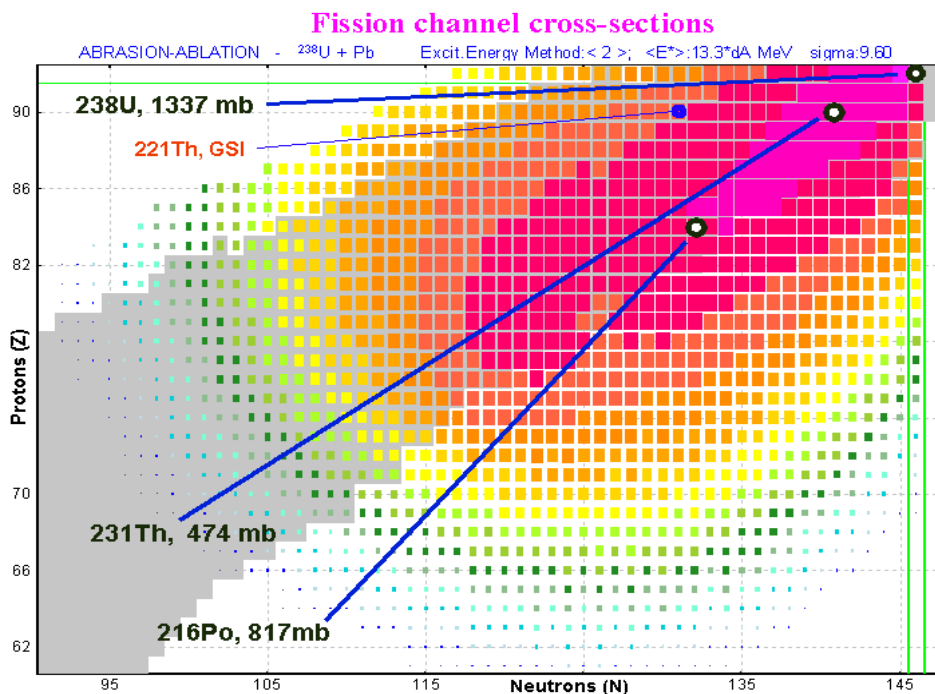
Fig.52 and Fig.53 show calculated fission excitation functions in the reaction  $^{238}\text{U}(80\text{AMeV})+\text{Be}$  and  $^{238}\text{U}(1\text{AGeV})+\text{Pb}$  respectively. It is possible to see from the inserts in these figures that EM fission dominates in the case of the lead target at relativistic energies. Fig.54 shows a 2D-plot of fission de-excitation channels after the abrasion of  $^{238}\text{U}(1\text{AGeV})$  by a lead target. Locations of the most probable fissile nuclei in the excitation energy regions are shown in the figure.



**Fig.52.** Calculated excitation distribution of fissile nuclei produced in the reaction  $^{238}\text{U}(80\text{A MeV})+\text{Be}$ . Parameters of excitation energy regions are shown in the insert.



**Fig.53.** Calculated excitation distribution of fissile nuclei produced in the reaction  $^{238}\text{U}(1\text{AGeV})+\text{Pb}$ . Parameters of excitation energy regions are shown in the insert.



**Fig.54.** Calculated fission de-excitation channels after the abrasion of  $^{238}\text{U}(1\text{AGeV})$  by a lead target. The most probable fissile nuclei in the excitation energy regions are shown in the figure.

$^{221}\text{Th}$  is the primary fissile nucleus for asymmetric fission from  $(^{238}\text{U}+p)$  at 1AGeV [Ber03].

### 1.5.1.3. Calculation of final fission fragment production

To calculate AF fission production for each excitation energy region the code uses the approach developed in the previous version for Coulomb fission [LISE71]:

- Calculation of the initial fission cross-section matrix ( $CS_{init}$ ) of production cross-sections for excited fragments uses the semi-empirical model [Ben98], but the charge distribution was modified in the new version (see chapter 1.5.1.3.1. Width of charge distribution).
- Post-scission nucleon emission. Based on the “LisFus” method [Tar03], the code calculates final cross-section matrices using the  $CS_{init}$  matrix, but in the new version the cascade procedure has been optimized for faster calculations (see 1.5.1.3.2. Modification of evaporation cascade subroutines).

Each of three excitation energy regions is considered as a separate reaction mechanism. But for cross-section, TKE, and nucleon emission plots, the calculation results of final production cross-section for each EER can be used together (see Fig.55).

Calculation of fission final cross-section production takes about *one and a half minutes* with the fission cross-section suppression value set equal to  $1e-9$  mb.

#### 1.5.1.3.1. Width of charge distribution

The width in proton number for fixed neutron number  $\sigma_{Z/N}$  in the semi-empirical model is calculated by using the following formula [Ben98 -Eq.24]:

$$\sigma_{Z/N}^2 = \frac{1}{2} \frac{\sqrt{E_{mac}(E_0^*, N)}}{\sqrt{\tilde{a}} C_{Z/N}} + k^2 \sigma_0^2, \quad /11/$$

where the term  $\sigma_0^2 = 0.4$  <sup>♠</sup>. The curvature  $C_{Z/N}$  defined in [Ben98] may be close to zero for some combinations of  $Z$  and  $N$  if using binding energy values from the AME2003 database. In this case LDM calculations without shell and pairing corrections are used for curvature calculations. The coefficient  $k$  initially being equal to 1 [Ben98] was set in the code to be equal to the ratio  $A_{CN}/N_{CN}$  following after relations [Sch00]:  $Z \sigma(N)_{[Z=const]} = N \sigma(Z)_{[N=const]} = A \sigma(Z)_{[A=const]}$ .

#### 1.5.1.3.2. Modification of evaporation cascade subroutines

The code temporarily sets the following parameters to calculate emission of light particles by excited fission fragments:

NPevap:	4	Tunneling:	Yes
Mode (Auto/Manual):	Manual	State density:	[C] (pairing + shell corrections)
De-excitation channels	n, p, $\alpha$	Acceleration Filter:	Yes

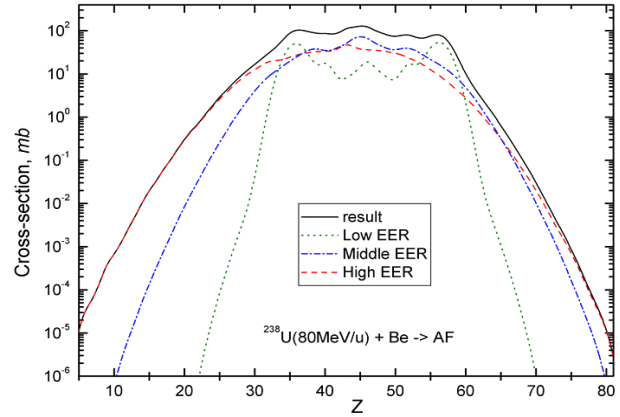


Fig.55. Calculated charge distributions of fission residues from the reaction  $^{238}\text{U}(1\text{AGeV})+\text{Be}$ . Parameters of excitation energy regions are shown in the insert of Fig.52.

<sup>♠</sup> in the paper [Ben98] it was mistakenly indicated  $\sigma_0 = 0.4$  instead  $\sigma_0^2 = 0.4$ . This value was extracted from isobaric charge distributions (i.e  $\sigma(Z)_{[A=const]}$ ) [Lan80].

Daughter excitation energy distribution calculate:	Qualitatively
Take into account unbound nuclei:	Yes

It was necessary to optimize the process of calculation in the case of Abrasion-Fission, because excitation energy is equal to several hundred MeV for the High EER, which takes significantly more time than in the case of Coulomb-Fission where the excitation energy is about 15-20 MeV. For this purpose an acceleration filter was developed to be used only for calculations of light particle emission by excited fission fragments. You can see from Table 6 that calculations without this filter take more than one hour!

**Table 6.** Statistical characteristics of the sum (three EER) neutron distribution of fission residues from the reaction  $^{238}\text{U}(80\text{A MeV})+\text{Be}$  depending on the dimension of evaporation distribution and use of the acceleration filter.

$\text{NP}_{\text{evap}}$	filter	$\langle N \rangle$	$\sigma_N$	Elapsed time
4	yes	64.97	12.77	80 sec
8	yes	65.07	12.75	140 sec
16	yes	64.35	12.80	15 min
4	no	64.66	12.79	11 min
8	no	64.90	12.67	35 min
16	no	64.43	12.84	> 1 hour

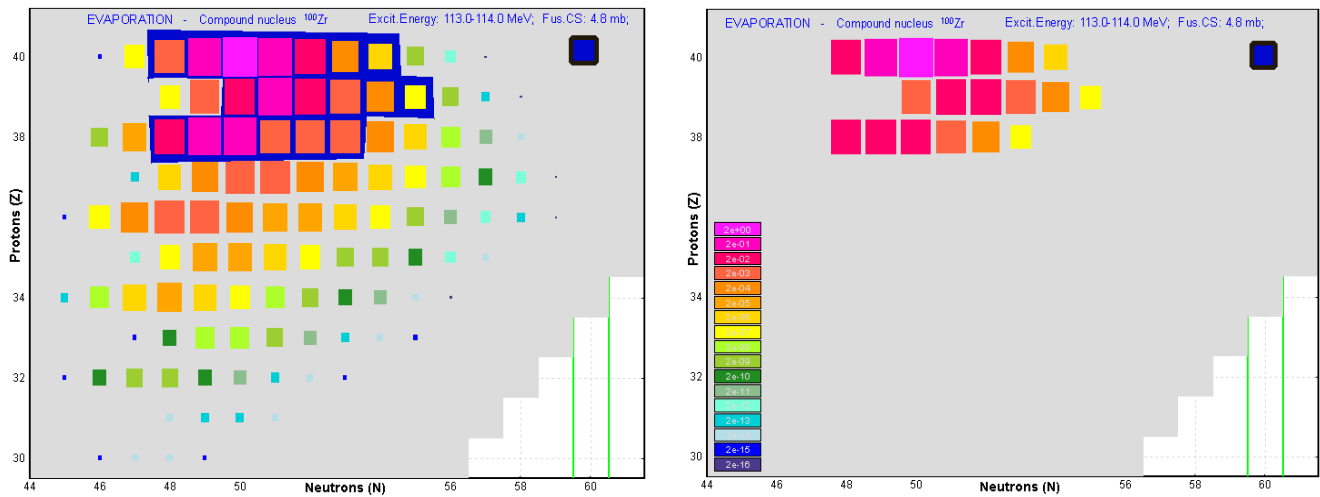
How does the acceleration filter work? The new parameter  $\sigma_{\text{lim}}$  has been added in the evaporation subroutine. At the beginning of the cascade this parameter is set equal to  $0.01 \sigma_{\text{init}}$  (initial production cross-section value from the CSinit matrix). The following constraints are checked:

- If  $\sigma_{\text{lim}} > 1e6 \sigma_{\text{Residual}}^i$  (final fragment cross-section of residual nucleus), then this final fragment is not included in the final matrices, and  $\sigma_{\text{Killed}} = \sigma_{\text{Killed}} + \sigma_{\text{Residual}}^i$ ;
- If  $\sigma_{\text{lim}} > 10 \sigma_{i\text{-decay}}^k$  ( $k$  decay channel of  $i$  excited intermediate nucleus), then the code cancels calculation in the  $k$  decay direction, and  $\sigma_{\text{Killed}} = \sigma_{\text{Killed}} + \sigma_{i\text{-decay}}^k$ ;
- If  $\sigma_{i\text{-sum}}$  (total production cross-section of  $i$  excited intermediate nucleus)  $> 50 \sigma_{i\text{-decay}}^k$ , then the code cancels calculation in the  $k$  decay direction, and  $\sigma_{\text{Killed}} = \sigma_{\text{Killed}} + \sigma_{i\text{-decay}}^k$ .

To show how and what the filter cuts, take from the CSinit matrix for example the  $^{100}\text{Zr}$  nucleus ( $E^* = 114$  MeV,  $\sigma = 4.8$  mb) produced in High EER fission (fissile nucleus  $^{220}\text{Rn}^*$ ,  $E^* = 232$  MeV,  $\sigma_{\text{fission}} = 476$  mb). Fig.56 shows  $^{100}\text{Zr}$  evaporation residues calculated with and without the filter.

This filter acts first of all against emission of alpha-particles and protons by low-excited nuclei in the neutron-rich region. In the process of calculating light particle emission from excited fission fragments, it is possible to see in the left bottom corner of the code a state line with the current status of the calculation:

Calculating Z=70 NumN=14 Killed=14.9%. The “NumN” parameter denotes the number of isotopes in the CSinit matrix for the currently calculating element, and the “Killed” parameter gives the average ratio  $\sigma_{\text{Killed}}/\sigma_{\text{init}}$  for this element. The filter cuts about 0-2 % for the Low EER, 1-5 % for Middle, and 5-16% for the High EER respectively.

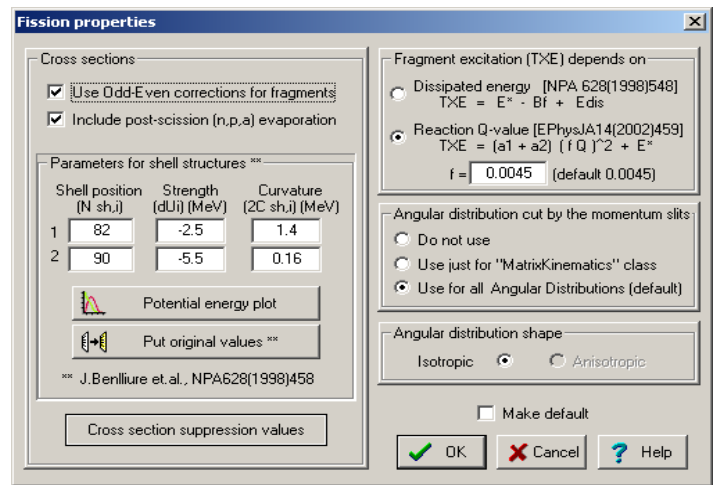


**Fig. 56.**  $^{100}\text{Zr}$  ( $E^* = 113 \text{ MeV}$ ,  $\sigma = 4.8 \text{ mb}$ ) evaporation residues calculated by the Evaporation calculator without/with the acceleration filter are shown in the left/right plot.

### 1.5.1.4. Additional settings

Tools to modify fission characteristics (Shell structures, TXE, angular distribution etc.) were moved from the Coulomb fission dialog to the separate dialog “Fission properties” (see Fig.57), which is accessible from the Abrasion-Fission and Coulomb Fission dialogs (see Fig.50).

It is possible from the Abrasion-Fission dialog to modify the settings of mechanisms involved in the production of the final fragment distribution:



**Fig. 57.** The “Fission properties” dialog.

**Table 7.**

Dialog	Properties	Daughter dialog
Fission properties dialog	Shell structures, TXE (excitation energy of fragment), angular distributions	Cross-section suppression values
Prefragment energy	Excitation energy for Abrasion-Ablation model to define fissile nuclei for EERs	
Evaporation settings	Dissipative effects in fission, break-up parameters to produce the fission excitation function	Fission barrier
Fission barrier dialog	Calculation of fission de-excitation channels	
Cross-section suppression values	To exclude low-probability events and to reduce the time of fragment cross-section calculation	

### 1.5.2. Kinematics

In order to calculate kinematics of Abrasion-Fission fragments, the code uses algorithms developed for the Coulomb version [LISE71]. Both *MCmethod* and *DistrMethod* can be used for these aims. We remind the reader that *DistrMethod* is the fast analytical method applied to calculate the fragment transmission through all optical blocks of the spectrometer. *MCmethod* has been developed for a qualitative analysis of fission fragment kinematics and is utilized in the Kinematics calculator.

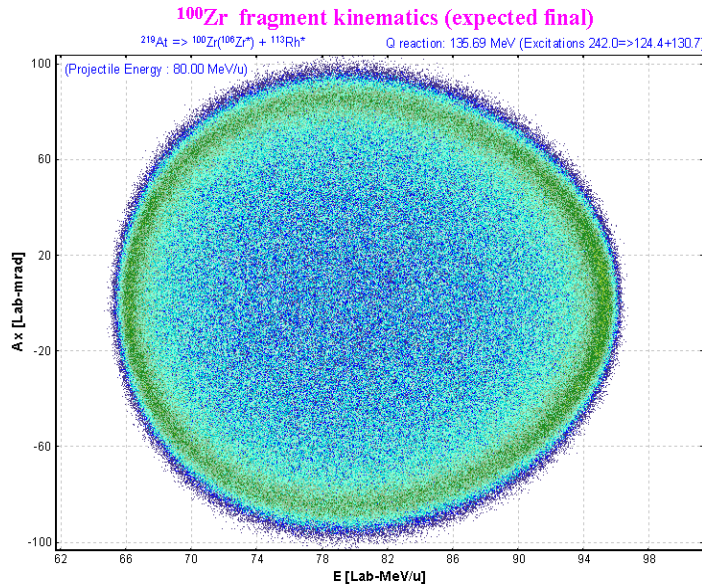
We shall show some examples of AF fragment kinematics calculation by both methods for different excitation energy regions, and also depending on angular acceptance and target thickness.

#### 1.5.2.1. Production of $^{100}\text{Zr}$

Let's again take the reaction  $^{238}\text{U}(80\text{A MeV})+\text{Be}$  with EERs defined in the insert of Fig.52. Initial emitances are  $\theta_x = \theta_y = 3.3\text{mrad}$  and  $\delta P=0.07\%$ . Set the target thickness equal to  $1\text{mg}/\text{cm}^2$ , and set the desired fragment to  $^{100}\text{Zr}$ , because this fragment may be produced by each EER:

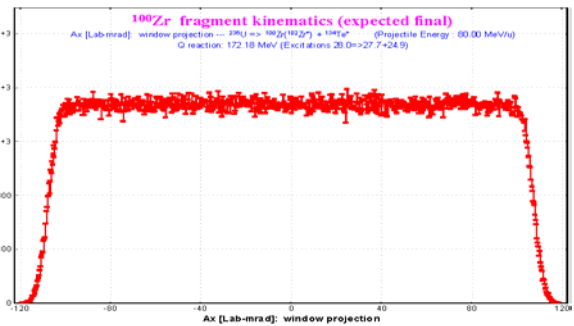
**Table 8.** Calculated production of  $^{100}\text{Zr}$  fission residues produced in the reaction  $^{238}\text{U}(80\text{A MeV})+\text{Be}$ .

EER	Fissile nucleus	$E^*$ MeV	Most probable excited fission fragment to produce $^{100}\text{Zr}$	Excitation energy ( $E^*$ ) of most probable excited fragment	$^{100}\text{Zr}$ production cross-section, mb
Low	$^{236}\text{U}$	28	$^{102}\text{Zr}$	27.7	10.7
Middle	$^{231}\text{Th}$	92	$^{104}\text{Zr}$	55.3	3.07
High	$^{219}\text{At}$	242	$^{106}\text{Zr}$	124.4	1.34



**Fig.58.** *MCmethod* (Monte Carlo) 2D-plot  $A_x$ (horizontal component of the angle in the laboratory frame) versus Energy per nucleon of  $^{100}\text{Zr}$  final fragments produced in fission of the  $^{219}\text{At}(E^*=242\text{MeV})$  nucleus.

**Fig.59.** Angular distributions of  $^{100}\text{Zr}$  fragments after the target calculated by the *DistrMethod* (analytical solution) for the reaction  $^{238}\text{U}(80\text{A MeV})+\text{Be}(1\text{mg}/\text{cm}^2)$ .



**Fig.60.** The projection of the 2D-plot in Fig.58 onto the  $A_x$  vertical axis.

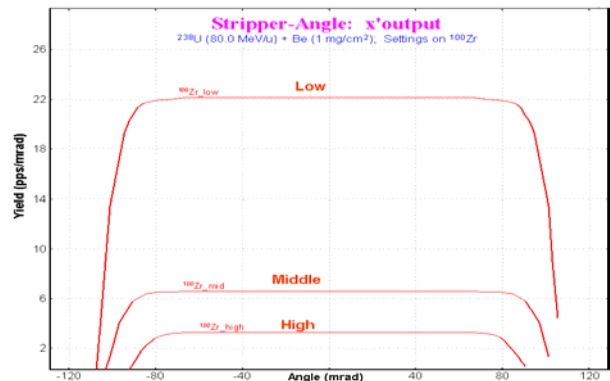
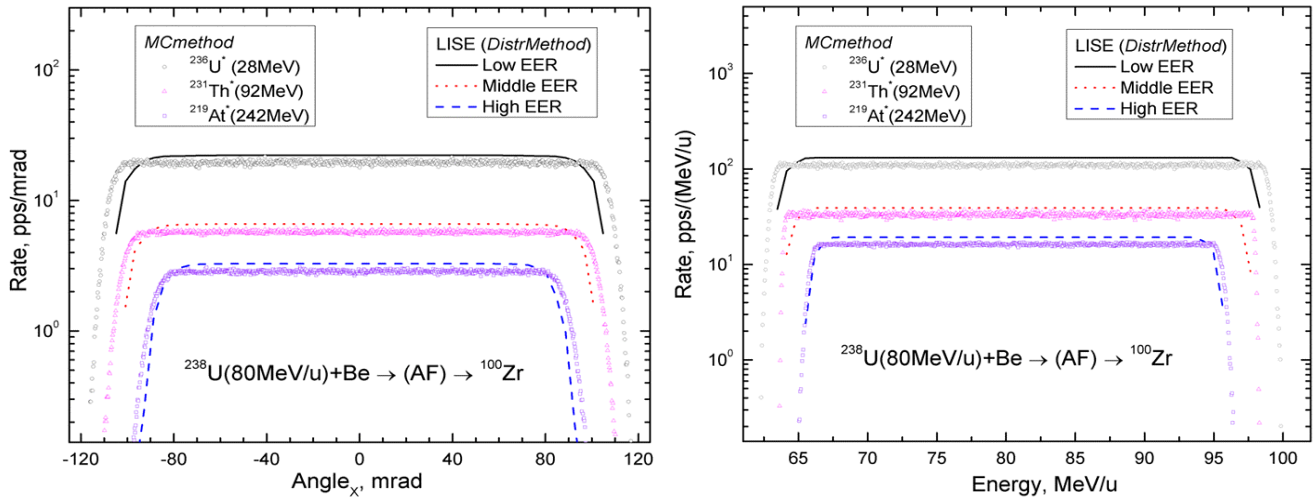


Fig.58 shows a kinematic Monte Carlo calculation of  $^{100}\text{Zr}$  final fragments produced in fission of the  $^{219}\text{At}(E^*=242\text{MeV})$  nucleus that corresponds to the High EER settings calculated for the AF reaction  $^{238}\text{U}(80\text{ MeV/u}) + \text{Be}(1\text{ mg/cm}^2)$ .

Fig.59 shows angular distributions of  $^{100}\text{Zr}$  fragments after the target, calculated for all of three EERs by the *DistrMethod* (analytical solution) for the reaction  $^{238}\text{U}(80\text{AMeV})+\text{Be}(1\text{mg/cm}^2)$ . This plot is the regular LISE plot developed to show transmission distributions through spectrometer blocks.

Fig.60 shows the projection of the 2D-plot (Fig.58) onto its vertical axis. Projections onto energy and angular axes of the 2D-plot of  $^{100}\text{Zr}$  fragment kinematics for different excited fragments done in this way are used to compare *DistrMethod* and *MCmethod* (see Fig.61). *MCmethod*'s angular and energy distributions produced by 2D-plot projections onto axes were normalized for Fig.61.



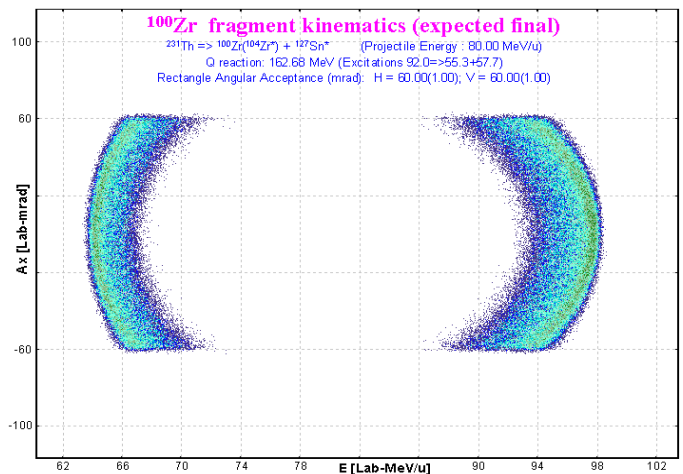
**Fig.61.** Matching of angular(left) and energy(right) distributions calculated by *DistrMethod* and *MCmethod* for the  $^{100}\text{Zr}$  final fragment produced by different excited fission fragments (or EERs).

### 1.5.2.2. Angular acceptance

Set the angular acceptances of the first optical block after the target to  $\pm 60\text{ mrad}$  in both directions and repeat the same calculation procedure as in the previous chapter.

Fig.62 shows a kinematics Monte Carlo calculation of  $^{100}\text{Zr}$  final fragments produced in fission of the  $^{231}\text{Th}(E^*=92\text{MeV})$  nucleus that corresponds to the Middle EER settings calculated for the reaction  $^{238}\text{U}(80\text{ MeV/u}) + \text{Be}(1\text{ mg/cm}^2)$ .

Table 9 shows, calculated by *MCmethod* and *DistrMethod*, angular transmissions of  $^{100}\text{Zr}$  fragments produced by different EERs in the reaction  $^{238}\text{U}(80\text{AMeV})+\text{Be}$ .



**Fig.62.** *MCmethod* (Monte Carlo) 2D-plot  $A_x$ (horizontal component of the angle in the laboratory frame) versus Energy per nucleon of  $^{100}\text{Zr}$  final fragments produced in fission of the  $^{231}\text{Th}(E^* = 92\text{ MeV})$ . Angular acceptances of the first optical block after the target are equal to  $\pm 60\text{ mrad}$  in both directions.



**Table 9.** Calculated by *MCmethod* and *DistrMethod*, transmission of  $^{100}\text{Zr}$  fragments produced by different EERs in the reaction  $^{238}\text{U}(80\text{A MeV})+\text{Be}$ . Angular acceptances of the first optical block after the target are equal to  $\pm 60$  mrad in both directions.

EER	Fissile nucleus	$E^*$ MeV	<i>MCmethod</i> Monte Carlo transmission, %	<i>DistrMethod</i> LISE transmission, %
Low	$^{236}\text{U}$	28	22.9	23.0
Middle	$^{231}\text{Th}$	92	26.0	25.2
High	$^{219}\text{At}$	242	36.5	33.6

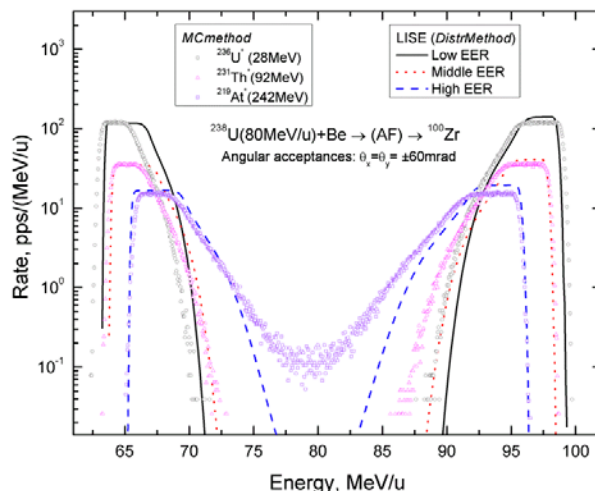
### 1.5.2.3. Thick target

Let's set the target thickness to  $150\text{ mg/cm}^2$  instead of the previous value of  $1\text{ mg/cm}^2$  and repeat the same calculation procedure as in the previous chapter.

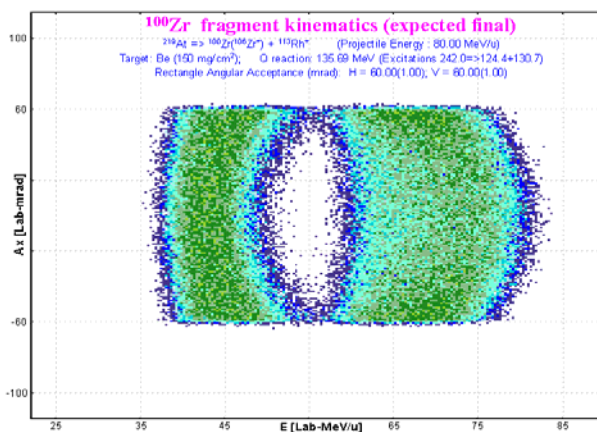
Fig.64 shows Monte Carlo kinematics of  $^{100}\text{Zr}$  final fragments, Table 10 shows transmission statistics, and Fig.65 shows comparable *MCmethod* and *DistrMethod* energy distributions of  $^{100}\text{Zr}$  fragments produced by different EERs in the reaction  $^{238}\text{U}(80\text{A MeV})+\text{Be}(150\text{ mg/cm}^2)$ . It is possible to see in Fig.65 a large discrepancy between angular distributions calculated by the *MCmethod* and *DistrMethod* models, because in the case of the *DistrMethod* the code assumes that the reaction takes place in the middle of the target.

**Table 10.** Calculated by *MCmethod* and *DistrMethod*, transmissions of  $^{100}\text{Zr}$  fragments produced by different EERs in the reaction  $^{238}\text{U}(80\text{A MeV})+\text{Be}(150\text{ mg/cm}^2)$ . Angular acceptances of the first optical block after the target are equal to  $\pm 60$  mrad in both directions.

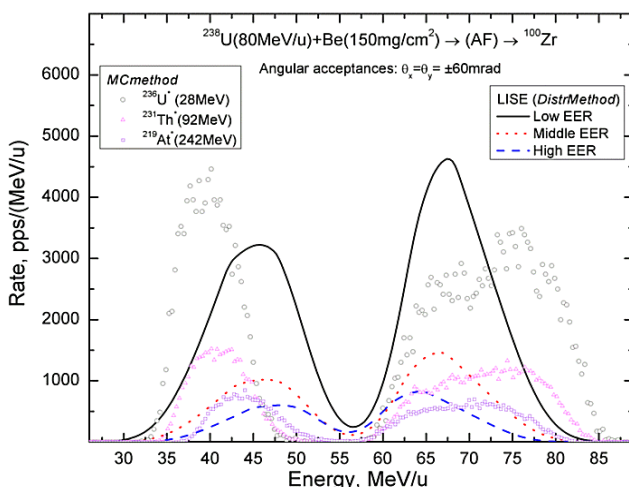
EER	Fissile nucleus	$E^*$ MeV	<i>MCmethod</i> MC transmission, %	<i>DistrMethod</i> LISE transmission, %
Low	$^{236}\text{U}$	28	17.9	14.9
Middle	$^{231}\text{Th}$	92	20.3	16.4
High	$^{219}\text{At}$	242	27.6	21.2



**Fig.63.** Comparison of energy distributions calculated by *DistrMethod* and *MCmethod* for the  $^{100}\text{Zr}$  final fragments produced by different excited fission fragments (or EERs).



**Fig.64.** Kinematics of  $^{100}\text{Zr}$  final fragments produced in fission of  $^{219}\text{At}$  ( $E^* = 242$  MeV). Angular acceptances of the first optical block after the target are equal to  $\pm 60$  mrad in both directions. Thickness of the Be-target is equal to  $150\text{ mg/cm}^2$ .



**Fig.65.** Matching of energy distributions in the case of a thick target.

### 1.5.3. Abrasion-Fission plots

Cross-section and TKE plot dialogs for the "Coulomb fission" reaction have been modified for the Abrasion-Fission mode and they are available in the menu "1D-plots". The complexity of the AF case lies in that AF is a result of three excitation energy regions, where each of them is an independent reaction mode for the program. It would be desirable to see them both separately and together. In connection with this, the cross-section and TKE dialogs were revamped (see Fig.66 and Fig.67). See examples of 2D cross-section plots in Fig.68.

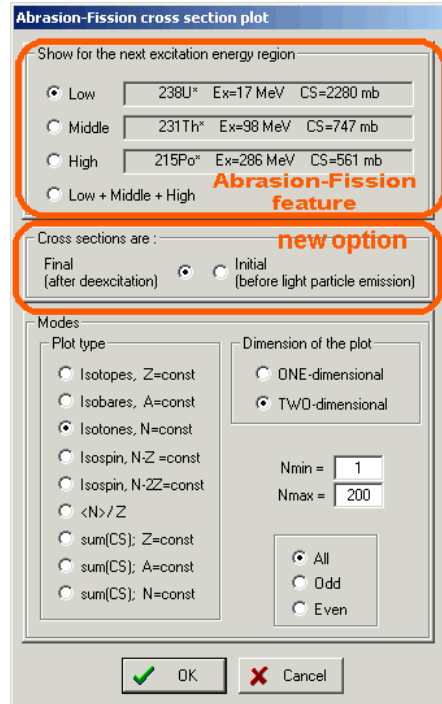


Fig.66. The "Abrasion-Fission cross-section plot" dialog.

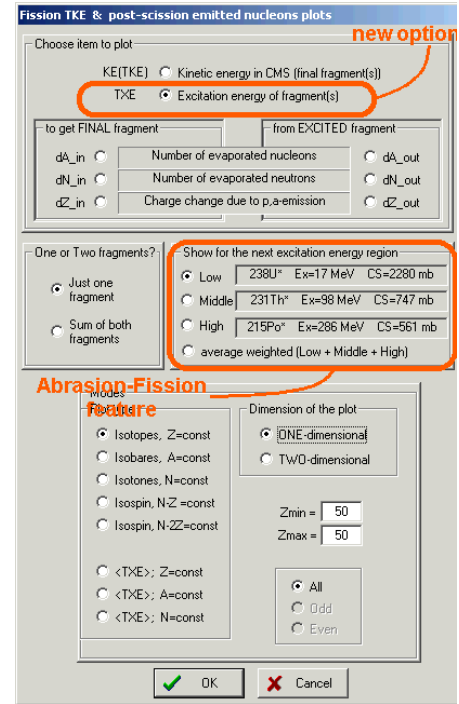


Fig.67. The "Fission TKE & post-scission emitted nucleons plot" dialog.

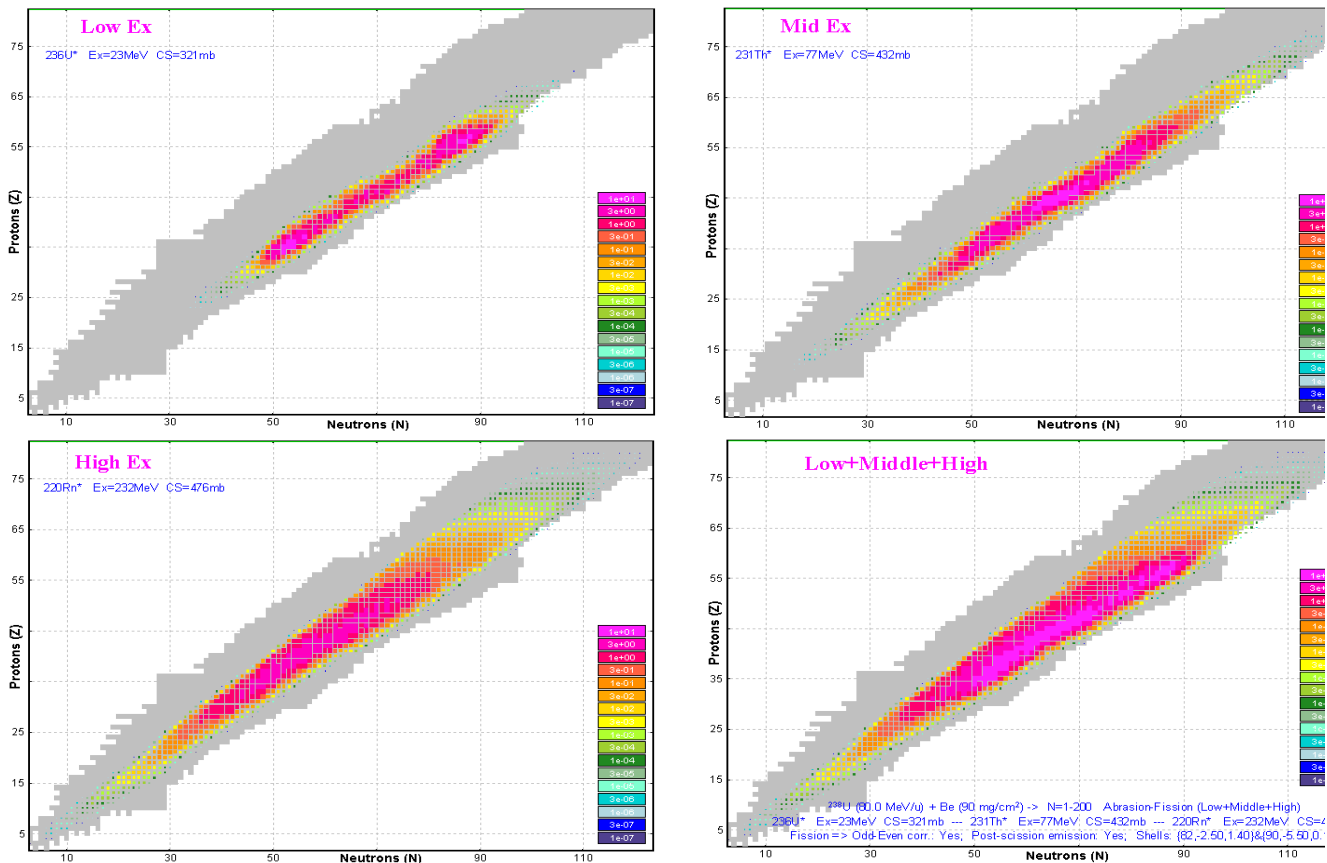


Fig.68. 2D fission fragment production cross-section plot for Low, Middle, High EERs and their sum (right bottom) for the reaction  $^{238}\text{U} (1\text{AGeV}) + \text{Be} (90 \text{ mg/cm}^2)$ . Projections on the vertical axis (Z) are shown in Fig.55.

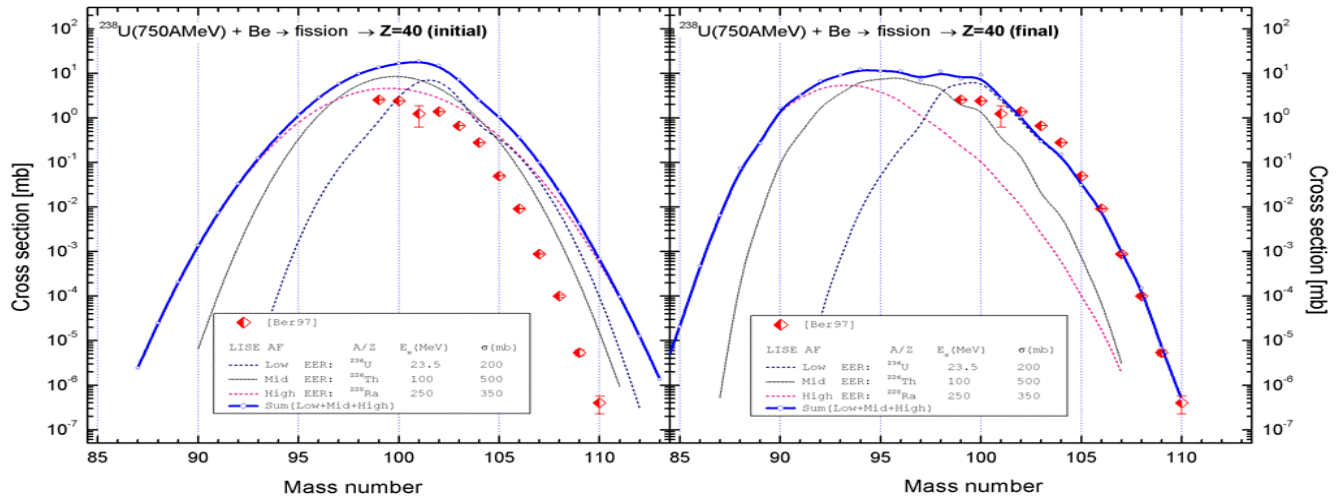
### 1.5.3.1. New plot options

New options to plot fission fragment distributions have been developed in the new version (see Fig.66 and Fig.67). These new options are also available in the Coulomb fission mode.

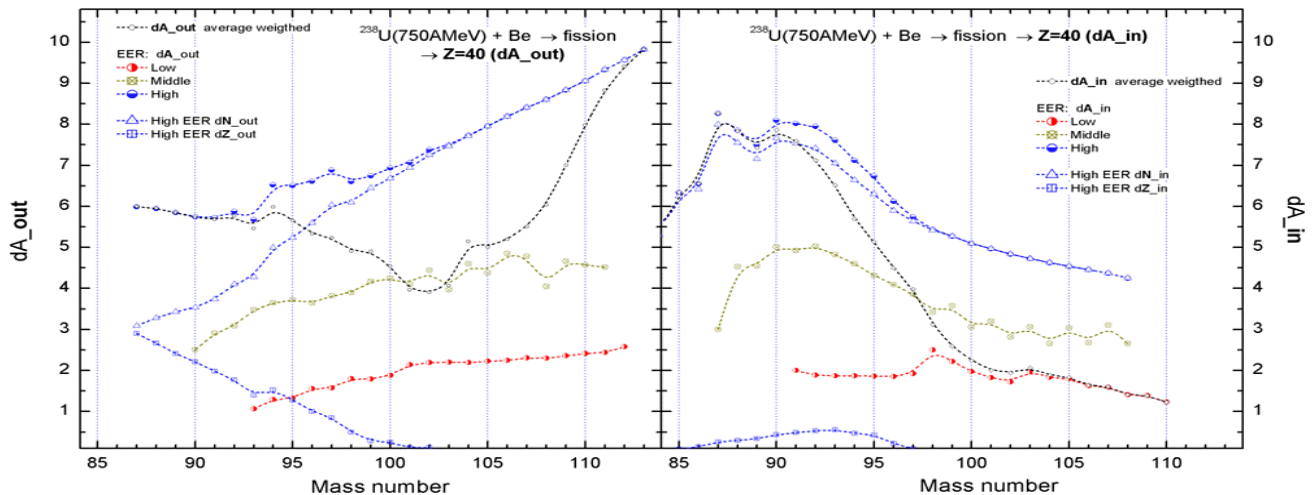
#### 1.5.3.1.1. Final (after de-excitation) and initial cross-section plots

In the new version the user can plot not only fission fragment cross-section distributions, when the fragments are already in a ground state, but also distributions immediately after fission before emission of light particles to release excitation energy. The  $^{238}\text{U}(750\text{AMeV})+\text{Be}$  reaction was used to illustrate this new possibility. The LISE parameters and a link with corresponding LISE++ file are given in chapter “1.5.9.4.  $^{238}\text{U}(750\text{AMeV}) + \text{Be}$ ”. Fig.69 shows the initial distribution of zirconium isotopes before and after emission of light particles. The experimental data [Ber97] are shown for comparison.

Fig.70 shows the mean quantity of nucleons emitted by excited Zirconium isotopes ( $dA_{out}$ ), and also the quantity of nucleons emitted before reaching a final fragment ( $dA_{in}$ ).



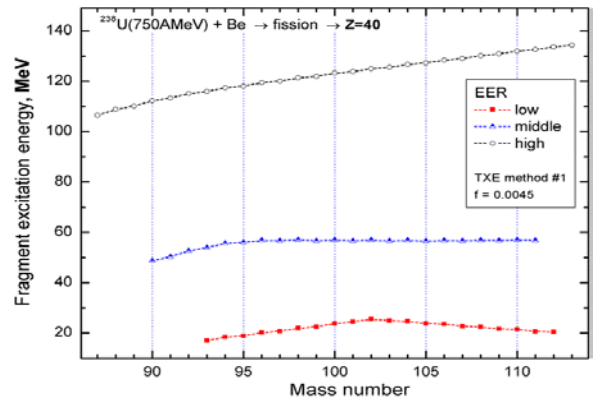
**Fig.69.** Initial (left plot) and final (right plot) Zirconium fission fragment distributions for different EERs in reaction  $^{238}\text{U}(750\text{AMeV})+\text{Be}$  reaction.



**Fig.70.** Left plot: Mean quantity of nucleons emitted by excited Zirconium fission fragments ( $dA_{out}$ ) produced in  $^{238}\text{U}(750\text{AMeV})+\text{Be}$  reaction. Right plot: Quantity of evaporated nucleons emitted before reaching a final fragment ( $dA_{in}$ ).

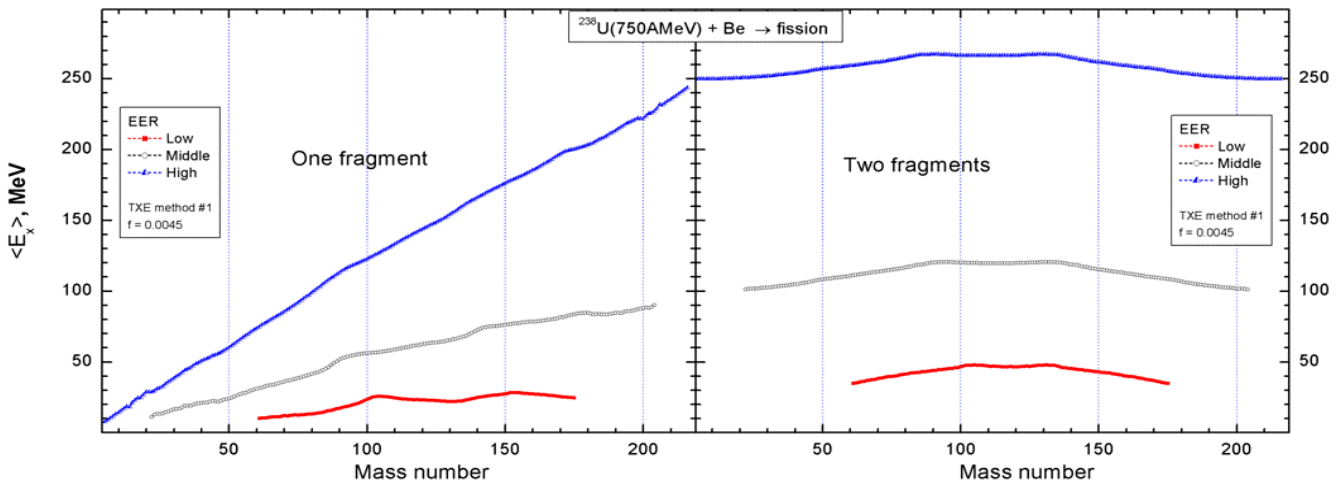
### 1.5.3.1.2. Excitation energy plot

The excitation energy plot is available through the dialog “Fission TKE & post-scission emitted nucleons plot” (Fig.67). The excitation energy plot of Zirconium isotopes produced in fission of  $^{238}\text{U}(750\text{AMeV})$  on a Be target is shown in Fig.71. The LISE parameters and a link with the corresponding LISE++ file are given in chapter “1.5.9.4.  $^{238}\text{U}(750\text{AMeV}) + \text{Be}$ ”.



**Fig. 71.** Excitation energy of Zirconium isotopes produced in fission of  $^{238}\text{U}(750\text{AMeV})$  on a Be target.

Fig.72 shows average isobar excitation energy plots of fission fragment for different EERs in the  $^{238}\text{U}(750\text{AMeV})+\text{Be}$  reaction.



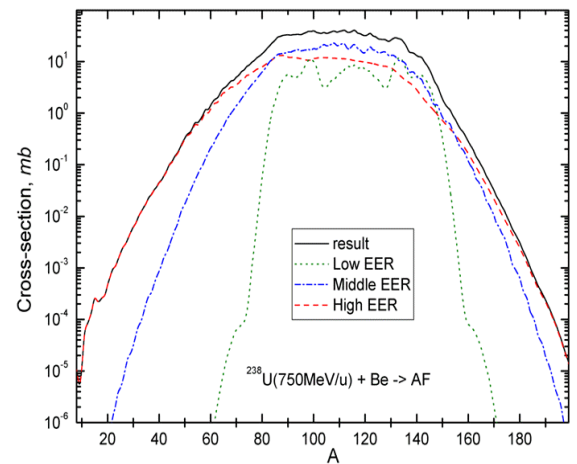
**Fig. 72.** Average isobar excitation energy of one (left plot) and two (right plot) fission fragment(s) for different EERs in the  $^{238}\text{U}(750\text{AMeV})+\text{Be}$  reaction.

### 1.5.4. Abrasion-Fission settings discussions

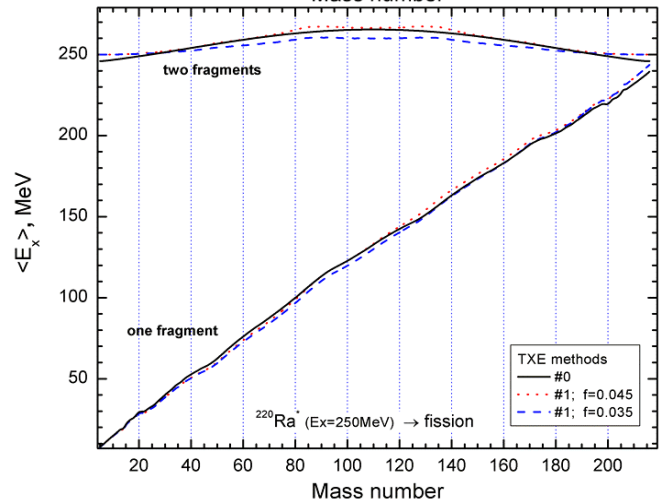
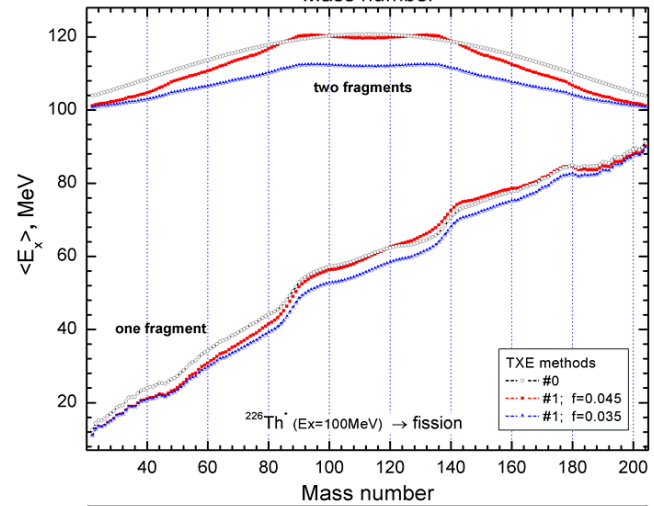
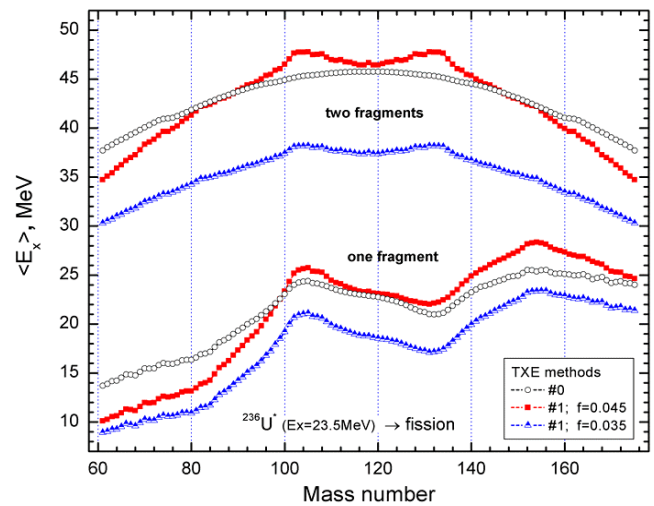
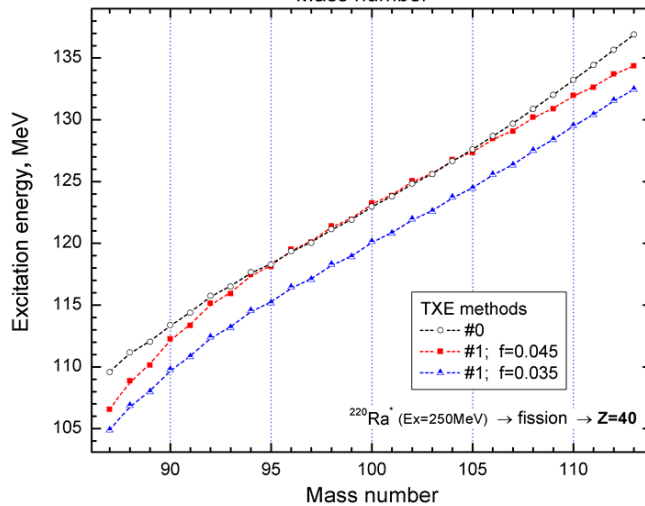
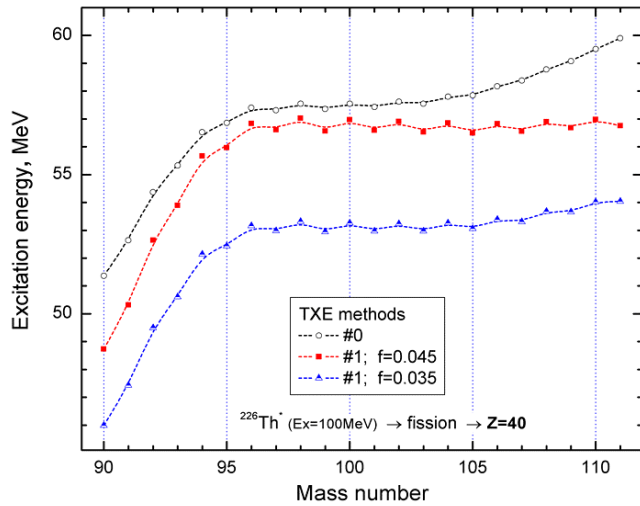
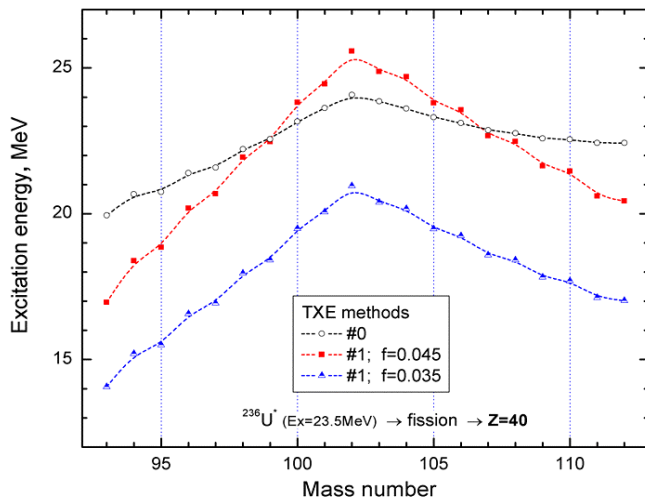
In this chapter we would like to show by example where and how Abrasion-Fission settings influence the final calculation results. Abrasion-Fission settings and where to access them are given in Table 7.

#### 1.5.4.1. Excitation energy of fission fragment (TXE)

Two models of fragment excitation energy (TXE) are included in LISE (see the “Fission properties” dialog in Fig.57). In the calculations for the TXE model based on Reaction Q-value (TXE #1), we will use two values, 0.0035 and 0.0045, for the  $f$  parameter. Calculated mass-distributions of fission fragments from  $^{238}\text{U}(750\text{MeV/u})+\text{Be}$  for different EERs are shown in Fig.73.

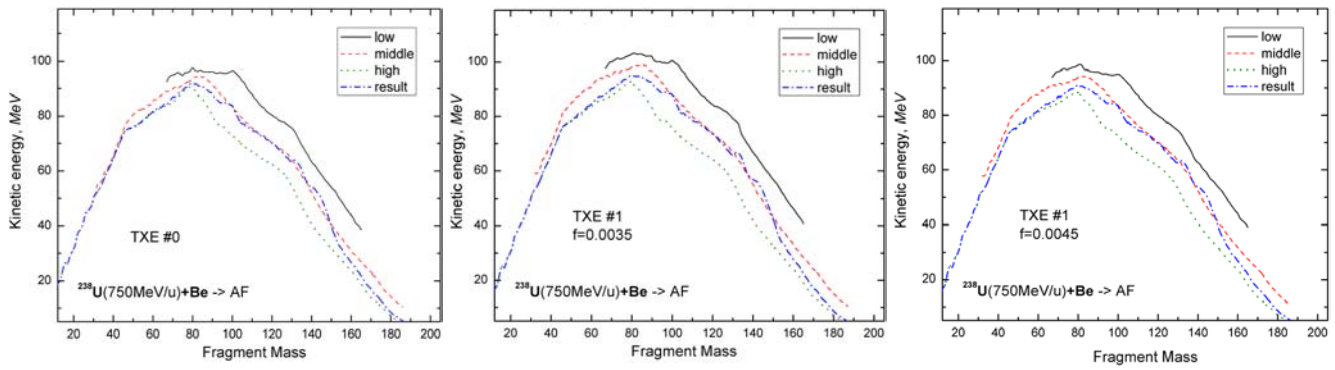


**Fig. 73.** Calculated mass distribution of fission fragments in  $^{238}\text{U}(750\text{MeV/u})+\text{Be}$  (TXE #1,  $f=0.0045$ ).

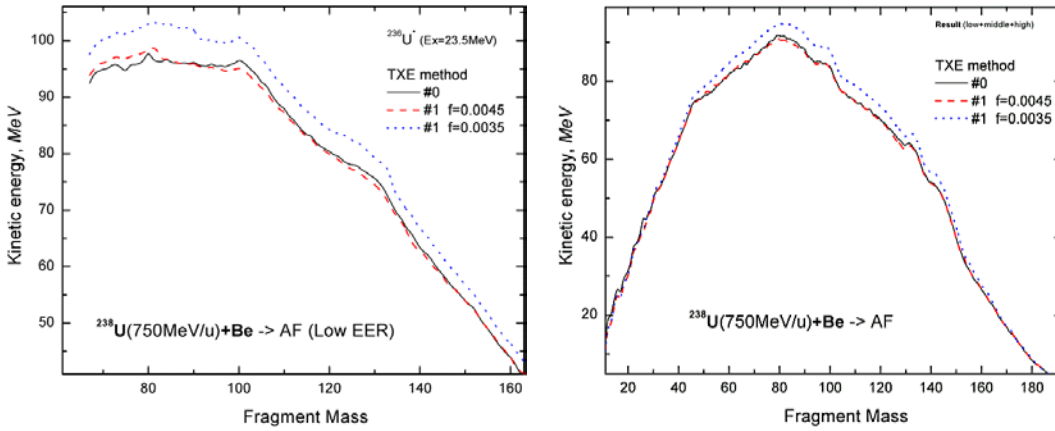


**Fig. 74.** Excitation energy of Zirconium fragments depending on an excitation energy method. Fragments are produced in fission of excited nuclei  $^{236}\text{U}$  ( $E_x=23.5\text{MeV}$ ) in top plot,  $^{226}\text{Th}$  ( $E_x=100\text{MeV}$ ) in middle plot, and  $^{220}\text{Ra}$  ( $E_x=250\text{MeV}$ ) in bottom plot. These excited nuclei correspond to EERs for the calculation of fission fragment production in the reaction  $^{238}\text{U}$  ( $750\text{MeV/u}$ )+Be.

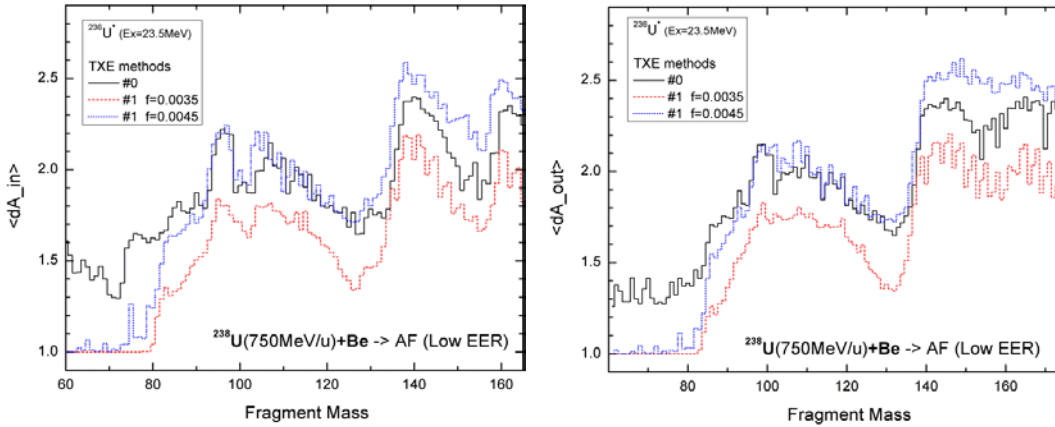
**Fig. 75.** Average weighted excitation energy of fragments depending on an excitation energy method. Fragments are produced in fission of excited nuclei  $^{236}\text{U}$  ( $E_x=23.5\text{MeV}$ ) in top plot,  $^{226}\text{Th}$  ( $E_x=100\text{MeV}$ ) in middle plot, and  $^{220}\text{Ra}$  ( $E_x=250\text{MeV}$ ) in bottom plot. These excited nuclei correspond to EERs for the calculation of fission fragment production in the reaction  $^{238}\text{U}$  ( $750\text{MeV/u}$ )+Be.



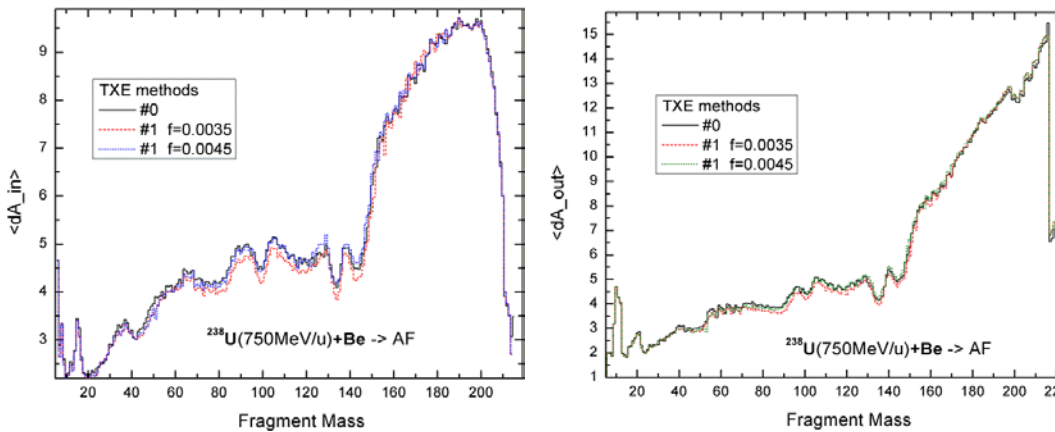
**Fig. 76.** Average kinetic energy of a fission fragment in the reaction  $^{238}\text{U}(750\text{MeV}/u)+\text{Be}$ . Left (TXE #0), middle (TXE #1,  $f=0.0035$ ), and right (TXE #1,  $f=0.0045$ ) plots show calculations for different EERs.



**Fig. 77.** Average kinetic energy of a fission fragment in the reaction  $^{238}\text{U}+\text{Be}$ . The left plot corresponds to the low EER [ $^{236}\text{U}$  ( $E_x=23.5\text{MeV}$ )], the right plot is the average weighted result of three EERs.



**Fig. 78.** Calculated average number of evaporated nucleons for / from a final / excited fragment produced by fission of the excited nucleus  $^{236}\text{U}$  ( $E_x=23.5\text{MeV}$ ).



**Fig. 79.** Calculated average number of evaporated nucleons for / from a final / excited fission fragment produced in the reaction  $^{238}\text{U}+\text{Be}$ .

Fig.74 shows excitation energy of Zirconium fragments and Fig.75 shows average weighted excitation energy of all fission fragments depending on the excitation energy method. Calculations were done for three different excited nuclei which correspond to EERs for the calculation of fission fragment production in reaction  $^{238}\text{U}$  (750MeV/u)+Be.

Fig.76 and Fig.77 show the average kinetic energy of a fission fragment in the reaction  $^{238}\text{U}$  (750MeV/u)+Be depending on the excitation energy method.

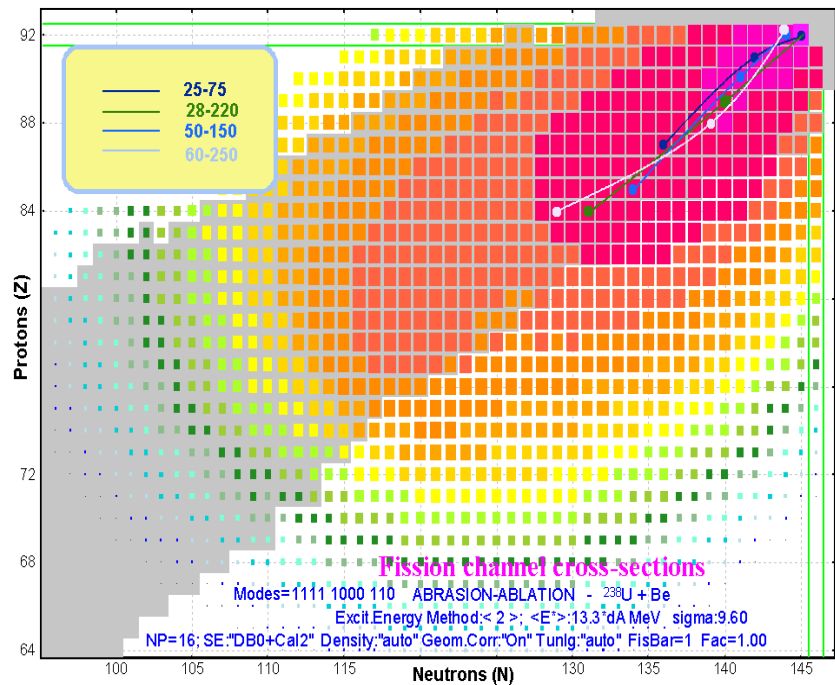
Fig.78 and Fig.79 show the calculated average number of evaporated nucleons for / from a final /excited fragment produced by fission of the excited nucleus  $^{236}\text{U}$  ( $E_x=23.5\text{MeV}$ ) and in the reaction  $^{238}\text{U}$ +Be.

It is possible to conclude from figures given above, that excitation energy values calculated by TXE method #1 ( $f=0.0045$ ) and method #0 are very close to each other if compared with method #1 ( $f=0.0035$ ). We recommend the use of method #1 ( $f=0.0045$ ).

### 1.5.4.2. Excitation energy region (EER) boundaries

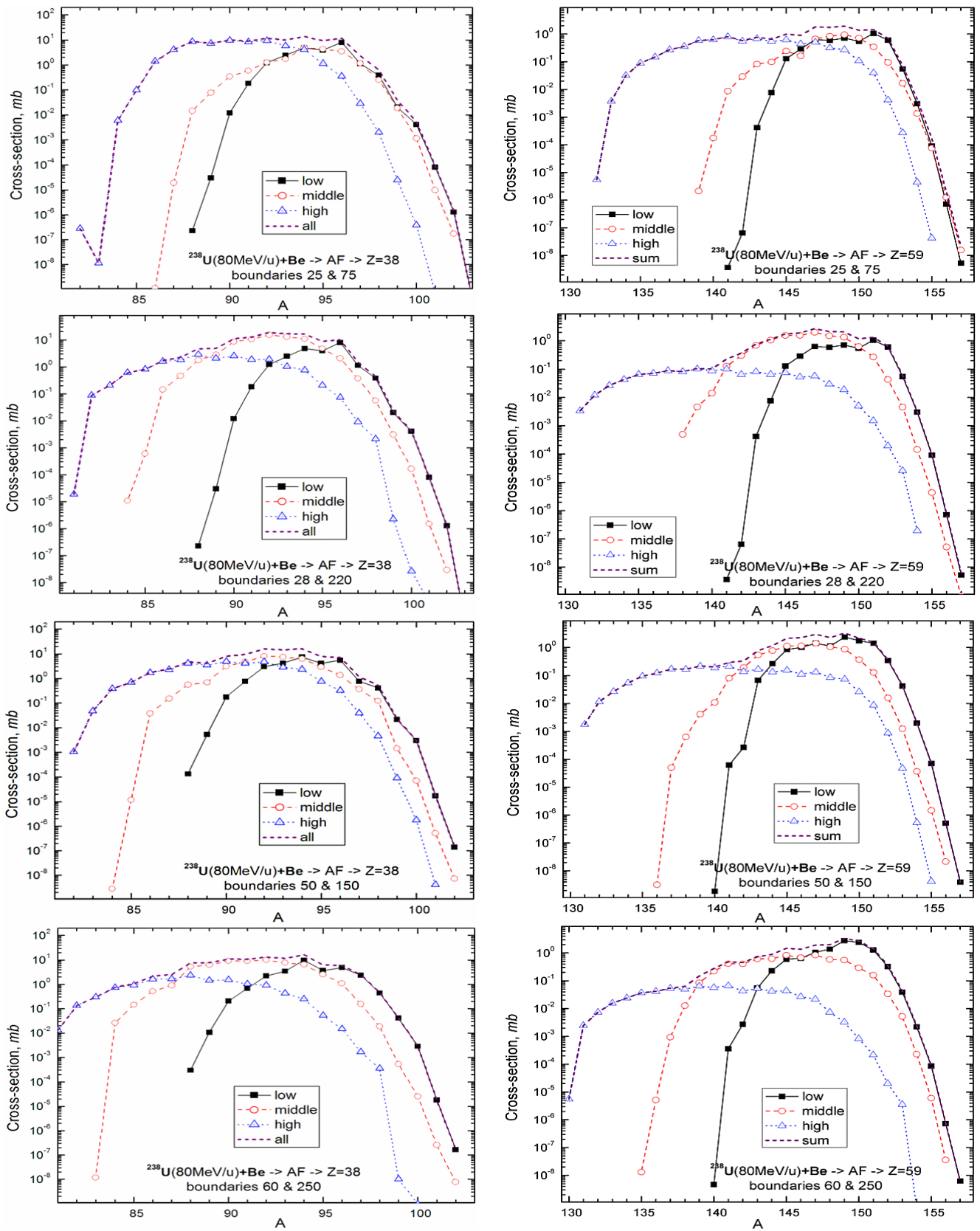
To see how boundary settings influence final fission fragment production, we chose four sets of boundaries to calculate EER characteristics (see Table 11). It is possible to visualize fissile nuclei for each boundary setting in Fig.80.

**Fig.80.** Fission de-excitation channel cross-sections calculated by the LISE Abrasion-Ablation model for the reaction  $^{238}\text{U}$ +Be. AA settings are shown in the figure. Circles correspond to the fissile nuclei of EERs given in Table 11



**Table 11.**

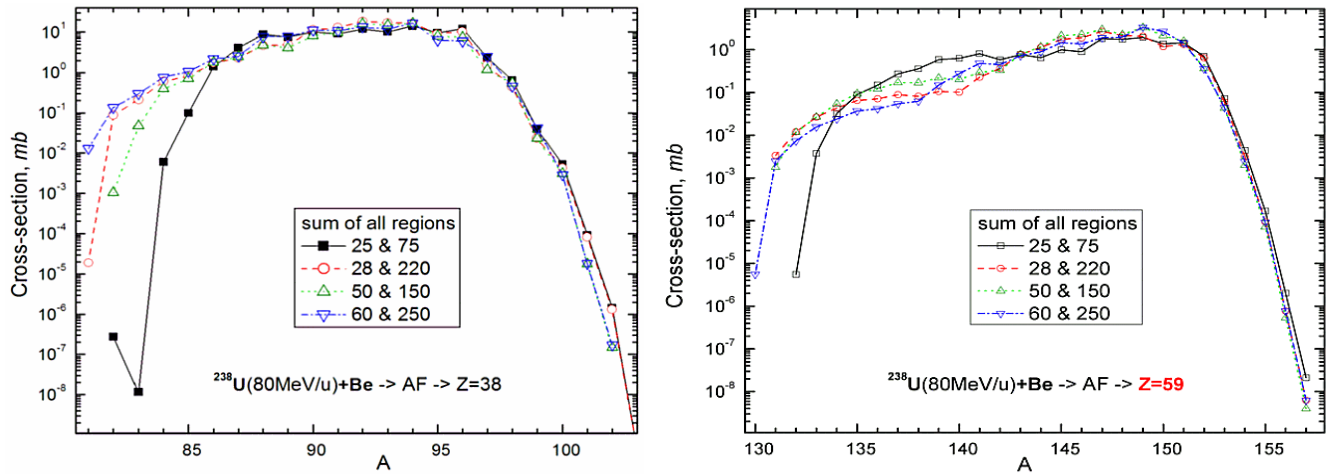
Boundaries		Low			Middle			High		
Left	Right	A, Z, N	$E^*$	$\sigma$	A, Z, N	$E^*$	$\sigma$	A, Z, N	$E^*$	$\sigma$
25	75	$^{237}_{92}\text{U}_{145}$	20.4	241.7	$^{234}_{91}\text{Pa}_{143}$	49.7	299.3	$^{223}_{87}\text{Fr}_{136}$	191.2	688.0
28	220	$^{237}_{92}\text{U}_{145}$	20.4	241.7	$^{229}_{89}\text{Ac}_{140}$	104.0	748.2	$^{215}_{84}\text{Po}_{131}$	288.4	239.0
50	150	$^{236}_{92}\text{U}_{144}$	28.3	409.7	$^{231}_{90}\text{Th}_{141}$	92.3	392.5	$^{219}_{85}\text{At}_{134}$	242.3	426.6
60	250	$^{236}_{92}\text{U}_{144}$	31.7	461.1	$^{227}_{88}\text{Ra}_{139}$	142.4	608.2	$^{213}_{84}\text{Po}_{129}$	314.8	159.6



**Fig.81.** Partial and total mass distributions of Strontium (left plots) and Praseodymium (right plots) fission fragments in the reaction  $^{238}\text{U}(80\text{MeV/u})+\text{Be}$  calculated for different sets of EER boundaries. See legends in plots.



Fig.81 shows partial and total mass distributions of Strontium and Praseodymium fission fragments in the reaction  $^{238}\text{U}(80\text{MeV/u})+\text{Be}$  calculated for different sets of EER boundaries. Fig.82 shows total mass distributions of Strontium and Praseodymium fission fragments in the reaction  $^{238}\text{U}(80\text{MeV/u})+\text{Be}$  calculated for different sets of EER boundaries given in Table 11.

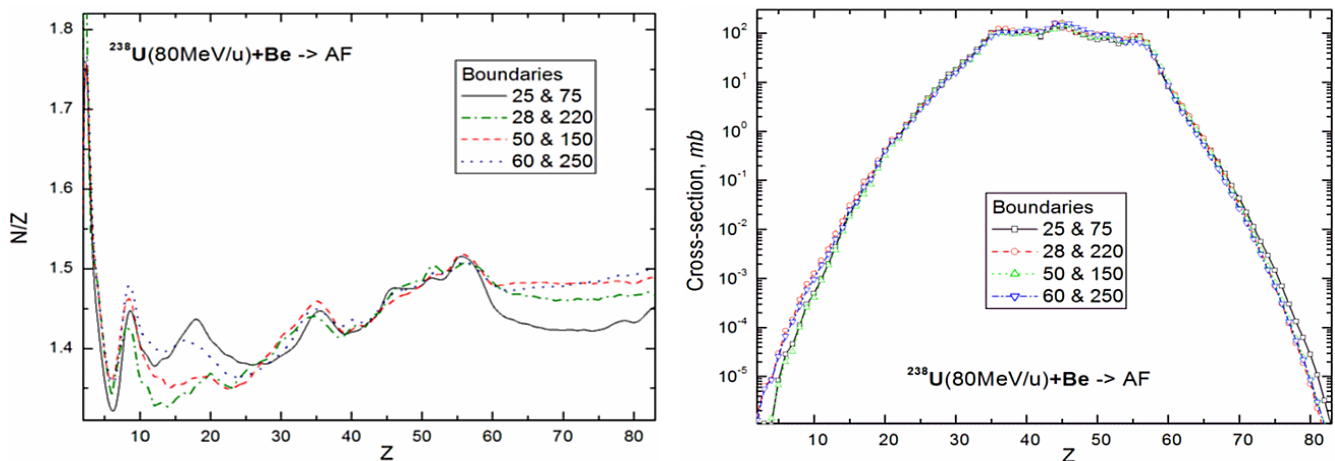


**Fig.82.** Total (sum of all regions) mass distributions of Strontium (left plot) and Praseodymium (right plot) fission fragments in the reaction  $^{238}\text{U}(80\text{MeV/u})+\text{Be}$  calculated for different sets of EER boundaries.

Based on Fig.81 and Fig.82 it is possible to make these three principal conclusions:

1. High left boundary (50 MeV in the third set and 60 MeV in the fourth set) leads to underestimation of super neutron-rich isotopes.
2. Low right boundary (75 MeV in the first set and even 150 MeV in the third set for Strontium isotopes) leads to LARGE underestimation of proton-rich isotopes (see left plot in Fig.82).
3. Large distance between boundaries (28 & 220 MeV in the second set and 60 & 250 MeV in the fourth) leads to a hole between High and Middle isotope cross-section distributions (see right plot in Fig.82).

Based on these conclusions we recommend the following boundaries<sup>♥</sup>: Left 30-40 MeV, Right 180-200 MeV. Fig.83 demonstrates the significant difference in N/Z ratio and element integrated distributions between boundary sets for elements with  $Z < 25$  and  $Z > 60$ .



**Fig.83.** N/Z ratio (left plot) and element integrated (right plot) distributions of fission fragments from ( $^{238}\text{U}+\text{Be}$ ).

<sup>♥</sup> Boundary positions depend on excitation energy per abraded nucleon, which is used by the Abrasion-Ablation model to define EER characteristics. In above examples the excitation energy was equal to 13.3 MeV/dA.

### 1.5.4.3. Excitation energy per abraded nucleon for Abrasion-Ablation

To calculate the fission de-excitation function after abrasion of a heavy projectile by a target in previous examples, the excitation energy value 13.3 MeV per abraded nucleon was used. This value is set by default in the code. What decay channel will follow after an abrasion is determined first of all by the value of excitation energy (see Fig.9). The analysis of excitation energy is the subject of very complicated theoretical and experimental research, and is not a subject of this chapter, where we only want to show the influence of the excitation energy value on fission fragment production. Excitation energy depends on the target material and projectile energy<sup>♦</sup>, as well as the reaction mechanism involved in fragment production, for example abrasion or INC (chapter 1.5.8. INC fission). We speak about the abrasion of a projectile and suggest simplistically that the excitation energy is proportional to the number of abraded nucleons without any dependence on the target material or projectile energy.

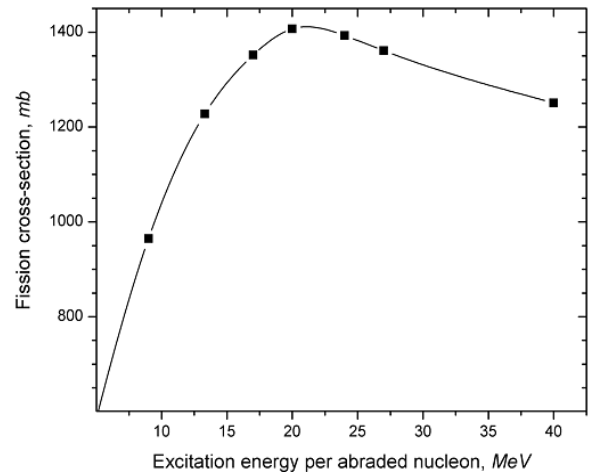
**Table 12.** EER characteristics as a function of excitation energy per abraded nucleon

per abr.nucleon		$\Sigma\sigma$ mb	boundaries		Low			Middle			High		
$E^*$	sigma		Left	Right	A, Z, N	$E^*$	$\sigma$	A, Z, N	$E^*$	$\sigma$	A, Z, N	$E^*$	$\sigma$
<b>9</b>	5	965	30	150	$^{236}_{92}\text{U}_{144}$	17.7	280.9	$^{228}_{89}\text{Ac}_{139}$	78.0	489.3	$^{210}_{83}\text{Bi}_{127}$	244.8	189.6
<b>13.3</b>	9.6	1228	30	180	$^{236}_{92}\text{U}_{144}$	23.5	312.8	$^{231}_{90}\text{Th}_{141}$	96.7	576.1	$^{217}_{85}\text{At}_{132}$	263.5	334.6
<b>27</b>	19	1361	45	200	$^{237}_{92}\text{U}_{145}$	38.7	292.4	$^{234}_{91}\text{Pa}_{143}$	114.5	573.2	$^{225}_{87}\text{Fr}_{138}$	320.8	489.9
<b>40</b>	28	1251	50	200	$^{236}_{92}\text{U}_{144}$	49.4	183.5	$^{234}_{91}\text{Pa}_{143}$	108.8	608.4	$^{228}_{89}\text{Ac}_{139}$	301.9	448.6

Table 12 shows EER characteristics calculated with different excitation energy values per abraded nucleon ( $E_{dA}^*$ ), which will be used for the following analysis of the influence of the excitation energy on fission fragment production. It is necessary to notice that with increasing  $E_{dA}^*$ , fissile nuclei become heavier. For example for Middle EER the masses of fissile nuclei are equal to 228, 231, 234, 234 for  $E_{dA}^*$  values of 9, 13.3, 27, 40 respectively, and for the High EER the masses are equal to 210, 217, 225, 228. It is explained that more abraded projectiles in the case of higher excitation energy proceed by the break-up channel. The following decay parameters were used for calculations:

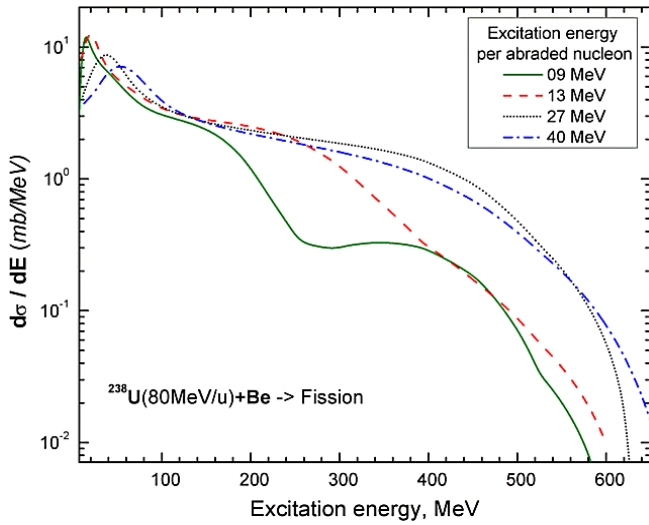
Channels:  $p, n, 2n, \alpha, \text{fission}, \text{break-up}$   
 Break-up:  $T(40)=6.0, T(200)=4.5$   
 Dissipation: "Kramers' factor"=NO and beta=1  
 BarFac=1 & mode: auto.

Fig.84 shows the fission de-excitation cross-section as a function of  $E_{dA}^*$ . A reduced experimental cross-section value of  $1.16 \pm 0.10$  barn [Rub96] corresponds to an excitation energy equal to 13 MeV/dA. We talk a little bit more about total cross-sections in chapter "1.5.9. Comparison with experiment".

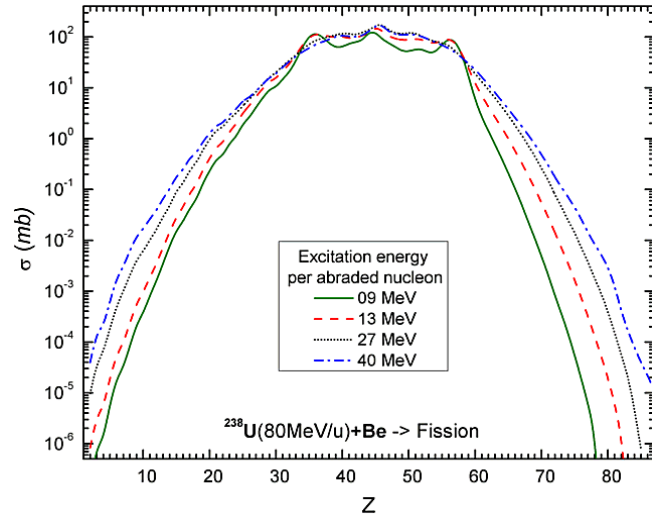


**Fig.84.** Fission de-excitation channel cross-section for  $^{238}\text{U} (80\text{MeV/u}) + \text{Be}$  as a function of excitation energy per abraded nucleon.

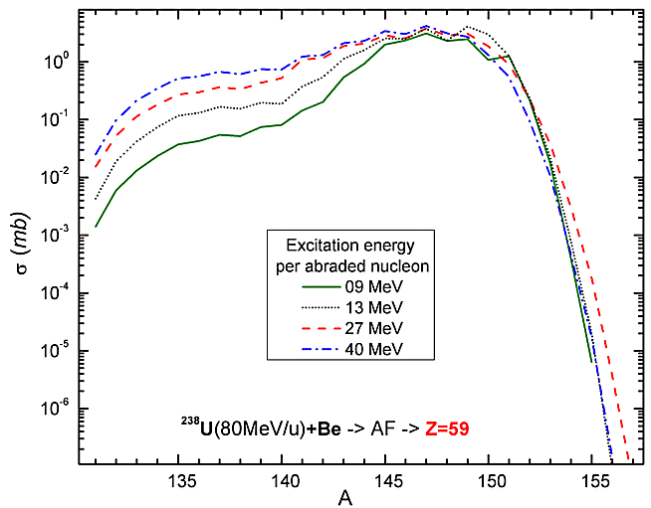
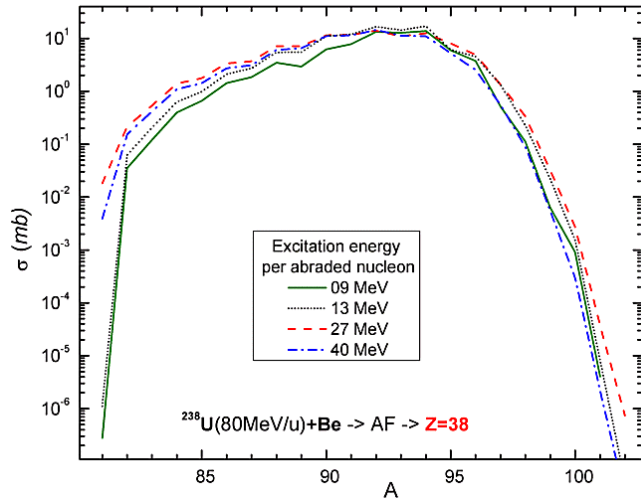
<sup>♦</sup> it is planned to make this analysis within the LISE development framework soon.



**Fig.85.** Fission de-excitation function for the reaction  $^{238}\text{U}+\text{Be}$  as a function of the excitation energy per abraded nucleon.



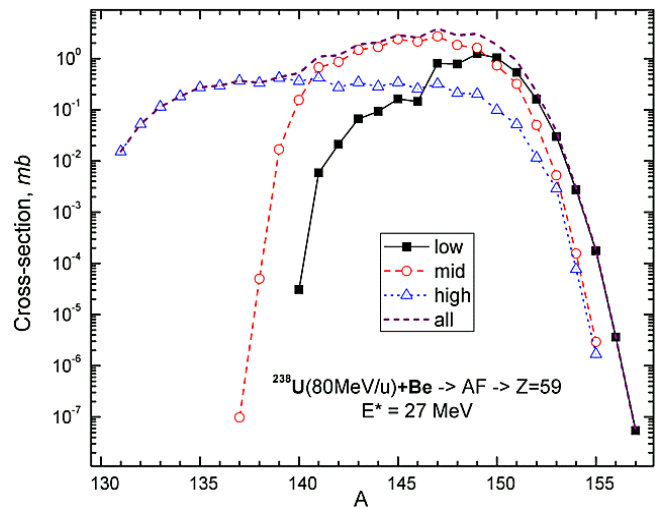
**Fig.86.** Elemental fission cross-sections for the reaction  $^{238}\text{U}(80\text{MeV})+\text{Be}$  as a function of  $E_{dA}^*$ .



**Fig.87.** Total (sum of all regions) mass distributions of Strontium (left plot) and Praseodymium (right plot) fission fragments in the reaction  $^{238}\text{U}(80\text{MeV/u})+\text{Be}$  calculated for different values of excitation energy per abraded nucleon.

Fig.85-87 demonstrate the influence of the excitation energy value in abrasion on fission de-excitation functions, elemental fission cross-sections, and mass distributions of Strontium and Praseodymium fission fragments in the reaction  $^{238}\text{U}(80\text{MeV/u})+\text{Be}$ .

Fig.88 shows partial and total mass distributions of Praseodymium fission fragments in the reaction  $^{238}\text{U}(80\text{MeV/u})+\text{Be}$  calculated for  $E_{dA}^* = 27 \text{ MeV/dA}$ .



**Fig.88.** Calculated mass distributions of Praseodymium fission fragments in the reaction  $^{238}\text{U}(80\text{MeV/u})+\text{Be}$ .

#### 1.5.4.4. Dissipation effects in fission

The influence of dissipation effects on the fission de-excitation functions has already been considered in chapter “1.2.2. Dissipation effects in fission”, where Fig.13 demonstrates how the total nuclear fission cross-section and the shape of the fission excitation functions can depend on the dissipation effects.

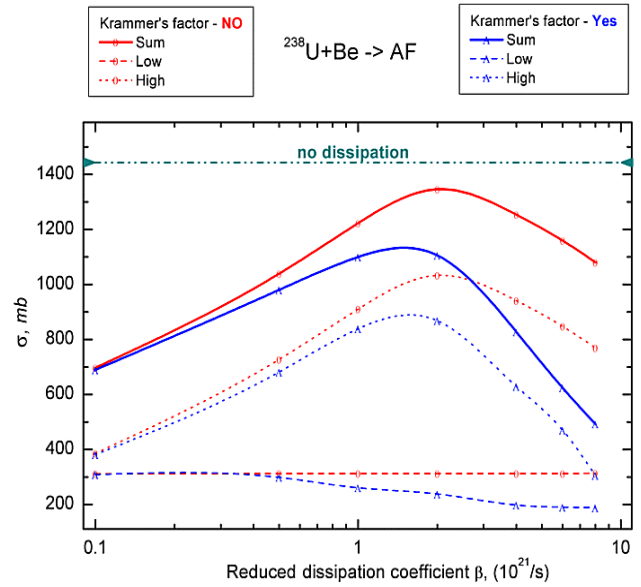
Here we would like to notice a correlation between the reduced dissipation parameter, Kramers’ factor, and the total fission cross-section. Recall that parameters for dissipation effects are in the “Evaporation options” dialog (see Fig.7, frame “A”).

Fig.89 and Fig.90 show fission cross-section and excitation energy of the High EER fissionable nucleus in the reaction  $^{238}\text{U}(80\text{MeV/u})+\text{Be}$  as a function of reduced dissipation coefficient. These calculations were done for the 2-EER model. The boundary between Low and High regions was set to 30 MeV. In the case of excitation energy per abraded nucleon equal to 13.3 MeV/dA it is recommended to use a reduced dissipation coefficient equal to  $1 \cdot 10^{21}/\text{s}$  and turn off Kramers’ factor to exclude dissipation effects at low-excitation energies.

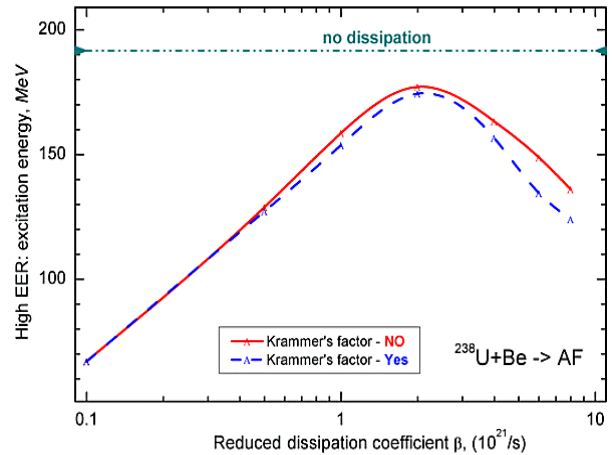
#### 1.5.4.5. Break-up de-excitation channel

The crucial role of the break-up channel has been already demonstrated in chapter 1.2.1.1.1. The dependence of break-up parameters (limiting temperature, diffuseness) on de-excitation channel cross-sections it is possible to see in Fig.91, based on calculation results given in Table 13. These calculations were done for the 3-EER model with boundaries 40 and 180 MeV. The excitation energy per abraded nucleon was set to 13.3 MeV/dA. It is possible to conclude for the limiting temperature “working” region (4-7 MeV) that:

- If we take dissipation effects into account, then the fission cross-sections do not depend on the limiting temperature. There is competition between break-up channels and light particle evaporation.
- If we do not take dissipation effects into account then light particle evaporation cross-sections do not depend on the limiting temperature. There is competition between break-up and fission de-excitation channels.



**Fig.89.** Fission cross-section in the reaction  $^{238}\text{U}(80\text{MeV/u})+\text{Be}$  as a function of reduced dissipation coefficient. Calculations were done for the 2-EER model. The boundary between Low and High regions was set to 30 MeV.



**Fig.90.** Excitation energy of the High EER fissionable nucleus in the reaction  $^{238}\text{U}(80\text{MeV/u})+\text{Be}$  as a function of reduced dissipation coefficient. Calculations were done for the 2-EER model. The boundary between Low and High regions was set to 30 MeV.

Table 13. Channel cross-sections as a function of the limiting temperature.

Break-up parameters			Dissipation <i>Use Step function</i>	High ERR Excit. en- ergy	AF cross-sections, [mb]		Evaporation calculator cross-section [barn]		
T A=40	T A=200	Diffuse- ness			High EER	Sum of EERs	Residues	Fission	Break-up
4.5	6	0.05	Yes	263.5	334.6	1223.5	0.904	1.18	0.604
4.5	6	<b>0.5</b>	Yes	256.4	275.6	1150.7	0.784	1.14	0.694
4.5	6	0.05	No	305.7	487.5	1464.2	0.721	1.44	0.603
3	3	0.05	Yes	200.1	127.3	1014.8	0.7	1.01	1.01
4	4	0.05	Yes	249	307.7	1196.6	0.838	1.16	0.702
5	5	0.05	Yes	282.4	362.4	1251.2	0.967	1.20	0.519
6	6	0.05	Yes	294.7	385.0	1273.9	1.09	1.22	0.372
7	7	0.05	Yes	294.9	387.1	1276.0	1.2	1.22	0.258
3	3	0.05	No	203.1	163.5	1079.9	0.658	1.09	1.01
4	4	0.05	No	263.8	473.1	1381.1	0.707	1.36	0.7
5	5	0.05	No	326	646.5	1554.5	0.728	1.53	0.517
6	6	0.05	No	359.5	798.4	1706.4	0.731	1.67	0.37
7	7	0.05	No	360.7	914.9	1822.9	0.733	1.79	0.257

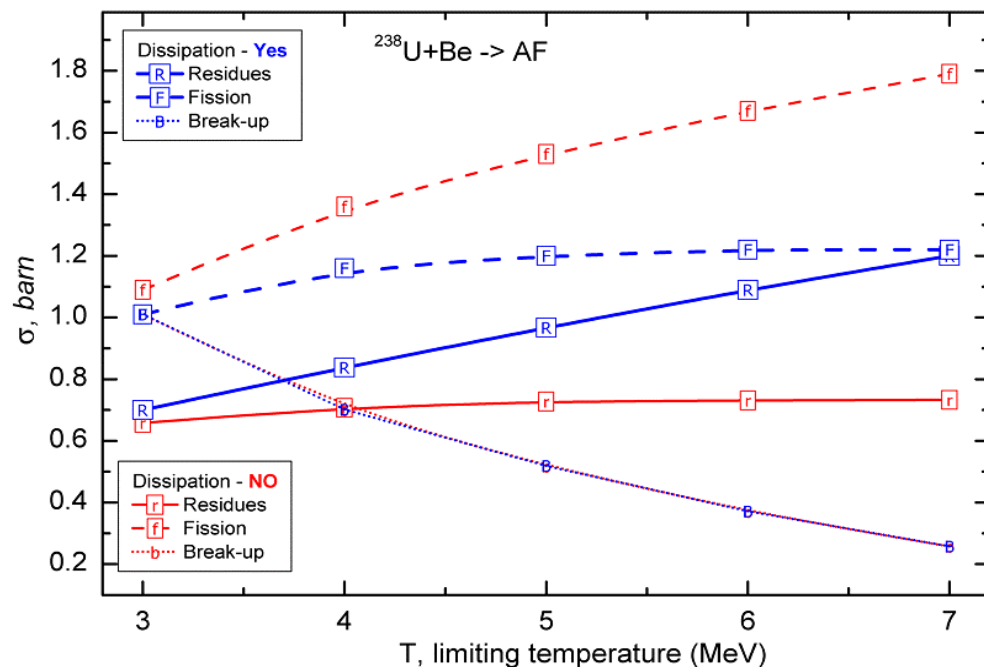


Fig.91. Fission cross-section in the reaction  $^{238}\text{U}(80\text{MeV/u})+\text{Be}$  as a function of reduced dissipation coefficient. Calculations were done for the 2-EER model. The boundary between Low and High regions was set to 30 MeV.

#### 1.5.4.6. Fission barrier

Correlation between the fission barrier and the fission de-excitation function has already been considered in chapter “1.3.5. Influence of corrections for fission barriers on abrasion-fission cross-sections”.

Increasing fission barrier height leads to a decrease of fission cross-sections and increasing light particle evaporation production.

### 1.5.4.7. Cross-section suppression coefficient

The cross-section suppression coefficient is applied to the initial fission cross-section matrix ( $CS_{init}$ ) of production cross-sections for excited fragments before the calculation of light particle emission. This coefficient is set by default to 1e-10mb. Using this coefficient decreases calculation time for cross-sections and frees the operating memory. With the coefficient equal to 1e-10 mb the code uses 90 seconds whereas for values 1e-15, 1e-20, and 1e-30 mb respectively, it uses 121, 142, and 206 seconds. It is necessary to note two moments:

- Decreasing the suppression coefficient does not lead similarly to low cross-sections for proton-rich fragments, because in the first place the acceleration filter (see “1.5.1.3.2. Modification of evaporation cascade subroutines”) works against low cross-section production after reaching the maximum of the final fragment distribution (see Fig.56).
- Secondary reactions contribution is very important in the case of Abrasion-Fission, and we recommend always using the SR option. As you will see in the next chapter, there is no difference between reduced cross-sections calculated with different cross-section limit values if the target is not very thin.

Fig.92 shows Tin fission fragment cross-sections for production in the reaction  $^{238}\text{U}+\text{Be}$  calculated for different cross-section suppression values.

### 1.5.4.8. Restore previous AF settings

If the user is working in the Abrasion-Fission reaction mode and changes the parameters of the target or the primary beam, then the program automatically

- ❑ initiates the AF EER settings,
- ❑ sends a message to the user (see Fig.93),
- ❑ shows AF settings by red colors in the Set-up window (see Fig.99).

If the user wants to go back to previous AF settings, it is necessary to open the “AF settings” dialog (for more details about it look at “1.5.6.2. Abrasion-Fission settings”) and click the “Restore previous settings” button to load the dialog of the same name, which shows the previous settings and prompts the user either to accept them or to refuse.

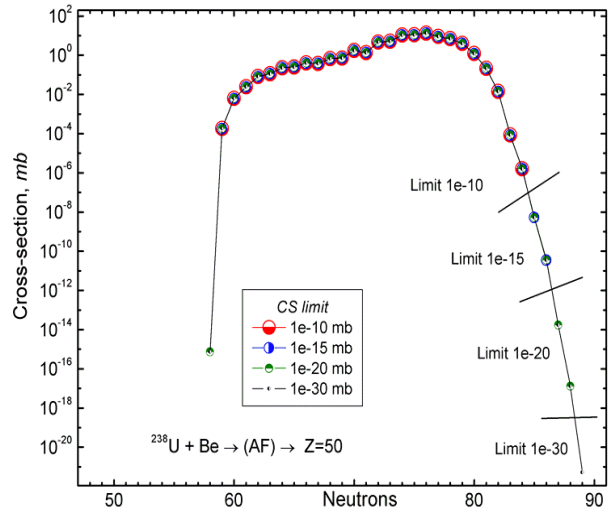


Fig.92. Calculated Tin fission fragment cross-sections for production in the reaction  $^{238}\text{U}+\text{Be}$ .

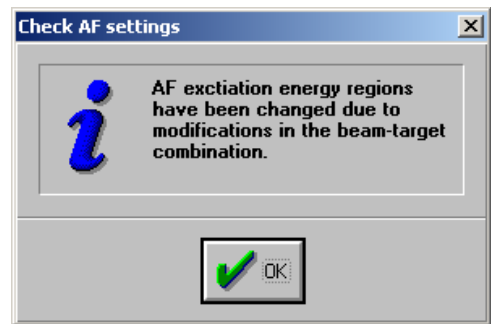


Fig.93.

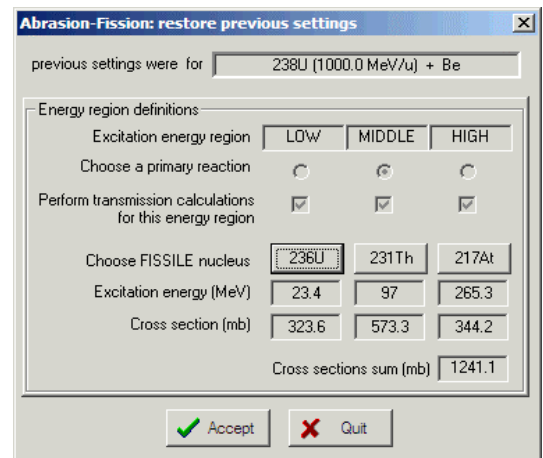


Fig.94. The “Restore previous AF settings” dialog.

### 1.5.5. Secondary reactions for Abrasion-Fission

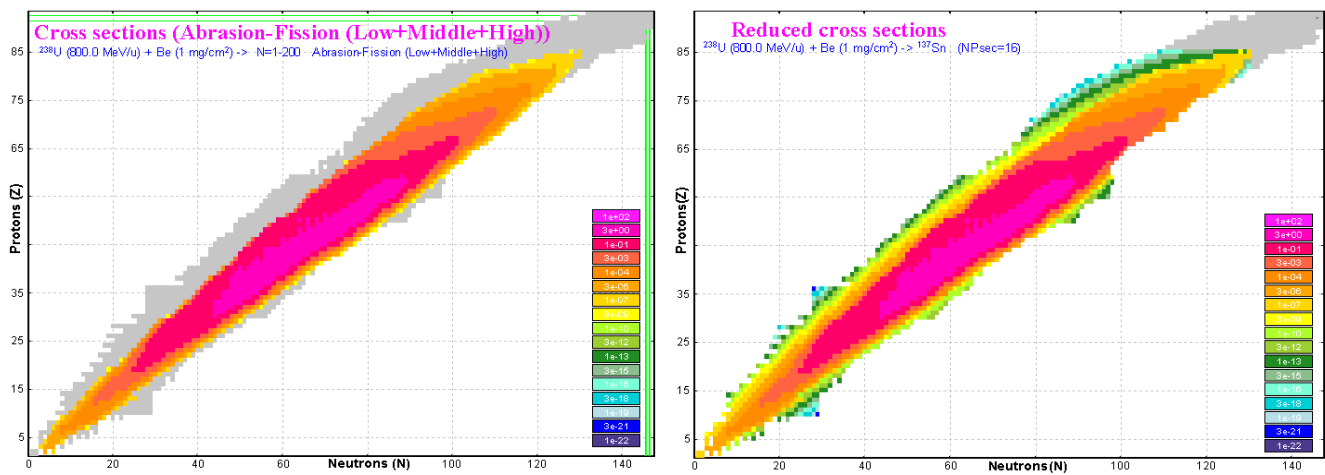
Secondary reactions are a very important component for fragments produced in fission with a low cross-section even in the case of a thin target. As it was already mentioned We recommend using the rectangle filter (bottom rectangle deltas are 30&30, top rectangle 0&0) for SR calculations and not setting the cross-section suppression coefficient very low, as you will see from the figures in this chapter.

Let's suggest that Middle EER is set as the primary reaction in the code. Then the reduced cross-section is calculated using Equation /10/, where  $\sigma_{\text{primary}}^*$  is equal to the production cross-section corresponding to the Middle EER. Total reduced cross-section is defined by the formula:

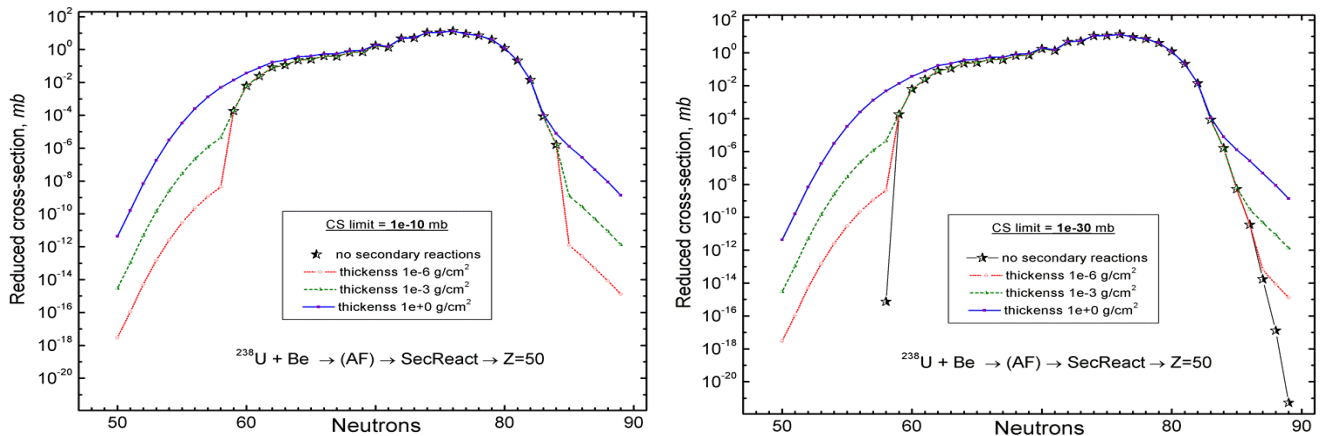
$$\sigma_{\text{total\_reduced}} = \sigma_{\text{Middle}}^* \cdot \tau_{\text{SR}} + \sigma_{\text{Low}} + \sigma_{\text{High}} \quad /12/$$

The reduced cross-section plot utility (1.4.2.1. Secondary Reactions plots: SR coefficients & reduced cross-sections) shows namely the total reduced cross-section values calculated based on Equation /12/.

Fig.95 shows in the left plot fission production cross-sections (sum of all three EER) in the reaction  $^{238}\text{U}(80\text{MeV/u})+\text{Be}$  calculated for cross-section suppression equal to  $1\text{e-}10$  mb and presents in the right plot total reduced cross-sections for the Be-target thickness equal to  $1\text{ mg/cm}^2$ .



**Fig.95.** Left plot: Fission production cross-sections (sum of all three EER) in the reaction  $^{238}\text{U}(80\text{MeV/u})+\text{Be}$  calculated for cross-section suppression equal to  $1\text{e-}10$  mb. Right plot: the same as the left plot but with SR contribution for the Be-target thickness equal to  $1\text{ mg/cm}^2$ .

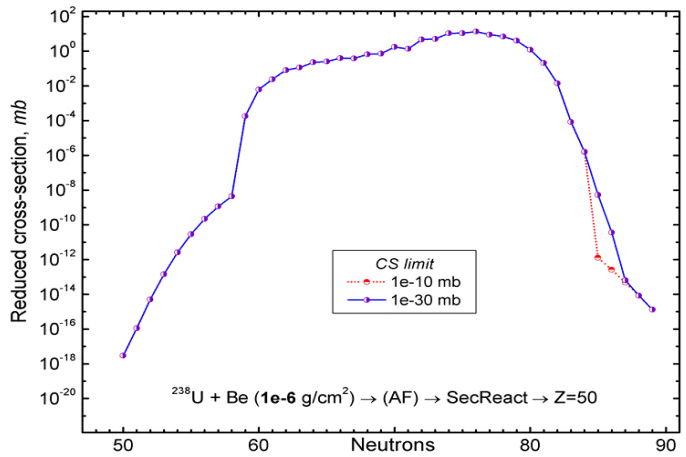


**Fig.96.** Total reduced production cross-sections of Tin fission fragments produced in the reaction  $^{238}\text{U}+\text{Be}$  as a function of the target thickness. Left plot corresponds to calculations with the cross-section suppression limit equal to  $1\text{e-}10$  mb, right plot similarly for a value  $1\text{e-}30$  mb.

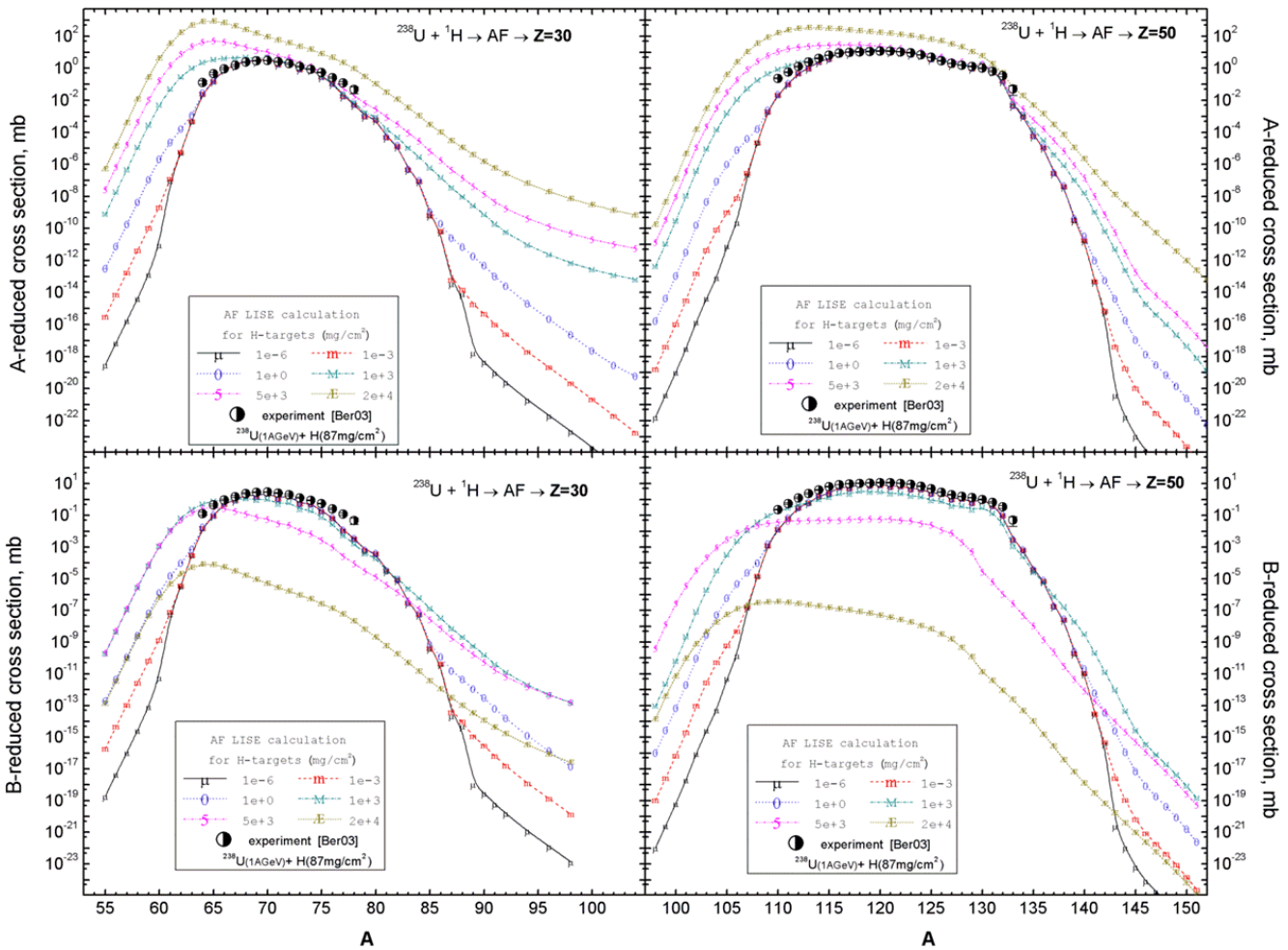
Fig.96 demonstrates how total reduced cross-sections of Tin fission fragments produced in the reaction  $^{238}\text{U}+\text{Be}$  depend on the target thickness.

Fig.97 shows total reduced production cross-sections of Tin fission fragments for two different suppression values in the case of a thin target ( $1\ \mu\text{g}/\text{cm}^2$ ). The small difference is observed just for two neutron-rich isotopes. With increasing target thickness (at least up to  $1\ \text{mg}/\text{cm}^2$ ) this discrepancy disappears.

Let's assume that we have a primary beam of  $^{238}\text{U}$  with very high energy to exclude "dead" layer of the target from calculations. Is there a limit for target thickness or, taking into account the contribution of secondary reactions, is the fragment production always continuously increasing in value? If this limit exists then where is it located?



**Fig.97.** Total reduced production cross-sections of Tin fission fragments produced in the reaction  $^{238}\text{U}+\text{Be}$  ( $1\ \mu\text{g}/\text{cm}^2$ ) as a function of the suppression limit.



**Fig.98.** A(top plots)- & B(bottom plots)- reduced (see text for details) production cross-sections of Zinc (left plots) and Tin (right plots) fission fragments produced in the reaction  $^{238}\text{U}(10\text{AGeV})+\text{p}$  as a function of the target thickness.



Fig.98 shows A- & B-reduced production cross-sections of Zinc and Tin fission fragments produced in the reaction  $^{238}\text{U}(10\text{AGeV}) + \text{p}$  as a function of the target thickness. AF EERs settings used for calculations are presented in chapter “1.5.9.5.  $^{238}\text{U}(1\text{AGeV}) + \text{p}$ ”. The A-reduced cross-section is equivalent to  $\sigma_{\text{total\_reduced}}$  from Equation /12/. The B-reduced cross-section is defined by the formula:

$$\sigma_{\text{reduced}}^B = \frac{R}{N_{\text{target}} \cdot I_{\text{beam}}}, \quad /13/$$

where  $R$  is the yield of fragment of interest after the target [1/s],  $N_{\text{target}}$  in the number of atoms in the target [1/cm<sup>2</sup>], and  $I_{\text{beam}}$  is the primary beam intensity [1/s]. The principal difference between “A” & “B” reduced cross-sections is contained in the reaction coefficient of losses, which exists in the B-reduced cross-section:  $\sigma_{\text{reduced}}^B = \sigma_{\text{reduced}}^A \cdot \mathcal{E}_{\text{reaction}}$ .

It is possible to see that the A-reduced cross-section increases with increased target thickness for Zinc isotopes as well as Tin isotopes due to secondary reactions contributions, and the largest gain is achieved for proton rich isotopes.

In the case of B-reduced cross-section it is possible to see that increasing target thickness in four times from 5 g/cm<sup>2</sup> up to 20g/cm<sup>2</sup> decreases reduced cross-sections by 3-4 orders of magnitude. It is possible to conclude that the optimal target thickness to produce the maximum rate of fragments for the reaction  $^{238}\text{U}(10\text{AGeV}) + \text{p}$  is about 1-3 g/cm<sup>2</sup>.

### ***1.5.6. Setting up LISE to calculate yield of AF products through the spectrometer***

Let’s start to acquaint ourselves with LISE settings for the Abrasion-Fission (AF) mechanism by an example. Assume we need to produce a  $^{81}\text{Zn}$  secondary beam using a primary beam of  $^{238}\text{U}^{86+}$  ions with energy 80 MeV/u at the NSCL/MSU.

#### ***1.5.6.1. Experiment settings***

Let’s assume in the beginning the simple case without charge states, without a wedge, using just one target, without secondary reactions, and with nonzero primary cross-sections. The first two steps are the same as for the case with other reaction mechanisms.

##### **1.5.6.1.1. Spectrometer choice**


Since we plan to use the A1900 fragment separator, we need to first configure LISE++ for this device. This is done as follows:

- a. Start the program LISE++
- b. Select the menu *File* → *Configuration* → *Load*
- c. Choose the file “A1900\_2005A.lcn” in the NSCL directory

##### **1.5.6.1.2. Primary beam, target, selected fragment**

- a. Set the projectile characteristics ( $^{238}\text{U}$ ,  $E=80$  MeV/u,  $Q=86+$ ) by clicking on the letter “P” of the label “Projectile” or alternatively selecting the menu *Settings* → *Projectile*.
- b. Set the desired fragment ( $^{81}\text{Zn}$ ) too if it hasn’t been done already by clicking on the “F” letter of the label “Fragment” or alternatively selecting the menu *Settings* → *Fragment*.
- c. The target (Be, 0.1 mm) can be entered directly by clicking on the “T” letter of the label “Target” or alternatively selecting the menu *Settings* → *Target*.

### 1.5.6.2. Abrasion-Fission settings

- Set the reaction mechanism (Abrasion-Fission) by clicking on the  or alternatively selecting the menu *Options* → *Production Mechanism*. After that you can see the AF frame where three fissile nuclei and their excitation energies are shown (see Fig.99).
- You need to recalculate the excitation regions parameters according to the beam and target characteristics. In order to make these changes you have to open the “Abrasion-Fission” dialog (see Fig.50) by clicking on the AF frame in the Set-up window (see Fig.100) or alternatively selecting the “Abrasion-Fission settings” button in the “Production mechanism” dialog through the menu *Options* → *Production Mechanism*.
- Make sure, that the break-up and fission de-excitation channels in the “Evaporation settings” are turned on. You can find more detailed information in the chapters about the “Abrasion-Fission” dialog, de-excitation, and fission default parameters. Now just click the multi-purpose button “*Calculate, Use ‘All’ in the code, Apply, Plot*” (see Fig.50) to calculate Abrasion-Fission settings for this beam-target combination to use in the following fragment yield calculations. It is recommended to set “Middle excitation energy region” as a primary reaction (see Fig.51). Click the “Ok” button to leave the dialog. Now you might see several changes in the Set-up window (see Fig.101).

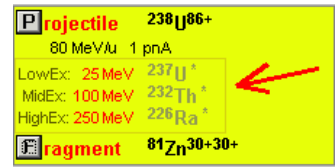


Fig.99. The Abrasion-Fission frame showing excitation regions.

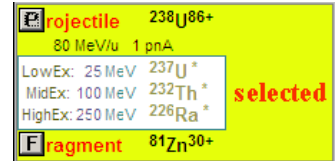
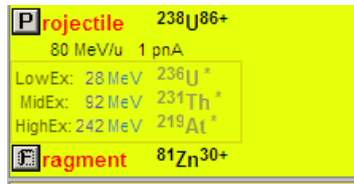





Fig.100. The Abrasion-Fission frame is selected by the mouse.

Fig.101. Parts of the Set-up window after AF settings calculations were done. Excitation energy strings color has been changed after modifications of AF settings. The initial color is red (see Fig.99).



### 1.5.6.3. Spectrometer tuning for the fragment of interest

- Set maximum possible momentum acceptance (5.07%) of the spectrometer using the “I2\_slits” block settings dialog through the Set-up window.
- Set the “Right peak” option in the “Calculate spectrometer settings using...” in the “Preferences” dialog by clicking  or selecting the menu *Options* → *Preferences*.

Calculate the fragment separator settings by clicking on  or selecting the menu *Calculations* → *Calculate the spectrometer for setting ion*. The code calculates spectrometer settings based on fragment kinematics of the primary reaction (AF-middle) you set. Therefore the code initially has to calculate AF-middle final fragment and excited fragment production cross-sections, which should be used in kinematics calculations. Kinematics of fission fragment calculations and spectrometer tuning are based on the same procedures as in the case of Coulomb fission. After the code runs, it will set the spectrometer and you can see in the Set-up window the number of AF-middle cross-sections . These cross-sections will be kept in the memory as long as the projectile & target combination, fission properties, and de-excitation properties have been not changed by the user.

### 1.5.6.4. Yield calculation

Calculate the yield of  $^{81}\text{Zn}$  for these settings by double right clicking on the corresponding nucleus in the table of nuclei. The code calculates consecutively the yields for all of three excitation energy regions (EER). Each EER represents a separate reaction mechanism in the code. This means the code first calculates rates for Middle EER, then changes the primary reaction to Low EER, calculates rates for this region, then High EER and finally comes back to Middle EER. Each EER has its own cross-section matrices, because the code checks cross-section matrices existence before yield calculations. If the matrices are absent for this reaction mechanism or the projectile and target combination or fission and de-excitation properties have been changed then the code calculates fission fragment production cross-sections for these new projectile-target-fission settings. The number of nonzero cross-sections for each EER kept in the memory is shown in the Set-up window (see in Fig.102).

<b>P</b> projectile	<b>238U92+</b>	AF lo
80 MeV/u	1 pnA	563
LowEx: 28 MeV	<b>236U+</b>	AF mi
MidEx: 92 MeV	<b>231Th+</b>	786
HighEx: 242 MeV	<b>219At+</b>	AF hi
		826
<b>F</b> ragment	<b>81Zn30+</b>	

Fig.102. The Abrasion-Fission frame showing excitation regions (EER) and the number of non-zero cross-sections for each EER.

Fig.103 shows statistics of  $^{81}\text{Zn}$  fragment production. Under the production line in the new version you can see two new lines: reaction mechanism name and sum of reactions. It is visible, that the  $^{81}\text{Zn}$  fragments have been produced in Middle and Low EER reactions. The  $^{81}\text{Zn}$  production cross-section for High EER is equal to zero.

statistics 81Zn			
81Zn		Beta- decay (Z=30, N=51)	
Q1 (D1)		30	30
Q2 (D2)		30	30
Q3 (D3)		30	30
Q4 (D4)		30	30
Production Rate	(pps)	9.77e-6	1.71e-4
Reaction		AF_mid	AF_low
Sum of reactions	(pps)	1.8e-4	1.8e-4
CS in the target	(mb)	4.39e-8	8.01e-7
Total transmission	(%)	2.879	2.758
Target	(%)	99.66	99.66

Fig.103. The statistics window of  $^{81}\text{Zn}$  fragment production.

The “Sum of reactions” result value has been included just in the new version and it is equal to the sum of the “Sum of charge states” values. The “Sum of charge states” values are the sum of all charge states produced for one fragment in ONE reaction.

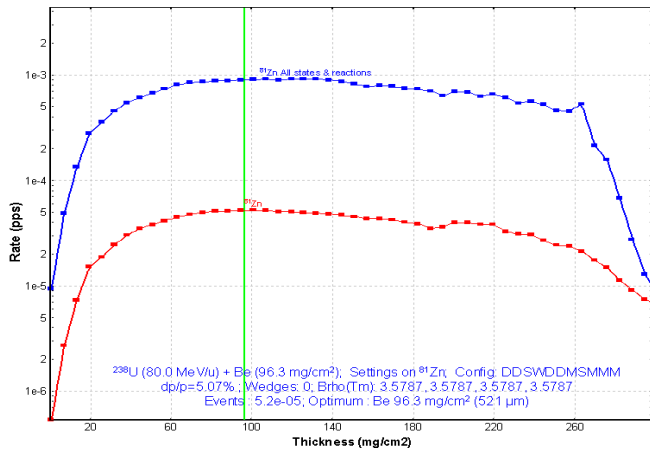
In total we have received a  $^{81}\text{Zn}$  fragment production rate equal to  $1.8\text{e-}4$  pps for 0.1 mm Be-target at the focal plane of the spectrometer.

### 1.5.6.5. Optimum target

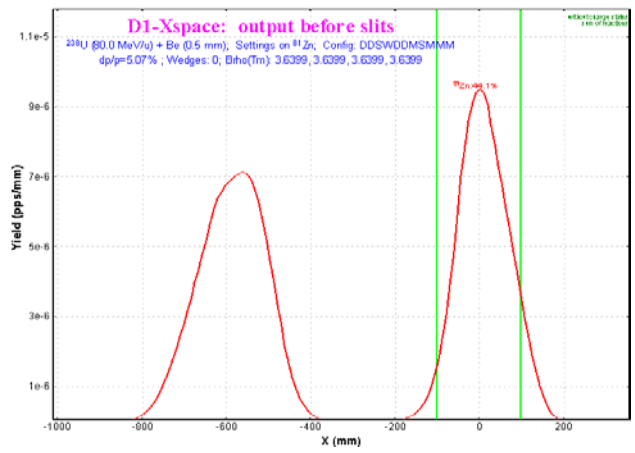
Let’s optimize the target thickness to produce the maximum production rate of  $^{81}\text{Zn}$  fragments by selecting the menu “Calculations → Optimum target”. Results of calculations are shown in Fig.104. The target thickness corresponding to maximum production rate (total:  $9.32\text{e-}4$ , Middle ERR:  $5.2\text{e-}5$ ) is equal to 0.52 mm.

Fig.105 shows the spatial distribution of  $^{81}\text{Zn}$  fission fragments in the dispersive focal plane after the first dipole. You can see the selection of the “Right” peak (corresponding to higher energy) of the fragment momentum distribution by the spectrometer.

**Note:** It is recommended to set such EER as the primary reaction that which contributes most to the fragment production rate. In the case of the reaction  $^{238}\text{U}(80\text{MeV/u}) + \text{Be} \rightarrow (\text{AF}) \rightarrow ^{81}\text{Zn}$  it is the Low EER (see Fig.103). In this case the spectrometer will be set following the kinematics of this reaction mechanism, and the secondary reaction coefficient is applied to the reaction mechanism with most intense production, which gives the most correct estimation of the secondary reactions’ contribution.



**Fig.104.**  $^{81}\text{Zn}$  fission fragment production rate in the reaction  $^{238}\text{U}(80\text{MeV})+\text{Be}$  as a function of the target thickness.



**Fig.105.** Spatial distribution of  $^{81}\text{Zn}$  fission fragments in the dispersive focal plane after the first dipole.

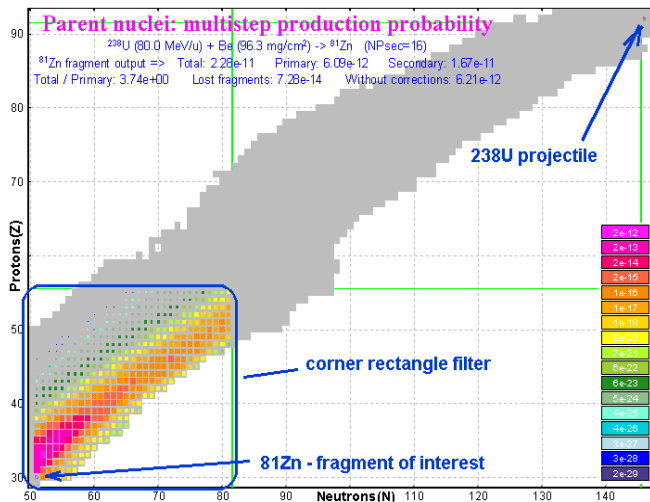
### 1.5.6.6. Secondary reactions

Let's turn on the secondary reactions contribution in the "SR" dialog by selecting the menu "Options → Secondary reaction in target". Set the Corner rectangle filter for all three procedures in the dialog. Use parameters  $\Delta N=30$  and  $\Delta Z=25$  for the bottom rectangle and 0 & 0 for the top rectangle of the corner filter in the case of fission (see 1.4.3.1.3. Application of acceleration filters). The SR contribution gives gain about four times even for this not so high energy of the primary beam (Fig.106).

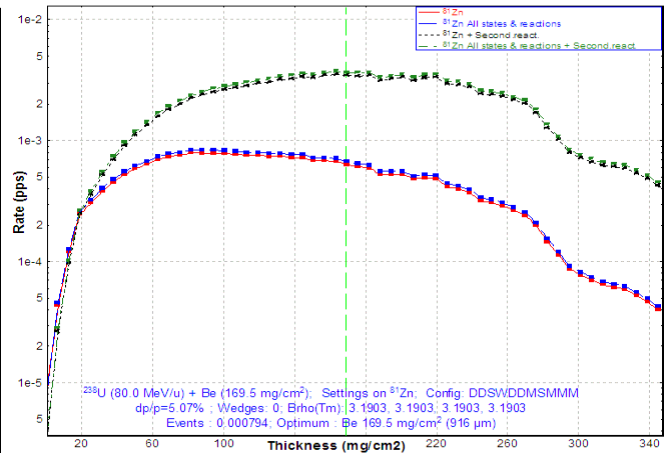
Statistics 81Zn			
81Zn		Beta- decay (2=30, N=51)	
Q1 (D1)		30	30
Q2 (D2)		30	30
Q3 (D3)		30	30
Q4 (D4)		30	30
Production Rate (pps)		5.36e-5	3.5e-3
Reaction		AF mid	AF low
Sum of reactions (pps)		3.55e-3	3.55e-3
CS in the target (mb)		4.39e-8	8.01e-7
Total transmission (%)		3.032	10.87
Target (%)		98.25	3.78e+2
X space transmission (%)		100	100
Y space transmission (%)		100	100
Unreacted in mater. (%)		98.25	98.25
Unstopped in mater. (%)		100	100
Secondary Reactions (coef)		1	3.85

**Fig.106.** The statistics window of  $^{81}\text{Zn}$  fragment production with taking into account the SR contribution.

Fig.107 shows the multi-step production probabilities to produce  $^{81}\text{Zn}$  from the primary reaction  $^{238}\text{U}(80\text{MeV/u})+\text{Be}(96\text{mg/cm}^2)\rightarrow\text{AF}$ . The corner rectangle filter is shown in the figure.



**Fig.107.** Multi-step production probabilities to produce  $^{81}\text{Zn}$  for the primary reaction  $^{238}\text{U}(80\text{MeV/u})+\text{Be}(96\text{mg/cm}^2)\rightarrow\text{AF}$ .



**Fig.108.**  $^{81}\text{Zn}$  fission fragment production rate for the reaction  $^{238}\text{U}(80\text{MeV})+\text{Be}$  as a function of the target thickness taking into account the SR contribution. The Low EER was set as the primary reaction to calculate  $^{81}\text{Zn}$  fission fragment production.

Fig.108 shows the optimum target thickness plot where the SR contribution was taken into account in the calculations. In the case of using SR contributions the target becomes significantly thicker (0.91 mm).

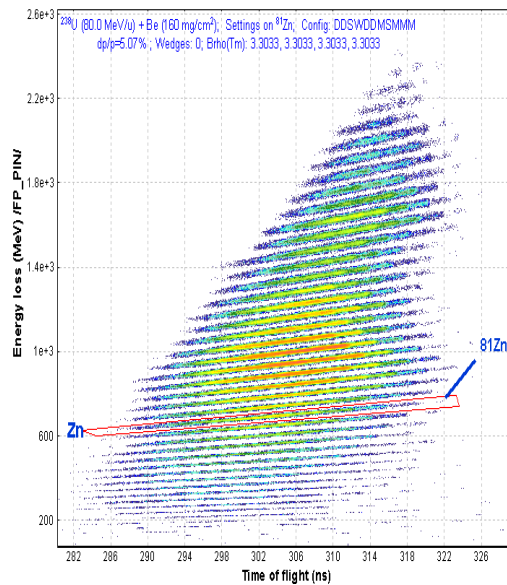
**Note:** It is necessary to notice that yield calculations become less precise when the amount of stopped fragments in the target exceeds 50 percent due to the analytical LISE fission approach. For example in the reaction  $^{238}\text{U}(80\text{A MeV})+\text{Be}$  this happens at thickness  $330\text{ mg/cm}^2$  (1.8 mm).

### 1.5.6.7. Cleaning

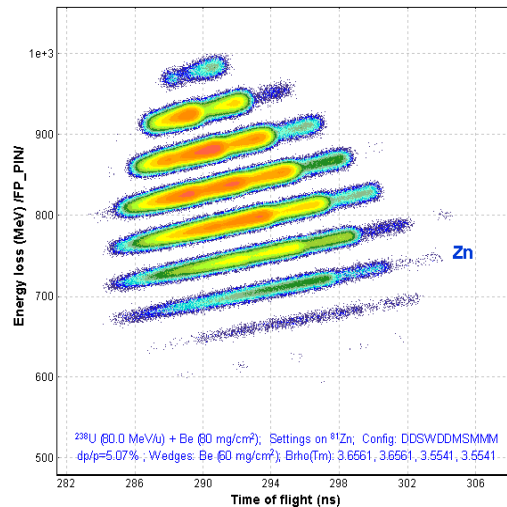
We need to think about purification of the secondary beam from background fragment production, because in a single run there are at once more than 1700 fragments (from different EERs) produced with a total yield of  $3.7\text{e}4$  pps. This is about  $10^7$  times more than the intensity of the  $^{81}\text{Zn}$  secondary beam (see Fig.109).

Let's set a wedge-profile achromatic Be-degrader ( $60\text{ mg/cm}^2$ ) in the intermediate dispersive focal plane I2 (*I2\_wedge*), while decreasing the target thickness down to  $80\text{ mg/cm}^2$  and setting the final slits *FP\_slits* to  $\pm 4\text{ mm}$ . Using the wedge we could decrease the total yield down to 630 pps (see Fig.110).

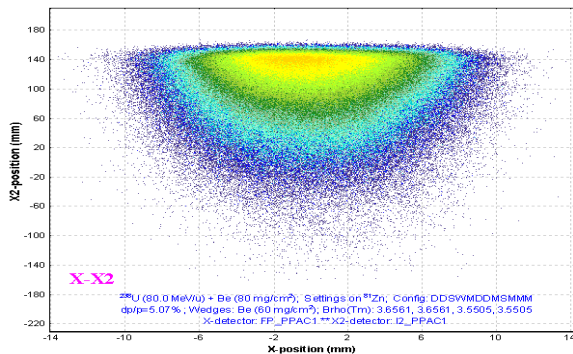
If we slightly increase the magnetic rigidity, it is possible to decrease background rates further without losing intensity of the fragment of interest, because the main background contribution is coming from low-energy intense isotopes (Fig.111 and Fig.112).



**Fig.109.** Two dimensional identification plot for fission fragments obtained in  $80\text{ MeV/u}$   $^{238}\text{U}+\text{Be}(160\text{mg/cm}^2)$  at the magnetic rigidity  $3.303\text{ Tm}$ . These statistics correspond to 2 seconds of acquisition. The intensity of the primary beam is equal to  $1\text{ pna}$ .



**Fig.110.** Two dimensional identification plot for fission fragments obtained in  $80\text{ MeV/u}$   $^{238}\text{U}+\text{Be}(80\text{mg/cm}^2)$  using an achromatic Be-wedge ( $60\text{mg/cm}^2$ ) in the dispersive intermediate focal plane I2. This statistics corresponds to 4.5 hours of acquisition.



**Fig.111.** 2D-plot of fission fragments. Abscissa axis: horizontal coordinate from PPAC in the final focal plane (*FP\_PPAC1*); ordinate axis: horizontal coordinate from PPAC in the intermediate dispersive focal plane (*I2\_PPAC1*).



**Fig.112.** Horizontal spatial distribution plot of fission fragments in the reaction  $^{238}\text{U}(80\text{MeV/u})+\text{Be}(80\text{mg/cm}^2)$  using an achromatic Be-wedge ( $60\text{mg/cm}^2$ ) in the intermediate dispersive focal plane (the dispersion is negative).

Let's decrease the momentum acceptance down to 1% and slightly increase the magnetic rigidity by 0.5% to get a 2D-plot with unambiguous identification in Fig.113.

Modifying wedge and target thicknesses as well as slits sizes at Image2 and the focal plane (FP) it is possible to more easily distinguish the secondary beam intensity and the better ratio between the fragment of interest and background.

### 1.5.6.8. Charge states



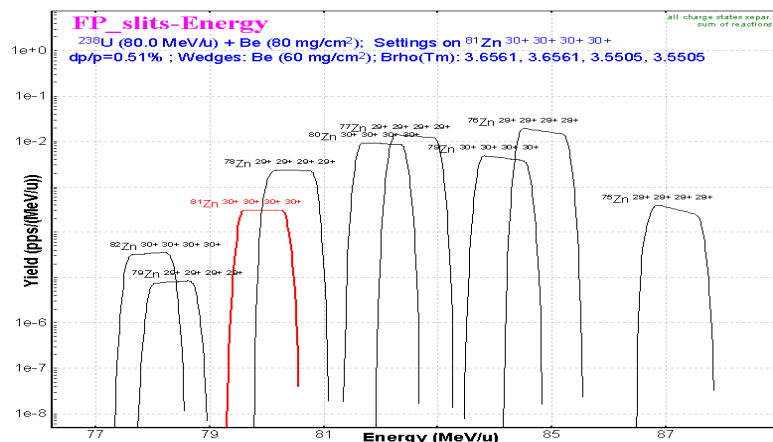
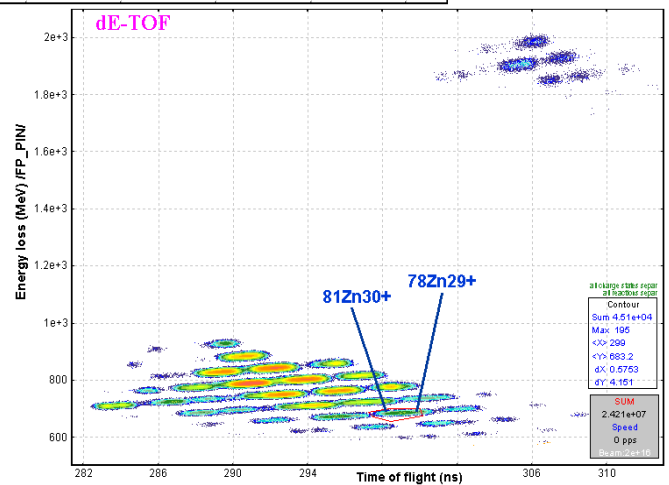
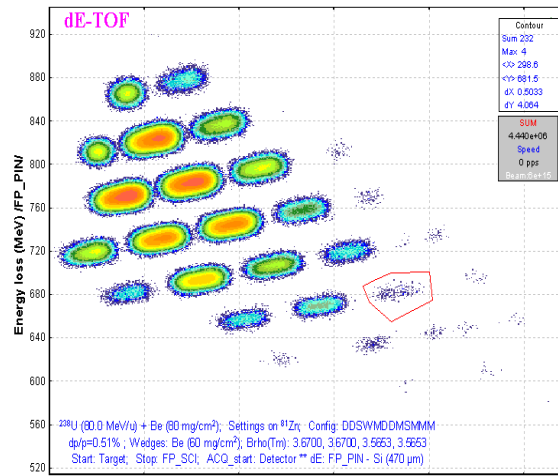
For the previous calculations, we guessed that all the fragments were completely charge stripped. But in reality the problem of charge states is important at this energy (80MeV/u) of a primary beam. In the case of the transmission calculation for charge states, we recommend limiting calculations to only a small region of isotopes using , where the fragments are expected; otherwise, in the case of transmission calculation of all isotopes , the calculation can take more than one hour. Let's turn on the charge state option in the "Preferences" dialog. Let's assume the spectrometer is tuned to fully stripped ions ( $^{81}\text{Zr}^{30+}$ ).

Fig.114 shows a two-dimensional *dE-ToF* identification plot for fission fragments obtained in the reaction  $^{238}\text{U}(80\text{MeV/u}) + \text{Be}(80\text{mg/cm}^2)$  using a Be-wedge ( $60\text{ mg/cm}^2$ ). Charge states and Secondary reactions options are turned on. If compared with Fig.113 you can see in the upper right corner the new group of heavy ions corresponding to elements with  $Z=47-52$ . The charge state of these fragments has been

changed by the wedge material from  $Q_{1,2} = Z-2$  to  $Q_{3,4} = Z-3$  or from  $Q_{1,2} = Z-1$  to  $Q_{3,4} = Z-2$ . Using this 2D-plot it is impossible now already to make an unambiguous identification because as you can see the  $^{81}\text{Zr}^{30+}$  and  $^{78}\text{Zn}^{29+}$  ions positions in the plot are overlapping (see also Fig.115). It is possible to make off-line separation using a third measured value, the total kinetic energy of the fragment (*TKE*).



### 1.5.6.9. Go to more exotic case of $^{83}\text{Zn}$

Let's set the  $^{83}\text{Zn}^{30+}$  ion as the setting fragment. The peculiarity of this fragment is the fact that the primary fission production cross-section is equal to zero<sup>♥</sup> for the fission fragment cross-section limit set to  $1\text{e-}10$  mb.

Fig.116 shows the optimum target thickness plot for  $^{83}\text{Zr}$  where the SR contribution and charge states distribution were taken into account in the calculations. No primary yield for  $^{83}\text{Zn}$  is shown in the plot because the primary fission fragment production cross-section is equal to zero (compare this with the optimum target thickness plot for  $^{81}\text{Zn}$  in Fig.108).

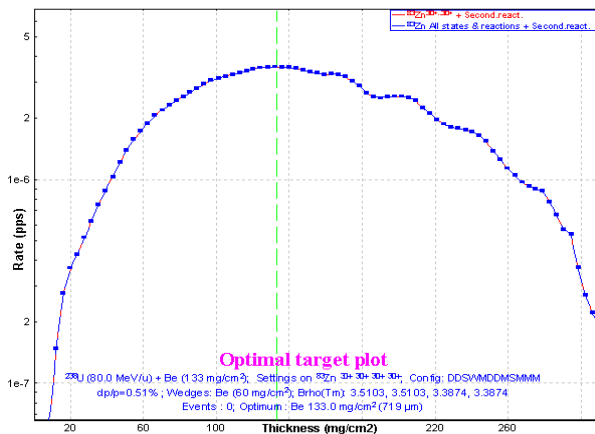


Fig.116.  $^{83}\text{Zn}$  fission fragment production rate as a function of target thickness.  $^{83}\text{Zn}$  primary fission production cross-section is equal to zero.

Statistics 83Zn	
83Zn Beta- decay (Z=30, N=53)	
Q1 (D1)	30
Q2 (D2)	30
Q3 (D3)	30
Q4 (D4)	30
Zero cross section has been changed due to secondary reactions!	
Production Rate (pps)	1.32e-5
Sum of charge states (pps)	1.32e-5
Reaction	AF_low
Sum of reactions (pps)	1.32e-5
CS in the target (mb)	1.77e-7
Total transmission (%)	0.135

Fig.117. The statistics window of  $^{83}\text{Zn}$  fragment production with the SR contribution.

The  $^{83}\text{Zn}$  production rate for a half-percent momentum acceptance is  $1.3\text{e-}5$  pps, suggesting that the reduced production cross-section is equal to  $1.8\text{e-}7$  mb (see Fig.117).

Fig.118 demonstrates production and identification of  $^{83}\text{Zn}$  fragment. See inserts in the plot for details.

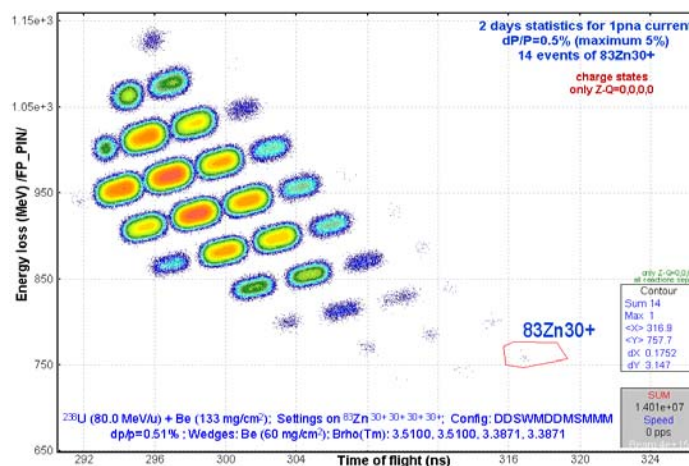


Fig.118. dE-ToF identification plot. See inserts in the plot for details.

### 1.5.6.10. Examples

All the previous examples of calculations are available as LISE files on the LISE-web site using the address: [http://groups.nsl.msu.edu/lise/7\\_5/examples/](http://groups.nsl.msu.edu/lise/7_5/examples/).

Calculation step	Corresponding figure	file
Target 0.1 mm	Fig.103	fission_example
Target 0.52 mm	Fig.104	fission_example_052mm
SR on	Fig.106	fission_example_SR
Calculation of All fragments	Fig.109	fission_example_SR_All
Wedge on	Fig.110	fission_example_wedge
Small acceptance	Fig.113	fission_example_wedge2
Charge states on	Fig.114	fission_example_wedge_charge_81Zn
83Zn – setting of fragment	Fig.116	fission_example_wedge_charge_83Zn

<sup>♥</sup> If we decrease the cross-section limit to  $1\text{e-}20$  mb we can get a  $^{83}\text{Zn}$  cross-section equal to  $1.3\text{e-}11$  mb.

### 1.5.7. LISE's options modifications connected with the AF mechanism

#### 1.5.7.1. New transmission parameter "Sum of reactions"

Abrasion-Fission is an especial case, because the products of the three excitation energy regions are all at once separated by the spectrometer. Each EER represents an independent reaction. But the user needs to receive a final summary answer. Therefore the new parameter "Sum of reactions" has been incorporated in the list of parameters.

Fig.119 shows statistics for  $^{132}\text{Sn}$  ions transmitted through two-dipoles of the system. As you can see there are 6 charge states for each EER fragment. The "Sum of reactions" parameter represents the sum of all charge states for all reaction mechanisms. The "Sum of charge states" parameter represents the sum of charge states for just ONE reaction mechanism.

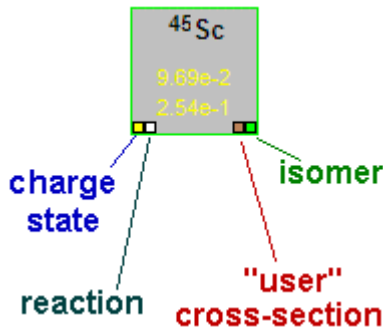


Fig.120. Isotope cell flags.

In the case of transmission calculated for the fragment produced in a reaction which is not set as primary, then the program draws a white small square in the left bottom corner of an isotope cell in the table of nuclides (see Fig.120). Information is given in the figure also by other flags, which can be displayed for certain isotopes.

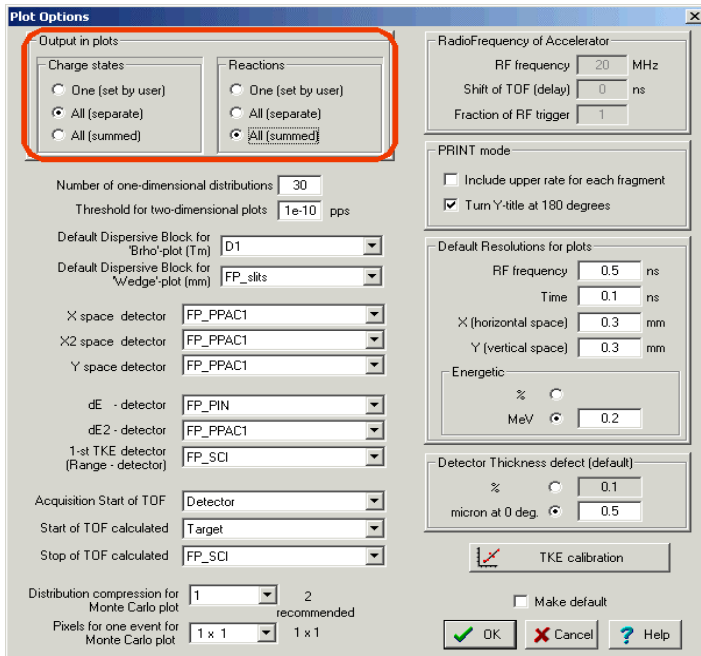


Fig.121. The "Plot options" dialog.

Beta- decay (Z=50, N=82)		132Sn	
O1 (D1)			
O2 (D2)			
Production Rate (pps)	1.19e-4	1.19e-4	1.19e-4
Sum of Charge states (pps)	5.14e-3	5.14e-3	5.14e-3
Sum of Reactions (pps)	6.27e+0	6.27e+0	6.27e+0
CS in the target (nb)	6.61e-6	6.61e-6	6.61e-6
Total transmission (%)	2.002	10.433	20.554
Target (%)	5.28	27.5	54.19
X space transmission (%)	100	100	100
Y space transmission (%)	100	100	100
Unreacted in mater. (%)	99.71	99.71	99.71
Q (Charge) ratio (%)	5.29	27.58	54.35
Unscattered in mater. (%)	100	100	100
D1 (%)	38.03	38.03	38.03
X angular transmission (%)	79.91	79.91	79.91
Y angular transmission (%)	47.59	47.59	47.59

Fig.119. Statistics window for  $^{132}\text{Sn}$  ions transmission. File [http://groups.nsl.msu.edu/lise/7\\_5/examples/new\\_parameter.lpp](http://groups.nsl.msu.edu/lise/7_5/examples/new_parameter.lpp)



Sometimes we need to see the dynamics of spatial or energy distributions just for one ion produced by the primary set reaction, but sometimes we are interested just in the sum distribution of all charge states and all reactions at the end of the spectrometer. For this purpose in the “Plot options” dialog, the possibility to define the mode for drawing the charge states and reaction mechanisms has been implemented.

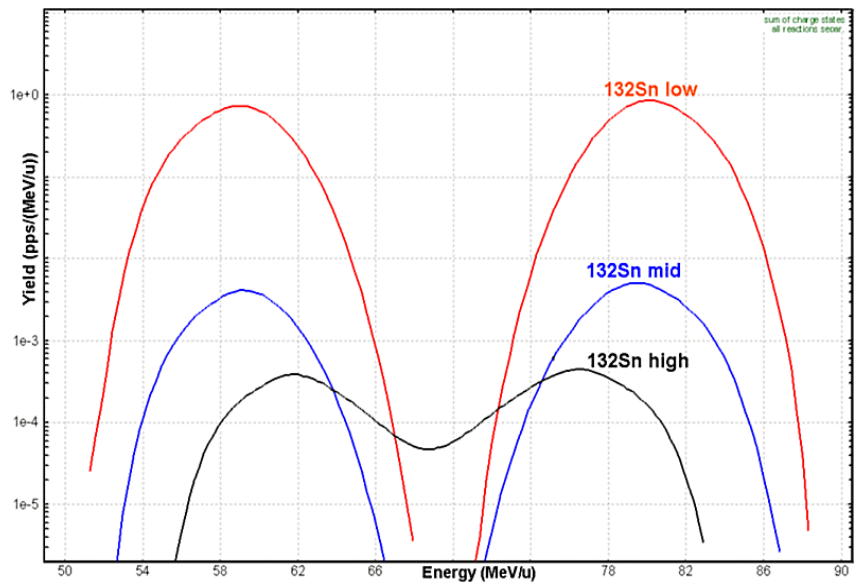
Fig.121 demonstrates the “Plot options” dialog where the red rectangle shows methods for plotting distributions from charge state and reaction settings. There are three modes for charge states as well as for reaction mechanism: One (set by user), All(separate), All (summed). This means there are 9 possible combinations, which are shown in Fig.124. Fig.122 shows energy distributions of  $^{132}\text{Sn}$  ions for the same experimental conditions as Fig.124 in the mode “Charge states: All(Summed) and Reactions: All(separate)”.

Some modifications connected with incorporation of the new parameter were done also to the “Transmission statistics” dialog (see Fig.123).

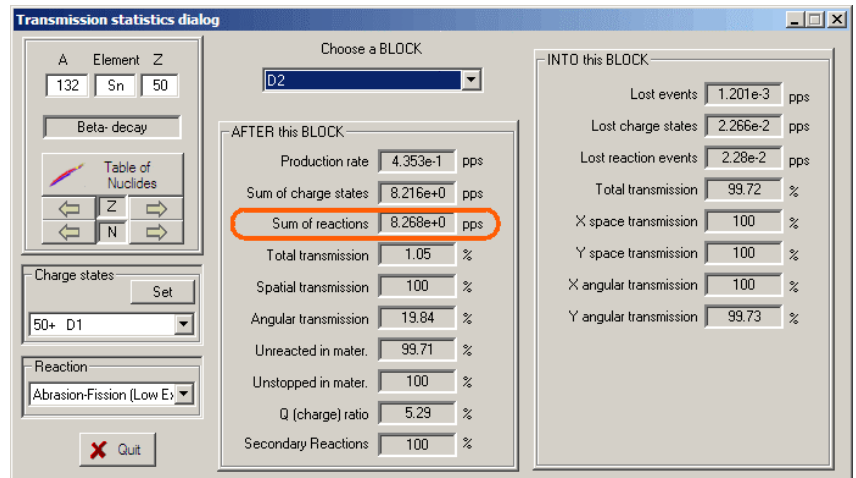
**NOTE:** The “All (summed)” mode cannot be applied for Debug distributions, Transmission characteristics plots, and 2D-plots. If distribution’s plot mode is set in the dialog as “All (summed)” then the code will use the “All (separate)” mode plot to draw the distributions.

**NOTE:** The envelope plot is created only in the “One (set by user)” mode.

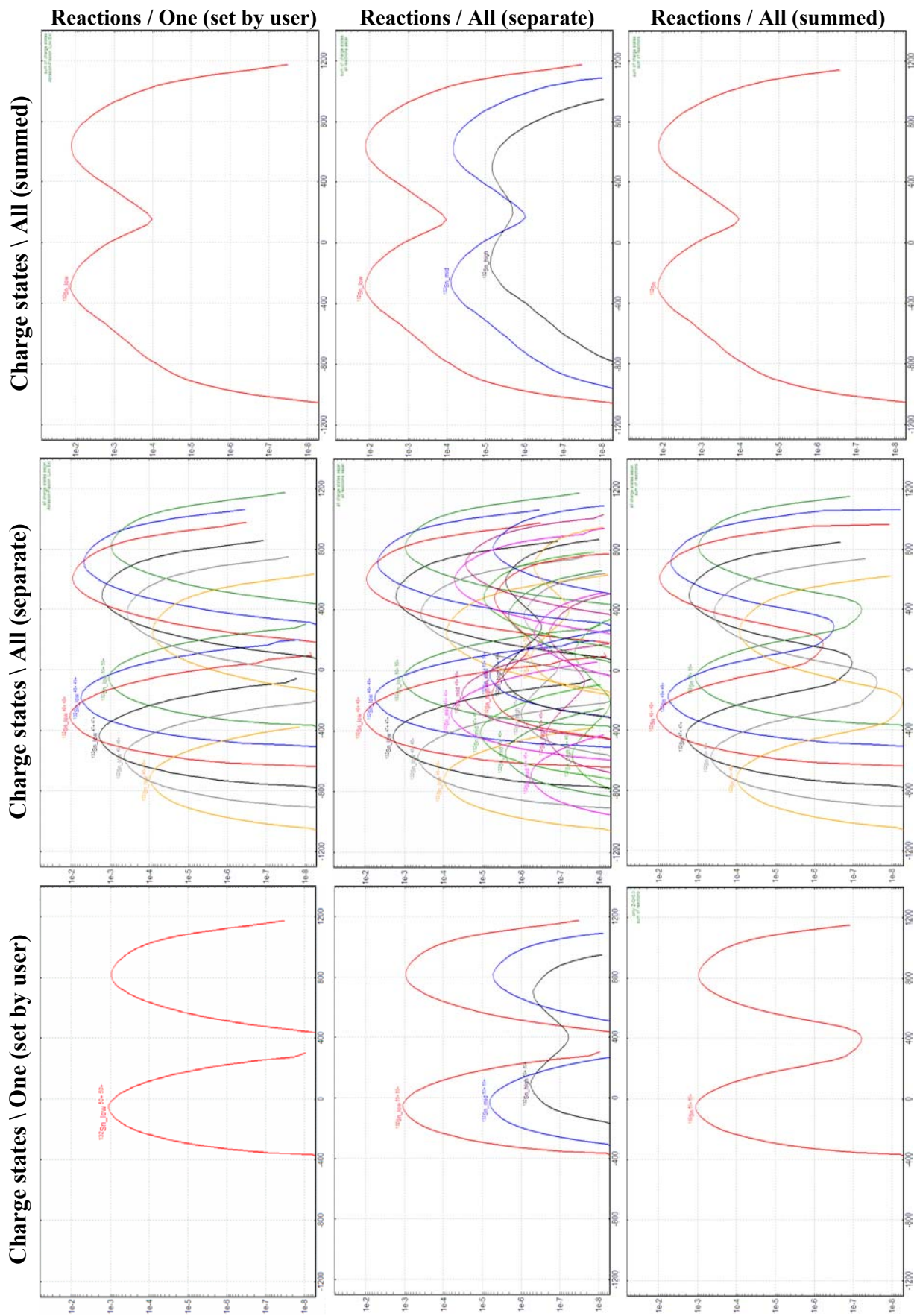
**NOTE:** The new version of the code does not support calculations done in the old-version code. The code asks the user for permission to recalculate. Also, the old-version code does not support the new format due to the new parameter “Sum of reactions”. Please pay attention.



**Fig.122.**  $^{132}\text{Sn}$  fragment energy distribution after the second dipole. Distributions are shown in the mode “Charge states: All(Summed) & Reactions: All(separate)”.



**Fig.123.** The “Transmission statistics” dialog.



**Fig.124.** Horizontal spatial distributions of  $^{132}\text{Sn}$  ions after the second dipole. File [http://groups.ncsl.msu.edu/lise/7\\_5/examples/new\\_parameter.lpp](http://groups.ncsl.msu.edu/lise/7_5/examples/new_parameter.lpp)

### 1.5.7.2. User cross-section file

As for other reactions the LISE++ code can support user cross-sections which can be loaded through the “Cross-section file” dialog (menu “Options”), but **it is necessary to remember** that an experimental cross-section value is the sum of all possible fissile nuclei.

**Important:** This means that you have to turn off two EERs from calculations and leave just one EER! It is better to use the Low EER if you are working in a neutron rich region (see Fig.125), or the High EER in the proton rich case. If you do not turn off the other two EERs as a result you will get the final production cross-section equal to the sum of an user and two EERs cross-section values.

Even when you use the user cross-section file the code calculates cross-sections which should be used for kinematics calculations to find an parent excited fragment. Also calculated cross-sections will be used to calculate the secondary reactions contribution from fragments whose cross-sections are absent in the user cross-section file.

**Note:** Do not forget that the new format of the cross-section file requires the reaction field: information about production reaction is keeping in file (for details see chapter “1.9.1. User cross-section file”).

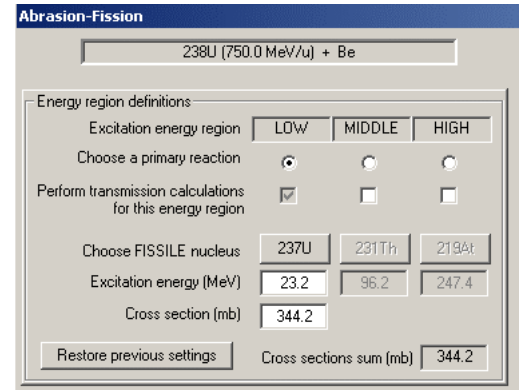


Fig.125. The fragment of the AF dialog in the case of work in the neutron rich region and using cross-section values from the file.

### 1.5.7.3. Transmission result file

Two new columns have been incorporated into the result transmission file due to creation of the Abrasion-Fission reaction mechanism. The first new column shows to what reaction this calculation result belongs (see frames “A” in Fig.126). The second new column shows the secondary reaction coefficient. It is necessary to note that the total transmission coefficient in the result file is different from the statistics window results due to a reduction by the secondary reaction coefficients to avoid values exceeding 100%.

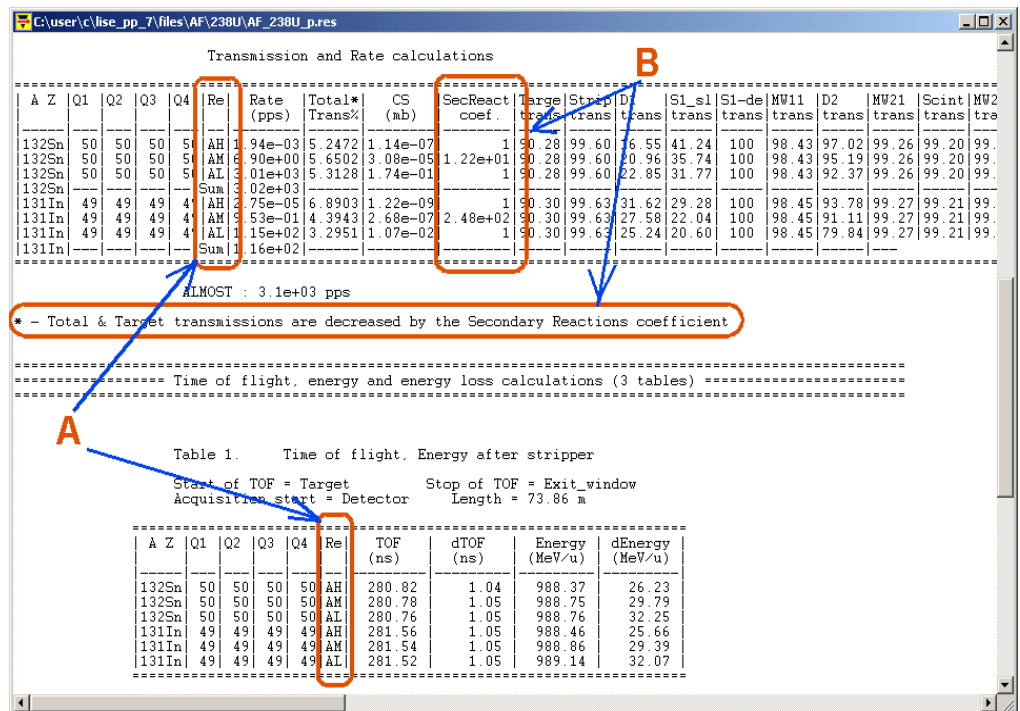
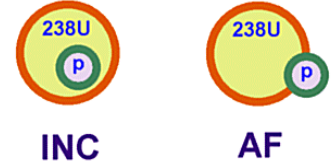


Fig.126. The fragment of the transmission result file listing.

### 1.5.8. INC fission

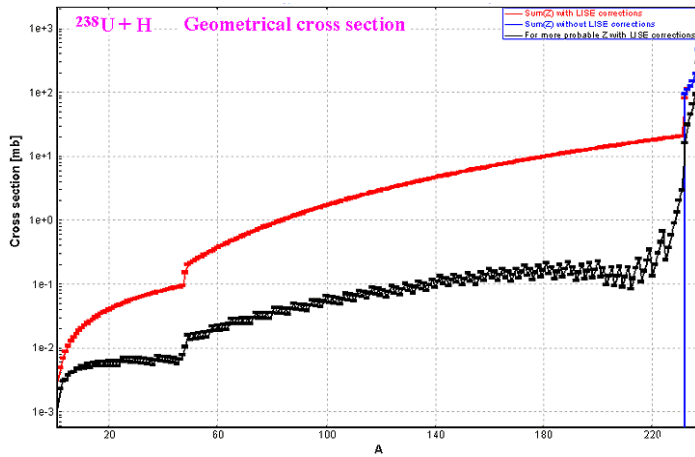
The application of the Abrasion-Ablation model to calculate EERs for induced fission of relativistic heavy projectiles by a light target requires an especial analysis. The use of AA is correct in the case of large impact parameters, but in the case when, geometrically speaking, the light target is completely overlapped by the incident projectile (see Fig.127), we assume another reaction mechanism, INC. The excitation energy of a fissile nucleus (or an excited prefragment in the case of evaporation) is higher in the case of INC, compared with Abrasion.



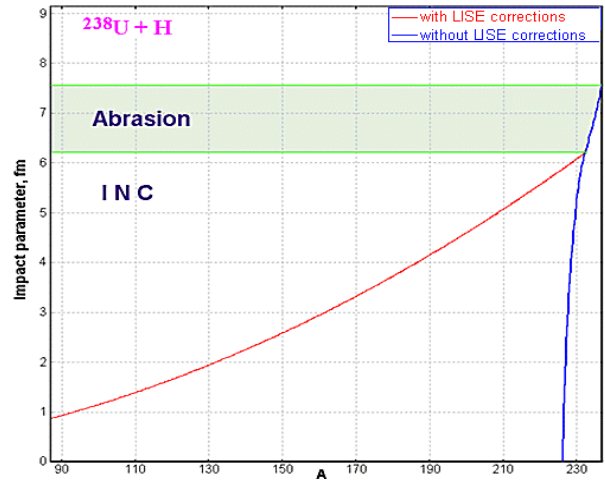
**Fig.127.** Schematic representation of INC and Abrasion from the impact parameter.

Special corrections were implemented for the geometrical AA model in the code to avoid a sharp fall in cross-sections (see Fig.128) and also to keep the sum of partial abrasion cross-sections equal to the geometrical cross-section:

$$\sigma_{geom} = \sum_{A=1}^{A_{proj}-1} \sigma_{abrasion}^{corrected}(A). \quad /14/$$



**Fig.128.** Prefragment production cross-sections as the result of abrasion of a  $^{238}\text{U}$  projectile by a proton target as a function of the prefragment mass. The blue(red) line shows LISE calculations without(with) LISE geometrical corrections. The black line shows the production cross-section of the most probable isotope using LISE geometrical corrections.



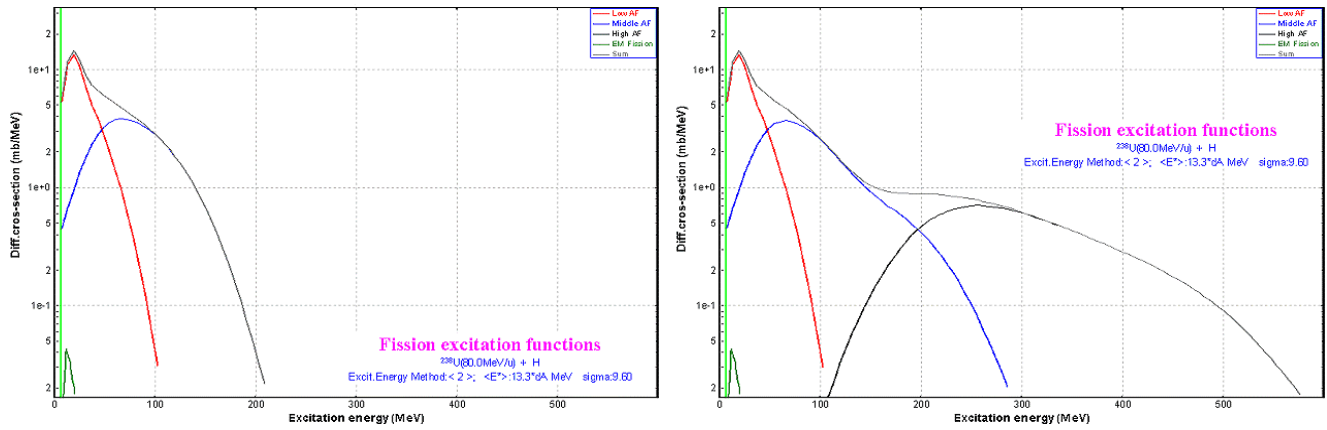
**Fig.129.** Correlation of the prefragment mass and the impact parameter in the reaction  $^{238}\text{U}+p$ . The blue(red) line shows LISE calculations without(with) LISE geometrical cross-sections.

We shall show in this chapter that it is possible to use the Abrasion-Fission model, with slight corrections, for light targets as well, assuming in this case that there is a combination of two processes: Abrasion (non-corrected) and INC (see Fig.129):

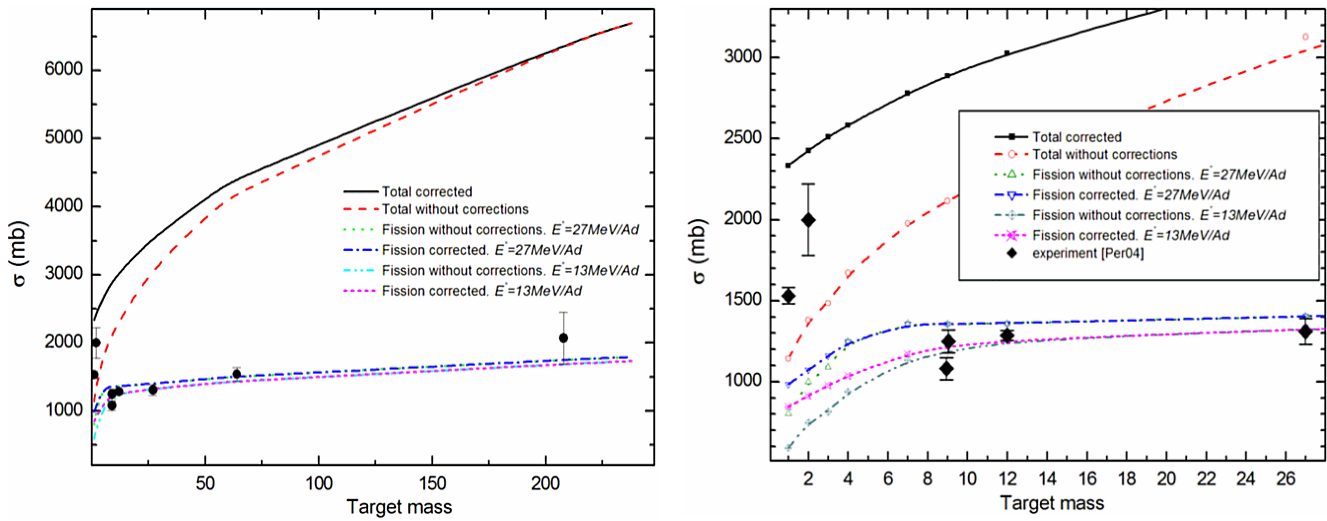
$$\sigma_{geom} = \sum_{A=1}^{A_{proj}-1} \sigma_{abrasion}^{non-corrected}(A) + \sigma_{INC} \quad /15/$$

Fig.130 shows how the LISE geometrical corrections are mirrored in the fission excitation function. The geometrical corrections considerably increase the high energy excitation contribution in fission. However, even these could not predict experimental fission cross-sections with light targets (Fig.131), which is probably explained by the following reasons:

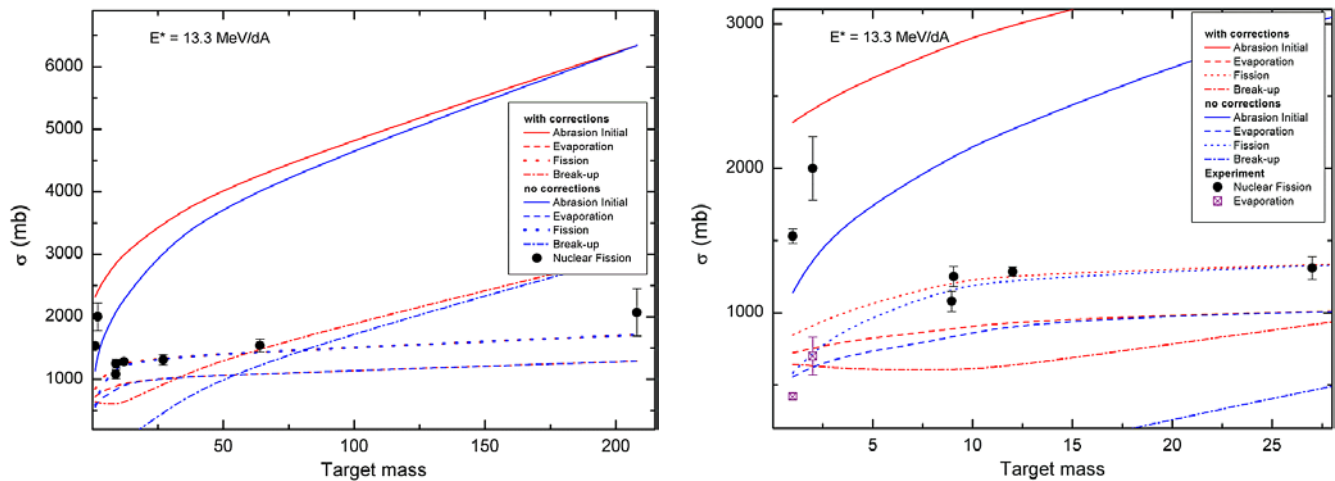
- Prefragments with the same mass are more excited in the INC case compared with Abrasion (corrected);
- AA (corrected) and INC distributions of prefragment production cross-sections have different shapes.



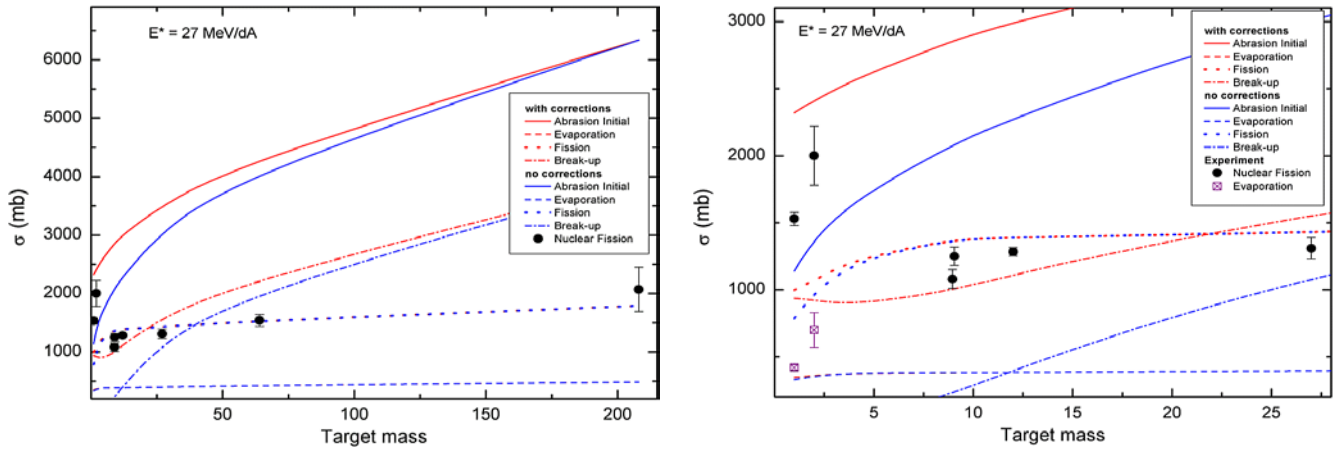
**Fig.130.** Left (Right) plot: fission excitation function calculated for the reaction  $^{238}\text{U}(1\text{AGeV}) + p$  without (with) LISE++ geometrical corrections.



**Fig.131.** Calculated total abrasion and summed abrasion-fission (with and without geometrical corrections for different excitation energies per abraded nucleon) cross-sections and experimental fission cross-sections (without EM component) as a function of the target mass for the projectile  $^{238}\text{U}(1\text{AGeV})$ . The right plot is the same as the left plot but with another abscissa axis scale to detail the light target region. Experimental data are taken from the works [Arm96,Rub96,Per04]. It is possible to see large disagreement between AF calculations and experimental data for proton and deuterium targets on the right plot that can be explained by the involvement of the other reaction mechanism (INC).



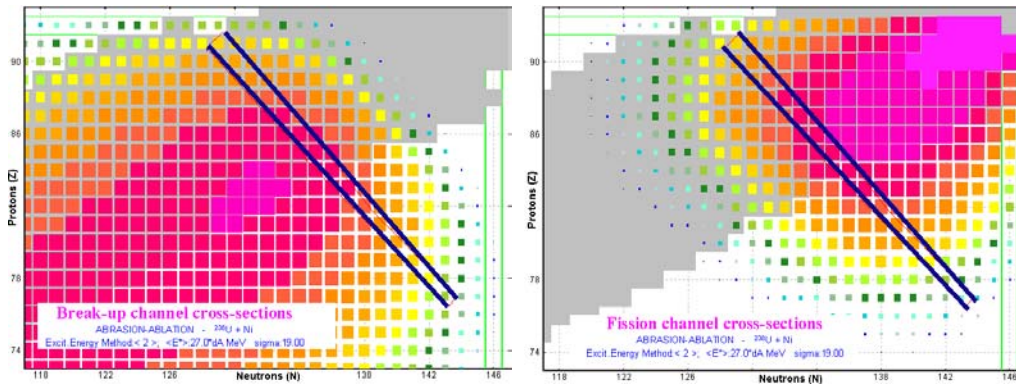
**Fig.132.** Calculated total abrasion and de-excitation channels cross-sections (with and without geometrical corrections for the excitation energy per abraded nucleon equal to 13.3 MeV/dA) and experimental fission (without EM component) and evaporation cross-sections as a function of the target mass for the projectile  $^{238}\text{U}(1\text{AGeV})$ .



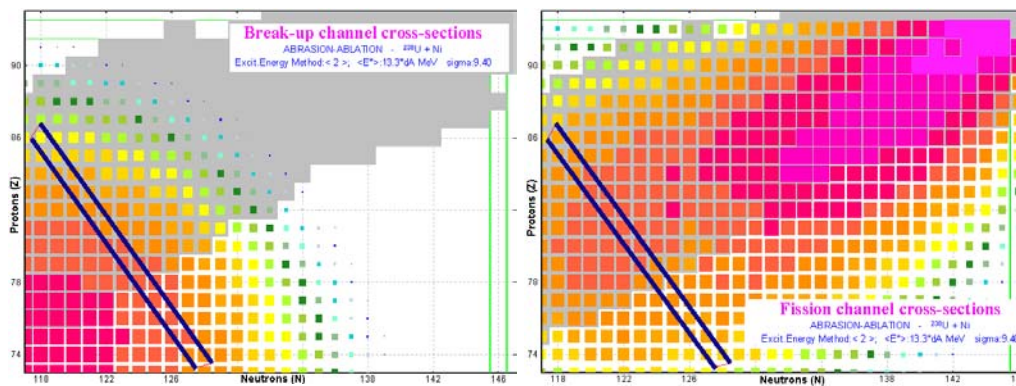
**Fig.133.** Calculated total abrasion and de-excitation channels cross-sections (with and without geometrical corrections for the excitation energy per abraded nucleon equal to 27 MeV/dA) and experimental fission (without EM component) and evaporation cross-sections as a function of the target mass for the projectile  $^{238}\text{U}(1\text{AGeV})$ .

Fig.132 and Fig.133 show experimental fission (without Coulomb fission contribution) and evaporation cross-sections and de-excitation channels after abrasion of  $^{238}\text{U}(1\text{AGeV})$  by the target calculated with and without geometrical corrections. Calculations for Fig.132 and Fig.133 correspond to excitation energies per abraded nucleon of 13.3 and 27 MeV/dA respectively. It is possible to conclude that there is good agreement between fission experimental results and AF calculations with  $E_0^* = 13.3$  MeV/dA for targets heavier than Beryllium, and between evaporation experimental results and calculations with  $E_0^* = 13.3$  MeV/dA.

👉 It is possible to conclude in the case of  $E_0^* = 13.3$  MeV/dA that the INC cross-section is shared between break-up and fission channels in the case of  $p$  and  $d$  targets. There is no contribution into the evaporation channel from the INC mechanism.



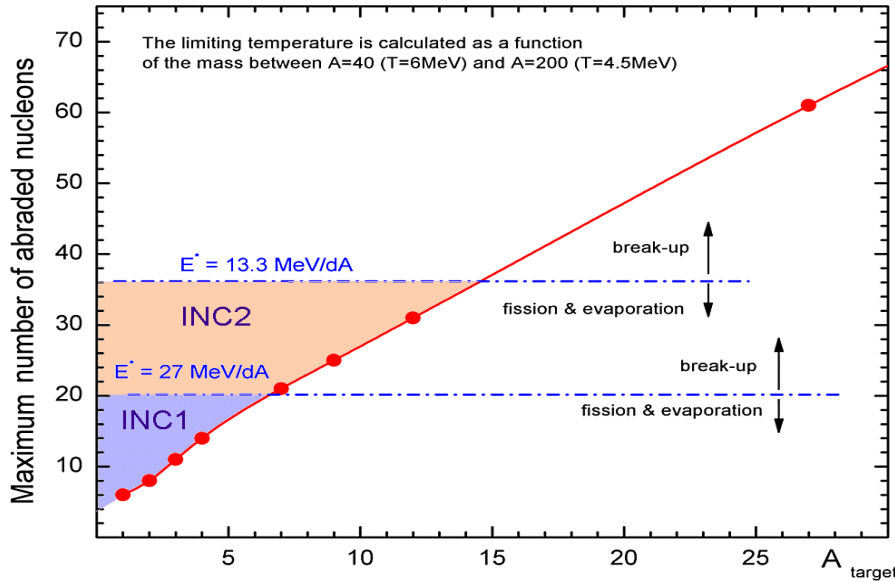
**Fig.134.** Break-up (left) and fission (right) channels for abrasion of a  $^{238}\text{U}(1\text{AGeV})$  projectile by a Ni target calculated with  $E_0^* = 27$  MeV/dA. The navy reference lines have the same position on both plots.



**Fig.135.** Break-up (left) and fission (right) channels for abrasion of a  $^{238}\text{U}(1\text{AGeV})$  projectile by a Ni target calculated with  $E_0^* = 13.3$  MeV/dA. The navy reference lines have the same position on both plots.

Using Fig.134 and Fig.135 it is possible to conclude, by depending on excitation energies per abraded nucleon, how many nucleons it is necessary to tear from the  $^{238}\text{U}$  projectile to make the break-up channel dominate over fission.

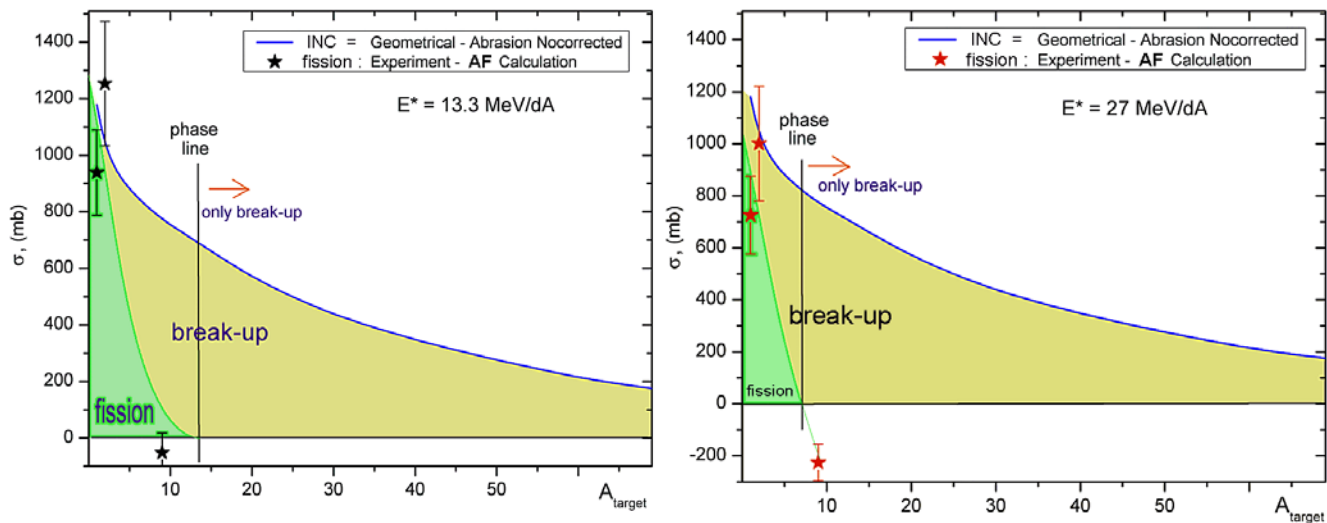
Fig.136 shows the maximum number of abraded nucleons from a  $^{238}\text{U}$  projectile as a function of the target mass calculated by the LISE++ Abrasion-Ablation model.



**Fig.136.** Maximum number of abraded nucleons from a  $^{238}\text{U}$  projectile as a function of the target mass calculated with the LISE++ geometrical abrasion-ablation model without LISE geometrical corrections. Two horizontal dash-dot lines corresponding to the two excitation energies (13 & 27 MeV/dA) denote regions where the break-up channel begins to dominate (see Fig.134 and Fig.135).

We suggest that in the INC-region both break-up and fission channels take place, below the blue line, (not including INC-region) fission and evaporation channels, and above the blue line (from definition of this line), just the break-up channel.

The number of abraded nucleons can be calculated by a fast analytical method using the expression for excitation energy  $E^* \cong a \cdot T_{lim}^2$ , where for masses  $A=200-220$  the parameter  $a$  is about  $27 \text{ MeV}^{-1}$ , and the limiting temperature is about  $4.4 \text{ MeV}$ . Therefore the excitation energy corresponding to the limiting temperature in this mass region is about  $530 \text{ MeV}$ . The excitation energy of prefragments in the Abrasion-Ablation model is proportional to the number of abraded nucleons and the  $E_0^*$  parameter. Therefore for  $E_0^* = 13.3 \text{ MeV/dA}$  we get  $dA \cong 39$ , and for  $E_0^* = 27 \text{ MeV/dA}$  similarly  $dA \cong 19$ .



**Fig.137.** INC cross-section as a function of target mass. Experimental fission cross-sections [Per04,Arm96,Rub96] are shown after subtraction of AF calculations without geometrical corrections. The phase line denotes a boundary above which only the break-up takes place (Fig.136). The left plot shows calculations done with  $E_0^* = 13.3 \text{ MeV/dA}$ , and the right plot similarly with  $E_0^* = 27 \text{ MeV/dA}$ .

Fig.137 shows the INC cross-section as a function of target mass. Using experimental points (after subtraction of the AF calculations without geometrical corrections) and phase lines we were trying to determine the fission component in the INC cross-section. It is possible to conclude the following:

- For  $E_0^*=13.3$  MeV/dA (left plot in Fig.137), it is possible to connect the reduced experimental points and the phase line. For  $p$  and  $d$  targets, de-excitation in the INC reaction mechanism goes through the fission channel; whereas in the case of Be-target and heavier it goes through the break-up de-excitation channel.
- For  $E_0^*=27$  MeV/dA (right plot in Fig.137) the reduced experimental value for a Be-target is not consistent with systematic error and can not be explained by the INC reaction mechanism.
- Experimental fission cross-sections for **He** and **Li targets** could considerably help with the further development of the model.
- A target of light mass, to which corresponds the lowest experimental fission cross-section, can serve as a test to estimate an excitation energy of the prefragment after abrasion (see Fig.136).

### 1.5.8.1. Recommended EER parameters for light targets in the LISE++ Abrasion-Fission model

Based on conclusions of the previous chapter we recommend using excitation energy of the prefragment after abrasion of  $E_0^*=13.3$  MeV/dA. Keeping values for Low and Middle EERs calculated by AA without LISE geometrical corrections, we are taking High EER from AA with these cross-sections. The next step is modification of the High EER cross-section assuming contributions from the INC process.

The code does not calculate AA+INC parameters. You can load already existing files, or enter EER parameters manually based on principles described below.

#### 1.5.8.1.1. Hydrogen target

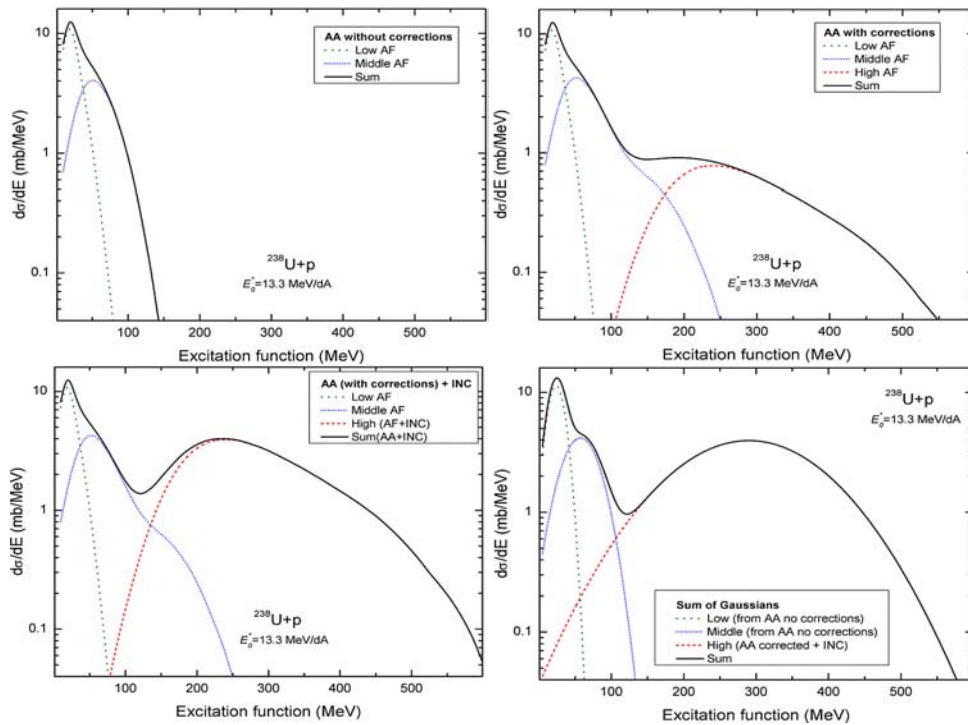
Fig.138 shows fission excitation functions and their EER components calculated by different methods for the reaction  $^{238}\text{U}(1\text{AGeV})+p$ . The EER parameters are given in Table 14. For the final summed fission cross-section of the AA+INC method we used the experimental value of 1530 mb [Ber03]. The Coulomb fission cross-section of a Hydrogen target for  $^{238}\text{U}(1000\text{AGeV})$  is less 1mb.

There is not a sharp boundary between low and middle excitation energy regions. In Bernas' experiment [Ber03] the asymmetrical fission cross-section was measured to be equal to  $105\pm 10\text{mb}$ . To reproduce this value in the code we have to set the low-energy boundary to 20 MeV, and the Low EER has the following parameters:  $^{237}_{92}\text{U}_{145}$ ,  $E^*=18.2\text{MeV}$ ,  $\sigma=157$  mb.

**Table 14.** EERs for the reaction  $^{238}\text{U}(1\text{AGeV})+p$  calculated by different methods. Region boundaries were set to 40 & 180 MeV.

Method	$\Sigma\sigma$ , mb	Low			Middle			High		
		$A, Z, N$	$E^*$	$\sigma$ , mb	$A, Z, N$	$E^*$	$\sigma$ , mb	$A, Z, N$	$E^*$	$\sigma$ , mb
AA without corrections	591.3	$^{236}_{92}\text{U}_{144}$	23.8	331.5	$^{234}_{91}\text{Pa}_{143}$	57.4	259.7			
AA with corrections	845.1	$^{236}_{92}\text{U}_{144}$	23.5	323.8	$^{232}_{90}\text{Th}_{142}$	75.7	352.1	$^{215}_{84}\text{Po}_{131}$	289.9	169.2
<b>AA + INC</b>	1530.5	$^{236}_{92}\text{U}_{144}$	23.8	331.5	$^{234}_{91}\text{Pa}_{143}$	57.4	259.7	$^{215}_{84}\text{Po}_{131}$	289.9	<b>939.3</b>





**Fig.138.** Fission excitation functions and their components calculated for the reaction  $^{238}\text{U}(1\text{AGeV}) + p$ .

Left top plot: without LISE++ geometrical corrections.

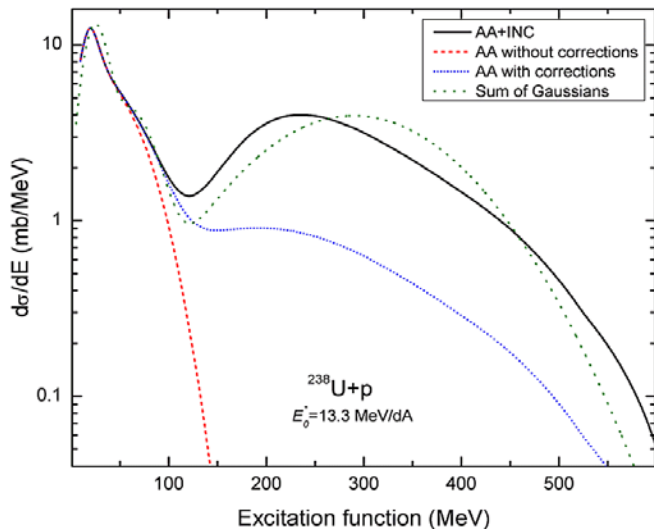
Right top: with corrections.

Left bottom: AA+INC. See Table 14 for details.

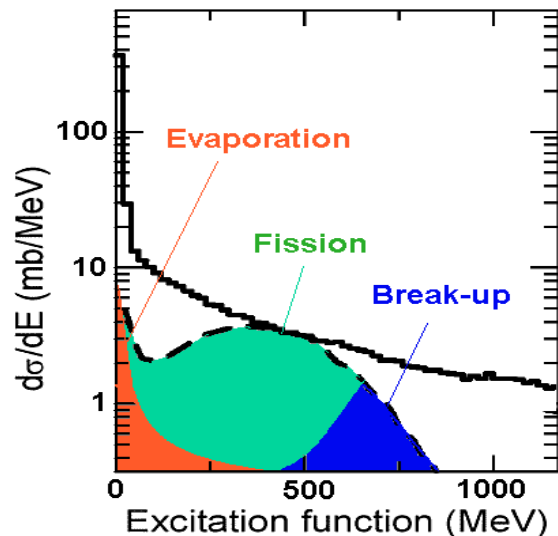
Right bottom: Sum of three normal distributions with EER parameters from AA+INC. The standard deviations of the distributions are taken from LISE calculations and are equal to 11.59, 24.85, and 94.7 MeV.

Fig.139 shows fission excitation functions calculated by different methods for the reaction  $^{238}\text{U}(1\text{AGeV}) + p$ . Compare the AA+INC excitation function with Fig.140. Fig.140 was modified to show qualitatively where break-up and evaporation de-excitation channels are located based on expected shapes and experimental cross-section values. Fission and total cross-sections were measured correspondingly  $1530 \pm 150$  and  $1990 \pm 170$  mb [Ber03], whereas in the reaction  $\bar{p}(1.2\text{ GeV}) + ^{238}\text{U}$ , reaction cross-section was measured to be  $2200 \pm 130$  mb [Gol96]. The geometrical cross-section is about 2.3 barn.

The file “examples/afission/AF\_238U\_p.lpp” with AA+INC settings is provided by the LISE installation package.



**Fig.139.** Fission excitation functions calculated by different methods for the reaction  $^{238}\text{U}(1\text{AGeV}) + p$ . Compare the AA+INC excitation function with the dashed line in Fig.140.



**Fig.140.** Total reaction cross-section as a function of the excitation energy induced right after the collision, before an eventual pre-equilibrium or break-up process and the consecutive sequential decay<sup>▲</sup>

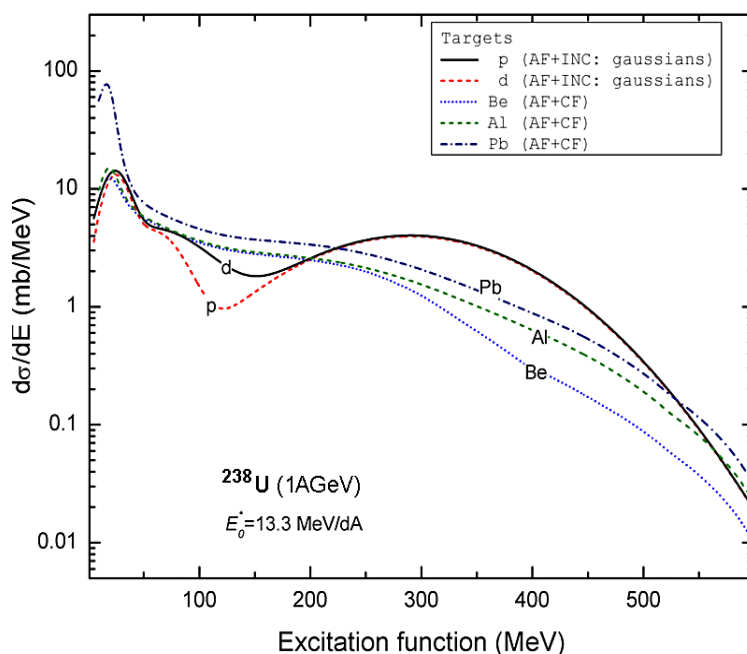
<sup>▲</sup> The dashed line corresponds to the reaction  $\bar{p}(1.2\text{ GeV}) + ^{238}\text{U}$  ( $\sigma_{\text{react}}=2200 \pm 130$  mb) measured in the work [Gol96]. The

### 1.5.8.1.2. Deuterium target

Table 15 shows fission EER parameters calculated by different methods for the reaction  $^{238}\text{U}(1\text{AGeV})+d$ . For the final summed fission cross-section of the AA+INC method we took 1700 mb in order not to exceed the geometrical cross-section when adding the evaporation cross-section:

Experiment	$\sigma$ , mb	$s(\sigma)$ , mb	Ref
Fission	2000	220	[Per04]
Evaporation	700	130	[Cas01]
Total	2700	350	[Per04]
Geom (calc)	2427		

**Table 15.** EERs for the reaction  $^{238}\text{U}(1\text{AGeV})+d$  calculated by different methods. Region boundaries were set to 40 & 180 MeV.



**Fig.141.** Fission excitation functions in the reaction of  $^{238}\text{U}(1\text{AGeV})$  with different targets.

Method	$\Sigma\sigma$ , mb	Low			Middle			High		
		A, Z, N	$E^*$	$\sigma$ , mb	A, Z, N	$E^*$	$\sigma$ , mb	A, Z, N	$E^*$	$\sigma$ , mb
AA without corrections	745.3	$^{236}_{92}\text{U}_{144}$	23.5	319.9	$^{232}_{90}\text{Th}_{142}$	74.6	425.4			
AA with corrections	912.5	$^{236}_{92}\text{U}_{144}$	23.5	319.3	$^{231}_{90}\text{Th}_{141}$	79.0	427.0	$^{215}_{84}\text{Po}_{131}$	290.2	166.2
<b>AA + INC</b>	<b>1700</b>	$^{236}_{92}\text{U}_{144}$	23.5	319.9	$^{232}_{90}\text{Th}_{142}$	74.6	425.4	$^{215}_{84}\text{Po}_{131}$	290.2	<b>954.7</b>

The file “examples/afission/AF\_238U\_d.lpp” with AA+INC settings is provided by the LISE installation package.

### 1.5.8.1.3. Targets with $Z \geq 2$

We recommend EER settings for light targets with  $Z \geq 2$  based on systematics in the right plot of Fig.132 and the left plot of Fig.137.

- He and Li targets: fission cross-sections should be about 1300 mb, and the INC fission contribution will be about 50% of the total INC cross-section.
- For targets with  $Z \geq 4$  it is not necessary to apply the INC fission contribution because, as it is possible to see in Fig.132, there is a good agreement between experimental values and calculations done with geometrical corrections for the excitation energy of the prefragment after abrasion  $E_0^* = 13.3 \text{ MeV/dA}$ .

Fig.141 shows fission excitation functions in the reaction  $^{238}\text{U}(1\text{AGeV})$  on different targets.

figure was imported from [Jur04] and then was updated.

### 1.5.9. Comparison with experimental data

Default AF settings (evaporation, fission, and excitation energy of prefragment) were used for comparisons with experimental data summed in Table 16.

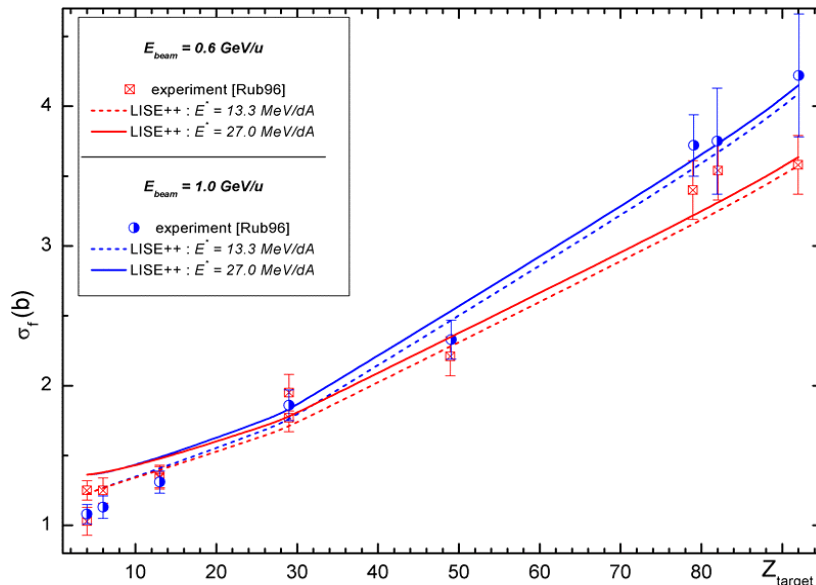
**Table 16.** Experimental works used for comparisons with LISE AF calculations.

Ref.	Reaction	Energy, AMeV	$\sigma_{EM}$	$\sigma_{fis}$ total	$\sigma_{fis}$ partial	$\sigma_{reaction}$ and others	TKE
Ber94	Pb( $^{238}\text{U}$ ,fis)	750			yes		
Aum95	Al,Cu,Pb( $^{238}\text{U}$ ,xn)	600,950			yes	yes	
Arm96	Pb,Be( $^{238}\text{U}$ ,fis)	750	yes	yes	yes	yes	
Hes96	Pb,Cu,Al( $^{238}\text{U}$ ,fis)	750		yes		yes	
Rub96	Be,C,Al,Cu,In,Au,U ( $^{238}\text{U}$ ,fis)	600, 1000	yes	yes			
Ber97	B,Pb( $^{238}\text{U}$ ,fis)	750	yes	yes			
End01	$^1\text{H}$ ( $^{208}\text{Pb}$ ,fis)	1000		yes	yes	yes	yes
End02	$^2\text{H}$ ( $^{208}\text{Pb}$ ,fis)	1000		yes	yes	yes	yes
Ben01	$^1\text{H}$ ( $^{197}\text{Au}$ ,fis)	800		yes	yes		yes
Ben02	$^1\text{H}$ ( $^{197}\text{Au}$ ,fis)	800		yes			
Ber03	$^1\text{H}$ ( $^{238}\text{U}$ ,fis)	1000		yes	yes	yes	yes
Tai03	$^1\text{H}$ ( $^{238}\text{U}$ ,evapor)	1000			yes	yes	
Arm04	p( $^{238}\text{U}$ ,spallation)	1000					

Analysis of experimental data (total nuclear fission cross-sections) on induced fission in reactions of relativistic  $^{238}\text{U}$  projectiles with light targets has already been done in chapter “1.5.8. INC fission”.

#### 1.5.9.1. Total fission cross-sections of $^{238}\text{U}$ at relativistic energies

Fig.142 shows the extracted experimental [Rub96 and references therein] total fission cross-sections as a function of the atomic number of the target at 0.6 and 1 GeV per nucleon. LISE calculations were done for two prefragment excitation energy values, 13.3 and 27 MeV/dA. The observed strong increase with  $Z_{target}$  is due to the electromagnetic contribution.



**Fig.142.** Total fission cross-sections of  $^{238}\text{U}$  at energies between 0.6 and 1 GeV per nucleon. See inset in the figure for details. LISE calculations were done for two prefragment excitation energy values. 13.3 and 27 MeV/dA.

### 1.5.9.2. $^{208}\text{Pb}(1\text{AGeV}) + p, d$

The aim in the present analysis is to find parameters of the LISE AF model to describe experimental fission fragment production cross-sections in the reactions  $^{208}\text{Pb}(1\text{AGeV}) + p, d$  [Enq01,Enq02], and thus to show that the program can be used for calculation of fission fragment yields in similar reactions. Table 17 shows parameters characterizing the fission process of the  $^{208}\text{Pb}(1\text{AGeV})+p$  [Enq01] and  $^{208}\text{Pb}(1\text{AGeV})+d$  [Enq02].

**Table 17.** Parameters characterizing the fission process of the  $^{208}\text{Pb}(1\text{AGeV})+p$  [Enq01] and  $^{208}\text{Pb}(1\text{AGeV})+d$  [Enq02] systems.

Reaction	$\sigma_{\text{fiss}}$ (mb)	$\bar{A}$	$\bar{Z}$	$\sigma_A$	$\sigma_Z$	$\bar{E}_{\text{kin}}$ (MeV)	$\sigma_{\text{frag}}$ (b)
$^{208}\text{Pb} + d$	$157 \pm 26^a$	$90.7 \pm 1.0$	$39.6 \pm 0.5$	$16.1 \pm 0.8$	$6.6 \pm 0.3$	$64 \pm 4$	$1.91 \pm 0.24^b$
$^{208}\text{Pb} + p$	$169 \pm 31^a$	$89.6 \pm 1.1$	$39.0 \pm 0.7$	$17.4 \pm 1.0$	$7.3 \pm 0.5$	$58 \pm 5$	$1.68 \pm 0.22^c$

<sup>a</sup> For elements from titanium (Z=22) to tellurium (Z=52).

<sup>b</sup> For elements from cesium (Z=52) to lead

<sup>c</sup> For elements from promethium (Z=61) to lead

The Abrasion-Ablation model cannot help us to get hints for the EER parameters; as it was developed for Abrasion-Fission in the case of uranium beams:

- The high fission barrier ( $\geq 20$  MeV) of nuclei with  $Z < 82$  makes it possible to exclude low excitation energy fission from calculations. Break-up energy in the region  $Z \leq 82$  is about 500 MeV from Fig.8.
- The maximum numbers of abraded nucleons from the geometrical AA model are equal to 7 for a proton target and 9 for a deuterium target. Without geometrical corrections, the AA model predicts very small fission cross-sections, 4.5 mb for a  $^2\text{H}$ -target (see Table 18) and 0.2 mb for a  $^1\text{H}$ -target (see Table 19).
- The AA model with geometrical correction shows that we can use just **ONE excitation energy region** with excitation energy about 300 MeV.

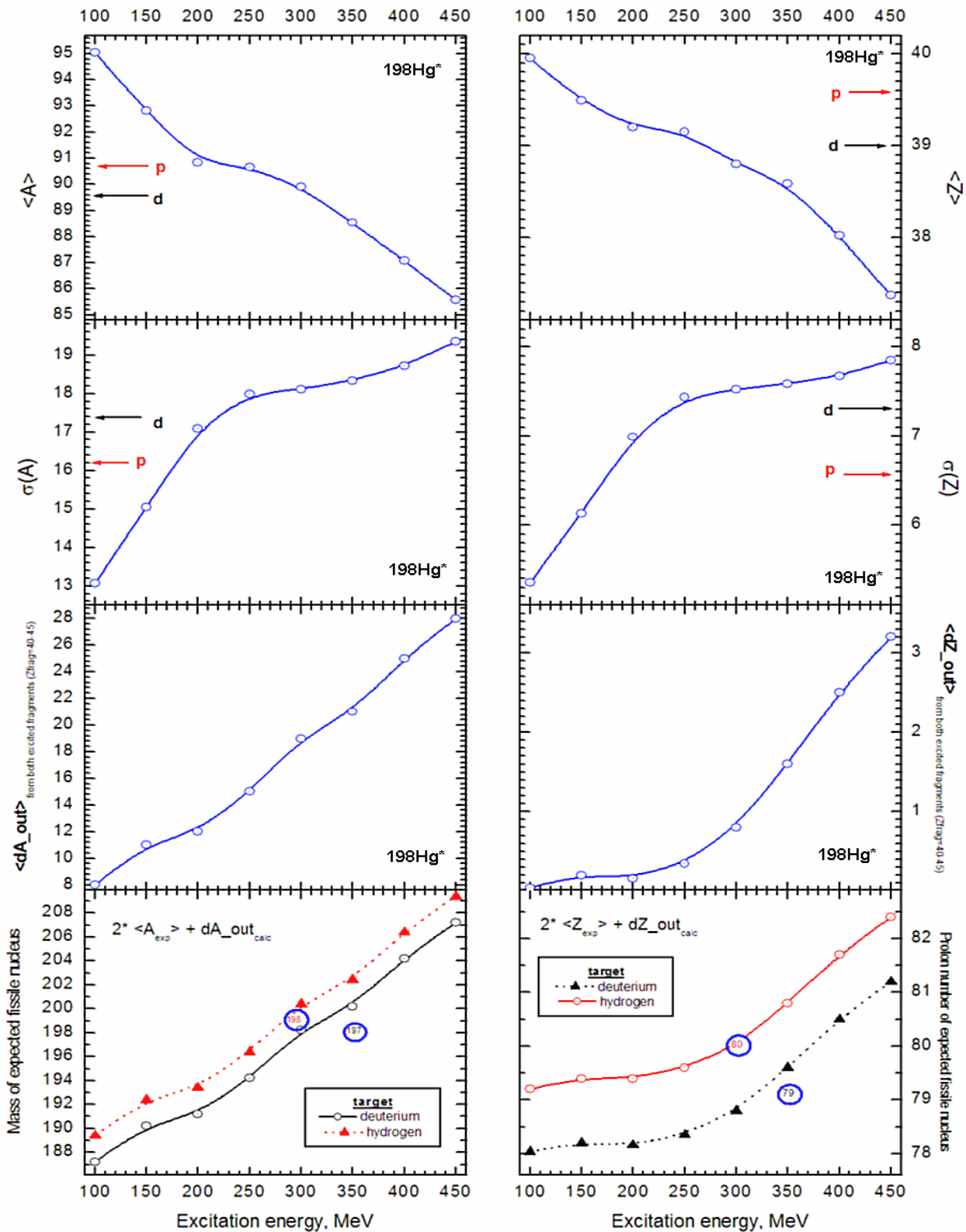
It is possible to conclude that the Abrasion-Fission cross-section is negligible in these reactions and that all fission events are due to the INC process.

**Table 18.** Calculated and recommended EERs for the reaction  $^{208}\text{Pb}(1\text{AGeV}) + d$ . The region boundaries were set to 40 & 180 MeV.

Method	$\Sigma\sigma$ , <i>mb</i>	Middle			High		
		<i>A, Z, N</i>	<i>E*</i>	$\sigma$ , <i>mb</i>	<i>A, Z, N</i>	<i>E*</i>	$\sigma$ , <i>mb</i>
AA without corrections	4.5	$^{198}_{80}\text{Hg}_{118}$	127.3	4.5			
AA with corrections	56.3	$^{197}_{80}\text{Hg}_{117}$	147.6	6.6	$^{184}_{75}\text{Re}_{109}$	305.3	49.7
<b>Recommended:</b> experiment	<b>200</b>	$^{197}_{79}\text{Au}_{120}$	<b>350</b>	<b>200</b>			

**Table 19.** Calculated and recommended EERs for the reaction  $^{208}\text{Pb}(1\text{AGeV}) + p$ . The region boundaries were set to 40 & 180 MeV.

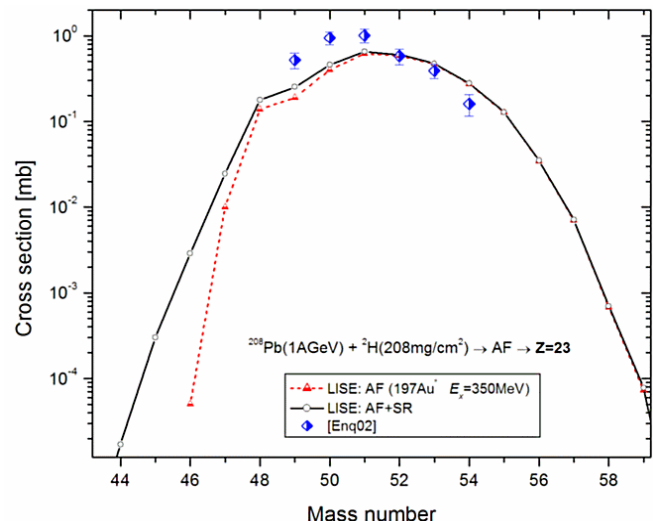
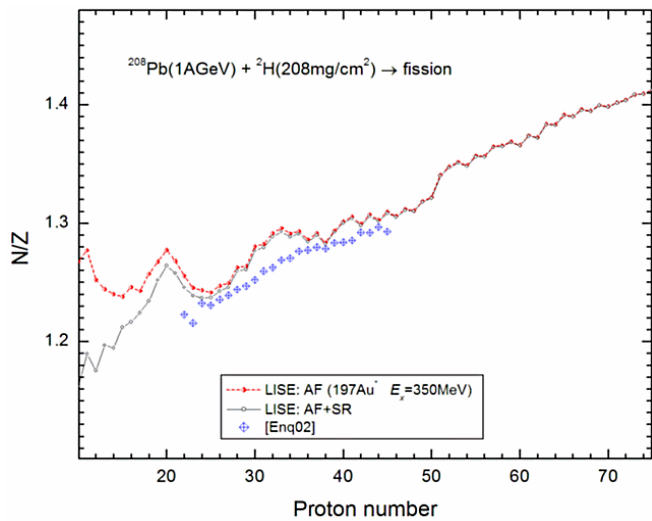
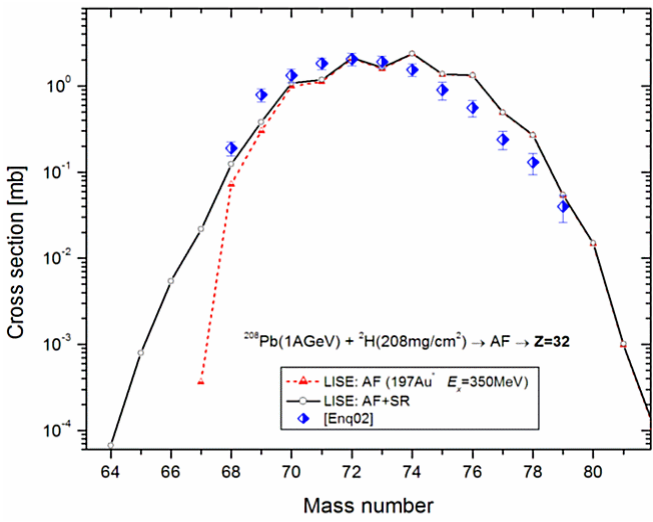
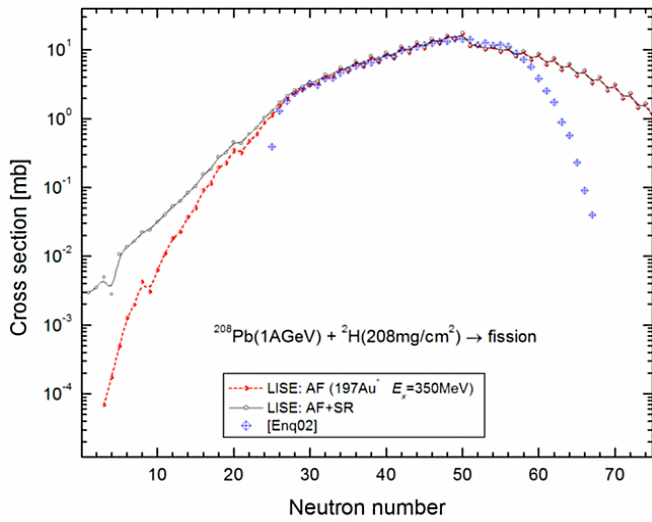
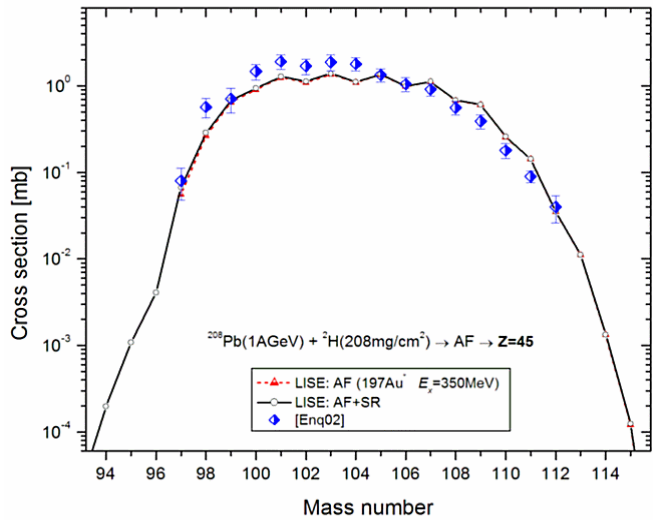
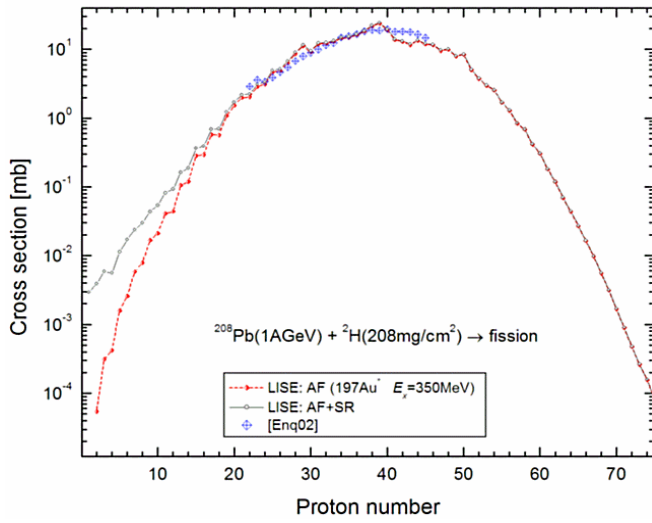
Method	$\Sigma\sigma$ , <i>mb</i>	Middle			High		
		<i>A, Z, N</i>	<i>E*</i>	$\sigma$ , <i>mb</i>	<i>A, Z, N</i>	<i>E*</i>	$\sigma$ , <i>mb</i>
AA without corrections	0.2	$^{198}_{80}\text{Hg}_{118}$	96	0.2			
AA with corrections	50.5	$^{197}_{80}\text{Hg}_{117}$	154.7	4.8	$^{184}_{75}\text{Re}_{109}$	304.4	50.5
<b>Recommended:</b> experiment	<b>175</b>	$^{198}_{80}\text{Hg}_{116}$	<b>300</b>	<b>175</b>			



**Fig.143.** Calculated  $^{198}\text{Hg}$  fission parameters as a function of excitation energy. The mean value of the mass and elemental distributions,  $\langle A \rangle$  and  $\langle Z \rangle$ , and their standard deviations,  $\sigma_A$  and  $\sigma_Z$ , are given in the two top rows. Arrows show experimental results on p- & d-targets [Enq01,Enq02].

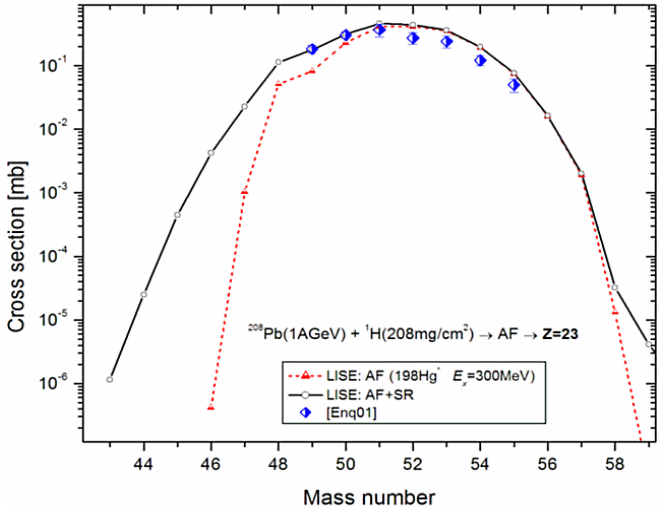
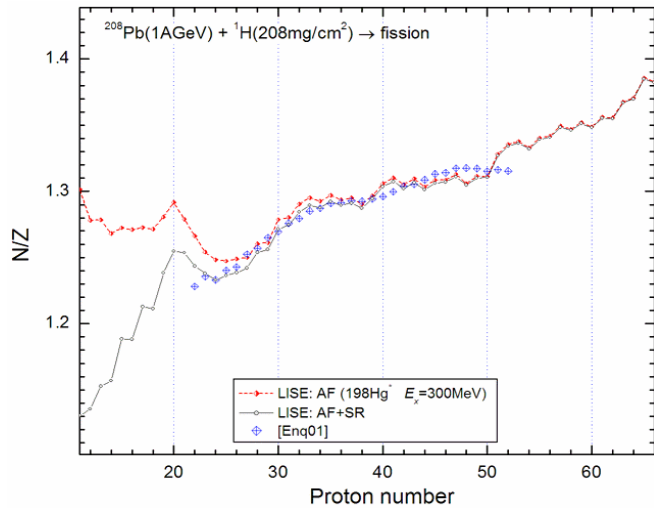
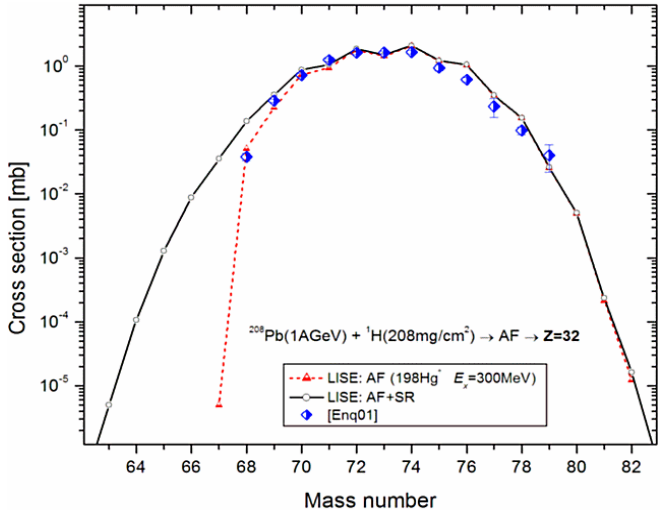
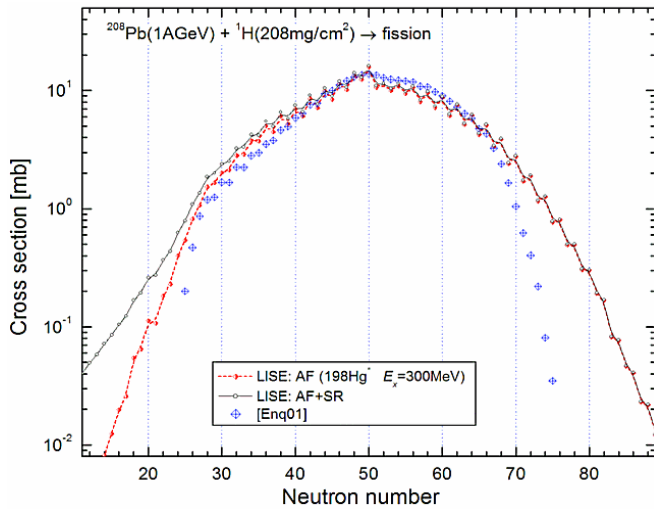
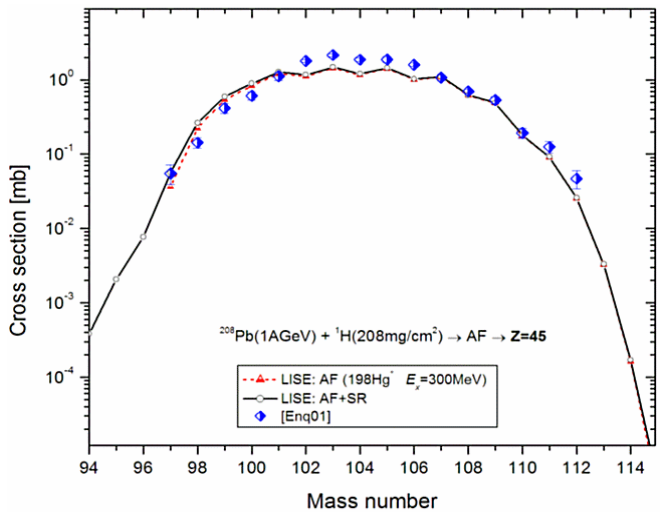
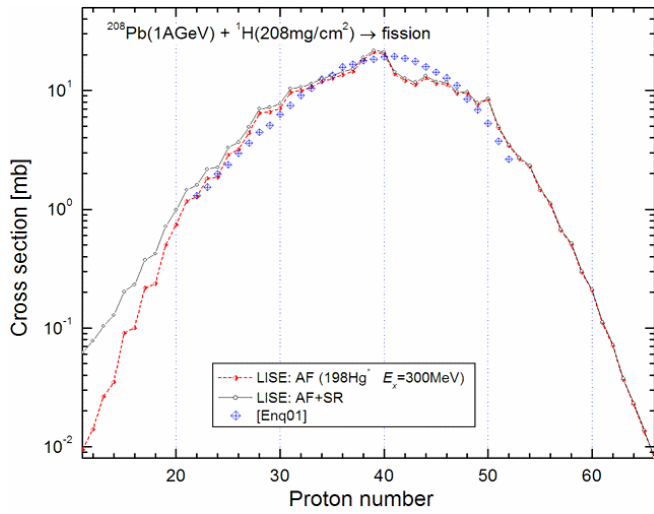
$\langle dA_{\text{out}} \rangle$  and  $\langle dZ_{\text{out}} \rangle$  plots show the mean values of emitted nucleons and protons respectively from both excited fragments before reaching their final states.

Bottom row: calculated mass and charge of the fission nucleus using experimental values of  $\langle A \rangle$  and  $\langle Z \rangle$  [Enq01,Enq02] and the calculated number of emitted nucleons and protons. Blue circles show values which give the best agreement with experimental results.



**Fig.144.** Experimental [Enq02] integrated distributions from spallation-fission reactions in  $^{208}\text{Pb}(1\text{AGeV})+d$  and calculated by LISE AF, assuming the fissile nucleus  $^{197}\text{Au}$  with  $E_x=350\text{ MeV}$ . Middle plot: no corrections were done for absent experimental results (compare with Fig.159).

**Fig.145.** Isotopic production cross-sections for spallation-fission products ( $Z=23,32,45$ ) from the reaction  $^{208}\text{Pb}(1\text{AGeV})+d$  obtained in work [Enq02] and calculated by LISE AF, assuming the fissile nucleus  $^{197}\text{Au}$  with  $E_x=350\text{ MeV}$ .

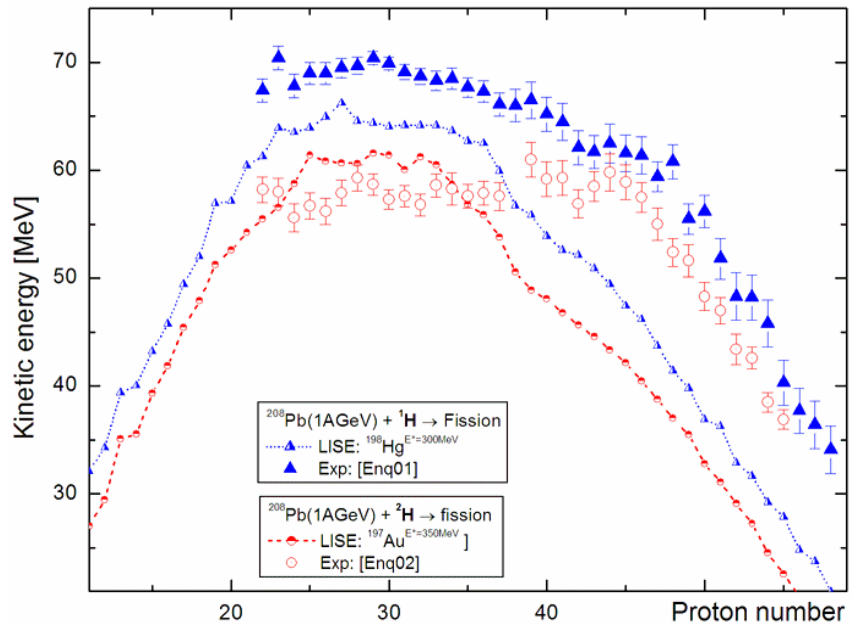


**Fig.146.** Experimental [Enq01] integrated distributions from spallation-fission reactions in  $^{208}\text{Pb}(1\text{AGeV})+p$  and calculated by LISE AF, assuming the fissile nucleus  $^{198}\text{Hg}$  with  $E_x=300\text{MeV}$ . Middle plot: no corrections were done for absent experimental results (compare with Fig.159).

**Fig.147.** Isotopic production cross-sections for spallation-fission products ( $Z=23,32,45$ ) from the reaction  $^{208}\text{Pb}(1\text{AGeV})+p$  obtained in work [Enq01] and calculated by LISE AF, assuming the fissile nucleus  $^{198}\text{Hg}$  with  $E_x=300\text{MeV}$ .

Fig.143 shows calculated  $^{198}\text{Hg}$  fission parameters as a function of excitation energy. Using the experimental fission characteristics from Table 17 and taking into account that an expected fissile nucleus has an excitation energy about 300-400 MeV.

Based on the fact that  $\sigma_A$  and  $\sigma_Z$  are larger in the case of a deuterium target and using calculations from Fig.143 it is possible to suggest that the excitation energy in the case of a deuterium target is about 50-100 MeV higher than in the case of a hydrogen target. Using the bottom pictures in Fig.143 it is possible to assume that fissile nuclei are found in the region  $A=196-200$  and  $Z=79-80$ . The comparison with experimental data has shown, that the best agreement is reached for  $^{198}\text{Hg}$  with  $E_x=300$  MeV in the case of a hydrogen target and for  $^{197}\text{Au}$  with  $E_x=350$  MeV in the case of a deuterium target.



**Fig.148.** Measured and calculated by LISE fission-fragment mean kinetic energies as a function of their proton number for the data of [Enq01 ,Enq02] ( $^{208}\text{Pb}(1\text{AGeV})+p,d$ ).

Fig.144 and Fig.146 show experimental integrated distributions from spallation-fission reactions in  $^{208}\text{Pb}(1\text{AGeV}) + ^2\text{H}, ^1\text{H}$  and calculated by LISE AF. Fig.145 and Fig.147 show isotopic production cross-sections of spallation-fission products ( $Z=23,32,45$ ) from the reaction  $^{208}\text{Pb}(1\text{AGeV}) + ^2\text{H}, ^1\text{H}$  obtained in work and calculated by LISE AF.

Fig.148 shows measured and calculated by LISE fission-fragment mean kinetic energies as a function of their proton number for the data of  $^{208}\text{Pb}(1\text{AGeV}) + p,d$ .

LISE++ files “AF\_208Pb\_p.lpp” and “AF\_208Pb\_d.lpp” contain experimental cross-section data for the reactions  $^{208}\text{Pb}(1\text{AGeV}) + p,d$  [Enq01,Enq02] and can be loaded from the site [http://groups.nsl.msui.edu/lise/7\\_5/examples/](http://groups.nsl.msui.edu/lise/7_5/examples/) or from the “\files\examples\afission\” directory.

**Note.** All this analysis of experimental fission fragment production cross-sections in the reactions  $^{208}\text{Pb}(1\text{AGeV}) + p,d$  was done using the previous version of the code without the first item in Equation /11/. We recommend repeating Fig.143 procedures to get new excitation energy regions. The new results probably will be slightly different from those given here.

Experimental data with the  $^{238}\text{U}$  beam were analyzed using with the “full” version of Equation /11/.



### 1.5.9.3. $^{238}\text{U}(1\text{A GeV}) + \text{Pb}$

To compare LISE calculations with experimental data for the reaction  $^{238}\text{U}+\text{Pb}$  we used the work [Enq99]. The experiment was performed at the GSI fragment separator. The primary beam of  $^{238}\text{U}$  with an energy of 1A GeV impinged on a 50.5 mg/cm<sup>2</sup> lead target. A secondary reaction contribution for this thin target (1.45e+20 atoms/cm<sup>2</sup>) is negligible. Reactions of U-projectiles on a lead target at this energy are characterized by a large contribution from Coulomb fission.

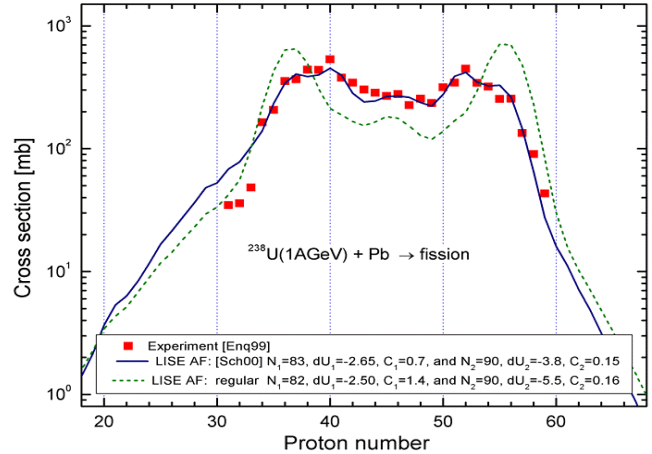
**Table 20.** EERs calculated by LISE and actually used for fission fragment yield calculations in the reaction  $^{238}\text{U}(1\text{A GeV})+\text{Pb}$ . Excitation energy of the prefragment after abrasion was set to  $E_0^* = 13.3 \text{ MeV/dA}$ .

Method	$\Sigma\sigma$ , mb	Low			Middle			High		
		A, Z, N	$E^*$	$\sigma$ , mb		$E^*$	$\sigma$ , mb	A, Z, N	$E^*$	$\sigma$ , mb
Abrasion-Ablation	3587.7	$^{238}_{92}\text{U}_{146}$	17.3	2279.9	$^{231}_{90}\text{Th}_{141}$	97.5	746.8	$^{215}_{84}\text{Po}_{131}$	286.1	561.1
Actually used for AF calculations	4080.0	$^{238}_{92}\text{U}_{146}$	17.3	2280	$^{230}_{90}\text{Th}_{140}$	100	500	$^{214}_{84}\text{Po}_{130}$	300	1300

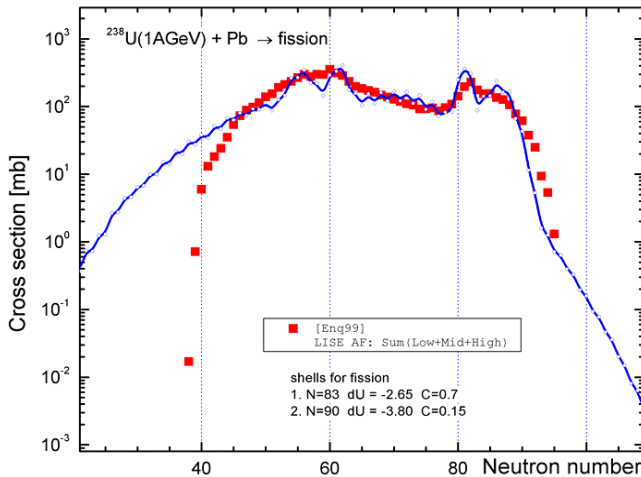
Calculated EER parameters for the reaction  $^{238}\text{U}(1\text{A GeV})+\text{Pb}$  are shown in Table 20. The file “AF\_238U\_Pb.lpp” containing experimental cross-section data [Enq99] can be loaded from the site [http://groups.nslc.msu.edu/lise/7\\_5/examples/](http://groups.nslc.msu.edu/lise/7_5/examples/).

Neutron shells for the semi-empirical fission model [Ben98] were changed in LISE for this analysis according to [Sch00]:  $N_1=83$ ,  $dU_1=-2.65$ ,  $C_1=0.7$ , and  $N_2=90$ ,  $dU_2=-3.8$ ,  $C_2=0.15$  (see Fig.149).

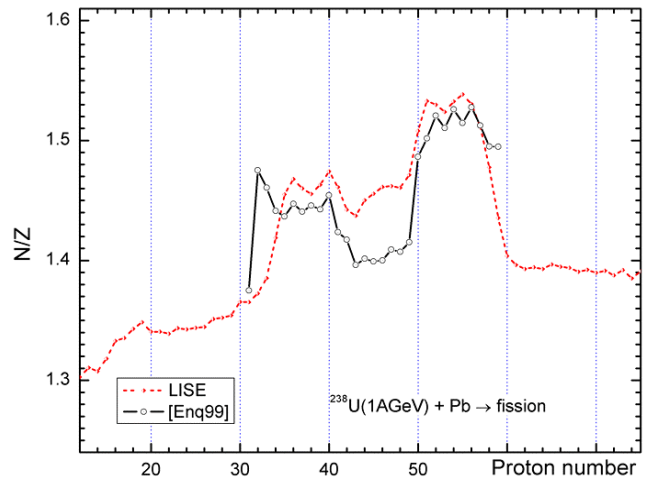
Comparison results between LISE calculation and experimental data [Enq99] are shown in Fig.150 (neutron fission cross-section), Fig.151 (N/Z ratio as a function of fragment proton number).



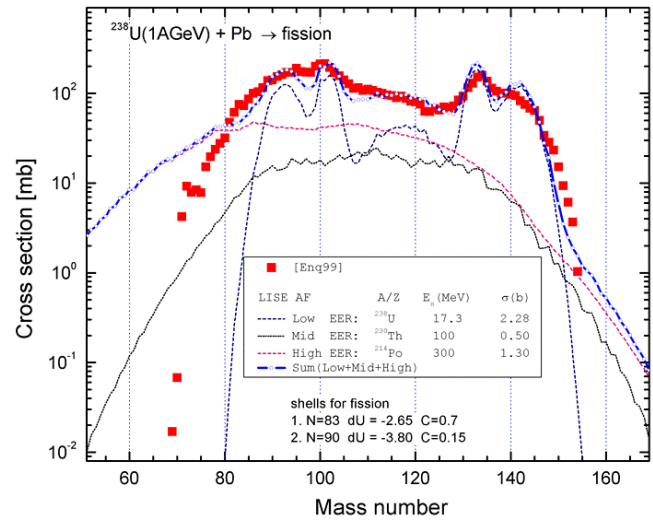
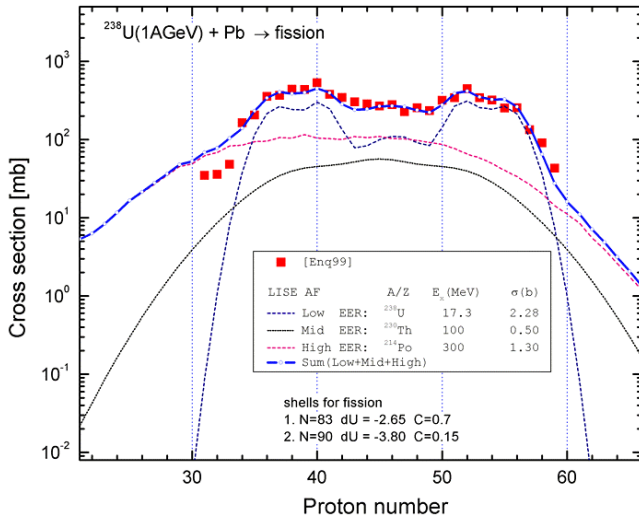
**Fig.149.** Experimental [Enq99] and calculated by LISE elemental fission cross-sections for the reaction  $^{238}\text{U}(1\text{A GeV})+\text{Pb}$ . LISE calculations were done with different parameters of the neutron shells of the fission model [Ben98].



**Fig.150.** Measured [Enq99] and calculated by LISE neutron fission cross-sections for the reaction  $^{238}\text{U}(1\text{A GeV})+\text{Pb}$ .

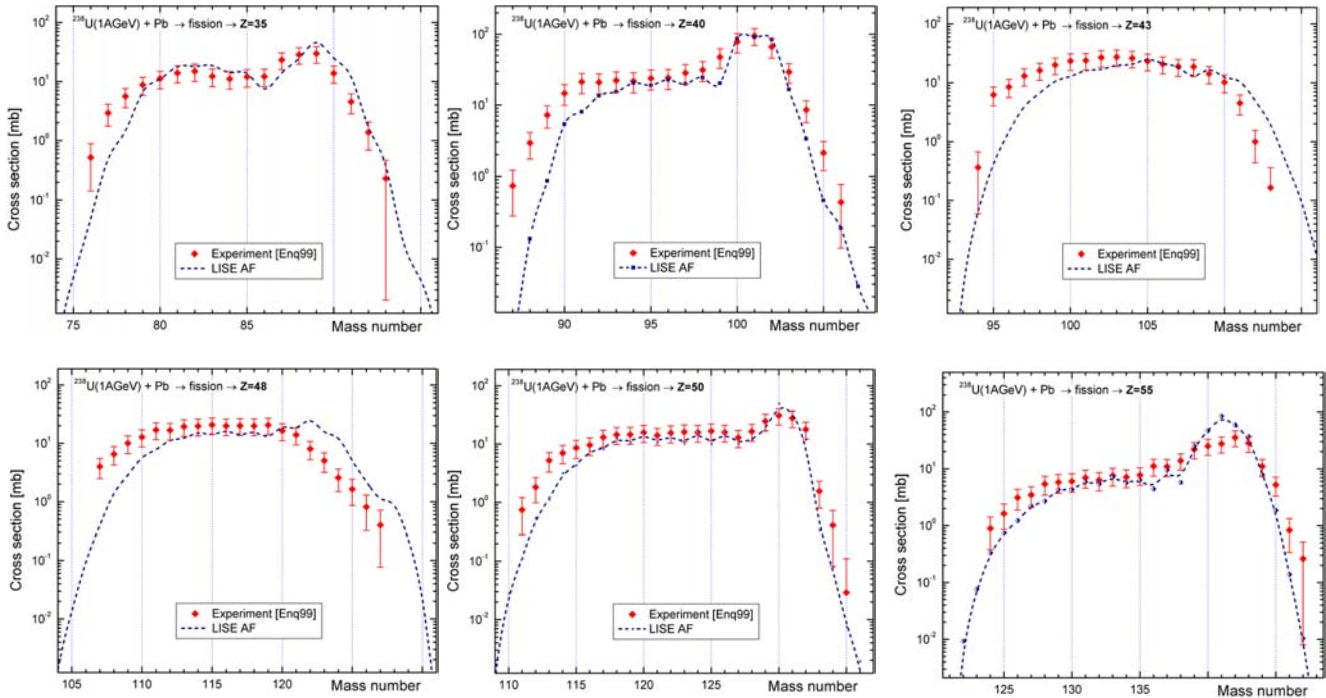


**Fig.151.** Experimental [Enq99] and calculated by LISE N/Z ratios as a function of their proton number for the reaction  $^{238}\text{U}(1\text{A GeV})+\text{Pb}$ .



**Fig.152.** Measured [Enq99] and calculated by LISE elemental fission cross-sections for the reaction  $^{238}\text{U}(1\text{AGeV})+\text{Pb}$ . Contributions from different EERs are shown in the plot also.

**Fig.153.** Experimental [Enq99] and calculated by LISE mass fission fragment cross-sections for the reaction  $^{238}\text{U}(1\text{AGeV})+\text{Pb}$ .



**Fig.154.** Isotopic production cross-sections for fission products ( $Z=35,40,43,48,50,55$ ) from the reaction  $^{238}\text{U}(1\text{AGeV})+\text{Pb}$  obtained in work [Enq99] and calculated by the LISE AF model for the excitation energy of the prefragment after abrasion  $E_0^* = 13.3 \text{ MeV/dA}$ . Load the “AF\_238U\_Pb.lpp” file for details.

Fig.152 (Fig.153) shows experimental and calculated by LISE elemental (mass) fission cross-sections for the reaction  $^{238}\text{U}(1\text{AGeV})+\text{Pb}$ . Contributions from different EERs are shown in the plots also.

Fig.154 shows isotopic production cross-sections for fission products ( $Z = 35, 40, 43, 48, 50, 55$ ) from the reaction  $^{238}\text{U}(1\text{AGeV})+\text{Pb}$  obtained in work [Enq99] and calculated by the LISE AF model.

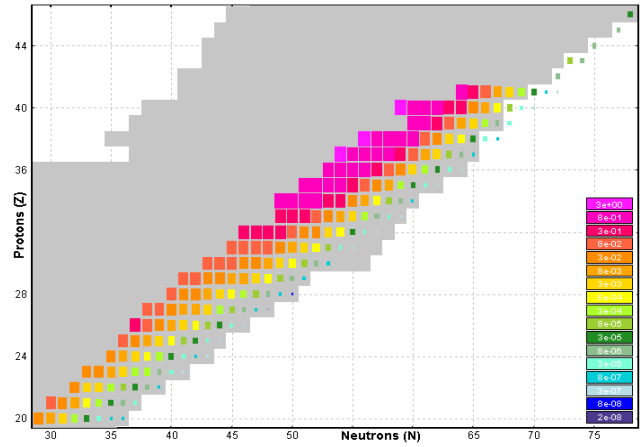
### 1.5.9.4. $^{238}\text{U}(750\text{AMeV}) + \text{Be}$

To compare LISE calculations with experimental data for the reaction  $^{238}\text{U}+\text{Be}$  we used the work [Ber97]. The experiment was performed at the GSI fragment separator. The primary beam of  $^{238}\text{U}$  with an energy of 750AMeV impinged on a 1 g/cm<sup>2</sup> beryllium target. A secondary reaction contribution in calculated cross-sections was not included for comparison with experimental data.

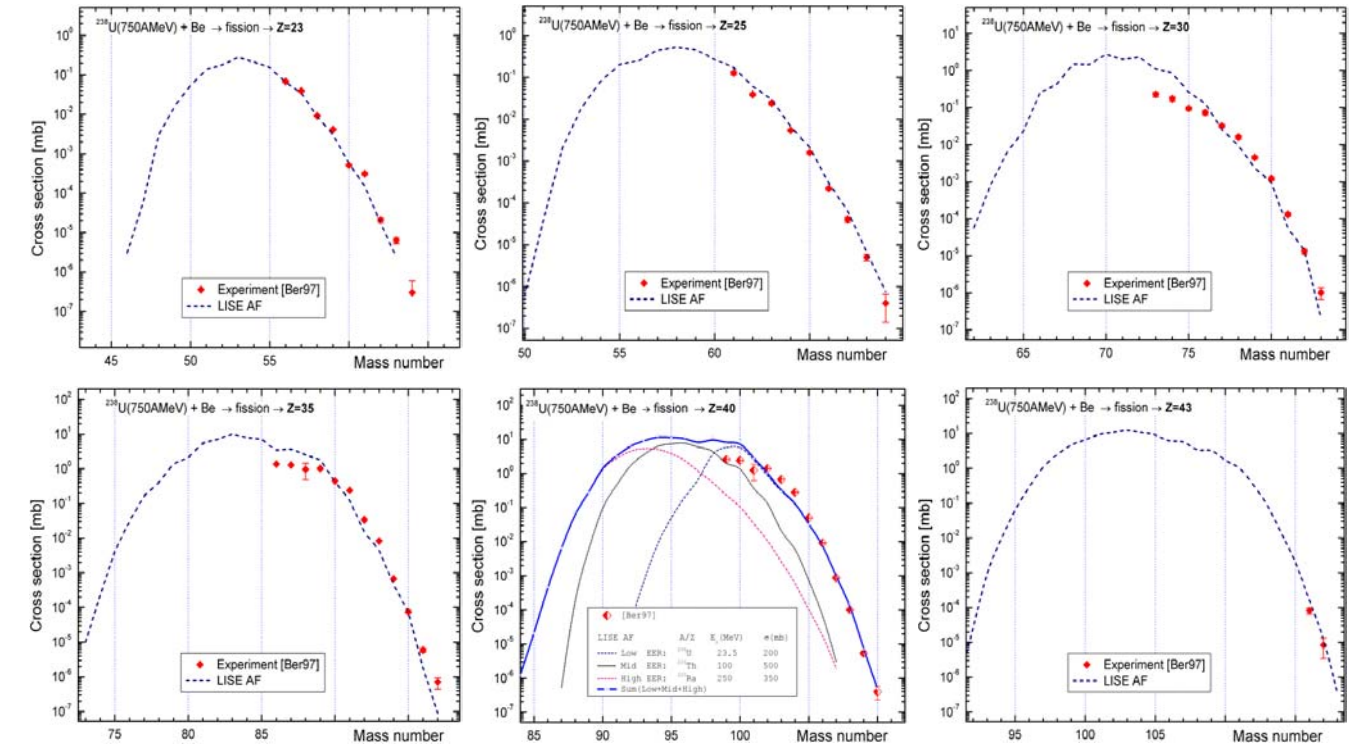
**Table 21.** EERs calculated by LISE and actually used for fission fragment yield calculations for the reaction  $^{238}\text{U}(750\text{ AMeV})+\text{Be}$ . The region boundaries were set to 40 & 180 MeV.  $E_0^* = 13.3\text{ MeV/dA}$ .

Method	$\Sigma\sigma$ , mb	Low			Middle			High		
		A, Z, N	$E^*$	$\sigma$ , mb	A, Z, N	$E^*$	$\sigma$ , mb	A, Z, N	$E^*$	$\sigma$ , mb
Abrasion-Ablation calculations	1207.5	$^{236}_{92}\text{U}_{144}$	23.4	323.2	$^{231}_{90}\text{Th}_{141}$	97.0	573.4	$^{218}_{85}\text{At}_{133}$	249	310.9
Actually used for AF calculations	1050.0	$^{236}_{92}\text{U}_{144}$	23.5	200	$^{226}_{90}\text{Th}_{136}$	100	500	$^{220}_{88}\text{Ra}_{132}$	250	350

EER parameters (AA calculated and actually used in fission production calculations) for the reaction  $^{238}\text{U}(750\text{AMeV})+\text{Be}$  are shown in Table 21. The LISE file “AF\_238U\_Be.lpp” with corresponding settings,



**Fig.155.** LISE two-dimensional plot of the experimental isotopic cross-sections for fission-fragments obtained in 750AMeV  $^{238}\text{U}+\text{Be}$  (Ber97).



**Fig.156.** Isotopic production cross-sections for fission products ( $Z=23,25,30,35,40,43$ ) from the reaction  $^{238}\text{U}(750\text{AMeV})+\text{Be}$  obtained in work [Ber97] and calculated by the LISE AF model for the excitation energy of the prefragment after abrasion  $E_0^* = 13.3\text{ MeV/dA}$ . Load the “AF\_238U\_Be.lpp” file for details.

which contains experimental cross-section data [Ber97], can be loaded from the site [http://groups.nsl.msu.edu/lise/7\\_5/examples/](http://groups.nsl.msu.edu/lise/7_5/examples/). As in the previous chapter, neutron shells for the semi-empirical fission model were set in LISE for this analysis according to [Sch00]:  $N_1=83$ ,  $dU_1=-2.65$ ,  $C_1=0.7$ , and  $N_2=90$ ,  $dU_2=-3.8$ ,  $C_2=0.15$ .

The experiment [Ber97] was devoted to the study of the neutron-rich side of the table of nuclides (see Fig.155). More than a hundred new nuclear species were identified including  $^{78}\text{Ni}$ , for which a cross-section of 300 pb was measured. Values of  $120\pm 40$  mb were found for the cross-section of  $^{238}\text{U}$  low excitation fission on Be. The total fission was measured cross-section to be 1.03 barn for the U/Be system [Hes96].

Fig.156 shows isotopic production cross-sections for fission products ( $Z=23,25,30,35,40,43$ ) from the reaction  $^{238}\text{U}(750\text{AmeV})+\text{Be}$  obtained in work [Ber97] and calculated by the LISE AF model.

### 1.5.9.5. $^{238}\text{U}(1\text{AGeV}) + p$

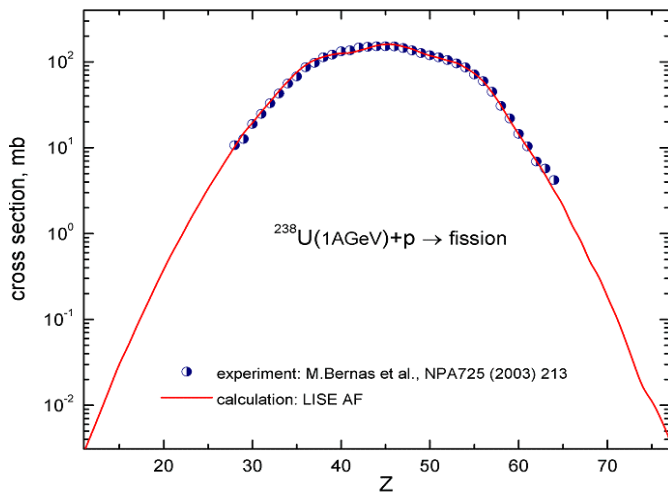
To compare LISE calculations with experimental data for the reaction  $^{238}\text{U}+p$  we used the work [Ber03]. The experiment was performed at the GSI fragment separator. The primary beam of  $^{238}\text{U}$  with an energy of 1AGeV impinged on a  $87.2\text{ mg/cm}^2$  liquid hydrogen target. The secondary reaction contribution in calculated cross-sections is shown for comparison with experimental data.

**Table 22.** EERs calculated by LISE and actually used for fission fragment yield calculations for the reaction  $^{238}\text{U}(1\text{ AGeV})+p$ . The region boundaries were set to 40 & 180 MeV.  $E_0^*=13.3\text{ MeV/dA}$ .

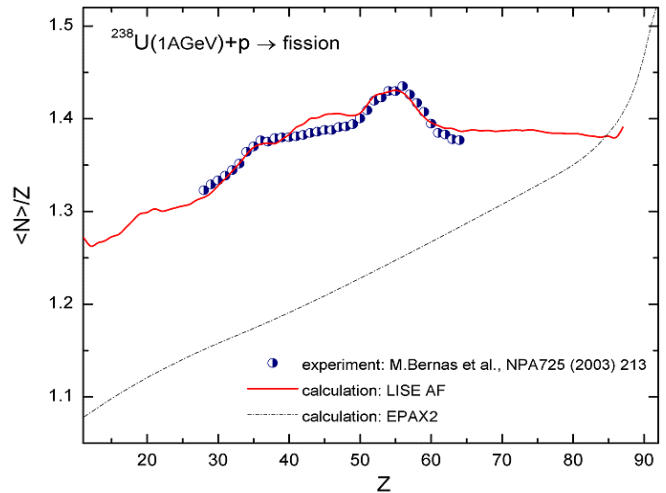
Method	$\Sigma\sigma$ mb	Low			Middle			High		
		$A, Z, N$	$E^*$	$\sigma, mb$	$A, Z, N$	$E^*$	$\sigma, mb$	$A, Z, N$	$E^*$	$\sigma, mb$
Abrasion-Ablation calculations	891.4	$^{237}_{92}\text{U}_{145}$	23.5	343.6	$^{232}_{90}\text{Th}_{142}$	75.3	373.9	$^{215}_{84}\text{Po}_{131}$	290	173.2
AF + INC fission (1.5.8.1.1. Hydrogen target)	1530.5	$^{236}_{92}\text{U}_{144}$	23.8	331.5	$^{234}_{91}\text{Pa}_{143}$	57.4	259.7	$^{215}_{84}\text{Po}_{131}$	289.9	939.3
calculations	<b>1550.0</b>	$^{236}_{92}\text{U}_{144}$	<b>23</b>	<b>150</b>	$^{226}_{90}\text{Th}_{136}$	<b>75</b>	<b>550</b>	$^{220}_{89}\text{Ac}_{131}$	<b>180</b>	<b>850</b>

EER parameters (AA calculated and actually used in fission production calculations) for the reaction  $^{238}\text{U}(1\text{AGeV}) + p$  are shown in Table 22. The LISE file “AF\_238U\_p.lpp” with corresponding settings, which contains experimental cross-section data [Ber03], can be loaded from the site [http://groups.nsl.msu.edu/lise/7\\_5/examples/](http://groups.nsl.msu.edu/lise/7_5/examples/). As in the previous chapter (except  $dU_1$  parameter), neutron shells for the semi-empirical fission model were set in LISE:  $N_1=83$ ,  $dU_1=-2.0$ ,  $C_1=0.7$ , and  $N_2=90$ ,  $dU_2=-3.8$ ,  $C_2=0.15$ .

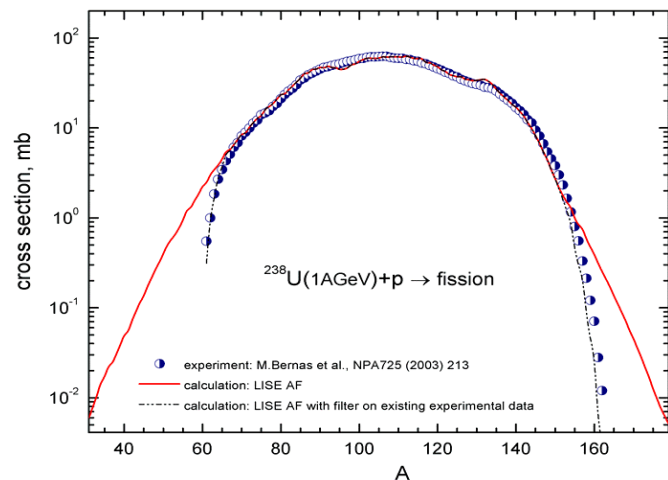
To get better agreement with experimental results we have made two global changes in EERs of “AF+INC” method: transfer  $\Delta\sigma=200$  mb from the Low EER to the Middle EER and change to more proton rich Middle and High fissile nuclei, from  $^{234}\text{Pa}$  ( $N/Z=1.57$ ) to  $^{226}\text{Th}$  ( $N/Z=1.51$ ) and from  $^{215}\text{Po}$  ( $N/Z=1.56$ ) to  $^{220}\text{Ac}$  ( $N/Z=1.48$ ) accordingly. It is probably that these changes can be explained by increasing the excitation energy per abraded nucleon as well as increasing dissipation influence through beta parameter (see Fig.13).



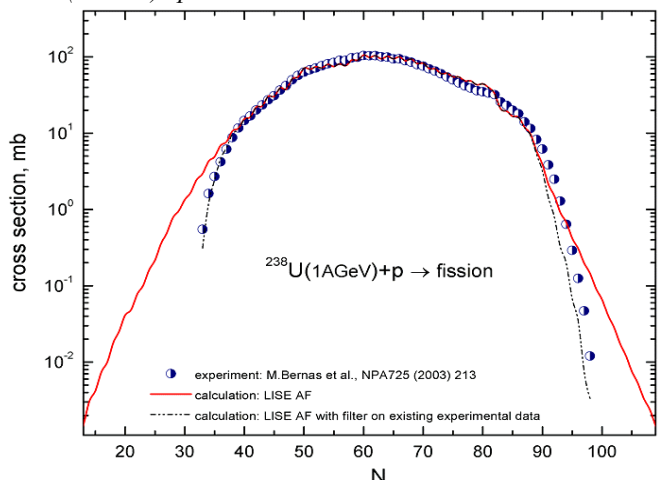
**Fig.157.** Measured [Ber03] and LISE calculated elemental fission cross-sections for the reaction  $^{238}\text{U}(1\text{AGeV})+p$ .



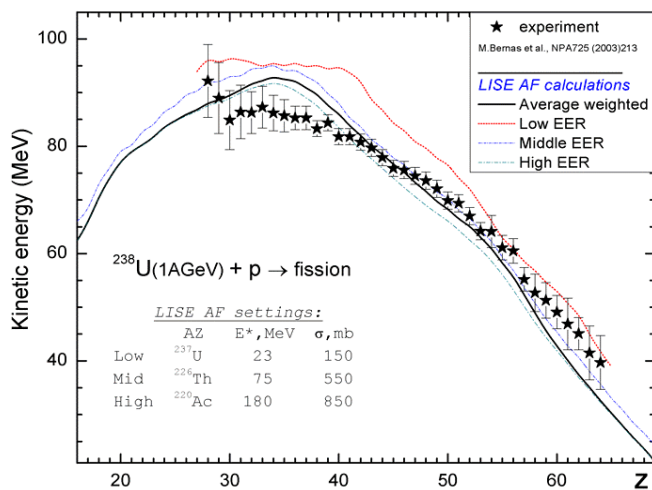
**Fig.158.** Experimental [Ber03] and LISE calculated  $N/Z$  ratios as a function of their proton number for the reaction  $^{238}\text{U}(1\text{AGeV})+p$ .



**Fig.159.** Measured [Ber03] and LISE calculated mass fission cross-sections for the reaction  $^{238}\text{U}(1\text{AGeV})+p$ . The dash-dot line represents calculated data filtered to existing experimental data ( $Z=28-64$ ).



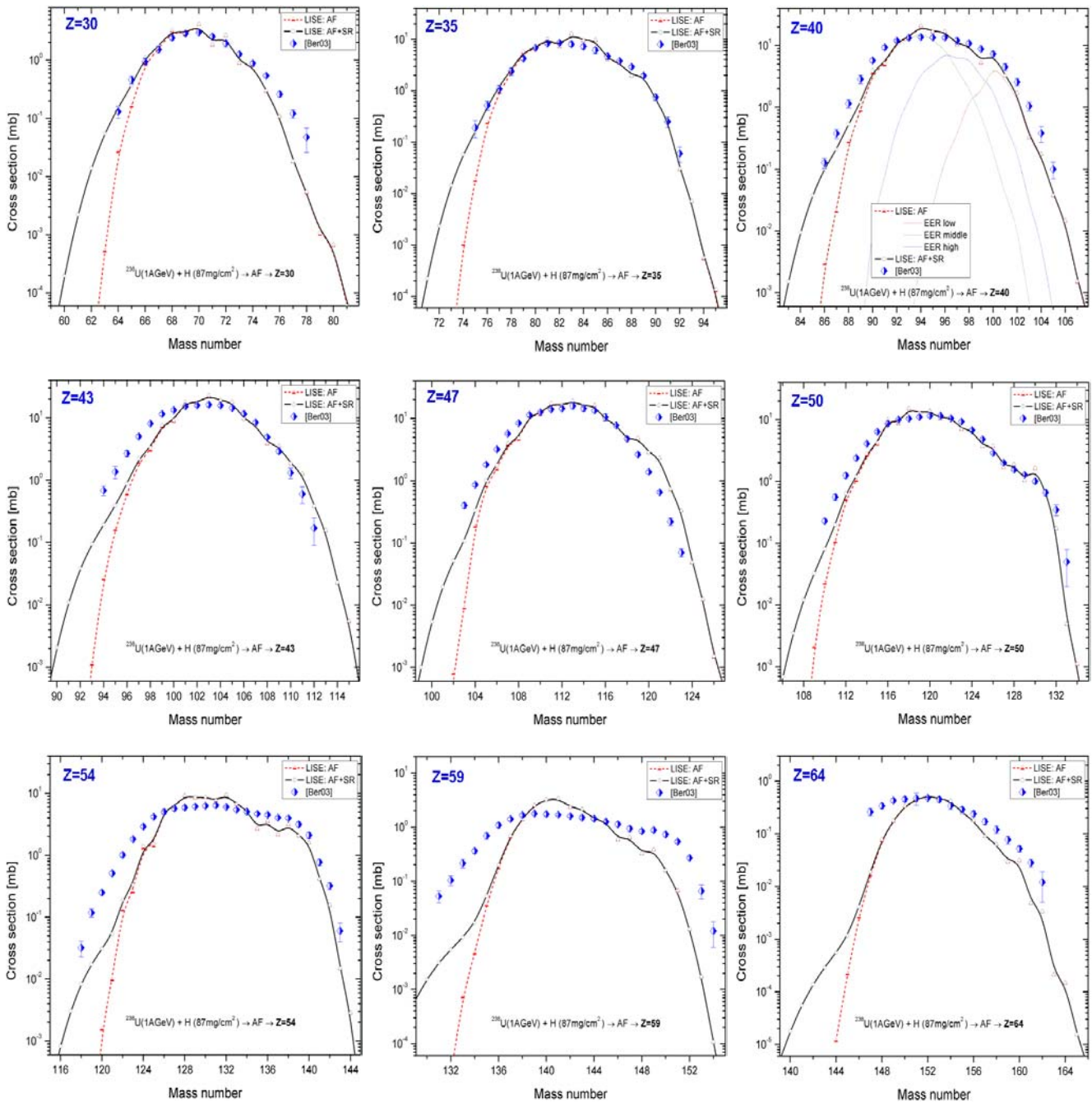
**Fig.160.** Experimental [Ber03] and LISE calculated neutron fission fragment cross-sections for the reaction  $^{238}\text{U}(1\text{AGeV})+p$ . The dash-dot line represents calculated data filtered to existing experimental data ( $Z=28-64$ ).



**Fig.161.** Measured and LISE calculated fission-fragment mean kinetic energies as a function of their proton for the data [Ber03] ( $^{238}\text{U}(1\text{AGeV})+p$ ).

Comparisons of results from LISE calculation and experimental data [Ber03] are shown in Fig.157 (elemental fission cross-section), Fig.158 ( $N/Z$  ratio as a function of fragment proton number), Fig.159 (mass fission cross-section), Fig.160 (neutron fission cross-section), and Fig.161 (fragment kinetic energy).

Fig.162 shows isotopic production cross-sections for fission products ( $Z = 30, 35, 40, 43, 47, 50, 54, 59, 64$ ) from the reaction  $^{238}\text{U}(1\text{AGeV})+p$  obtained in work [Ber03] and calculated by the LISE AF model.



**Fig.162.** Isotopic production cross-sections for fission products ( $Z=30,35,40,43,47,50,54,59,64$ ) from the reaction  $^{238}\text{U}(1\text{AGeV})+p$  obtained in work [Ber03] and calculated by the LISE AF model. Load the “AF\_238U\_p.lpp” file for details.

Six example files devoted to Abrasion-Fission are included in the LISE installation package:

- |                |                |
|----------------|----------------|
| AF_208Pb_d.lpp | AF_208Pb_p.lpp |
| AF_238U_p.lpp  | AF_238U_d.lpp  |
| AF_238U_Be.lpp | AF_238U_Pb.lpp |

The user can load them from the “files\examples\afission\” directory.

## 1.6. New utilities

### 1.6.1. User cross-section analysis using Abrasion-Ablation model

The purpose of the new utility is to find parameters for the prefragment excitation energy distribution (mean value and deviation) which best correspond to experimental data. The “user cross-section analysis” can be loaded from the “Utilities” menu (see Fig.163).

The analysis might be run if the following four conditions are satisfied:

1. The “Projectile fragmentation” reaction mode is selected;
2. Abrasion-ablation is the selected production cross-section method;
3. There are more than two user cross-sections in memory;
4. The “File” cross-section option is set to “on” in the “Options” dialog.

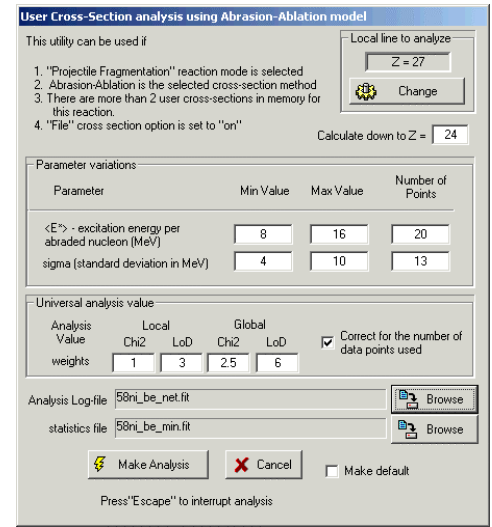


Fig.163. The “User cross-sections analysis” dialog.

If one of these conditions is not fulfilled then an error message will appear in the bottom of the dialog instead of the line “Press Escape to interrupt analysis” (see Fig.163).

Before running the analysis the user has to define the following parameters:

1. “Local line to analyze” - click the corresponding button to define the set of data important for you (for example the neutron removal line). It may be  $Z$ ,  $N$ ,  $A$ , or  $N-Z$  lines. The code compares experimental data and calculated values separately for the global set of data and for the local line defined by the user (see for details chapter “3.2. User CS in plots” [http://groups.nsl.msu.edu/lise/6\\_4/lise++\\_6\\_4.pdf](http://groups.nsl.msu.edu/lise/6_4/lise++_6_4.pdf)).
2. “Calculate down to  $Z$ ” - initially is set to 1, but if you want to make the analysis faster and you do not need light elements’ cross-sections then it may be increased. Obviously it is better to set this parameter greater than or equal to the lowest charge value of experimental data.
3. Minimal and maximal values of excitation energy and its deviation as well as the number of calculated points ( $N_{\langle E^* \rangle}$  and  $N_{\text{sigma}}$ ) for both cases.
4. “Weights of analysis value” – determines contribution of each of the four calculated values in the final result:

$$Final = w_1 \cdot Lo\chi^2_{\text{local}} + w_2 \cdot LoD_{\text{local}} + w_3 \cdot Lo\chi^2_{\text{total}} + w_4 \cdot LoD_{\text{total}} \quad /16/$$

where  $Lo\chi^2 = \ln(\chi^2)$  and  $LoD = \sum_{i=1}^N |\log_{10}(y_{\text{exp}}) - \log_{10}(y_{\text{calc}})| / N$ .

If the “Correct for the number of data points used” checkbox is set to “on” then the code calculates the  $Lo\chi^2$  value in the following way:  $Lo\chi^2 = \ln(\chi^2/N)$ , where  $N$  is the number of points used for the analysis.

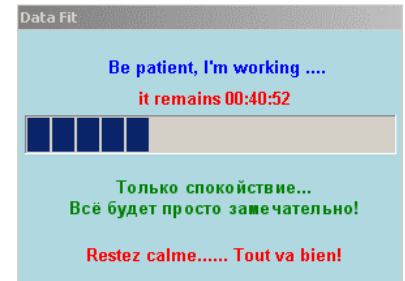
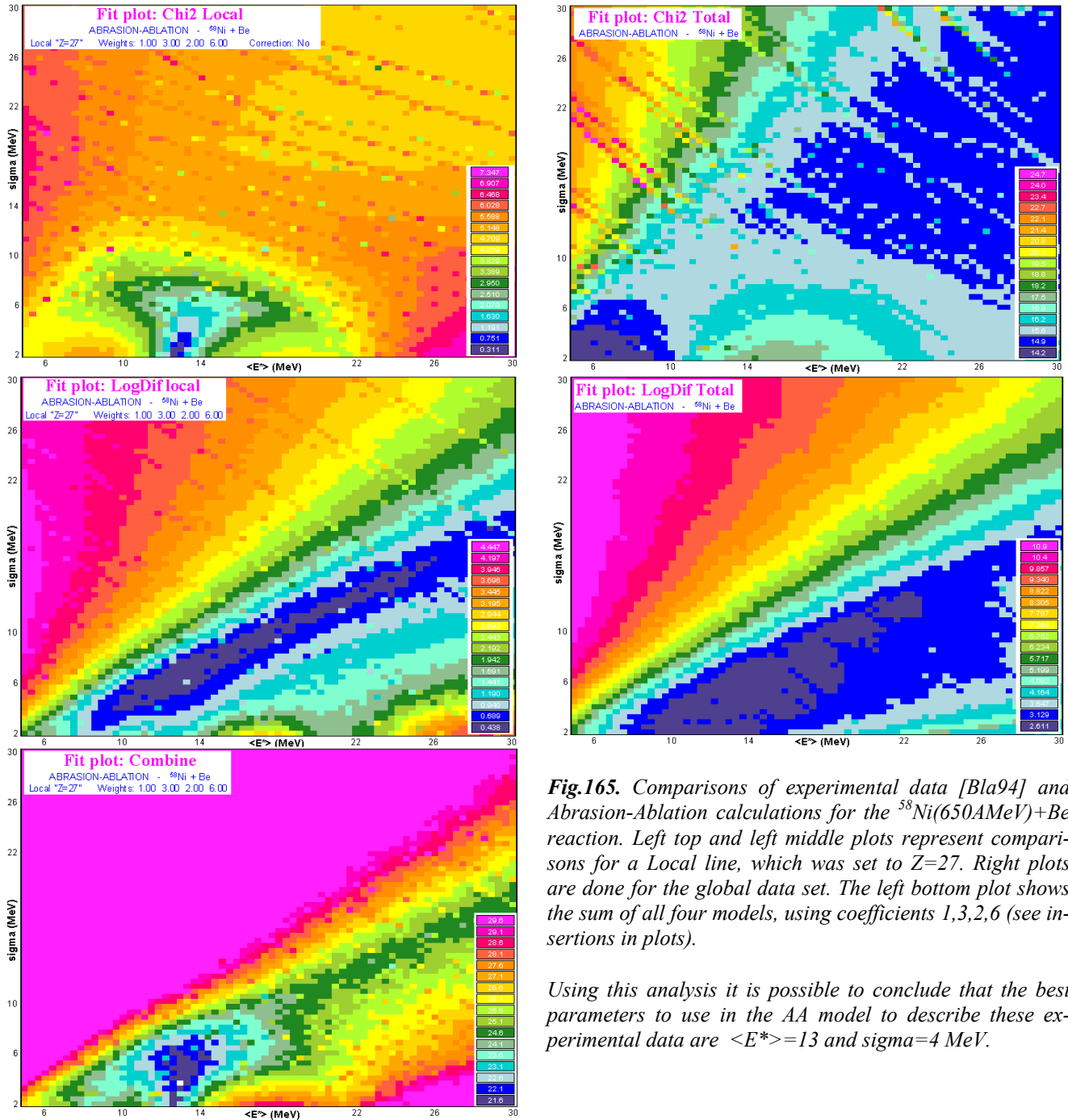


Fig.164.

The program will run the Abrasion-Ablation model  $N_{\langle E^* \rangle} \times N_{\text{sigma}}$  times after the user clicks the “Make analysis” button. During the calculation process the information window shows approximately how much time is remaining (see Fig.164).



**Fig.165.** Comparisons of experimental data [Bla94] and Abrasion-Ablation calculations for the  $^{58}\text{Ni}(650\text{AMeV})+\text{Be}$  reaction. Left top and left middle plots represent comparisons for a Local line, which was set to  $Z=27$ . Right plots are done for the global data set. The left bottom plot shows the sum of all four models, using coefficients 1,3,2,6 (see insertions in plots).

Using this analysis it is possible to conclude that the best parameters to use in the AA model to describe these experimental data are  $\langle E^* \rangle = 13$  and  $\text{sigma} = 4$  MeV.

After calculations are completed the program creates five two-dimensional plots (see Fig.165), four of them correspond to  $Lo\chi^2_{\text{local}}$ ,  $LoD_{\text{local}}$ ,  $Lo\chi^2_{\text{total}}$ ,  $LoD_{\text{total}}$  values and one represents the final result based on Equation /16/. The code also creates two text files, a statistics file and a log file, for each calculation. An analysis log-file shows calculated values for each combination “Energy-Sigma”; hereafter this file can be used by other programs (for example Excel or Origin) to determine optimum weights of mod-



els. The statistics file gives minimum values and their coordinates (energy, sigma) for each of the five models:

model	minimum	Energy	Sigma	maximum
Chi2 L	3.111e-01	12.61	2.00	7.787e+00
LD L	4.384e-01	12.25	6.06	4.698e+00
Chi2 T	1.425e+01	5.72	2.81	2.535e+01
LD T	2.611e+00	12.25	3.22	1.141e+01
comb T	2.153e+01	12.97	3.62	4.741e+01

**Note:** The code automatically uses a linear scale for two-dimensional plots using the minimum and maximum calculated values. It is recommended to decrease the step in the “Linear scale” dialog manually to get a more detailed picture as was shown in Fig.165.

### 1.6.1.1. AA parameters corresponding to EPAX

There was a question: what parameters should be set in the AA model in order for its calculation results to corresponded to EPAX calculations for different combinations of primary beam and production target?

In order to conduct this analysis using the new utility it is necessary to do the following steps:

- ❑ Set a very thin target thickness;
- ❑ Set the EPAX2.15 parameterization as the model for fragmentation production cross-sections in the “Production mechanism” dialog;
- ❑ Calculate reduced cross-sections and save them in a user CS file (extension \*.cs2) using the “Secondary reactions” dialog;
- ❑ Load the obtained file into the operating memory through the “User CS file” dialog;
- ❑ Open the “User cross-sections analysis using Abrasion-Ablation model” (see Fig.163) dialog and begin the analysis.

**Table 23.** AA parameters obtained to match EPAX results for different projectile & beam combinations.

Beam	Target	$E_x \pm d(E_x)$	$\sigma_{Ex} \pm d(\sigma)$	Minimum prefragment mass	Local line and limit for calculations	Minimum mass corresponding to local line	Special case
<sup>124</sup> Sn	Be	25.9 <sup>2.6</sup>	13.5 <sup>3.4</sup>	101	Z = Zb-4 = 46	91	✓
<sup>112</sup> Sn	Be	12.3 <sup>1.6</sup>	7.4 <sup>1.4</sup>	90	Z = Zb-4 = 46	91	
<sup>112</sup> Sn	Ta	11.8 <sup>1.0</sup>	7.4 <sup>0.9</sup>	4	Z = Zb-4 = 46	91	
<sup>86</sup> Kr	Be	19.7 <sup>0.7</sup>	10.0 <sup>1.8</sup>	66	Z = Zb-6 = 30	55	✓
<sup>86</sup> Kr	Be	17.9 <sup>0.6</sup>	13.0 <sup>0.6</sup>	66	Z = Zb-2 = 34	64	
<sup>86</sup> Kr	Ta	20.6 <sup>3.1</sup>	10.8 <sup>2.9</sup>	1	Z = Zb-6 = 30	55	
<sup>78</sup> Kr	Be	14.2 <sup>0.7</sup>	9.8 <sup>1.2</sup>	58	Z = Zb-6 = 30	55	
<sup>78</sup> Kr	Ta	12.4 <sup>1.3</sup>	8.6 <sup>1.2</sup>	1	Z = Zb-6 = 30	55	
<sup>64</sup> Ni	Be	11.6 <sup>1.2</sup>	7.0 <sup>1.3</sup>	45	Z = Zb-6 = 22	39	
<sup>58</sup> Ni	Be	11.7 <sup>1.2</sup>	6.0 <sup>1.3</sup>	39	Z = Zb-6 = 22	39	
<sup>48</sup> Ca	Be	13.2 <sup>1.4</sup>	9.3 <sup>1.0</sup>	30	Z = Zb-6 = 14	22	
<sup>48</sup> Ca	Be	10.2 <sup>1.5</sup>	10.3 <sup>1.3</sup>	30	Z = Zb-2 = 18	31	
<sup>40</sup> Ca	Be	9.7 <sup>1.1</sup>	4.4 <sup>1.7</sup>	23	Z = Zb-6 = 14	22	
<sup>40</sup> Ar	Be	6.1 <sup>1.5</sup>	3.3 <sup>1.9</sup>	23	Z = Zb-6 = 12	20	
<sup>36</sup> Ar	Be	8.9 <sup>0.7</sup>	4.8 <sup>1.7</sup>	19	Z = Zb-6 = 12	20	

AA parameters obtained to match EPAX results for  $^{36,40}\text{Ar}$ ,  $^{40,48}\text{Ca}$ ,  $^{58,64}\text{Ni}$ ,  $^{78,86}\text{Kr}$ ,  $^{112,124}\text{Sn}$  projectiles on Be and Ta targets are shown in Table 23.

The following options and parameters of the AA model were kept in the analysis:

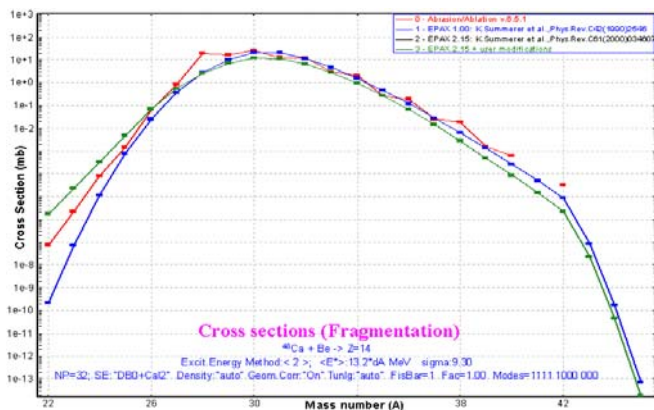
Dimension of evaporation:	32	Geom. corrections:	No
Decay Modes:	1n,2n,1p,2p, $\alpha$	BarFac:	1
State density:	C	Masses:	Database0 + LDM2
Take into account unbound nuclei:	Yes	Excitation energy:	Method "C" without LISE geometrical corrections

The parameters of User CS matching by the AA model were used:

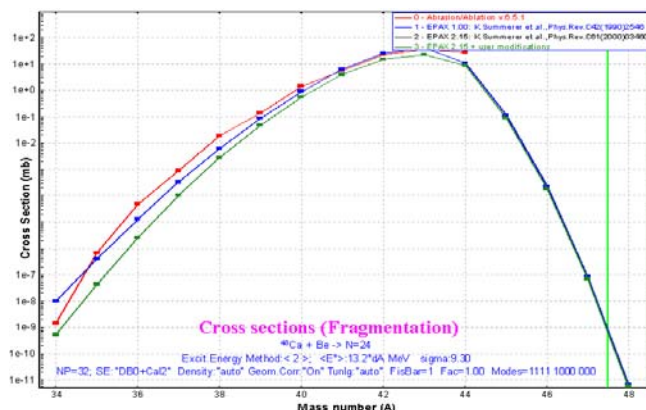
Excitation energy ( $E_x$ ):	5-35 MeV, 70 points	Weights:	1,2,3,6
Sigma of $E_x$ distribution	2-25 MeV, 70 points	Corrections for the number of data points:	Yes
Local line to analyze	Z=Zb-6 (*)	Calculate down to Z	Zb-6 (*)

\* where Zb is the atomic number of the projectile. There are several combinations where Z=Zb-4 and Zb-2 were used for the analysis (Table 23).

Fig.166 and Fig.167 show calculated cross-sections of Silicon isotopes and isotones N=24 produced in  $^{48}\text{Ca}$  fragmentation on a Be target. Parameters  $E_x=13.2$  and  $\sigma=9.3$ , according to Table 23, were used for AA calculations. Fig.168 shows four combined plots resultant from matching AA and EPAX calculations for reactions  $^{64}\text{Ni}+\text{Be}$ ,  $^{124}\text{Sn}+\text{Be}$ ,  $^{112}\text{Sn}+\text{Be}$ , Ta. Fit by double gaussian function was used to define  $E_x$  and  $\sigma$  positions as well as to obtain their standard deviations.



**Fig.166.** Calculated cross-sections of Silicon isotopes produced in  $^{48}\text{Ca}$  fragmentation on a Be target. Parameters  $E_x=13.2$  and  $\sigma=9.3$ , according to Table 23, were used for AA calculations.



**Fig.167.** Calculated cross-sections of isotones N=24 produced in  $^{48}\text{Ca}$  fragmentation on a Be target. Parameters  $E_x=13.2$  and  $\sigma=9.3$ , according to Table 23, were used for AA calculations.

The “Minimum prefragment mass” column represents the minimum mass of excited prefragment which can be obtained from the projectile due to abrasion by the target nucleus.

The special case mark shows cases when the minimum of prefragment mass number is more than 7 units greater than the minimum mass number corresponding to the local line. These cases correspond to light (Be) target and neutron-rich beams ( $^{48}\text{Ca}$ ,  $^{86}\text{Kr}$ ,  $^{124}\text{Sn}$ ). For these cases the AA model (peripheral process) is not valid, because it is impossible to reproduce light masses without additional LISE geometrical corrections or a significant increase of the excitation energy to reproduce EPAX calculations. For example the INC (central collisions) model should be used to describe these data.

Data shown in Table 23 are plotted in Fig.169 as excitation energy versus width of excitation energy distribution and in Fig.170 as excitation energy as a function of projectile element number. From these figures it is possible to select out two data sets, “Regular” and “Neutron-rich”.

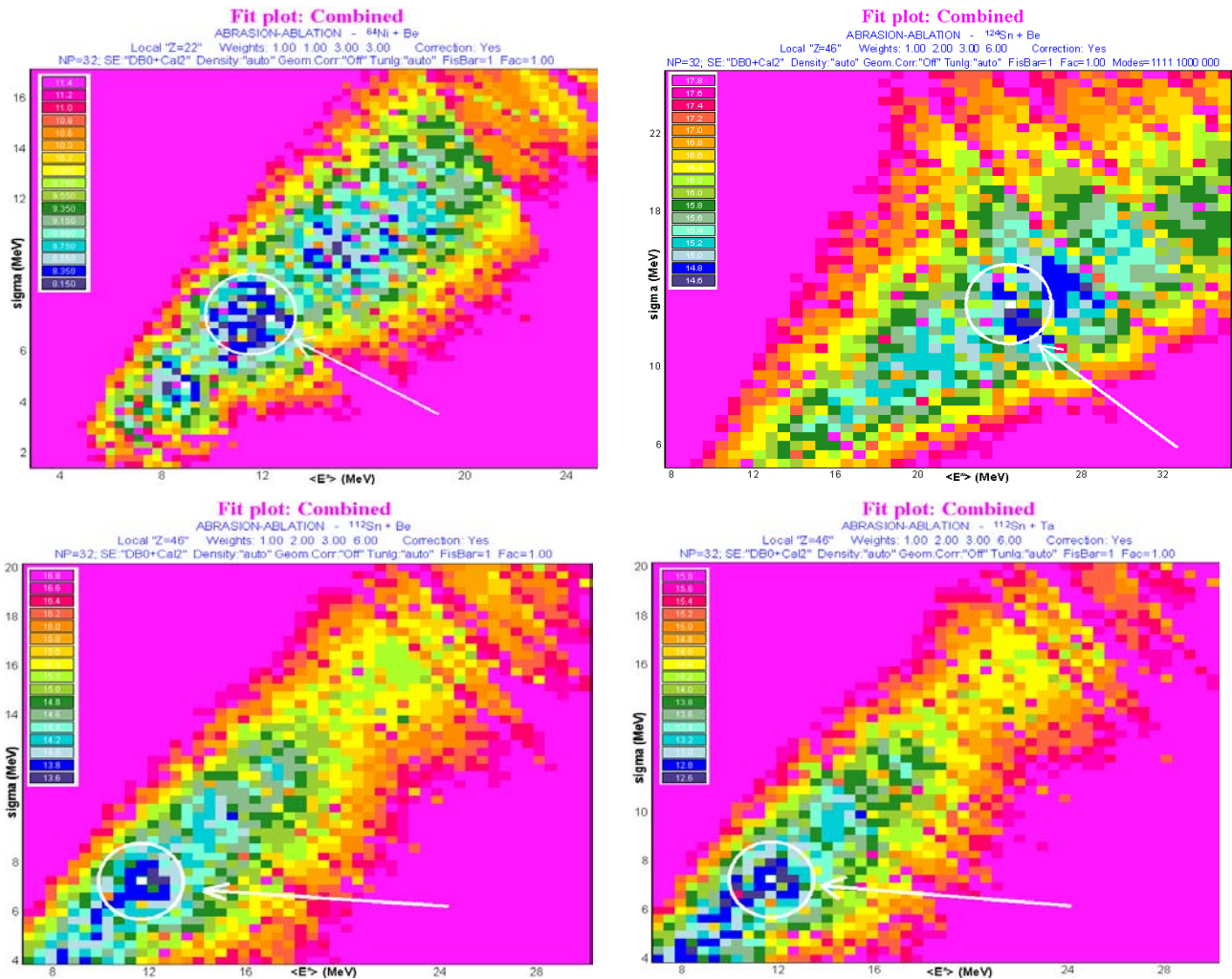
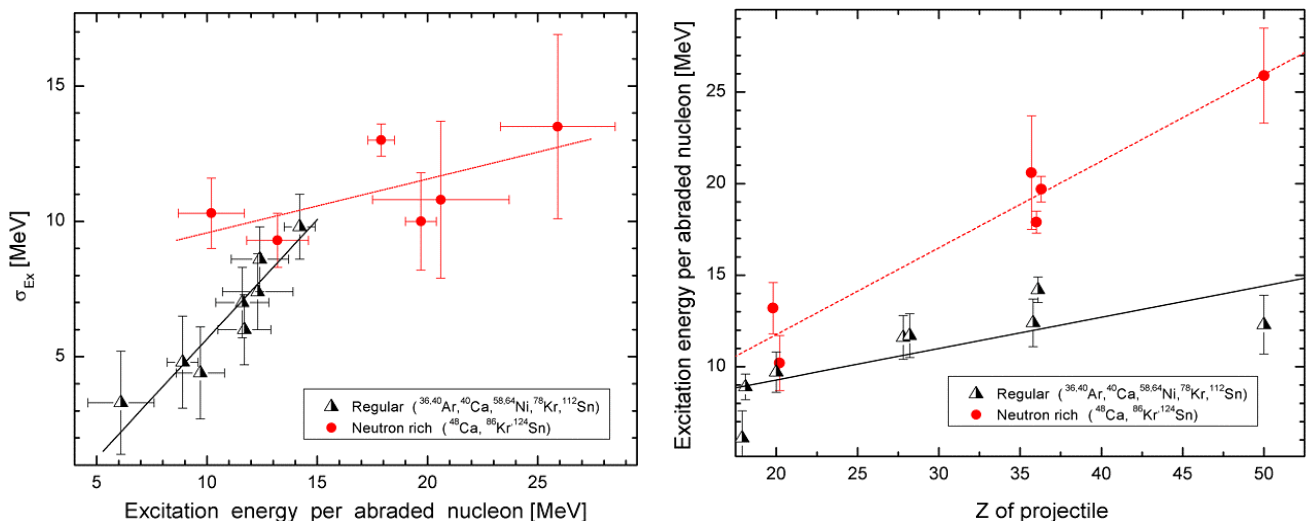


Fig.168. The Combined plots resultant from matching AA and EPAX calculations for reactions  $^{64}\text{Ni} + \text{Be}$  (left top plot),  $^{124}\text{Sn} + \text{Be}$  (right top plot),  $^{112}\text{Sn} + \text{Be}$  (left bottom plot), and  $^{112}\text{Sn} + \text{Ta}$  (right bottom plot). White circles show approximately the data regions which were fitted by the double gaussian function.



**Fig.169.** Widths versus mean values of excitation energy from distributions from Table 23 obtained by matching EPAX values with the AA model.

**Fig.170.** Excitation energies per abraded nucleon from Table 23 versus projectile element number obtained by matching EPAX values with the AA model.

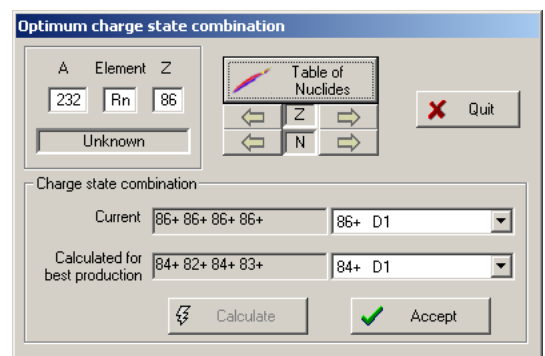
Black solid and dashed red lines are linear fits of “regular” and “neutron rich” datasets respectively. Fit parameters are shown in Table 24.

**Table 24.** Results of the linear fit ( $Y = A*X + B$ ) of data sets in Fig.169 and Fig.170.

Plot	Data set	A Slope value	dA standard error	B Intercept value	dB standard error	R Correlation coefficient	SD Standard deviation of the fit
Fig.169	Neutron rich	0.474	0.059	2.289	2.050	0.97	1.52
Fig.169	Regular	0.171	0.061	5.861	1.903	0.75	1.80
Fig.170	Neutron rich	0.199	0.116	7.585	2.157	0.65	1.45
Fig.170	Regular	0.817	0.126	-2.458	1.404	0.94	0.84

### 1.6.2. Optimum charge state combination

To which charge state combination is it necessary to set the spectrometer to produce the maximum fragment rate at the end of the spectrometer? In order to find a solution the user must determine the average ion charge state of the fragment after each “material & dispersive block” combination (for example blocks “Target” and “Dipole D1”). Try to find a combination for the example file “charge\_state\_optimum.lpp” (the file can be found in [http://groups.nsl.msui.edu/lise/7\\_5/examples/](http://groups.nsl.msui.edu/lise/7_5/examples/)). This example was made especially so that before each of four dipoles the setting fragment passes through materials with different atomic number.



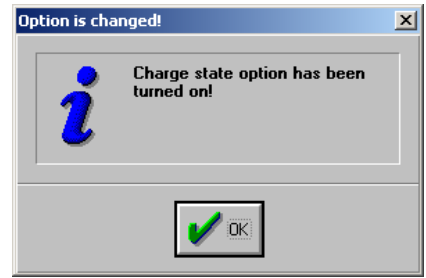
**Fig.171.** The “Optimum charge state combination” dialog (from the “Calculations” menu). Calculations were done for the example file “charge\_state\_optimum.lpp”.

The new utility “Optimum charge state combination” (see Fig.171), which can help to the user to solve this problem, has been incorporated into the code and is available in the “Calculations” menu. This utility is especially relevant for calculation of optimum target thickness, because the charge state combination is a function of target thickness. In the next chapters we will demonstrate the capabilities of the new utility for other utilities.

After loading the dialog it is necessary to choose the isotope of interest and click the “Calculate” button. How does the code look for the best combination?

1. It saves all settings of optical blocks;
2. The charge state option is turned on (if initially it was turned off);
3. The code sorts out all possible charge state combinations. The spectrometer is tuned for each combination;
4. The program finds a charge state combination giving maximum output and displays the result in the dialog (see Fig.171).

If the user clicks the “Cancel” button then all previous settings are restored. To set the new settings based on these calculations it is necessary to click the “Accept” button. If the user has decided to accept these values, and the charge state option was initially turned off in the program, the program remains in the “charge state on” mode, and the user receives a message on it (see Fig.172).



*Fig.172.*

### 1.6.3. Charge state combination calculation for the optimal target thickness utility

The utility to determine the optimum charge state combination (see the previous chapter) has been incorporated into the subroutine for optimal target thickness calculations. In order to use this option the user has to select the corresponding checkbox in the “Choose fragment” dialog of the optimal target thickness utility (see Fig.173).

We will demonstrate this new possibility using the example “optimum\_target\_and\_charge\_states.lpp” (the file can be found in [http://groups.nsl.msu.edu/lise/7\\_5/examples/](http://groups.nsl.msu.edu/lise/7_5/examples/)).

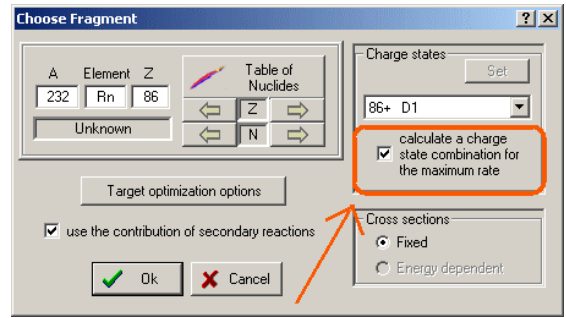


Fig.173. The “Choose fragment” dialog for the optimal target thickness utility.

Why do we need this utility? Suppose that we do not know what is the best charge state combination to get the maximum rate, and we take the fully stripped fragment because the target is “light” (Lithium) and the primary beam energy is high enough (400MeV/u). Running the optimal target thickness utility in the regular mode we get that the optimum thickness is about 600 mg/cm<sup>2</sup> (see Fig.174). We expect only about 20 events per second of the setting fragment for the given charge state combination.

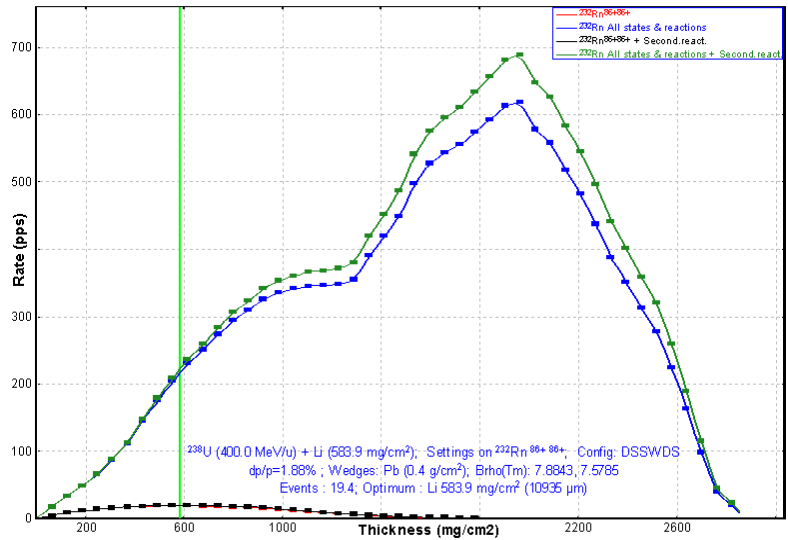


Fig.174. Rate of <sup>232</sup>Rn ions as a function of the target thickness. The spectrometer was tuned on the <sup>232</sup>Rn<sup>86+86+</sup> ion.

Determination of the optimal target thickness with searching the charge state combinations consists of three steps.

**First step:** Calculation of target thickness without charge states (see Fig.175). Usually the code uses the dependence of fragment rate on target thickness to define the optimum thickness; in this case the fragment rate is decreased by the standard deviation ( $\sigma_{\text{charge}}$ ) of the charge state distribution, which is calculated for various average fragment energies after the target (stripper). If  $\sigma_{\text{charge}}$  is less 0.5 then the value 0.5 is used instead  $\sigma_{\text{charge}}$ .

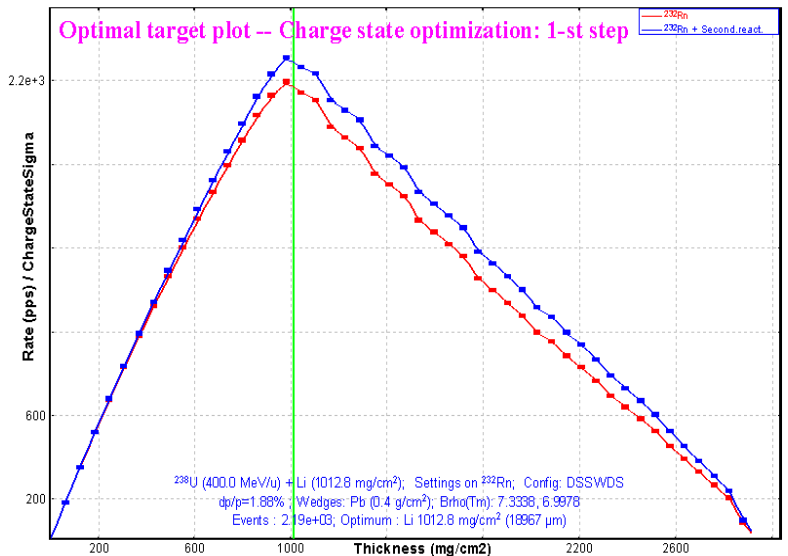


Fig.175. Optimal target thickness & Charge state optimization. Step 1: calculation of reduced fragment yield without charge states.

**Second step:** The program calculates an optimum charge state combination for the target thickness (1.01 g/cm<sup>2</sup>) obtained on the first step. Using the “2nd step optimization” dialog (see Fig.176) the user can click one of the following buttons:

- ❑ Cancel: leave the dialog and restore previous settings;
- ❑ Accept: accept the charge state combination (afterwards, leave the dialog or continue calculations);
- ❑ 3<sup>rd</sup> step: Accept the charge state combination and repeat optimum target calculations.

If no option is selected within 5 seconds, then the program automatically starts the third step of calculations.

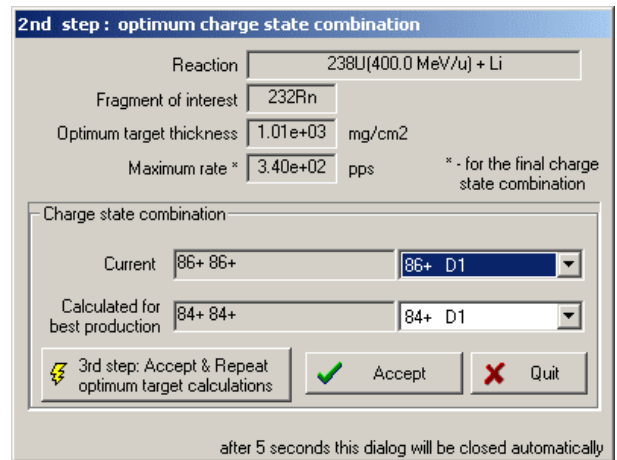
**Third step:** The program calculates an optimum target thickness for the charge state combination (84+ 84+) obtained on the second step. The final thickness is equal to 1.285 g/cm<sup>2</sup>, which corresponds to 342 events per second of the <sup>232</sup>Rn<sup>84+84+</sup> ions without secondary reactions contribution (see Fig.177).

Actually the yield difference for thicknesses 1.01 and 1.28 g/cm<sup>2</sup> obtained respectively on the first and third steps is insignificant (see Fig.177), and moreover if we take the sum of all charge states then the value 1.1g/cm<sup>2</sup> is preferable. Due to this fact the user can skip the third step, using only the first two steps as was done for the “Rate & transmission calculation batch mode” utility (see the next chapter).

### 1.6.3.1. Target optimization options

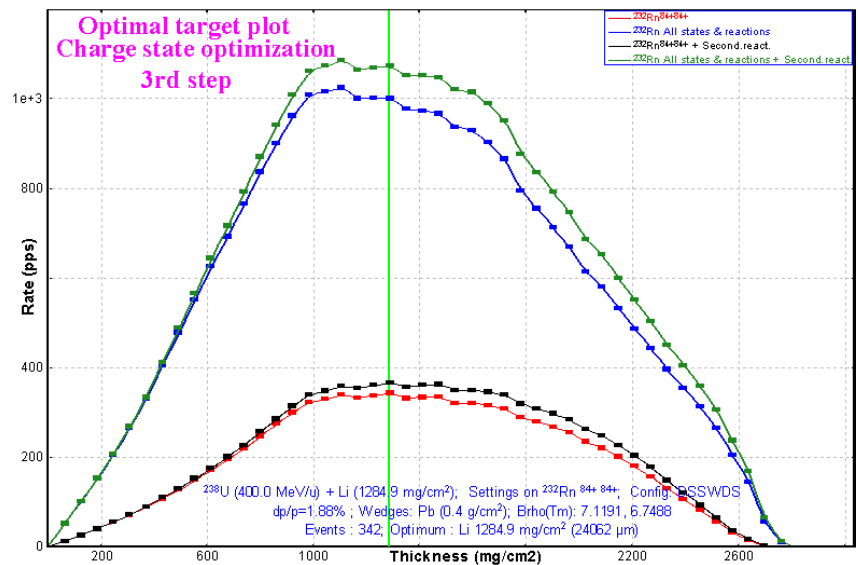
Several items connected with target optimization were moved from the “Preferences” dialog (the “Options” menu) into the new “Target optimization options” dialog (see Fig.178). This dialog is available in a few different places:

- ❑ The “Preferences” dialog (menu “Options”);
- ❑ The “Choose nucleus for Target optimization” dialog (see Fig.173) (menu “Calculations”);
- ❑ The “Rate & transmission calculation: batch mode” dialog (see Fig.180) (menu “Utilities”).



**Fig.176.** Optimal target thickness & Charge state optimization.

Step 2: calculation of optimum charge state combination for the target thickness obtained on the first step.



**Fig.177.** Optimal target thickness & Charge state optimization.

Step 3: calculation of fragment yield with charge states combination obtained on the second step.

The new parameter “Method to search optimal target” has been incorporated into the code and can be changed in the “Target optimization options” dialog. The next chapter is devoted to this new parameter.

### 1.6.3.2. Optimal target searching methods

The plot of calculated yields as a function of target thickness is the result of the target optimization process. This plot contains four curves when taking into account secondary reactions’ contributions in yield calculations. The new version allows the user to choose what curve will be used to define the optimal target. Fig.179 shows calculated target yields as a function of target thickness. Vertical lines show maximum values of distributions. Depending on the choice of searching mode in the “Target optimization options” dialog (see Fig.178) the final answer can be any one of these four maxima.

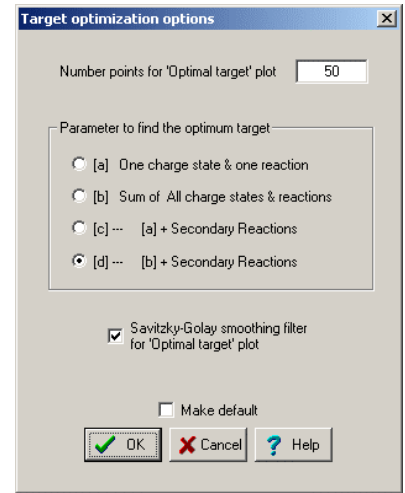


Fig.178. The “Target optimization options” dialog.

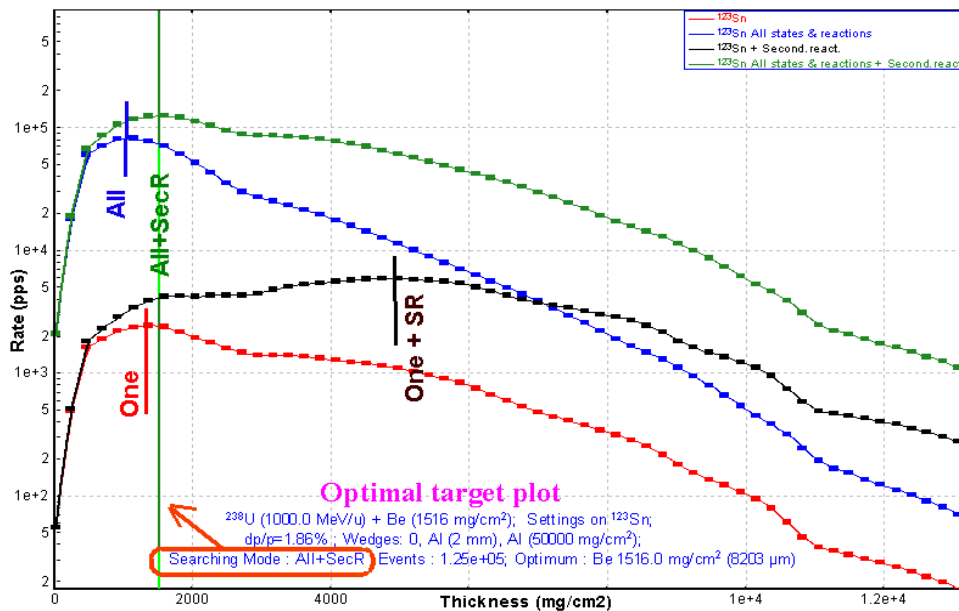


Fig.179. Calculated target yields as a function of target thickness for the production of  $^{123}\text{Sn}$  from fission of a  $^{238}\text{U}$  beam on a Be target. Short vertical lines show the maximum of each of the curves.

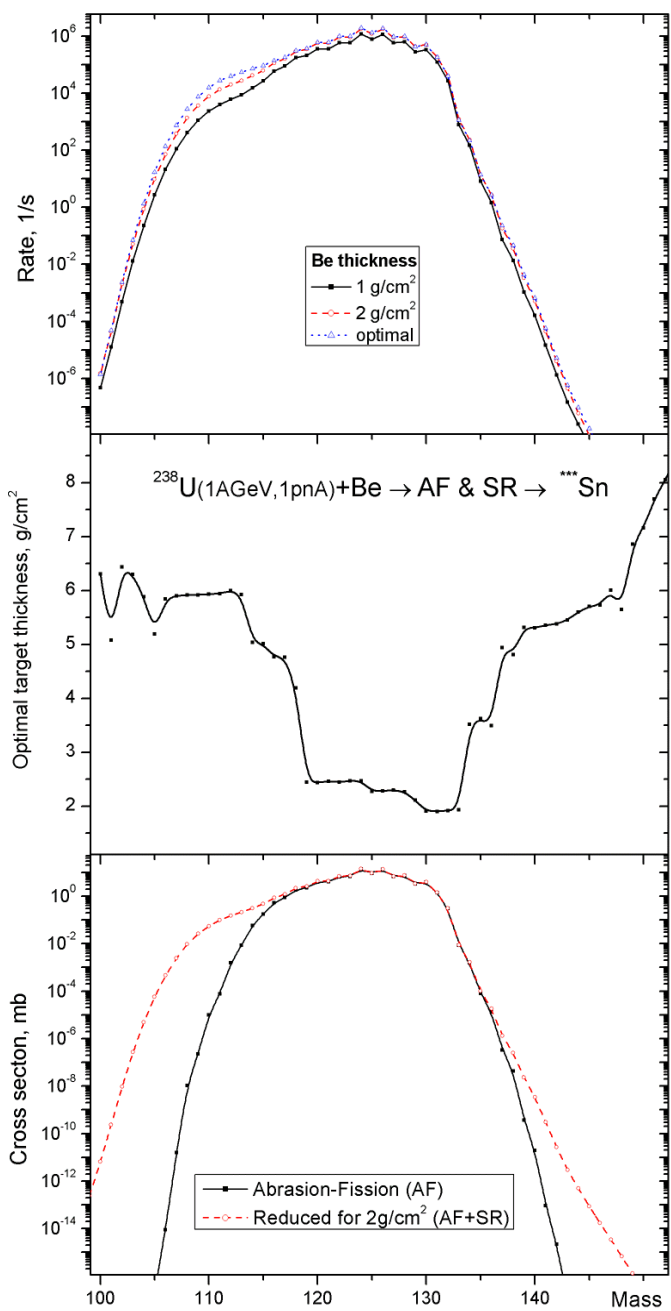
### 1.6.4. Rate & transmission calculation batch mode

The new utility “Rate & transmission batch mode” available via the “Utilities” menu has been incorporated into the code to run a long-term calculation task with different options. Using this utility, the user can obtain a text file with calculated parameters (optimum target thickness, best charge state combination, yield, transmission and secondary reactions contribution coefficients) for each fragment of a nuclide rectangle set in the “Rate & transmission batch mode” dialog (see Fig.180).

Before running the LISE++ code in the batch-mode it is necessary to:

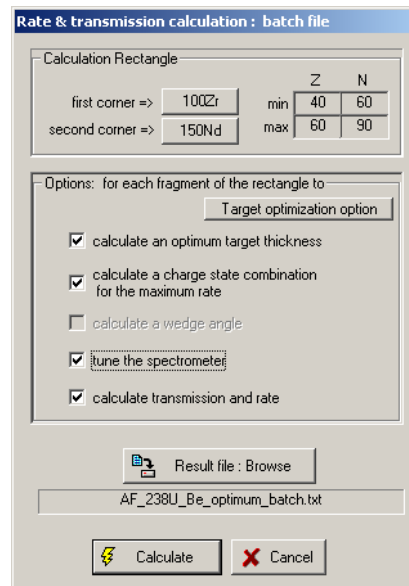
1. set a nuclide rectangle choosing two opposite corners (see the “Calculation rectangle” frame in Fig.180);
2. choose options which will be applied in the calculation process for each fragment of the nuclide rectangle;
3. set the name of the file where information will be saved.





**Fig.181.** Top plot: Calculated rates of Tin isotopes produced in the fission of  $^{238}\text{U}(1\text{AGeV}, 1\text{pnA})$  on a Be-target taking into account secondary reactions' contributions. Calculations were done for target thickness equal to  $1\text{ g/cm}^2$ ,  $2\text{ g/cm}^2$ , and for optimal thickness calculated to obtain the maximum yield of given isotope (see the middle plot).

Bottom plot: Calculated AF and reduced cross-sections (assuming the thickness  $2\text{ g/cm}^2$ ) of Tin isotopes produced in the fission of  $^{238}\text{U}(1\text{AGeV}, 1\text{pnA})$  on a Be-target.



**Fig.180.** The “Rate & transmission calculation: batch mode” dialog.

This new utility allows one to calculate the optimal target thicknesses for a large region of nuclides, which would be tiresome if done manually using the “Optimal target” utility from the “Calculations” menu. Thus using the batch mode utility, the top and middle plots in Fig.181 have been created. An unexpected result was obtained for optimal target thicknesses to produce Tin isotopes in the fission of  $^{238}\text{U}(1\text{AGeV})$  on a Be-target (see the middle plot in Fig.181). For Tin isotopes with masses 119-133 the optimal target thickness is about  $2\text{ g/cm}^2$ , whereas for lighter and heavier isotopes the optimal target becomes considerably thicker. It is possible to explain this by looking at the bottom plot in Fig.181, which shows calculated AF and reduced cross-sections (assuming a thickness  $2\text{ g/cm}^2$ ) of Tin isotopes produced in the fission of  $^{238}\text{U}(1\text{AGeV})$  on a Be-target. The secondary reactions contribution dominates for the proton-rich side from mass about 117, and for the neutron-rich side from the mass about 135. If production of isotopes happens mostly from secondary reactions' contributions, then certainly we need to increase the target thickness, whereas increasing target thickness in the case of masses 119-133 leads to decreasing transmission. The example file

“[AF 238U Be batch mode for Tin isotopes.lpp](#)” was used to prepare the plots in Fig.181.

### 1.6.5. Target and wedge optimization

The utility to determinate the optimum target and wedge combination has been incorporated into the new version. The user defines himself what is more important to him in the final result: intensity or purity through the use of weights. The utility is available in the “Calculations” menu.

Firstly, the user has to choose a fragment of interest as well as turning on/off the “charge state optimization” and “Secondary reactions contribution” options using the dialog shown in Fig.173.

The second step is setting the optimization process parameters in the “Target & wedge optimization” dialog (see Fig.182).

The “**Keep value**” combobox is initially set to “no keep value”. This means that settings of all optical blocks can be recalculated to provide the maximum transmission of the setting fragment. The user can choose to keep an optical dispersive block value for the transmission calculations. In this case other optical blocks settings will be recalculated for the setting fragment based on this kept value.

*Note:* If the “calculate the charge state combination” option has been turned on in the first step, then the “Keep value” combobox won’t be available.

The “**Wedge block**” combobox allows the user to select a wedge block whose thickness will be modified in the optimization process. The combobox is initially assigned to the enabled wedge block, which is the first one in the spectrometer line. If there are no enabled wedge blocks then this combobox is not available and neither are wedge thickness cells.

Target and wedge thickness ranges as well as number of thickness sets can be defined in the “**Material thickness**” block. The product of target and wedge set numbers defines how many times the code will change the spectrometer settings: target and wedge settings, and subsequent spectrometer tuning for the setting fragment. These changes can be seen in the “Setup” window during the optimization process.

When the user loads the “Target & Wedge optimization” dialog, the code calculates minimum and maximum thickness values automatically in the following way: the code calculates setting fragment and projectile ranges in the target in both cases suggesting an energy of the primary beam when taking into account the stripper thickness. The maximum range value ( $R_{max}$ ) is used to define minimum (5% of  $R_{max}$ ) and maximum (80% of  $R_{max}$ ) thickness for the optimization process. The wedge material is used instead of the target material to define the maximum range by the same way as was done for the target, but minimum and maximum values are defined in this case as (1% of  $R_{max}$ ) and (70% of  $R_{max}$ ) respectively. If you want to recalculate material range values manually at the next dialog loading then press the “**Calculate Max & Min values**” button.

The “Isotope Rectangle for calculations” allows one to define how many nuclei  $N_{isotopes} = (2 \cdot dP + 1) \cdot (2 \cdot dN + 1)$  surrounding the fragment of interest will be included in transmission calculations. We define the **purity** value as equal to the ratio of the intensity of the setting fragment to the sum of all calculated isotope yields:

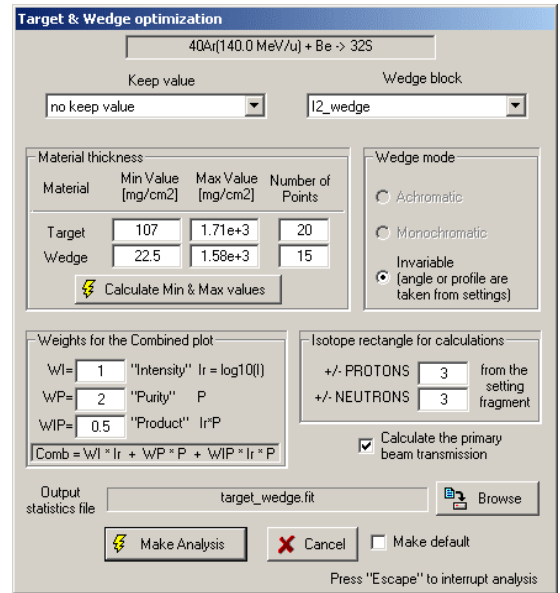
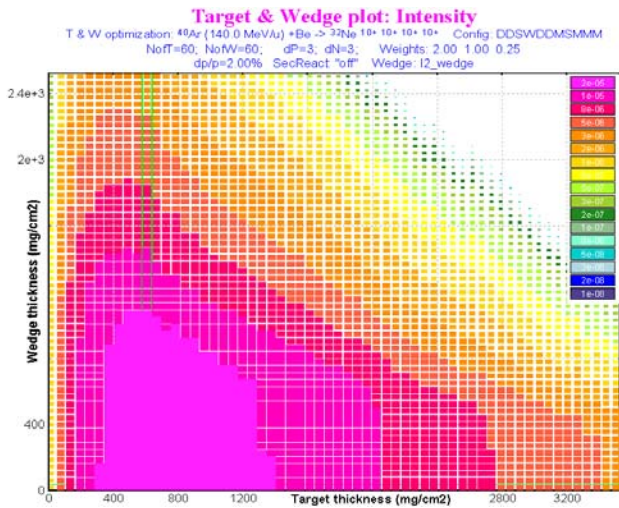


Fig.182. The “Target & Wedge optimization” dialog.

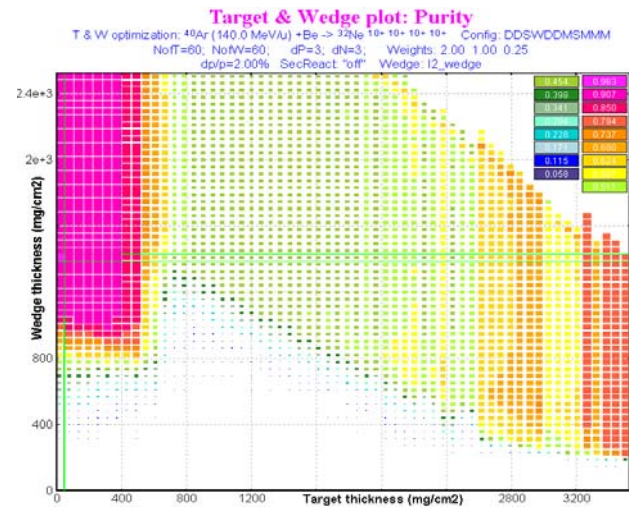
$$Purity(Z, N) = \frac{Rate(Z, N)}{Rate(Z_{beam}, N_{beam}) + \sum_{i=Z-dP}^{Z+dP} \sum_{k=N-dN}^{N+dN} Rate(i, k)} \quad /17/$$

A large area for the “Isotope rectangle” leads to more precise calculation of the purity value, but obviously takes more time. It is also recommended to calculate the primary beam transmission. This option is turned on by default.

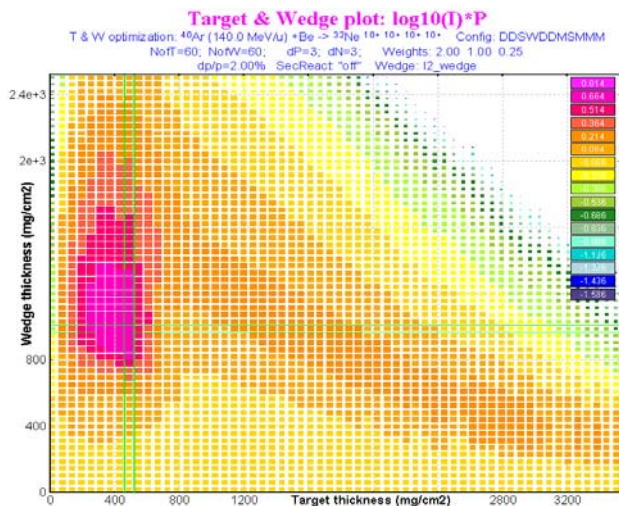
After the user has defined the optimization parameters, the optimization process is started by clicking the “Make analysis” button. The optimization process can be canceled by pressing “Escape”. The information window shows approximately how much time is remaining (similar to Fig.164).



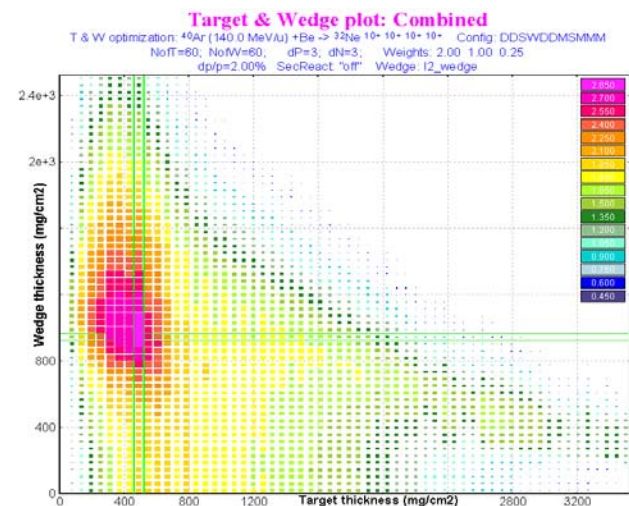
**Fig.183.** The “Target & Wedge *Intensity*” plot for  $^{32}\text{Ne}$  isotopes produced in  $^{40}\text{Ar}(140\text{MeV})+\text{Be}$  and selected by the A1900 spectrometer with 2% momentum acceptance.



**Fig.184.** The “Target & Wedge *Purity*” plot for  $^{32}\text{Ne}$  isotopes produced in  $^{40}\text{Ar}(140\text{MeV})+\text{Be}$ . The “Isotope rectangle” values were set to  $dP=3$  and  $dN=3$ .



**Fig.185.** The “Target & Wedge *IP*” plot for the same optimization process as in Fig.183 and Fig.184.



**Fig.186.** The “Target & Wedge *Combined*” plot. Weights are equal to 2, 1.5, 0.25 for Ir, P, and IP values.

Four plots (Intensity, Purity, IP, Combined) and one text file (the filename can be changed by the user using the “Browse” button) will be created and displayed for the user as a result of the optimization.

The 1<sup>st</sup> plot “**Intensity**” shows the calculated  $Rate(Z, N)$  value from target and wedge thicknesses (Fig.183). The 2<sup>nd</sup> plot “**Purity**” (Fig.184) show calculated  $Purity(Z, N)$  values according to Eq./17/.

The program calculates 4 reduced values (*Ir*, *P*, *IP*, *Combined*) based on these two plots.

**Ir** : intensity normalized reduced value. First we calculate the array of reduced values  $I_{it,iw} = \log_{10} [\text{Rate}(t_{ib}, w_{iw})]$ , where *t* is the target thickness value, *w* is the wedge thickness,  $it=1,2..N_{target}$ ,  $iw=1,2..N_{wedge}$ . The next step is normalization  $Ir_{it,iw} = I_{it,iw} / \max(I)$ .

**P** : purity normalized value  $P_{it,iw} = \text{purity}_{it,iw} / \max(\text{purity})$ .

**IP**: product of **Ir** and **P** values. As the product of two normalized values, any **IP** array element cannot be more than 1. The **IP** value plot is the third optimization result plot (see Fig.185).

**Combined** : sum of products **Ir**, **P** and **IP** values with their weights (*WI*, *WP*, *WIP*):

$$\text{Combined} = Ir \cdot WI + P \cdot WP + IP \cdot WIP, \quad /18/$$

where weight values should be defined by the user in the “Target & wedge optimization” dialog (see Fig.182) before optimization. The **Combined** value plot is the fourth optimization result plot (see Fig.186). Combined values cannot be more than the sum of weights (*WI*, *WP*, *WIP*).

The green horizontal and vertical lines on plots show the maximum value included in this plot.

The text file contains information about calculated intensity, purity and all reduced values for each target & wedge combination used in the optimization process (see Fig.187). Information about a maximum value for each plot and their location (target and wedge thicknesses) are shown at the bottom of this file (see Table 25 and Table 26). This output statistics file can be used by other programs (for example Excel or Origin) for subsequent analysis.

N	Target	Wedge	Rate	Purity	RateN	PurityN	IP_N	Combined
0	1.000e+01	1.000e+01	4.587e-01	1.015e-01	-5.671e-01	1.015e-01	-5.758e-02	-2.917e-01
1	1.000e+01	1.426e+02	4.538e-01	1.313e-01	-5.718e-01	1.313e-01	-7.506e-02	-2.151e-01
2	1.000e+01	2.753e+02	4.518e-01	2.782e-01	-5.737e-01	2.782e-01	-1.596e-01	1.811e-01
3	1.000e+01	4.079e+02	4.397e-01	4.182e-01	-5.855e-01	4.182e-01	-2.449e-01	5.467e-01
4	1.000e+01	5.405e+02	4.348e-01	5.860e-01	-5.904e-01	5.861e-01	-3.460e-01	9.949e-01
5	1.000e+01	6.732e+02	4.271e-01	8.040e-01	-5.981e-01	8.041e-01	-4.809e-01	1.574e-01
6	1.000e+01	8.058e+02	4.139e-01	9.280e-01	-6.055e-01	9.281e-01	-5.619e-01	1.898e-01
7	1.000e+01	9.384e+02	4.132e-01	9.795e-01	-6.125e-01	9.796e-01	-6.000e-01	2.026e-01
8	1.000e+01	1.071e+03	4.073e-01	9.961e-01	-6.187e-01	9.962e-01	-6.163e-01	2.062e-01
9	1.000e+01	1.204e+03	3.911e-01	9.992e-01	-6.363e-01	9.993e-01	-6.359e-01	2.044e-01
10	1.000e+01	1.336e+03	3.611e-01	9.997e-01	-6.710e-01	9.998e-01	-6.708e-01	1.993e-01
11	1.000e+01	1.469e+03	3.170e-01	9.997e-01	-7.275e-01	9.998e-01	-7.274e-01	1.908e-01
12	1.000e+01	1.602e+03	2.733e-01	9.997e-01	-7.920e-01	9.998e-01	-7.918e-01	1.812e-01
13	1.000e+01	1.734e+03	2.341e-01	9.997e-01	-8.592e-01	9.998e-01	-8.590e-01	1.711e-01
14	1.000e+01	1.867e+03	1.994e-01	9.997e-01	-9.290e-01	9.998e-01	-9.288e-01	1.606e-01
15	1.000e+01	1.999e+03	1.700e-01	9.997e-01	-9.982e-01	9.998e-01	-9.980e-01	1.502e-01
16	1.000e+01	2.132e+03	1.445e-01	9.997e-01	-1.069e+00	9.998e-01	-1.069e+00	1.396e-01
17	1.000e+01	2.265e+03	1.231e-01	9.997e-01	-1.138e+00	9.998e-01	-1.138e+00	1.292e-01
18	1.000e+01	2.397e+03	1.042e-01	9.997e-01	-1.211e+00	9.998e-01	-1.211e+00	1.183e-01
19	1.000e+01	2.530e+03	8.752e-02	9.997e-01	-1.287e+00	9.998e-01	-1.286e+00	1.070e-01
20	1.616e+02	1.000e+01	7.070e+00	9.506e-02	6.208e-01	9.507e-02	5.902e-02	9.355e-01
21	1.616e+02	1.426e+02	6.992e+00	1.352e-01	6.160e-01	1.352e-01	8.328e-02	1.063e-01
22	1.616e+02	2.753e+02	6.806e+00	2.963e-01	6.042e-01	2.964e-01	1.791e-01	1.583e-01
23	1.616e+02	4.079e+02	6.784e+00	4.300e-01	6.028e-01	4.300e-01	2.592e-01	2.022e-01

**Fig.187.** LISE window showing the output statistics file containing the optimization process protocol and statistics information.

**Table 25.** Maximum values for each plot (Fig.183, Fig.184, Fig.185, Fig.186) and their location (target and wedge thicknesses). All this information is kept at the bottom of the output statistics file (see Fig.187).

Plot	Maximum value	Target (mg/cm <sup>2</sup> )	Wedge (mg/cm <sup>2</sup> )
Intensity	<b>2.726e-05</b>	6.098e+02	2.000e+01
Purity	<b>9.633e-01</b>	2.000e+01	1.407e+03
IP	<b>7.974e-01</b>	4.919e+02	9.868e+02
Combined	<b>2.896e+00</b>	4.919e+02	9.447e+02

**Table 26.** Intensity, Purity, and IP values corresponding to target and wedge thickness values when the Combined value reaches the maximum.

Model	Combined
Intensity	<b>2.260e-05</b>
Purity	<b>8.295e-01</b>
IP	<b>7.911e-01</b>

**Recommendations:**

Before the optimization process it is recommended to set wedge angle close to the value which corresponds to the optimal wedge thickness value (or use curved profile degrader – the best choice!)

Set “wedge selection” slits (I4 for A1900 for example) to a value corresponding to 95% of the wedge selection transmission for the optimal target and wedge combination.

If you do not know at least approximately these values then run the optimization process twice:

- run the first time with small  $N_{target}$  and  $N_{wedge}$ ,

- then set wedge angle and slits using calculated target and wedge combination using the combined plot,
- increase  $N_{target}$  and  $N_{wedge}$ ,
- narrow the target and wedge thickness regions around the expected location of the optimum combination,
- run the optimization process again.

### 1.6.5.1. Secondary Reactions contribution option

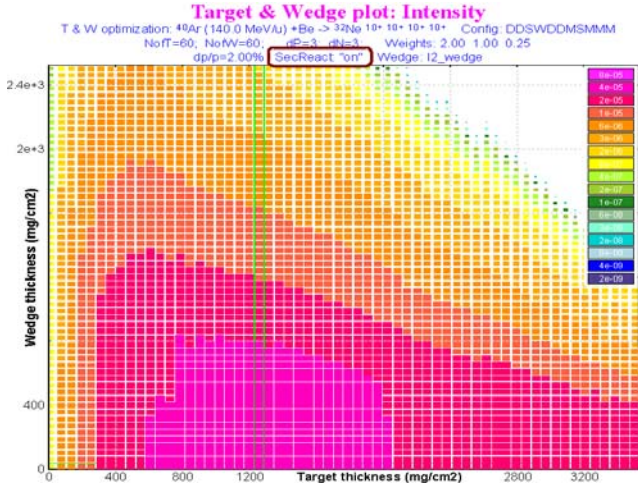


Fig.188. The “Target & Wedge Intensity” plot the same as Fig.183 but with SR contributions.

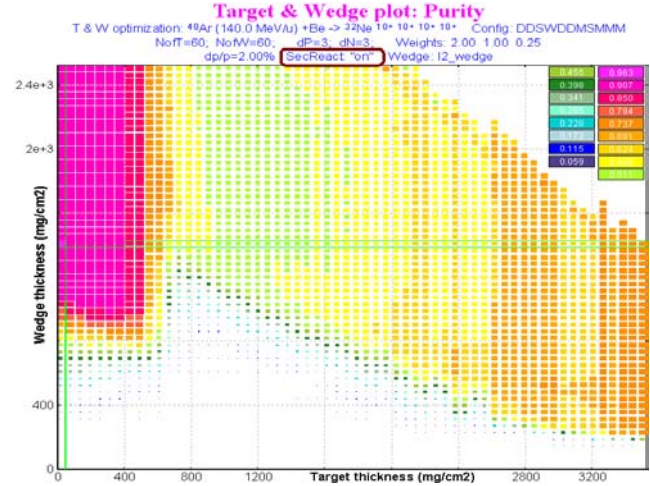


Fig.189. The “Target & Wedge Purity” plot the same as Fig.184 but with SR contributions.

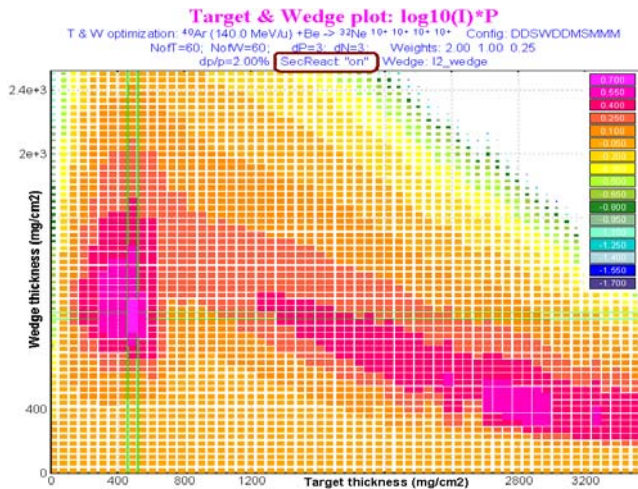


Fig.190. The “Target & Wedge IP” the same as Fig.185 but with SR contributions.

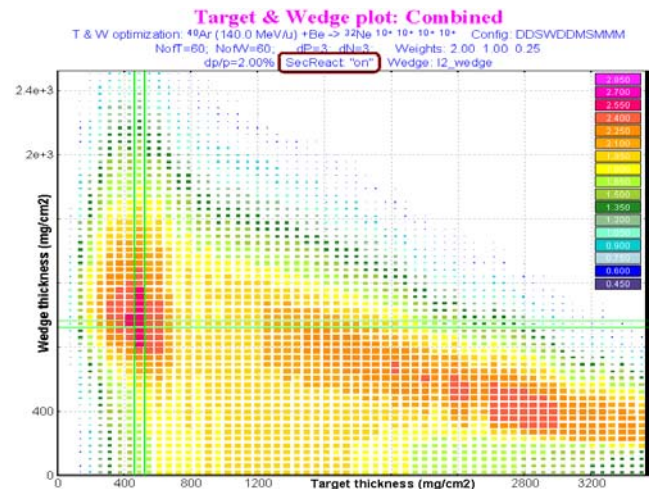


Fig.191. The “Target & Wedge Combined” plot the same as Fig.186 but with SR contributions.

Fig.188-191 show result plots for the same settings which were used in the previous chapter for the  $^{32}\text{Ne}$  optimization process but in this case including the secondary reactions contribution. Compare these plots with Fig.183-186. Statistics information for the optimization process with SR contribution is shown in Table 27 and Table 28. Compare this information with data in Table 25 and Table 26.

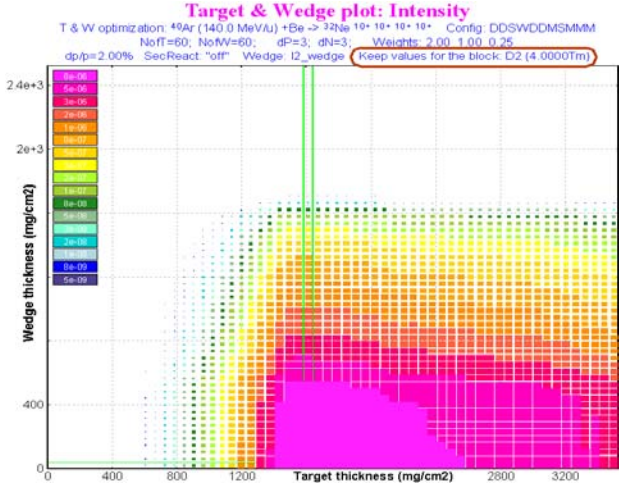
Table 27. Maximum values for each plot (Fig.188-191) and their location (target and wedge thicknesses).

Plot	Maximum value	Target (mg/cm <sup>2</sup> )	Wedge (mg/cm <sup>2</sup> )
Intensity	4.895e-05	1.259e+03	2.000e+01
Purity	9.633e-01	2.000e+01	1.407e+03
IP	7.171e-01	4.919e+02	9.868e+02
Combined	2.686e+00	4.919e+02	9.447e+02

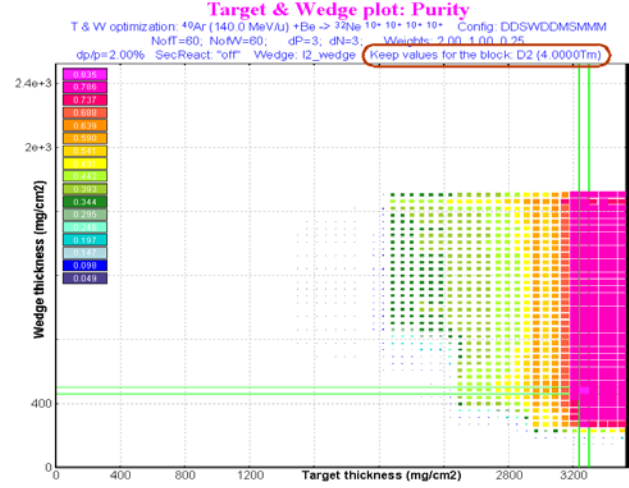
Table 28. Values corresponding to the maximum Combined value.

Model	Combined
Intensity	3.202e-05
Purity	8.433e-01
IP	7.142e-01

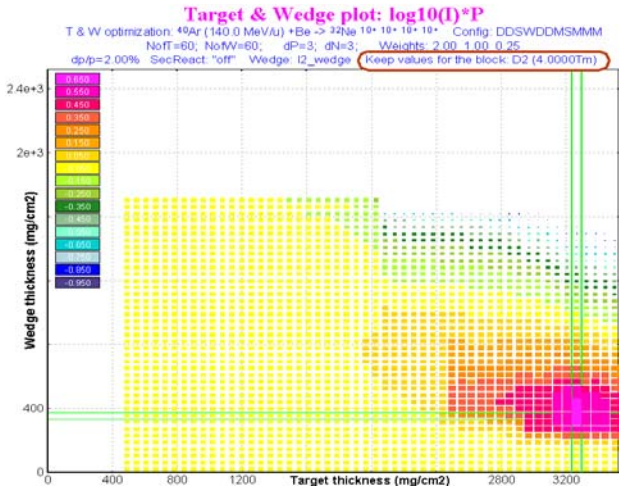
### 1.6.5.2. “Keep value” parameter



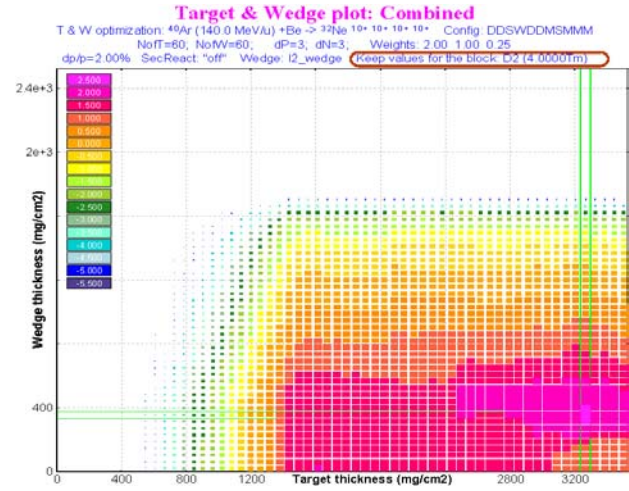
**Fig.192.** The “Target & Wedge *Intensity*” plot the same as Fig.183 but the second dipole value was kept equal to 4.0 Tm.



**Fig.193.** The “Target & Wedge *Purity*” plot the same as Fig.184 but the second dipole value was kept equal to 4.0 Tm.



**Fig.194.** The “Target & Wedge *IP*” the same as Fig.185 but the second dipole value was kept equal to 4.0 Tm.



**Fig.195.** The “Target & Wedge *Combined*” plot the same as Fig.186 but the second dipole value was kept equal to 4.0 Tm.

Fig.192-195 show result plots for the same settings which were used for Fig.183-186 but in this case the second dipole value was kept equal to 4.0 Tm. Compare these plots with Fig.183-186. Statistics information for the optimization process with SR contribution is shown in Table 29 and Table 30. Compare this information with data in Table 25 and Table 26.

**Table 29.** Maximum values for each plot (Fig.192-195) and their location (target and wedge thicknesses).

Plot	Maximum value	Target (mg/cm <sup>2</sup> )	Wedge (mg/cm <sup>2</sup> )
Intensity	1.166e-05	1.613e+03	2.000e+01
Purity	8.353e-01	3.264e+03	4.824e+02
IP	6.669e-01	3.264e+03	3.563e+02
Combined	2.507e+00	3.264e+03	3.563e+02

**Table 30.** Values corresponding to the maximum Combined value.

Model	Combined
Intensity	5.567e-06
Purity	8.205e-01
IP	6.669e-01

**Note:** The “Charge state optimization” and the “keep value” options cannot be used simultaneously in the target & wedge optimization process.

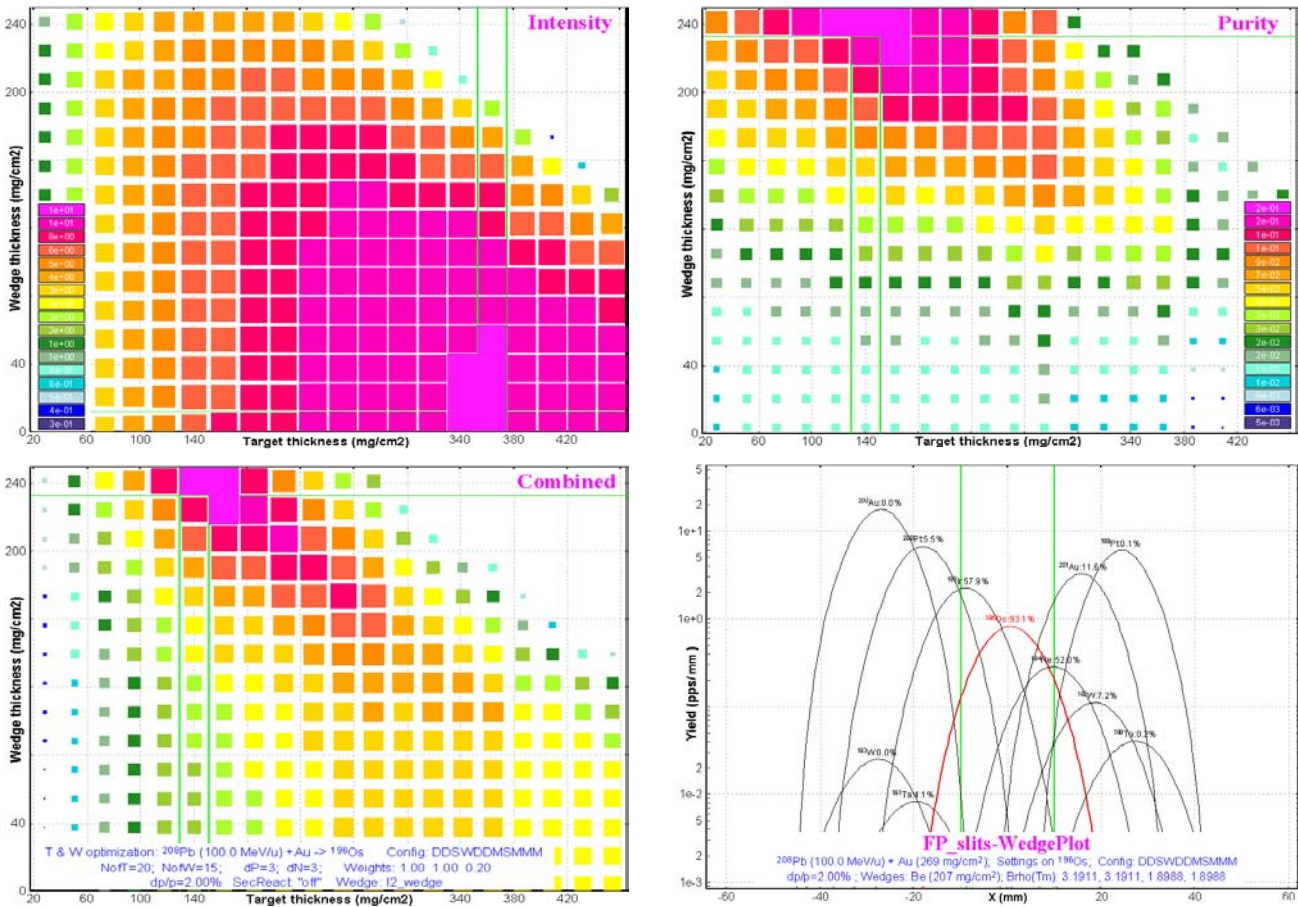
### 1.6.5.3. Target and wedge optimization for charge states

In this chapter we shall calculate the target-wedge combination for the  $^{208}\text{Pb}$  (100 MeV/u) + Au  $\rightarrow$   $^{196}\text{Os}$  reaction considering three different situation:

- without charge states;
- the separator is tuned to only one charge state combination (fully stripped);
- with spectrometer tuned to the charge state combination giving maximum yield of the setting fragment.

Now we shall analyze all three cases. The A1900 fragment separator ( $\Delta p/p=2\%$ ) and the achromatic curved profile Be-degrader will be used to determine the optimum target-wedge combination.

#### 1.6.5.3.1. No charge states



**Fig.196.** The Intensity (left top), Purity (right top), and Combined (left bottom) target-wedge optimization plots for the  $^{208}\text{Pb}$ (100 MeV/u) + Au  $\rightarrow$   $^{196}\text{Os}$  reaction assuming no charge states are included. The wedge selection plot (right bottom) shows spatial distributions of separated fragments at the end of the spectrometer. Calculations were done for target and wedge thicknesses equal to 269 and 207 mg/cm<sup>2</sup> respectively. Plot statistics are given in Table 31 and Table 32.

**Table 31.** Maximum values for the target-wedge optimization plots on Fig.196 and their location (target and wedge thicknesses).

Plot	Maximum value	Target (mg/cm <sup>2</sup> )	Wedge (mg/cm <sup>2</sup> )
Intensity	1.308e+01	3.644e+02	3.440e+00
Purity	2.697e-01	1.403e+02	2.410e+02
IP	5.579e-01	1.627e+02	2.240e+02

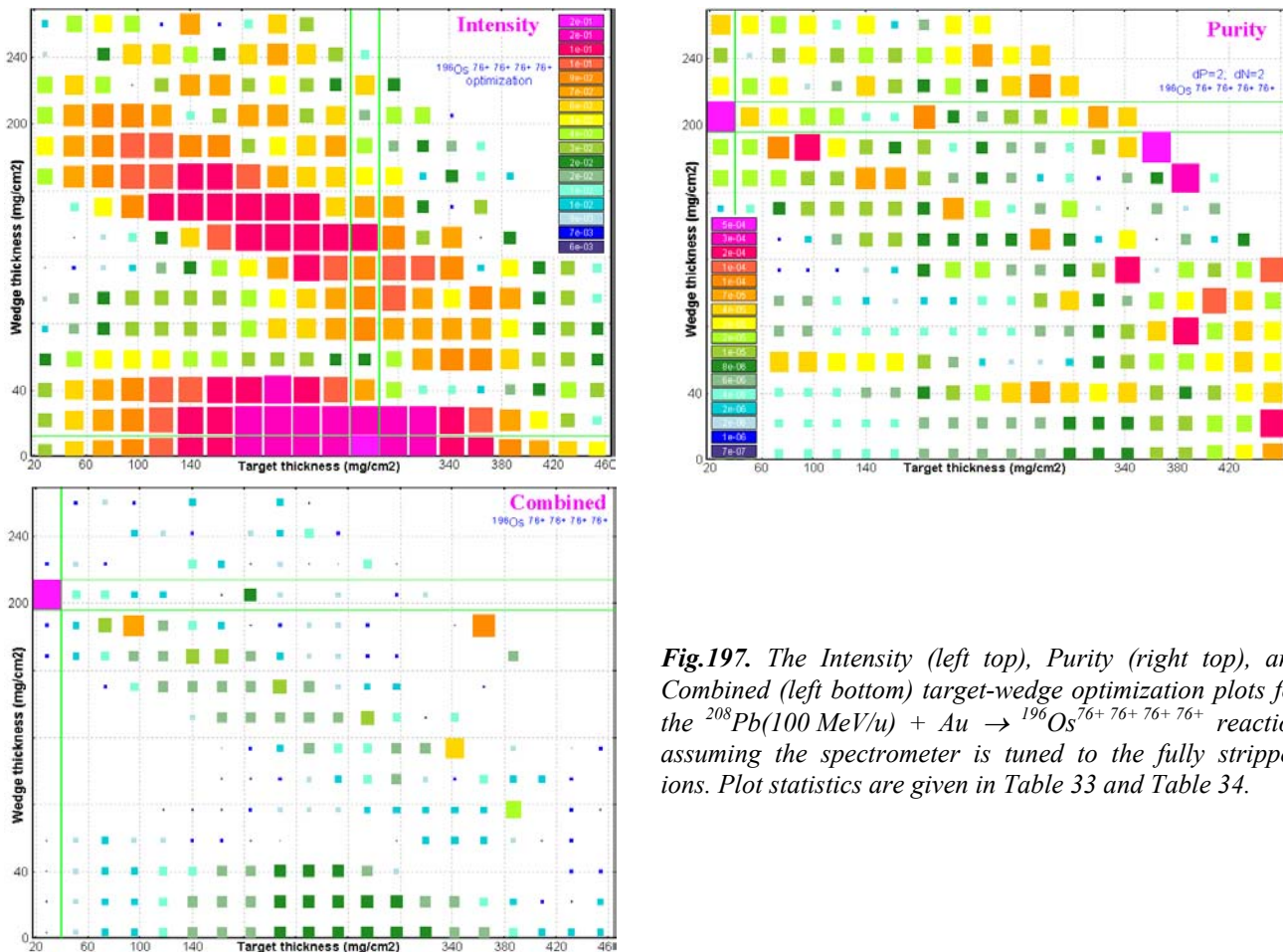
**Table 32.** Values corresponding to the maximum Combined value.

Model	Combined
Intensity	4.542e+00
Purity	2.697e-01
IP	5.407e-01

Combined	1.649e+00	1.403e+02	2.410e+02
----------	-----------	-----------	-----------

### 1.6.5.3.2. Spectrometer tuned to only one charge state combination

The target-wedge optimization plots in the case of the spectrometer tuned to fully stripped ions are shown in Fig.197. On the Intensity plot (Fig.197) it is possible to see the second island of maximum values in the region: target thickness is about 140-240 mg/cm<sup>2</sup> and 120-160 mg/cm<sup>2</sup> for wedge thickness. This island corresponds to transmission of ions with charge state 75+75+74+74+ even though the spectrometer is tuned to fully stripped ions. Transmission of fully stripped ions in this thickness region is equal to zero.



**Fig.197.** The Intensity (left top), Purity (right top), and Combined (left bottom) target-wedge optimization plots for the  $^{208}\text{Pb}(100\text{ MeV}/u) + \text{Au} \rightarrow ^{196}\text{Os}^{76+76+76+76+}$  reaction assuming the spectrometer is tuned to the fully stripped ions. Plot statistics are given in Table 33 and Table 34.

Such sharp peaks on the Purity plot (Fig.197) are explained by the very small yield of the isotope of interest (0.001-0.01%) in contrast to background and also by the small area ( $dN=2$ ,  $dP=2$ ) taken for the background calculation. As soon as yield of more intense neighbor background isotope decreases due to momentum or “wedge” selections, the setting fragment purity increases sharply. The picture will be smoothed by increasing the isotope rectangle size (for example  $dN=4$ ,  $dP=4$ ). Such a small size of the isotope rectangle is made desirable by the time spent on the optimization. So for your general information, the calculations take about 7-11 hours for this reaction with the charge state option turned on, the rectangle size equal to ( $dN=2$ ,  $dP=2$ ) and target and wedge thickness steps both equal to 20.

**Table 33.** Maximum values for each plot on Fig.197 and their location (target and wedge thicknesses).

Plot	Maximum value	Target (mg/cm <sup>2</sup> )	Wedge (mg/cm <sup>2</sup> )
Intensity	2.313e-01	2.748e+02	3.440e+00
Purity	6.046e-04	2.830e+01	2.050e+02
IP	3.182e-01	9.552e+01	1.867e+02
Combined	3.549e+00	2.830e+01	2.050e+02

**Table 34.** Values corresponding to the maximum Combined value.

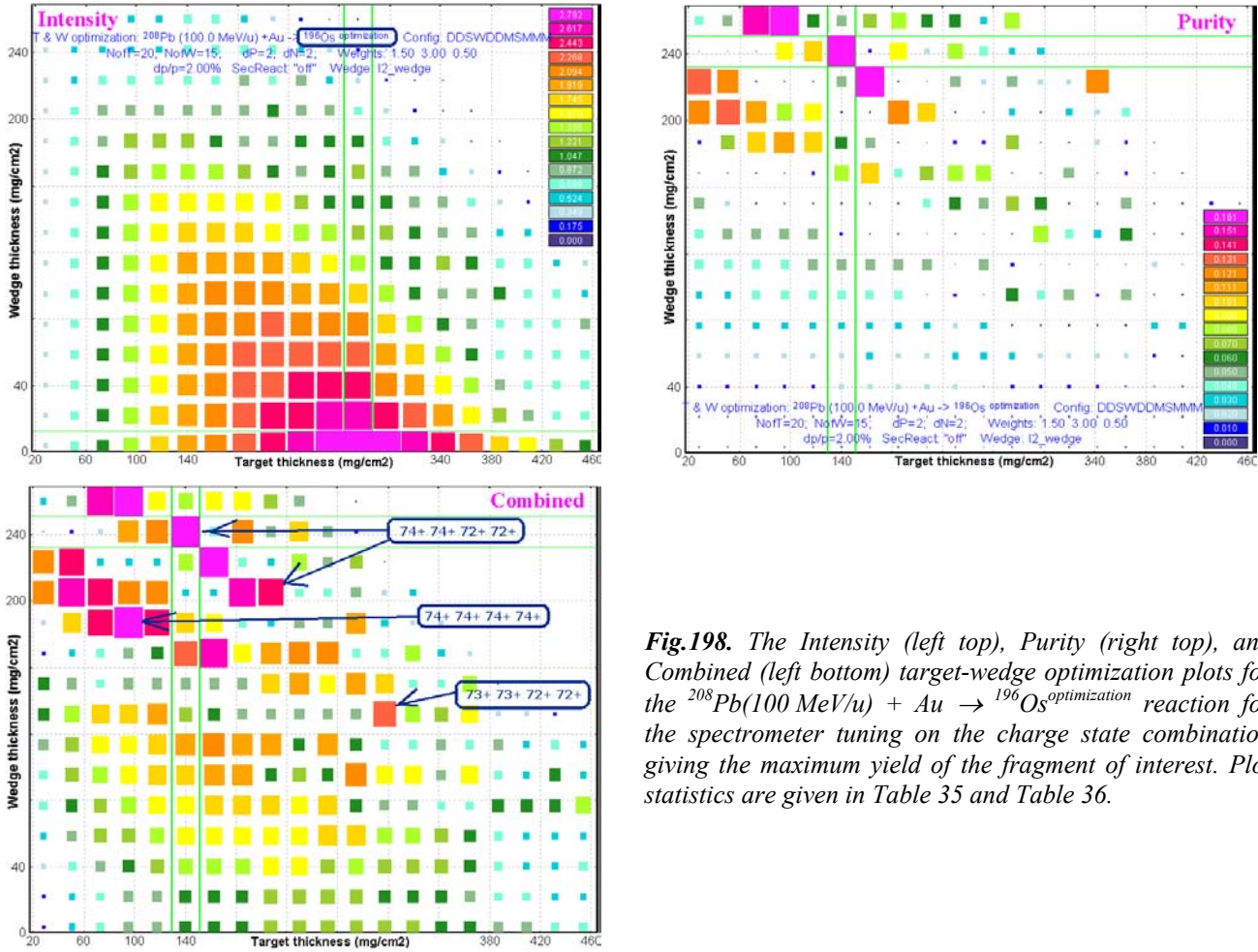
Model	Combined
Intensity	4.350e-02
Purity	6.046e-04
IP	2.744e-01



Combined	3.549e+00	2.830e+01	2.050e+02
----------	-----------	-----------	-----------

### 1.6.5.3.3. Optimization of the charge state combination

The target-wedge optimization plots in the case of tuning the spectrometer on the best charge state combination to produce a maximum yield of the fragment of interest are shown in Fig.198. The best charge state combinations for different target and wedge thicknesses are shown in the Combined plot (Fig.198).



**Fig.198.** The Intensity (left top), Purity (right top), and Combined (left bottom) target-wedge optimization plots for the  $^{208}\text{Pb}(100\text{ MeV}/u) + \text{Au} \rightarrow ^{196}\text{Os}_{\text{optimization}}$  reaction for the spectrometer tuning on the charge state combination giving the maximum yield of the fragment of interest. Plot statistics are given in Table 35 and Table 36.

Sharp peaks in the Purity plot have the same nature (very small purity and small isotope rectangle size) as in the previous section devoted to the spectrometer tuned to just one charge state.

**Table 35.** Plot maximum values on Fig.198 and their location (target and wedge thicknesses).

Plot	Maximum value	Target (mg/cm <sup>2</sup> )	Wedge (mg/cm <sup>2</sup> )
Intensity	2.966e+00	2.748e+02	3.440e+00
Purity	1.709e-01	1.403e+02	2.417e+02
IP	4.416e-01	1.627e+02	2.233e+02
Combined	3.857e+00	1.403e+02	2.417e+02

**Table 36.** Values corresponding to the maximum Combined value.

Model	Combined
Intensity	7.959e-01
Purity	1.709e-01
IP	4.286e-01

### 1.6.5.3.4. Results

It should be noted that the target and wedge thickness values calculated for the combined plot in the case charge state optimization are exactly the same as those produced for the case without charge states (see Table 37). These cells are selected by yellow background color.

**Table 37.** Combined plot statistics from Tables 31-36 and Fig.199.

Method	No charge states	One charge state	Charge state optimization	Charge state optimization*	Charge state optimization** (Fig.199)
Isotope rectangle ( $\pm dN, \pm dP$ )	3, 3	2, 2	<b>2, 2</b>	<b>4, 4</b>	<b>5, 5</b>
Target (mg/cm <sup>2</sup> )	<b>140.3</b>	28.3	<b>140.3</b>	112.9	158.3
Wedge (mg/cm <sup>2</sup> )	<b>241.0</b>	205.0	<b>241.7</b>	248.9	220.5
Intensity	4.542e+00	4.350e-02	7.959e-01	5.054e-1	6.79e-1
Purity	0.270	6.046e-04	0.171	0.0468	0.02605
IP	5.41e-01	2.74e-01	4.29e-01	5.04e-01	8.62e-01

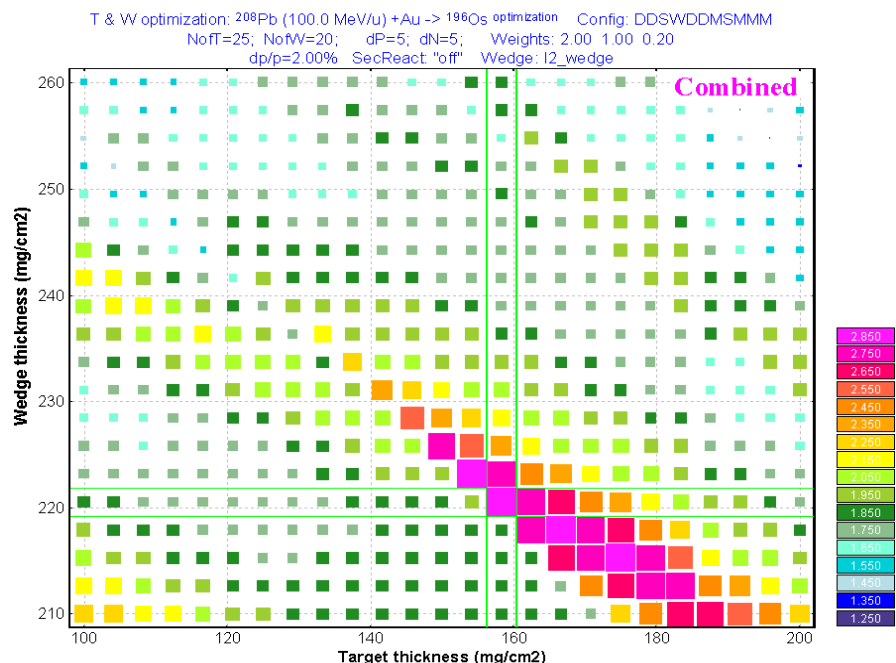
\* Target range: 70-220 mg/cm<sup>2</sup>, *NofT*=15; Wedge range: 160-260 mg/cm<sup>2</sup>, *NofW*=10; Weights: 1, 1, 0.2.

\*\* Target range: 100-200 mg/cm<sup>2</sup>, *NofT*=25; Wedge range: 210-260 mg/cm<sup>2</sup>, *NofW*=20; Weights: 2, 1, 0.2. See results in Fig.199.

**Recommendation:**

By analogy with the one-dimensional case (see chapter 1.6.3. Charge state combination calculation for the optimal target thickness utility) in order to decrease target-wedge optimization time for the case of optimum charge state combination calculations it is recommended to do the following:

- Find the best target-wedge combination without charge states;
- Turn on the charge state option (The “Preference” dialog);
- Check on the “Charge state optimization” checkbox (see Fig.173);
- Set the target and wedge search area with the center obtained in the step without charge states;
- Reduce the target and wedge search area. For example if the previous thickness range was 100 – 3000 mg/cm<sup>2</sup> at 30 steps (*NofT* or *NofW*), and the thickness value from the optimization without charge states was 1700 mg/cm<sup>2</sup>, then set the range 1500 – 1900 mg/cm<sup>2</sup> at 9 steps;
- Make *dN* and *dP* large enough to avoid the “sharp peak” effect in the case of low purity of the fragment of interest;
- Increase the “Intensity” weight in the case of “sharp” peaks to decrease their influence on the combined plot.



**Fig.199.** The Combined target-wedge optimization plot for the <sup>208</sup>Pb(100 MeV/u) + Au → <sup>196</sup>Os optimization reaction for the spectrometer tuned to the charge state combination giving the maximum yield of the fragment of interest. Plot statistics are given in Table 37.

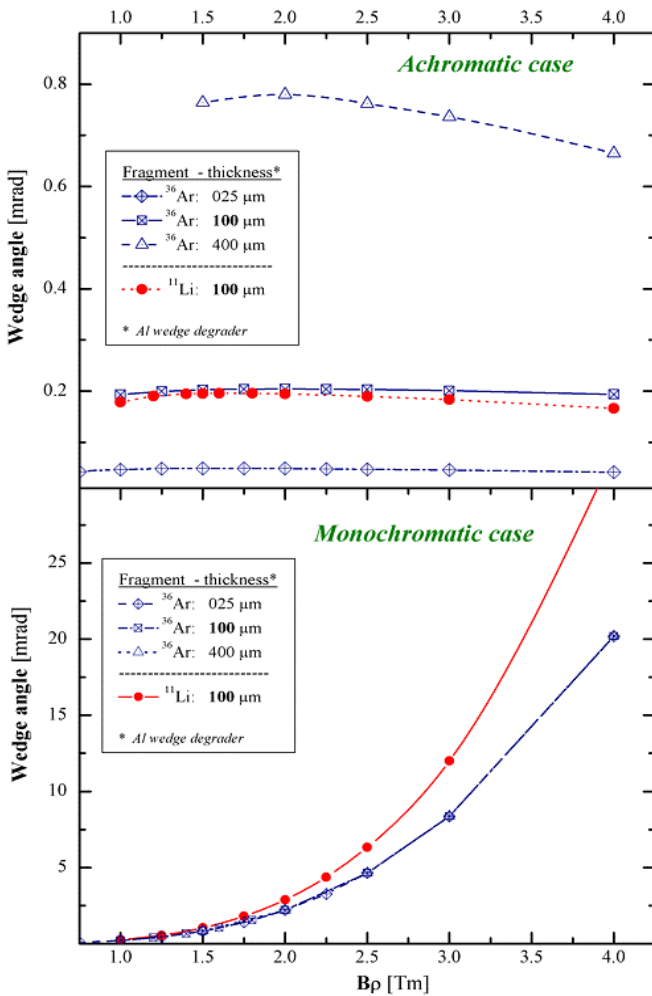
The following parameters were used for calculations:  
 Target range: 100-200 mg/cm<sup>2</sup>, *NofT*=25;  
 Wedge range: 210-260 mg/cm<sup>2</sup>, *NofW*=20;  
 Weights: 2, 1, 0.2

### 1.6.5.4. Wedge-shape and curved profile degraders properties

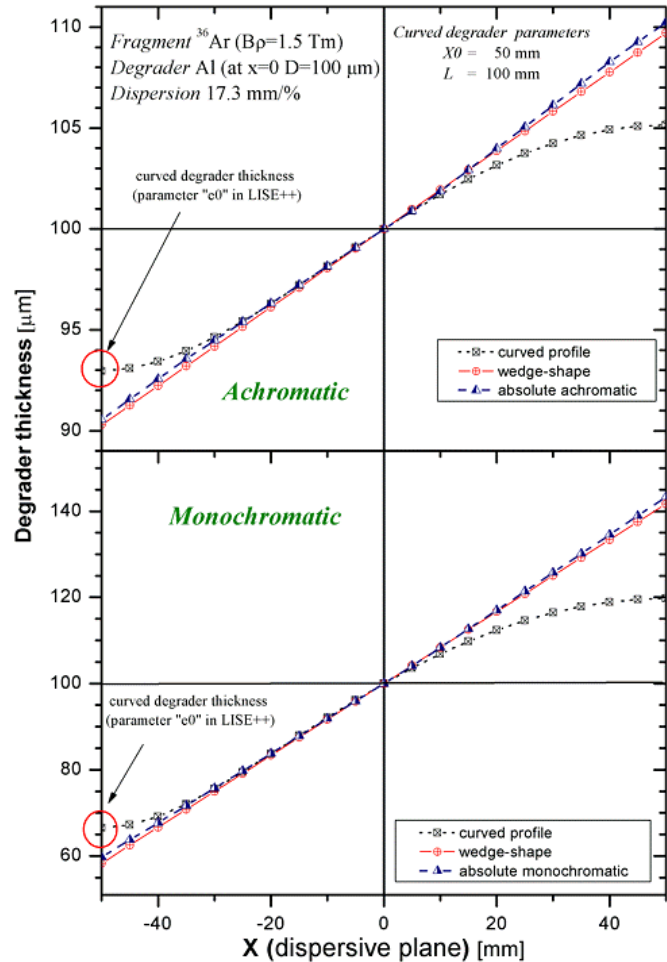
We need an analysis of wedge-shape and curved profile degraders properties to know what kind of degrader can be used in the dispersive focal plane for the “Optimum target” and the “Optimum target and wedge” utilities because, for example, the user may wish to have an achromatic focus at the end of spectrometer independently from the target or wedge thickness. Must we recalculate a wedge angle on each calculation step? Or will achromatic properties be retained if we change the target thickness?

Fig.200 shows the angle of several wedge-shape Al-degraders as a function of magnetic rigidity for isotopes of  $^{36}\text{Ar}$  and  $^{11}\text{Li}$  in the achromatic and monochromatic modes. From this figure **it is possible to conclude** the following for the **achromatic mode**:

- The angle of achromatic wedge is mostly a **function of a degrader thickness and a momentum dispersion**;
- The angle of wedge-shape degrader **does not change** much for a fixed degrader thickness **for different energies and different isotopes**;
- This means that **it is possible to keep one angle value** (calculated just once to be achromatic at one point) for all calculation steps in the **“Optimal target” utility in the achromatic mode** thus saving all achromatic properties.



**Fig.200.** The angle of several wedge-shape Al-degraders as a function of magnetic rigidity for isotopes of  $^{36}\text{Ar}$  and  $^{11}\text{Li}$  in the achromatic mode on the top plot and the monochromatic mode accordingly on the bottom one. The momentum dispersion in the wedge position is equal to 17.3 mm/%.



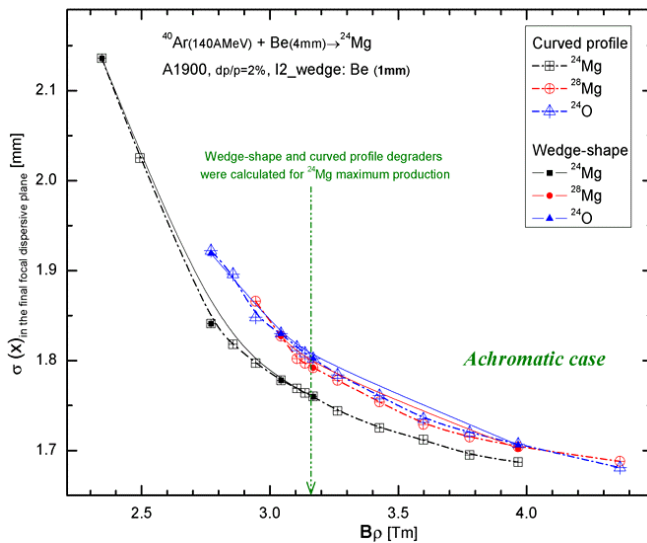
**Fig.201.** The effective thickness of degraders in the dispersive focal plane as a function of a horizontal coordinate in the achromatic mode on the top plot and the monochromatic mode accordingly on the bottom one. Calculations were done for the  $^{36}\text{Ar}$  fragment at  $Bp = 1.5 \text{ Tm}$ .

It is possible to conclude the following from Fig.200 for the **monochromatic mode**:

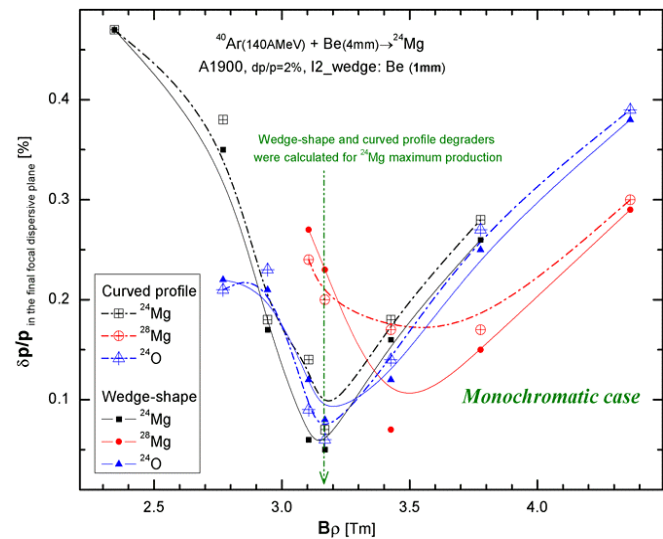
- The angle of wedge-shape degrader **does not change** much for other degrader **thicknesses**;
- The angle of monochromatic wedge mostly is a **function of a fragment and its energy**;
- This means that it is **not possible to keep one angle value** for all calculation steps in the **“Optimal target” utility in the monochromatic mode** while keeping all monochromatic properties.

Fig.201 shows the effective thickness of degraders in the dispersive focal plane as a function of a horizontal coordinate in the achromatic and monochromatic modes. From plots on this figure it is possible to make two statements:

- The wedge-shape degrader is more close to absolute achromatic (monochromatic) degrader than the curved profile degrader. This is an evident advantage of wedge-shape degraders over the curved profile degrader.
- **Edge aberrations in Curved Profile Degraded:** To avoid large deviations from the ideal achromatic (monochromatic) degrader on the wings of the curved profile degrader (CPD) it is necessary to build the CPD on a long base. For example if momentum slit size is  $\pm 20$  mm, than the CPD base (parameter  $L$ ) should be 2-3 times longer and equal to 80-120 mm.



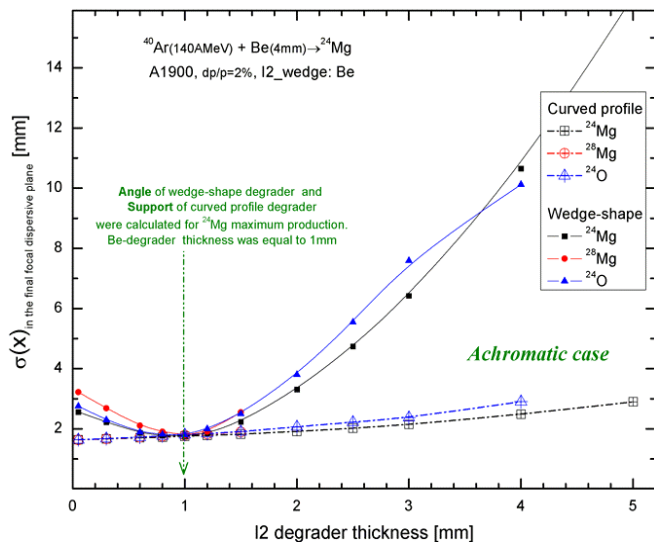
**Fig.202.** The  $^{24,28}\text{Mg}$ , and  $^{24}\text{O}$  fragment spot sizes in the final focal plane of the A1900 spectrometer for the wedge-shape and curved profile Be-degraders (1mm) as a function of magnetic rigidity. The wedge-shape angle and curved profile support were calculated for the **achromatic** mode at the  $B\rho$ -value corresponding to  $^{24}\text{Mg}$  maximum production.



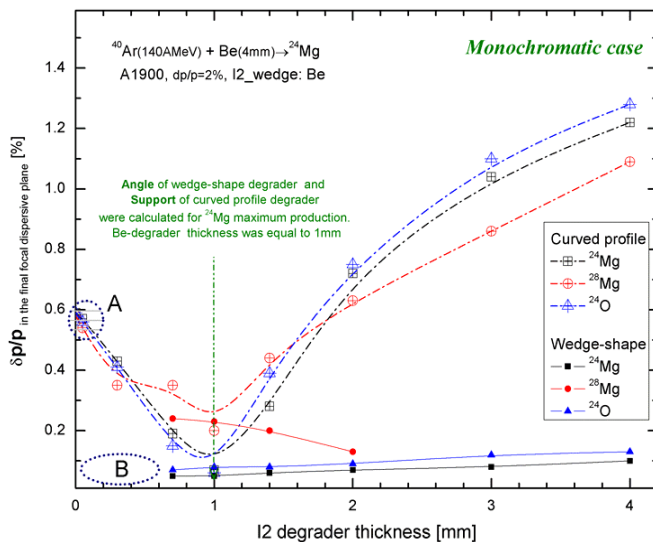
**Fig.203.** The  $^{24,28}\text{Mg}$ , and  $^{24}\text{O}$  fragment momentum widths in the final focal plane of the A1900 spectrometer for the wedge-shape and curved profile Be-degraders (1mm) as a function of magnetic rigidity. The wedge-shape angle and curved profile support were calculated for the **monochromatic** mode at the  $B\rho$ -value corresponding to  $^{24}\text{Mg}$  maximum production.

Fig.202 and Fig.203 show the  $^{24,28}\text{Mg}$ , and  $^{24}\text{O}$  fragment spot sizes (achromatic mode) and momentum widths (monochromatic mode) respectively in the final focal plane of the A1900 spectrometer for the wedge-shape and curved profile Be-degraders (1mm) as a function of magnetic rigidity. It is visible from Fig.202 that calculation results for both types of degrader are identical at magnetic rigidity values of 2.5-5 Tm. At the same time from Fig.203 it is visible, that the monochromatic effect is lost with changes of the magnetic rigidity value. Therefore, as for wedge-shape degrader, we can conclude the following for CPD:

- it is **possible to keep one curved profile support** (calculated just once to be achromatic in one point) for all calculation steps in the **“Optimal target” utility** in the **achromatic mode**, thus saving all achromatic properties;
- It is **not possible to keep one curved profile support** for all calculation steps in the **“Optimal target” utility** in the **monochromatic mode**.
- It is necessary to note that the **momentum width** in the case of using **wedge-shape degrader** in the monochromatic mode is **better** than in the case of the CPD (see Fig.203); this is explained by CPD edge aberrations.



**Fig.204.** The  $^{24,28}\text{Mg}$ , and  $^{24}\text{O}$  fragment spot sizes in the final focal plane of the A1900 spectrometer for the wedge-shape and curved profile Be-degraders (1mm) as a function of degrader thickness. The wedge-shape angle and curved profile support were calculated **ONCE** for the **achromatic mode** at the  $B\rho$ -value corresponding to  $^{24}\text{Mg}$  maximum production and were used for all degrader thickness points.



**Fig.205.** The  $^{24,28}\text{Mg}$ , and  $^{24}\text{O}$  fragment momentum widths in the final focal plane of the A1900 spectrometer for the wedge-shape and curved profile Be-degraders (1mm) as a function of degrader thickness. The wedge-shape angle and curved profile support were calculated **ONCE** for the **monochromatic mode** at the  $B\rho$ -value corresponding to  $^{24}\text{Mg}$  maximum production and were used for all degrader thickness points.

Fig.204 and Fig.205 show  $^{24,28}\text{Mg}$ , and  $^{24}\text{O}$  fragment spot sizes (achromatic mode) and momentum resolutions (monochromatic mode) respectively in the final focal plane of the A1900 spectrometer for the wedge-shape and curved profile Be-degraders as a function of degrader thickness. Wedge-shape angles and curved profile supports for both figures were calculated **ONCE** at the  $B\rho$ -value corresponding to  $^{24}\text{Mg}$  maximum production and were used for all degrader thickness points. It is visible from Fig.204 that the CPD keeps its achromatic properties at change of degrader thickness for one curved profile support, whereas the wedge-shape degrader on the contrary does not keep them if changing degrader thickness and keeping the wedge angle. For the monochromatic case the situation is changed: the wedge-shape degrader saves monochromatic properties at change of degrader thickness, and the CPT does not. Therefore it is possible to conclude based on that said above:

- It is **not possible to keep one angle value** (calculated just once to be achromatic in one point) and it is **possible to keep one curved profile support** for all calculation steps in the **“Optimal target & wedge” utility** in the **achromatic mode** thus saving all achromatic properties.
- It is **not possible to keep one angle value** and **one curved profile support** for all calculation steps in the **“Optimal target & wedge” utility** in the **monochromatic mode**.

**Recommendation:** use the curved profile degrader for the **“Optimal Target and Wedge” utility!**

For details see the analysis for wedge-shape degrader in chapter 1.6.5.5.1. Acceptance.

But it is possible to use a wedge-shape degrader for the monochromatic mode if the “keep value” parameter is on, or by other words the fragment energy before the wedge is constant for all calculation steps.

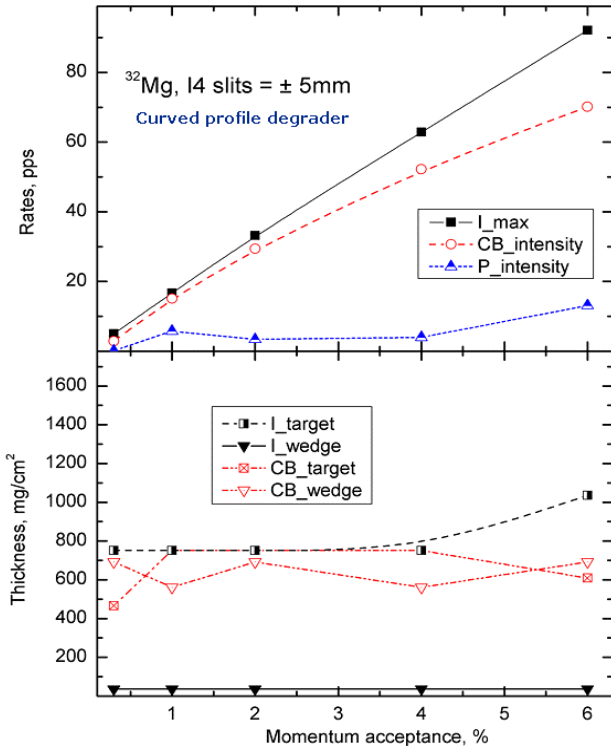
### 1.6.5.5. Setting discussions

In this chapter we shall analyze an influence of momentum acceptance, “wedge selection” slits, type of degrader (CPD and wedge-shape), and fragment nature (using as examples isobars A=32) on the optimum target and wedge combination for the  $^{40}\text{Ar}(140\text{MeV/u})+\text{Be}$  reaction using the A1900 fragment separator. The following parameter designations are used in figures in this chapter:

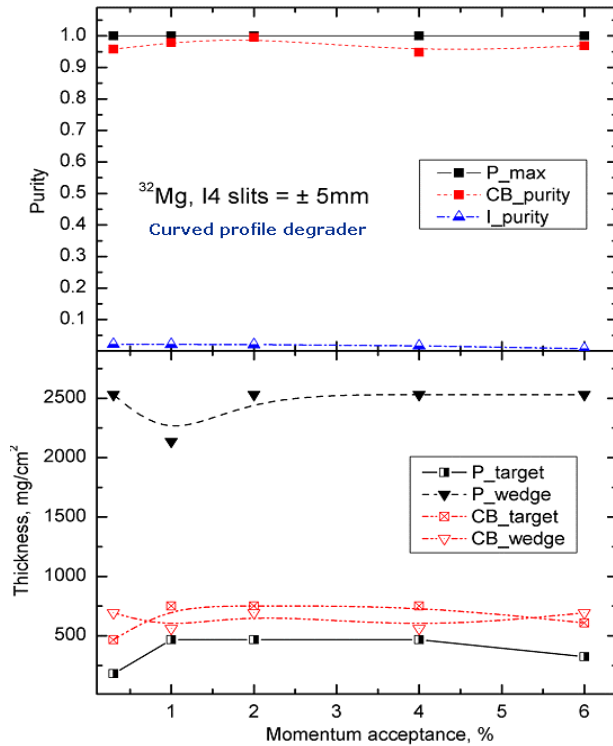
**Table 38.** Parameter designations for figures in this chapter.

1D-plot	Designation for 1D-plots	Origin 2D plot	Description of parameter
<b>Y-axis</b>	<b>Parameter</b>		
Intensity	I_max	Intensity	Maximum intensity value
	CB_intensity	Combined	Intensity corresponding to the largest Combined value
	P_intensity	Purity	Intensity corresponding to P_max
Purity	P_max	Purity	Maximum purity value
	CB_purity	Combined	Purity corresponding to the largest Combined value
	I_purity	Intensity	Purity corresponding to I_max
Thickness	I_target	Intensity	Target thickness corresponding to I_max
	I_wedge	Intensity	Wedge thickness corresponding to I_max
	P_target	Purity	Target thickness corresponding to P_max
	P_wedge	Purity	Wedge thickness corresponding to P_max
	CB_target	Combined	Target thickness corresponding to the largest Combined value
	CB_wedge	Combined	Wedge thickness corresponding to the largest Combined value

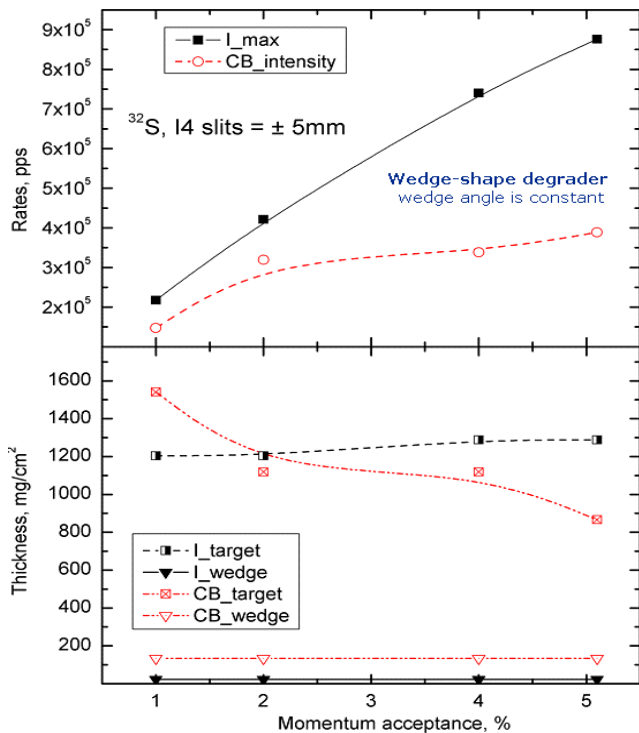
#### 1.6.5.5.1. Acceptance



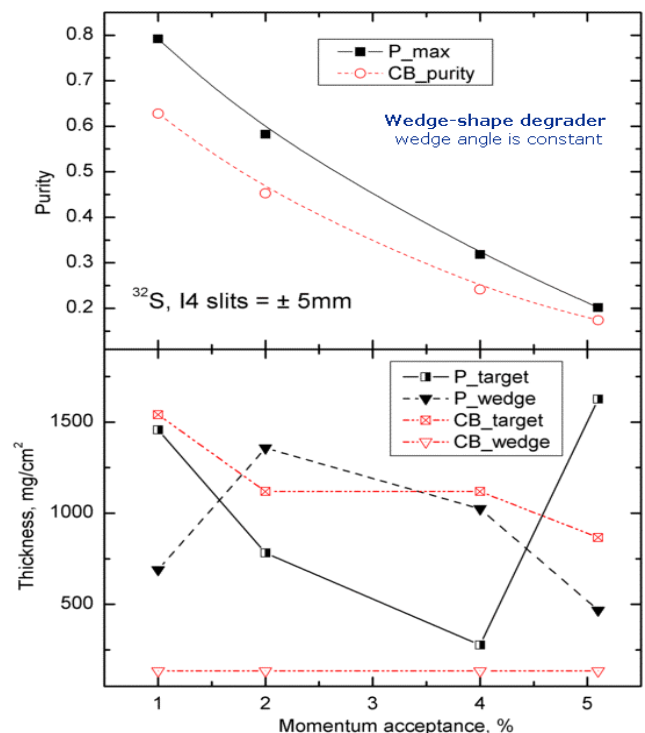
**Fig.206.** Top plot: The  $^{32}\text{Mg}$  fragment maximum possible production rate ( $I_{\text{max}}$ ) and the rate corresponding to the largest Combined value ( $\text{CB}_{\text{intensity}}$ ) versus the A1900 momentum acceptance. Bottom plot: Target and wedge thicknesses corresponding to rate curves in the top plot.



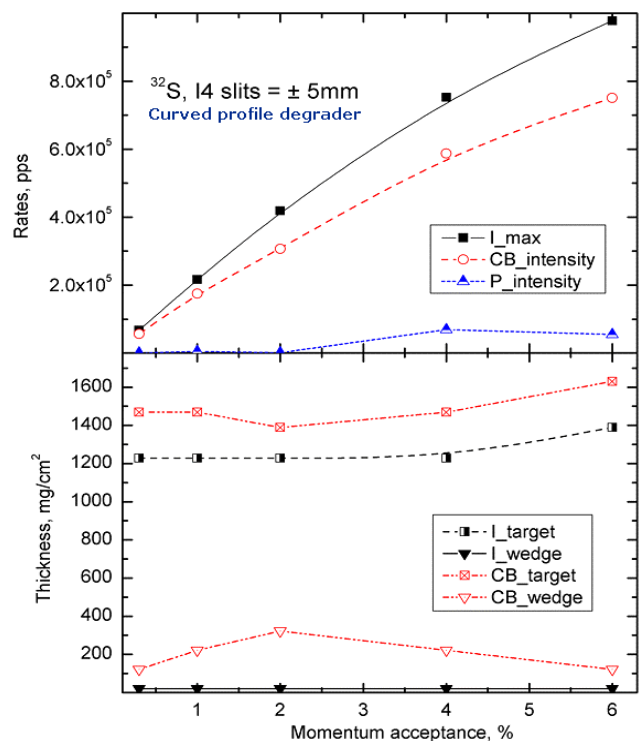
**Fig.207.** Top plot: The  $^{32}\text{Mg}$  fragment maximum possible purity and the purity corresponding to the largest Combined value versus the A1900 momentum acceptance. Bottom plot: Target and wedge thicknesses corresponding to rate curves in the top plot. Calculations were done with the curved profile degrader.



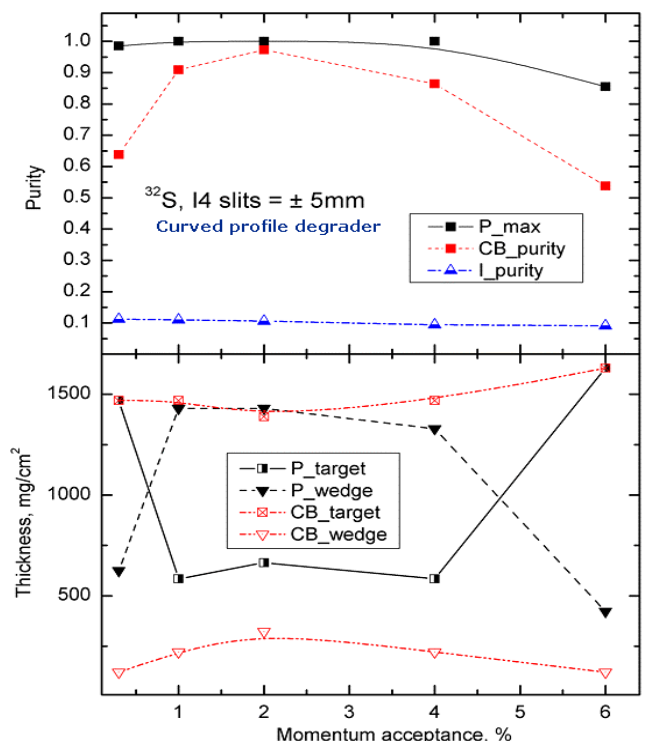
**Fig. 208.** Top plot: The  $^{32}S$  fragment maximum possible production rate ( $I_{max}$ ) and the rate corresponding to the largest Combined value ( $CB_{intensity}$ ) versus the A1900 momentum acceptance. Calculations were done with the *wedge-shape degrader*.



**Fig. 209.** Top plot: The  $^{32}S$  fragment maximum possible purity and the purity corresponding to the largest Combined value versus the A1900 momentum acceptance. Calculations were done with the *wedge-shape degrader*.



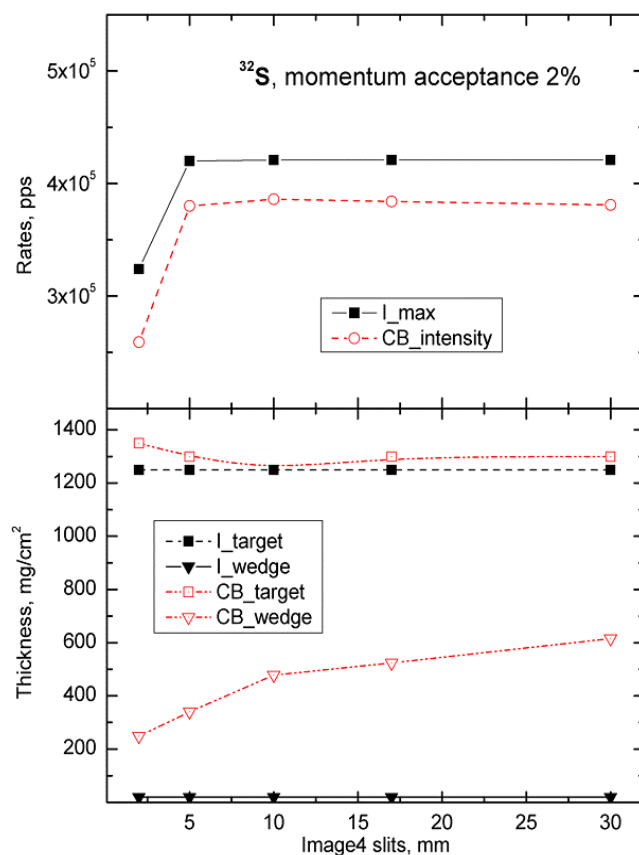
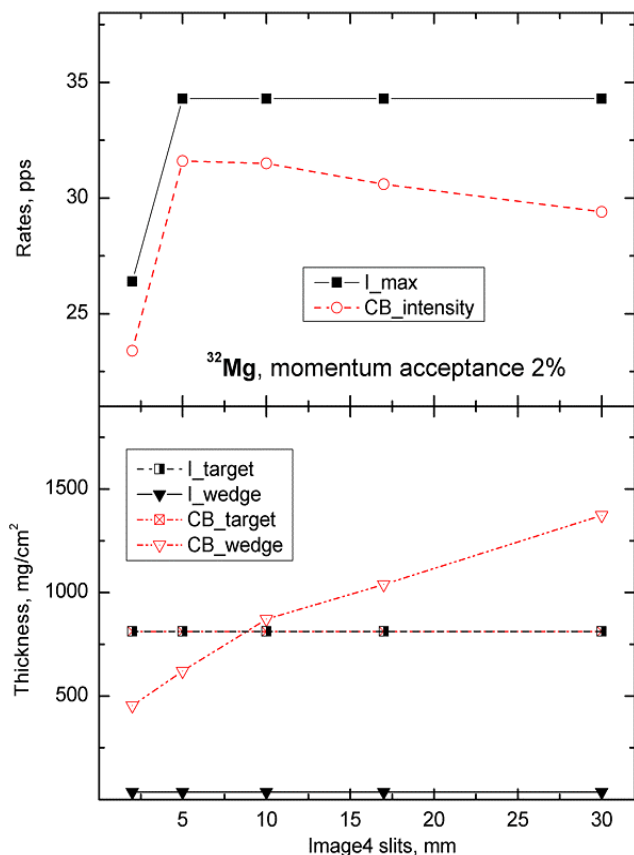
**Fig. 210.** Top plot: The  $^{32}S$  fragment maximum possible production rate ( $I_{max}$ ) and the rate corresponding to the largest Combined value ( $CB_{intensity}$ ) versus the A1900 momentum acceptance. Calculations were done with the *curved profile degrader*.



**Fig. 211.** Top plot: The  $^{32}S$  fragment maximum possible purity and the purity corresponding to the largest Combined value versus the A1900 momentum acceptance. Calculations were done with the *curved profile degrader*.

### 1.6.5.5.2. Wedge selection slits

Fig.212 and Fig.213 show maximum and optimum production rate of the  $^{32}\text{Mg}$  and  $^{32}\text{S}$  fragments as well as corresponding target and wedge thickness values. We do not comment on these results, but leave this process for the reader.



**Fig.212.** Top plot: The  $^{32}\text{Mg}$  fragment maximum possible production rate ( $I_{\text{max}}$ ) and rate corresponding to the largest Combined value (intensity) versus size of the Image4 slit.

Bottom plot: Target and wedge thicknesses corresponding to production rate curves in the top plot.

Calculations were done with the **curved profile degrader**.

**Fig.213.** Top plot: The  $^{32}\text{S}$  fragment maximum possible production rate ( $I_{\text{max}}$ ) and rate corresponding to the largest Combined value (intensity) versus size of the Image4 slit.

Bottom plot: Target and wedge thicknesses corresponding to production rate curves in the top plot.

Calculations were done with the **curved profile degrader**.

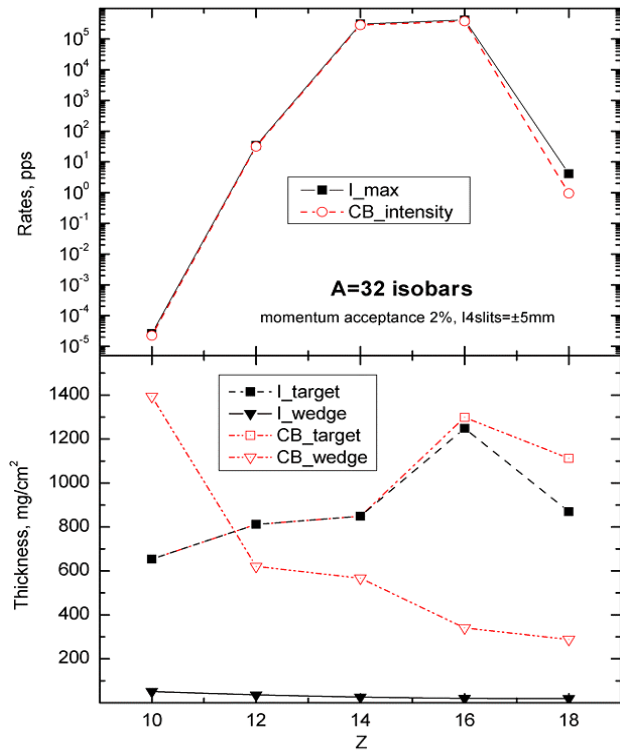
### 1.6.5.5.3. Isobars A=32

Fig.214 and Fig.215 show maximum and optimum production rate and purity of isobars A=32 as well as corresponding target and wedge thickness values.

Fig.216 shows the Combined target-wedge optimization plots for isobars A=32.

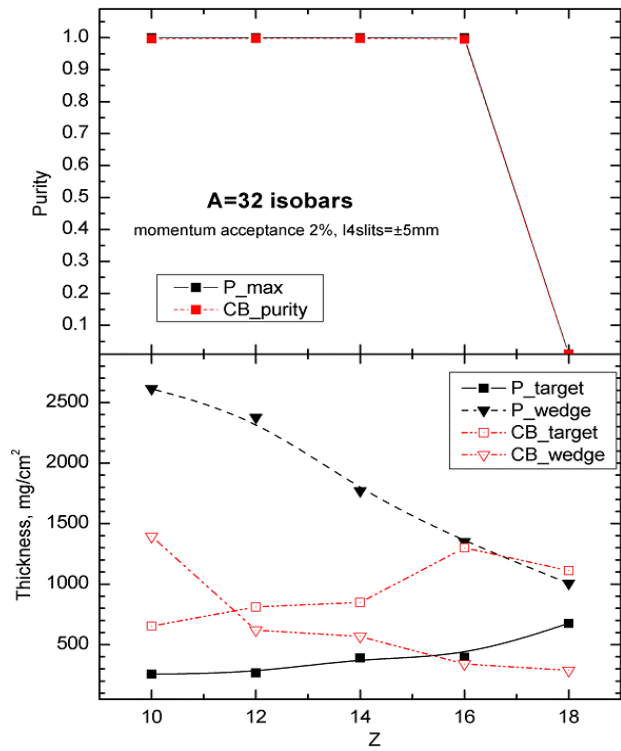
These calculations were done for the  $^{40}\text{Ar}(140\text{MeV/u})+\text{Be}$  reaction using the A1900 fragment separator with the momentum acceptance being equal to 2% and on Image4 slits size of  $\pm 5\text{mm}$ . The curved profile degrader was used in calculations in the intermediate dispersive focal plane.





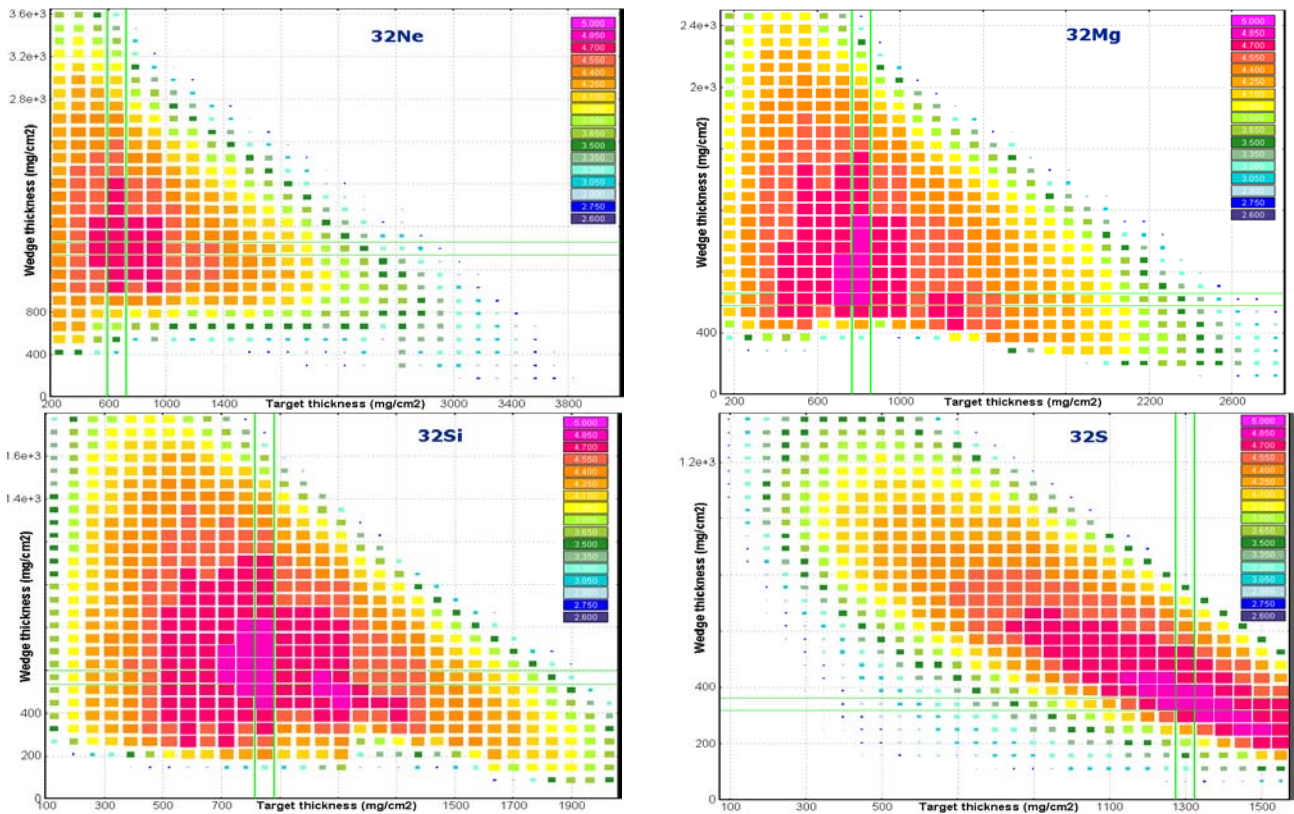
**Fig.214.** Top plot: The fragment maximum possible production rate ( $I_{max}$ ) and rate corresponding to the largest Combined value (intensity) for isobars  $A=32$ .

Bottom plot: Target and wedge thicknesses corresponding to production rate curves in the top plot.



**Fig.215.** Top plot: The fragment maximum possible purity and purity corresponding to the largest Combined value for isobars  $A=32$ .

Bottom plot: Target and wedge thicknesses corresponding to production rate curves in the top plot.



**Fig.216.** The Combined target-wedge optimization plots for isobars  $A=32$ .

## 1.7. Masses. AME2003

The new evaluation of atomic masses AME2003 [AME03] has been incorporated into the LISE++ code (version 7.2) replacing the previous nuclide mass database [Aud95]. Errors of nuclide characteristics also have been added in the database and might be edited or plotted (see Fig.217 and Fig.218).

Accurate predictions of the production cross-sections of rare isotopes are important in the study of astrophysical processes and in the location of the drip-lines. Reaction models involved in the LISE++ code as *Abrasion - Ab-lation*, *LisFus* (fusion – evaporation models), and *Coulomb fission* rely on parameterization of the nuclear masses. This may lead to large inaccuracies in the case of discrepancies between mass parameterization and the experimental masses.

Representation of nuclei as liquid drops has been very successful in predicting their properties and masses, especially those along the valley of stability. However, a large discrepancy is observed between the classical LD mass formula and experimental values due to the shell structure. LISE++ uses a new mass formula with shell crossing (see [http://groups.nsl.msu.edu/lise/6\\_1/lise++\\_6.htm#\\_Toc26162476](http://groups.nsl.msu.edu/lise/6_1/lise++_6.htm#_Toc26162476)). A new LDM fit with shell crossing corrections has been performed using the new evaluation of atomic masses.

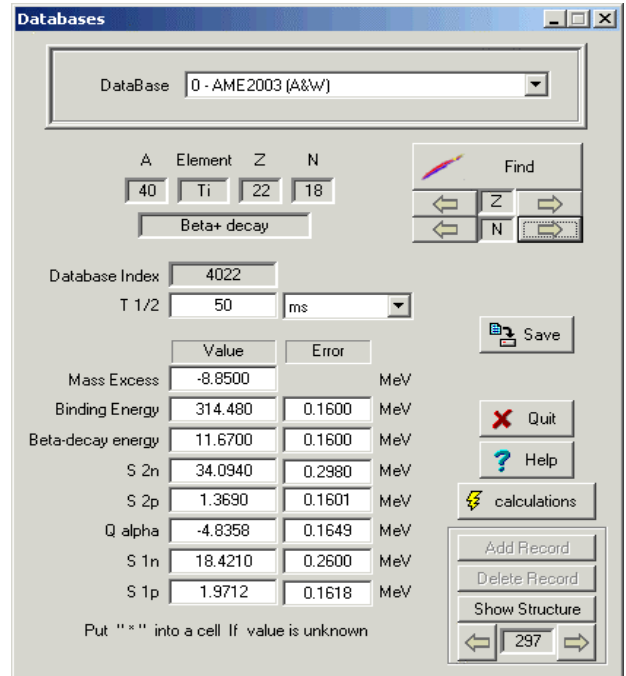


Fig.217. The “Databases” dialog. The new version allows to work (edit, plot) with isotope value errors.

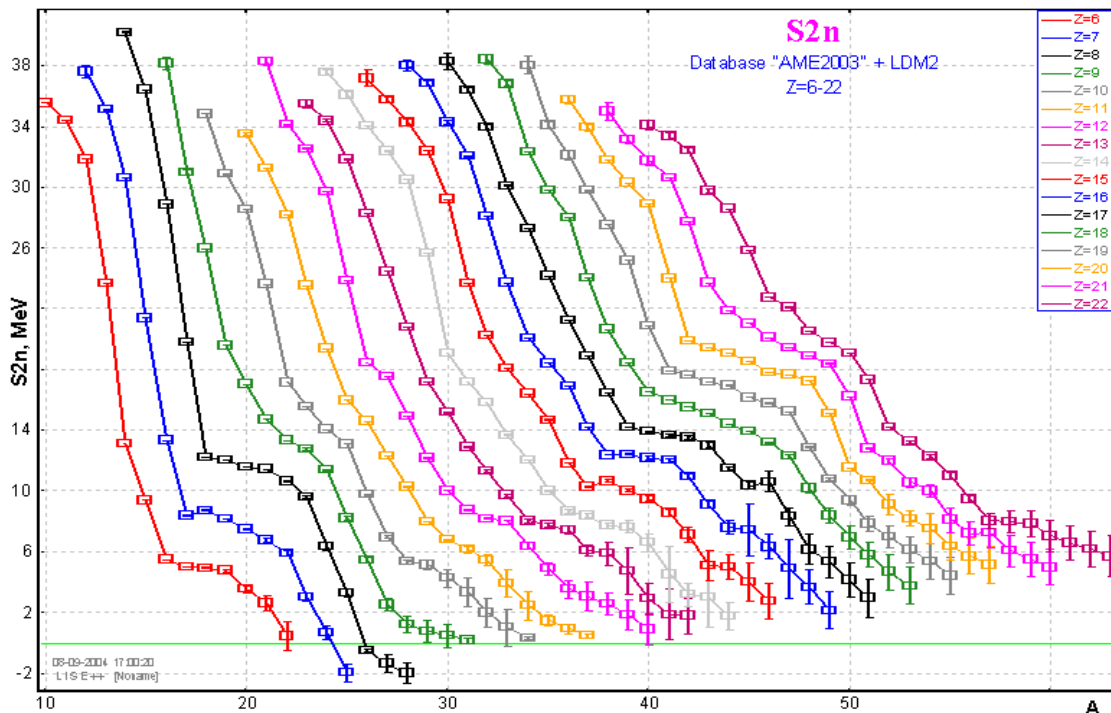


Fig.218. Two neutron separation energy of elements with atomic numbers 6-22 plotted by the LISE++ code.

### 1.7.1. New mass excess files in the LISE package

The new mass excess files “user\_mass\_excess\_TUYY.lme” (Z=1-112), “HFB8.lme” (Z=8-120), and “HFB9.lme” (Z=8-110) are provided in the LISE installation package.

The “user\_mass\_excess\_TUYY.lme” file is created based on the empirical mass formula with proton-neutron interaction by Takahiro Tachibana, Masahiro Uno, Masami Yamada, and So Yamada [Hau88]. The data were extracted from the page <http://www.phys.nthu.edu.tw/~nap/toimass.html>.

The mass excess files “HFB8.lme” and “HFB9.lme” [HFB9] are based on the Hartree-Fock-Bogoliubov + PLN method and were obtained from <http://www-astro.ulb.ac.be/Nucdata/Masses/hfb8-plain> and <http://www-astro.ulb.ac.be/Nucdata/Masses/hfb9-plain> accordingly.

*Note:* It is recommended to use AME2003 + LISE LDM#2 values for regular calculations with LISE++. The TUYY mass excess file can be used as an alternative file for comparison and to show predicted masses very far from the stability line (so called “unknown” isotopes. See the next chapter for details) where the shell crossing corrections for LDM#2 do not act.

### 1.7.2. "Unknown" - new type of isotope designation for the table of nuclides

*“There is no clear definition of the dripline...”*

M.Thoennessen [Tho04]

There are several different definitions of drip-line in the “Reaching the limits of nuclear stability” review [Tho04]. We are not going to discuss them, but we need to introduce some definitions to characterize the new type of isotope designation for the table of nuclides in the LISE++ code.

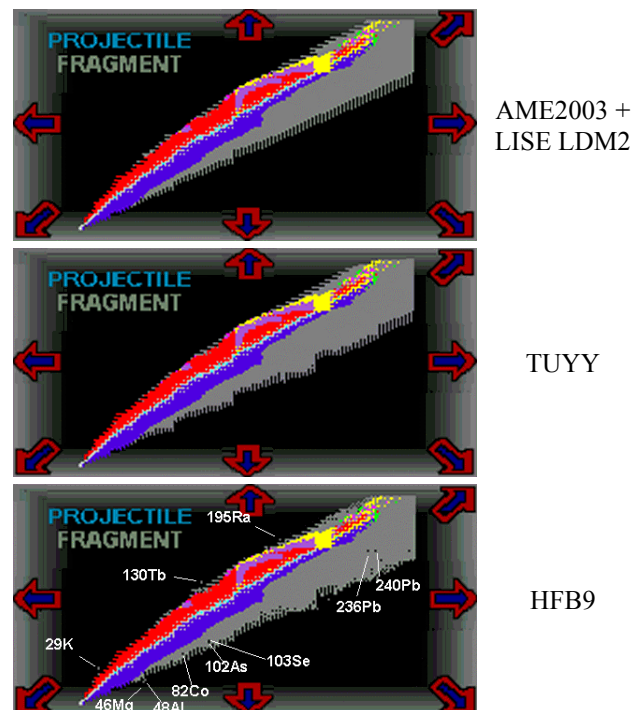
But for a start we answer on the question:

#### Why do we need new type of designation?

1. Show to LISE’s users nuclei which are possibly particle bound based on theoretical predictions (see Fig.219);
2. Use this type of isotopes in transmission calculations (see Fig.220);
3. Use this type of isotopes for Database plots, because the code is looking for extremities to plot isotope characteristics (see Fig.226);
4. Calculate and keep in the memory AA and AF cross-sections and secondary reactions contribution for this type of isotopes.

#### 1.7.2.1. Particle bound, quasi bound and unbound nuclei

The new type of isotope designation “Unknown” means that the isotope was initially set as “doesn’t exist” (black color), but if the user run a mass model



**Fig.219.** The LISE’s navigation scheme with different sets of “unknown” isotopes calculated by different models.

which predicts this isotope be **particle bound**, then the code changed the state of this nuclide from “Doesn’t exist” to “Unknown”. Unknown isotopes are marked by gray color in the table of nuclides (see Fig.220) and the navigation scheme (see Fig.219).

We use the following definitions in the code:

“**particle bound**” if **all four** separation energies ( $S_{1n}$ ,  $S_{2n}$ ,  $S_{1p}$ ,  $S_{2p}$ ) are positive<sup>♦</sup>.

“**particle quasi bound**” if all statements are valid:

$$\begin{aligned} S_{1n} > 0, & \quad S_{1p} + V_{B0\_p} > 0, \\ S_{2n} > 0, & \quad S_{2p} + V_{B0\_2p} > 0, \\ & \quad Q_\alpha - V_{B0\_a} < 0, \end{aligned}$$

but at least one from  $S_{1p}$  or  $S_{2p}$  separation energies is negative ( $S_{1p} < 0$  or  $S_{2p} < 0$ ).

“**particle unbound**” if one of these five statements is valid:

$$\begin{aligned} S_{1n} < 0, & \quad S_{1p} + V_{B0\_p} < 0, \\ S_{2n} < 0, & \quad S_{2p} + V_{B0\_2p} < 0, \\ & \quad Q_\alpha - V_{B0\_a} > 0; \end{aligned}$$

Fig.221 visually demonstrates the arrangement of these conditions. With increasing angular momentum these levels will move up. The “Absolute zero” value shows a level below which an isotope is always particle unbound at any angular momentum. The “Particle quasi bound” expression has appeared because for small but negative values of separation energies an isotope can be found to be particle bound (in other words can be identified in an experimental way) due to the Coulomb barrier, for example B.Blank and collaborators work [Bla00] where  $^{48}\text{Ni}$  isotopes were unambiguously identified:

Decay mode	Separation energy		$V_{B0}$
	AME2003	TUYY	
1p	-0.4050 ( $\pm 0.711$ )	-0.1610	5.73
2p	-3.0650 ( $\pm 0.615$ )	-2.8321	10.55

Particle bound properties (or decay modes) calculated from database or mass formula it is possible to see in the “Isotopes” dialog (see fragment “C” in Fig.223). Depending on isotope properties, the “Particle absolutely unbound” state can be marked as “2p+CB unbound”, “1p+CB unbound”, “alpha+CB unbound”, “1n unbound”, or “2n unbound”, and the “Particle quasi bound” state can be seen as “1p unbound” or “2p unbound”. Recall that just **particle bound isotopes** can be moved from the “doesn’t exist” state to the “unknown” state as a result of searching by the code.

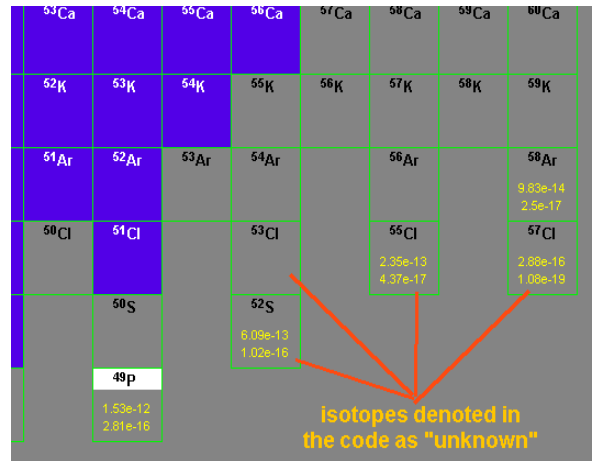


Fig.220. Fragment of the LISE nuclide table where transmission calculation results are shown for unknown isotopes.

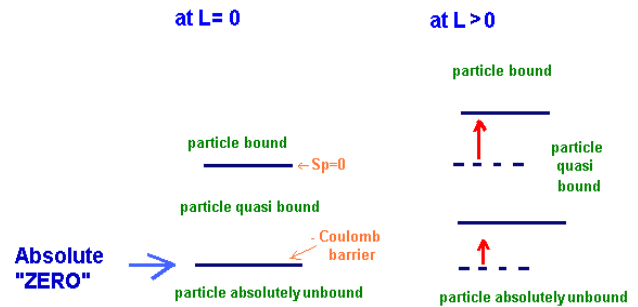


Fig.221. Scheme for particle bound, quasi bound and unbound definitions.

<sup>♦</sup> it has been decided to assign the “particle bound” property for nuclei with  $Q_\alpha - V_{B0\_a} < 0$  and  $Q_\alpha > 0$  when the code searches “unknown” isotopes.

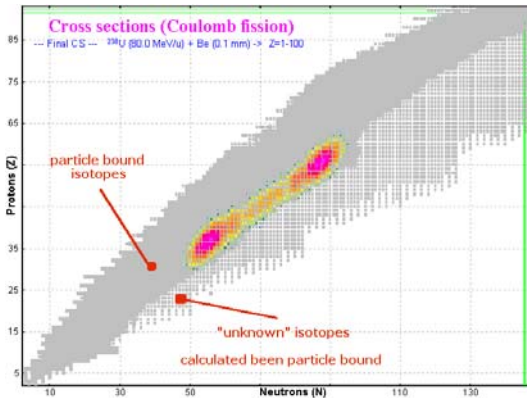


Fig.222. Designation of particle bound and "unknown" nuclides on 2D plots.

mass excess file (marked "A" in Fig.224) and set the "1 User's ME" item as mass method (marked "B").

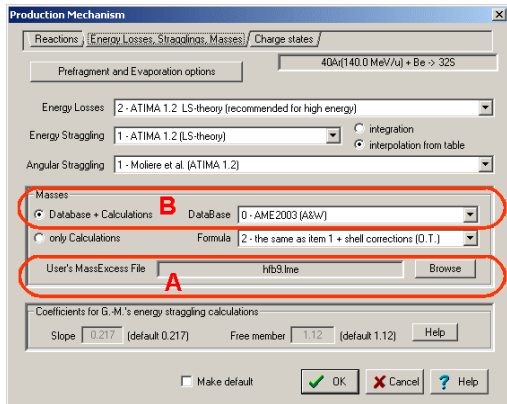


Fig.224. The "Masses" panel of the "Production mechanism" dialog.

### 1.7.2.2. How to load information from the user mass excess file in the navigation scheme

In order to reload information in the navigation scheme (Fig.219) it is necessary to load the "Production mechanism" dialog from the "Options" menu. For example to use the HFB9 model, it is necessary to choose the "hfb9.lme" file as the user

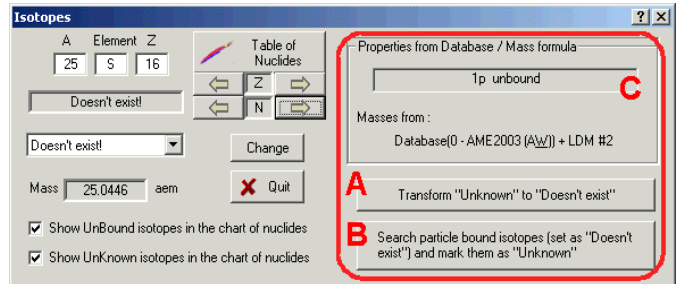


Fig.223. The "Isotopes" dialog.

Load the "Isotopes" dialog (see Fig.223) from the "Options" menu. Click the button "Transform 'Unknown' to 'Doesn't exist'" (marked "A" in Fig.223) to clean the navigation table from previous calculations. Click the "Search particles.." button (marked "B" in Fig.223) to find particle bound isotopes and move some of them which marked as "doesn't exist" into "unknown" state (see result of this operation in Fig.219).

The LISE installation package contains the "table.iso" file with information for the table of nuclides where "unknown" isotopes have already been set based on the TUYU model.

### 1.7.2.3. Modifications in the database plot

The new version allows one to plot all calculations by different methods in one plot with different options. See Fig.225 and Fig.226 for modification details.

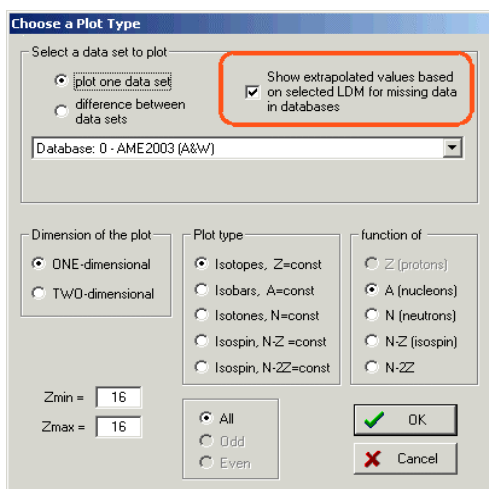


Fig.225. The "Database Plot options" dialog.

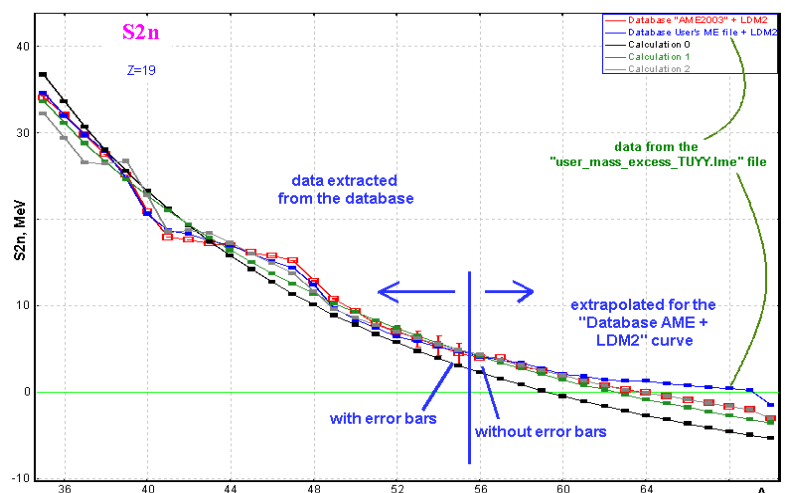


Fig.226. Two neutrons separation energy of Potassium isotopes.

## 1.8. LISE++ block structure development

### 1.8.1. New material block: FaradayCup



Fig.227. A portion of the "Set-up" dialog showing the "Faraday cup" block button.

The new material block "FaradayCup" was incorporated in the program (see Fig.227). Primary goal of the FaradayCup block (by analogy with reality) to stop transmission calculation in it. Initially the program guesses the FaradayCup block is made from W-material of  $10^7$  millimeters. If we put a regular material block with the same thickness, and any optical block will be somewhere behind this block then the code will

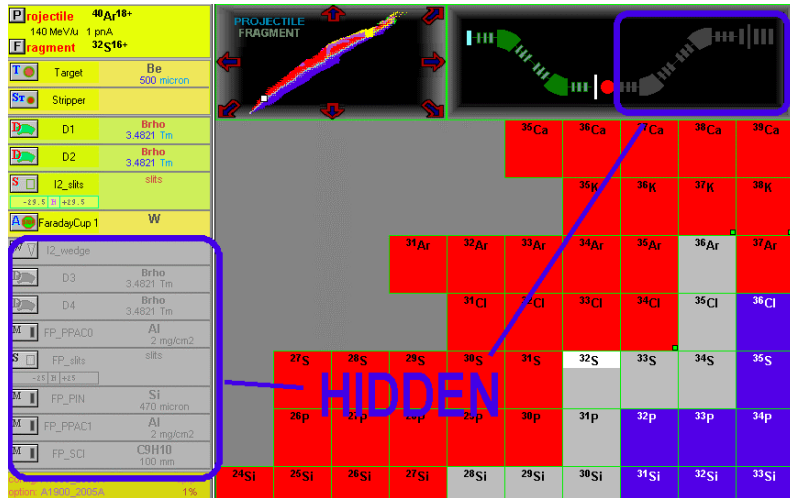


Fig.228. A portion of the LISE window demonstrating the "FaradayCup" block action.

show transmission 0%. The code assumes no more blocks (see Fig.228) behind the FaradayCup block and shows transmission from the target up to the FaradayCup block (see Fig.229). In addition, no materials are shown in the Physical calculator behind the Faraday cup.

If identification detectors were set behind the FaradayCup block in the Plot options" dialog then calculations will be done just up to the FaradayCup block, and the FaradayCup block will be used instead of these identification detectors.

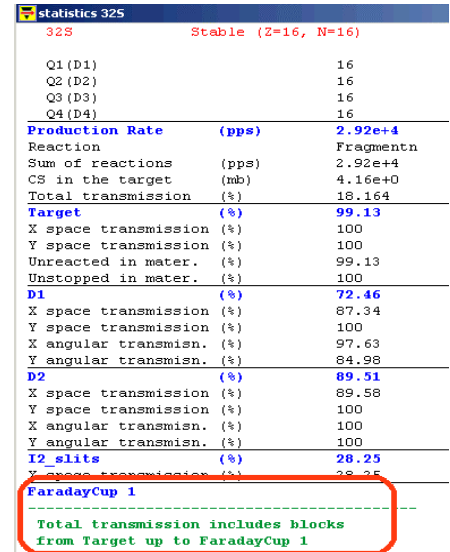


Fig.229. Transmission statistics window. Calculation were done up to the FaradayCup block. It is possible to see in the bottom of figure the message about blocks involved in calculations.

### 1.8.2. Append blocks in the current open configuration from other LISE files

The new version allows the create of new configurations by appending blocks from an existing file (\*.lpp or \*.lcn) into the current open document through the "File" menu (Fig.230). The user has to specify a location where new blocks will be inserted (see Fig.231).

Fig.232 shows a spectrometer built by the "Append blocks" command.

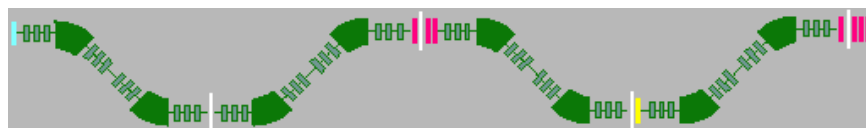


Fig.232. The spectrometer consisting of two A1900 fragment-separators built with the help of the "Append blocks from file" command.

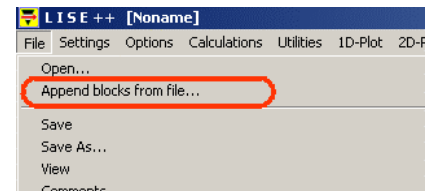


Fig.230. The new command "Append blocks from file" in the "File" menu.

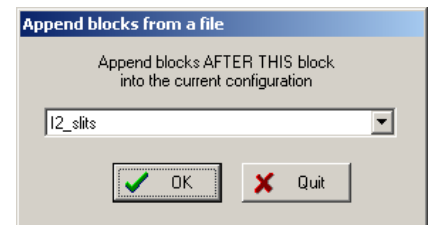


Fig.231.

## 1.9. Different

### 1.9.1. User cross-section file

The extension of user cross-section file accepted by the LISE++ code, depends on in what application the file was created:

Extension	Application	Type of cross-sections
*.cs	LISE++: the cross-section file dialog	All calculated by LISE++ reaction mechanism models: Abrasion-ablation, Fusion-residues, Abrasion-Fission, Coulomb fission
*.cs2	LISE++: the secondary reactions dialog	<b>Reduced</b> (sum of all process involved in fragment production including secondary reactions contribution)
*.cs4	PACE4	Fusion-residues

#### 1.9.1.1. User cross-section file: reaction property

The format of user cross-section file has been changed in the new version. The new data field “Reaction” was added in the user cross-section record in the code to keep in the operating memory as well as in the cross-section file.

The fifth column in the user CS file (see the “Cross-section file format” frame in Fig.233) shows a reaction label to assign this cross-section record to determine reaction. The new version allows one to keep user cross-sections in the memory for different reaction mechanisms. The reaction field should begin with the letter “R”, and the next number shows the reaction type.

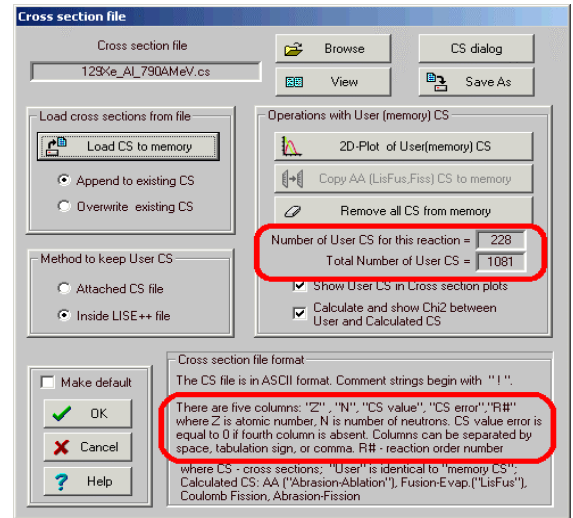


Fig.233. The “User cross-section file” dialog.

Index	Reaction	Index	Reaction
R0	Fragmentation	R4	Abrasion-Fission (Low Ex)
R1	Fusion -> Residual	R5	Abrasion-Fission (Mid Ex)
R2	Fusion -> Fission	R6	Abrasion-Fission (High Ex)
R3	Coulomb fission	R8	ISOL method

If the reaction field is omitted in a CS file, then the CS records will be assigned to the current reaction set in the code. When the user saves a CS file, the reaction field is always written in a user cross-section file (if the “Method to keep User CS” is set as “Attached CS file”) or in the LISE document currently opened (option “Inside LISE++ file”).

Using the “Cross-sections” dialog (see Fig.234) it is possible to list and edit user cross-sections for any reaction independently from the current reaction mechanism set in the code.

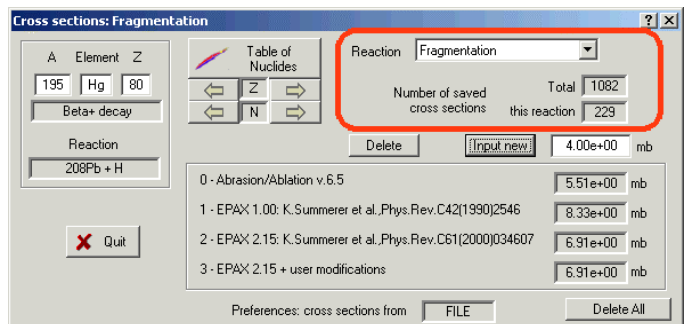
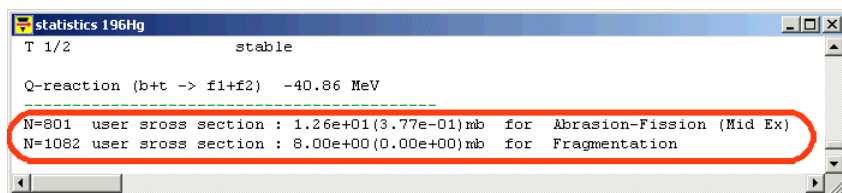


Fig.234. The “Cross-sections” dialog.

Presence of a user cross-section for an isotope can be also seen in the table of nuclides (see red and blue squares in Fig.235) as well as in the statistics window (see Fig.236).



**Fig.235.** The  $^{196}\text{Hg}$  isotope square of the table of nuclides. The red square in left bottom corner shows that there is a user cross-section in the memory and this cross-section value is applied for current calculations. The blue square shows the existence of a user cross-section value for a reaction mechanism, which is not currently being used.



**Fig.236.** Portion of the transmission statistics window showing not only the presence of user cross-sections in the memory for this isotope, but their details as well.

### 1.9.1.2. User file of reduced cross-sections

There is a very simple method to make your work with the code faster: do not repeat AF and secondary reactions calculations using a file with reduced CS. The User file of Reduced CS consists of three columns (no CS error and reaction columns).

- ❑ First it is necessary to calculate all AF cross-sections, then all secondary reactions contribution coefficients.
- ❑ Afterwards you have to save the calculated reduced cross-section values using the Secondary reactions dialog. Reduced cross-section is the sum of cross-sections of all EERs including the secondary reactions contribution.
- ❑ Turn off secondary reactions and leave just one working EER in the Abrasion-Fission dialog.
- ❑ Load the user file with reduced CS as a regular user CS file in the “Cross-section file” dialog.

**NOTE:** If you are saving calculated cross-sections in AF mode then remember that cross-sections will be saved JUST for ONE current excitation energy region.

**NOTE:** If you load an experimental AF cross-section file then you have to leave one EER and turn off the two other one because the experimental cross-section is the sum of cross-sections from all fissile nuclei.

### 1.9.1.3. CS files in LISE++ package

The new version installation package contains new user CS files for reactions of  $^{238}\text{U}$  and  $^{208}\text{Pb}$  beams with different targets.

**Table 39.** The “LISE\CrossSections-PublishedData” directory listing of files with published experimental cross-section values.

Subdirectory	File name	Reference
	129Xe_Al_790AMeV	[Rei98]
	136Xe_Al_760AMeV	[Zei92]
	40Ar_Be_1AGeV	[Oza00]
	40Ar_C_240AMeV	[Sym79]
	48Ca-Ta_90AMeV	[Not02]
	58Ni_Be_650AMeV	[Bla94]
208Pb\	208Pb_1H_1AGeV_evap	[Enq01]
	208Pb_1H_1AGeV_fission	[Enq01]
	208Pb_2H_1AGeV_evap	[Enq02]
	208Pb_2H_1AGeV_fission	[Enq02]
238U\	238U_Be_750AMeV_fission	[Ber97]
	238U_Pb_1AGeV_fission	[Enq99]
	238U_Pb_1AGeV_fragmentation	[Enq99]
	238U_p_1AGeV_fission	[Ber03]
	238U_p_1AGeV_spallation	[Tai03]



We recommend erasing the “LISE\CrossSections\PublishedData” directory before installation of the version 7.5 because locations of several CS files from previous versions were changed.

### 1.9.2. Curved profile degrader modifications

The new version is able to keep all properties of the curved profile inside the LISE++ file (\*.lpp). In the previous version the user could only attach a curved profile file to a LISE++ file.

The new version supports curved profile files created by the previous versions.

The “Current profile” is a separate class in the code which belongs to the Wedge class. Initially, when the code loads, “Current profile” does not exist. To create the “Current profile” the user has to load the Wedge dialog and run the Curved profile utility (see Fig.237).

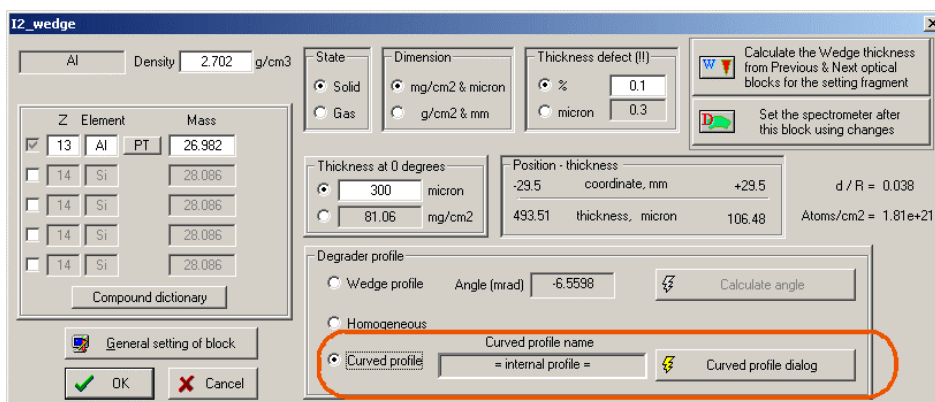


Fig.237. The Wedge dialog.

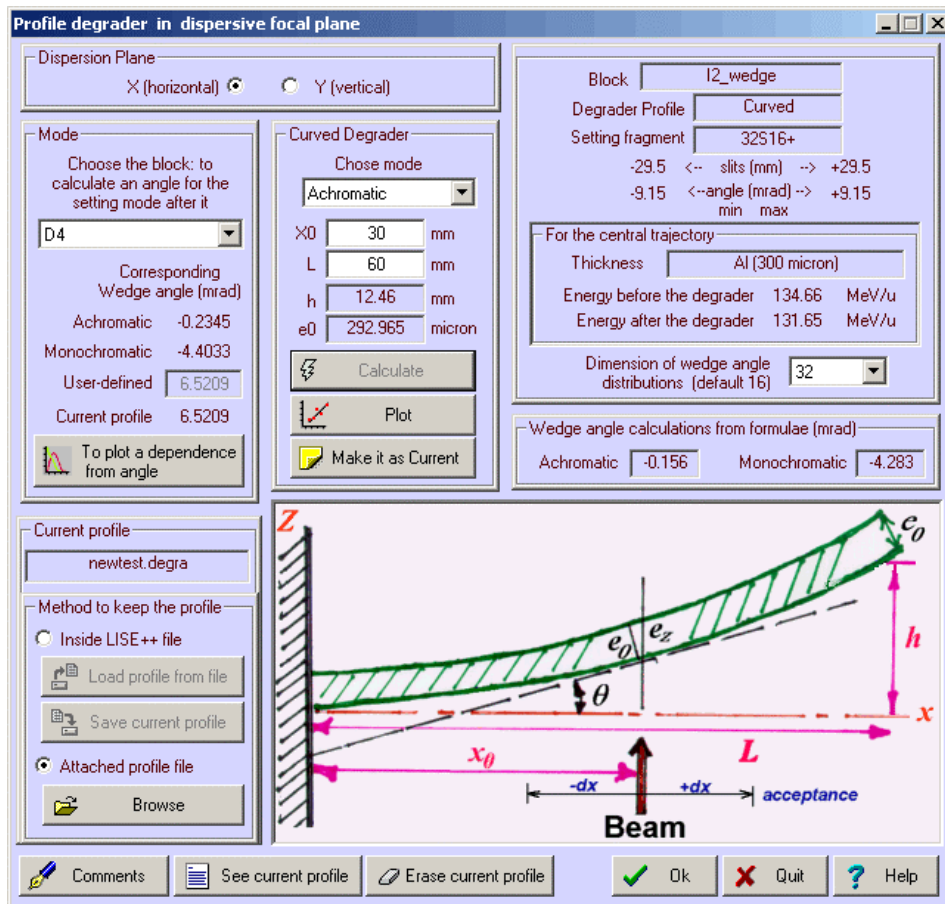
There are three possible variations in the “Curved profile name” message window (see Fig.237):

1. no current profile!
2. = internal profile =
3. the name of an attached curved degrader file (as in previous versions)

To create a new “current profile” the user has to complete the following steps (see Fig.238):

- a. Choose the block: to calculate the angle for the setting mode after it (for example “D4”);
- b. Choose the mode (Acromatic, Monochromatic, User-Deifned);
- c. Define X0 & L;
- d. Click the “Calculate” button;
- e. Choose the method to keep “current profile” (Inside LISE++ or the attached file);
- f. Click the “Make it current” button if calculations complete without any warnings;

You can make some comments, which will be saved together with the profile in LISE++ file as well as in the attached file in the corresponding mode. Do not correct curved degrader files (or LISE++ files) manually by text editors. The code checks a special structure of file and you can get an error message if, for example, you modified the comment line number 4 where the code keeps the settings of the “current profile” such as distribution dimension size.



*Fig.238. The Curved profile degrader dialog.*

**Load profile from file** – load a profile from an external file “\*.degra” to be the current profile. This works only if the “method to keep profile” is set to “Inside LISE++ file”

**Save current profile** – save the current profile to an external file “\*.degra”. This works only if the “method to keep profile” is set to “Inside LISE++ file”

**Browse** – load a profile from an external file and accept it as the current profile (only for mode “Attached profile file”). When you open a LISE++ file where the wedge block has a reference to an attached curved profile file, the code automatically loads the curved profile into the current profile.

“LISE/degrader” is the default directory for curved profile files.

Use the **Erase current profile** button if you want to use the Wedge profile mode and do not want to keep curved profile settings in a LISE file.

If the user quits the Wedge dialog pressing “Cancel” then all wedge settings, including curved profile, settings will be restored.

Even if the user chooses the “Wedge profile” for degrader profile mode, the existing current curved profile **will be kept** in the code and saved in LISE++. To avoid this you have to erase the “current profile” in the “Curved profile degrader” dialog.


### 1.9.3. Logotypes and references

In the version 7.5 by clicking on a logotype in the left bottom corner of the code the user can load a web site connected with this logotype. Logotypes of laboratories and scientific organizations, which have made or are making contributions to the development of the program, each appear 6 seconds.

Logotype	Organization	WEB address
	FLNR Dubna Russia	<a href="http://flerovlab.jinr.ru/flnr/">http://flerovlab.jinr.ru/flnr/</a>
	JINR Dubna Russia	<a href="http://www.jinr.ru/">http://www.jinr.ru/</a>
	GANIL Caen France	<a href="http://www.ganil.fr/">http://www.ganil.fr/</a>
	IPN Orsay France	<a href="http://ipnweb.in2p3.fr/">http://ipnweb.in2p3.fr/</a>
	CEA France	<a href="http://www.cea.fr/">http://www.cea.fr/</a>
	IN2P3 France	<a href="http://www.in2p3.fr/">http://www.in2p3.fr/</a>
	NSCL East Lansing USA	<a href="http://www.nscl.msu.edu/">http://www.nscl.msu.edu/</a>
	MSU East Lansing USA	<a href="http://www.msu.edu/">http://www.msu.edu/</a>
	National Science Foundation USA	<a href="http://www.nsf.gov/div/index.jsp?org=PHY">http://www.nsf.gov/div/index.jsp?org=PHY</a>
	Department of Energy USA	<a href="http://www.sc.doe.gov/np/">http://www.sc.doe.gov/np/</a>
	GSI Darmstadt Germany	<a href="http://www.gsi.de/">http://www.gsi.de/</a>

## 1.9.4. 2D-plots: contours & projections

### 1.9.4.1. Contour dialog

In the new version during work with Monte Carlo or cross-section 2D-plots it is possible to take advantage of some new utilities: contours and projections. Using the icon  in the 2D-plot toolbar the user can load the Contour dialog (see Fig.239) to begin creation of a new contour, to save a contour from the operating memory in a file or to load a contour from a file. Only one contour can be in memory. The extension of contour files is “\*.contour”, and by default the contour files are found in the “LISE\Spectra” directory.

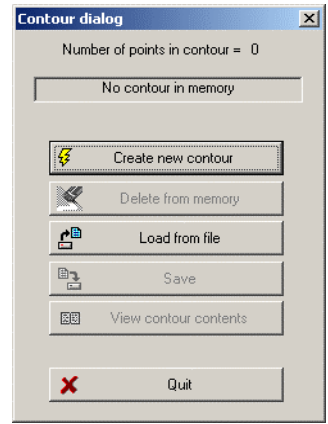


Fig.239. The Contour dialog. No contours in memory.

Fig.240 and Fig.241 show contour examples for 2D cross-section and Monte Carlo plots respectively.

In the case of a 2D cross-section plot (Fig.240) the rectangle with coordinates  $X \pm dX$ ,  $Y \pm dY$  will be inside of the contour (or for window projections in the slice created by user zoom) if the central point (X,Y) is found inside the contour if even the contour line crosses this rectangle.

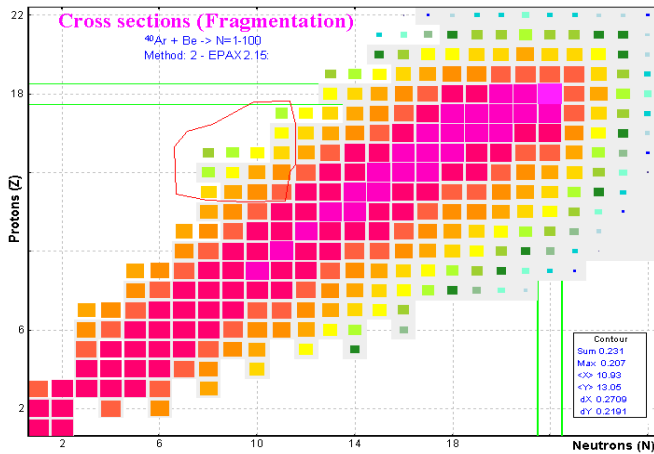


Fig.240. The contour example for a 2D cross-section plot.

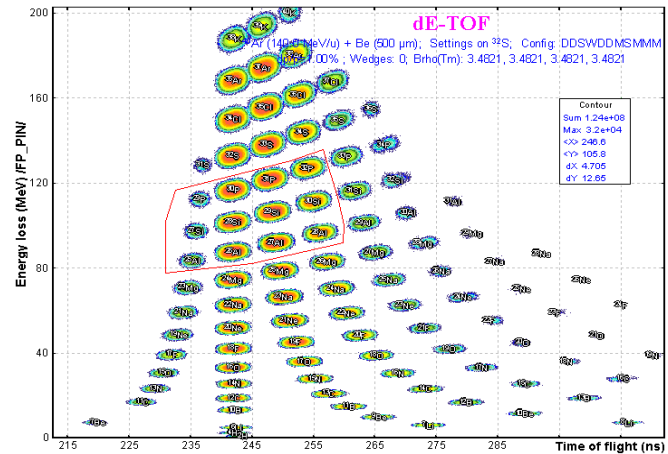


Fig.241. The contour example for a Monte Carlo plot.

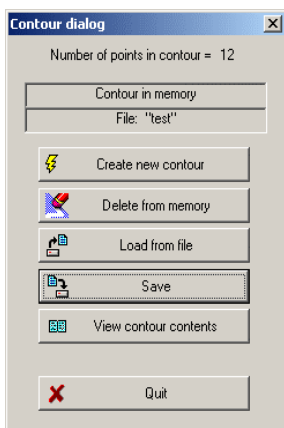


Fig.242. The Contour dialog. The “Test” contour in the memory.


If the contour already exists in memory the Contour dialog looks as shown in Fig.242. The user can manipulate a contour in memory: save, view, erase. The contour content is shown in Fig.243.

#### 1.9.4.1.1. Window and contour projections on an axis for 2D Cross-section plot

The screenshot shows a window titled 'Contour contents'. It displays the following information: '02-08-2005 16:04:55 Version 7.4.166', 'Plot name : Cross sections (Fragmentation)', 'X-axis: Neutrons (N)', 'Y-axis: Protons (Z)', and 'Number of points: 12'. Below this is a list of 12 data points with their X and Y coordinates.

Point	X (Neutrons)	Y (Protons)
1	6.578	15.346
2	6.6353	12.908
3	7.8938	12.601
4	9.5242	12.506
5	11.126	12.553
6	11.326	14.045
7	11.555	14.4
8	11.526	16.459
9	11.326	17.642
10	9.8102	17.595
11	8.1226	16.459
12	7.1215	16.104

Fig.243. Contents of the contour file.

Clicking the  icon in the 2D-plot toolbar the user loads the “Projections” dialog (Fig.244) to select the type of projection: on what axis (horizontal or vertical) as well as what data (for the contour or for the whole window). Fig.245 shows the projection of the contour in Fig.241 on the horizontal axis.

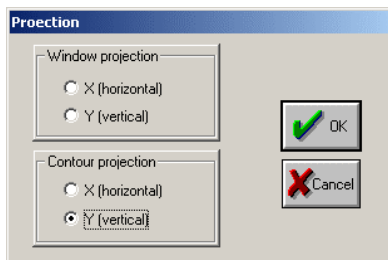


Fig.244. The Projection dialog.

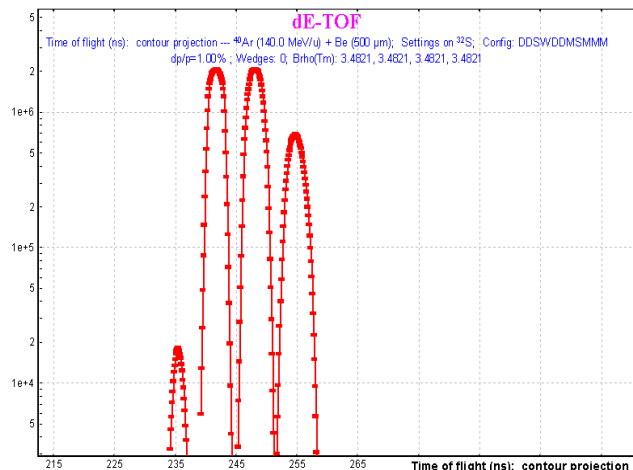


Fig.245. The horizontal projection of the contour in Fig.241.

### 1.9.5. Fission channel for the fusion-evaporation excitation function plot

Initially the Fusion-Residue reaction mechanism was incorporated into the code disregarding the fission deexcitation channel of the excited compound nucleus. In the new version the fission channel was included in the list of possible deexcitation channels, and in connection with this, the fission channel was also added in the fusion-residue excitation function plot. The user can turn on/off the fission channel in the “Fusion cross-section plot” dialog (Fig.246).

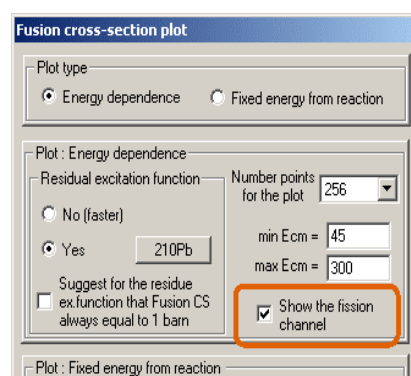


Fig.247 shows the  $^{210}\text{Pb}$  excitation function in the reaction  $^{12}\text{C} + ^{208}\text{Pb}$ .

Fig.246. Portion of the “Fusion cross-section plot” dialog.

**Note:** The fission channel calculation may increase the time to calculate fusion-residues excitation function, because in the previous version if the fusion-residues cross-section became very small with increasing excitation energy then the evaporation cascade automatically was stopped, even if the last point (“max Ecm” in Fig.246) was not yet reached. In the case of fission the calculation always goes to the last point.

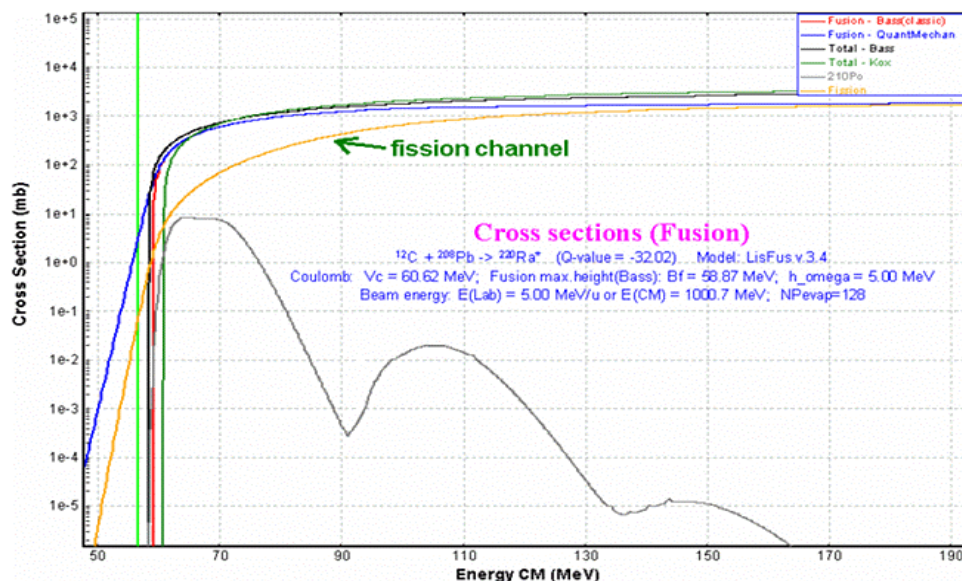


Fig.247.  $^{210}\text{Pb}$  excitation function in the reaction  $^{12}\text{C} + ^{208}\text{Pb}$ .

### 1.9.6. Abrasion-Ablation: fast mode for heavy projectiles

In the new version it is possible to speed up the cross-section calculation process when using the Abrasion-Ablation model for heavy projectiles, taking into account secondary reactions contributions. The principal difference between the fast mode of AA and the regular is the dimension of the evaporation distributions, which is equal to 8 for the fast mode of AA. It is impossible to manually set such a small value in the “Evaporation options” dialog.

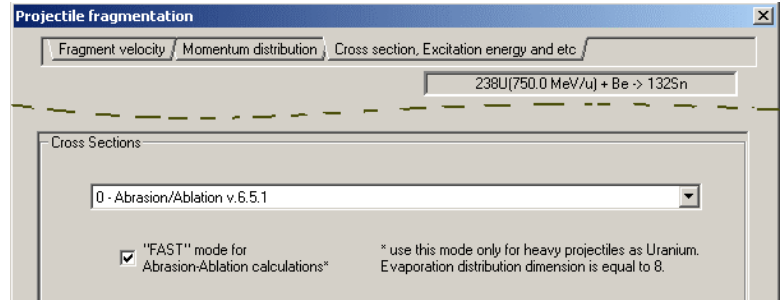


Fig.248. Fragment of the “Projectile fragmentation” dialog.

To select the AA fast mode it is necessary to choose the AA model and set the flag in the “fast mode” checkbox in the “Projectile fragmentation” dialog (Fig.248).



Fig.249. Fragment of the “Set-up” window.

The following messages, when fragmentation is set as the reaction mechanism in the code, will be shown in the left bottom corner of the code, depending on the model to being used to calculate the production cross-section (see Fig.249):

Cross-section model	Message
EPAX	Fragmentation
Abrasion-Ablation	Fragmentation-AA
Fast mode of Abrasion-Ablation	Fragmentation-AA fast

### 1.9.7. The "About" dialog modifications

The “About” dialog contains the information on the LISE and LISE++ codes official publication, which can be used for citation. Clicking on one of the selected papers (Fig.250) will load it in your default browser.

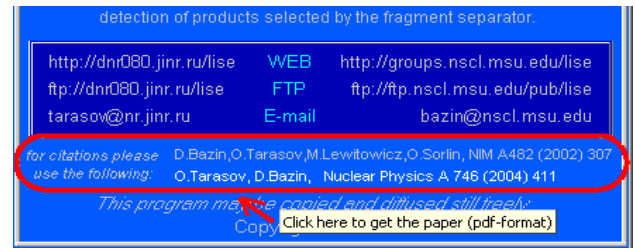


Fig.250. Portion of the “About LISE++” dialog.

### 1.9.8. PACE4: User's limits for Angular and Energy distributions of residues

The PACE4 code after ending calculation displayed energy and angular distribution tables just for the 15 most intense fusion residual nuclei. This restriction was caused by the limited operating memory and output file size, and decreased the time necessary for calculation and sorting. However, some remarks from the users have arrived encouraging the inclusion of low intensity products as well. We have decided not to increase the number of tables to solve this problem, but to give to the user the possibility to choose products to be displayed based on their intensity. The user determines the intensity window in the first dialog (right bottom corner of this dialog) of the program (see Fig.251).

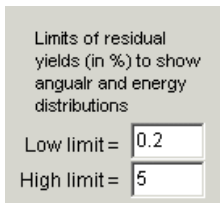


Fig.251.

### 1.9.9. Gas density dialog

Be very careful with the gas density calculation using the “Gas density” dialog! The calculations will be correct only for a molecular formula (see Fig.252). This dialog cannot be used for a gas mixture!

In the case of a gas mixture, to correctly calculate energy loss in material or interaction cross-sections it is better to enter a percentage ratio, but the gas density should be input **manually**. Let's consider a case of the ionization chamber filled by gas mixture of Argon (90%) and butylene (10%). The “Gas density” dialog will automatically

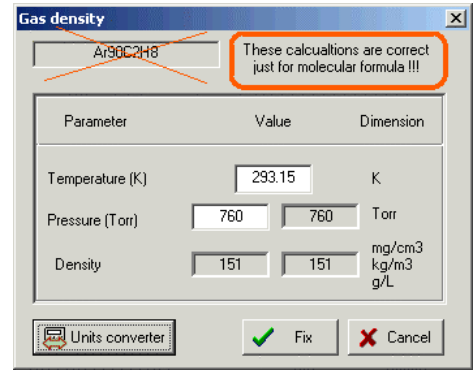


Fig.252. The “Gas density” dialog.

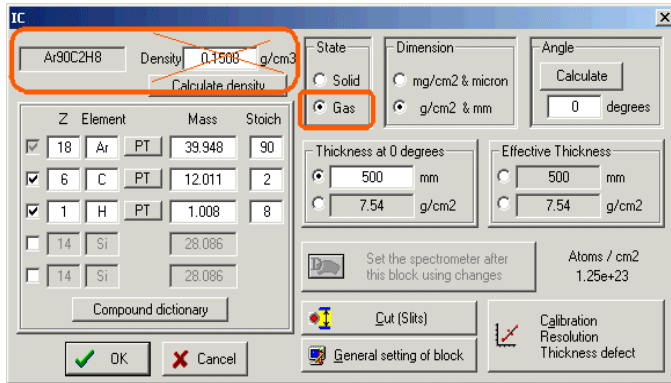


Fig.253. The “Material Thickness” dialog

calculate for you the density value of 0.1508 g/cm<sup>3</sup> (see Fig.253). However, the density of this mixture should actually be near to argon density (0.0016608 g/cm<sup>3</sup> at P=760 Torr). Therefore, it is recommended in the case of gas mixture at the beginning to input the mixture components and percentages, and then manually to input a density value, because if the percentage or components were changed then the program automatically calculates the density.

### 1.9.10. Block labels for the transport envelope

Block labels were incorporated for the envelope transport plots (Fig.254).

### 1.9.11. Drift block

It is possible to have drift block parameters shown in the Set-up window (Fig.255).

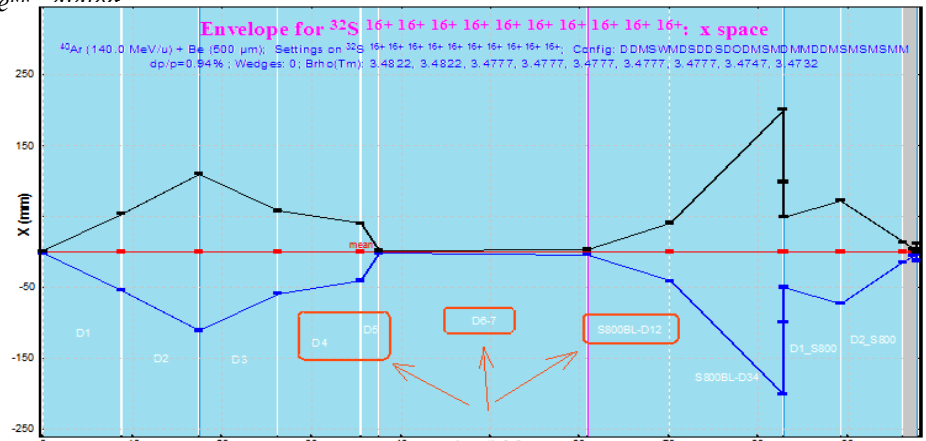


Fig.254. The <sup>32</sup>S transport envelope.

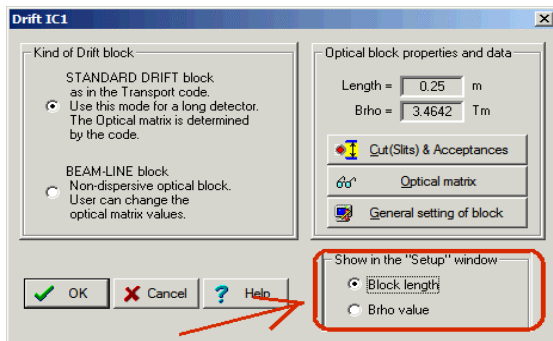
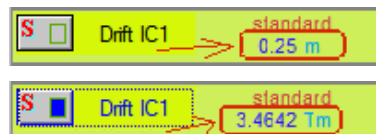


Fig.255. The “Drift block” dialog and drift block parameters in the “Set-up” window.



### 1.9.12. Compound targets for AA calculations, fusion-residues and fission reactions

The new version allows one to use a compound target for AA calculations, fusion-evaporation and fission reactions. The user can select what target component will be used for cross-section calculations (see Fig.256). Just one material component can be used for this purpose.

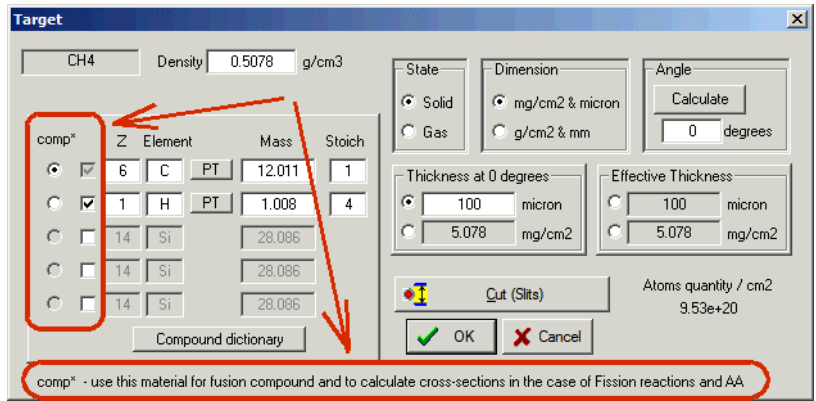


Fig.256. The “Target” dialog for compound material for fission reactions.

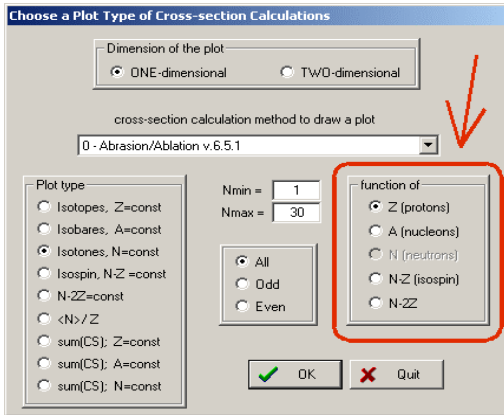


Fig.257. The “Cross-section plot” dialog.

### 1.9.13. Choice of horizontal axis for 2D-plots

All dialogs connected to 2D-plots (cross-sections, isotope database values, transmission values etc) were modified to give an opportunity to choose a horizontal axis from the list of axes possible for this plot type (Fig.257).

This novelty was incorporated into the program just before the completion of this documentation. For this reason almost all plot dialogs in the documentation were shown in the old style.

### 1.9.14. Version numbers

Version 7.2 devoted to implementation of the AME2003 database was the latest announced version. However we used the version number 7.3.\* just for the NSCL internal purpose to keep the program without global modifications, only for bug corrections. Version number 7.4.\* was used temporarily for global development of the code.

If a previous version (below 7.5) saved file contains calculation results, then the code (v.7.5) recalculates them due to changes in the list of transmission coefficients and implementation of the total reaction yield value.

### 1.9.15. LISE user statistics

Fig.435 shows in which countries there is interest in LISE++. The statistics correspond to the past two years, and are based on identified visits of the LISE sites<sup>♦</sup> (Fig.258).

Fig.260 shows statistics among US universities and laboratories.

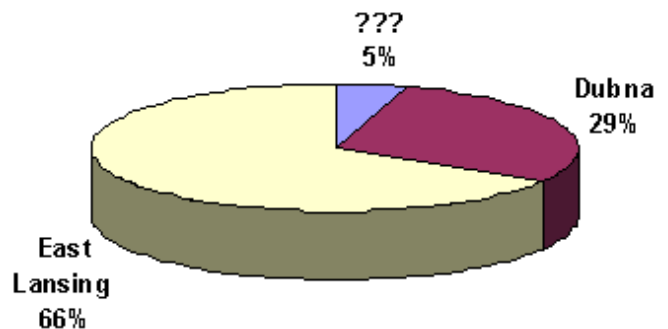
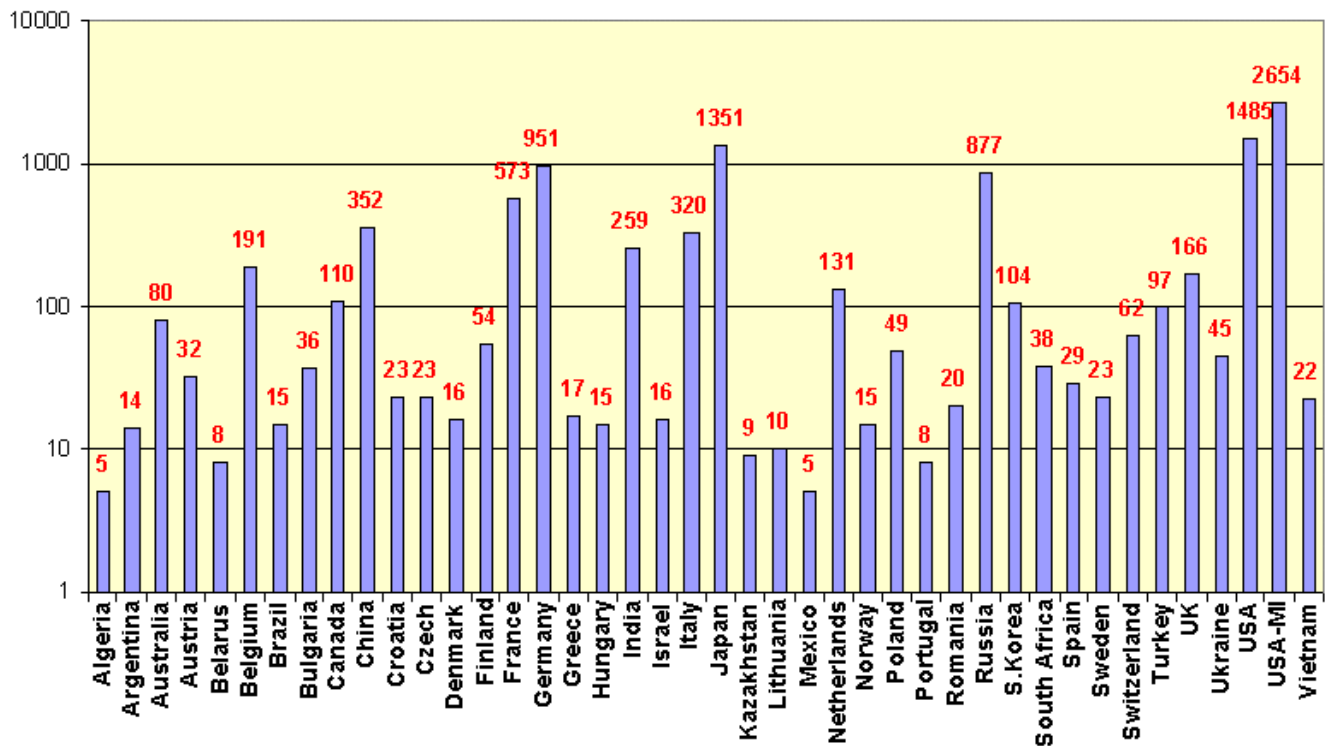


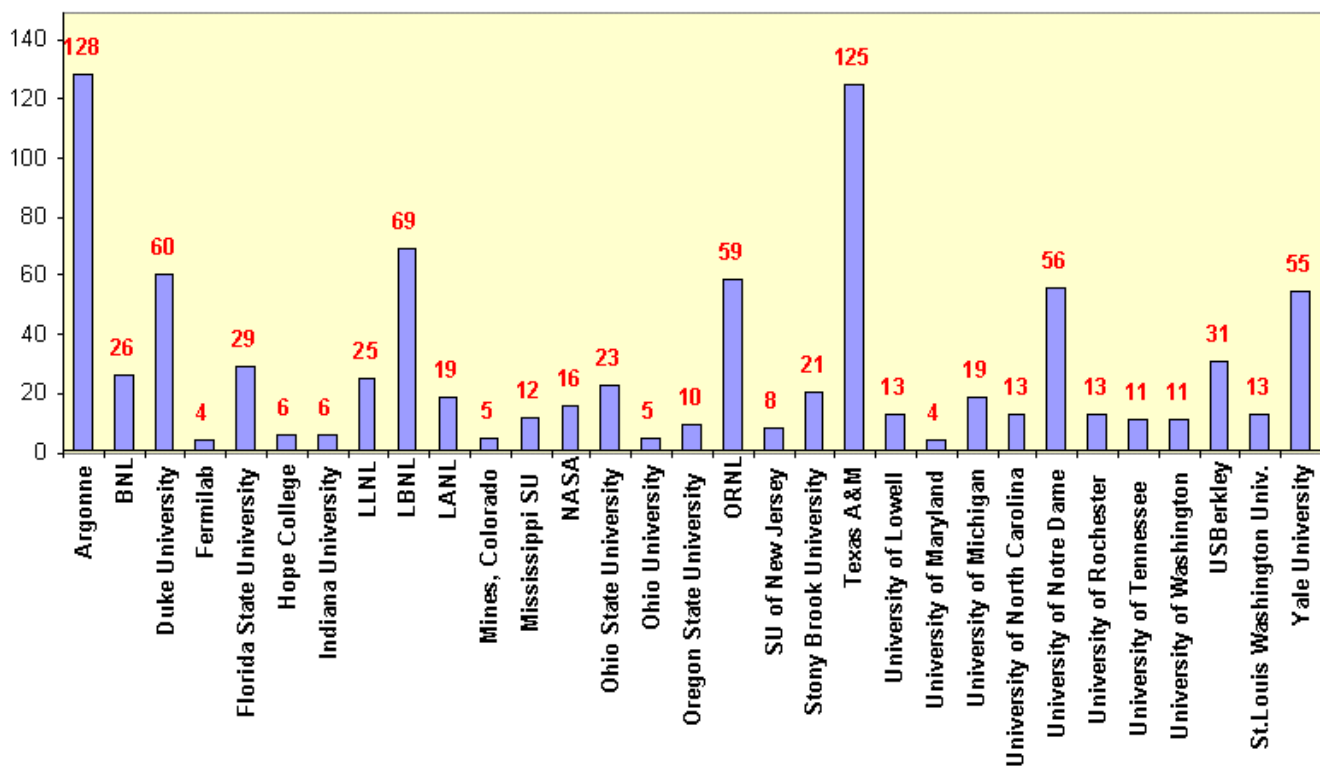
Fig.258. Statistics between LISE sites.

<sup>♦</sup> Due to temporary problems with the work of dnr080 server (at Dubna) about 30-40 percent of all hits were lost.





**Fig.259.** User statistics for the LISE web sites. The “USA” label refers to number of hits excluding MSU & NSCL contributions. The “USA-MI” label includes just hits from MSU or NSCL. Statistics are shown whenever the number of hits was more than 4.



**Fig.260.** User statistics of the LISE web sites for US universities and laboratories (without MSU and NSCL). Statistics are shown if the number of hits was more than 3.

## 1.10. User requests and bugs report

There are several corrections and user requests what we want to note.

### 1.10.1. Corrections

<ul style="list-style-type: none"> <li>▪ <i>Optical matrix: validation procedure of input value;</i></li> <li>▪ <i>Fusion-residue transmission: cross-section calculation procedure.</i></li> </ul> <p style="text-align: right;">D.Morrissey (NSCL)</p>	<i>Fixed</i>
<ul style="list-style-type: none"> <li>▪ <i>The Range plot subroutine.</i></li> <li>▪ <i>The “Block material” dialog.</i></li> <li>▪ <i>Universal parameterization (low limit for separation energy)</i></li> <li>▪ <i>Wedge angle calculation</i></li> </ul> <p style="text-align: right;">M.Haussman (NSCL)</p>	<i>Fixed</i>
<ul style="list-style-type: none"> <li>▪ <i>Calculation of charge state distribution after the target &amp; stripper in the non-equilibrium mode.</i></li> <li>▪ <i>Surviving probability: weight error.</i></li> </ul> <p style="text-align: right;">H.Weik (GSI)</p>	<i>Fixed</i>
<ul style="list-style-type: none"> <li>▪ <i>Charge states for Monte Carlo plots.</i></li> <li>▪ <i>The Envelope plot.</i></li> <li>▪ <i>Reactions in target (surviving coefficient) for light target.</i></li> <li>▪ <i>Correction in the Set-up window refresh procedure</i></li> </ul> <p style="text-align: right;">OT</p>	<i>Fixed</i>
<p><i>Kantele’s Spectrometric calculator: subroutines ICCK and ICCTot.</i></p> <p style="text-align: right;">A.Andreev (TRIUMF)</p>	<i>Fixed</i>
<p><i>Gas density calculator</i></p> <p style="text-align: right;">OT, S.Lukyanov (Dubna&amp;NSCL)</p>	<i>See chapter 1.9.9.</i>
<p><i>2D-ellipse plot</i></p> <p style="text-align: right;">S.Lukyanov(Dubna&amp;NSCL), OT</p>	The same problem with the "Goodies" dialog and result files. <i>Fixed.</i>
<p><i>Angular straggling (plane – space)</i></p> <p style="text-align: right;">Sam Austin (NSCL)</p>	<i>Fixed</i>
<p><i>Set-up window redraw process for target inclination</i></p> <p style="text-align: right;">L.Perrot, F.de Oliviera, C.Stodel (GANIL)</p>	Very old and confused bug ☹ <i>Fixed</i>
<p><i>Memory leaks</i></p> <p style="text-align: right;">OT M.Haussman (NSCL)</p>	Serious bugs which can result in code crash in the batch mode. <i>99% Fixed</i>
<p><i>Joint fusion residue and primary beam transmission</i></p> <p><a href="http://groups.nsl.msu.edu/lise/7_5/examples/fusion_and_primary_beam.lpp">http://groups.nsl.msu.edu/lise/7_5/examples/fusion_and_primary_beam.lpp</a></p> <p style="text-align: right;">Z.Podolyak (Surrey)</p>	<i>Fixed. See Fig.261.</i>

statistics <sup>136</sup> Xe									
<sup>136</sup> Xe Stable (Z=54, N=82)									
Q1 (stripper)		51	50	49	48	48	47	46	
Production Rate (pps)		1.51e-4	1.99e+0	2.02e+3	5.16e-14	3.14e+5	9.74e-12	1.17e+7	4.63e-10
Sum of charge states (pps)		6.25e+9	6.25e+9	6.25e+9	6.48e-7	6.25e+9	6.48e-7	6.25e+9	6.48e-7
Reaction		BEAM	BEAM	BEAM	FusRes	BEAM	FusRes	BEAM	FusRes
Sum of reactions (pps)		0.23e75	0.23e75	0.23e75	0.23e75	0.23e75	0.23e75	0.23e75	0.23e75
CS in the target (mb)		beam	beam	beam	beam	beam	beam	beam	beam
Total transmission (%)		2.42e-12	3.18e-8	3.23e-5	7.96e-6	0.005	0.002	0.187	0.072

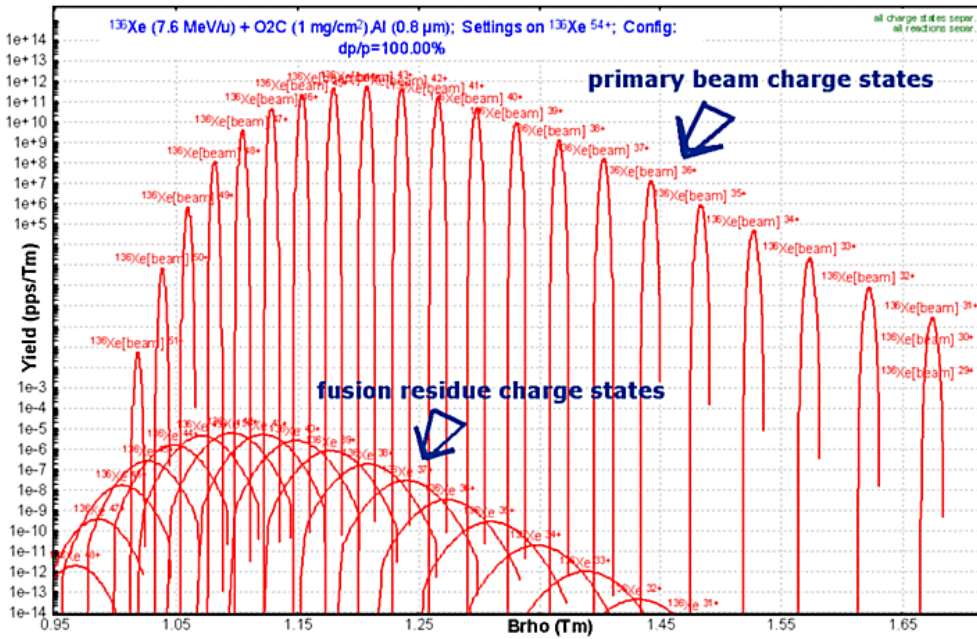


Fig.261. A portion of the statistics window (top plot) and  $B\rho$  distribution plot (bottom plot) of the  $^{136}\text{Xe}$  ions produced in  $^{136}\text{Xe}(7.6\text{MeV/u}) + \text{CO}_2(1\text{mg/cm}^2) + \text{Al}(0.8\mu\text{m})$ .

### 1.10.2. User requests

Keeping the curved profile degrader in the LISE++ file. The A1900 group (NSCL)	Modified. See chapter 1.9.2.
PACE4: User's limits for Angular and Energy distributions of residues. L.Penescu (GANIL), Andrey Blazhev (University of Sofia)	Implemented. See chapter 1.9.8.
Transport envelope: block labels. D.Morrissey (NSCL)	Implemented. See chapter 1.9.10.
Drift block: $B\rho$ -value in the Set-up window. D.Morrissey (NSCL)	Implemented. See chapter 1.9.11.
Compound target for the fusion-residues reaction. A.Semchenkov (GSI)	Modified. See chapter 1.9.12.
Choice of horizontal axis for 2D-plot. M.Thoennessen (NSCL)	Modified. See chapter 1.9.13.
New FRS configurations: "FRS - TA-Cave C.lcn", "FRS - TA-ESR.lcn", "Super-FRS.lcn", "FRS- TA-S4 new standard.lcn". H.Weick (GSI)	Implemented in the LISE installation package.

## **1.11. Next steps development**

### **1.11.1. First priority**

#### ***Long-term***

- Secondary reactions in wedge; secondary target block
- Monte Carlo transmission

#### ***Short-term***

- Compilation of LISE documentation based on all LISE version announcements.
- New reaction mechanism: Binary reactions (just kinematics)
- New block: RF kicker (deflector system for proton-rich fragments).
- New block: Solenoid (selection due to angular distribution).
- Create more help-files.

### **1.11.2. Second priority task**

- LISE++ paper
- Abrasion-Fission paper
- Fusion-Fission reaction mechanism
- Possibility to use the angular momentum in fusion-fission & residues calculations.

### **1.11.3. Third priority task**

- Alternative models to calculate fission fragment distributions
- Three-body kinematics calculator
- Charge state distribution model for low energies.
- Wedge (including curved profile wedge) inclination.
- "Water" wedge procedure (wedge with one moving plane and filled by liquid).
- Development of the spallation mechanism in the code.
- Development of a database of experimental data from various fission and fragmentation experiments.
- Create the possibility to insert a material before the target. (to take into account energy loss, straggling, charge states)
- Develop a subroutine to calculate a reduced dispersion for large values of  $dp/p$ .
- Abrasion-Ablation as a function of the primary beam energy (as done for momentum distribution of products of projectile fragmentation)

## ***Acknowledgements***

The authors thank Mr. Matthew Amthor for carefully proofreading this manual.

We are grateful to Prof. Brad Sherrill for continuous support and guidance. Fruitful discussions with Prof. Michael Thoennessen and Prof. Dave Morrissey are gratefully acknowledged.

The LISE++ authors thank Dr. Jorge Pereira Conca for help in developing the Abrasion-Fission model.

We are very appreciative of Dr. Marc Hausmann, Dr. Helmut Weik, and the A1900 staff for so intensely using the code and bugs searching.

Thanks to everyone who sent wishes and remarks allowing the modification of the LISE++ code for the best possible performance.

## 2. Version 7.1: Coulomb Fission

### 2.1. Introduction

High-energy secondary-beam facilities such as GSI, RIA, and RIBF provide the technical equipment for a new kind of fission experiment [Sch01]. Fission properties of short-lived nuclei can be investigated in inverse kinematics. A new model of fast analytical calculation of fission fragment transmission through a fragment separator has been developed in the framework of the code LISE++.

The reaction mechanism determines the excitation energy, deformation and angular momentum of the fissioning system. Here is an attempt to classify fission reaction mechanisms:

1. spontaneous fission;
2. photofission;
3. Coulomb (electro-magnetic) and electron fission;
4. fusion-fission (fast fission, quasifission);
5. fission induced by nuclear reactions (proton-induced, spallation and etc).

However from the point of view of the LISE++ code only the following fission reactions are interesting to simulate fragment transmission through a fragment-separator:

1. Coulomb (electro-magnetic) fission;
2. fusion-fission;
3. abrasion-fission (spallation in inverse kinematics).

This version devoted to the new reaction mechanism “Coulomb Fission” has been developed in LISE++ mainly based on GSI experience. The two other fission mechanisms will also be developed soon in LISE++.

In the development of this new reaction mechanism in the LISE++ framework it is possible to distinguish the following principal directions:

- Kinematics of reaction products;
- Production cross-section of fragments
- Spectrometer tuning to the fragment of interest to produce maximal rate (or purification).

The next three chapters are devoted to these questions. The kinematics of fission products was realized in two different ways: Monte Carlo method<sup>†</sup> and LISE “classical”method<sup>‡</sup>.

The following assumptions were made for Coulomb fission:

- The angular momentum of the fissile nucleus is equal to 0;
- The spatial distribution of fragments is isotropic as a consequence of the previous assumption;
- Fission takes place without preliminary emission of light particles from the projectile;
- The primary beam energy is high enough to assume that  $\text{tg}(\theta) \approx \theta$ , where  $\theta$  is the angle between beam and fragment directions in the case of *DistrMethod*.

---

<sup>†</sup> *MCmethod* – Monte Carlo method of fission fragment kinematics.

<sup>‡</sup> *DistrMethod* – analytical distribution solution using transport integral theory.

## 2.2. Fission fragment kinematics at intermediate and high energies

### 2.2.1. Kinematical description

The kinematics of the fission process is characterized by the fact that the velocity vectors of the fission residues populate a **narrow shell of a sphere in the frame of the fissioning nucleus**. The radius of this sphere  $V_f$  is defined by the Coulomb repulsion between both fission fragments. In the case of reactions induced by relativistic heavy ions, the transformation into the laboratory frame leads to an **ellipsoidal distribution** which will characterize the angular distribution of fission residues [Ben02, Amb96].

An example of the velocity spectrum is shown in Fig.262b [Ber03]. Two narrow asymmetric peaks are observed roughly equidistant from velocity zero, i.e. the projectile velocity. Velocities are defined in reference to the beam direction i.e. forwardly and backwardly emitted fragments have positive and negative velocities, respectively. Velocity vectors of a specific isotope populate a thin spherical shell in the fissioning system. The sphere is pictured in Fig.262a [Ber03] by a circle, the cut of the sphere by a plane which contains the beam. Only forward and backward cups of the sphere, defined by the angular acceptance  $\alpha$  of the Fragment Recoil Separator, are transmitted, and the longitudinal projections of their velocity distributions are shaping the two peaks (Fig.262 b).

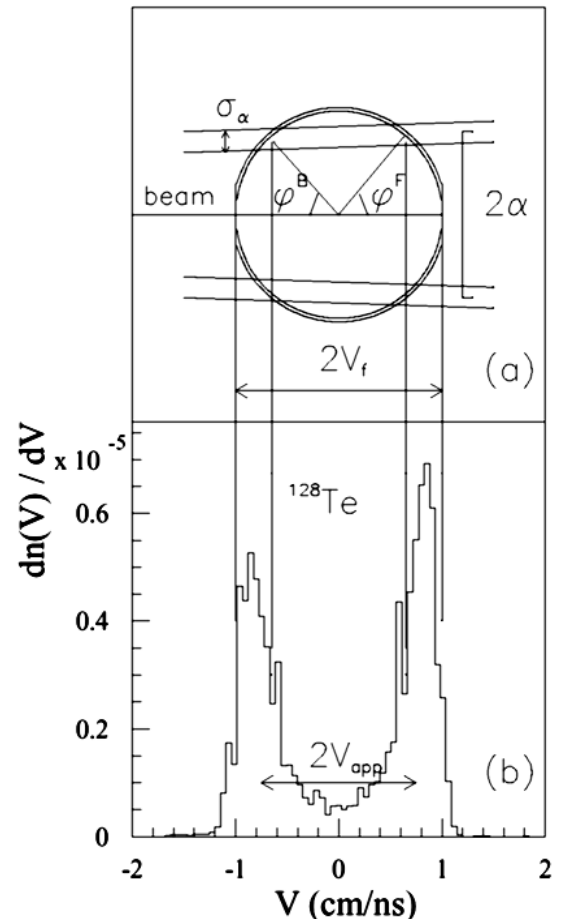
Two different methods for fission fragment kinematics are available in LISE++: *MCmethod* and *DistrMethod*.

*DistrMethod* is the fast analytical method applied to calculate the fragment transmission through all optical blocks of the spectrometer. *MCmethod* has been developed for a qualitative analysis of fission fragment kinematics and utilized in the Kinematics calculator.

*Note:* The user is setting the excited fission fragment then the code calculates expected final fragment in the case of *MCmethod*, but the situation is opposite in the case of *DistrMethod*: the user is setting the final fragment in ground state and then find out expected excited fragment as result of splitting the projectile nucleus.

### 2.2.2. Monte Carlo simulation of fission fragment angular and energy transmissions

To get Monte Carlo simulation of fission fragment transmission it is necessary to click on the button “2D fragment plot” from the “Kinematics calculator” dialog (see Fig.263) in the mode “BREAKUP (FISSION)”. Q-value of the reaction should be positive, else this button is disabled.



**Fig.262.** a) Schematic view of the experimental parameters shaping the measured velocity spectrum in the frame of the fissioning system.  $V_f$  the fission-fragment velocity,  $\alpha$  is the angular acceptance of the FRS, and  $\sigma_\alpha$  its variance.  $\phi^{B,F}$  are the corresponding emission angles of fission fragments in the fissioning system in forward and backward directions, respectively. b) Velocity spectrum of  $^{128}\text{Te}$  in the frame of the fissioning system. The velocity  $V = 0$  refers to the projectile frame [Ber03].

The first version of fission fragment kinematics Monte Carlo simulation was done just for angular and energy transmissions assuming:

- manual settings of fragment excitation energy;
- target thickness equal to zero (see Fig.264).

In the dialog it was possible to set:

- The energy, horizontal and vertical angular emittances;
- The angular acceptance shape;
- The horizontal and vertical angular values and their variance<sup>1</sup>;
- The center of energy silts and their size in %.

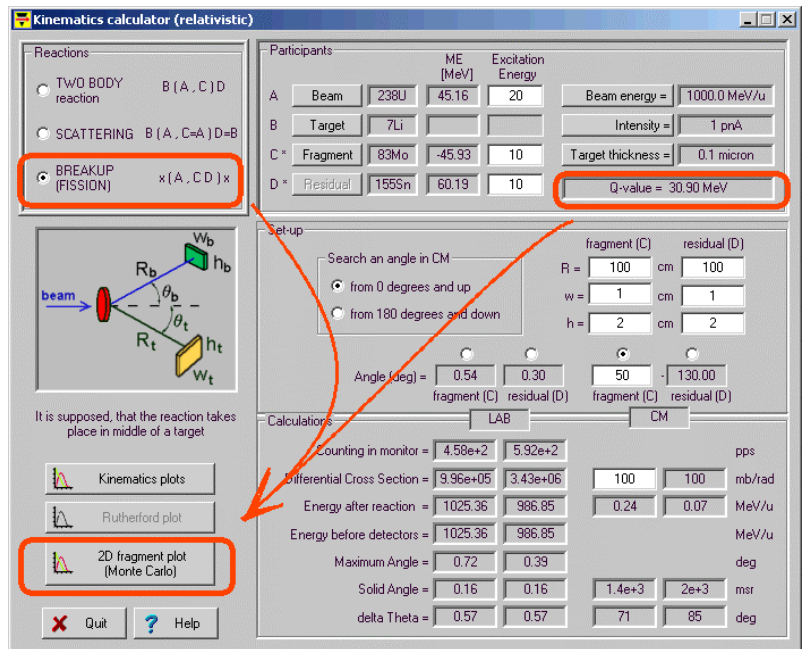


Fig.263. The “Kinematics calculator” dialog.

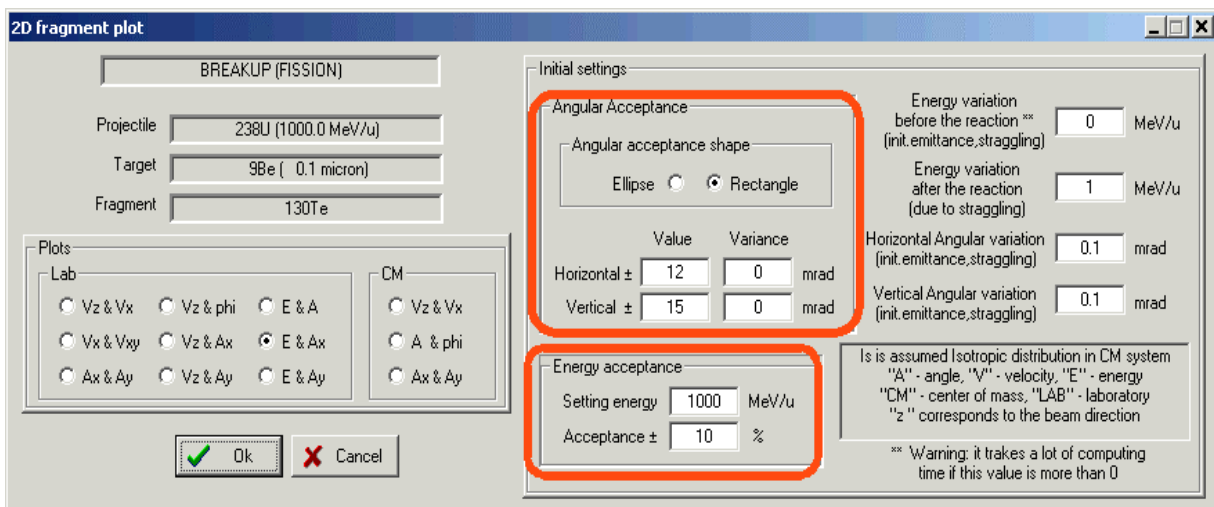


Fig.264. The “2D fragment plot” dialog (version 6.6).

There are twelve different 2D plots that can be done. Nine of them are in the laboratory frame, and the three other are in the center-of-mass system. All reaction settings and excitation energies can be entered in the “Kinematics calculator” dialog.

*Note:* A positive value of the energy variation before reaction reduces the calculation speed because the code needs to recalculate all initial kinematics angular and energy distributions for each fission event. Otherwise initial distributions are calculated only once at the beginning of calculations.

<sup>1</sup> It has been done It was made by analogy to work of M.Bernas et al.[Ber03], but actually an angular acceptance is constant value, and the idem variations can be explained by the initial angular emittance of a beam, and angular straggling of the beam and the fragment in the target.



An example of the Monte Carlo simulation plot of fission fragment transmission is shown in Fig.265. In the right gray box it is possible to see an angular and energy acceptance transmission result. The projection of the plot in Fig.265 on the horizontal axis ( $V_z$ ) is shown in Fig.266.

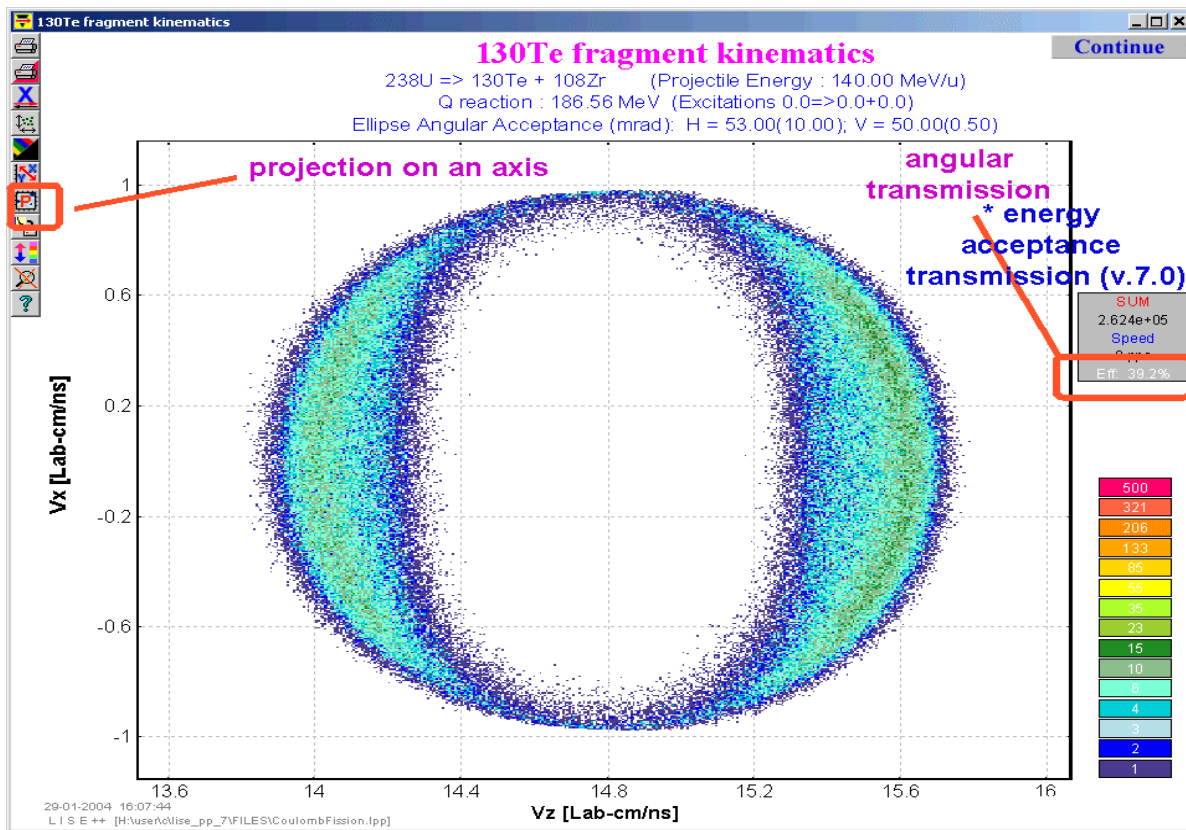


Fig.265. Monte Carlo simulation: 2d-identification plot  $V_x$  versus  $V_z$  in the laboratory frame.

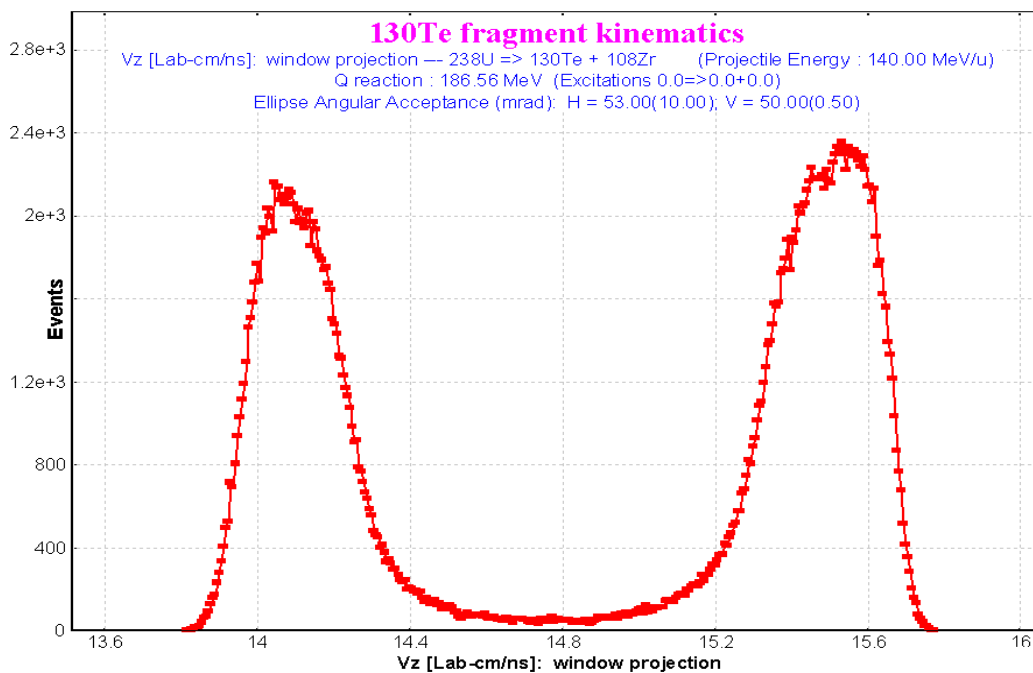
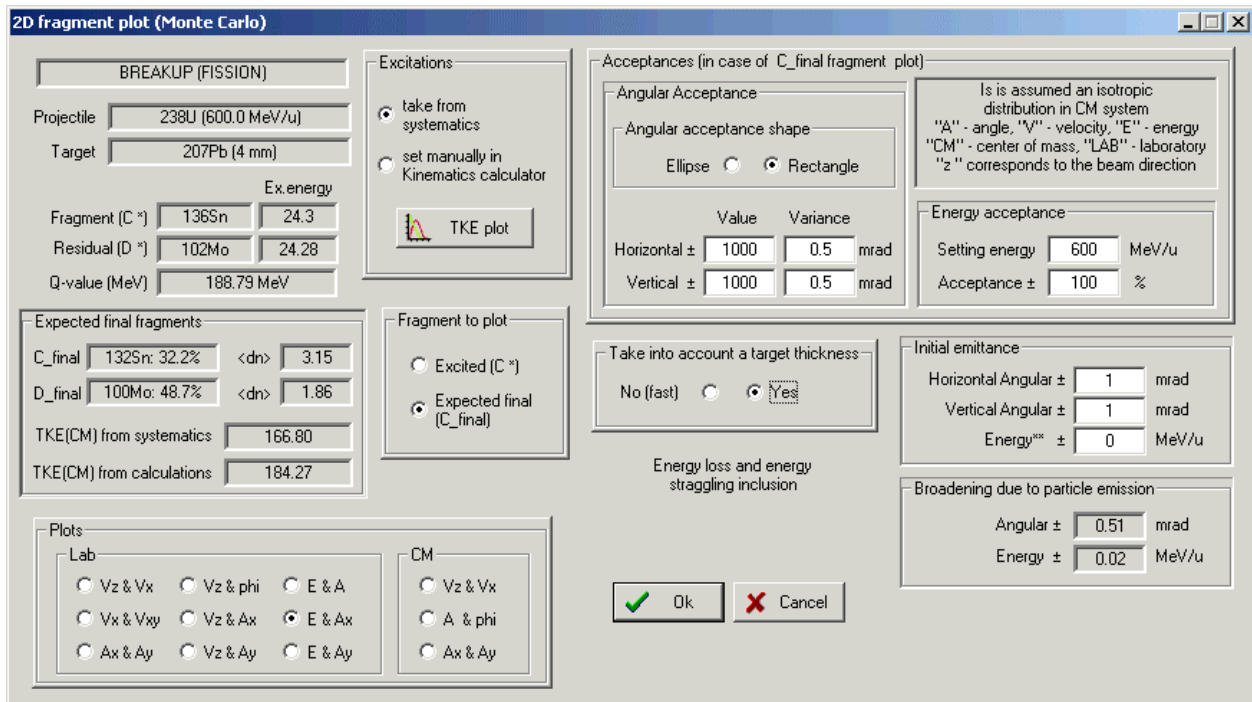


Fig.266. The projection of the plot (Fig.265) onto the  $V_z$  horizontal axis.

### 2.2.2.1. 2D fragment plot (Monte Carlo) – version 7.1

The old MCmethod (v.6.6) calculates the transmission of an excited fragment through a dipole after projectile fission in a target of zero thickness which physically is not correct. Fragment excitation energies were set manually in the Kinematics Calculator. In the new version of dialog the following options are now available (see Fig.267):

1. Taking into account a target thickness;
2. Only fragments in the ground state can be used for transmission calculations;
3. Fragment excitation energies can be taken from systematics in view of the initial excitation energy of the fissioning particle;
4. Broadening of the spatial distributions due to emission of light particles.



**Fig.267.** The “2D fragment plot” dialog (version 7.1). Initial excitation energy of fissioning nucleus  $^{238}\text{U}$  is equal to 50 MeV

There is the calculation algorithm for a nonzero target thickness and excitation energies taken from systematics:

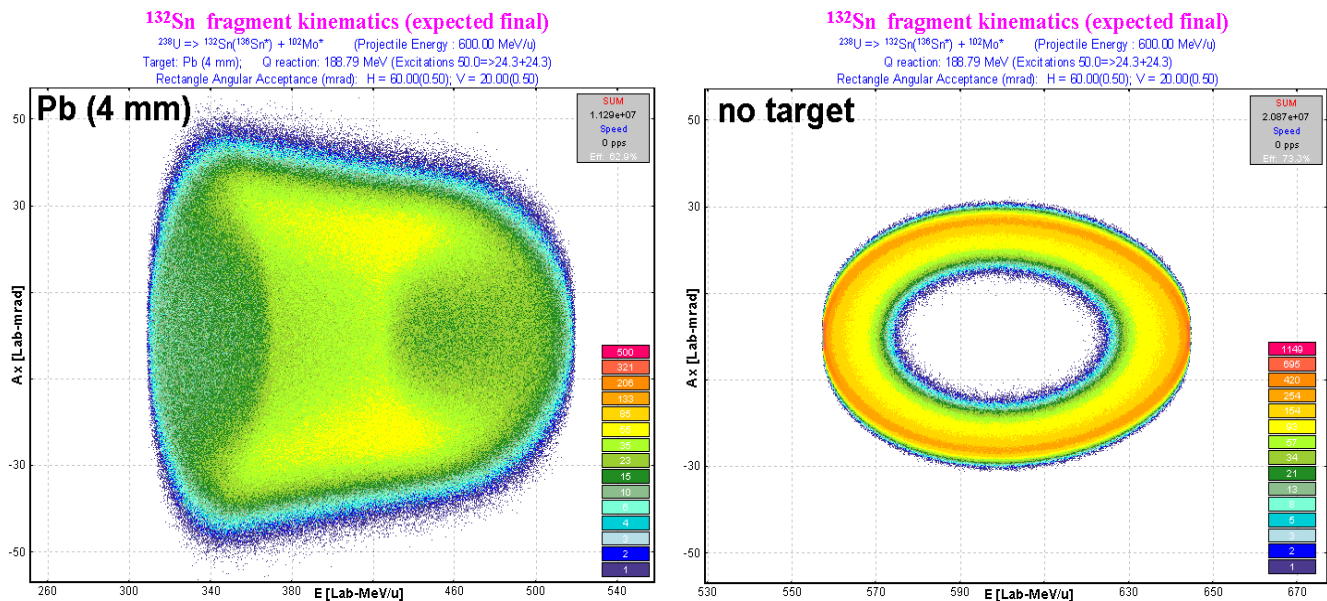
1. Initial settings:  $E0$  (beam energy),  $Ex(A^*)$  (excitation energy),  $\alpha_x=0$ ,  $\alpha_y=0$ .
2. Choosing an initial emittance  $d(\alpha_x1)$ ,  $d(\alpha_y1)$ :  $E0 \otimes dE \Rightarrow E1$ ;
3. Choosing a place  $X$  of reaction in the target ( $0 \leq X \leq T$ , with the target thickness  $T$ ).
4. Calculation of projectile energy loss in the target  $dE2$  (thickness  $X$ ) and drawing an energy straggling  $d(dE3)$ :  $E1 - (dE2 \otimes d(dE3)) \Rightarrow E4$ . Angular straggling  $d(\alpha_x2)$ ,  $d(\alpha_y2)$ ;
5. Calculation of excitation energy of fragments  $Ex(C^*)$  and  $Ex(D^*)$  using initial excitation energy, and the energy dissipation systematic.
6. Construction of Relativistic Kinematics class with input parameters:
  - $A^*$ ,  $C^*$ ,  $D^*$  ( $A$  – input,  $C$ ,  $D$  – output, the sign “\*” means excited);

- E4 – energy of the fissioning projectile at the time of reaction;
  - Excitation energies:  $Ex(A^*)$ ,  $Ex(C^*)$ ,  $Ex(D^*)$ .
7. Choosing angles of emission of fragment C\* in the centre-of-mass system (CMS).
  8. Transformation of angles and energy from the CMS to the lab system:  $E5$ ,  $\alpha x3$ ;  $\alpha y4$ ;
  9. Calculation of the final fragments  $C_f$  &  $D_f$  in their ground states.
  10. Calculation of broadening values caused by the emission of light particles  $dE6$ ,  $d(\alpha x6)$ ,  $d(\alpha y6)$ ,  $E5 \otimes dE6 \Rightarrow E7$ .
  11. Calculation of fragment ( $C_f$ ) energy loss  $dE8$  in the remaining target thickness  $T-X$  and choosing an energy straggling  $d(dE9)$ :  $E7 - (dE8 \otimes d(dE9)) \Rightarrow E10$ . Angular straggling  $d(\alpha x7)$ ,  $d(\alpha y8)$ .
  12. Drawing fragment direction of fragment  $\alpha x3 \otimes [d(\alpha x1), d(\alpha x2), d(\alpha x6), d(\alpha x7)] \Rightarrow \alpha x12$ ,  $\alpha y3 \otimes [d(\alpha y1), d(\alpha y2), d(\alpha y6), d(\alpha y7)] \Rightarrow \alpha y12$ .
  13. Analysis of energy and angular transmission with  $\alpha x12$ ,  $\alpha y12$ ,  $E10$ .

where the expression “ $A \otimes B$ ” denotes drawing value with mean value A and standard deviation B.

### 2.2.2.2. Using target thickness

Two 2D-plots of  $A_x$  (horizontal component of the angle in the laboratory frame) versus energy per nucleon of  $^{132}\text{Sn}$  final fragment after  $^{238}\text{U}(600 \text{ MeV/u})$  fission are shown in Fig.268. Acceptances settings are given in Fig.267. The left picture represents case of a Pb target with 4 mm thickness; the right plot was created for a zero target thickness. The initial excitation energy of the fissioning nucleus  $^{238}\text{U}$  is equal to 50 MeV. Transmissions are equal to 63% and 73%, respectively, in the case of the 4 mm target and zero thickness. The projections of the 2D plots from Fig.268 on horizontal and vertical axes are shown in Fig.269.



**Fig.268.** 2D-plots  $A_x$ (horizontal component of the angle in the laboratory frame) versus Energy per nucleon of  $^{132}\text{Sn}$  final fragment after  $^{238}\text{U}(600\text{MeV/u})$  fission. Acceptances settings are shown in Fig.267. The left picture represents case of using a Pb target thickness of 4mm, the right plot was obtained for the case of a zero thickness target. Initial excitation energy of fissioning nucleus  $^{238}\text{U}$  is equal to 50 MeV.

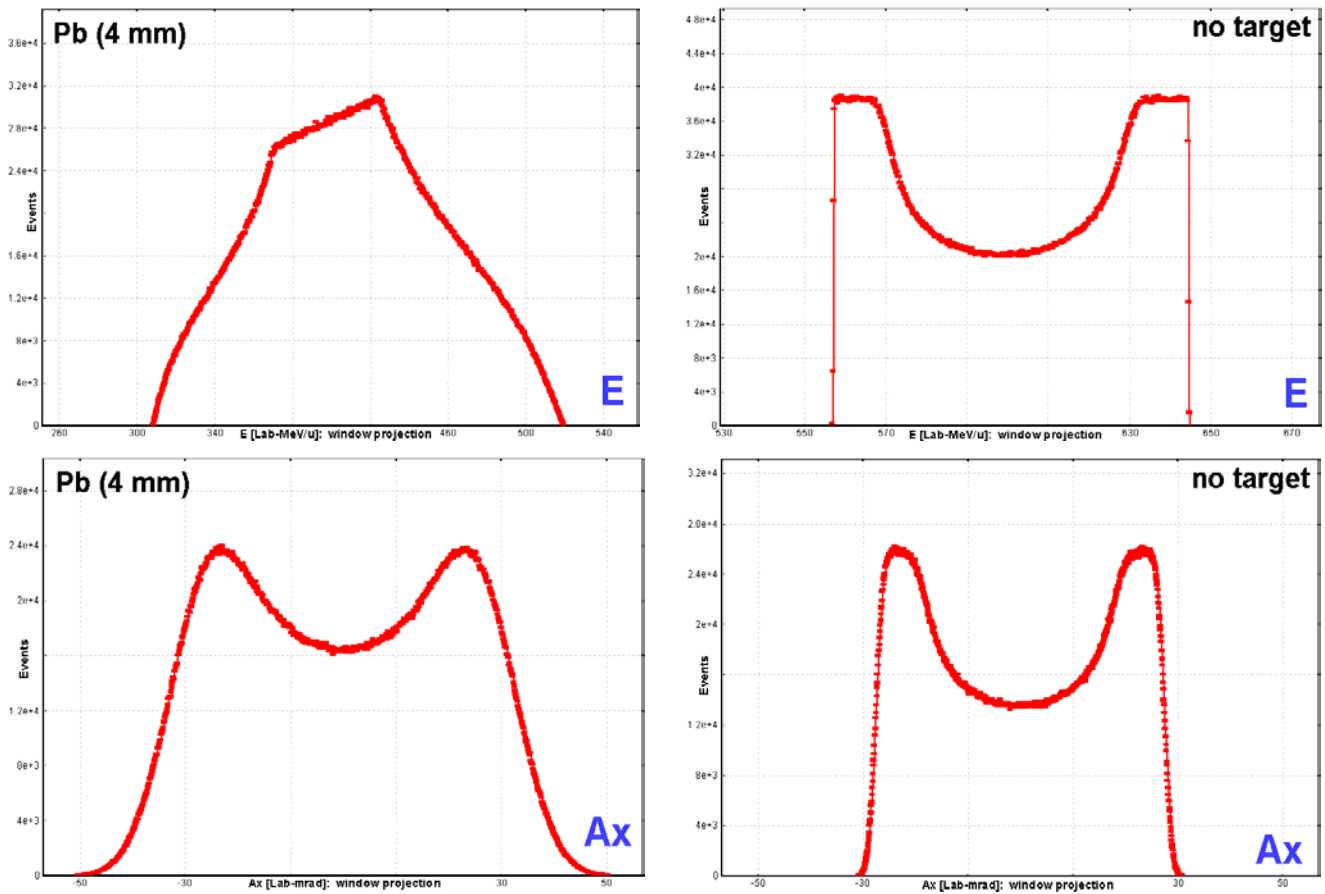


Fig.269. Projections of 2D plots from Fig.268 on the horizontal and vertical axes.

### 2.2.2.2.1. MCmethod calculation speed

The Monte Carlo method gives a very qualitative analysis, but the basic problem is the amount of time spent for the calculations. For comparison some estimations of the MC calculation speed were done. MCmethod can be applied for single estimations, but for fast results for simulations with many nuclei it may be preferable to use the analytical methods (see table).

Method	Rates (events per second)	Time to calculate transmission of one nucleus
<i>MCmethod:</i> with zero thickness target	~40 000 (for 100% transmission)	To get the right plot in Fig.268 ~ 10 minutes
<i>MCmethod:</i> take into account thickness target	~2 000 (for 100% transmission)	To get the left plot in Fig.268 ~ 2 hours
<i>DistrMethod</i>	<i>for the same conditions as for MC method test above</i>	For NP=16: 0.15 sec For NP=32: 0.22 sec For NP=64: 0.35 sec

Note: increase the number of pixels for one event for the Monte Carlo plot in the “Plot options” dialog to get more “intense” MC plot faster.

### 2.2.2.3. Excitation energies

If the option “take from systematic” is set in the “Excitation energy” box of the “2D-fragment plot” dialog (see Fig.267), then the excitation energy of the fragments is taken as the sum of the excitation energy above the barrier and intrinsic excitation energy  $E_{dis}$  [Ben98]:

$$TXE = E_x(C^*) + E_x(D^*) = E_x(A^*) - B_f + E_{dis} \quad /19/$$

where  $B_f$  is the height of the fission barrier, and  $E_{dis}$  is parameterized in the following way [Wil86]:

$$E_{dis} = 3.53 \left( Z_{CN}^2 / A_{CN} - 34.25 \right). \quad /20/$$

The final excitation energy is attributed to the fission proportionally to their level density parameters basing on thermal equilibrium as one approaches scission [Bis70], or in other words, the nuclear temperatures of C\* & D\* fragments are equal  $T(C^*) = T(D^*)$ . We refer to this TXE method as “dissipated energy” method.

The user can select the second alternative definition of the total excitation energy (“Qvalue” method) by H.R.Faust [Fau02] in the “Fission properties” dialog:

$$TXE = E_x(A^*) + (a_{C^*} + a_{D^*}) \cdot (\bar{f} \cdot Q)^2 \quad /21/$$

where  $a_{C^*}$  and  $a_{D^*}$  are the level density parameters for the excited fragment C\* and D\*,  $Q$  is the reaction Q-value, and  $\bar{f}$  is the constant connecting fragment excitation and  $Q$ -value. The value for  $\bar{f}$  was estimated to be equal to 0.0045 [Fau02].

### 2.2.2.4. Expected final fragment

Expected final fragments ( $C_{final}$  and  $D_{final}$ ) are calculated by the “LisFus” evaporation model in the fast mode. The fast mode of the “LisFus” model assumes the following features:

- Number points in evaporation distributions depends from excitation energy of the fragment:

$$NP_{evap} = \begin{cases} 16 & \text{if } E^* \leq 10 \text{ MeV} \\ 8 & \text{if } 10 < E^* \leq 100 \text{ MeV} \\ 4 & \text{if } E^* > 100 \text{ MeV} \end{cases}$$

- There are only four decay modes: n,2n,p, $\alpha$ .
- If the probability to get a daughter nucleus is less than 0.001 then this nucleus is excluded from the subsequent calculations.

The code finds the most probable final fragment and the average number of emitted nucleons which are shown in the “2D-fragment plot” dialog (see Fig.267).

Use of the “LisFus” method to define the number of post-scission nucleons is a big **advantage** of the LISE++ code which allows to observe shell effects in the TKE distribution, and enables the user to estimate qualitatively the final fission fragment faster instead of using post-scission neutron emission systematic which does not work well in a wide region of excitation energy for different fragment mass.

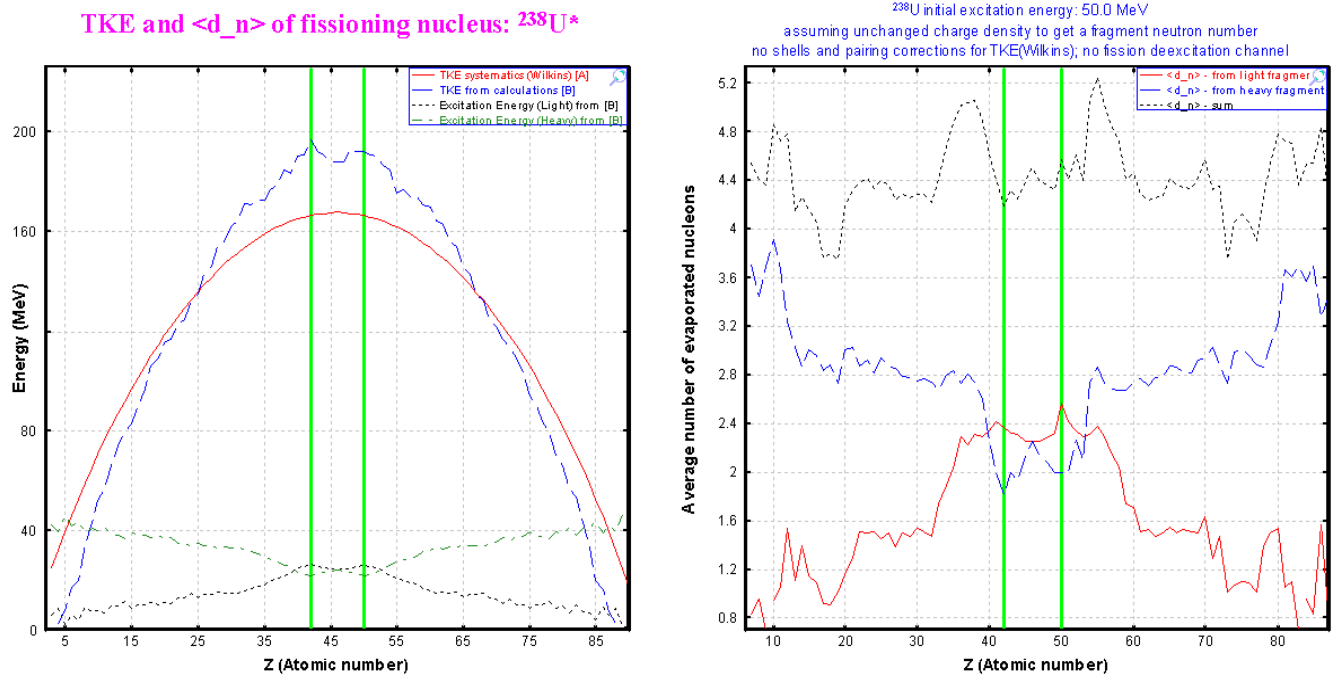
### 2.2.2.5. Total kinetic energy of fission fragments

A plot of total kinetic energy of fission fragments is available in the “2D fragment plot (Monte Carlo)” dialog. The sum of the kinetic energy of two fragments in their final states is calculated assuming an unchanged charge density of the fissile nucleus to get a fragment neutron number (see Fig.270). By analogy with work [Sch00] LISE’s TKE calculations are compared in Fig.270 with a prediction of the liquid-drop-model without taking shell effects into account [Wil76]:

$$TKE = \frac{Z_1 \cdot Z_2 \cdot e^2}{D} \text{ with} \quad /22/$$

$$D = r_0 \cdot A_1^{1/3} \left(1 + \frac{2}{3} \beta_1\right) + r_0 \cdot A_2^{1/3} \left(1 + \frac{2}{3} \beta_2\right) + d, \quad /23/$$

where the quadrupole deformation is  $\beta_1 = \beta_2 = 0.625$ , and the tip distance is  $d = 2$  fm. Average number of evaporated post-scission nucleons and the distribution of excitation energy in the fragments also are shown in Fig.270. Descriptions of other possibilities to plot total kinetic energy distributions ( $\langle TKE \rangle$  and TKE versus various observables in 1D- and 2D-formats) can be viewed in chapter 2.4.3.



**Fig.270.** Plots of the total kinetic energy and the average number of evaporated post-scission nucleons versus the atomic number of one fragment for the fissioning nucleus  $^{238}\text{U}$  ( $E_x=50$  MeV). The “Dissipated energy” TXE method (#0) was used for the calculations.

### 2.2.2.6. Fragment distribution to plot

There are two possibilities to choose when plotting a fragment distribution: final fragment in ground state or excited fragment before emission of nucleons. The excited fragment mode is not compatible with “using target thickness” mode. The code automatically sets the target option into “no target” mode.

### 2.2.2.7. Broadening due to particle emission

Angular and energy broadening values due to evaporation of nucleons from the excited fragment are shown in the dialog box in the “final fragment to plot” mode.

### 2.2.3. Fission kinematics used by the LISE “distribution” method (DistrMethod)

In order to calculate the kinematics of the final fission fragment by LISE’s “distribution” approach the code is looking for the most probable excited fragment for a given final fragment (see chapter 2.4.2.1.). LISE++ estimates the excitation energies of both fragments and then uses classes of the Relativistic Kinematics Calculator to fill matrices and distributions of the “MatrixKinematics” class.

This chapter describes in details the class “MatrixKinematics”, and how to use debug plots. It is recommended for beginning users to skip this chapter and to proceed to chapter 2.2.4.

#### 2.2.3.1. Class “MatrixKinematics”: fission kinematics by LISE “distribution” method

The class “MatrixKinematics” has been developed to calculate fission kinematics transmission by means of the LISE’s “distribution” approach. The Monte Carlo transmission simulation supports two angular acceptance shapes (ellipse and rectangle) whereas “MatrixKinematics” uses only a rectangle shape.

Let’s define  $\theta_x = x' = AX$ , where  $\theta_x$  – is the horizontal component of an angle  $\theta$  between the fragment direction and the beam axis in the laboratory frame which is calculated as  $\theta_x = \text{atan}(\tan(\theta) \cos(\varphi))$  ( $0 \leq \varphi \leq \pi$ ). At intermediate and high energies it is possible to assume  $\theta_x = \theta \cos(\varphi)$  to simplify Jacobian matrix for the transformation from  $d^2\sigma/(d\Omega)$  to  $d^2\sigma/(d\theta_x d\theta_y)$ .

##### 2.2.3.1.1. AX&AY matrices

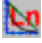

The base of the “MatrixKinematics” class is four AX&AY matrices of size  $(NP+1) \times (NP+1)$ , where  $NP$  is the current dimension of LISE’s distributions which can be changed in the “Preferences” dialog. For the fission fragment transmission it is recommended to use 32 or 64, because is more time consuming than projectile fragmentation transmission calculations.

Horizontal (Vertical) axis  $i$ -value is equal to  $AXmax$  ( $2i / NP-1$ ), where  $AXmax$  ( $AYmax$ ) is the maximal possible value of angle  $\theta_x$  ( $\theta_y$ ), and  $i = [0, 1 \dots, NP]$ . The first two matrices are “intensity” matrices in “Forward” and “Backward” directions. The matrix value corresponds to the differential cross-section  $d^2\sigma/(d\theta_x d\theta_y)$  which is calculated assuming isotropic spatial distribution in the center of mass. The sum of both “intensity” matrices is identical to the plot “Ax&Ay” in the Laboratory system in Monte Carlo simulations (see Fig.264). The other two matrices are “energy” matrices in “Forward” and “Backward” directions. The matrix value corresponds to the energy of a fragment emitted at angles  $(\theta_x, \theta_y)$  in the Laboratory frame. The division into forward and backward matrices was made because each pair  $(\theta_x, \theta_y)$  correspond two meanings of energy.

Ax&Ay matrices can be viewed through the dialog “BI” after the transmission calculations done in the debug mode. Matrices will be saved as files in the directory “\spectres” if the “Debugging mode” option in the “Preferences” has been turned on dialog and after executing the code to calculate fission fragment transmission. After every cutting of angular distributions several files will be created. For example after first cutting into the horizontal acceptance component ( $\pm 12\text{mrad}$ ) the following files will be created:

“minten00.spa”	forward “intensity” matrix
“minten_b01.spa”	backward “intensity” matrix
“menergy02.spa”	forward “energy” matrix
“menergy_b03.spa”	backward “energy” matrix

The next file for vertical acceptance is “minten05.spa”. Matrices are saved in the NSCL ASCII two-dimensional spectrum and can be viewed in the dialog “BI”.

It is better to plot the “Intensity” matrices in logarithmic scale (default), and “Energy” matrices in the linear scale. To plot the matrix in linear scale it is necessary to turn off the logarithmic scale using  and set the initial values of the linear scale mode using the icon . Forward “intensity” and “energy” matrices are shown in Fig.271 and Fig.272. For example in the case of forward “energy” matrix in the file “CoulombFissionExample.lpp” the parameters were: minimal value=994 and step=5 (see Fig.272).

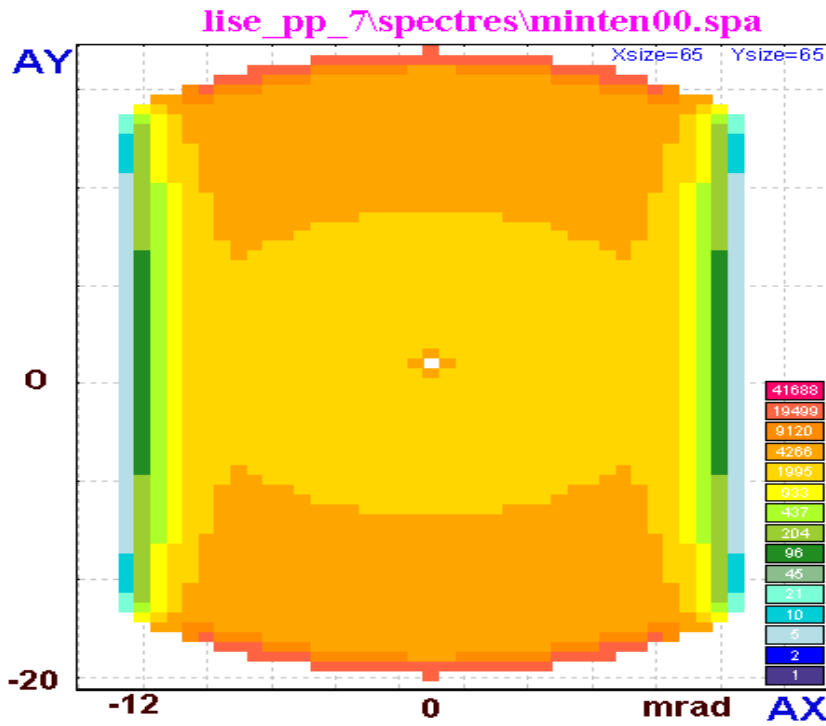


Fig.271. The forward “intensity” matrix after cutting by a horizontal rectangle shape acceptance equal to  $\pm 12$  mrad.

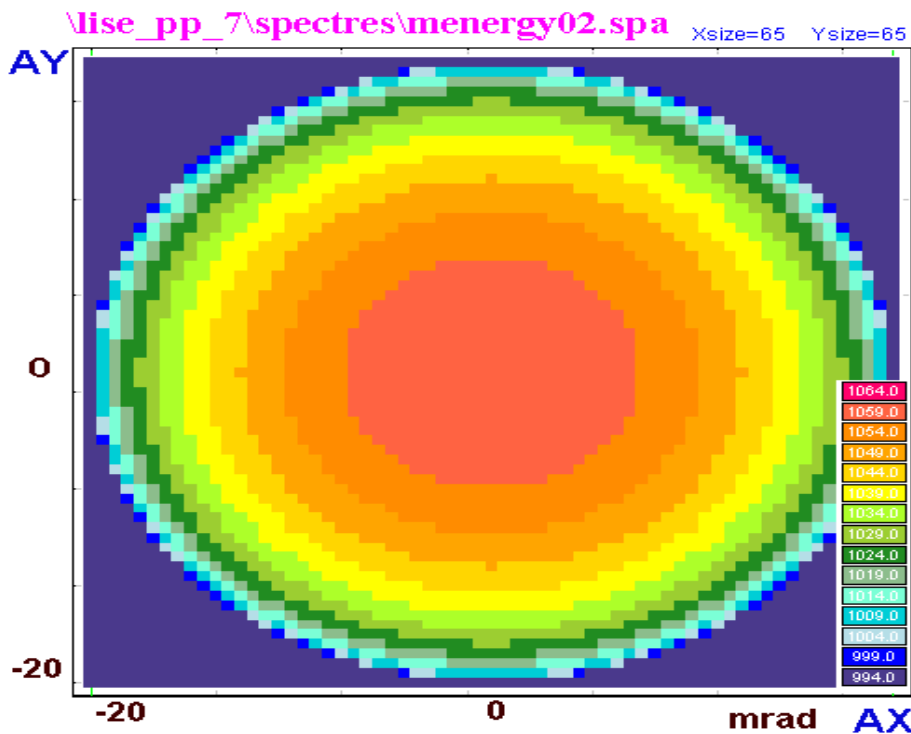


Fig.272. The forward “energy” matrix.



### 2.2.3.1.2. “Base” and “Acquired” distributions

Two sets of three one-dimensional distributions are used to get information from the “MatrixKinematics” class to the LISE transmission calculation subroutines. The first set, named “Base”, is created as a result of integration using matrices AX&AY. There are two “angular” (*AdisX* and *AdisY*) and one “energy” (*disE*) distributions which represent cross-section distributions correspondingly  $(d\sigma/d\theta_X)_{i\Delta\theta_X}$ ,  $(d\sigma/d\theta_Y)_{i\Delta\theta_Y}$ , and  $(d\sigma/dE)_{i\Delta E}$ . It is possible to express the *i*-th value of *AdisX* distribution in the follow terms:

$$AdisX_i = \int_{-AY_{max}}^{+AY_{max}} \int_{AX_i}^{AX_i+\Delta_X} \left[ \left( \frac{d^2\sigma}{d\theta_X d\theta_Y} \right)_{forward} + \left( \frac{d^2\sigma}{d\theta_X d\theta_Y} \right)_{backward} \right] d\theta_X d\theta_Y, \quad /24/$$

$$disE_i = \int_{-AY_{max}}^{+AY_{max}} \int_{-AX_{max}}^{+AX_{max}} \int_{E_i}^{E_i+\Delta_E} \left[ \left( \frac{d^2\sigma}{d\theta_X d\theta_Y} \right)_{forward} \cdot \delta(E - fE(\theta_X, \theta_Y)_{forward}) + \left( \frac{d^2\sigma}{d\theta_X d\theta_Y} \right)_{backward} \cdot \delta(E - fE(\theta_X, \theta_Y)_{backward}) \right] dE d\theta_X d\theta_Y, \quad /25/$$

where  $d^2\sigma/(d\theta_X d\theta_Y)$  values are taken from “intensity” matrices, and  $fE(\theta_X, \theta_Y)$  values are taken from “energy” matrices.

The second set of distributions is called “acquired” and serves to take into account the following components:

- angular and energy straggling in the target and in materials;
- initial energy and angular emittance;
- energy broadening in the target due to different energy loss of the projectile and the fragment;
- energy broadening in the target due to different initial energy in the reaction kinematics.

*Note:* More detailed description of the given distributions, and also explanation on how angular and power selection works will be given in the next chapter.

### 2.2.3.2. Fission kinematics debug distributions

Debugging distribution plots are enabled with the menu “1D-plot → Debug distributions”. Actually “debugging” distributions were done to show how the class “DF4” is working. For example, a “real” momentum distribution (which the user can see in the momentum plot is “1D-plot → Momentum distributions”) is the result of three distributions “I(P)”, “-dP(P)”, “+dP(P)” from the “debugging distributions” plot. But this topic is not devoted to the class “DF4”, and fission fragment debugging distributions will be considered here. Fission kinematics distribution can be seen in the reaction mode “Coulomb-Fission” through the menu “1D-plot → Debug distributions”, but the option “Fission mode” has to be chosen first in the “Debug plot mode” dialog (see Fig.273).

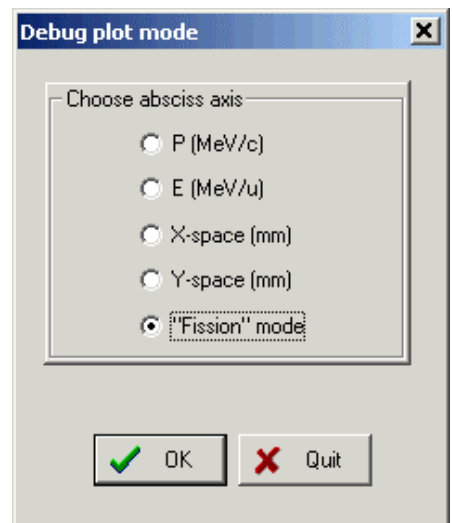


Fig.273. The “Debug plot” dialog.

### Stripper-DebugFission

<sup>238</sup>U 1000.0 MeV/u + Be (1 mm); Settings on <sup>130</sup>Te; Config: DSWMDMMMWSDMSMMMMMSMMW  
 dp/p=3.09% ; Wedges: 0, Al (2 mm), Al (50000 mg/cm<sup>2</sup>); Brho(Tm): 14.5381, 14.4476, 14.1400, 14.0964

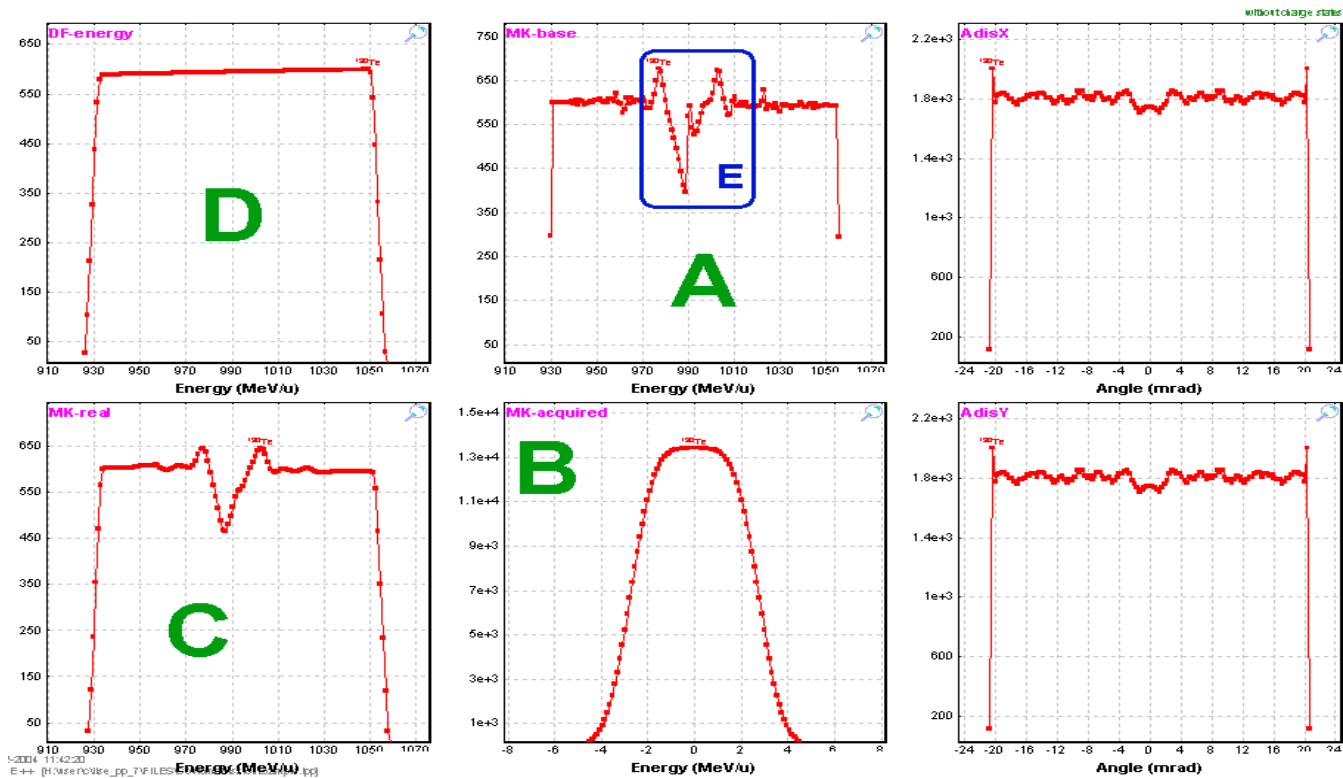


Fig.274. Fission debug distributions after the stripper (Initial settings of the file “CoulombFissionExample.lpp”).

### D1-DebugFission

<sup>238</sup>U 1000.0 MeV/u + Be (1 mm); Settings on <sup>130</sup>Te; Config: DSWMDMMMWSDMSMMMMMSMMW  
 dp/p=3.09% ; Wedges: 0, Al (2 mm), Al (50000 mg/cm<sup>2</sup>); Brho(Tm): 14.5381, 14.4476, 14.1400, 14.0964

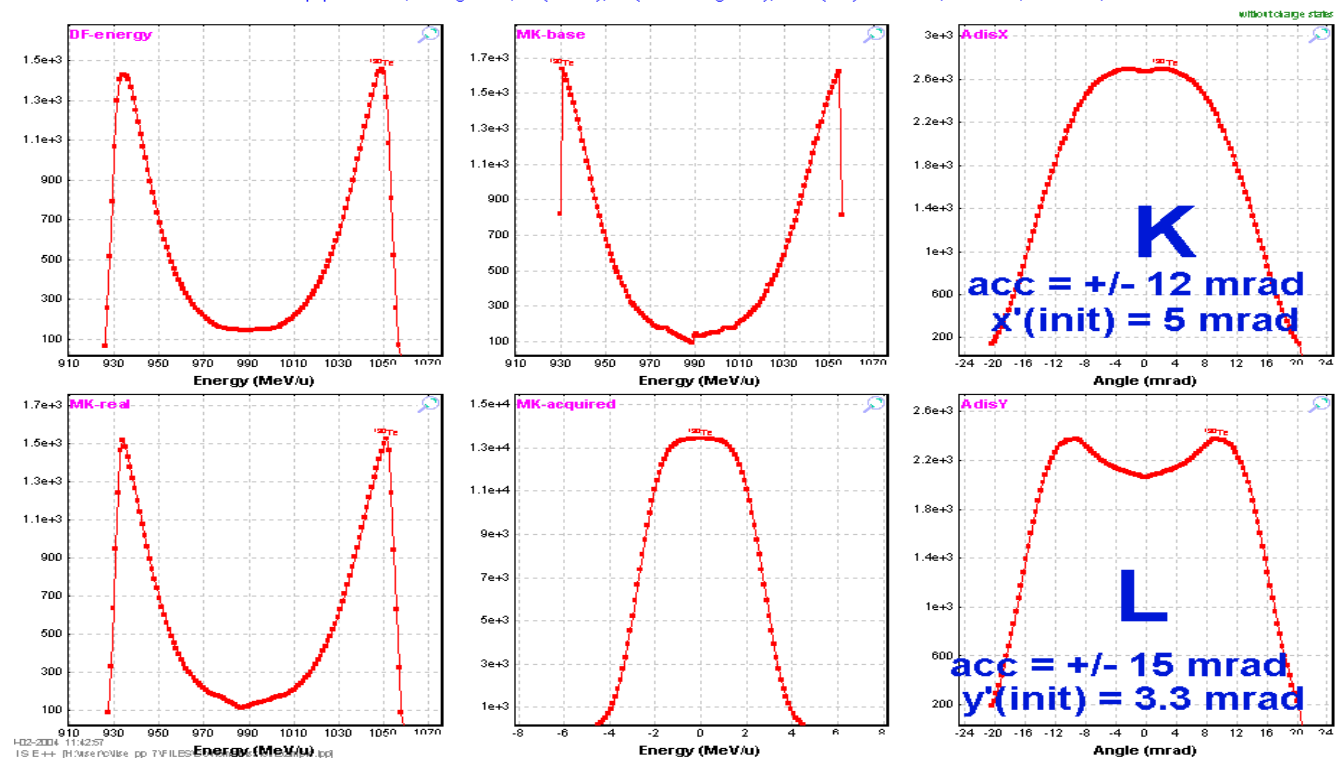


Fig.275. Fission debug distributions after the First dipole (the same settings as in Fig.274).

Fission kinematics debug distributions after the stripper and the first dipole are shown in Fig.274 and Fig.275 for initial settings of the file “*CoulombFissionExample.lpp*” ( $NP=128$  for plots). Plot designations in these figures are next:

Letter	Alternative signature in plot	Distribution
A	MK-base	<i>disE</i> (from class “ <i>MatrixKinematics</i> ”)
B	MK-acquired	<i>acquiredE</i> (from class “ <i>MatrixKinematics</i> ”)
C	MK-real	<i>disE</i> $\otimes$ <i>acquiredE</i>
D	DF-energy	<i>I(E)</i> of DF debugging plot (mode “E” in Fig.273)
K	AdisX	<i>AdisX</i> (from class “ <i>MatrixKinematics</i> ”)
L	AdisY	<i>AdisY</i> (from class “ <i>MatrixKinematics</i> ”)

The blue color rectangle marked by “E” indicates the region where “*MatrixKinematics*” can not reproduce the energy distribution well due to “edge” effects at values where the intensity is maximal (see Fig.271). With increased dimension of the distributions (NP) this effect becomes less. However this problem has been solved by the “filter” method incorporated into the code.

*How it works?*

1. Angular acceptance subroutine creates the special “gate” distribution based on:
  - Rectangle shape angular acceptance with  $(\theta/\theta)^{-1}$  coefficient (global) of the previous optics block (or “1” if there are not optical blocks before);
  - Acquired angular distribution (from class “*MatrixKinematics*”);
  - Components  $(\theta/X)\cdot X$  and  $(\theta/P)\cdot P$ .
2. This “gate” distribution is applied to both “intensity” matrices (it is possible to see the result of “intensity” matrix cut by the gate distribution in Fig.271).
3. Creation of new “base” distributions *AdisX*, *AdisY*, *disE* (see Fig.275)
4. Calculation of new distribution “C”. (Let’s call it “ $C_{new}$ ”).
5. The code creates the filter distribution  $Filter(i) = C_{new}(i)/C_{old}(i)$ . Edge effects are washed out in the new “filter” distribution. It is clear that  $0 \leq Filter(i) \leq 1$  for each  $i$ -point.
6. The “filter” distribution is applied to *I(E)* distribution of the DF distributions (left top plot).

Fission kinematics debug distributions after the stripper and the first dipole for thicker target (15 mm instead 1mm in Fig.274 and Fig.275) for comparison are shown in Fig.276 and Fig.277.

### Stripper-DebugFission

$^{238}\text{U}$  1000.0 MeV/u + Be (15 mm); Settings on  $^{130}\text{Te}$ ; Config: DSWMDMMMWSDMSDMMMMMMSMMW  
 dp/p=3.09% ; Wedges: 0, Al (2 mm), Al (50000 mg/cm<sup>2</sup>); Brho(Tm): 12.8595, 12.7627, 12.4323, 12.3853

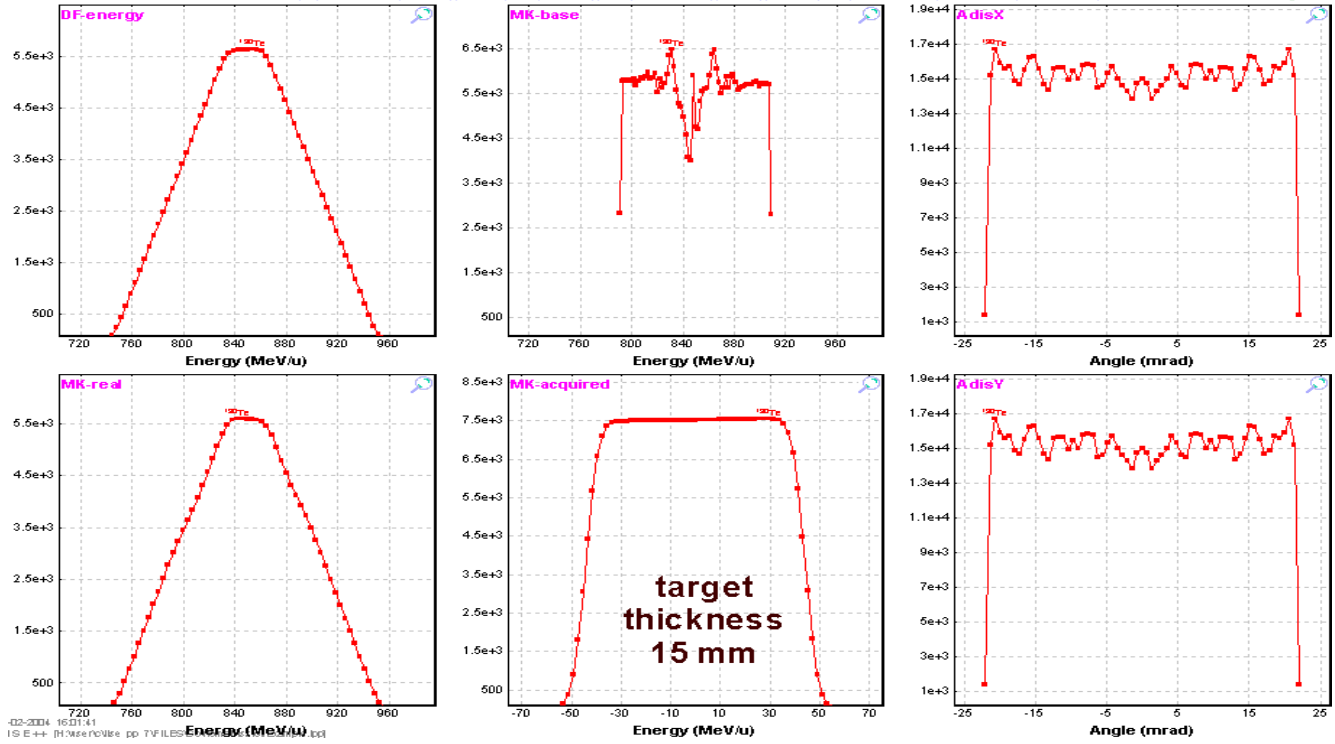


Fig.276. Fission debug distributions after the stripper. Target thickness is equal to 15 mm.

### D1-DebugFission

$^{238}\text{U}$  1000.0 MeV/u + Be (15 mm); Settings on  $^{130}\text{Te}$ ; Config: DSWMDMMMWSDMSDMMMMMMSMMW  
 dp/p=3.09% ; Wedges: 0, Al (2 mm), Al (50000 mg/cm<sup>2</sup>); Brho(Tm): 12.8595, 12.7627, 12.4323, 12.3853

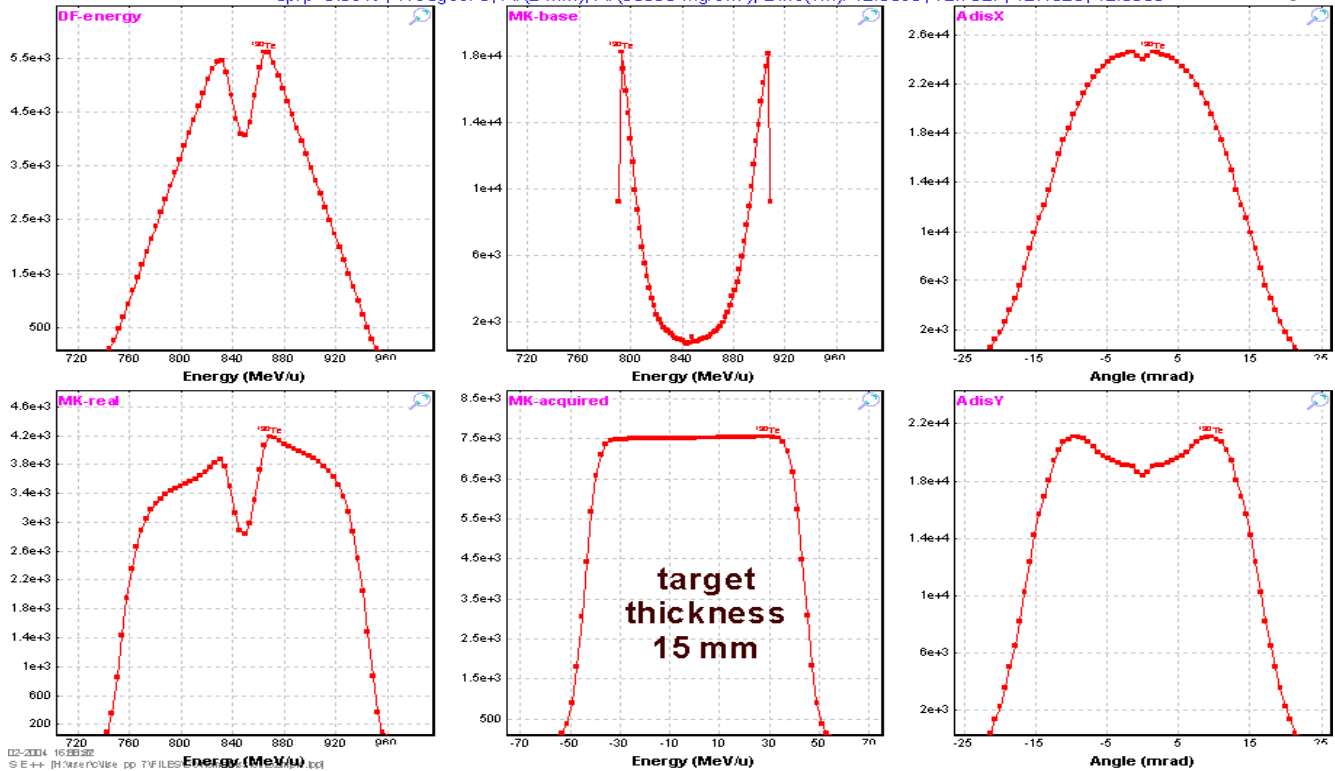


Fig.277. Fission debug distributions after the First dipole (the same settings as in Fig.276).

Fig.278 demonstrates the influence of an initial angular emittance on the shape of angular distributions and the “base” energy distribution after cutting by the first dipole. The thin target (0.1mg/cm<sup>2</sup>) was used in calculations shown in this figure.

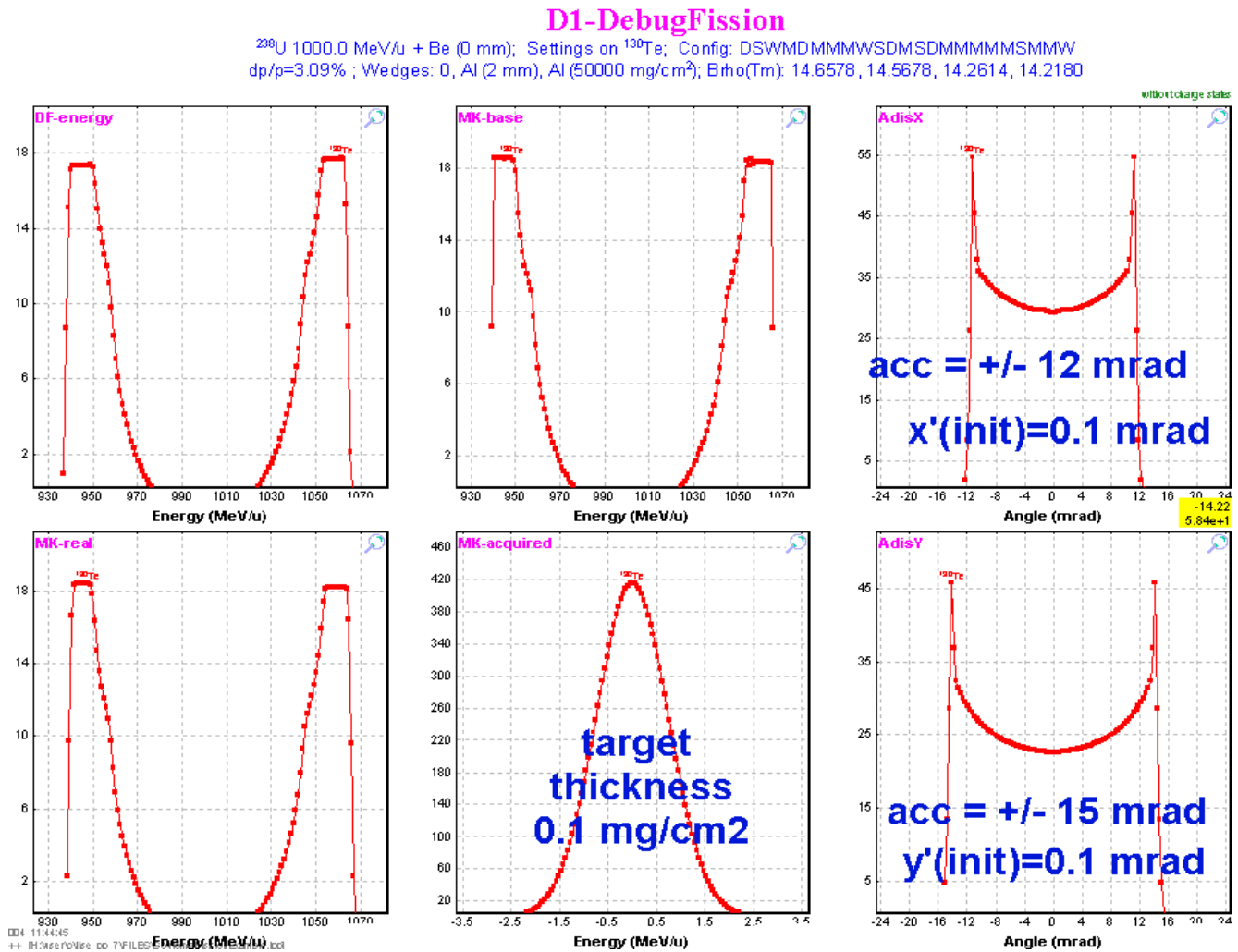


Fig.278. Fission debug distributions after the First dipole in the case of the thin target and a zero initial angular emittance.

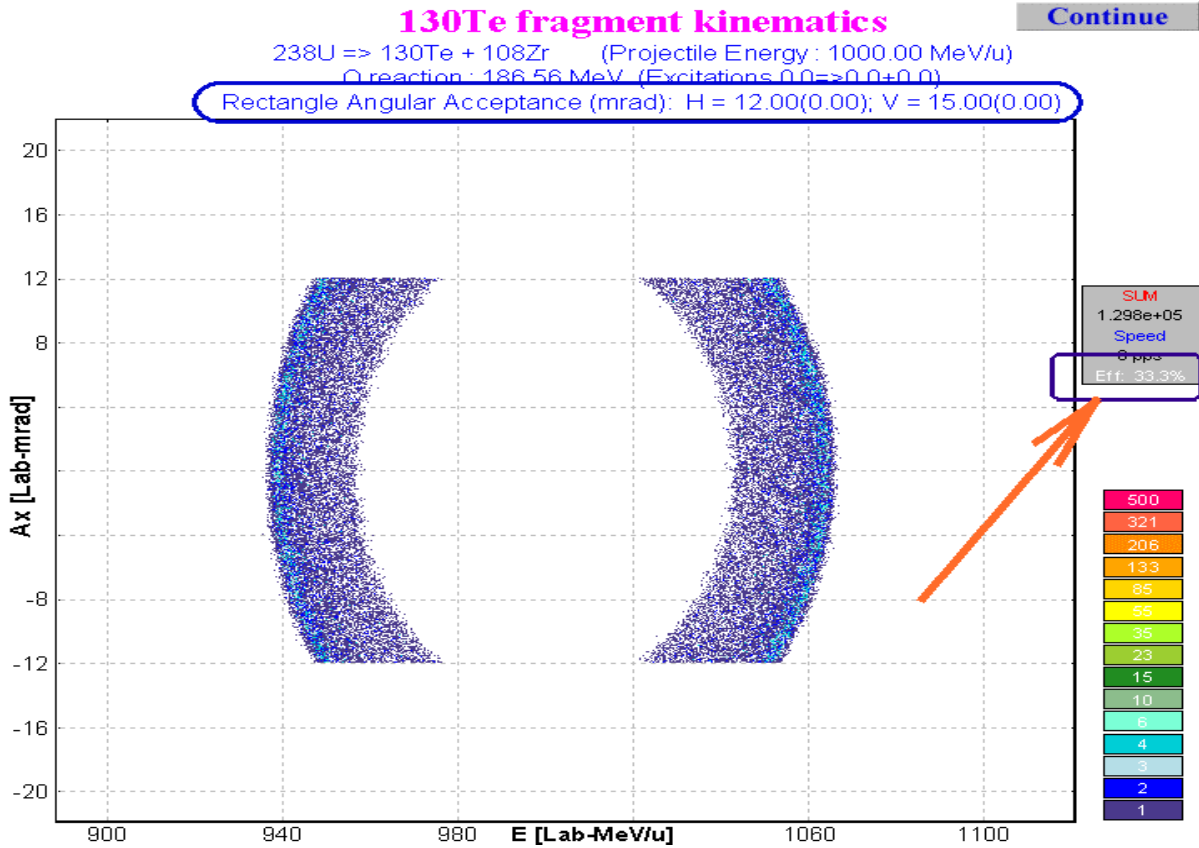
### 2.2.4. Comparison of calculations using the Monte Carlo method and the “MatrixKinematics” class

The Monte Carlo method is a powerful tool for modeling, but sometimes the amount of time spent to get enough statistics makes it more beneficial to use fast analytical methods. However for the analytical solution it is necessary to make some assumptions (simplifications), and also to develop new methods (algorithms) and to confirm them by experimental results. In these cases Monte Carlo method plays an irreplaceable role to check assumptions. The transmission results of a fission fragment for calculations corresponding to Fig.278 are shown in Fig.279. It is possible to see

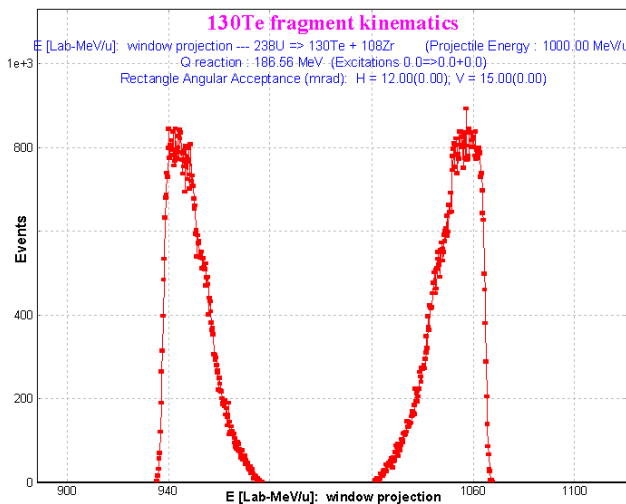
statistics <sup>130</sup> Te		
<sup>130</sup> Te	Stable (Z=52, N=78)	
Q1 (D1)		52
Q2 (D2)		52
Q3 (D3)		52
Q4 (D4)		52
<b>Production Rate</b>	(pps)	<b>4.31e+0</b>
Sum of charge states	(pps)	4.31e+0
CS in the target	(mb)	1e+0
Total transmission	(%)	10.313
<b>Target</b>	(%)	<b>100</b>
Unreacted in mater.	(%)	100
Unstopped in mater.	(%)	100
<b>D1</b>	(%)	<b>33.44</b>
X angular transmiss.	(%)	58.78
Y angular transmiss.	(%)	57.37
<b>S1 slits</b>	(%)	<b>50.53</b>
X space transmission	(%)	50.53
<b>MW11</b>	(%)	<b>98.59</b>
Unreacted in mater.	(%)	98.59
Unstopped in mater.	(%)	100
<b>D2</b>	(%)	<b>82.95</b>
--		-- --

Fig.279. Statistics window corresponding to calculations shown in Fig.278.

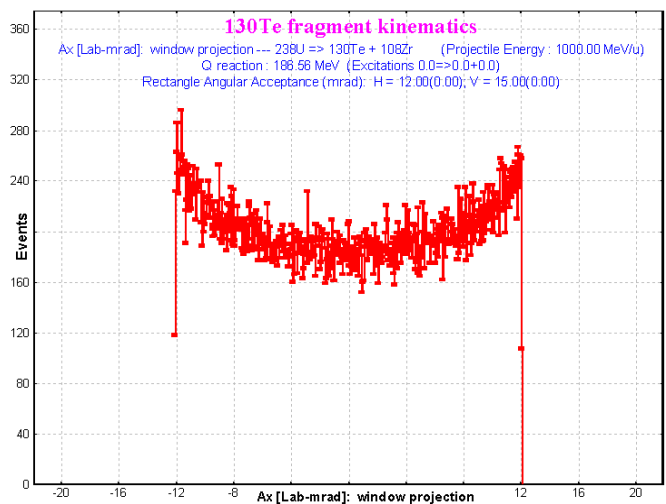
from the figure that the transmission through dipole D1 is 33,44 percent. Monte Carlo simulations for the same settings as in Fig.278 for the rectangle shape acceptance are shown in Fig.280. Transmission in the case of Monte Carlo method is equal to 33,3% (see figure). Projections on the horizontal and vertical axis are given in Fig.281 and Fig.282. The energy distribution plot created by the Monte Carlo method in Fig.281 corresponds to the top middle plot in Fig.278 (*MK-base*), and accordingly the X-angular distribution plot in Fig.282 corresponds to the top right plot (*AdisX*).



**Fig.280.** Two-dimensional plot Energy versus  $A_x$  with the same settings as in Fig.278.



**Fig.281.** Energy distribution as result of the projection of the two-dimensional plot on the horizontal axis in Fig.280.



**Fig.282.** X-Angular distribution as result of the projection of the two-dimensional plot on the vertical axis in Fig.280.

### 2.2.5. Angular distribution cut by the momentum slits

In the previous chapters we have considered energy distribution cuts by the angular acceptance. But it is necessary to discuss the opposite case: cutting angular distribution by means of the momentum slits. It could be very important for the case of a relatively large angular acceptance and small momentum acceptance. It is also important for transmission calculation to avoid a cut of an already truncated region that could lead to an underestimation of the transmission.

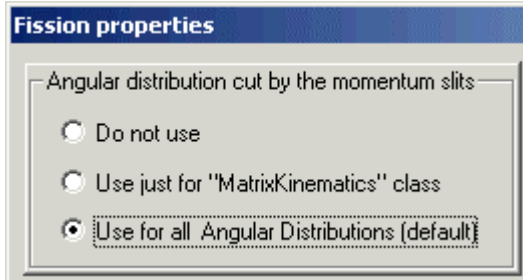


Fig.283. The “Fission properties” dialog fragment.

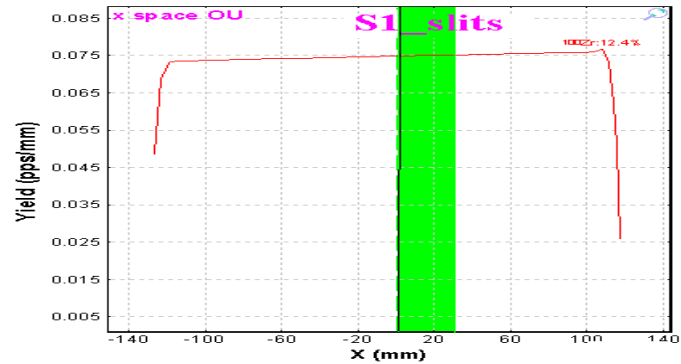


Fig.284. Fission fragment horizontal spatial distribution in the block “S1\_slits”. Momentum slits are shown by the green band.

A method of cutting the angular distribution by momentum slits can be selected in the “Fission properties” dialog (see Fig.283) which is available for reaction “CoulombFission” through the “Production mechanism” dialog. All of these three options will be shown in examples using the file [http://groups.nsl.msu.edu/lise/7\\_1/examples/CoulombFissionEnergyCutting.lpp](http://groups.nsl.msu.edu/lise/7_1/examples/CoulombFissionEnergyCutting.lpp). The spectrometer is set to the mean value of the fission fragment momentum distribution, but slits “S1” were set out to (0÷30) mm (see Fig.284).

#### 2.2.5.1. Angular distribution cut by the momentum slits: option “Do not use”

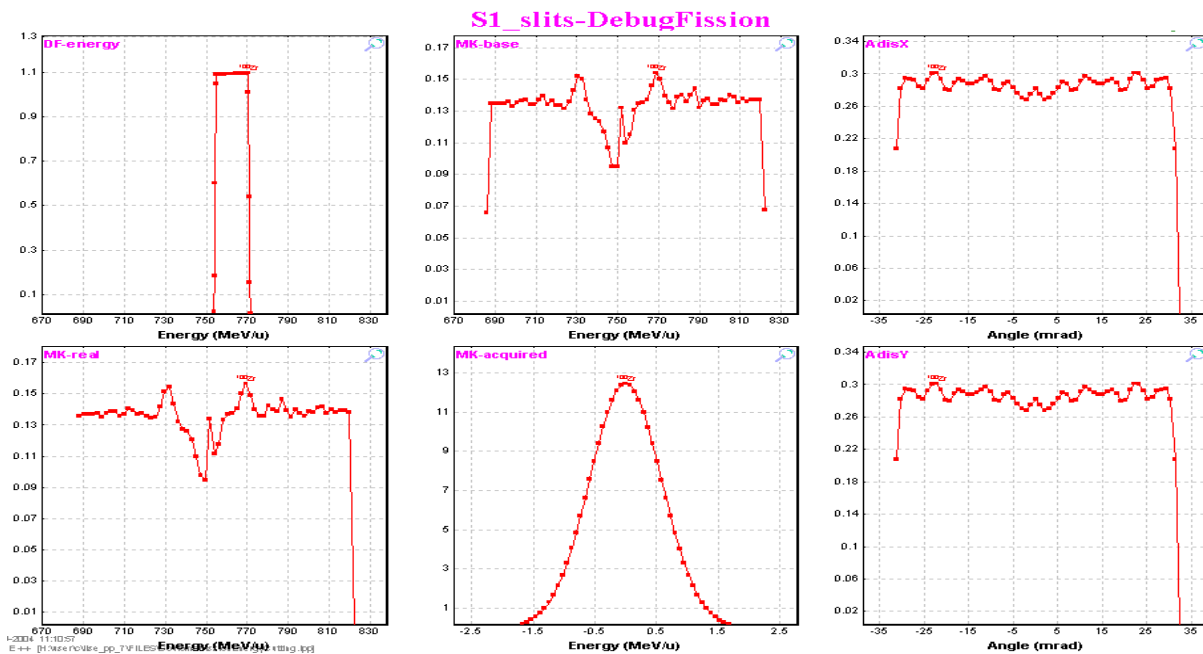
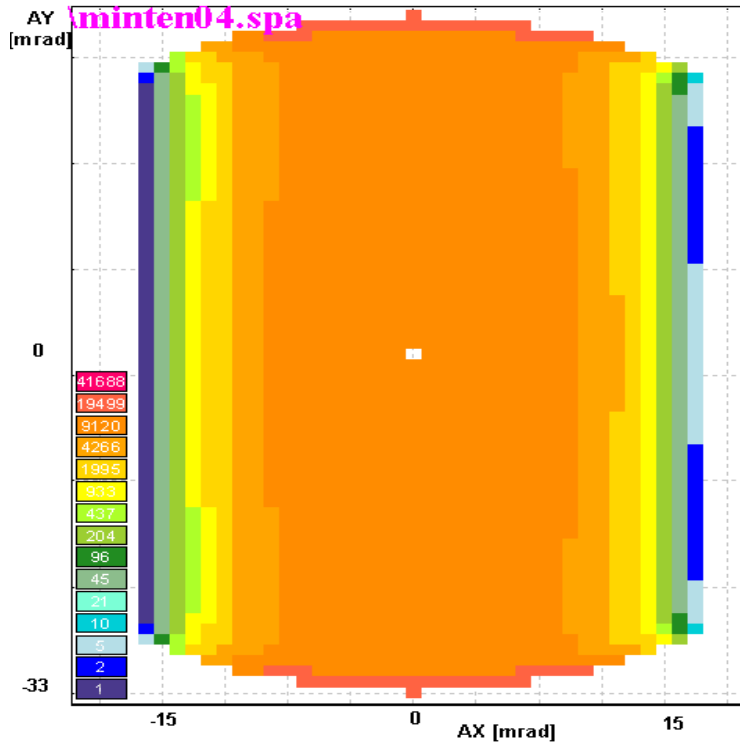
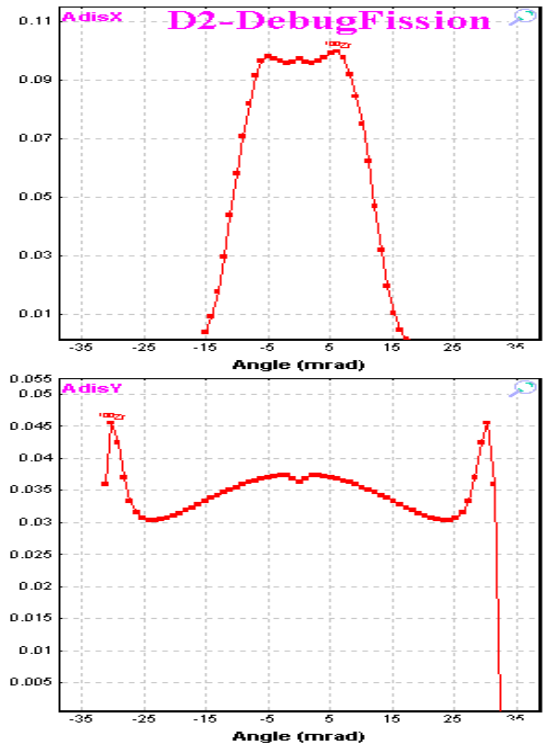


Fig.285. Fission debugging distributions after the “Slits\_S1” block. No cuts are observed for angular distributions.

Fission debugging distributions after the “Slits\_S1” block for the mode “DO NOT USE” are shown in Fig.285. No cuts are observed for angular distributions and as consequence the “energy” filter in the left bottom plot has not been changed after this block. *It is necessary to note that the backward “intensity” matrix area is positive.* The **forward** ”intensity” matrix after the block “Dipole D2” is shown in Fig.286. Projections on axes of forward and rear “intensity” matrices sum are shown in Fig.287.



**Fig.286.** The **forward** ”intensity” matrix after the block “Dipole D2”. Projections on axes of forward and backward “intensity” matrices sum are shown in Fig.287.



**Fig.287.** AdisX & AdisY angular debug distributions after the block “Dipole D2”.



### 2.2.5.2. Angular distribution cut by the momentum slits: option “Use for MatrixKinematics class”

The first cut by the spectrometer takes place at the momentum slits “S1”. The second cut occurs by the angular acceptance of the dipole “D2”. The backward “intensity” matrix area is equal to 0 due to the settings of the spectrometer (in middle of the fission fragment momentum distribution) and slits (0 ÷ 30 mm). The **forward** ”intensity” matrices after the slits “ S1” and the dipole “D2” are shown in Fig.288 and Fig.290 correspondingly.

Fission debugging distributions after the slits “S1” and the dipole “D2” for the mode “Use for MatrixKinematic class” are shown in Fig.289 and Fig.291.

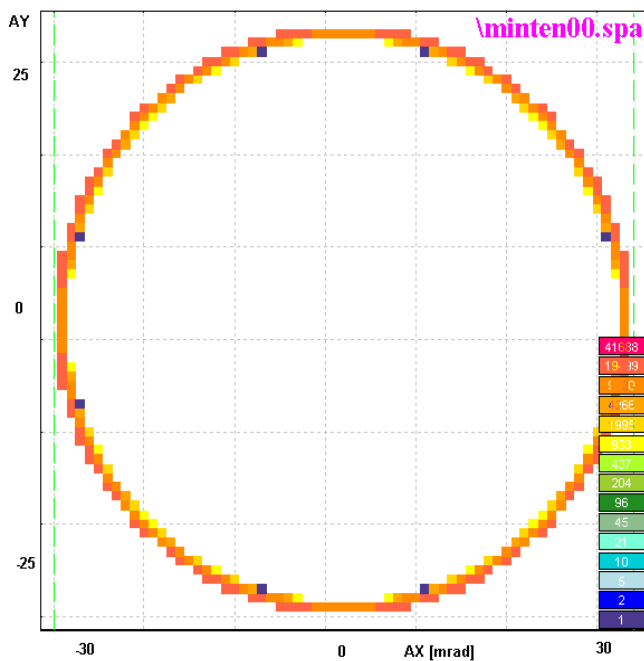


Fig.288. The forward ”intensity” matrix after the slits “ S1”.

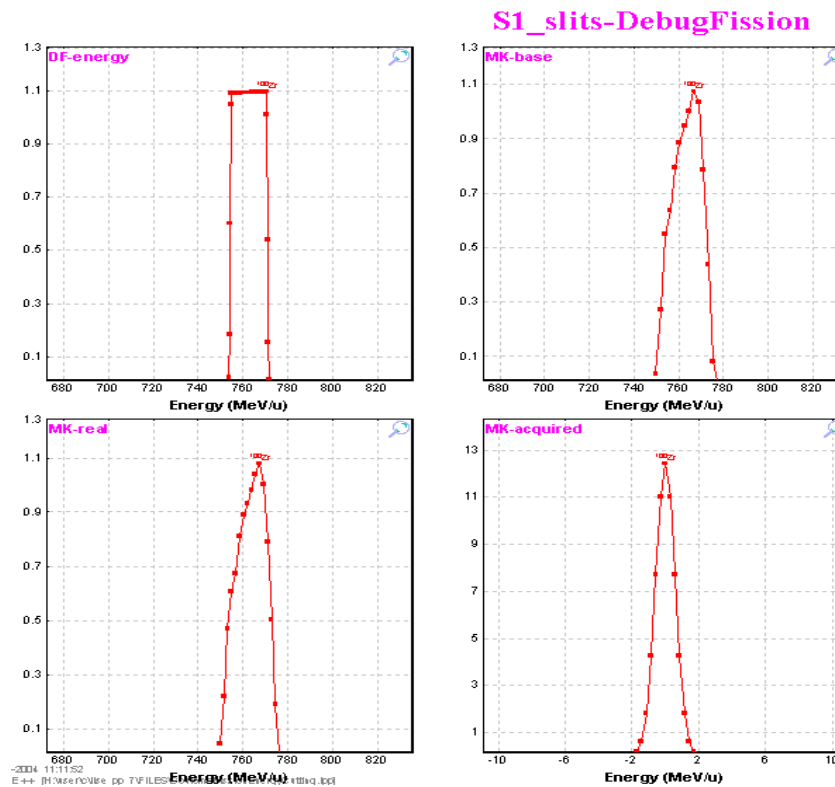
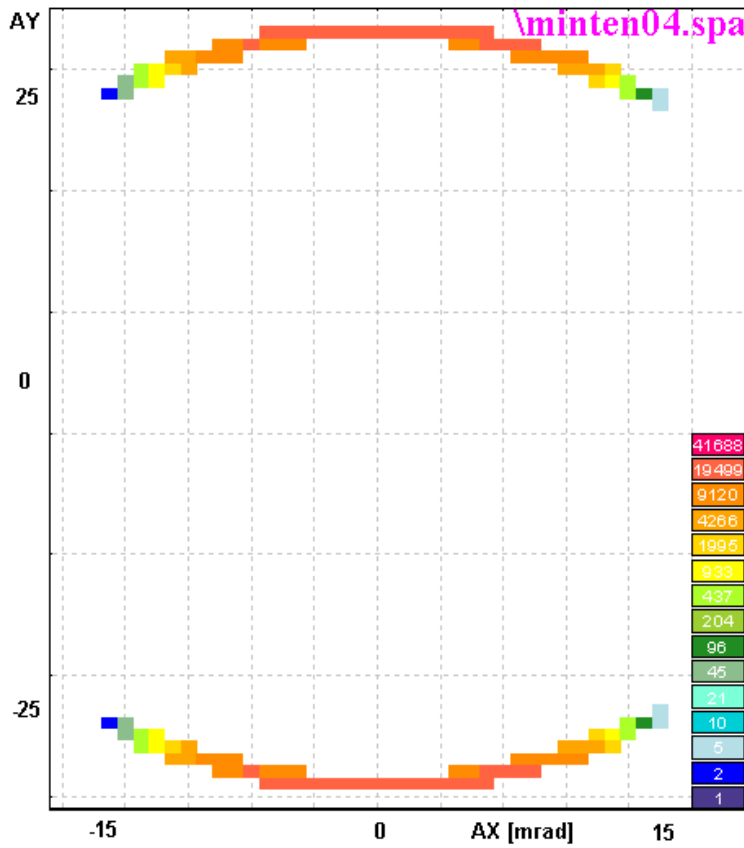
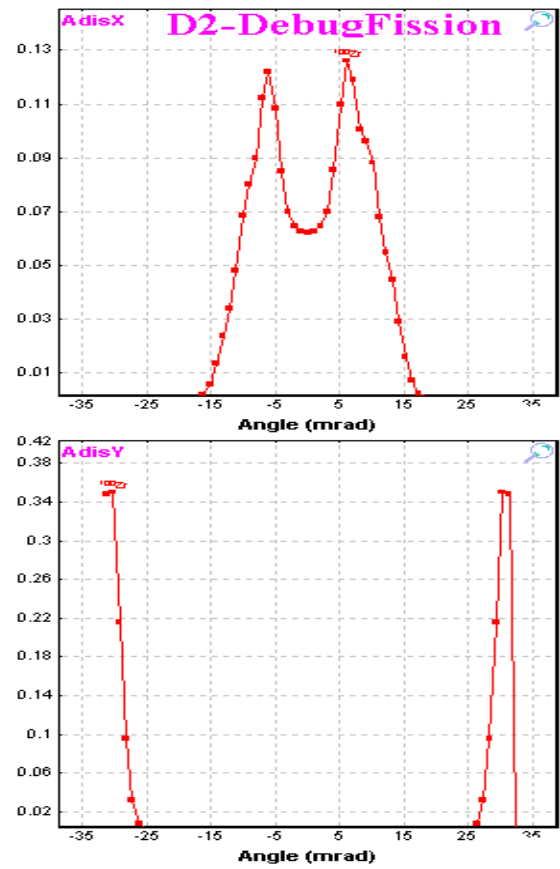


Fig.289. Fission debugging distributions after the “Slits\_S1” block. (Compare with Fig.285 to see difference).



**Fig.290.** The forward "intensity" matrix after the dipole "D2". Projections on axes of this matrix are shown in Fig.291.

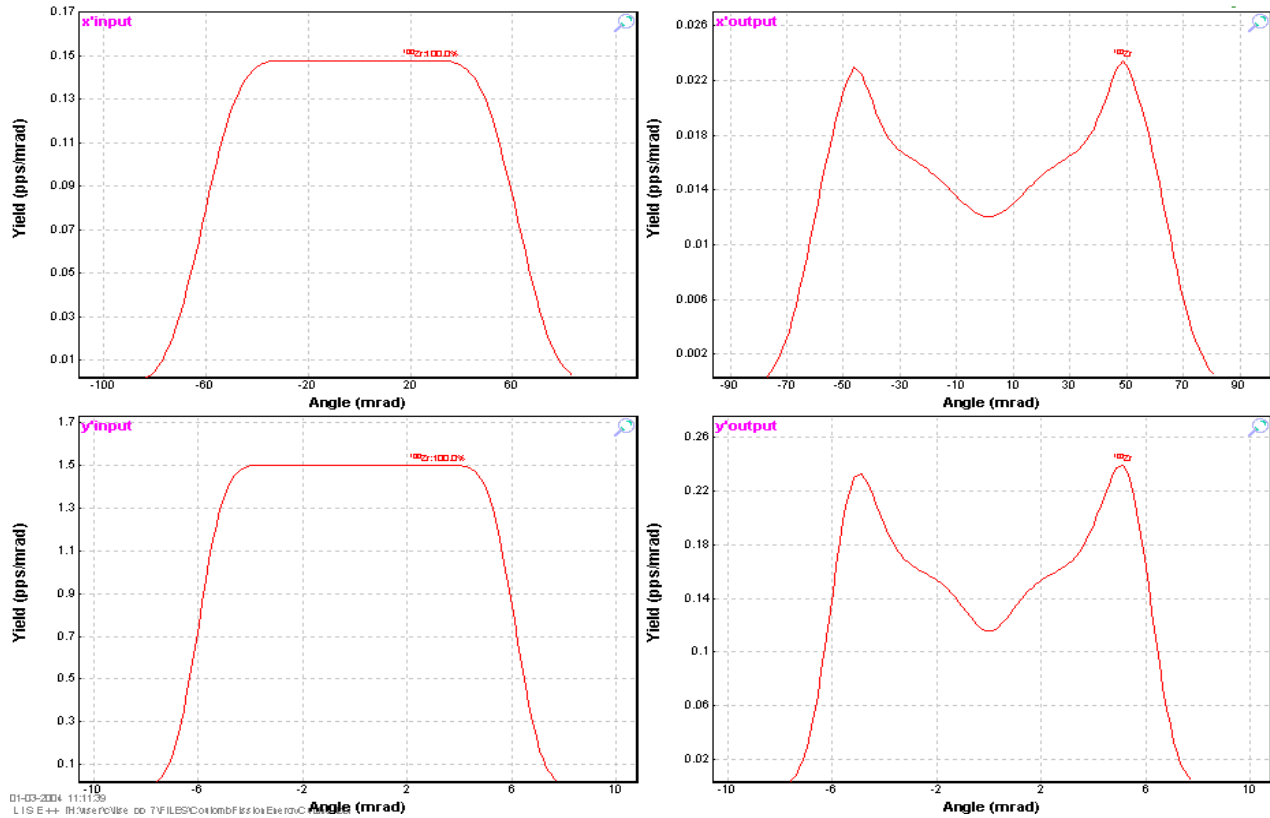


**Fig.291.** AdisX & AdisY angular debug distributions after the block "Dipole D2".

### 2.2.5.3. Angular distribution cut by the momentum slits: option "Use for All distributions"

Angular distributions before/after the slits "S1" in the mode "Use for All distributions" are shown in Fig.292. For other modes (see Fig.283) output distributions are identical to input distributions.

## S1\_slits-Angle



**Fig.292.** “Input”/“Output” angular distributions before/after the slits “S1” for the mode “Use for All distributions”. The output distributions are identical to input distributions for other modes of option “Angular distribution cut by the momentum slits”.

The “Use for All distributions” mode is recommended to use in calculations. The “Angular distribution cut by the momentum slits” option is used for the debug purposes, and also for demonstrating the influences of energy cutting for angular distributions and how it apparently reflects on the transmission of the fragment through the spectrometer. Transmission values for  $^{100}\text{Zr}$  fragment<sup>Y</sup> are presented in the following table for different modes of the “Angular distribution cut by the momentum slits” option:

Mode	After “Slits1” [%]	After fragment separator, [%]
Do not use	12.28	1.821
Use for “MatrixKinematics” class	12.28	0.696
Use for All distributions	12.28	0.696

<sup>Y</sup> file [http://groups.nslc.msu.edu/lise/7\\_1/examples/CoulombFissionEnergyCutting.lpp](http://groups.nslc.msu.edu/lise/7_1/examples/CoulombFissionEnergyCutting.lpp). Energy distribution cutting descends due to Slits1.

## 2.3. Coulomb fission fragment production cross-sections

### 2.3.1. Electromagnetic fission cross-section

A study of the processes generated by the electromagnetic interaction in relativistic nuclear, and atomic collisions by C.Bertulani and G.Baur [Ber88] has been used to calculate the excitation energy function for fission.

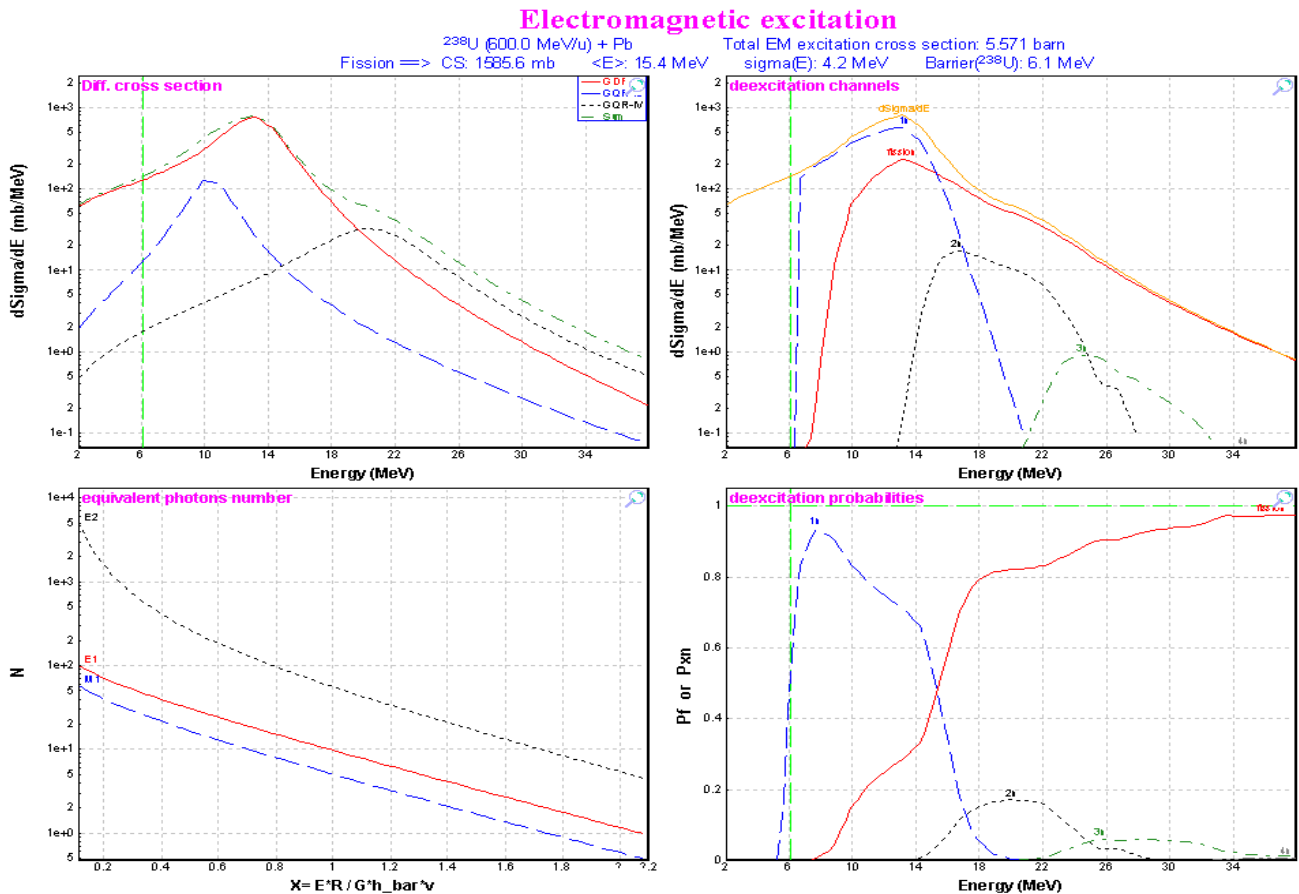
#### 2.3.1.1. Electromagnetic excitation

The differential cross-section for electromagnetic excitation is given by [Ber88, equation 2.7.11]:

$$\frac{d\sigma_{em}}{dE_\gamma} = \frac{n_{E1}}{E_\gamma} \cdot \sigma_\gamma^{E1} + \frac{n_{E2}}{E_\gamma} \cdot (\sigma_{\gamma,1}^{E2} + \sigma_{\gamma,2}^{E2}) \quad /26/$$

with  $n_{E1}$ ,  $n_{E2}$  being the number of equivalent photons per MeV for electric dipole and quadrupole excitations respectively.  $\sigma_\gamma^{E1}$ ,  $\sigma_{\gamma,i}^{E2}$  are the photon absorption cross-sections for giant E1 and E2 excitations, where for E2 excitations  $i=1$  is isoscalar and  $i=2$  is isovector giant quadrupole resonances.

Multiple excitations of the quadrupole resonances are neglected.



**Fig.293. Top left:** Differential cross-sections of GDR (red solid curve), GQR(IS) (blue dashed curve), and GQR(IV) (black dot curve) excitations in  $^{238}\text{U}$  as calculated from the equivalent photon spectrum representing a  $^{208}\text{Pb}$  nucleus at 600 MeV/u. The green dot-dashed curve is obtained by summing-up the different contributions. **Bottom left:** Equivalent photon number per unit projectile charge, for E1, M1, and E2 radiation. **Top right:** Deexcitation channels for  $^{238}\text{U}$  nuclei at 600 MeV/u excited by a lead target. The solid red curve represents fission decay. The blue dashed line represents 1n-decay channel, black dotted and green dot-dashed curves correspondingly 2n- and 3n-decay channels. **Bottom right:** the same as the top right but in the frame of probabilities.

### 2.3.1.1.1. Equivalent photon spectrum

The probability for a certain electromagnetic process in a relativistic nuclear collision to occur, in terms of the cross-sections for the same process generated by an equivalent pulse of light, is given as

$$P(b) = \int I(\omega, b) \sigma_{\gamma}(\hbar\omega) d(\hbar\omega) = \int n(\omega, b) \sigma_{\gamma}(\omega) \frac{d\omega}{\omega}, \quad /27/$$

where  $b$  is the impact parameter,  $\sigma_{\gamma}(\omega)$  is the photo cross-section for the photon energy  $E_{\gamma} = \hbar\omega$ , and the integral runs over all the frequency spectrum of the virtual radiation. The quantities  $n(\omega, b)$  can be interpreted as the number of equivalent photons incident on the target per unit area. The equivalent photon numbers are obtained from expressions 2.5.5 a-c in [Ber88] and can be plotted<sup>w</sup> by LISE++ (see left bottom plot in Fig.293) from the “Fission properties” dialog. (see Fig.294). The “Fission properties” dialog is available through the menu “Options → Production mechanism” if the mode “Coulomb Fission” is set.

### 2.3.1.1.2. Giant dipole resonance

The parameterization from work [Ilj92] for giant E1 excitation in equation /26/ has been used:

$$\sigma_{\gamma}^{E1} = \frac{\sigma_0}{1 + (E_{\gamma}^2 - E_R^2)^2 / (E_{\gamma} \cdot \Gamma_R)^2},$$

where the empirical parameters of the giant dipole resonance have the values  $\sigma_0=2.5A$  (in mb),  $\Gamma_R=0.3E_R$ , and  $E_R=40.3 \cdot A^{-0.2}$  (in MeV).

### 2.3.1.1.3. Giant quadrupole resonance

For quadrupole excitation, the isoscalar as well as the isovector giant quadrupole resonances are calculated following [Gre97, Sch00]:

$$\sigma_{\gamma, i}^{E2}(E_{\gamma}) = \frac{2}{\pi \Gamma_i} \frac{\sum_{E2} E_{\gamma}^2}{1 + (E_{\gamma}^2 - E_{i \max}^2)^2 / (E_{\gamma} \cdot \Gamma_i)^2} w_i, \quad /29/$$

with  $i=1,2$  denoting isoscalar and isovector mode, respectively.  $\sum_{E2}$  represents the sum rule for E2-absorption:

$$\sum_{E2} = \int \frac{\sigma_{\gamma}^{E2}}{E^2} dE = 2.2 \cdot 10^{-4} Z A^{2/3} \text{ mb/MeV}. \quad /30/$$

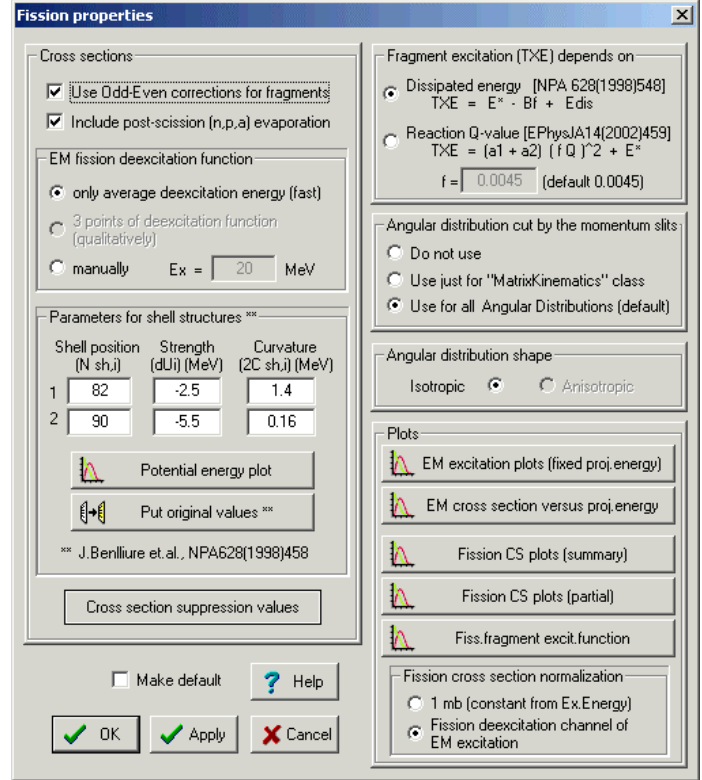


Fig.294. The “Fission properties” dialog. /28/

<sup>w</sup> the button “EM excitation plots (fixed proj.energy)”

The parameters in equation /29/ are chosen to be

$$\begin{aligned}
 w_1 &= Z/A, & w_2 &= N/A, \\
 E_{1,\max} &= 64.7 \cdot A^{-1/3} \text{ MeV}, & E_{2,\max} &= 130 \cdot A^{-1/3} \text{ MeV}, \\
 \Gamma_1 &= 17.5 \cdot A^{-1/3} \text{ MeV}, & \Gamma_2 &= 10.5 - 0.073 \cdot A^{2/3} - 0.00174 \cdot A^{4/3} \text{ MeV}.
 \end{aligned}$$

Differential cross-sections of GDR and GQR excitations in  $^{238}\text{U}$  as calculated from the equivalent photon spectrum representing a  $^{208}\text{Pb}$  nucleus at 600 MeV/u are shown in Fig.293 (top left plot).

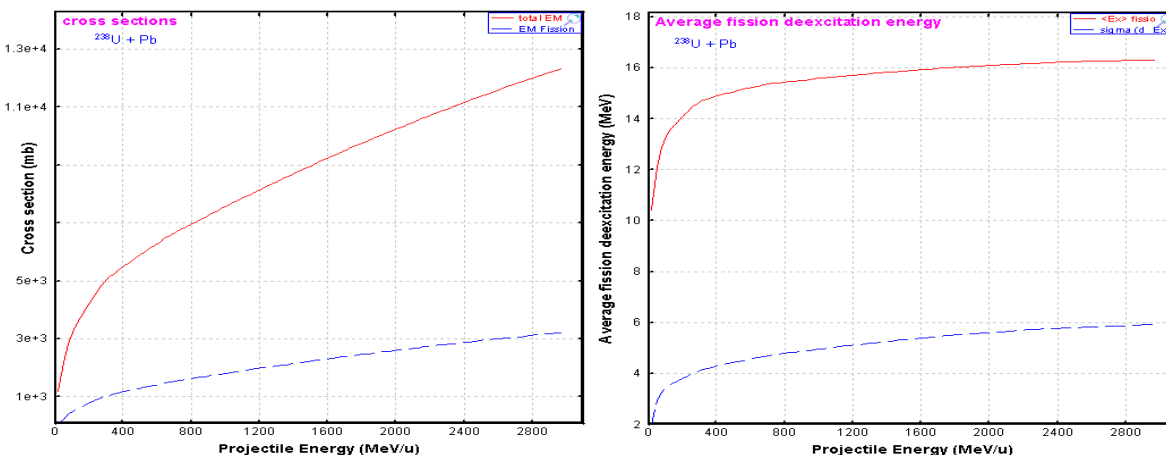
### 2.3.1.2. Fission deexcitation channel

Excitations exceeding the fission barrier may lead to fission. The code using the “LisFus” evaporation model calculates a fission probability to get the differential fission cross-section  $d\sigma^f/dE$  to use in the following fission fragment production cross-sections. Deexcitation channels for  $^{238}\text{U}$  nuclei at 600 MeV/u excited by a lead target are shown in right plots of Fig.293. The following settings are used in the “LisFus” model automatically to calculate fission differential cross-section:

State Density: “C”	Tunneling: <i>Yes</i>
Mode (manual/auto): <i>manual</i>	Use unstable: <i>Yes</i>
Mode (qualitatively/fast): <i>qualitatively</i>	Decay modes: <b>n, p, <math>\alpha</math>, fission, <math>\gamma</math></b>
Dimension of evaporation distributions	$E^* - B_f > 30$
4, if	$8 < E^* - B_f \leq 30$
8, if	$E^* - B_f \leq 8$
16, if	

### 2.3.1.3. Dependences of average excitation energy and EM fission cross-section from beam energy

The user can plot distributions of the average excitation energy and EM fission cross-section from the projectile energy using the “EM cross-section versus proj.energy” button in the “Fission properties” dialog. Fig.295 represents the case  $^{238}\text{U}+\text{Pb}$ . In Fig.295. The linear dependences of cross-sections and average value  $\langle E^* \rangle$  are observed at the projectile energy above 200 MeV/u.



**Fig.295. Left plot:** calculated total electromagnetic and fission electromagnetic cross-sections from the  $^{238}\text{U}$  projectile energy in the case of a lead target. **Right plot:** Average value and standard deviation distributions of differential fission electromagnetic cross-section from the  $^{238}\text{U}$  projectile energy in the case of a lead target.

### 2.3.2. A semi-empirical model of the fission-fragment properties

Fission, especially at low excitation energy, is a very complicated process which is far from being fully understood [Ben97]. The influence of nuclear structure on the fission process is manifested in the observed mass distributions. Models for the description of nuclear fission which are able to reproduce measured fission fragment distributions with considerable success. Some models use parameters which are individually adjusted to the experimental distributions of each system.

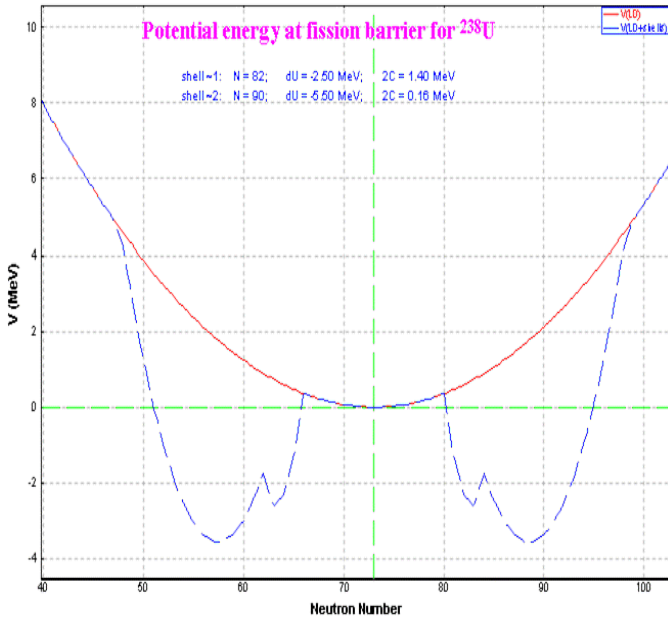
The LISE++ code uses a semi-empirical model of J. Benlliure [Ben97] based on a version of the abrasion-ablation model which describes the formation of excited prefragment due to the nuclear collisions and their consecutive decay. The competition between evaporation of different light particles and fission is computed with the “LisFus” evaporation model.

The semi-empirical description of the fission process presented in Benlliure’s model has some similarities with previously published approaches, e.g. [Itk86, Itk88], but in contrast to those, B.’s model describes the fission properties of a large number of fissioning nuclei over a wide range of excitation energies.

For a given excitation energy  $E$ , the yield  $Y(E, N)$  of fission fragments with neutron number  $N$  is calculated by the statistical weight of transition states above the conditional potential barrier:

$$Y(E, N) = \frac{\int_0^{E-V(N)} \rho_N(U) dU}{\sum_{N=0}^{N_{CN}} \int_0^{E-V(N)} \rho_N(U) dU}, \quad /31/$$

where  $V(N)$  is the height of the conditional potential barrier for a given mass-asymmetric deformation,  $\rho_N$  is the level densities for an energy  $U$  above this potential and  $N_{CN}$  is the neutron number of the fissioning nucleus.



**Fig.296.** Potential energy at the fission barrier for  $^{238}\text{U}$ , as a function of mass asymmetry expressed by the neutron number.

#### 2.3.2.1. Potential energy at the fission barrier

The total potential energy at the fission barrier is given by the sum of five contributions:

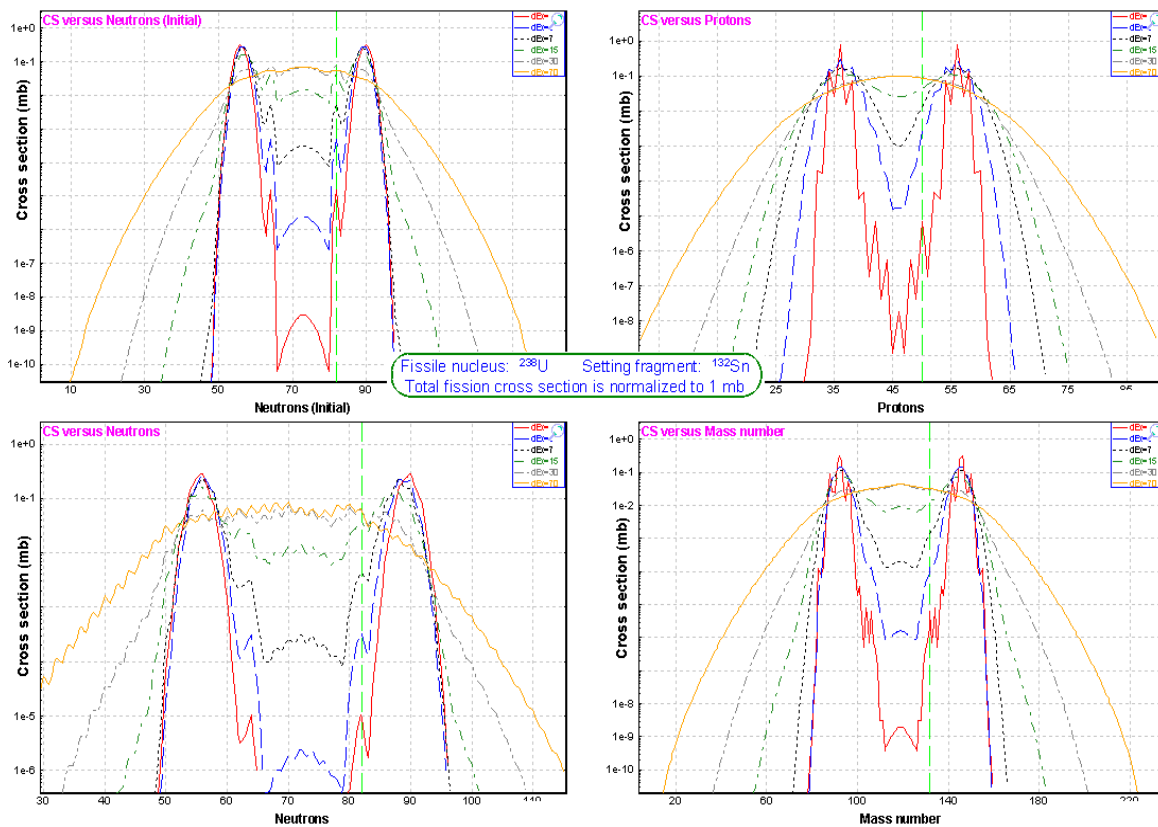
$$V(N) = V_{mac}(N) + V_{sh,1}(N) + V_{sh,1}(N_{CN} - N) + V_{sh,2}(N) + V_{sh,2}(N_{CN} - N) \quad /32/$$

where  $V_{mac}$  is the symmetric component defined by the liquid-drop description by means of a parabolic function. This parabola is modulated by two neutron shells, located at mass asymmetries corresponding to the neutron shells  $V_{sh,1}$  and  $V_{sh,2}$  in the nascent fragments.

The macroscopic part of the potential energy at the fission barrier as a function of the mass-asymmetry degree of freedom has been taken by J.B. from experiment [Itk88]. Parameters for shell structures can be modified in LISE++ in the “Fission properties” dialog (see Fig.294). The code takes default (initial) values for shell description from [Ben98]. A dependence of potential energy at the fission barrier from the neutron number can be plotted from the “Fission properties” dialog (see Fig.296).

### 2.3.2.2. Pairing corrections

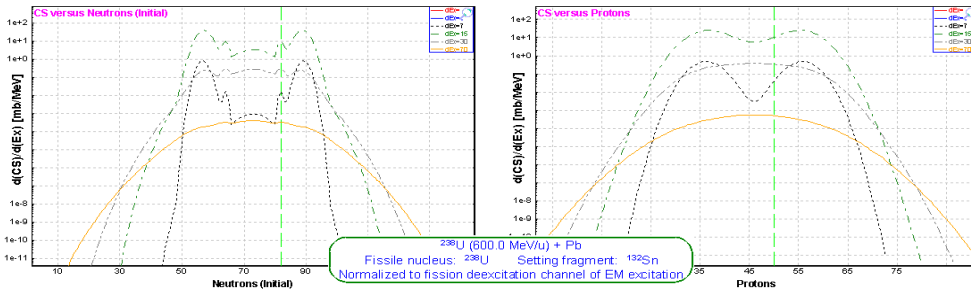
Pairing (or odd-even) corrections have been done in the code in accordance with [Ben98]. Odd-even corrections can be turned off in the “Fission properties” dialog. Using the “Fission cross-section plot (summary)” button the cross-section distributions versus the fragment neutron number, atomic number and mass for different excitation energies can be plotted (see Fig.297 and Fig.298). Left top plots in both figures represent cross-section distributions without odd-even corrections and post-scission nucleon emission. Cross-section in Fig.297 were normalized to 1 mb, whereas they were normalized to the EM fission excitation function in Fig.298.



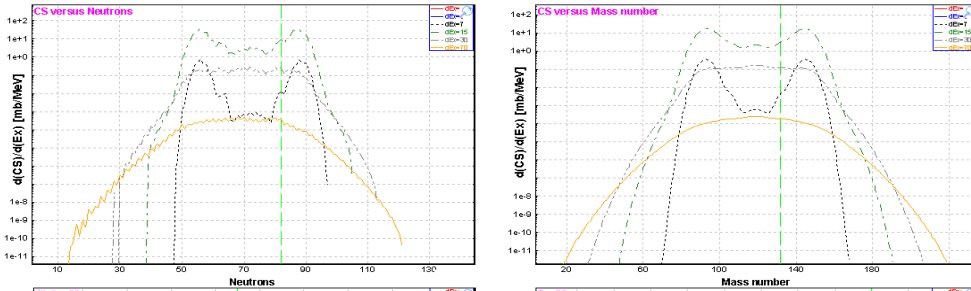
**Fig.297.** Calculated fission fragment production cross-sections for different excitation energies. Cross-sections were normalized to 1 mb. **Left top plot:** initial distributions (without odd-even corrections and post-scission nucleon emission) versus the fragment neutron number. **Left bottom:** final (after using odd-even corrections and post-scission nucleon emission) cross-section distributions versus the fragment neutron number. **Right top:** final cross-section distributions versus the fragment atomic number. **Right bottom:** final cross-section distributions versus the fragment mass.

Partial cross-section distributions of isotones  $N=82$ , isotopes  $Z=50$  and isobars  $A=132$  for different excitation energies can be plotted using the “Fission cross-section (partial)” button (see Fig.299 and Fig.300).

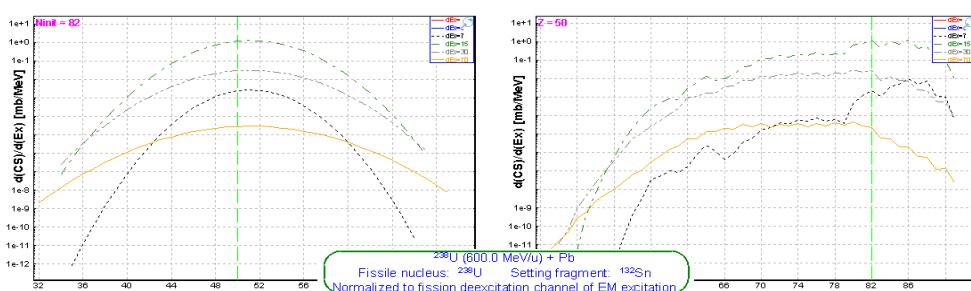
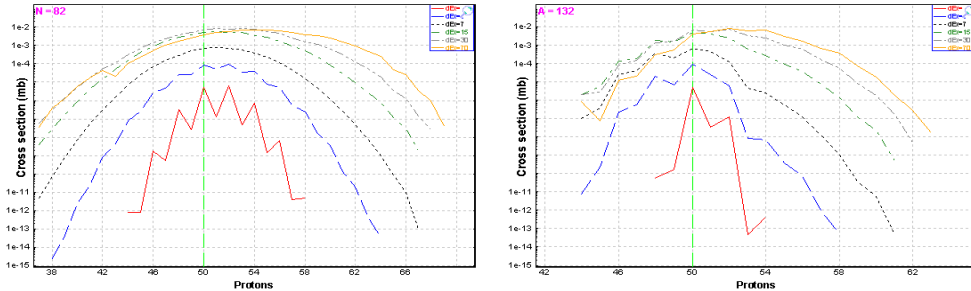
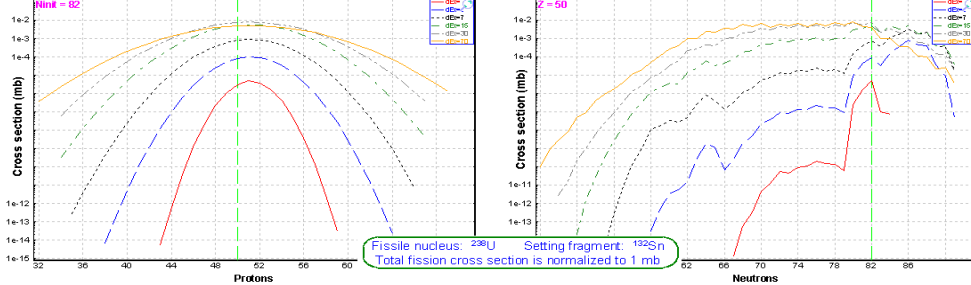




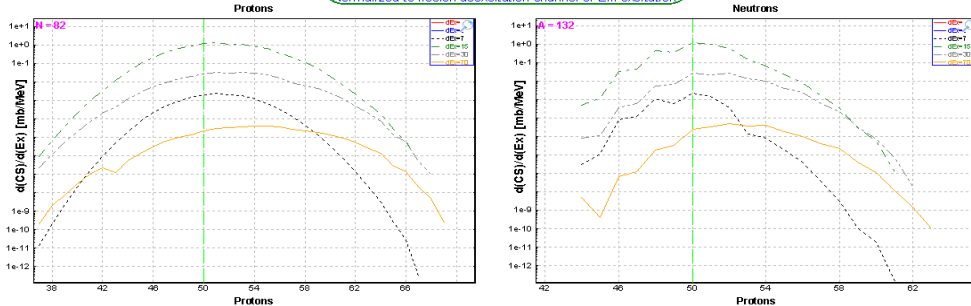
**Fig.298.** The same as Fig.297 but normalized to EM fission excitation function for the combination  $^{238}\text{U}(600\text{MeV/u}) + \text{Pb}$ .



**Fig.299.** Calculated partial fission fragment production cross-sections for different excitation energies. Cross-sections were normalized to 1 mb. **Left top plot:** initial distributions (without odd-even corrections and post-scission nucleon emission) for isotones  $N=82$ . **Left bottom:** final (after using odd-even corrections and post-scission nucleon emission) cross-section distributions for isotones  $N=82$ . **Right top:** final CS distributions for isotopes  $Z=50$ . **Right bottom:** final CS distributions for isobars  $A=132$ .



**Fig.300.** The same as Fig.299 but normalized to EM fission excitation function for the combination  $^{238}\text{U}(600\text{MeV/u}) + \text{Pb}$ .



### 2.3.2.3. Post-scission nucleon emission

The part of post-scission nucleon\* emission due to the deformation of the fission products and its evolution with the excitation energy was taken into account. But in contrast with [Ben98] where the mean post-scission neutron number  $\nu(A)$  due to deformation was obtained as a parameterization of data the LISE++ code uses the “LisFus” model (fast version) to calculate the final fragment in ground state.

The excitation energy of the fragment after scission is defined by way as it was already described in chapter 2.2.2.3. The following settings automatically are used in the “LisFus” model to calculate post-scission nucleon emission:

- State Density: “C”
- Mode (manual/auto): *manual*
- Mode (qualitatively/fast): *fast*
- Dimension of evaporation distributions: *4*
- Tunneling: *Yes*
- Use unstable: *Yes*
- Decay modes: **n, p,  $\alpha$**

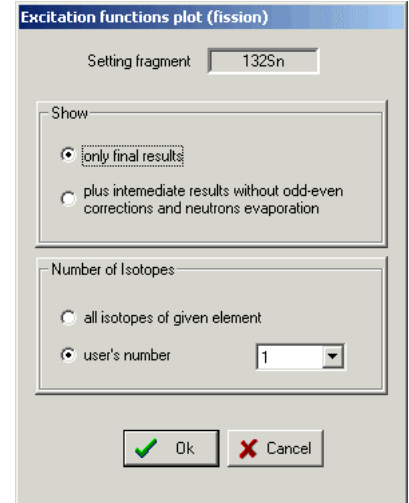


Fig.301.

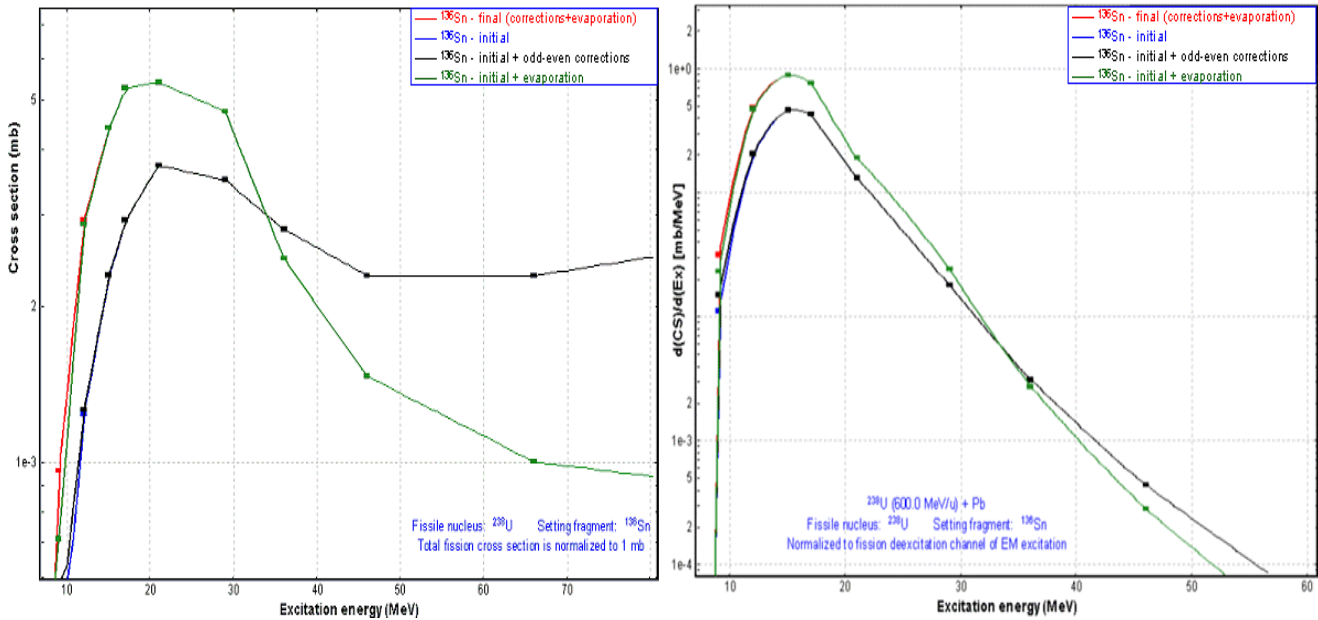
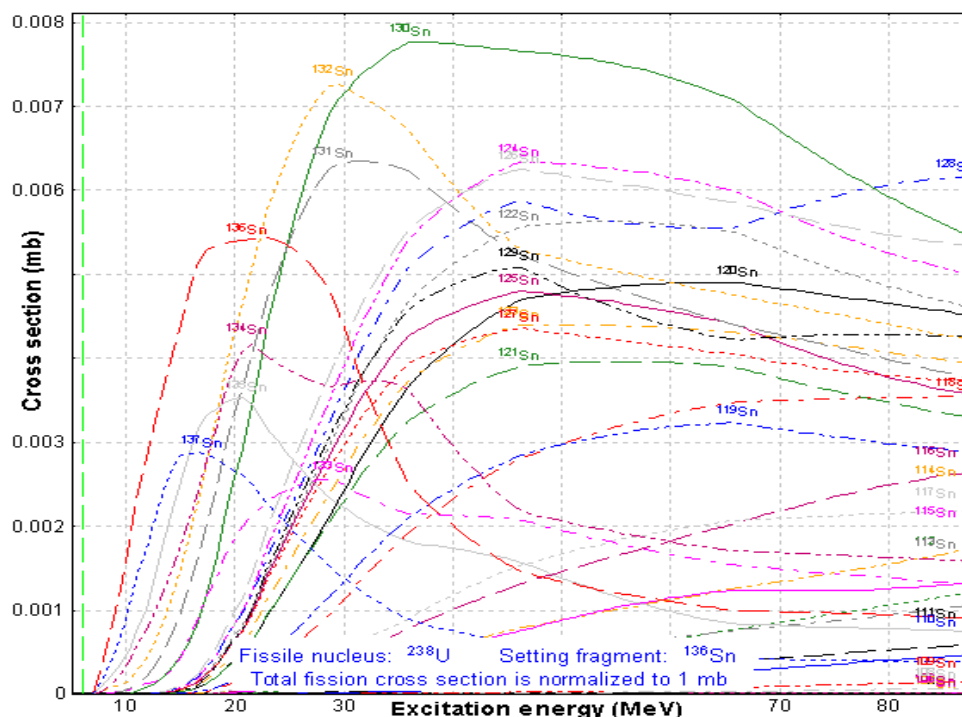


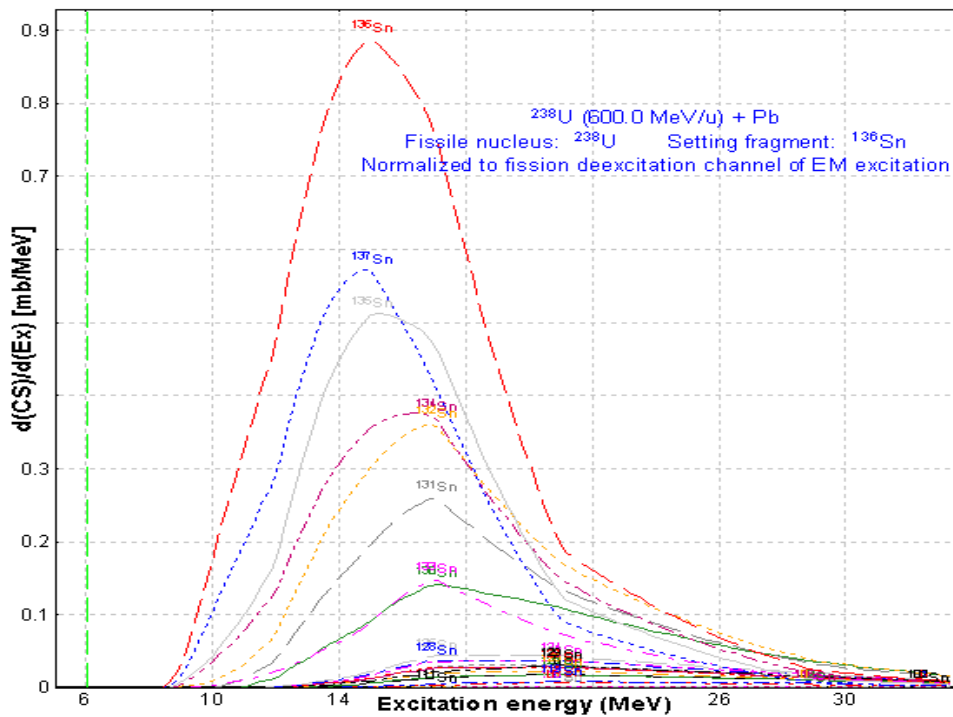
Fig.302. Excitation functions of the final fragment  $^{136}\text{Sn}$  for the combination  $^{238}\text{U}(600\text{ MeV/u})+\text{Pb}$ . The blue curve represents the excitation function without pairing corrections and post-scission nucleon emission. The black curve shows pairing corrections, and the green line correspondingly shows contribution of nucleon emission. The red curve includes pairing corrections and nucleon evaporation. After 15 MeV the red curve coincides with the green one, and the blue curve coincides with the black one. Left plot: total fission cross-section was normalized to 1 mb. Right plot: normalization has been done on the electromagnetic fission channel.

\* LISE++ calculates also alpha and proton emission for high excitation energies how (will be shown lately). This is the reason why the expression “nucleon emission” is used in this work instead “neutron emission”.

Pairing corrections and post-scission nucleon emission can be turned off in the “Fission properties” dialog to see the contribution of these processes. Pairing corrections play the relevant role close to the fission barrier as can be seen in Fig.297-300, whereas the contribution of nucleon emission is necessary considering at excitation energies of several tens MeV, as is shown in figures of excitation function of tin isotopes (see Fig.302-304). Excitation function plot of fission fragment is available through the “Fission properties” dialog using the “*Fiss.fragment excit.function*” button which allows the user to get the “Excitation functions plot (fission)” dialog (see Fig.301) where the user can chose options for a excitation function plot.



**Fig.303.** Excitation functions of tin isotopes for the combination  $^{238}\text{U}$  (600 MeV/u) + Pb. Total fission cross-section was normalized to 1 mb.



**Fig.304.** The same as Fig.303 but normalization has been done on the electromagnetic fission channel.

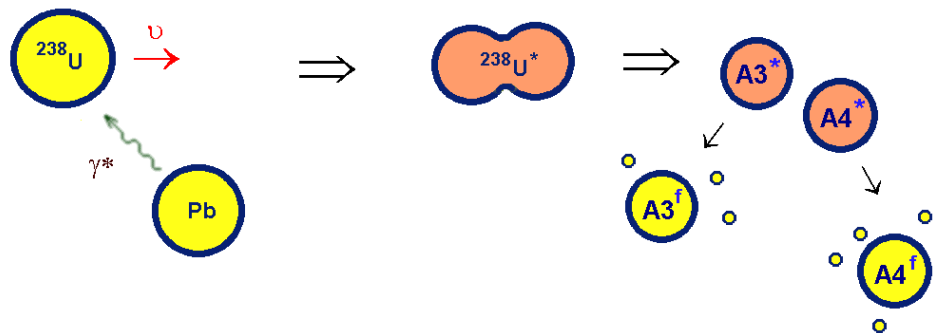
### 2.3.3. How it works in LISE++?

Before the explanation how fission fragment production cross-sections are calculated in the code it is necessary to give some definitions, including the fission cross-section matrix (FCSM).

#### 2.3.3.1. Fission cross-section matrix (FCSM).

The fission cross-section matrix represents an array of float values (32 bits) of dimension ( $Z_{max} \times N_{max}$ ) where  $Z_{max}$  is the maximum  $Z$  possible to be used in the code (130) and  $N_{max}$  is the maximum number of neutrons in an element possible in the code (200). The class “FissionCS” responsible for fission fragment production cross-sections has **6 FCSM which are kept in the memory**. These matrices contain the following values for each isotope:

1. Final fragment production cross-sections,
2. Excited fragment production cross-sections,
3.  $dA_{out}$ ,
4.  $dA_{in}$ ,
5.  $dN_{out}$ ,
6.  $dN_{in}$ .



**Fig.305.** Coulomb fission schematic.

Coulomb fission schematic is shown in Fig.305, where  $A^*$  is the excited fragment, and  $A^f$  the final fragment in ground state. Then  $dA = A^* - A^f$  is the number of emitted nucleons, and  $dN$  is the number of emitted neutrons from the excited nucleus. Let's define  $dA_{in}$ ,  $dA_{out}$  as:

**Table 40.**  $dA_{in}$  &  $dA_{out}$  definitions.

1.  $dA_{in}$  is the value used only for the **final** fragment and equal to average number on nucleons emitted by excited fragments to **get the final fragment**

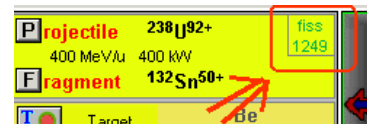
$$dA_{in}(A_3^f) = \frac{\sum_j \sigma(A_{3j}^* \rightarrow A_3^f) \cdot dA_{3j}}{\sum_j \sigma(A_{3j}^* \rightarrow A_3^f)}$$

2.  $dA_{out}$  is the value used only for the **excited** fragment and equal to average number on nucleons emitted **by the excited fragment**

$$dA_{out}(A_3^*) = \frac{\sum_j \sigma(A_3^* \rightarrow A_{3j}^f) \cdot dA_{3j}}{\sum_j \sigma(A_3^* \rightarrow A_{3j}^f)}$$

### 2.3.3.2. Fission fragment cross-section for transmission calculations

1. The program assumes that the reaction takes place in middle of the target. In connection with that the EM cross-section depends on the primary beam energy. Therefore the first step is the calculation of the primary beam energy in the middle of the target.
2. Total fission cross-section and average excitation energy:
  - a. Calculation of differential electromagnetic cross-section (chapter 2.3.1.1.).
  - b. Deexcitation fission function  $d\sigma^f/d(E^*)$  (chapter 2.3.1.2.).
  - c. Calculation of statistical parameters of the deexcitation fission function: mean value  $\langle E^* \rangle$ , and area  $\sigma^f$ .
3. Calculation of an initial fission cross-section matrix ( $CS_{init}$ ) of production cross-sections excited fragments using the semi-empirical model [Ben98] (see chapter 2.3.2.). The code takes into account unbound nuclei as well for this stage of the calculations. **The single criterion is that the Q-value of the reaction reaction should be positive<sup>♦</sup>!**
4. Post-scission nucleon emission: The code calculates the final 5 FCSM matrices based on equations /19,20/ using the  $CS_{init}$  matrix. If a final production cross section of a fragment is less than the suppression value then the final fragment is excluded from matrices. As explained previously, fission fragment cross sections are kept in the operating memory and are being used for the next calculations. The number of calculated cross sections can be seen in the “Setup” window (see Fig.306).



**Fig.306.**

All four stages together take no more than 5 seconds. But if some of the initial settings have been changed in the program then the code recalculates the cross section again (see chapter 2.3.3.4.). Final cross sections can be visualized as 1D- or 2D-plots (see chapter 2.4.)

<sup>♦</sup> ME(fissile nucleus)+  $E^* > ME(A3^*)+ME(A4^*)$  (see Fig.305)

### 2.3.3.3. Suppression values for fission production cross-sections

To exclude low-probability events and therefore to reduce the time of transmission calculation the user can set a threshold for fragment production cross-sections. The fragment cross section is excluded from FCSM matrices if the fragment production cross-section is less than the product of the total fission cross-section and the suppression value. The threshold can be changed in the “Fission cross section suppression values” (see Fig.307) which is accessible through the “Fission properties” dialog (see Fig.294).

### 2.3.3.4. Recalculation of fission fragment cross-sections

The matrixes are automatically recalculated, if at least one of the following program settings is changed:

Projectile	Mass or Atomic number ( $A, Z$ )
	Primary beam energy has been changed by <b>10%</b>
Target	Mass or Atomic number ( $A, Z$ )
	Target thickness has been changed by <b>10%</b>
Fission options	Post-scission nucleon emission: on/off
	Pairing correction - on/off
	Suppression value for fission cross-sections
	Shells characteristics (chapter 2.3.2.1.)
	Excitation energy method and parameter $\bar{f}$ (chapter 2.2.2.3.)
General	Mass formula
Evaporation options	Parameter “ <i>BarFac</i> ”
	Evaporation Odd-Even Delta parameter
	Fission Odd-Even Delta parameter

### 2.3.3.5. File of fission fragment cross-sections

The code has been modified to support reading/writing of fission fragment production cross-sections into/from the cross section file. Using the “Cross section file” dialog (the menu “Options”, see Fig.308) it is possible to copy calculated fission cross section to the “User memory” (frame #1 in Fig.308) array to be saved after in the file. The “User memory” cross sections can be plotted (see Fig.309) through the “Cross section file” dialog (frame #2 in Fig.308). The cross section file can be used to avoid a recalculation of the fission cross section by the code or to load experimental cross sections into the code.

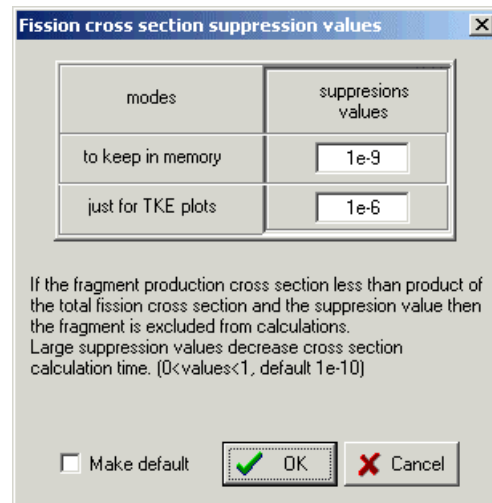
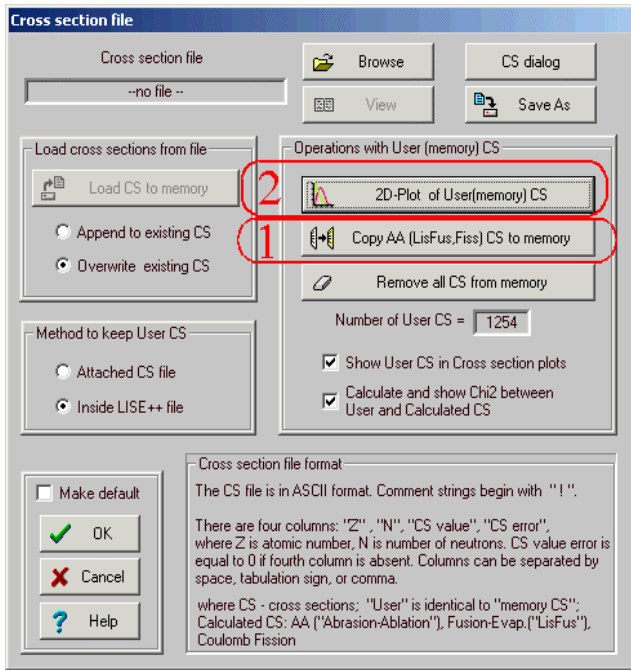
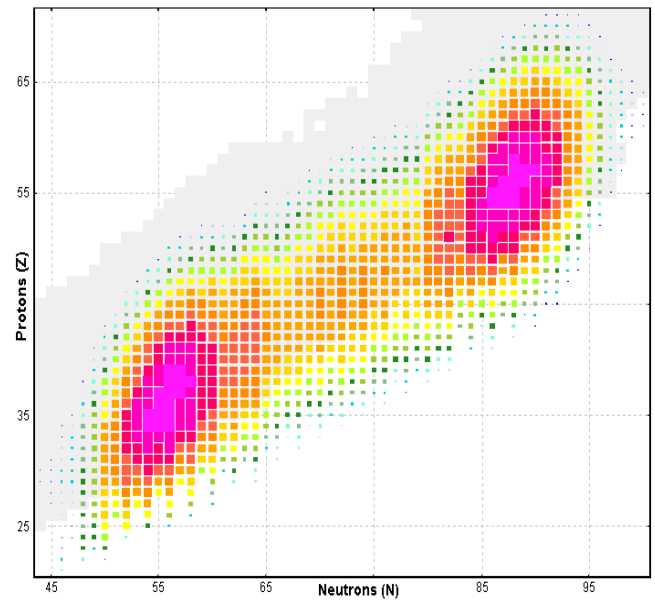


Fig.307. The “Fission cross-section suppression values” dialog.



**Fig.308.** The “Cross-section file” dialog.



**Fig.309.** Two-dimensional plot of “User memory” cross-sections created by the “Cross section file dialog for the reaction  $^{238}\text{U}(400\text{ MeV/u})+\text{Be}(12\text{ mg/cm}^2)$ .

### 2.3.3.6. Simulation of “abrasion-fission” (nuclear fission)

It is possible to set manually the excitation energy to use in cross section calculations and fission fragment kinematics. The user can roughly simulate “abrasion-fission” fragment kinematics if the option “manually” in the “Excitation energy” frame of the “Fission properties” dialog is set and 60-80 MeV as an excitation energy of the projectile is used. But in any case the total fission cross section can be calculated from the EM fission excitation function. It is necessary to remember and make normalization of the fragment rate later.

## 2.4. Plots for “Coulomb fission” mode (menu 1D-plot)

### 2.4.1. Cross-sections

To see the fission fragment production cross section distribution plot it is necessary to load the “Fission cross-section plot options” dialog (see Fig.310) which is available in the menu "1D-plots => Cross-section distributions" of the "Coulomb fission" reaction mode. The “Fission cross section plot options” dialog gives two options to plot cross sections distributions depending on excitation energy.

“EM fission cross-section”: the code takes two average excitation energies and fission cross-section values calculated assuming the Coulomb fission mechanism from the initial reaction parameters set in the code: primary beam ( $A, Z, E$ ) and target ( $A, Z$ , thickness). In this case the user can plot fission fragment production cross-sections used by the code in transmission calculations.

“Differential cross-sections”: it is possible to input manually differential fission cross-section and excitation energy values. In this case the code gives a hint to user as to what the differential EM fission cross-section corresponds to the input excitation energy.

#### 2.4.1.1. “EM fission cross-section” option

Calculated production cross-sections for the reaction  $^{238}\text{U}(600\text{ MeV/u}) + \text{Pb}(1\text{g/cm}^2)$  are presented in Fig.311. The excitation energy for CS calculations has been calculated as the mean value of the differential EM fission cross section and is equal to 15.4 MeV. Post-scission nucleon emission has been taken into account.

Figures 312-314 have been created using 1D-dimensional plot types “ $\text{sum}(\text{CS}); N=\text{const}$ ”, “ $\text{sum}(\text{CS}); A=\text{const}$ ”, and “ $\text{sum}(\text{CS}); Z=\text{const}$ ”, for different initial conditions (Position of the second shell, Post-scission nucleon emission) and saving calculated cross-section distributions into files.

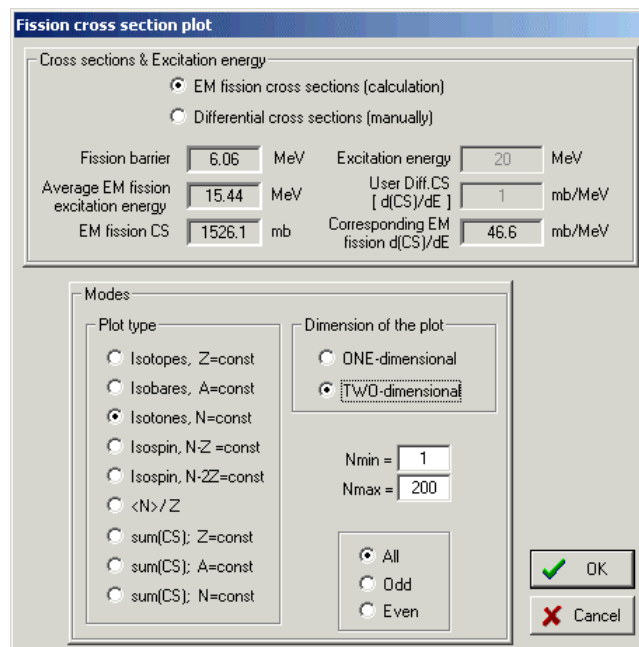


Fig.310. The “Fission cross section plot options” dialog.

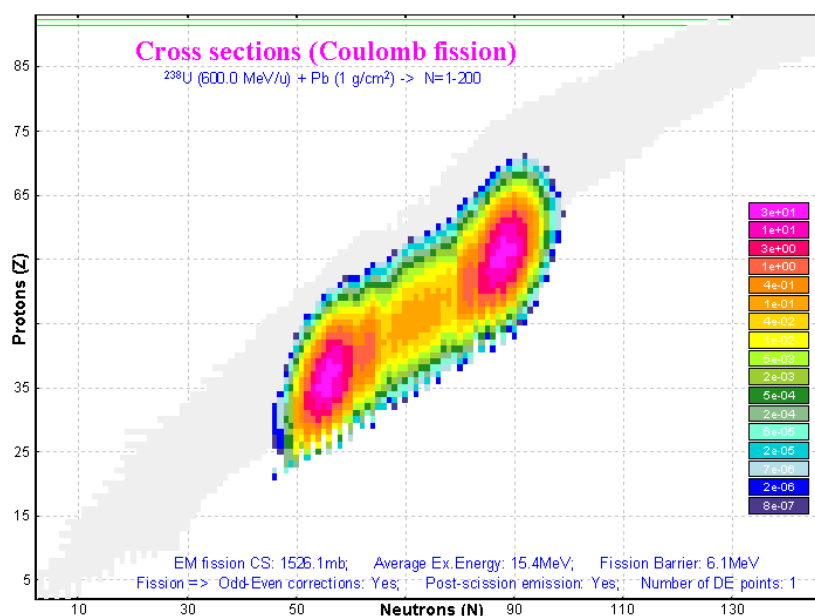
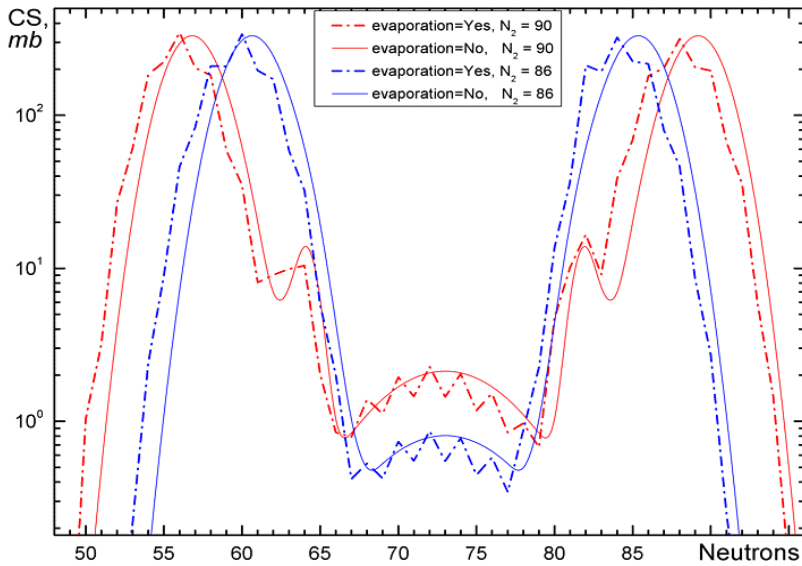


Fig.311. Calculated production cross-sections for the reaction  $^{238}\text{U}(600\text{MeV/u}) + \text{Pb}(1\text{g/cm}^2)$ . Default shell settings (chapter 2.3.2.1.) were applied. The cross section suppression value was set to  $1e-9$ .



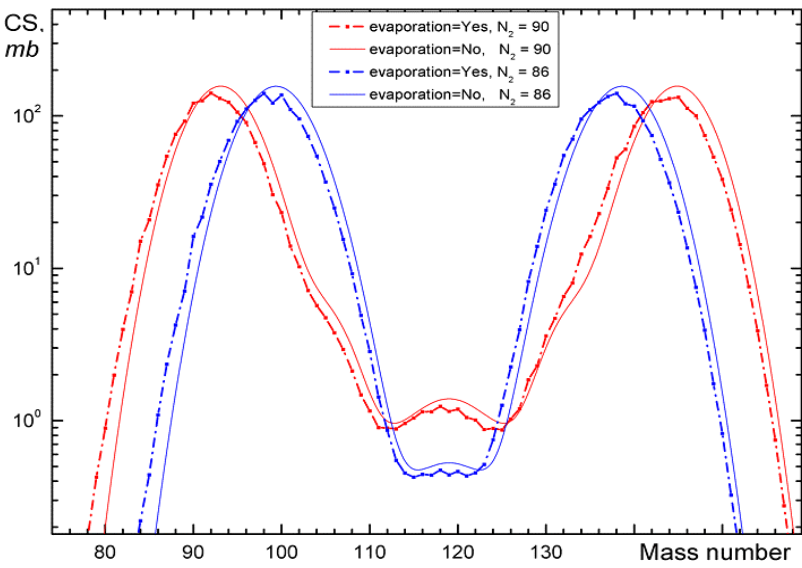


**Fig.312.** Calculated production cross-sections for the reaction  $^{238}\text{U}(600\text{MeV/u}) + \text{Pb}(1\text{g/cm}^2)$  versus fragment **neutron** number.

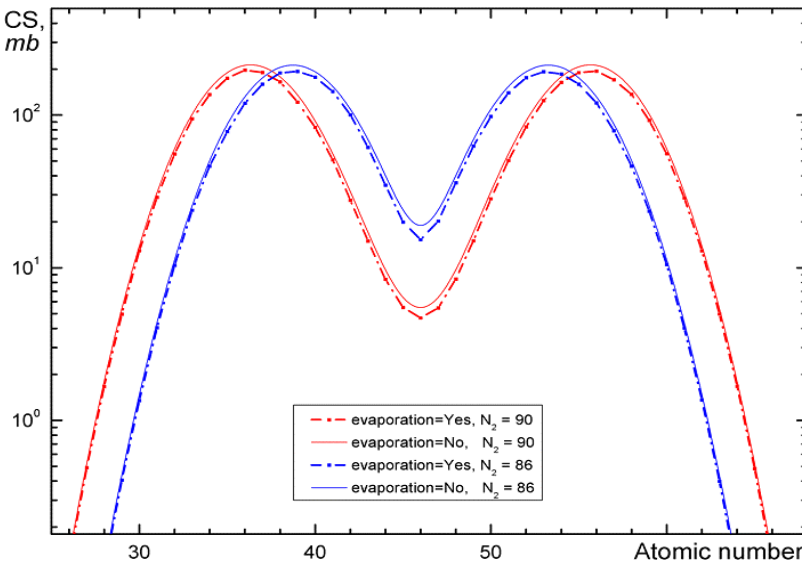
Default shell settings (chapter 2.3.2.1.) were applied. The cross section suppression value was set to  $1e-9$ .

Red (blue) curves correspond to the position of the second shell at  $N_2=90$  (86).

Solid (dot-dashed) curves correspond to calculations without (with) taking into account post-scission nucleon emission.



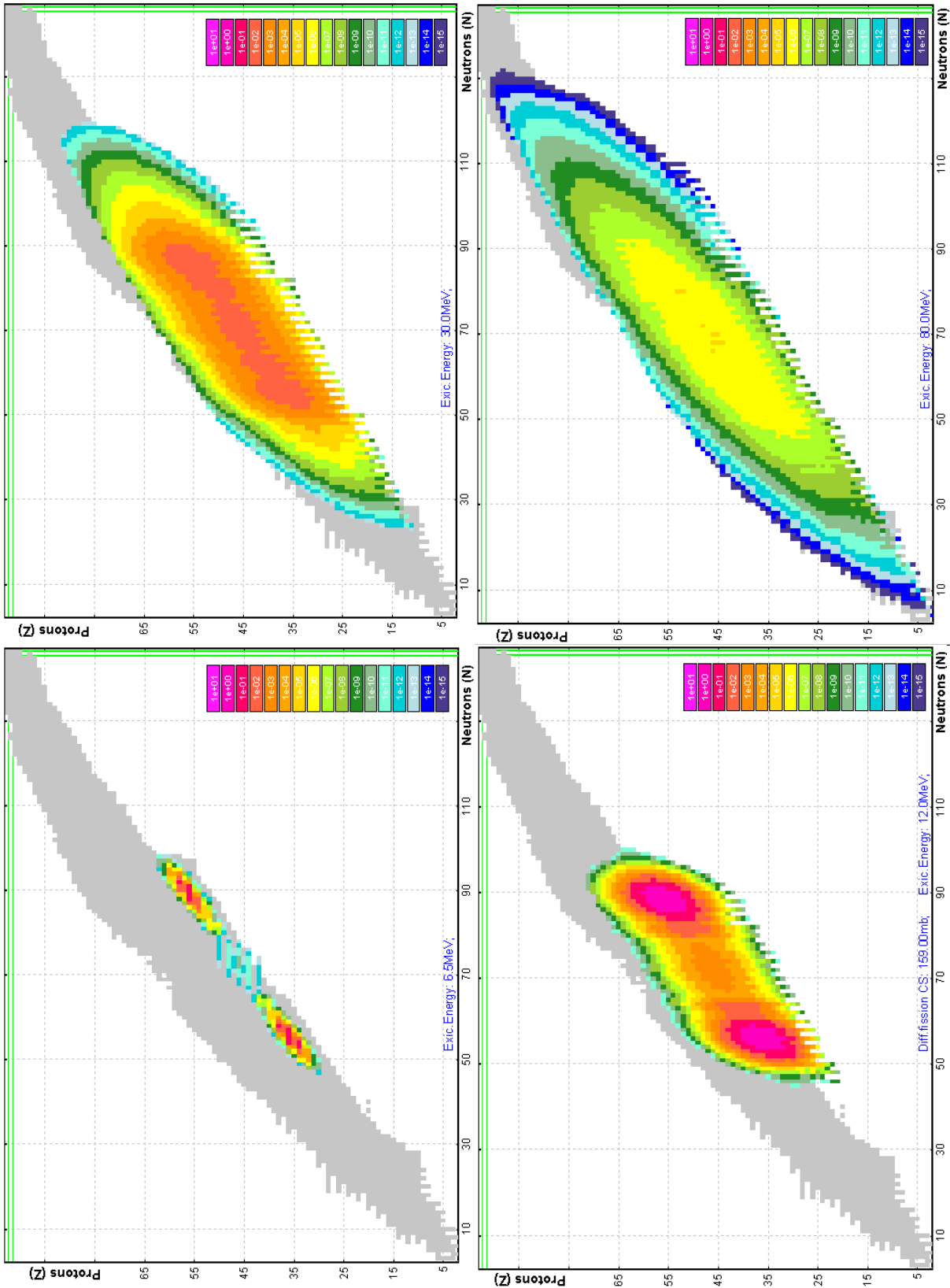
**Fig.313.** The same as Fig.312 but versus the fragment **mass** number.



**Fig.314.** The same as Fig.312 but versus the fragment **atomic** number.

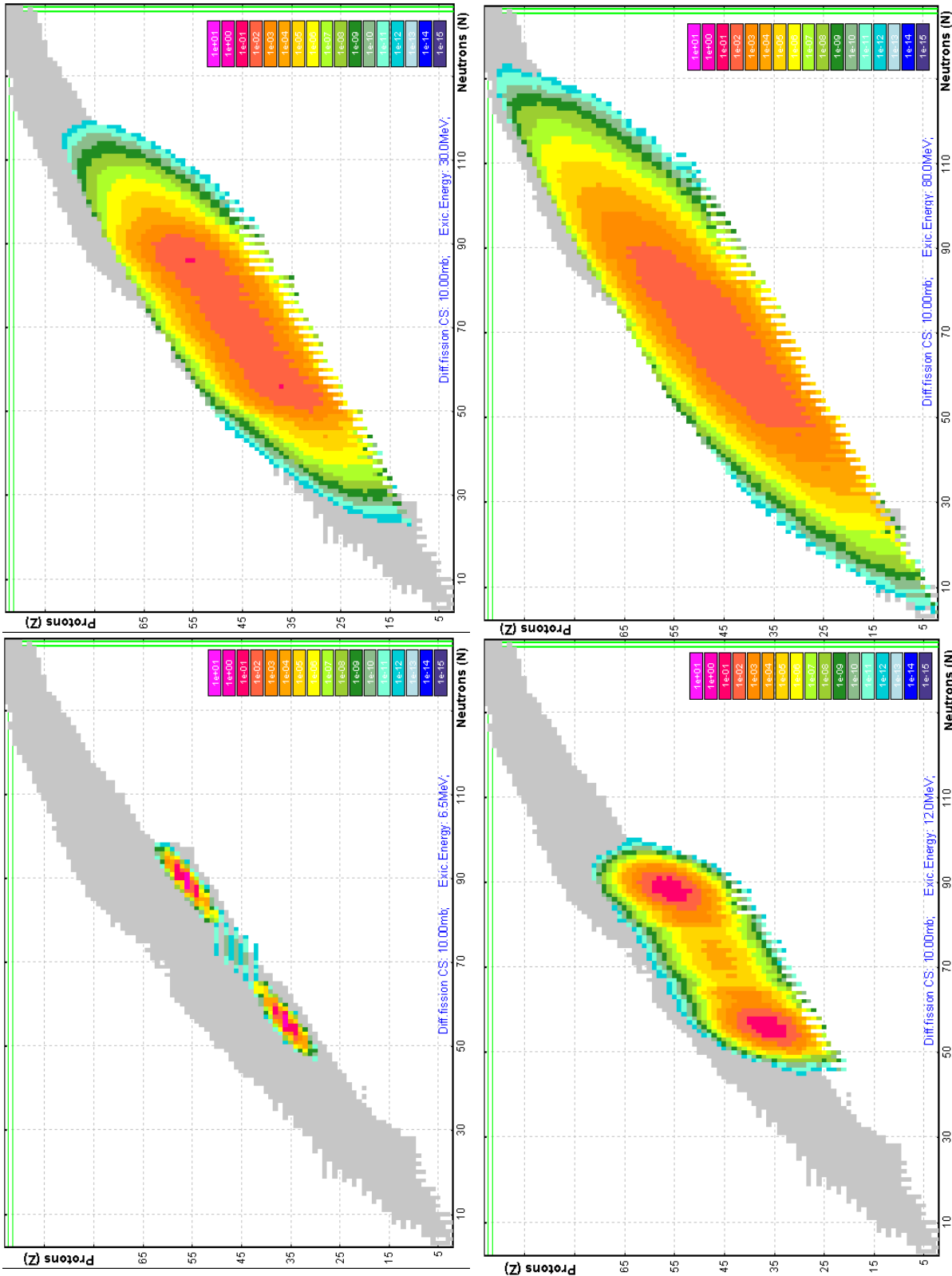
### 2.4.1.2. "Differential cross-section" option

Calculated fission fragment differential cross sections for the fissile nucleus  $^{238}\text{U}$  for different excitation energies (6.5, 12, 30, and 80 MeV) are shown in Fig.315 and Fig.316.



**Fig.315.** Calculated fission fragment differential cross sections for the fissile nucleus  $^{238}\text{U}$  for different excitation energies: left top 6.5 MeV, left bottom 12 MeV, right top 30 MeV, right bottom 80 MeV. The total fission cross section is normalized to the EM fission deexcitation function of the reaction  $^{238}\text{U}(600\text{MeV}/u) + \text{Pb}(1\text{g}/\text{cm}^2)$ .

The total fission cross section in Fig.315 is normalized to the EM fission deexcitation function of the reaction  $^{238}\text{U}(600\text{MeV/u}) + \text{Pb}(1\text{g/cm}^2)$ , and in Fig.316 correspondingly normalized to 10 mb. Z-scale for all plots in the figures was set the same ( $1\text{e-}15 \div 1\text{e+}01$  with the logarithm step equal to 10 between colors). LISE++ default fission properties setting was used for these calculations.



**Fig.316.** Calculated fission fragment differential cross sections for the fissile nucleus  $^{238}\text{U}$  for different excitation energies: left top 6.5 MeV, left bottom 12 MeV, right top 30 MeV, right bottom 80 MeV. The total fission cross section is normalized to 10 mb

### 2.4.2. Total kinetic energy and post-scission nucleon emission plots

Total kinetic energy and post-scission nucleon emission plots are available from the menu "1D-plots ⇒ Velocity after reaction / TKE (for fission)" in the "Coulomb fission" reaction mode. The "Fission TKE & post-scission emitted nucleons plots" dialog (see Fig.317) has two principal modes:

- 1) Kinetic energy in CMS (*TKE*);
- 2) Number of evaporated nucleons ( $dA_{in}$ ,  $dN_{in}$ ,  $dZ_{in}$ ,  $dA_{out}$ ,  $dN_{out}$ ,  $dZ_{out}$ ). See the definitions  $dA_{in}$  and  $dA_{out}$  in chapter 2.3.3.1.

The "Excitation energy modes" frame in the plot options is identical to the "Fission cross sections plot options" dialog from the previous chapter.

"One or Two fragments?": it is possible to plot values corresponding to one fragment (kinetic energy in CMS or number of evaporated nucleons), or in the sum of this fragment with the conjugate fragment. In the case of *TKE* and  $dX_{in}$  the code is looking for a conjugate final fragment, in the case of  $dA_{out}$  correspondingly the code is looking for an excited fragment:

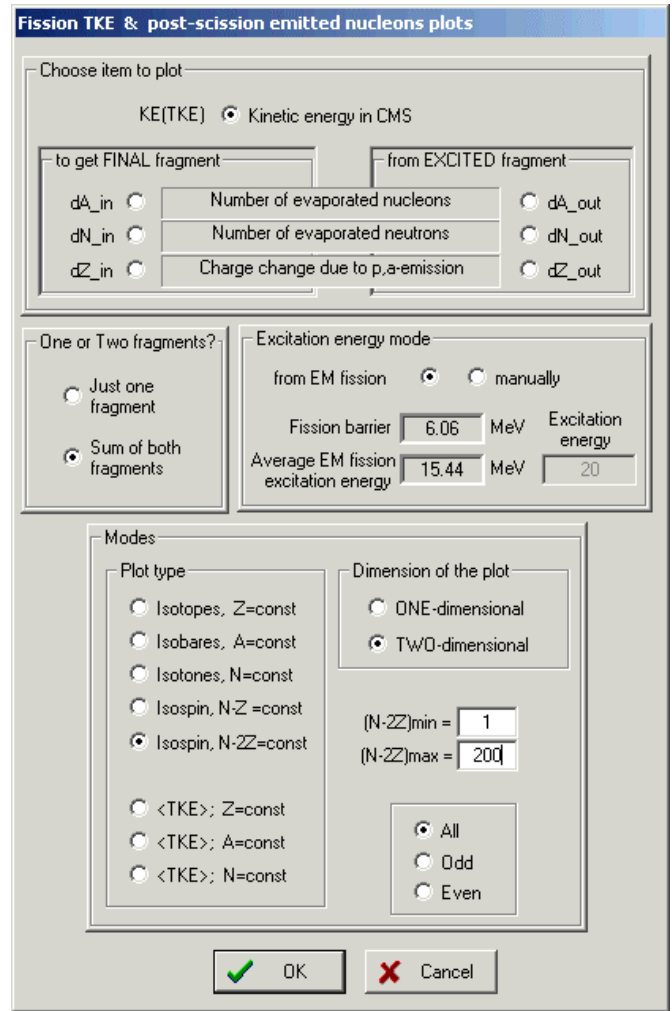


Fig.317. The "Fission TKE & post-scission emitted nucleons plots options" dialog.

Table 41.

mode	"Just for one fragment"	"Sum of both fragments"
$dA_{in}$	$dA_{in}(A_3^f)$	$dA_{in}(A_3^f) + dA_{in}(A_4^f)$
$dA_{out}$	$dA_{out}(A_3^*)$	$dA_{out}(A_3^*) + dA_{out}(A_4^*)$

#### 2.4.2.1. Calculation of conjugate final fragment

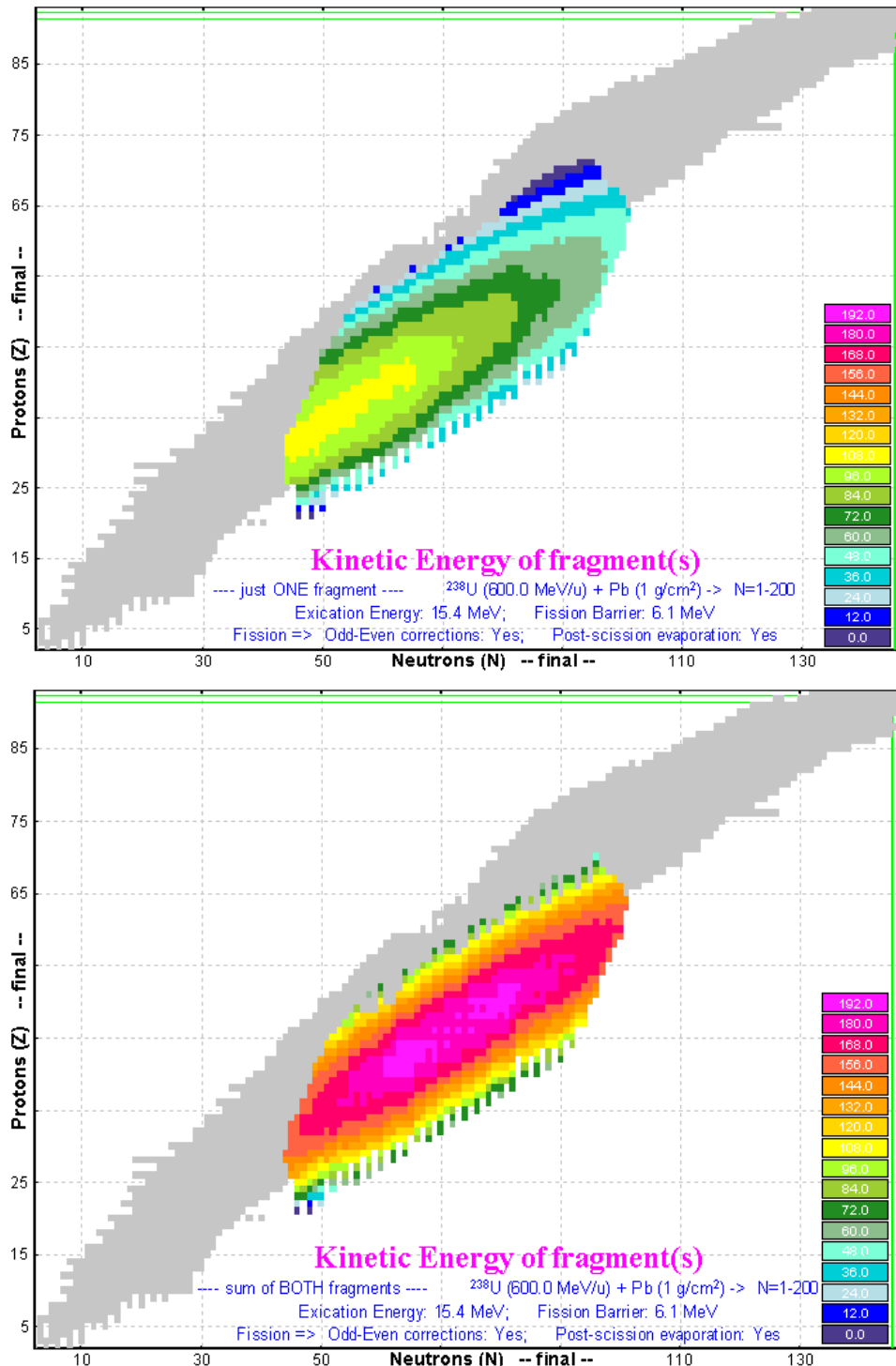
For the plots in mode "Sum of both fragments" it is necessary to find a conjugate final fragment. The code is looking for an expected conjugate final fragment making the next steps with use of 4 FCSM matrices ( $dA_{out}$ ,  $dA_{in}$ ,  $dN_{out}$ ,  $dN_{in}$ )<sup>♦</sup>:

	Initial	FCSM matrices		Result (more probable)
1	$A_3^f$	$dA_{in}(A_3^f)$ & $dN_{in}(A_3^f)$	⇒	$A_3^*$
2	$A_3^*$	Fissile nucleus	⇒	$A_4^*$
3	$A_4^*$	$dA_{out}(A_4^*)$ & $dN_{out}(A_4^*)$	⇒	$A_4^f$

<sup>♦</sup> See chapter 2.3.3.1.

### 2.4.3. Kinetic energy plots

Two-dimensional calculated kinetic energy plots for different excitation energies are shown in Fig.318 ( $E^* = 15.4$  MeV) and Fig.319 ( $E^* = 80$  MeV). Calculations of kinetic energies for Fig.319 were done with and without taking into account post-scission nucleon emission. To avoid the contribution of fragments with low-probability production it is possible to set the threshold for TKE plots in the dialog “Fission cross section suppression values” dialog (see Fig.307).

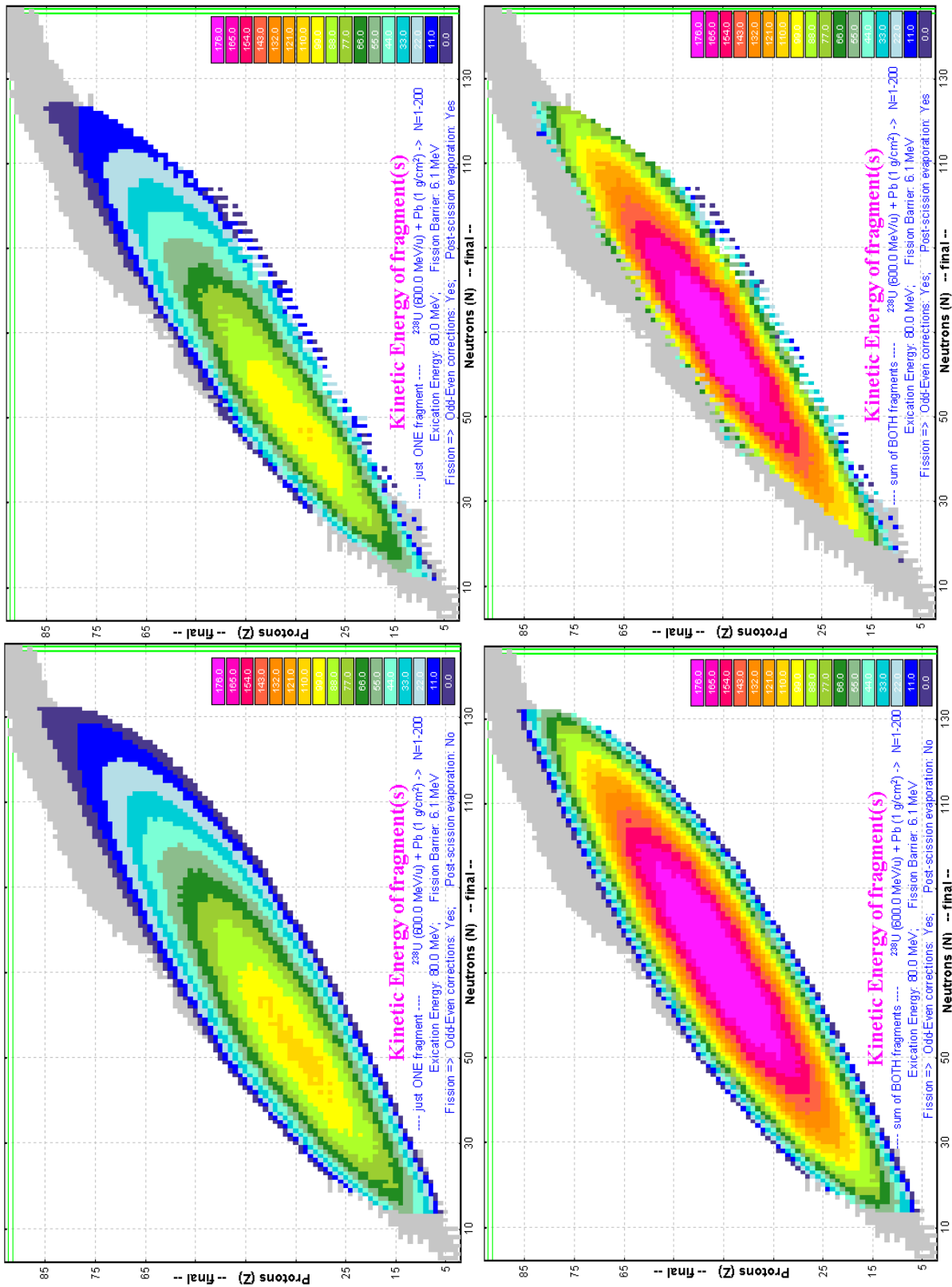


**Fig.318.** Calculated kinetic energies of one final fragment (top plot) and both final fragments (bottom plot) for the fissile nucleus  $^{238}\text{U}$  with excitation energy equal to 15.4 MeV that corresponds to the average energy of the EM fission deexcitation function for the reaction  $^{238}\text{U}(600\text{MeV/u}) + \text{Pb}(1\text{g/cm}^2)$ .

LISE++ default shell settings for fission were applied and post-scission nucleon evaporation has been taken into account. Z-scales for both plots are the same ( $0 \div 192$  with the linear step equal to 12 between colors).

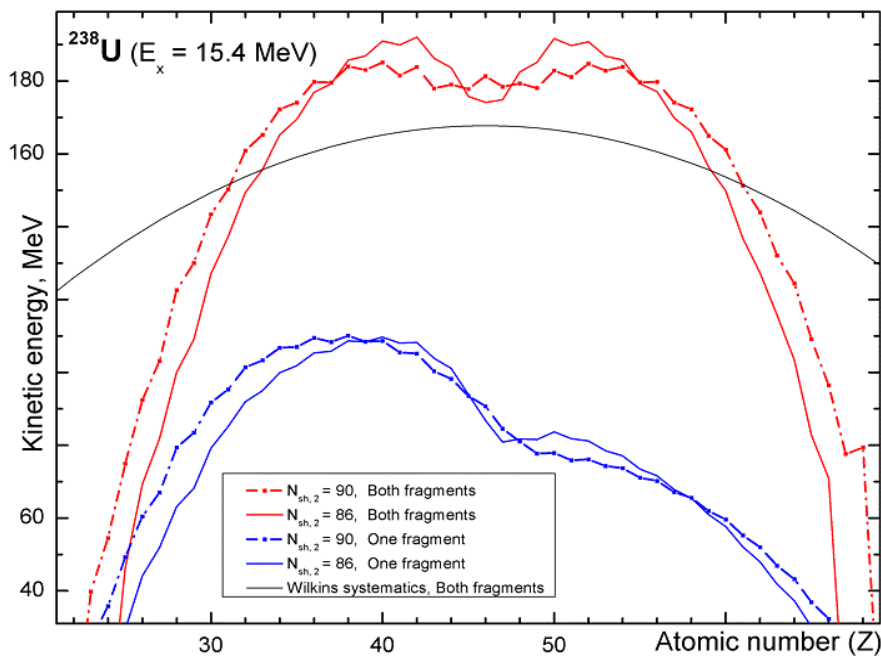
Suppression values used for these calculations:  
 “Keep in memory”  $1e-10$   
 “For TKE plot”  $1e-7$

TKE plot suppression value can be changed in the “Fission cross section suppression values” dialog (see Fig.307).



**Fig.319.** Calculated kinetic energies of one final fragment (top plots) and both final fragments (bottom) for the fissile nucleus  $^{238}\text{U}$  with excitation energy equal to 80 MeV. Calculations for left (right) plots were done without (with) taking into account post-scission nucleon emission.

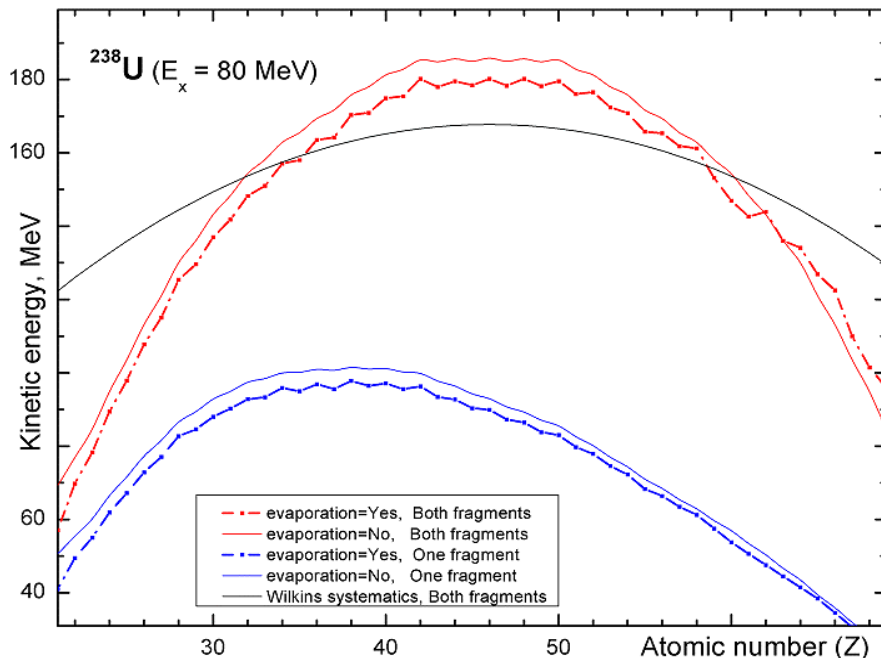
Calculated mean kinetic energies as a function of the fission-fragment neutron number in fission of the excited nucleus  $^{238}\text{U}$  are shown in Fig.320 ( $E^* = 15.4$  MeV) and Fig.321 ( $E^* = 80$  MeV). Fig.320 and Fig.321 have been created using 1D-dimensional plot types “sum(CS);Z=const”.



**Fig.320.** Calculated mean kinetic energies as a function of the fission-fragment neutron number in fission of the excited nucleus  $^{238}\text{U}$  with excitation energy equal to **15.4 MeV**. The red curves represent the sum of kinetic energies of both final fragments (TKE), the blue curves correspondingly kinetic energy of one final fragment. The dot-dashed curves were done for the position of second shell at  $N_2=90$  whereas the solid lines were done assuming  $N_2=86$ .

Wilkins's model [Wil76] is shown by black solid curve ( $\beta_1=\beta_2=0.625$ ;  $d=2\text{fm}$ ).

The "Dissipated energy" TXE method (#0) was used for calculations.



**Fig.321.** Calculated mean kinetic energies as a function of the fission-fragment neutron number in fission of the excited nucleus  $^{238}\text{U}$  with excitation energy equal to **80 MeV**. The red curves represent the sum of kinetic energies of both final fragments (TKE), the blue curves correspondingly kinetic energy of one final fragment. The dot-dashed (solid) curves were done with (without) taking into account post-scission nucleon emission.

Wilkins's model is shown by black solid curve ( $\beta_1=\beta_2=0.625$ ;  $d=2\text{fm}$ ).

The "Dissipated energy" TXE method (0) was used for calculations.

#### 2.4.4. Plot of evaporated nucleon yields

Calculated number of emitted nucleons ( $dA$ ), number of emitted neutrons ( $dN$ ), and charge change ( $dZ$ ) for / from **one / both final / excited** fragment(s) for the fissile nucleus  $^{238}\text{U}$  with the excitation energies equal to **15.4 and 80 MeV** are shown in Fig.322-324. LISE++ default shell settings for fission were applied for these calculations. CS suppression value was equal to  $1e-10$ .

In the case of the excitation energy equal to 15.4 MeV (Fig.322) the number of evaporated nucleons is equal to the number of evaporated neutrons or in other words the charge change is absent in this low-energy region.

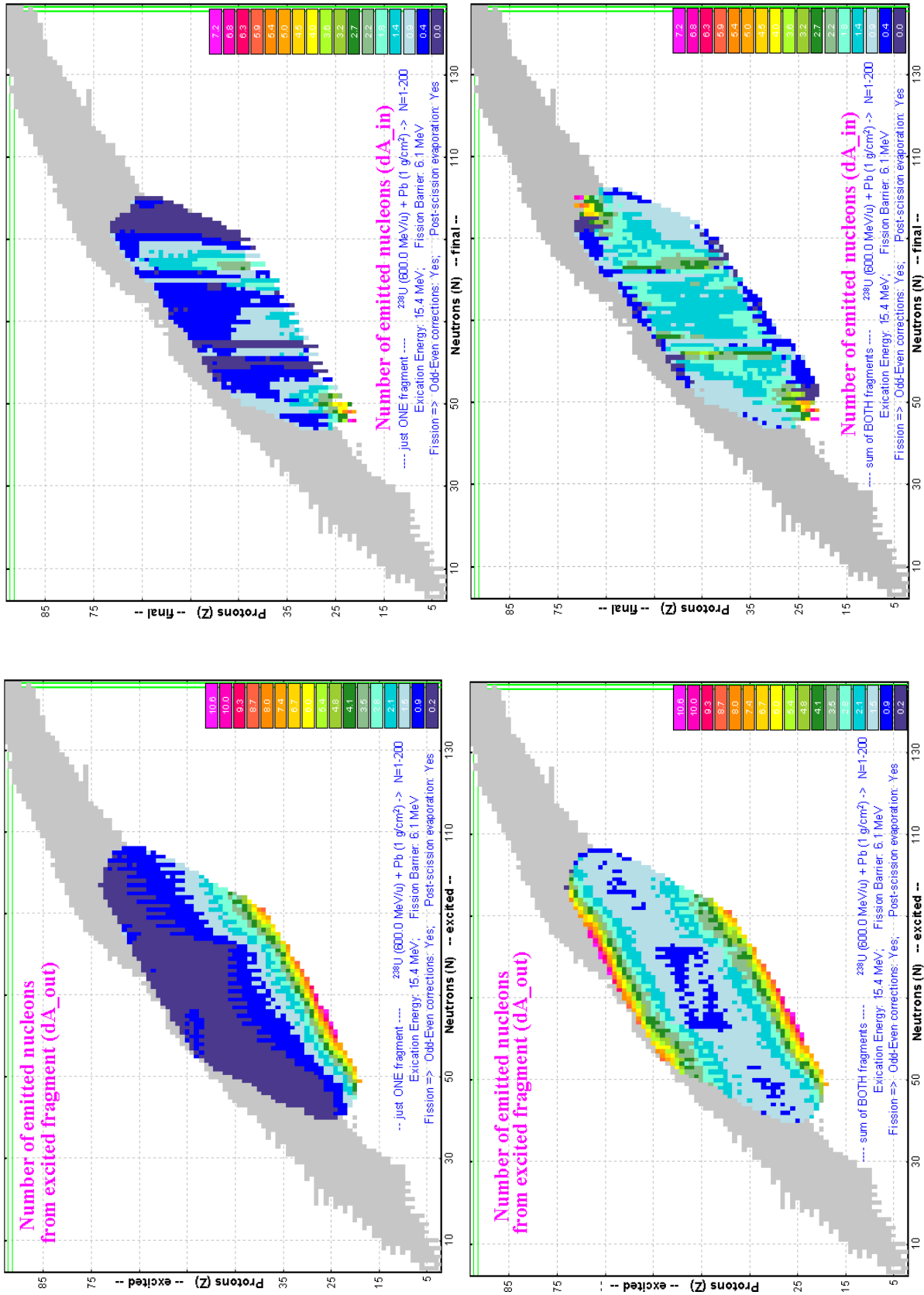


Fig.322. Calculated number of emitted neutrons *for / from one fragment* (top plots) and both *final fragments* (bottom plots) for the fissile nucleus  $^{238}\text{U}$  with the excitation energy equal to 15.4 MeV. Calculations for *left / right* plots were done for *excited / final* nuclei (*OUT / IN*-modes).



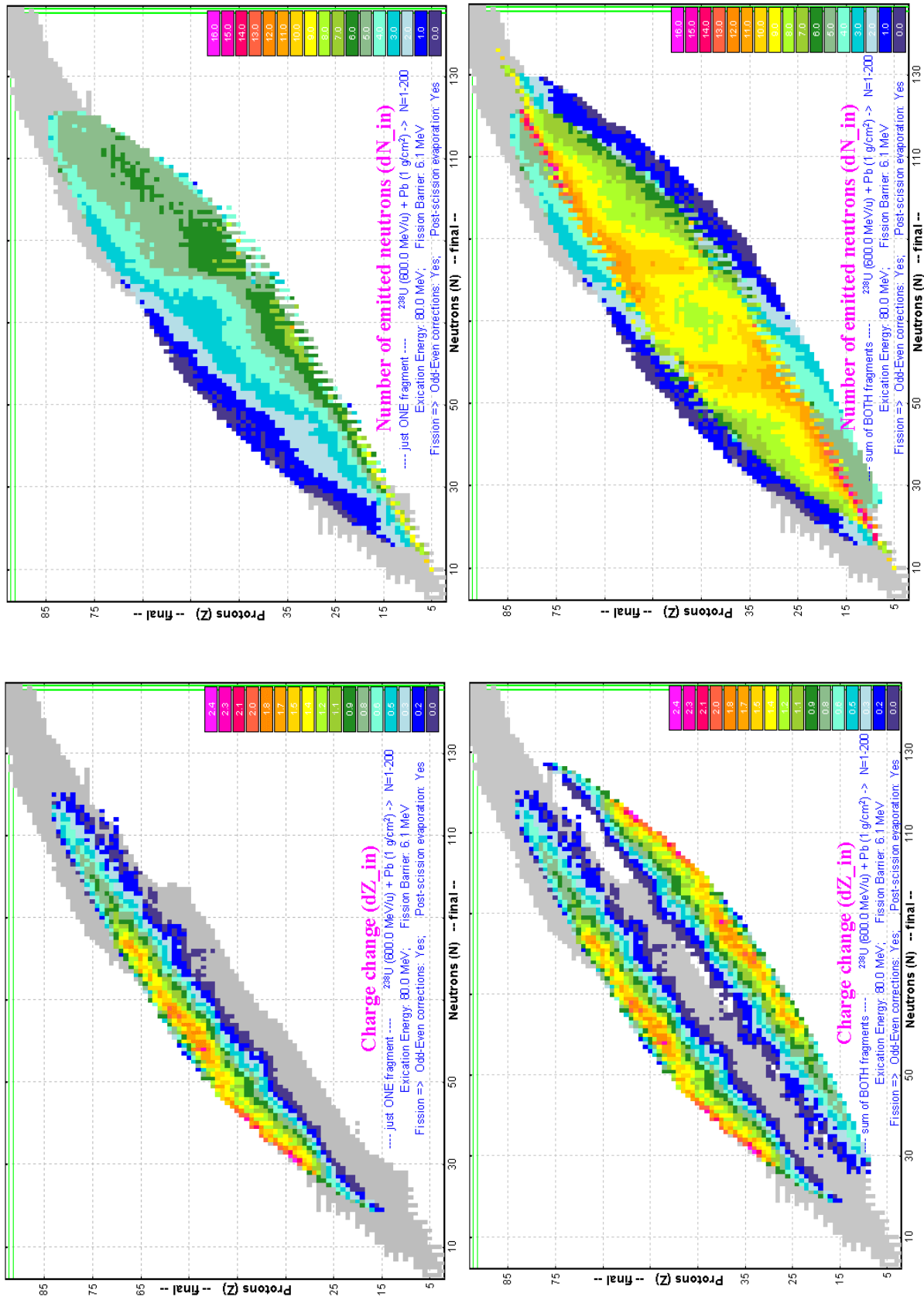


Fig. 323. Calculated number of emitted neutrons for one final fragment (right top plot) and both final fragments (right bottom plot) and charge change for one final fragment (left top plot) and both final fragments (left bottom plot) for the fissile nucleus  $^{238}\text{U}$  with the excitation energy equal to 80 MeV.

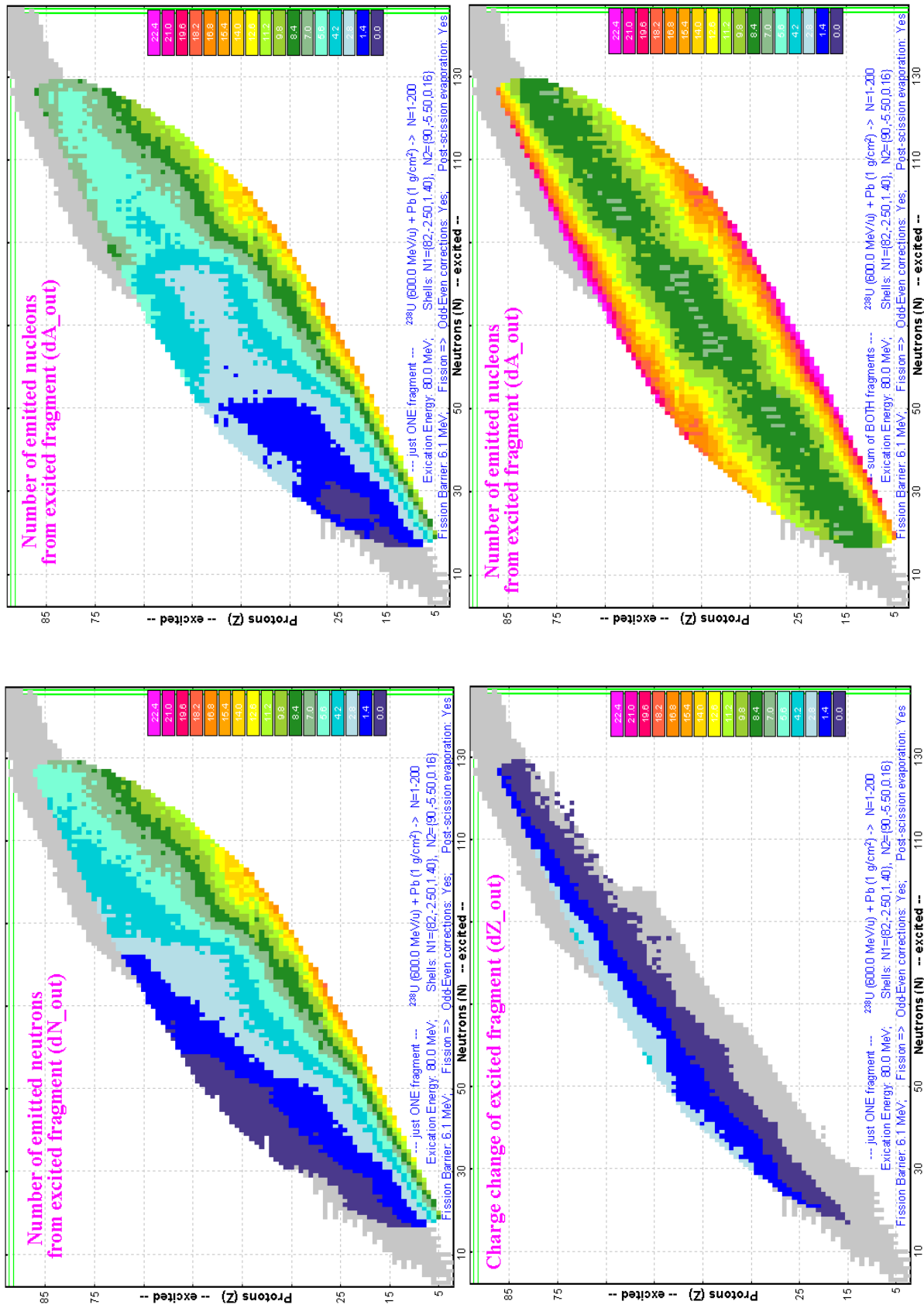
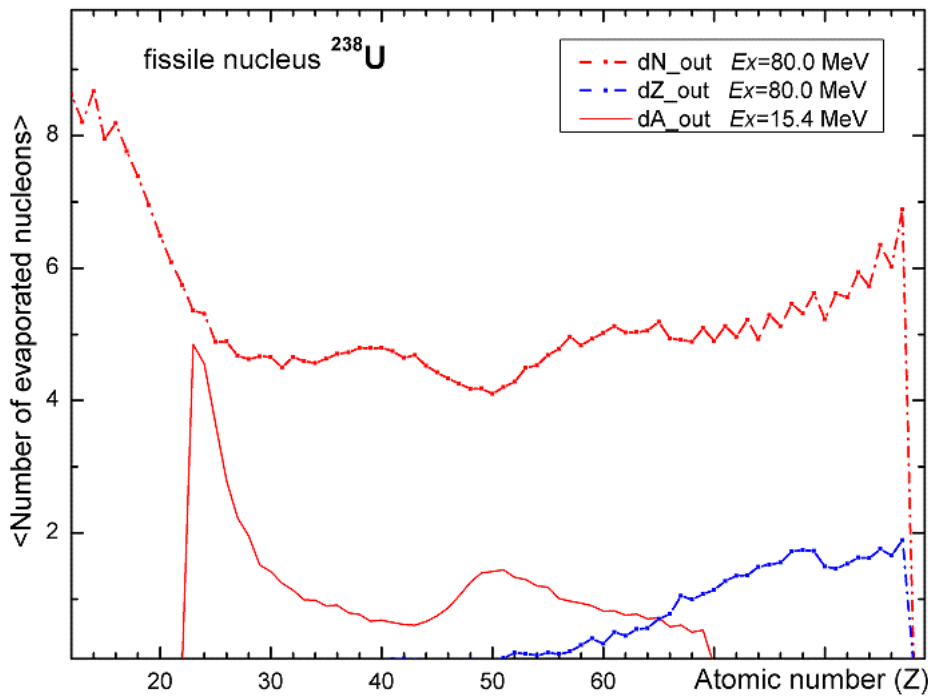


Fig.324. Calculated number of emitted neutrons from one excited fragment (left top plot), charge change of one excited fragment (left bottom plot), number of emitted protons from one excited fragment (right top plot) and both final fragments (right bottom plot) for the fissile nucleus  $^{238}\text{U}$  with the excitation energy equal to 80 MeV.

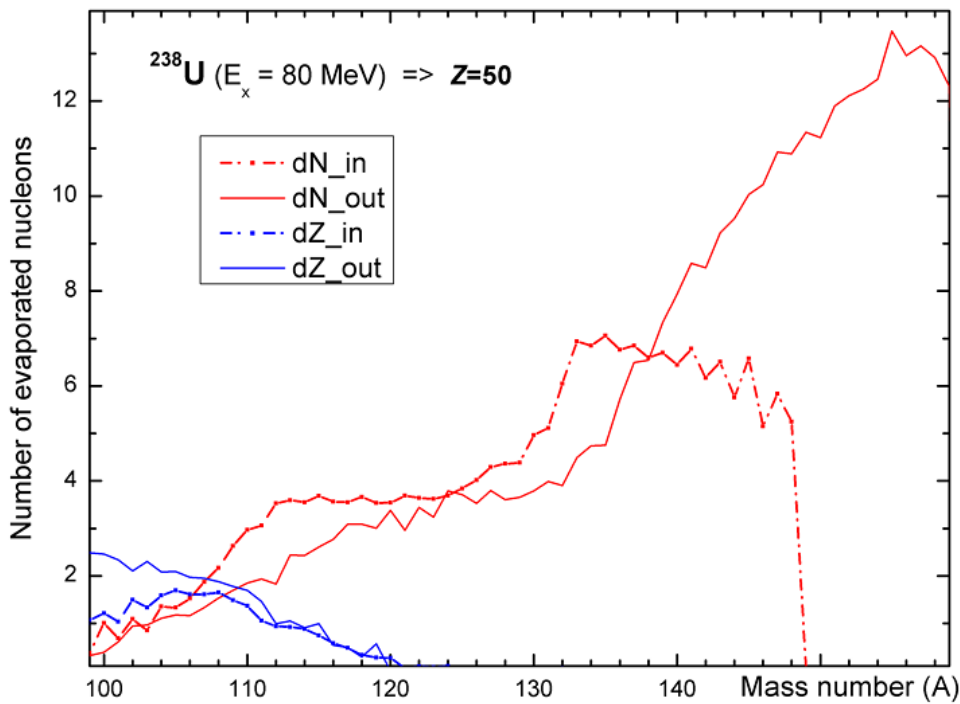


**Fig.325.**

Red solid curve: calculated mean number of evaporated nucleons as a function of the excited fission-fragment atomic number in fission of the excited nucleus  $^{238}\text{U}$  with excitation energy equal to 15.4 MeV.

Red dot-dashed curve: calculated mean number of evaporated neutrons as a function of the excited fission-fragment atomic number in fission of the excited nucleus  $^{238}\text{U}$  with excitation energy equal to 80 MeV.

Blue dot-dashed curve: calculated charge change as a function of the excited fission-fragment atomic number in fission of the excited nucleus  $^{238}\text{U}$  with excitation energy equal to 80 MeV.



**Fig.326.** Calculated number of evaporated neutrons for/from final/excited fission tin fragment and calculated charge change as a function of the fission-fragment mass number in fission of the excited nucleus  $^{238}\text{U}$  with excitation energy equal to 80 MeV.

The “Dissipated energy” TXE method (0) was used for calculations.

## 2.5. Spectrometer settings in the case of fission

### 2.5.1. Fission fragment momentum distribution and spectrometer settings

In the case of a thin target the energy distribution of the fission fragment has a rectangle shape. Without cutting by angular acceptance it is reasonable to assume the spectrometer is set to the center of the energy distribution of the fragment as was done previously in the case of fusion-evaporation and projectile fragmentation.

However, if the angular distribution of the fragments exceeds the size of angular acceptance, then the resulting energy distribution can have a two peaked shape. In this case tuning of the spectrometer on the centre of energy distribution can give the minimal fragment output. Therefore it is necessary to consider additional possibilities of spectrometer tuning. The two new settings mode (“left peak” and “right peak”) have been developed for the case of fission reactions (see Fig.327). The default method to tune the spectrometer in the fission case is “right peak” (as on more intense peak).

Understanding how the program searches for these peaks is very important, so that user can confidently choose the tuning mode for a concrete case:

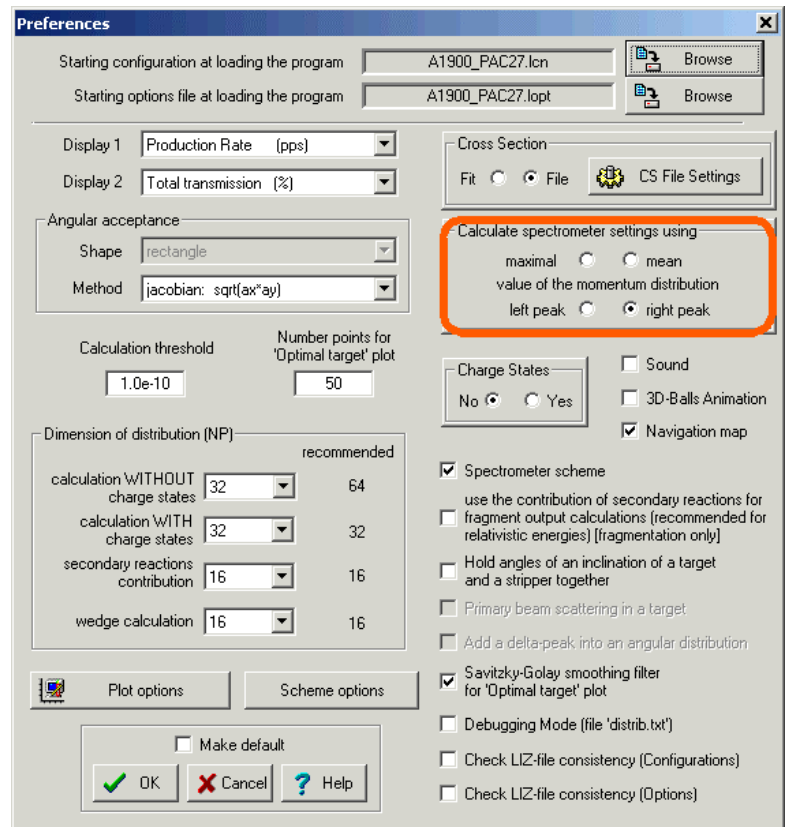
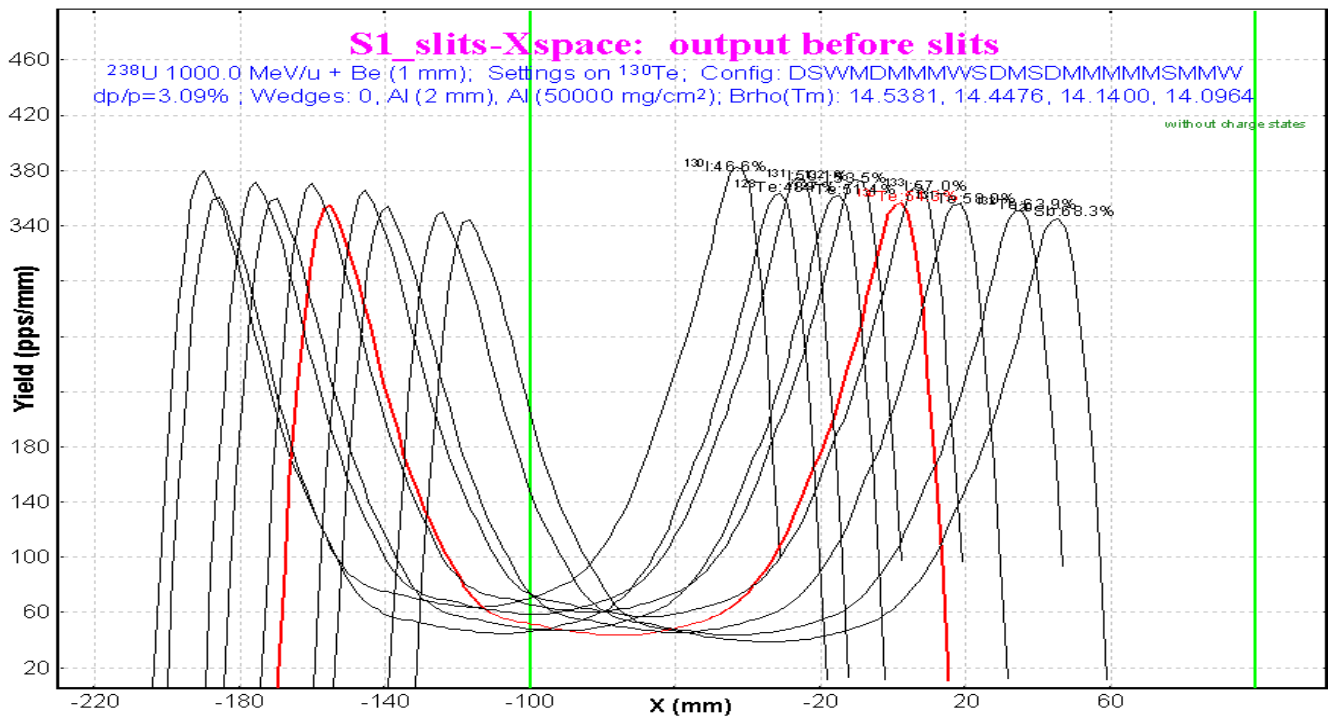


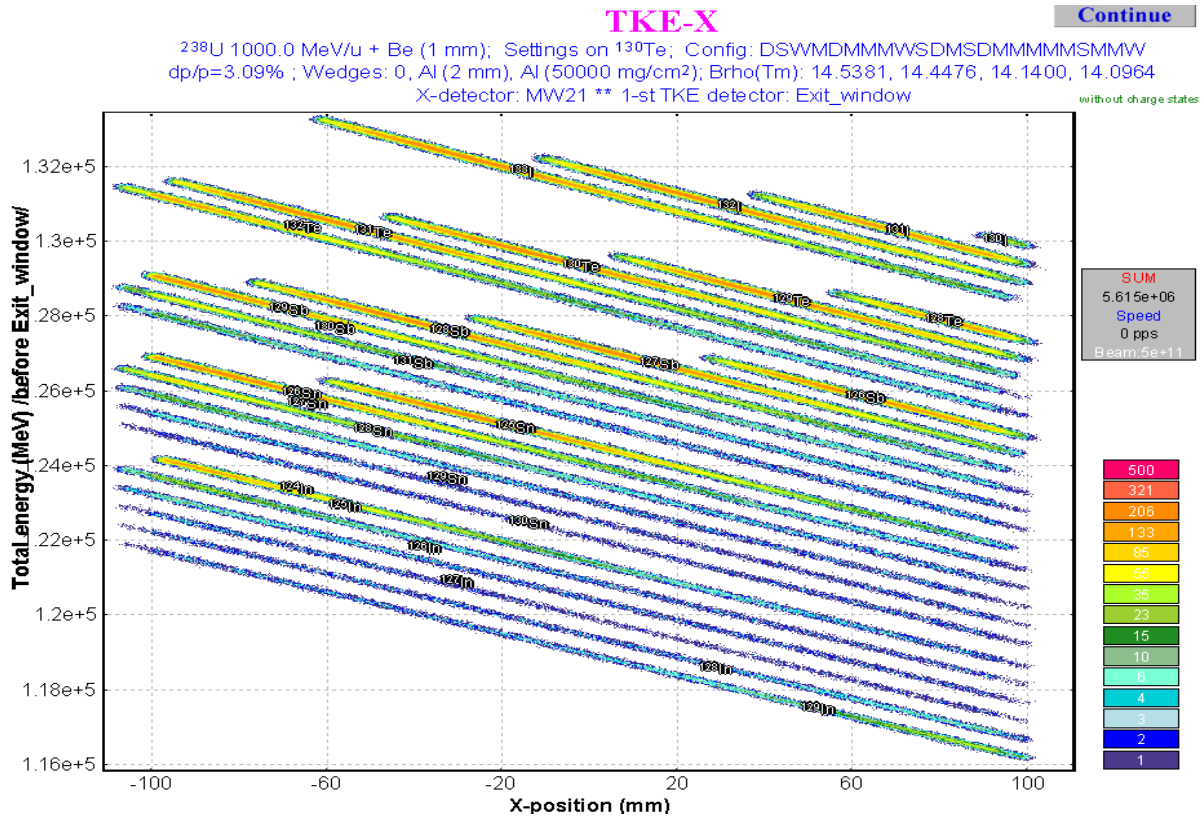
Fig.327. The “Preferences” dialog.

1. Ax&Ay matrices and distributions of “MatrixKinematics” class are calculated after the stripper.
2. The code is looking for minimal values of production  $w=Acc \cdot (\theta/\theta)^{-1}$  in horizontal and vertical directions, where  $Acc$  is the angular acceptance of the optic block in given direction,  $(\theta/\theta)$  is angular magnification coefficient from the “global” matrix of the previous optic block (or it is equal to 1 if there are not optical blocks before).
3. The special “gate” distribution is the convolution of energy “acquired” distribution after stripper and rectangle distribution with the width equal to  $w$ ;
4. The next steps are identical to “filter” method steps 2-6 to get  $I(E)$  of DF distribution (see chapter 2.2.3.2. ).
5. The code searches position of the right and left peaks of  $I(E)$  of DF distribution.

The “CoulombFissionExample.lpp” demonstration file for “CoulombFission” reaction mechanism has been created and is located in the directory “\Files\Examples”. The following discussion and examples are based on this file. Fig.328 shows the horizontal spatial selection of fission fragments by slits the S1, and the two-dimensional identification plot of fission fragments is presented in Fig.329.



**Fig.328.** Horizontal spatial selection of fission fragments by the slits S1. The spectrometer is set to the right peak of  $^{130}\text{Te}$  momentum distribution.

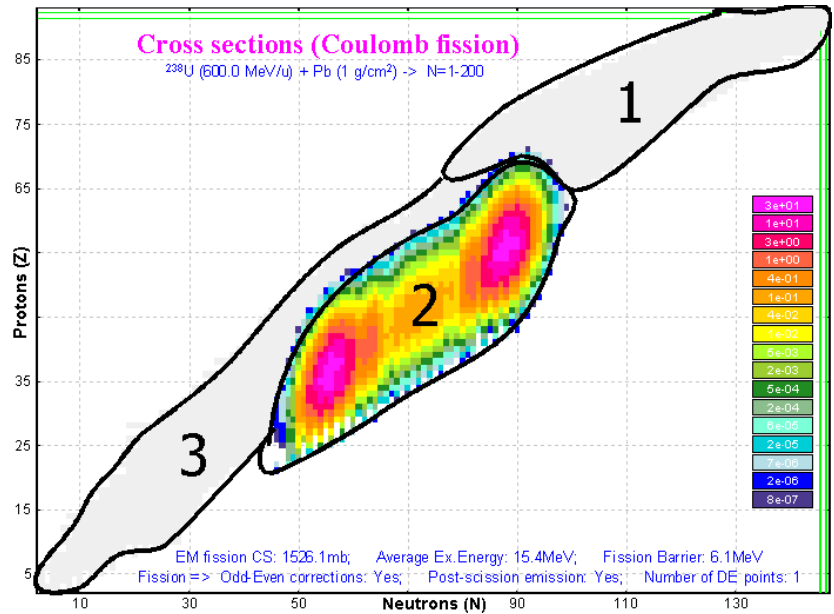


**Fig.329.** Two-dimensional identification plot "X&TKE". Spectrometer configuration and detector used for identification are shown on the picture.

### 2.5.2. Secondary reactions in the target

A subroutine of secondary reactions in target calculations has been adapted for Coulomb fission reactions. There are some relevant differences in case of secondary reactions for the “fragmentation” and “fission” reaction modes. Some of them we would like to point out:

1. For fragmentation, the cross-section of any isotope with neutron or atomic numbers less (or equal to) than correspondent numbers of the projectile is not equal to zero. Whereas in the Coulomb fission case cross-sections are equal to zero in regions 1 & 3 shown in Fig.330.
2. For fragmentation a “secondary” parent nucleus given a maximum contribution in the final fragment is located in 2-3 nucleons up on the line “projectile-final fragment”, whereas if for a final fragment in the region #3 for the fission case a maximum secondary parent nucleus is located in the region #2 in Fig.330.



**Fig.330.** Calculated production cross-sections for the reaction  $^{238}\text{U}(600\text{MeV/u}) + \text{Pb}(1\text{g/cm}^2)$ .

Reactions to get maximum rate for the  $^{238}\text{U}(600\text{MeV/u})$  projectile on a lead target are given in Table 42.

**Table 42.** Reactions to get maximum rate for the  $^{238}\text{U}(600\text{MeV/u})$  projectile on a lead target (without taking into account the abrasion-fission reaction). Regions are denoted in Fig.330.

Region	For thin target	For thick target
#1	fragmentation	1 <sup>st</sup> step: fragmentation, 2 <sup>nd</sup> step: fragmentation
#2	EM fission	EM fission
#3	fragmentation	1 <sup>st</sup> step: EM fission, 2 <sup>nd</sup> step: fragmentation

In order to apply the secondary reactions contribution, the code uses a coefficient to the primary production cross-section. However, as was already mentioned the initial cross sections in region #3 are equal to 0 in the Coulomb fission case. This disadvantage should be overcome in the next version. As a temporary solution it is possible to set very low suppression value for fission cross-sections that increases calculation time. As well as secondary reactions, the calculation procedure should be optimized for speed. This it is very important in the case of a projectile as heavy as Uranium.

### 2.5.3. Optimal thickness target calculations

The fission-fragment production cross section depends upon the projectile energy. If a target thickness has changed by at least 10 percent then the cross-sections will be recalculated. The user can switch off the option of cross-section recalculation in the case of the optimum target thickness calculation. It is assumed in this case that the reaction takes place in the beginning of the target.

Dependences of  $^{78}\text{Ni}$  fragment rate from the Pb-target thickness in EM fission of  $^{233}\text{U}$  (400MeV/u) are shown in Fig.332. In the case of energy dependent calculations the maximum of  $^{78}\text{Ni}$  fragment distribution with energy dependent cross-sections calculations is given on the left and its amplitude is less than for constant cross-section calculations. The plot of a cross-section versus a target thickness is created (see Fig.333) if the “Cross section energy dependent” option is selected in the “Choose fragment” dialog (see Fig.331).

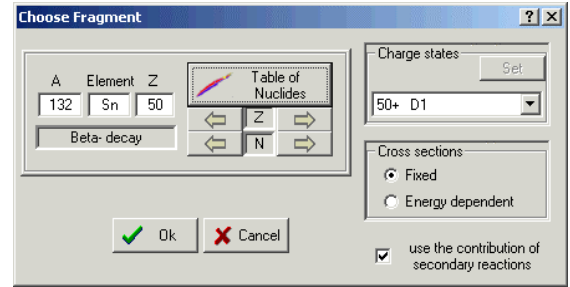


Fig.331. The “Choose fragment” dialog for optimum target thickness calculations.

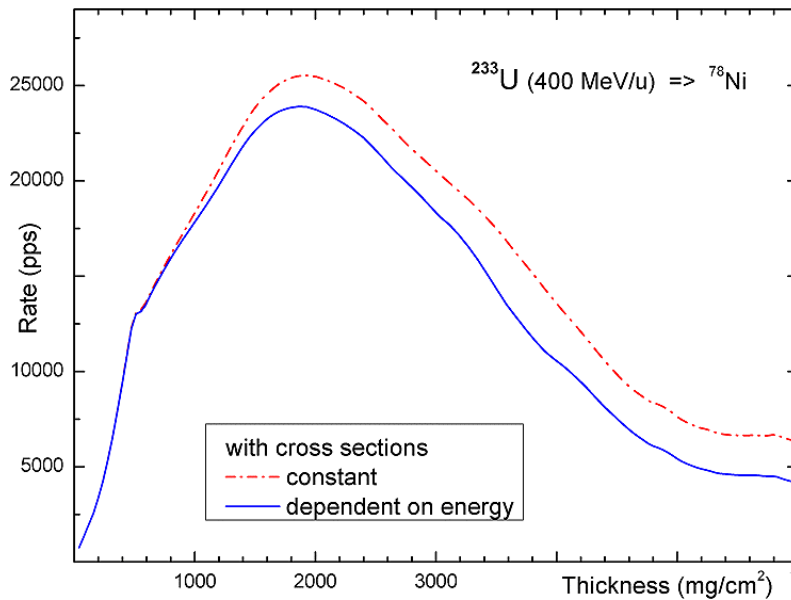


Fig.332.  $^{78}\text{Ni}$  fission-fragment rates in the final focal plane of a fragment-separator from EM fission of  $^{233}\text{U}$  (400MeV/u) versus a target thickness. The red dot-dashed (blue solid) line has been calculated assuming fission-fragment production cross-section being constant (dependent) from the projectile beam.

200 thickness values for the optimal target thickness calculations were used. The dimension of transmission distributions was set to 64. Savitzky-Golay smoothing filter was applied for both curves.

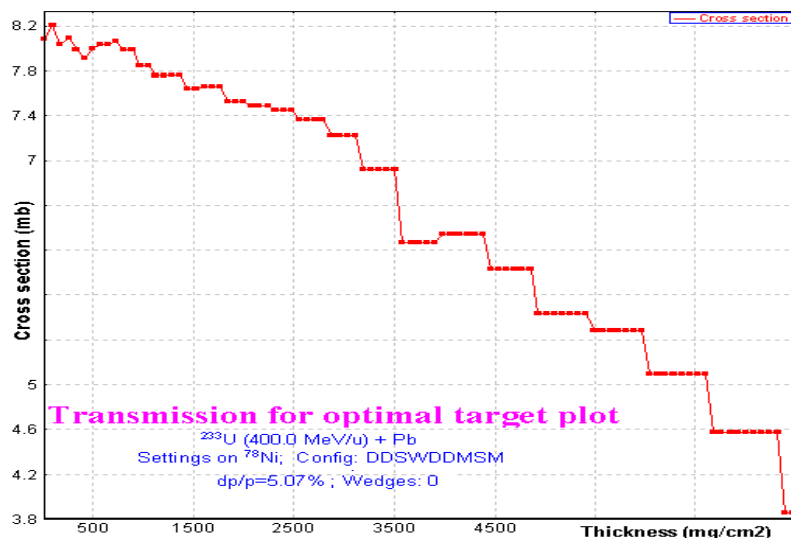
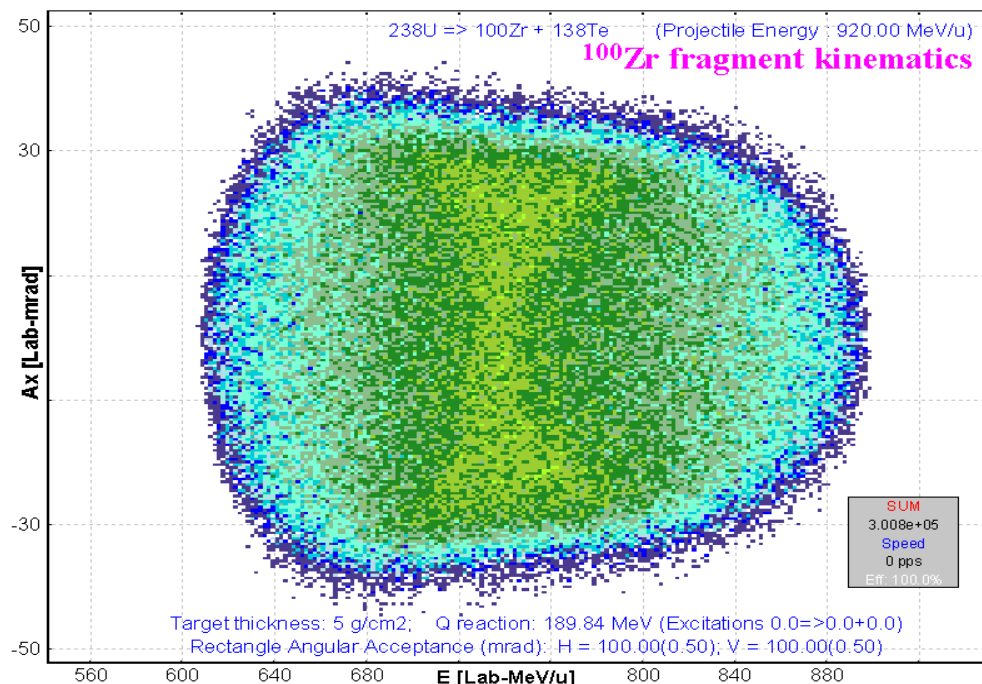


Fig.333.  $^{78}\text{Ni}$  fragment-fission production cross-section in EM fission of  $^{233}\text{U}$  (400MeV/u) in the middle of the target versus a target thickness. The “teeth” structure of the curve is explained by the fact that cross-sections are recalculated after 10% change of the target thickness.

## 2.6. Comparisons of LISE calculations with experimental data and the MOCADI code

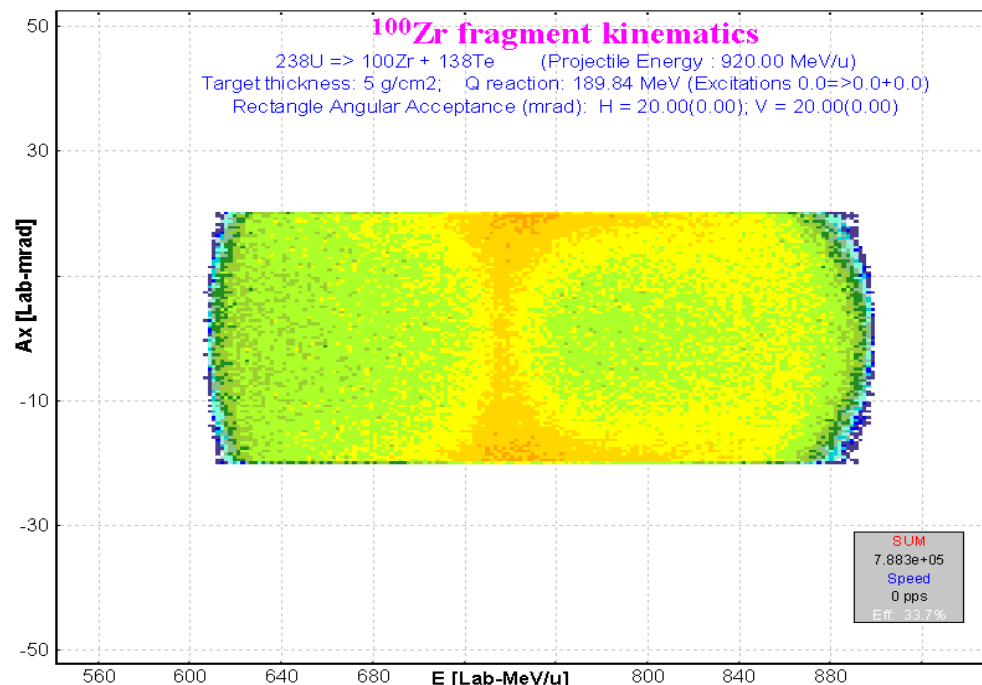
### 2.6.1. Kinematics calculation in the case of thick targets

Calculation comparisons of *DistrMethod* and *MCmethod* methods of the LISE++ program and the MOCADI [Wei04] program were made depending on energy of a primary beam and target thickness. The MOCADI calculations were done by Dr.H.Weick (GSI). In this chapter the comparison will be presented for the case of a thick Pb target ( $5\text{g/cm}^2$ ) and primary beam  $^{238}\text{U}$  with energy  $920\text{ MeV/u}$  for the final fragment  $^{100}\text{Zr}$ . Two-dimension plots created by the LISE++ code (*MCmethod*) are shown in Fig.334 for 100% angular transmission, and for angular acceptances  $H=\pm 20$  &  $V=\pm 20\text{ mrad}$  in Fig.335.



**Fig.334.** LISE++ *MCmethod* calculations. 2D-plot “Energy- $\theta_x$ ” of the fission-fragment  $^{100}\text{Zr}$  in the reaction  $^{238}\text{U}(920\text{MeV/u})+\text{Pb}(5\text{g/cm}^2)$

Angular transmission of the fragment is 100%.

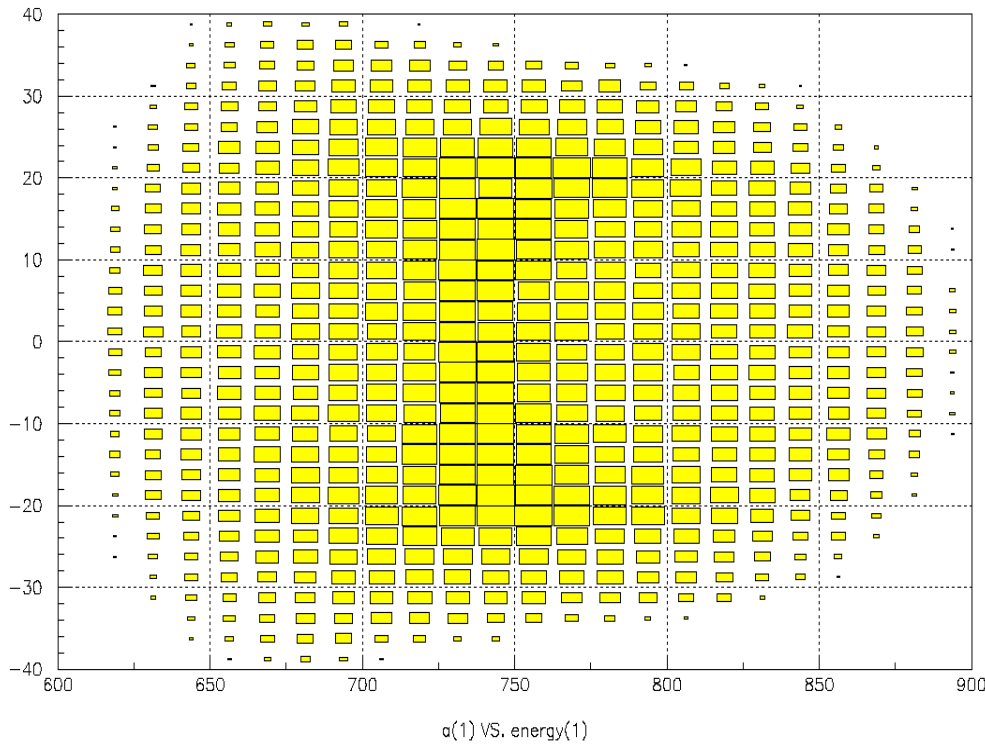


**Fig.335.** LISE++ *MCmethod* calculations. 2D-plot “Energy- $\theta_x$ ” of the fission-fragment  $^{100}\text{Zr}$  in the reaction  $^{238}\text{U}(920\text{MeV/u})+\text{Pb}(5\text{g/cm}^2)$

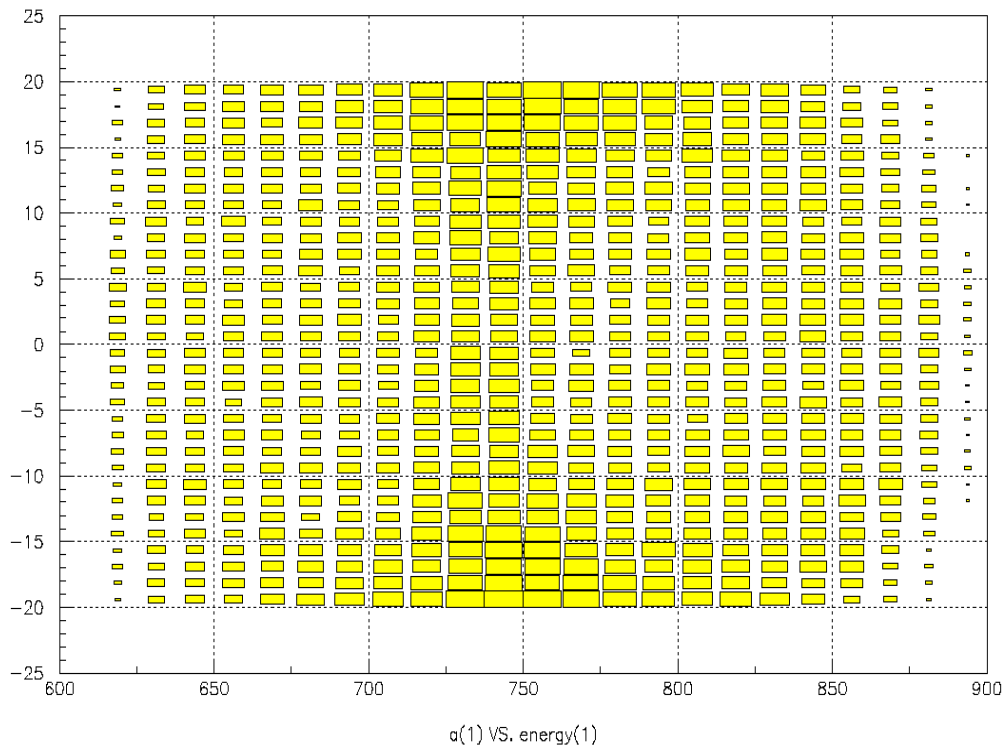
Angular acceptances:  
 $H = \pm 20$  &  $V = \pm 20\text{ mrad}$ .  
 Angular transmission of the fragment is 33.6%.



MOCADI's calculations corresponded to the same conditions as were done for Fig.334 and Fig.335 are shown accordingly in Fig.336 and Fig.337.

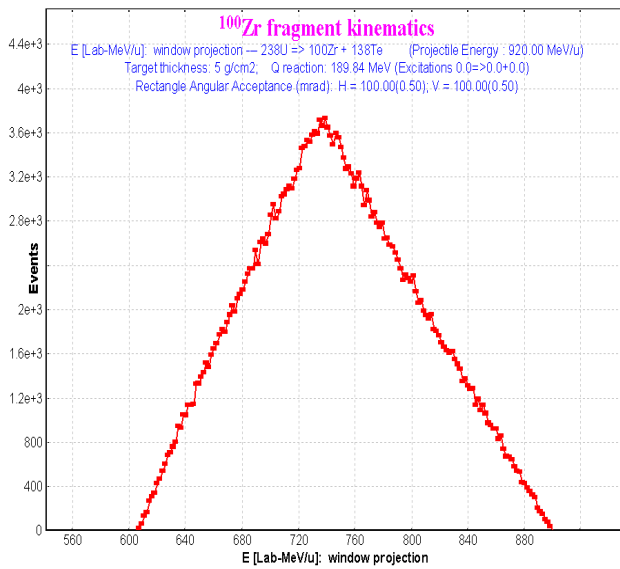


**Fig.336.** MOCADI calculations. The same conditions as in Fig.334.

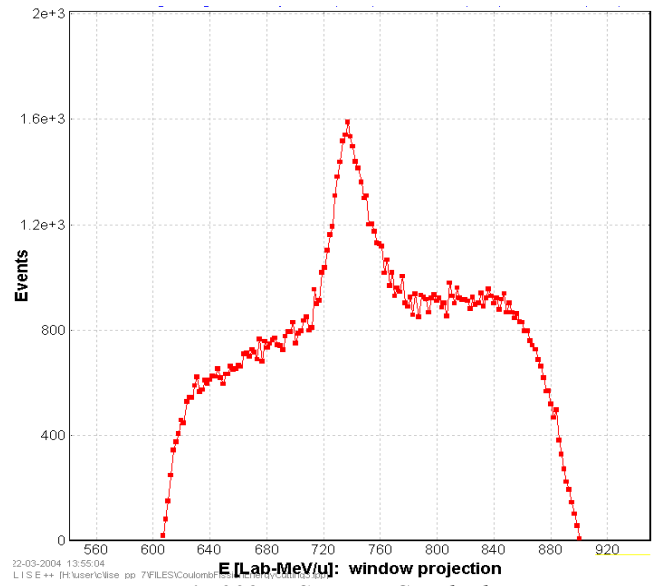


**Fig.337.** MOCADI calculations. The same conditions as in Fig.335.

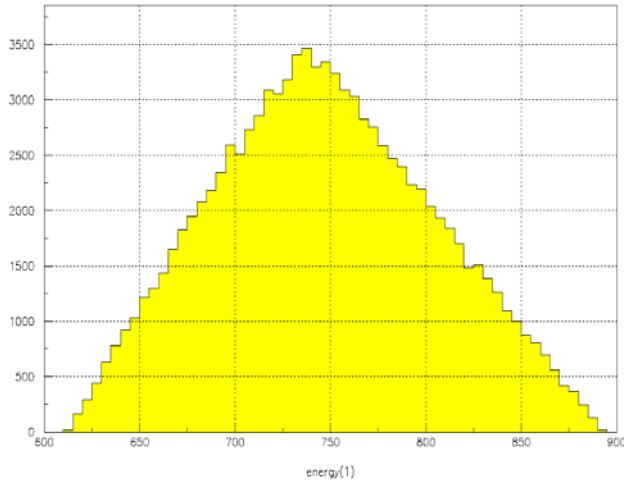
Horizontal projections of Fig.334-337 are shown correspondingly in Fig.338-341. Calculated energy distributions by LISE++ *DistrMethod* are shown in Fig.342 (without angular acceptance) and Fig.343 (for angular acceptances  $H=\pm 20$  &  $V=\pm 20$  mrad). Transmission coefficients in the case of limited angular acceptances are almost the same for all three methods (about 34%).



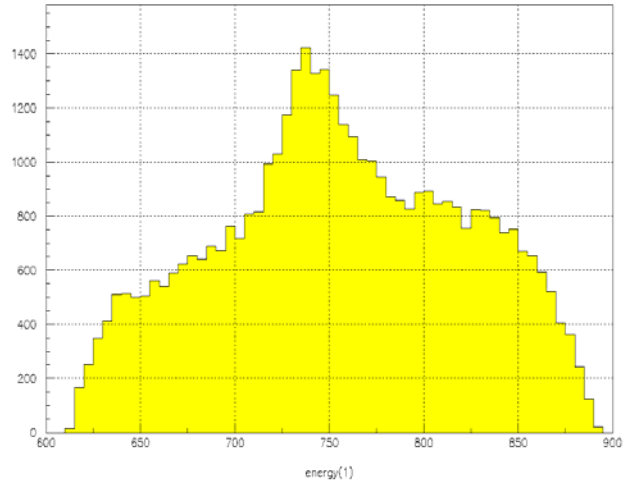
**Fig.338. LISE++ MCmethod.**  
Projection of Fig.334 on the horizontal axis.



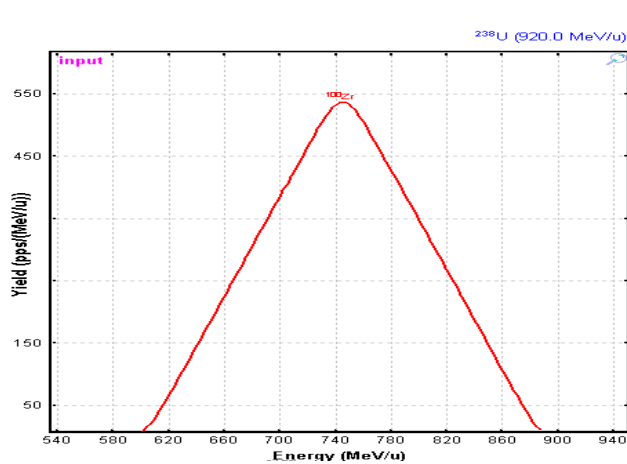
**Fig.339. LISE++ MCmethod.**  
Projection of Fig.335 on the horizontal axis.



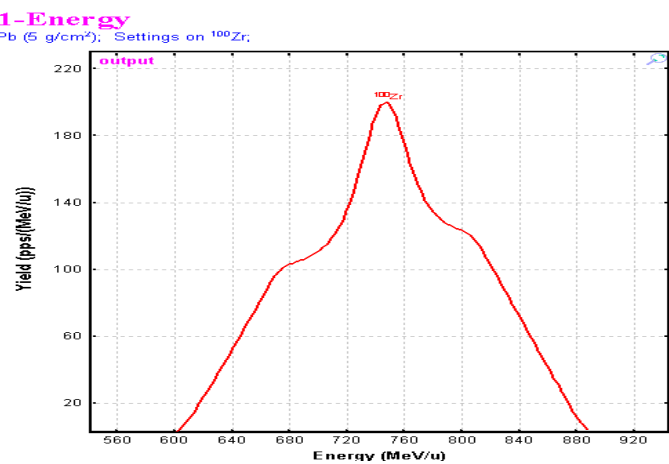
**Fig.340. MOCADI.** Projection of Fig.336 on the horizontal axis.



**Fig.341. MOCADI.** Projection of Fig.337 on the horizontal axis.



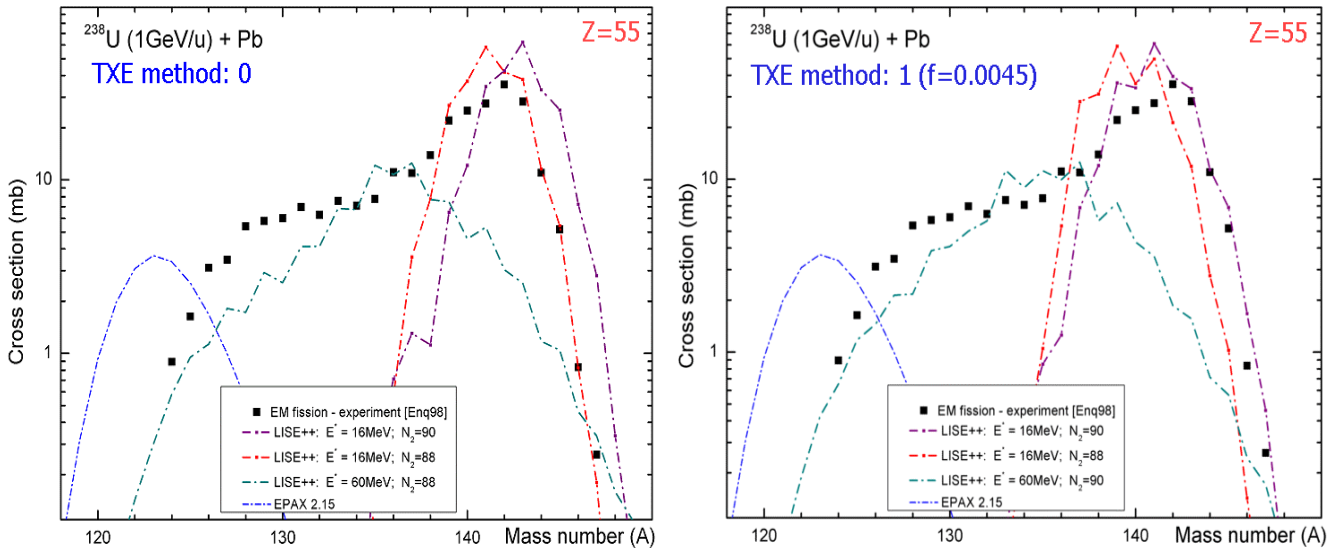
**Fig.342.** Calculated energy distribution by LISE++ DistrMethod of  $^{100}\text{Zr}$  in the EM fission reaction  $^{238}\text{U}(920\text{MeV/u}) + \text{Pb}(5\text{g/cm}^2)$  Angular transmission of the fragment is 100%.



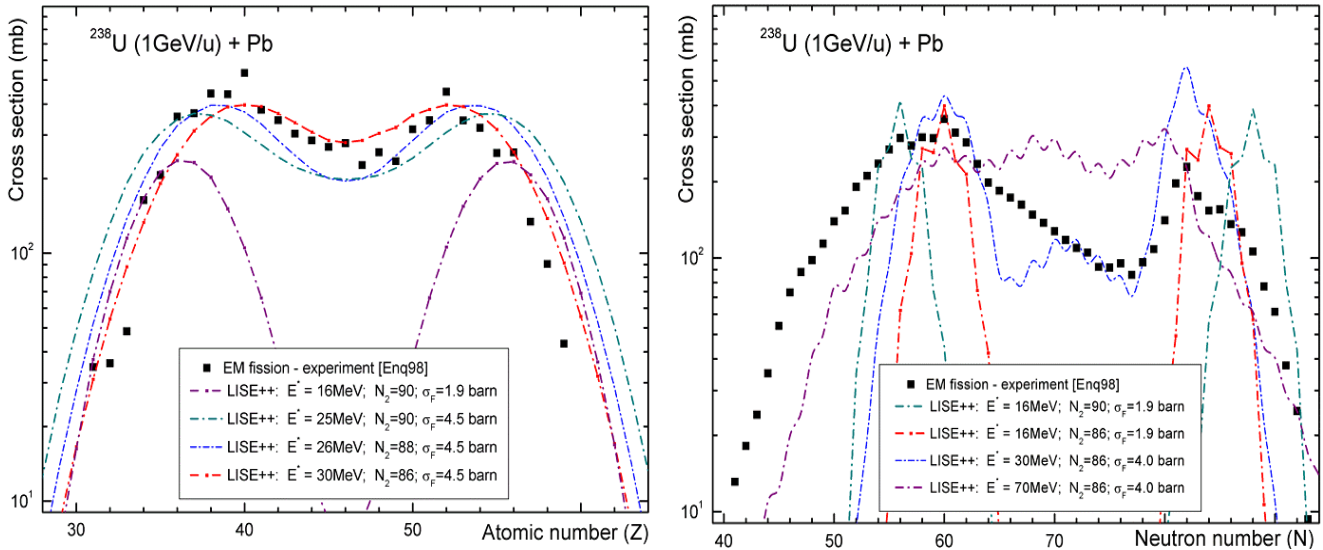
**Fig.343.** Calculated energy distribution by LISE++ DistrMethod of  $^{100}\text{Zr}$  in the EM fission reaction  $^{238}\text{U}(920\text{MeV/u}) + \text{Pb}(5\text{g/cm}^2)$ . Angular acceptances:  $H=\pm 20$  &  $V=\pm 20$  mrad. Angular transmission of the fragment is

### 2.6.2. Fission-fragment production cross-sections

Experimental production cross-section of cesium isotopes (black squares) with a uranium beam (1GeV/u) on a lead target [Enq99] and calculations done by the LISE++ code using different TXE methods are shown in Fig.344. Experimental cross-sections are available in the cross-section file “238U\_Pb\_1AgeV\_fission.cs” in the “\CrossSections\PublishedData” directory. Integrated experimental and calculated fission-fragment production cross-sections for the same reaction are shown in Fig.345.



**Fig.344.** Experimental production cross-section of cesium isotopes (black squares) with a uranium beam (1GeV/u) in a lead target [Enq99]. Cross sections calculated with the TXE method set to 0 (“Dissipated energy”) are shown in left plot, and with the TXE method to set 1 (“Qvalue”) correspondingly on right plot. See details on plots. Fragmentation parameterization EPAX2.15 is shown on both plots by blue dotted-dash line.



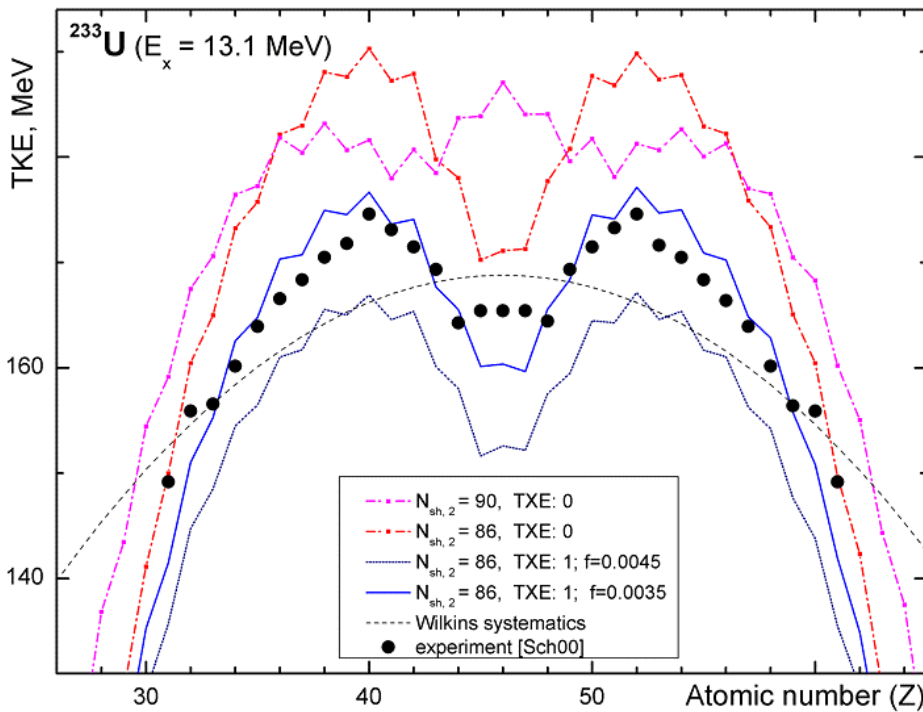
**Fig.345.** Experimental (black solid squares) integrated nuclear-charge (left plot) and neutron number (right plot) cross-sections for EM fission of  $^{238}\text{U}(1\text{GeV/u})$  in a lead target [Enq99]. See details for calculation curves in plots. The “Dissipated energy” TXE method (0) was used for calculations.

It is possible to make the following conclusions from the comparison of calculations and experimental data in Fig.344 and Fig.345:

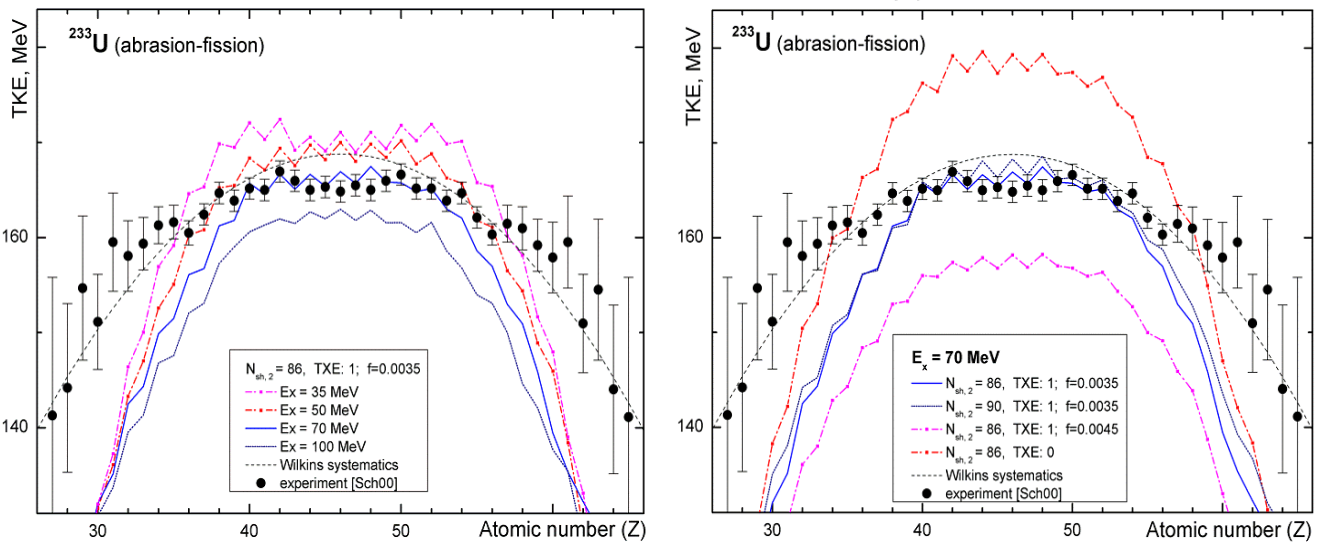
1. LISE uses only the average excitation energy of the EM fission excitation function ( $\langle E_x \rangle = 16$  MeV for Fig.344) for cross section calculations. In this context the experimental cross sections are well described by the calculations only at small excitation energies (neutron-rich isotopes). In the next version, cross-sections will be calculated from several excitation energy points of the EM fission excitation function (for example see right plot in Fig.302).
2. *Left plot in Fig.345:* it is necessary to incorporate in the code the new  $\delta Z$ -development of GSI’s group to reproduce more accurately nuclear charge odd-even effects.
3. Experimental cross-section of cesium isotopes (Fig.344) can be reproduced just partially by calculations with different excitation energies but with the constant total fission cross-sections. In order to reproduce experimental integrated cross-sections (Fig.345) the total EM fission cross-section was increased, that points out a significant “abrasion-fission” contribution in fission-fragment production cross-sections.

### 2.6.3. TKE comparisons

The total kinetic energy fission fragment spectra as a function of the nuclear charge corresponding to fission of  $^{233}\text{U}$  at 420 MeV/u [Sch00] are shown in Fig.346 (lead target) and Fig.347 (plastic target). Calculations for the excitation energy equal to 13.1 MeV (corresponds to the average energy of the EM fission excitation function in the reaction  $^{233}\text{U}(420 \text{ MeV/u})+\text{Pb}$ ) are shown in Fig.346. TKE calculations using the TXE method #1 (“Qvalue”) with the  $f$ -parameter equal to 0.0035 depending on the excitation energy of the  $^{233}\text{U}$  fissile nucleus are shown in the left plot of Fig.347, and TKE calculations with excitation energy equal to 70 MeV for different models are shown in right plot of Fig.347.



**Fig.346.** The total kinetic energy as a function of the nuclear charge of the fission fragments. Experimental (black circles) values of every element correspond to fission of  $^{233}\text{U}$  having passed the lead target at 420 MeV/u [Sch00]. Calculations were done the excitation energy equal to 13.1 MeV what corresponds to the average energy of the EM fission excitation function in the reaction  $^{233}\text{U}(420\text{ MeV/u}) + \text{Pb}$ . See details for calculated curves in plots.



**Fig.347.** The total kinetic energy as a function of the nuclear charge of the fission fragments. The experimental spectrum (black circles) corresponds to fission of  $^{233}\text{U}$  induced by nuclear interactions with a plastic target [Sch00]. TKE calculations using the TXE method #1 (“Qvalue”) with the  $f$ -parameter equal to 0.0035 depending on excitation energy are shown in left plot. TKE calculations with excitation energy equal to 70 MeV depending on different models are shown in right plot. See details for calculation curves in plots.


It is possible to make the following conclusions from comparisons between calculations and experimental data in Fig.346 and Fig.347:

1. Calculation with the shell position  $N_{\text{shell},2}$  equal to 86 better describes experimental data than 88 and 90 the case of low excitation energies of  $^{233}\text{U}$  fissile nucleus (see Fig.346).
2. The best agreement with data is observed for calculations done with the TXE model set to 1 (“Qvalue”) with the  $f$ -parameter equal to 0.0035 and assuming  $N_{\text{shell},2}$  equal to 86 (see Fig.346).

3. A difference between experimental data and the calculated curve (TXE method #1 with  $f=0.0035$ ) for elements  $Z=45-47$  in Fig.346 can be explained by the “abrasion-fission” contribution.
4. An influence of the  $N_{\text{shell},2}$  shell location is washed out at high excitation energies (right plot in Fig.347).
5. A good agreement with experimental data is achieved for calculations with the TXE model #1 for the  $f$ -parameter equal to 0.0035 at an excitation energy equal to 70 MeV (left plot in Fig.347).
6. For excitation energy equal to 70 MeV the best normalization for different TXE models is observed for the model #1 with the  $f$ -parameter equal to 0.0035 (right plot in Fig.347).
7. There is discrepancy between calculations and experimental data in the edges of distribution ( $Z<34$  and  $Z>68$ ) in the “abrasion-fission” reaction. One reason could be an inaccurate mass excess calculation for unbound super neutron-rich isotopes. The new masses (AME2003) will be incorporated in the next version of the code, as well as mass model parameters will be reconsidered.

## 2.7. Other

### 2.7.1. Projection on an axis in Monte Carlo plots

In all Monte Carlo two-dimensional plots beginning from the version 6.5.5 the user can create a projection on horizontal or vertical axes using the icon  in the plot toolbar. The plot projections in horizontal and vertical axes are shown in Fig.269.

### 2.7.2. Equilibrium thickness calculation methods in the Production dialog

In the previous version of the code the equilibrium thickness in the Physical calculator was calculated using the “Charge” code algorithm. In the new version the user can select a method of equilibrium thickness calculation for the “Physical calculator” in the “Charge States” frame of the “Production mechanism” dialog. The default calculation method is the “Global” code algorithm.

### 2.7.3. Navigation map: projectile & fragment

In case of the fragmentation reaction the “setting fragment” is found “close to” the primary beam. However, in case of fission the projectile is found in top of the table of nuclides, whereas the fragment uses to locate in middle of the table. For fast navigating (and also precise) in the new version, to be moved cross the table of isotopes, two buttons

“projectile” and “fragment” have been incorporated in the navigation window (see Fig.348. The mouse cursor changes at an intake of the mouse to these buttons.

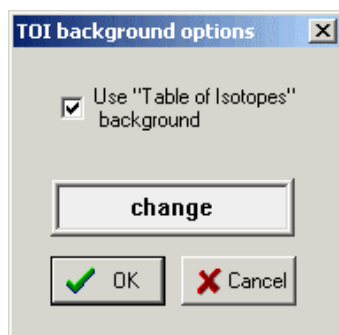


Fig.349.

### 2.7.4. "Table of nuclides" background

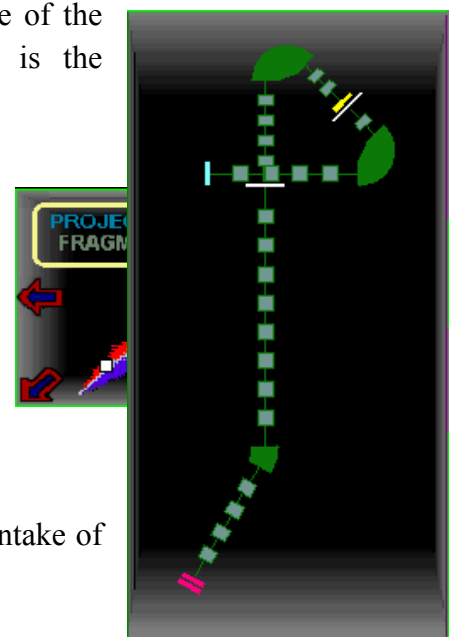



Fig.350. The “Alpha-D2” configuration file.

“Table of nuclides” background is available now for 2D cross-section (and several other) plots (for example Fig.318). Using the icon  in the plot toolbar the user can load the “TOI background options” where it is possible to change the background color or turn off this option (see Fig.349).

### 2.7.5. New configuration files

The new LISE++ configuration files have been added to the installation package:

Directory	Config-file	Thanks to
GANIL	Alpha	A.Lopez, B.Jacquot
GANIL	Alpha-D2 (see Fig.350)	
NSCL	A1900_2004A	A.Stolz

The “Alpha-D2” scheme options are next: initial angle = 0; width = 3, height = 6, margins =30 (Fig.350).

### 2.7.6. Charge state suppression values

Suppression values can be set to increase the calculation speed for transmission of ions with different charge values. In the previous version some constant coefficients were also used, but the new version gives to the user a possibility to change these suppression values from the “Charge state suppression values” dialog (Fig.351). This dialog is available through the “Charge states” frame of the “Production mechanism” dialog. Let assume there is a spectrometer with  $n$  dipoles and before every dipole a material with non-zero thickness is located. The code calculates charge state transmission  $n$  times through this spectrometer if the “charge state calculation” option is turn on. The ion will be excluded from transmission calculations if one of conditions is true:

1. if  $\exists i$  that  $\xi_i < S_{individual}$ , where  $i \in [1, n]$
2.  $\prod_{i=1}^n \xi_i < S_{global}$

where  $\xi_i$  is the charge state probability after  $n$ -material, and  $S_k$  are the suppression coefficients (see Fig.351).

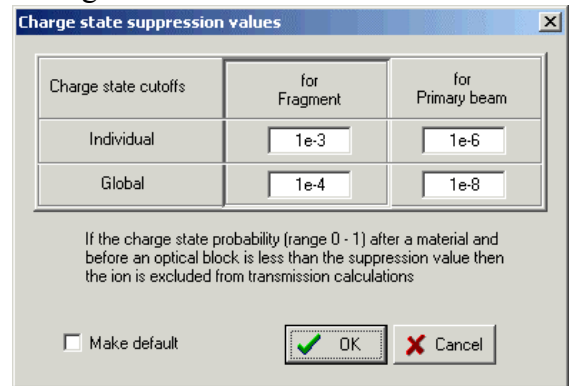


Fig.351. The “charge state suppression values” dialog.

### 2.7.7. Rate Calculator

A utility for the fast calculation of production rates has been developed using MS Excel and the LISE code dynamical libraries. It was named *Rate Calculator* and represents 7MB Excel file. To use the intensity calculator it is necessary:

1. Set the security priority in Excel to “low” or “medium” for the use of LISE’s macros (the menu “Tools→Macros→Security”).
2. Load the “LISE.xls” file from the LISE root directory.

The “*RateCalculator.xls*” file can be downloaded from the following directories of the LISE-ftp sites:

<ftp://dnr080.jinr.ru/lise/different/>\* and <ftp://ftp.nslc.msu.edu/pub/lise/different/>.

The Rate Calculator file contains 11 sheets but the user can make changes (input data) only\* in several cells (marked by special color) in the “MAIN” sheet (see Fig.352). A plot in the “PLOT” sheet (Fig.353) is automatically recalculated if the setting fragment has been changed in the “MAIN” sheet. Press the “Rescale plot” button to adapt new boundaries for the horizontal axis. Nine other sheets contain data bases of different reactions: fragmentation of  $^{48}\text{Ca}$ ,  $^{86}\text{Kr}$ ,  $^{112}\text{Sn}$ ,  $^{124}\text{Sn}$ ,  $^{124}\text{Xe}$ ,  $^{208}\text{Pb}$ ,  $^{238}\text{U}$  projectiles and fission of  $^{238}\text{U}$  nucleus with excitation energies equal to 16 and 70 MeV that correspond to average excitation energies of Coulomb fission (CF) and abrasion-fission (AF) respectively.

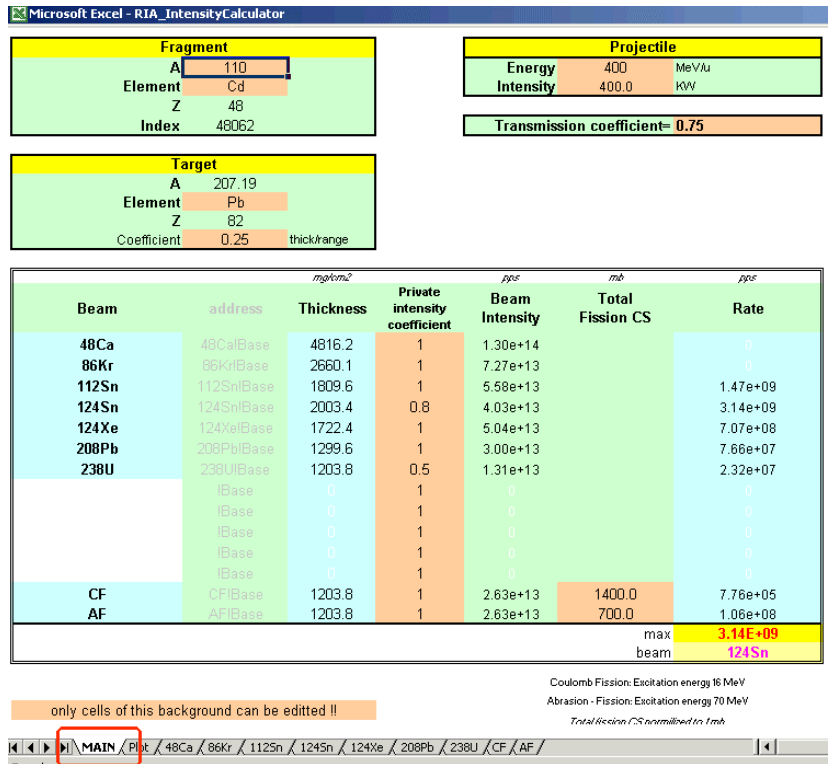
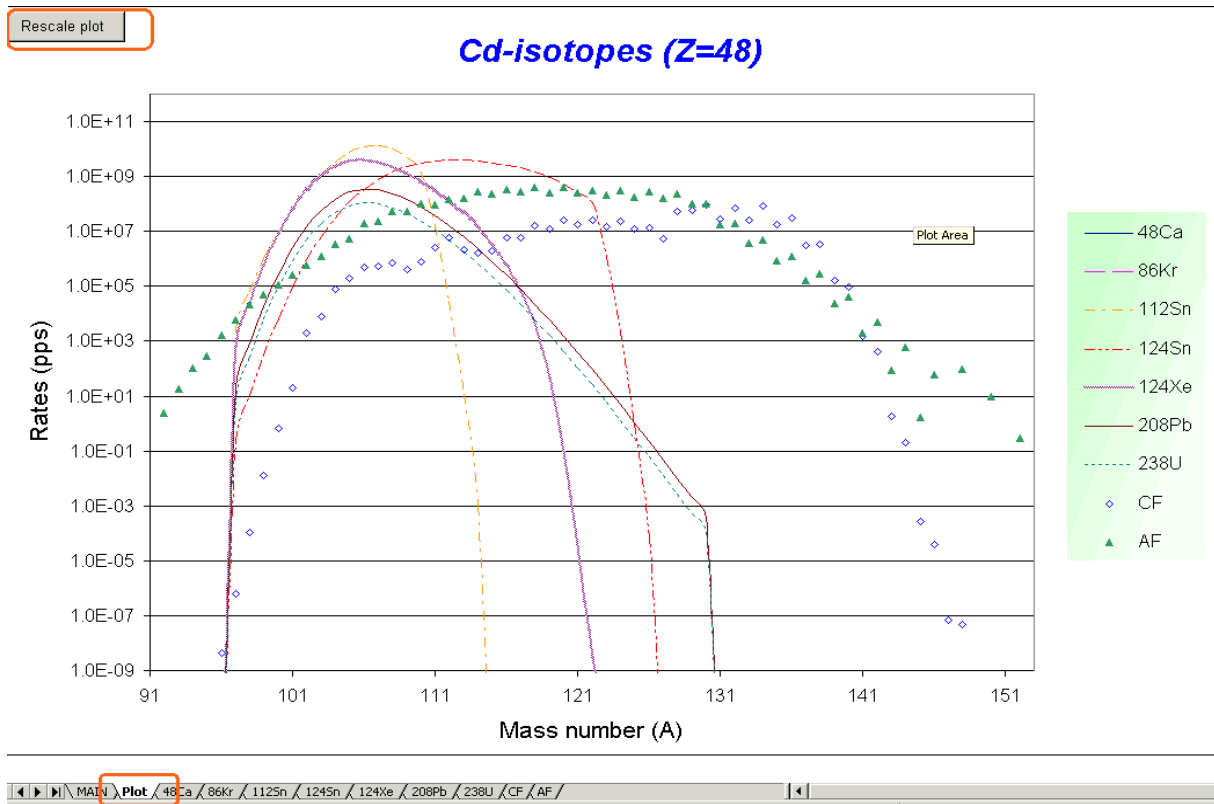


Fig.352. The “MAIN” sheet of the “RateCalculator.xls” file.

\* Dubna's ftp-server doesn't support Netscape's orders. Sorry.

\* Actually the user can unprotect sheets without a password using the menu “Tools → Protection → Unprotect sheet”.





**Fig.353.** The “Plot” sheet of the “RateCalculator.xls” file.

Fragment production cross-section are automatically recalculated if the atomic or mass numbers of the target are changed for fragmentation reactions. Fission-fragment cross-sections were deduced from the LISE code and normalized to the total fission cross-section equal to 1mb. The user has to set manually total fission cross-section if the target is changed. EM total fission cross section can be taken from LISE++ calculations (see Fig.293). For example the total EM fission cross-section in the reaction  $^{238}\text{U}(400\text{MeV/u})+\text{Pb}$  is equal to 1320 mb.

The effective target thickness is equal to the product of  $Coefficient_{(thick/range)}$  and the range of the projectile in the target material. The target and the projectile energy are set by the user in the “MAIN” sheet. An intensity is set in KW and then it transformed to the particle per second dimension (for every projectile with taking into account the private intensity coefficient”) (see Fig.352). Using the beam intensity [pps], the target thickness [ $\text{mg}/\text{cm}^2$ ], and the production cross-section [mb] MS Excel calculates the rate of the fragment. The transmission coefficient is unique for all fragments and entered by the user manually.

### 2.7.8. 2D-plot “Range-X”

2D-Plot	Database
Plot dE-TOF	
Plot TKE-TOF	
Plot dE-TKE	
Plot dE-dE2	
Plot dE-X	
Plot dE-Y	
Plot TKE-X	
Plot TKE-Y	
Plot TOF-X	
Plot TOF-Y	
Plot X-Y	
Plot X-X2	
Plot Z-A/Q	
<b>Plot Range-X</b>	
Plot Options	

A new 2D-plot “Range-X” can be plotted in the new version of the code through the “2D-plot” menu (see Fig.354). The X-coordinate is taken from “X-space” detector, and the “Range” detector is assumed to be the same as the TKE-detector (Fig.355). Examples of “Range-X” plot are shown in Fig.356 (in case of 2nd achromatic wedge) and Fig.357 (in case of 2nd monochromatic wedge) for “A1900-gas cell” configuration file. The vertical green line shows the thickness of the range detector.

Fig.354.

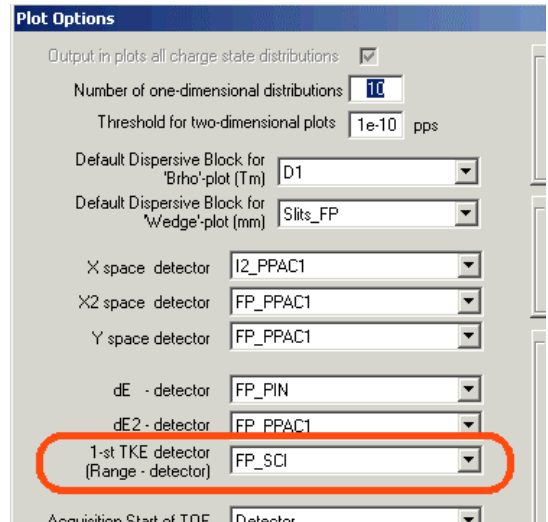


Fig.355. Fragment of the “Plot options” dialog.

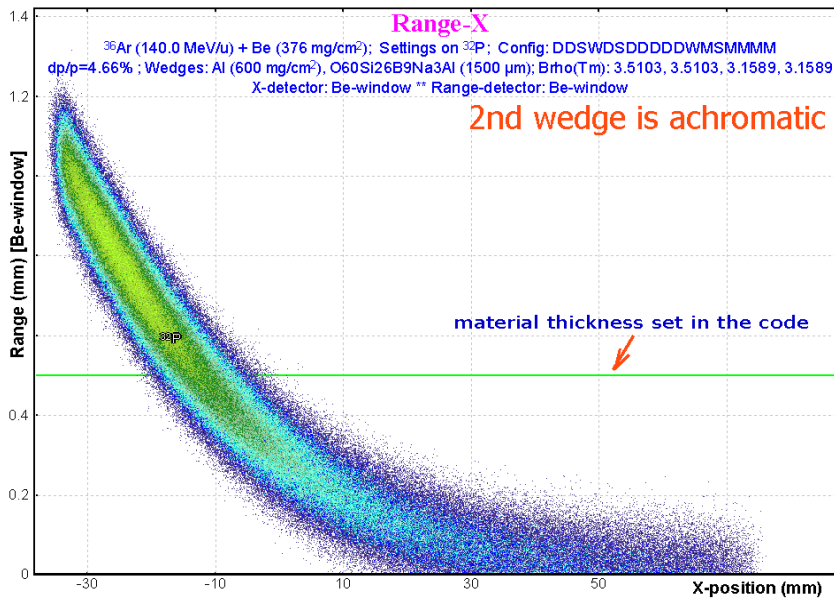


Fig.356. “Range-X” plot calculated for the “A1900-gas cell” configuration file in the case of 2<sup>nd</sup> achromatic wedge.

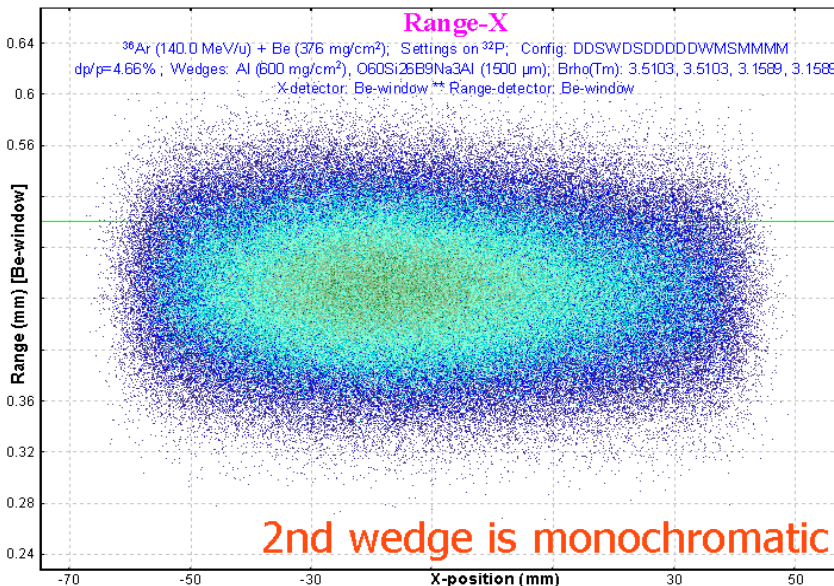
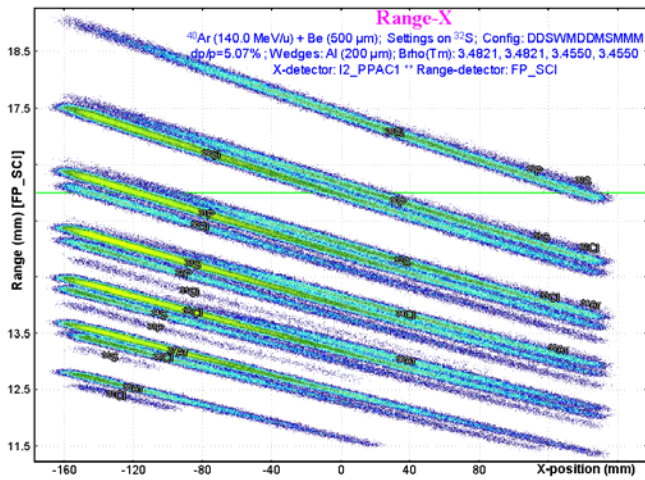
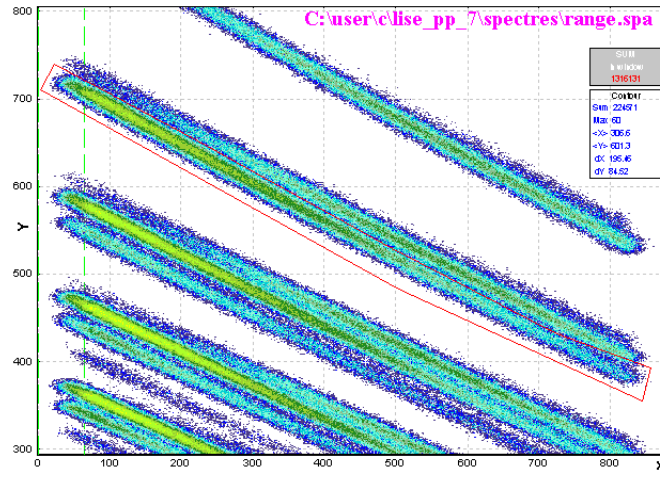


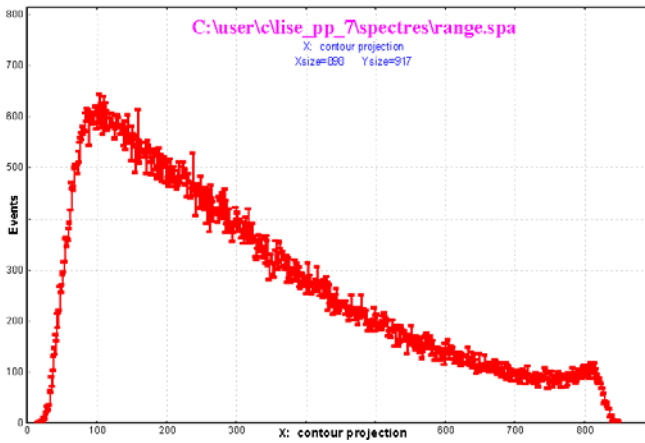
Fig.357. “Range-X” plot calculated for the “A1900-gas cell” configuration file in the case of 2<sup>nd</sup> monochromatic wedge.



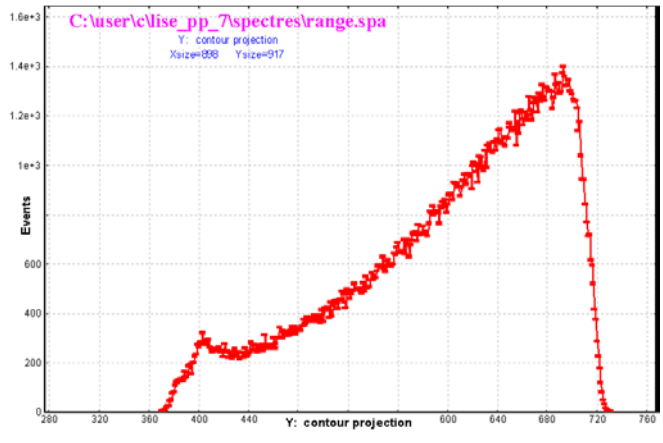
**Fig.358.** “Range-X” plot for the A1900 configuration file with Al-wedge (200micron) in I2. X-coordinate is taken from PPAC in intermediate dispersive focal plane. The “Range” detector is a scintillator in the final focal plane.



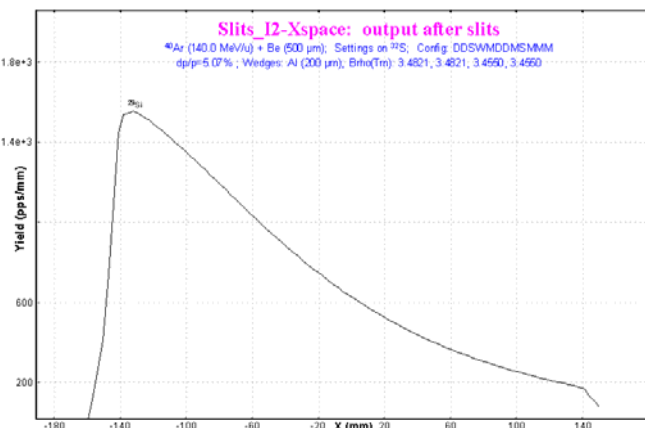
**Fig.359.** The 2D-plot reproduced by the “BI” dialog from the file saved by MC plot package for Fig.358.



**Fig.360.** A contour projection (Fig.359) on the horizontal axis (X-coordinate in the dispersive focal plane).



**Fig.361.** A contour projection (Fig.359) on the vertical axis (Range in the focal plane scintillator).



**Fig.362.** LISE++ analytical calculation of the  $^{29}\text{Si}$  fragment spatial distribution (compare with Fig.360).

## 2.8. Bug and remark report

<p>No messages, no Brho recalculations in the case of very thick target</p> <p style="text-align: right;">A.Stolz (NSCL)</p>	<p>Brho-value of the first optical block now is set to 0 in the case of very thick target. The user will get a message. <i>Fixed.</i></p>
<p>Zero transmission of the primary beam through the spectrometer in the case of a zero thickness target.</p> <p style="text-align: right;">M.Mocko (NSCL)</p>	<p>The code does not calculate charge state production for primary beam, fragment production and etc. in the case of a zero thickness target by analogy with experiment. <i>Fixed.</i></p>
<p>1. Curved profile wedge corrections then slits a little bit more than spatial distribution in the block.</p> <p>2. Problem with charge state calculations.</p> <p>3. Logarithm error for very small argument.</p> <p style="text-align: right;">T.Bauman (NSCL)</p>	<p><i>All of them fixed.</i></p>
<p>Program crash in the case of continuous decreasing the main window to zero size</p> <p>Ask to make: the "Physical Calculator" is not hiding together with LISE main window</p> <p style="text-align: right;">A.Miller(NSCL)</p>	<p><i>Fixed</i></p> <p><i>Done</i></p>
<p>Equilibrium thickness in the Physical calculator</p> <p style="text-align: right;">W.Lynch (NSCL)</p>	<p>See chapter 2.7.2.</p>
<p>Small angular acceptance problems for fission fragment kinematics.</p> <p style="text-align: right;">H.Weik (GSI)</p>	<p><i>Fixed. It was also corrected for "fragmentation" case.</i></p>

## 2.9. Next steps development

### *Short-term plans for Coulomb fission*

1. Reconsider the secondary reactions calculation mechanism in the target in case of Coulomb fission;
2. Use more points (now just one point) for the EM fission excitation function in the fission-fragment production cross-sections;
3. Incorporate the new model of fission-fragment yields prediction of V.A.Rubcheya & J.Äystö [Rub03] as alternative to the model of [Ben98].

### *Long-term plans*

1. Development of the abrasion-fission (nuclear fission) mechanism in the code;
2. Incorporation of Atomic Mass Evaluation (AME2003) database for more precise mass calculations;
3. Develop a procedure to take into account secondary reactions in a wedge.

## ***Acknowledgements***

The authors thank [Dr. Alexandra Gade](#) and [Mr. Anthony Nettleton](#) for carefully proof reading this manual.

Further, the authors gratefully acknowledge [Dr. Helmut Weick's](#) fruitful remarks, his careful checking LISE++ calculations in fission fragment kinematics, and MOCADI calculations performed by him to compare with LISE simulations.

The LISE++ authors thank [Prof. Carlos Bertulani](#) for the help in developing EM cross-sections procedures in the program.

We are grateful to [Prof. Brad Sherrill](#) for continuous support and guidance. Fruitful discussions with [Prof. Michael Thoennessen](#) are gratefully acknowledged.

## 3. Version 6.5: ISOL method

### 3.1. ISOL method

The code does not simulate processes in the ISOL-target (number of produced fragments, diffusion, extraction time etc). The new method is a combination of the so-called ISOL method of production and separation of radioactive nuclei with the classical method of mass analysis. This new method named “ISOL-method” has been incorporated to estimate fragment transmission through a spectrometer, and help with spectrometer tuning. Using LISE++ graphical utilities the user can observe spatial and energy distributions after any optical block.

The ISOL mode can be set in the “Production mechanism” dialog (menu “Options”). The buttons “Target”, “Stripper”, and “Setting fragment” are absent in this mode. The user can only set parameters of the projectile and choose a spectrometer configuration. Nuclei produced in nuclear reactions are emitted from an ECR ion source at energy  $E = qU$ , where  $q$  is the ion charge of nuclide, and  $U$  is the voltage in  $kV$ . For this mode the new possibility of entering the energy in  $kV$  has been developed (see Fig.363).

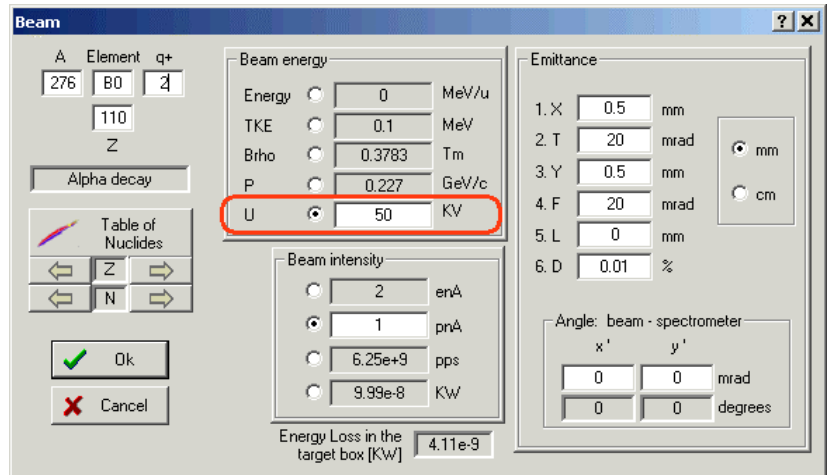



Fig.363. The “Beam” dialog.

The next step is the calculation of spectrometer settings for the chosen projectile using the button  in the toolbar or calling the command “Calculate the spectrometer for setting ion” from the menu “Calculations”.

statistics 277B0		
277B0	Alpha decay (Z=110, N=167)	
Q1 (M1)		1
Q2 (M2)		1
Q3 (M3)		1
Q4 (ElecDip)		1
<b>Production Rate</b>	<b>(pps)</b>	<b>2.78e+9</b>
Sum of charge states	(pps)	2.78e+9
<b>Intensity Coefficient</b>		<b>1e+0</b>
Total transmission	(%)	44.489
<b>Target</b>	<b>(%)</b>	<b>100</b>
Unreacted in mater.	(%)	100
Unstopped in mater.	(%)	100
<b>M1</b>	<b>(%)</b>	<b>47.86</b>

Fig.364. The transmission statistic window.

“Cross Section file” dialog. The intensity coefficient should be proportional to the production cross section of the given nuclide and the coefficient of extraction from ECR. It is possible to use the PACE4 code (or “LisFus” model) to estimate the production cross sections. The file with calculated cross sections can be loaded as intensity coefficients using the “Cross section file” dialog (see documentation for version 6.4).

### 3.1.1. Mass separator “MASHA”

The configuration file of the mass separator MASHA [Oga03] operating in “ISOL-mode” has been created and incorporated in the LISE++ installation package:

LISE++ file: *Files\examples\MASHA.lpp*

Configuration file: *Config\Dubna\MASHA.lcn*

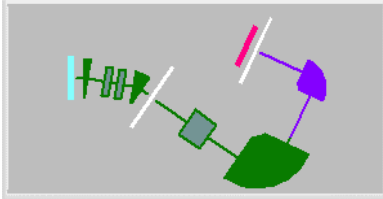


Fig.366. LISE++ scheme of MASHA separator.

The separator MASHA set-up window and its scheme are shown in Fig.365 and Fig.366. The MASHA configuration file provides by calibration files of magnetic dipoles that help the user to tune the mass separator.

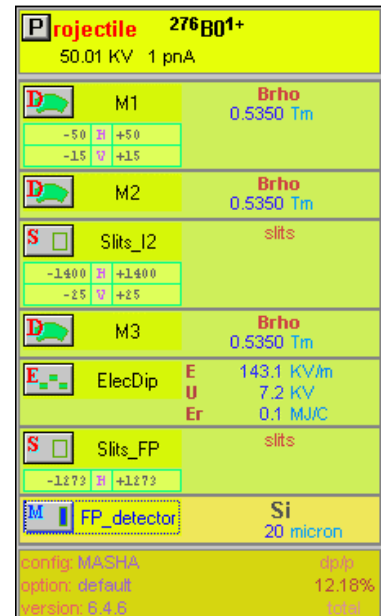


Fig.365. MASHA separator set-up window.

Envelopes of  $^{276}\text{B}0^{1+}$  and  $^{275}\text{B}0^{1+}$  nuclides through the MASHA mass separator tuned on the ion  $^{276}\text{B}0^{1+}$  are shown in Fig.367. The projectile initial emittance used in that calculation was the following:  $x=y=0.5\text{ mm}$ ,  $\theta=\varphi=20\text{ mrad}$ ,  $dp/p=0.01\%$ . Some examples of fragment transmission calculation under different initial conditions are presented in Fig.368.

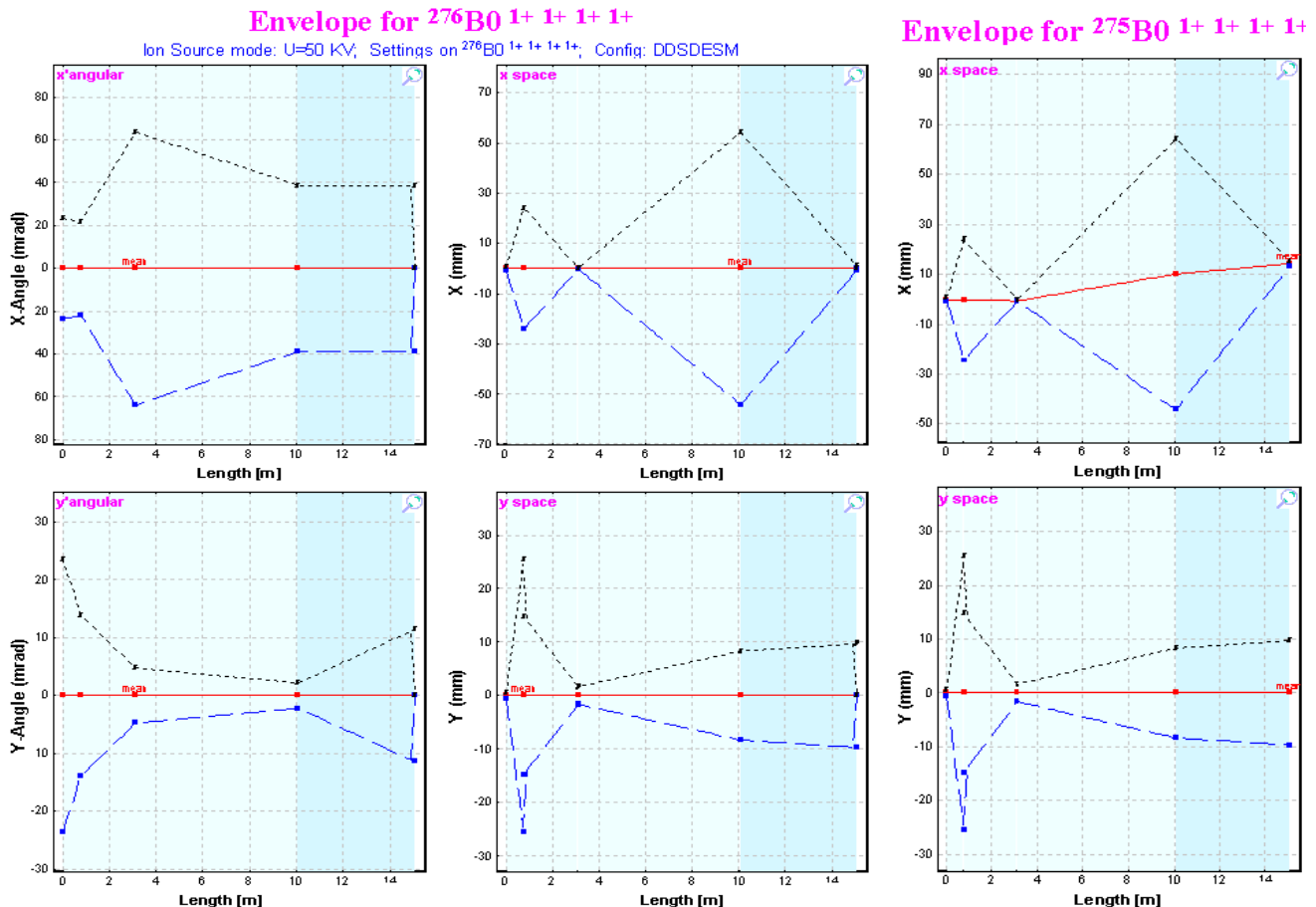
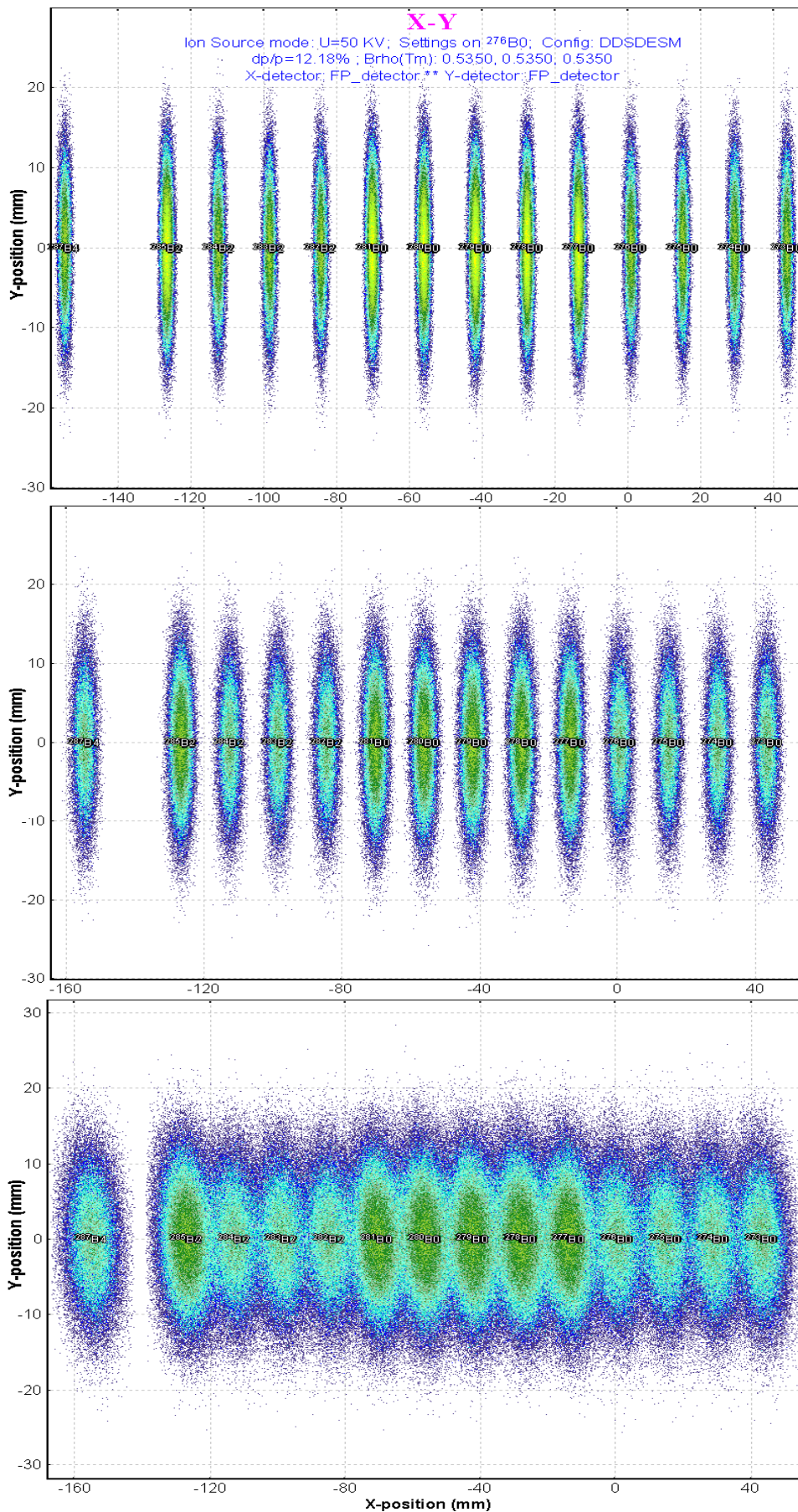


Fig.367. Envelopes of  $^{276}\text{B}0^{1+}$  and  $^{275}\text{B}0^{1+}$  nuclides through the MASHA mass separator tuned on the ion  $^{276}\text{B}0^{1+}$ .



**Fig.368.** Two-dimensional identification plots of nuclides transmitted through the mass separator and registered by the final focal plane position-sensitive detector. The spectrometer is set to  $^{276}\text{B}0^{1+}$ .

The top figure corresponds to the projectile initial emittance  $x=y=0.5$  mm,  $\theta=\varphi=20$  mrad,  $dp/p=0.01\%$ ;

the middle figure to  $x=2.5$  mm,  $y=0.5$  mm,  $\theta=\varphi=20$  mrad,  $dp/p=0.01\%$ ;

the bottom plot to  $x=y=0.5$  mm,  $\theta=\varphi=20$  mrad,  $dp/p=0.05\%$ .



### 3.1.2. Charge states

It is recommended to turn the “Charge state” option off, because the output of ions with a charge more than 1+ is small in this energy region (some tenth of KeV). Moreover, other charge states will be suppressed by the spectrometer, which is tuned on ions with 1+. The next example proves this statement. For this purpose it is necessary to turn off all slits and turn on the “Charge state” option. For the ISOL method the code assumes that the output of ions with charge  $q=(n+1)+$  is 10 times less than the output of ions with charge  $q=n+$  (see Fig.369). In this case ions with different charge will be easily differentiated in the plots (see Fig.370). In the figure it is visible that the ions with  $q=2+$  are located away from  $q=1+$  by two meters, much greater than the sizes of the detector. Moreover charges with  $q > 1$  will not go through the first dipole. It is easy to check this statement.

276B0 Alpha decay (Z=110, N=166)							
Q1 (M1)	7	6	5	4	3	2	1
Q2 (M2)	7	6	5	4	3	2	1
Q3 (M3)	7	6	5	4	3	2	1
Q4 (ElecDip)	7	6	5	4	3	2	1
<b>Production Rate (pps)</b>	<b>7.36e+2</b>	<b>1.08e+4</b>	<b>1.43e+5</b>	<b>1.77e+6</b>	<b>2.1e+7</b>	<b>2.37e+8</b>	<b>2.48e+9</b>
Sum of charge states (pps)	2.74e+9	2.74e+9	2.74e+9	2.74e+9	2.74e+9	2.74e+9	2.74e+9
Intensity Coefficient	1e+0	1e+0	1e+0	1e+0	1e+0	1e+0	1e+0
Total transmission (%)	0	0	0.002	0.028	0.337	3.795	39.684
<b>Target (%)</b>	<b>0</b>	<b>0.001</b>	<b>0.009</b>	<b>0.09</b>	<b>0.9</b>	<b>9</b>	<b>90</b>
Unreacted in mater. (%)	100	100	100	100	100	100	100
<b>Q (Charge) ratio (%)</b>	<b>0</b>	<b>0.001</b>	<b>0.009</b>	<b>0.09</b>	<b>0.9</b>	<b>9</b>	<b>90</b>
Unstopped in mater. (%)	100	100	100	100	100	100	100
<b>M1 (%)</b>	<b>48.47</b>	<b>48.47</b>	<b>48.47</b>	<b>48.47</b>	<b>48.47</b>	<b>48.47</b>	<b>48.47</b>
Y space transmission (%)	61.07	61.07	61.07	61.07	61.07	61.07	61.07
X angular transmism. (%)	100	100	100	100	100	100	100
Y angular transmism. (%)	79.36	79.36	79.36	79.36	79.36	79.36	79.36
<b>M2 (%)</b>	<b>92.04</b>	<b>60.87</b>	<b>71.53</b>	<b>83.49</b>	<b>94.39</b>	<b>99.73</b>	<b>100</b>
X angular transmism. (%)	52.04	60.87	71.53	83.49	94.39	99.73	100
Y angular transmism. (%)	100	100	100	100	100	100	100
<b>Slits_I2 (%)</b>	<b>100</b>	<b>100</b>	<b>100</b>	<b>100</b>	<b>100</b>	<b>100</b>	<b>100</b>
Y space transmission (%)	100	100	100	100	100	100	100
<b>M3 (%)</b>	<b>51.91</b>	<b>65.28</b>	<b>73.22</b>	<b>77.9</b>	<b>81.74</b>	<b>87.23</b>	<b>90.98</b>
X angular transmism. (%)	51.91	65.28	73.22	77.9	81.74	87.23	90.98
Y angular transmism. (%)	100	100	100	100	100	100	100
<b>ElecDip (%)</b>	<b>100</b>	<b>100</b>	<b>100</b>	<b>100</b>	<b>100</b>	<b>100</b>	<b>100</b>
<b>Slits_FP (%)</b>	<b>100</b>	<b>100</b>	<b>100</b>	<b>100</b>	<b>100</b>	<b>100</b>	<b>100</b>
Y space transmission (%)	100	100	100	100	100	100	100
<b>FP_detector (%)</b>	<b>0</b>	<b>0</b>	<b>0</b>	<b>0</b>	<b>0</b>	<b>0</b>	<b>0</b>
Unreacted in mater. (%)	100	100	100	100	100	100	100
Unstopped in mater. (%)	0	0	0	0	0	0	0
reaction	ISOL	ISOL	ISOL	ISOL	ISOL	ISOL	ISOL

Fig.369. The transmission statistic window.

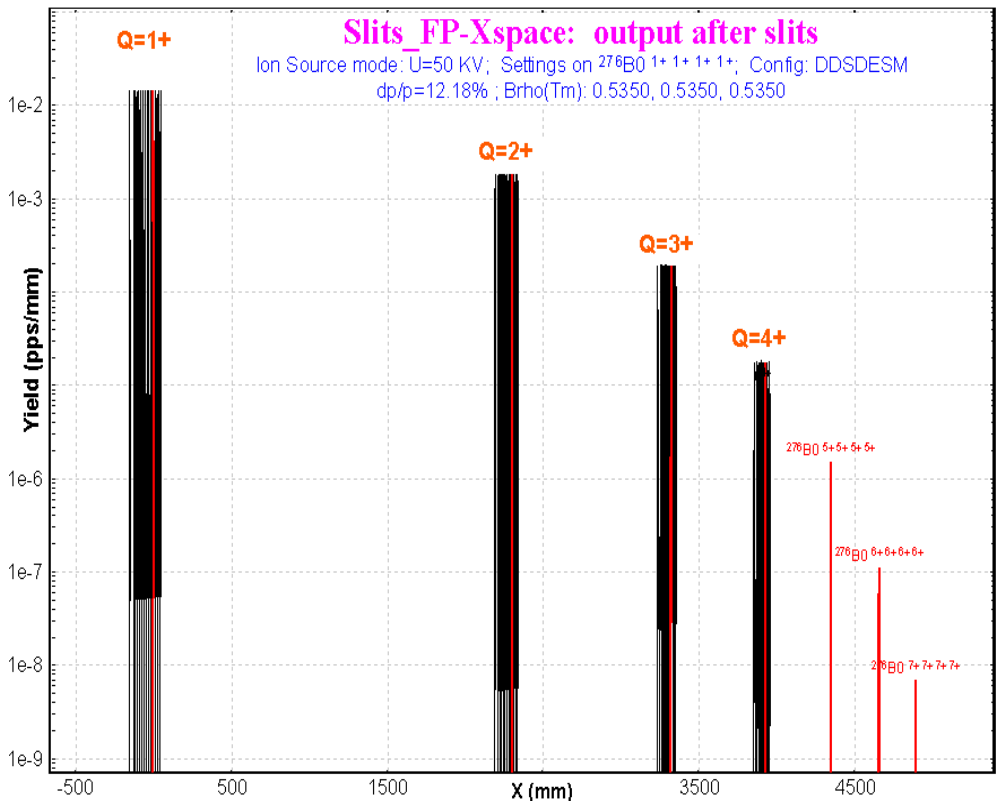


Fig.370. Horizontal spatial distribution of ions in the final focal plane of mass separator MASHA. Spectrometer settings are shown in the figure.

### 3.2. Other

#### 3.2.1. Electric dipole: separation plane

A “Separation plane” frame has been added to the “Electric dipole” dialog (see Fig.371) to select the plane where the electric rigidity selection is applied ( $E$ -plane). The magnetic rigidity selection is applied to the perpendicular plane ( $M$ -plane). This modification was introduced because of a specific case in the MASHA spectrometer where after the electrical dipole both dispersions in vertical and horizontal planes are not equal to zero.

#### 3.2.2. Wedge angle dialog

Wedge angle calculations basing on formulae have been added to the “Wedge angle” dialog (Fig.372). The code calculates the transfer matrix between the wedge block and the point chosen in the dialog to get the spatial magnification and dispersion coefficients. This method of wedge angle calculation does not take into account materials which can be located between the wedge and the final point.

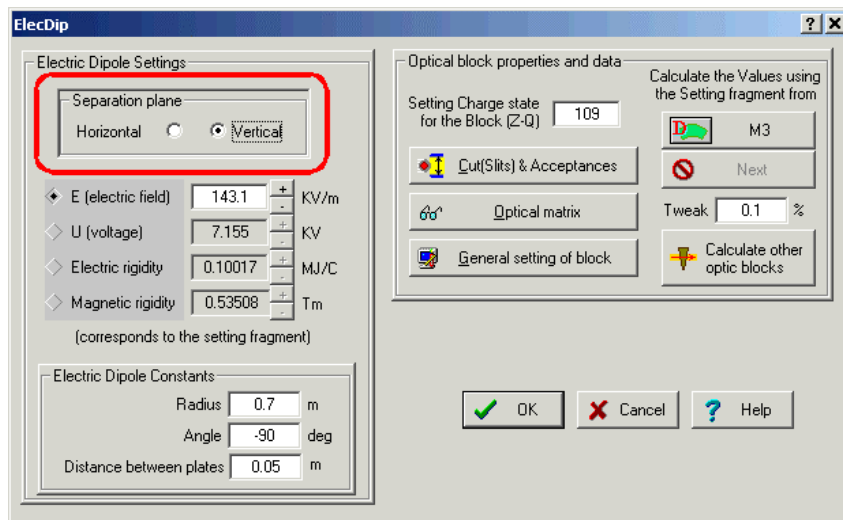


Fig.371. The “Electric dipole” dialog.

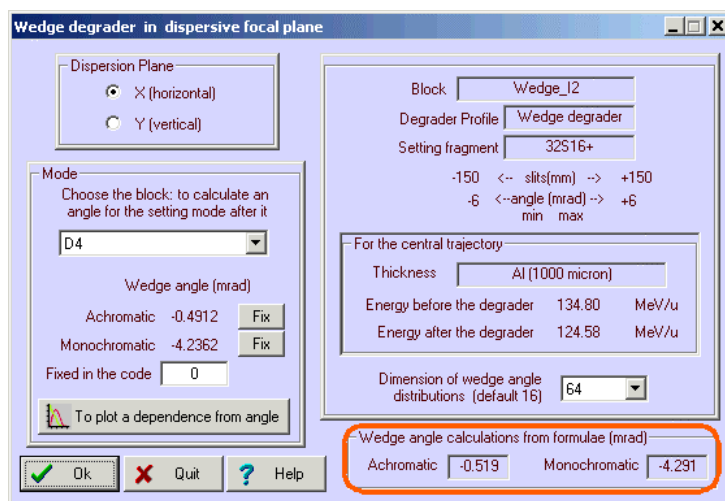


Fig.372. The “Wedge angle” dialog.

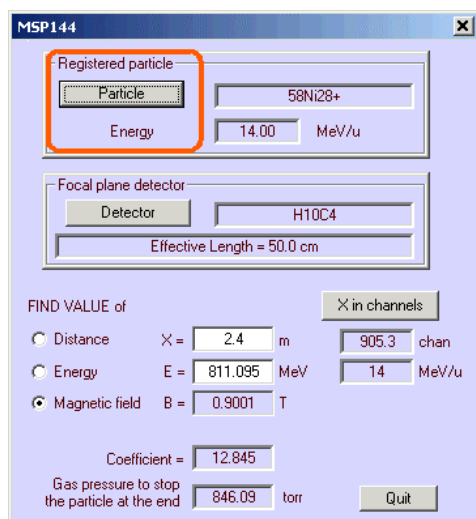


Fig.373. The MSP144 dialog

#### 3.2.3. MSP-144 modification

The possibility to input a projectile energy in the MSP144 dialog was developed (see Fig.373). The algorithm to search the magnetic field  $B$  from  $E$  and  $X$  has been corrected.

### Acknowledgements

The authors gratefully acknowledge Dr.V.Shchepunov (Dubna & Oak Ridge) for help with the development of the MASHA spectrometer configuration for LISE++.

## 4. Version 6.4

### 4.1. LISE for “unprivileged” users

The program “LISE” was initially developed for Personal Computer (PC) under DOS, and then Windows 95 and 98. With these systems, the user of PC was the absolute owner of the computer. Nowadays the multitask operational systems Windows 2000 & XP are installed on the majority of PCs. LISE++ is mostly used in laboratories, where PC users usually have no administrative privileges, and the following problems are encountered:

- It is impossible to load the program under WinXP because the file “*lise.dbf*” is set to read-only by the system;
- It is forbidden to save LISE user files in the directory “Program files\LISE\files”, as well as to keep user settings of the code;
- The programs “Charge”, “PACE4”, and “BI” can not be loaded because it is impossible to open temporary files in the directory “Program files\LISE”.

All of the above-mentioned problems were solved in the new version. However the possibility to install the code without administrative privileges in a user directory (creating a temporary directory for unzipped files) has been removed.

#### 4.1.1. The “\user\MyDocuments\LISE” directory

What happens now, when the user loads the program, after it has been installed by the administrator? The program tries to open the file “*lise.ini*” for writing. If the attempt is unsuccessful, the user is automatically considered without privileges, and the program uses the directory “\user\MyDocuments\LISE” as LISE's working directory. If this directory is missing, the code will create the directory “LISE” and subdirectories “files”, “config”, “bin”, “options” etc. The program copies configuration, setting, degrader files from the directory “Program Files\LISE ” (default) in “\user\MyDocuments\LISE\”. The User's ME file is created in the directory “bin”. All users have then own settings of the program, as well as the nuclide file and User's ME. The database A&W95 remains common for all users, and is protected from changes.

The program compares the versions of the files in the directory “MyDocuments\LISE” to the current version of the program each time at loading. LISE++ will copy the updated files in the directory “MyDocuments\LISE” in case of a new version has been installed.

#### 4.1.1.1. Using the folder “My Documents” for users with administrative privileges

If users with administrative privileges want to keep their settings in the “MyDocuments\LISE” directory they have to set the file “*lise.ini*” to “Read only”. In this case ALL users will work from their “MyDocuments\LISE” directories.

#### 4.1.2. "Charge", "Global", "PACE4" & "BI" for "unprivileged" users

The programs "Charge", "Global", "PACE4" also check the possibility to create files in the default directory. If the attempt is unsuccessful these programs create temporary files and read & write result files in the directory "MyDocuments\LISE\files".

#### 4.2. User's Mass-Excess file

Masses of isotopes are used everywhere in the program from energy losses of ions in matter to the Brho-analyzer. It is important to use correct values of masses in evaporation cascade (*Abrasion-Ablation* and *LisFus* models), as well as in the kinematic calculator. In the previous versions masses were taken from the mass database [A&W95]. There are some disadvantages of using this database:

- If a mass excess value is changed then it is necessary to change all other cells manually;
- There is no calculated suggested value in the dialog "Database" for an isotope which is missing in the database;
- Only one database "lise.dbf" can be used.

In the new version of LISE++ it is possible to use other databases of masses: the user's mass excess file (UME). This file only stores mass excess value of isotopes, and other isotope characteristics that are calculated by the code. Therefore the UME file has much smaller size than the database A&W95. The UME file is called by default "user\_mass\_excess.lme" and found in the "\bin" directory. If the UME file is missing, then LISE++ will create a new UME file using information from the database A&W95.

##### 4.2.1. Use of mass models

The user can choose a UME file to be used in the code in the "Production mechanism" dialog (see region "A" in Fig.374). In this dialog the user can determine a mass model to be used in future calculations. There are 9 available combinations (see region "B" in Fig.374):

1. Database+Calculations: one of two mass databases (A&W95 or UME file) + one of three available LDM to extrapolate masses of nuclei missing in the database.
2. Calculations only: one of three LDM formulas.

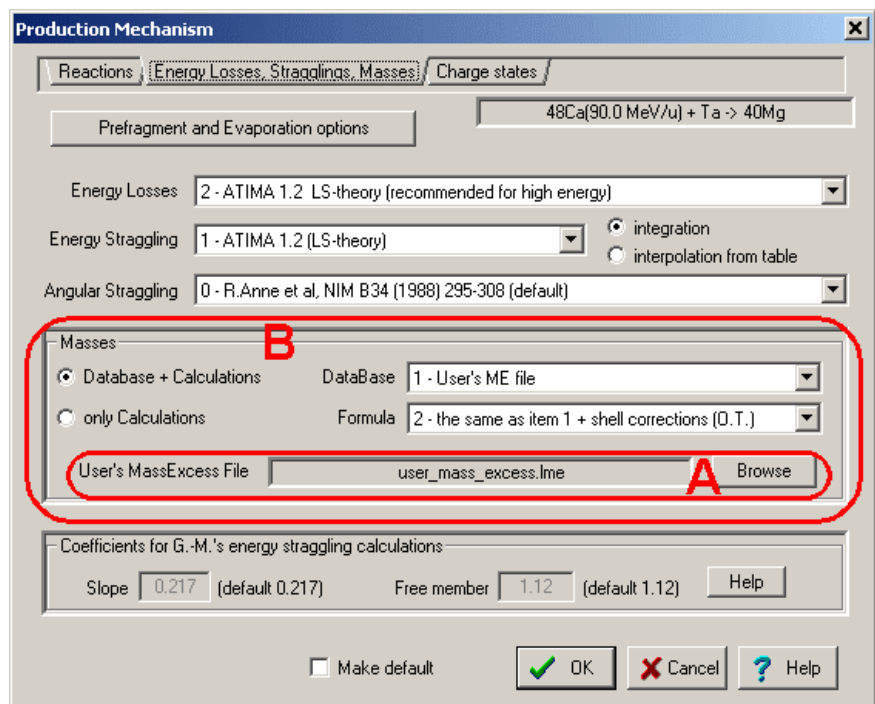


Fig.374. The "Production mechanism" dialog: choose a mass model.

### 4.2.2. UME file format

The format of the UME file is simple. It is an ASCII file that consists of two columns separated by one of several possible separation characters (tabulation sign, comma, or space). The first column is the isotope (Z,N) index in format Z×1000+N. The second column is the mass excess value of this isotope in MeV. The ME value can be written in exponent form, or in floating point format.

### 4.2.3. UME file editing

New records in the UME file and changes of already existing data can be performed through the “Database” dialog from the menu “Database” (see Fig.375). The user has to choose the database mode “1-User’s ME file” to obtain access to the UME file data. There are three possible states of the data (see rectangle “C” in Fig.375):

1. Data from User's ME file.
2. ME value has been modified.
3. LDM calculation.

The two first states show an already existing record. In the third state the data the isotope is missing in the UME file, and calculated values are shown in the dialog. Click "Add record" to add the calculated value for this isotope to the UME file. After the record is created it is possible to edit the mass excess value for this isotope.

The new database of Audi & Wapstra (edition 2003) will soon be incorporated. Mass excess errors will also be used in the code (at least for plots). Mass excess errors will be recorded in the UME file as the third column.

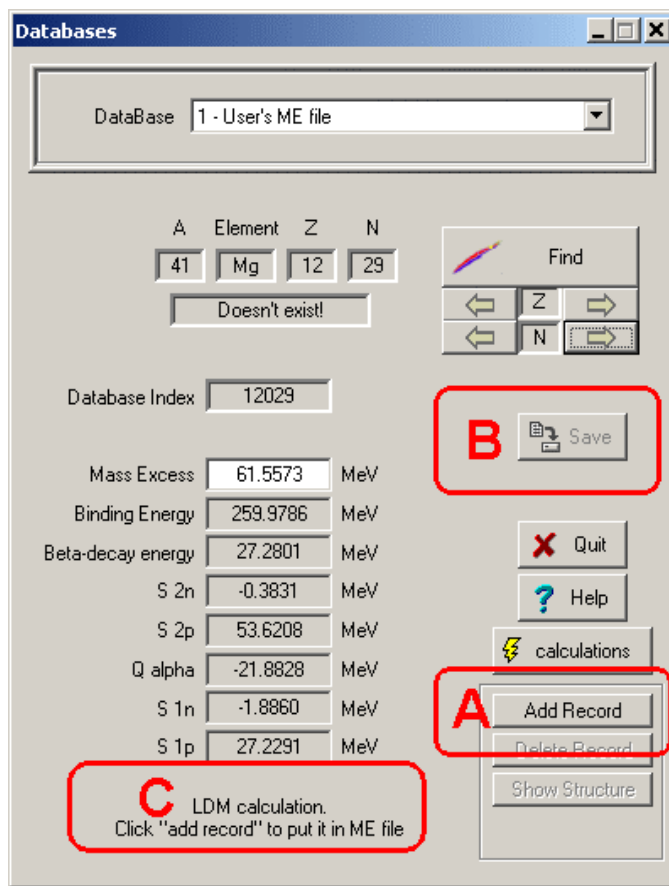


Fig.375. The “Databases” dialog in the UME file mode.

⚡ When you are editing a mass excess value don’t forget that isotope characteristics such as separation energies of neutrons or protons are also changed in the neighboring nuclei. For example, the work [Sar00]: the measured masses of particle-bound isotopes <sup>34,35</sup>Mg equal 9220(330) and 17540(1000) respectively. If one puts these values in the “Database” then <sup>35</sup>Mg isotope becomes unbound by 249 KeV against one neutron emission because of the large error bar on the measurements.

⚡ Important details about the UME file are given in the sections in relation with the user’s privileges (4.1. LISE for “unprivileged” users) and the separation energy determination through production cross-section (4.4.8. Cross-section & minimum separation energy dependence).

### 4.3. User's cross-section file

Even if the user had the cross-sections file obtained from experimental data or calculation by other programs it is possible to input cross-sections manually in the LISE++ program to be used in calculations. The new version allows users to read/write cross-section values from/to the Cross-section File (CSF).

All CSF operations are available if the option “Fit/File” in the box “Cross-section” in the “Preference” dialog is set to “File” (see Fig.376). Using the button “CS File settings” from the “Preference” dialog (Fig.376) or the menu “Options->Cross-section file” the user can load the “CSF dialog” (see Fig.377) to provide operations with the CSF.

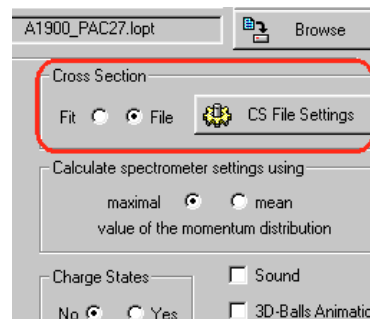


Fig.376. The “Cross-section” block in the “Preference” dialog.

The “Browse” button allows users to connect to the CSF. To **load** CS values from the connected file in the memory it is necessary to click the “Load” button. There are two options to load data:

- **Append:** already existing data in memory are saved; missing data are added in memory.
- **Overwrite:** if CS data already exist for given isotope then it will be overwritten.

Use the “Remove All CS from memory” button if it is necessary to remove all data from the memory before loading data from the CSF.

If the number of user CS (or in other words “CS in memory”) is not equal to zero then the “Save as” button is available. It is possible to save the data in a file with other name than the connected CSF. The connected CSF is left as the same in any case. The number of used CS is shown the dialog.

The format of CSF is simple and shown in the dialog. PACE4’s CSF can be used by the LISE++, but the file has the special header which is read by LISE++ to show PACE4 settings applied to provide these calculations.

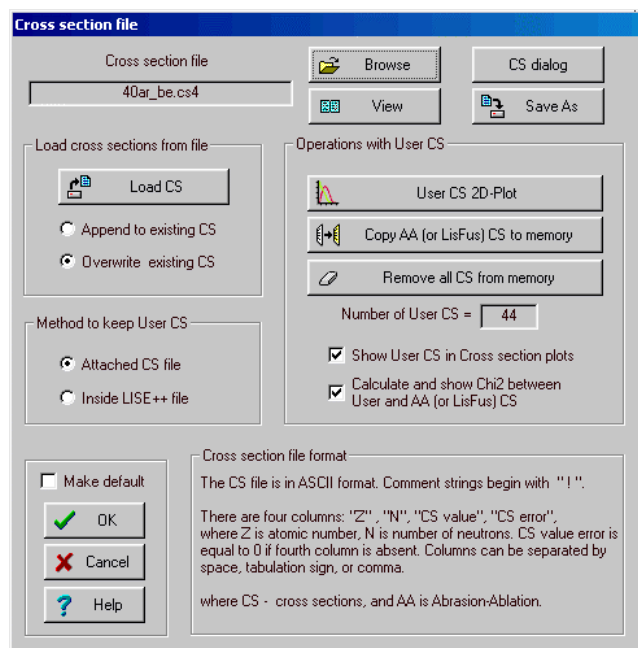


Fig.377. The “Cross-section file” dialog.

There is brief description of some buttons:

- **View:** to visualize contents of the connected file;
- **CS dialog:** to get the “Cross-sections” dialog to see cross-sections calculated by LISE++ and to modify user CS;
- **User CS 2D-plot:** to plot cross-section values loaded to memory. This command is available if at least one CS value is loaded to the memory;

- **Copy AA or (LisFus) CS to memory:** if Abrasion-Ablation or LisFus models were used to calculate CS then the user can copy them to memory (by OVERWRITE method!!). This button is not available if the number of AA (or LisFus) cross-sections is equal to zero.

☞ For fast work it is preferably to load AA (or LisFus) calculated values from “fast” CS memory then recalculate them again.

### 4.3.1. Methods to keep user CS

There are two methods to save CS values in files to use them the future:

- Inside LISE++ file: CS values are saved inside LISE++ file as it has been done in the previous versions. In this case the data increase LISE++ file size and can not be used by other applications (by default).
- Attached file: Data are kept in the connected CSF. The CSF is saved when the user clicks the button “Save As” in the “CSF” dialog *OR* the LISE++ file is saved in the disk. When the LISE++ file with the attached CSF is loading, the CS data are automatically loading from the CSF to the memory. It is possible to see the name of the connected file in the “Setup” window (see Fig.378) if the number of memory (User’s) cross-sections is positive, the option “Cross-sections” is set to the value “File” (see Fig.376), and the method to keep user CS is set to “Attached CS file”.

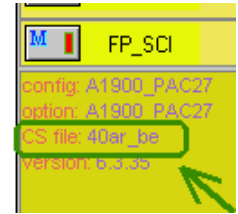


Fig.378. The fragment of the “Setup” window shown the connected CS file.

### 4.3.2. User CS in plots

User CS data are plotted (Fig.379) if the option “Show User CS in Cross-sections plot” is set in the “CSF” dialog (see Fig.377). Errors of user CS data are plotted also if they are different from zero (see fragment “A” in Fig.379). Chi-square calculation results between User CS and AA (LisFus) calculations appear in the right bottom corner of the plot if the option “Chi-square” is set in the “CSF” dialog, and at least one isotope from memory CS exist for which AA calculations was done. The value “LoD” shows an average deviation in log-scale  $LoD = \sum_{i=1}^N |\log_{10}(y_{exp}) - \log_{10}(y_{calc})| / N$

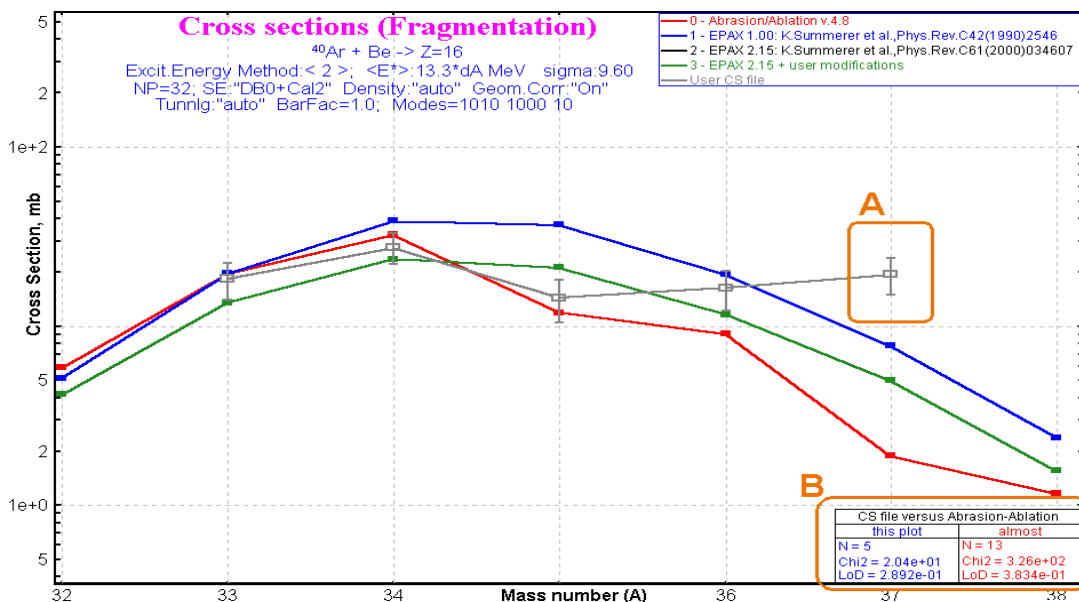


Fig.379. The cross-section production plot for Z=16 in the reaction  $^{40}\text{Ar}+\text{Be}$ .

#### 4.4. Abrasion-Ablation revision

The AA model has undergone significant updates in the new version, both for the first part of model (excitation energy), as well as for the evaporation cascade. The new options, new plots have been implemented, and some corrections were done. The algorithm of determination of excitation energy parameters compared with experimental data is presented. All this is presented in this chapter step by step using examples. At the end of the chapter the comparisons of experimental data and calculations for several primary beams are shown. Three step fragmentation process and separation energy determination through production cross-section of fragment are discussed.

##### 4.4.1. Evaporation cascade

To understand the AA new features it is better to begin with the “Evaporation calculator” in the mode “Excited nucleus evaporation” (see Fig.380, step 1). Let's consider an  $^{40}\text{Ar}$  nucleus (step 2 in Fig.380) with excitation 40-45 MeV (rectangle distribution). To observe the complete evolution of the cascade, set the final nucleus also to  $^{40}\text{Ar}$  (step 3). To begin calculations use the button “Calculation” (step 4). To get the plots as shown in Fig.381 and Fig.382 use the button “Excitation energy plot” (step 5).

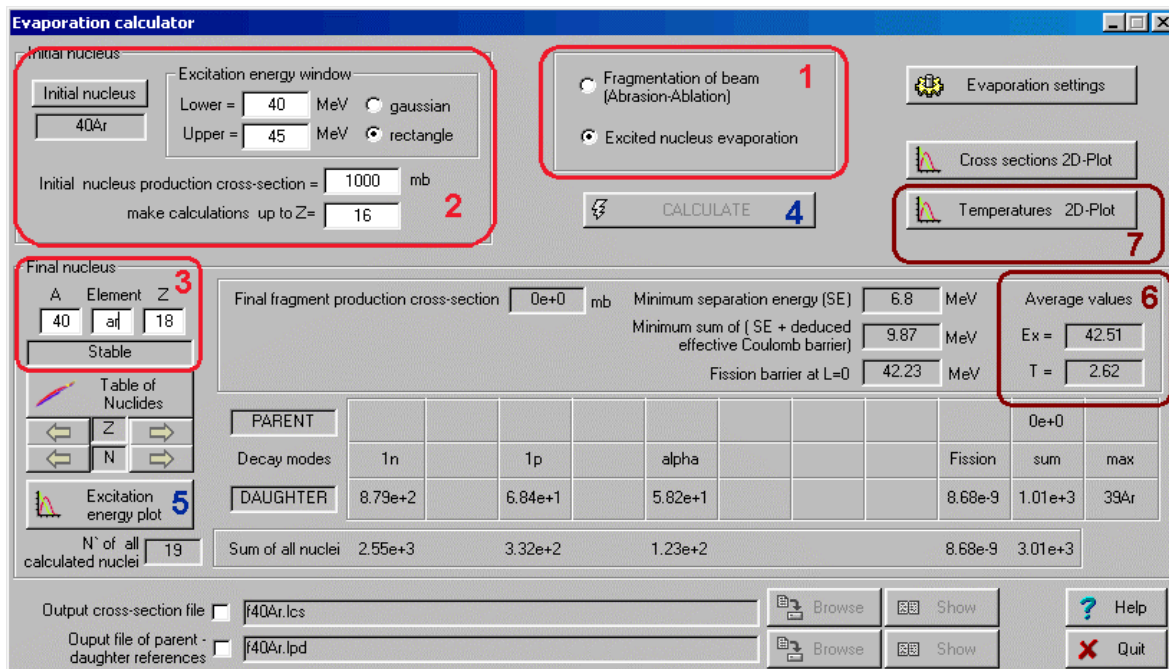
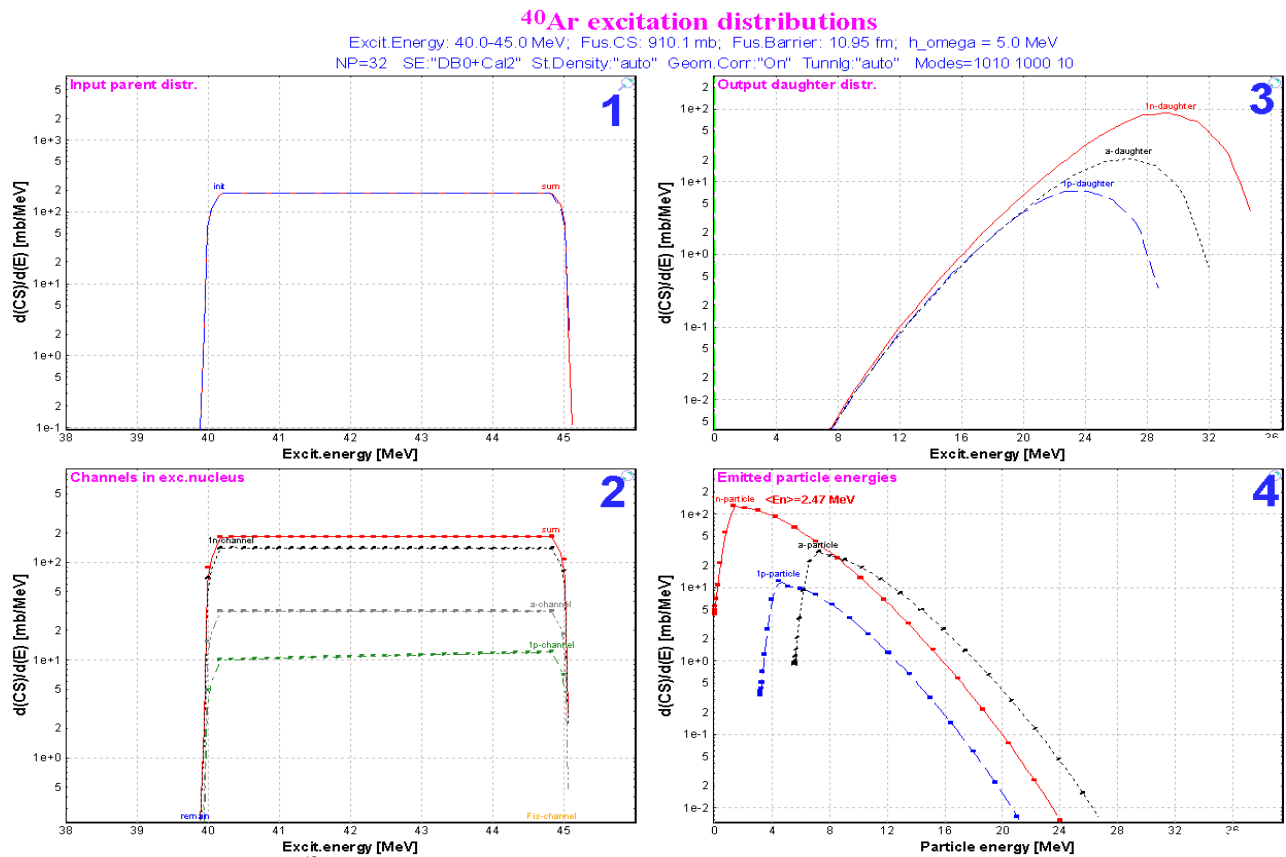


Fig.380. The “Evaporation calculator” dialog in the mode of “Excited nucleus evaporation”.

1. The left top plots in Fig.381 and Fig.382 represent the sum of initial and parent excitation energy distributions. In the case of Fig.381 there are not parent distributions, because the sum distribution is equal to initial one defined as a rectangle from 40-45 MeV in the Evaporation calculator.
2. The left bottom plots in Fig.381 and Fig.382 are new in the new version and show the evaporation channels in the excited nucleus. The area painted in dark blue shows the cross-section of the residue production. All the cross-section to the right of this area goes to the daughter nuclei. The “sum” dis-



tributions in the left figures are identical. However, the top figure shows how it was produced, and the bottom figure how it breaks up.



**Fig.381.** <sup>40</sup>Ar excitation distribution plots created from the Evaporation calculator.

### $^{38}\text{Cl}$ excitation distributions

Excit.Energy: 40.0-45.0 MeV; Fus.CS: 910.1 mb; EVAPORATION - Initial nucleus  $^{40}\text{Ar}$   
 NP=32 SE="DB0+Cal2" St.Density:"auto" Geom.Corr:"On" Tunnelg:"auto" Modes=1010 1000 10

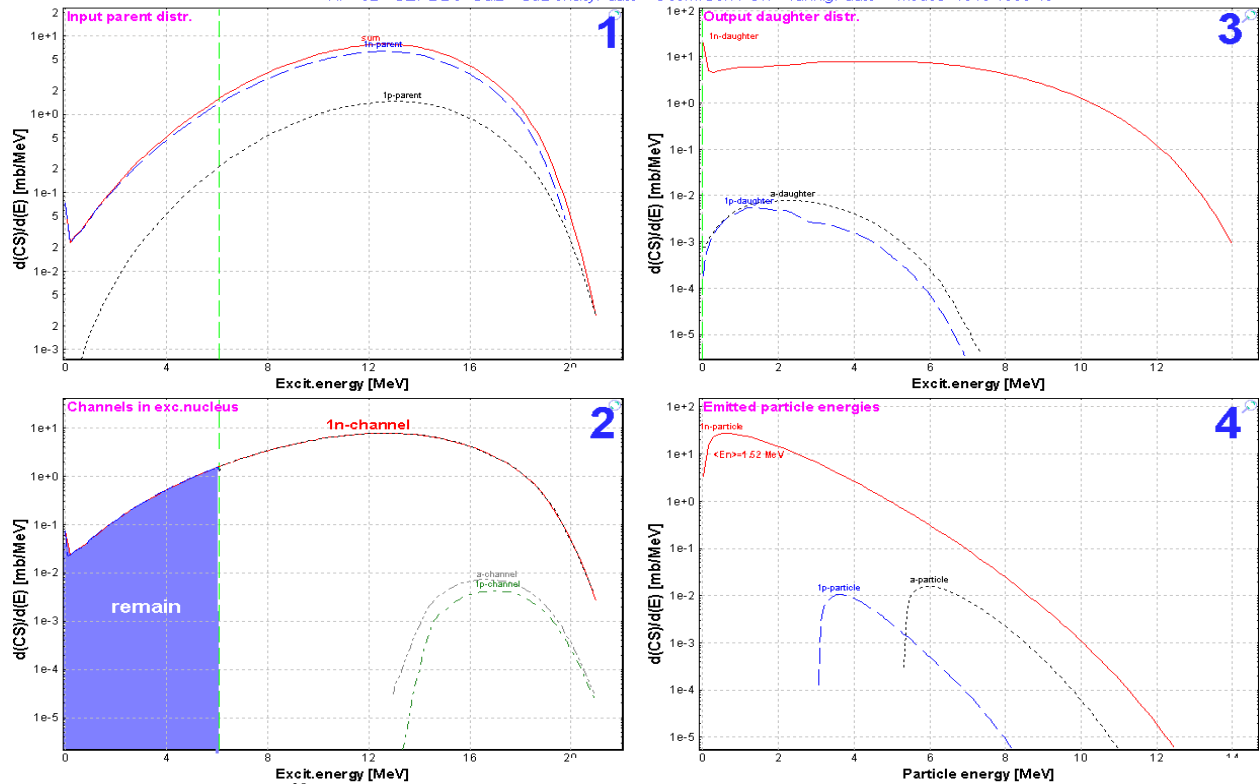


Fig.382.  $^{38}\text{Cl}$  excitation distribution plots created from the Evaporation calculator.

The green vertical lines on the left plots show the minimum separation energy and the minimal sum of separation energy and effective coulomb barrier. If the minimal separation energy is less than zero (in case of proton-rich nuclei or heavy nuclei), then the fission barrier is shown instead of the minimal separation energy.

- The right top plots in Fig.381 and Fig.382 show the excitation energy distributions in daughter nuclei.
- The right bottom plots are also new in the program and show the energy distribution of emitted particles. Using these plots it is possible to estimate the average energy of evaporated neutrons to be compared with experimental result of temperature measurements. The mean values of the average neutron energy are shown in the right bottom plots of Fig.381 and Fig.382.

The areas under the same name distributions in plots 2,3,4 (Fig.381 and Fig.382) are normalized on the one value which determines the cross-section of the evaporation channel.

To estimate the channel widths the code uses the average values of evaporated particles. However to create the daughter excitation energy distributions the code can

A) use the time-consuming qualitative approach using energy distribution of evaporated particles as it has been done for plots Fig.381 and Fig.382, or

B) apply an average energy value of emitted particles as shown in Fig.383. This new option can be applied for the highly excited heavy nuclei to make calculations faster.

It is possible to choose the calculation mode of the daughter excitation energy distribution in the “Evaporation (Prefragment) options dialog” (see Fig.384, “A”).

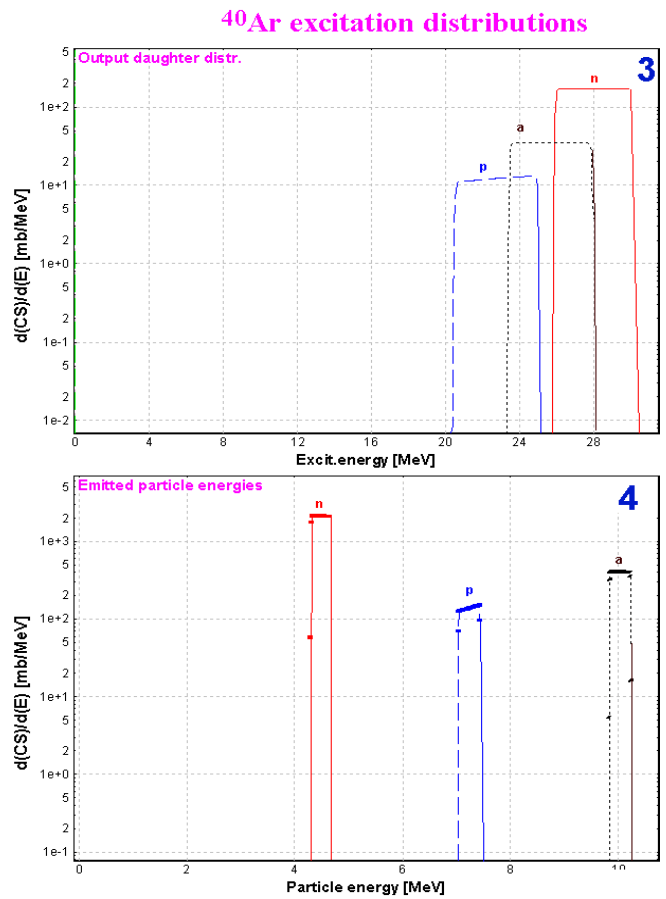


Fig.383. The  $^{40}\text{Ar}$  excitation distributions plots are the same as right plots in Fig.381, but the daughter excitation energy distributions were calculated using the average value of emitted particles.

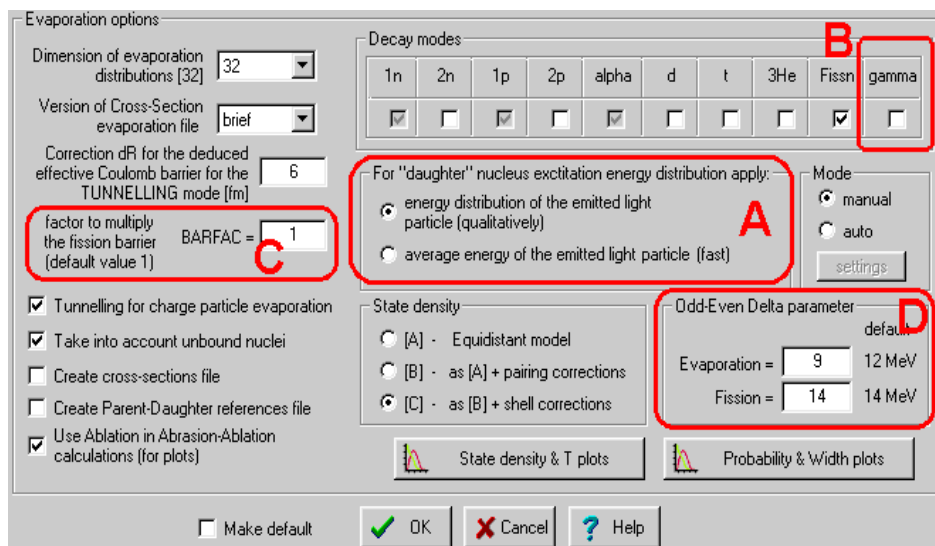


Fig.384. The Evaporation (Prefragment) options dialog

#### 4.4.2. Corrections of low energy region

##### 4.4.2.1. Level density

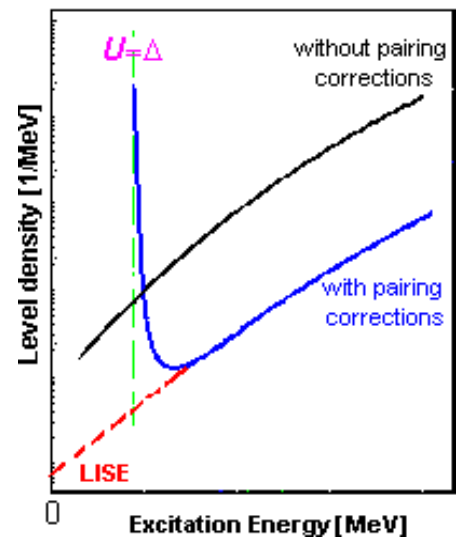
The nuclear level density (non-collective nuclear internal excitations) is described by the Fermi-gas expression [Ilj92]:

$$\rho(U) = \frac{1}{12} \sqrt{\pi} a^{-1/4} (U - \Delta)^{-5/4} \exp$$

where  $a$  is the level density parameter, and  $\Delta$  is the pairing energy. Let's consider the behavior of that expression at small energies (see the blue curve in Fig.385):

- It is invalid for energy  $U < \Delta$ ;
- It has a minimum at  $U_{\min} = \frac{25}{16}a + \Delta$  (assuming that  $a$  is independent from  $U$ );
- It diverges to infinity when  $U$  comes nearer to a point  $\Delta$  ( $U > \Delta$ ).

The pairing energy  $\Delta$  explains the fact that for even-even nuclei the first excited level is relatively high. At lower level density the value  $\Delta$  is assumed to be equal to 0. The levels density is used to calculate the evaporation channel, but in the case of an excitation energy lower than  $\Delta$  it follows from equation /33/ that this channel is closed. Let's consider the case of a particle-unbound nucleus with populated low-energy state (for example  $^{25}\text{O}$  in Fig.386). The neutron evaporation channel from  $^{25}\text{O}$  is closed as the level density of  $^{24}\text{O}$  nucleus is equal to zero for such small excitation energy, and therefore the unbound nucleus becomes artificially particle-bound. It means that the possibility to go in the ground state of the daughter nucleus is missing. To avoid this problem, a linear extrapolation of level densities has been implemented in the code LISE++ from zero up to the energy  $U_B = \frac{3 \cdot 25}{16}a + \Delta$  using the values at points  $U_B$  and  $U_B + 2$  MeV (red curve in Fig.385).



**Fig.385.** Plot of level density versus excitation energy. The blue curve shows the calculation by formula /33/ with pairing corrections. LISE's extrapolation is shown by the red curve.



**Fig.386.** Example of slightly excited particle-unbound nucleus. The left picture shows the restriction of  $n$ -evaporation channel in the case  $\rho=0$  based on expression /33/. On the right picture the level density is not equal to 0 according to LISE's extrapolation, consequently the  $n$ -evaporation channel is allowed.

#### 4.4.2.2. Temperature

The same problems as with the level density at low energies appear in the case of the temperature calculation with the implementation of the pairing correction  $\Delta$ :

$$T(U) = \sqrt{(U - \Delta)/a} \quad /34/.$$

The temperature for an excitation energy lower than  $\Delta$  should be small, but not equal to 0. Experimental data cited in the work [Ilj92] have chosen the criterion  $U - \Delta \geq 2\text{MeV}$ . Keeping the same distance  $s$  (2 MeV) from the value  $\Delta$  it was decided to enter in the code LISE++ a function  $f(U)$  which satisfies the following:

1. the function  $f(U)$  is continuous in the region  $0 \div (\Delta+s)$ ;
2.  $f(0)=0$ , and  $f(U)>0$  for  $U>0$  and  $U<(\Delta+s)$
3.  $f(\Delta+s)=T(\Delta+s)$ , and  $f'(\Delta+s)=T'(\Delta+s)$ ;

A polynomial of second order was chosen as the simplest choice. The polynomial coefficients are determined using the second and third criteria. The resulting temperature dependence from excitation energy is shown in Fig.387.

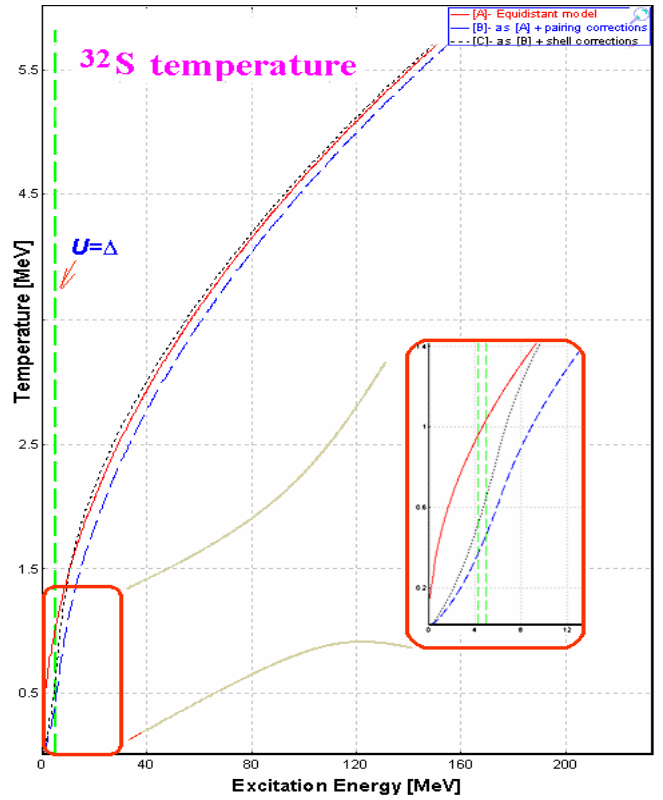


Fig.387.  $^{32}\text{S}$  temperature dependence from excitation energy.

#### 4.4.3. $\gamma$ -channel in evaporation cascade

At first approximation the nucleus angular momentum was neglected and it was assumed that dipole  $E1$ -transitions are the main source of  $\gamma$ -quanta from highly-excited nuclei. In the statistical model for the partial width  $\Gamma_\gamma$  the following expression is used:

$$\Gamma_\gamma(U_L) = \frac{3}{(\pi\hbar c)^2} \frac{1}{\rho_0(U_0)} \int_{U_L}^{U_0} \sigma_\gamma(E) \rho_\gamma(U_0 - E) E^2 dE \quad /35/$$

where  $E$  is the energy of  $\gamma$ -quantum,  $U_0$  is the excitation energy of nucleus,  $\sigma_\gamma(E)$  is the dipole photoabsorption cross-section. The total partial  $\gamma$ -width is used to calculate for  $U_L=0$ . A probability to emit **one**  $\gamma$ -quantum with the remaining excitation energy in the nucleus minus the minimum separation energy  $S_{min}$  in the nucleus can be calculated taking  $U_L$  equal to  $U_0 - S_{min}$ . In other words the  $\Gamma_\gamma(U_0 - S_{min})$  defines the survival cross-section of this excited nucleus. If the  $\gamma$ -channel is switched off and  $U_0 < S_{min}$  the code assumes no more decay (see the left bottom plot in Fig.382). A zero value is used in  $\Gamma_\gamma(0)$  for partial widths calculation in the “Widths plot” in the “Evaporation option (Prefragment)” dialog. The gamma-channel has been implemented in the evaporation cascade in the new version (see Fig.384, fragment “B”). In this mode the low limit  $U_L$  is taken equal to  $U_0 - S_{min}$  for  $\Gamma_\gamma(U_L)$  calculations. It is advised to use this option carefully because the  $\gamma$ -channel assumes an  $E1$ -transition, and rotational and vibrational collective enhancements, as well as angular momentum are not taken into account in the code. Therefore the gamma-channel is turned off by default.

#### 4.4.4. Calculation of temperature in Evaporation calculator

The Evaporation calculator dialog has been modified to show the temperature of the excited nucleus. The average temperature shown in Fig.380 (region 6) is calculated based on the average value of the excitation energy distribution. It is possible to see a small difference between this calculated value and the temperature extracted from the average kinetic energy of neutrons (see the right bottom plots in Fig.381 and Fig.382.). Using the button “Temperatures 2D-plot” (Fig.380, region 7) the user can visualize a temperature map of all nuclei participating in the evaporation cascade (see Fig.388), as well as to compare the temperature map with the cross-section plot (see Fig.389).

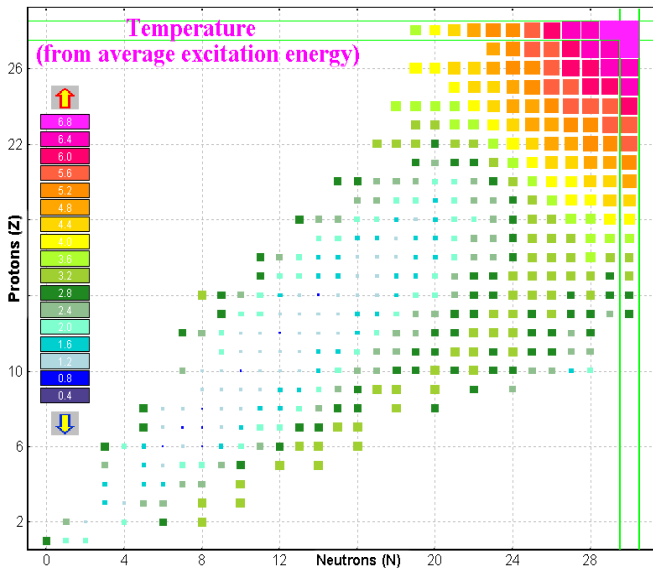


Fig.388. Temperature plot of  $^{58}\text{Ni}$  nucleus deexcitation ( $E_x=400\text{MeV}$ ).

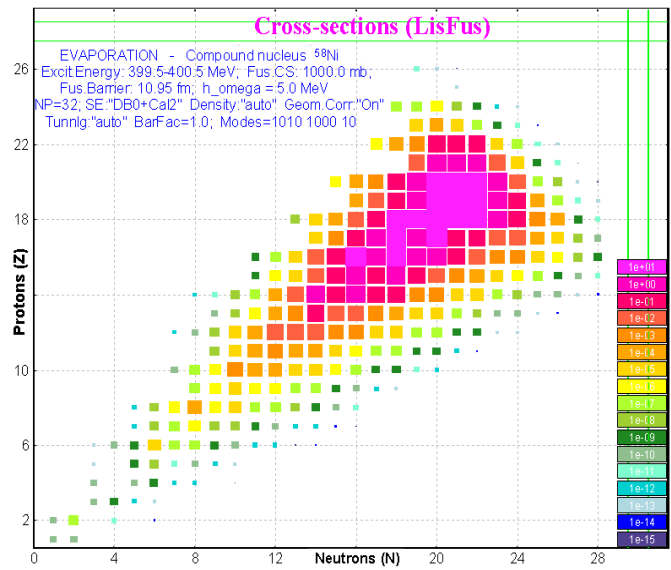


Fig.389. Residues production cross-section plot in the case of excited nucleus  $^{58}\text{Ni}$  ( $E_x=400\text{MeV}$ ).

#### 4.4.5. “BarFac” - fission barrier coefficient

The fission barrier coefficient “BarFac” (By analogy with the program PACE) has been added in the Evaporation option dialog (see Fig.384, fragment “C”). The “BarFac” value is taken as a factor to multiply the fission barrier. The experimental [Oga98] fusion-evaporation cross-sections for reactions  $^{48}\text{Ca}(^{206}\text{Pb},1-3n)$  and  $^{48}\text{Ca}(^{208}\text{Pb},2n)$  and “LisFus” calculations are shown in Fig.390. The “BarFac” value was set to 3.9 (!) in the LisFus calculations to be compared with the  $^{48}\text{Ca}(^{206}\text{Pb},2n)$  experimental data. This emphasizes the necessity to reconsider the fission barrier model in the program.

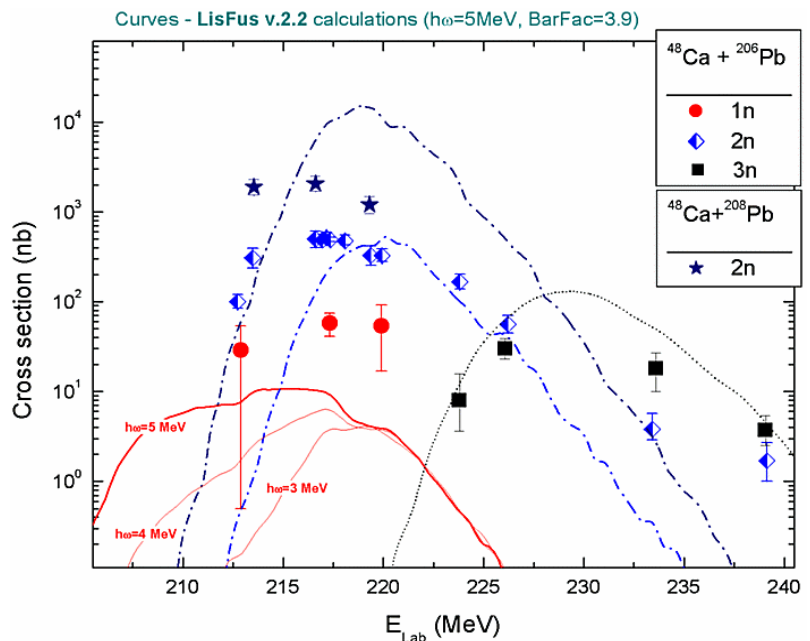


Fig.390. The experimental [Oga98] fusion-evaporation cross-sections for reactions  $^{48}\text{Ca}(^{206}\text{Pb},1-3n)$  and  $^{48}\text{Ca}(^{208}\text{Pb},2n)$ . The curves are showing the “LisFus” calculations used with the settings: BarFac=3.9,  $h\omega=5\text{MeV}$ .

#### 4.4.6. Excitation energy of prefragment

The method “C” of prefragment excitation energy has been modified in the new version in order to TRY to describe the excitation energy distribution proposed by K.-H.Schmidt et al. [Sch02] and shown in Fig.391. The boundary between two regions called “L” and “H” can be built from the atomic number  $Z$  as well as the mass number  $A$  (see Fig.392).

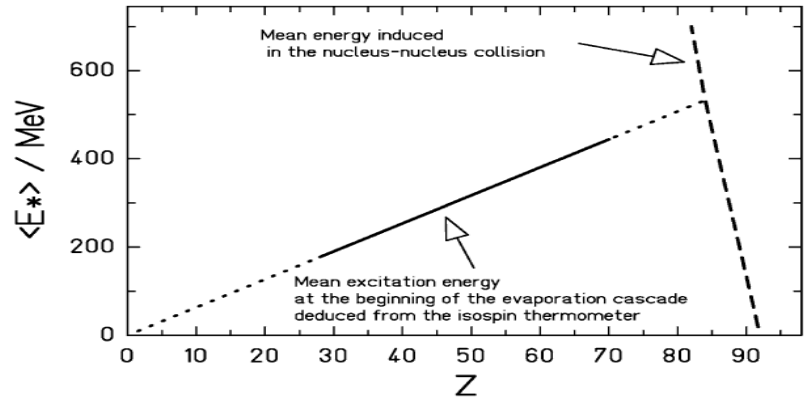


Fig.391. Schematic presentation of the initial energy induced in the abrasion stage and of the mean excitation energy at the beginning of the evaporation cascade after fragmentation of  $^{238}\text{U}$  in a lead target [Sch02].

The mean value and width of excitation energy distributions can be expressed by a second order polynomial. Actually just coefficient of the first order is used then a second order coefficient and a free member are equal to zero in these polynomials.

The plot of temperature versus mass number has been implemented in the code to help choose and set the excitation energy model (see right bottom plot in Fig.393). The modified model “C” of prefragment excitation energy in “L”-region is set to a temperature equal to 3.4 MeV (see Fig.393), that corresponds to an excitation energy  $E_x=1.6 \cdot A$ .

It is possible to turn on/off the LISE corrections for the Geometrical AA model (see fragment “C” in Fig.392). The left bottom plot shows cross-section values versus the prefragment mass with the LISE corrections (red and black curves) and without them (blue curve).

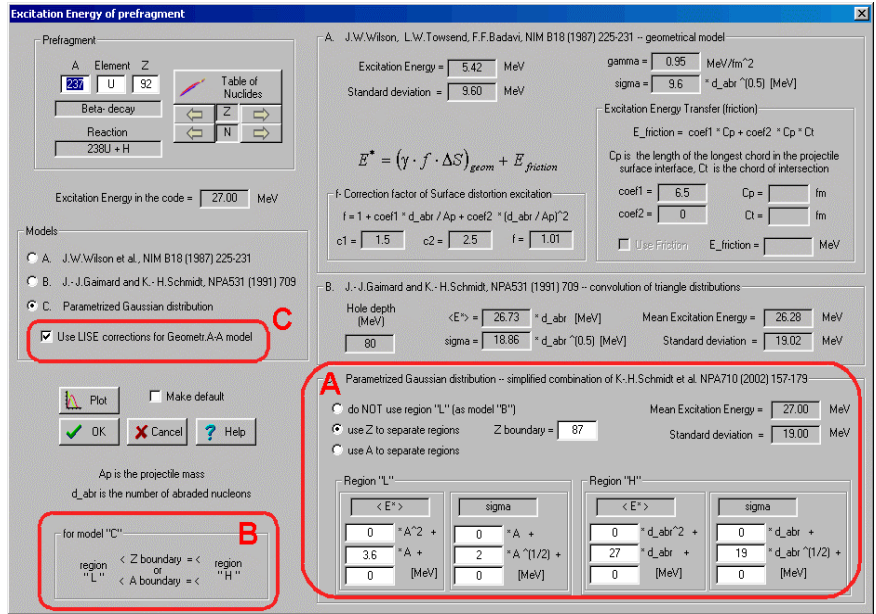


Fig.392. The “Excitation energy of prefragment” dialog.

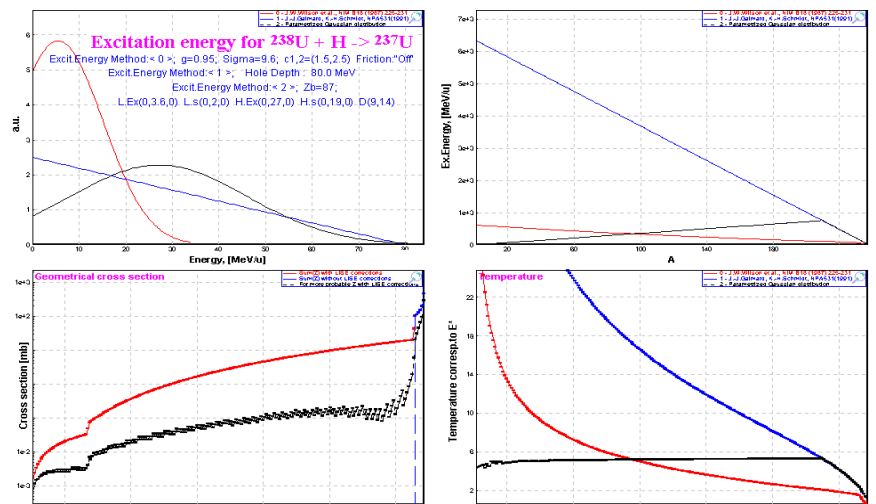


Fig.393. Excitation energy and temperature plots created from the “PREFRAGMENT excitation energy” dialog.

#### 4.4.7. Comparison with experimental data

In order to compare experimental results in LISE++ with calculations it is necessary:

- Save experimental production cross-section values in the CSF (4.3. User's cross-section file).
- Load cross-section values from the User CSF to memory to be used in LISE++.
- Create cross-section plots to see comparison results (*Chi2* or *LoD*) between calculated and experimental cross-sections (see fragment "B" in Fig.379)

It is planned to create a possibility to use a batch-file in LISE++ with different initial settings to fit experimental data. The user can adjust the parameters only manually in this version.

##### 4.4.7.1. <sup>58</sup>Ni+Be

Experimental results from works done in GSI [Bla94] and NSCL [Moc03] (preliminary) were used for analysis. A primary beam of <sup>58</sup>Ni at 650 MeV/nucleon was used to measure production cross-section of proton-rich fragments in GSI, whereas the beam energy in NSCL experiment to study neutron-rich fragments was 140 MeV/nucleon. 152 production cross-section values in the region of atomic number  $Z=10-28$  were analyzed. The minimization of the reduced parameter  $RP=[Chi2+(LoD-0.1)\cdot 2000]$  (for *LoD* definition see 4.3.2. User CS in plots) is used to obtain the AA parameters for this set of experimental data.

The next options and parameters of AA model were kept in analysis:

Dimension of evaporation:	32	Geom. corrections:	yes
Decay Modes:	1n,2n,1p,2p, $\alpha$	BarFac:	1
State density:	C	Masses:	Database1 + LDM2
Take into account unbound nuclei:	Yes	Excitation energy method:	C

##### 4.4.7.1.1. Step 1: Excitation energy

An average excitation energy of 27 MeV per abraded nucleon was used in the work [Bla94] to reproduce the experimental data. Six different values of excitation energy 27, 20, 16.5, 13, 9.5, 7 were used in our analysis. The values  $\sigma$  were searched from the minimum of *RP* value for each of excitation energy value. The minimum of *RP* value is reached for  $\langle E \rangle = 9.5$ , and  $\sigma = 5$  with the excitation energy option "Don't use region "L"".

Excitation energy model "C"		Tunneling	Odd-even shift	Results		
$\langle E \rangle$	$\sigma$	$dR$	$\Delta_0$	<i>Chi2</i>	<i>LoD</i>	<i>RP</i>
<b>27</b>	<b>19.1</b>	Auto	12	1010	0.4997	<b>1809</b>
<b>9.5</b>	<b>5</b>	Auto	12	794	0.4367	<b>1467</b>

Where  $dR$  and  $\Delta_0$  are described in the next chapters.

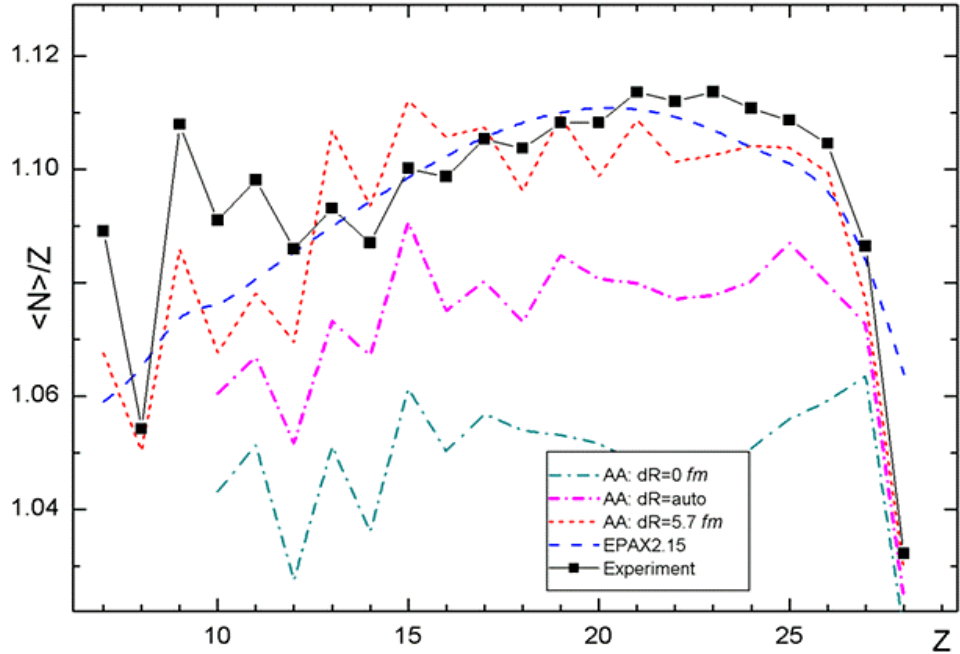
**Conclusion 1:** An average excitation energy is considerably less than it was found in the work [Bla94].



#### 4.4.7.1.2. Step 2: Deduced effective Coulomb barrier

The  $dR$  correction for the deduced effective Coulomb barrier for tunneling model was determined to be equal to 6 fm in work [Ben98]. Increasing the effective barrier (by decreasing  $dR$ ) leads to increasing reduced minimum separation energy for proton-rich isotopes and as a consequence the increase of production cross-section of this fragment. In the first versions of AA-model in LISE it was assumed that  $dR$  correction is equal to 0 for light prefragments. The parameterization for  $dR$ -value was proposed for “AUTO-mode” ([http://groups.nsl.msu.edu/lise/5\\_8/lise\\_5\\_8.html#g1](http://groups.nsl.msu.edu/lise/5_8/lise_5_8.html#g1)).

The large discrepancy (see Fig.394) was noted for proton rich fragments from visual comparison of AA calculations (after the first step) and experimental data what can be corrected by the effective reduced Coulomb barrier. The option “AUTO-mode” was used in the first step to calculate  $dR$  value. This correction calculated by “AUTOmode” is equal to 2.7 in mass region 50. In the second step AUTOmode was switched off, and the correction  $dR$  was set manually.



**Fig.394.** Experimental data neutron-over-proton ratios of heavy fragmentation-evaporation residues produced in the fragmentation of  $^{58}\text{Ni}+\text{Be}$  in comparison with the results of EPAX 2.15 and LISE++ Abrasion-Ablation 5.0 using different values of the correction radius  $dR$ .

Excitation energy model “C”		Tunneling	Odd-even shift	Results		
$\langle E \rangle$	$\sigma$	$dR$	$\Delta_0$	$\text{Chi}2$	$\text{LoD}$	<b><math>RP</math></b>
<b>8.5</b>	<b>4.6</b>	<b>5.75</b>	12	340	0.2887	<b>717</b>

The final fit value  $dR$  is close to results of analysis [Ben98]. It is recommended in the future LISE++ AA calculations to use the fixed value of  $dR$  correction instead “AUTOmode” option. Difference in definition of value  $dR$  between versions v.5.8 and v.6.4 can be explained by the total revision Abrasion-Ablation model done in the latest versions.

**Conclusion 2.** The correction of effective Coulomb barrier is not dependent on mass fragment and its value is found to be equal to about 6 fm, as what determined early in work [Ben98].

#### 4.4.7.1.3. Step 3: Effect of pairing correlations

The resulting washing-out of pairing correlations was parameterized by Ignatyuk et al. [Ign85]. For the differences between odd-odd, odd-mass and even-even nuclei it was proposed a backshift using the pairing gap  $D_0 \approx \Delta_0/\sqrt{A}$ , where  $\Delta_0 = 12 \text{ MeV}$ . It is possible to edit this parameter as well as the shift in the case of fission channel in the new version of LISE++ (see Fig.384, region “D”).

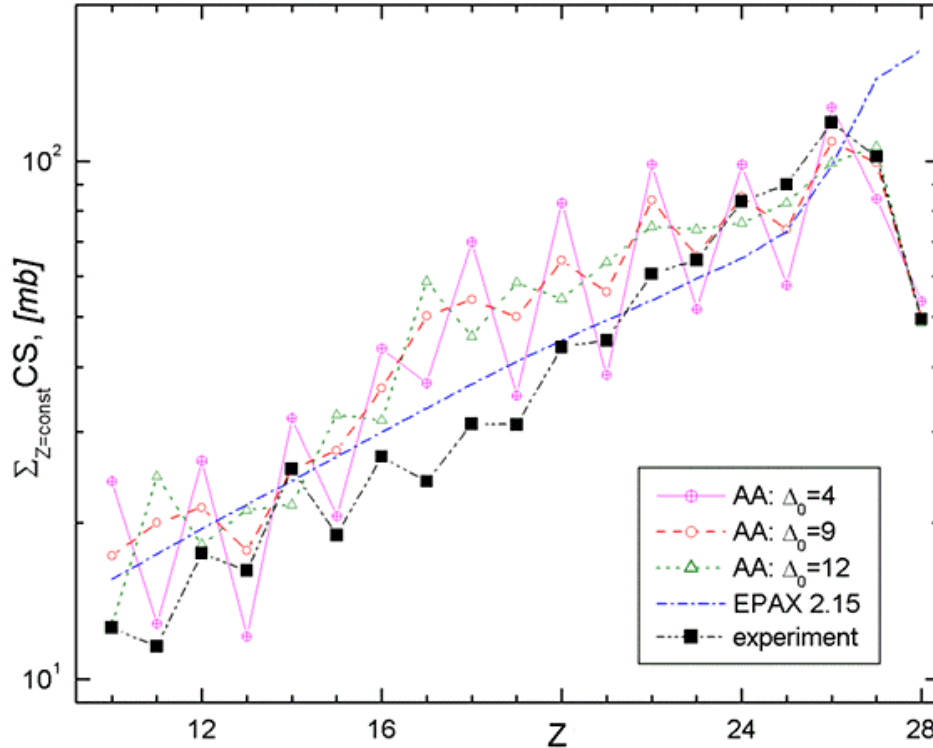


Fig.395. Plot of the value  $f(Z) = \sum_i \sigma(A_i, Z)$  versus the atomic number in the reaction  $^{58}\text{Ni}+\text{Bi}$ .

Abarasion-Ablation calculations were done using different odd-even shift parameter  $\Delta_0$ .

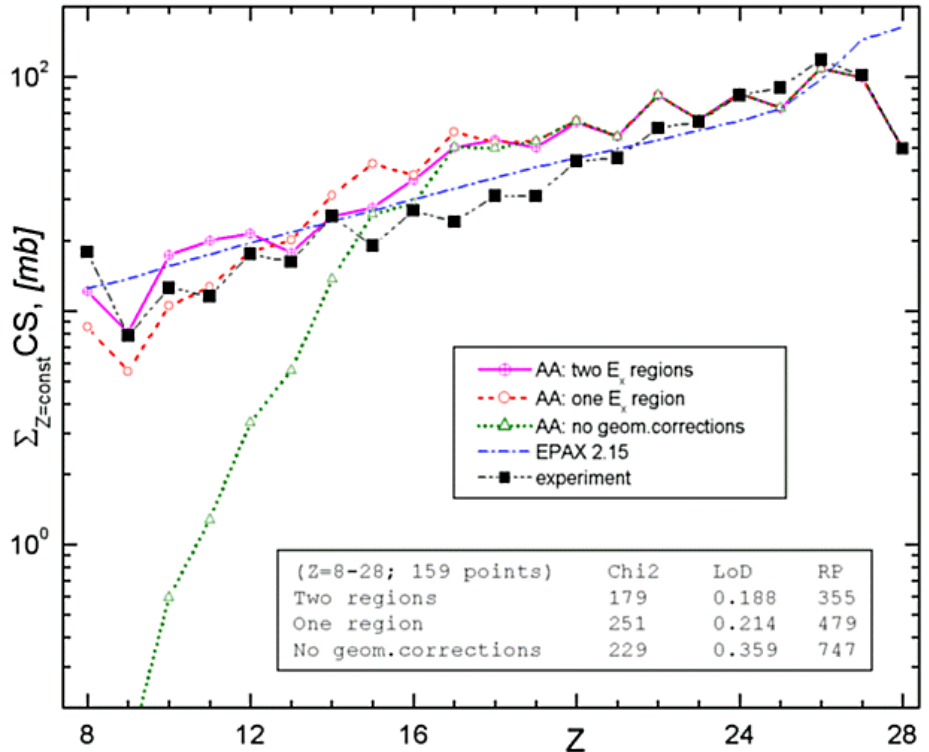
It was noticed from plots that some even elements have output less than their odd neighbors (for example see Fig.395). It is possible to explain by “over”washing-out of pairing correlations. The minimum of *RP* value in the case of odd-even shift  $\Delta_0$  modification has been reached for parameters shown in the following table:

Excitation energy model “C”		Tunneling	Odd-even shift	Results		
$\langle E \rangle$	$\sigma$	<i>DR</i>	$\Delta_0$	<i>Chi2</i>	<i>LoD</i>	<b><i>RP</i></b>
<b>9.0</b>	<b>5.0</b>	5.8	<b>9</b>	212	0.2062	<b>424</b>

**Conclusion 3.** The odd-even shift parameter  $\Delta_0$  should be lower in the fragmentation of  $^{58}\text{Ni}$  on Be-target (see Fig.395) than it was proposed by Ignatyuk [Ign85].

#### 4.4.7.1.4. Step 4: Use of two excitation energy regions

The definition of two excitation energy regions in the first time was given by K.-H.Schmidt et al. [Sch02] for an explanation of the three stage model then the temperature of 5 MeV is reached in the abrasion, and the break-up sets in. In the case of the fragmentation of  $^{58}\text{Ni}$  on Be target after the third step of minimization presented in this work the large discrepancies between experimental results and Abrasion-Ablation calculations are observed in the region  $Z=8\div 12$ . It is necessary to note that the LISE geometrical corrections were applied in the previous steps to avoid a jump (see Fig.396) caused of that a geometrical cross-section of a prefragment with mass 37 and lower in the case of the “light” beryllium target is equal to zero. The same model of two excitation energy regions as shown in Fig.391 was used in the step 4 to improve cross-section calculations of light mass fragments.



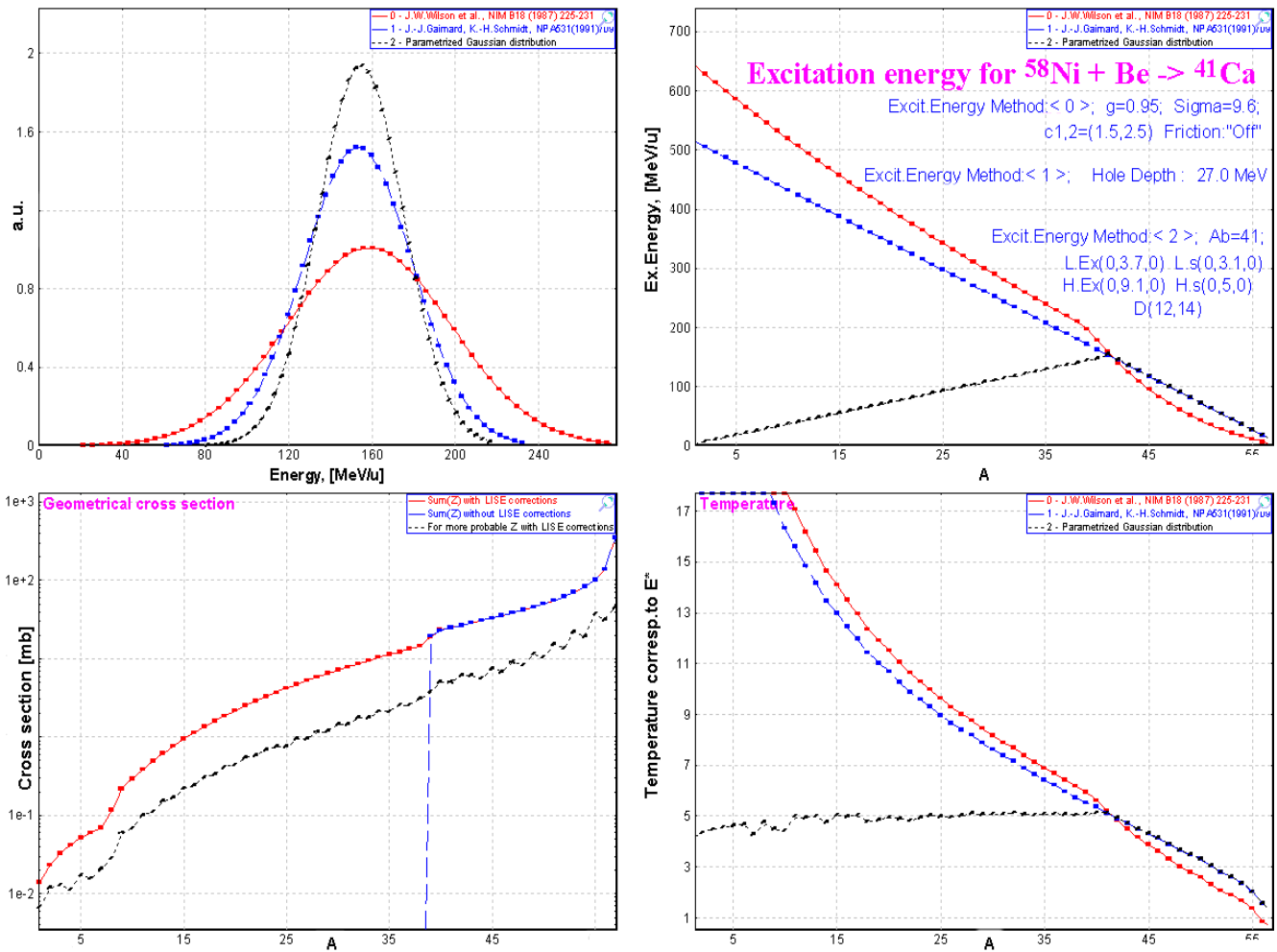
**Fig.396.** The same as Fig.395 but Abrasion-Ablation calculations were done using one-region and two region excitation models. For one-region model calculations were done with and without LISE geometrical corrections for light targets.

The border between two regions was found for prefragment mass equal to 41. The minimization results are the following:

Excitation energy model “C”				Tunneling	shift	Results			
“H” region		“L” region		Ab	$dR$	$\Delta_0$	Chi2 N=152	LoD	RP
$\langle E \rangle$	$\sigma$	$\langle E \rangle$	$\sigma$						
9.1	5.	3.7	3.1	41	5.7	9	176	0.1890	354

**Conclusion 4.** The implementation of the second excitation energy region considerably reduces RP-value and improves a quality of cross-section calculations in the region of light mass fragments.

In this connection it is interesting to see the influence of the two excitation energy regions model in the case of “heavy” target where geometrical corrections are not needed.



**Fig.397.** Excitation energy and temperature plots created from the “Prefragment excitation energy” dialog after the fourth step of minimization with the final settings of excitation energy

Fig.397 demonstrates final excitation energy and temperature distributions obtained as a result of minimization. Two surprising and interesting observations can be taken out from this figure:

1. The temperature in the left excitation energy region is about **5 MeV** (see the right bottom plot in Fig.397) what in K.-H.Schmidt three stage model corresponds to the temperature for the break-up set in.
2. Average values and standard deviations of excitation energy of both regions in the boundary point are approximately equal (see Table 43) though they were modified independently in minimization process!

**Table 43.** Excitation energy values at the boundary point  $A=41$ .

Excitation energy	“L” - region		“H” - region	
Mean value	$\langle E \rangle = 3.7$	$\langle E_{tot} \rangle = \langle E \rangle \cdot A_{pf} = \mathbf{152}$	$\langle E \rangle = 9.1$	$\langle E_{tot} \rangle = \langle E \rangle \cdot A_{abr} = \mathbf{155}$
Standard deviation	$\sigma = 3.1$	$\sigma_{tot} = \sigma \cdot \sqrt{A} = \mathbf{19.9}$	$\sigma = 5.0$	$\sigma_{tot} = \sigma \cdot \sqrt{A_{abr}} = \mathbf{20.6}$

#### 4.4.7.1.5. Results

Minimization results for isotopes and for isotones are given in Table 44. It is possible to see that the principal discrepancy in minimization is observed for isotopes in the rectangle with  $Z=17-19$  and  $N=17-20$ . The sum of  $chi2$  result for these 12 nuclei makes half of total sum of  $chi2$  for 159 nuclei. Nowadays we are not ready to explain this appearance.

Table 44. Final minimization results

Z	Points	Chi2	LoD	RP1
28	8	4.47	0.163	24
27	8	11.9	0.165	38
26	11	2.24	0.117	7
25	10	4.86	0.107	9
24	12	2.72	0.129	10
23	11	7.08	0.144	20
22	14	15.5	0.206	42
21	12	7.77	0.260	47
20	11	27.4	0.375	103
19	6	17.2	0.265	83
18	7	16.2	0.240	69
17	8	27.1	0.336	108
16	6	7.52	0.124	25
15	5	7.76	0.246	58
14	4	0.832	0.092	1
13	4	1.33	0.098	5
12	5	1.81	0.079	1
11	4	9.15	0.181	55
10	4	3.42	0.148	25

N	Points	Chi2	LoD	RP1
30	7	6.31	0.203	32
29	9	3.16	0.200	23
28	9	12.3	0.297	56
27	9	2.7	0.207	24
26	9	2.81	0.138	12
25	9	4.13	0.133	13
24	11	11.1	0.179	29
23	12	12.2	0.220	37
22	11	13	0.172	30
21	11	7.12	0.149	18
20	10	38	0.292	90
19	10	23.1	0.213	54
18	6	16.6	0.279	72
17	5	6.33	0.188	34
16	5	0.342	0.100	1
15	4	2.37	0.126	13
14	4	0.21	0.036	-11

A comparison of experimental data and calculated by EPAX2.15 and LISE ++ AA is given in Fig.398. LISE++ file with final settings and experimental cross-sections (attached file) is located in NSCL web-server: [http://groups.nscl.msu.edu/lise/6\\_4/examples/58ni\\_be.lpp](http://groups.nscl.msu.edu/lise/6_4/examples/58ni_be.lpp)

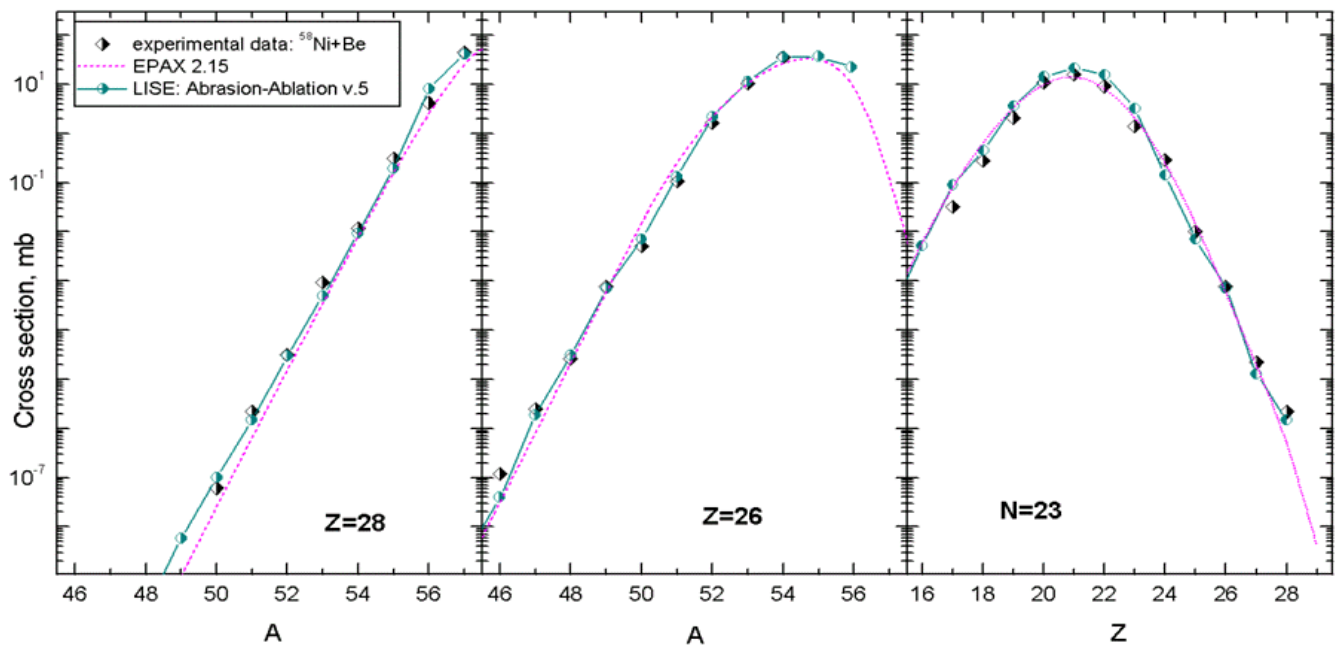
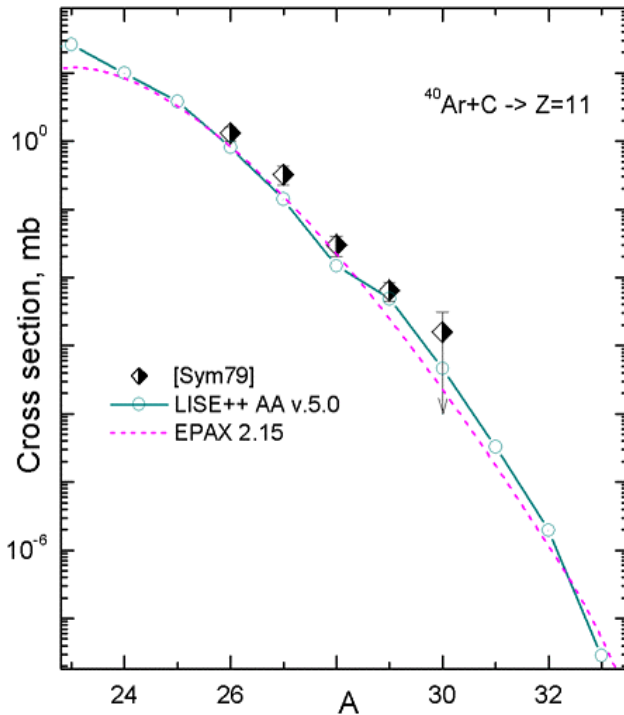


Fig.398. Experimental [Bla94, Moc03] and calculated (EPAX2.15 & LISE++ Abrasion-Ablation v.5) production cross-section of nickel isotopes (left), iron isotopes (middle plot), and isotones  $N=23$  (right plot) in the reaction  $^{58}\text{Ni}+\text{Be}$  (140MeV/u & 650 MeV/u).

#### 4.4.7.2. $^{40}\text{Ar} + \text{Be}, \text{C}$

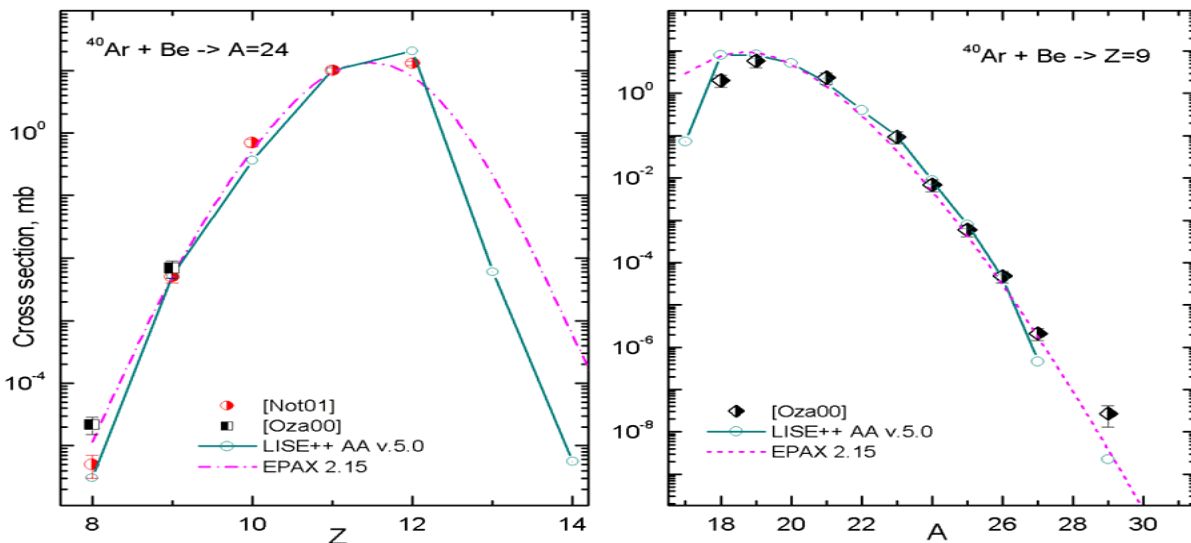
Experimental cross-sections in the fragmentation of a nucleus  $^{40}\text{Ar}$  in different targets [Sym79, Oza00, Not01] were compared with LISE++ AA calculations using the settings obtained in previous chapter for the fragmentation of  $^{58}\text{Ni}$ . Experimental [Sym79] and calculated production cross-sections of sodium isotopes with a carbon target are shown Fig.399. Experimental production cross-sections of isobars  $A=24$  and fluorine isotopes in the reaction  $^{40}\text{Ar}$  (1GeV/u) + Be [Oza00] and  $^{40}\text{Ar}$  (90MeV/u) + Be [Not01] are shown in Fig.400.

Due to the small number of published data points, it is difficult to carry out a comprehensive analysis in the case of the fragmentation of  $^{40}\text{Ar}$ . Instead the AA settings obtained for the case of the fragmentation of  $^{58}\text{Ni}$  are used and the calculation well describe the experimental data as shown in Fig.399 and Fig.400:



**Fig.399.** Experimental [Sym79] and calculated (EPAX2.15 & LISE++ Abrasion-Ablation v.5.) production cross-section of sodium isotopes in the reaction  $^{40}\text{Ar} + \text{C}$  (205 MeV/u).

Ex. energy model "C"		Tunl.	shift	modes	Results		
$\langle E \rangle$	$\sigma$	$\Delta_0$	$dR$		$N$	$\text{Chi}2$	$\text{LoD}$
9.1	5.0	9	5.6	n,p,2p, $\alpha$	18	25.4	0.3062



**Fig.400.** Experimental [Oza00, Not01] and calculated (EPAX2.15 & LISE++ Abrasion-Ablation v.5.) production cross-section of isobars  $A=24$  (left plot), and fluorine isotopes (right plot) in the reaction  $^{40}\text{Ar} + \text{Be}$ .

### 4.4.7.3. Other experimental data

Analysis of some experimental data with AA calculations is still in progress. Experimental data [Tai03] and calculated (EPAX2.15 & LISE++ Abrasion-Ablation v.5) production cross-section of uranium isotopes in the spallation reaction  $^{238}\text{U} + p$  at 1 AGeV are shown in Fig.401. Plots in Fig.401 demonstrate the influence of “hole energy” (Excitation energy method “B”) and “BarFac” values on production cross-sections.

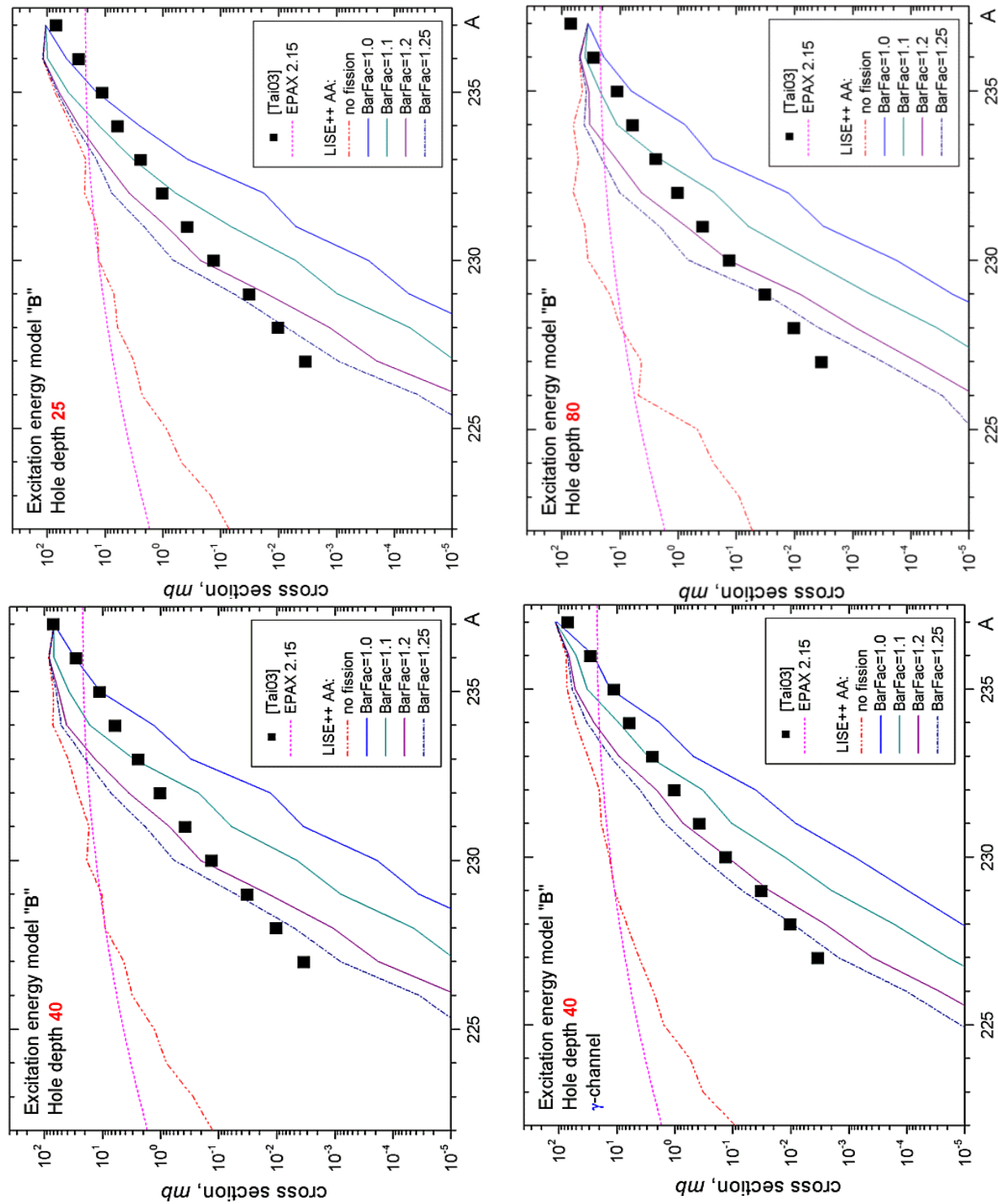


Fig.401. Experimental [Tai03] and calculated (EPAX2.15 & LISE++ Abrasion-Ablation v.5) production cross-section of uranium isotopes in the spallation reaction  $^{238}\text{U} + p$  at 1 AGeV.

The model settings applied for calculations in Fig.401 are listed below:

Ex. energy model “B” <i>Hole depth</i>	NP Dimension	Tunl $\Delta_0$	Shift <i>dR</i>	Modes	Density
25,40,80	64	12	5.7	n,p, $\alpha$ ,fission	“C”

From comparison with experimental data it is possible to make conclusion about necessary updating of the fission barrier depending on the angular moment of a nucleus [Jon97].

Some experimental data applied in LISE++ AA analysis can be found in the directory “CrossSections\PublishedData”. Most of these data was ported from the personal site of Dr.K.-H.Schmidt (<http://www-w2k.gsi.de/kschmidt/data.htm>).

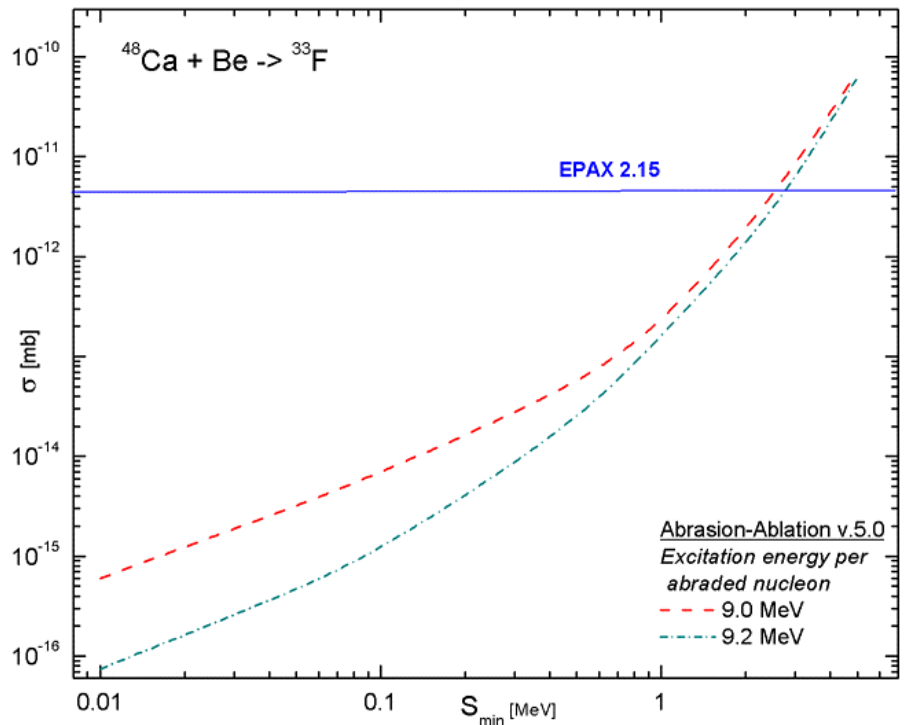
Contents of the directory “CrossSections\PublishedData”:

40Ar_Be_1AGeV.cs	[Oza00]	40Ar_C_240AMeV.cs	[Sym79]
58ni_be_650AMeV.cs	[Bla94]	129Xe_Al_790AMeV.cs	[Rei98]
136Xe_Al_760AMeV.cs	[Zei92]	238U_Pb_1AGeV_fragmentation.cs	[Enq99]
238U_p_spallation.cs	[Tai03]	238U_Pb_1AGeV_fission.cs	[Enq99]
<i>It is planned to add</i>			
<sup>208</sup> Pb (1GeV/u) +Cu	[Jon98]	<sup>36</sup> S (75MeV/u) +Be, Ta	[Tar97]
<sup>197</sup> Au (950MeV/u) +Be	[Ben99]		

#### 4.4.8. Cross-section & minimum separation energy dependence

A model to relate the experimental cross-sections to neutron separation energies for nuclei far from stability has been proposed by W.A.Friedman and M.B.Tsang [Fri03]. The procedure is based on determining cross section production of nuclei by projectile fragmentation. An Abrasion-Ablation analysis leads to a cross section prediction which is sensitive to the neutron separation energy. LISE++ can be used for such kind of purposes. Moreover it would be desirable to note a number of LISE++ features for this analysis:

- Possibility quickly to change a mass excess of a nucleus in the mode “UME file” using the “Databases” dialog (see Fig.375)
- Fast analytical LISE++ Abrasion-Ablation model which is “transparent” for the user.



**Fig.402.** The predicted cross-sections to produce a nucleus <sup>33</sup>F from fragmentation of <sup>48</sup>Ca with Be target as a function of the separation energy for <sup>33</sup>F nucleus. LISE++ AA settings for the fragmentation of <sup>58</sup>Ni with Be target (chapter 4.4.7.1.) were used to predict cross-sections.



- The built-in database of measured masses [A&W95].

The predicted cross-sections to produce a nucleus  $^{33}\text{F}$  from fragmentation of  $^{48}\text{Ca}$  with Be target as a function of the separation energy for  $^{33}\text{F}$  nucleus are shown in Fig.402. LISE++ AA settings for the fragmentation of  $^{58}\text{Ni}$  with Be target (chapter 4.4.7.1.) were used to predict cross-sections. The dimension ( $NP$ ) of evaporation distributions was equal to 64, and just one excitation energy region was used in this analysis.

☞ It is necessary to remember that the accuracy of separation energy estimation depends from accuracy of mass measurement of neighbor nuclei used in calculations. It is recommended to use the dimension of evaporation distributions more than 32. For small separation energy the quality of estimation depends very much from LISE++ AA settings (see the energy region 0.01÷0.3 MeV in Fig.402).

#### 4.4.9. Three step Abrasion-Ablation model

LISE++ Abrasion-Ablation model uses excitation energy models which can not reproduce the following experimental facts:

- Difference between production cross-sections with different target at intermediate energies. Production cross-sections for neutron-rich isotopes for the primary beam at energies 50-200 MeV/u [Tar97] with heavy targets are larger than with light targets.
- Production cross-section dependence from the primary beam energy. With increase of primary beam energy from 50 MeV/u [Tar98] to relativistic energies the neutron-rich production cross-sections decrease.

These observations can be explained by an assumption that the excitation energy in the case of heavy targets and low incident energies is lower than the excitation energy in the case of light targets and high incident energies. The release of excitation energy is larger with an increase of the abrasion time. The abrasion time is proportional to the velocity of fragment and the target size.

In this connection it is suggested to implement three step Abrasion-Ablation in LISE++ where the release of excitation energy is calculated in the intermediate step.

Three step fragmentation model has already been successfully applied to the description of momentum distributions by the Universal parameterization in LISE++ ([http://groups.nscl.msu.edu/lise/doc/universal\\_param.ppt](http://groups.nscl.msu.edu/lise/doc/universal_param.ppt)). It was assumed that between abrasion and ablation an intermediate step “**friction**” exists due to kinetic energy loss, exchange of nucleons, and transformation into the internal degrees of freedom. The exponential attenuation is implemented to momentum distribution of fragments due to friction.

## 4.5. Other

### 4.5.1. Drift block in the Beam analyzer dialog

The possibility to insert a drift block after a dipole has been added in the dialog “Brho analyzer” (see Fig.403,404).

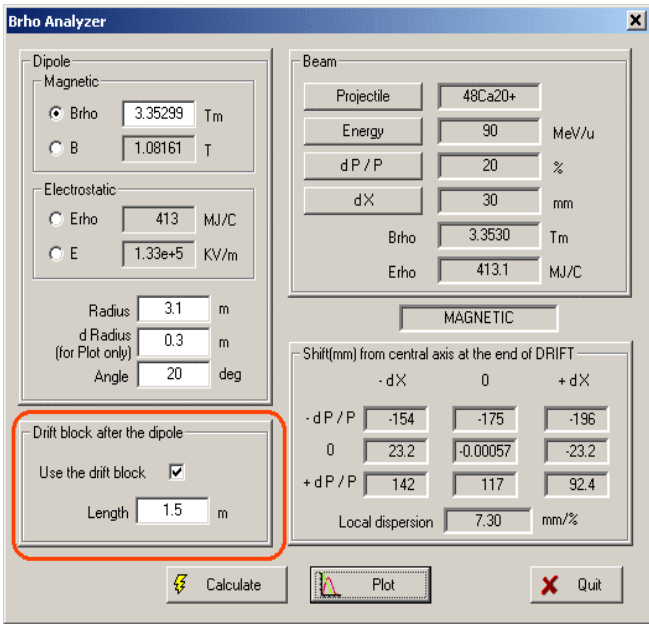


Fig.403. The “Brho analyzer” dialog

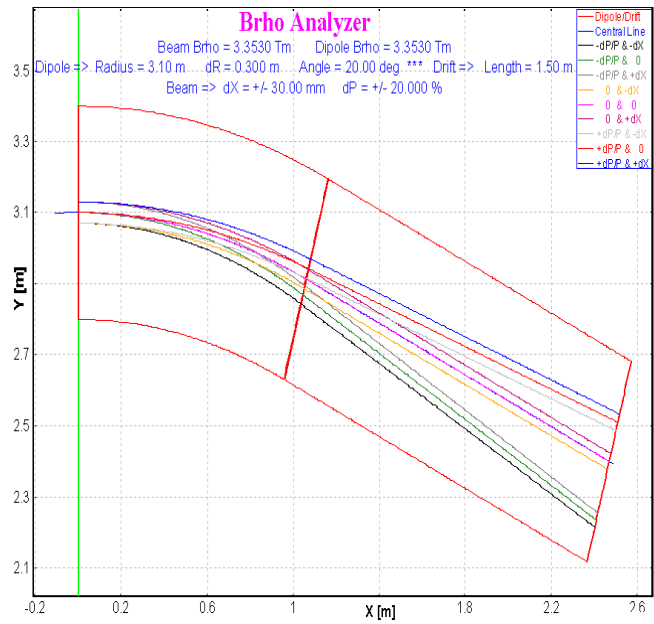


Fig.404. “Brho analyzer” plot with the drift option on.

#### 4.5.2. New options for cross-section plot

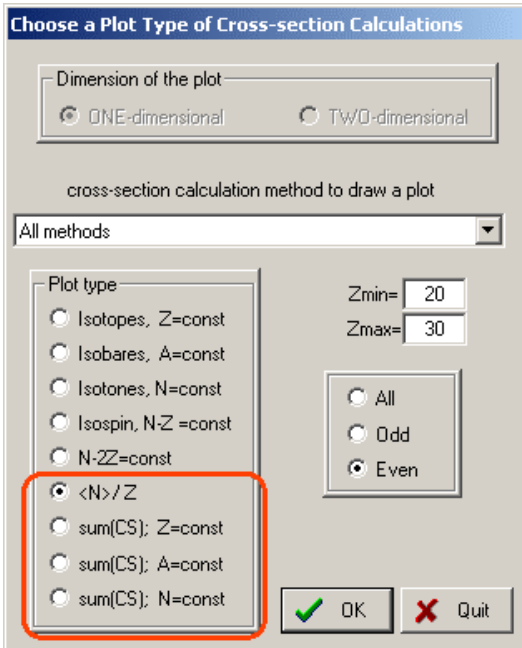


Fig.405. The cross-sections plot dialog with new options marked by the red rectangle.

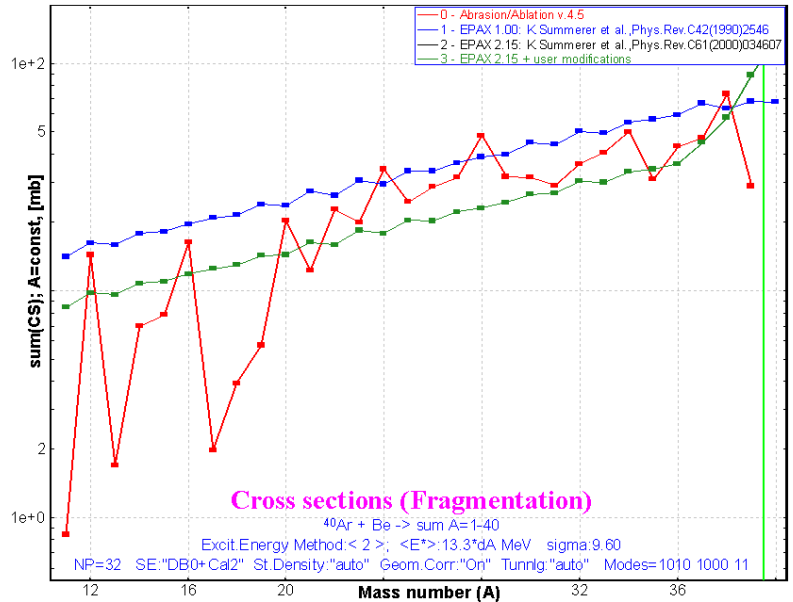


Fig.406. Example of “ $sum(CS_A)$ ” cross-section plot in the reaction  $^{40}\text{Ar} + \text{Be}$ .

Four new options to create cross-section plots have been added in LISE++ (see Fig.405 and Fig.406).

#### 4.5.3. Writing files from the “Statistics” windows

There are two available “statistics” window in LISE++: the first one is the window of transmissions of fragment when the user clicks the right button of the mouse on an isotope in the table of nuclides, and the second can be created from a one-dimensional plot using the icon to show the statistical parameters of

distributions. The new version allows users to write the contents of these windows into a file by clicking on the button “File Save”.

#### 4.5.4. PACE4 modifications

##### 4.5.4.1. Number of cascades

The maximum number of cascades has been increased to 1 million. The previous limit was due to short integers (< 32768) used in the file “PACE4.evt”. This limit was removed using integer (4 words) format. Increasing the number of cascades increases not only the calculation speed, but also memory allocated for the “event” array (65 MB in the case of one million cascades), as well as the size of the working file (for example, the size of this file is about 635 MB (!!!) in the case of one million cascades for the reaction  $^{48}\text{Ca}+^{124}\text{Sn}$  with a primary beam energy at  $E_{lab}=200\text{ MeV}$ ). If the fusion cross-section is 1 barn, using 1 million of cascades it is possible to reach the 1 nb limit.

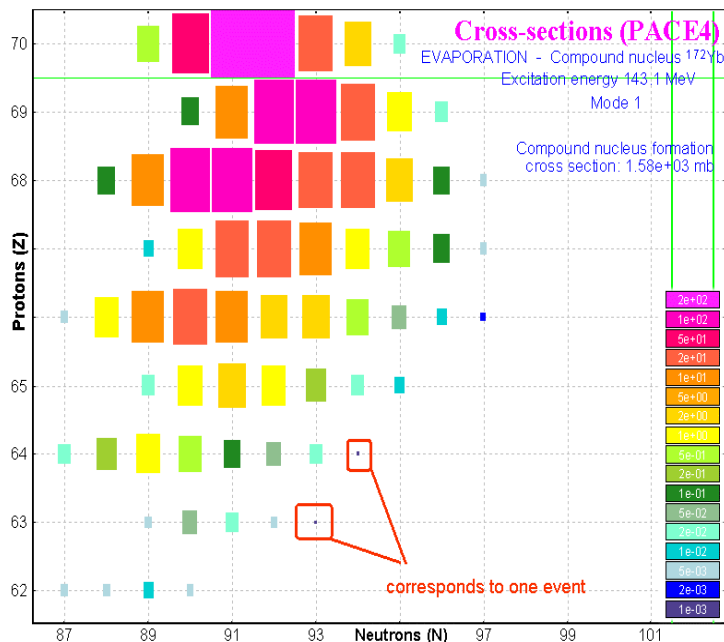


Fig.407. PACE4 calculations (1 million of cascades) for the reaction  $^{48}\text{Ca}(200\text{MeV})+^{124}\text{Sn}$ .

##### 4.5.4.2. BarFac modifications

The “BarFac” parameter determinates the fission barrier characteristics and can be modified in the first dialog of the code PACE4. The program assumes the A.J.Sierk modified rotating liquid drop barrier if the atomic number of the compound is one of these values: 68,76,84. For other atomic number of the compound the code uses a rotating liquid drop fission barrier from the work [Coh63].

- If BarFac is positive the value will be taken as a spin for the desired zero spin fission barrier.
- If BarFac is negative, its absolute value will be taken as a factor to the fission barrier.

It is planned to implement in the code PACE4 (as well as in LISE++) a new model of fission barrier which allows to calculate more correctly the fission barrier, in particular for compound nuclei heavier than uranium.

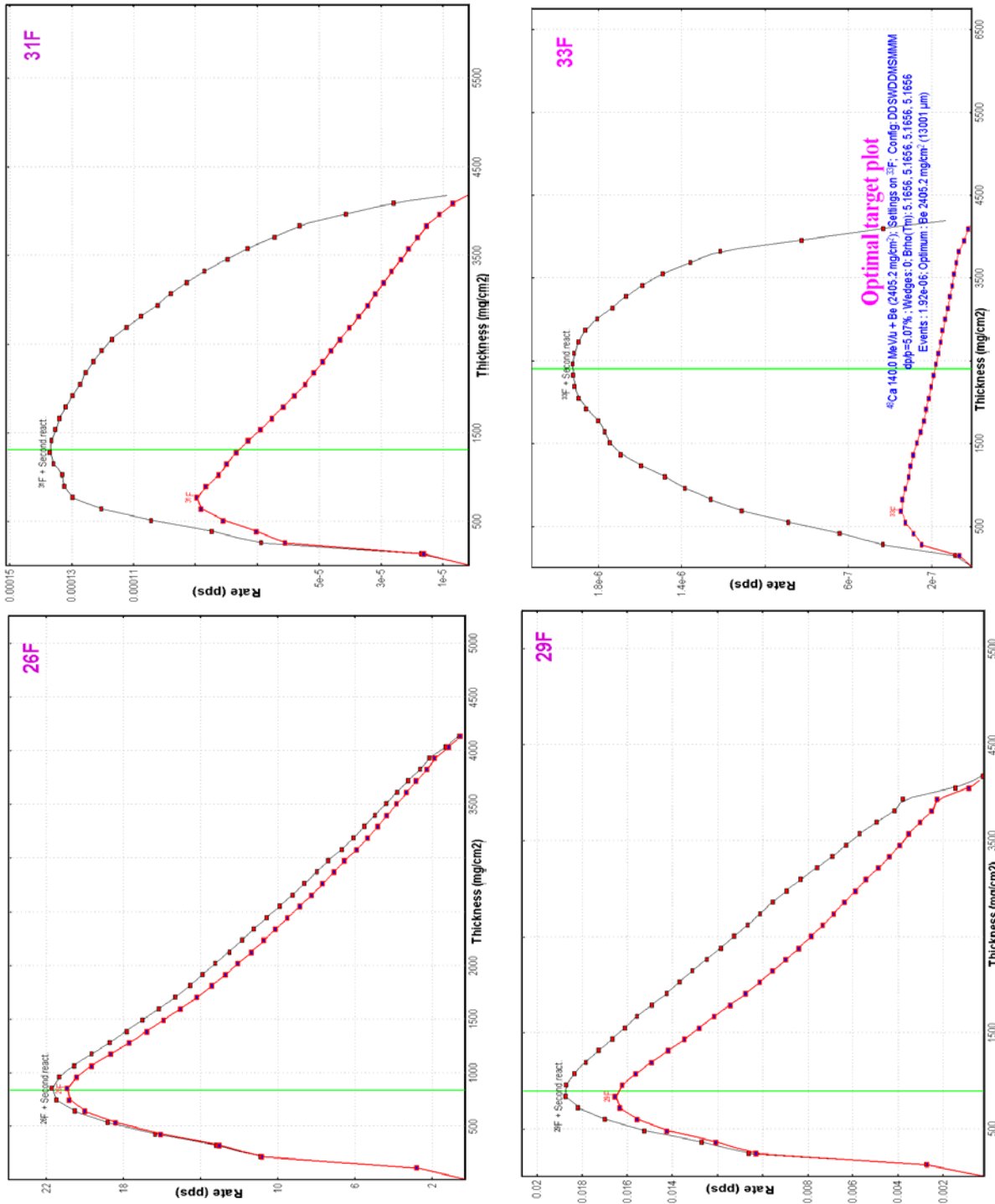
##### 4.5.4.3. Cross-section file

The format of PACE4 cross-section files has been changed. The new extension of PACE4 is “\*.cs4”, whereas for all User CSF the extension is “\*.cs”. PACE4 CSF is saved by default in the directory “LISE\CrossSections”. In the previous versions cross-sections were saved in the same directory where the PACE4 input file was located.

##### 4.5.5. Secondary reactions (in target) corrections



The procedure to calculate the contribution from secondary reactions in the target into the final counting rate of fragments has been revised. As marked earlier in the LISE documentation the contribution of sec-

ondary reactions is reasonable for energies above 500 MeV/u. These estimations were made for  $^{28}\text{O}$  and  $^{29}\text{F}$ . However, for more neutron-rich isotopes, it is possible to get considerable fields from secondary reactions at much lower energies as for example 140 MeV per nucleon shown in Fig.408. For example, a factor 2 can be gained for the particle bound  $^{31}\text{F}$  isotope (see Fig.408).



**Fig.408.** Optimal target thickness calculation plots for the fluorine neutron-rich isotopes  $^{26,29,31,33}\text{F}$  in the reaction  $^{48}\text{Ca}(140\text{MeV/u}, 1\text{pnA})+\text{Be}$  using the A1900 fragment separator. The black top curves represent the rates of fragment of interest taking into account secondary reactions in the target, the red bottom curves without contribution of secondary reactions. Calculations were done using the EPAX 2.15 parameterization.

#### 4.5.6. Configuration files

RIKEN	RIPS.lcn (T.Kubo)	corrected
NSCL	A1900-N4-gas_cell.lcn (D.Morrissey)	corrected
	A1900 – 4 dipoles.lcn	The same as A1900_PAC27.lcn
	BL+S800_d0.lcn (former S800_d0.lcn) BL+S800_dm.lcn (former S800_dm.lcn)	
	New configuration: S800.lcn	

#### 4.5.7. Bug report

<i>Two-dimensional “ellipse” plot</i> L.Sobotka (WU)	Shift of fragment peak position in the case of “ellipse” drawing mode for two-dimensional plots. <i>Fixed.</i>
<i>LISE’s file reading</i> K.Starosta (NSCL)	Wrong reading of slit parameters if the slit had different left and right positions. <i>Fixed.</i>
<i>Fusion cross-section calculations in versions 6.3.15-21</i> P.Sugathan (NSC, New Delhi)	The code crashed in fusion-residue mode in the process of residue transmission calculation. It happened due to a recent change of reaction order. <i>Fixed.</i>
<i>Slit &amp; Acceptance settings dialog</i> M.Hausmann (LANL)	The code didn’t restore previous settings and kept changed values then the button “Cancel” was pressed. <i>Fixed.</i>
<i>Fragment energy after reaction and Width of momentum distributions at relativistic energies</i> H.Weik (GSI)	This is a serious problem for relativistic energies, which was not taken into account before for intermediate energies. Calculated fragment momentum distribution is narrower than actually should be. <i>Fixed.</i> <i>In connection to this bug all calculations done by the previous versions will be repeated at loading.</i>
<i>Secondary reactions (in target) corrections</i>	See chapter 4.5.5. Secondary reactions (in target) corrections.

*All user’s remarks, wishes are welcome!*

#### Acknowledgements

The authors gratefully acknowledge Dr.H.Weik and Prof.M.Tsang for help with the development of LISE++.

## 5. Version 6.3

### 5.1. Charge states calculations

#### 5.1.1. "GLOBAL" (charge states calculations)

GLOBAL is a program to calculate ionic charge-state distributions of projectiles traversing solid and gaseous targets. The program was developed for the interaction of projectiles having a nuclear charge larger than 28 with any target. Details of the underlying physics as well as of a comparison between experiment and predictions by GLOBAL can be found in [Sch98]. The main advantages of the code comparing with the "Charge" code for example appear the next features:

- possibilities to calculate charge states up to 28;
- take into account energy loss of incoming particle in matter.

In the following, a short description of the program as well as of the underlying physics is given in <http://www-aix.gsi.de/~scheid/GLOBAL.readme.html>. Some fragments of this file are given below.

The different parameters are:

- For the projectile: The nuclear charge  $Z$ , the mass number  $A$ , the number of orbital electrons  $Q_e$ , and the incident energy  $E/A$ .
- For the target: The nuclear charge  $Z$ , the mass number  $A$ , and the target thickness  $D$ .
- Projectile  $Z$  and target  $Z$  can be given using the element symbol.

The program proposes for each change of either the charge  $Z$  or the mass  $A$  a new values for the respective other parameter. The projectile mass number  $A$  determines only the energy loss and should be in reasonable limits with respect to the nuclear charge  $Z$ . The charge state  $Q_e$  is limited to  $Q_e = 0 \div 28$ . This includes K, L, and M shells.

The energy can vary between 30 MeV/u and 2000 MeV/u. The low-energy limit is defined by the applicability of the atomic cross-section calculations, whereas the high-energy limit is due to the energy-loss relations. If, during the calculations, the program reaches the low-energy limit, it stops. The target charge and mass can be changed between  $Z=1$  and  $Z=96$  with the respective mass numbers. The thickness is limited by the number of integration steps possible ( $1.e9$ ), i.e. the maximum allowed target thickness depends on the target material, but is of the order of  $100\text{g/cm}^2$ .

There are three different basic output options:




1. The charge state distribution of a projectile as defined by the projectile parameters at the exit of the target.
2. The charge state distribution of the projectile after having reached the equilibrium charge-state distribution.
3. The user can follow the charge-state evolution of the projectile throughout the target.

In order to facilitate comparison for different projectiles, incident energies, numbers of incident orbital electrons, targets, or target thicknesses, one can use loops over these different parameters. In this case, the

user can specify the range of the scan. For the incident energy and the target thickness, the program takes the value from the menu as the maximum loop value. For the projectiles and targets, all elements up to  $Z=96$  can be scanned, one for the incident number of orbital electrons values of up to 28 are possible. For the basic option of charge-state evolution, the user can influence the amount of adata output (Frequency of Output) by choosing an output after ten integration steps, after hundred, thousand, or ten thousand integration steps. During the integration through the target, the program takes into account the energy loss of the projectile in the target material.

### 5.1.1.1. "GLOBAL" for "Windows"

The code "Global" has been translated in C++ and is now part of the "LISE++" package. The original source code (FORTRAN) was kindly provided by colleagues from GSI. The dynamical library "LISE\_Global.dll" contains charge state calculations which can be used in different applications such as the LISE code or MS Excel. This library is found in the windows\system32 directory.

The "Global" code (executable version for Windows) can be loaded by clicking the icon  in the toolbar or in the menu "Utilities". The program can also be loaded from LISE's folder using the Start → Programs on the desktop menu. The program interface window is shown in Fig.409. The calculation results are saved by default in the file "untitled.goutput". The user can save he input data to a file  (extension of input file is "ginput"). The result file gets the same name as the input file with the extension "goutput". The results can be printed immediately from the code .

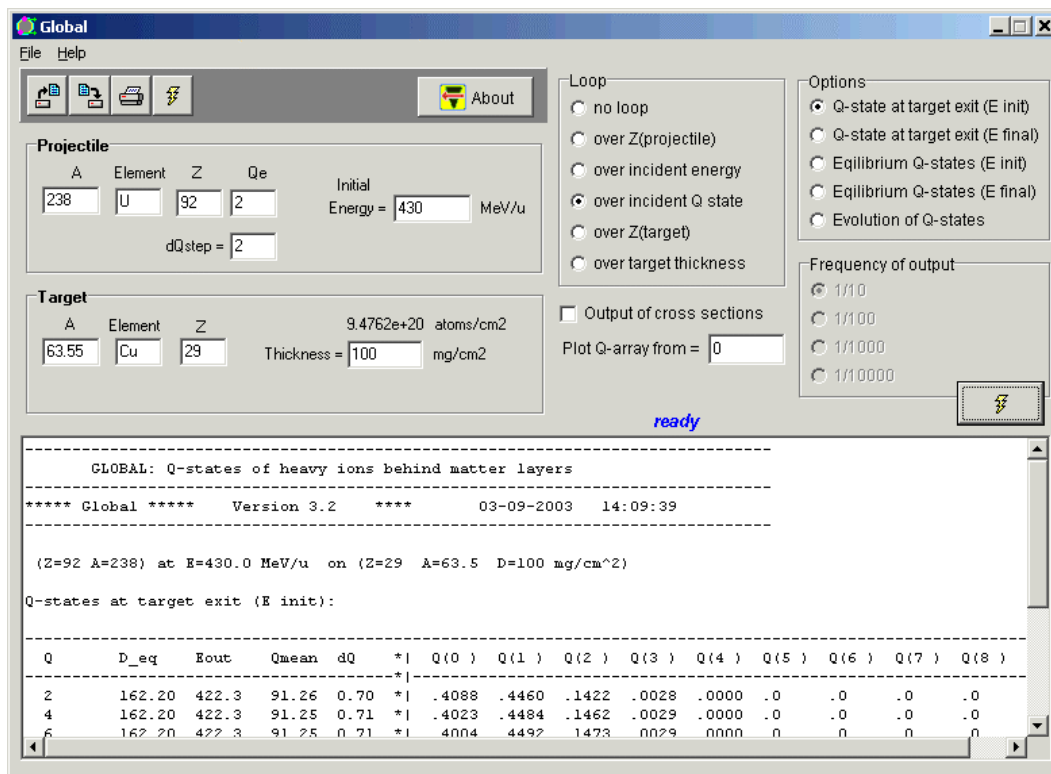


Fig.409. The "Global" code (version for MS Windows) in action.

The C++ code has preserved the features of the original version and added some new possibilities which are presented in chapter 5.1.1.4.

### 5.1.1.2. Use of GLOBAL's calculations in LISE++

The new version of LISE++ uses Global's subroutines on the fragment transmission calculations with some restrictions connected with the low energy limit (30 MeV/u) of Global's calculations. Two new methods of charge states calculations have been implemented in LISE++. The first one (number 3 in LISE's charge state calculation method) uses Winger's calculations for the low energy region, and Global's calculations for the energy region above the upper boundary (UP). The upper boundary default value is 70 MeV/u. The user can change the UP value via the "Production mechanism" dialog (see Fig.410). The possible values of UB are in the energy range 35-100 MeV/u. In the intermediate energy interval 30-UB MeV/u the charge states are calculated using a linear combination of both methods proportionally to energy to insure a smooth transition between the two calculations:

$$P(Q_i) = \sum_{k=1}^2 P_k(Q_i) \cdot W_k, \text{ where } W_1 = \frac{UP - E}{UP - 30} \text{ and } W_2 = \frac{E - 30}{UP - 30}, \quad /36/$$

where  $E$  is the projectile energy after the material in MeV/u, the index 1 corresponds to the low energy method (Winger), and the index 2 to Global. Another new method (number 4 in LISE++) uses Leon's method for low energy calculations instead of Winger's.

There is also a low limit for the atomic number of the fragment in Global's calculations. If the atomic number of the fragment is lower than this limit (default value of Z-limit is 29) then the low energy method (Winger's or Leon's) will be used instead of Global to calculate the Q-states.

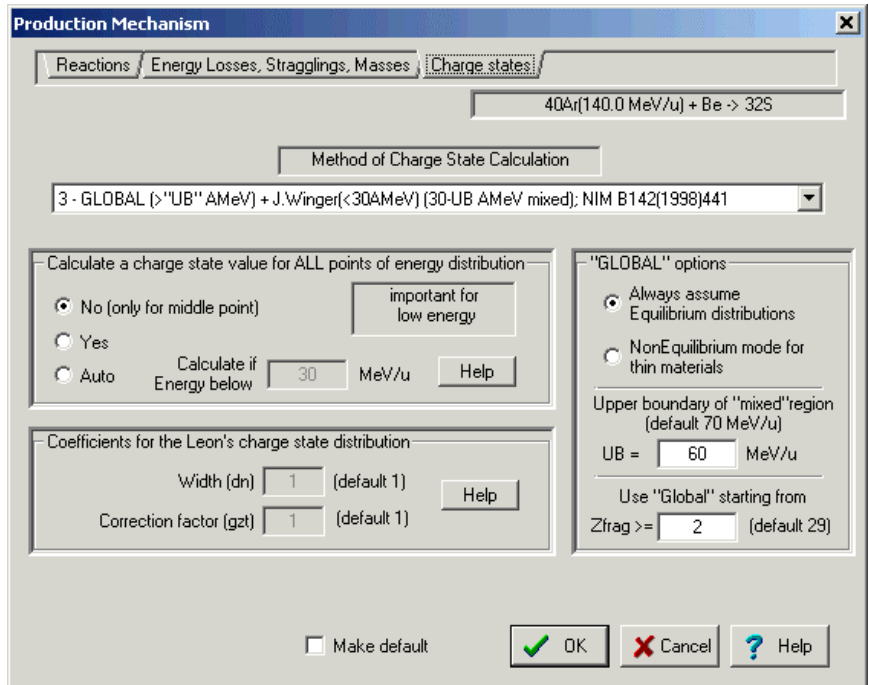


Fig.410. The Charge state panel of the Production mechanism dialog.

Since version 4.6 LISE calculates the charge state ratio for each point of the energy distribution after the target (stripper) ([http://groups.nsl.msu.edu/lise/4\\_6/lise\\_4\\_6.html#g2](http://groups.nsl.msu.edu/lise/4_6/lise_4_6.html#g2)). It is rather important for energies below 50 MeV per nucleon, whereas for high energy it is possible to assume that the charge state ratio is homogeneous for all points of the energy distribution after the target. The new version can avoid this time-consuming calculation for high energy and gives the possibility to choose the energy region in which to apply the charge state calculation to each point of the energy distribution (see the "Calculate a charge state value for ALL points of energy distribution" box in Fig.410).



It is possible to calculate the nonequilibrium charge state distributions after a material using Global's method. The user can set "NonEquilibrium" mode also via the "Production mechanism" dialog (see the right bottom box in Fig.410). More details about this mode in chapter 5.1.3.

### 5.1.1.3. "GLOBAL" in LISE.XLS

GlobalCode(ZmQ\_out; Aparticle; Zparticle; ZmQ\_in; Energy; Atarget; Ztarget; Thickness; Option; Fast)

names		Description
ZmQ_out=	103	Option (see bottom table)
Aparticle=	238	Mass of projectile
Zparticle=	92	Element number of proj.
ZmQ_in=	2	initial input charge
Energy=	300	MeV/u (init or final : depends from option)
Atarget=	63.55	Mass of target
Ztarget=	29	Element number of target
Thickness=	300	mg/cm2
Option=	3	0/1- at target (Einit/Efinal); 2/3 -equilibrium (Einit/Efinal)
Fast=	2	0-slow / 1-fast / 2 -superfast
<b>RESULT=</b>	<b>312.35</b>	

E init : initial energy of projectile before Equilibrium thickness  
 E final : final energy of projectile after Equilibrium thickness

Options		RESULT	Description	Dimens
ZmQ_out=	103	312.354	Energy after/before target	MeV/u
ZmQ_out=	102	139.378	Equilibrium thickness	mg/cm2
ZmQ_out=	101	0.763	dQ /st. deviation/	
ZmQ_out=	100	90.797	<Q> /average/	
ZmQ_out=	0	0.18847	Z - Q = 0	part
ZmQ_out=	1	0.44164	Z - Q = 1	part
ZmQ_out=	2	0.34914	Z - Q = 2	part
ZmQ_out=	3	0.02016	Z - Q = 3	part
ZmQ_out=	4	0.00056	Z - Q = 4	part
ZmQ_out=	5	0.00000	Z - Q = 5	part
ZmQ_out=	6	0.00000	Z - Q = 6	part
ZmQ_out=	27	0.00000	Z - Q = 6	part
		<b>1.0000</b>		

If result is equal -776,-777 or -778 --- you got error!  
 check input parameters

Base \ Global \ ChargeStates -> MeanValue \ Z -> data \ data -> Z \ parameters /

Fig.411. The sheet "Global" of the file "LISE.xls" demonstrating uses of the Global code in Excel

The sheet "Global" of the file "LISE.xls" (Fig.411) is an example how the user can use the Global program in Excel, including calculations of nonequilibrium processes. In fact it is possible to consider this sheet as the shell of Global in Excel, the user can get any result in a cell by setting the corresponding index. The indexes 0-27 correspond to charges Z-Q, and the meaning of indexes 100-103 are shown in (Fig.411). By analogy to the program LISE the methods 3 (Global+Winger) and 4 (Global+Leon) also are accessible in EXCEL. Examples of use of these functions (ChargeState, ChargeState\_Option, Charge\_Qmean, Charge\_dQ) are shown in the sheet "Base" (Fig.412). However these methods always assume equilibrium processes. To calculate nonequilibrium process, use the function "GlobalCode".

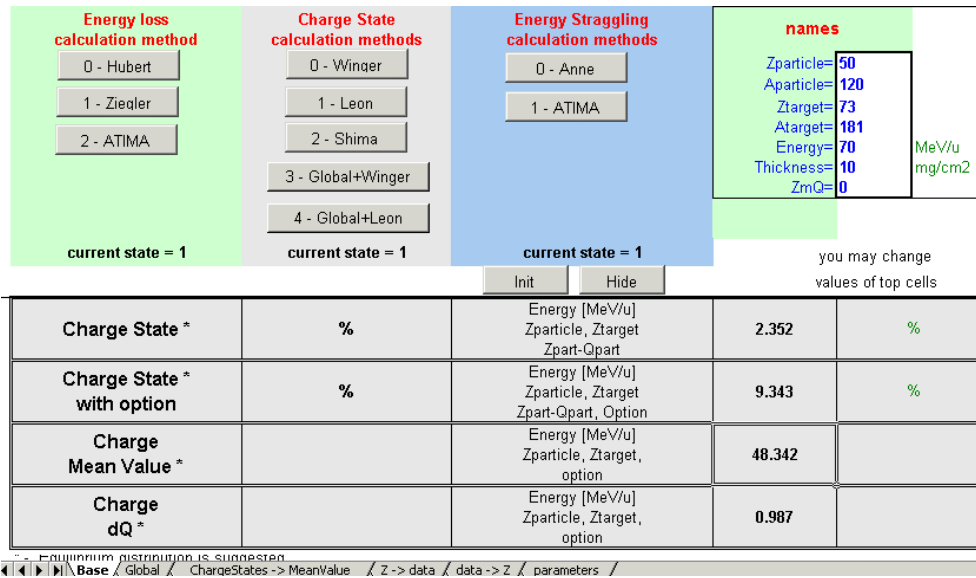


Fig.412. The sheet “Base” of the file “LISE.xls”.

### 5.1.1.4. GLOBAL’s new features

#### 5.1.1.4.1. Options for final energy projectile

By default the Global code calculates Q-states for the energy before the material. The final energy is calculated based on the material thickness. However the LISE code always needs the charge state distributions after the material assuming the equilibrium distributions. Two new options have been incorporated into Global to calculate the Q-state at target exit and the Equilibrium Q-states when the user gives the final energy after the material. The code calculates the initial energy of projectile before the target and shows this value in the results window of the code. LISE inputs to Global the final energy after the material, the thickness of material and initial Q-states distribution before the material in order to calculate nonequilibrium Q-states. **The initial Q-states distribution is a the new option** in Global because the original code used just one initial charge state.

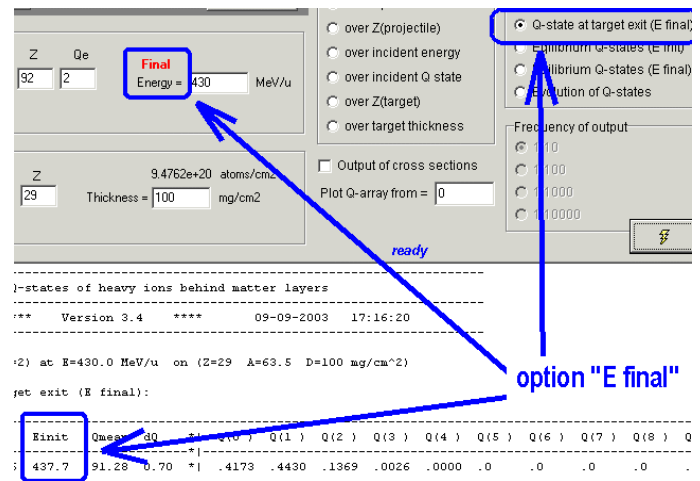


Fig.413. The “Global” code with the option “Q-states: Energy final”.

#### 5.1.1.4.2. Optimization for a thick target

An optimization of the calculations is done in the program in case of a thick target. It is based on the assumption that it is not necessary to calculate the Q-states for all points of a thick target, but only the equilibrium Q-states at the end of the target. This procedure goes as follows:

- Calculate the equilibrium thickness for the initial energy. If the target thickness is three times less than the equilibrium thickness, then the program does a regular calculation.
- Calculate the final energy  $E_{final}$  after the target and the range  $R_0$  in the material corresponding to this energy.

- Calculate the equilibrium thickness  $T_{equil}$  for  $E_{final}$ .
- Calculate the energy  $E_{3d}$  corresponding to the range  $R_0 + 3 \cdot T_{equil}$ .
- Calculate Q-states with the initial energy  $E_{3d}$  for the target with thickness  $3 \cdot T_{equil}$ .

The optimization allows not only to speed up calculations but also to avoid critical cases, when the program reaches the maximum possible number of cycles for the given accuracy of calculations, and stops calculating.

#### 5.1.1.4.3. Calculations for a projectile with atomic number lower than 29

As already mentioned the Global code was developed for projectiles with the atomic number greater than 28. The program has been modified to overcome this restriction<sup>2</sup>. The default value of Z-limit in LISE++ for Global's calculations is 29.

The **principal** modifications done to use projectiles with  $Z < 29$  (for those who know Global's source) are the following:

<p><i>Subroutine "GLOBAL"</i></p>	<ul style="list-style-type: none"> <li>• <code>J = min(ZF-1, J);</code> // (dimension of Q-arrays)</li> <li>• to determine the step of calculations instead</li> </ul> <p><i>"AUX = DE / NT / MIS;" to insert</i></p> <pre> if( J &lt; 10 )AUX = DE / NT / KIS; else if( J &lt; 28 ) AUX = DE / NT / LIS; else     AUX = DE / NT / MIS; </pre>
<p><i>Subroutine "CROSS"</i> conditions to calculate KRD &amp; LRD</p>	<pre> KRD = (ZF&gt;2 ? (LIU-KIB)/(KEX*LIU+KMETA) : 0); LRD = (ZF&gt;10 ? (MIU-LIU)/(LEX*MIU+LMETA) : 0); </pre>
<p><i>Subroutine "CAPCROSS"</i> exclude negative values of reduced Z1 &amp; Z2 from the loop</p>	<pre> for(.....) { ... if(Z1&lt;=0    Z2&lt;=0) {     CEIK[JP][JT]=0;     continue; } ... } </pre>
<p><i>Subroutine "IONICRO"</i> comment the strings</p>	<pre> // if( SMIU == 0. ) SMIU = 1.E10; // if( SMIS == 0. ) SMIS = 1.E10; </pre>

Global's calculations for light projectile are found in good agreement with experimental results, as well as with the Charge program results. Examples will be given in chapter 5.4.1.

#### 5.1.2. Q-state calculations: optimization for speed

With increasing number of optical blocks in a spectrometer the CPU time for transmission calculation is obviously increased, especially in case the "charge states" option is turned on. The simplest way to reduce the CPU time is to limit the number of points of the transmission distribution in the "Preferences" dialog, at the expense of the quality of calculations (by default 32 if the option "charge states" is on). Two alternative ways to accelerate the transmission calculation for different charge states of the fragment have been implemented.

<sup>2</sup> However the user gets a warning message in the Global code if he uses a projectile with an atomic number less than 29.

### 5.1.2.1. Tabulation of Q-states

The code is able to save 65 results of Q-states results in memory (**only equilibrium** charge states can be used!). The tabulation set records the initial parameters (fragment mass, fragment atomic number, energy after material, target atomic number, and charge state model number) and an array of Q-states. Before calculating Q-states the program searches a record with identical initial parameters in the tabulation sets. If the record is not found then the charge states are calculated and kept in the tabulation sets.

### 5.1.2.2. Restrictions for improbable Q-states

The code has been modified to exclude fragments with low probability of charge states from ion transmission calculation. An ion ( $Z-Q = X_1, X_2, \dots, X_n$ ) is excluded from the next calculations if the probability of any charge state  $X_i$  of the ion after a material before an optical block is less  $1e-4$ . Also this ion can be excluded if the production of all its charge states  $\prod_{i=1}^n X_i$  is less than  $1e-7$ . For the primary beam ions these restrictions are set to  $1e-7$  (for one charge state) and  $1e-10$  (for all charge states).

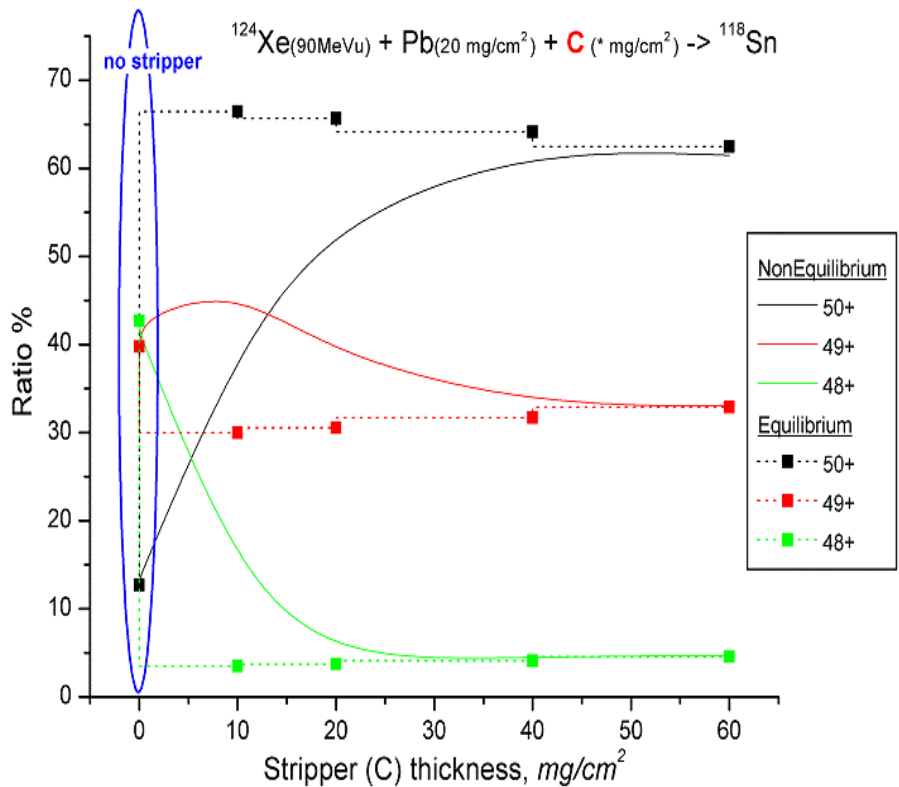
### 5.1.3. Nonequilibrium charge state calculations

Nonequilibrium charge state calculations are available now in the code LISE based on GLOBAL's library. Nonequilibrium calculations can be used if all the following conditions are fulfilled:

1. The charge state model is 3 (Global+Winger) or 4 (Global+Leon);
2. Nonequilibrium mode is enabled on in the "Global's option" box of the "Production mechanism" dialog;
3. The final energy  $E_{final}$  after the material is greater than the value of  $UB$  (upper boundary) set in the "Global's option" box;
4. The fragment atomic number is more than  $Z-limit$  set in the "Global's option" box.

The code always assumes equilibrium Q-states in the mixed area ( $30 \div UB$  MeV/u).

The charge states are always assumed in equilibrium after the target, for the following reasons:



**Fig.414.** Charge state evolution of the fragment  $^{118}\text{Sn}$  after a C-stripper as a function of its thickness for equilibrium and nonequilibrium cases in the reaction  $^{124}\text{Xe} (90 \text{ MeV/u}) + \text{Pb}(20\text{mg}/\text{cm}^2) + \text{C}(x \text{ mg}/\text{cm}^2)$ .

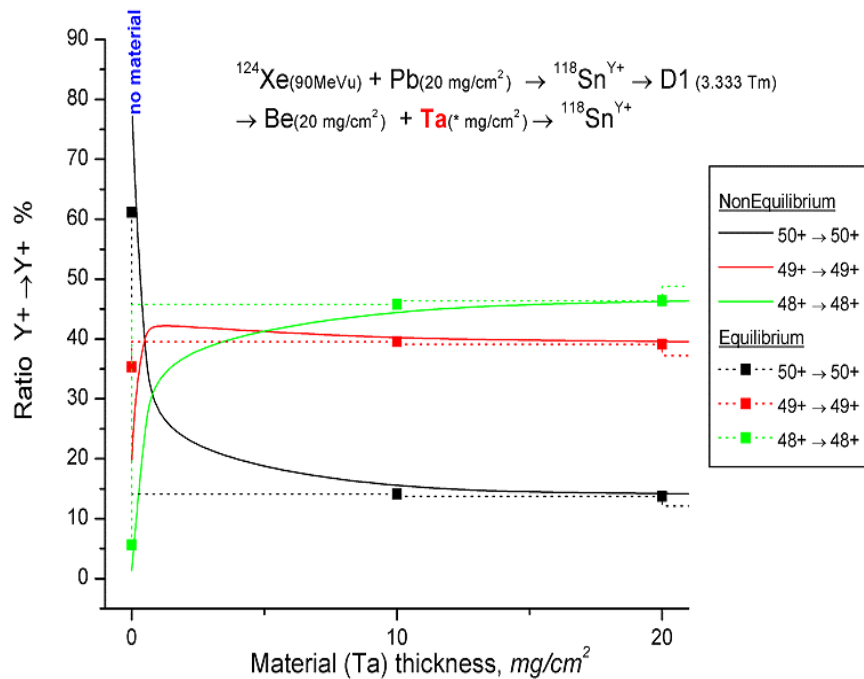
- As a rule the thickness of a target is more than the equilibrium thickness;
- It is too complex to calculate an initial charge state of the fragment at the instant of the reaction.

Therefore nonequilibrium Q-states are only calculated for a stripper after target and for materials located between optical blocks.

**Note:** nonequilibrium Q-states are not tabulated in memory, therefore the speed of transmission calculations in nonequilibrium Q-states mode is lower. Moreover, if some materials are located between optical blocks then the program calculates the Q-states after the last material in the equilibrium mode, and for **each** material in the nonequilibrium mode.

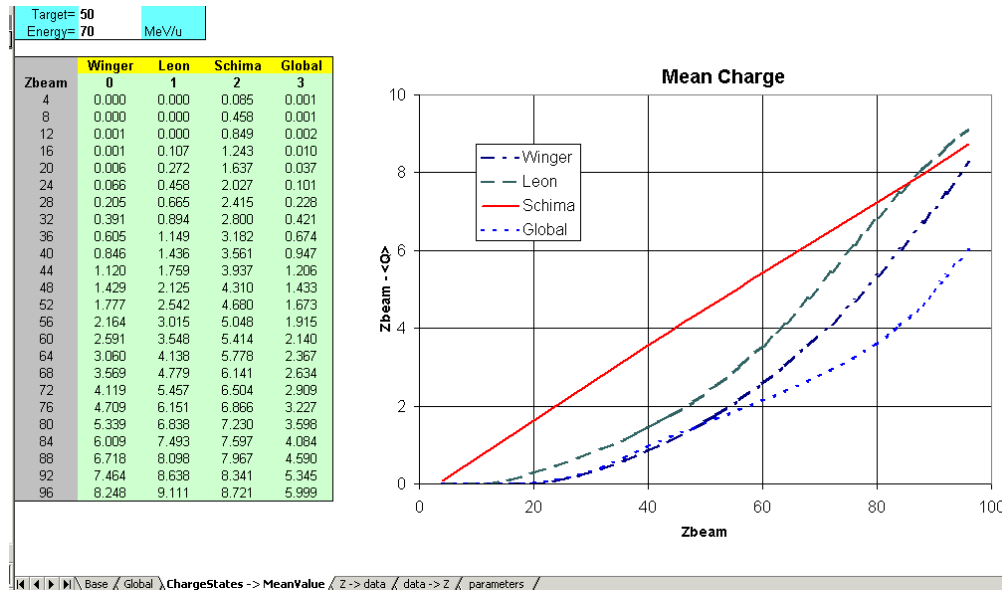
As an example, the charge state evolution of the fragment  $^{118}\text{Sn}$  after a C-stripper as a function of its thickness for Equilibrium and Nonequilibrium cases are shown in Fig.414, and after a material between optic blocks in Fig.415. The LISE++ file for these examples is located on the LISE web-site at: [http://groups.nslc.msu.edu/lise/6\\_3/examples/charge\\_test.lpp](http://groups.nslc.msu.edu/lise/6_3/examples/charge_test.lpp)

**Fig.415.** Charge state evolution of the ions  $^{118}\text{Sn}^{Y+Y+}$  after a Ta-material as a function of its thickness for equilibrium and nonequilibrium cases in the reaction  $^{124}\text{Xe} (90 \text{ MeV/u}) + \text{Pb}(20 \text{ mg/cm}^2) \rightarrow \text{Dipole} \rightarrow \text{Be}(20 \text{ mg/cm}^2) + \text{Ta}(x \text{ mg/cm}^2)$ .



#### 5.1.4. Excel: new sheet and functions with charge states

Additional utilities have been created in the LISE.xls file. The new sheet “ChargeStates → MeanValue” allows to plot the mean values of the charge state distribution versus the atomic number of the projectile. It is possible to enter the energy of the projectile and the target atomic number to get the mean value of the equilibrium charge state distribution with different models (see Fig.416).



**Fig.416.** The sheet “ChargeStates → MeanValue” of the file “LISE.xls”. It is possible to enter the energy of the projectile and the target atomic number to get mean value of the equilibrium charge state distribution with different models.

The functions *EnergyLossInMatter\_option*, *RangelnMatter\_option*, *ChargeState\_option*, *Charge\_Qmean*, *Charge\_dQ* have been implemented in the library of LISE.xls. The first three functions are identical to *EnergyLossInMatter*, *RangelnMatter*, *ChargeState*, but require to specify a model. The functions *Charge\_Qmean* and *Charge\_dQ* calculate the mean value and the dispersion of the charge state distribution.

*Note:* To use built-in LISE functions in Excel you have to set the options:

- Tools → Macro → Security → ”Low” or ”Medium”.
- Switch on the option “macros enabled” then load the Excel file in the security mode ”Medium”.

### 5.1.5. Equilibrium thickness plot

The “Equilibrium thickness versus projectile energy” plot can be viewed in LISE++ (menu “Utilities”). Two models calculate the equilibrium thickness: one from the Global code and the other from Thierberger’s [Thi85] definition of the equilibrium thickness in the code “Charge”. An example of the equilibrium thickness plot for the projectile  $^{208}\text{Pb}$  in Be is shown in Fig.417.

### 5.1.6. Physical Calculator Charge state values ( $\langle Q \rangle$ , $\Delta Q$ )

The Physical calculator dialog in the new version of the code shows the statistical characteristics of the equilibrium charge state distribution as well as the value of equilibrium thickness (see Fig.418). The equilibrium thickness is calculated based on Thierberger’s definition of the equilibrium from the Charge code.

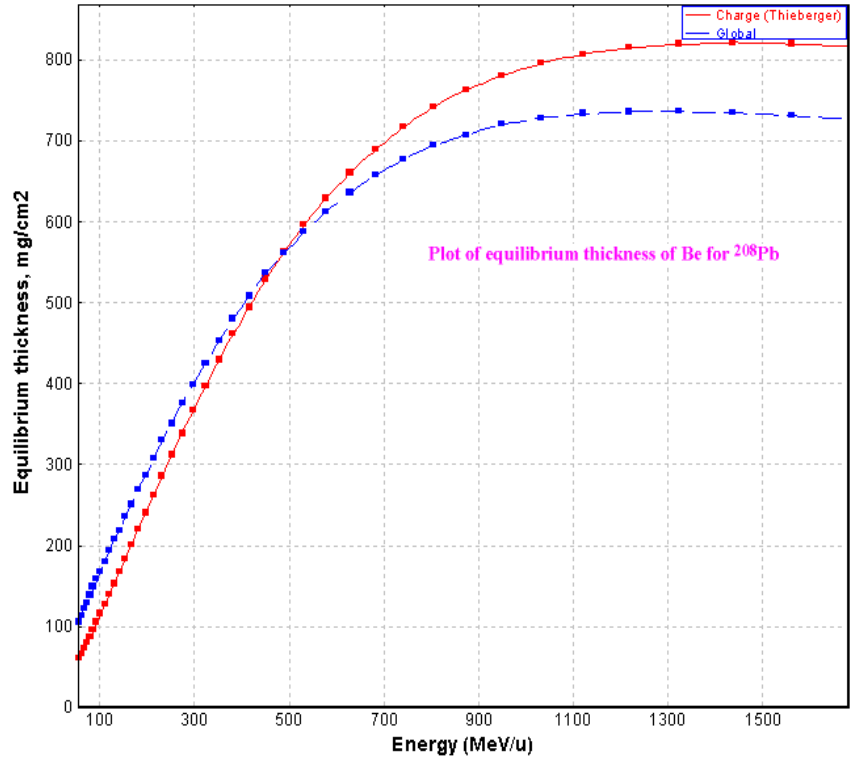


Fig.417. Equilibrium thickness of Be as a function of energy for a  $^{208}\text{Pb}$  projectile.

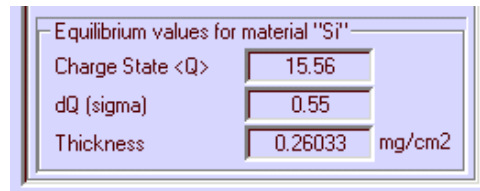


Fig.418. Fragment of the “Physical calculator” window with the results of equilibrium charge state distribution and equilibrium thickness of material. The thickness of material for the charge state calculation is assumed to be equal to 0.

## 5.2. Modification of evaporation calculations

### 5.2.1. Level density calculations

Level densities and decay widths from the statistical analysis of A.Iljinov et al [Ilj92] have been incorporated in LISE++. The code calculates decay widths instead of width ratios as was done in the previous version. This modification is necessary in order to add the fission channel in the evaporation cascade. The option to use shell corrections has been added to calculate the level density (see frame A in Fig.419).

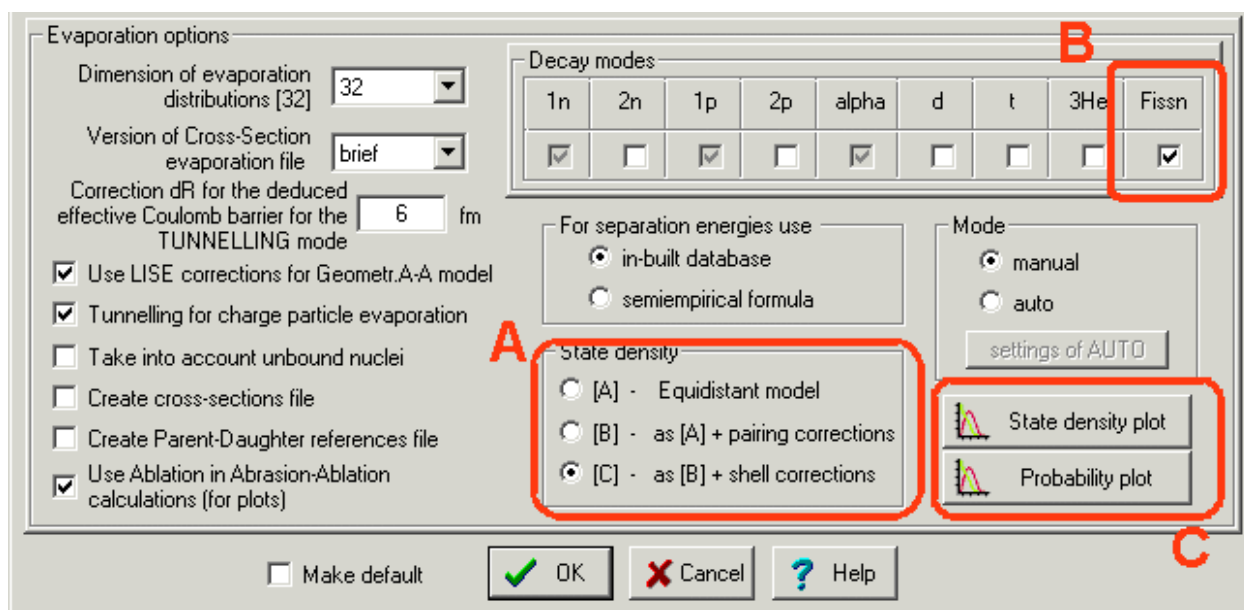


Fig.419. The “Evaporation options” dialog

The shell corrections are calculated without collective effects following the results of level density analysis of Myers-Swiatecki shell corrections where the asymptotic level density parameter  $\gamma$  is equal to  $\tilde{\alpha}/0.46A^{4/3}$  (see Table 3 in [Ilj92]).

Due to these modifications it is recommended to use the new values shown in Table 45 in the mode “AUTO” (see the “Settings of AUTO” dialog)

Table 45. Recommended values for the mode “Auto” of evaporation calculations.

	Abrasion-Ablation	Fusion-Evaporation	Previous value
Take into account unbound nuclei with A less than	40	300	40
Include pairing and shell corrections for nuclei with A greater than	2	2	70

#### 5.2.1.1. Level density and temperature plots

Level density and temperature versus an excitation energy plots can be viewed from the “Evaporation options” dialog (see frame C in Fig.419). The plots are drawn for all of three modes of state density available in LISE++: A) Equidistant model, B) “A” + pairing corrections, c) “C” + shell corrections, to give the user a possibility to compare them (see Fig.420).



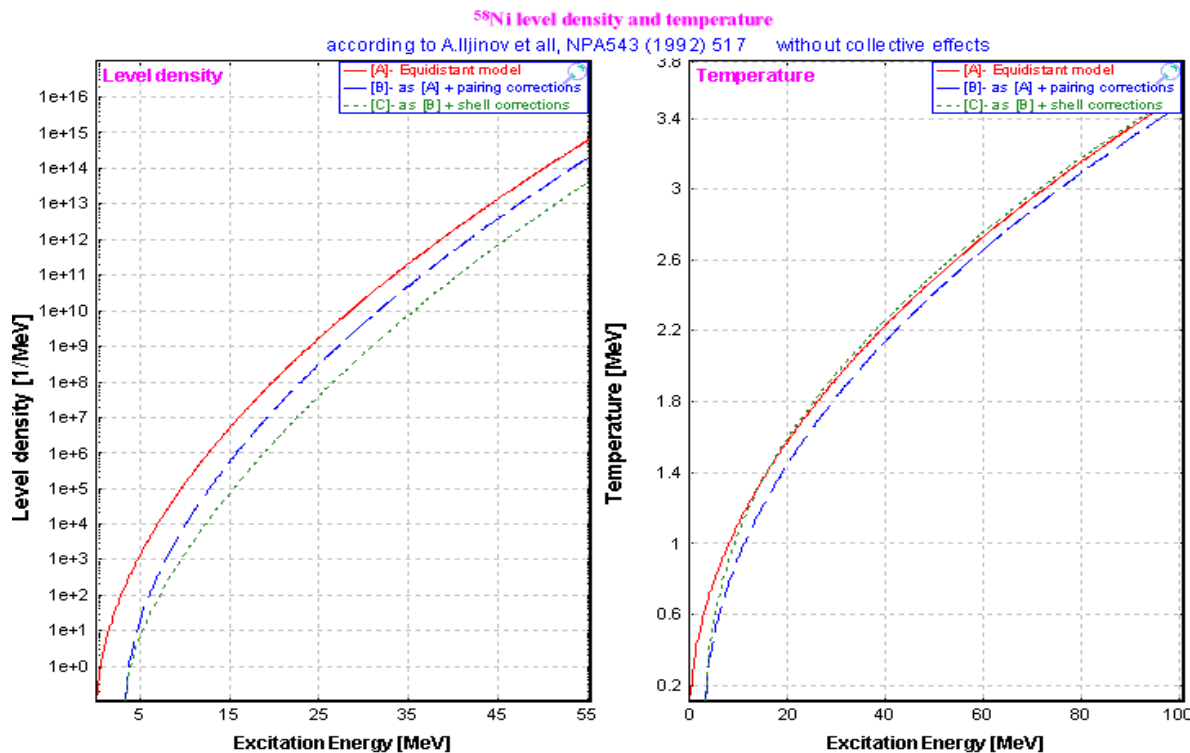


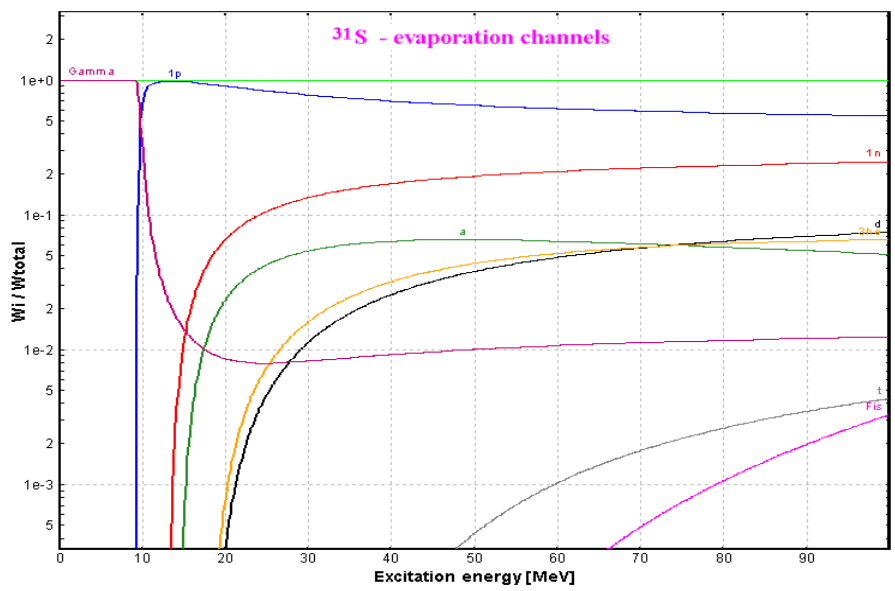
Fig.420. <sup>58</sup>Ni level density and temperature versus excitation energy.

### 5.2.2. Fission channel in evaporation cascade

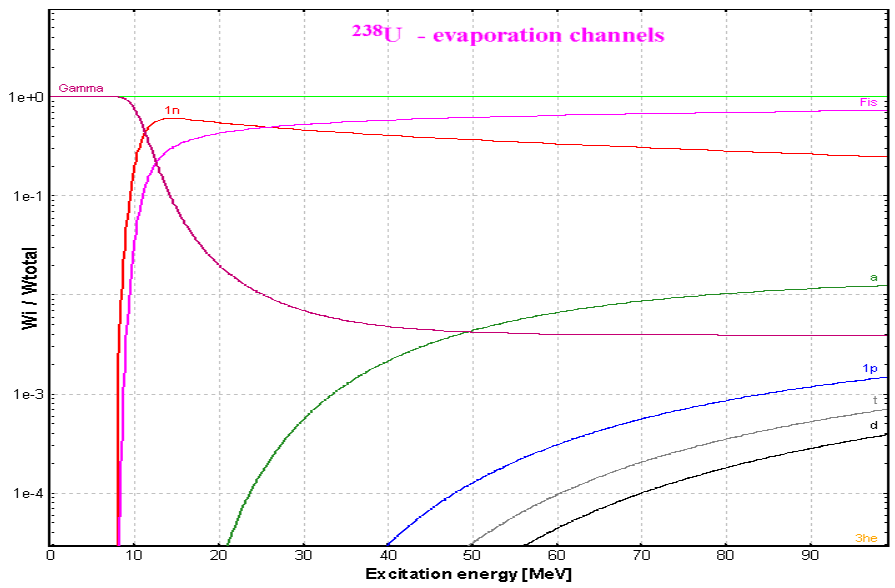
A fission channel has been added to the family of decay channels of LISE evaporation calculations, and is very important for excited heavy nuclei where fission is a dominant channel. The code does not take into account the angular momentum of the decaying nucleus in fission. The fission width is calculated according to the article [Ilj92]. The subroutine FISROT [Coh63] of the PACE code is used to calculate the fission barrier. It is possible to see the fission barrier value in the “Evaporation calculator” dialog. LISE uses the fission channel to determine the production cross section of evaporation residues, but the code does not calculate the transmission of fission fragments and therefore fission fragments. To use the fission channel in evaporation calculations the user has to check the fission checkbox in the decay modes frame (see frame B in Fig.419)

### 5.2.3. Plot of decay channel probabilities

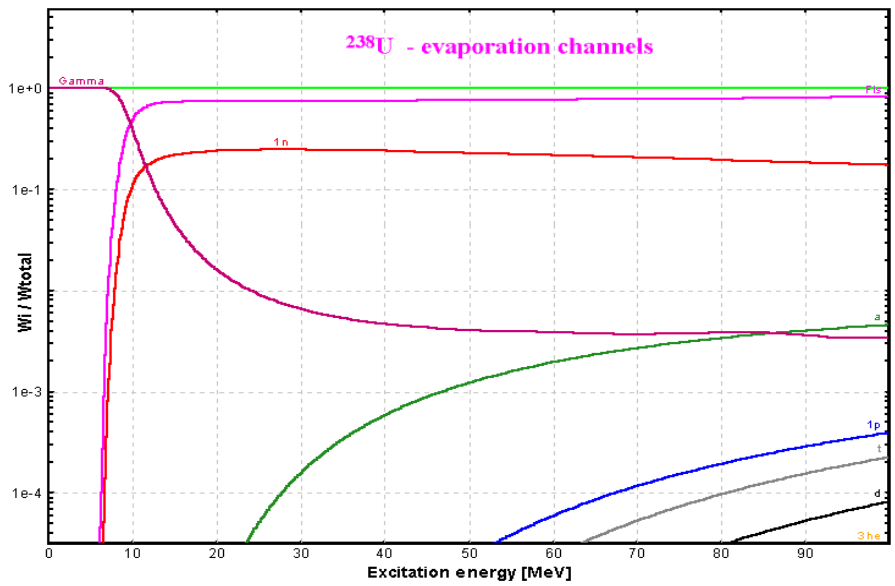
The energy dependence of decay channel probabilities can be plotted from the “Evaporation options” dialog by pressing on the “Probability plot” button. The plot is very useful to estimate the dominant channels and also to see the influence of different level density modes. Plots of the decay channel probabilities of <sup>31</sup>S and <sup>238</sup>U are presented in Fig. 421-423. Energy dependences in Fig.421 and 422 were calculated using the level density mode “C” (with pairing and shell corrections), the energy dependence in Fig.423 was calculated for the level density mode “A” (without any corrections).



**Fig.421.** Energy dependence of light particle and gamma emission probabilities for  $^{31}\text{S}$ . Calculations were performed using the level density mode “C” (pairing and shell corrections included).



**Fig.422.** Energy dependence of light particle and gamma emission probabilities for  $^{238}\text{U}$ . Calculations were performed using the level density mode “C” (pairing and shell corrections included).



**Fig.423.** Energy dependence of light particle and gamma emission probabilities for  $^{238}\text{U}$ . Calculations were performed using the level density mode “A”.

### 5.3. Other

#### 5.3.1. New angular transmission method

A new method to calculate the fragment angular transmission has been incorporated in LISE after discussions on how to analytically calculate the angular transmission depending on the shape of the angular acceptance. The LISE original method (named “jacobian”) is as follows:

- The fragment angular distribution  $d\sigma/d\Omega$  is transformed to the distribution  $d\sigma/d\theta$ .
- The angular transmission is equal to the ratio:

$$\varepsilon(m) = \int_0^m \left( \frac{d\sigma}{d\theta} \right) d\theta \bigg/ \int_0^{\pi/2} \left( \frac{d\sigma}{d\theta} \right) d\theta, \quad /37/$$

where  $m$  is the angular acceptance of the device. If the horizontal  $m_X$  and vertical acceptances  $m_Y$  are different then the code uses a geometrical average value  $\varepsilon = \sqrt{\varepsilon(m_X) \cdot \varepsilon(m_Y)}$  as total angular transmission.

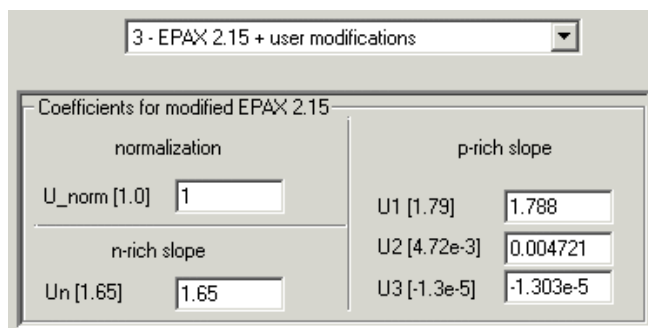
The new angular transmission labeled “projection” method is equal to  $\varepsilon = \zeta(m_X) \cdot \zeta(m_Y)$ , where  $\zeta(m)$  is defined by the relation:

$$\zeta(m) = \int_{-m}^m \left( \frac{d\sigma}{d\Omega} \right) d\theta \bigg/ \int_{-\pi/2}^{\pi/2} \left( \frac{d\sigma}{d\Omega} \right) d\theta. \quad /38/$$

The results from both methods are almost always identical. It is possible to interpret these two methods via the acceptance shape: the “jacobian” method corresponds to an oval acceptance, whereas the “projection” method corresponds to a rectangular acceptance. The angular transmission method can be selected in the “Preference” dialog. The “jacobian” method is chosen by default.



#### 5.3.2. Possibility to modify EPAX 2.15

The version 6.3 of LISE allows to adjust 5 parameters of EPAX 2.15 (model number 3 which can be selected in the “Projectile fragmentation” dialog – see Fig.424.). The parameters are named according to the article [Sum00]. Using this option it is possible to achieve better agreement between calculated values and experimental results and to fragment cross section based on actual measurements. Five parameters can be modified: three of them are used for to proton-rich nuclei, one for neutron-rich nuclei, and the last one to normalize all cross sections.



**Fig.424.** Fragment of the “Projectile fragmentation” dialog showing the new option of projectile fragmentation cross sections.

### 5.3.3. Monte Carlo plot saving and use by the "BI" code

The two-dimensional spectra created by the Monte Carlo method can be saved in ASCII formats: three columns file (\*.dat, \*.txt) or NCSL 2d-spectrum (\*.spa). It is possible to use the saved spectra (\*.dat, \*.txt) in several graphical software (for example Microcalc Origin) to build plots or to load spectra in the NSCL acquisition and analysis software (\*.spa). To save the two-dimensional Monte Carlo spectrum, click the icon  after the Monte Carlo acquisition has been stopped (Fig.425). Saved Monte Carlo spectra can be loaded in the Bi code  (see Fig.426). It is then possible to create contours to see the statistical characteristics of the peaks and make projections on horizontal and vertical axis. An example of a contour for a Monte Carlo spectrum is shown in Fig.426, and the projection of this contour on the vertical axis is shown in Fig.427.

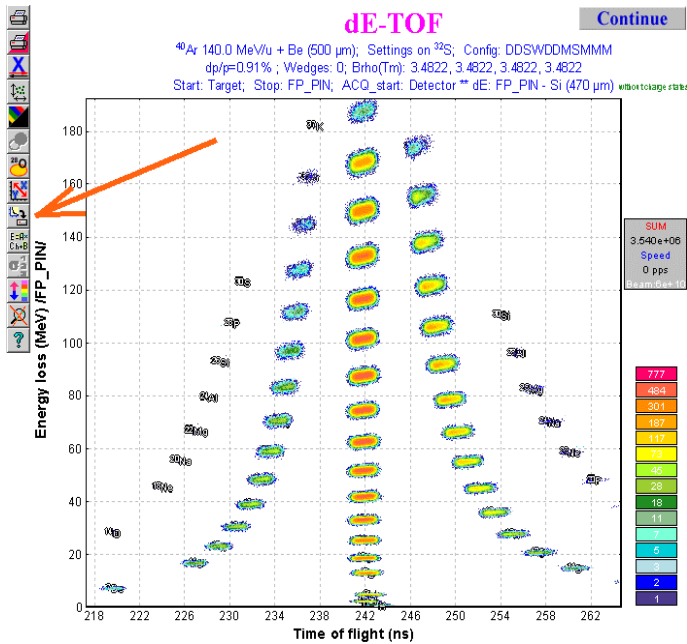


Fig.425. Monte Carlo identification plot.

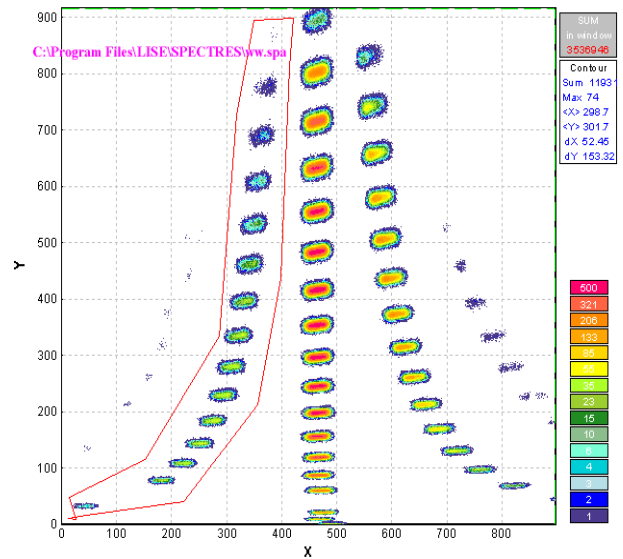


Fig.426. Input spectrum in the BI code. The spectrum was created from Monte Carlo plot (see Fig.425).

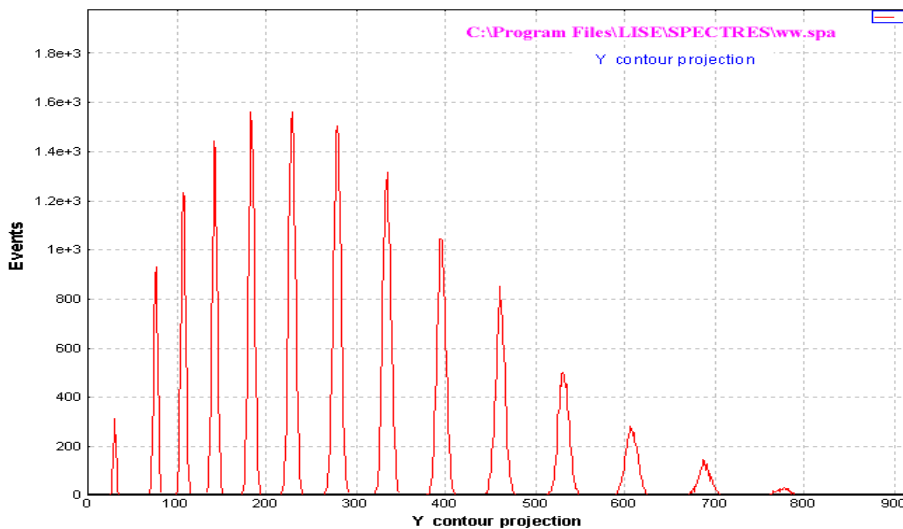


Fig.427. Vertical projection of the contour in Fig.426.

### 5.3.4. New configurations

Configuration	Subdirectory	Scientist who assisted to create or created the configuration
A1900_PAC27.lcn	NSCL	A.Stolz
RIPS	RIKEN	K.Yoneda
MSP-144*	Dubna	R.Kalpakchieva
ACCULINNA	Dubna	S.Stepantsov
Combas	Dubna	Yu.Sereda
FRS - new standard.lcn FRS - ESR.lcn FRS - FB07E to S8.lcn Super-FRS.lcn	GSI	H.Weik

\*The MSP-144 dialog was moved from the Kinematics calculator to the Utilities menu.

### 5.3.5. Bug corrections

<p><i>Thickness dialog</i></p> <p>A.Stolz (NSCL)</p>	<p>The program rounded the thickness value in the material dialogs and was saving to the file only up to two digits after a decimal point.</p> <p>Rounding is now not made in material dialogs. Up to 6 digits after the decimal point are deduced.</p> <p>In the Setup window 7 characters are allocated for the material thickness (for example 500.233 or 1.678e+9)</p>
<p><i>Integration method of energy straggling calculations</i></p> <p>H.Weik (GSI)</p>	<p>For thick enough materials a large difference in energy straggling was noticed when using the integration method. This is corrected but an insignificant deviation is still observed, therefore it is recommended to use the tabulation method for energy straggling calculations.</p>
<p><i>Problems with Windows XP</i></p> <p>H.Weik (GSI), T.Kibedi (Australian Nat.Univ.)</p>	<p>The program is not loaded if the user has regular privileges but no administrative privileges. This is caused because the program tries to open a database file both for reading, and writing. In the new version the program checks the possibility to open the database file for writing. If forbidden, the file opens only for reading.</p>
<p><i>Database access in the PACE4 code</i></p> <p>G.Savard (Argonne)</p>	<p>After modifying the access to the database (look above) in some cases the program (LISE and PACE) did not open the database file and used the built-in procedures. This is corrected</p>
<p><i>Energy straggling for Monte Carlo plots</i></p> <p>A.Stolz (NSCL)</p>	<p>Problem corrected. Remember: detector resolution, material defect, timing resolution, and straggling are responsible for the peak width in an identification plot. Set all resolutions and defects to 0 to see the straggling contribution. You can also see the straggling contribution if choose the mode (2) "No energy straggling" in the "Reaction mechanism" dialog.</p>

## 5.4. Comparison between LISE calculations and experimental results

It is often asked what models describe better the fragment momentum distributions, charge state distributions, production cross sections, etc. Obviously it depends on the energy of the projectile and from the reaction mechanisms involved in the fragment production process. In this chapter comparisons of experimental results with calculations of the program LISE are presented for different models in LISE. The analysis is carried out for charge states distributions, parallel fragment momentum distributions, and production cross sections in the next sections.

### 5.4.1. Charge state distributions

NSCL experimental data for different energy regions have been used for charge state analysis.

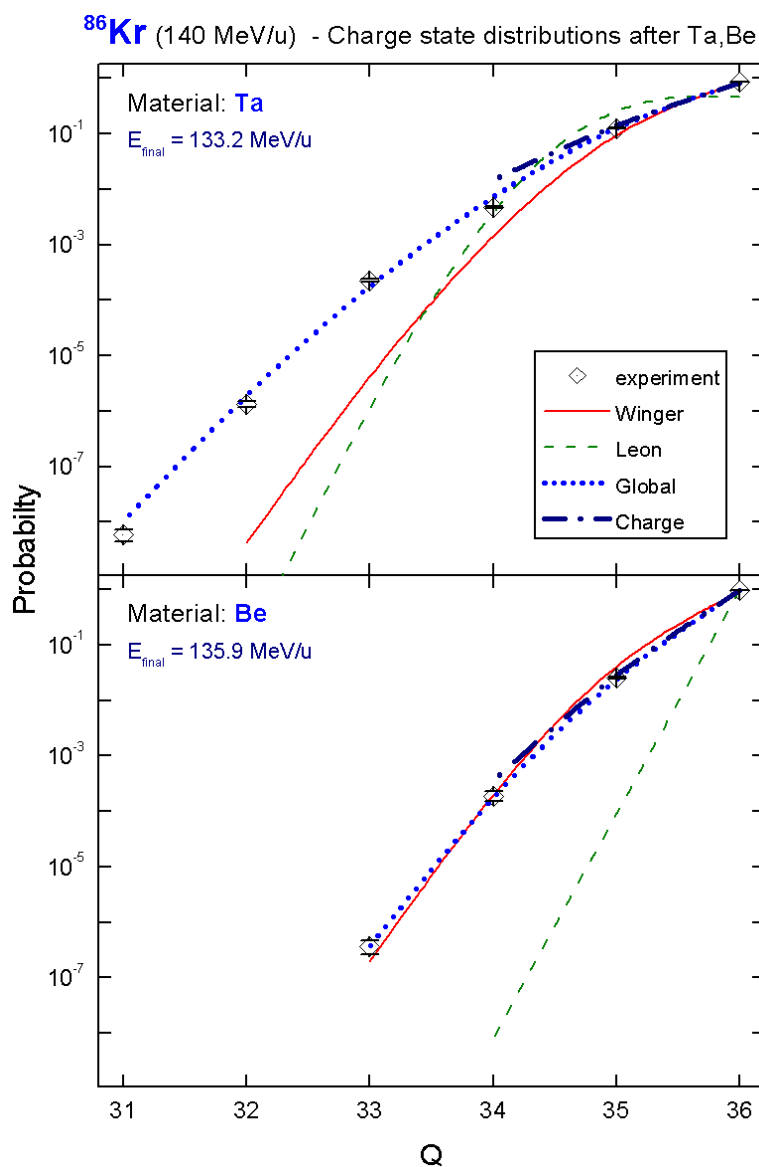
$^{86}\text{Kr}$  (140 MeV/u) equilibrium charge states distributions [Tsa03] after Ta-target (energy after the target 133.2 MeV/u) and Be-target (energy after the target 135.9 MeV/u) are shown in Fig.428.

$^{58}\text{Ni}$  (140 MeV/u) equilibrium charge states distributions [Tsa03] after Au, Ta, Nb, and Be are shown in Fig.429. The energies after targets are shown in the plots.

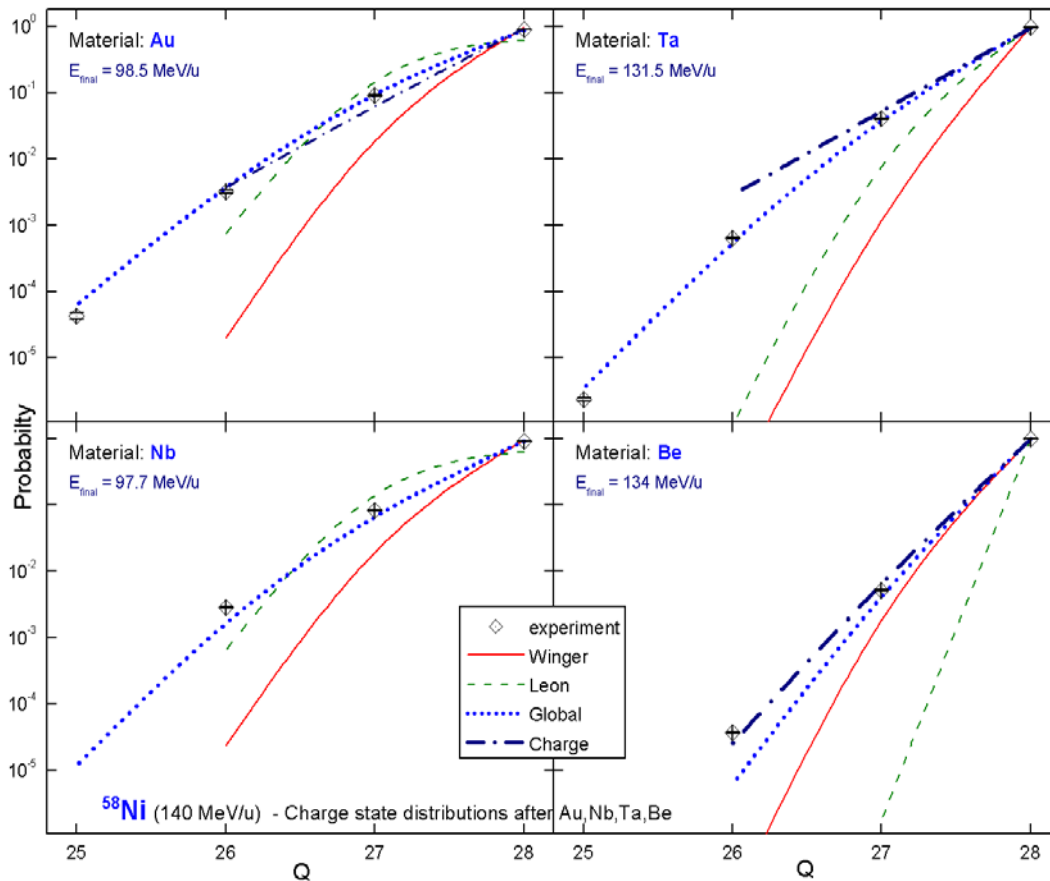
The equilibrium charge states distributions of  $^{136}\text{Xe}^{21+}$  (10.85MeV/u),  $^{124}\text{Xe}^{20+}$  (12.25MeV/u),  $^{86}\text{Kr}^{14+}$  (12.3MeV/u) after a carbon foil [A1903] are shown in Fig.430 (Global and Charge do not calculate at energies lower than 30 MeV/u). The foil thicknesses are shown in the plots.

Looking at these figures it is possible to conclude that in the energy region of 90 to 150 MeV/u the Global model gives the best agreement with the data. The Charge code also gives a quite good agreement but calculates just three charge states ( $Z-Q=0,1,2$ ).

For lower energies Winger and Leon give a good agreement, and Schima calculations are unsuitable for this energy region.

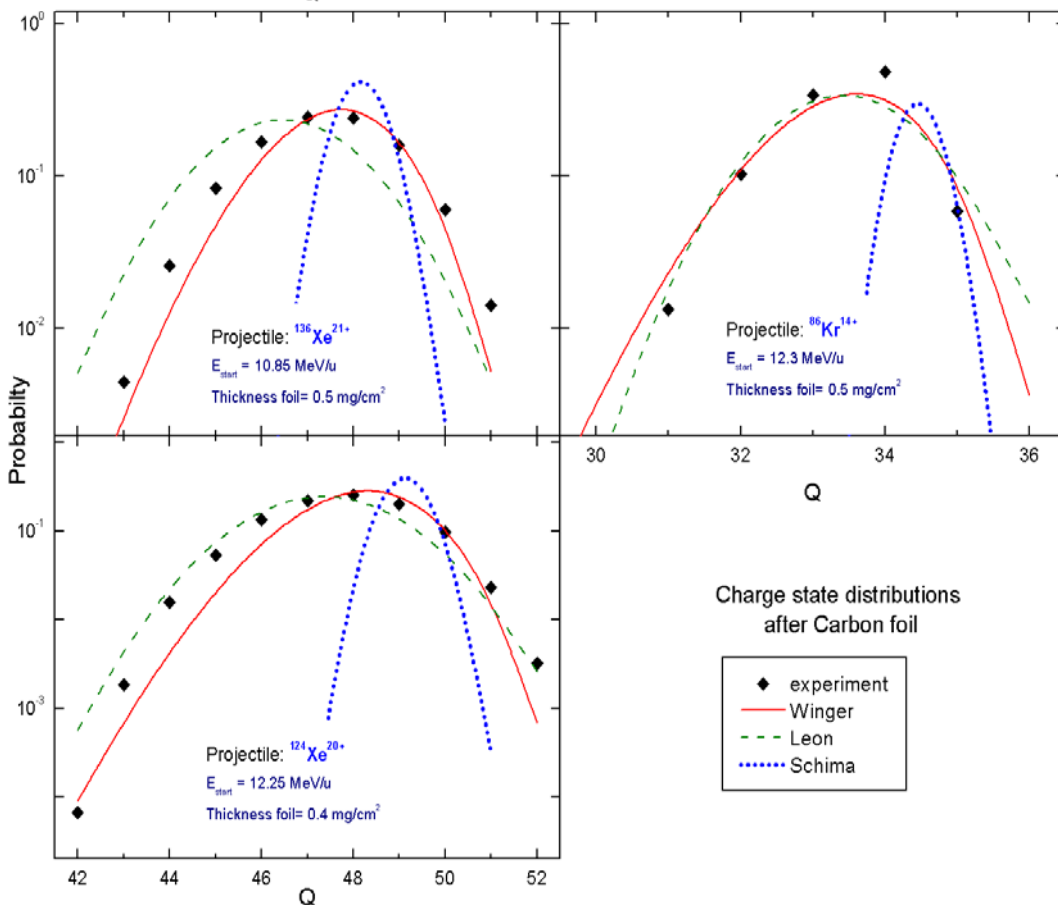


**Fig.428.**  $^{86}\text{Kr}$  equilibrium charge states distributions [Tsa03] after Ta-target (top picture) and Be-target (bottom picture). The energies after the Ta and Be targets are 133.2 MeV/u and 135.9 MeV/u respectively.



**Fig.429.**  
 $^{58}\text{Ni}$  (140 MeV/u)  
 equilibrium charge  
 states distributions  
 [Tsa03] after  
 Au (top left),  
 Ta (top right),  
 Nb (bottom left),  
 Be (bottom right).

Energies after materi-  
 als are shown in the  
 plots.

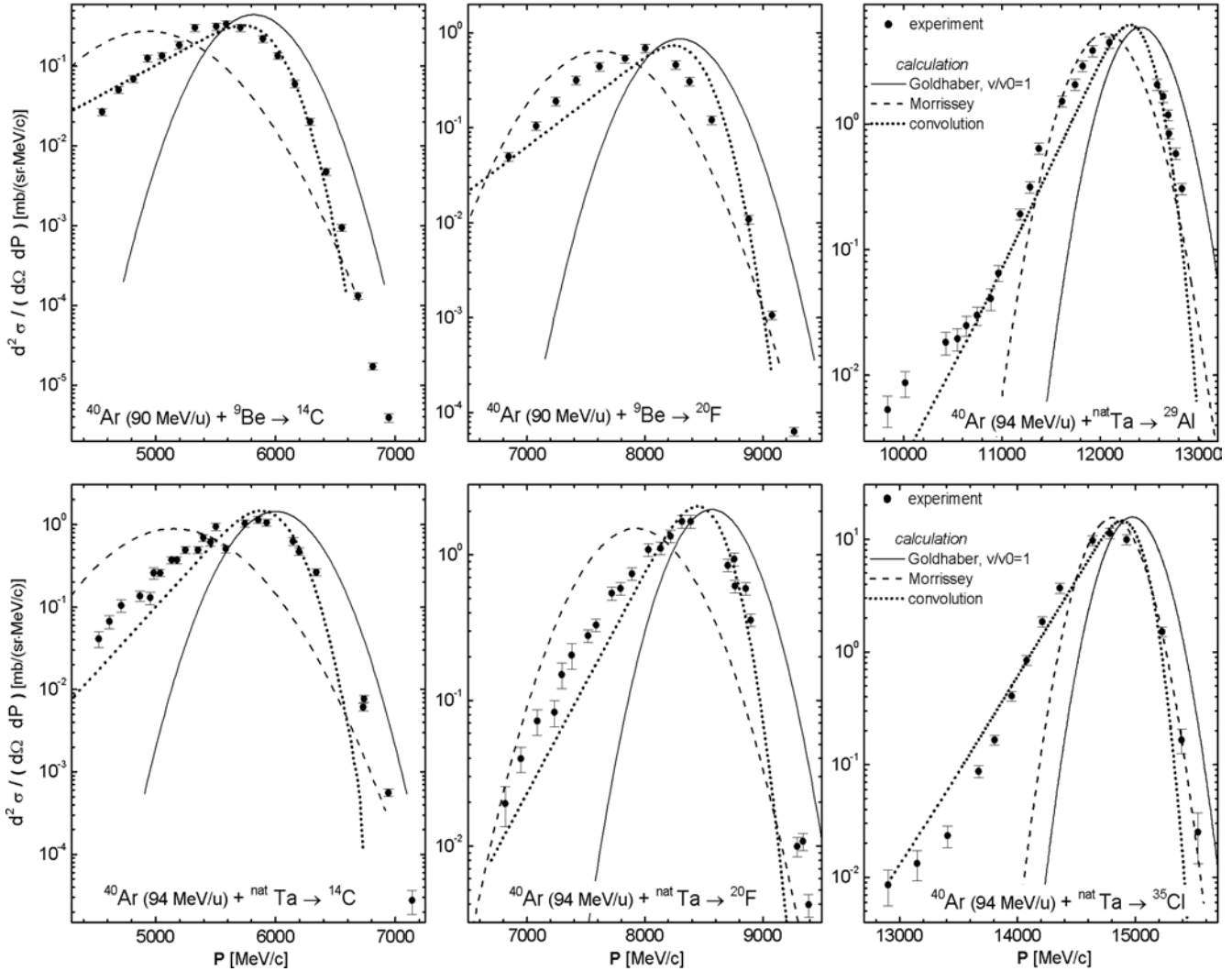


**Fig.430.** Equilibrium  
 charge states  
 distributions of  
 $^{136}\text{Xe}^{21+}$  (10.85MeV/u)  
 (top left),  
 $^{124}\text{Xe}^{20+}$  (12.25MeV/u)  
 (bottom left),  
 $^{86}\text{Kr}^{14+}$  (12.3MeV/u)  
 (top right)  
 after a carbon foil  
 [A1903].

Foil thicknesses are  
 shown in the plots.

### 5.4.2. Fragment parallel momentum distributions

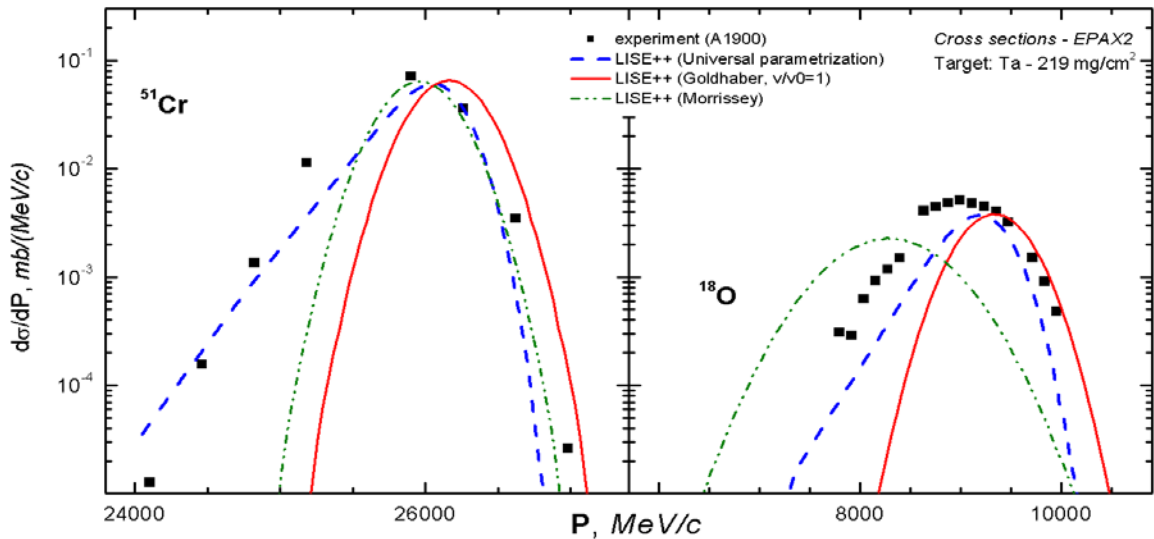
Recent experimental results [Mom02] from RIKEN on the study of production cross sections and momentum distribution of projectile fragmentation products in the reactions  $^{40}\text{Ar} + \text{Ta}$  and  $^{40}\text{Ar} + \text{Be}$  at 90 MeV per nucleon are compared to the models in Fig.431. The differential cross section distributions were calculated with LISE++ normalized on the area of the experimental spectra. The sum of surface excess and mass difference was used for the separation energy in the convolution method. Corrections for target thickness have been applied following [Mom02].



**Fig.431.** Experimental spectra of  $^{14}\text{C}$ ,  $^{20}\text{F}$  produced in  $^{40}\text{Ar} + \text{Be}$  [Mom02] and  $^{14}\text{C}$ ,  $^{20}\text{F}$ ,  $^{29}\text{Al}$ ,  $^{35}\text{Cl}$  resulting from  $^{40}\text{Ar} + \text{Ta}$ . The calculated spectra using Goldhaber's model with fragment to projectile velocity ratio equal to 1 are indicated by solid lines. Dashed lines represents the momentum distributions with widths and mean velocity based on Morrissey's systematics and the convolution model calculations are shown by dotted lines.

NSCL experimental results [Tsa03] on the study of production cross sections and the momentum distribution of projectile fragmentation products in the reactions  $^{58}\text{Ni} + \text{Ta}$  at 140 MeV per nucleon are compared to the models in Fig.432. The differential cross section distributions were calculated with LISE++ based on cross section calculations by EPAX 2.15.



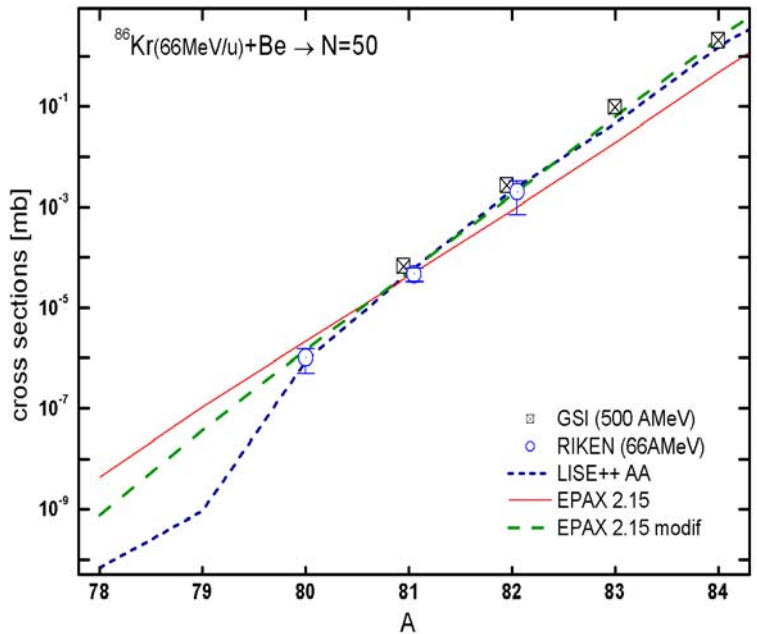


**Fig.432.** Experimental spectra of  $^{18}\text{O}$ ,  $^{51}\text{Cr}$  produced in  $^{58}\text{Ni}(140\text{MeV/u}) + \text{Ta}$  [Tsa03]. The calculated spectra using Goldhaber's model with fragment to projectile velocity ratio equal to 1 are indicated by solid lines. Dashed lines represents the momentum distributions with widths and mean velocity based on Morrissey's systematics and the convolution model calculations are shown by dotted lines.

These figures show that in the energy region of 90 of 150 MeV/u the Universal parameterization based on the 3-step projectile fragmentation model gives a better agreement with the experimental data.

#### 5.4.3. LISE Abrasion-Ablation model

The Abrasion-Ablation model implemented in LISE++ is used to predict production cross sections. However to correctly reproduce experimental cross sections it is necessary to calculate precisely the excitation energy of the prefragment. Some examples of AA calculations and their comparisons with experimental data are given below. The production cross sections of  $N=50$  isotones in the reaction  $^{86}\text{Kr}(66\text{MeV/u}) + \text{Be}$  [Aoi02] as a function of mass number are shown in Fig.433. The parameters of the Abrasion-Ablation model and modified EPAX2.15 are given in Tables 46 and 47 respectively. The LISE file for the example is located on the LISE website



**Fig.433.** Production cross sections of  $N=50$  isotones as a function of mass number. See text for details.

[http://groups.nsl.msu.edu/lise/6\\_3/examples/86kr\\_80zn.lpp](http://groups.nsl.msu.edu/lise/6_3/examples/86kr_80zn.lpp).

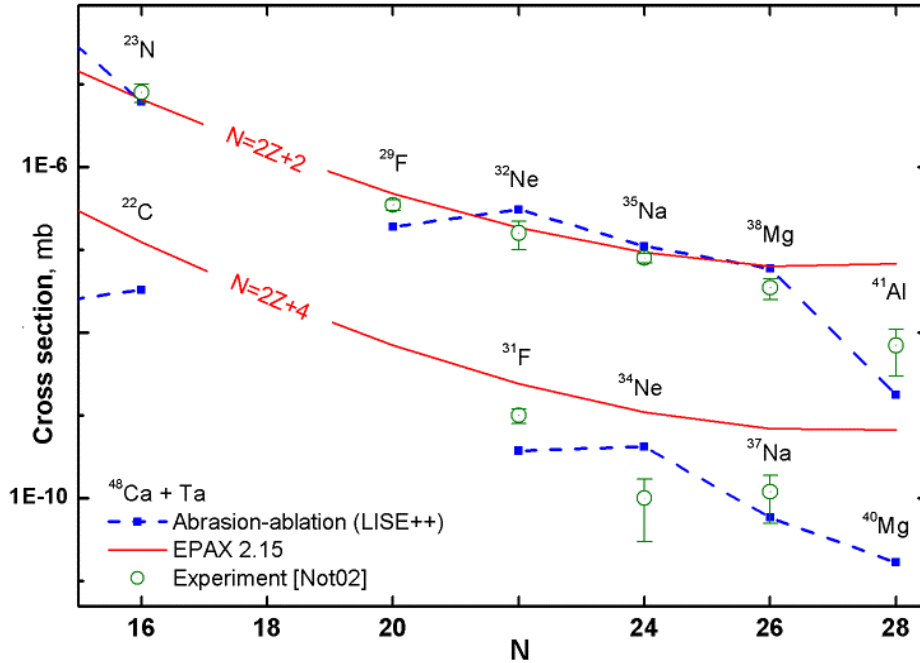
**Table 46.** Parameters of Abrasion-Ablation model used in calculations of Fig.433.

LISE++ version	6.3	State density	Shell+Pairing
Distribution dimension (NP)	64	Option "unbound"	auto
Hole depth (MeV)	48	Decay modes	All (8)
Excitation energy method	1	Tunneling	auto

**Table 47.** Parameters of "EPAX 2.15 modified" in Fig.433.

Changed parameter	New value	EPAX 2.15 value
U_norm	6	1
Un	1.73	1.65

The experimental and calculated production cross sections of various isotopes in the reaction  $^{48}\text{Ca}$  (90MeV/u)+Be are shown in Fig.434. These results have been already shown in the LISE++ documentation v.6.1. A difference of almost two-orders magnitude is observed between the abrasion-ablation model and the EPAX parameterization for the  $^{40}\text{Mg}$  production cross-section. The parameters used for the Abrasion-Ablation model are given in Table 48.



**Fig.434.** Experimental [Not02,Sak97], calculated by the LISE abrasion-ablation model (blue dash curve) and EPAX parameterization (red solid curve) production cross sections of neutron-rich isotopes in the reaction  $^{48}\text{Ca}+\text{Ta}$  versus neutron number. Binding energies from the database+LDM2 have been used for the Abrasion-Ablation calculations.

**Table 48.** Parameters of Abrasion-Ablation model used in calculations of Fig.434.

LISE++ version	6.1	State density	auto
Excitation energy method	2	Tunneling	auto
Distribution dimension (NP)	64	Option "unbound"	auto
$\langle E^* \rangle$ (MeV)	16.5 dA	Decay modes	All (8)
$\delta E$ (MeV)	9.6		

## 5.5. Status of the code

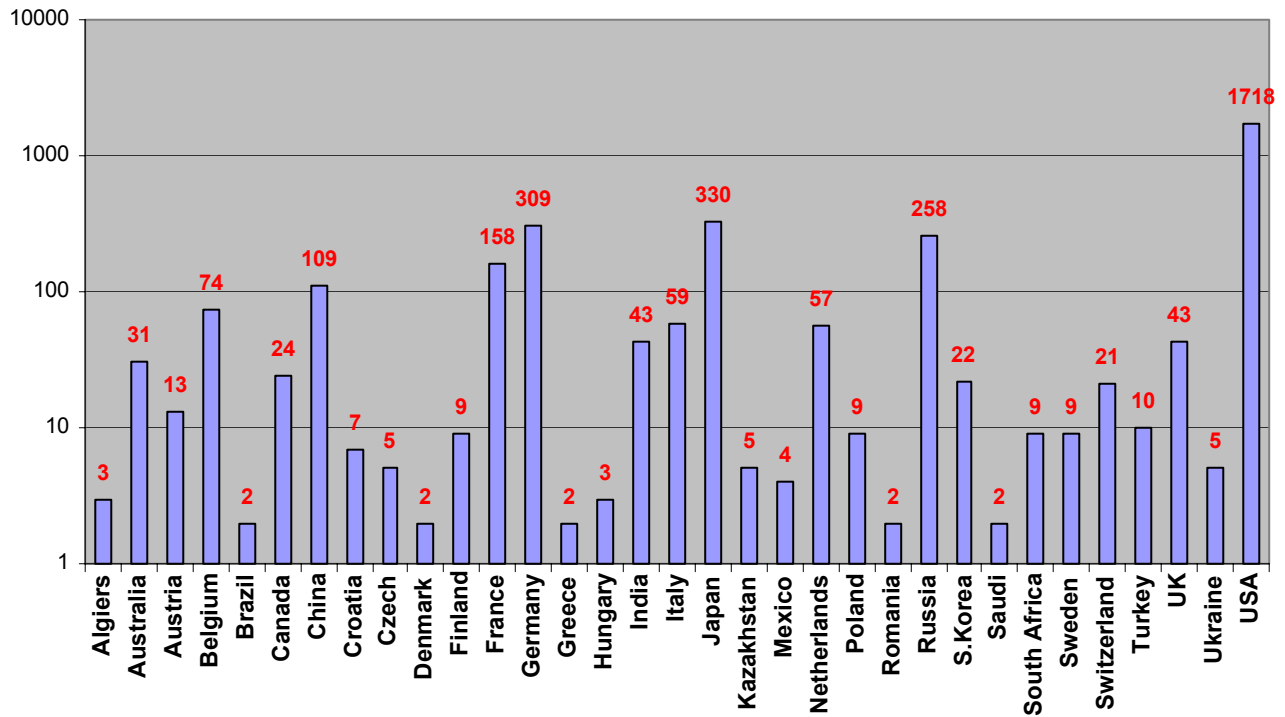
### 5.5.1. LISE tutorial

A tutorial for LISE++ was created for the RIA Summer School at NSCL / Michigan State University on August 2003. This tutorial shows step by step how to prepare for producing a radioactive beam of  $^{22}\text{Al}$  to be used in an implantation experiment where the  $\beta$ -delayed proton decay of this nucleus is to be studied. This tutorial can be loaded using the following links:

<http://groups.nslc.msu.edu/lise/doc/tutorial.pdf> or <http://dnr080.jinr.ru/lise/doc/tutorial.pdf>.

### 5.5.2. User statistics

Fig.435 shows in which countries there is interest to LISE++. The statistics corresponds to the past year, and are based on identified visits of sites of the LISE code. Due to temporary problems with the work of dnr080 server (at Dubna) about 40 percents of hits are not registered.



*Fig.435. User statistics of the LISE web sites for the past year. Countries with one hit were excluded. More than half the statistics for USA is from NSCL, for Germany GSI, for Japan RIKEN, and for Russia JINR.*

### 5.5.3. Future perspectives for LISE++ (version 6.4)


- Develop fission products kinematics in LISE++.
- Incorporate a new reaction mechanism: **Fission**.

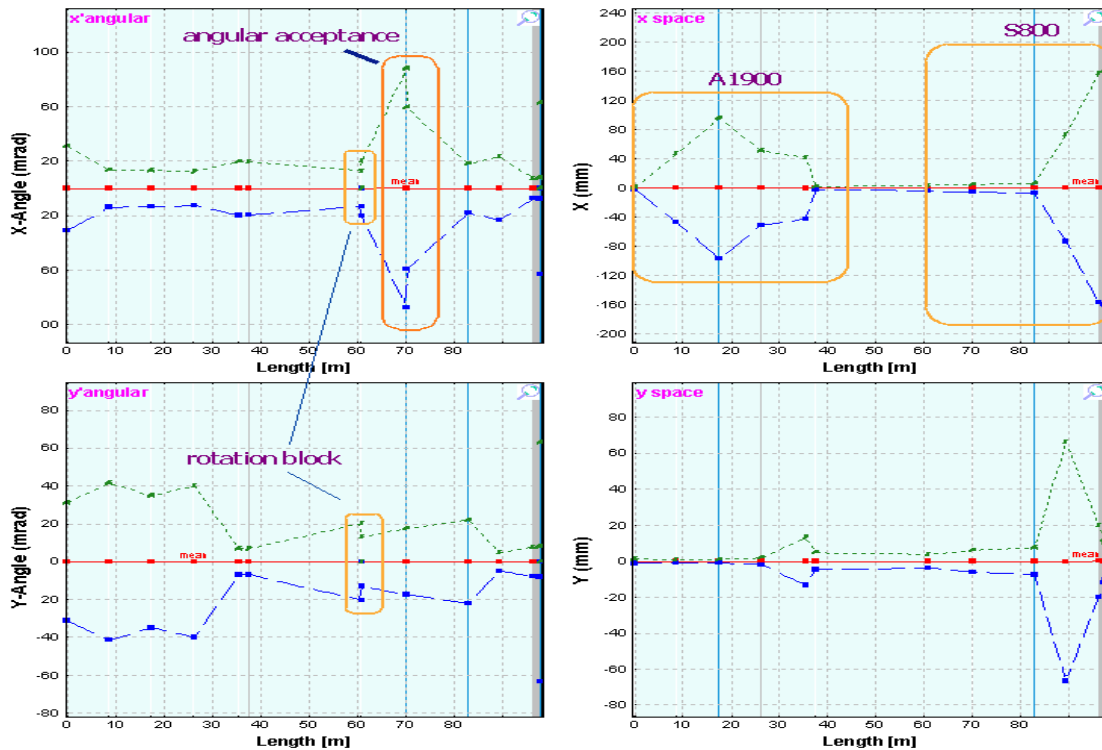
### Acknowledgements

The authors gratefully acknowledge Prof. Carlos Bertulani, Prof. Filomena Nunes, Dr. Helmut Weik and Dr. Ken Yoneda for fruitful help with the development of LISE++.

## 6. Version 6.2

### 6.1. Transport envelope calculation package

The envelope calculation package permits to visualize the dynamics of changes in distributions along the spectrometer. Use the menu “Plot->Envelope Plot” or the icon  in the toolbar to load the new utility. The code builds envelope plots for horizontal and vertical angular distributions, horizontal and vertical spatial distributions, and energy and momentum distributions (see Fig.436). The code extracts the mean value of the distribution (red line in Fig.436) at the beginning and at the end of each block. Green and blue lines show left and right positions corresponding to the half-maximum amplitudes of these distributions.



**Fig.436.**  $^{32}\text{S}$  envelope for the configuration A1900\_S800\_d0. The spectrometer is set to the fragment  $^{32}\text{S}$ . The round rectangle “angular acceptance” shows the cut of horizontal angular distribution by the acceptance of the second part of s800 beam-line spectrometer.

**Fig.437.**  $^{32}\text{S}$  horizontal spatial distribution envelope for the configuration described in Fig.436, but the spectrometer set to a 3% higher magnetic rigidity.

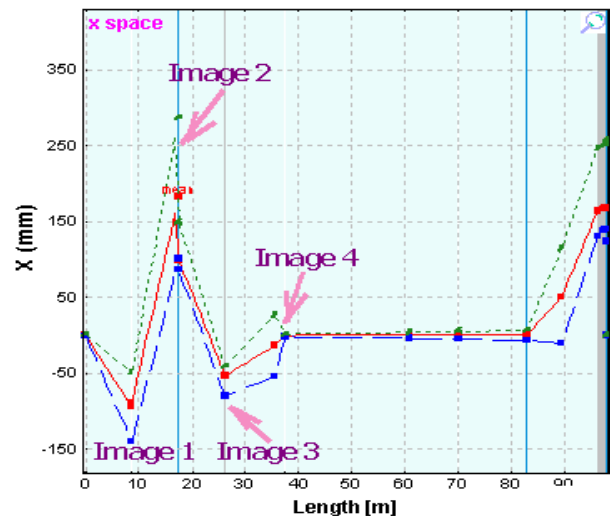



Fig.437 shows for comparison the  $^{32}\text{S}$  horizontal spatial distribution for the spectrometer tuned to magnetic rigidity 3% above the  $^{32}\text{S}$  optimal value (Fig.436).

The envelope package allows to debug the code calculations, to see the evolution of the distributions and their changes due to energy loss in materials (wedge) and the influence of slits.

Use “zoom” plot to see evolution momentum or energy distributions between detectors.

## 6.2. Code “Charge”

“CHARGE” is a user program developed at GSI which calculates atomic charge-changing cross sections, charge-state evolutions, and equilibrium-charge-state distributions for bare, H-, and He-like relativistic heavy ions penetrating through matter. The code “Charge” [Sch98] has been translated into C++ and is now part of the “LISE++” package. The source code (FORTRAN) was kindly provided by colleagues from GSI. The “Charge” code can be loaded by using the icon  in the toolbar or the menu “Utilities”. The program interface window is shown in Fig.439. “Equilibrium thickness versus projectile energy” plot (Fig.438) can be

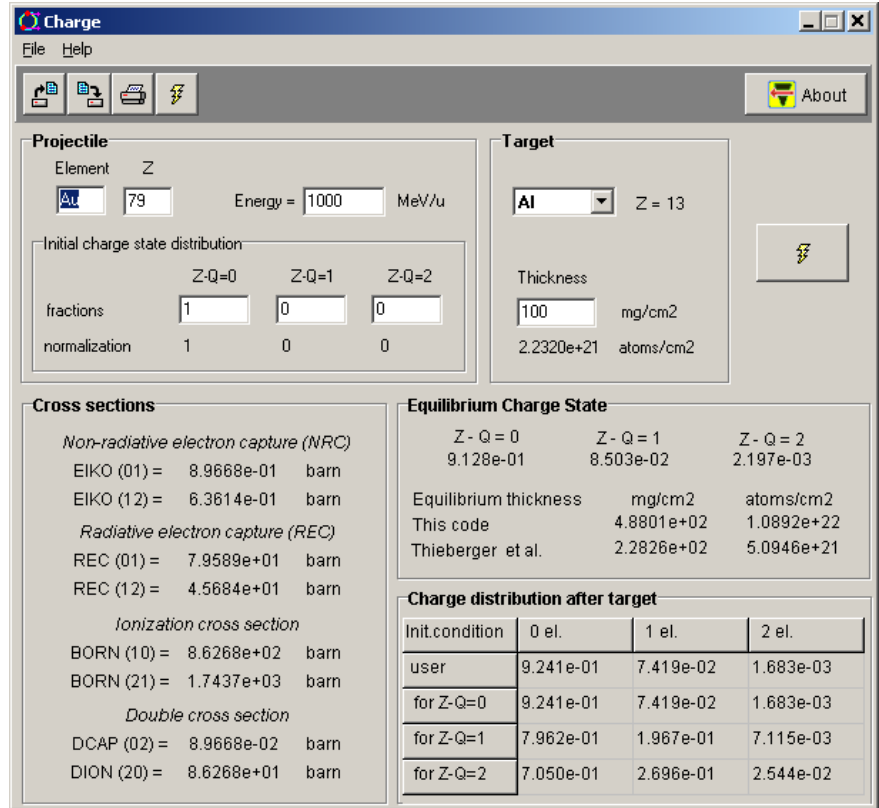


Fig.439. The “Charge” code (version for MS Windows) is in action

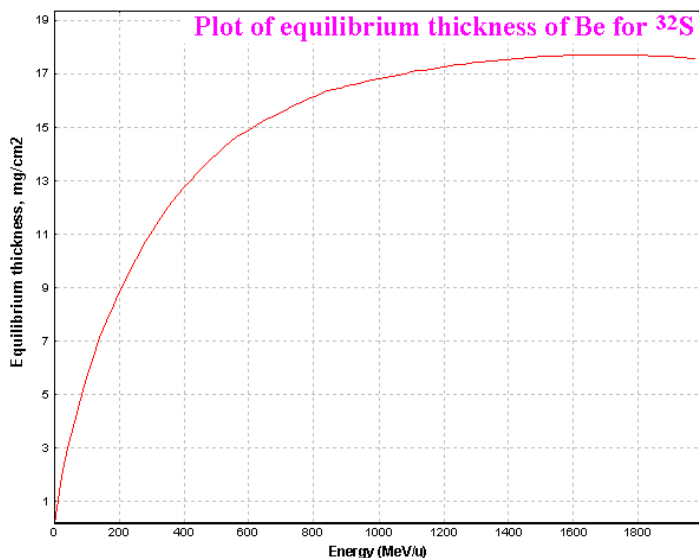


Fig.438. Equilibrium thickness for  $^{32}\text{S}$  in material Be.

loaded in LISE++ (menu “Utilities”). LISE++ uses Thierberger’s [Thi85] definition of the equilibrium thickness from the code “Charge”.

It is possible also to see the equilibrium thickness value in the “Physical calculator”.

The program “Global” [Sch98] will be soon adapted for “Windows” and will be used in LISE++ for calculations of charge states distributions.

### 6.3. Brho (Erho) analyzer dialog

The Brho / Erho analyzer dialog is developed to calculate and plot a trajectory of ions in the magnetic / electrical dipoles depending on energy and emittance of beam and settings of the dipole. The utility can help to calculate a position for a primary beam trap in the chamber dipole to avoid scattering of a primary beam on walls of the dipole chamber. The dialog is loaded from the menu "Utilities → Brho Analyzer". The Brho (Erho) analyzer supports magnetic and electric dipoles. The dialog in the “magnetic dipole” mode is shown in Fig.440. The switching between modes is made by choice of a field of dipole. The “magnetic dipole” mode is chosen in case of input of  $B\rho$  or  $B$  values, in the case of  $E\rho$  or  $E$  values, accordingly the “electrostatic dipole” mode will be applied. The user can see the mode used in the window “A” of the dialog (see Fig.440). An example of the “electrostatic dipole” mode is presented in the chapter “6.4.2. Electrostatic dipole”.

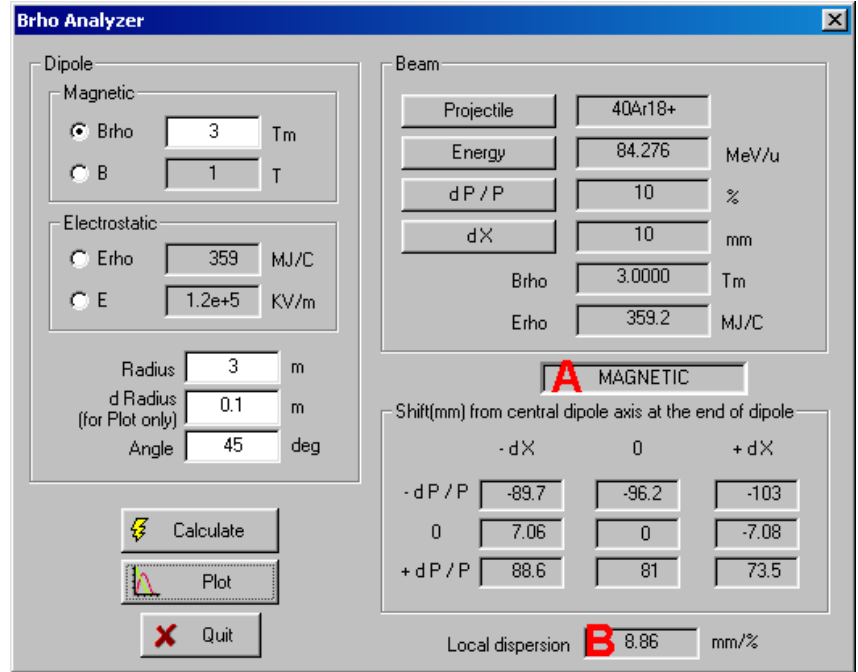


Fig.440. Brho(Erho) analyzer dialog in action of “magnetic” mode.

It is always assumed, that the incoming beam is parallel to an optical axis of spectrometer. The Brho analyzer calculates a local dispersion in the end of the dipole by using relations:

$$D = \frac{X_{+dP/P} - X_{-dP/P}}{2 \cdot dP/P} [mm / \%] \quad dP/P \neq 0 \text{ and } (X_{+dP/P} \cdot X_{-dP/P}) < 0 \quad /39/$$

$$D = \frac{X_{P_{beam}}}{P_{beam} / P_0 - 1} \cdot 100 [mm / \%] \quad dP/P \rightarrow 0 \text{ or } (X_{+dP/P} \cdot X_{-dP/P}) > 0, \quad /40/$$

where  $P_{beam}$  is the user’s adjusted momentum of the beam projectile,  $P_0$  is the momentum of projectile corresponding to the dipole central line. Local dispersion is given in the field marked by “B” (see Fig.440).

The program calculates 9 trajectories proceeding from combinations of 2 sets with three parameters characterizing beam ( $-dX$ , 0,  $+dX$ ) and ( $-dP/P$ , 0,  $+dP/P$ ). Numerical values in the exit of the dipole can be visualized in the dialog window. The sequence of steps is given next:

- Determine beam characteristics (mass, charge, energy and emittance ( $dP/P$  and  $dX$ ),
- Choose magnet entry field and enter the value,
- Enter the dipole parameters: radius, half-width of dipole chamber ( $d\_radius$ ), and angle ( $d\_radius$  is used only to show a chamber boundaries on the plot),

- Press the “Calculate” button to calculate trajectories, and then “Plot” to draw calculated trajectories.

As an example trajectories calculated for four different initial conditions are shown in Fig.441.

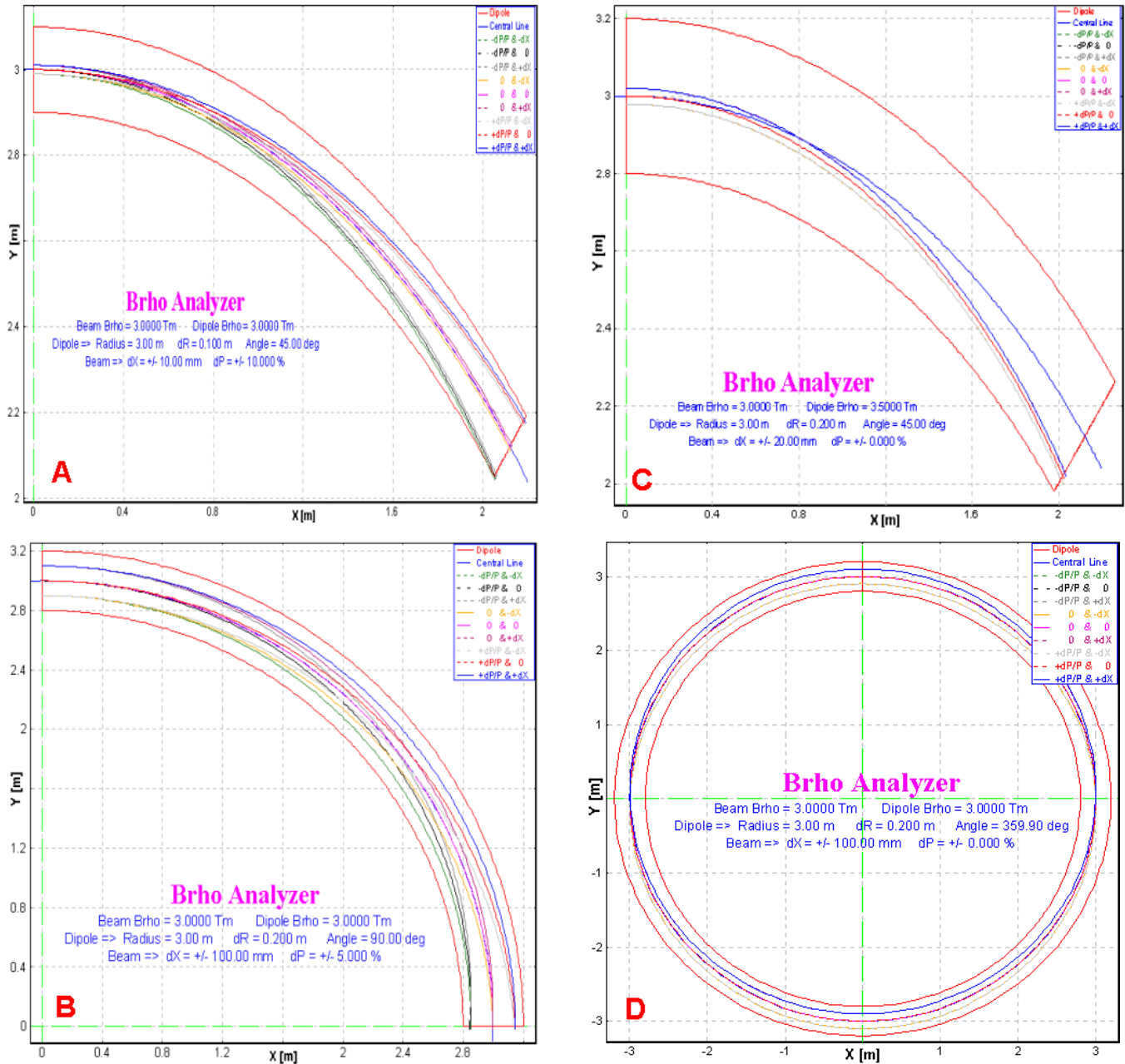


Fig.441. Brho analyzer plots for four different initial conditions. Initial conditions are listed in Table 49.

Table 49. Initial parameters of the primary beam and dipole settings for Fig.441.

Plot	Beam Brho, Tm	Dipole Brho, Tm	R m	DR m	Angle degree	dX ± mm	dP ± %
A	3.0	3.0	3	0.1	45	10	10
B	3.0	3.0	3	0.2	90	100	5
C	3.0	3.5	3	0.2	45	20	0

D	3.0	3.0	3	0.2	360	<b>100</b>	0
---	-----	-----	---	-----	-----	------------	---



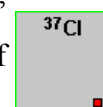
## 6.4. New optical blocks

Three new optic blocks based on magnetic dipoles have been developed:

- Compensating dipole
- Electric dipole
- Gas-filled magnetic dipole.

Electric dipole and gas-filled magnetic dipole blocks (as well as configuration files created on their base) are still under construction and will be more developed and optimized very soon in the experimental groups in operating conditions.

All three new blocks are intended for low-energy beam applications. In this context the further development of reaction models (fusion-evaporation, fission) is planned, and also use of charge state models at significantly lower energies. Please note, that the user can enter a production cross-section manually, instead of use “LisFus” model calculations. For this purpose it is necessary to set the option “File” in the dialog “Options⇒Preferences” and enter a cross section value in the dialog “Cross sections” (menu “Options”). The red square in the right bottom corner of an isotope cell in the table of nuclides indicates that a cross section value from a file is used.



### 6.4.1. Compensating dipole

Compensating dipole block has already been realized in the code LISE as the block “D6” ([http://groups.nsl.msu.edu/lise/3\\_4/lise\\_3\\_4.html](http://groups.nsl.msu.edu/lise/3_4/lise_3_4.html)). This block represents a magnet on a platform that it is possible to incline, so that the global dispersion after the block will be equal to zero. In the LISE++ code the compensating dipole may be used now after dispersive block (not only after the Wien velocity filter as it was done in the code LISE) to compensate global dispersion. The compensating dipole block can be used for the spectrometer MARS (TAMU), and for LISE3 and VAMOS at GANIL. Compensating dipole characteristics in the “Set-up” window is shown in Fig.442, where  $Br$  is the magnetic rigidity (Brho) [Tm],  $A$  is the inclination angle of the magnet [deg],  $DG$  is the global dispersion behind this block [mm/%].

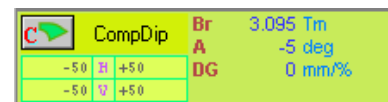


Fig.442. Compensating dipole in the “Set-up” window.

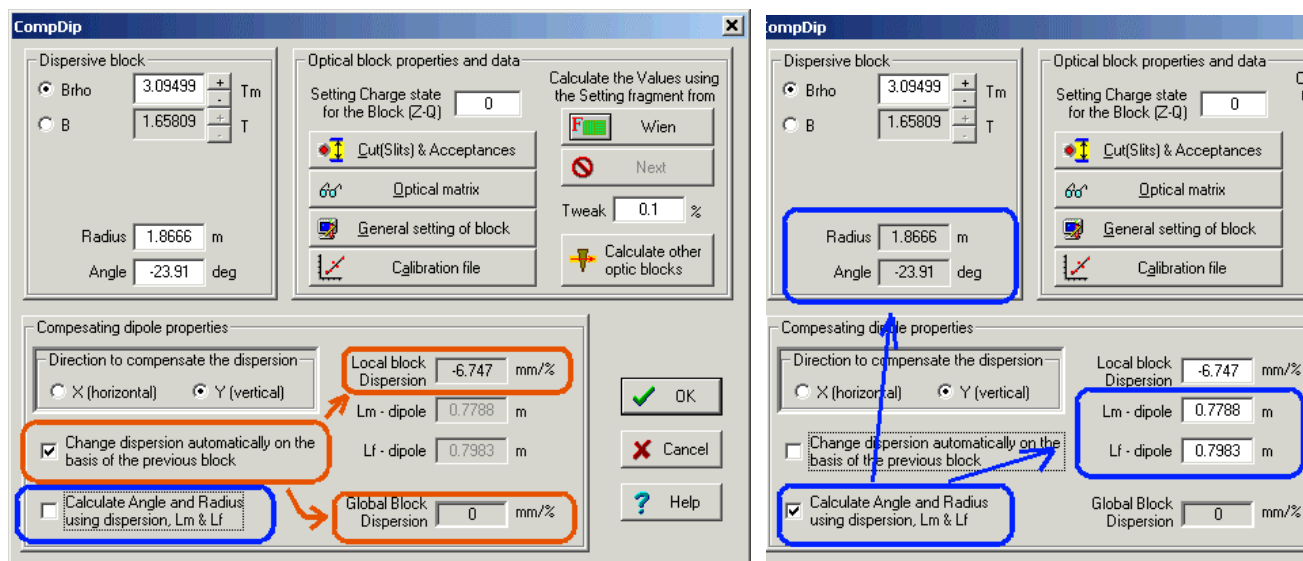


Fig.443. The compensating dipole dialog. Left and right picture show different modes of compensating dipole settings.

Some new features have been added. It is now also possible to input the local dispersion manually as well as the radius and the angle of the dipole (see Fig.443). The configuration file “LISE3.lcn” for the LISE spectrometer with Wien velocity filter and the compensating dipole D6 is included in the standard LISE++ package. An example of a simulation using the LISE3 configuration is shown in Fig.444.

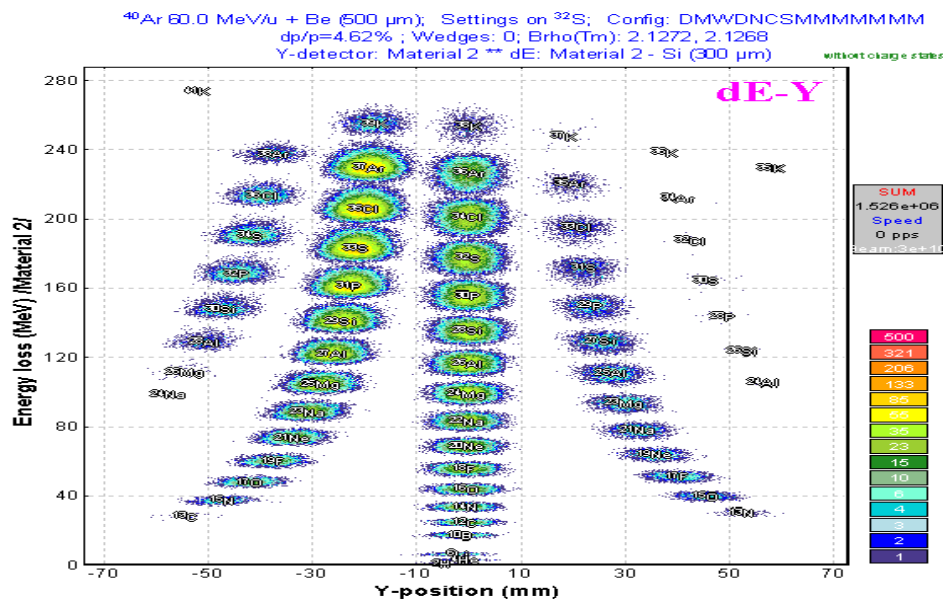


Fig.444. Plot of energy loss versus vertical position in final focal plane for the LISE3 configuration file. The vertical plane represents a selection with A/Q dispersion.

6.4.1.1. MARS spectrometer configuration

A preliminary configuration (file “TAMU-MARS.lcn”) for the MARS spectrometer [Tri89] has been developed. The scheme of the spectrometer is shown in Fig.445. An example to produce the secondary beam of ions <sup>8</sup>He with the MARS spectrometer is provided in the file “TAMU-Mars\_8He.lpp”. The two-dimensional particle identification plot and the selection plot to produce <sup>8</sup>He secondary beam are shown in Fig.446 and 447. It is planned to optimize the MARS configuration in future experiments.

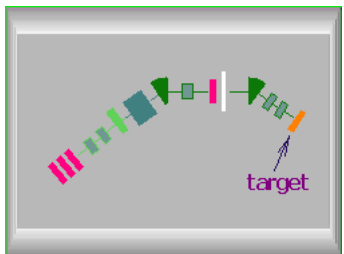


Fig.445. MARS spectrometer scheme

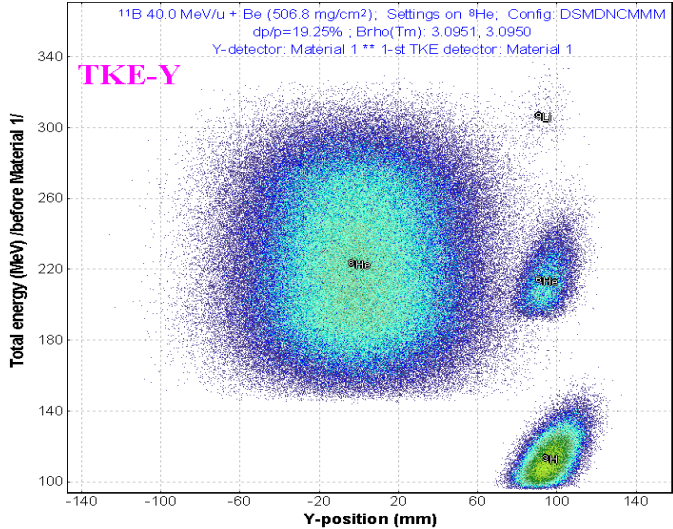


Fig.446. The plot of total kinetic energy versus vertical position in the final focal plane of the MARS spectrometer set to produce the secondary beam of <sup>8</sup>He.

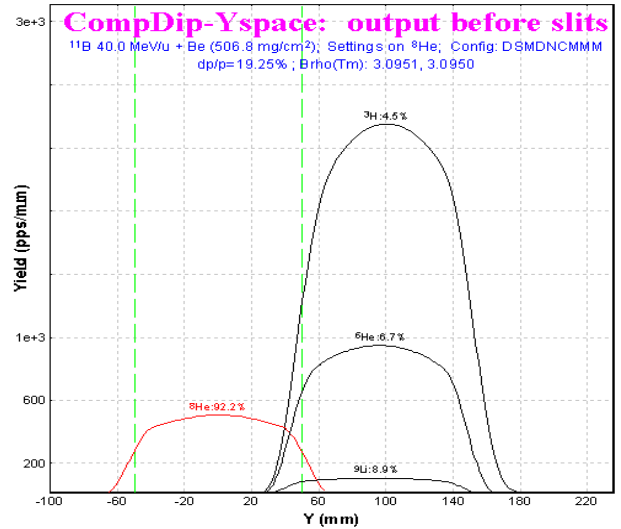


Fig.447. Vertical selection plot after the compensating dipole.

### 6.4.2. Electrostatic dipole

The new physical value “electric rigidity” (“Erho”) has been added to physical values family of the code. Electric rigidity represents multiplication of electric field and dipole radius, and is characterized the settings of electrostatic dipole in analogy to the magnetic dipole and magnetic rigidity. Electric rigidity can be calculated as other physical values (Energy of projectile, Range, Brho etc) by means of the “Physical calculator” dialog.

The code assumes that electric field in the electrostatic dipole is always uniform and is equal to  $U/d$ , where  $U$  is the voltage, and  $d$  is the gap between plates. Electric dipole window in the “Set-up” window is shown in Fig.448, where  $E$  is the electric field [KV/m],  $U$  is the voltage [KV],  $Er$  is the electric rigidity [MJ/C]. The Electrostatic dipole dialog is shown in Fig.449. The edit cell “Magnetic rigidity” in this dialog serves just to show the corresponding value for setting fragment (residual) and helps in the case of the combination of magnetic dipole and electrostatic dipole.

E	ED1	E	3440.9 KV/m
		U	516.1 KV
		Er	11.29 MJ/C
-100	+100		
-90	+90		

Fig.448. Electrostatic dipole window in the “Set-up”.

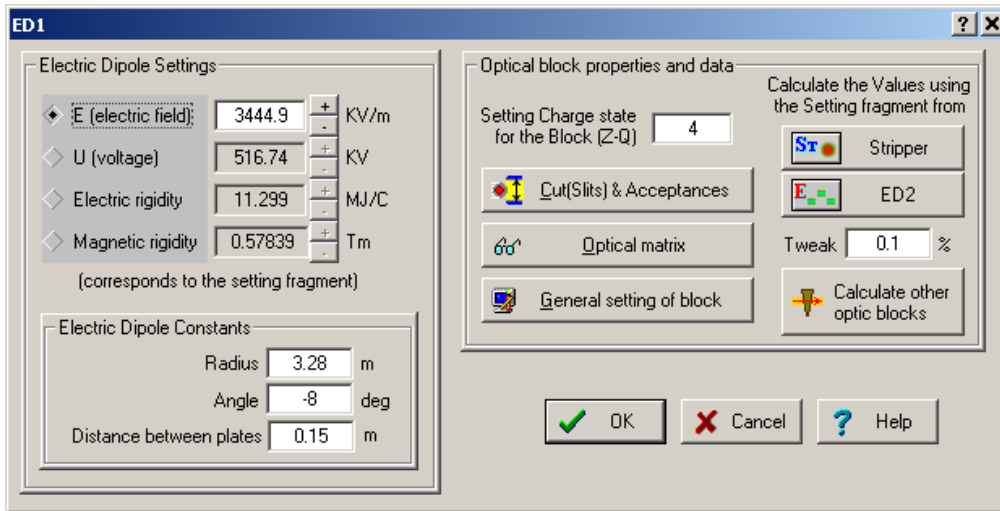


Fig.449. The Electrostatic dipole dialog.

Projectile trajectories in an electric dipole (as well as in a magnetic dipole) can be plotted in the dialog “Brho analyzer” (see chapter “6.3. Brho (Erho) analyzer dialog”). Similar to other optic dispersive blocks the electric dipole block uses the optical transport matrix with the dispersion determined by relation  $x/(\Delta P/P)$ . The code calculates the momentum of the ion ( $P_{\text{dipole}}$ ) from the electric dipole settings. The spatial component  $x_P$  is calculated based on the dispersion, fragment momentum distribution, and  $P_{\text{dipole}}$ . The application of electric dipole mode in LISE++ is given in the following chapter on by example of the kinematic separator VASSILISSA.

#### 6.4.2.1. The kinematic separator “VASSILISSA” configuration

The LISE++ configuration file (LISE/config/Dubna/vassilissa.lcn) of the kinematic separator VASSILISSA has been created using the article [Yer94] and TRANSPORT code file for this separator which was kindly provided by V.Schepunov. The scheme of the spectrometer is shown in Fig.450. As in [Yer94] the reaction  $^{22}\text{Ne}(100\text{MeV}) + ^{197}\text{Au}(0.35\text{mg}/\text{cm}^2) \rightarrow ^{215}\text{Ac} + 4n$  was chosen to calculate the recoil

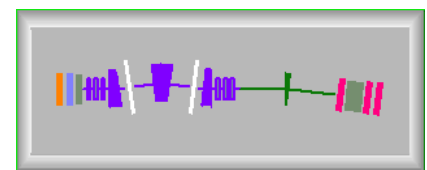


Fig.450. The VASSILISSA separator scheme

transmission for separator. The file “vassilissa\_22ne\_Au\_charge\_states.lpp” with these settings is included in LISE++ package and can be found in the directory “LISE\files”.

### 6.4.2.2. Tuning the spectrometer for fusion-evaporation residue

Procedure to calculate the rate of fusion-evaporation products:

- Set “Fusion->Residual” as reaction in the dialog “Production mechanism”;
- Select your spectrometer in the directory “LISE\Config” (or create new one);
- Enter the primary beam characteristics in the dialog “Projectile (Beam);
- Enter the target characteristics;
- Enter the stripper (after target) characteristics, if stripper thickness is not 0;
- Set the option “Charge states” ON in the dialog “Preferences”;
- Check energy loss, charge states and other calculation methods used in the code. For lower energy (less 10 MeV/u) it is recommended to use the following methods:

Charge states calculation	Leon [1] or Shima [2]
Energy Loss calculation	Ziegler [1]
Energy straggling	Atima [1]
Angular straggling	Particle Data Group [2]

- Select the fragment (residue) of interest (don’t enter charge states now);
- Click the button “Compound” in the setup window of the code to get the fusion-residue information window (see Fig.451) to see calculations of charge states, energies etc.

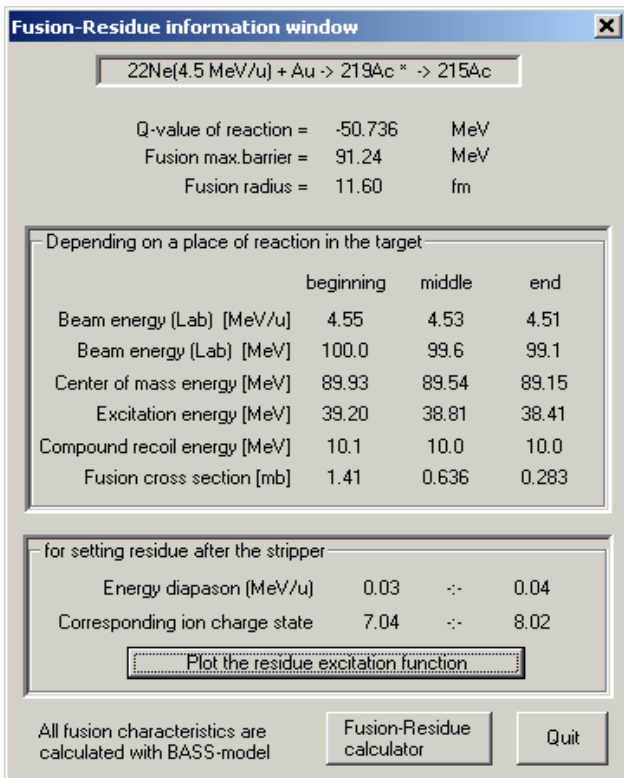


Fig.451. The fusion-residue information window for the reaction  $^{22}\text{Ne}(100\text{MeV}) + ^{197}\text{Au}(0.35\text{ mg/cm}^2) \rightarrow ^{215}\text{Ac} + 4n$ .

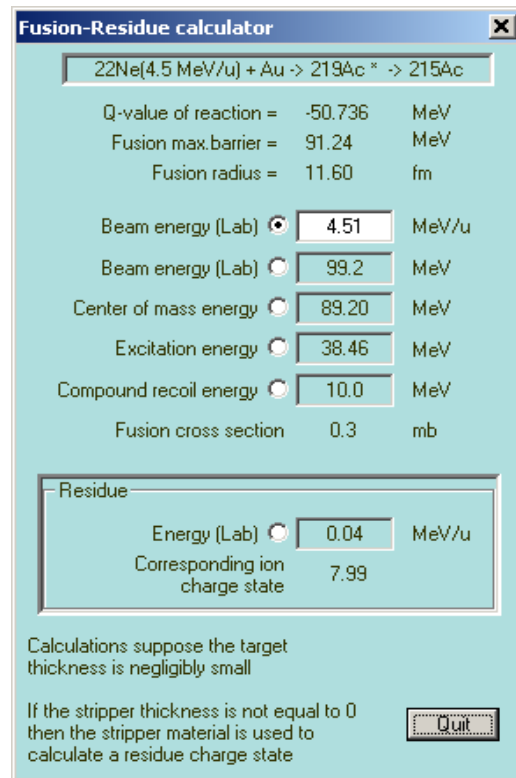




Fig.452. The fusion-residue calculator can be loaded from the fusion-residue information window or from the menu “Calculations”.

- Depending on the corresponding charge state of the ion after the target (stripper) shown in the fusion-residue information window enter the charge state of the residual through the dialog “Setting fragment (residue)”. Please keep in mind that it is also possible to estimate a charge state using the fusion-residue calculator (Fig.452);
- Calculate the spectrometer settings for the selected ion using the menu “Calculation” or the icon  in the toolbar;
- Calculate the selected ion transmission and rate by mouse right click over an isotope of interest or using the menu “Calculation→Transmission”. If production cross section was not yet calculated or has not been entered manually, then the program will offer (see Fig.453) to calculate (A) the production cross section with the help of the LisFus model (without fission channel), or enter them manually (B). The user can enter 1. already known cross section, 2. calculate them using the PACE4 code , 3. enter any number, only to estimate a transmission.

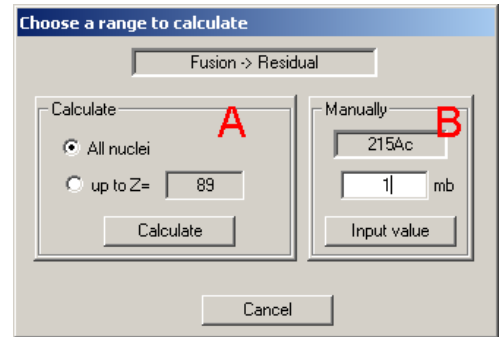


Fig.453.

#### 6.4.2.3. Choice of charge state of ion to set the spectrometer

The mean ionic charge of  $^{215}\text{Ac}$  after a carbon stripper is shown in Fig.454. It is possible to see that Winger’s model (blue line) predicts a high value of ionic charge in the low energy region. Leon’s (black line) and Schima’s (green line) models are close to each other for low energies, however Shima’s model underestimates a charge state with increasing energy. Therefore the model of Leon is recommended for calculations of charge states in the region between 0.5-5 MeV/u.

The comparison of various models of charge state calculations with experiments, and also energy regions of applications of models will be summarized in the next version documentation.

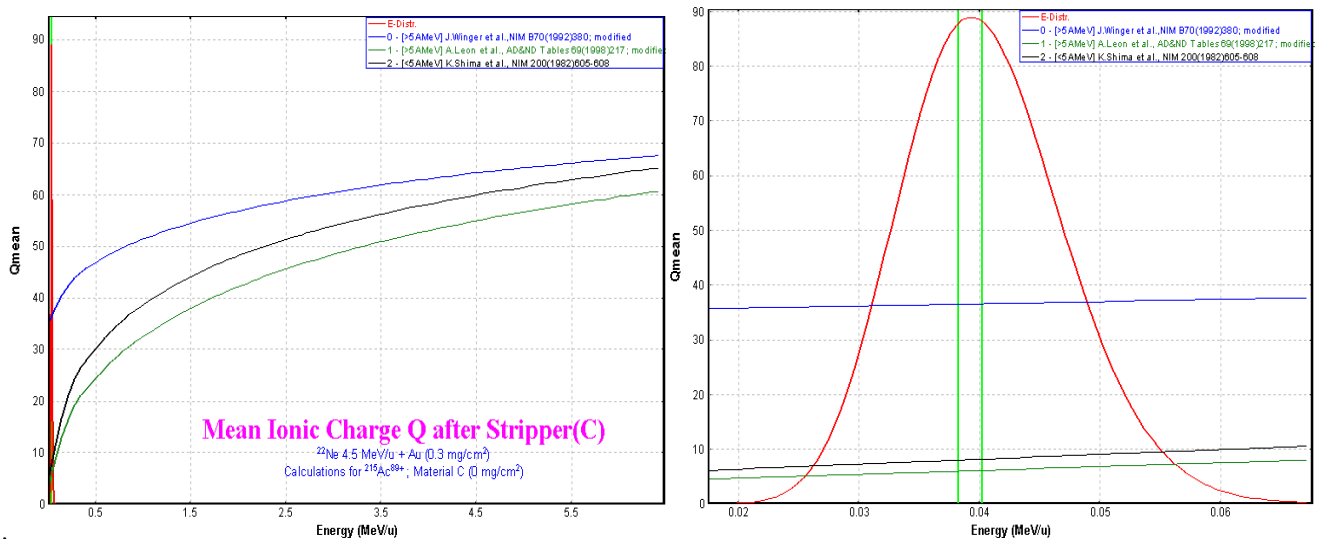
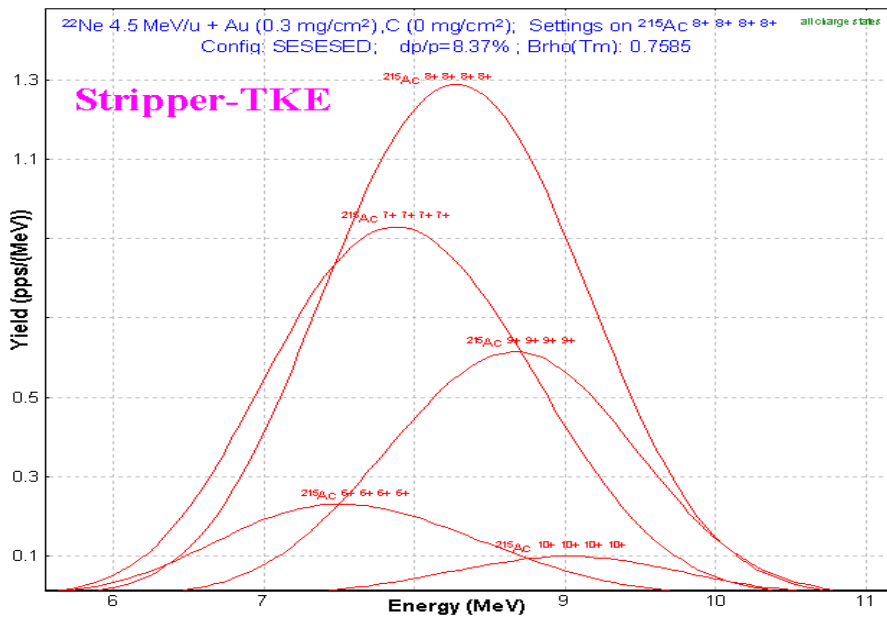


Fig.454. Mean ionic charge of  $^{215}\text{Ac}$  after a carbon stripper on the left plot shows in the energy diapason 0.0 – 6.0 MeV/u. The right plot is the same for the energy diapason 0.02 ÷ 0.07 MeV/u. The energy distribution of  $^{215}\text{Ac}$  residue after the stripper is indicated by the red line. The energy distribution of different charge states of  $^{215}\text{Ac}$  is shown in Fig.455.



**Fig.455.** Energy distribution of different charge states of  $^{215}\text{Ac}$  residuals after a carbon stripper in the reaction  $^{22}\text{Ne}(100\text{MeV}) + ^{197}\text{Au}(0.35\text{ mg/cm}^2) \rightarrow ^{215}\text{Ac} + 4n$ . The carbon foil ( $0.35\text{ mg/cm}^2$ ) is placed after the target to reset the charge distribution to equilibrium.  $^{215}\text{Ac}^{8+}$  dominates the charge state distribution.

#### 6.4.2.4. Calculation of energy and angular distribution of fusion-evaporation residues

Fig.456 and Fig.457 compare evaporation residuals energy and angular distributions calculated by LISE++ and calculated using a Monte Carlo computer code [Yer94]. In the case of LISE++ all distributions have been calculated after a carbon stripper. The reactions used for the calculations are listed in Table 50. For LISE++ calculations the option “Charge state” was set off to sum all charge state distributions. LISE files for the examples discussed in the figure are located in LISE web-site:

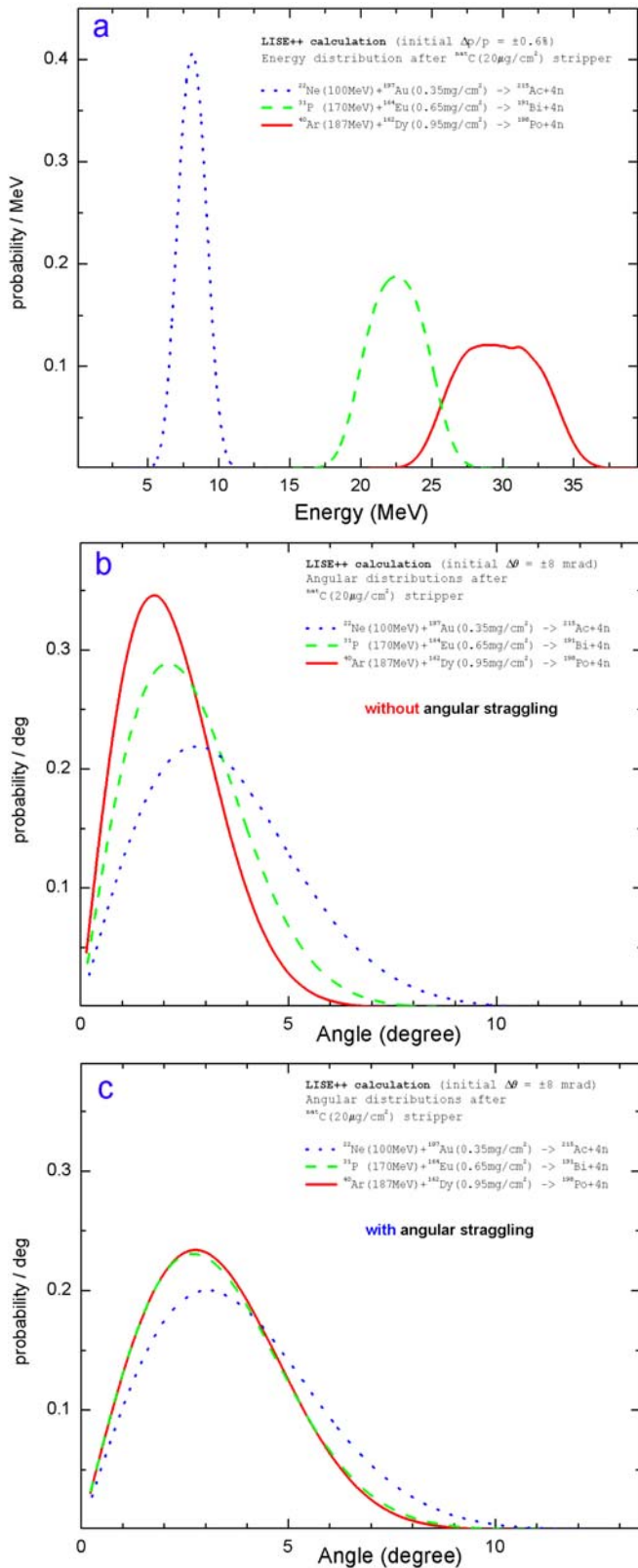
[http://www.nsl.msui.edu/lise/6\\_2/examples/vassilissa\\_22ne\\_au.lpp](http://www.nsl.msui.edu/lise/6_2/examples/vassilissa_22ne_au.lpp)  
[http://www.nsl.msui.edu/lise/6\\_2/examples/vassilissa\\_31p\\_164er.lpp](http://www.nsl.msui.edu/lise/6_2/examples/vassilissa_31p_164er.lpp)  
[http://www.nsl.msui.edu/lise/6\\_2/examples/vassilissa\\_40ar\\_162dy.lpp](http://www.nsl.msui.edu/lise/6_2/examples/vassilissa_40ar_162dy.lpp)

LISE++ uses  $(d\sigma/d\Omega)_{x,y}$  “plane” (projection) angular distributions for transmission calculations. This means regular LISE’s angular distributions (which the user can see in the plots) have been transformed to  $(d\sigma/d\Omega)$  “space” distributions and then into distributions  $(d\sigma/d\theta)$  to be compared with Monte Carlo calculations [Yer94]. In order to show a contribution of angular straggling calculations have been performed with and without angular straggling (see Fig.456 b & c). Angular straggling and the lateral range at low energies are discussed in the chapter “6.5.4. Angular straggling”.

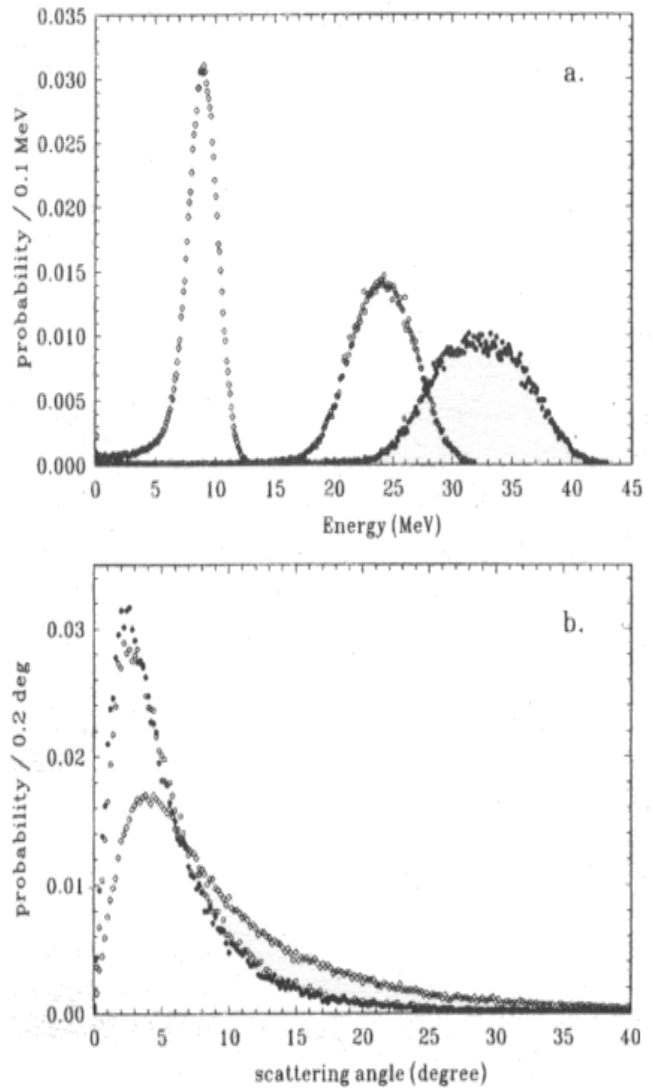
#### 6.4.2.5. Suppression of the primary beam

Suppression of the primary beam is a more principal task in the region of nuclei with subnanobarn cross sections in heavy ions fusion-evaporation reactions. In this context it is necessary to take into account all possible factors capable to render influences on transmission/suppression of the primary beam. The current version of the code assumes energy and spatial broadening of the primary beam due to energy and angular straggling, but it does not take into account actual scattering of the beam in the target. In later versions of LISE++ it is planned to include a possibility to use a scattering primary beam. The initial emittance of the primary beam used to calculate transmission was set the following:

$$x = y = \pm 2.5 \text{ mm}, x' = y' = \pm 8 \text{ mrad}, dP/P = \pm 0.6 \text{ \%}.$$



**Fig.456.** LISE++ calculated energy (a), scattering angle without straggling contribution (b) and scattering angle with straggling contribution (c) distributions after the STRIPPER for evaporation residuals from the reactions listed in Table 50. See text for details.



**Fig.457.** Calculated energy (a) and angular (b) distributions [Yer94] for evaporation residuals from the reactions given in Table 50.

**Table 50.** Designations for Fig.456 and Fig.457

for Fig.45 6	for Fig.45 7	reaction
•••	◇	$^{22}\text{Ne}(100\text{MeV}) + ^{197}\text{Au}(0.35\text{ mg/cm}^2) \rightarrow ^{215}\text{Ac} + 4n$
---	○	$^{31}\text{P}(170\text{MeV}) + ^{164}\text{Er}(0.65\text{ mg/cm}^2) \rightarrow ^{191}\text{Bi} + 4n$
—	●	$^{40}\text{Ar}(187\text{MeV}) + ^{162}\text{Dy}(0.95\text{ mg/cm}^2) \rightarrow ^{198}\text{Po} + 4n$

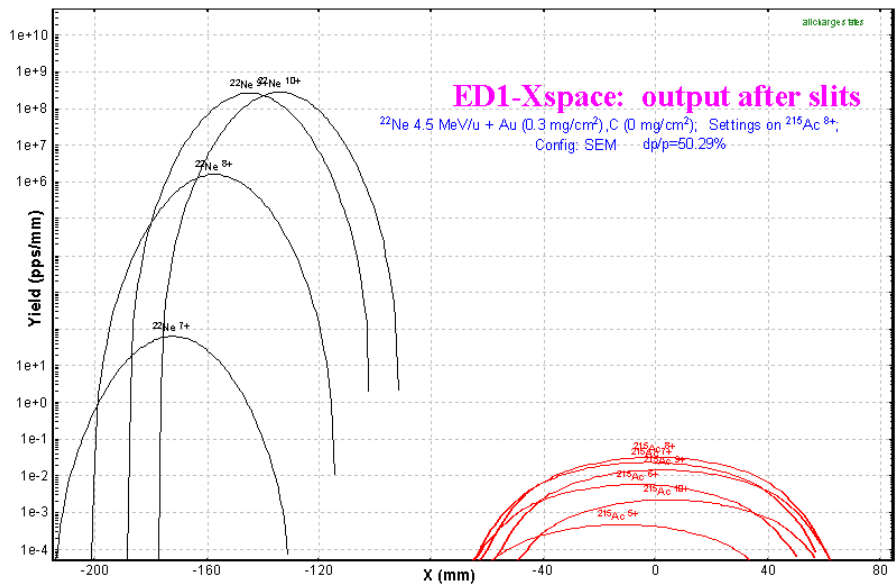


Fig.458. Horizontal distributions of  $^{215}\text{Ac}$  residuals (red) and primary beam charge states (black) after the first electric dipole. See a text for details.

The horizontal distributions of charge states of  $^{215}\text{Ac}$  residual and primary beam particles from the reaction  $^{22}\text{Ne}(100\text{MeV}) + ^{197}\text{Au}(0.35 \text{ mg/cm}^2)$  after the first electric dipole of VASSILISSA separator are shown in Fig.458. The separator is set to the ion  $^{215}\text{Ac}^{8+}$ . All blocks behind the first dipole in the separator configuration were set disable to get the primary beam horizontal distributions in Fig.458. The distributions were calculated assuming the dispersion being **position independent** from position in the horizontal plane.

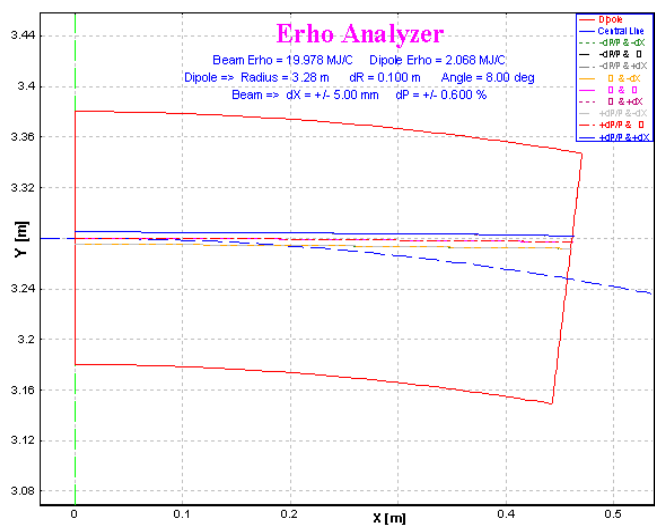
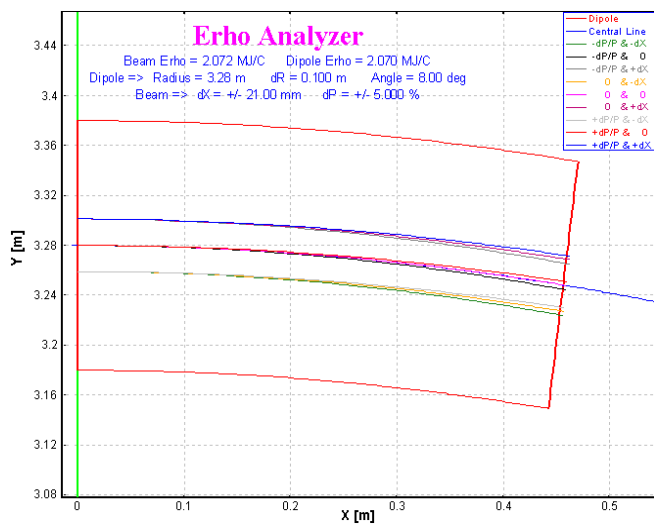
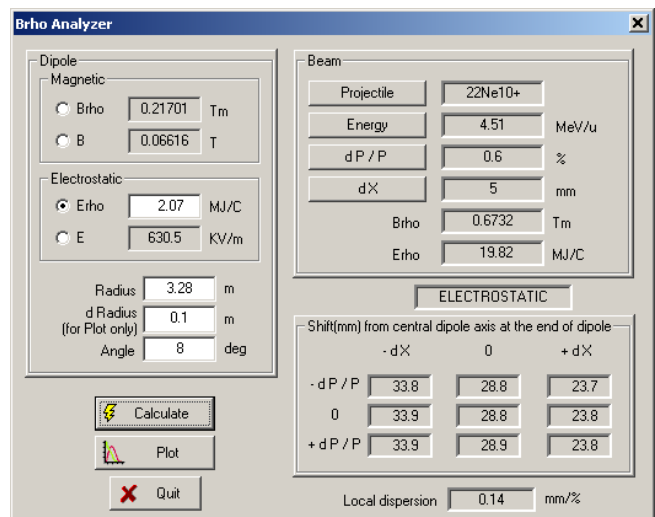
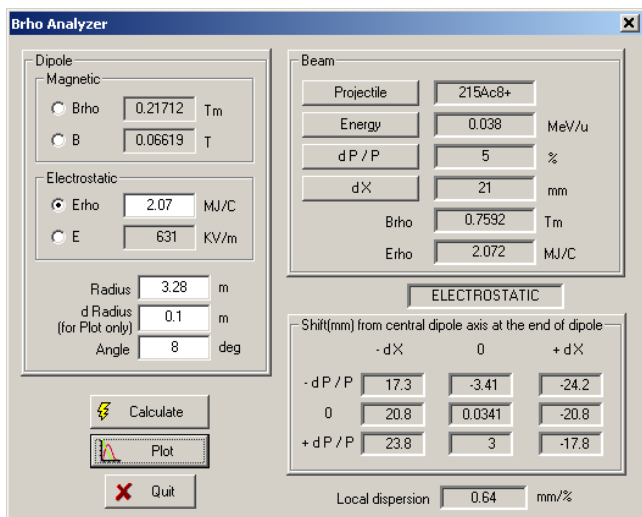
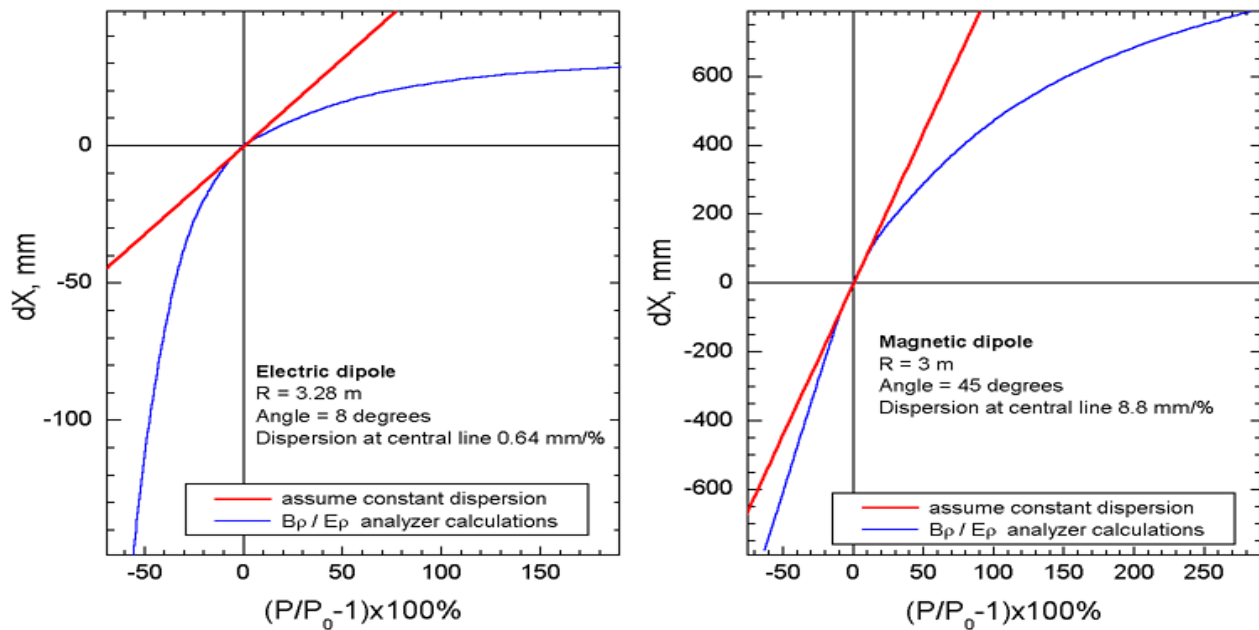


Fig.459. Trajectory calculations for the residual  $^{215}\text{Ac}^{8+}$  (left plots) and the primary beam charge state  $^{22}\text{Ne}^{10+}$  (right plots) by the Brho(Erho) analyzer for the first dipole tuned to  $^{215}\text{Ac}^{8+}$  in the reaction  $^{22}\text{Ne}(100\text{MeV}) + ^{197}\text{Au}(0.35 \text{ mg/cm}^2)$ .



It is easily seen from the picture that it is possible to separate residuals from the primary beam after the dipole. It is valid to consider a constant dispersion close to the central optical line for several percents of value  $dP/P$ . To show this statement and to determine a dispersion further away from a primary beam position in the dipole exit the calculations were made with the help of the Brho(Erho) analyzer. Initial conditions (energies, emittances) and calculated trajectories for the residual  $^{215}\text{Ac}^{8+}$  and the primary beam charge state  $^{22}\text{Ne}^{10+}$  are shown in Fig.459. It is obvious, that local dispersion in the case of  $^{215}\text{Ac}$  is equal to 0.64 mm/% confirmed also by TRANSPORT (look the first dipole optical matrix in the configuration file), however in the case of primary beam the dispersion is equal to 0.14 mm/% and a shift of the primary beam from the optical axis results in 28 mm instead of 130 mm calculated by LISE++ assuming a constant dispersion. The residue  $^{215}\text{Ac}^{8+}$  settings of the first dipole corresponds to an energy of 0.47 MeV/u for the primary beam charge state  $^{22}\text{Ne}^{10+}$ . The ratio of the primary beam momentum after the reaction and the momentum from dipole setting  $P_{(22\text{Ne})}/P_{\text{dipole}(22\text{Ne}^{10+})}$  is approximately equal to 3. Fig.460 shows calculated distributions of the horizontal position at the exit of the dipole from the ratio  $P/P_0$  for electric and magnetic dipoles.



**Fig.460.** Horizontal position at the exit of dipole versus ratio  $(P/P_0-1)\cdot 100\%$  for electric (left) and magnetic (right) dipoles. Brho analyzer calculations are shown by blue color. Red lines show a shift from the central optical line assuming a constant dispersion.

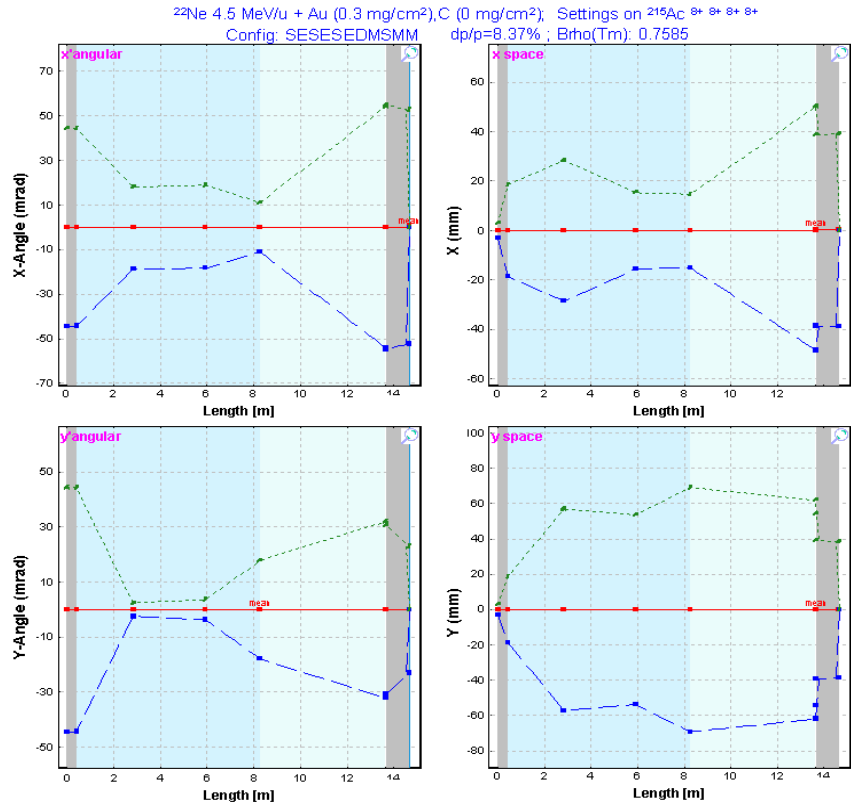
In order to predict correctly the separation of residues and the primary beam it is planned to implement the following options:

- To add an opportunity to include a drift block after the dipole in the Brho(Erho) analyzer;
- To develop a subroutine to calculate a reduced dispersion for large values of  $dP/P$ ;
- To insert a drift block between the two first dipoles in the configuration of the VASSILISSA separator to obtain a separation of residues from a primary beam.

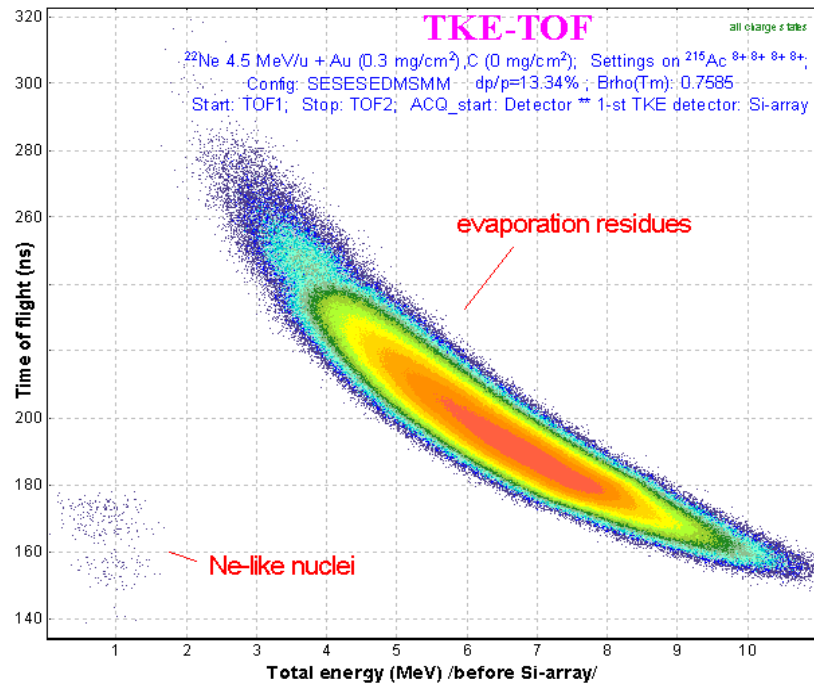
### 6.4.2.6. Residue transmission calculation

An example of the transmission residues in the VASSILISSA separator from the reaction  $^{22}\text{Ne}(100\text{MeV}) + ^{197}\text{Au}(0.35\text{ mg/cm}^2) \rightarrow ^{215}\text{Ac}^{8+}$  is given in the file “vassilissa\_22ne\_au\_states.lpp” which is included in LISE++ package. The  $^{215}\text{Ac}^{8+}$  envelope is shown in Fig.461.

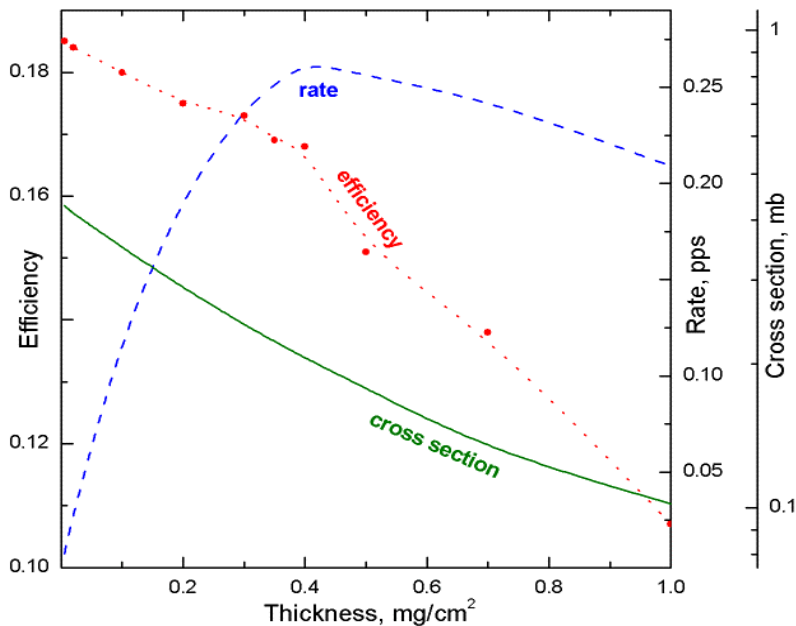
The spectrum time-of-flight versus total energy at the VASSILISSA focal plane calculated by LISE++ is shown in Fig.462. The separator was optimized to get the maximum rate of  $^{215}\text{Ac}^{8+}$  residues. Ne-like nuclei production cross sections were entered manually. Production cross sections of residues have been calculated within the LisFus model with the option quantum-mechanical transmission probability for the barrier. The curvature parameter  $h\omega$  was set to 3 MeV. Chapter “6.6. Sub-barrier fusion cross-section” provides more details on this option. Also this chapter presents results for residue production cross sections calculated within various reaction models and a comparison to experimental results. The separation efficiency, production cross section of residue  $^{215}\text{Ac}$ , and rate of all charge states of residue  $^{215}\text{Ac}$  as a functions of the target thickness are shown in Fig.463.



**Fig.461.**  $^{215}\text{Ac}^{8+}$  envelope in the reaction  $^{22}\text{Ne}(100\text{MeV}) + ^{197}\text{Au}(0.35\text{ mg/cm}^2)$  with the VASSILISSA separator. The separator was set to the ion  $^{215}\text{Ac}^{8+}$ .



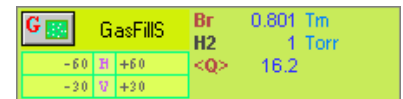
**Fig.462.** Time-of-flight versus energy spectrum at the VASSILISSA focal plane calculated by LISE++ for the reaction  $^{22}\text{Ne}(100\text{MeV}) + ^{197}\text{Au}(0.35\text{ mg/cm}^2)$ .



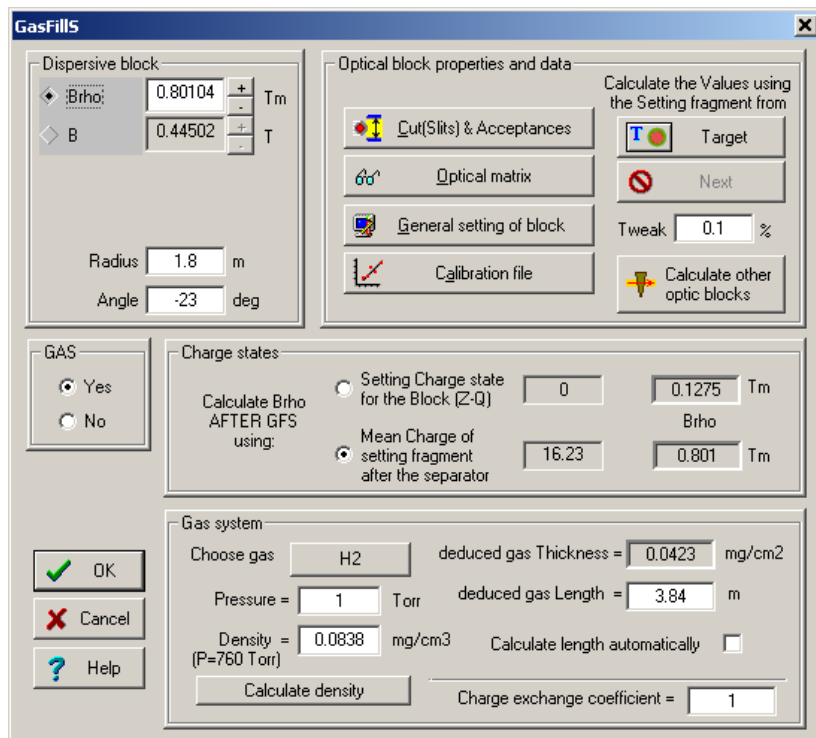
**Fig.463.** Separation efficiency, production cross section of  $^{215}\text{Ac}$ , and rate of all charge states of the residue  $^{215}\text{Ac}$  as function of the target thickness calculated by LISE++ for the VASSILISSA separator in the reaction  $^{22}\text{Ne}(100\text{MeV}) + ^{197}\text{Au}$ . Cross sections are calculated considering the energy of the primary beam in the middle of the target using the LisFus model ( $h\omega = 3 \text{ MeV}$ ). The efficiency is the ratio of all charge states of  $^{215}\text{Ac}$  at the final focal plane of VASSILISSA separator relative to the number of  $^{215}\text{Ac}$  nuclei produced in the target. The separator was always tuned to the ion  $^{215}\text{Ac}^{8+}$ .

### 6.4.3. Gas-filled magnetic dipole

The gas-filled magnetic block is a more complicated optical block in the code and consists of two classes: magnetic dipole and compound materials. The gas-filled dipole window in the “Set-up” window is shown in Fig.464, where  $Br$  is the magnetic rigidity [T m], the middle string classifies the gas in the dipole and its pressure [Torr], and the bottom line shows a charge state value to which the dipole set, or a mean charge state of the setting fragment after the dipole, if this option was set. The gas-filled dipole dialog is shown in Fig.465.



**Fig.464.** Gas-filled dipole window in the “Set-up”.



**Fig.465.** The gas-filled dipole dialog.

The gas-filled dipole is acting as a regular magnetic dipole if the option “GAS” was set to “No” (see Fig.465). In that case the user can see the message “no gas” in the middle string of the gas-filled dipole window in the “Set-up” window (see Fig.464). In the case of no gas different charge states of an isotope end up in different spots after a dipole compared to a magnetic dipole. But if the option “Gas” is set to “Yes” and even the pressure is equal to 0 Torr, the code is suggesting equilibrium of charge states within the gas, and all charge states of one isotope have the same spatial distributions.

It is recommended:

- To use the gas-filled dipole option “Charge states” to set “Mean charge”. The option “charge state Z-Q” is applied for debugging purposes or in the case of no gas in the dipole. If the option “Charge States” in the code is set to “Off” (dialog “Preferences”) then the field “charge state Z-Q” in the gas-filled dipole is disabled. The code automatically recalculates magnetic rigidity values corresponding to different charge state options and shows them in the dialog. If you want to set one of these values to the dipole setting it is necessary to click the button of the previous block (for example in Fig.465 this button is called “Target”);
- To turn off the charge state option in the code if you use just a gas-filled dipole without any other optical dispersive blocks. This avoids time-consuming calculations. If you use other blocks (a magnetic dipole or Wien velocity filter for example) then turn on the charge state option.

It is possible to enter the gas density (for pressure equal 760 Torr) manually or to calculate it (button “Calculate density”) by using the new subroutine of the gas density calculation (see the chapter “6.5.1. Gas density calculations in the dialog "Material"”).

It is known that the  $B\rho$ -resolution is mainly determined by statistics of charge-exchanging collisions, multiple scattering, velocity dispersion and beam optics. The code takes into account energy loss, angular and energy straggling of the fragments in the gas assuming the gas as regular material with reduced thickness calculated using the length of the block and the density of gas. The contribution of charge-changing collisions is given by M.Paul et al.[Pau89]:

$$\Delta x = k_{exch} \cdot Disp \cdot \frac{\Delta q}{\bar{q}} \cdot \frac{100\%}{\sqrt{N_{targ}} \sigma} [mm], \quad /41/$$

where  $N_{targ}$  is the number of atoms in gas [ $1/cm^2$ ],  $Disp$  is the dispersion [ $mm/\%$ ],  $\bar{q}$  is the mean charge of ion after the gas,  $\Delta q$  is the standard deviation of a mean value of the charge distribution,  $k_{exch}$  is the coefficient used in LISE++ with a default value equal to 1 (see “Charge Exchange Coefficient” Fig.465), and  $\sigma$  is the charge-changing cross section [ $cm^2$ ] which is calculated by using the empirical scaling rule developed by A.Schlachter et al.[Sch83].

### 6.4.3.1. Gas pressure optimization plot

The choice of the gas pressure in a gas-filled separator plays a crucial role for the spatial resolution in the final focal plane of separator. The utility to optimize the gas pressure has been developed in the framework of the LISE++ code. Use the menu “Utilities → Gas pressure optimization for gas-filled dipole” to start the gas pressure optimization (see Fig.466). Different characteristic calculation results versus gas pressure are shown in Fig.467. LISE++ calculated widths in the focal plane of the gas-filled separator as a function of the gas pressure (nitrogen) for  $^{41}K$ ,  $^{58}Ni$ , and  $^{126}Te$  ions at the specified incident energies are given Fig.468.

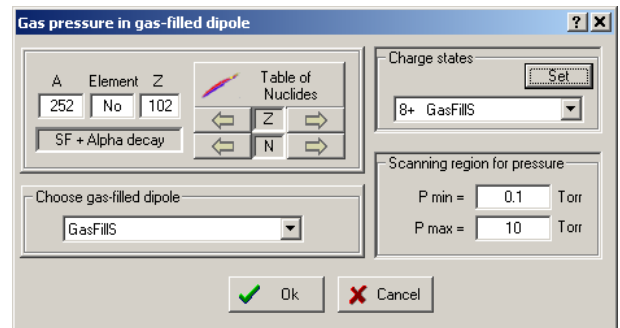


Fig.466. The dialog to initialize gas pressure optimization calculations.

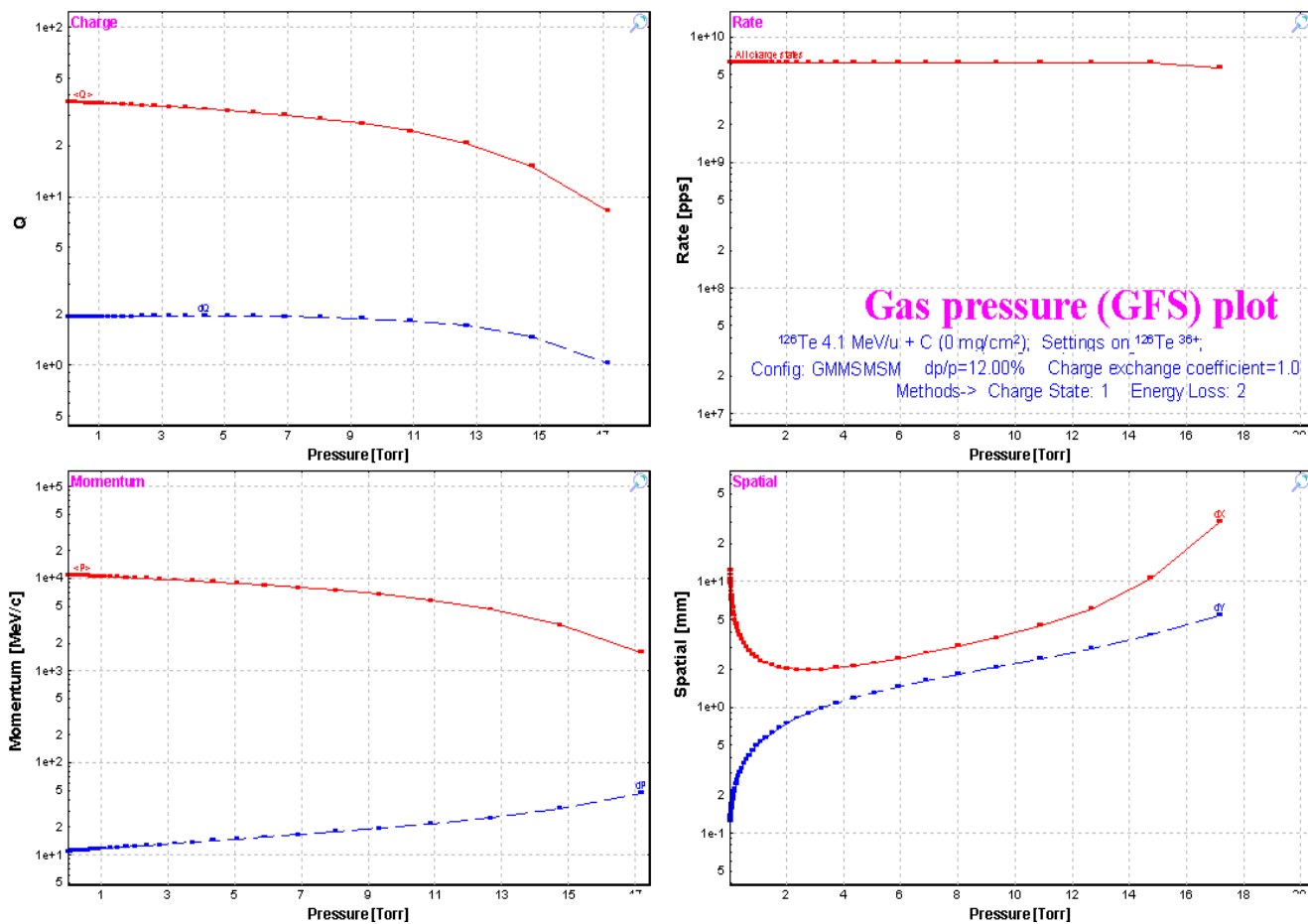


Fig.467. The gas pressure optimization plot.

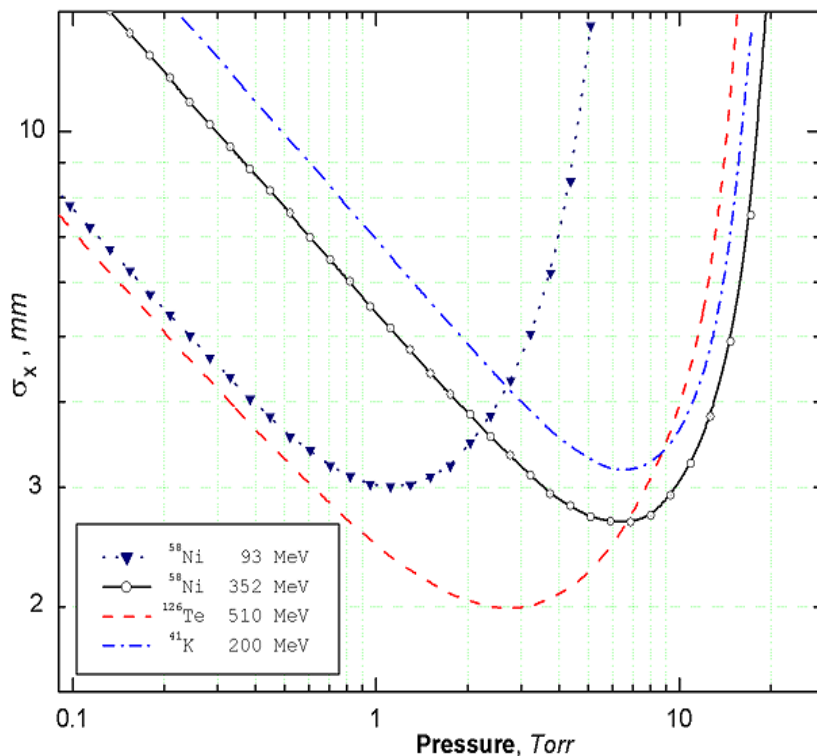


Fig.468. LISE++ calculated widths in the focal plane of the gas-filled separator as a function of the gas pressure (nitrogen) for  $^{41}\text{K}$ ,  $^{58}\text{Ni}$ , and  $^{126}\text{Te}$  ions at the specified incident energies. The incident ions were chosen to compare to the paper [Pau89]. To calculate this plot the incident ions were assumed as primary beam. The dipole length was set to 3 meters, and the target thickness equal zero was used. The optical matrix of the separator is unitary except for the dispersion which is equal to 10 mm/%. The primary beam emittance was set to  $x=y=\pm 0.1\text{mm}$ ,  $x'=y'=\pm 0.1\text{mrad}$ ,  $dP/P=\pm 0.1\%$ . The example discussed in the figure can be found on the LISE web-site:

[http://www.nslc.msu.edu/lise/6\\_2/examples/paper\\_gfs.lpp](http://www.nslc.msu.edu/lise/6_2/examples/paper_gfs.lpp)

### 6.4.3.2. The Dubna GFS configuration

The LISE++ configuration file (Lise/config/Dubna/Dubna\_GFS.lcn) of the Dubna gas-filled separator has been created parameters given an using the articles [Oga98] and [Sub02]. However it is still necessary to correct the op-



Fig.469. Dubna gas-filled separator scheme

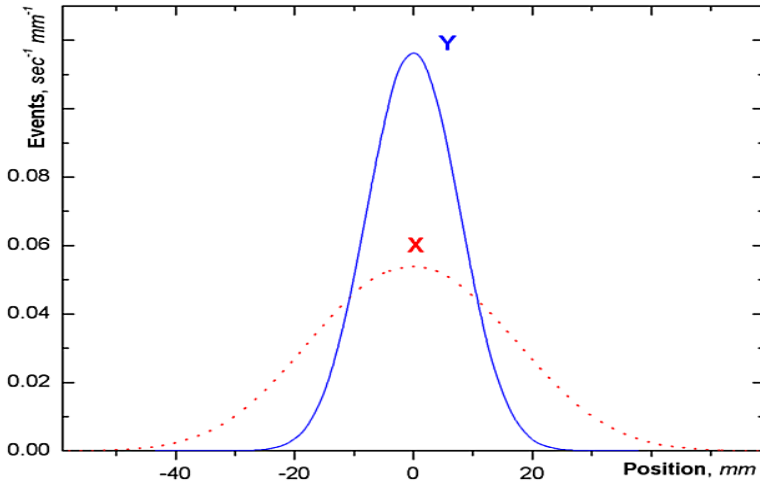


Fig.470. Horizontal and vertical focal-plane position spectra in the reaction  $^{48}\text{Ca}(217\text{MeV})+^{206}\text{Pb} \rightarrow ^{252}\text{No}+2n$  calculated by LISE++.

tical matrix of the dipole. The scheme of the spectrometer is shown in Fig.469. Spatial distributions of  $^{252}\text{No}$  residues at the focal plane of the separator are given in Fig.470. This example of the transmission residues in the Dubna gas-filled separator from the reaction  $^{48}\text{Ca}(217\text{MeV})+^{206}\text{Pb}(0.4\text{ mg/cm}^2) \rightarrow ^{252}\text{Ac}$  can be found in the file “Lise/Files/Dubna\_GFS.lpp” which is included in LISE++ package.

## 6.5. New features and Corrections

### 6.5.1. Gas density calculations in the dialog "Material"

LISE++ has a database containing various densities for materials in a solid state. In case of gases it is difficult to create a similar database of densities because the gas density depends on pressure and temperature. In this context the gas density dialog was created (see Fig.471), in which the user can enter parameters of the environment (gas and pressure) to calculate the density of a gas. The dialog is loaded from the material dialog in the mode “Gas” (Fig.472). Also in the mode “Gas” the user can enter parameters of a molecular gas. The units converter can be called from the gas density dialog to transform units of temperature or pressure.

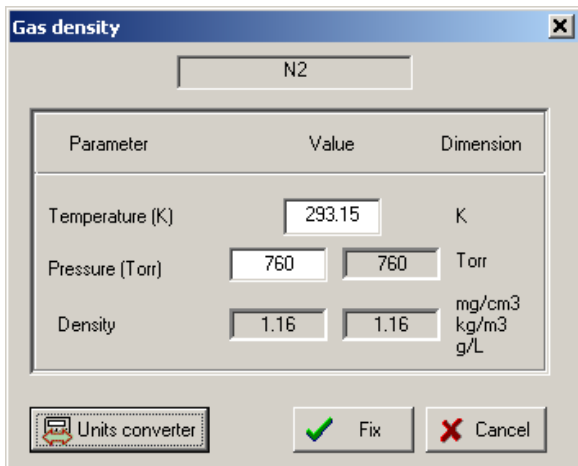


Fig.471. Gas density dialog.

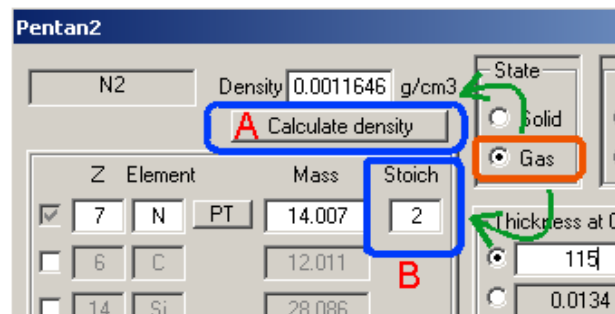


Fig.472. The segment of the material dialog in the mode “Gas”. The button “Calculate density” (letter “A”) and the field “Stoich.” (letter “B”) to enter a molecular gas appear in the mode “Gas” of the material dialog.

### 6.5.2. The “Beam” dialog: several possibilities to enter a beam energy

The opportunity was created to set the energy of the primary beam in the “Beam” dialog (see Fig.473) through various equivalent physical quantities. So for example in the region of intermediate energies it is convenient to enter the energy in MeV per nucleon, while for low energies it is common to quote the total kinetic energy of the projectile.

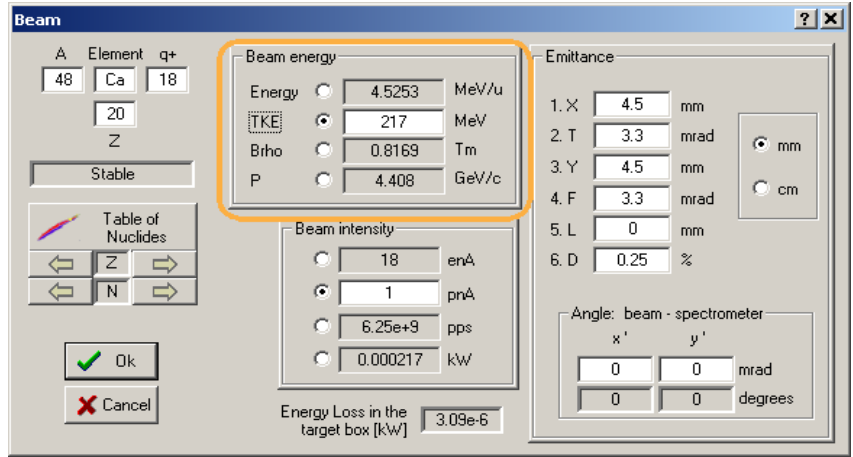


Fig.473. The Beam dialog.

### 6.5.3. Spectrometer setting for the primary beam in the fusion mode

In case of fusion-evaporation reactions the program considers the entered primary beam particle as product of the reaction. If the user sets a nucleus as fragment (residue) in the regular way, then the program will apply the cross section, and angular as well as momentum distributions calculations assuming a fusion-evaporation reaction. However it is often desired to see the trajectory and the transmission of the primary beam particles. For this purpose it is possible to set the primary beam as fragment in the menu “Settings → Tune the spectrometer for primary beam”. The message “=beam=” will appear close to fragment settings in the Set-up window (see Fig.474). The program automatically calculates the spectrometer settings optimal for the primary beam transmission. Charge states of the primary beam for the spectrometer can be entered using the optical block dialogs.

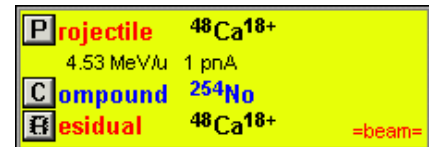


Fig.474. The fragment of the Set-up window in the case when the primary beam is set as setting fragment.

### 6.5.4. Angular straggling

A new method [PDG00] to calculate angular straggling has been added to the program. The opportunity to perform calculations without contributions of angular and energy straggling (for debugging purposes) are included in the program (see the dialog “reaction mechanism”). The user now can compare different models for angular straggling versus projectile energy using the menu “Utilities → Plot of angular straggling in the material”.

For calculations of angular straggling at small energies arises the question at what energy the formula remains valid? So in the work [Dio89] it was assumed that using the model is correct only if the scattering angle is below 10 degrees. The use of the Born approximation is expected to be valid when the born parameter  $\alpha_B$  is much smaller than unity. In the nonrelativistic approximation this condition is satisfied if

$$\alpha_B \sim \frac{Z_1 \cdot Z_2}{137\beta} \ll 1. \quad /42/$$

However, R. Anne et al [Ann88] have shown that experimental results obtained in the reaction  $^{100}\text{Mo}(23.8\text{MeV/u})+\text{Au}$  ( $\alpha_B=109.2$ ) are in the good agreement with the calculations. To avoid problems

with calculations at energies close to zero (when the angular straggling value begins to become infinite) the following restriction for the energy is applied:

$$E_{limit} = \frac{Z_t \cdot Z_p}{2 \cdot A_p \cdot A_t^{0.55}} [MeV/u], \quad /43/$$

where  $Z_t, Z_p$  are the atomic number for the target and projectile and  $A_t, A_p$  are their mass numbers respectively. The coefficient has been chosen so that the lateral range is always monotonically increasing for increasing energy and every combination of projectile and target. The plot of the fragment range in material (see menu "Utilities") was used for this purpose. Angular straggling models use  $E_{limit}$  for calculations for projectile energies below  $E_{limit}$ .

### 6.5.5. Corrections and changes

Some updates and corrections have been included in version 6.2 compared to the previous version. Items affected by the changes are listed below:

- Monte Carlo 2D plot,
- Wedge dialog,
- Momentum distribution after the stripper,
- Rotation block transmission,
- The Optic Block Dialog,
- Total Kinetic energy plot (1D) from the menu "Plot → Total kinetic energy distributions" (see Fig.475),
- LISE++ file (\*.lpp) for option "charge state is ON",
- Angular transmission calculations.

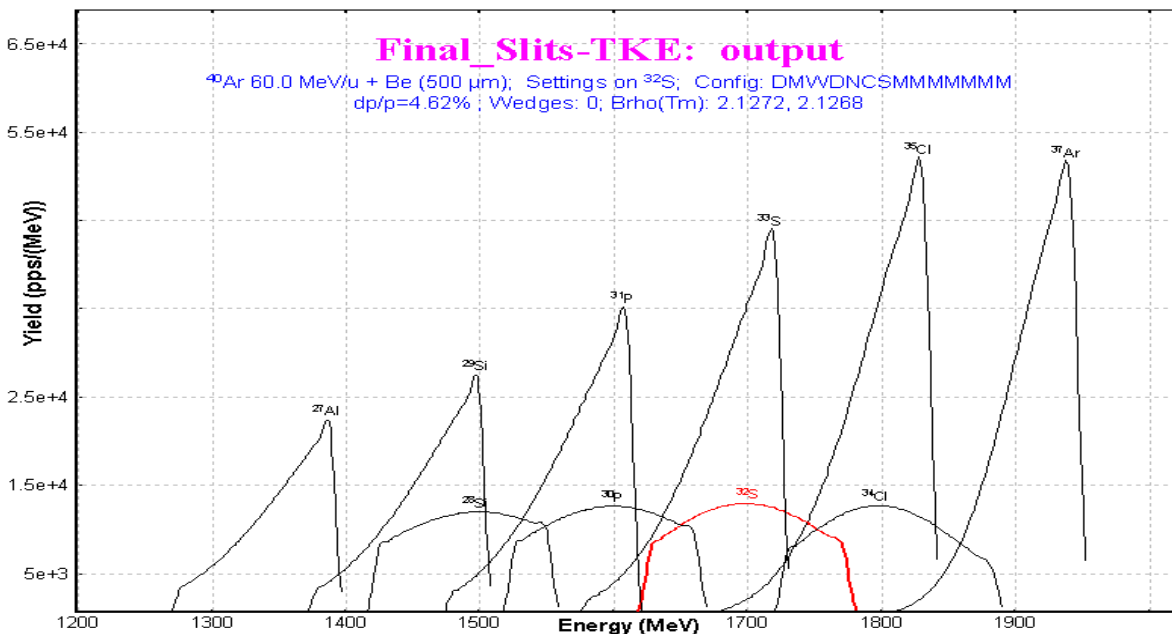


Fig.475. Total kinetic energy distribution plot.



## 6.6. Sub-barrier fusion cross-section

The possibility to calculate sub-barrier fusion cross section is available now in the PACE4 code as well as in the LisFus model. There is a brief introduction for the quantum-mechanical approach used in the codes. The cross section for the compound-nucleus formation is given as

$$\sigma = \pi \tilde{\lambda}^2 \sum_{l=0}^{\infty} (2l+1) T_l, \quad /44/$$

where  $T_l$  is the transmission coefficient for the  $l$ th partial wave:

$$T_l = \left\{ 1 + \exp \left[ \frac{l - l_{\max}}{\Delta} \right] \right\}^{-1}, \quad /45/$$

with  $\Delta$  as diffuseness parameter and  $l_{\max}$  as the maximum angular momentum determined by the total fusion cross section. This approach was used in the code PACE [Gav80]. For the study of fusion reactions below the Coulomb barrier it is necessary to use the quantum-mechanical transmission probability instead of the classical solution to describe the experimental data. For a one-dimensional barrier it is assumed that the potential barrier can be replaced by a parabola:

$$V_0(r) = V_{B0} - \frac{1}{2} \mu^2 \omega^2 (r - r_0)^2, \quad /46/$$

where  $V_{B0}$  is the barrier height and  $\omega$  is a measure of the curvature of the  $s$ -wave potential barrier. The transmission probability can be calculated following [Hil53]

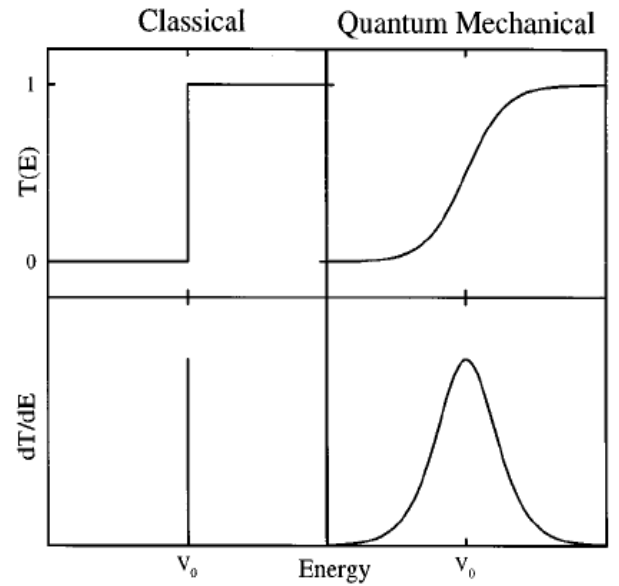
$$T_0(E) = \left\{ 1 + \exp \left[ \frac{2\pi(V_{B0} - E)}{\hbar\omega} \right] \right\}^{-1}. \quad /47/$$

In a completely classical treatment,  $T_0$  is unity above the barrier and zero below, as shown in Fig.476. Quantum mechanically the  $dT_0(E)/dE$  delta function peak is broadened [Bal98] as the transmission probability smoothly evolves from zero at energies far below the barrier to unity for energies far above the barrier (see Fig.476).

It is possible to approximate the  $l$  dependence of the transmission probability at a given energy by simply shifting the energy [Bal98]:

$$T_l \cong T_0 \left\{ E - \frac{l(l+1) \hbar^2}{2\mu R^2(E)} \right\}, \quad /48/$$

where  $\mu R^2(E)$  characterizes an effective moment of inertia. Approximating  $R(E)$  by  $r_0$  and inserting the penetration probability for the parabolic barrier, one obtains an approximate expression for the cross section [Won73]:



**Fig.476.** Classical (on the left) and quantum-mechanical (on the right) transmission probabilities for a one-dimensional potential barrier [Bal98].

$$\sigma(E) = \frac{\hbar\omega r_0^2}{2E} \log \left\{ 1 + \exp \left[ \frac{2\pi(E - V_{B0})}{\hbar\omega} \right] \right\}. \quad /49/$$

In the classical limit, where  $\omega \rightarrow 0$  or  $E \gg V_{B0}$ , Equation /49/ reduces to the standard geometrical result:

$$\sigma(E) = \pi r_0^2 \left( 1 - \frac{V_{B0}}{E} \right). \quad /50/$$

The user can choose the calculation method of the transmission probability for a potential barrier in the “Fusion-evaporation settings” dialog (see Fig.477) in LISE++. The default value of the curvature parameter is equal to 5 MeV. The same option exists in the PACE4 code in the “Card 2-1” dialog. Cross section calculations by the PACE4 program and the LisFus model for the example reaction  $^{197}\text{Au}(^{22}\text{Ne}, 3-6n)$  using the quantum-mechanical transmission probability for the potential barrier are given in Fig.478 and Fig.479. This reaction was already used for residue transmission calculations in chapter “6.4.2.6. Residue transmission calculation” compared to experimental results from the paper [Yer94].

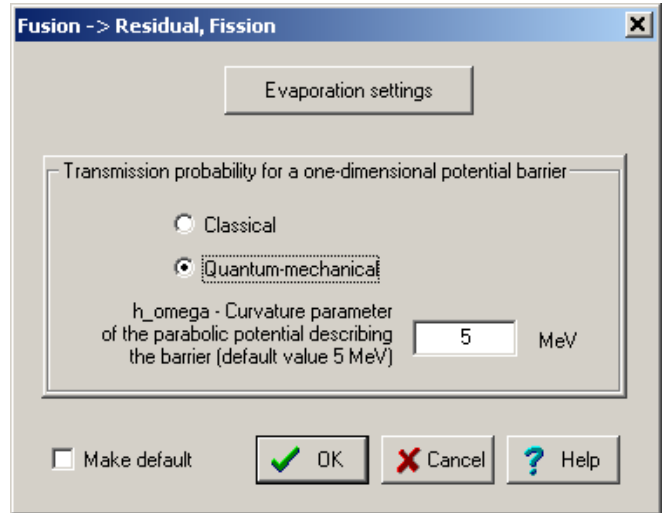


Fig.477. The dialog of fusion-evaporation settings

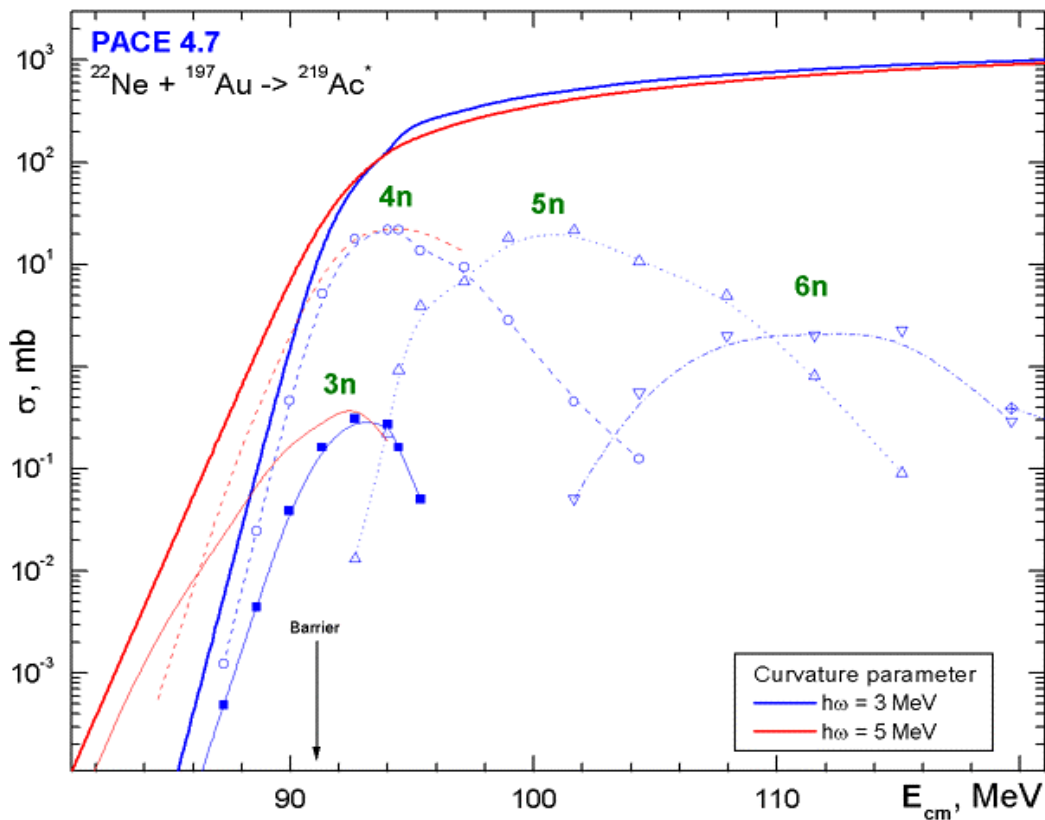


Fig.478. PACE calculated fusion-evaporation cross sections for the reaction  $^{197}\text{Au}(^{22}\text{Ne}, 3-6n)$  using the quantum-mechanical transmission probability for the potential barrier using the two different values of the curvature parameter 3 and 5 MeV.

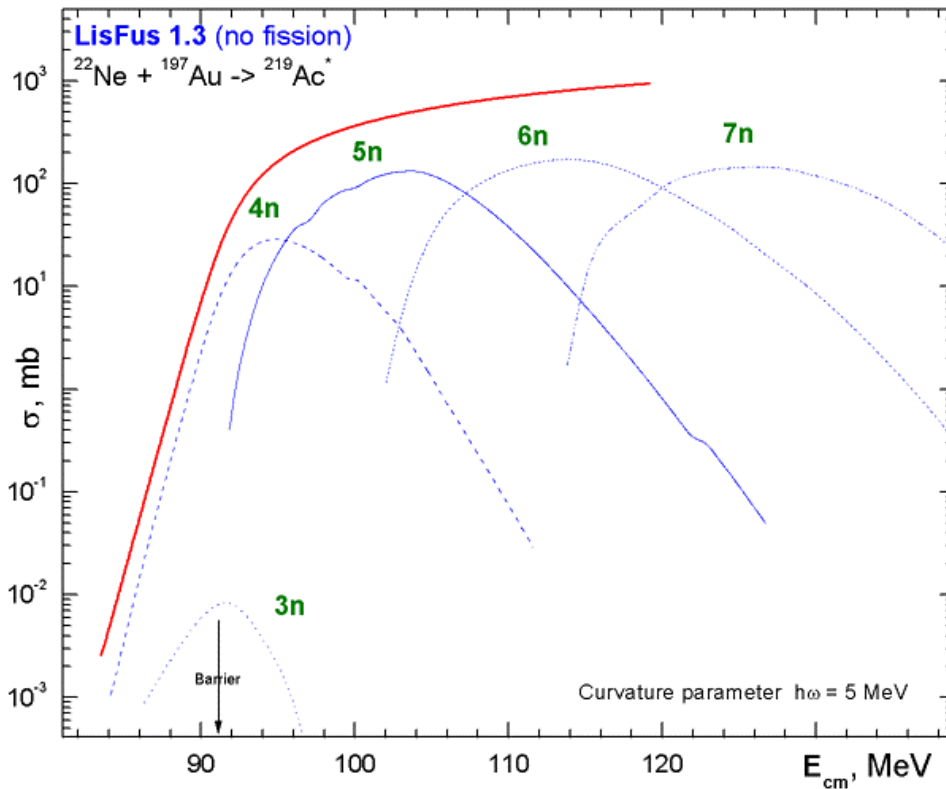



Fig.479. LisFus calculated fusion-evaporation cross sections for the reaction  $^{197}\text{Au}(^{22}\text{Ne},3-7n)$  using the quantum-mechanical transmission probability for the potential barrier with the curvature parameter equal to 5 MeV.

### 6.7. The code “BI” development

The program “BI” for the automatic search of two-dimensional peaks has undergone a number of changes: cycles optimization, some corrections, and help support has been included.

Contour and projection utilities allowing to work with experimental spectra have also been added. The user can create a contour using the icon  in the toolbar of the plot window while displaying an experimental two-dimen-

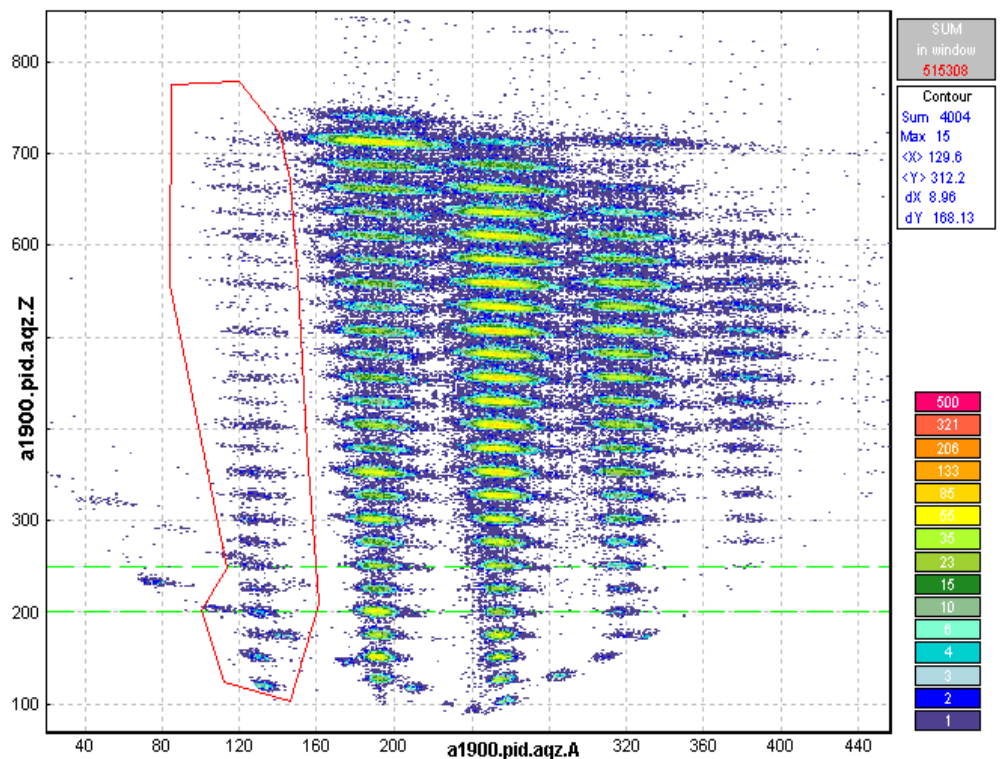
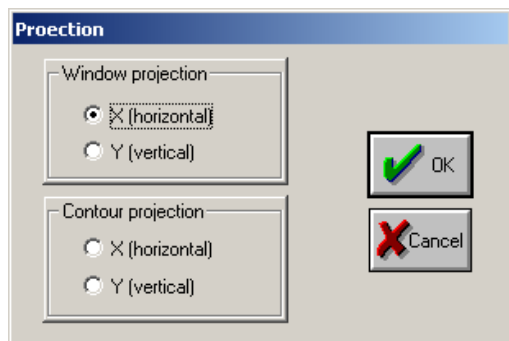




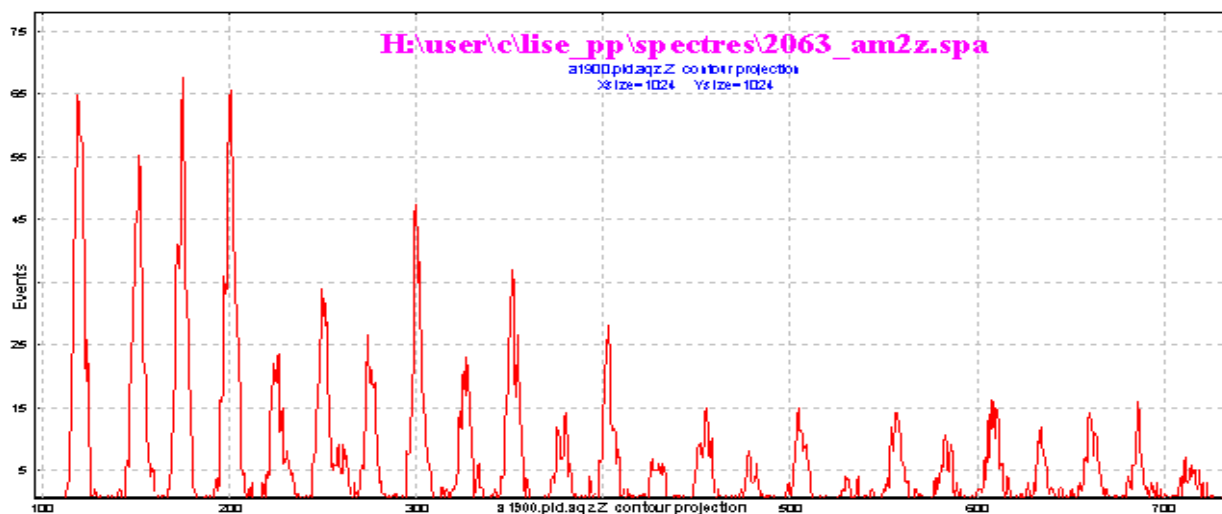
Fig.480. Example of a contour in a two-dimensional particle identification plot. Statistic characteristics of the data within the contour are shown in the top right window.



*Fig.481. The projection dialog.*

sional spectrum. By pressing the left mouse button, the user can add a new point of a contour, while pressing the right mouse key closes the contour. Statistic characteristics of the data within the contour will appear in the top right window of the plot (see Fig.480). The contour can be used in the case of low intensity two-dimensional peaks or bad separation between them. Under these conditions the program cannot identify peaks automatically. The user can manually get the peak characteristics or create a contour projection on one of axes.

By pressing the icon  the user loads the projection dialog (see Fig.481) which prompts to choose a method to create a projected spectrum. The projection of the contour in Fig.480 on the vertical axis is shown in Fig.482. The one-dimensional spectrum can be saved as a file using the icon  for a further analysis by the code “Bi” in the one-dimensional peak search mode.



*Fig.482. One-dimensional spectrum obtained from the contour projection (see Fig.480) onto the vertical axis.*

### 6.8. Future perspectives for LISE++ (version 6.3)

- Incorporate the “Global” code in the LISE++ package.
- Add the fission channel in the LisFus model.
- Develop fission products kinematics in LISE++.
- Incorporate a new reaction mechanism: **Fission**.

### Acknowledgements

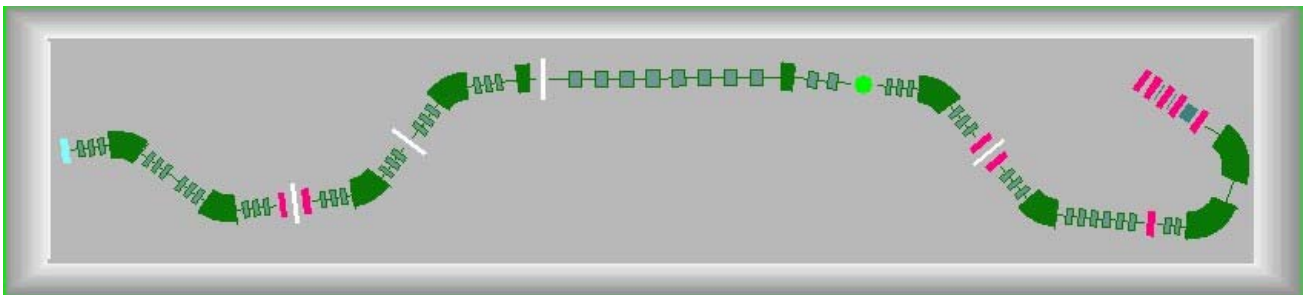
The LISE++ authors thank Dr. Alexandra Gade for carefully proof reading this documentation.

Further, the authors gratefully acknowledge Dr.Helmut Weik’s fruitful remarks, suggestions, and help with the development of LISE++.

We are grateful to Prof. Dave Morrissey for the idea to include a Brho analyzer.

**7. Version 6.1**

Block structure: designing own spectrometer



## 7.1. Introduction

**LISE++** is the new generation of the LISE code, which **allows the creation of a spectrometer through the use of different “blocks”**. A “block” can be a dipole (dispersive block), a material (i.e. a given thickness for a detector), a piece of beampipe, etc. The original LISE was restricted to a configuration consisting of two dipoles, a wedge, and a velocity filter. The number of blocks used to create a spectrometer in LISE++ is limited by operating memory of your PC and your imagination. The code has an improved interface, new utilities were added, and the spectrometer scheme in the program allows quick editing of blocks.

### 7.1.1. How to download LISE++

As with LISE, LISE++ is distributed freely and is accessible through ftp-servers in East Lansing (<ftp://ftp.nslc.msu.edu/pub/lise/>) and Dubna (<ftp://dnr080.jinr.ru/lise/>). Dubna ftp-server does not support Netscape. Contents of the LISE ftp site and detailed information about downloadable files can be found in <ftp://ftp.nslc.msu.edu/pub/lise/readme>.

The new version LISE++ should be installed in the previous LISE directory as to not duplicate certain files (for example the mass database). The previous version will still work if this is done.

♣ *If you have already installed one of LISE++ (6.0.\*\*\*) beta versions, it is strongly recommended to re-install it with the newest version.*

### 7.1.2. New file formats

The LISE++ program has a new file format for all of the files it uses and creates. The extensions of these files were changed to avoid overlap with files of the LISE program. Three new types of files were added: a file containing a profile of a curved degrader, a file containing calibrations of dispersive optical blocks, and a matrix file. The new extensions are given in table 51.

*Table 51. File extensions used by LISE and LISE++.*

Type of file	LISE	LISE++	Default directory
Regular	liz	lpp	/files
Configuration (set-up)	lcf	lcn	/config
Option	opt	lopt	/options
Degrader	-	degra	/degrader
Calibration	-	cal	/calibrations
Matrix	-	mat	/files

*Note: The regular LISE++ file (extension "lpp") consists of the Configuration file (lcn), the some sections of the Option file (lopt), the experiment settings and calculation results:*

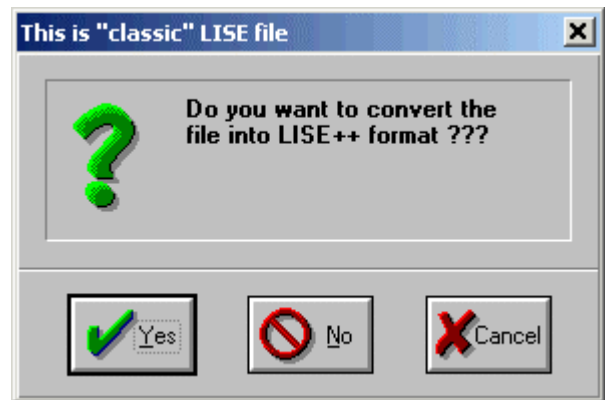
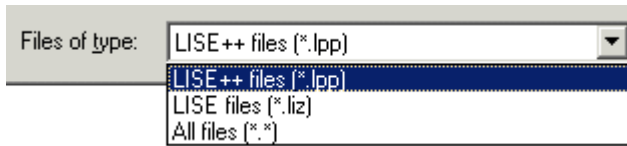
$$LPP = LCN + LOPT + \text{Experiment settings} + \text{Calculation results}$$

File names of calibration and degrader files are saved in the configuration file.

*Note: Upon starting, the code reads the LISE.INI file which contains the default configuration and options file names, as well as the list of most recent files. The code loads the default configuration file and the default options files. If these files are absent the user is informed and the standard LISE settings are used. The user can set the default configuration and option files in the dialog "Preferences".*

### 7.1.3. Support of “classic” LISE files

LISE++ can read all old-format files (regular, configuration, option), but **it only saves just in its own format**. If you choose old-format files (for example “liz” instead “lpp”) the code will propose to recalculate transmissions of fragments and then ask if you want to save this file in the LISE++ format.



☞ LISE++ also will show a message about a new momentum acceptance. It is described in detail in the chapter 7.3.1.1.3.

☞ If you used a LISE++ (6.0.\*\*\*) beta version, and the configuration files A1900-4dipoles.lcn and A1900-2dipoles.lcn are found in the directory “<LISE>\config”, then it is necessary to delete them. Corrected A1900’s configuration files are found in the directory “<LISE>\config\NSCL”.

### 7.2. Designing your own spectrometer

The “classic” LISE code uses **only one** configuration of a spectrometer consisting of two dipoles:

**LISE “classic”:** Target + Stripper ⇒ Dipole1 ⇒ Wedge ⇒ Dipole2 ⇒ Velocity Filter ⇒ 7 materials

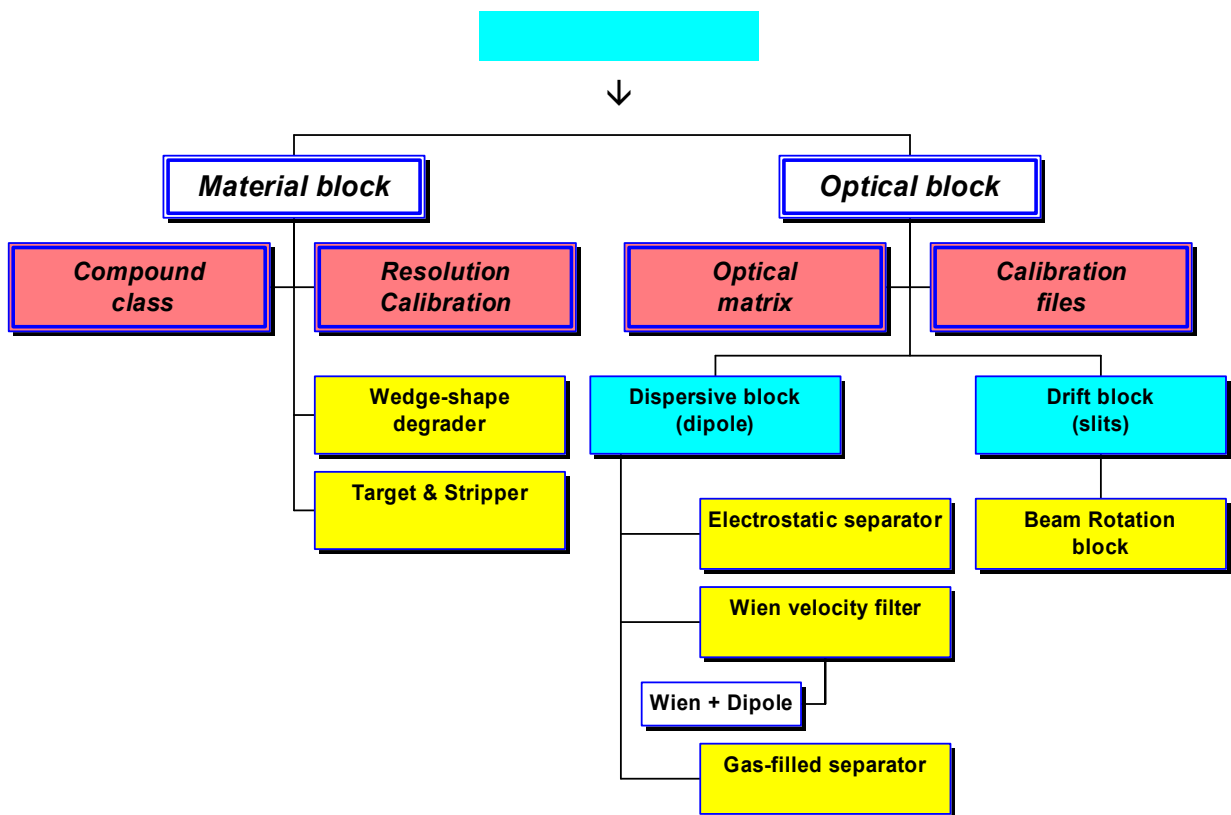












Fig.483. LISE++ block hierarchy

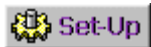
There were a lot requests from users to increase a number of materials, to put a velocity filter in beginning of a spectrometer, to put additional materials between dipoles, etc. All this is now possible in LISE++. The user can choose and place blocks in the spectrometer at own their discretion.

The main class “BLOCK” in the program is inherited by classes “Material” and “Optical” (see Fig.483). The basic properties and methods of these two classes will be considered in this chapter. Currently, LISE++ has eight blocks and three more block are under development (Table 52).

*Table 52. LISE++ blocks.*

<u>Types</u>	<u>Available blocks:</u>	<u>Under construction:</u>
<b>Material</b>	<ul style="list-style-type: none"> <li>❖ Target </li> <li>❖ Stripper </li> <li>❖ Wedge-shape degrader </li> <li>❖ Material (detector) </li> </ul>	<ul style="list-style-type: none"> <li>➤ Secondary target</li> </ul>
<b>Optical</b>	<ul style="list-style-type: none"> <li>❖ Dispersive (dipole) </li> <li>❖ Wien velocity filter </li> <li>❖ Drift block </li> <li>❖ Beam rotation </li> </ul>	<ul style="list-style-type: none"> <li>➤ Gas-filled separator </li> <li>➤ Electrostatic separator </li> </ul>

### 7.2.1. Set-up dialog: new main feature




Pressing on the button “Setup” in the toolbar (or through the menu “Settings ⇒ Spectrometer designing”) brings up a dialog “Spectrometer designing” (Fig.484) and allows you to begin designing a fragment separator. This is the main new feature of LISE++.

The first two positions are occupied by the blocks “Target” and “Stripper”. There are fixed, it is impossible to delete or move them.

#### Insert a new block:

- In the column “Block” of the window (“A” in Fig.484 - *Spectrometer window*) click on an existing block, which you want to insert a new block before or after;
- Choose an insert method “before” or “after” (“B” in Fig.484),
- In the frame “Insert block” (“C” in Fig.484) click on the icon of the block you wish to insert.

#### Delete block:

- Select a block you want to delete in the *Spectrometer window*,
- Press on the button .

#### Move block:

- Select a block you want to move in the *Spectrometer window*,



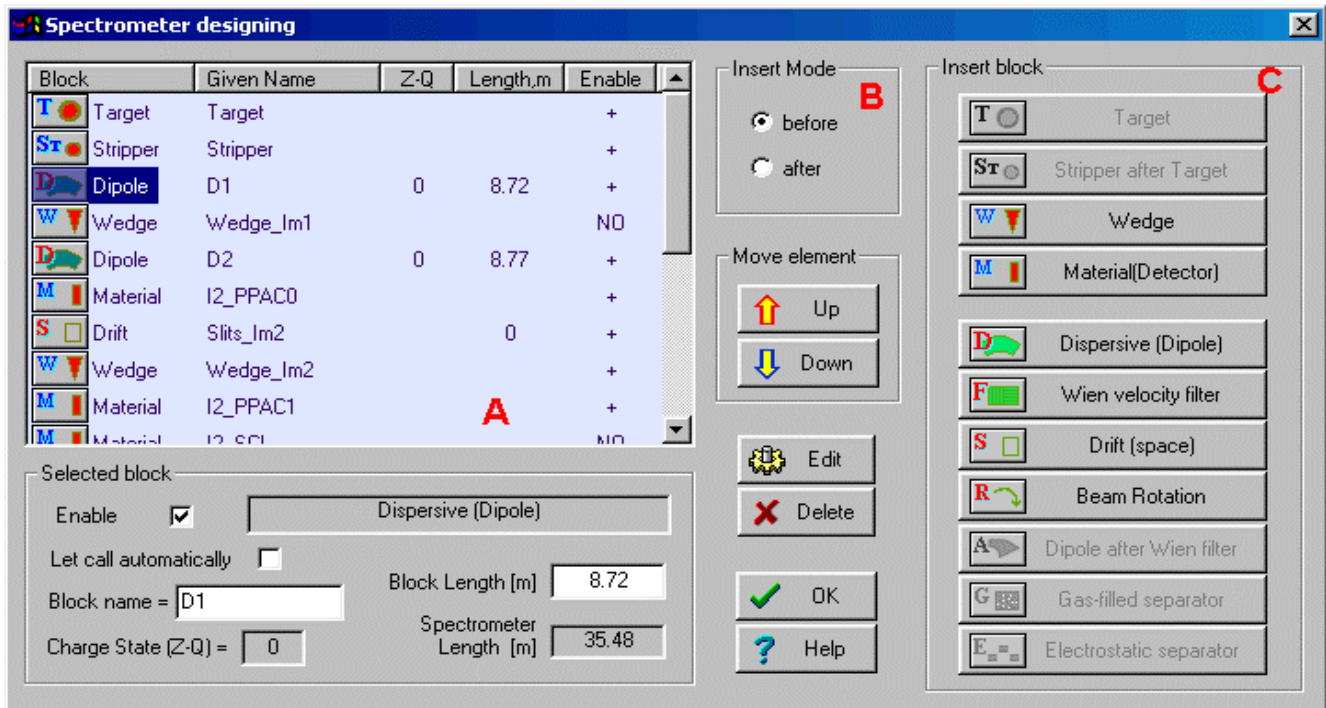
- Press on a button “Up” or “Down” in the frame “Move element”.

**Edit block:**

- Select a block you want to edit in the *Spectrometer window*,
- Press on the button  Edit.

or

- Double click, using the left mouse button, on the block you want to edit in the *Spectrometer window*.



*Fig.484. The dialog “Spectrometer designing” is the first step designing fragment separator.*

It is possible to edit some properties of the selected block in the frame “Selected block” in the bottom left corner of the dialog.

Checkbox “**Enable**”:

all new blocks are available automatically. It is impossible to disable the blocks “Target” and “Stripper”. If a block is set to disable, then this block is not shown in the Setup window and in the spectrometer scheme and the message “NO” will appear opposite this block in the column “Enable” of Spectrometer window of the dialog. A disabled block is not taken into account in transmission and spectrometer optic calculations.

☞ It is possible to change mode (“enable / disable”) of a block **only** in the dialog “Spectrometer designing”.

**Checkbox “Let call automatically”:**

- **On:** the block name is called automatically using the name of the block type and its order number in the spectrometer;
- **Off:** the block name may be entered manually. It is desired to input short names (less than 10 characters) to avoid a name truncation in the Setup window;
- All new blocks are called automatically.

**Block name:** The name of the block appears in all dialogs and menus connected with this block. If the option “Let call automatically” is set “Off”, then the user can input a new name for the block. It is recommended to name the block so that it is clear from the name where the block is located. For example the name “Slits\_Im2” is used to describe a drift block in the mode “slits” found in the location “Image2”.

**Block length:** the code uses a material block with zero length for the spectrometer length and time-of-flight calculations. Just optical blocks may have a length to determinate a spectrometer length and calculate time-of-flight. More on the length of optical blocks will be mentioned later in more detail.

**Charge State (Z-Q):** if the option “Charge states” (in the dialog “Preferences”) is set, and this is an optical dispersive block, then the cell “Charge state” is enabled and you can edit the charge state value for the setting fragment. More details about charge state calculations and their transmission is found in chapter 7.4.2.

*⚠ All operations in the dialog will be carried out without an opportunity to restore a former configuration. In other words the operation UNDO does not work in this dialogue. All changes will be shown in the “Setup window” of the code and in the spectrometer scheme only after leaving this dialogue.*

### 7.2.2. Scheme of spectrometer

The spectrometer scheme is a convenient innovation found in the new version (Fig.485). The program draws the spectrometer scheme on the basis of the blocks, entered by the user. The user can exclude or include this option in the dialog “Preference”.

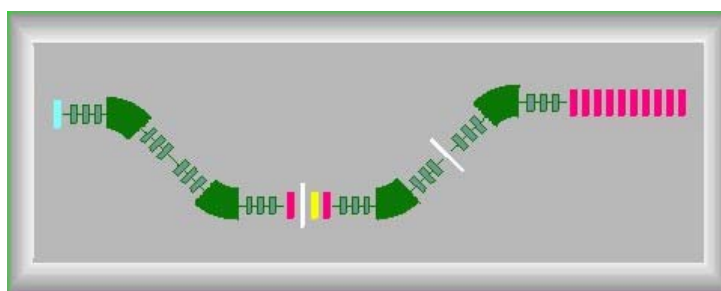


Fig.485. The spectrometer scheme.

The number of dispersive block quadruples in your spectrometer can be changed in the dialog “General Block Settings” (see Fig.486) which is available through the dialog of block properties editing. Quadruples are properties of dispersive blocks (dipole, velocity filter). Quadruples are used just for the spectrometer scheme.

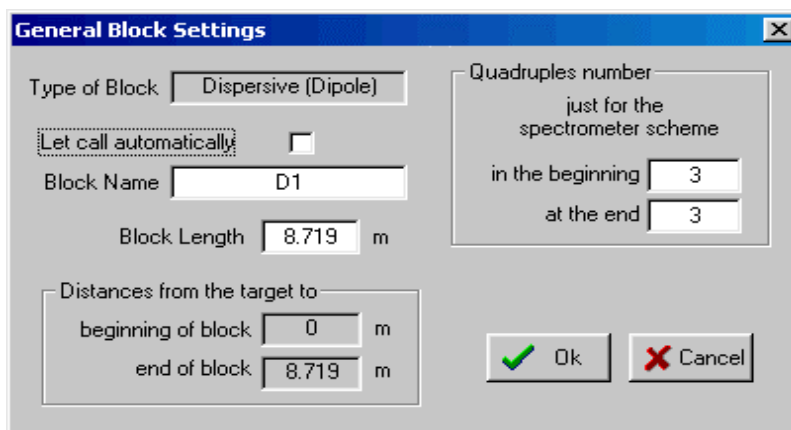


Fig.486. The “General block settings” dialog.

The user must be careful to set the correct length of dispersive block, which includes the quadruples and dipole(s). The dispersive block length should be always more than the dipole length, equal to the product of the radius of the dipole(s) and the angle (in radians). The difference between these lengths is the total length of the quadruples in that block.

- The user can select a block on the spectrometer scheme by moving the mouse over it (turning the block dark blue), thus selecting it and allowing the user to click on it to bring up a dialog.
- To Edit block properties: click on the selected block once using the left mouse button.
- To Edit block acceptances and slits: click on the selected block once using the right mouse button.
- Drift blocks in the mode “Slits” (block length is equal to 0) is shown by thin long line perpendicular to the beam axis. In other words the length of the drawn block is proportional to its real length.
- Materials with zero thickness are not shown in the scheme.

### 7.2.2.1. Settings of spectrometer scheme

It is possible to change properties of the spectrometer scheme using the dialog “Spectrometer scheme options” (see Fig.487) which can be loaded through the dialog “Preferences”.

The user can:

- Input an initial angle of the spectrometer,
- Set sizes of the scheme in units of the dimension of the isotope cells of the chart of nuclides,
- Change the background layout for the scheme,
- Change colors.

To change a color it is necessary to select a block using the listbox in the frame “Block color in scheme” and then click on the window “Change”.

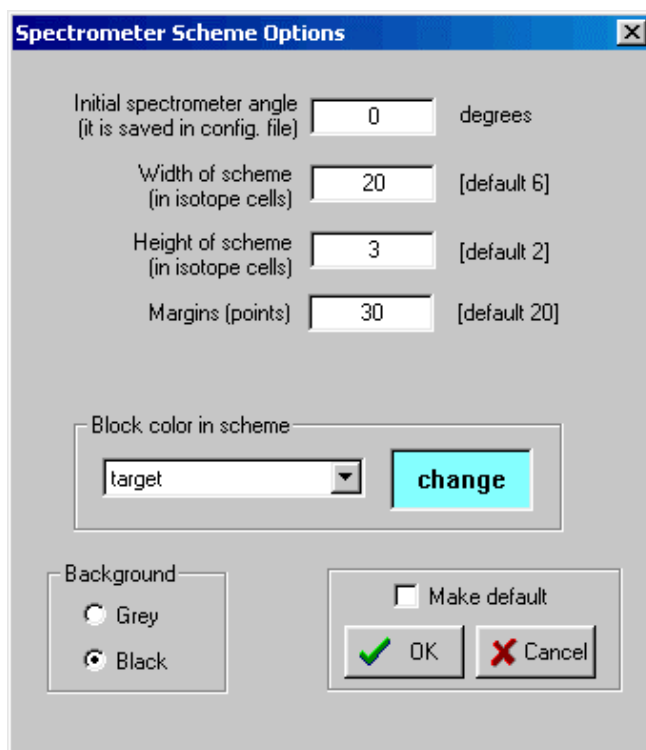


Fig.487. The “Spectrometer Scheme Options” dialog.

## 7.3. Description of Blocks and their properties

### 7.3.1. Optical block

The hierarchy of optical blocks is shown in Table 53.

Table 53. The hierarchy of optical blocks.

Class	Derived from class	New principal properties	Blocks from this class
Optical block	LISE++ block	<ul style="list-style-type: none"> <li>• Optical matrix</li> <li>• Slits &amp; Acceptances</li> </ul>	<ul style="list-style-type: none"> <li>• Drift</li> <li>• Beam rotation</li> </ul>
Dispersive block	Optical block	<ul style="list-style-type: none"> <li>• Computational setting values</li> <li>• Calibration file</li> <li>• Setting charge state</li> </ul>	<ul style="list-style-type: none"> <li>• Dipole</li> <li>• Wien velocity filter</li> </ul>

The description of classes is explained in the text. First the methods used in a class will be described for each class, then blocks used for constructing the spectrometer on the basis of a given class will be explained.


### 7.3.1.1. Optical block: properties and methods

#### 7.3.1.1.1. Optical matrix of LISE++ block

The “Optical matrix” class is based on a class “matrix” of constant, 6×6, dimension and has the capability of transforming matrix elements of different units ( $mm \Leftrightarrow cm$ ). LISE++ has two optical matrices for each optical block: “global” and “local”. The local matrix belongs just to one block and does not depend on other blocks. The program keeps all local matrices in configuration files. This is so the insert/removal of a new block in/from a spectrometer does not change the matrices of other blocks. The global matrix of the block is computed on the basis of ALL the previous blocks and the local matrix of this block. It is possible to present  $i$  global matrix calculations as recursive equation:

$$G_i = L_i \times G_{i-1} ,$$

Where  $G$  is the global matrix, and  $L$  is the local matrix. The global matrix of the first optical block is equal to its local matrix. The program uses elements from both matrices in fragment transmission calculations. The code automatically recalculates all global matrices if one of local matrices changed.

Clicking the button  in the dialog of optical block properties allows the user to load the dialog “Optical matrix” to edit block matrices (see Fig.488). The user can enter the data in different dimensions  $mm \Leftrightarrow cm$ , and into different matrices  $Local \Leftrightarrow Global$ . For this purpose using keys the user can choose mode, convenient for him. The matrix opposite to the one the user changed will be automatically recalculated on the basis of the just entered and previous matrices. If you enter the data in a global matrix, you should be sure, that the previous global matrix is computed correctly. If you input global matrices, start editing from the first matrix of a spectrometer.

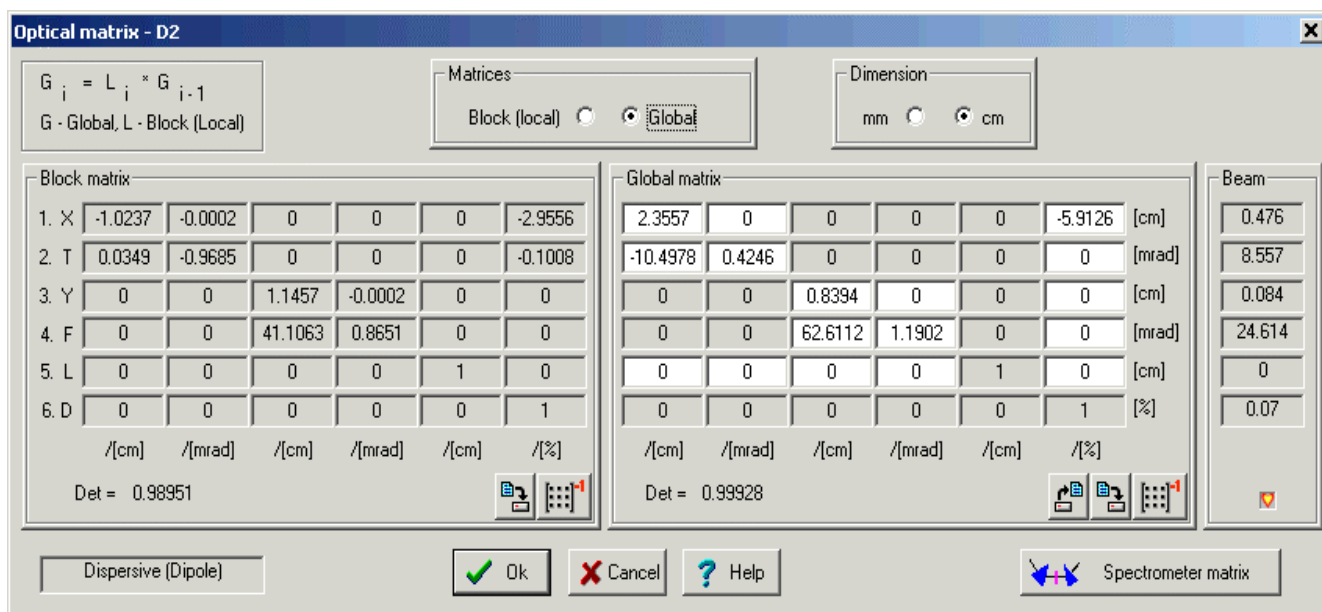

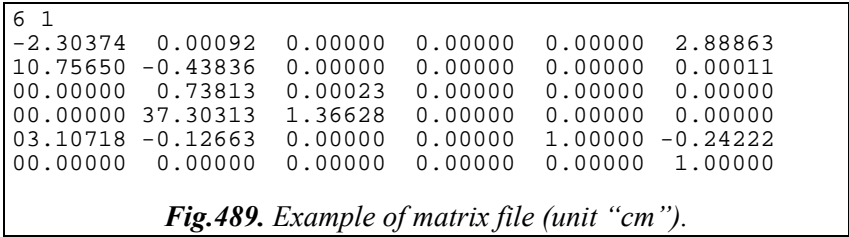


Fig.488. The “Optical matrix” dialog.



In the LISE “classic” version the user could only edit local matrices. LISE++ not only allows you to edit local and global matrices by element as described above, but also allows to you input entire matrices using matrix files. Inserting matrices into the program LISE++ from the program TRANSPORT [Bro80] can be done using the following steps:

- Choose a matrix corresponding to the block you want to change in the TRANSPORT result file and copy it to a new file.
- Save the file with extension “mat”.
- Create a new blank line in the file before the matrix elements. The first line of a file has to contain two numbers. The first shows matrix dimension (matrix is always supposed to be a square matrix). The second value is the dimension. 0 corresponds to “mm”, 1 corresponds to “cm”. If the second number is missed, by default it is supposed to be equal zero. The first line of the TRANSPORT matrix file should contain “6 1” (see Fig.489). The next six lines are matrix elements corresponding to the rows of the matrix. A separator between elements can be tabs, spaces, commas, or semicolons.
- In the “Optic matrix” dialog click on “Global” to go to the mode of global matrix editing. Click on the button  to load the file you just created. The default directory of matrix files is “<LISE++>\FILES”.



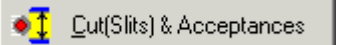
**Fig.489.** Example of matrix file (unit “cm”).

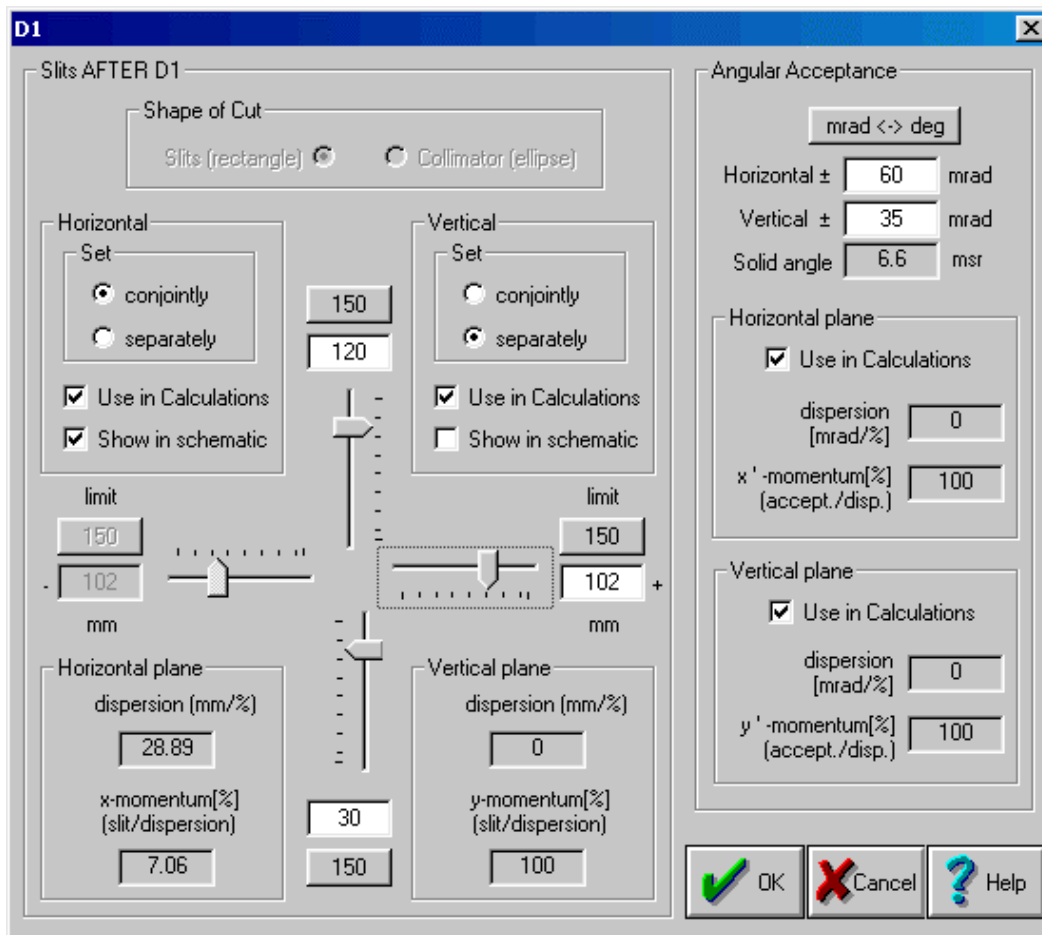
The dialogs of optical matrices depend on the block, and their features will be further explained in later sections. Reading of data in the matrix dialogs is not instantaneous, but it takes approximately 1 second in which you can see a blinking heart in the lower right corner of the dialog.

- ❖ To save a matrix in a file it is necessary to press the button  under the matrix. The program saves the file as well as saving the units (mm/cm).
- ❖ To get an inverse matrix press the button .

♠ One way to check if the input values are corrected when then you are editing a matrix is to calculate the determinant. The determinant of an optical matrix should always be about 1. The determinant of a matrix is automatically calculated and displayed in the lower left, below the matrix.

**7.3.1.1.2. Acceptances and slits**

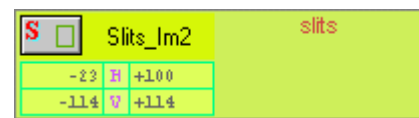
In the “classic” LISE program there was just one dialog for all the slits and acceptances of the spectrometer. In LISE++ each block (excluding “Rotation beam”, “Stripper”, and “Wedge” blocks) has its own “Slits & Acceptance” dialog (see Fig.490), which is available by clicking in the dialog of the optical block properties through the button .



*Fig.490. The “Slits & Acceptance” dialog.*

The editing of slit sizes is more visual and convenient in the new version, as well as the use of slits is closer to the reality of an experiment. The maximum slit size is defined by the user. In LISE++ it is not possible to input a moment acceptance that frequently resulted in fallacy earlier. The momentum acceptance is now determined by the slit size and dispersion ( $x/\delta$ ). Also, the program can calculate a momentum acceptance from the angular dispersion ( $\theta/\delta$ ) and angular acceptance and takes that into account in transmission calculations. It plays an important role in case of small dispersion ( $x/\delta$ ) and large angular dispersion (for example: block “Slits\_S800BL” in the configuration file “A1900+S800\_d0.lcn”).

If the checkbox “Use in calculations” is off then the program keeps the slits settings, but does not use in the calculations. The program shows the slit size in the “Set-up” window (see Fig.491 on the right) if the checkbox “Show in schematics” is set.

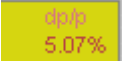


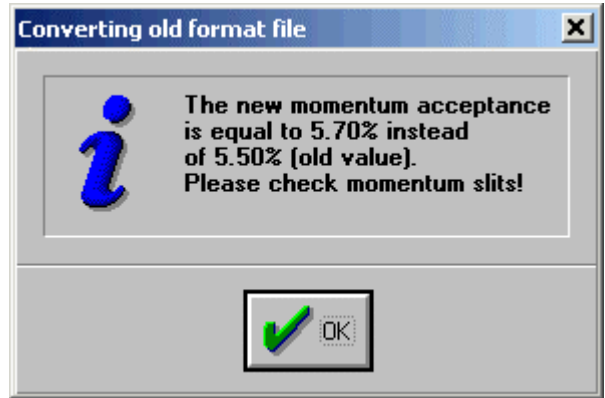
*Fig.491. The Set-up window fragment.*

### Important

- If the block has working slits then the Slits are found **AFTER** the **optical** block and **BEFORE** the **material** block (like support of detector)
- Angular acceptance is applied on the **BEGINNING** of the block

### 7.3.1.1.3. Momentum acceptance of spectrometer

The program searches for the smallest acceptance in all the blocks and takes that for total momentum acceptance of spectrometer (TMAS). The program shows the TMAS in the top right corner of the Information window . In reading in old (LISE) files, where the slit size of slits was set using a momentum acceptance, LISE++ will display the message indicating the former momentum acceptance value and new TMAS.



⚡ There are specific cases when the real TMAS actually will be more than shown by the program. The “double acceptance effect” is explained in chapter 7.3.4.5.

### 7.3.1.2. Blocks from optical class

#### 7.3.1.2.1. Drift block

A drift space is a field-free region through which the beam passes. There are three types of drift block classes (see Fig.492):

- ❖ **Standard drift** block (as in the TRANSPORT code [Bro80]): Use this mode for a finite length detector in place of a detector with zero length in the spectrometer length calculation. The optical matrix is determined by the code on the base of block length.
- ❖ **Beam-line** block: non-dispersive optical block. User can change the optical matrix values.
- ❖ **Slits** mode: if the block length is equal to zero without dependence from a above-mentioned mode. The optical matrix of block in this mode is unitary.

It is possible to see the mode of a drift block in the Set-up window (see Fig.491). As well as in the spectrometer scheme “Slits” has different designation from other modes of drift blocks. Some cells will be blocked from input in editing an optical matrix.

⚡ Increasing number blocks you decrease transmission calculation speed. Despite that, it is recommended to use drift blocks in the mode Slits (more visual, fast access, is closer to a reality) instead of setting slits in the block “Dipole” for example.

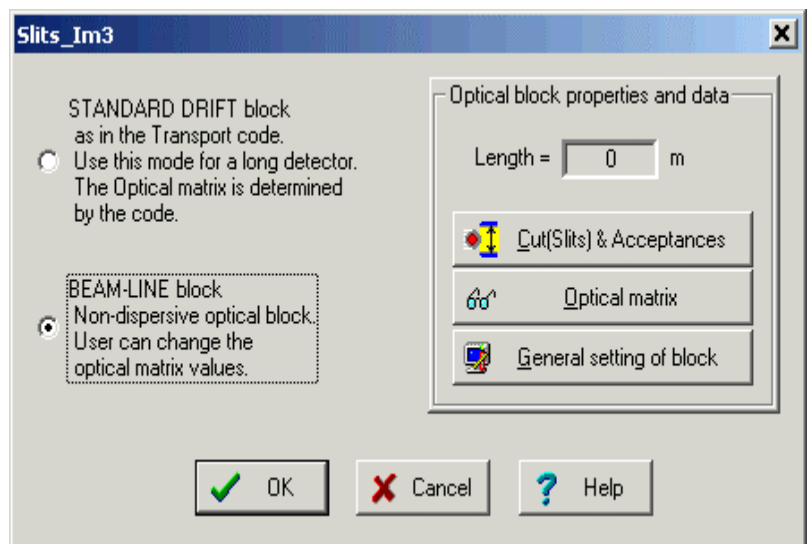


Fig.492. The “Drift block” dialog.

### 7.3.1.2.2. Rotation beam block

The transverse coordinates  $x$  and  $y$  may be rotated through an angle 90, 180, and 270 degrees about the  $z$  axis (the axis tangent to the central trajectory at the point of question) as done in the program TRANSPORT [Bro80]: type code 20.0. The “Rotate beam” block (see Fig.493) does not support slit properties. The “Rotation beam” block is shown by a circle on the spectrometer scheme. The code automatically recalculates the local optic matrix of the block. The user cannot edit matrix values.

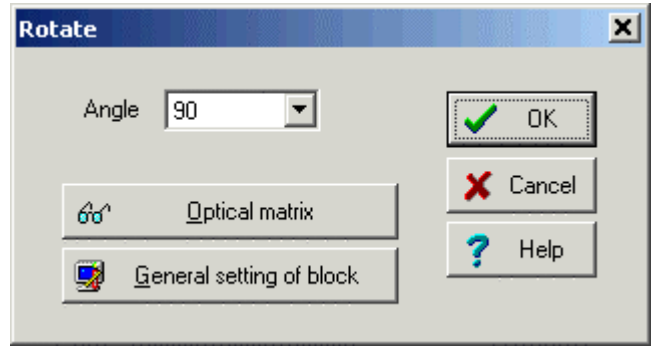


Fig.493. The “Rotate beam” dialog.

The block is used at transitions of one plane to another. For example, the A1900 spectrometer is in a horizontal plane, and then the beam follows the S800 beam-line which is in a vertical plane.

### 7.3.2. Dispersive block

Optical dispersive blocks are electromagnetic separation devices. Only Dispersive optical blocks determine the setting of the spectrometer on a certain fragment.

#### 7.3.2.1. Properties and methods

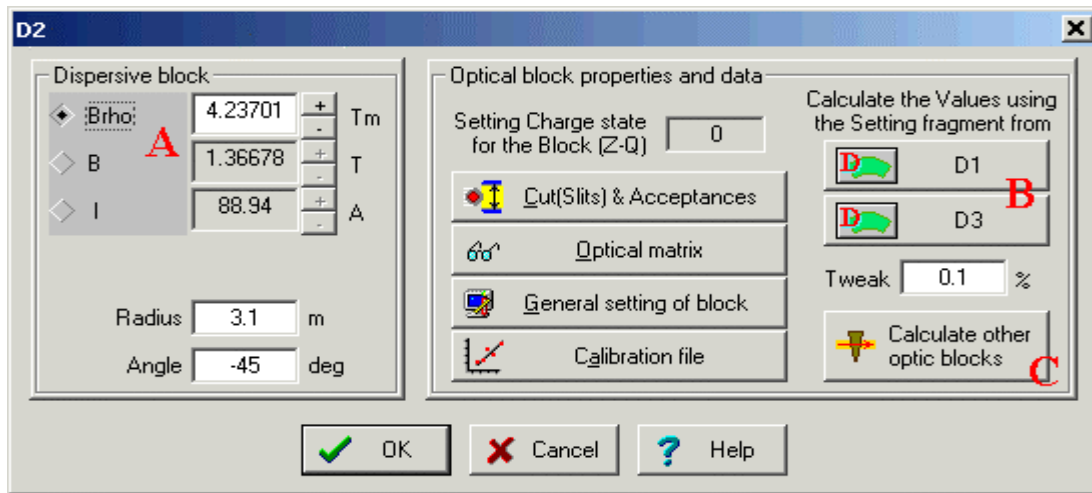
##### 7.3.2.1.1. Computational values (fields)

Classification of electromagnetic separation devices (LISE++ dispersive blocks) and their selection methods is given in Table 54. Magnetic (electrical) fields of dispersive blocks can be calculated by the code, as well as the user can enter manually field values. The basic difference of dispersive blocks from optical blocks is that the adjustment of the fields of these blocks result in a change in the trajectory of particles and therefore their separation in space. When the spectrometer is “set” on a fragment, it means that the magnetic (electrical) rigidity of a particle coincides with magnetic (electrical) rigidity of electromagnetic devices in the central trajectory. The magnetic field (for a magnetic dipole) is calculated from the magnetic rigidity of the device using a dipole radius. If a calibration file (see the next chapter for a definition of the calibration file) is entered, then the electric current ( $I$ ) is also taken into account.

Table 54. Electromagnetic separation devices.


Separation device	Changeable field	Strength	Selection by
Magnetic dipole	Magnetic (B[T])	$\vec{F} = q\vec{v} \times \vec{B}$	Magnetic rigidity $B\rho = \frac{mv}{q}$ [T·m]
Electric dipole	Electric (E [kV/m])	$\vec{F} = q\vec{E}$	Electric rigidity $E\rho = \frac{mv^2}{q}$ [J/C]
E-cross-B filter	Magnetic (B[T]) Electric (E [kV/m])	$\vec{F} = \vec{F}_B + \vec{F}_E$	Velocity





**Fig.494.** The “Dispersive block” dialog.

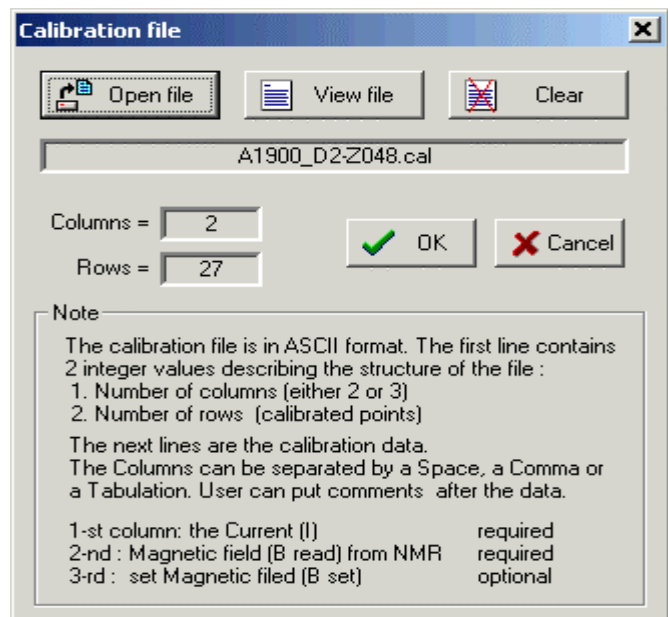
You can do the things listed below using the options in the “dispersive block” dialog pictured in Fig.494:

- You can manually change the magnetic field and the electric current using the dialog (see Fig.494 “A”). The magnetic rigidity will be changed automatically.
- You can calculate a rigidity of the block for a given setting fragment depending on a previous or following dispersive block values with the materials between them taken into account (Fig.494 “B”).
- You can use the rigidity value of the block to calculate the field values of all the other dispersive blocks in the spectrometer (Fig.494 “C”).
- Clicking on the button  in the toolbar or calling the command “Calculate the spectrometer for setting ion” from the menu “Calculations”, the program will calculate rigidity values of spectrometer blocks for the setting fragment.

### 7.3.2.1.2. Calibration file

The interrelation between a magnetic field and an electric current can be entered for the block through a calibration file. In actuality, experimenters use electric currents to set a desirable magnetic field or in other words to establish desirable magnetic rigidity. Entering a value of the electric current in the Dispersive block dialog, you can estimate expected magnetic rigidity.

Calibration dialogs were done in the LISE classic version just for two defined spectrometers. Moreover the user could not change calibration values. LISE++ allows you to use calibration files for all of the dispersive blocks.



**Fig.495.** The “Calibration file” dialog.

The format for the calibration file is rather simple. You can see the format description in The “Calibration file” dialog (Fig.495). The program uses a cubic spline to get a value in region indicated in the file. The code uses a linear extrapolation if the searched value exceeds the determinate region.

$B_{read}$  is a measured value from an electromagnetic device (for example a NMR probe).

$B_{set}$  is established using the calibration. The program uses the  $B_{read}$  value to calculate a magnetic rigidity. If just one calibration between the magnetic field and electric current is entered, then  $B=B_{read}=B_{set}$ .

### 7.3.2.2. Dispersive block on the base of Magnetic dipole

The program uses the definition of a “Dispersive block” instead of simply a “Magnetic dipole” to underline that this block is a system with one optical matrix but consists of quadruples, drifts, and magnetic dipoles. The “Dispersive block” dialog is presented in Fig.494. The basic characteristics and properties were described above in the text.

The order of distribution and transmission calculations in the dispersive blocks is given in chapter 7.4.1.

### 7.3.2.3. Wien velocity filter

LISE++ assumes the velocity filter is a standard dispersive block with the optical matrix and all other properties and methods. This redefinition in comparison with the “classical” version allows the use of the filter anywhere in the spectrometer. Velocity dispersion through the filter depends on the mass and charge of a particle and is function of the particles energy. The most important difference between the filter and a magnetic dipole is that dispersive elements of the local optical matrix are recalculated for each fragment and energy anew for the Wien velocity filter.

The filter operates with two fields. Therefore to adjust the filter on a one fragment, you should keep one field constant (see the frame ”Select constant field” in Fig.496) and change the other field. In a reality the electrical field is kept constant, while the magnetic field is changed.

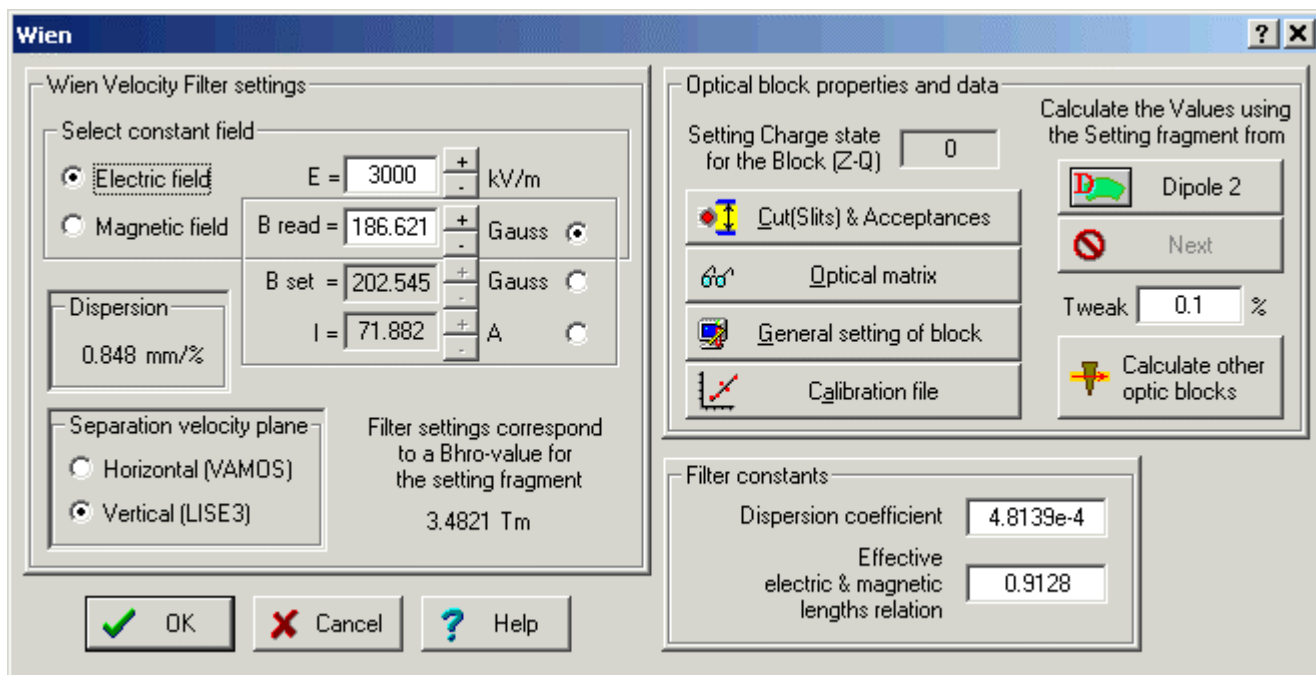


Fig.496. The “Wien velocity filter” dialog.

The LISE code has three parameters to define the filter of velocity:

- eElen - Effective electric length,
- eMlen - Magnetic effective length,
- rrf - Real/Read field.

There is just one parameter “Effective electric & magnetic length relation (EMLR)” in the LISE++ (see the frame ”Filter constants” in Fig.496), which is a combination of three of these LISE parameters using the formula:  $EMLR = eElen \cdot rrf / eMlen$ .

#### 7.3.2.4. Compensating dipole after the Wien velocity filter

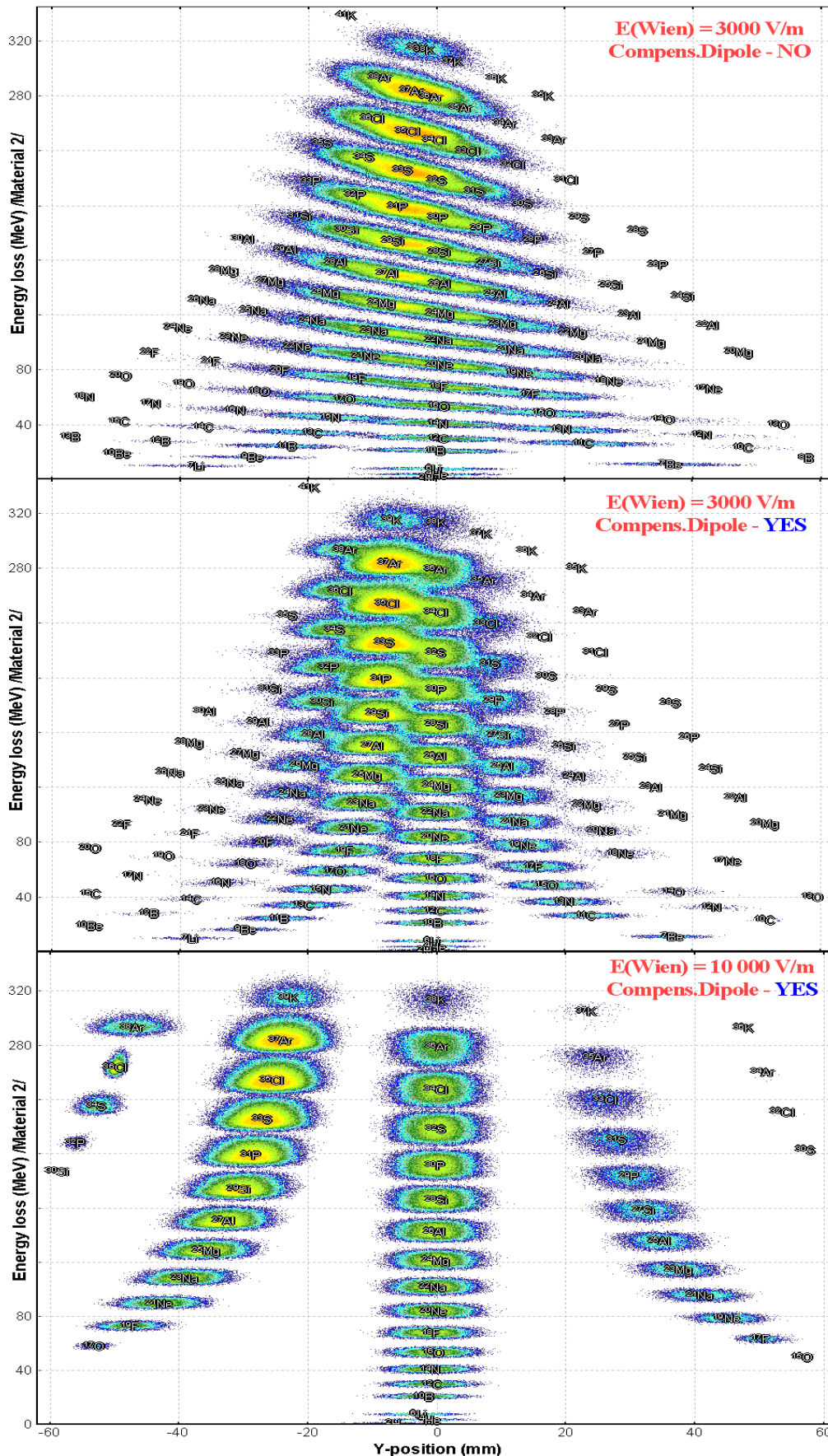
It is planned to develop a dialog for a compensating dipole after the Wien velocity filter as in LISE (it was named dipole D6). The compensating dipole is a dispersive block assigned to compensate the velocity dispersion after the Wien velocity filter. Using the compensating dipole it is possible to get the A/Q dispersion. The main advantage of A/Q selection is absence of a momentum (velocity) dispersion which allows you to use the large momentum emittance of the secondary beam. However, you can simulate the compensating dipole in LISE++ already now. To do so, you have to put a dispersive block after the Wien velocity filter and manually input a dispersion of the block to compensate the filter dispersion, such that after the compensating block the global dispersion is equal to zero. Fig.497 shows selections by the system “velocity filter ⊗ dipole” for different values of the electric field of the velocity filter. This example is accessible through the LISE web-site: [http://groups.nsl.msui.edu/lise/6\\_1/examples/lise\\_wien\\_d6.lpp](http://groups.nsl.msui.edu/lise/6_1/examples/lise_wien_d6.lpp)

#### 7.3.3. Material blocks

Material blocks were created on the basis of the LISE++ **Block** class and the LISE **Compound** class. There are four existing blocks (Target, Stripper, Material, Wedge) and one (Secondary target) still under development. Material blocks properties are given in Table 55.

Table 55. Properties of Material blocks.

Property / Block	Target		Wedge	Material	Secondary target
Calculation of primary fragments production		+			+
Calculation of secondary reactions	+				
Attenuation due to reactions	+	+	+		+
General setting dialog			+		
Slits before block					+
Calibration & Resolution				+	
Detector mode for two-dimensional plot				+	
Detector mode for TOF calculation				+	
Thickness defect			+	+	+
Option: to set the spectrometer down part			+	+	+
Inclination of material	+				+
Wedge property			+		+



**Fig.497.** *dE-Y simulation spectra for the reaction  $^{40}\text{Ar} + \text{Be}(500 \mu\text{m})$  with  $^{32}\text{S}$  as the setting fragment. The LISE spectrometer ( $\Delta p/p=4.6\%$ ), Wien velocity filter and the compensating dipole were used in the calculations. LISE velocity filter selects fragments in the vertical plane. Energy loss calculations were done through a  $300 \mu\text{m}$  silicon detector located behind the compensating dipole.*

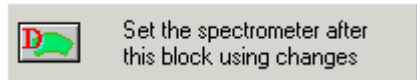
*Upper plot shows the vertical selection of fragments after the velocity filter without the compensating dipole.*

*Middle and lower plots show the vertical selection of fragments using the compensating dipole for different values of the electric field of the velocity filter.*

New dimensions (**mm** and **g/cm<sup>2</sup>**) were added in LISE++ to avoid it excess characters. The user can choose system of measurement units in the frame “Dimensions” of the “Material block” dialog (see Fig.498).

Material (detector) and Target blocks own the optical blocks property: **Slits**. To correspond to a reality, the supports of a material act as slits and therefore are ahead of the block. The slits used in the program have the rectangular form. Use of oval slits is planned in the future.

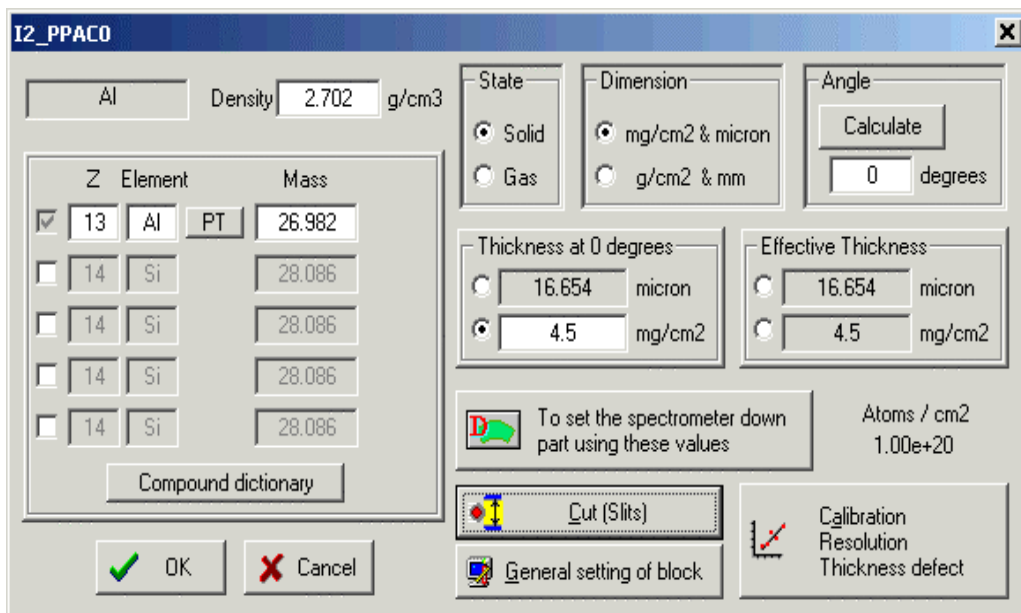
It is possible to calculate field values of optical dispersive blocks located in the spectrometer after a material, after change of material thickness in blocks Material and Wedge using the button “Set ...”.



The calculations will be made using the values of the Dispersive block before the material with the new thickness of this material taken into account. The material block is not shown in the spectrometer scheme if the material thickness is equal to zero. In the Set-up window a blank space is shown instead of zero.

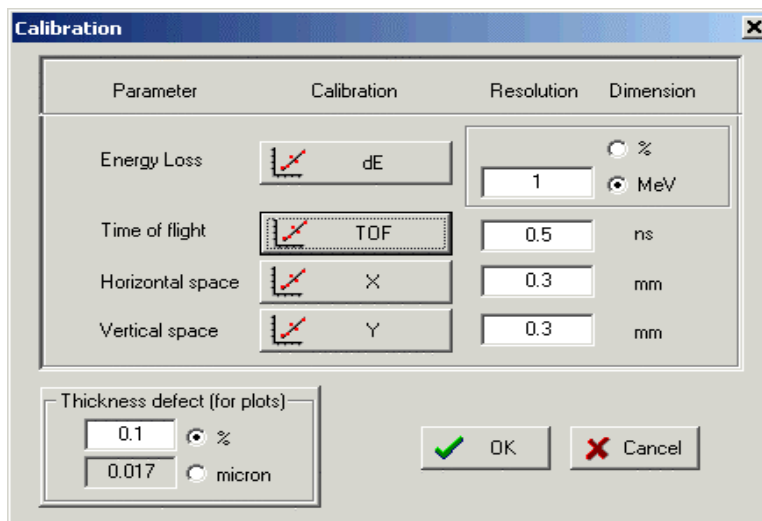
### 7.3.3.1. Material (detector) block: properties and methods

Only Material (detector) block (Fig.498) can be used for the two-dimensional plots. This block has properties of real detectors: calibrations and resolutions (energetic, timing, spatial).



**Fig.498.** The “Material(detector) block” dialog.

It is possible using the button “Calibration, Resolution, Thickness defect” of the Material dialog to get an access to the dialog of material properties editing (Fig.499). The detector resolution is used only for drawing the two-dimensional plots. The defect of material thickness is used for transmission calculations and therefore the effect from it is observed on the plots also. Total kinetic energy calibration is available in the Plot options dialog.



**Fig.499.** The dialog of detector properties settings: calibration, resolution, and thickness defect.

### 7.3.4. Degradar in the dispersive focal plane

LISE++ supports three types of degrader profiles: wedge profile, homogeneous (a simple material), and curved profile. To calculate a wedge angle or a curved profile, the code uses the modes: achromatic and monochromatic. Also you can enter an angle manually, or have the code calculate a wedge angle for you (see the frame “Degradar profile” in Fig.500).

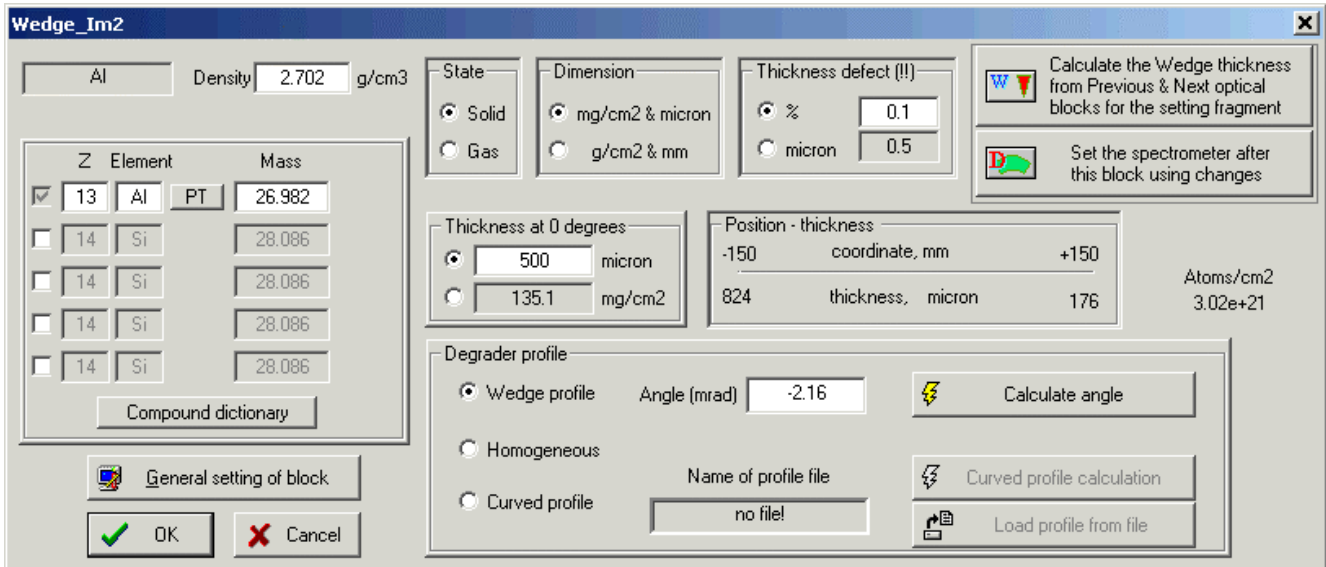


Fig.500. The “Wedge (Degradar in the dispersive focal plane)” dialog.

Coordinate (X) in the frame “Position-thickness” is defined as smallest slit between the previous and next dispersive blocks. These coordinates determinate maximal possible angle of wedge:

$$\text{Angle}_{\text{limit}} = \arctan \left( \frac{\text{Thickness}_{\text{central trajectory}} [\text{mm}]}{\text{Slit} [\text{mm}] / 2} \right) \text{ (see Fig.501).}$$

☞ The angle of the wedge is not recalculated automatically as in the classical version. The angle of the wedge or the curved profile are always kept such that they correspond to the reality of an experiment.

LISE++ has a large set of warnings in the case of wrong data entry in the Wedge dialog. The user gets messages if:

- There is not a slit between the previous and next dispersive blocks.
- A slit is larger than a profile degrader size.
- The setting fragment is stopped in the material.
- A curved degrader profile has been chosen, but a filename of curved profile is absent.
- The angle of the wedge exceeds the maximum possible angle.

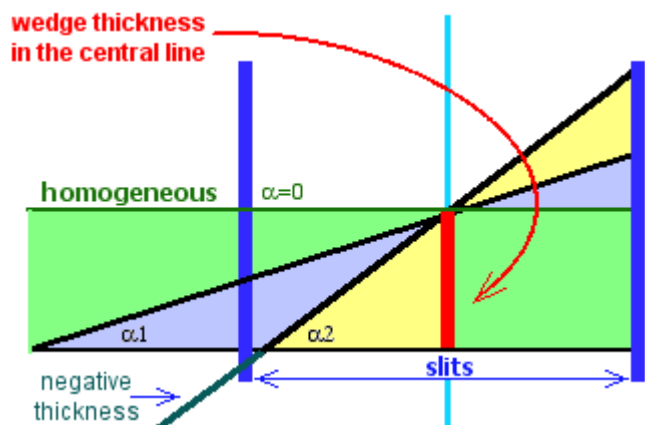
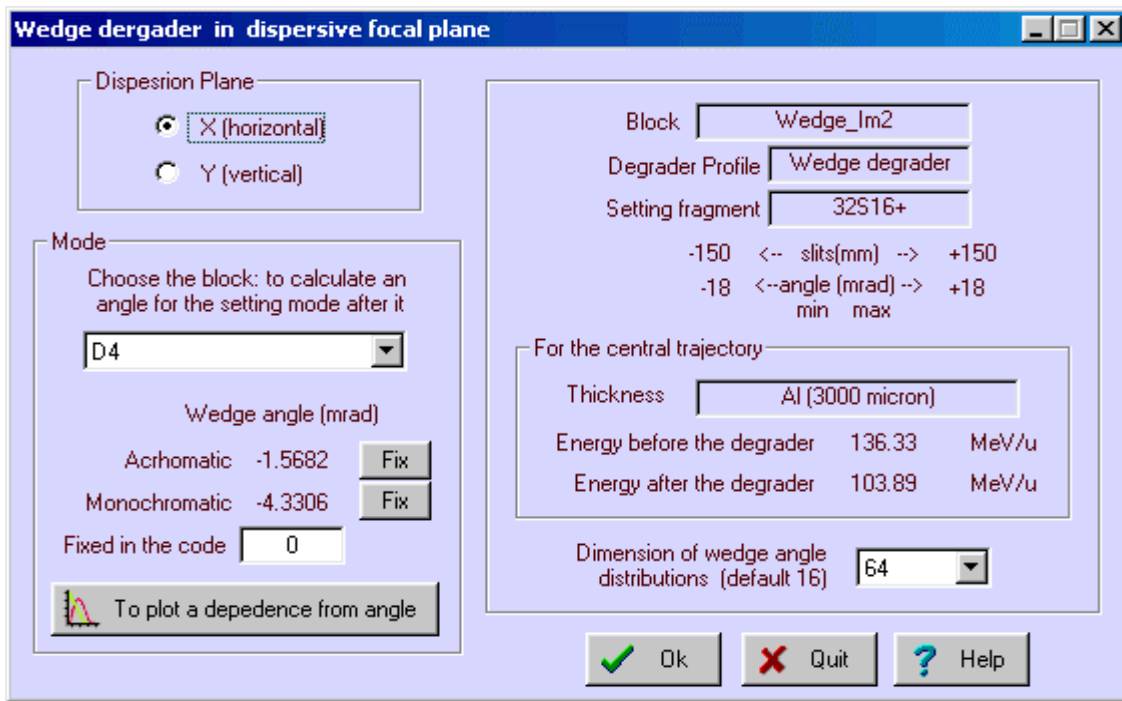


Fig.501. Scheme of wedge angle calculation.

### 7.3.4.1. Wedge angle calculation

LISE++ can calculate a wedge angle from the conditions that the wedge must be achromatic or monochromatic after the block defined by the user. In the classical version the wedge is found between two dipoles and the angle is calculated for the focal plane after the second dipole. In LISE++ a wedge can be placed in anywhere.

It is necessary in the frame “Mode” to choose the block after which conditions will be applied. If you press one of the keys “Fix” or enter a value into “Fixed in the code” cell manually (Fig.502) than the program uses one of calculated angles in the further calculations.



**Fig.502.** The wedge angle calculation dialog.

LISE++ calculates the wedge angle when this dialog is loading or when one of the parameters (block, number of points in distribution) changed. The code determinates the minimal ( $\alpha_{\min}$ ) and maximal ( $\alpha_{\max}$ ) values of angle (as well as  $\text{Angle}_{\text{limit}}$  from the previous section). The program  $N+1$  times calculates a setting fragment transmission changing a wedge angle for the value  $(\alpha_{\max} - \alpha_{\min}) / N$ . As a result of these calculations the program fills four distributions which can be plotted by clicking “to plot a dependence from angle” in the frame “Mode”. The received wedge angular distributions are shown in Fig.503. A description the wedge angular distribution is shown in Table 56.

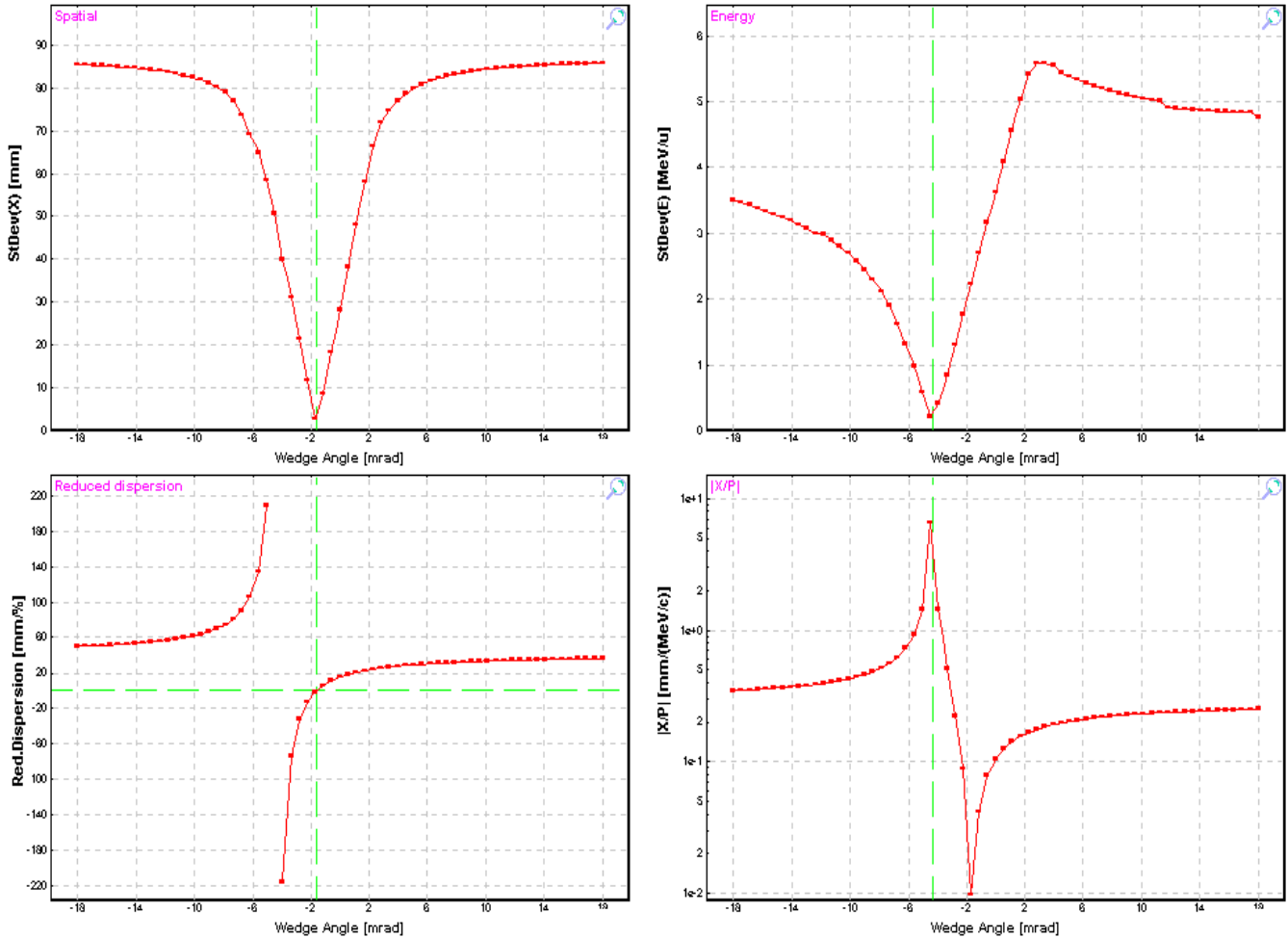
**Table 56.** Wedge angular distributions.

Distribution after setting block	Position in the plot (Fig.503)	Mode	Condition to find an angle	Use to define an angle
Spatial – Sd.Dev.(X)	upper left	achromatic	minimum	Yes
Reduced dispersion	lower left	achromatic	equal to 0	
Energetic – St.Dev.(E)	upper right	monochromatic	minimum	Yes
Relation  X/P  from debug distributions (chapter 7.7.3.)	lower right	monochromatic	maximum	

## Wedge\_Im2 calculations for D4

<sup>40</sup>Ar 140.0 MeV/u + Be (500 μm); Settings on <sup>32</sup>S; Config: DDMSWMDSDMMMMMMMMMM  
 dp/p=5.07% ; Wedges: Al (3000 μm); Brho(Tm): 3.4821, 3.4821, 3.0101, 3.0101

Horizontal direction



*Fig.503. Wedge angular distributions.*

The code seeks minimums in spatial and energetic distributions. The code defines angles using neighboring points of these minimal points by a simple expression. To get more precise wedge angles, it is necessary to increase the number of points in the wedge angular distributions. A default value of the distribution dimension is defined in the dialog “Preferences”.

Press the key “Escape” once if you want to break calculations.

If the code didn’t find a solution for one of a mode or you interrupted then you will see a string “???” instead of a calculated angle value.

Button “To plot a dependence from angle” will be inaccessible if

- Calculations were interrupted
- The transmission of the setting fragment after chosen block is equal to zero for all points of the wedge angular distributions.



### 7.3.4.2. Possible problems in wedge angle calculation

Working with the beta-version many users had questions and problems with wedge angle calculations. On the basis of their remarks, the program was modified to display messages indicating why a wedge angle was not is calculated. See Table 57 for messages problems, reasons then to correct the problem.

**Table 57.** Possible problems in wedge angle calculation and methods of their elimination.

LISE++ message	Problem	Reasons	How to correct
Spectrometer is not set for the isotope of interest	Transmission of the isotope of interest after the setting block is equal to 0	The wedge thickness has been changed, but the user forgot to recalculate block values of the spectrometer after this block	<ul style="list-style-type: none"> <li>Return to the wedge dialog,</li> <li>Click the button “to set the spectrometer ...”</li> </ul>
		Spectrometer has not been set on the isotope of interest	<ul style="list-style-type: none"> <li>Leave the wedge dialog,</li> <li>Calculate spectrometer.</li> </ul>
		Wedge thickness is too thick	<ul style="list-style-type: none"> <li>Return to the wedge dialog,</li> <li>Decrease wedge thickness,</li> <li>Set the spectrometer.</li> </ul>
		Thickness of material located between wedge and the setting block is too thick	<ul style="list-style-type: none"> <li>Leave the wedge dialog,</li> <li>Change material,</li> <li>Calculate spectrometer</li> </ul>
try to increase maximum (min) angle by closing slits or making the wedge thicker	There is not minimum in the wedge spatial or energetic distributions (then see angle distribution plots)	Achromatic or Monochromatic angles are bigger than the maximum possible angle. This is a frequent problem.	try to increase the maximum possible angle by closing slits or making thicker the wedge
		Slit size of one of the blocks after the wedge up to the selected plane is smaller than the spatial distribution of fragment of interest	<ul style="list-style-type: none"> <li>Leave the wedge dialog,</li> <li>Check all slits after the wedge</li> </ul>
		Dispersion is wrong	Check optical matrices; check that the correct dispersion plane direction was chosen
		There is not a dispersive block after the wedge and the setting plane. In this case it is possible to calculate a wedge angle in monochromatic mode, but not in achromatic mode.	
The wedge thickness is equal to 0!	No comments... it is clear	<ul style="list-style-type: none"> <li>Input a positive value in the edit cell of wedge thickness,</li> <li>Click button “to set the spectrometer...” to calculate spectrometer down parts for new wedge thickness</li> <li>And try to calculate angle once more.</li> </ul>	

### 7.3.4.3. Curve profile degrader

LISE ++ has a new profile of degrader that can be used for transmission calculations: a curved profile degrader. If in the classical version only a wedge shape degrader was applied to transmission calculations, but in the new version a curved profile degrader also can be applied for transmission calculations.

A curved degrader consists of a foil and a support for this foil. Having calculated a profile for the support, the user can save it in a file and use it in further calculations.

In reality, a support for a curved degrader can hold many different thickness degrader (foil). Therefore, LISE++ has the capability to let you use the same support for several different thickness degraders.

The support can be designed with use of the “Curve profile degrader” dialog (Fig.504).

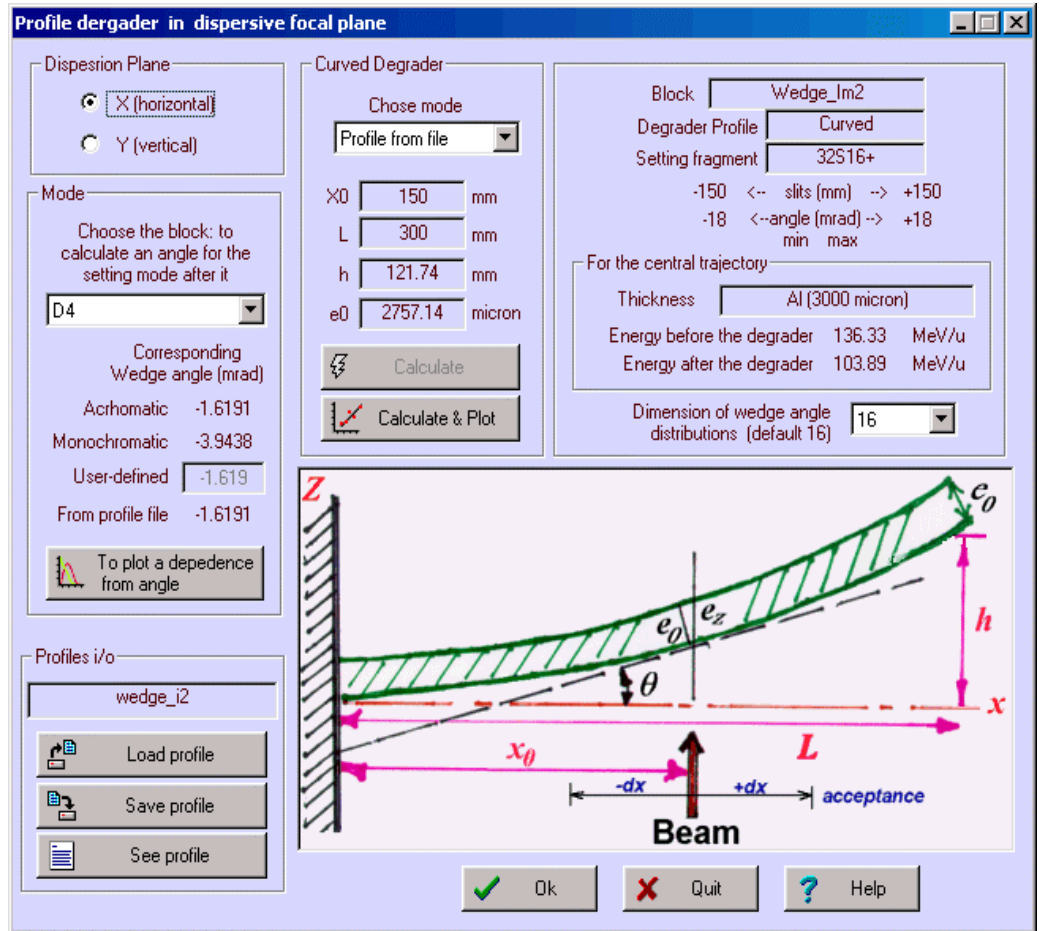


Fig.504. The “Curve profile degrader” dialog.

- By analogy to the “Wedge angle calculation” dialog (Fig.502), the user should select a block and mode.
- It is necessary to define support parameters  $X$  and  $L$ . A degrader length should be approximately the slits size.
- Pressing on the button “Calculate & Plot”, the program will calculate a support of curved degrader.
- Save the calculated profile in a file.

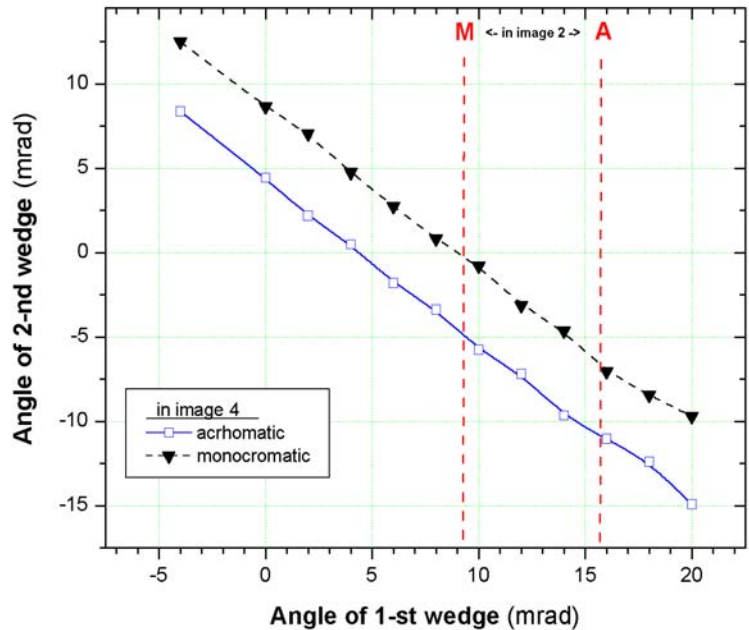
The user can load already created structures from a disk. The parameters of a support from a file will be shown in the dialog and can be visualized in the plot. It is possible to see the corresponding wedge angle from profile file in the dialog. This angle is calculated on the basis of the support and a material used at this moment in the wedge block. The files of supports have the extension “degra” and are by default in the directory “\degrader”.

### 7.3.4.4. Use of two wedges

The new version has the opportunity to use multiple wedges at once. Examples of ways to use two wedges are:

1. Select an isotope of interest using an achromatic wedge to partially eliminate impurities. Then use a monochromatic wedge to get a monoenergetic secondary beam without impurities at the end of spectrometer.
2. To eliminate (by the second wedge) products of secondary reactions from the first wedge. This is very useful for particles at relativistic energies.
3. To increase the spectrometer momentum acceptance (see the next chapter).

Dependences between angles of two wedges for different modes are shown in Fig.505. The 1st wedge is found in Image 1, and is calculated to be achromatic or monochromatic for Image 2. The 2nd wedge is found in Image 3, and is calculated to be achromatic or monochromatic for Image 4. The configuration “A1900-4dipoles” is used in calculations. Two vertical red lines show angles of the 1<sup>st</sup> wedge to be monochromatic and achromatic in Image 2. Blue and black lines are angles of both wedges to be achromatic and monochromatic in Image 4.



**Fig.505.** Dependences between angles of two wedges for different modes. (See text for details)

In this configuration wedge angles can be written by:

Achromatic mode in Image4	$\alpha_1 + \alpha_2 \cong 5 \text{ mrad},$
Monochromatic mode in Image4	$\alpha_1 + \alpha_2 \cong 10 \text{ mrad}.$

### 7.3.4.5. Double acceptance effect

The use of two wedges can result in an effect, which we have named the “double acceptance effect”. The “A1900-4dipoles” configuration is used. The calculated momentum acceptances in Image1, Image2, and Image 3 are equal to 5.07%, 10.39 %, and 5.07% respectively. Therefore, the momentum acceptance of the spectrometer is equal to 5.07%, which the user can see in the Information window. Let’s consider the reaction  $^{36}\text{S}(140\text{MeV}/u, 100\text{pna})+\text{Be}(1\text{g}/\text{cm}^2)$  with  $^{30}\text{Ne}$  as the setting fragment.  $^{30}\text{Ne}$ ’s rate at the end of the spectrometer is equal to **3.3e+1 pps**, and only 54 % of all fragments pass through the slits in Image2. Now let’s put a wedge (Be,  $0.7\text{g}/\text{cm}^2$ ) in Image1 and choose the angle of the wedge (22.5mrad) which is the maximum possible from the slits. The wedge is not achromatic; it works as a lens focusing on Image2.  $^{30}\text{Ne}$ ’s rate at the end of the spectrometer is equal to **5.6e+1 pps**, and 98% transmission through the slits in

Image2. Now the momentum acceptance of the spectrometer is determined by the slits in Image1, instead of by the slits in Image2, and therefore the rate has doubled.

If a degrader is put in Image 3 that is identical to the wedge in Image1 and an angle is calculated to be achromatic for Image4 (angle = -14 mrad), it is possible to select  $^{30}\text{Ne}$  from the impurities which comprise about 65% of the beam.

Calculation results for configurations with different numbers of wedges are shown in Table 58. From this table it follows that the best selection is reached when the wedge is found in a plane with maximal dispersion. But in this case the rate is lower, but the quality of a secondary beam (emittance, purification) is much better, than in the case of the use of two wedges. As always there is the balance between quantity and quality.

*Table 58. Calculation results for configurations with different numbers of wedges.*

Configuration		2 wedges	1 thin wedge	1 thick wedge	
First Wedge	Location	Image1	Image2	Image2	
	Thickness	Be 0.7 g/cm <sup>2</sup>	Be 0.7 g/cm <sup>2</sup>	Be 1.4 g/cm <sup>2</sup>	
	Angle (mrad)	Achromatic	40.3	-2.05	-4.13
		Monochromatic	22.0	-10.85	-10.76
		abs.maximal	22.72	22.72	45.42
fixed in the code		22.5	-2.1	-4.1628	
Second wedge	location	Image3	-	-	
	Thickness	Be 0.7 g/cm <sup>2</sup>			
	Angle (mrad)	achromatic	-13.7		
		monochromatic	-0.38		
		Abs.maximal	22.72		
fixed in the code		-13.7			
$^{30}\text{Ne}$ transmission in Image2 slits		97.2%	54.2%	54.2%	
Slits in final focal plane (Image4), mm		-4/+8	-6/+6	-9/+9	
Total rate		65	36	28	
For $^{30}\text{Ne}$ setting fragment	Rate, pps	<b>42</b>	<b>31</b>	<b>28</b>	
	Purification%	<b>65%</b>	<b>87%</b>	<b>100%</b>	
	Energy, MeV/u	85.7	100.5	85.8	
	Standard Deviation (before slits in Image4)	Energy, MeV/u	4.4	2.9	2.5
		X, mm	4.5	1.9	2.5
		Y, mm	1.13	1.13	1.13
		$\theta$ , mrad	15	15	15
		$\phi$ , mrad	18	18	18

The LISE++ files with these calculations are accessible through the LISE web-site:

[http://groups.nsl.msu.edu/lise/6\\_1/examples/double\\_acceptance\\_1wedge.lpp](http://groups.nsl.msu.edu/lise/6_1/examples/double_acceptance_1wedge.lpp)  
[http://groups.nsl.msu.edu/lise/6\\_1/examples/double\\_acceptance\\_2wedges.lpp](http://groups.nsl.msu.edu/lise/6_1/examples/double_acceptance_2wedges.lpp)

## 7.4. Transmission and fragment output calculations

The program calculates transmission from the target and finishing last block, but total transmission value is determined by **last optical block**. The user can see the message about blocks used for calculation of total transmission in the “Statistics” window (Fig.506). The program considers that the particle has stopped in the spectrometer if after last optical block the transmission is equal to zero.

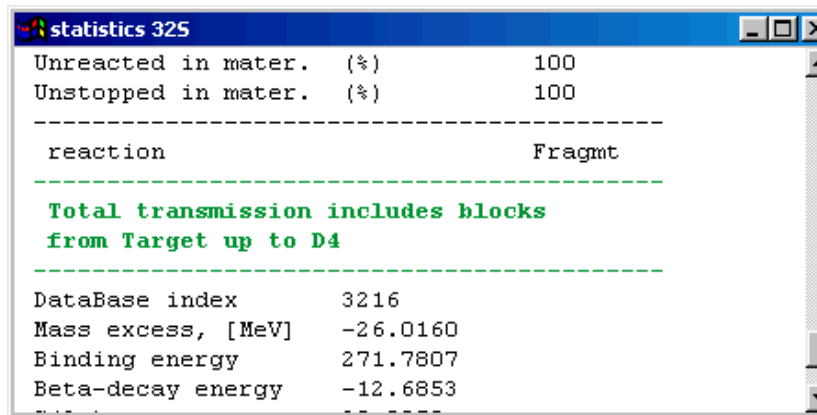


Fig.506. Fragment of statistics window.

☞ If a telescope, with certain slits in front of it, is placed in the end of the spectrometer, losses on the slits will not enter in the total transmission value. For example, FP\_PIN detector after dipole 4 has its own slits of  $\pm 25$  mm in the configuration A1900-4dipoles. But the dipole D4 slits are equal to  $\pm 150$  mm. A loss of rate on FP\_PIN slits is expected, but it will be not incorporated to the total transmission value.

☞ Let's suggest a scenario in which all secondary particles are stopped a telescope in the end of the spectrometer. If an optical block is put after the telescope then transmission of all particles will be equal to 0, and the code suggests no events were transmitted through the spectrometer.

### 7.4.1. Transmission calculation in a block

The orders of distribution transformation and transmission calculations in the dispersive and material blocks are given in Table 59.

Table 59. Transmission calculation order in block.

Optical block	Material block
1. Angular acceptance: <ul style="list-style-type: none"> <li>☐ Transmission value calculation,</li> <li>☐ Cutting of angular distributions.</li> </ul> 2. Optical matrix application for spatial distributions.           3. Spatial slits at the end of a block: <ul style="list-style-type: none"> <li>☐ Transmission value calculation,</li> <li>☐ Cutting of spatial, momentum and angular distributions.</li> </ul> 4. Optical matrix application for angular distributions.	1. Spatial slits before a block: <ul style="list-style-type: none"> <li>☐ Transmission value calculation,</li> <li>☐ Cutting of spatial, momentum and angular distributions.</li> </ul> 2. Passing through the material. Transformation of energetic distributions.           3. Angular straggling application for angular distributions.

### 7.4.1.1. Transmission statistics

By moving the mouse pointer to an isotope cell in the nuclide chart and pressing the right button of the mouse the user can calculate the transmission and rate of a selected isotope and its statistics window will pop up (Fig.507). Transmission results are shown block by block in the new version. Lines divide the blocks. The total block transmission is shown in dark blue. In the new version the user can automatically see the block in which the particle has stopped (see the green oval in Fig.507), if the total transmission in that block is equal to zero.

The user can load the transmission dialog analysis (Fig.508), using the button “Analysis” from the statistics window or the command in the menu “Calculations ⇒ Transmission”.

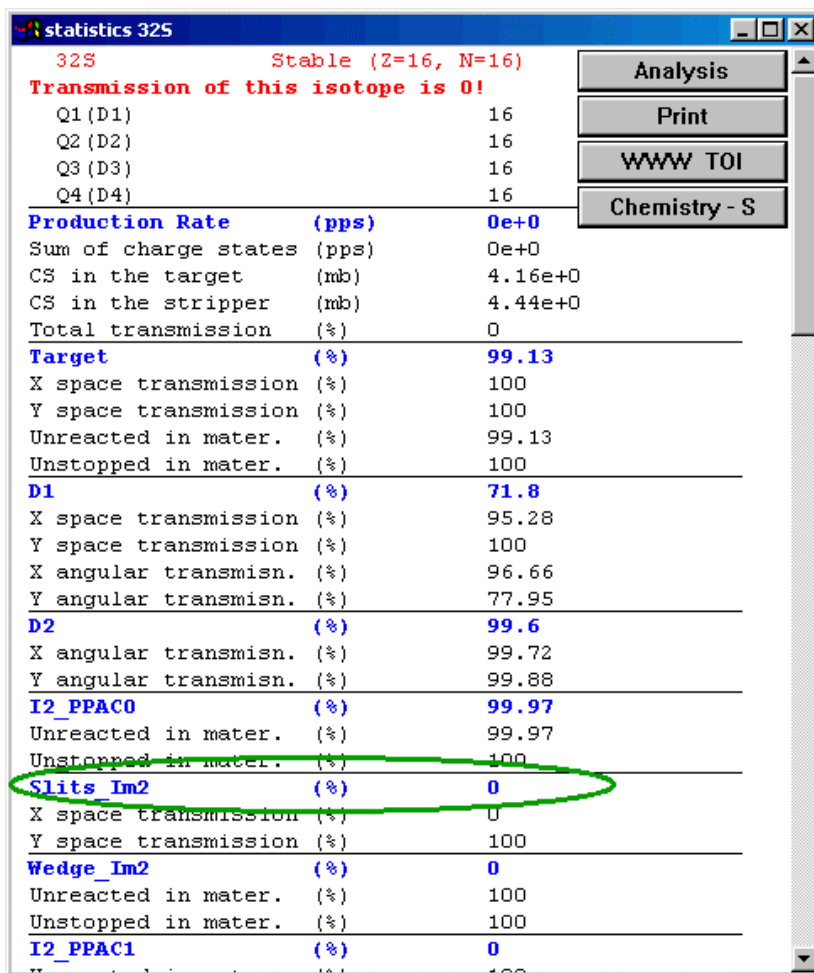
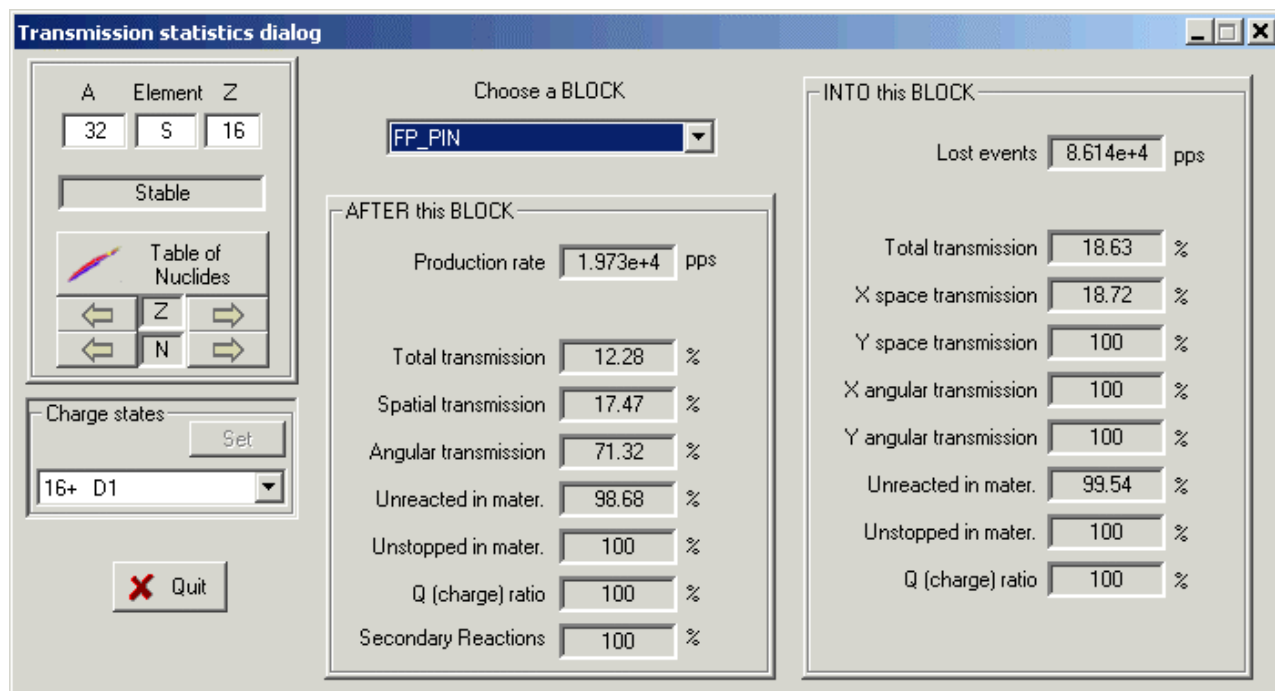


Fig.507. Fragment of statistics window.

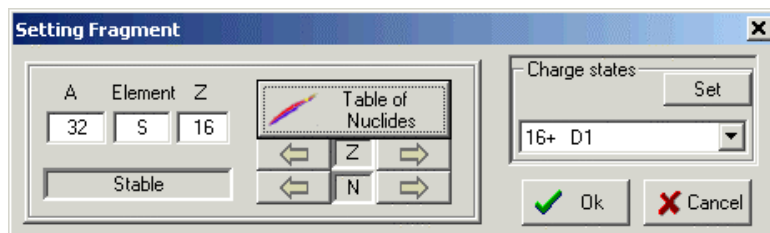


*Fig.508. The transmission analysis dialog.*

### 7.4.2. Charge states

The number of charge states of the setting fragment is equal to the number of dispersive blocks. The n charge state of a block is defined in the code as Z-Q, where Q is the n charge state of setting fragment (see table on the right). The magnetic (electric) rigidity of the block is recalculated on the basis of its charge state setting.

Dispersive block order	$I$	$2$	$N$
Charge state of setting fragment	$Q_1$	$Q_2$	$Q_N$
Charge state of block	$Z-Q_1$	$Z-Q_2$	$Z-Q_N$



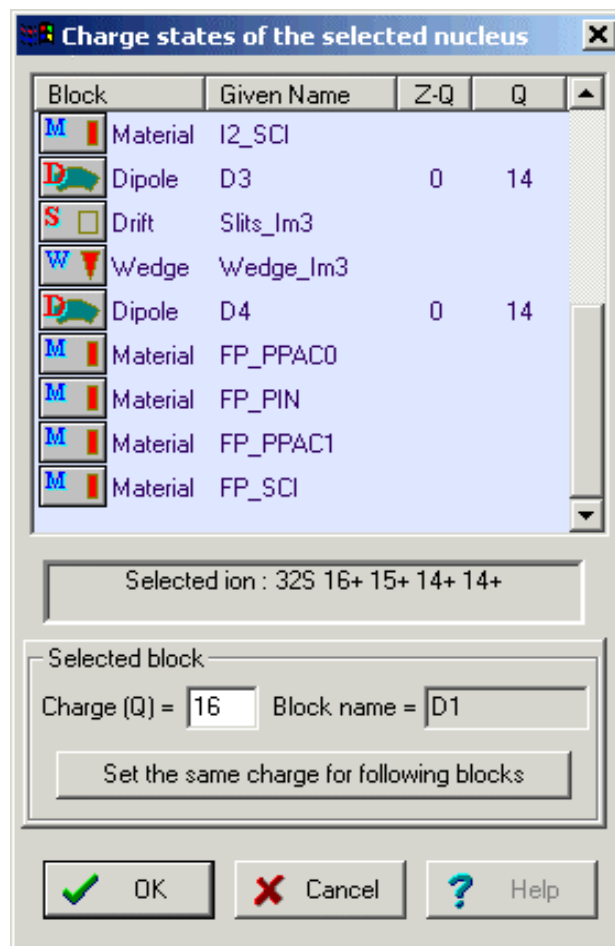
*Fig.509. The “Setting fragment” dialog.*

If the option “charge state” is set in the code, the user can replace a block charge state in the dialog of block properties editing (see for example Fig.494). If the user changes the charge state of the block then the code also changes the corresponding charge state of the setting fragment. After leaving the dialog it is possible to see the new charge settings in the Set-up window or in the status bar of the program

Z-Q=1,4,6,0

If there is a necessity to set more than one charge state, it can be made through the spectrometer setup dialog (chapter 7.2.1.) or through the setting fragment dialog (Fig.509.). The dialog of charge state settings (Fig.510) can be loaded using the button “Set” in the “Charge states” frame of the setting fragment dialog (Fig.509.).

In LISE++ you can have as many blocks as you want and you can enter the charge state for each block. For convenience, you can assign the value of the selected block to all further blocks.



*Fig.510. Dialog of charge states settings.*

The default value of the transmission distribution dimension in the charge state mode has been decreased to a value of 32 in comparison with the “classical” version (64). This is to facilitate more complicated transmission calculations. It is possible to change this value in the dialog “Preferences”.

### 7.4.3. Results file

In connection with global reconstruction of the program, the result file also has undergone a number of serious changes. As before, the user can create, look and print a result file through the menu “File ⇒ Results”. The file will be saved with the same name as the name of the LISE++ file in the same directory, but with the extension “res”.



The result file contains calculations of energy losses and times of flight along with *standard deviations*. The same subroutine used to create the result file is used to calculate values (using the resolution of detectors) in the dialog “Goodies” and in the ellipse mode of two-dimensional plots.

Structure of the result file is:

- Header: brief spectrometer configuration and basic options,
- Table 0: Transmission and Rate calculations,
- Table 1. Time of flight, Energy after stripper,
- Table 2. Energy after blocks,
- Table 3. Energy loss in materials.

☞ *Be careful when printing a result file. The width of the page depends proportionally on the quantity of blocks in the spectrometer. Print in landscape mode instead of portrait, or use a word-processor to prepare the file for printing.*

### 7.4.4. Previous isotope area rectangle

It is possible just once to choose a rectangle of isotopes of interest to calculate their transmission by the button “Calculate area of nuclei” , and to repeat calculations with this rectangle again by clicking the button “Previous calculated area”  in the toolbar. The new version saves the previous isotope rectangle in the LISE++ file. After loading the file, the user can use the button “Previous calculated area” without additional definition. If you want to change what isotopes are calculated, just click on “Calculate area of nuclei” again.

## 7.5. Improved mass formula with shell crossing corrections.

Accurate predictions of the production cross-sections of rare isotopes are important in the study of astrophysical processes and in the location of drip-lines. Reaction models as the abrasion-ablation, statistical multifragmentation or fusion-evaporation models rely on parameterization of the nuclear masses. This may lead to large inaccuracies in the case of discrepancies between mass parameterization and the experimental masses.



Representation of nuclei as liquid drops has been very successful in predicting their properties and masses, especially those along the valley of stability. However, a large discrepancy is observed for the classical Liquid Drop Mass formula and experimental values due to the shell structure. LISE++ uses a new mass formula with shell crossing corrections.

The most commonly used Liquid Drop Mass (LDM) formula (first developed by Von Weizsaecker) is where the nucleus binding energy is presented by sum of the terms shown in the table below:

Volume	Surface	Coulomb	Symmetry	Pairing
$aV \cdot A$	$-aS \cdot A^{2/3}$	$-aC \cdot Z^2 / A^{1/3}$	$-aSym \cdot (2A-Z)^2/A$	$\delta \cdot A^{-1/2}$

Where Z and A are the charge and mass number; aV, aS, aC, aSym,  $\delta$  are coefficients; delta is equal to + $\delta$  for Z and N are even, and - $\delta$  for Z and N are odd, and zero for A is odd. Let's name this formula by LDM0.

Meyers and Swiatecki [Mye66] have generalized this expression for the more general case of distorted nuclei:

Volume	Surface	Coulomb	Coulomb_X	Pairing
$aV \cdot A \cdot (1 - aVx \cdot x)$	$-aS \cdot A^{2/3} (1 - aSx \cdot x)$	$-aC \cdot Z^2 / A^{1/3}$	$Acx \cdot Z^2 / A$	$\delta \cdot A^{-power}$

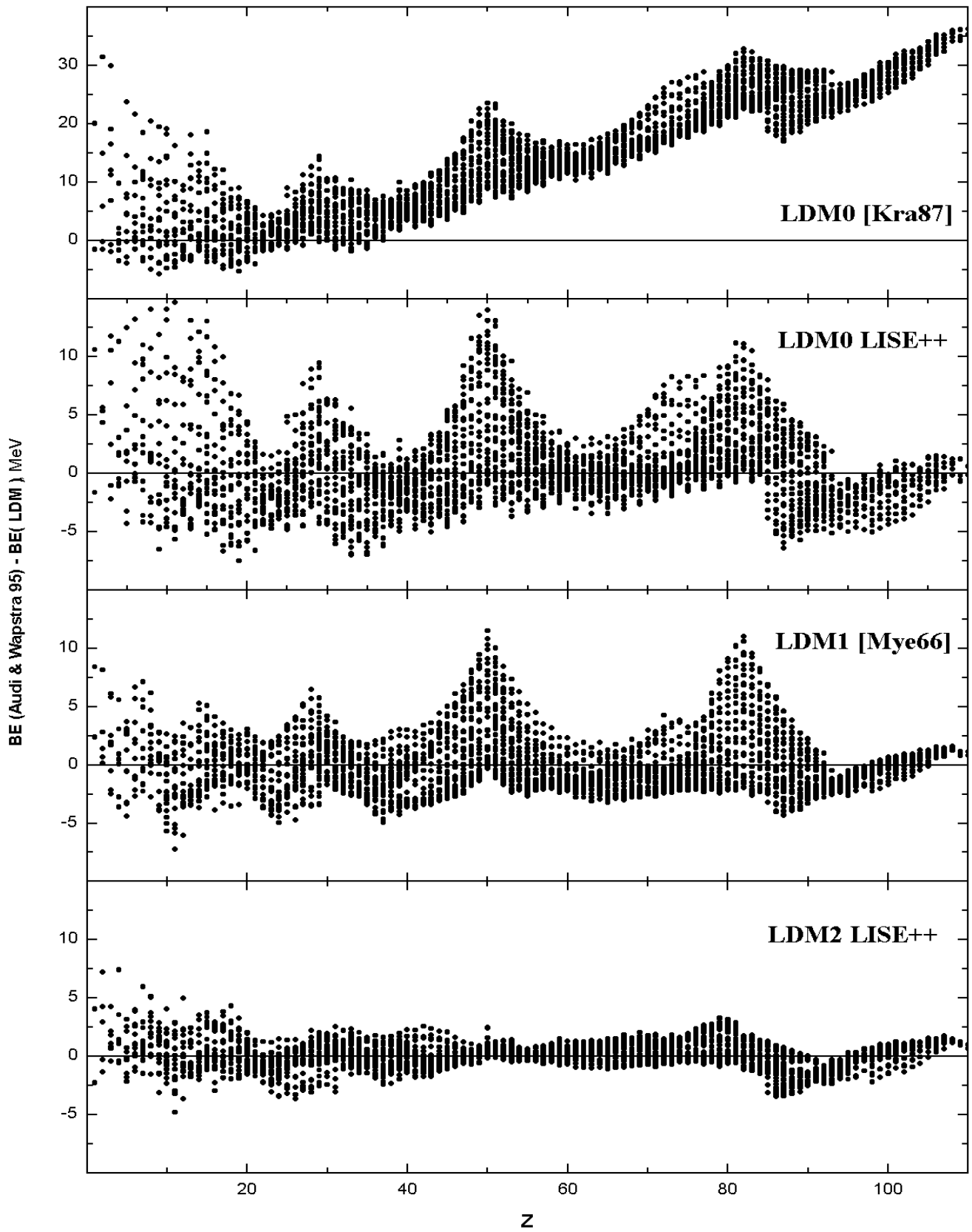
Where x is  $((A-2Z)/A)^2$ ; aSx, aVx, aCx are the coefficients; the term Symmetry is equal to 0 in this formula, aSx and aVx suggested to be equal. Let's name this formula by LDM1.

The formula LDM2 represents the formula LDM1 with shell crossing corrections, which are described in the next chapter. Table 60 shows parameters for all these models including a new fit of parameters using the LDM0 formula (LDM0 LISE++). Fig.511 shows differences between binding energies from experimental masses [Aud95] and different LDM parameterizations.

**Table 60.** Parameters of different LDM parameterizations and their  $\chi^2$  with experimentally deduced binding energies (2810 recommended values [Aud95] have been used).

Parameter/model	LDM0 [Kra87]	LDM0 LISE++	LDM1 [Mye66]	LDM2 LISE++
<b>aV</b>	15.5	15.32	15.677	15.6453
<b>aS</b>	16.8	16.297	18.56	19.002
<b>aC</b>	0.72	0.6877	0.717	0.7153
<b>aSym</b>	23	22.4243		
<b>delta</b>	34	10.122	11	4.39935
<b>power</b>	-0.75	-0.5	-0.5	-0.28764
<b>aVx</b>			1.79	1.7382
<b>aSx</b>			1.79	1.6266

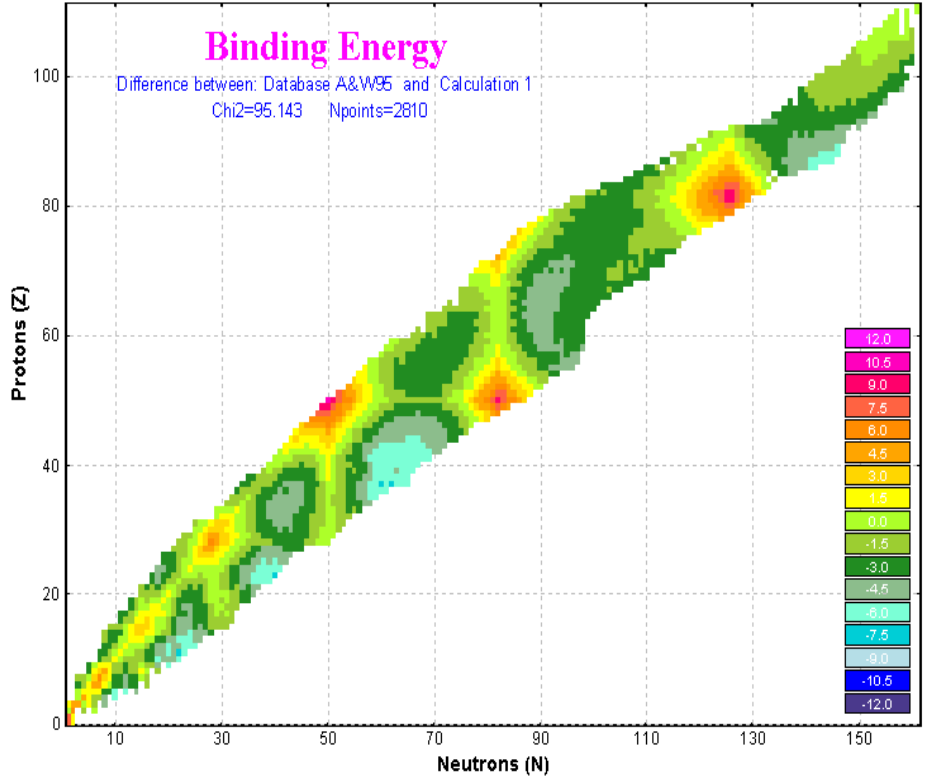
<b>aCx</b>			1.2111	1.6345
<b>(BE) <math>\chi^2</math></b>	<b>863.8</b>	<b>157.3</b>	<b>95.1</b>	<b>20.1</b>



*Fig.511. Differences between binding energies from experimental masses [Aud95] and different LDM parameterizations.*

### 7.5.1. Shell crossing corrections

It is clearly visible from Fig.512, that the largest difference between experimental binding energies and calculated LDM1 parameterization is observed on crossings of shells. Fig.511 shows (LDM0 LISE++ and LDM1 plots), that most of these deviations for shells 28, 50 and 82 have the form close to Lorentz distribution. It is necessary to note, that these triangular deviations influence fitting throughout the chart of nuclides. Attempts to smooth these “triangle” effects and then to make a new parameterization are undertaken with the use of “two-dimensional” Lorentz distribution. A finite area that is to be corrected is defined in the code. To avoid overshooting on the boundary of the area to be corrected the difference between the Lorentz functions at this point and the boundary point are taken. The section of code used to calculate the shell correction is shown below Fig.512. Table 61 contains parameters of shell corrections of the LDM2 model. It is possible to appreciate the contribution of shell crossings corrections comparing  $\chi^2$  of different models in Table 60.



**Fig.512.** Differences between binding energies of the inbuilt database and LDM1 parameterization.

```
//=====
double ShellCorrect(int Z, int N, int Zshell, int Nshell,
                    double Amp, double width,
                    double length, double coef)
{
double v = (fabs(N-Nshell)/coef + fabs(Z-Zshell))/width;
double vl = length/width;

return( v < vl ? Amp * (1/(v*v + 1) - 1/(vl*vl + 1)) : 0);
}
//=====
```

**Table 61.** Parameters of LDM2 shell crossings corrections.

Z	N	Amp	width	length	coef
82	126	11.85	8.15	23.090	0.878
50	82	12.84	8.21	21.382	0.878
28	50	6.24	9.30	16.294	0.878
20	28	2.13	6.89	12.165	0.878
82	82	17.99	9.38	20.960	0.942
50	50	12.26	8.91	21.841	0.942
28	28	7.33	6.65	16.804	0.942
20	20	5.40	2.02	3.332	0.942
16	16	5.14	2.71	6.909	0.942
14	14	4.88	2.39	11.253	0.942
8	8	20.75	3.43	2.500	0.942
6	6	18.57	3.04	2.500	0.942
2	2	17.08	2.41	2.500	0.942

### 7.5.2. Use of LDM parameterizations in LISE++

The parameterizations LDM0 (LISE++), LDM1 and LDM2 are used in the code and named correspondingly *Calculation 0*, *Calculation 1*, and *Calculation 2*. Mass calculations are used:

- To extrapolate mass of nuclei absent in the inbuilt database. These masses are kept in the operating memory and used for calculations every time the code needs an isotope mass. The extrapolated mass of a nucleus is equal to:

$$M_{A,Z} = LDM(A,Z) + \sum_{i=1}^3 (M_{A_i,Z_i} - LDM(A_i,Z_i)),$$

where the nuclei  $(A_i, Z_i)$  are the closest known nuclei, in the database, to the unknown nuclei of interest.

- To calculate widths of different channels of particle emissions in the Abrasion-Ablation or “Lis-Fus” models if option “*for separation energies use*” is set to “*semiempirical formula*” in the “Setting of Prefragment and Evaporation calculations” dialog.

In the “Production mechanism” dialog it is possible to choose one of LDM parameterizations in order to use it in calculations mentioned above. From the “Database” dialog it is possible to load the “Calculations” dialog (Fig.513), which with the user can see isotope characteristics calculated by various models. Using the “Database” dialog and LDM models plot options (Fig.514), the user can construct not only different model distributions, but also differences between distributions of various models (see for example Fig.512).

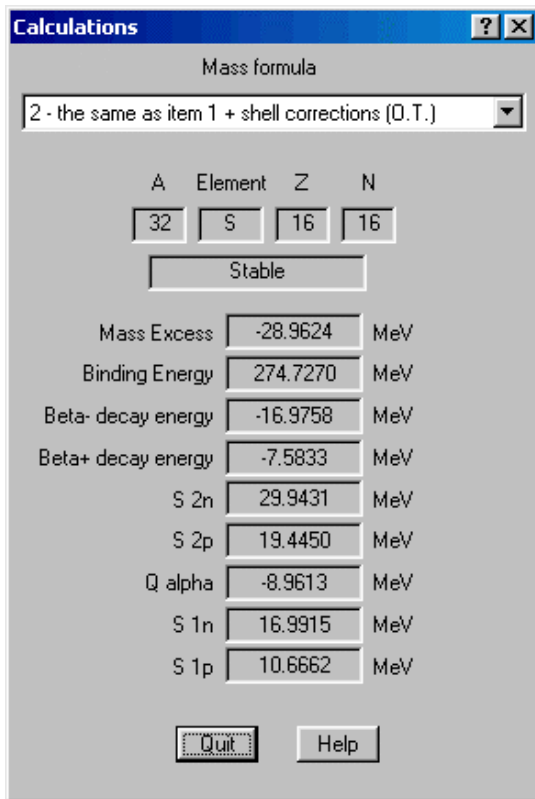


Fig.513. The mass calculations dialog.

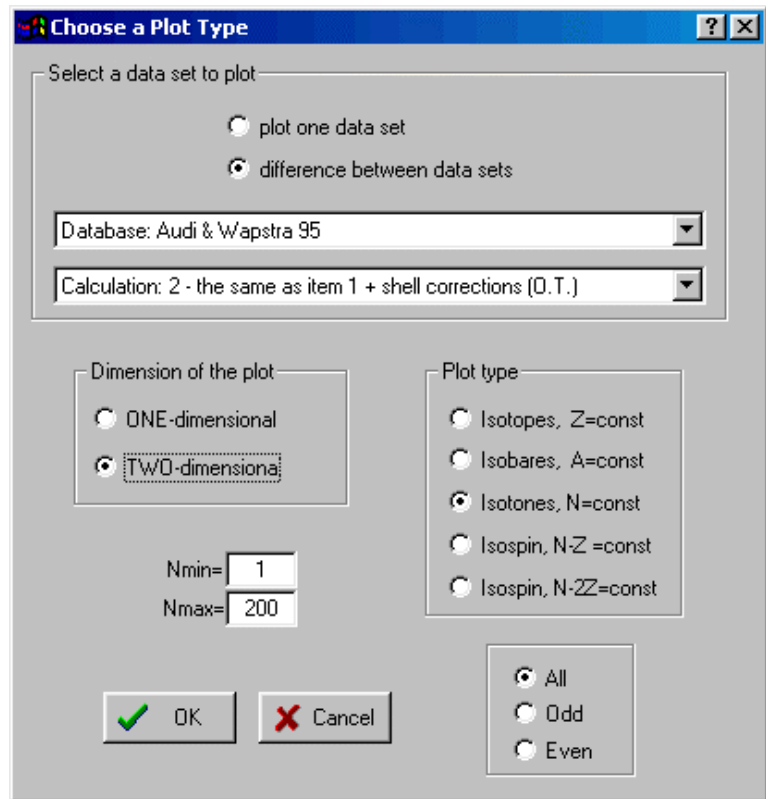
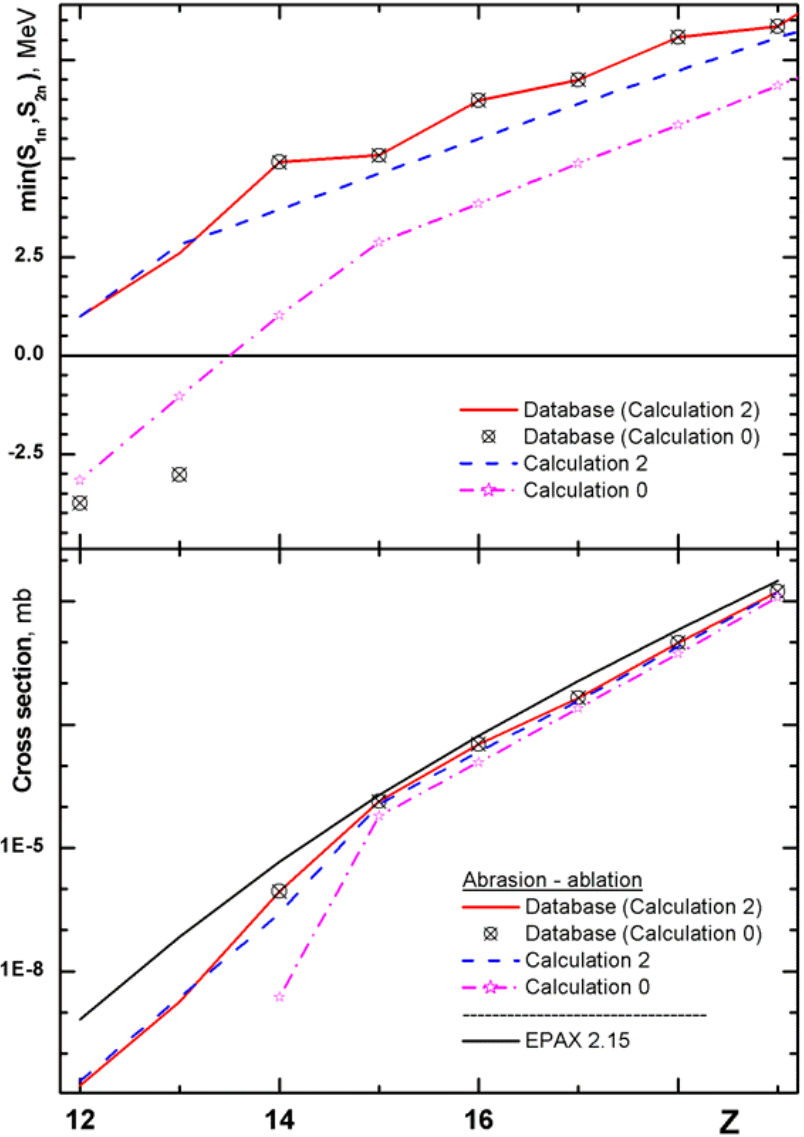


Fig.514. Database and LDM models plot options dialog

### 7.5.3. LDM parameterizations and accuracy of cross-section calculations

The dependences of minimum neutron separation energy ( $\min\{S_{1n}, S_{2n}\}$ ) and the production cross-sections of  $N=28$  isotones versus the charge number are plotted in Fig.515. Isotopes  $^{40}\text{Mg}$  and  $^{41}\text{Al}$  are unbound in calculations using *Calculation 0* and they are bound when using *Calculation 2*, as is visible from the figure.  $^{41}\text{Al}$  was observed in experiment [Not02], but  $^{40}\text{Mg}$  has not been observed, probably because of a small production cross section (see Fig.516). It is clear from the bottom plot of Fig.515 that the importance of accurate mass calculations becomes important close to the drip-line where the separation energy of a neutron or two neutrons close to zero. The plots indicate that it is possible to estimate the value of binding energy given experimental cross sections.

Experimental and calculated production cross-sections of  $N=28$  isotones are shown in Fig.516. A difference of almost two-orders magnitude is observed between the abrasion-ablation model and EPAX parameterization in the  $^{40}\text{Mg}$  production cross-section. It is necessary to note, that it corresponds to the minimal separation energy to 1 MeV (see Fig.515), calculated by the LDM2. If the binding energy is even less, the cross section will decrease.



**Fig.515.** Dependences of minimal neutron separation energy ( $\min\{S_{1n}, S_{2n}\}$ ) of  $N=28$  isotones versus the charge number are shown in the top figure. Abbreviation “database (calculation  $x$ )” means that database values have been used for known masses and the LDM $x$  parameterization was used to extrapolate unknown masses from the database.

Calculated production cross-section of  $N=28$  isotones in the reaction  $^{48}\text{Ca}+Ta$  are presented in the bottom plot. Parameters of the abrasion-ablation model used in calculations are shown in Table 62.

**Table 62.** Parameters of Abrasion-Ablation model were used in calculations in Fig.516.

Excitation energy method	2	Tunneling	auto
Distribution dimension (NP)	64	Option "unbound"	auto
$\langle E^* \rangle$ (MeV)	16.5 dA	Decay modes	All (8)
$\delta E$ (MeV)	9.6	State density	auto

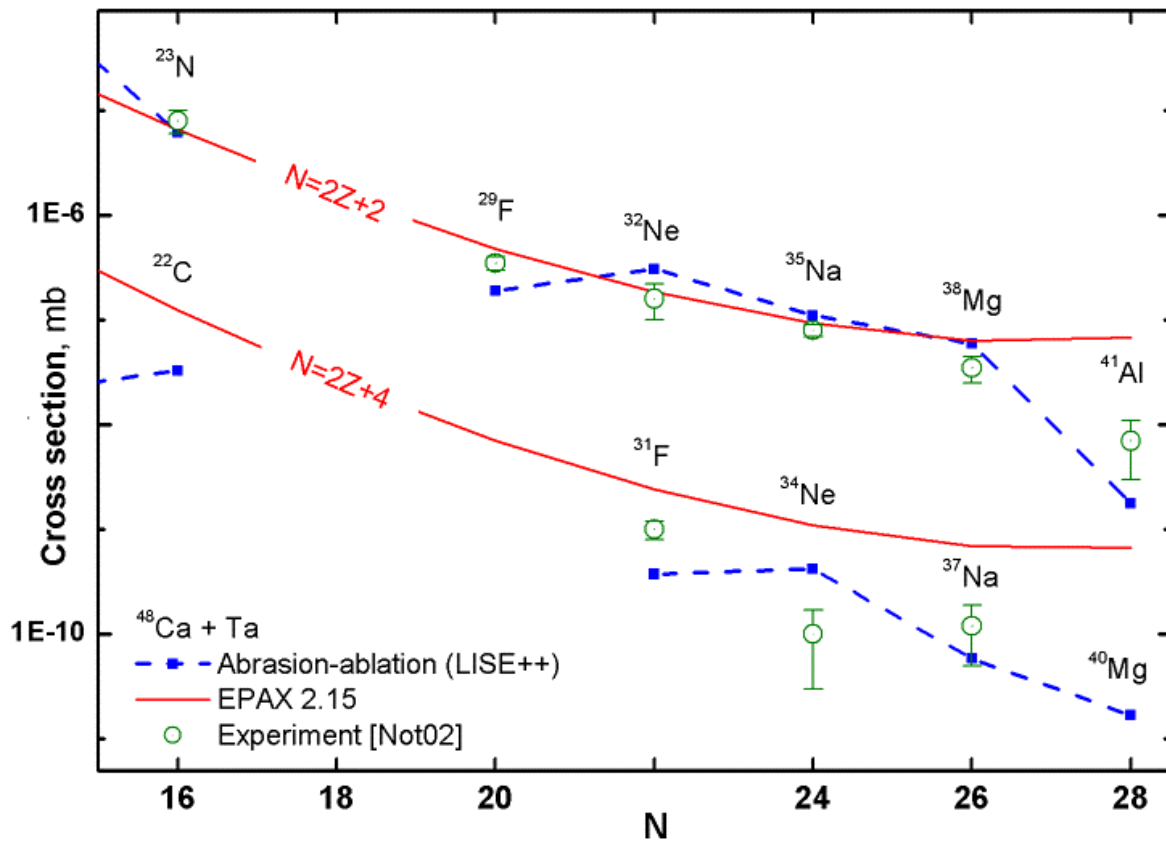


Fig.516. Experimental [Not02,Sak97], calculated by the LISE abrasion-ablation model (blue dash curve) and EPAX parameterization (red solid curve) production cross sections of neutron-rich isotopes in the reaction  $^{48}\text{Ca}+\text{Ta}$  versus neutron number. Binding energies from the database+LDM2 have been used for abrasion-ablation calculations.

More detailed description of improved mass parameterizations will be given in the upcoming paper [Sou02].

## 7.6. Updating and new utilities

### 7.6.1. Emittance of beam

In LISE++ the beam emittance frame has been moved to the beam dialog (Fig.517). This location is more logical. In LISE the frame was located in the spectrometer optical matrices dialog.

In the new version the user can set an angle between the beam and the spectrometer not only in a horizontal plane, but also in the vertical plane.

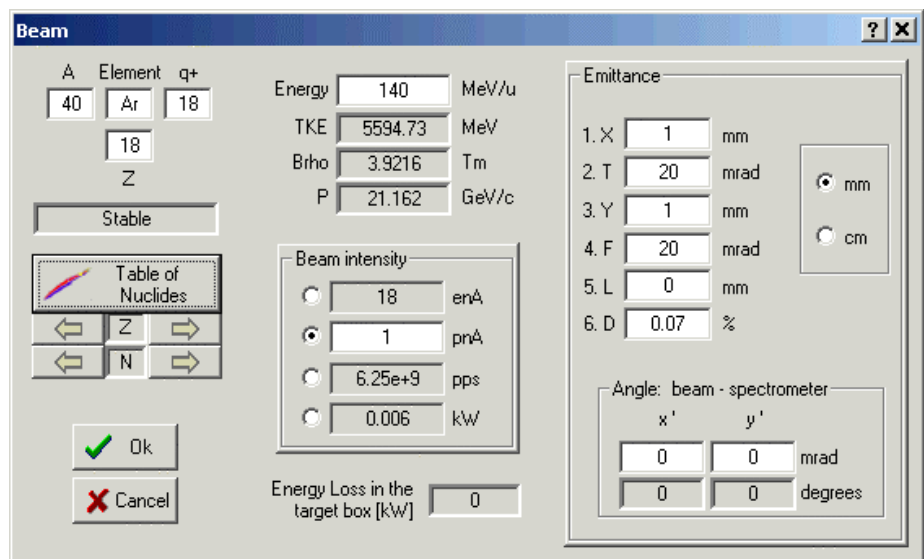
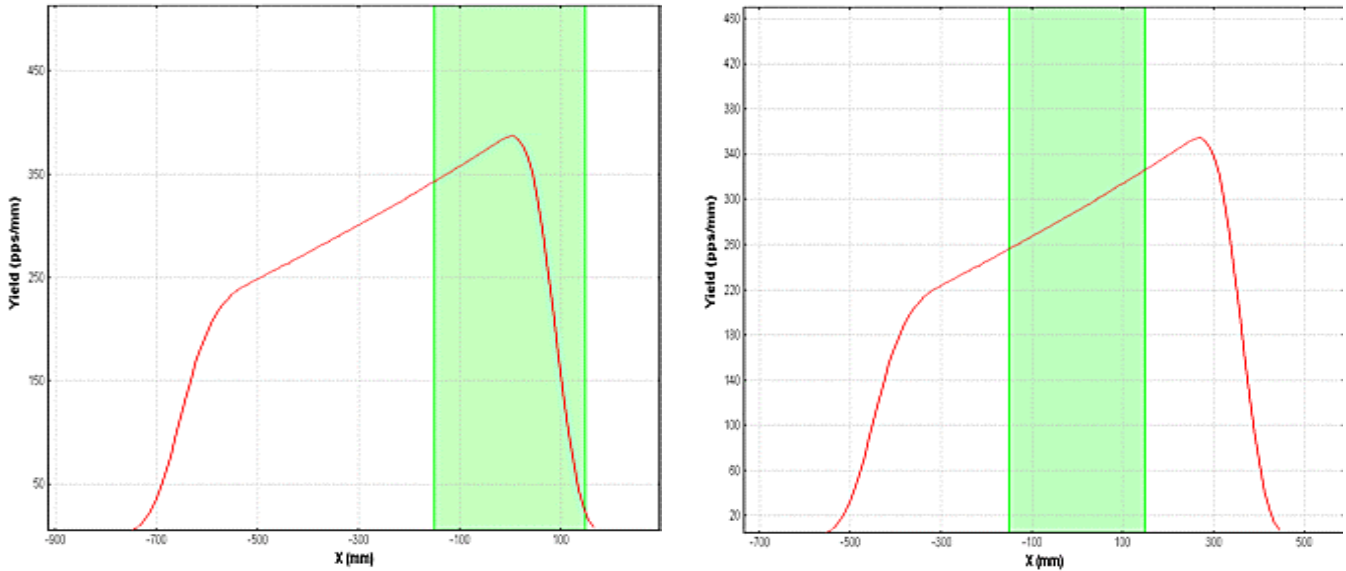


Fig.517. The "Beam" dialog.

### 7.6.2. Preferences

In LISE++ the dialog “Preferences” has got a number of new options some of them already were described above. There are just some words about the new option “Calculate spectrometer setting using maximal or mean value of the momentum distribution”. The rigidity can be calculated using one of conditions (see Fig.518):

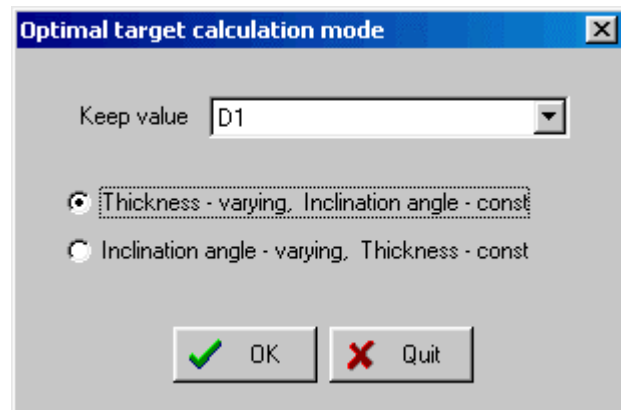
- The maximum of momentum distribution corresponds to the central line of the spectrometer (left plot),
- The average of momentum distribution is in the central line (right plot). This is the new feature of the code. The program LISE assumed only the first case for calculations.



**Fig.518.** Momentum distribution of a setting fragment in the dispersive focal plane. The block momentum acceptance is shown by green color. The spectrometer is set on the maximal value of momentum distribution in the left figure and on the mean value correspondingly in the right plot.

### 7.6.3. Optimum target

In LISE++ the different modes of target thickness and angle inclination calculations were joined to one dialog (see Fig.519). The user can keep constant a value of any dispersive blocks to calculate a target thickness corresponding to the block value.

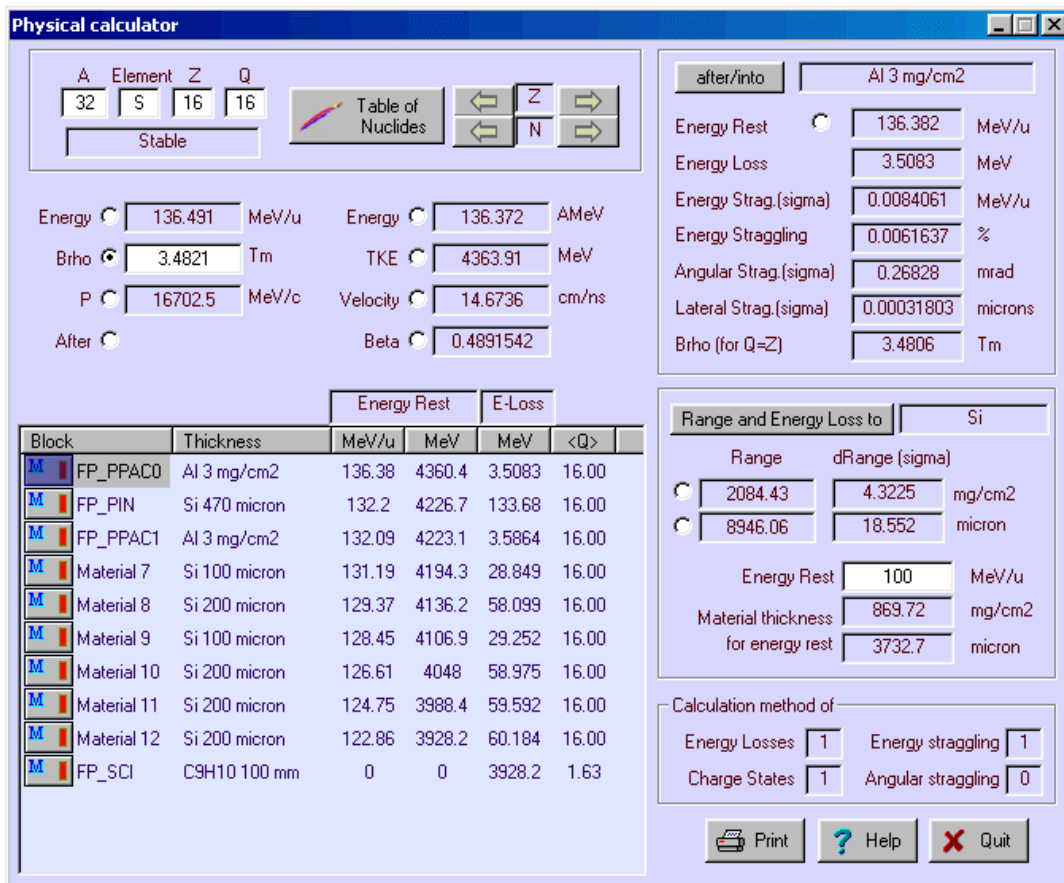


**Fig.519.** The “Optimal target calculation mode” dialog.

### 7.6.4. Dialogs Goodies & Physical calculator

In the dialog “Goodies” the code calculates *standard deviations* of times of flight and energy loss in materials. Momentum acceptance and detector (timing, energy) resolutions are taken into account.





**Fig.520. Physical calculator.**

The Physical calculator of LISE++ can calculate energy loss throughout unlimited number of detectors (see Fig.520). The number of detectors in LISE was limited to seven. It is possible to edit materials without leaving the physical calculator dialog by clicking on an icon of a detector in the window of materials.

☞ *The window of material blocks contains only materials located after the last optical block.*

Lateral straggling through materials is included in the physical calculator, which is calculated on the basis of angular straggling and the detector length. The lateral straggling of fragments through a material is taken into account in fragment transmission calculations. The biggest effect of lateral straggling can be seen in for gas detectors.

### 7.6.5. Matrix calculator

☐ The matrix calculator is new in LISE++. Using this new utility (Fig.521) it is possible to do the following matrix computing operations with matrices:

#### *One matrix operation*

- Inverse
- Transpose
- Transform to Up triangular
- Transform to Down triangular
- Product by constant value
- Determinant calculation

#### *Two matrix operations*

- Product of two matrices
- Sum of two matrices

The calculator supports only square matrixes by dimensions from 2 up to 6. To do an operations with two matrixes, the second matrix should be stored in memory (M). The matrixes can be read / saved from / in a matrix file. The format of the matrix file was given in the chapter 7.3.1.1.1.

☞ *The calculator does not support optical matrix dimensions (mm/cm).*

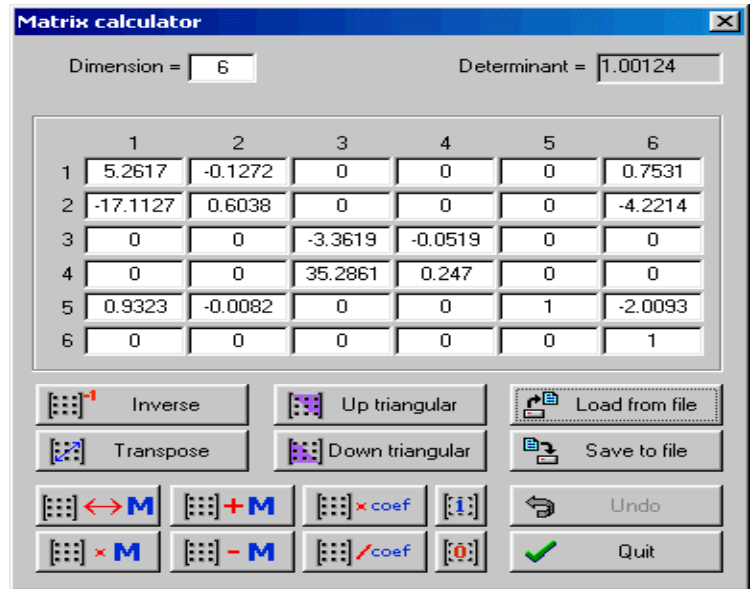


Fig.521. Matrix calculator

### 7.6.6. Range optimizer – Gas cell utility

The ability to calculate the thickness (or inclination angle) of a degrader used to slow beam particles to alter their stopping distance into a gas cell is developed in LISE++. Let us suppose, that a beam of ions after a dipole through a monochromatic wedge, to make a monoenergetic beam. An adjustable degrader is located behind the monochromatic wedge (Fig.522). The thickness of the adjustable degrader can be changed to achieve a maximal ratio of particles stopped in the gas cell to the sum of particles stopped before the gas cell and those that pass through it completely. The thickness of the adjustable degrader is varied by changing the angle of the degrader. The utility can calculate an optimum inclination angle or thickness of a degrader, keeping the other fixed (see Fig.523).

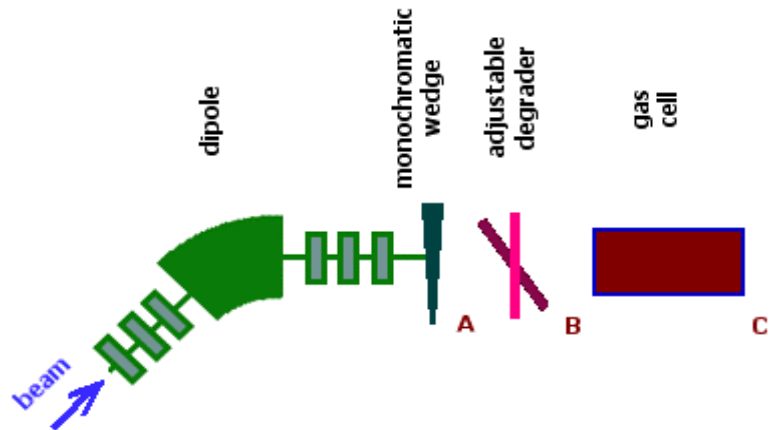


Fig.522. Range optimizer block scheme.

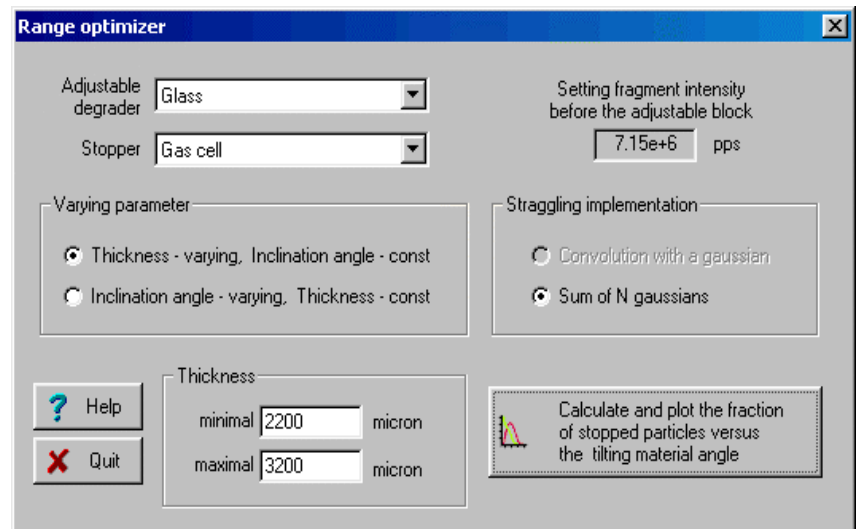
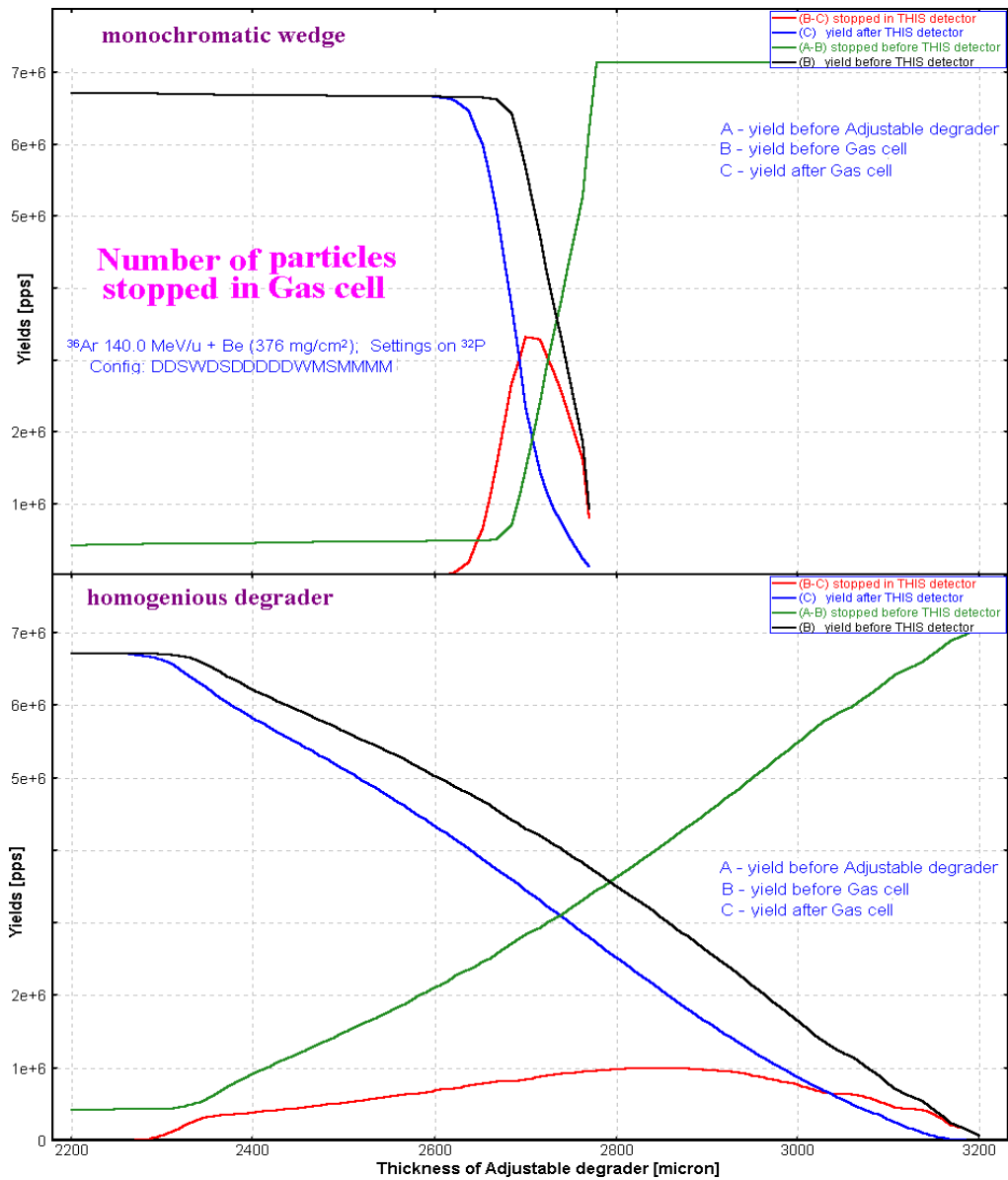


Fig.523. The “Range optimizer” dialog.

The user has to choose, in the range optimizer dialog, the adjustable degrader material, the stopper material and the minimum and maximum thicknesses of the adjustable degrader. The code automatically suggests the minimum and maximum thicknesses of the adjustable degrader equal to zero and the range of the particle in the adjustable degrader respectively. The number of points used to calculate the optimal thickness (inclination angle) is equal to the number of points for the optimal thickness target calculation utility defined in the Preferences dialog.

The number of particles stopped in the gas cell versus the thickness of the adjustable degrader for two different wedges before the adjustable degrader are shown in Fig.524. It is visible from the figure that it is possible to set the adjustable degrader, using the monochromatic wedge, to stop 3.5 times more particles in the gas cell if a homogeneous degrader is used.



**Fig.524.** Number of particles stopped in the gas cell versus the thickness of adjustable degrader for two different wedges before the adjustable degrader (see the scheme in Fig.522). The case of the monochromatic wedge is shown in top plot, the homogeneous degrader is given in the bottom plot.

### 7.6.7. LISE for Excel

The new version of LISE.xls allows you to make a fast identification of isotopes and a calibration of experimental registered parameters during an experiment. For calibration and identification LISE.xls uses the configuration:

Dipole  $\Rightarrow$  Wedge  $\Rightarrow$  Dipole  $\Rightarrow$  dE-detector  $\Rightarrow$  TKE-detector

Initially, it is necessary to input parameters of a set-up (lengths of dispersive blocks, dE-detector properties, etc) and perform calibrations of time-of-flight and energy loss in the dE and TKE detectors.

You can use the new utility in two directions:

- Input parameters A, Z, Q1 and Q2 of the isotope of interest and input the Brho values to get energy loss and time-of-flight data in channels (upper picture in Fig.525);
- Input experimental data in channels to get physical values (energy loss and time-of-flight) and identification of the ion (lower picture in Fig.525).

You can only edit cells with a light grey background (see Fig.525). Other cells are write protected.

Brho1= 3.5000	
Brho2= 3.5000	
32S 16+16+	
A	32
Z	16
Q1	16
Q2	16

		section		
		first	second	final
Energy	MeV/A	137.58	137.58	137.58
beta		0.491	0.491	0.491
gamma		1.148	1.148	1.148
TOF	ns	118.86	122.31	241.18
TKE	MeV	4402.6	4402.6	4402.6
az	(for bz=0)			7.6476

A,Z,Q -> channels

		acquisition				plot			
		phys.value	channel	min	max	range	dim	range	channel
RF1.1	241.18 ns	970.0	0	4095	4095	10	1024	242.5	
RF1.2	241.18 ns	2717.6	0	4095	4095	10	1024	679.6	
RF2.1	241.18 ns	907.6	0	4095	4095	10	1024	227.0	
RF2.2	241.18 ns	2623.4	0	4095	4095	10	1024	656.0	
pin.E	132.66 MeV	726.0	0	4095	4095	10	1024	181.5	
sci.DE	4161.5 MeV	1314.9	0	16383	16383	10	1024	82.2	

Brho1= 3.5
Brho2= 3.5

channels -> A,Z,Q

		plot			acquisition										
		channel	dim	range	min	max	range	channel	phys.value	beta	AoQ	Z	AoQ * Z	Q	AoQ * Q
RF1.1	242.5	10	1024	0	4095	4095	969.8	241.18 ns	0.4907	2.000	16.00	32.00	15.61	31.22	
RF1.2	679.6	10	1024	0	4095	4095	2717.7	241.17 ns	0.4907	2.000	16.00	32.00	15.61	31.22	
RF2.1	227	10	1024	0	4095	4095	907.8	241.17 ns	0.4907	2.000	16.00	32.00	15.61	31.22	
RF2.2	656	10	1024	0	4095	4095	2623.4	241.18 ns	0.4907	2.000	16.00	32.00	15.61	31.22	
pin.E	181.5	10	1024	0	4095	4095	725.8	132.63 MeV							
sci.DE	82.2	10	1024	0	16383	16383	1315.1	4162.26 MeV							

TKE = 4294.89 MeV

Fig.525. New identification tables of LISE.xls.

New transformation functions (Energy  $\Leftrightarrow$  Momentum, Brho  $\Leftrightarrow$  Momentum) and some new statistic functions (integration, etc) have been incorporated in the LISE.xls package. One improvement is that LISE.xls can handle unphysical inputs (i.e. a negative value for a material thickness).

## 6.7. Cyrillic and Hex-style converter

The new utility “Cyrillic converter” (Fig.526) has been developed to convert one Cyrillic character set to another. The Converter was made using the free distributed converter source (for MS-DOS) by Serge Bajin (bsv@cntc.dubna.su). The text converter supports formats: KOI8, Alternative 866, Windows-1251, ISO 8859-5 and can be loaded from the Units converter. This utility has been made in free time from work :)

This converter can be useful for people who are not burdened by problems of Cyrillic character set conversion because the utility also allows converting Hex-style text (=EF=F0) and HTML symbols (and....;) to normal text.

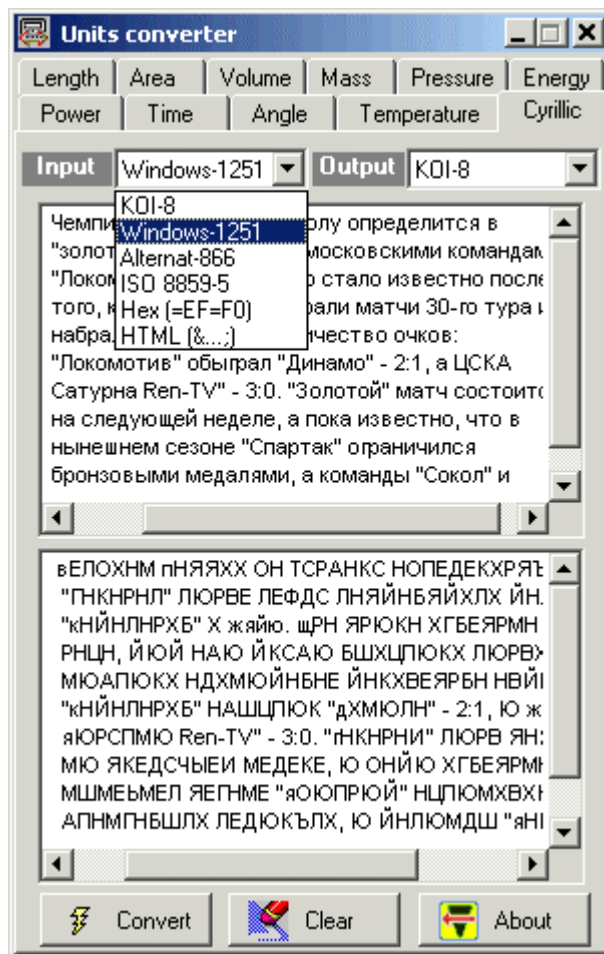


Fig.526. Cyrillic and Hex-style converter.

## 7.7. Plots

The program can plot angular, spatial, energy and momentum distributions before and after every block, as well as inside a dispersive block. It permits to the user to look at how the dynamics of distributions change from block to block. Two-dimensional plots allow the user to see correlations between parameters (dE, TKE, TOF, X, Y) in detectors with the resolution of detectors taking into account.

### 7.7.1. Transmission plots




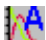
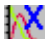



One-dimensional selection plots can be found through the menu “Plots” or the LISE++ toolbar. Table 63 shows different types of selection plots. Momentum and Vertical special selection plots are available **only** from the menu “Plots”. By clicking the icon of any of the plots (except for the Brho and Wedge selection plots) in the toolbar you get the menu of available blocks for which can be constructed the plot. The Brho and Wedge selection plots are drawn immediately, without this menu, for blocks, which were set in the dialog “Plot options” (Fig.527). If the plot selection window has more than one plot then you can use the button  inside the plot in which you want to zoom. A window with one selected plot will be created. It is possible to load the dialog “Plot options” using the button  in the toolbar or through the menu “Plot->Plot Options”.

Table 63. Selection plots.

Plot name	Number of distribution plots in window	note
 Block selection	<ol style="list-style-type: none"> <li>x' angular (I)</li> <li>y' angular (I)</li> <li>x spatial (OU)</li> <li>y spatial (OU)</li> <li>Momentum (OC)</li> <li>Energy (OC)</li> </ol>	Designations in the plot: I - input O - output U - uncut C - cut
 Angular	<ol style="list-style-type: none"> <li>x' angular (I)</li> <li>y' angular (I)</li> <li>x' angular (O)</li> <li>y' angular (O)</li> </ol>	
 Spatial (horizontal)	<ol style="list-style-type: none"> <li>x spatial (I)</li> <li>x spatial (OU)</li> <li>x spatial (OC)</li> </ol>	<i>X spatial (OU) is not shown for materials and for dispersive blocks without slits.</i>
 Energy	<ol style="list-style-type: none"> <li>Energy (I)</li> <li>Energy(OC)</li> </ol>	
 Brho selection	Momentum (OU) [Tm]	<i>You have to select a block for the plot in the "Plot options" dialog (Fig.527).</i>
 Wedge selection	X or Y spatial (OU) [mm]	

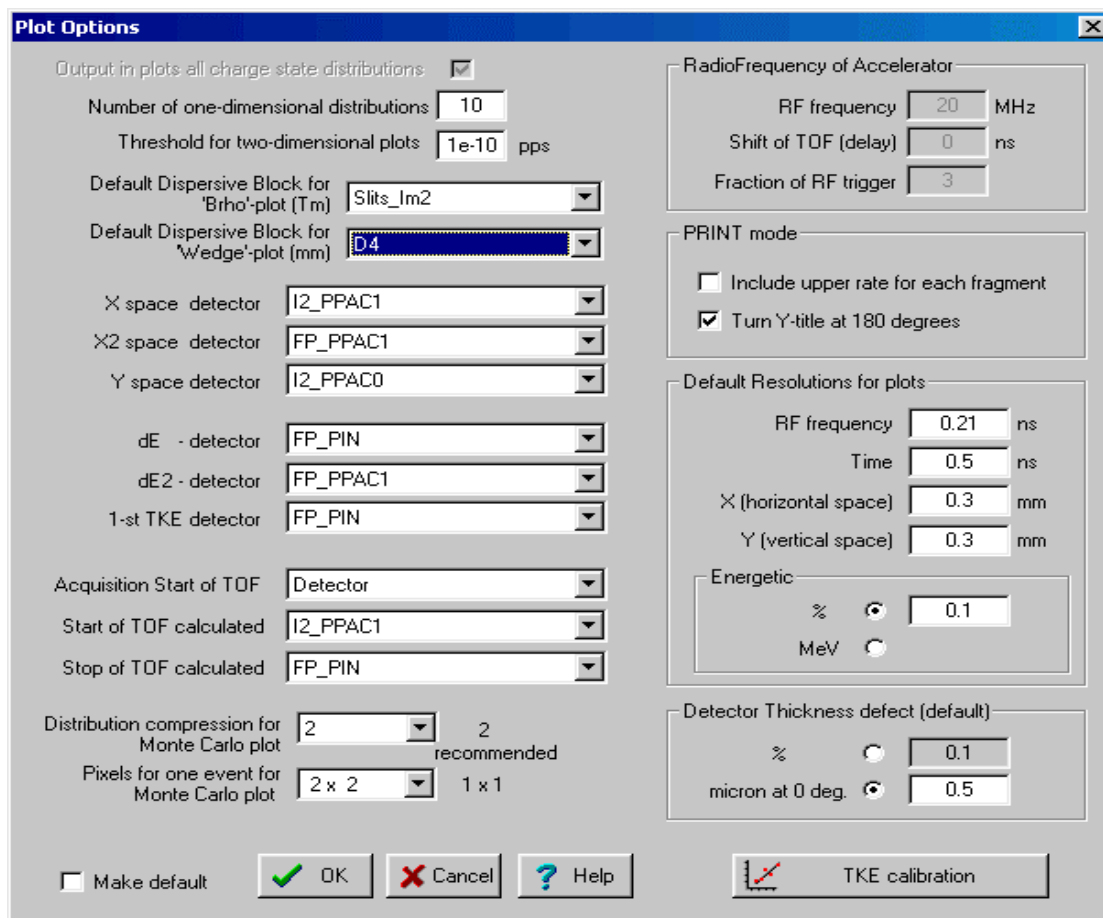


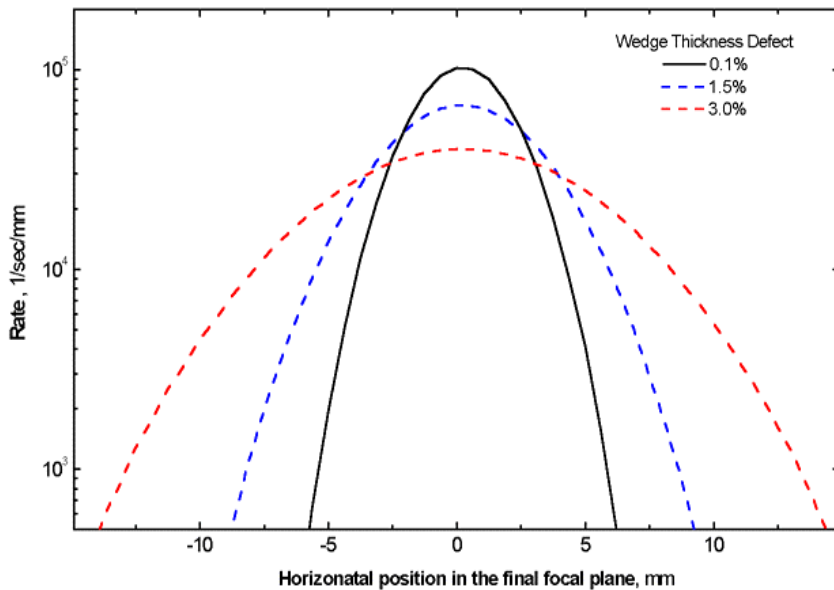
Fig.527. The "Plot options" dialog.

### 7.7.2. Two-dimensional plots

The use of experimental data from different detectors to build a two-dimensional plot is a large advantage of LISE++. For example, you can build a two-dimensional plot using the X-coordinate from a PPAC located in Image2 and an energy loss value from a PIN-detector located after the last optical block. First you have to set in the "Plot options" dialog (Fig.527) "PPAC in Image2" as the X-detector and "PIN-detector" as the dE-detector. Then you click on plot "dE-X" from the menu "Plots" to create the plot. Material (detector) blocks only can be used to make two-dimensional plots.

The code uses a trigger for data acquisition taken from a detector. For "ellipse" mode drawing of two-dimensional plots, the first detector found in the beam line is used. For Monte Carlo simulations the last detector is used to start an acquisition.

Energy, time, and spatial resolutions of a detector are used when calculating standard deviations of measured values in two-dimensional plots. The defect (percent error) of a material thickness is used in two-dimensional plots as well as in fragment transmission calculations. You can see the increase in a peak width with a larger detector resolution or larger material thickness defect.



Be careful when you input the defect of a wedge thickness located in the dispersive plane. The effect on your fragment distribution can be large (see Fig.528).

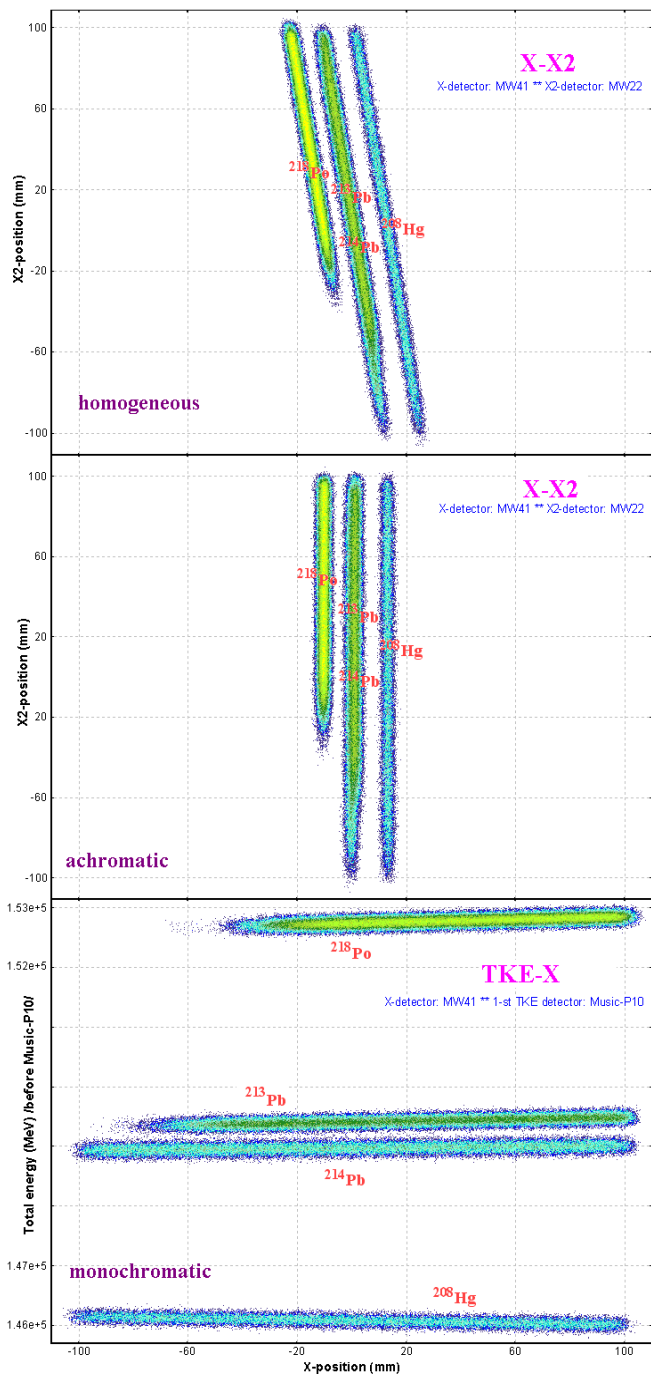
**Fig.528.** "Wedge selection" distributions in the focal plane of A1900 spectrometer for different wedge thickness defects (0.1%, 1.5%, and 3.0%). Calculations were done with the reaction  $^{40}\text{Ar}(140\text{ MeV/u}) + \text{Be}(500\text{ mg/cm}^2)$  for setting fragment  $^{32}\text{S}$  with an achromatic wedge (Be 300 mg/cm<sup>2</sup>) located in Image 2.

### 7.7.3. Debug distributions

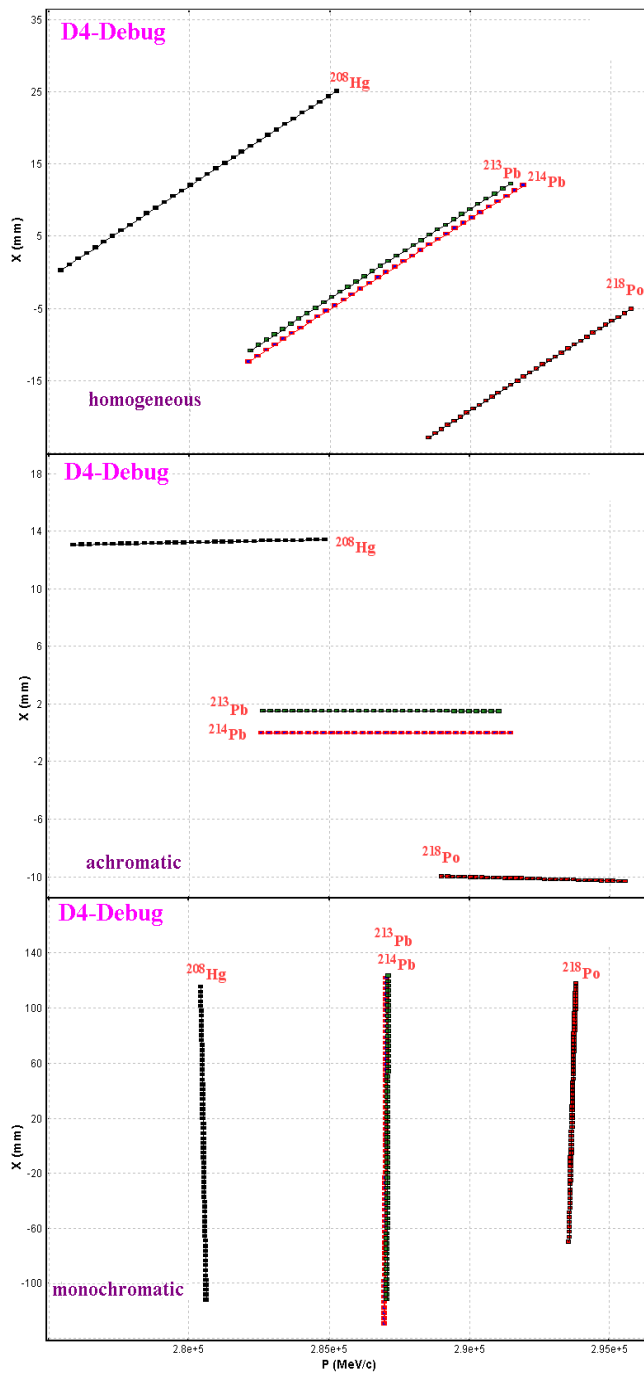
Debug distributions serve to check transmission calculations and transformations of distributions and represents an ideal transformation of the momentum to a coordinate. The given distribution ( $P \Rightarrow x$ ) is used in convolutions with spatial ( $x$ ) and angular ( $\theta \Rightarrow x$ ) components to get an output spatial distribution after a block. Using debug distributions it is easy to see the dependence of distributions on wedge shape. Debug distributions also can be used for calculation of achromatic or monochromatic wedges (see the lower right plot in Fig.503).

Fig.529 shows two-dimensional spectra for the reaction  $^{238}\text{U}(1\text{ GeV/u}) + \text{Be}(3.5\text{ g/cm}^2) \Rightarrow ^{214}\text{Pb}$  with a Al 1 g/cm<sup>2</sup> wedge found between the 2nd and 3rd dipoles of the fragment separator FRS. The spectra are calculated for different wedge shapes. Fig.530 shows debug distributions after the 4<sup>th</sup> dipole for the same reaction as in Fig.529. Only calculations for isotopes  $^{208}\text{Hg}$ ,  $^{213,214}\text{Pb}$ ,  $^{218}\text{Po}$  are shown in the plots for illustration purposes. This example is available through the LISE web-site: [http://groups.nslc.msu.edu/lise/6\\_1/examples/214pb.lpp](http://groups.nslc.msu.edu/lise/6_1/examples/214pb.lpp)

The debug information window (the menu “Plot⇒Debug information”) as well as debug distribution plots are only used for the developers of the program to control calculations of standard deviations of the main characteristics of debug distributions.



**Fig.529.** Monte Carlo method simulations for different shapes of wedge located between the second and third dipoles of the fragment-separator FRS (GSI). The position detector MW22 is found in the dispersive focal plane between the 2nd and 3rd dipoles, the detectors MW41 and Music-P10 are located after the 4<sup>th</sup> dipole. See details in text.



**Fig.530.** Debug distributions ( $X \leftrightarrow P$ ) after the fourth dipole of the fragment-separator FRS (GSI) for different shapes of wedge located between the second and third dipoles. The wedge shapes are labeled on the plots. See details in text.



## 7.8. Future developments of LISE++

- Develop new dispersive blocks: **gas-filled, electrostatic separators, compensating dipole** after the Wien velocity filter.
- Create LISE++ configuration files for spectrometers in GANIL, Dubna, RIKEN, Texas A&M, etc. The authors hope to have help from experts of these laboratories for specific information (transport files, location and characteristics of detectors, emittance of primary beam, etc.).
- Add a subroutine of fusion cross-section calculations below the Coulomb barrier in the PACE4 code and the LisFus model of LISE++.
- Incorporate a new reaction mechanism: **Fission** (*principal task* for 2003 FY)
- Develop a new material block: **secondary target**
- Continue work under “Universal parameterization of momentum distribution of projectile fragmentation products”.
- Write a guide, “First steps” for beginners.
- Write full LISE++ documentation.
- Develop the “Beam analyzer” dialog to plot beam trajectories in dipoles.

## Acknowledgements

LISE++ authors gratefully acknowledge Dr.Helmut Weik’s fruitful remarks, suggestions, and help with the development of LISE++. Special thanks to Helmut for continually checking the code.

LISE++ authors thank Heather Olliver for carefully proof reading this manual.

Fruitful discussions with Prof.Betty Tsang on the improved mass formula (chapter 7.5.) and with Dr.Leo Weissman on the gas cell range optimizer (chapter 7.6.6.) are gratefully acknowledged.

The authors are grateful to the entire National Superconducting Cyclotron Laboratory for fruitful remarks, comments and checking of preliminary versions of LISE++.

# THE CODE LISE

Last version 5.15  
March 08, 2002

O.Tarasov<sup>1,2</sup>, D.Bazin<sup>1</sup>, M.Lewitowicz<sup>3</sup>, O.Sorlin<sup>4</sup>

<sup>1</sup> NSCL-Cyclotron Laboratory, Michigan State University, East Lansing, MI 48824-1321, USA

<sup>2</sup> Flerov Laboratory of Nuclear Reactions, JINR, 141980 Dubna, Moscow region, Russia

<sup>3</sup> Grand Accélérateur National d'Ions Lourds, BP 5027, 14076 Caen Cedex 5, France

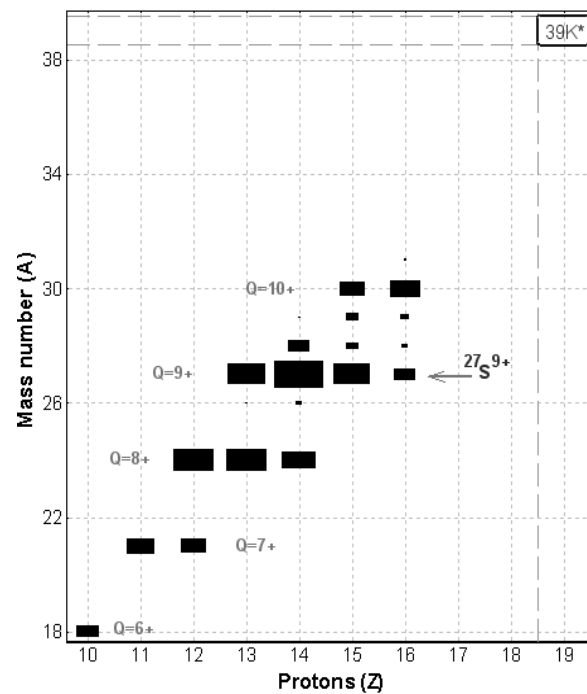
<sup>4</sup> Institut de Physique Nucléaire, CNRS-IN2P3, 91406 Orsay, France



## 8. Fusion - version 5.15

East Lansing  
08-MAR-2002

### Fusion residue transmission



Plot of transmitted residues calculated by the LISE program for the reaction  $^{12}\text{C}(37\text{ MeV/u}) + \text{Al}(4\text{ mg/cm}^2)$ . Calculations were performed for the LISE spectrometer with the Wien velocity filter ( $E=2000\text{ kV/m}$ ) set on the ion  $^{27}\text{S}^{9+}$ .

## 8.1. How to calculate fusion residue transmission (step by step)

A new fusion-evaporation model “LisFus” for the fast calculations of fusion residue cross sections has been developed. This model is based on the Bass fusion cross-section algorithm [Bas74], the evaporation cascade code of Gaimard and Schmidt’s Abrasion-Ablation model [Gai91], and the transport integral theory [Baz94]. The user has also the possibility to use fusion residue cross sections calculated by the program PACE, which has been incorporated in the LISE package. The code PACE [Gav80] (**P**rojection **A**ngular-momentum **C**oupled **E**vaporation) is a modified version of JULIAN - the Hillman-Eyal evaporation code using a Monte-Carlo method coupling angular momentum. The program LISE has now the possibility to calculate the transmission of fusion residues through a fragment separator. The transmission calculations have to be performed following the steps described below:

1. Choosing reaction type
2. Beam, Target, Residue settings
3. Options
4. Residue excitation function
5. Setting of residue ion charge
6. Target thickness
7. Separation

### 8.1.1. Choosing Reaction type

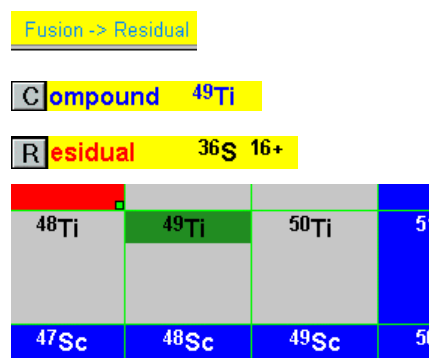
Choose the “Fusion → Residue” option in the “Production mechanism” dialog (menu “Options”). There are no other settings for the “Fusion → Residue” reaction in this. At this point the SETUP window will show:

A message “Fusion → Residue”

A new “C”ompound button

A “R”esidual button instead of “S”etting Fragment

The Compound cell in the table of nuclides is marked in green



### 8.1.2. Beam, Target, Residue settings

Input of next values:

<i>Beam</i>	A, Z, Q	<i>Example</i>
	Energy	$^{40}\text{Ar}^{18+}$
	Intensity	15 MeV/u
<i>Target</i>	A, Z (! No composite target!!!)	1000 enA
	Thickness should be close to 0	$^9\text{Be}$
<i>Residue</i>	A, Z	50 micron
		$^{42}\text{Ca}$

The user can input an expected thickness target value if he or she is sure that this thickness will be satisfactory for this beam-target-residue combination, but it is recommended to calculate a thickness value by following the next steps.

### 8.1.3. Options

#### 8.1.3.1. The “Preferences” dialog

For fusion residue reactions it is strongly recommended to **SET** the “Charge State” option **ON!** To decrease the calculation time (fusion calculations take more time than fragmentation) it is recommended to use the following values:

Calculation WITH charge states  $\leq 64$   
 Number points for 'Optimal target' plot  $\approx 32$

#### 8.1.3.2. The “Prefragment search and Evaporation options” dialog

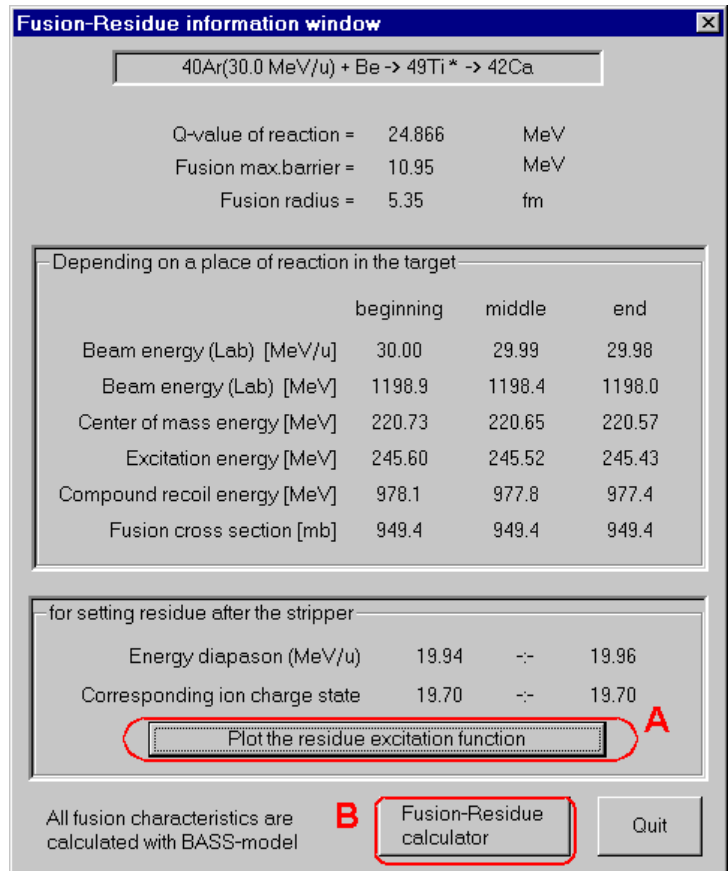
The “Prefragment search” part of this dialog will be blocked when the reaction “Fusion→residue” has been chosen. For fast calculations it is recommended to use

Only three basic mode of decay           proton, neutron, alpha  
 Dimension of evaporation distribution    32  
 Modes Auto/Manual                        auto

### 8.1.4. Residue excitation function

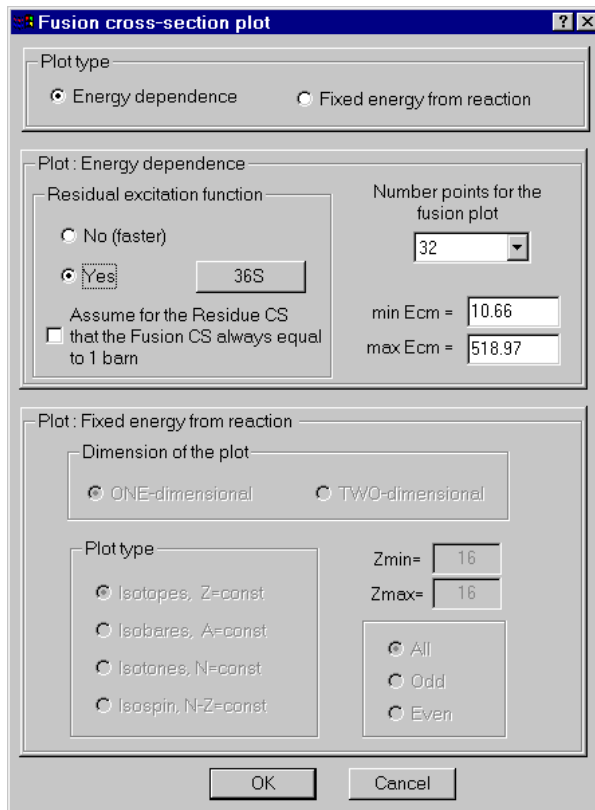
The next task is to determinate the excitation energy value of the compound nucleus corresponding to the maximum of the residue production cross section. To do this the user can load the subroutine to plot the excitation function one of two possible ways: from the “Fusion-residue information window” dialog (see Fig.531, item A), or from the “Plots → Cross section distributions” menu. If the reaction mode “Fusion → Residue” is selected, the “Cross sections” dialog (menu “Options”), and the “Cross section Plot” dialog (menu “Plots”, see Fig.532) will correspond to the fusion-residue reaction.

As an example the excitation function of the  $^{42}\text{Ca}$  residue from the  $^{49}\text{Ti}$  compound is shown in Fig.533 (it takes only 20 seconds on average to perform these calculations!!!).

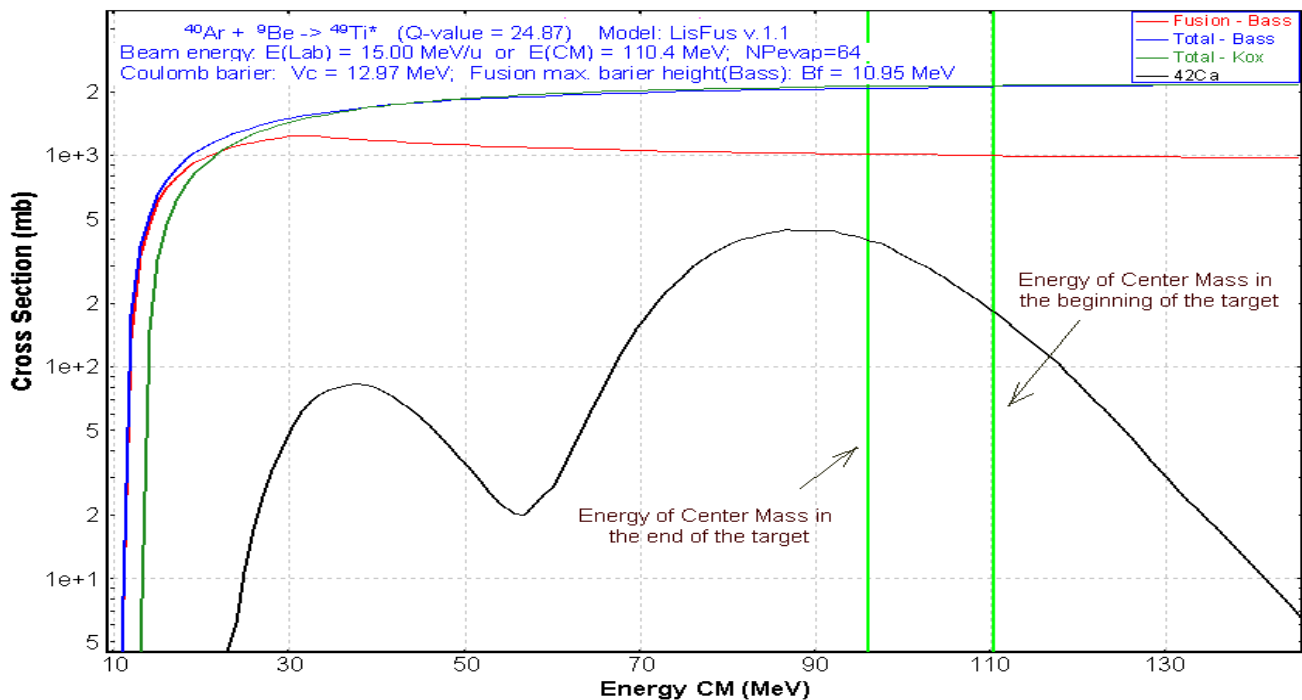


**Fig.531.** The Fusion-Residue information window. It is activated by clicking the “C” compound button in the SETUP window (see chapter 8.1.1.).

**Fig.532.** The “Fusion cross section plot” dialog. To obtain the excitation function of a residue the user has to choose the options “Energy dependence” and “Calculate a residue excitation function – YES”. The recommended number of points for the fusion plot is 32.



**Note:** It is possible to skip this step if the “Cross sections from file” option in the “Preferences” dialog is set, and set the input cross section value for the chosen residue independent from energy in the “Cross sections” dialog (menu “Options”). The program will automatically try to calculate “LisFus” fusion-residue cross sections and show them in the “Cross sections” dialog, but the user can break out of the calculation by clicking Cancel in the “Choose a range to calculate” dialog and input his or her own cross section value.




**Fig.533.** The excitation function of  $^{42}\text{Ca}$  residues from the  $^{49}\text{Ti}$  compound is shown (black curve). Fusion, Total (Bass), and Total (Kox) cross section distributions for the reaction  $^{40}\text{Ar} + ^9\text{Be}$  are shown respectively in red, blue and green colors. The vertical green lines indicate the energy in center of mass at the beginning and the end of the target respectively. The two-peak shape of the  $^{42}\text{Ca}$  excitation function can be explained by the domination of the  $\alpha$ -channel from intermediate nucleus  $^{46}\text{Ti}$  at an energy of 40 MeV (in CM), whereas at an energy of 100 MeV the final residue is created by p- & n-channels (see “Evaporation calculator” for details). This phenomenon has been seen also by Michael Thoennessen using the programs EVAP (UNIX-version of the PACE code) and CASCADE.

### 8.1.5. Setting of residue ion charge

In the case of fusion reactions attention should be paid to the ionic charge of the residue, as fusion reactions take place at lower energies than fragmentation. The present step is to estimate the ionic charge after the target based on the excitation function obtained during the previous step. For this purpose a Fusion-Residue calculator has been developed (see Fig.534). In our example the maximum cross section for  $^{42}\text{Ca}$  production from Fig.533 corresponds to 90 MeV (CM). The ion charge of the residue obtained at this energy is equal to 19.04 using the Fusion-Residue calculator. The initial beam energy in our example is higher and it is assumed that the energy lost in the target slows the beam down to the optimum energy of 12.23 MeV/u. To increase the yield of a residue the target thickness can be increased, which will lower the charge state even further. Thus it is better to round off the ionic charge to the smallest integer.

The calculated ion charge of the residue (i.e.  $^{42}\text{Ca}^{19+}$ ) has to be entered in the Residue setting dialog (“R”esidual button in the “SETUP” window, see chapter 8.1.1.).

### 8.1.6. Target thickness

The subroutine “Optimal target plot” (menu “Calculations”) is used to get the maximum rate of the chosen residue. The target thickness calculations for the residue  $^{42}\text{Ca}^{19+}$  are shown in Fig.535. The user can click the  button to put the calculated values into the program settings.

This step is the most time consuming. A benchmark table (Table 64) for various configurations is given below. A Pentium III (600 MHz, 128MB RAM) computer has been used for the calculations.

Table 64.

Dimension of evaporation distributions	N. points for optimal plot	Dimension of transmission distributions	Evaporation channels	Setting residue	Time, sec	coef
32	32	64	3	$^{42}\text{Ca}^{19+}$	46	1
32	64	64	3	$^{42}\text{Ca}^{19+}$	80	1.74
64	32	64	3	$^{42}\text{Ca}^{19+}$	89	1.93
32	32	64	8	$^{42}\text{Ca}^{19+}$	70	1.52
32	32	128	3	$^{42}\text{Ca}^{19+}$	65	1.41
32	32	64	3	$^{35}\text{Ar}^{17+}$	72	1.57
64	64	128	8	$^{42}\text{Ca}^{19+}$	360	7.83

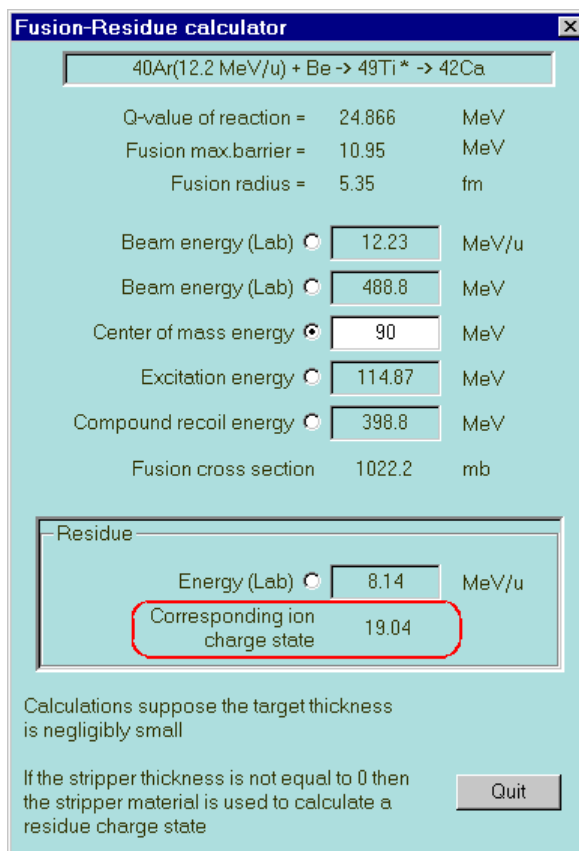
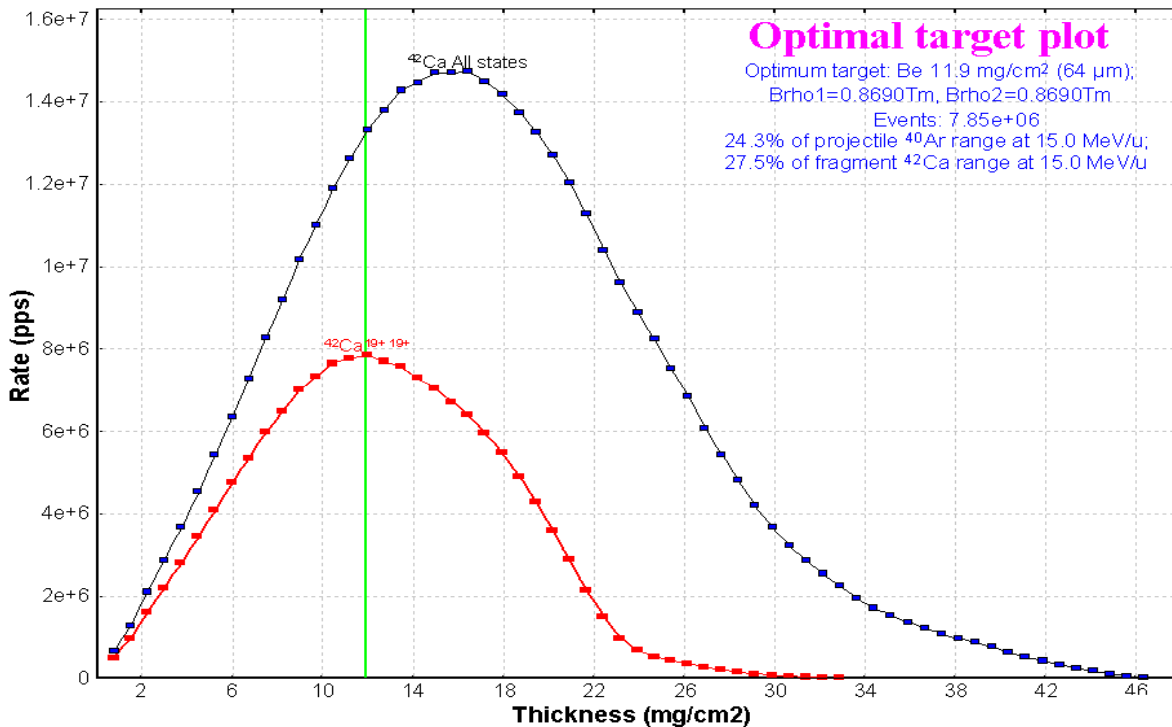


Fig.534. The “Fusion-Residue calculator” dialog helps the user to get transformations from one of six fusion→residue reaction characteristics to the others. This dialog can be activated from the “Fusion information” window (see Fig.531, item B), or via the “Calculations” menu.



**Fig.535.** Yield of the  $^{42}\text{Ca}^{19+19+}$  ion (red line) as a function of target thickness in the reaction  $^{40}\text{Ar}(15\text{ MeV/u})+\text{Be} \rightarrow ^{49}\text{Ti}^* \rightarrow ^{42}\text{Ca}$ . The blue line corresponds to the sum of all charge states of  $^{42}\text{Ca}$  when the fragment separator is tuned on  $^{42}\text{Ca}^{19+19+}$ .

### 8.1.7. Separation

The final step is the calculation of the selection of the chosen residual by the separation devices to maximize transmission and purity. In today's version, four methods of separation are available in the program LISE: magnetic rigidity, energy loss in a wedge located in the dispersive focal plane, Wien velocity filter, and combination of a Wien filter and a dipole. The most popular method of separation for small energies is velocity separation (velocity filter). At small energies using energy loss in a wedge is ruled out. In the future electrostatic and gas-filled separators will be available in the program LISE. A comparison of different methods of selection is shown in Table 65 and Fig.536, where it is apparent that the "Velocity Filter + Dipole D6" (VAMOS) method gives the best results: best purification and highest intensity of the chosen residue.

**Table 65.** Comparison of the performance of different kinds of low-energy residue selection.

Selection	Output of $^{42}\text{Ca}^{19+}$ [1/s]	Sum output of all ions [1/s]
Dipole (dp/p=3%)	4.1e+6	1.7e+7
Dipole & Wien	2.0e+6	2.4e+6
Dipole & Wien+D6	4.1e+6	4.3e+6
Wien+D6 (VAMOS)	2.4e+7	2.6e+7



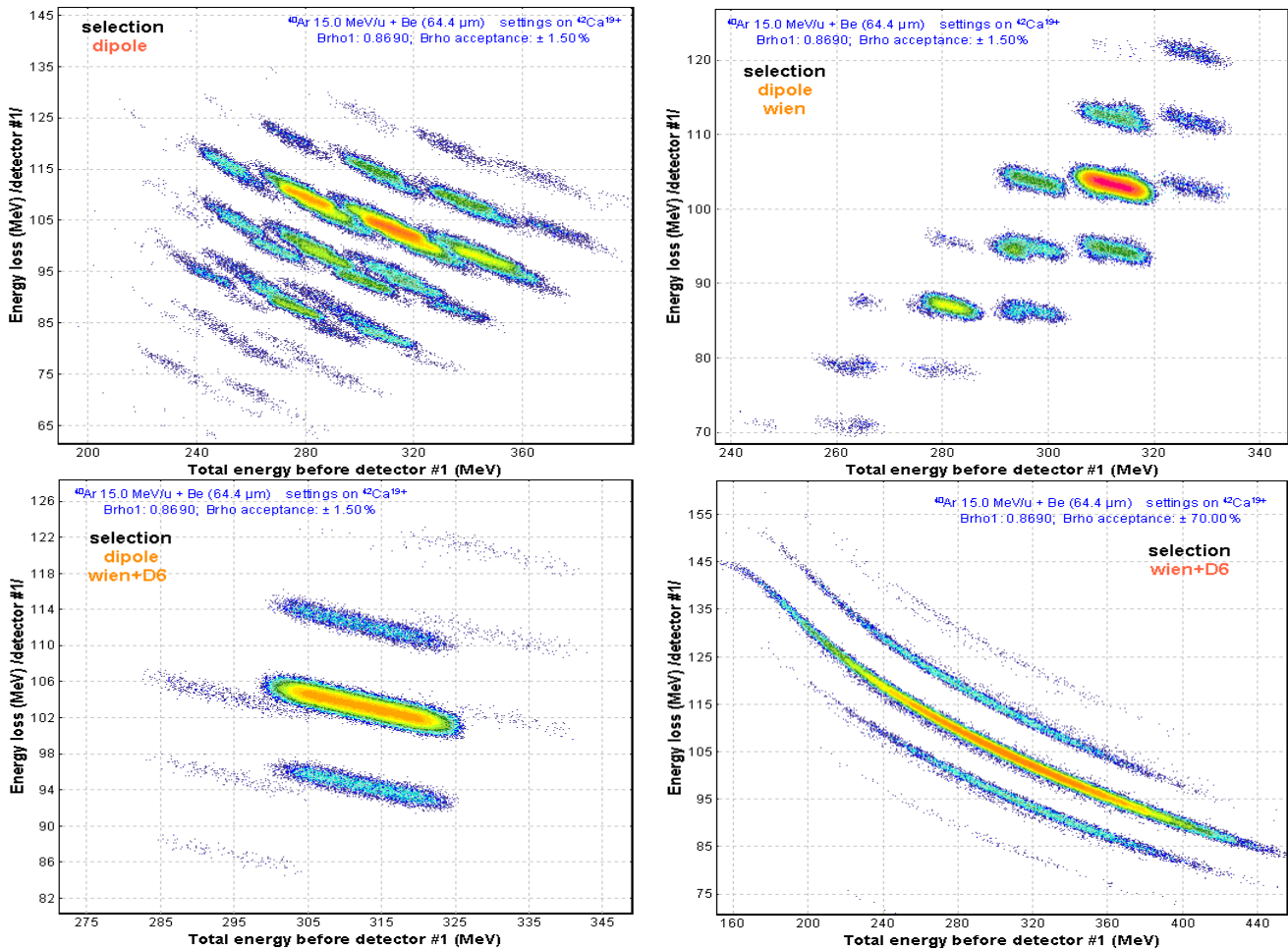


Fig.536.  $\Delta E$ - $E$  plots for different types of selection. The most intense peak on all pictures corresponds to the ion  $^{42}\text{Ca}^{19+}$ .

## 8.2. Characteristics of fusion residue calculations

The yield of reaction products ( $I_{sec}$ ) selected by a fragment separator depends from the primary beam intensity ( $I_{beam}$ ), the number of atoms in the target ( $N$ ), the production cross section ( $CS$ ), and the transmission ( $coef$ ) through the fragment separator:  $I_{sec} = I_{beam} \cdot CS \cdot N \cdot coef$ . Assuming  $I_{beam}$  and  $N$  are constant the remaining parameters to calculate are the cross section of residue production and the transmission. In order to calculate the transmission it is necessary to know:

- The kinematics distributions
  - Momentum distribution (average velocity and momentum distribution width for gaussian distributions)
  - Angular distributions (widths of parallel and perpendicular momentum distributions)
- The charge state distribution of the residue (calculated as for fragmentation reactions)

This chapter is devoted to the principles of cross section and kinematics distribution calculations.

## 8.2.1. Kinematics distributions of fusion residues

### 8.2.1.1. Momentum distribution

The residue velocity after reaction (fusion and evaporation of light particles) is assumed to be equal to the compound nucleus recoil velocity. A Maxwell distribution of velocities is used to calculate the root-mean-square velocity after evaporation of light particles. To simplify calculations and to get the result in an analytical form it was assumed that:

- Each step represent only one-nucleon evaporation
- The excitation energy of the daughter nucleus on each step is a delta function
- The separation energy of one nucleon is equal to  $(ME_{\text{compound}} - ME_{\text{residue}})/(A_{\text{compound}} - A_{\text{residue}})$

In this case it is possible to consider the final distribution as the convolution of  $(A_{\text{compound}} - A_{\text{residue}})$  gaussian distributions with  $\sigma_i = \sqrt{\tau_i / aem} / A_i$ . Thus the width of the final gaussian distribution is equal to

$$\sigma_f^2 = \sum_{i=A_{\text{compound}}-1}^{A_{\text{residue}}} \sigma_i^2 \text{ and the root-mean square velocity is determined as } \bar{v}_f^2 = 3\sigma_f^2 \text{ (the parallel and perpendicular components of the momentum distribution are } \bar{v}_{\parallel f}^2 = \sigma_f^2 \text{ and } \bar{v}_{\perp f}^2 = 2\sigma_f^2 \text{ respectively).}$$

The initial excitation energy of the compound nuclei is taken as the average of excitation energy between the beginning and the end of the target. A root-mean-square velocity calculation subroutine has been added to the PACE4 program for the “beam & target” mode to check this assumption (see Fig.537).

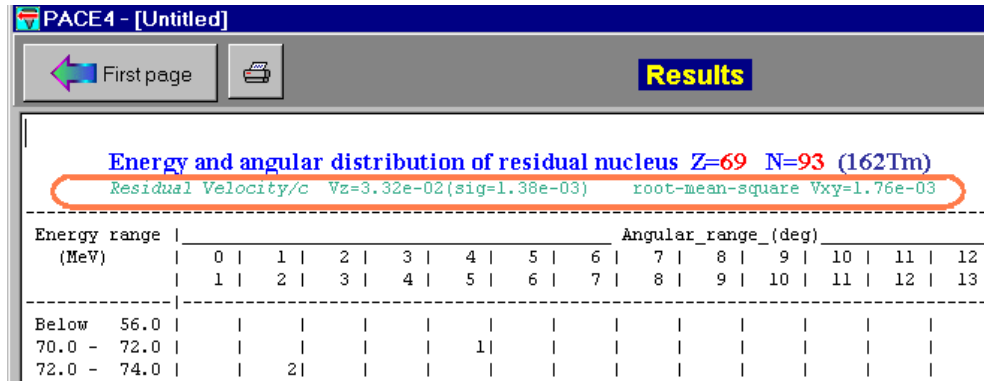
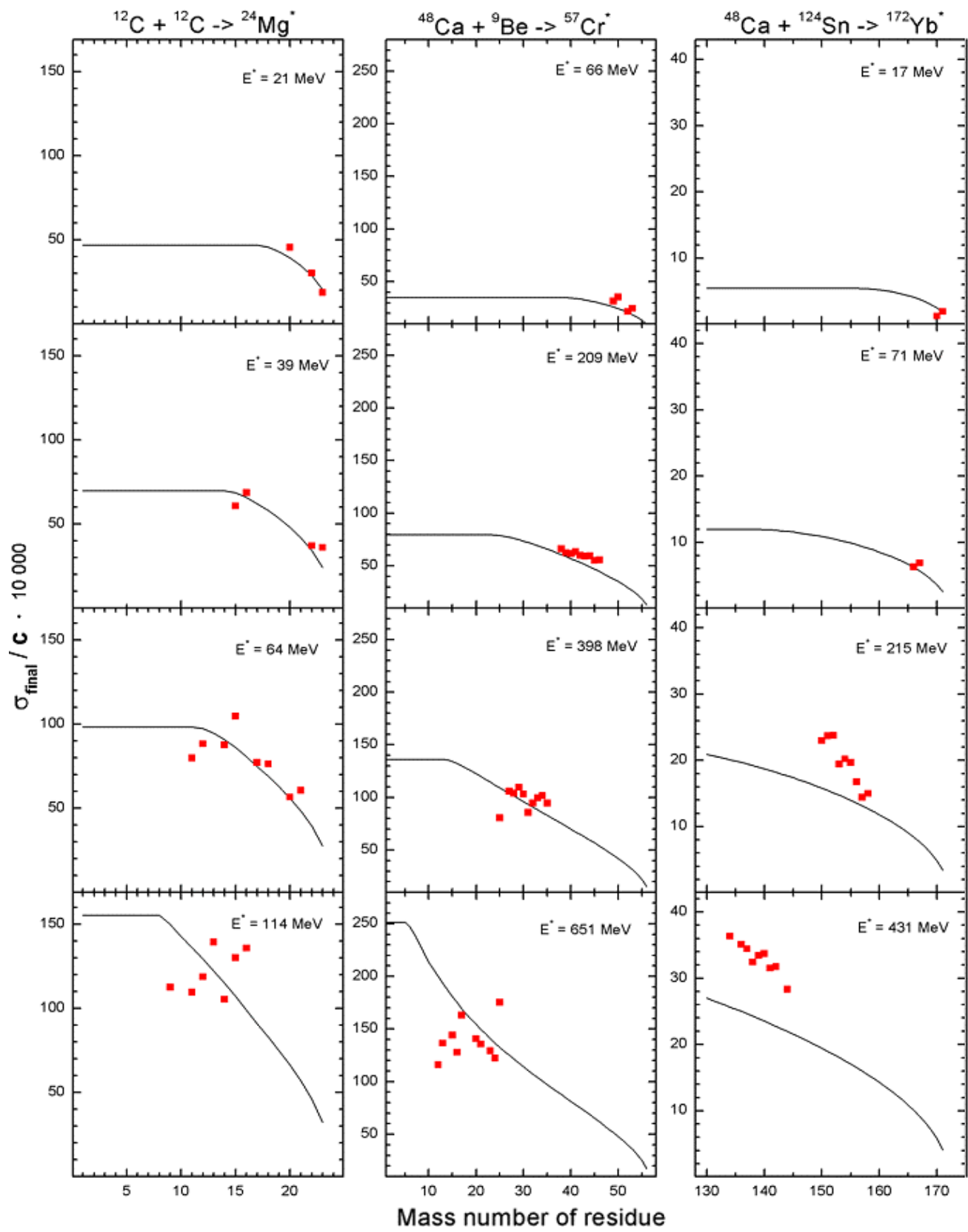


Fig.537. Fragment of the PACE4 result window. The results of the root-mean square velocity subroutine are shown in a red rounded rectangle.

Comparisons between the LISE and PACE4 calculations were made for different combinations of “beam & target & excitation energy”. The residue velocity calculations performed by the PACE4 program using a Monte Carlo method are close to the LISE simplified model (see examples in Fig.538). Some discrepancies are observed for high excitation energies of heavy compounds (see the right bottom plot in Fig.538) but for the fast calculations performed in the LISE program the agreement is acceptable. The results from the PACE program were used only for nuclei which output exceeded three hundred events.

### 8.2.2. Angular distributions

Angular distributions in the center of mass system are assumed isotropic. The calculated widths of longitudinal and transverse momentum distributions are used with the formula from the work [Bor83] to get the angular distributions of residues.




**Fig. 538.** The widths of velocity distribution versus the mass number of residue calculated by the PACE4 code (red rectangle) and the LISE program (black curve) for three different reactions  $^{12}\text{C}+^{12}\text{C}$  (left),  $^{48}\text{Ca}+^9\text{Be}$  (middle), and  $^{48}\text{Ca}+^{124}\text{Sn}$  (right) at several excitation energies.

### 8.2.3. Fusion residue cross sections

The program assumes that the targets used are thin enough and that the cross section of residue formation is constant within the target thickness. Since the calculation of the cross section is the most time consuming, this assumption greatly shortens the overall calculation time. The program is performing the following steps to calculate the cross section of a fusion residue:

- The target is divided into N slices (N is the dimension of the evaporation distribution defined in the “Search of prefragment and evaporation options” dialog)
- The energy of the primary beam ( $E_i$ ) is calculated for each slice i of target thickness due to energy loss
- The excitation energy of the compound nucleus ( $E_i^*$ ) is calculated from the primary beam energy ( $E_i$ );
- The fusion cross section ( $\sigma_i$ ) is calculated;
- The  $\sigma(E^*)$  distribution (N+1 points) is filled with values of  $\sigma_i$  and  $E_i^*$ ;
- The area of this distribution is normalized to the average value  $\bar{\sigma} = \frac{\sum_{i=0}^N \sigma_i}{N+1}$
- This excitation function of compound nucleus is used as initial distribution to calculate the cross sections of residues with the help of the Abrasion-Ablation evaporation subroutine.

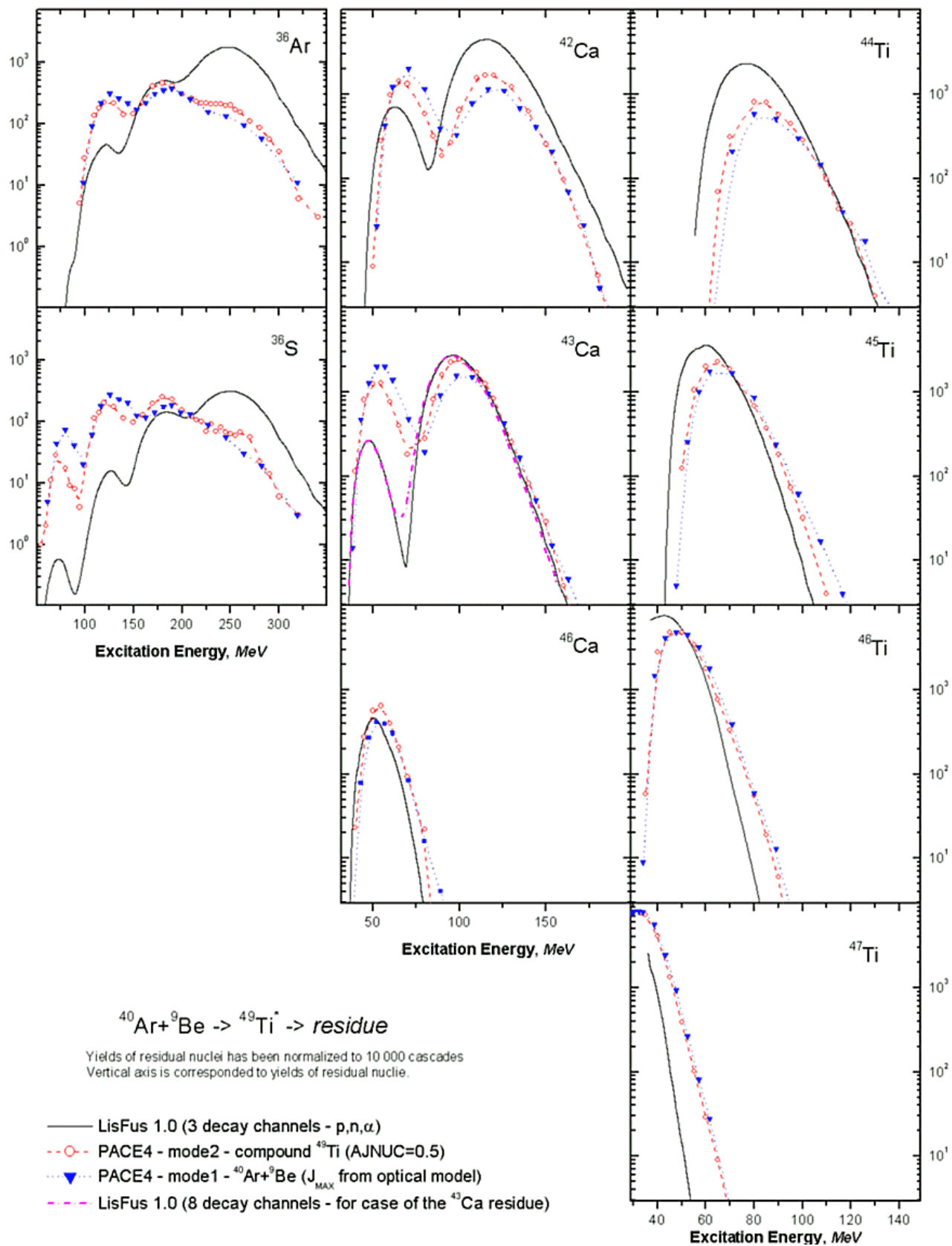
It is possible to see the evolution of the excitation functions using the Evaporation calculator in the mode “Excited nucleus evaporation”.

In order to avoid long calculation times the program asks a minimum atomic number (Z) down to which to calculate the cross sections. The user can interrupt the calculations at any time by pressing the Escape key. In the case of the optimum thickness calculation the program automatically considers the cascade only down to the nucleus of interest. All values of calculated cross sections are kept in memory. The number of kept cross sections is displayed in the “Setup” window . These cross sections are not saved in the LIZ-file and are erased from memory if the following changes are made:

- Type of reaction, projectile or target
- Coefficients used for evaporation calculation
- Number of evaporation channels
- Dimension of evaporation distributions
- If the target thickness or the beam energy have been changed by at least 2%

#### 8.2.3.1. Comparison between LISE and PACE4 fusion residue cross sections

The main advantage of the LISE code calculations (“LisFus”) of residue formation cross section is the speed. The user can get the excitation function in a short time (typically less than one minute, if the residue is close to the compound nucleus, and the dimension of distributions is not too high). Only such type of fast calculations is suitable for the computation of the transmission and yield of fusion residues in a reasonable time.



**Fig.539.** Excitation functions of  $^{36}\text{S}$ ,  $^{36}\text{Ar}$ ,  $^{42,43,46}\text{Ca}$ ,  $^{44,46,46,47}\text{Ti}$  fusion residues in the reaction  $^{40}\text{Ar} + ^9\text{Be}$  are shown. The fusion barrier is equal to 10.95 MeV. The  $Q$ -value of the fusion reaction is equal to 24.87 MeV.

In order to test the validity of the approximations used in the LisFus model, comparisons with calculations from the PACE program were made for the reaction  $^{40}\text{Ar} + ^9\text{B}$  at various energies of the primary beam. The maximum angular momentum was taken from the optical model used in the PACE4 calculations. The calculations for the  $^{49}\text{Ti}$  excited compound nucleus were carried out at a maximum spin of  $0.5 \hbar$ . The excitation functions of some residues from the reaction  $^{40}\text{Ar} + ^9\text{Be}$  are shown in Fig.539. Overall there is a quite good agreement between the calculations from the LisFus model and the PACE4 program except for the titanium isotopes. All excitation functions of the LisFus model for titanium isotopes have a systematic shift in the region of low excitation energies. This can be explained by the fact that at small excitation energies the program PACE predicts the deexcitation of nuclei by emission of gamma-rays, whereas in the LisFus model this decay channel is not included, as the only evaporation channels are emission of light particles.

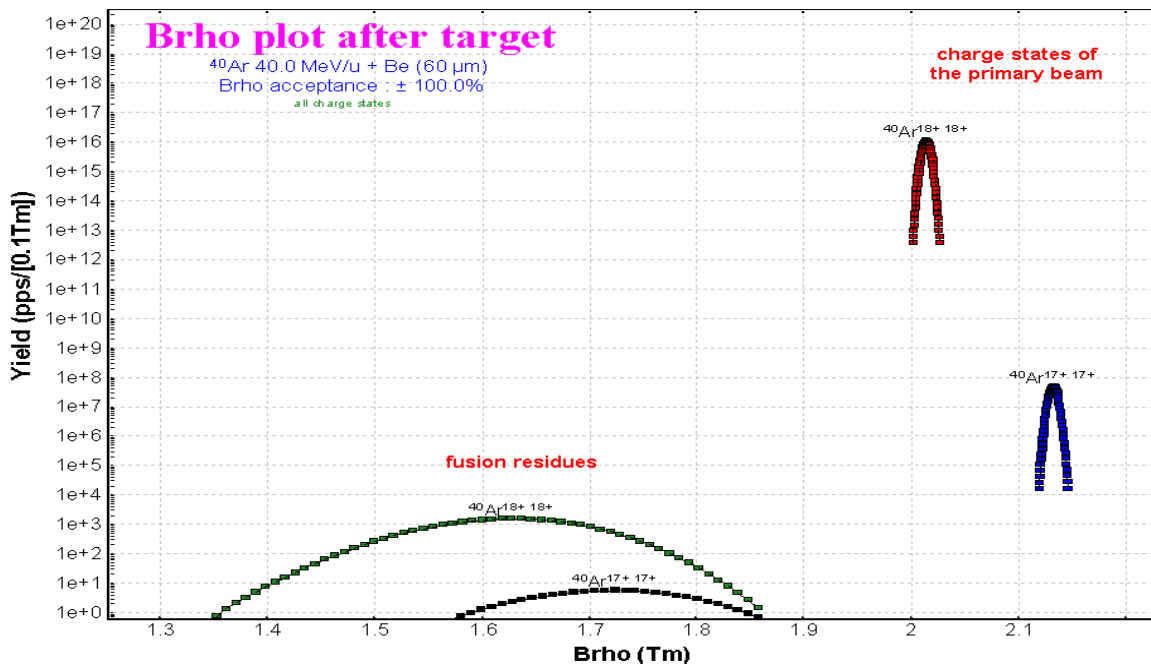
#### 8.2.4. Transmission of the primary beam

If the primary beam is among the transmitted in fusion residue mode, then the LISE program automatically switches to the fragmentation mode to calculate the transmission of the primary beam. It then returns in the fusion residue mode to get the transmission of this nucleus assuming it arose from the de-excitation of the compound nucleus.

The user can get the transmission window corresponding to the primary beam by clicking the right button of the mouse on the primary beam cell in the table of nuclides (see Fig.540). Both types of reactions can be seen, assuming that their transmission is not equal to zero. A label indicating what kind of reaction is responsible for the given charge states of the nucleus has been added after the transmission parameter number 24 (see the rounded rectangle in Fig.540). This option has been made especially to prevent from sending the primary beam into the detectors. The magnetic rigidity distributions of the transmitted charge states of  $^{40}\text{Ar}$  ion are shown in Fig.541.

statistics 40Ar				
40Ar		Stable (Z=18, N=22)		
Qt	18	17	18	17
Qw	18	17	18	17
Energy after 2-nd dipole, MeV/	26.35	23.54	26.35	23.54
00 Angular transmission (%)	100.00%	100.00%	52.40%	52.40%
01 Brho transmission (%)	100.00%	100.00%	100.00%	100.00%
02 Wedge transmission (%)	100.00%	100.00%	100.00%	100.00%
03 Wien transmission (%)	100.00%	100.00%	100.00%	100.00%
04 Total transmission (%)	99.86%	99.86%	52.32%	52.32%
05 Cross section (mb)	1.3e+06	1.3e+06	9.2e-05	9.2e-05
06 Qtarget ratio (%)	100.00%	0.00%	99.60%	0.40%
07 Qwedge ratio (%)	100.00%	100.00%	100.00%	100.00%
08 Production rate (pps)	3.5e+11	1.7e+03	1.2e+01	4.9e-02
09 Sum of charge states (pps)	3.5e+11	3.5e+11	3.5e+11	3.5e+11
10 Y Brho transmission (%)	100.00%	100.00%	100.00%	100.00%
11 Y Wedge transmission (%)	100.00%	100.00%	100.00%	100.00%
12 No 'dead' target (%)	100.00%	100.00%	100.00%	100.00%
13 X-target ang.transmis.(%)	100.00%	100.00%	62.85%	62.85%
14 Y-target ang.transmis.(%)	100.00%	100.00%	46.94%	46.94%
15 X-wedge ang.transmis.(%)	100.00%	100.00%	97.38%	97.38%
16 Y-wedge ang.transmis.(%)	100.00%	100.00%	95.57%	95.57%
17 X-wien ang.transmis.(%)	100.00%	100.00%	100.00%	100.00%
18 Y-wien ang.transmis.(%)	100.00%	100.00%	100.00%	100.00%
19 X-target slits (%)	100.00%	100.00%	100.00%	100.00%
20 Y-target slits (%)	100.00%	100.00%	100.00%	100.00%
21 CS in stripper (mb)	1.0e+20	1.0e+20	0.0e+00	0.0e+00
22 Reactions in Target (%)	0.14%	0.14%	0.15%	0.15%
23 Reactions in Wedge (%)	0.00%	0.00%	0.00%	0.00%
24 Second.Reactions /coef/	1.0e+00	1.0e+00	1.0e+00	1.0e+00
reaction	Fragmt	Fragmt	FusRes	FusRes

Fig.540. The transmission window of  $^{40}\text{Ar}$  nucleus.

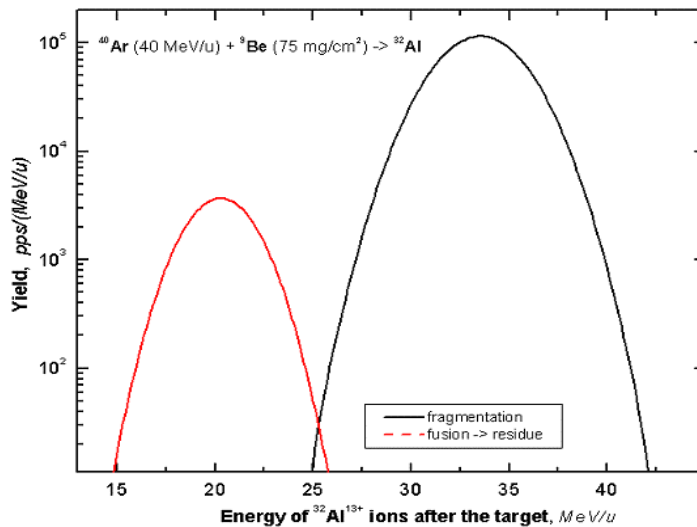


**Fig.541.** Magnetic rigidity distributions of charge states of the  $^{40}\text{Ar}$  nucleus after the target in the reaction  $^{40}\text{Ar}$  (40 MeV/u) + Be (60 microns). The charge states of the primary beam calculated in fragmentation mode dominate in this setting of the fragment separator.

It is also interesting to compare the outputs of fragmentation and fusion-evaporation reaction products and their energy distribution not only for the case of the primary beam, but for other nuclei as well. Performing this comparison requires the following conditions:

- The energy of the primary beam should neither be too high, so that the cross section for fusion-evaporation is still significant, nor too low, so that projectile fragmentation can still occur
- The overlap region between fragmentation and fusion-evaporation corresponds usually to a residue far enough from the compound nucleus, where the excitation energy of the compound is high
- Both reactions coexist only for light targets where the compound is not too far from the primary beam
- The nucleus of interest to be produced from projectile fragmentation must have less neutrons and protons than the primary beam

As an example the reaction  $^{40}\text{Ar}$  (40MeV/u) +  $^9\text{Be}$  (75mg/cm<sup>2</sup>)  $\rightarrow$   $^{32}\text{Al}$  has been chosen. The energy distributions of the  $^{32}\text{Al}$  ions after the target for both types of reactions are shown in Fig.542. For this case the products from both reactions can be well separated in the experiment. The velocity of the projectile fragment was assumed to be equal to the beam velocity and the Goldhaber momentum distributions were used to calculate the  $^{32}\text{Al}$  energy distribution for the fragmentation reaction.



**Fig.542.** Energy distributions of  $^{32}\text{Al}$  ions after the target in the reaction  $^{40}\text{Ar}$  (40 MeV/u) + Be (75 mg/cm<sup>2</sup>). The energy distribution for the fragmentation reaction is shown by the black curve, and for the fusion residue reaction by the red curve.

### 8.3. Other topics

#### 8.3.1. Two-dimensional plots for cross sections, transmission and database characteristics

It is now possible to build two-dimensional plots of cross sections, transmission and database characteristics. Before plotting the data the user can choose in the dialogs what kind of plot he or she wishes. An example of a two-dimensional plot is shown in Fig.543.

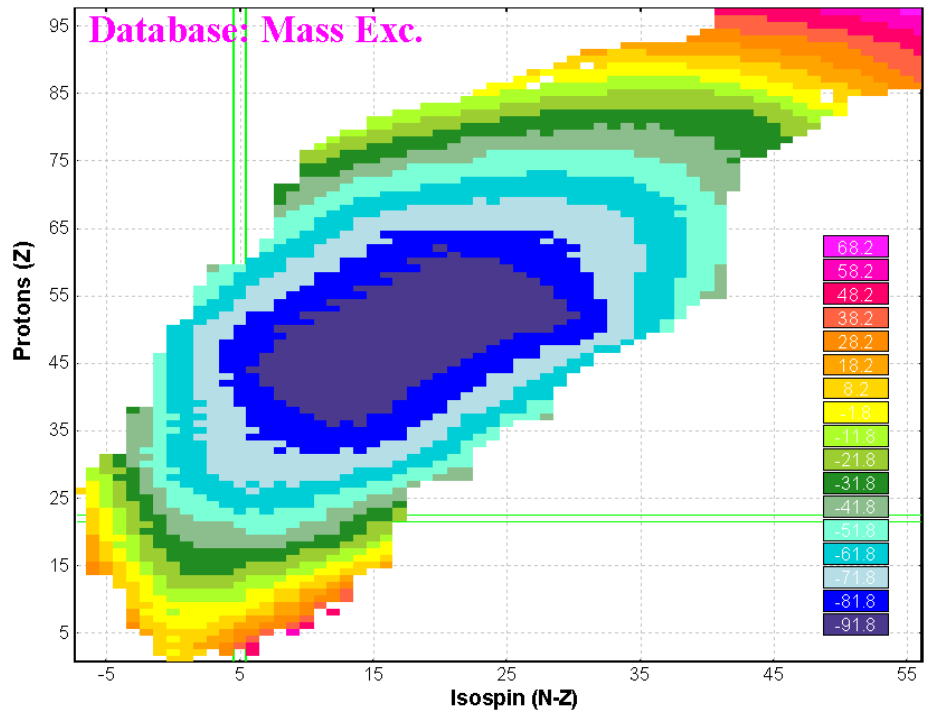


Fig.543. Mass excess values in a two-dimensional plot from the built-in database.

#### 8.3.2. Modification of evaporation calculation procedure

A considerable change has taken place in the calculation of the daughter nuclei excitation functions of the evaporation cascade model. In the previous versions it was assumed that each i-th point of an intermediate nucleus excitation function had only one projection in the daughter nucleus excitation function:

#### <sup>49</sup>Ti excitation distributions

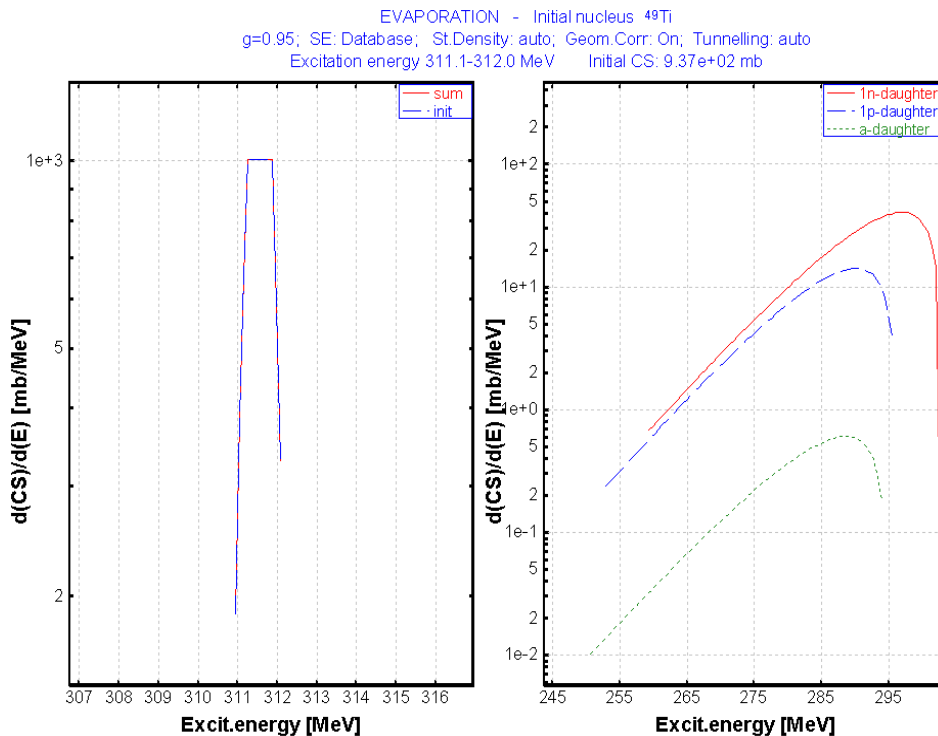


Fig.544. The initial excitation function of the <sup>49</sup>Ti parent nucleus (left picture) is chosen close to a delta-function, and its daughters excitation functions calculated with the new method (right picture).



$$(E_{daugh}^*)_i = (E_{parent}^*)_i - S - B - 2\tau_i, \quad /51/$$

where  $S$  is the separation energy,  $B$  is the reduced coulomb barrier in the case of a charge particle evaporation, and  $\tau$  is the temperature of the daughter nucleus. The value in this  $i$ -th point of the daughter distribution was equal to the multiplication of the  $i$ -th value of the intermediate nucleus and the probability for this daughter evaporation channel:

$$f[(E_{daugh}^*)_i] = \phi[(E_{parent}^*)_i] \cdot P(E_{parent}^*)_i. \quad /52/$$

In the new version each  $i$ -th point of parent distribution is represented as a distribution following the Maxwell law with the an area normalization of /52/. Then all  $NP_{evap}+1$  partial daughter distributions are summed up to one final daughter distribution. The final result is shown in Fig.544. The initial excitation function was chosen as a very narrow rectangle (close to a delta function).

### 8.3.3. LISE.xls – stopping power functions

Stopping power functions (dE/dx) have been incorporated in the *lise.xls.dll* library and can be loaded as a function in Excel through the *LISE.xls* file (see Fig.545).

The screenshot shows the LISE.xls Excel window with four main panels: Energy loss calculation methods (Hubert, Ziegler, ATIMA), Charge State calculation methods (Winger, Leon, Shima), Energy Straggling calculation methods (Anne, ATIMA), and a names panel with input fields for Zparticle, Aparticle, Ztarget, Atarget, Energy, Thickness, and ZmQ. Below these panels are 'Init' and 'Hide' buttons and a note: 'you may change values of top cells'. At the bottom is a table with columns: function, return, parameters, and example.

function	return	parameters	example
StragglingRange	range straggling in material [mg/cm2]	Zparticle, Aparticle Energy [MeV/u] Ztarget	0.809 mg/cm2
Stopping power	Hubert - option=0	Zparticle, Aparticle Energy [MeV/u] Ztarget	2.46206 MeV/(mg/cm2)
Stopping power	Zigler - option=1	Zparticle, Aparticle Energy [MeV/u] Ztarget	2.54668 MeV/(mg/cm2)
Stopping power	Atima - option=2	Zparticle, Aparticle Energy [MeV/u] Ztarget	2.48435 MeV/(mg/cm2)
Stopping power	Atima without LS - option=3	Zparticle, Aparticle Energy [MeV/u] Ztarget	2.57521 MeV/(mg/cm2)

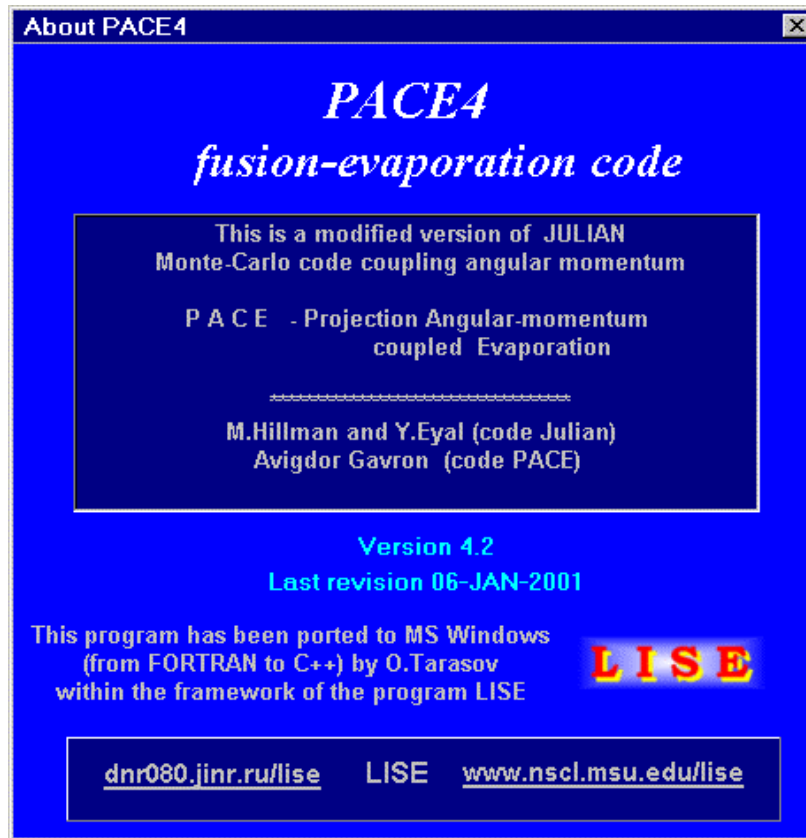
Fig.545. Fragment of the Excel window. The block with new functions “Stopping power” is indicated by the red rounded rectangle.

### Acknowledgement

Fruitful discussions with A.Andreev, and M.Toennessen are gratefully acknowledged.

## 9. PACE4 - version 5.13

East Lansing  
15-JAN-2002

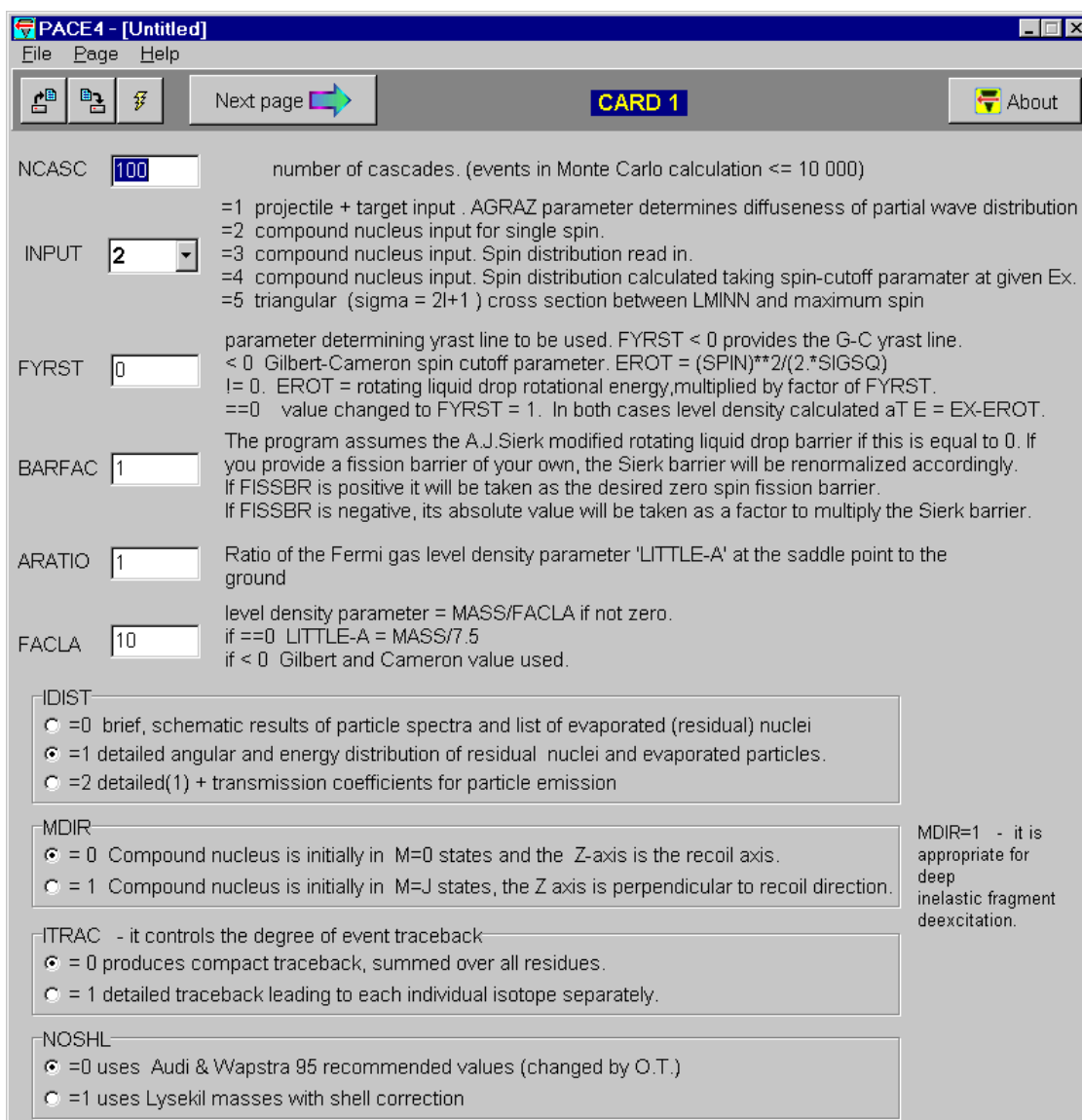


## 9.1. PACE4

### 9.1.1. Introduction

The program PACE has been incorporated (after approbation by the authors) in the LISE package. The expansion of the program LISE to other reaction mechanisms has motivated the attachment of the program PACE. The code PACE (developed by A.Gavron [Gav80]) is a modified version of JULIAN - the Hillman-Eyal evaporation code. PACE (Projection Angular-momentum Coupled Evaporation) is a Monte-Carlo code coupling angular momentum. This code has been ported to MS Windows from FORTRAN to C++. The FORTRAN (original PACE3) and C (PACE4) source files can be found at the following ftp-address [ftp://ftp.nslcl.msu.edu/lise/PACE\\_source](ftp://ftp.nslcl.msu.edu/lise/PACE_source).

### 9.1.2. Modifications



The screenshot shows a window titled "PACE4 - [Untitled]" with a menu bar (File, Page, Help) and a toolbar with icons for file operations and a "Next page" button. The main area is labeled "CARD 1" and contains several input fields and radio button groups with descriptive text.

**NCASC**  number of cascades. (events in Monte Carlo calculation  $\leq 10\,000$ )

**INPUT**    
=1 projectile + target input. AGRAZ parameter determines diffuseness of partial wave distribution  
=2 compound nucleus input for single spin.  
=3 compound nucleus input. Spin distribution read in.  
=4 compound nucleus input. Spin distribution calculated taking spin-cutoff parameter at given Ex.  
=5 triangular ( $\sigma = 2l+1$ ) cross section between LMINN and maximum spin

**FYRST**    
parameter determining yrast line to be used. FYRST  $< 0$  provides the G-C yrast line.  
 $< 0$  Gilbert-Cameron spin cutoff parameter.  $EROT = (SPIN)**2/(2.*SIGSQ)$   
 $l=0$ . EROT = rotating liquid drop rotational energy, multiplied by factor of FYRST.  
=0 value changed to FYRST = 1. In both cases level density calculated at  $T E = EX-EROT$ .

**BARFAC**    
The program assumes the A.J.Sierk modified rotating liquid drop barrier if this is equal to 0. If you provide a fission barrier of your own, the Sierk barrier will be renormalized accordingly. If FISSBR is positive it will be taken as the desired zero spin fission barrier. If FISSBR is negative, its absolute value will be taken as a factor to multiply the Sierk barrier.

**ARATIO**    
Ratio of the Fermi gas level density parameter 'LITTLE-A' at the saddle point to the ground

**FACLA**    
level density parameter =  $MASS/FACLA$  if not zero.  
if =0 LITTLE-A =  $MASS/7.5$   
if  $< 0$  Gilbert and Cameron value used.

**IDIST**

- =0 brief, schematic results of particle spectra and list of evaporated (residual) nuclei
- =1 detailed angular and energy distribution of residual nuclei and evaporated particles.
- =2 detailed(1) + transmission coefficients for particle emission

**MDIR**

- =0 Compound nucleus is initially in  $M=0$  states and the Z-axis is the recoil axis.
- =1 Compound nucleus is initially in  $M=J$  states, the Z axis is perpendicular to recoil direction.

**ITRAC** - it controls the degree of event traceback

- =0 produces compact traceback, summed over all residues.
- =1 detailed traceback leading to each individual isotope separately.

**NOSHL**

- =0 uses Audi & Wapstra 95 recommended values (changed by O.T.)
- =1 uses Lysekil masses with shell correction

MDIR=1 - it is appropriate for deep inelastic fragment deexcitation.

Fig.546. The first input card of the code PACE4.

The program PACE has a user-friendly interface in the MS Windows system, where the user can enter information directly in dialogs (see Fig.546), in which the explanation for each parameter is displayed. The entered information is written to files with the extension “in”, compatible with the previous versions. The database of recommended values for binding energies [Aud95] was added into the program (see Fig.547). In the new version it possible to calculate up to 10000 cascades at the maximum excitation energy of 2000 MeV the compound nucleus. The calculation results are displayed and formatted in a scrollable window (see Fig.549). The result file is saved in the format “rtf” and can be printed from the program. The user can select (as in the original

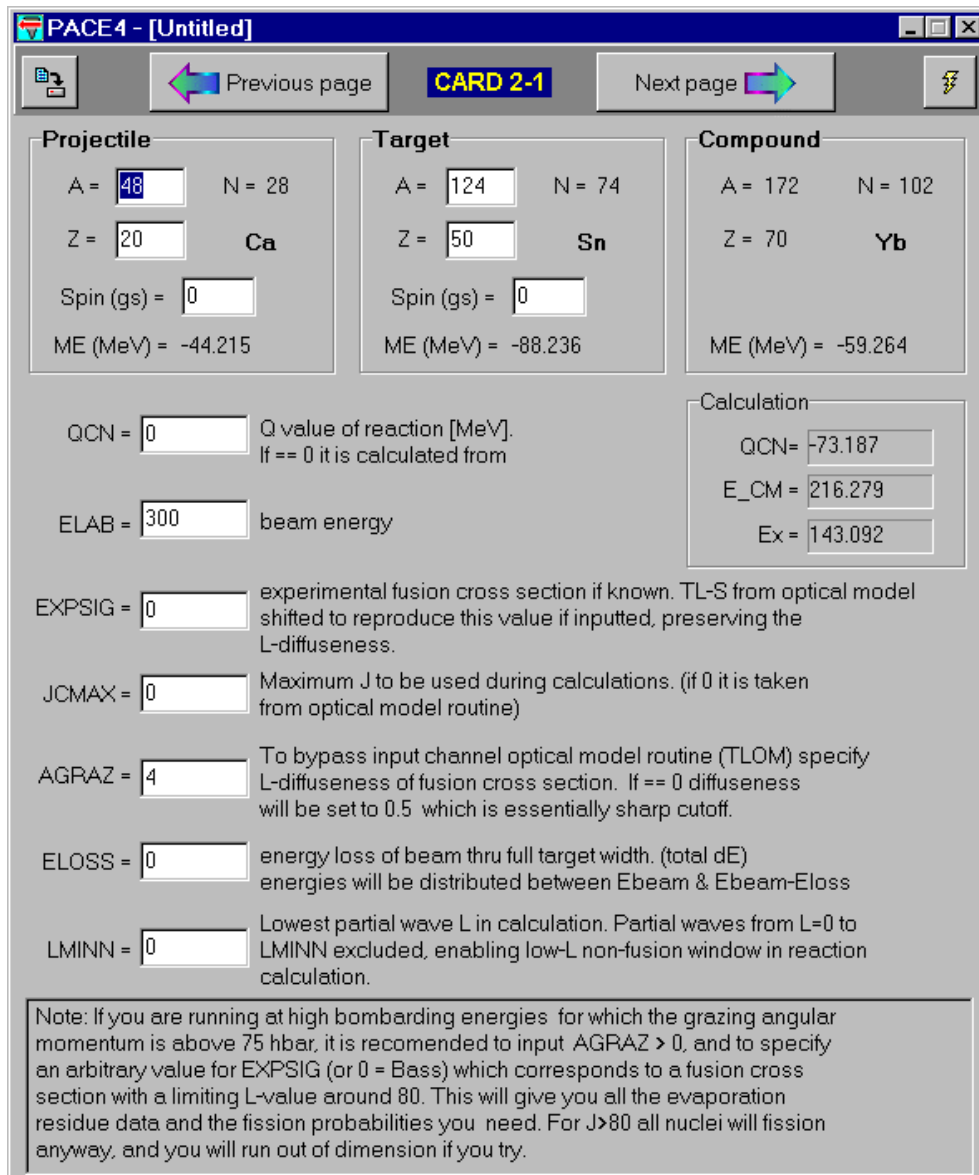


Fig.547. The second card of the PACE4 code for the projectile and target mode.

but the possibility to input nucleus levels in this version is not available.

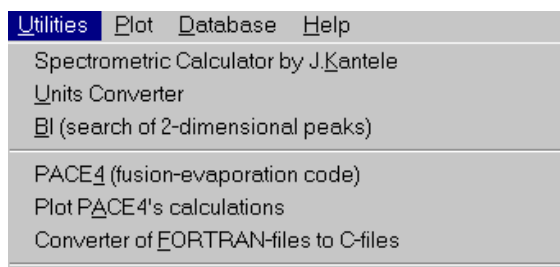


Fig.548. The fragment of the menu “Utilities”.

The program can be launched directly from the program LISE through the “Utilities” menu (see Fig.548). The user can also use the program PACE4 separately from the LISE package by clicking on the icon from the LISE folder (Start menu).

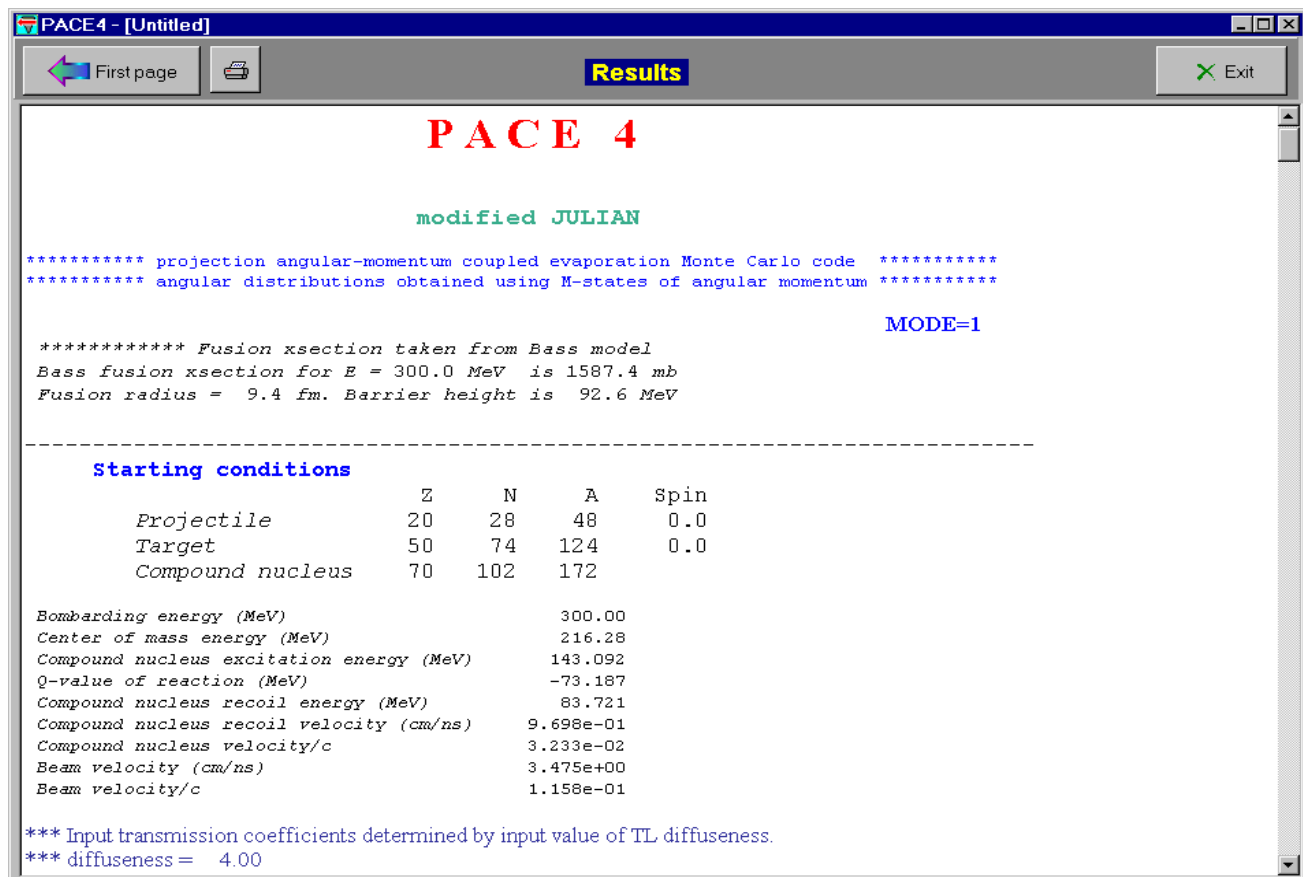


Fig.549. The window of PACE4 calculation results.

### 9.1.3. Visualization of PACE4 calculations

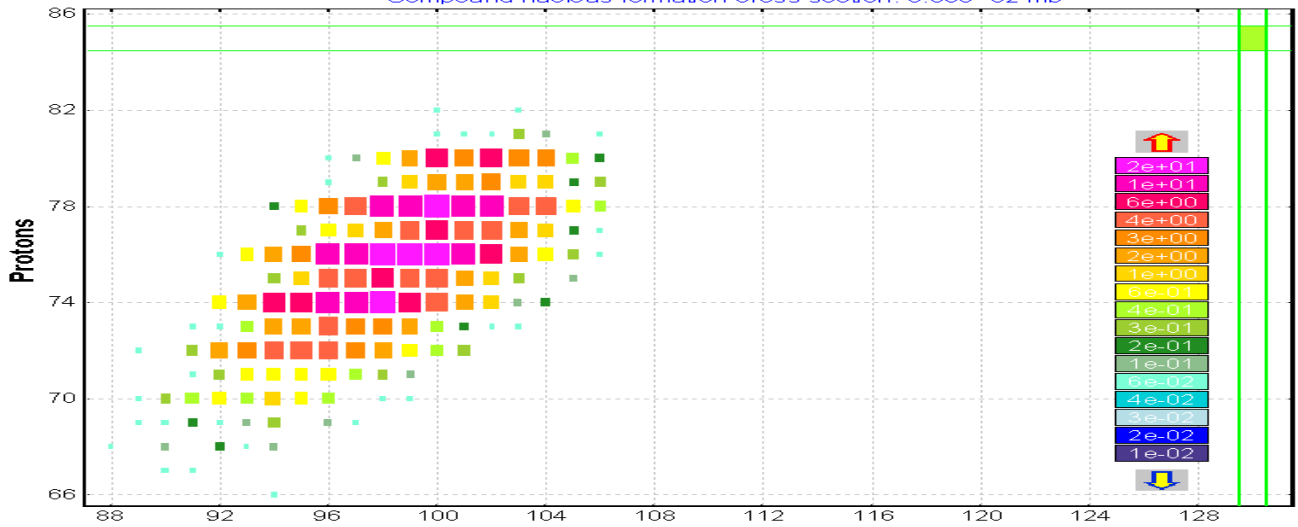
The PACE4 calculation results can be plotted within the framework of the program LISE. For this purpose it is necessary to load the cross-sections file (extension “cs”, default directory is <LISE>/files), which was created by the program. The plots are obtained of selecting the menu “Utilities -> Plots PACE4 results” (see Fig.548). Examples of this plot are shown in Fig.550 and 551.

### 9.1.4. Comparisons of PACE4 and LISE AA-model calculations

Comparisons of PACE4 and LISE AA-model calculations for the compound nucleus  $^{215}\text{At}$  are presented in Fig.550 (Excitation energy 500 MeV) and Fig.551 (Excitation energy 50 MeV). The upper plots on these figures are the PACE4 calculations, the middle plots the LISE built-in abrasion-ablation (AA) model [Gai91] plotted using the same scales for X, Y, and Z. The lower plots are the same as the middle plots, but using free scales for X, Y, and Z. It is apparent that for high excitation energies there is a large difference between the two models, caused by the large angular momentum, which is ignored by the LISE AA model. The advantages of PACE4 calculations are the possibility to calculate gamma-emission and fission channels, to take into account the angular momentum (important for high excitation energies), whereas the LISE AA-model assumes an angular momentum of zero. However, the LISE AA-model allows to calculate very small cross-sections quickly due to the analytical approach of that calculation, compared to programs using the Monte Carlo method.

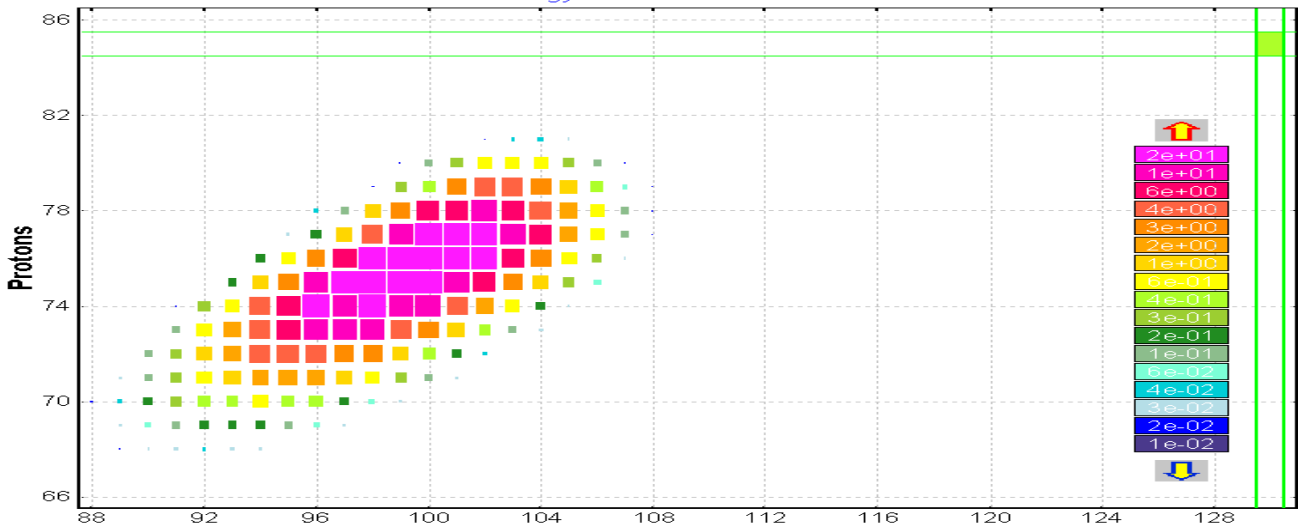
**PACE4**

EVAPORATION - Compound nucleus  $^{215}\text{Ar}$ ; Mode 4  
Excitation energy 500.0 MeV; Max.compound nucleus spin 100.0 hbar  
Compound nucleus formation cross section:  $6.60\text{e}+02$  mb



**LISE**

EVAPORATION - Compound nucleus  $^{215}\text{Ar}$   
 $g=0.95$ ; SE: Database; St.Density: auto; Geom.Corr: On; Tunnelling: auto  
Excitation energy 480.0-520.0 MeV Initial CS:  $6.60\text{e}+02$  mb



**LISE**

EVAPORATION - Compound nucleus  $^{215}\text{Ar}$   
 $g=0.95$ ; SE: Database; St.Density: auto; Geom.Corr: On; Tunnelling: auto  
Excitation energy 480.0-520.0 MeV Initial CS:  $6.60\text{e}+02$  mb

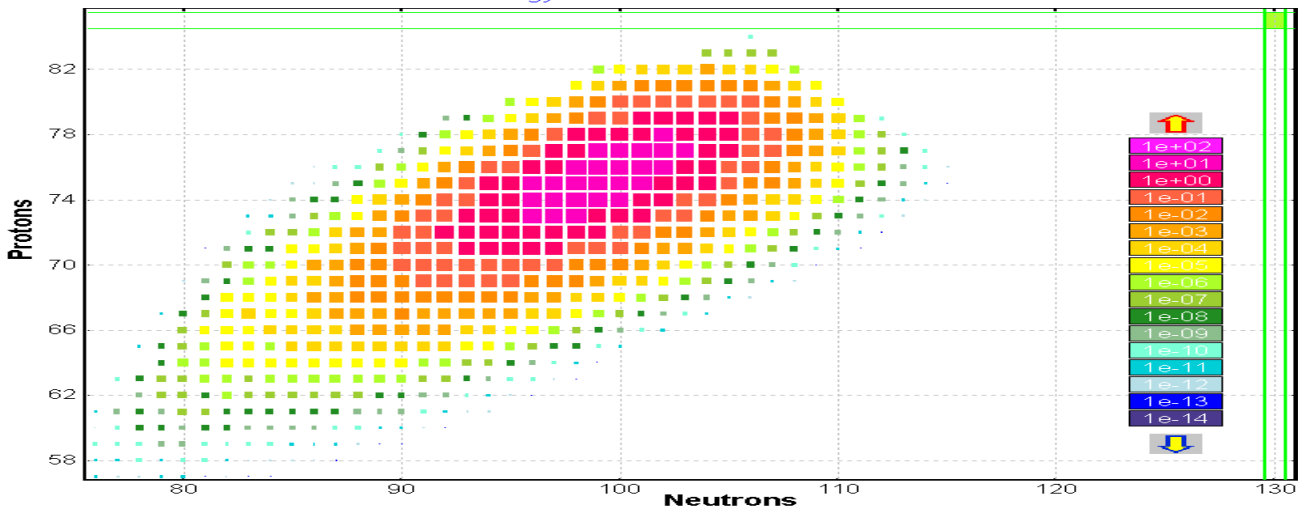


Fig.550.  $^{215}\text{Ar}$  ( $E_x=500$  MeV) evaporation results (see details in the text).

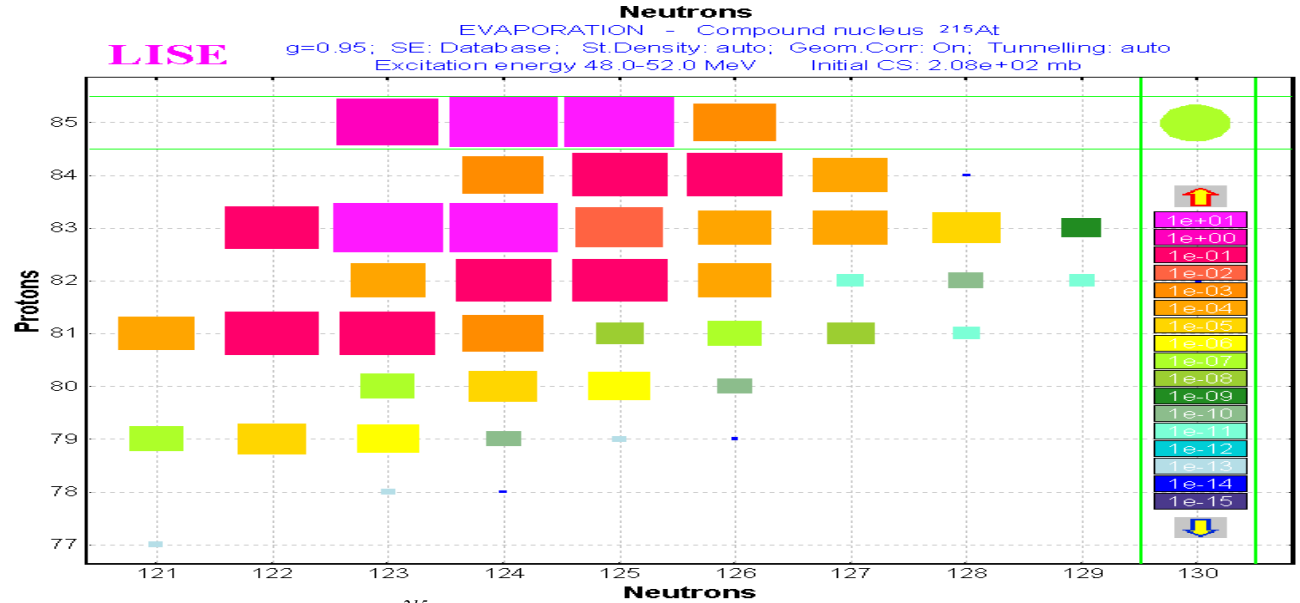
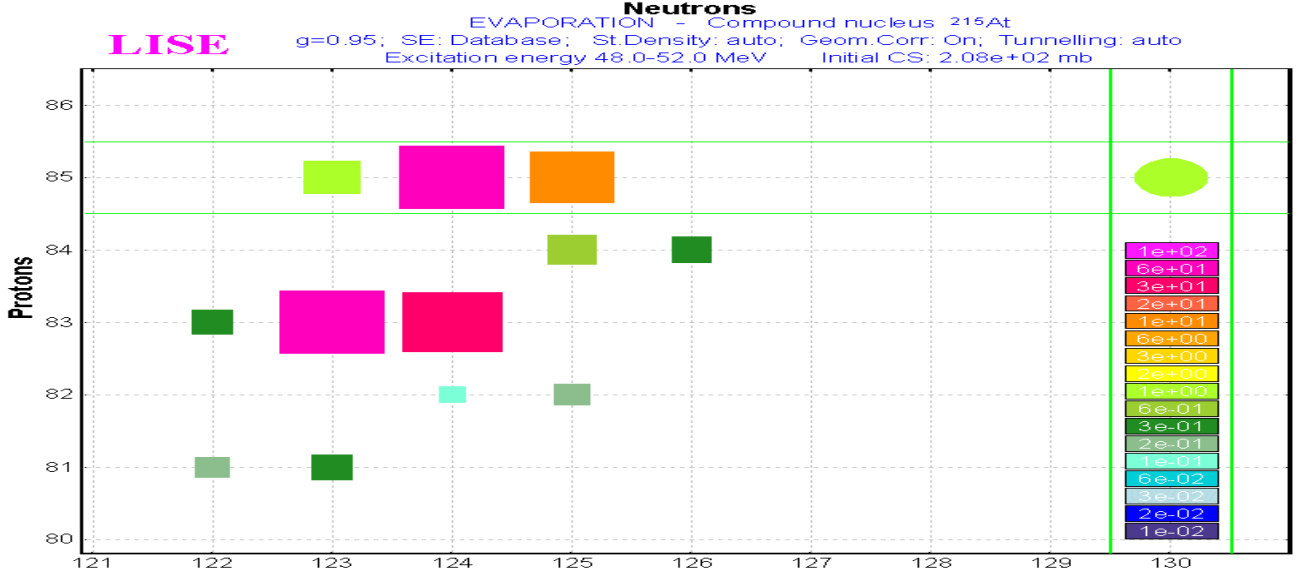
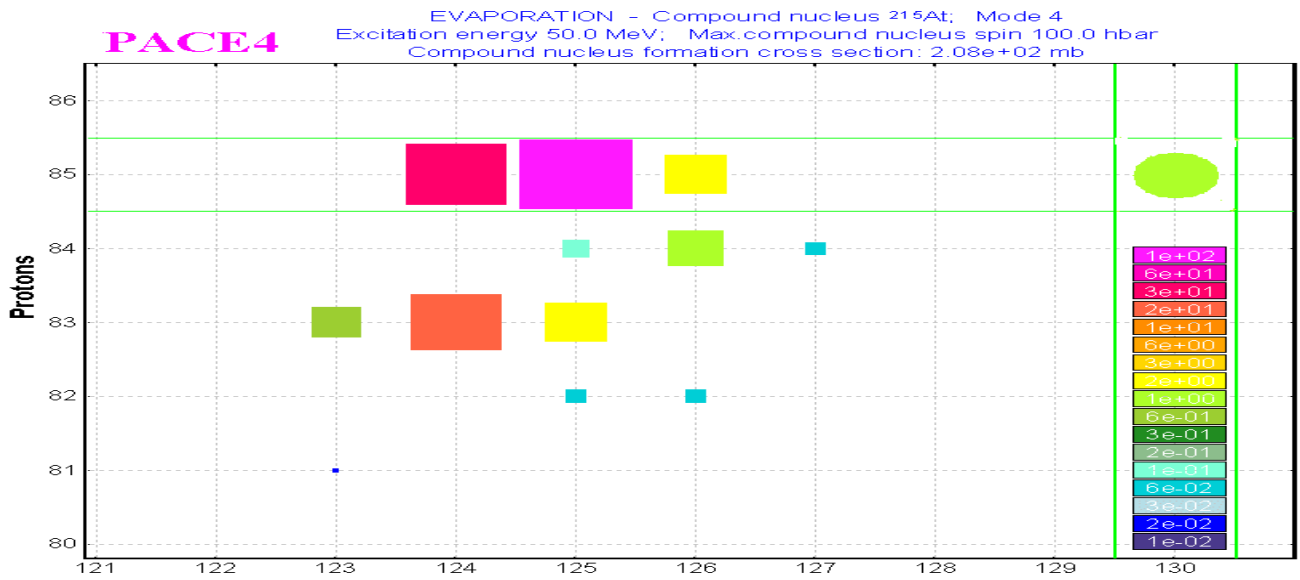


Fig.551.  $^{215}\text{Ar}$  ( $E_x=50$  MeV) evaporation results (see details in the text).

## 9.2. Option & Configuration files

In order to save and restore the settings (spectrometer characteristics, experiment settings, options of reaction mechanism, entered cross-sections, calculated transmissions and rates) the user uses standard LIZE-files with the extension “**liz**”. However it is very often necessary to apply other set-ups or options of reaction mechanism to some already existing calculations. To do this the code has now the possibility to read an OPTION-file (extension “**opt**”) as well as a CONFIGURATION-file (extension “**lcf**”). This chapter tries to explain the structure of these files and the new modifications made on the basis of numerous remarks from users.

### 9.2.1. Structure of files

#### 9.2.1.1. Configuration file (LCF-extension)

The fragment-separator characteristics are saved in this file (subdirectory “**config**”). There are four sections:

Section	Parameter
Object	All slits of spectrometer;
Acceptances	Momentum and angular acceptances of spectrometer;
Optics	Beam characteristics, dipole radius, optic matrices of each part of spectrometer, distances;
Wien_filter	Velocity filter characteristics.

#### 9.2.1.2. Option file (OPT-extension)

Calculation parameters, visualization options, reaction mechanism options and others are saved in this file (subdirectory “**options**”). There are 14 sections:

Section	Parameter	Save also in LIZ-file
Distribution	Distributions dimension	Yes
Display	3d-animation, navigation, sound and etc	No
	Charge State (Yes/No), Cross Section (Fit/File), Secondary Reactions(Yes/No), threshold=1.0e-10	Yes
Resolution	Energy, Time, and spatial resolutions; Material defect	Yes
Plots	Plot options, Monte Carlo options and etc	No
Evaporation	Evaporation options: distribution dimension, modes of decay	Yes
	Option: Create reference files (Yes/No)	No
EvapAuto	Parameters of evaporation auto mode	Yes
Excitation	Excitation energy dialogue settings	Yes
Mechanism	Charge State Method, Energy Loss Method, Energy and Angular straggling methods, Cross Section method	Yes
Velocity	Fragment velocity calculation methods and their parameters	Yes
Momentum	Widths of momentum distribution methods and their parameters	Yes
Friedman	Parameters of Friedman’s momentum distribution	Yes
Convolution	Parameters of Convolution method of momentum distribution	Yes
Internet	Internet options	No
MSP144	Characteristic of MSP144 spectrometer	Yes



### 9.2.1.3. Data file (LIZ-extension)

The regular LIZE-file (extension “**liz**”) consists of the Configuration file (**lcf**), the sections of the Option file (**opt**) mentioned in the table (see sec.9.2.1.2.), the experiment settings and calculation results:

$$\mathbf{LIZ = LCF + OPT + Experiment\ settings + Calculation\ results}$$

The experiment settings include the characteristics of the beam, target, stripper, wedge, and materials. The names of the configuration and option files are also saved in the LIZ-file.

### 9.2.2. New features

Upon starting, the code reads the LIZE.INI file which contains the default configuration and options file names, as well as the list of most recent files. The code loads the default configuration file, and the default options files. If these files are absent the user is informed and the standard LIZE settings are used.

The user can set the default configurations in the dialog “Preferences” (see Fig.552). In the new version the possibility to choose a default option file has been added (see the rounded rectangle on Fig.552).

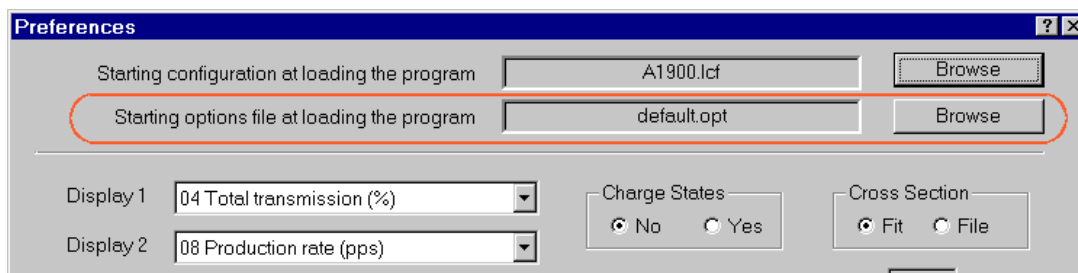


Fig.552. Fragment of the dialog “Preferences”.

The current configuration and options files are displayed in the window “SETUP” (see Fig.553).

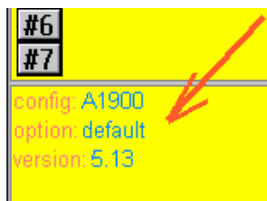


Fig.553. Fragment of window “Setup”.

After loading the LIZ-file the code checks the existence of the options and configuration files from their names saved in this LIZ-file. If one of these files is absent the user is warned and the string “????” is displayed in the window “Setup” instead of a file name. Note that it is necessary to set the option “Check LIZ-file consistency” in the “Preferences” dialog.

**Important!** When the user clicks the button “MAKE DEFAULT” and then “OK” the current options will be saved in the options file with the name shown in the

window “Setup”.

## 9.3. File converter from Fortran to C

The necessity to port software from one programming language to another arises quite for programmers. In the field of physics it is connected to the fact that the most popular programming language among physicists was (and still probably is) FORTRAN. As a rule all programs made for computers with multi-task systems were started from a command line. However with the fast intrusion of personal computers and CPU speeds superior to that 10-year old VAX- and UNIX-computers it quite often makes sense to port these programs to the most commonly used language nowadays, which is C or PASCAL. To facilitate

the work of programmers a file converter from FORTRAN to C was built. This converter is certainly not ideal: the user should still itself edit the C-file, but most labor-consuming operations are taken care of in the converter:

1. Comments;
2. Logical operators And, Or, Equal etc.;
3. Operands “Mod” and “^” changed to corresponding “%” and “pow”;
4. Operators “Go To” and their corresponding labels;
5. Operators “then”, “else”, “do”, “continue”;
6. Junction of lines by the disjointed identifier in 6-th position of line (FORTRAN-case), attachment of the character “;” at the end of line (C-case);
7. Identification of FORTRAN in-built function and replacement on corresponding C-functions;
8. Arrays (replacement of parentheses, splitting of multi-dimensional arrays)
9. Subroutines etc.

The user’s main work after converting consists in the editing of COMMON-blocks, checking of DO-loops, and functions built by the user. The size of the FORTRAN file should not exceed 64 kB. An example of how the converter works is presented in Fig.554.

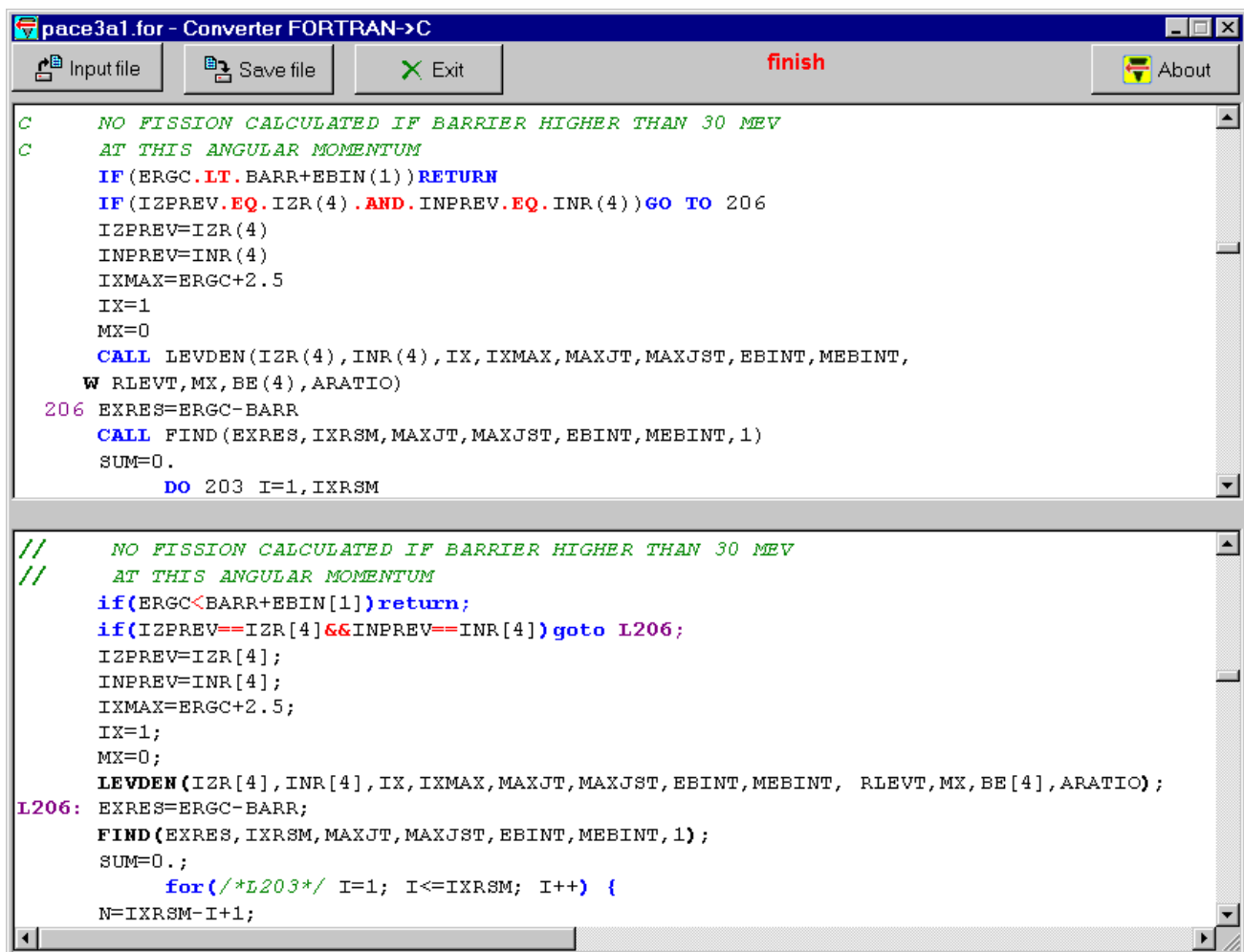


Fig.554. Converter of FORTRAN-files to C.

## 9.4. Other

### 9.4.1. Modernization of the Abrasion-Ablation model

The analytical form of parent and daughter distributions has been modified. All distributions have now an exponent base to reproduce the low-energy part better. New modifications allow to input a delta-function as the input excitation energy distribution (see Fig.555). It is recommended to put the evaporation distributions dimension to 64 instead 32 for better quality calculations.

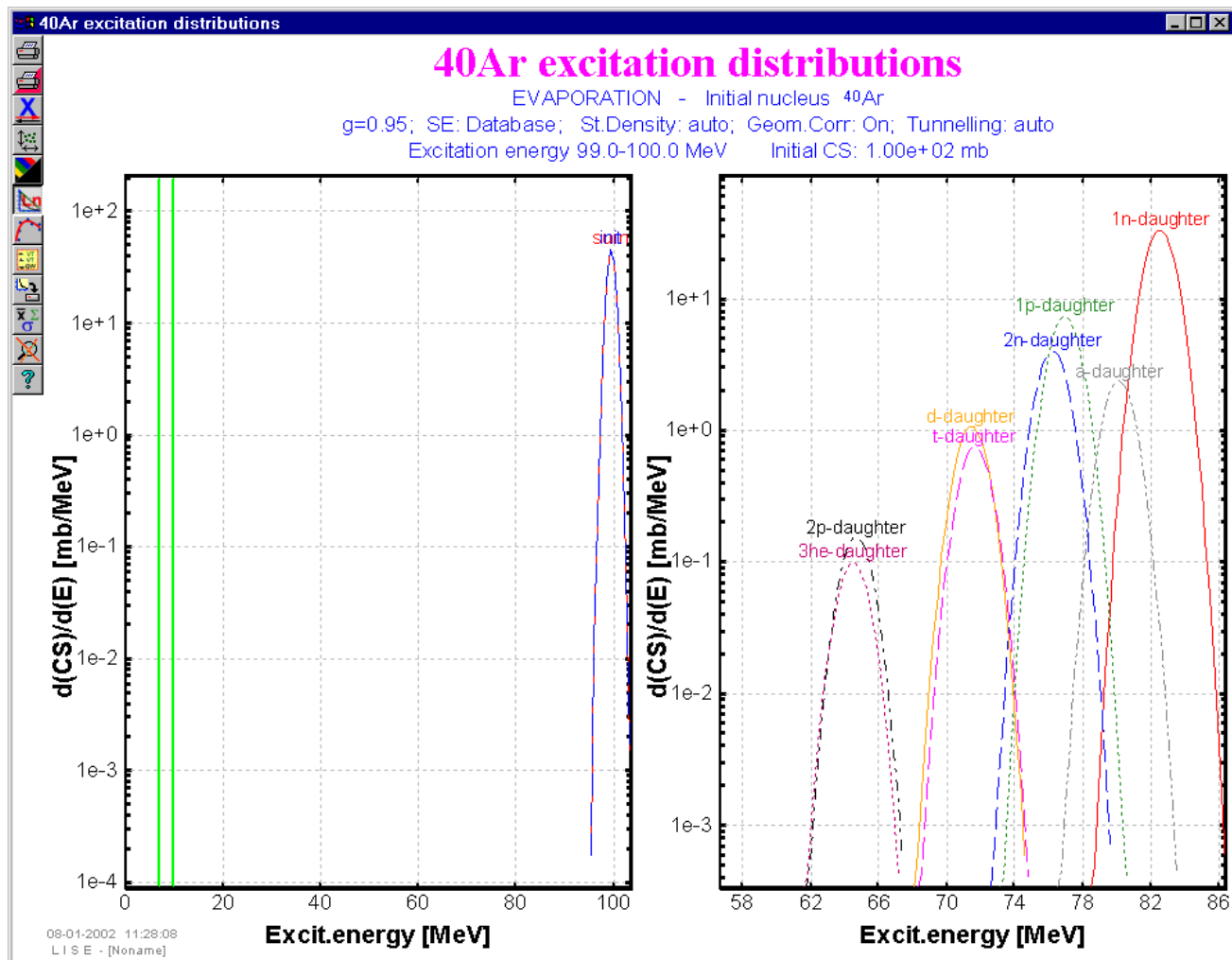
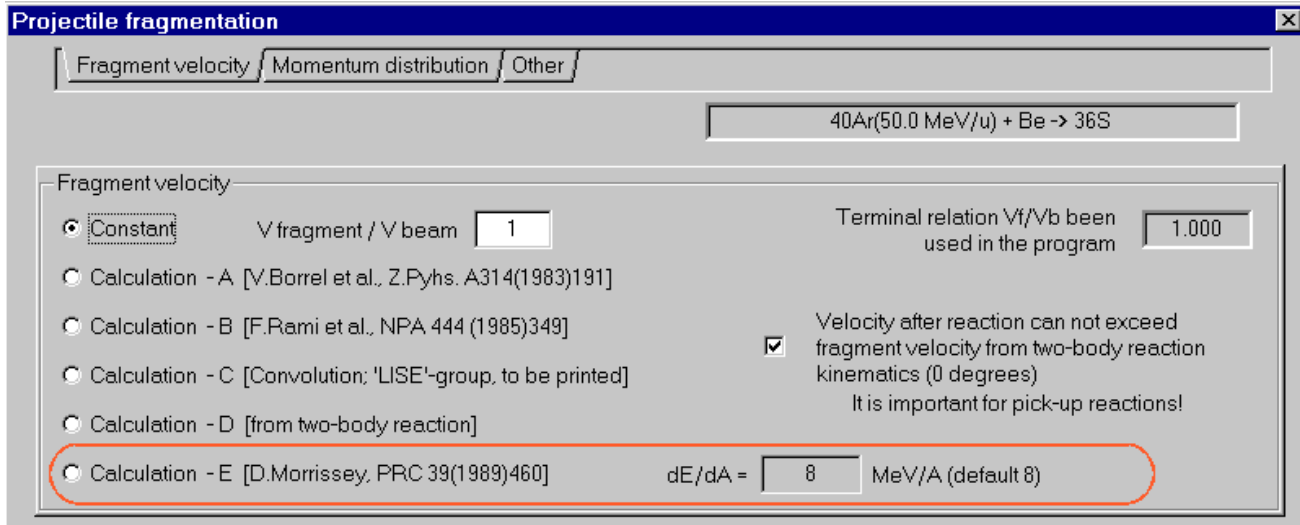


Fig.555.  $^{40}\text{Ar}$  distributions (initial distribution – left plot, daughter distributions –right plot) are shown for the case of an  $^{40}\text{Ar}$  initial excitation energy from 99 to 100 MeV.

### 9.4.2. New NSCL ftp-address

The NSCL download address has changed! The new address is <ftp://ftp.nsl.msu.edu/lise/>. The LISE site and the LISE's subroutine to obtain the new version automatically have been modified.

### 9.4.3. New model for projectile fragmentation velocity



**Fig.556.** Part of the “Projectile fragmentation” dialog. The new method to calculate the fragment velocity is outlined by a red rounded rectangle. Detailed information of this new method can be found in the reference [Mor89.]

### 9.4.4. Changes in the Utilities menu

The code **”BI”** (from the menu *BI*), **”Spectroscopic calculator of J.Kantele”** and **”Units converter”** (from the menu *Calculations*) have been moved to the menu *Utilities* (see Fig.548). Also the new items **”PACE4”**, **”Plot PACE4’s calculations”** and **”Converter of FORTRAN-files to C”** have been incorporated to the menu *Utilities* as well.

### 9.4.5. LISE code references

The article “The program LISE: a simulation of fragment separators” (D.Bazin, M.Lewitowicz, O.Sorlin, O.Tarasov) has been accepted in NIM A. The reference is NIMA 41218.

A brief version of this article has been published in the proceedings of the Sixteenth International conference “Cyclotrons and their applications”, 13-17 May 2001, East Lansing, Editor F.Marti, AIP conference proceedings, Vol.60, p.417.

### 9.4.6. Future steps of the LISE code development

1. Fusion reactions (compound cross sections, evaporation, kinematics) and transmission of residual through a fragment separator;
2. Block-structure that the User can combine to form any fragment separator from different sections (dispersive section, velocity filter, electrostatic separators and gas-filled separators ...).

## 10. version N`5.9-10

[www.nsl.msu.edu/lise](http://www.nsl.msu.edu/lise)  
[dnr080.jinr.ru/lise](http://dnr080.jinr.ru/lise)

18-Oct-2001  
Dubna

### *The Nuclear Spectrometry Handbook of J.Kantele*

#### *10.0.1. The Nuclear Spectrometry Handbook of J.Kantele - version 5.10*

The new utility is developed on the basis of **the Handbook of nuclear spectrometry of J.Kantele** (Academic Press Limited, 24-28 Oval Road, London NW1 7DX, Copyright 1995) within the framework of the program LISE (see Fig.557). Nowadays there are transferred from the handbook package in language C++ and are adapted under Windows 46 programs from 60. In a near future the translation of all other programs is planned.

**Spectrometric calculator of J.Kantele**

Menu: ElecStop | Electron | Elem | EtoPos | FermiFun | FermiOld | FK\_Energ | FK\_EnPos | FK\_Momen | GammaFun | GamSpeed | HalfLife | HlonLoss | HlonStop | ICCK | ICCTot | Ion | IgFT\_bet | IgFT\_EcB | LlonLoss | LlonStop | LlonTran | LIStop | MathPack | Metag | Monopole | MulScatt | NegaShap | Omega | OmegaGen | OmegalPF | PosiShap | QuickRan | Qvalues | Reaction | Recoil | Rutherf | Screeneg | ScreenPos | SolidAng | TargHeat | WeighAve | Z\_A\_rel | Z\_eff | Z\_per\_A | Act | AnaState | AttGamma | Barrier | CaptuRat | ChrgStat | Clebsch | CompNucl | Compton | ConverSI | ConvertE | CurveFit | Doppler

**Doppler shift**

photon  
 electron

Energy (keV) = 1000  
Angle (degr) = 45

moving atom/nucleus

Energy (MeV) = 18.6  
Mass number, A = 100  
 v/c = 0.02

Doppler shift, delta E = **14.142** keV  
Shifted energy, E (full) = **1014.142** keV

**Thermal Doppler broadening**

Energy of gamma = 1000 keV  
Mass number, A = 100  
Temperature (C) = 30


delta E = **1.247** eV  
(= Doppler broadening, no shift in energy)

The doppler energy-shift of photons and conversion electrons emitted by moving atoms/nuclei. The recoil effects are ignored, since they are, in practical cases, negligible as compared with the Doppler shifts. The code also calculates the Doppler broadening of a photon line-width due to the thermal motion of the atoms in a source.

About  
List of programs  
Units converter  
LISE  
Exit

Page index: 13

Fig.557. The view of the Nuclear spectrometry handbook

The new utility is available in the menu "Calculations" or the icon  in the toolbar of the LISE code. Also the Handbook can be started from the folder LISE in the START-Programs menu.

#### ***10.0.1.1. About The Handbook***

**Academic Press - Physics:** <http://www.academicpress.com/physics/atomic.html>

**The Handbook of nuclear spectrometry of J.Kantele:** <http://www.apcatalog.com/cgi-bin/AP?ISBN=0123964407&LOCATION=US&FORM=FORM2>

***Juhani Kantele University of Jyväskylä, Finland***

Edited by **Juha Aysto** *University of Jyväskylä, Finland*

##### **10.0.1.1.1. General description**

The **Handbook of Nuclear Spectrometry** distills material from many disparate sources and brings widely applicable nuclear spectrometry information into an easily accessible form. The **Handbook** is divided into two parts. **Part I** consists of the text which covers such fundamental topics as atomic phenomena, interaction of radiation with matter, and beta-ray, conversion-electron, and gamma-ray spectrometry. To complement the text, **Part II** is a series of practical computer programs provided on an accompanying diskette. **Part II** is written in Microsoft BASICA and provides the user with a way to modify programs to meet their own specific needs. **The Handbook** includes formulae, tables, graphs, and extensive references which make it an invaluable resource for post-graduate nuclear science students, as well as nuclear physicists and chemists.

##### **10.0.1.1.2. Key Features**

This text includes

- Examples, to give an order-of-magnitude picture of phenomena
- Graphs, for obtaining a quick approximation of a quantity
- References, to **Part II** (the accompanying computer program) to aid in the use of the codes found in the text
- Comments, to clarify important points
- Simple rules of thumb
- References, to works containing more-detailed information on a given subject

##### **10.0.1.1.3. Contents:**

**Part I: Introduction. Fundamental Physical Constants. Elements, Isotopes, and Materials:** Elements, Isotopes, Masses, Mass Tables and Q Values. Electron Binding Energies and Atomic Level Widths. Phenomena within the Atomic Electron Shells. Properties of Some Frequently Used Composite Materials. Neutron Activation Sensitivities of Elements. **Irradiation Yields and Decaying Sources. Beta Decay:** Basic Phenomena and Energy Relations. Conservation Laws and Selection Rules. Shapes and Intensities of Continuous Beta Spectra. Electron Capture, Capture Ratios and EC/Positron Competition.  $\log_{10} ft$  Values. Higher-Order Phenomena. **Decay of Excited States:** Gamma-ray Emission and E0 Transitions. Internal Conversion (IC). Internal Pair Formation (IPF). **Interaction of Radiation with Matter.** Gamma- and X-ray Interactions. Electron Interactions. Interaction of Swift Ions with Matter. Production of X-rays

and Delta-rays (Electrons). Neutron Interaction with Matter: Shielding. **Radiation Detection.** Some General Concepts. Special Detector/Spectrometer Types. Radiation Damage of Detectors and Materials. Statistics in Data Collection. Coincidence Measurements. **Brief Review of Methods of Gamma-ray Spectrometry.** Types of Gamma-ray Spectrometers. Comparison of Efficiencies of NaI(Tl) and Germanium Detectors. Background Gamma-rays. **Beta-ray and Conversion-electron Spectrometry:** Electron in Electric and Magnetic Fields. General Properties of Magnetic Beta-ray Spectrometers. Magnetic Electron Transporters in In-beam Spectrometry. **Calibration Standards** Gamma-ray Energy and Intensity Standards. Gamma-ray and Electron Energy and Intensity Standards. Alpha Decay Energy Standards. Absolute Standards and Determination of Their Strengths. **Nuclear Reaction Experiments.** Energetics of Nuclear Reactions. Some Selected Nuclear Reactions. Miscellaneous Procedures in the Use of an Accelerator. Lifetime Measurements. Recoil and Doppler Effects in Nuclear Spectrometry. **Some Special Methods--Brief Description and References. Systematics of Nuclear Data--List of References. Key Articles on Selected Topics of Nuclear Structure. Appendix: Items for a Computer-aided Experiment Logbook. References.**

### 10.0.1.2. List of programs

N	Program	Description
1	<b>Act</b>	Production of Radioactive Nuclei
2	<b>AnaState</b>	Coulomb Displacement and Excitation Energies
3	<b>AttGamma</b>	Attenuation of Photon Beams
4	<b>AttQuick</b>	Simple Formula for Photon Half-thickness Estimate
5	<b>Barrier</b>	Coulomb and Interaction Barrier Heights for Heavy Ions
6	<b>CaptuRat</b>	Capture Ratios in Electron-capture Decay
7	<b>ChrgStat</b>	Average Equilibrium Charge-state of Swift Heavy Ions in Matter
8	<b>Clebsch</b>	Clebsch-Gordan (Vector-coupling) Coefficients
9	<b>CompNucl</b>	Velocity, Kinetic and Excitation Energy of a Compound Nucleus
10	<b>Compton</b>	Parameters in Compton Scattering
11	<b>ConverSI</b>	Conversion of 10 Quantities to Different Units
12	<b>ConvertE</b>	Flexible Conversion of Units of Electron Energy and Momentum
13	<b>CurveFit</b>	Fitting of Several Types of Curves
14	<b>Doppler</b>	Doppler Shifts and Thermal Doppler Broadening
15	<b>ElecStop</b>	Ranges and Stopping Powers for Monokinetic Electrons
16	<b>Electron</b>	Speed, Bp and Ranges of Electrons
17	<b>Elem</b>	Electron Binding and X-ray Energies
18	<b>EtoPos</b>	Electron-capture to Positron-emission Ratios
19	<b>FermiFun</b>	"Proper" Fermi (Coulomb) Functions for $\beta^-$ and $\beta^+$ Decays
20	<b>FermiOld</b>	Traditional Fermi (Coulomb) Functions for $\beta^-$ and $\beta^+$ Decays
21	<b>FK-Energ</b>	Fermi-Kurie Analysis of Electron Energy Spectrum
22	<b>FK-EnPos</b>	Fermi-Kurie Analysis of Positron Energy Spectrum
23	<b>FK-Momen</b>	Fermi-Kurie Analysis of Electron Momentum Spectrum
24	<b>GammaFun</b>	Calculation of Modulus of Gamma Function

25	<b>GamSpeed</b>	Weisskopf Estimates of Gamma-ray Half-lives and Global Predictions for $B(E2; \uparrow)$ for the First $2^+$ State
26	<b>HalfLife</b>	Half-life of Single-component Decay
27	<b>HIonLoss</b>	Energy Loss of Heavy Ions in Matter Layer
28	<b>HIonStop</b>	Ranges and Stopping Powers of Heavy Ions
29	<b>ICCK</b>	Internal-conversion Coefficients for the $K$ Shell
30	<b>ICCTot</b>	Total Internal-conversion Coefficients
31	<b>Ion</b>	Ion Velocities and Magnetic Rigidities
32	<b>lgFT-bet</b>	Determination of $\log ft$ Values in $\beta^-$ Decay
33	<b>lgFT-EcB</b>	Calculation of $\log ft$ Values in Electron Capture and $\beta^-$ Decay
34	<b>LIonLoss</b>	Energy Loss of Light Ions (H, He) in Matter Layer
35	<b>LIonStop</b>	Ranges and Stopping Powers of H and He Ions
36	<b>LionTran</b>	Residual and Deposited Energies in Light-ion Transmission
37	<b>LIStop</b>	Approximate Light-ion Ranges and Stopping Powers
38	<b>MathPack</b>	Simple Mathematics Programs and Formulae
39	<b>Matters</b>	Quick Reference Table on Properties of Some Materials
40	<b>Metag</b>	Fissility and SF Half-lives of Shape Isomers
41	<b>Monopole</b>	$X(E0/E2)$ , $B(E2)$ and $\rho^2$ in E0/E2 Transitions
42	<b>MulScatt</b>	Rms Angle for Multiple Scattering of Charged Particles
43	<b>NegaShap</b>	Shapes of Allowed $\beta^-$ Energy Spectra
44	<b>Omega</b>	Electronic Factors $\Omega$ for E0 Transitions
45	<b>OmegaGen</b>	General, Simplified $\Omega_{kl}$ Calculations
46	<b>OmegaIPF</b>	Electronic Factors $\Omega_{IPF}$ for E0 Transitions
47	<b>PosiShap</b>	Shapes of Allowed Positron Energy Spectra
48	<b>QuickRan</b>	Simple Program for Electron Ranges $R(ex)$ and $R(99)$
49	<b>Qvalues</b>	Nuclear Reaction $Q$ Value Calculation
50	<b>Reaction</b>	Kinematics of Simple Nuclear Reactions
51	<b>Recoil</b>	Recoil Effects in Gamma-, Beta-, Electron and Alpha-emission and in Spontaneous Fission
52	<b>Rutherf</b>	Rutherford Scattering Cross-sections
53	<b>Screeneg</b>	Screening Correction for Electron Fermi Functions
54	<b>SreenPos</b>	Screening Correction for Positron Fermi Functions
55	<b>SolidAng</b>	Solid-Angle Calculation in Simple Cases
56	<b>TargHeat</b>	Beam Heating and Temperature of Self-supporting Foil
57	<b>WeighAve</b>	Calculation of Weighted Averages
58	<b>Z-A-rel</b>	Atomic Weight of Element $Z$
59	<b>Z-eff</b>	Effective $Z$ Values of Compounds in Electron Stopping
60	<b>Z-per-A</b>	Most Stable $Z$ and Ratio $Z/A$ for Isobar $A$



### 10.0.2. MSP144 focal plane detector

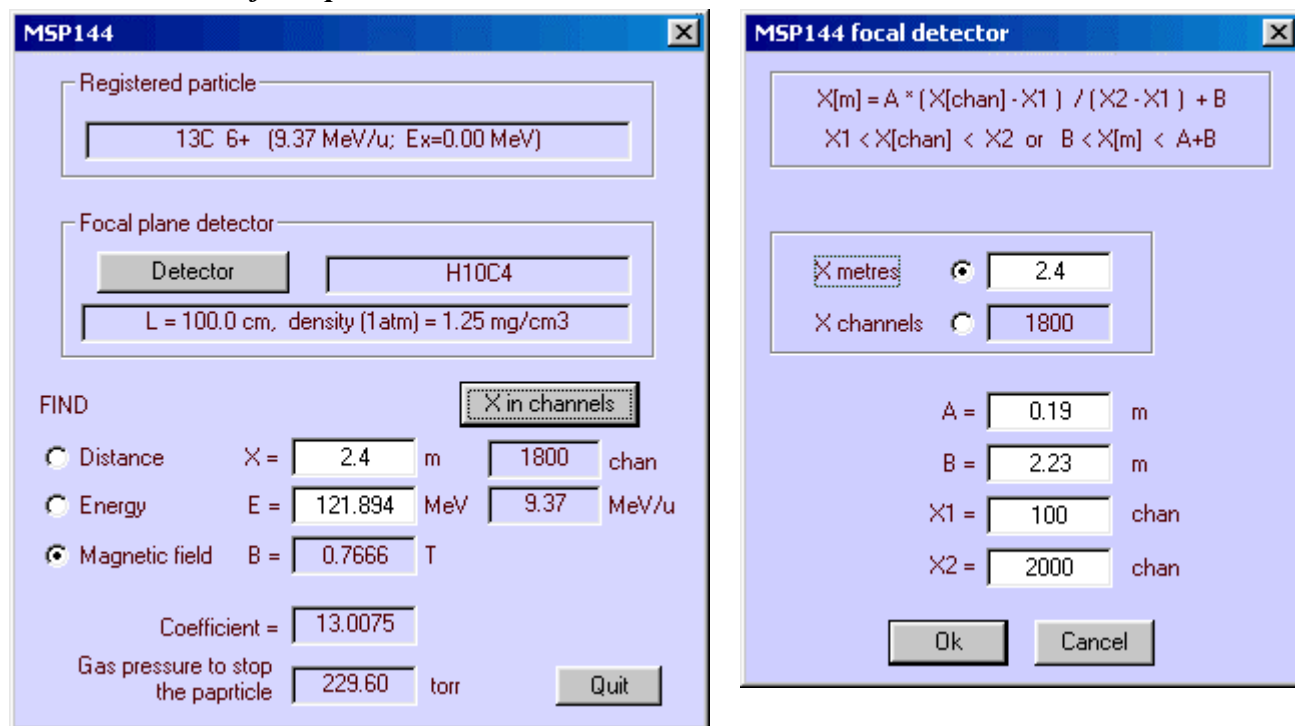


Fig.558. The MSP144 focal plane detector dialogs.

Calculations of settings of the MSP144 focal plane detector are available via the Kinematics calculator clicking the button "MSP144" (see Fig.558). All settings of the focal plane detector (Gas density, gas material, detector length, calibrations) are saved only in the file "lise.ini".

### 10.0.3. Chemical properties of element

The user gets a window of statistics clicking by the right key of the mouse on the isotope rectangle on the table of the nuclides. Pressing on the button "Chemistry" in the statistics window, the user will get the information (see Fig.560) on chemical properties of the given element from the site <http://environmentalchemistry.com/yogi/periodic>.

### 10.0.4. Units Converter – version 5.9

The "Units Converter" calculates the values of the following quantities in several different units: **Length, Area, Volume, Mass, Pressure, Energy, Power, Time, Angle, Temperature** (see Fig.559).

The program is developed on the basis of **the Handbook**

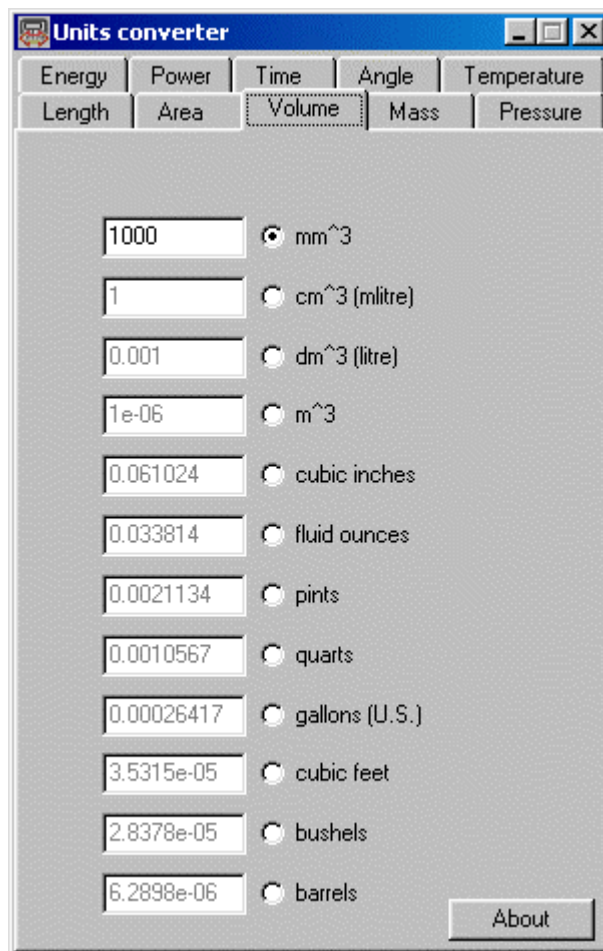

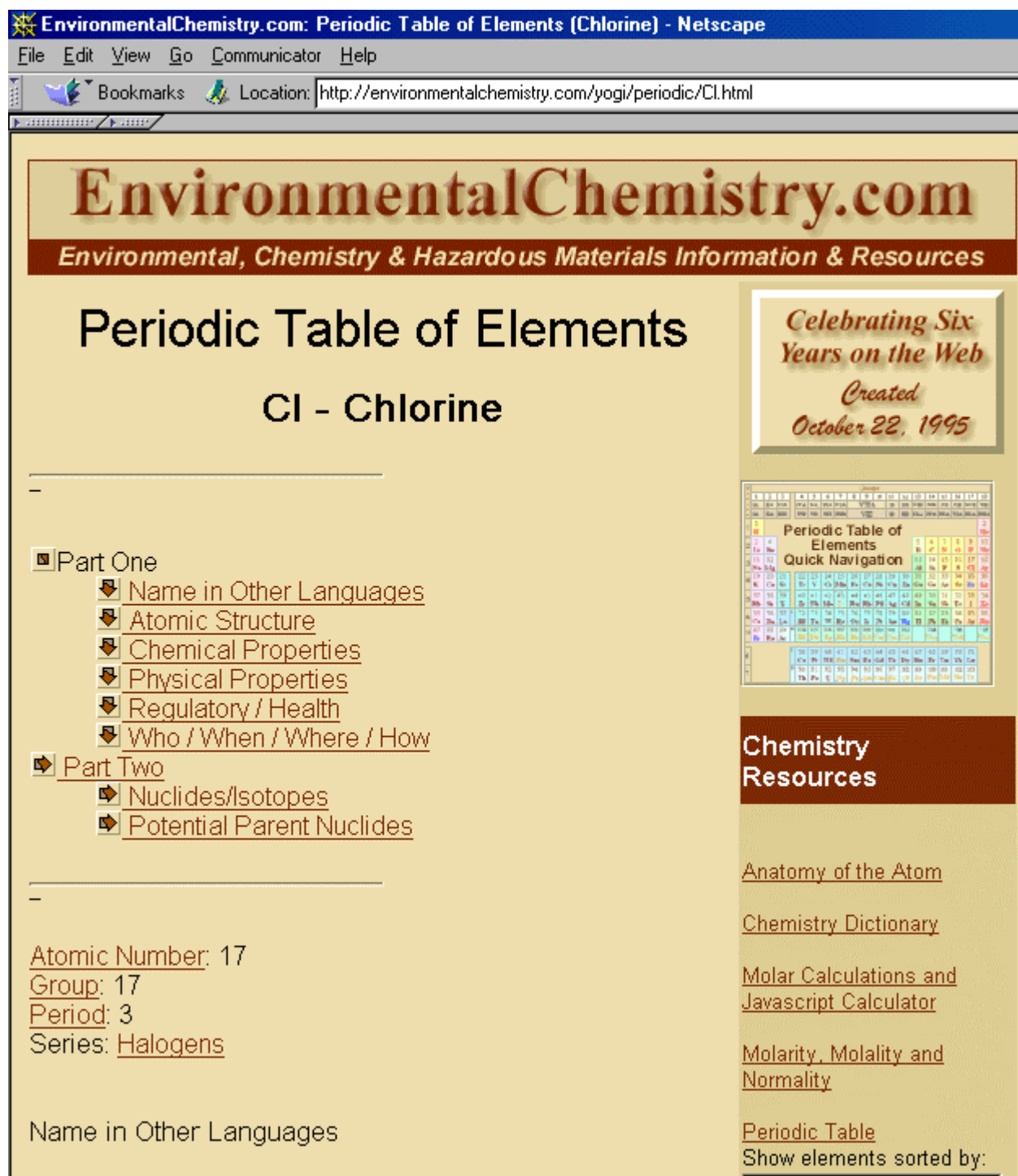


Fig.559. Units converter.

**of nuclear spectrometry of J.Kantele** (Academic Press Limited , 24-28 Oval Road, London NW1 7DX, Copyright 1995 ) within the framework of the program LISE.

The new utility is available in the menu "Calculations" or the icon  in the toolbar of the LISE code.

*The bug in Kinematics calculator has been checked. (15-SEP-2001)*



**EnvironmentalChemistry.com**  
*Environmental, Chemistry & Hazardous Materials Information & Resources*

## Periodic Table of Elements

### Cl - Chlorine

Part One

- [Name in Other Languages](#)
- [Atomic Structure](#)
- [Chemical Properties](#)
- [Physical Properties](#)
- [Regulatory / Health](#)
- [Who / When / Where / How](#)

Part Two

- [Nuclides/Isotopes](#)
- [Potential Parent Nuclides](#)

Atomic Number: 17  
Group: 17  
Period: 3  
Series: [Halogens](#)

Name in Other Languages

**Chemistry Resources**

- [Anatomy of the Atom](#)
- [Chemistry Dictionary](#)
- [Molar Calculations and Javascript Calculator](#)
- [Molarity, Molality and Normality](#)
- [Periodic Table](#)
- Show elements sorted by:

*Celebrating Six Years on the Web*  
*Created October 22, 1995*

Periodic Table of Elements Quick Navigation

**Fig.560.** Chemical properties of element via the site <http://environmentalchemistry.com/yogi/periodic>.

# 11. version N`5.8

## 11.1. Auto mode for the abrasion-ablation model

As it was shown in version 5.4 there are various recommended meanings of Abrasion-Ablation model options depending on the prefragment mass. However it is inconvenient to enter values each time when changing the projectile-target combination. In this connection, in the new version the opportunity of automatic input of options was entered depending on the prefragment mass. An opportunity of manual input options is kept, too. The dialog “Settings of prefragment” is shown in Fig.561, where the choice of auto or manual modes is outlined by a red rectangle. The tunneling, choice of state density, unbound nuclei and geometrical corrections blocks are not accessible in the case of the automatic mode. The program automatically puts values defined by the user in the dialog “Settings of AUTO mode” (see Fig.562). The parameter  $dR$  has been fitted by a parabolic dependence on the value  $(A_{pf})^{1/3}$ , so for mass  $A=200$  the value  $dR$  is equal to  $6\text{ fm}$ , for mass  $A=2$  accordingly it is equal to  $0\text{ fm}$  (two points  $A=40$  and  $58$  have been used also, see the documentation of version 5.4).

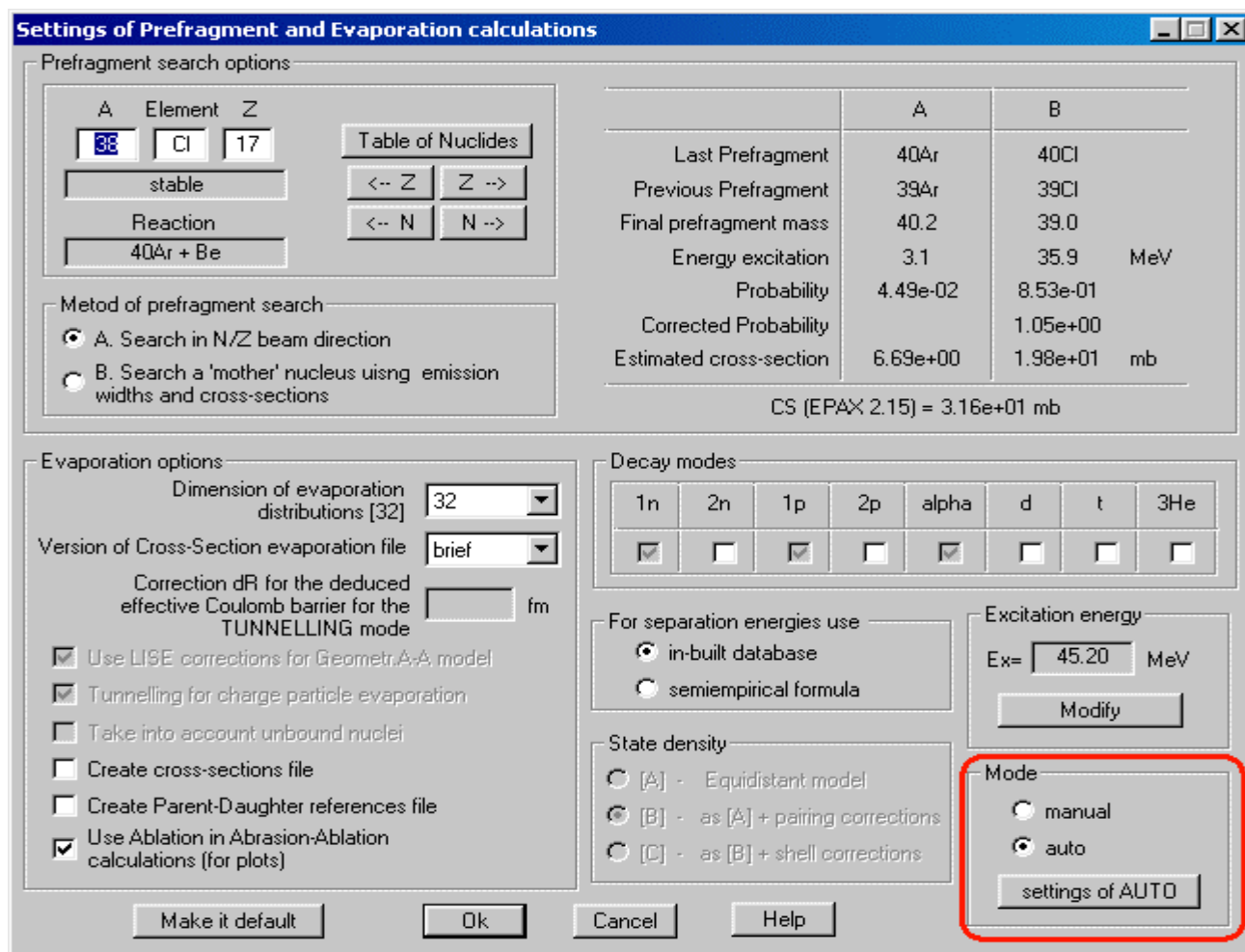


Fig.561. The dialog “Settings of Prefragment and Evaporation calculations”.

Further the improvement of automatic adjustments for excitation energy and state density is supposed.

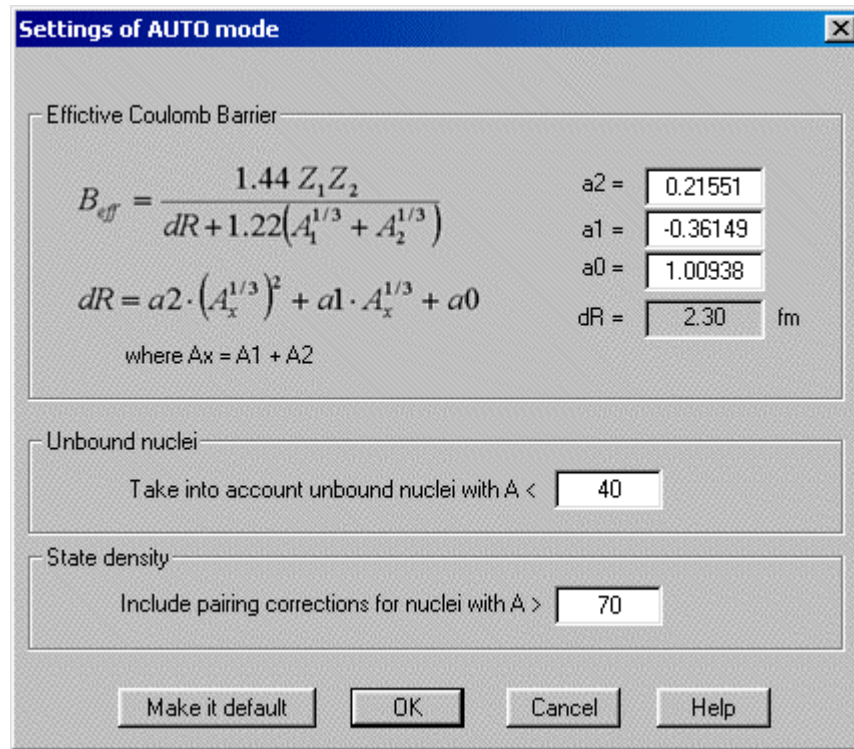


Fig.562. The new dialog "Setting of AUTO mode for evaporation options".

## 11.2. On-line LISE analysis of experimental plots

Into the concept of the program LISE development enters not only input of new tools (new models of reaction mechanisms, etc.) able to help physicists in the prediction of products' outputs, but also further development of the mechanism of experimental data analysis. In the new version the apparatus for work with experimental spectra obtained by the program BI was developed. The analysis of experimental two-dimensional peaks can be divided into 4 stages:

**The first stage** is reading an experimental spectrum by the program BI. An example of such a spectrum is shown in Fig.564-1. This spectrum is obtained with the spectrometer A1900 (NSCL MSU) in the reaction  $^{18}\text{O}$  (120AMeV) + Be (this experiment is discussed in more detail in the chapter "Version 5.5").

**The second stage** is the determination of the program-BI parameters for the analysis of the initial spectrum, and the analysis itself. The program creates a text file with the found peaks and an output spectrum with the found peaks in the format of the initial spectrum (Fig.564-2).

**The third stage** is the new stage, which helps the user to avoid unnecessary peaks and also to initialize "good" peaks. After search of peaks by clicking on the button "Plot" in the dialog "BI" the user gets an output spectrum (Fig.564-3), where the determined peaks are shown by ellipses

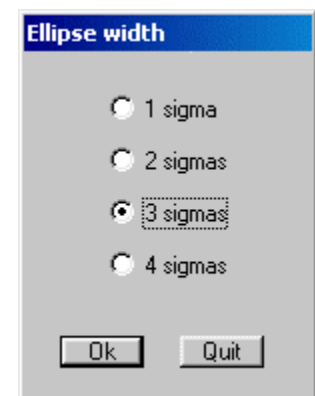

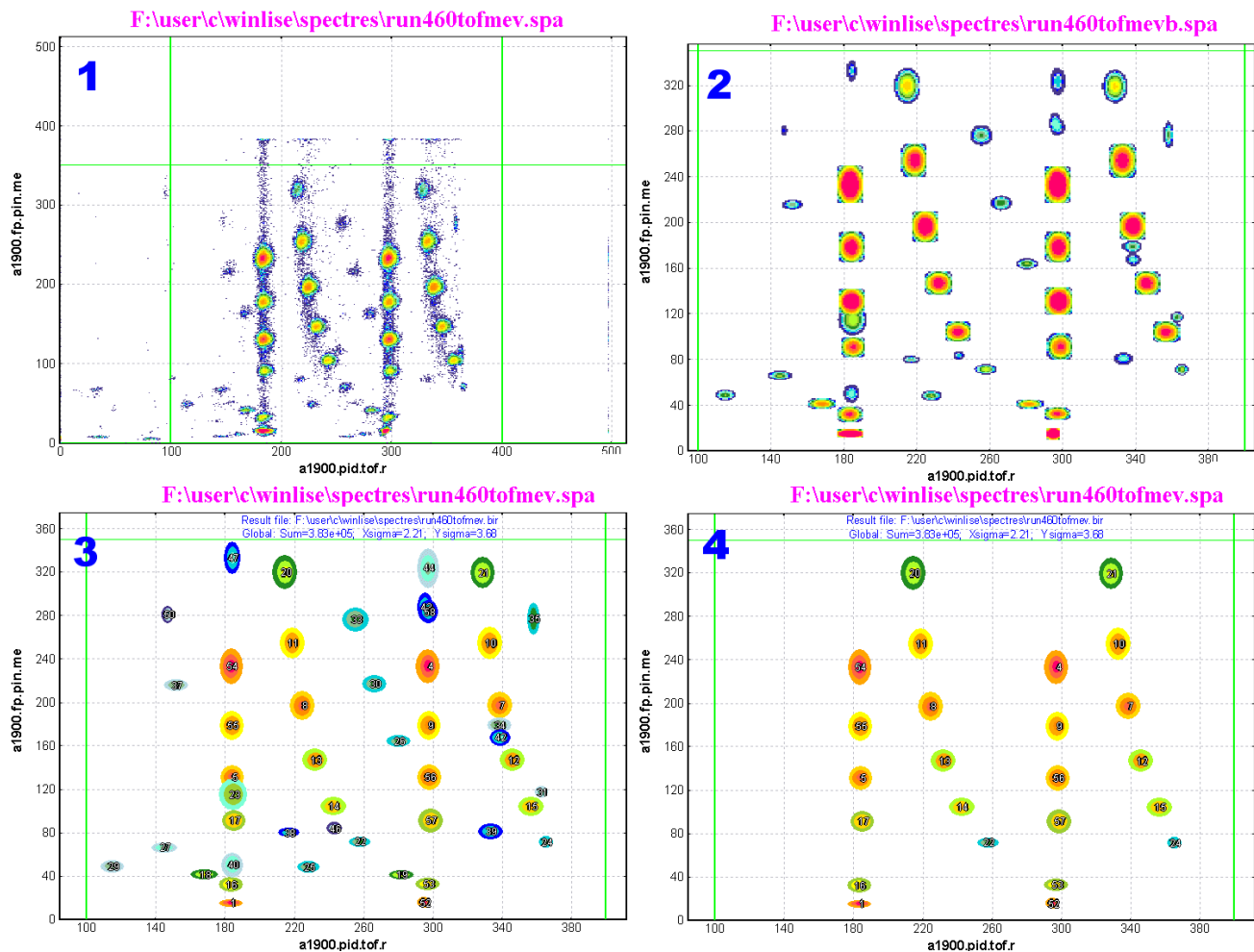



Fig.563. The dialog of ellipse size.

with serial numbers. The semi-axes of ellipses by default are equal to three standard deviations ( $\sigma$ ) found by the program BI. However, the user can redefine their size pressing the icon  (see Fig.563). The double clicking of the right button of the mouse on a peak allows editing this peak. The user can switch off the peak using the checkbox “Available” and/or give a name (see Fig.565). The new spectrum obtained after selection from the previous spectrum (Fig.564-3) is shown in Fig.564-4.



*Fig.564. Analysis of an experimental two-dimensional spectrum in the program.*

**The fourth stage** is recording selected peaks on a disk (clicking the icon ) and reading them by another program (for example MS Excel).

Within 10 minutes the user gets the table with found selected peaks with the characteristics (average values, standard deviations, area) that can be used for the further analysis (cross sections, momentum distributions, calibrations, etc.).

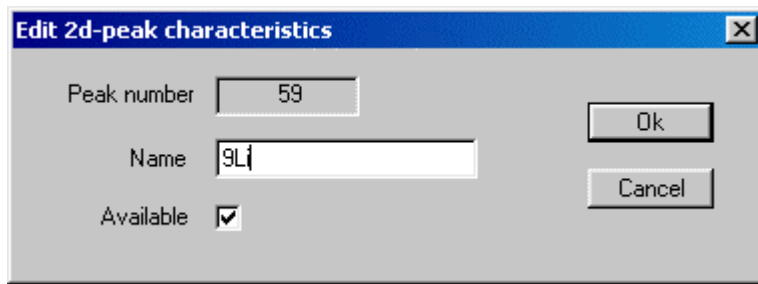


Fig.565. The dialog of editing peak characteristics.

### 11.3. Calculation of the Wedge thickness

The opportunity of calculation of a material thickness appropriate for an initial kinetic energy and an energy after this material was specially entered in the Physical Calculator earlier. However, as experience has shown, some users have difficulties when calculating the wedge thickness for known input and output energies. In this connection, the opportunity to calculate the wedge thickness for the defined fragment proceeding from the values of the magnetic rigidities  $B\rho_1$  and  $B\rho_2$  has been created in the dialog “Degrader in Dispersive Focal Plane”.

To calculate the wedge thickness it is necessary beforehand to input the values of the magnetic rigidities (items 1 and 2 in Fig.566) and to press afterwards on the key “Calculate thickness” in the dialog “Degrader in Dispersive Focal Plane” (item 3 in Fig.566).

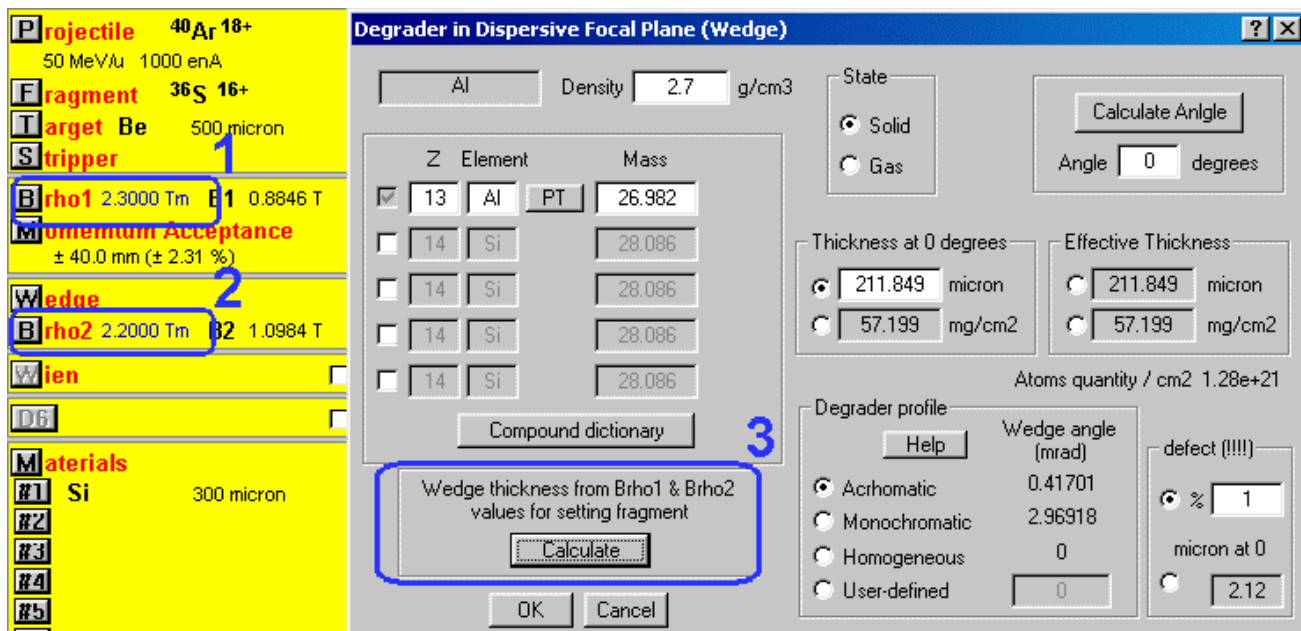


Fig.566. Calculation of the wedge thickness for the defined fragment from the magnetic rigidities  $B\rho_1$  and  $B\rho_2$ .

## 12. LISE & Excel - version 5.7

The opportunity of using the LISE huge computing luggage by other programs has appeared in the new version of the LISE code. Some subroutines were replaced from the module LISE.EXE in separate libraries (\*.DLL), and can be executed from these libraries by other programs. The modules of calculation of energy losses in matter, range in materials, stragglings of range and energy losses, and also empirical

The screenshot shows the Microsoft Excel interface for the 'lise.xls' file. The spreadsheet is organized into several functional areas:

- Energy loss calculation method:** Includes buttons for '0 - Hubert', '1 - Ziegler', and '2 - ATIMA'. The current state is set to 1.
- Charge State calculation methods:** Includes buttons for '0 - Winder', '1 - Leon', and '2 - Shima'. The current state is set to 1.
- Energy Stragglings calculation methods:** Includes buttons for '0 - Anne' and '1 - ATIMA'. The current state is set to 1.
- names:** A box containing parameters: Zparticle=18, Aparticle=40, Ztarget=73, Atarget=181, Energy=35 (MeV/u), Thickness=10 (mg/cm2), and ZmQ=0.
- Control:** 'Init' and 'Hide' buttons are located below the calculation sections.
- Table:** A table with columns: function, return, parameters, and example. It lists various calculation functions and their corresponding return values and parameters.

function	return	parameters	example
Energy Loss In Matter	Rest energy in MeV/u	Zparticle, Aparticle Energy [MeV/u] Ztarget Thickness [mg/cm2]	34.36 MeV/u
Range In Matter	Range in mg/cm2	Zparticle, Aparticle Energy [MeV/u] Ztarget	357.08 mg/cm2
StragglingsEnergy	energy stragglings in material [MeV/u]	Zparticle, Aparticle Energy [MeV/u] Ztarget Thickness [mg/cm2]	0.012 MeV/u
StragglingsRange	range stragglings in material [mg/cm2]	Zparticle, Aparticle Energy [MeV/u] Ztarget	0.809 mg/cm2
Charge State	%	Energy [MeV/u] Zparticle, Ztarget Zpart-Qpart	44.6 %
Mass	get element mass	Z	39.948
Show_Z	Element Name -> Z (int)	Element Name	18
Show_Element	Rest energy in MeV/u	Zparticle, Aparticle Energy [MeV/u] Ztarget Thickness [mg/cm2]	Ar
Mg2Mkm	mg/cm2 -> microns	Thickness [mg/cm2] Ztarget	6.024 micron
Mkm2Mg	microns -> mg/cm2	Thickness [micron] Ztarget	10 mg/cm2

Fig.567. The file "LISE.xls".

parameterization of cross sections (EPAX 2.15) can now be used for calculations in sheets of MS Excel. It is necessary to notice, that such opportunity exists only for the versions of the program LISE installed in a standard way, instead of taken from the “open version” directory. New libraries will be placed by the install program in the directory windows/system (OS Windows 98/Me) or windows/system32 (OS Windows NT/2000) in the case of a standard way installation. In the program LISE package there is the file LISE.XLS (version MS Excel 8 or higher), which is placed in the root LISE directory and for which the icon from the starting menu of the program LISE is created. This file contains connections (via Visual Basic) with libraries of the program LISE (see Fig.567). Also this file contains one sheet with examples of all functions available in these libraries. At loading the given file the window will appear with a question: to include/avoid macro-functions, on what you should include macros, if you want to use the LISE luggage.

If you want to use functions of the program LISE in other Excel files, the file LISE.XLS should be loaded previously. Then the user should execute the Excel command “Insert function” (shift F3), and choose a function necessary for you from the list of functions determined by the user (for example “lise.xls!EnergyLossInMatter”).

With use of these libraries the user can create sheets with various amount of detectors (reminder: in the program the maximum quantity of detectors is equal to 7), to use the tables for calibrations, etc., using thus all the power of Excel. An example of such a file is found at the address: [http://dnr080.jinr.ru/lise/-5\\_8/lise\\_example.xls](http://dnr080.jinr.ru/lise/-5_8/lise_example.xls). Only do not forget to earlier load the file LISE.XLS.



## 13. LISE & Internet - version 5.6

The program has received in the new version an access to databases through the Internet (databases of Isomers and TOI), and also utilities of automatic informing of the new version of the program and connection with sites of the LISE program.

### 13.1. Access to databases

The LISE program has the built-in database (Audi & Wapstra 95) of nuclide characteristics (separation energies, half-lives etc.). However the user frequently requires more extensive information during the preparation of experiment and its realization. Supplement of the program LISE by other databases can essentially change the size of the program. Thus as the majority of users of the program have access to the Internet, it was decided to approach the appropriate databases directly by the program.

#### 13.1.1. Isomer database

Nuclei having isomeric states are marked on the table of nuclides in the program by green rectangle in the left bottom corner (see Fig.568, item A). The information about isomeric states is taken from the database located on the site of the LISE spectrometer ([www.ganil.fr/LISE](http://www.ganil.fr/LISE)). This database has been created by Dr.Jean-Michel Dugas. The user gets a window of statistics clicking by the right key of the mouse on the isotope rectangle on the table of the nuclides. If the isotope has an isomeric state, in this window the button “Isomer” (see Fig.568, item B) will appear. Pressing this button, the information from the GANIL site will be loaded into default browser (Fig.569). The information about isomers is accessible for isotopes with mass less than 84.

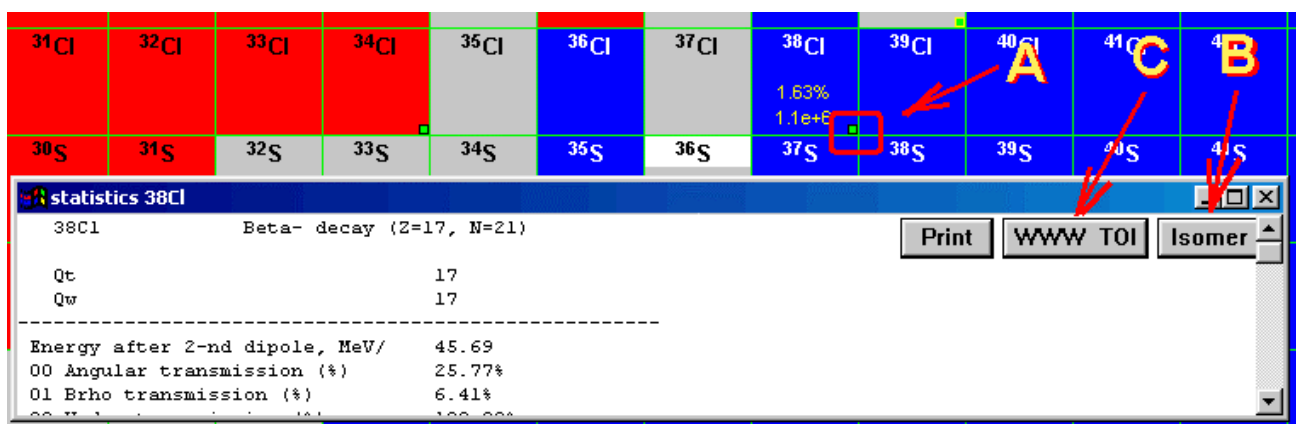


Fig.568. The window of transmission characteristics of  $^{38}\text{Cl}$ .

#### 13.1.2. TOI

Pressing on the button “WWW TOI” (see Fig.568, item C) in the statistics window, the user will get the information on the given isotope from the database TOI located on the site in Sweden (see Fig.570).

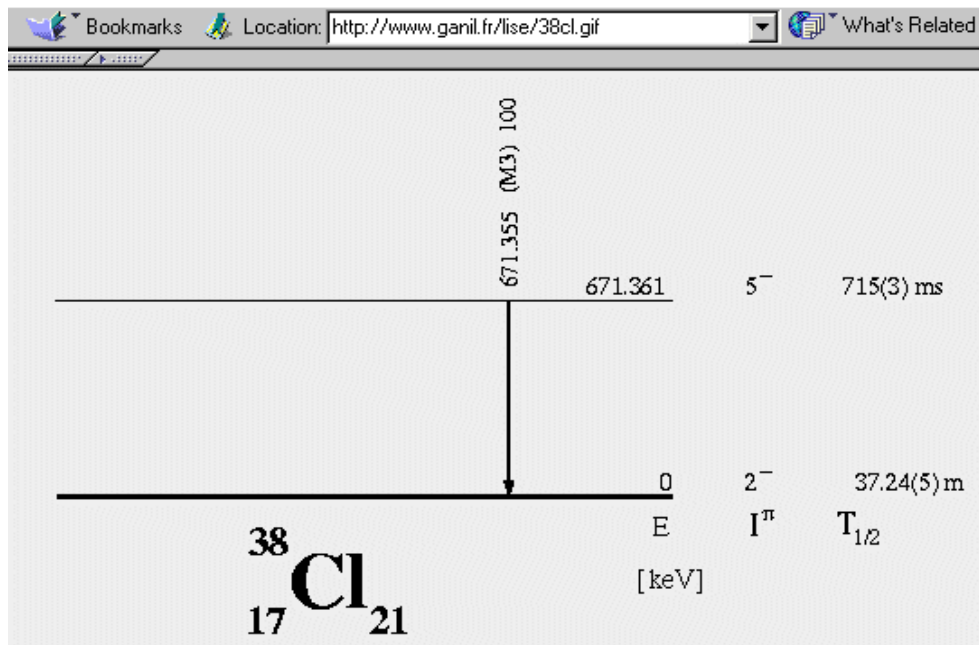


Fig.569. Scheme of  $^{38}\text{Cl}$  isomeric decay from the LISE site (France).

WWW Table of Radioactive Isotopes

$^{38}_{17}\text{Cl}_{21}$

<b>Half life:</b>	37.24 m 5
<b>J<math>\pi</math>:</b>	2-
<b>S<sub>n</sub> (keV):</b>	6107.78 10
<b>S<sub>p</sub> (keV):</b>	10190.7 3
<b>Prod. mode:</b>	Fast neutron activation Thermal neutron activation
<b>ENSDF citation:</b>	NP A521,1 (1990)
<b>Literature cut-off date:</b>	1-Jun-1990
<b>Author(s):</b>	P.M. Endt
<b>References since cut-off:</b>	<a href="#">38Cl decay from 1990-98 (NSR)</a>

**Decay properties:**

Mode	Branching (%)	Q-value (keV)	References
$\beta^-$	100	4916.8 5	<a href="#">86Wa22</a> <a href="#">90En08</a>

**Data sets:**

Mode	Data set name	Display data
------	---------------	--------------

Fig.570. Information about the isotope  $^{38}\text{Cl}$  from the TOI database located in Sweden.

### 13.2. Check to the new version

An access to the Internet utilities of the program LISE is realized through the menu “Help” (see Fig.571). The user can in the dialog “Check to the new version of the code” (Fig.572):

- choose a web-site to check presence of the new version, and also to see the documentation about changes of the program;
- choose a ftp-server to download the new version of the program;
- establish a time interval when the program automatically checks presence of the new version;
- see documentation about changes of the program.

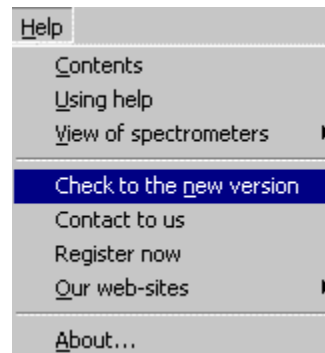


Fig.571. The menu “Help”: access to internet utilities.

At loading, the program automatically checks a date of check, if the date has already expired, the dialog “Check to the new version of the code” is automatically loaded. The dialogue is not closed at detection of the new version and there is a message that there is a new version, in case of absence of the new version the dialog is automatically closed.

Unfortunately one issue has not been yet solved - at which the program undergoes a crash. It is connected with the absence of access to the Internet when the code checks the new version. The Internet access block was realized with the compiler Builder 5.0, whereas the program is compiled by Borland 5.02 OWL. But in any case the program will replace the date of check and at the subsequent start the program will be loaded without automatic check to the new version.

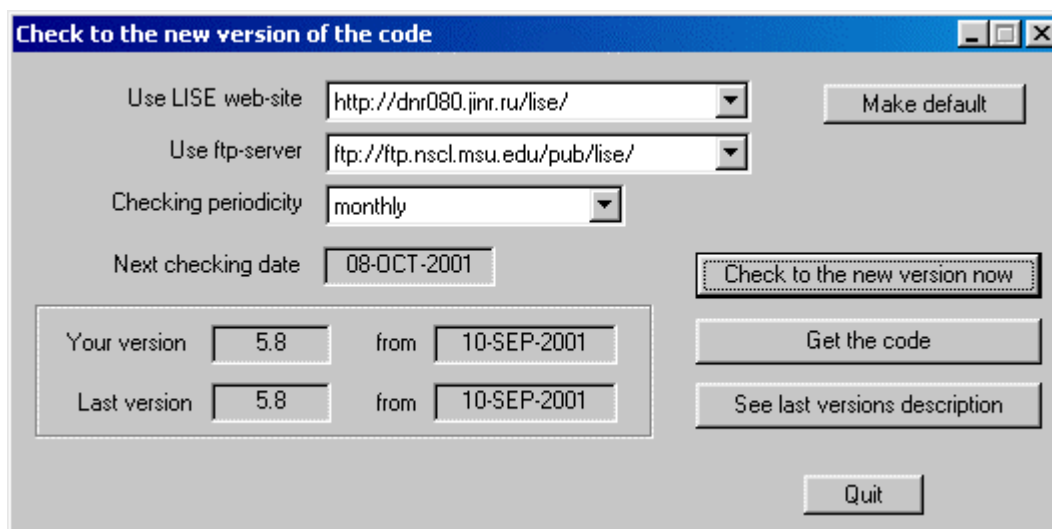


Fig.572. The dialog “Check to the new version of the code”.

### 13.3. Mail and registration from the code

From the menu “Help” the user may (see Fig.571)

- Send an e-mail with remarks or problems to the authors of the code;
- Register on the LISE sites to get information about new versions;
- Visit the LISE sites at East Lansing or Dubna.

## 14. version N`5.5

### 14.1. Brho Scanning Plot

A new utility to help the experimenter in the analysis of the experimental information was developed in the new version. Frequently in experiments there is a necessity of scanning of reaction-products outputs depending on magnetic rigidity. The given procedure will be carried out for study of momentum distribution and production cross sections, and also for obtaining spectrometer settings for an optimum output of the fragment of interest (maximal output, best relation of setting fragment to background, etc.). Also the scanning represents the large interest from the point of view of comparison of the calculations done within the LISE program with the experimental data, which in turn allows modifying the parameters of models in the program for the best agreement with experiment.

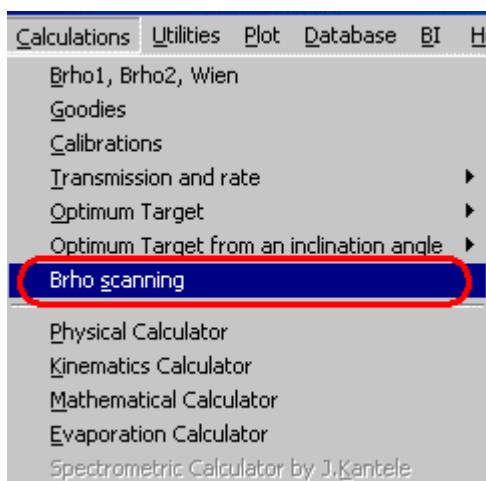



Fig.573. The menu Calculations and new utility "Brho Scanning"



Fig.574. The dialog "Brho Scanning".

The user has access to the utility "Brho scanning" through the menu "Calculation" (see Fig.573). A fragment of interest and range of scanning are determined in the dialog "Brho scanning" (see Fig.574). The number of points for scanning is the same as for the optimum thickness target calculation plot and can be changed through the dialog "Preferences". After creation of the "Brho scanning" plot (Fig.576), the calculated distribution can be kept in a file  and is used for the further analysis.

#### 14.1.1. Comparison of calculations with experimental data

New possibilities of the code: *Brho scanning* and *On-line LISE analysis of experimental plots* (version 5.8) were used recently in the analysis of experimental data obtained in the experiment at NSCL with the spectrometer A1900 using the reaction  $^{18}\text{O}(120 \text{ AMeV})+\text{Be}(1166 \text{ mg/cm}^2)$ . Experimental spectra were analyzed by the program BI, after some unnecessary peaks were eliminated in the LISE program, and the

resulting files were transmitted to Excel and later after an analysis to Origin. 18 brho scanning files for different momentum distribution models and for different setting fragments were created by the LISE code and transmitted to Origin, too. You may see the result plots in Fig.575. Using the new utilities accelerates the analysis by a factor of ten! The complete analysis took less than two working days of one physicist!!!

$^{18}\text{O}$  (120 AMeV, 1pna) + Be (1166 mg/cm<sup>2</sup>)

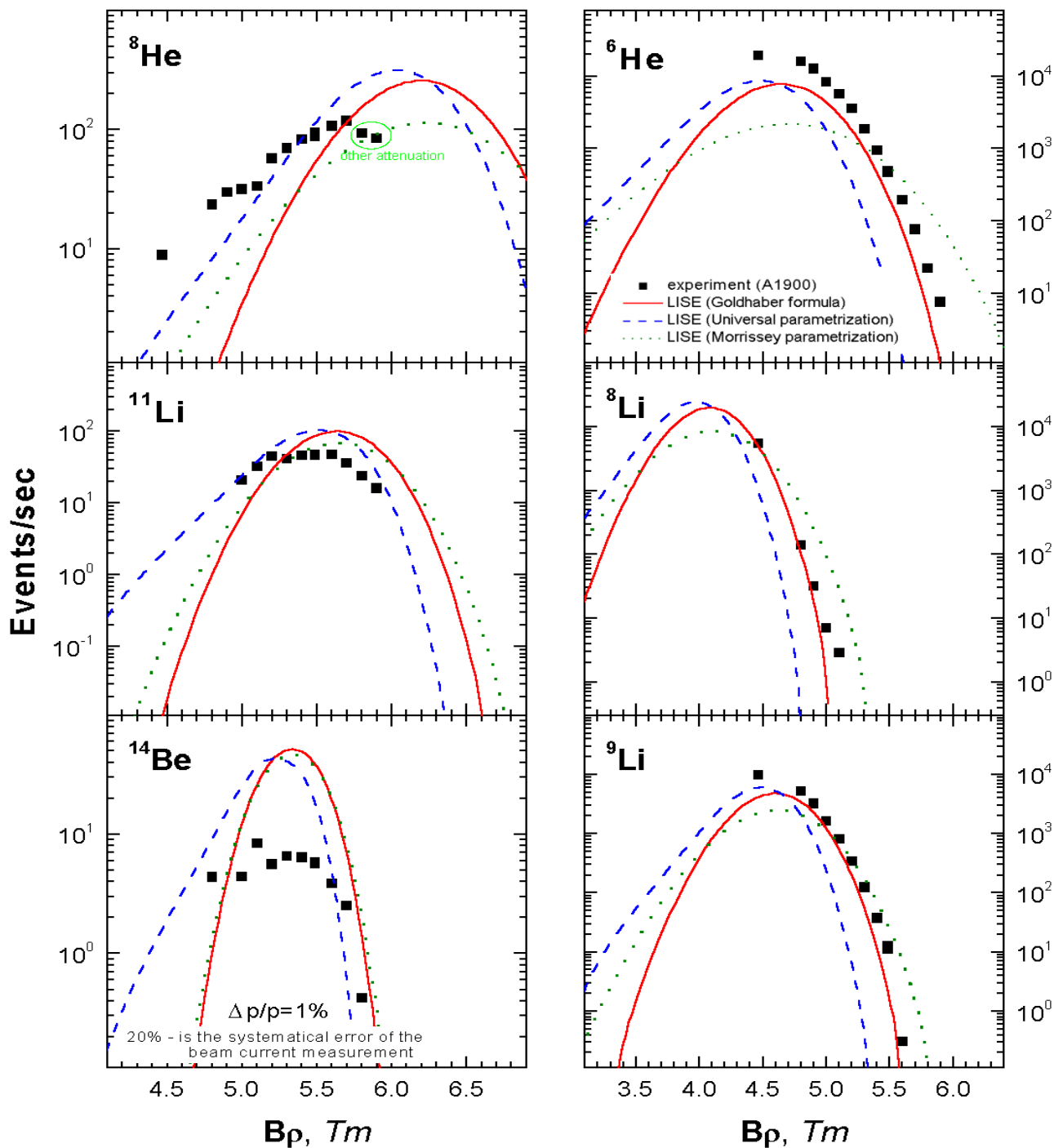
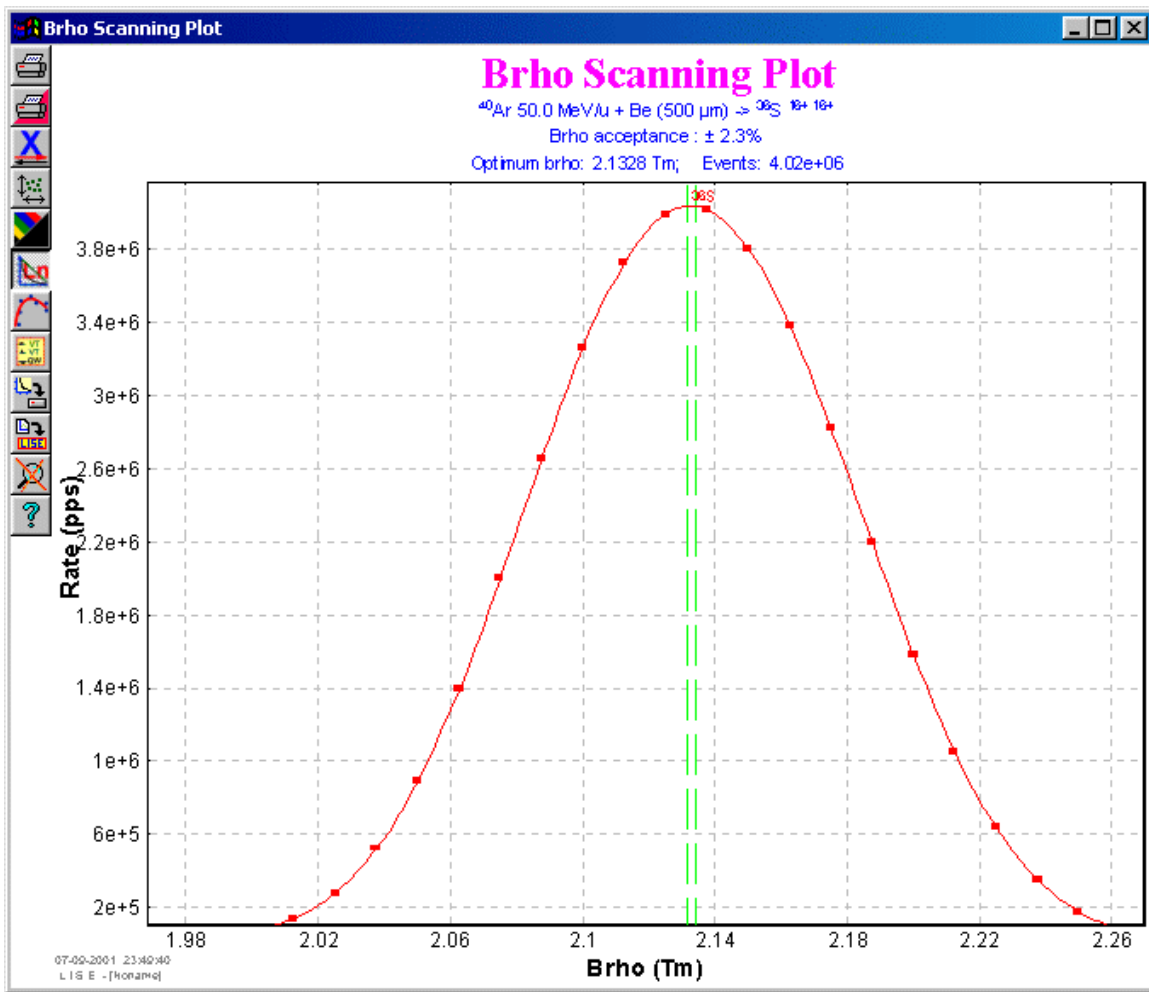


Fig.575. Brho scanning plots for isotopes <sup>6,8</sup>He, <sup>8,9,11</sup>Li, <sup>14</sup>Be in the reaction <sup>18</sup>O(120 AMeV)+Be(1166 mg/cm<sup>2</sup>).



**Fig.576.** The Brho scanning plot for the selected fragment  $^{36}\text{S}$ .

## 14.2. Options files

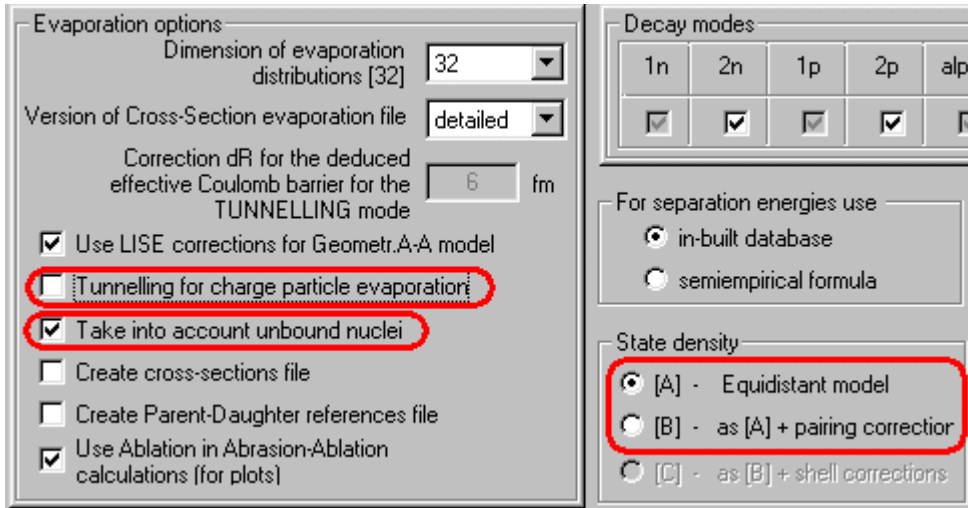
All LISE in-built setting after clicking the button “Make it default” are saved in the file LISE.INI. However, from experience sometimes physicists work on one computer with the LISE code but with different settings. In the new version there is a possibility to create an option file of options, which is found in the directory OPTIONS. The user should use the menu “File” in order to save or to load private settings in/from the option file.

## 14.3. Print of the dialogs “Physical Calculator” and “Goodies”

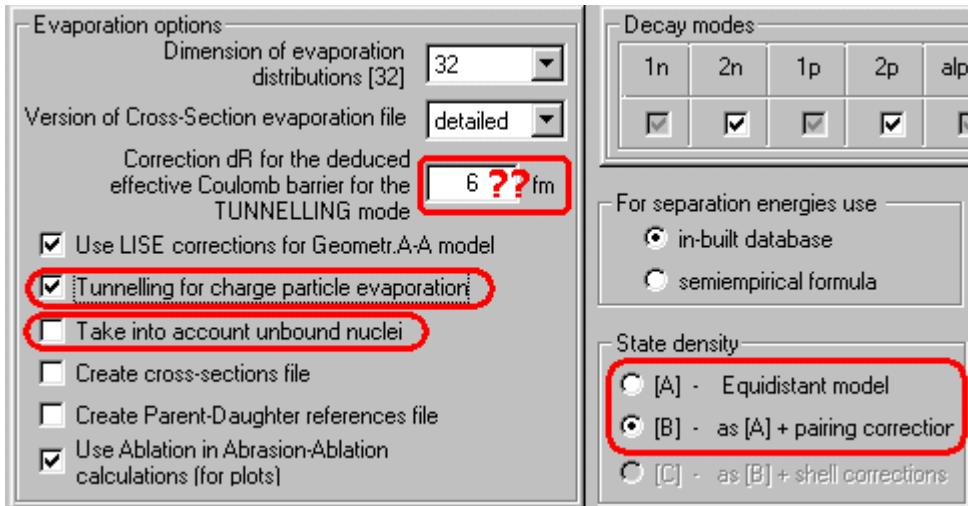
Opportunity of printing the dialogs “Physical calculator” and “Goodies” directly from the program has now been realized. The button "Print" existed since these dialogues were created, but print of dialogs was not possible, which often caused questions and inconvenience to the LISE users. We are glad to inform, that this lack is now corrected.

## 15. Abrasion-Ablation v.1.3 – version 5.4

In the new version of the program the mathematical apparatus to use the Abrasion-Ablation model was considerably altered. Omitting details of transformations, we shall note only options for this model depending on beam projectile mass. The recommended configurations for Abrasion-Ablation calculations in the case of a beam of light ions are shown in Fig.577, and for a beam of heavy ions in Fig.578.



*Fig.577. The recommended configuration for Abrasion-Ablation calculations in the case of a beam of **light** ions.*



*Fig.578. The recommended configuration for Abrasion-Ablation calculations in the case of a beam of **heavy** ions.*

For light projectiles the factor  $dR$  is set to 0, that is equivalent to switching-off the correction on the tunneling effect. It is necessary to parameterize  $dR$  as a function of projectile mass. From comparison with EPAX parameterization [Sum00] this parameter is less than 1 for the  $^{40}\text{Ar}$  beam, is equal to 3 for  $^{58}\text{Ni}$  beam and 5 for  $^{197}\text{Au}$  beam correspondingly. This parameter is important for predictions of proton-rich isotopes.

In Fig.579-583, Results of Abrasion-Ablation calculations are compared to calculations with different EPAX parameterizations for reactions  $^{197}\text{Au}+\text{Al}$ ,  $^{58}\text{Ni}+\text{Ni}$  and  $^{40}\text{Ar}+\text{Ni}$ .

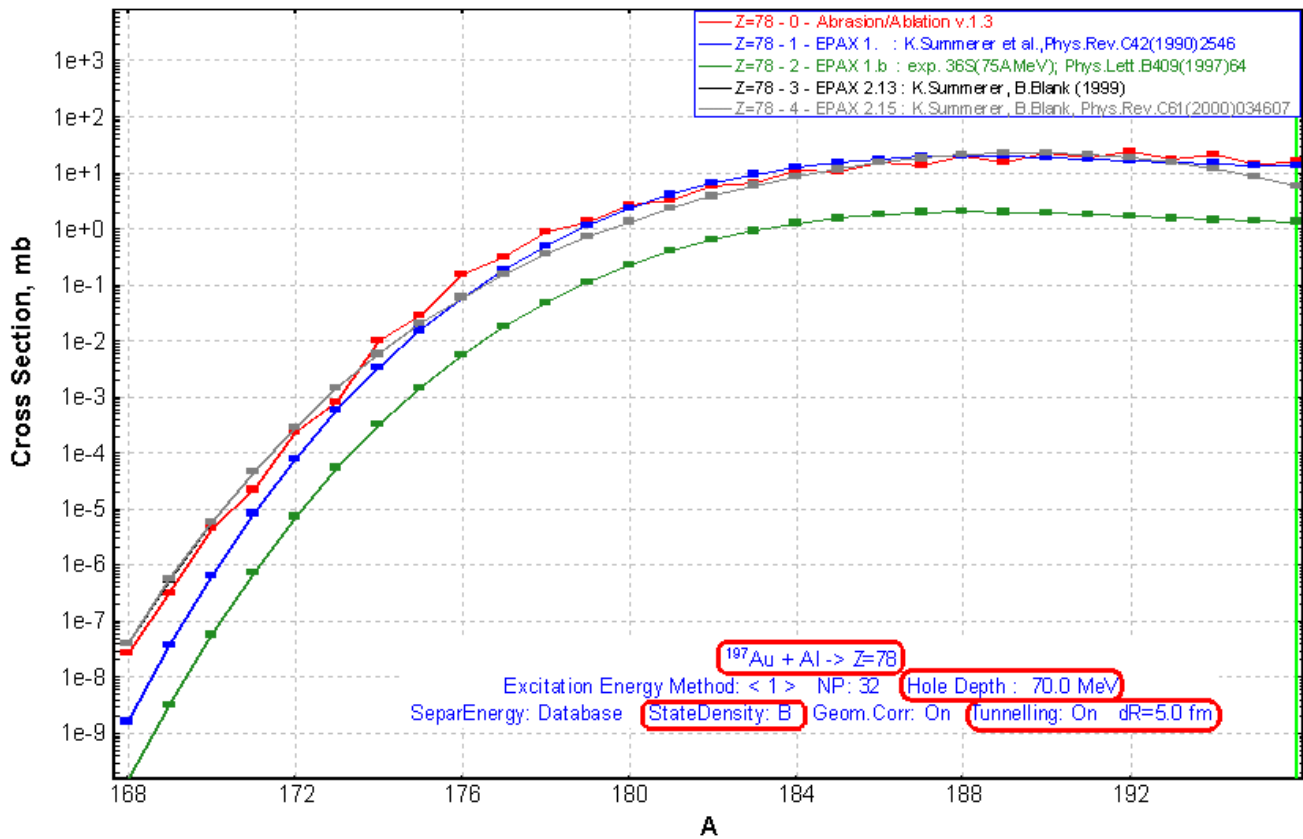


Fig.579. Production cross-sections of Pt-isotopes in the reaction  $^{197}\text{Au} + \text{Al}$ .

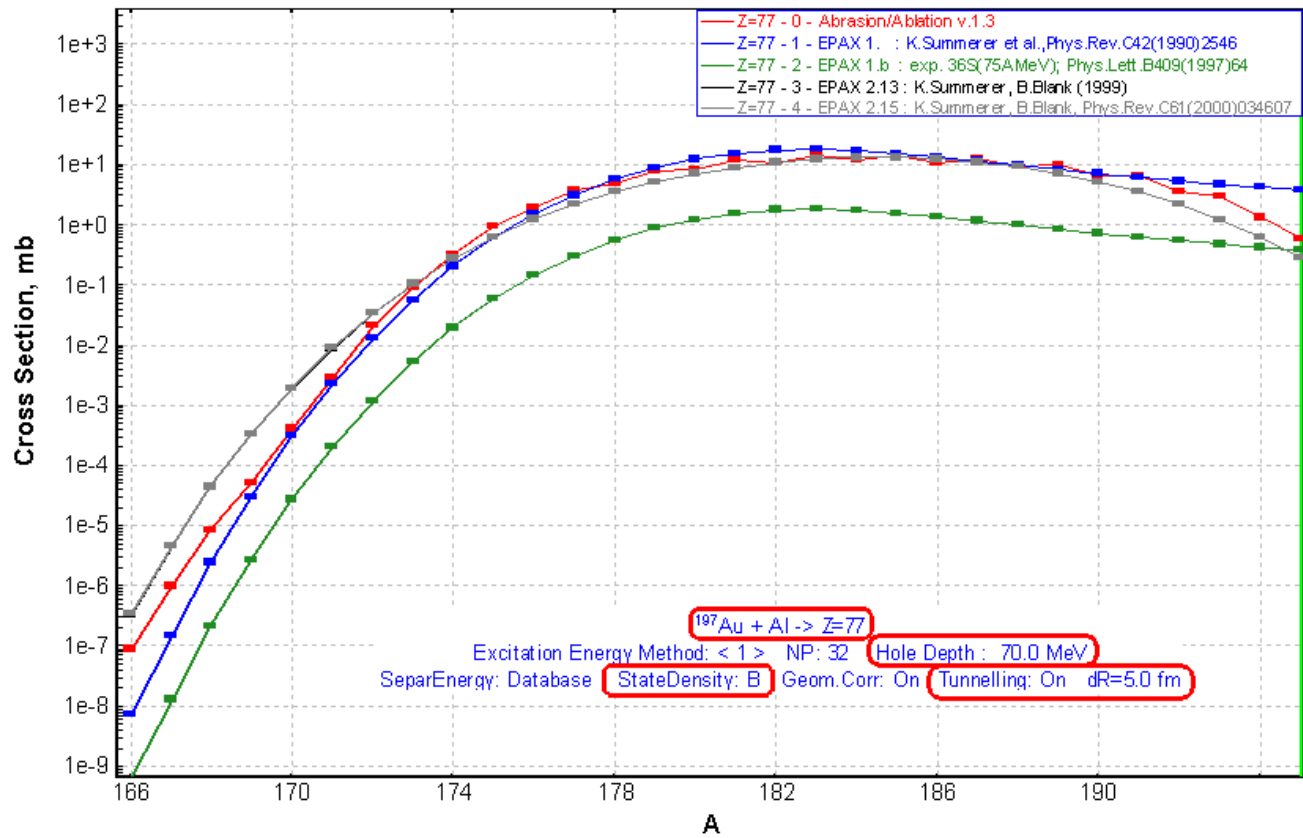


Fig.580. Production cross-sections of Ir-isotopes in the reaction  $^{197}\text{Au} + \text{Al}$ .



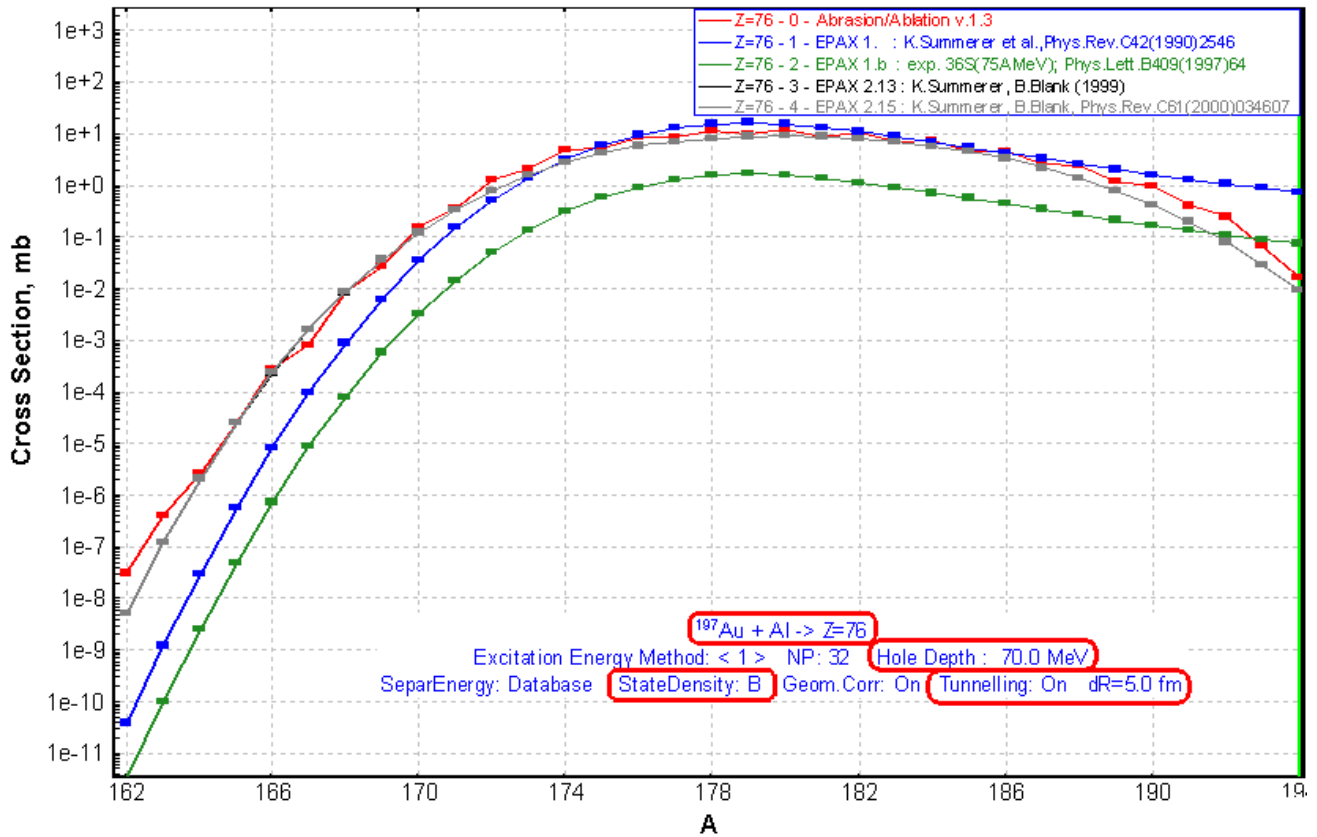


Fig.581. Production cross-sections of Os-isotopes in the reaction  $^{197}\text{Au}+\text{Al}$ .

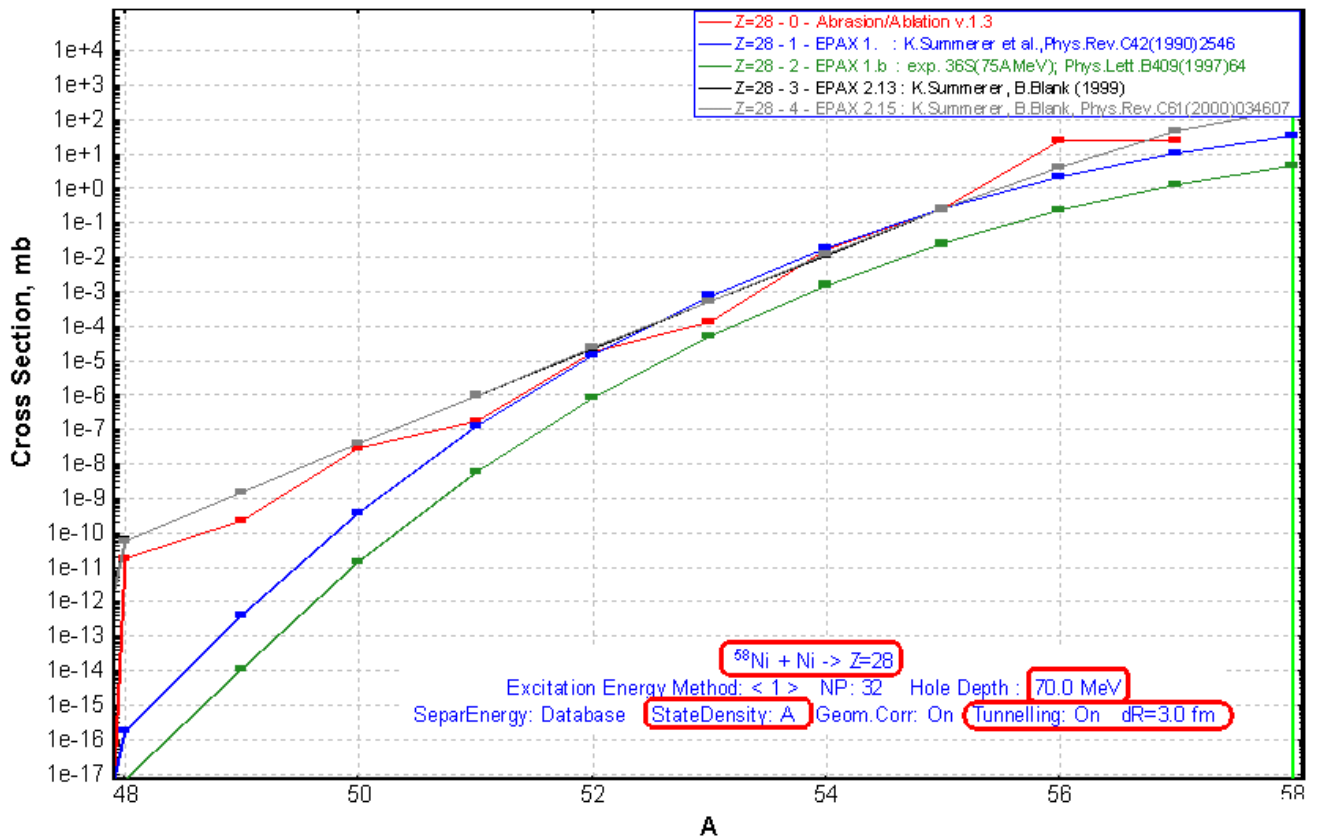


Fig.582. Production cross-sections of Ni-isotopes in the reaction  $^{58}\text{Ni}+\text{Ni}$ .

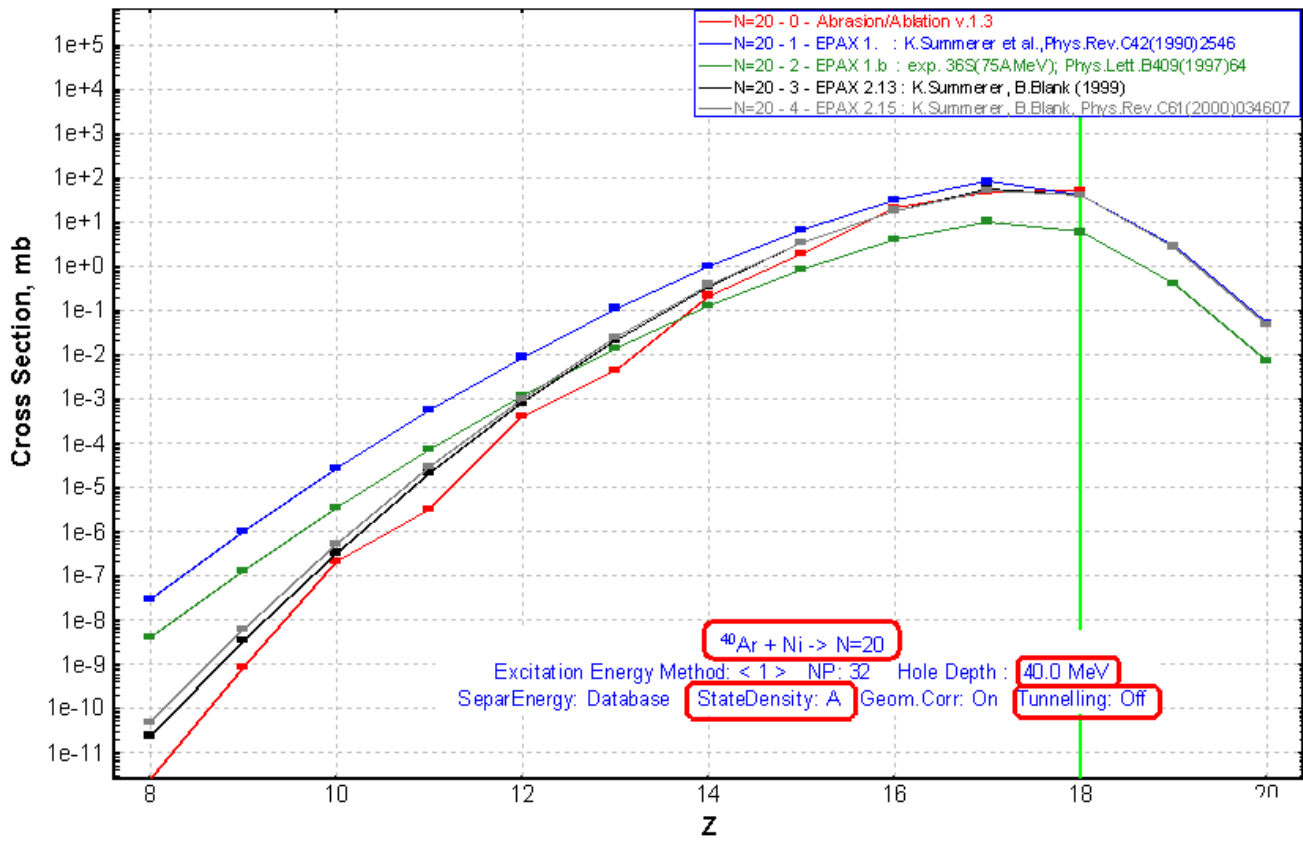


Fig.583. Production cross-sections of  $N=20$  isotones in the reaction  $^{40}\text{Ar}+\text{Ni}$ .

## 16. Prefragment Excitation Energy – version 5.3

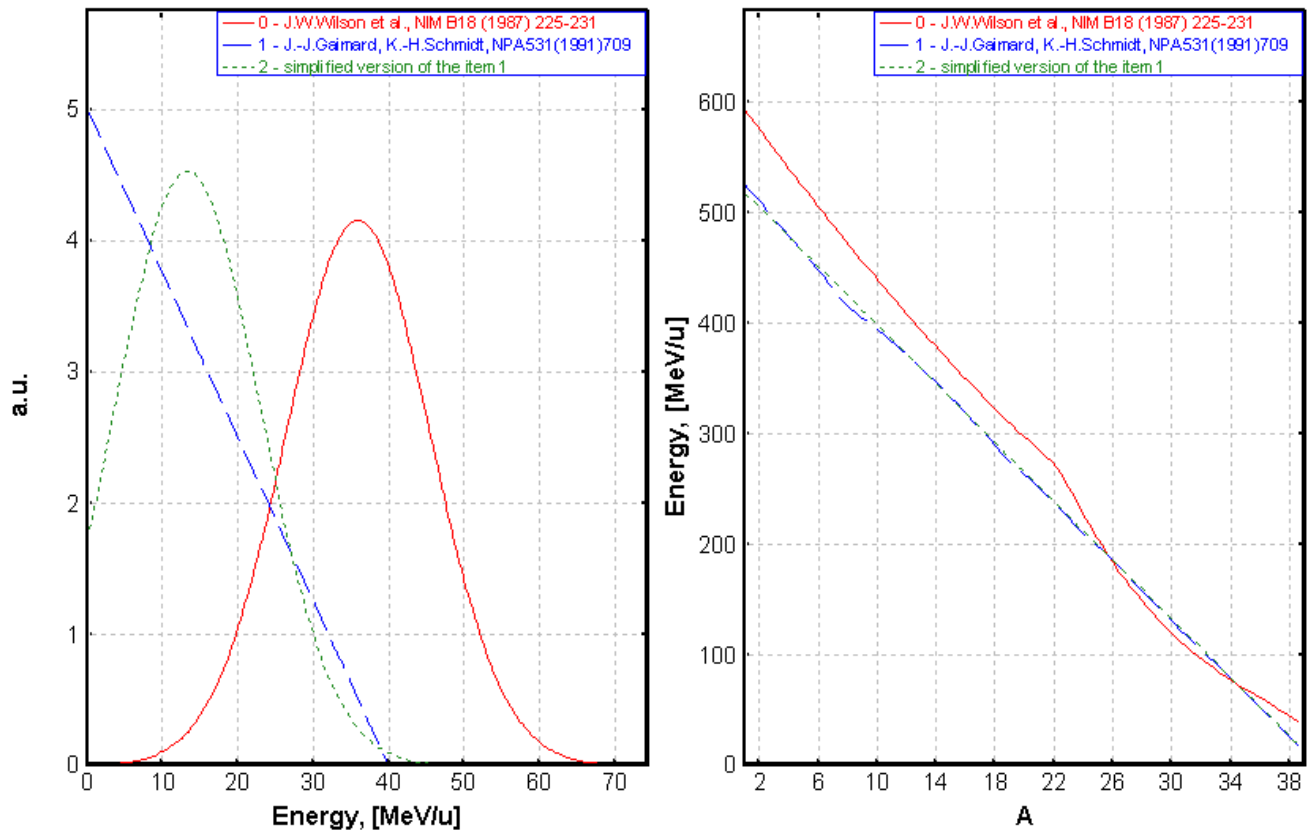
The geometrical model with the friction correction [Wil87] was used in the previous versions to calculate the prefragment excitation energy for Abrasion-Ablation. In the new version two methods were incorporated (see Fig.584). The first (B in Fig.584) is based on the statistical hole-energy model. The energy distribution of the prefragments with more nucleons removed is given by the convolution of several linear distributions [Gai91]. The second method (C in Fig.584) represents a simplified algorithm ref.[Gai91] where a gaussian distribution is used instead of convolution. The gaussian parameters (center and width) are derived from the convolution method. Alternatively, one can be entered the width parameter in the geometrical method (A in Fig.584).

In the new version the user can compare these methods using the button “Plot” in the dialog “Prefragment Excitation Energy”. The distributions of excitation energy of a selected isotope (left part) and the function of excitation energy from a prefragment mass (right part) are shown in Fig.585.

**Fig.584.** The “Production menu” dialog. The section setting energy losses and straggling calculation methods.

# Excitation energy for $^{40}\text{Ar} + \text{Be} \rightarrow ^{39}\text{Ar}$

< 0 > -  $g=0.95$   $\sigma=9.60$   $c1=1.50$   $c2=2.50$  Friction: On  $cf1=6.5$   $cf2=0.0$   
< 1 > - Hole Depth = 40.0  
< 2 > -  $\langle E^* \rangle = 13.30$   $\sigma = 9.60$



**Fig.585.** The distributions of excitation energy of a selected isotope (left part) and the function of excitation energy from a prefragment mass (right part) are shown.

## 17. Start configuration – version 5.2

In the previous versions the user could load his own configurations (spectrometer, reaction mechanism and so on) through working files with extension “liz”, which he has saved before. By default the configuration of the LISE spectrometer and standard settings (on an example the reaction product speed is always equal to beam ion speed) was loaded. In the new version of the program all settings made in dialogs “Preferences”, “Production mechanism”, “Prefragment search and Evaporation properties”, “Excitation energy of prefragment”, “Plot options”, “Convolution (Universal parameterization), “Friedman’s momentum distribution width” can be kept in the file “LISE.INI”. Data values in the file “LISE.INI” will be loaded at the start of program. This way, the user can keep by default a spectrometer configuration (see A in Fig.10). To save the current parameters in the file “LISE.INI”, the user has to press the button “Make it default” (see B in Fig.10). This button will be then disabled. Then the user should press the button “OK”.

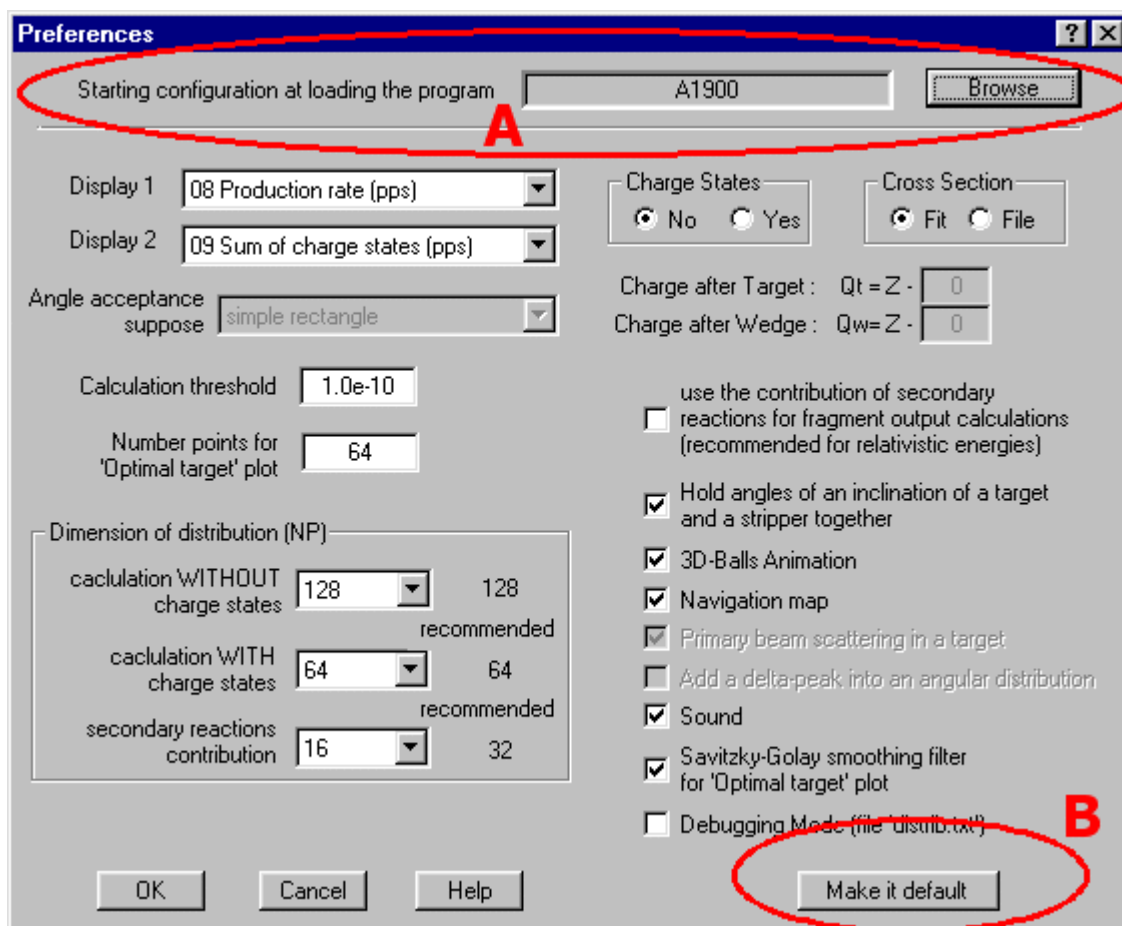
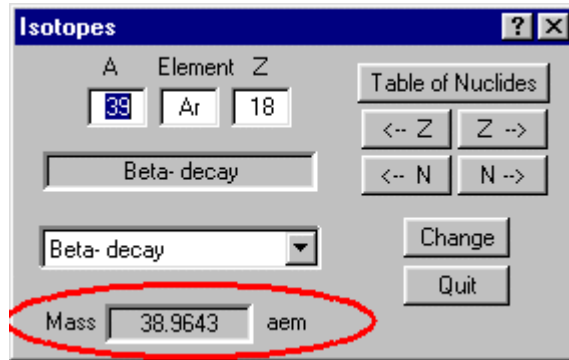


Fig.586. The “Preferneces” dialog.

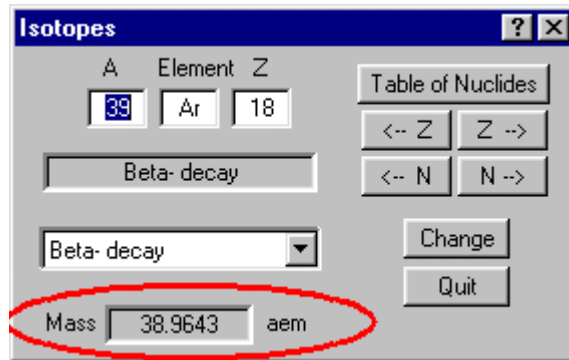
## 18. Transformation AMeV to MeV/u – version 5.1

With the advance in computing it is possible now to keep in operative memory an array of binding energy of all isotopes. The new version has the option to input beam energy in MeV/u (see A in Fig.587. The “Physical calculator” dialog.



*Fig.588. The user can see an isotope mass in the “Isotopes” dialog.*

) in addition to AMeV (see B in Fig.587. The “Physical calculator” dialog.



*Fig.588. The user can see an isotope mass in the “Isotopes” dialog.*

). Values are read from the database file when the program is loaded. The calculations are faster in this case, because there is no need to address constantly to a database storing on a disk. The user can see an isotope mass in the “Isotopes” dialog (see Fig.588).

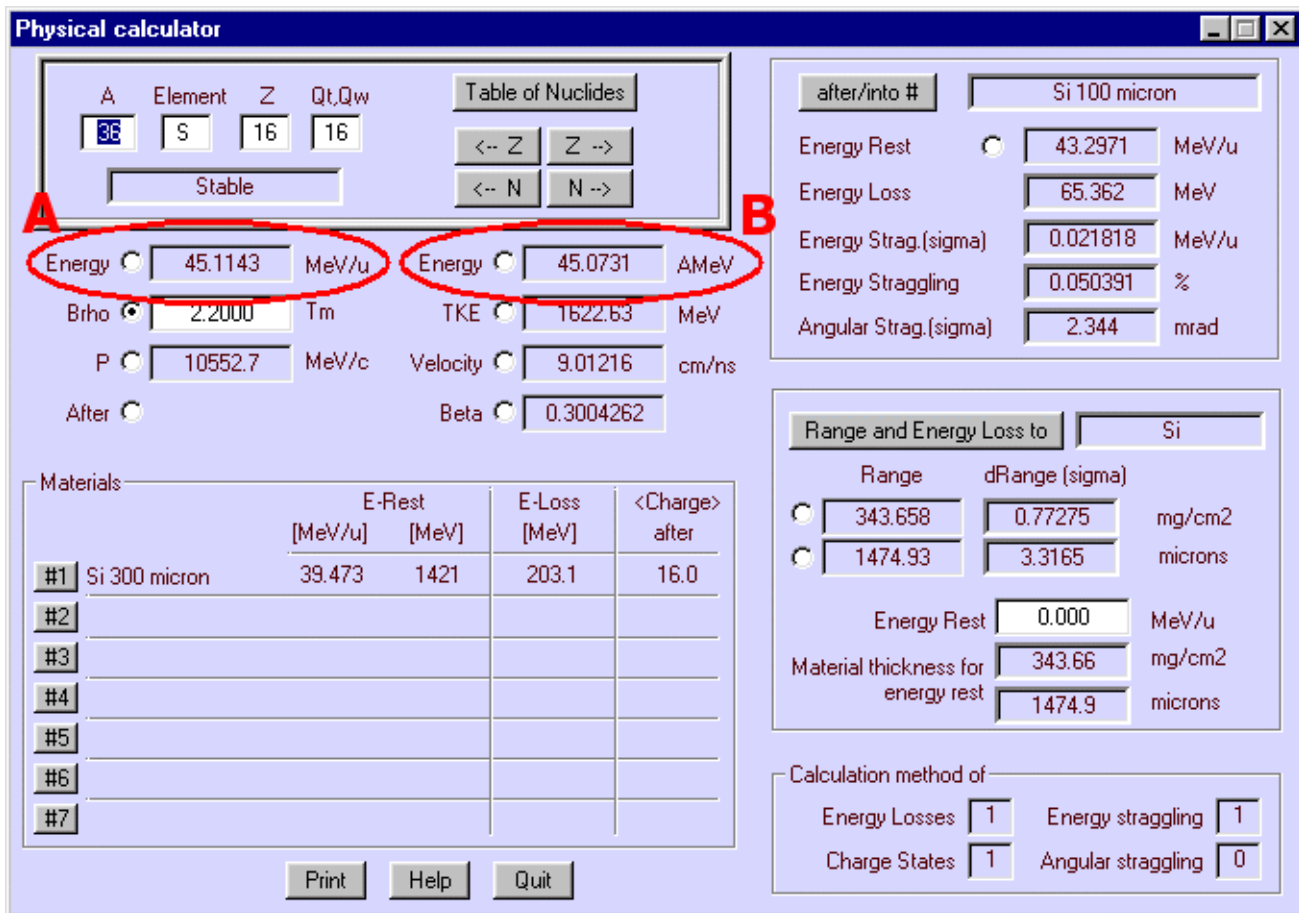


Fig.587. The "Physical calculator" dialog.

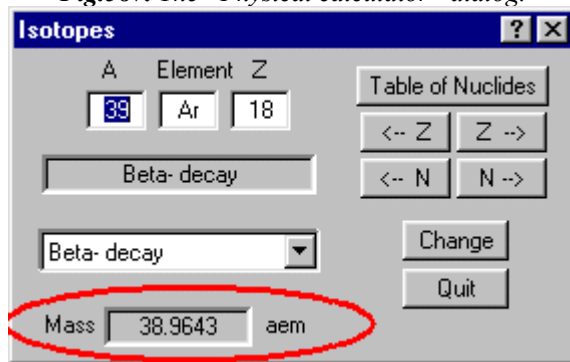


Fig.588. The user can see an isotope mass in the "Isotopes" dialog.

## 19. version 4.20

[www.nsl.msu.edu/lise](http://www.nsl.msu.edu/lise)  
[dnr080.jinr.ru/lise](http://dnr080.jinr.ru/lise)

East Lansing  
15-JUN-2001

### ATIMA Calculations of energy loss and straggling in matter

#### 19.1. ATIMA (**A**Tomic **I**nteraction with **M**atter)

Some of the ATIMA subroutines (Version 1.2) have been incorporated into the new version of the LISE code. ATIMA is a user program developed at GSI, which calculates various physical quantities characterizing the slowing-down of protons and heavy ions in matter for specific kinetic energies ranging from 1 keV/u to 500 GeV/u, such as

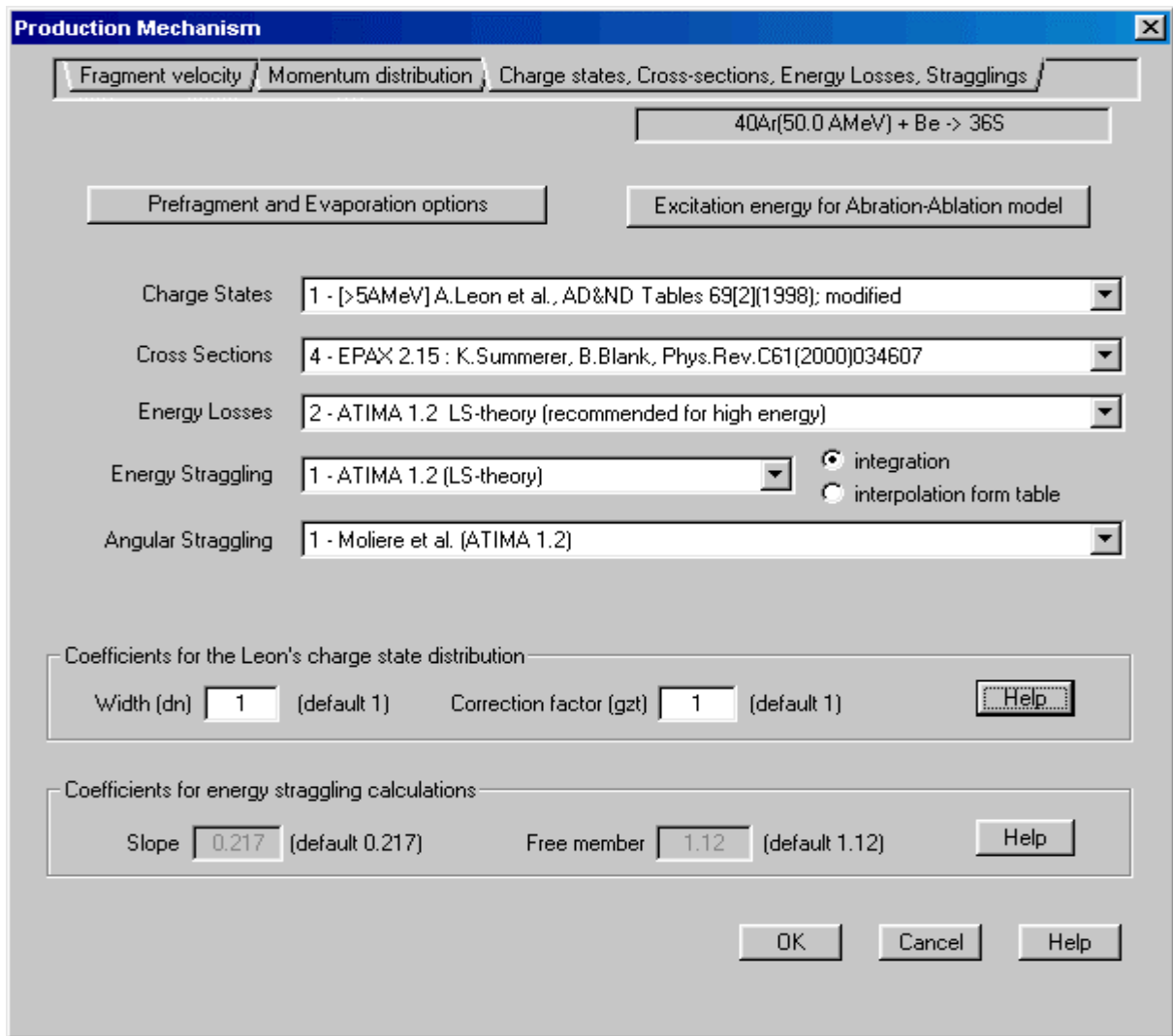
- stopping power,
- energy loss,
- energy-loss straggling,
- angular straggling,
- range,
- range straggling and others.

ATIMA is available under UNIX. The FORTRAN source of ATIMA has been transformed to C, and was optimized to exclude creating range files for spline procedures. Please report your suggestions for ATIMA via electronic mail to either [h.geissel@gsi.de](mailto:h.geissel@gsi.de) or [c.scheidenberger@gsi.de](mailto:c.scheidenberger@gsi.de) or [h.weick@gsi.de](mailto:h.weick@gsi.de). The web-site of this code is <http://www-aix.gsi.de/~scheid/ATIMA1.html>.

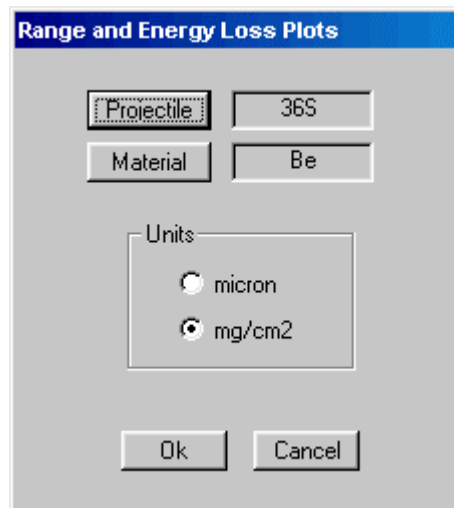
More details about the physics used in the ATIMA calculations can be found in the following references [Lin96, Sch98, Wei00].

New energy loss and straggling calculation method settings are available via the “Production mechanism” dialog box (see Fig.589).





*Fig.589. The “Production menu” dialog. The section setting energy losses and straggling calculation methods.*



*Fig.590. The dialog setting the projectile-target combination to plot range or energy loss distributions versus energy.*

## 19.2. Stopping power. Energy loss.

Four stopping power calculation methods are available in the LISE code (the abbreviation is like in the code):

- 0 - [Hub90],
- 1 - [Zie85],
- 2 - ATIMA 1.2,
- 3 - ATIMA 1.2 without LS-correction".

The “ATIMA 1.2 without LS-correction” method was incorporated to show the influence of the LS-correction. After the various tests for different energies and projectile-target combinations we **recommend** to use for calculations the following methods:

- At low and intermediate energies (up to 100-300 AMeV), and also for gaseous targets the method “1” [Zie85],
- For high energies (from 150 AMeV and higher) accordingly the method “2” (ATIMA 1.2).

The user can plot energy loss distributions as a function of energy using the “Plot of Fragment Energy Loss (dE/dx) in Target versus Energy” item in the Utilities menu (see Fig.591).

In previous versions the user could create this plot only for a combination beam-target given in the “Projectile” and “Target” menus. In the new version the user can set the necessary combination and choose units (micron or mg/cm<sup>2</sup>) directly ahead of plot creation via a dialog shown in Fig.590.

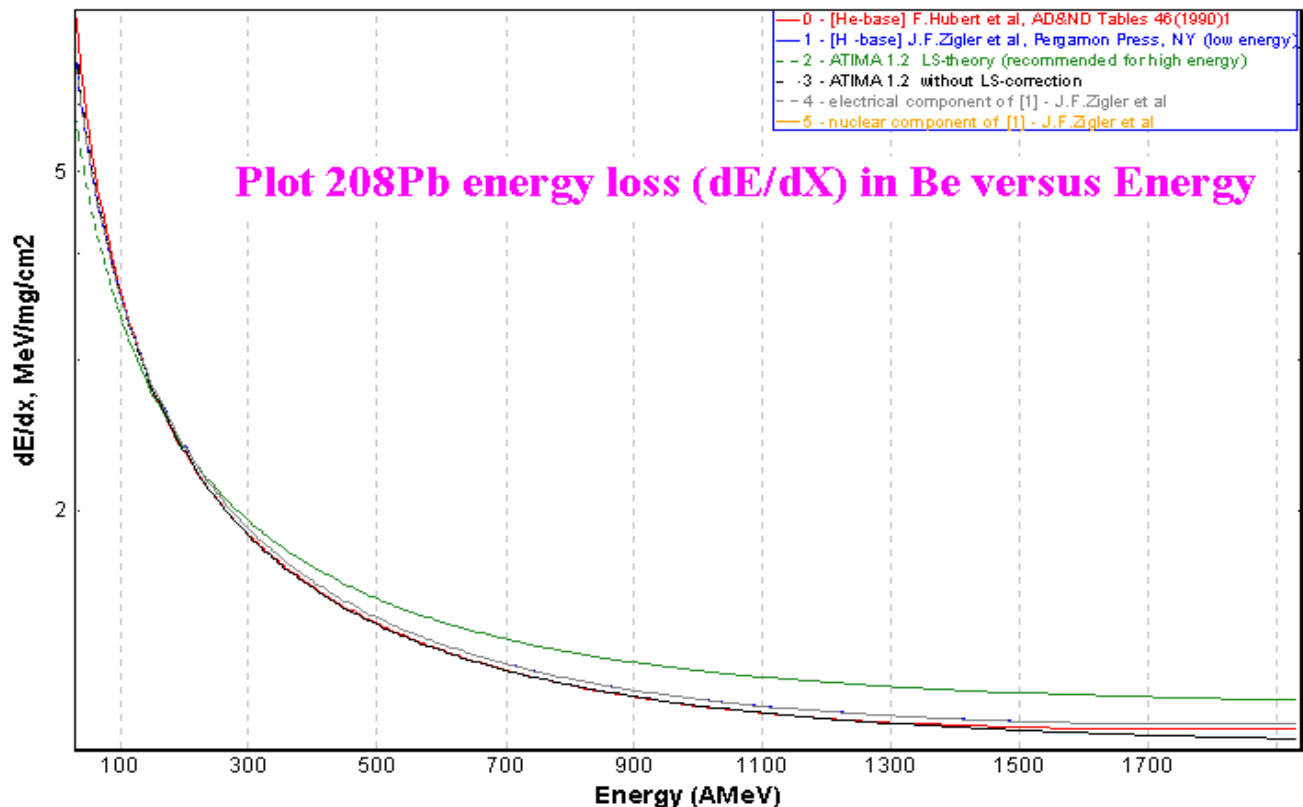


Fig.591. <sup>208</sup>Pb energy losses in Be calculated by different methods.

### 19.3. Ranges

The calculation of energy loss in material is most efficiently performed using a backward interpolation on a table of range calculations. The LISE code is capable to fill ten tables for different combinations (particle, target, calculation method) and to save them in memory in cyclic order. In other words the 11-th combination will be written down in the table instead the first one. This procedure accelerates calculation of run and losses of energy. The user can plot range distributions from energy using the “Plot of Range in Target versus Energy” item in the Utilities menu (see Fig.592).

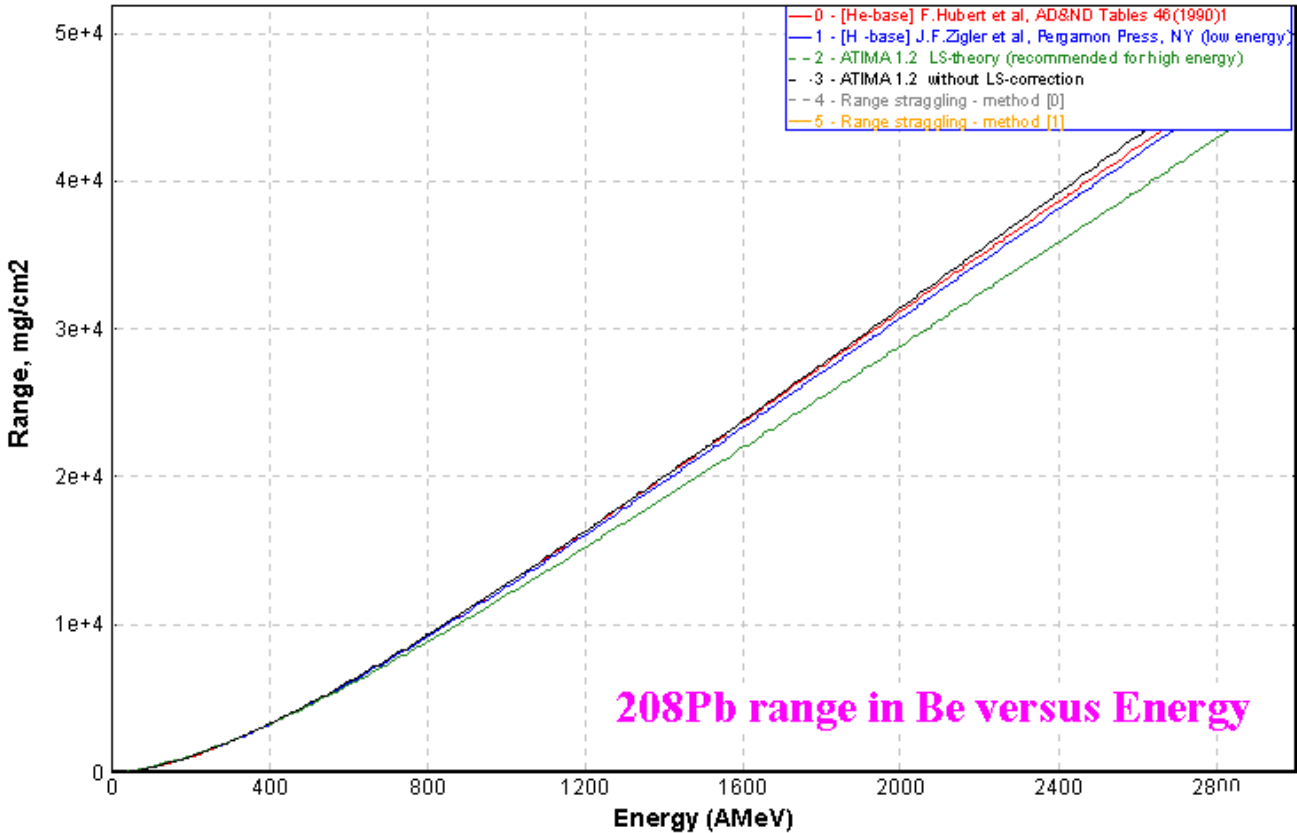


Fig.592.  $^{208}\text{Pb}$  ranges in Be calculated by different methods.

### 19.4. Energy-loss and ranges straggling

The LISE code has got a new method for calculating energy-loss straggling (which is based on the ATIMA subroutines) in addition to the [Gui86] method, already existing in the program. The Methods of range straggling calculation were reconsidered. Now the user has two opportunities:

1. Values for range straggling are calculated once from 10 KeV up to 3 GeV/A, and are kept in a table in analogy to the range tables. In LISE this method is referred to as "interpolation from table" (see Fig.589);
2. The second method is called "direct integration": the thickness of the material after which it is necessary to determine the straggling is divided into N parts. The projectile energy is calculated after each such material layer. The final straggling is equal to the square root of the sum of the intermediate values:

$$\Delta E = \sqrt{\sum_{i=1}^N \left[ \frac{dS^2}{dx} \cdot \Delta x_i \right]}$$

/53/

It is **recommended** to use the ATIMA subroutines to calculate energy-loss straggling using the method "interpolation from table". The user can plot range distributions as a function of energy using the "Plot of Range in Target versus Energy" item in the "Utilities" menu as in the case plot ranges (see Fig.593).

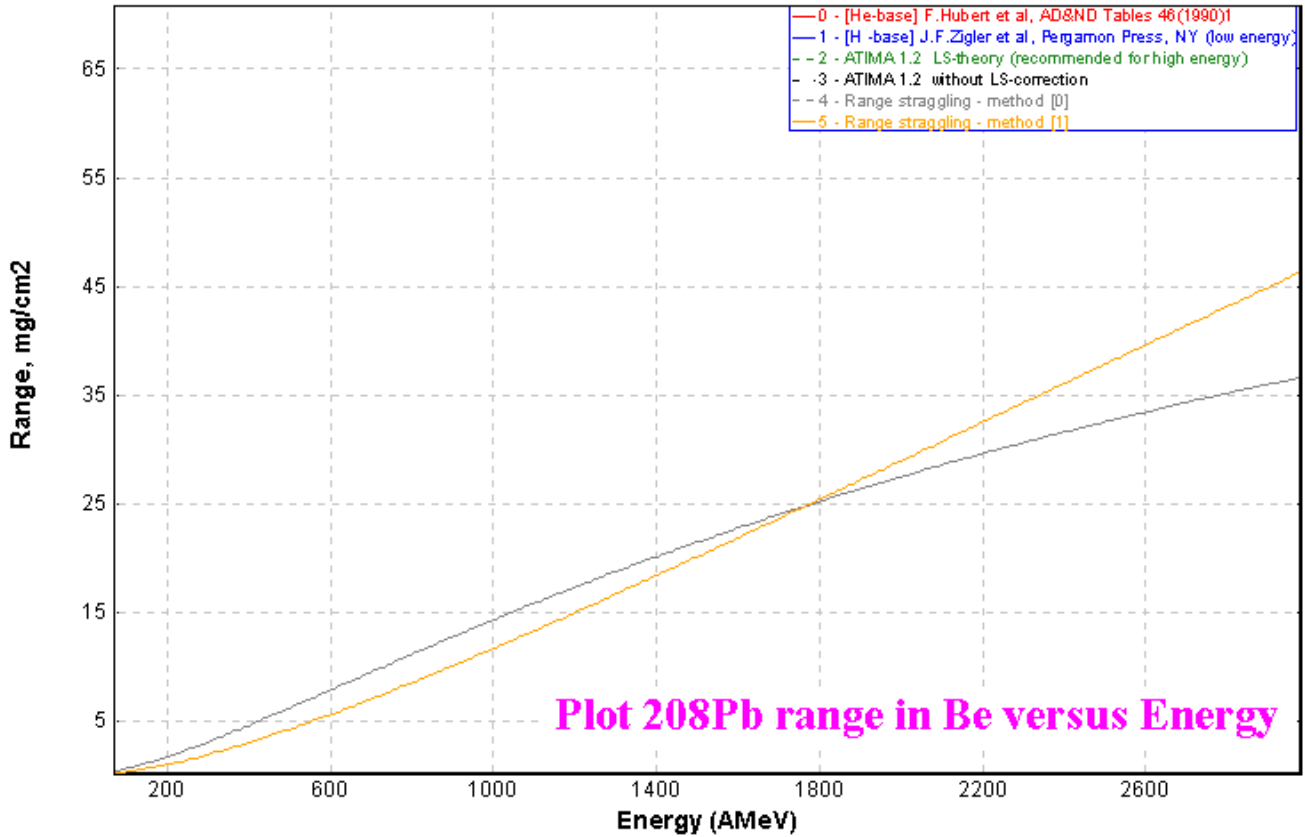


Fig.593. <sup>208</sup>Pb range straggling in Be calculated by different methods.

### 19.4.1. Angular straggling

Two methods to calculate the angular straggling are available in the program LISE: [Ann88] and [Par98]. It is recommended to use the [Ann88] method.

## 19.5. Miscellaneous

### 19.5.1. Range plot

Plot "Range in material" subroutines have been reconsidered. In the new version are used table range straggling instead "integration" method in previous versions.

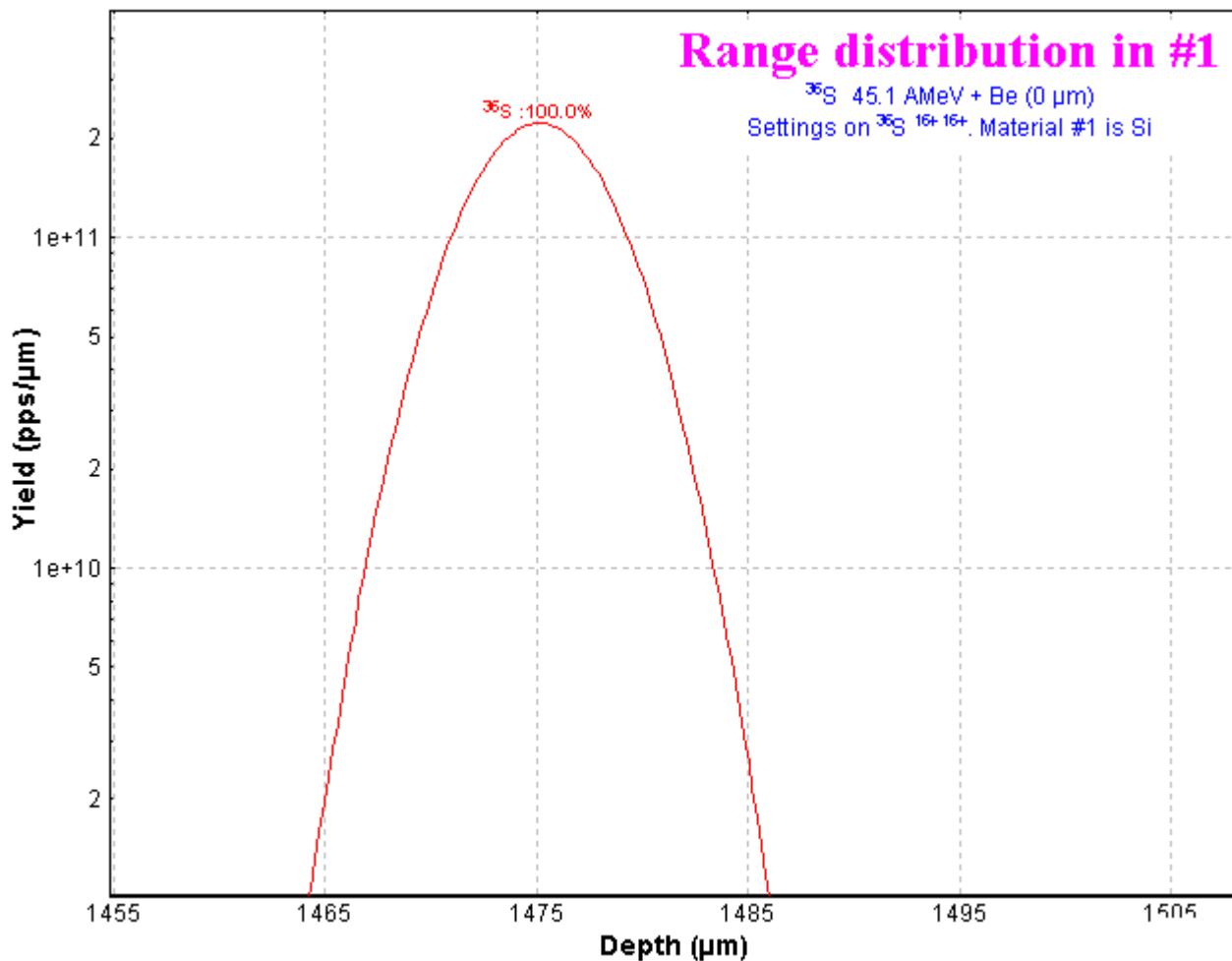


Fig.594.  $^{36}\text{S}$  Range distribution in Si. Initial energy distribution of  $^{36}\text{S}$  is delta-function at 45.1 AMeV.

Statistics							
Range distribution in #1							
36S 45.1 AMeV + Be (0 μm)							
Settings on 36S 16+ 16+. Material #1 is Si							
Plot 1							
N	distribution	x-mean	x-max	max	deviation	FWHM	area
1	36S :100.0%	1475	1475	2.219e+11	3.315	7.812	1.845e+12

Fig.595.

Statistical characteristics of range distribution (Fig.594) are shown in Fig.595. Compare these values with Physical calculator calculations in Fig.596 for the same case.

### 19.5.2. Physical Calculator

A range straggling is available in the Physical calculator dialog (see A in Fig.596). Methods used to calculate energy loss, straggling, charge states distributions the can observe also (see b in Fig.596)

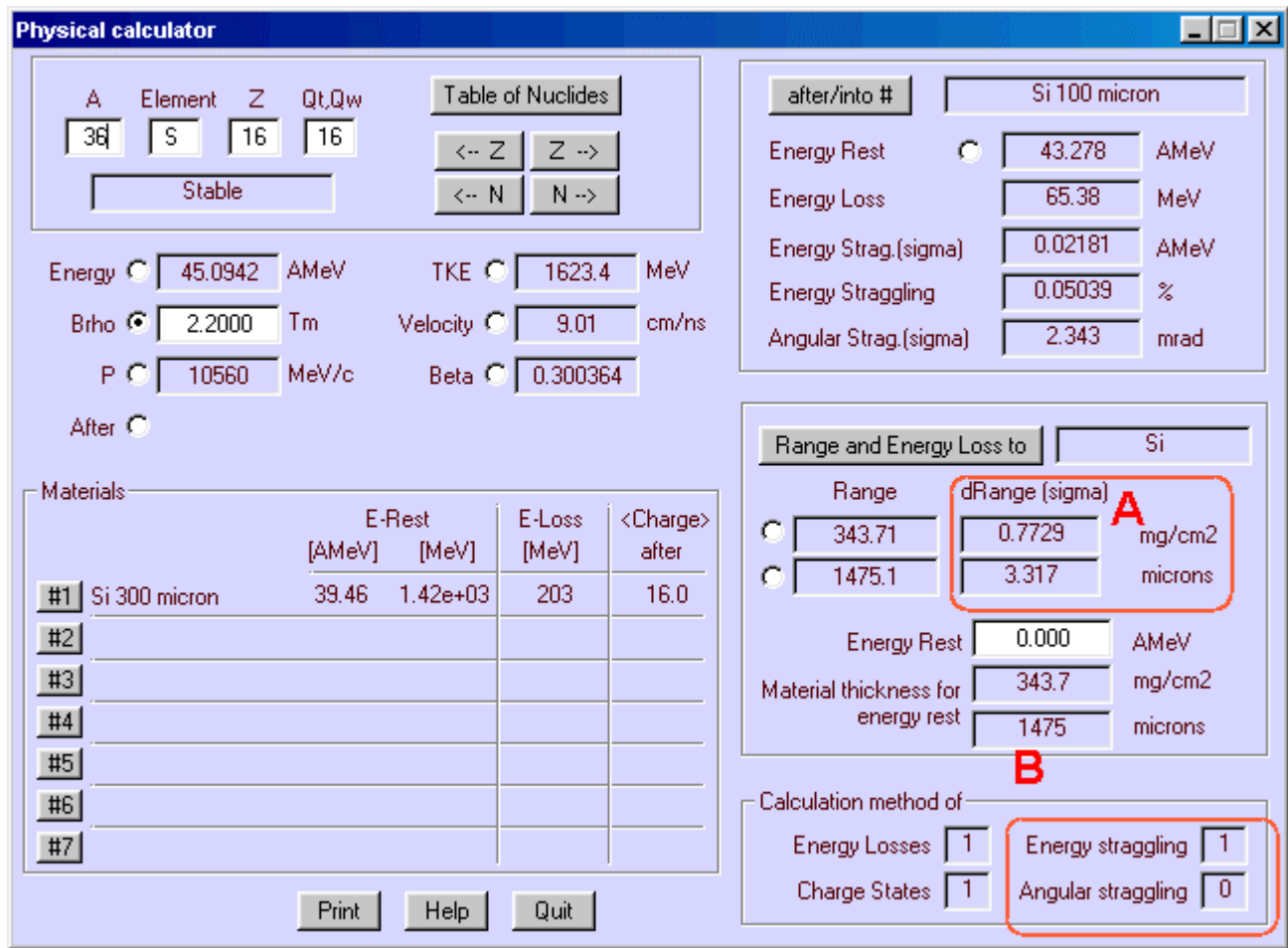


Fig.596. The Physical calculator dialog.

### Acknowledgement

The LISE program authors thank Dr.H.Weick and Prof.H.Geissel for the help rendered at adaptation of the ATIMA program in our program, and also for the useful remarks at work above the documentation of this version, and also hope for the further cooperation in development of the LISE program.

# 20. version 4.18

East Lansing  
12-JUN-2001

## Evaporation Calculator Abrasion-Ablation Model

### 20.1. Introduction

Various versions of the EPAX parameterization [Sum00] have been used to calculate projectile fragmentation cross-sections. The basic advantages of the parameterization are the following:

- Simple and fast calculations of real cross-sections using good enough approximation;
- Direct (one-step) calculation.

However, there are some disadvantages:

- No target dependence;
- The parameterization does not reproduce observed odd-even effects
- Parameterization estimations are inexact for lightest nuclei and nuclei near the drip-lines.

In further developments of the program LISE other kinds of reaction, in addition to projectile fragmentation will be introduced. One candidate is complete fusion with subsequent evaporation and/or fission. These reactions require an in built procedure for calculating light particle evaporation by exited nuclei.

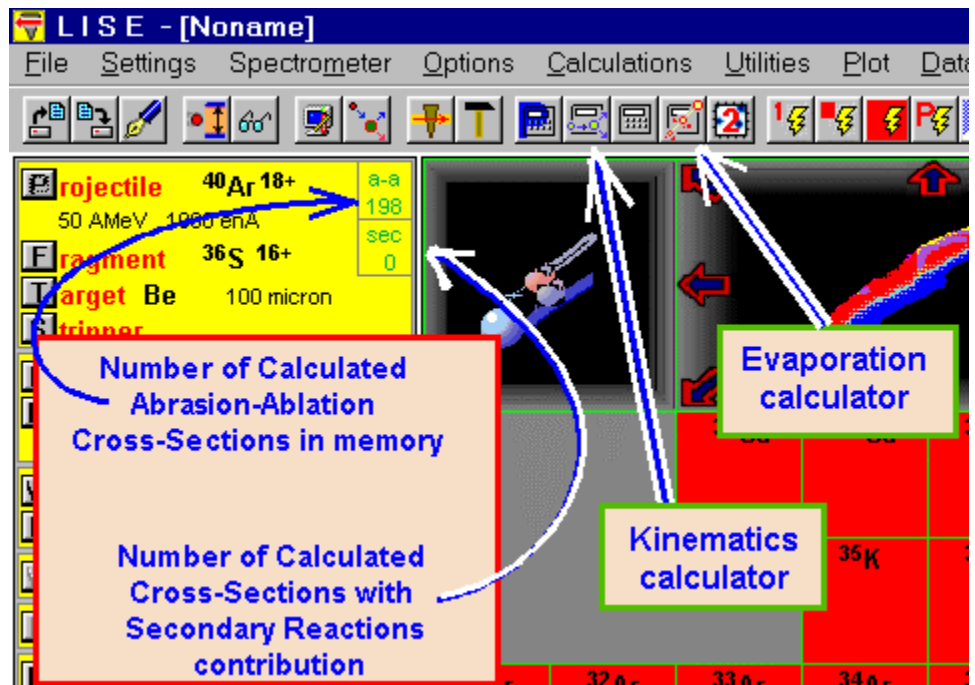



Fig.597. Icons of Kinematics and Evaporation calculators.

This has resulted the creation of a new calculator called “Evaporation Calculator” [Chapter 20.2.]. Using this new tool the user can calculate the production cross-sections of different nuclei as a result of deexcitation of an excited nucleus. This calculator is based on the work by [Gai91]. The introduction of the evaporation algorithm allows incorporation of an additional method for calculating projectile fragmentation cross section using an Abrasion-Ablation model [Chapter 20.3.].

## 20.2. Evaporation Calculator

The Evaporation calculator is available in the Calculations menu or via the icon  in the toolbar (see Fig.597). The “Evaporation Calculator” dialog is shown in Fig.598. The production of  $^{32}\text{Mg}$  nucleus from deexcitation of  $^{40}\text{Ar}$  is presented in this figure as an example. The excitation energy distribution of  $^{40}\text{Ar}$  in this example is gaussian, with the excitation energy window (50 MeV, 100 MeV) as the left and right points at the gaussian half-height.

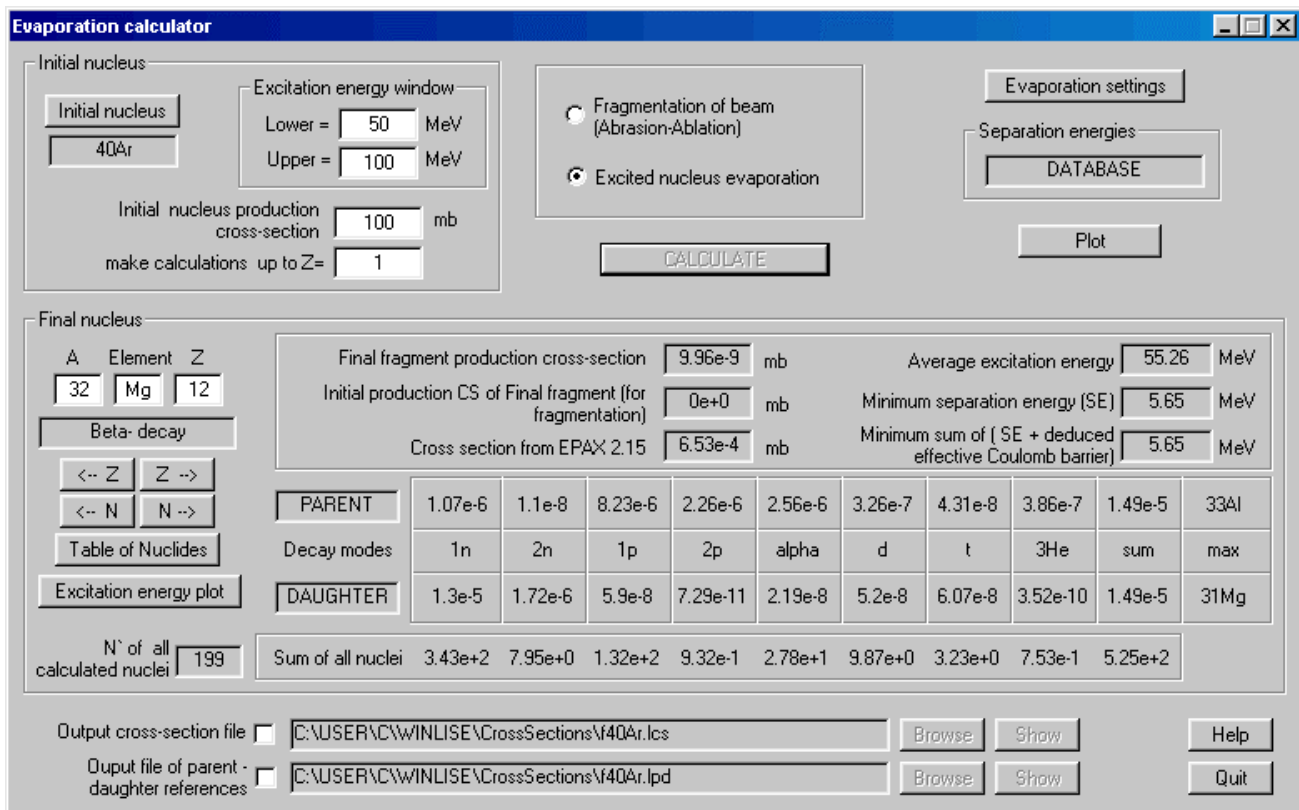


Fig.598. The “Evaporation Calculator” dialog (Excited  $^{40}\text{Ar}$  nucleus evaporation example).

The basic differences between the work [Gai91] and the LISE algorithm are the following:

- **J.-J.Gaimard & K.-H.Schmidt [Gai91]** - determines average values ( $A$ ,  $I$ ) of a final daughter nucleus with the normal distribution of width  $\tau$ .
- **The LISE code** assumes that each nucleus is individual. The program sums all input (parent) energy distributions (including initial abrasion cross-section for fragmentation). Then it calculates output (daughter) distributions and determines the part of the input distributions that was not in-

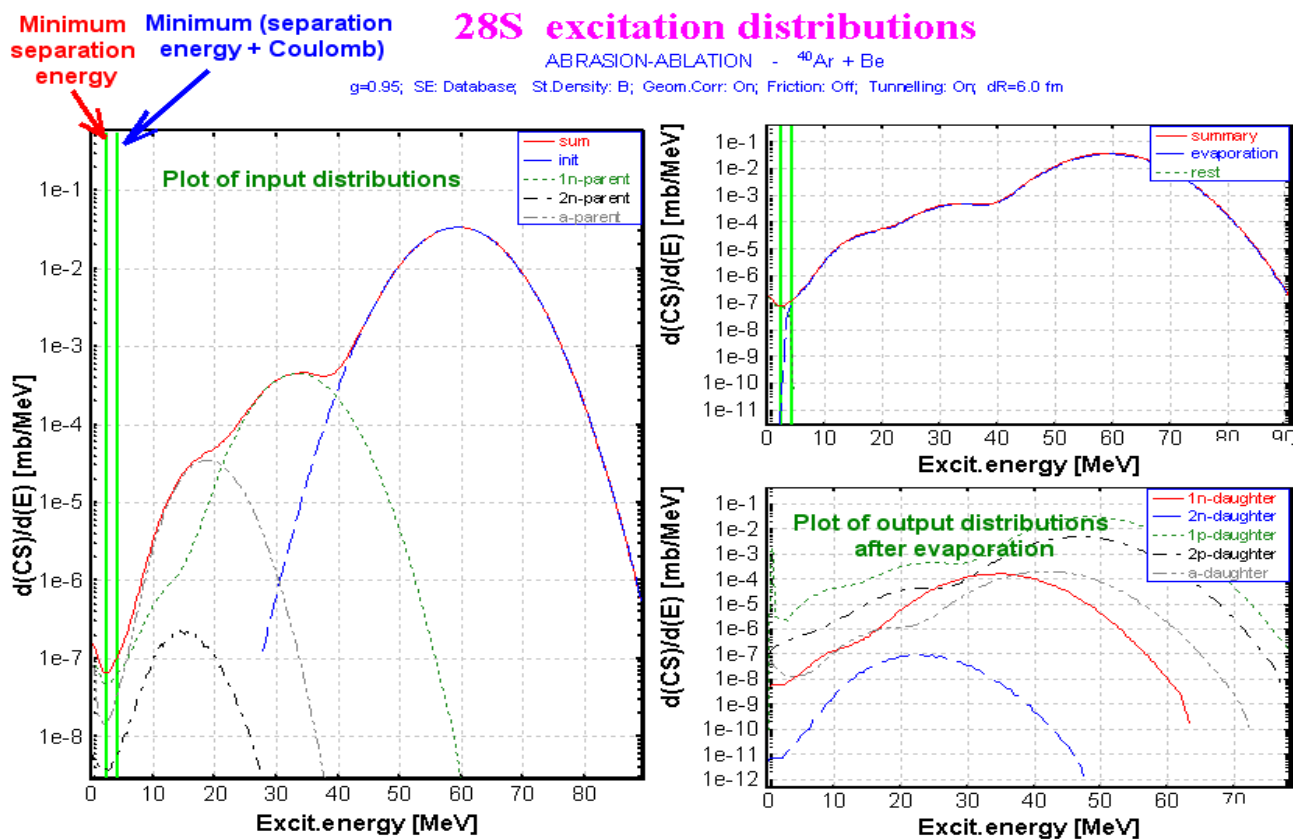


cluded in the output. The area of this part of input distribution is equal to the production cross-section of this nucleus as a result of the deexcitation of the initial nucleus (see Fig.599).

In this sense the LISE method is **unique**: it carries in itself the best features of Monte Carlo evaporation programs (energy distributions, odd-even effects, "individuality" of each nucleus) and one of the advantages of analytical methods [Gai91] - fast calculations.

### 20.2.1. Evaporation calculator plots

The user can observe results of the evaporation calculator using plots of input and output energy distributions for a given nucleus (see Fig.599) and a two-dimensional plot of cross-sections (see Fig.600). The 2D-dimensional plot is a new feature in the program. The data is represented by rectangles centered at N (neutrons) and Z (protons), where the cross-section value depends on color and size of the rectangle. The user can change the display modes of rectangles (see Fig.601), and also change the scale (see Fig.602).



**Fig.599.** Parent (input) and Daughter(output) distributions of  $^{28}\text{S}$  nucleus in the reaction  $^{40}\text{Ar}+\text{Be}$ . These plots are available via the "Excitation energy plots" button in the "Evaporation calculator" dialog.

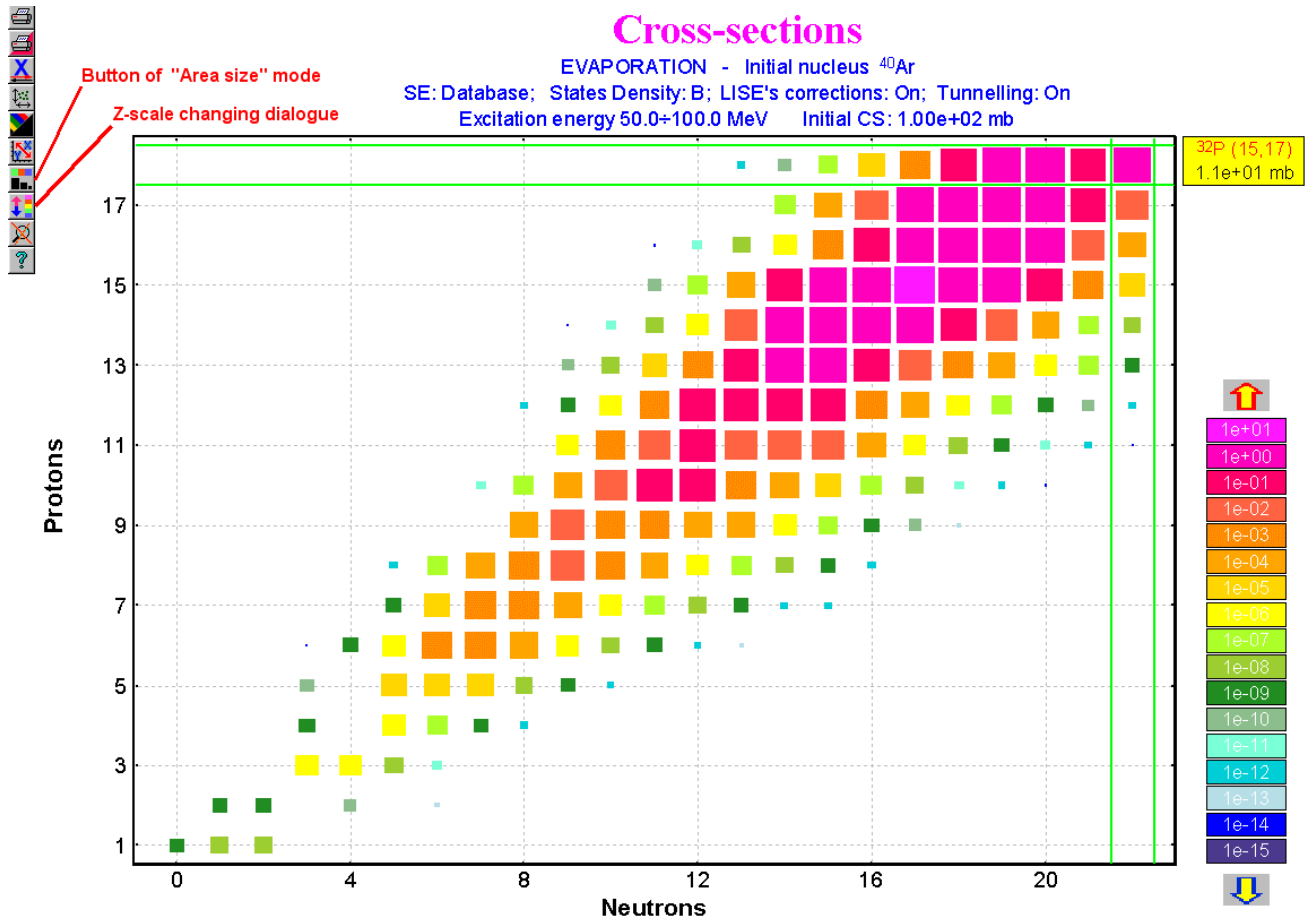


Fig.600. The bi-dimensional plot of production cross-sections of nuclei as a result of  $^{40}\text{Ar}$  deexcitation.

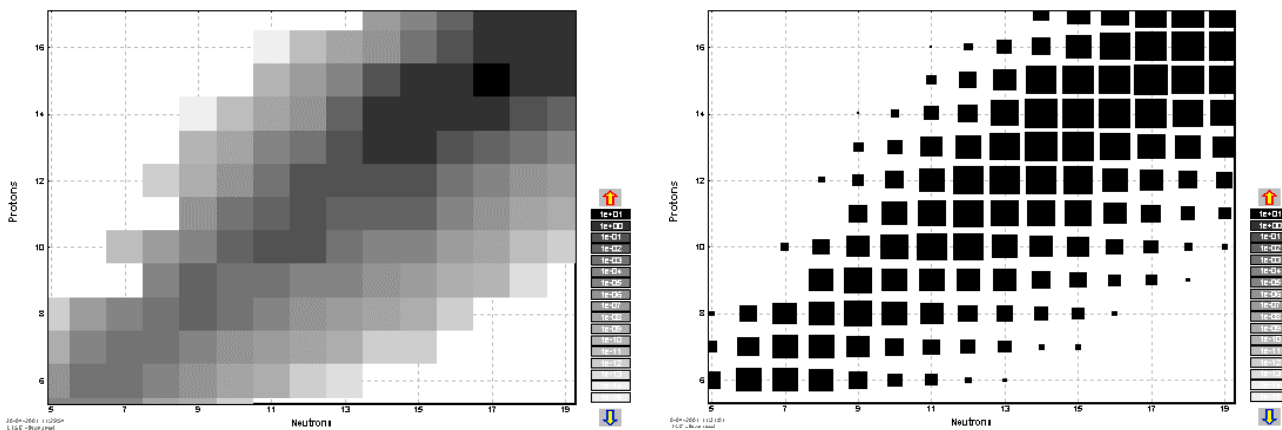


Fig.601. Different presentation modes of the new bi-dimensional plot.

### 20.2.2. Evaporation settings

The “Evaporation settings” dialog (see Fig.603) can be accessed from the “Evaporation calculator” dialog or from the “Options” menu. Eight decay modes are available in the code. The user can not change three of them (p,n, $\alpha$ ). Other modes may be switched on or off. It is not recommended to use  $^3\text{He}$  and t –decays as their contributions are insignificant, and increases calculation speed. The user can test this by performing calculations with various options.

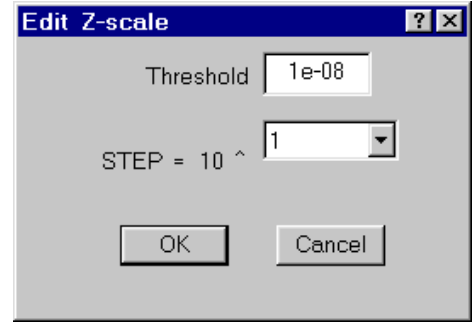


Fig.602. The dialog “Edit Z-scale”.

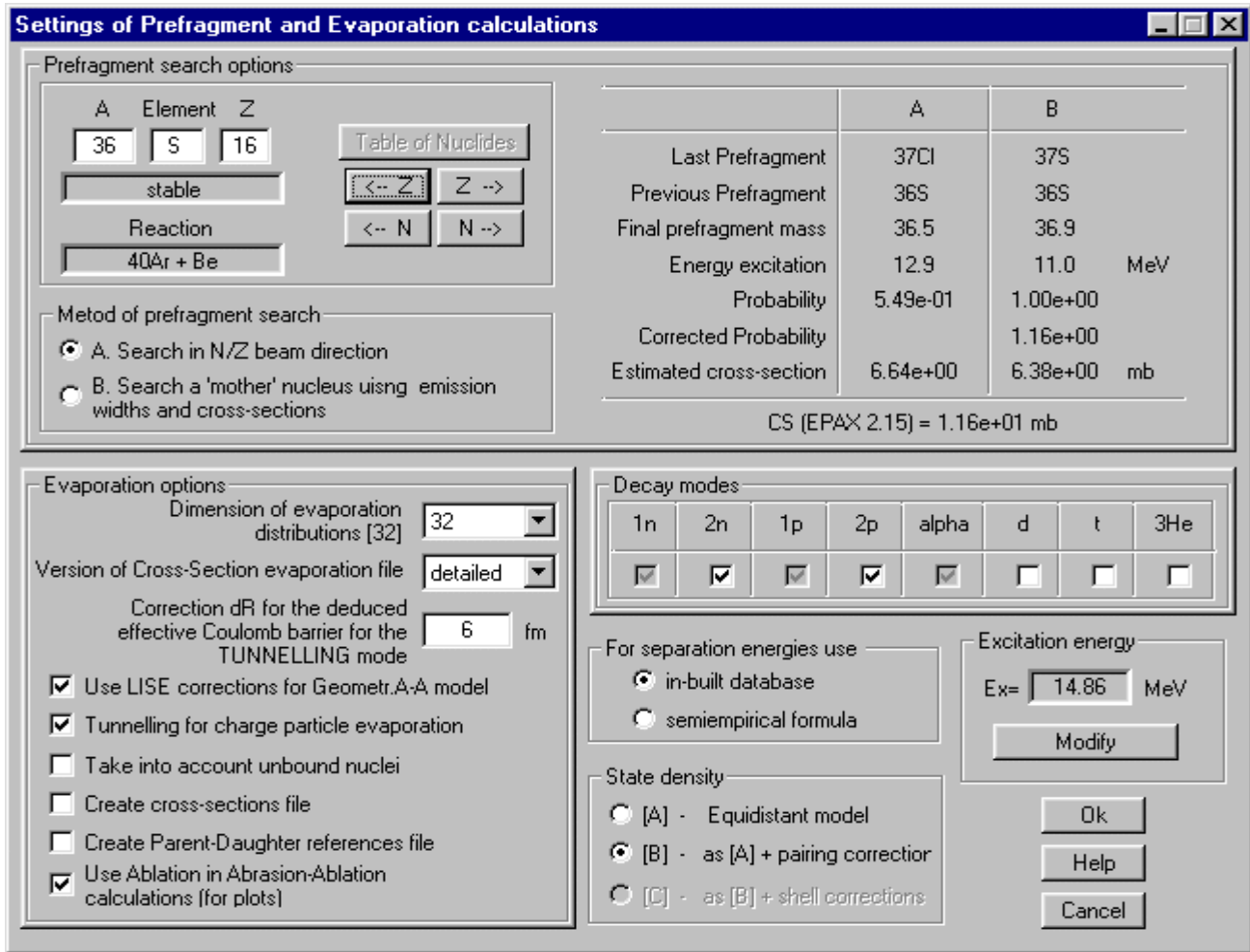


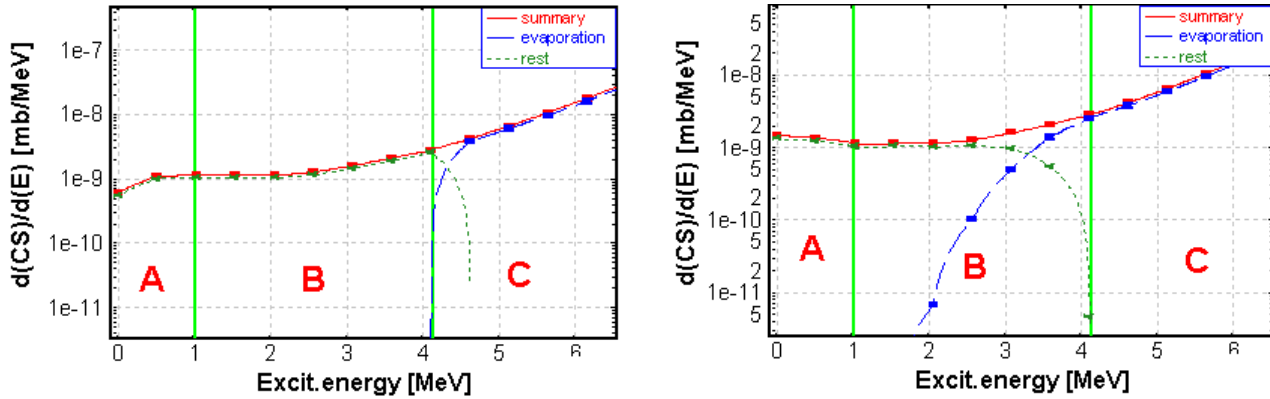
Fig.603. Settings of Prefragment and Evaporation calculations. (Recommended values are shown)

#### 20.2.2.1. Tunneling for charge particles

In Fig.599 and Fig.604 plots are shown with two green vertical lines corresponding to the minimum separation energy (left line) and the minimum sum of the separation energy and the effective Coulomb barrier (right line). The part of the distribution (A) located to the left of a line does not undergo evaporation (see Fig.604). The deexcitation proceeds by emission of  $\gamma$ -rays. It is also assumed, that the part of the distribution between these two lines (B) does not undergo the further evaporation (see Fig.604, left plot). The effective

barrier assumes a shift of the right line to the left, assuming a tunneling effect. The default value  $dR = 6 \text{ fm}$  is taken from work [Ben98]. The effective Coulomb barrier is written as:

$$B_{eff} = \frac{1.44 Z_1 Z_2}{dR + 1.22(A_1^{1/3} + A_2^{1/3})}. \quad /54/$$



**Fig.604.** Excitation energy distribution plots. The left plot shows the calculation principle in the LISE code. The right plot is an idealized case, which is still in a stage of development.

In Fig.604 (right plot) an example of a real situation including a tunneling effect is shown (*this is still in a stage of development*). Not all part would remain in the given fragment in this case in the B zone. The standard Coulomb barrier is used in this case:

$$B = \frac{1.438 Z_1 Z_2}{0.5 + 1.36(A_1^{1/3} + A_2^{1/3})}. \quad /55/$$

The use of the effective barrier can have various consequences. For example, when the sum of the separation energy and the Coulomb barrier is positive, the nucleus is bound. However it is not excluded that at the same time the sum of the separation energy and the effective Coulomb barrier is negative (as the effective Coulomb barrier is less the standard barrier). In this case the nucleus is unbound and the program will show zero cross-section for its production.

#### 20.2.2.2. Option to take into account unbound nuclei

This option includes calculating unbound nuclei via evaporations channels, for example, the most probable path of  $^{32}\text{Ne}$  nucleus deexcitation is  $^{32}\text{Ne}^* \rightarrow ^{31}\text{Ne} \rightarrow ^{30}\text{Ne}$  in the  $^{40}\text{Ar} + \text{Be}$  reaction. This option brings contribution for nuclei near the drip-lines. Cross-sections of  $^{24}\text{O}$ ,  $^{29}\text{F}$ ,  $^{30}\text{Ne}$  are increased about 1-3% with this option from a test in the  $^{40}\text{Ar} + \text{Be}$  reaction.

### 20.3. Geometrical Abrasion-Ablation Model

In the LISE code, a simple theory of fragmentation based upon a two-step abrasion/ablation model is presented [Wil87]. The abrasion process accounts for removal of nuclear matter in the overlap region of the colliding ions. An average transmission factor is used for the projectile and target nuclei at a given impact parameter to account for the finite meanfree path in nuclear matter. The ions are treated otherwise on a geometrical basis assuming uniform spheres. The surface distortion excitation energy of the projectile

prefragment following abrasion of nucleons is calculated from the clean-cut abrasion formalism of [Gos77]. Wilson’s model also includes (see Chapter 20.3.1.2. Excitation energy):

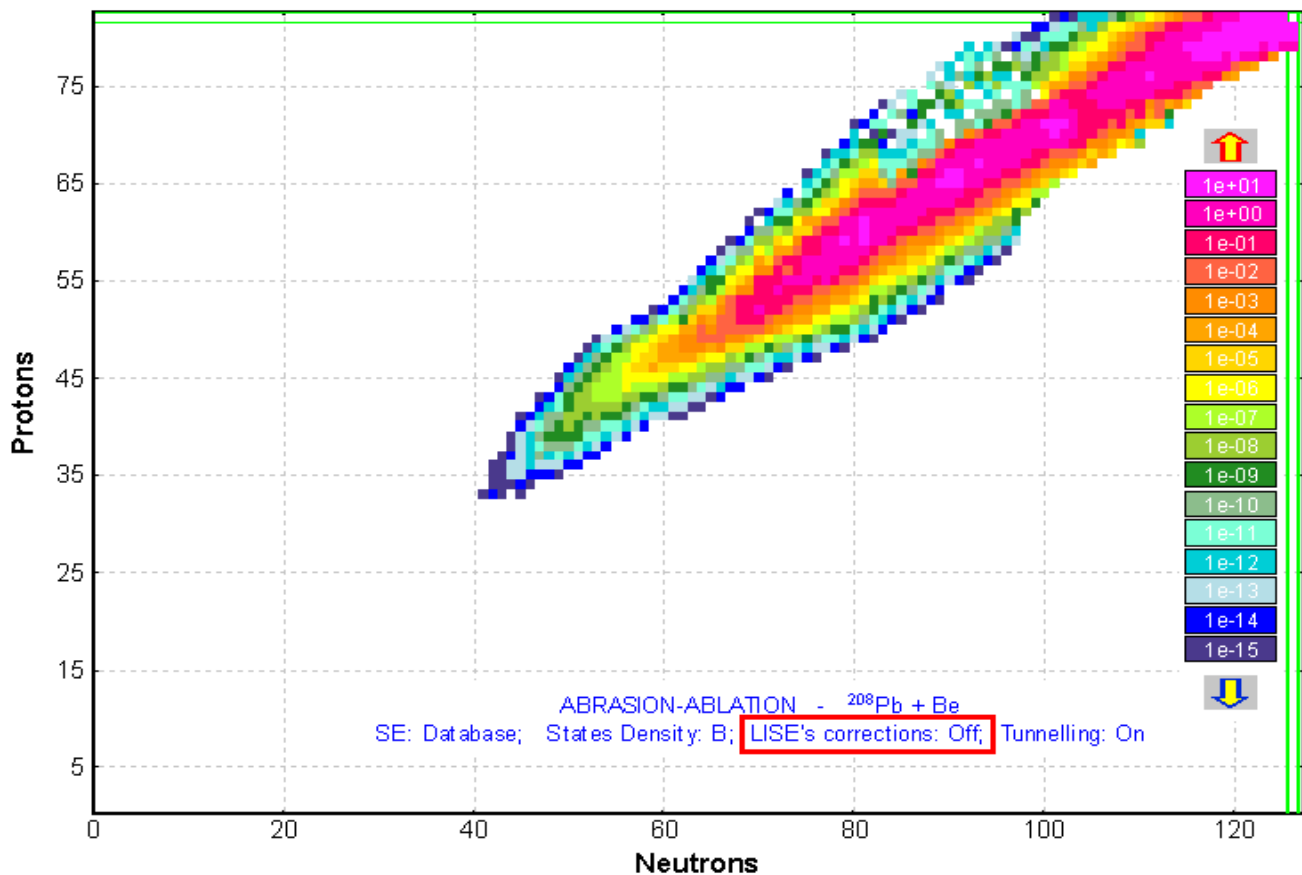
- The excitation energy correction factor when large portions of the nucleus are removed in the collisions;
- The transfer of kinetic energy of relative motion across the intersecting boundary of the two ions (friction).

### 20.3.1. Abrasion-Ablation settings

User may access the abrasion-ablation setting via the “Evaporation settings” dialog (see Fig.603).

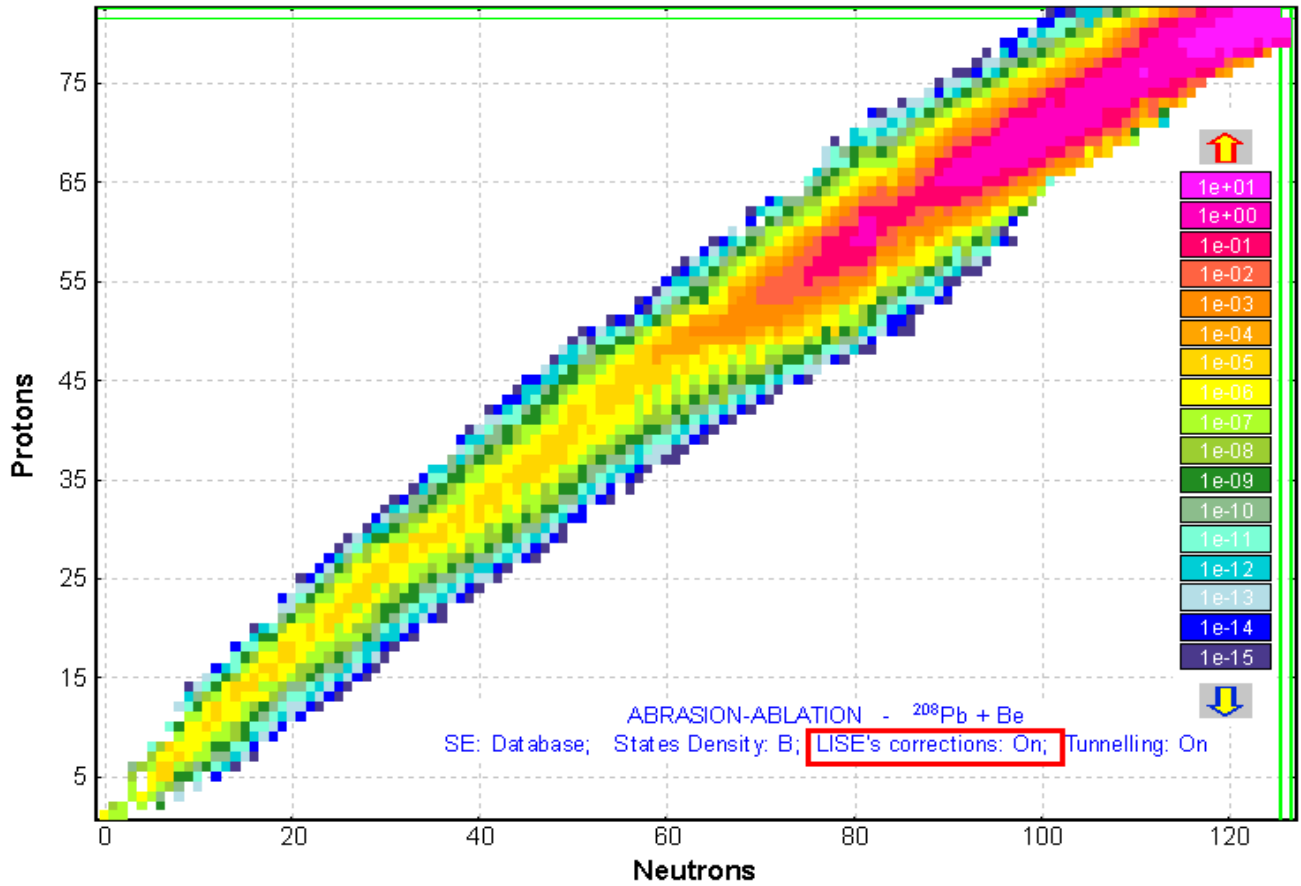
#### 20.3.1.1. LISE corrections

There are restrictions some in the geometrical abrasion-ablation model when light target are used. For example, it is impossible to get a prefragment mass less than 22 in the  $^{40}\text{Ar}+\text{Be}$  reaction. In other words the target cannot in this geometrical assumption make an aperture in a particle more than the volume proportional to mass 18 nucleons. Further prefragment deexcitation will not allow to be lowered more than on 5 units, though in experiments all spectrum of elements inclusive up to hydrogen is observed (see Fig.605). Corrections have been incorporated in the program LISE to solve this restriction. The code extrapolates exponentially the dependences of cross-sections and excitation energies from the prefragment mass in the



**Fig.605.** Cross-sections plot for the  $^{208}\text{Pb} + \text{Be}$  reaction. LISE corrections for Geometrical Abrasion-Ablation model are switched OFF.

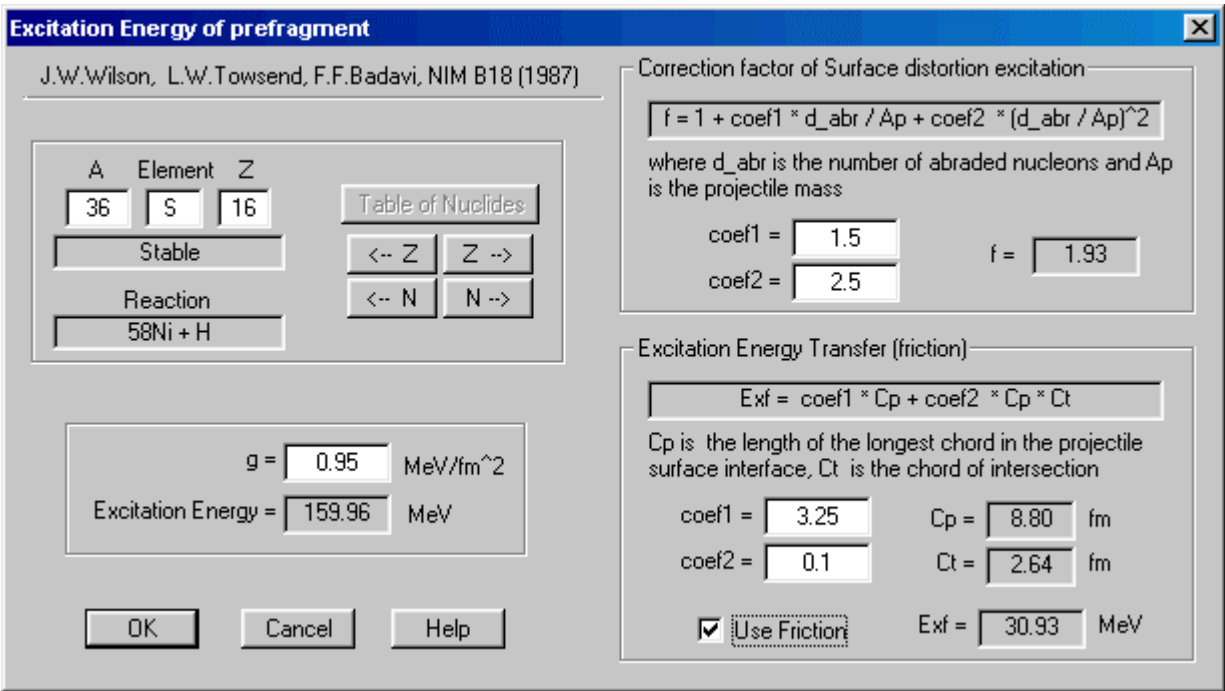
break point in a lightest targets case (Fig.606).



**Fig.606.** Cross-sections plot for the  $^{208}\text{Pb} + \text{Be}$  reaction. LISE corrections for Geometrical Abrasion-Ablation model are switched ON.

### 20.3.1.2. Excitation energy

The user can vary excitation energy options in the “Excitation energy of prefragment” dialog (Fig.607). This dialog is available the “Options” menu or the “Evaporation settings” dialog (see Fig.603). The excitation energy calculation is based on the work of [Wil87].



**Fig.607.** Prefragment excitation energy settings.

The user can change coefficients of correction factors in this dialog. Original coefficients in the work [Wil87] for correction factor expression (17) are 15 and 25. We assume, that these coefficients are erroneous. Real values should be in the range of 1.5 and 2.5 correspondingly. For example, if to suggest a projectile half-part abrasion the correction factor will be equal to 14.75! Comparing excitation energy with the work [Gai91], more realistic value of the correction factor should be about 2.

Two additional methods of excitation energy calculation are planned in the next version. The first method is based on the diabatic model [Gai91] (convolutions of several linear distributions), the second one is a simplified approach from the first method:

$$\langle E^* \rangle = C_1 \cdot \Delta A_{abr}, \quad \sigma^2 = 9.6^2 \cdot \Delta A_{abr} . \quad /56/$$

Cross-sections calculated by the abrasion-ablation model may be used for other calculations into the program (see Fig.608). Cross-sections are saved in the memory (see Fig.597) and will be recalculated if the projectile (target) is changed.

# Cross sections

$^{86}\text{Kr} + \text{Ni} \rightarrow Z=28$

$g=0.95$ ; SE: Database; St.Density: B; Geom.Corr: On; Friction: On; Tunnelling: On;  $dR=6.0$  fm

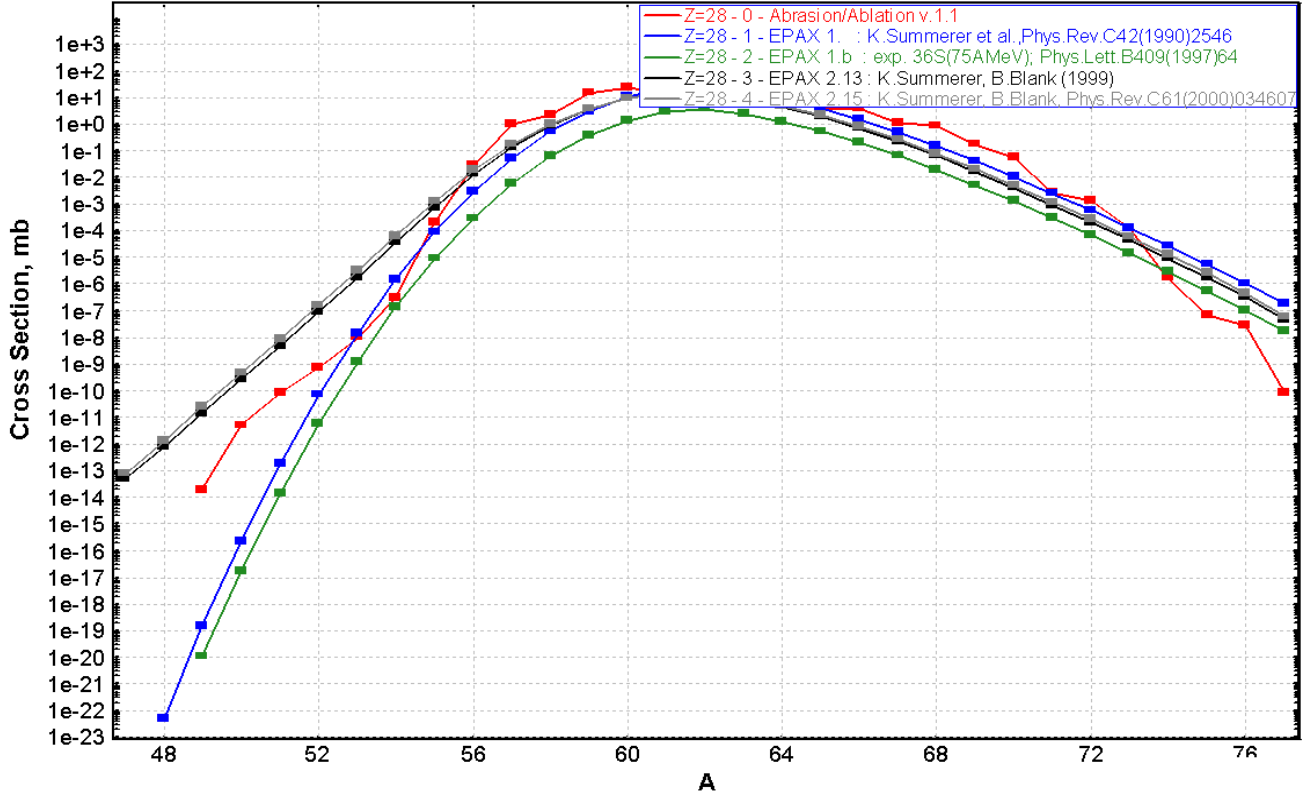


Fig.608. Prefragment excitation energy settings

## Epilogue.

All remarks, comments for the Evaporation calculator and Abrasion-Ablation model **are welcome!**



# 21. version 4.17

East Lansing  
09-JUN-2001

## Relativistic Kinematics Calculator

### 21.1. Short review of the Kinematics Calculators in previous versions of the code

The purpose of these calculators is to help physicists quickly get visual information on various characteristics of nuclear reaction, in particular about the kinematics of the reaction products. In previous versions the following utilities for kinematics calculation were already available:


1. Version 4.0.30 – Reaction kinematics (two body) relativistic calculations  
[http://www.nsl.msue.edu/lise/4\\_0\\_30/lise\\_4\\_0\\_30.html](http://www.nsl.msue.edu/lise/4_0_30/lise_4_0_30.html)
2. Version 4.13 - Scattering calculator  
[http://www.nsl.msue.edu/lise/4\\_13/lise\\_4\\_13.htm#g2](http://www.nsl.msue.edu/lise/4_13/lise_4_13.htm#g2)

However users of the LISE program stated the following:

- Calculations of break-up reactions kinematics;
- Possibility to enter the excitation energy for the particle and the target in the Scattering calculator;
- Errors in the calculations of scattered particles rates in detectors (Scattering calculator) were noticed.

In the new version these utilities were incorporated in one unique “Kinematics Calculator”, which includes all features from both calculators as well as new options.

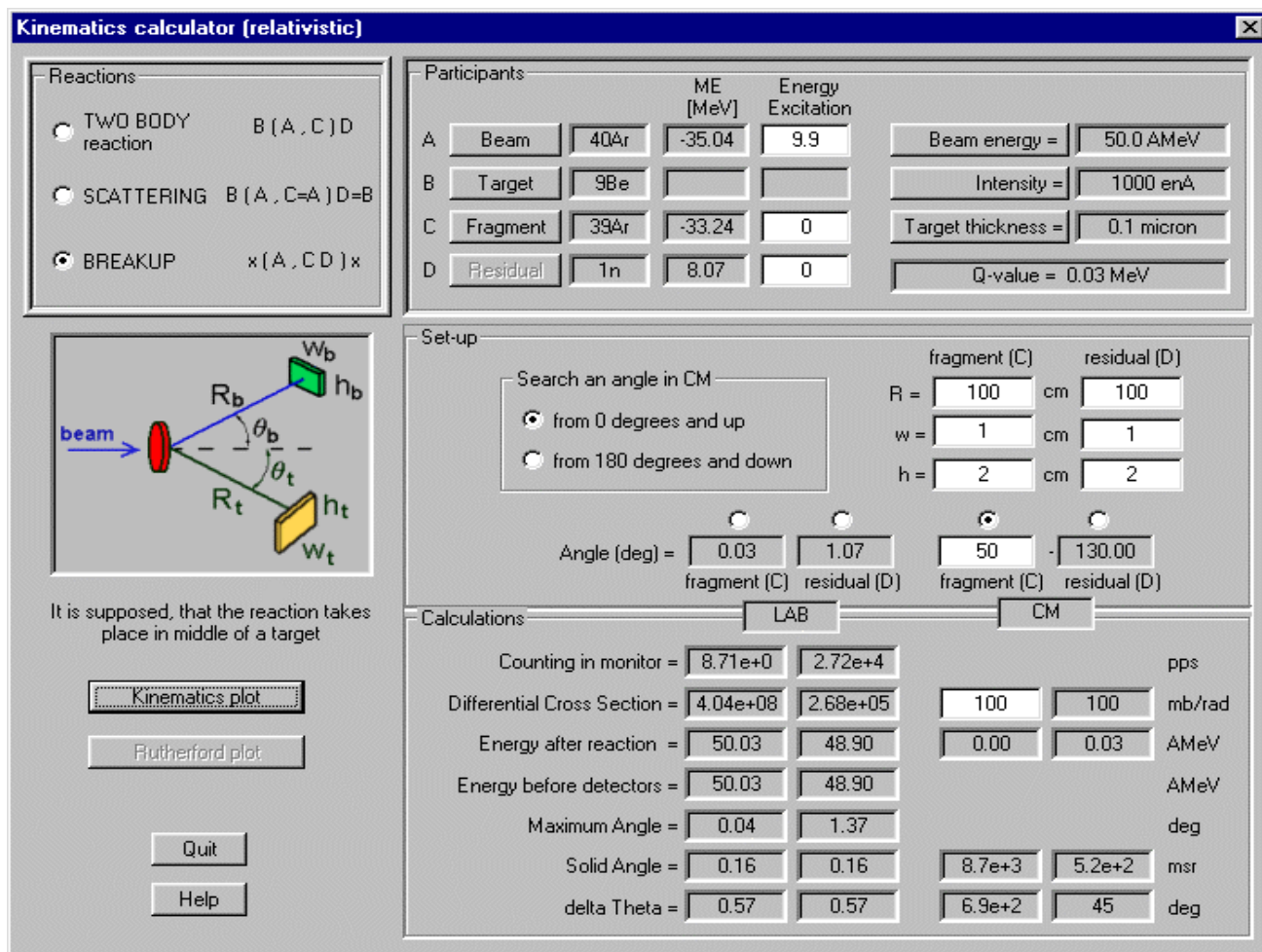
### 21.2. Kinematics Calculator

The new “Kinematics Calculator” is available in the “Calculations” menu or via the icon  in the toolbar. The “Kinematics Dialog” is shown in Fig.609. In this dialog the user can choose one from three types of reactions. For convenience all participants of the reaction are designated by letters and the possible types of reactions are shown.

New features:

1. The kinematics calculation of break-up reactions was added (see Fig.610). Note that for break-up reaction the Q-value has to be greater than zero! (otherwise the reaction will not occur);
2. Possibility to enter of the excitation energy of all participants;

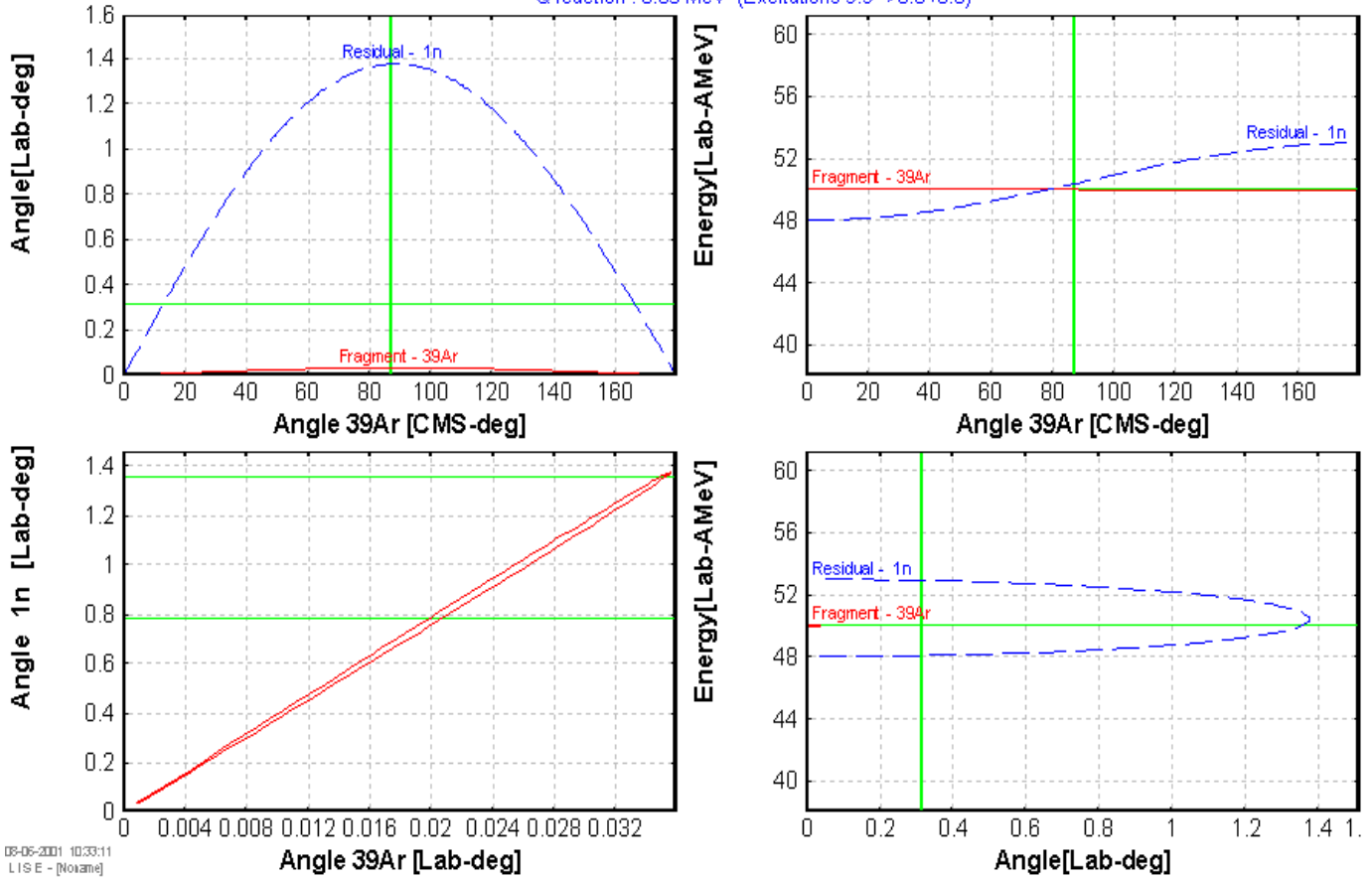
- Possibility to enter the parameters of beam and target directly from the dialog (in previous versions it was necessary to leave the dialog);
- Possibility to use to use a detector system for break-up and two-body reactions also (before it was only for scattering). However it is necessary manually to set the differential cross-sections in these cases;
- Some errors have been corrected.



*Fig.609. Kinematics Calculator*

## Reaction's Kinematics

$^{40}\text{Ar} \Rightarrow ^{39}\text{Ar} + n$      $\times (^{40}\text{Ar}, ^{39}\text{Ar} + n) \times$   
 Projectile Energy : 50.00 AMeV  
 Q reaction : 0.03 MeV (Excitations 9.9=>0.0+0.0)



**Fig.610.** Kinematics calculations plot for break-up of  $^{40}\text{Ar}^*$  (50AMeV) to  $^{39}\text{Ar}$  and  $n$ .

### 21.3. Miscellaneous

#### 21.3.1. Simultaneous and separate changes of horizontal slits

In previous versions it was assumed, that the slits in dispersive and first focal planes were symmetric, whereas the slits after the velocity filter could establish could be moved independently. In the new version the user can get all horizontal slits independently (see Fig.611). To use this feature the user has to choose the mode “Separately” (compare “A” and “B” in Fig.611).

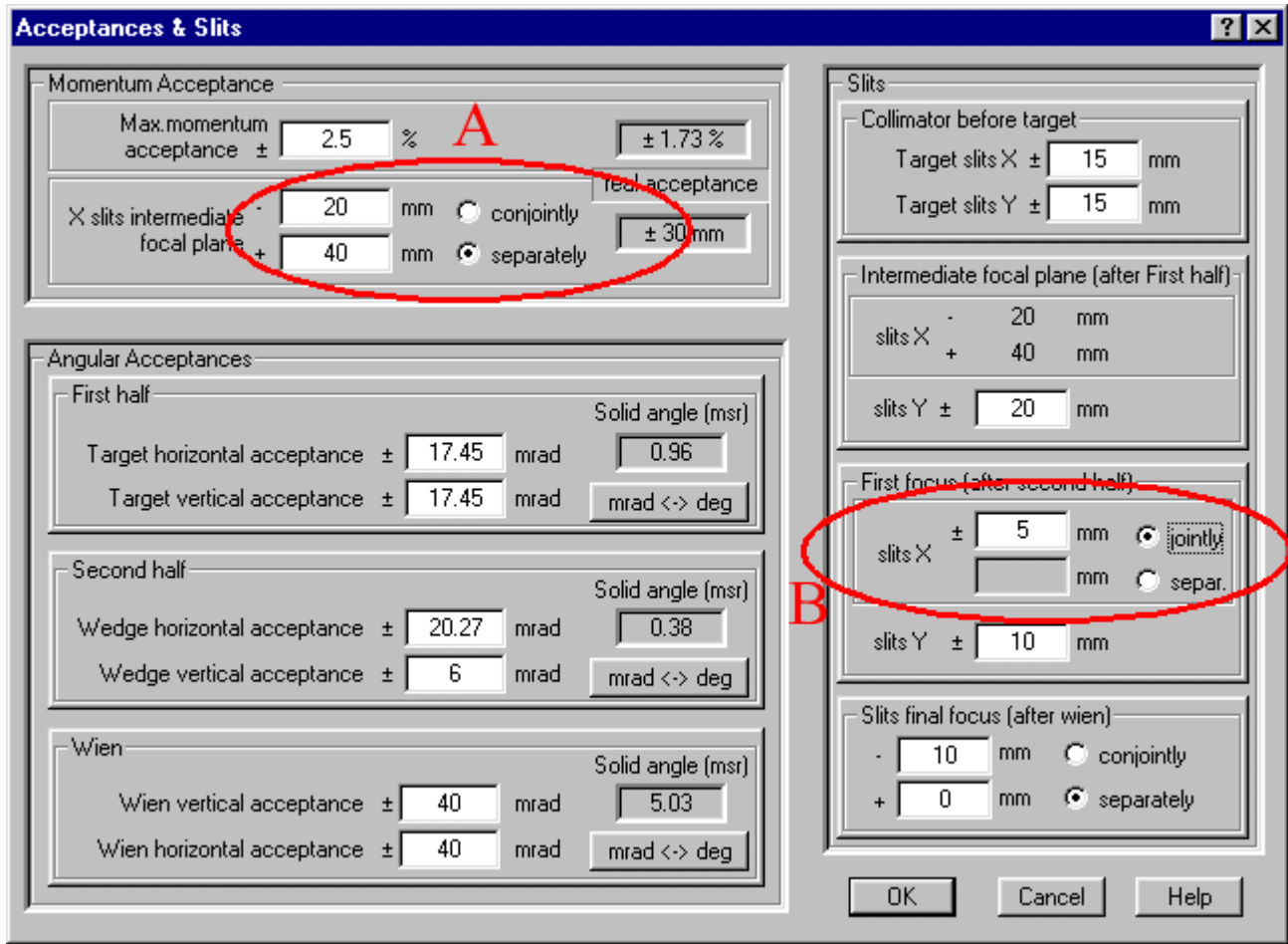


Fig.611. The "Acceptances & Slits" dialog.

### 21.3.2. Stepping of dipole values

In the new version the user can increase or reduce (see A in Fig.612) the magnetic rigidity and magnetic field by percentage set by the user (B in Fig.612). The same feature exists now for all calibration dialogs as well.

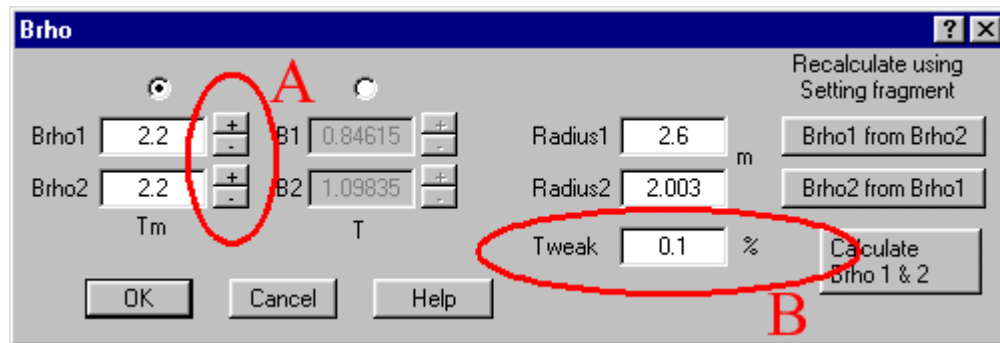


Fig.612.  $B\rho$ -values setting dialog.


### 21.3.3. Dimension of Secondary reactions distributions

The user can set the dimension of distributions of secondary reactions contributions in the OPTIONS menu > Preference. By increasing the dimension the user improves calculations quality, but loses in speed. The default value is set to the minimal value (16).

### 21.3.4. Accelerator Radio Frequency fraction for dE-TOF plot

In the menu PLOT-> OPTIONS it is possible to set an accelerator radio-frequency fraction for dE-TOF plot. The default value is 1. NSCL scientists use for this kind of plots to prevent the folding of the time-of-flight on the spectrum with fraction equal to 2.

### 21.3.5. Statistical characteristics of plot distributions

 - A new icon has been added in the toolbar for some one-dimensional plots. By clicking on this icon the user may get all statistical characteristics of plot distributions – (x-mean, x-max, y-max, standard deviation, FWHM and area).

### 21.3.6. Bugs

Some bugs have been corrected:

1. Coefficient of “Dead” thickness in the mode of “Charge states”.
2. Nuclear binding energy calculation.
3. Code crash in universal momentum distribution parameterization for light nuclei (H, He).
4. Savitsky-Golay smoothing filter for optimal target thickness calculations.

#### 21.3.6.1. Error in the list of recently used file.

A bug in the “files” menu was sometimes observed (see Fig.613).

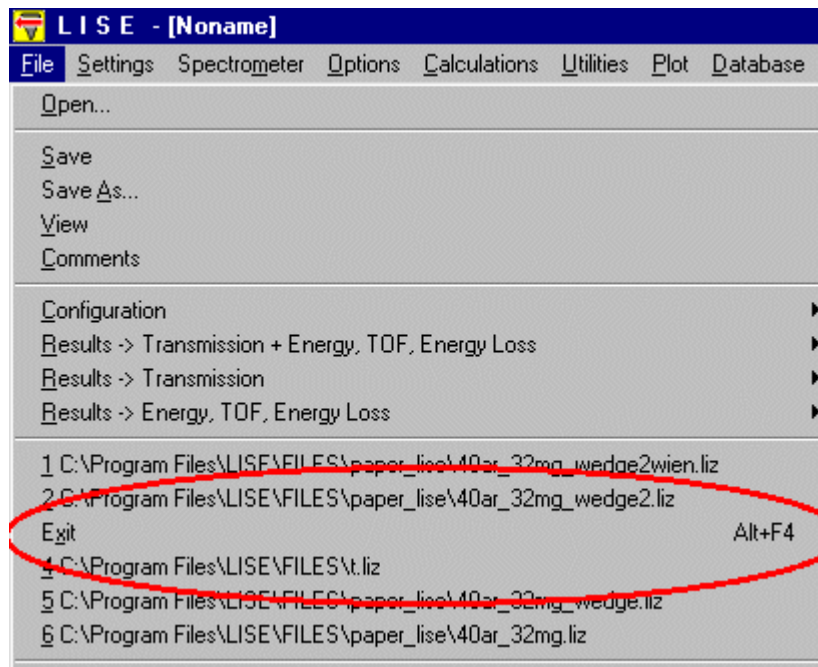


Fig.613. The bug in the FILES menu.

To correct this unpleasant incident, it is necessary to edit the file LISE.ini, which is in the LISE root directory (standard path is c:\program files\lise). The mistake is caused by MRU section (see below the

fragment of “lise.ini”, the MRU2 value corresponds a zero line). To correct this problem, it is necessary to enter a filename on the blank line (preferably a LISE file :-). This mistake will be corrected in the near feature.

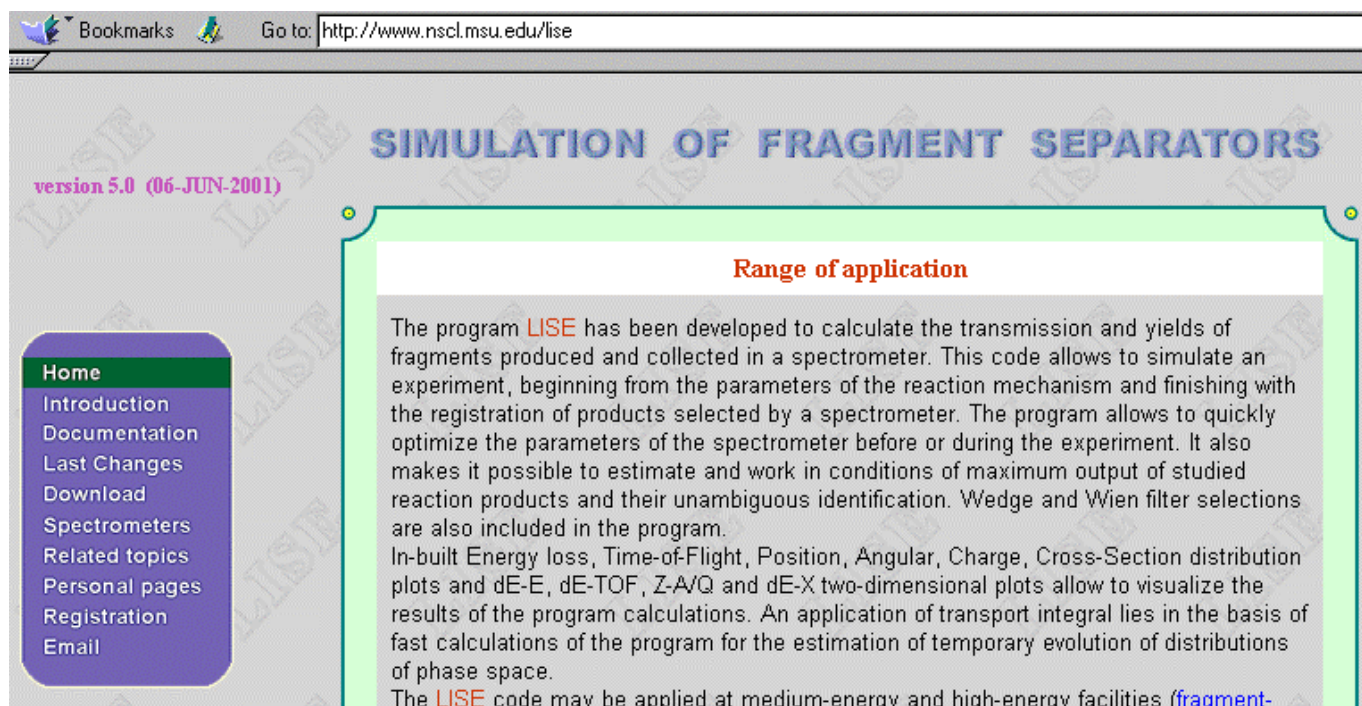
```
[MRU]
Count=6
MRU0=C:\Program Files\LISE\FILES\paper_lise\40ar_32mg_wedge2wien.liz
MRU1=C:\Program Files\LISE\FILES\paper_lise\40ar_32mg_wedge2.liz
MRU2=
MRU3=C:\Program Files\LISE\FILES\t.liz
MRU4=C:\Program Files\LISE\FILES\paper_lise\40ar_32mg_wedge.liz
MRU5=C:\Program Files\LISE\FILES\paper_lise\40ar_32mg.liz
```

## 22. version 4.16

[www.nscl.msu.edu/lise](http://www.nscl.msu.edu/lise)  
[dnr080.jinr.ru/lise](http://dnr080.jinr.ru/lise)

East Lansing  
07-JUN-2001

### WEB sites Code installation



Bookmarks Go to: <http://www.nscl.msu.edu/lise>

## SIMULATION OF FRAGMENT SEPARATORS

version 5.0 (06-JUN-2001)

- Home
- Introduction
- Documentation
- Last Changes
- Download
- Spectrometers
- Related topics
- Personal pages
- Registration
- Email

### Range of application

The program **LISE** has been developed to calculate the transmission and yields of fragments produced and collected in a spectrometer. This code allows to simulate an experiment, beginning from the parameters of the reaction mechanism and finishing with the registration of products selected by a spectrometer. The program allows to quickly optimize the parameters of the spectrometer before or during the experiment. It also makes it possible to estimate and work in conditions of maximum output of studied reaction products and their unambiguous identification. Wedge and Wien filter selections are also included in the program.

In-built Energy loss, Time-of-Flight, Position, Angular, Charge, Cross-Section distribution plots and dE-E, dE-TOF, Z-A/Q and dE-X two-dimensional plots allow to visualize the results of the program calculations. An application of transport integral lies in the basis of fast calculations of the program for the estimation of temporary evolution of distributions of phase space.

The **LISE** code may be applied at medium-energy and high-energy facilities ([fragment-](#)

### 22.1. LISE web sites

The LISE home site in Dubna (<http://dnr080.jinr.ru/lise>) has been updated in connection with the numerous remarks concerning slow down loading of this site due to the use of bulky Java-applets (at least for Windows NT and Windows2000). The new site is made without frames and is adapted under the monitor

with the resolution 800x600. Users can obtain detailed information about the program, and also load the new version in a new site.

The new home page (<http://www.nscl.msu.edu/lise>) was created in East Lansing (UNIX server 433 MHz Alpha with 700 MB of RAM). The given page is completely mirror to the Dubna LISE site.

The Dubna LISE site is run on a PC-based server (Pentium 200 MHz, 32 MB, OS Windows 98), that is much slower than the NSCL server.

The new version 5.0 of the program was dated to June 6 on Internet. However documentation on previous versions (4.17-4.20) will be sent to registered users in a near future.

#### **4.17 - Relativistic Kinematics Calculator**

#### **4.18 - Evaporation Calculator and Abration-Ablation model**

#### **4.19 - New Utilities and Correction of bugs**

#### **4.20 - Program ATIMA. Calculations of energy losses and stragglings in materials.**

## **22.2. Installation**

Users can access the ftp servers through the program LISE home pages in order to download the program:

East-Lansing, USA	<a href="ftp://ftp.nscl.msu.edu/pub/lise">ftp://ftp.nscl.msu.edu/pub/lise</a>
Dubna, Russia	<a href="ftp://dnr080.jinr.ru/lise">ftp://dnr080.jinr.ru/lise</a>

Try to connect from your web browser. If this method does not work, it is recommended to use an FTP tool such as WS\_FTP (available from <http://www.ipswitch.com>).

Users who are connected to the local networks of JINR and NSCL can download the program at the following addresses:

East-Lansing, USA	Nscl_user -> \\ Cycpc85
Dubna, Russia	FLNR -> \\ Tarasov586

### **22.2.1. LISE installation for Windows NT or Windows 2000 without administrator privileges**

During normal installation the setup program needs access to a temporary directory, and also has to be able to write in the table registers. However, to write in the table registers in systems Windows NT and Windows 2000 the user has to have the appropriate privileges, otherwise he will get an error during installation.

To be able to install the program without administrator privileges, the user can copy an already “open” (unpacked) version. That version is located at the following address:

[ftp://ftp.nscl.msu.edu/pub/lise/open\\_version](ftp://ftp.nscl.msu.edu/pub/lise/open_version)

The user should simply copy the contents of this directory on his computer, and directly run the program LISE.EXE.



### ***22.2.2. Getting things in order in the LISE directory and LISE menu***

Each new version of the program had its own setup program, and was installed on top of the old version. With the new versions some new files have appeared, and some have disappeared or were renamed. As a result:

1. In the CONFIG directory both old and new configuration files with different names are present for the same fragment separators;
2. For each new version a WORD file to describe the modifications was added. In the new version the description is in the file LISE.DOC, although the old files still are there.
3. In the program LISE menu (Start Menu - > Programs - > LISE) there should be only three shortcuts:
  - LISE.exe (executive file)
  - LISE.doc (WORD file)
  - LISE web site (html reference)

In the former versions a shortcut was created for each WORD file describing the modification. In addition these files were renamed for each different versions. As a result many unnecessary references have appeared.

We ask the users to do the following three operations **BEFORE INSTALLATION of the NEW VERSION**:

1. remove all files and subdirectories in the CONFIG directory (standard path is c:\program files\lise\config)
2. remove all files and subdirectories in the DOC directory (standard path is c:\program files\lise\doc)
3. remove all files and subdirectories the following directory: < WINDOWS DIRECTORY > \All users\profiles\Start menu\programs\LISE (or same) to remove shortcut icons.

## 23. Versions 4.14, 4.15

East Lansing  
23-MAR-2001

### Plot calibration utilities NSCL & The LISE code

#### 23.1. Plot calibration utilities – version 4.15

Physicists get in experiments the data in relative channels, then translate them proceeding from given calibration in real physical values. On the contrary the program does all calculations and creates the plots in absolute physical values. For comparison of calculations with experimental data a physicist was obliged with the calculator quickly to recalculate these plots. In the old versions under DOS the program allowed to deduce in channels for the plot dE-TOF. In the new version of the program it has been incorporated a

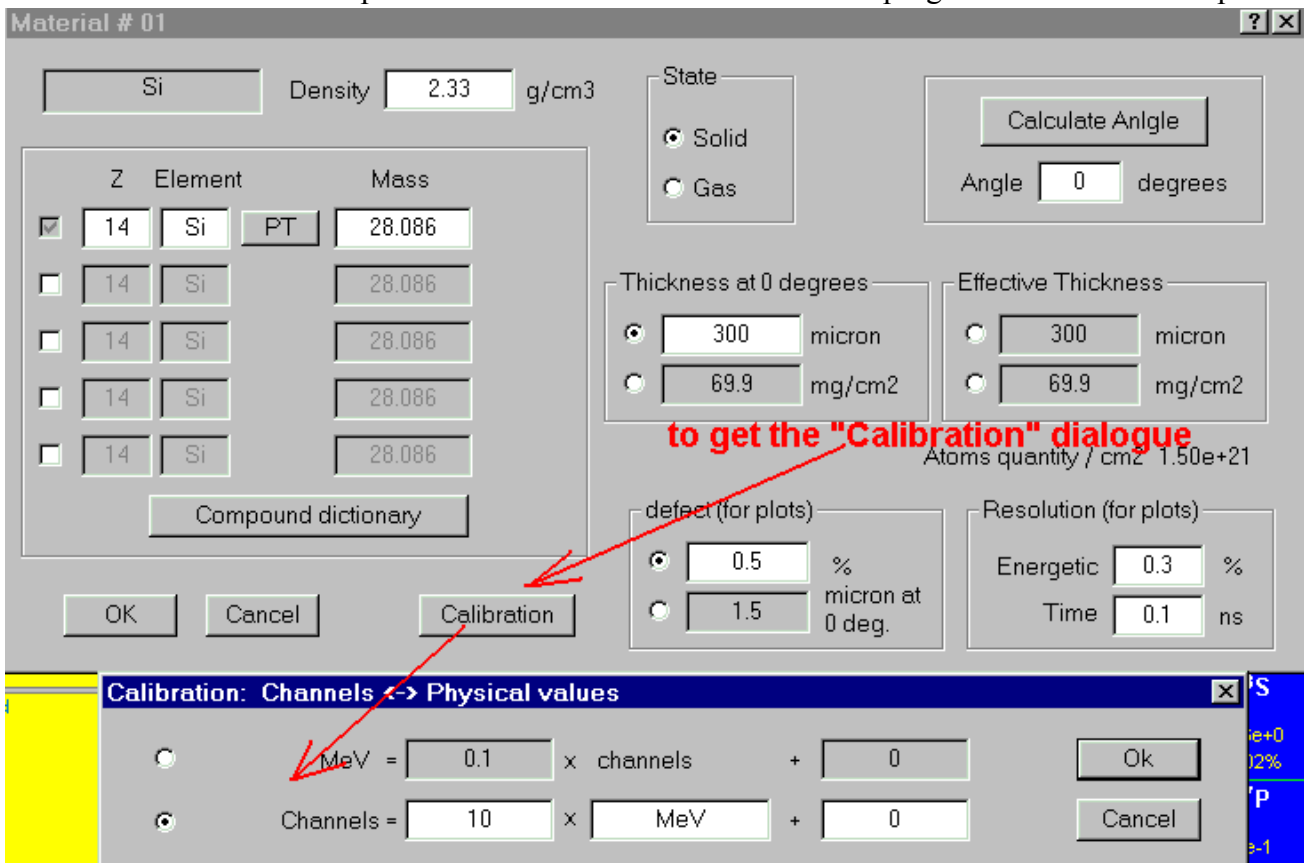


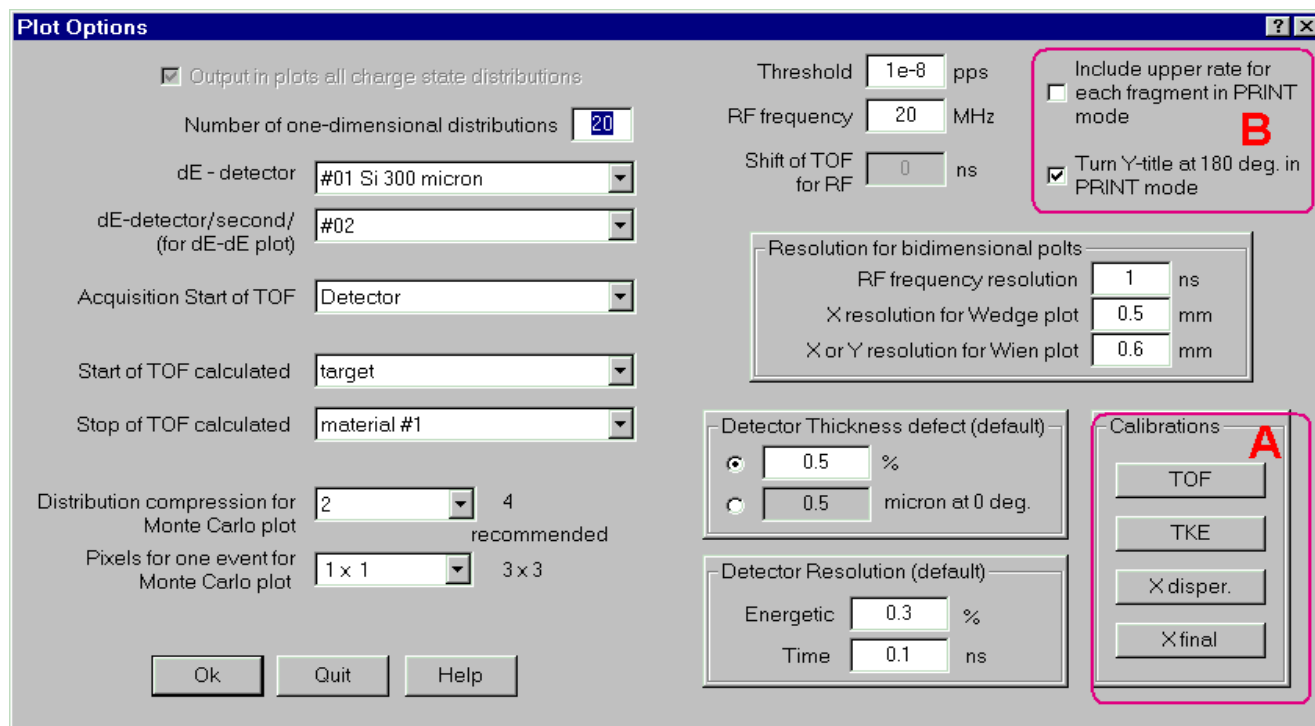
Fig.614. Input of calibration values of a material (detector).

possibility to input calibrations of 7 materials (detectors) and next 4 parameters: time of flight (TOF), total kinetic energy (TKE), horizontal distributions in disperse and final focal planes. All calibration values are kept in LISE-files.

### 23.1.1. Calibration of physical parameters

Calibration values for materials (detectors) are entered through the dialogue "Material", then the button "Calibration". The user can enter given as calibration of physical values through channels, so channels through physical values with the help of switching of a direction of input (see Fig.614). A name of dimension of physical value also can be modified (in the given figure the dimension is "MeV").

Input of calibration values for parameters TOF, TKE, Xdisp, and Xfinal is carried out through the dialogue "Plot options" (menu "Plots") (see Fig.615, the box A).



**Fig.615.** The dialogue "Plot options". The box A is showing the panel for input of calibration values for parameters TOF, Tke, Xdisp, Xfinal. The box B is showing new options to print plots.

### 23.1.2. Two-dimensional plots in the "calibration" mode

At work with two-dimensional plots a new window exists in the new version, where the relative channels values are displayed on the basis of entered calibrated values (see A in Fig.616). This innovation works as well as standard mode, and with Monte-Carlo method. Also all calibration values are transformed and in case of change of a direction of a horizontal axis, or change of axes X and Y.

The user can change calibration values directly at work with the given plot, pressing on an icon that is shown by the arrow C in Fig.616. As a result of this action there is the dialogue "Plot's Calibration" (see

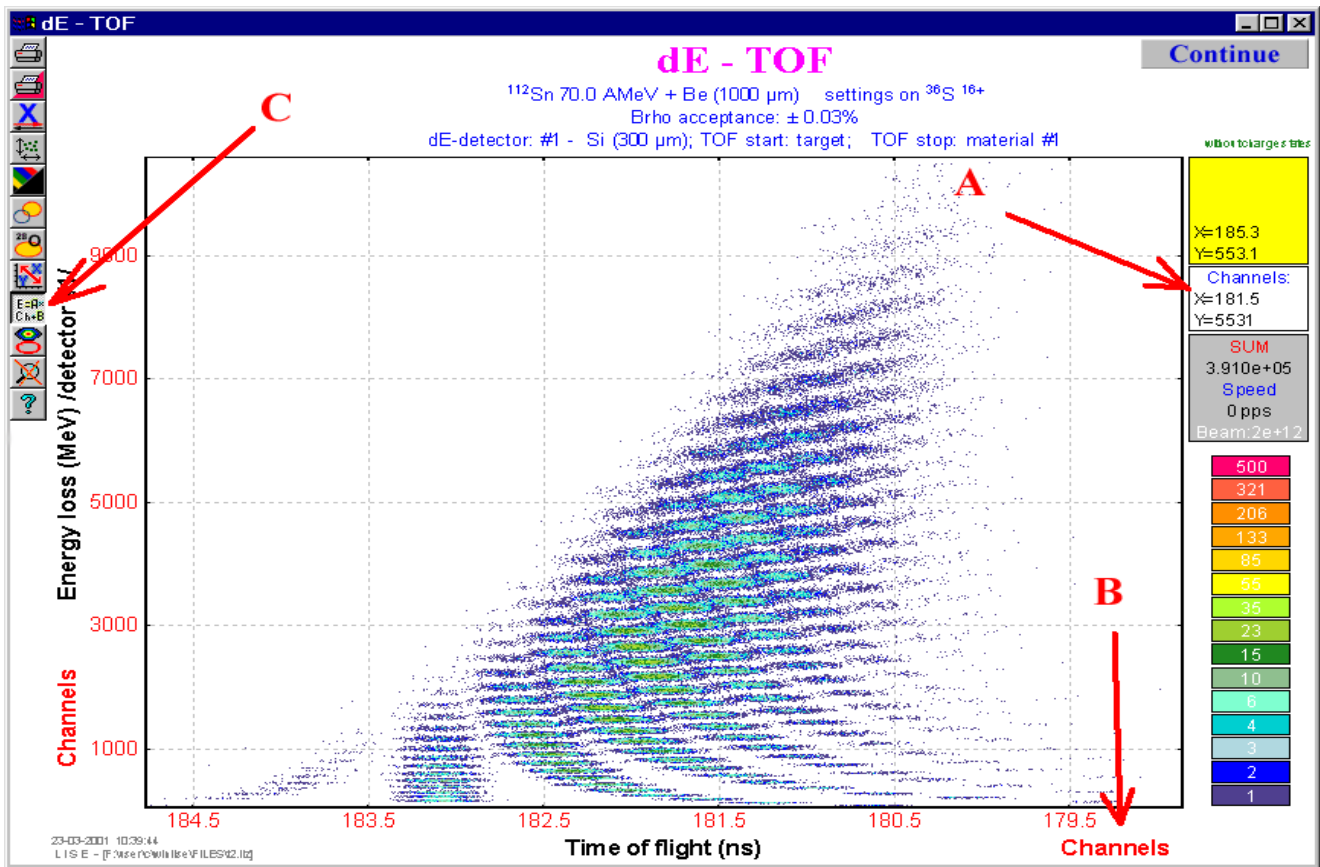


Fig.616. The bi-dimensional plot dE-TOF. New calibration possibilities are marked by arrows. For details see the text.

Fig.617). Besides that the user can change calibration, he also can put an option, that the axes were in channels designed on the basis of calibration that facilitate comparison of the experimental plots with designed by the program LISE. If the user has chosen an option of a conclusion given in channels, there is an inscription Channels in red color, and the digits on an axis also are deduced in red color (see Fig.616, arrow B).

### 23.1.3. New options of plots

In the early versions of the LISE program a fragment rate was always typed also to the right of a fragment name at output of two-dimensional plots on a printer. It was caused by that it were earlier used black-and-white printers to print. Now color printers are used everywhere. The user can switch off this possibility and print a plot without rates value (see Fig.615, box B).

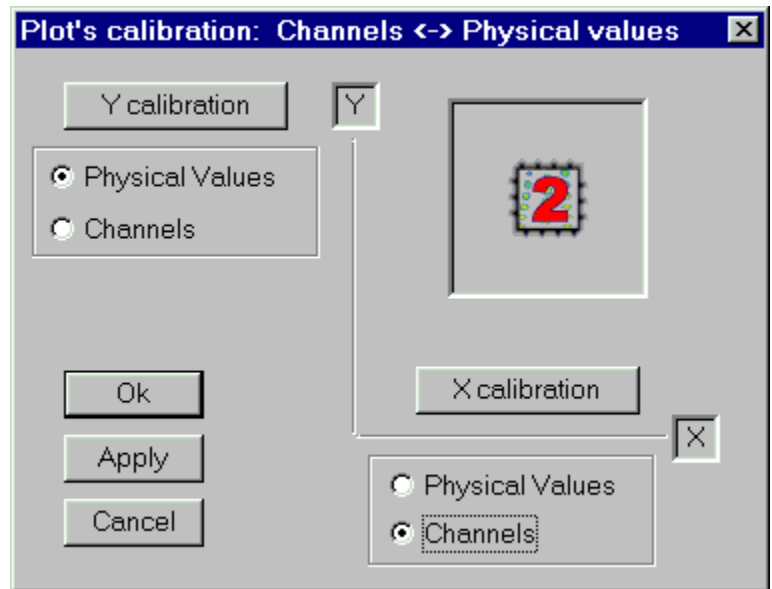


Fig.617. The dialogue "Plot's calibration" allows to change calibration values and to choose a method to draw axis's values (physical values or channels).

Unfortunately, the vertical inscriptions for various systems are deduced on the printer not as they are visible on the screen. The inscriptions are developed on 180 degrees sometimes in PRINT mode. To explain it was more hardly, than to make simply option of turn of the name of a vertical axis in PRINT mode (see Fig.615, box B). So for GANIL and JINR this option should be switched off, and for NSCL is on the contrary included. However user always can himself check up and choose an option inherent for his system.

### 23.2. NSCL & The LISE code - version 4.14

The user may get the scheme of new A1900 spectrometer using the menu “Help -> A1900 spectrometer”.

#### 23.2.1. Calibration of A1900's dipoles

As well as for setups LISE and M5678 (JINR) the calibration values of magnetic dipoles were entered for the A1900 spectrometer. Through the menu “Utilities -> A1900 calibration <PLAN>” the User may get the scheme of the A1900 spectrometer, where he can with the help of buttons choose a necessary dipole. The values can be entered as in tesla-meters, tesla, and amperes at the request of the user.

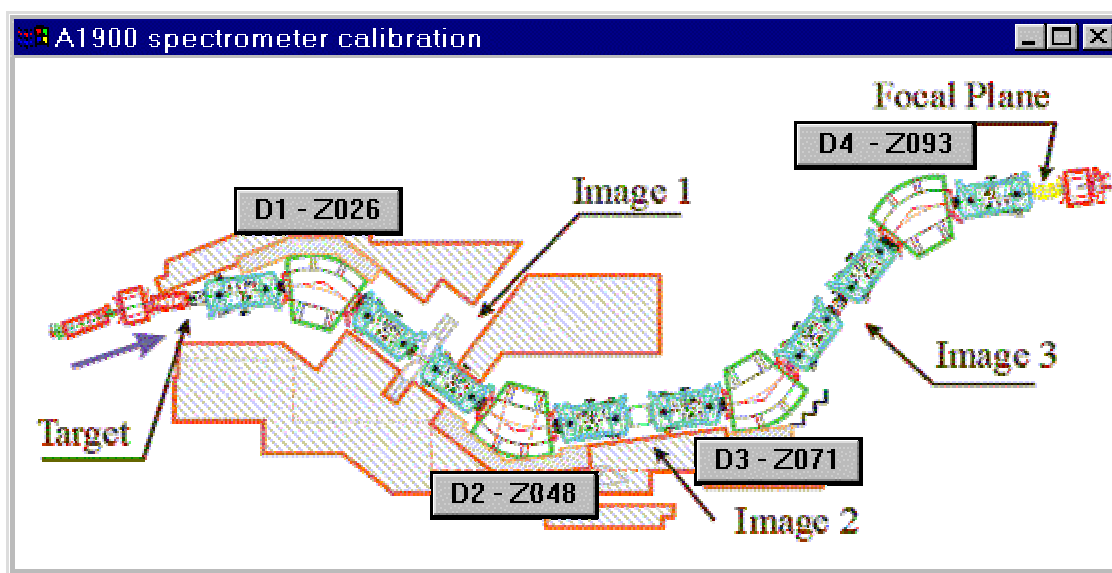


Fig.618. The A1900 spectrometer scheme with dipole calibration buttons.

#### 23.2.2. Support of NSCL specters

In the new version the opportunity to show on the screen spectra in a format NSCL-ACSII has appeared. The given spectra can be as well as one-dimensional, and two-dimensional. Thus in-built program BI can distinguish spectra of the given format to search peaks. The binary format of NSCL spectra will be entered into the program in a near future.

#### 23.2.3. Balls animation for Windows NT

Problem of palettes arising under Windows NT system at last was solved. Thus fans of the given operating system can be glad by this ball's animation.

#### ***23.2.4. Optimization of Monte-Carlo plots***

It was marked, the system takes away time from the LISE program on enough fast computers in a mode of a spectra acquisition by a method of Monte-Carlo. It was possible to be convinced visually, when the speed of a acquisition falls gradually from 20 thousand per second up to 1 thousand per second. In the new version the subroutine of a spectrum output by a Monte Carlo method was modified, that allows to have the greatest priority and to achieve speed of a set up to 45 thousand events per second for the computer Pentium III with frequency 600 MHz.

Algorithm of event drawing on the screen also was modernized, that essentially has allowed to reduce of a spectrum portrayal time.

## 24. Versions 4.10, 4.11, 4.12, 4.13

Dubna  
23.02.2001

### Scattering calculator Mass-separator mode BI code Prefragment search

#### 24.1. Preprint of LISE paper

It is our pleasure to inform, that after long years of work the preprint of the paper on the LISE code has been submitted to Nuclear Instruments and Methods B: “The program LISE: a simulation of fragment separators”. The preprint of the LISE paper (Preprint NSCL MSU, MSUCL-1187, January 2001) is available as a pdf file (<ftp://ftp.nscl.msu.edu/pub/lise/LISE.pdf>, <ftp://dnr080.jinr.ru/LISE/LISE.pdf>) or as a PostScript file (<ftp://ftp.nscl.msu.edu/pub/lise/LISE.ps>) (be patient, it is 120 Mbytes!).

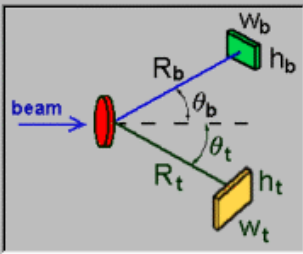
*ABSTRACT: This paper is a description of the program LISE, which simulates the operation of fragment separators, used in the production of radioactive beams via fragmentation. The various aspects of the physical phenomena involved in the production of such radioactive beams are discussed. They include fragmentation cross sections, energy losses in materials, ionic charge state distributions, as well as ion optics calculations and acceptance effects. Among the goals of this program is a highly user-friendly environment, designed not only to forecast intensities and purities for planning future experiments, but also as a tuning tool during experiments where its results can be quickly compared to on-line data. In addition, several general purpose tools such as a physical parameters calculator, a database of nuclei properties, and relativistic two body kinematics calculations make it also attractive in experiments where radioactive beams are not involved. After a general description of fragment separators, the principles underlying the calculations are presented, followed by a practical description of the program and its many features. Finally, a few examples of calculations are compared to on-line data, both qualitatively and quantitatively.*

#### 24.2. Scattering calculator – version 4.13

Continuing the tradition of developing the program of physical calculators, in the new version the calculator of a scattering process was created. The access to this calculator is carried out through the menu: *Calculation -> Scattering Calculator*. The given calculator is a powerful and convenient tool for estimations of Coulomb scattering cross-sections, energies of scattered particles, both in the laboratory frame, and in the center-of-mass system. The calculator also allows to estimate the maximal scattered angle of particles in the laboratory frame, and also to estimate the rate of scattered particles in the detectors. The scattering angle can be input by one of four possible ways, picking thus the frame and scattered particle. The user can at once see the results of calculations for the given angle in the calculator (Fig.619), and also to con-

struct the plots (Fig.620) Dependences of energies and angles in the laboratory frame on the scattering angle in the center-of-mass system are displayed: ( $\theta_{LAB} = f(\theta_{CM})$ ) and  $Energy_{LAB} = f(\theta_{CM})$ , and also plots  $\theta_{LAB} = f(\theta_{LAB})$  and  $Energy_{LAB} = f(\theta_{LAB})$ . Also the user can construct the plots of cross-sections of Coulomb scattering, both in the center-of-mass system, and in the laboratory frame (Fig.621).

**Scattering calculator (relativistic)**



Settings

Beam Target  
 6He(25.0 AMeV, 1000 enA) + H (100 micron)

Energy Excitation = 0 MeV 0  
 R = 100 cm 100  
 w = 2 cm 2  
 h = 2 cm 2

Angle (deg) = 7.05 19.65 140.00 - 40.00

projectile target projectile target  
 LAB CM

Calculations

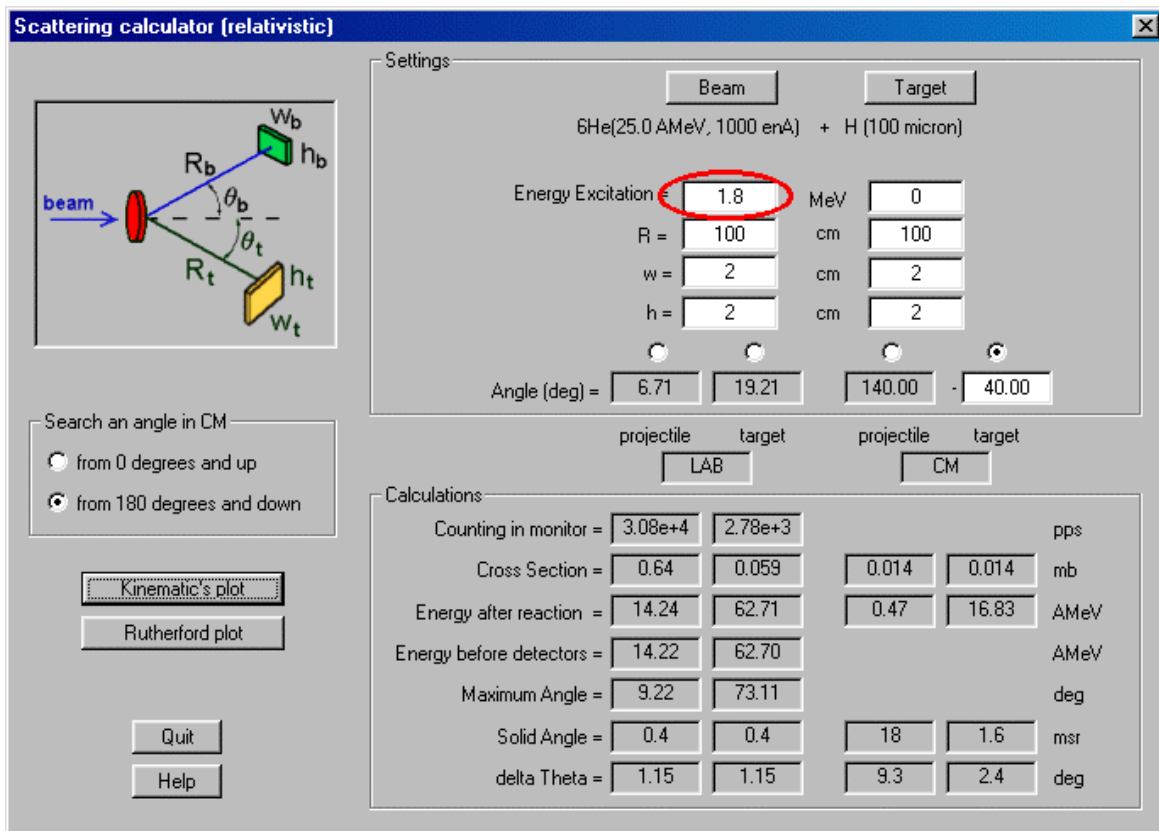
Counting in monitor =	2.8e+4	2.66e+3			pps
Cross Section =	0.58	0.056	0.014	0.014	mb
Energy after reaction =	14.07	65.50	0.52	18.37	AMeV
Energy before detectors =	14.06	65.49			AMeV
Maximum Angle =	9.64	89.99			deg
Solid Angle =	0.4	0.4	16	1.6	m sr
delta Theta =	1.15	1.15	8.9	2.3	deg

Search an angle in CM  
 from 0 degrees and up  
 from 180 degrees and down

Kinematic's plot  
 Rutherford plot

Quit  
 Help

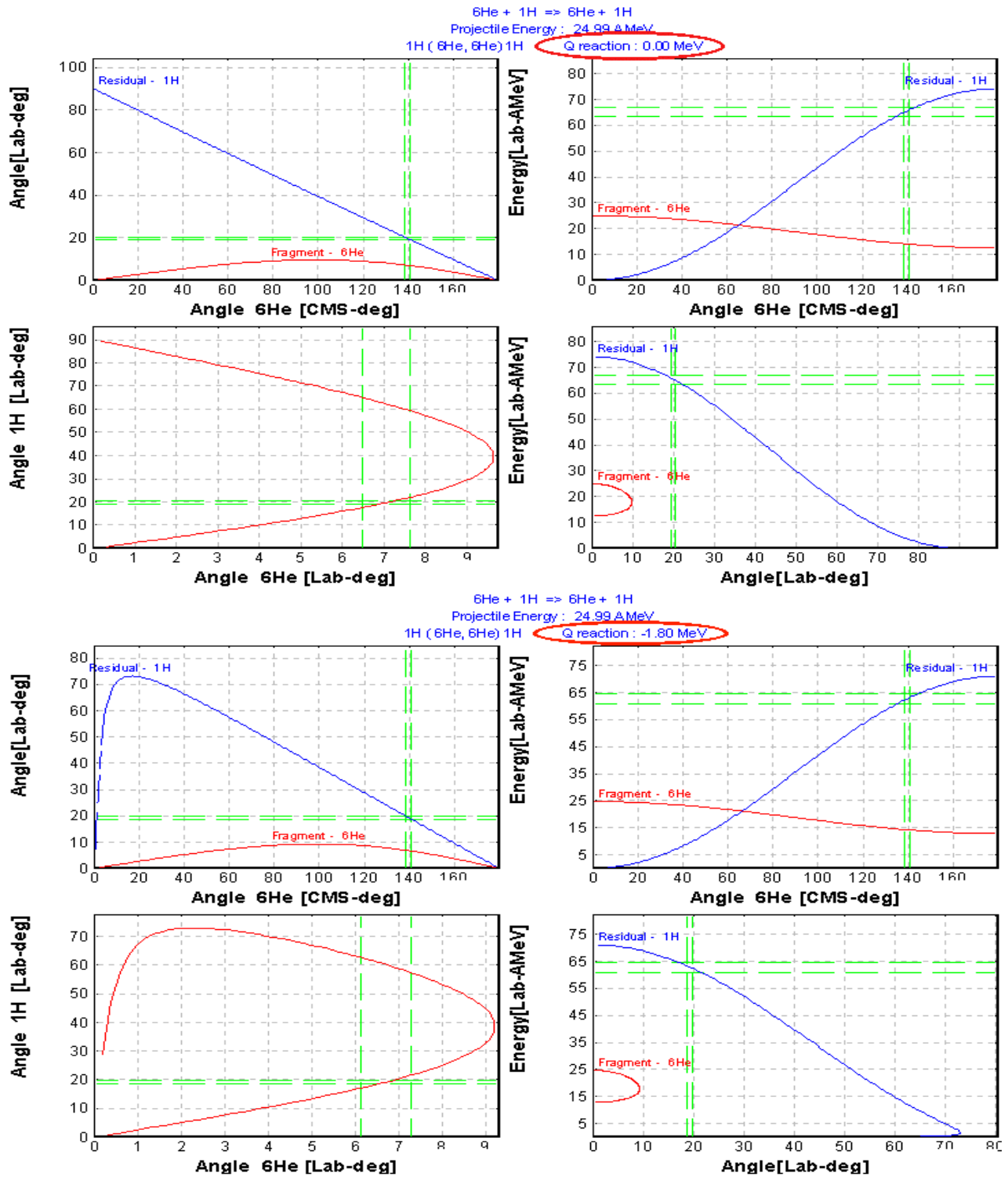




**Fig. 619.** Calculations made by the Scattering calculator for  ${}^6\text{He}$  (25 AMeV) on hydrogen at an angle of 140 degrees in the center-of-mass system for the ground state  ${}^6\text{He}$  (upper figure) and in case of excitation of the 1.8 MeV state (bottom figure).

In a series of cases for one scattering angle in the laboratory frame there can correspond two scattering angles in the center-of-mass system (as for example, for  ${}^6\text{He}$  on Fig.620). In such cases the user should set a direction of searching of the relevant angle in the center-of-mass system, if the initial angle is input in laboratory system. In the basis of the calculator lie the relativistic evaluations. The user can be convinced of it in case of the scattering of two identical particles at small energies (about some MeV per a nucleon) and at higher energies.

## Reaction's Kinematics



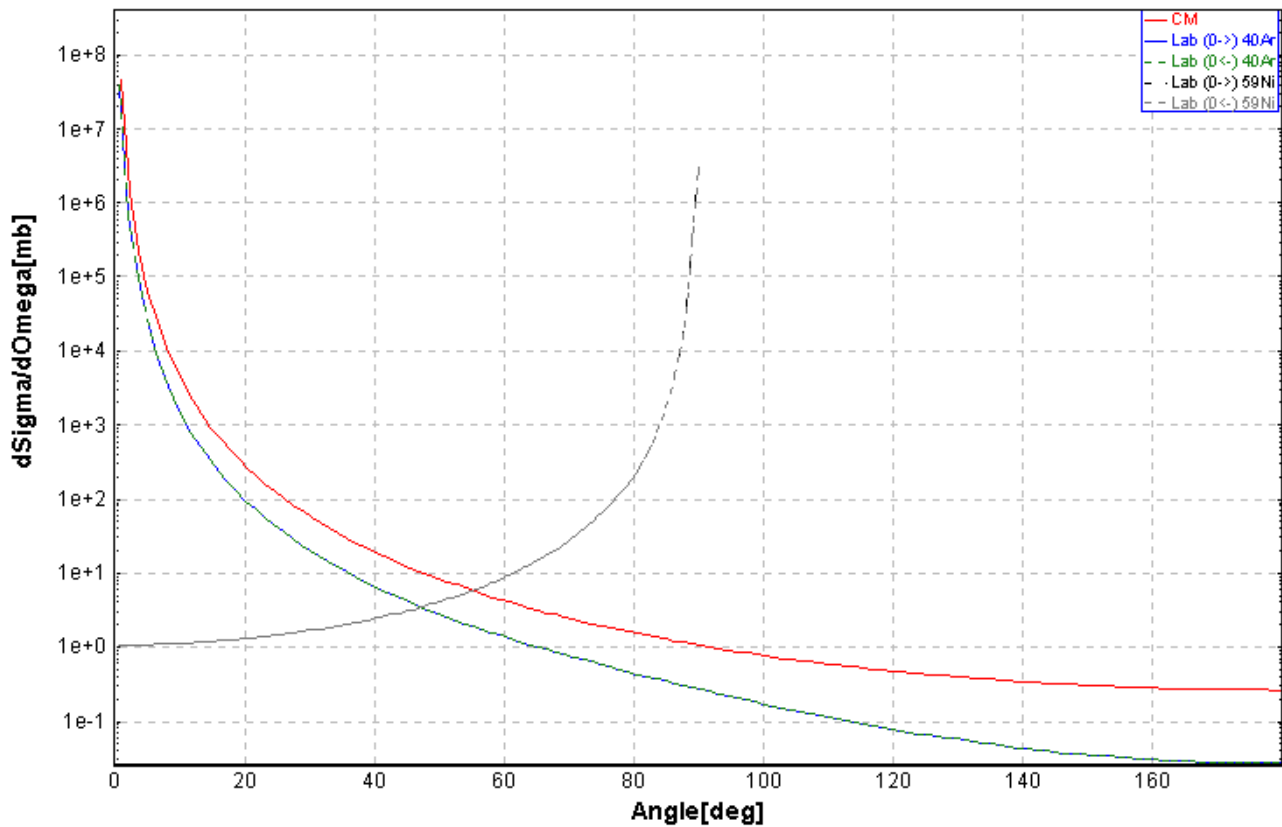
*Fig.620. Angular and energy dependences for the scattering of  ${}^6\text{He}$  (25A MeV) on hydrogen for the ground state  ${}^6\text{He}$  (upper figure) and in the case of excitation of the 1.8 MeV state (bottom figure).*

## Rutherford scattering

40Ar + 59Ni => 40Ar + 59Ni

Projectile Energy : 46.88 A.MeV

59Ni(40Ar,40Ar)59Ni    Q reaction : 0.00 MeV



**Fig.621.** Differential cross-sections of Coulomb scattering of  $^{40}\text{Ar}$  (46.7A MeV) + Ni in various frames.

In the calculations it is supposed, that the beam particle undergoes scattering in the middle of a target in view of losses of energy in the first half of the target. Further on, before registration in the detector both particles also lose kinetic energy in the target of width  $t/2/\cos(\theta_{\text{LAB}})$ , where  $t$  is the thickness of the target. The target is considered homogeneous so as to avoid complicated calculations with a composite target.

One convenience is also the opportunity of the assignment of excitation in one of the scattered particles. So on Fig.619 and Fig.620 the examples of scattering for the reaction  $^6\text{He}(25\text{A MeV}) + \text{H}$  without excitation  $^6\text{He}$  and for excitation  $^6\text{He}$  to 1.8 MeV are given (it is certainly supposed, that the nucleus does not collapse, though we know, that  $^6\text{He}$  is unstable at excitation of a level  $2^+$ ).

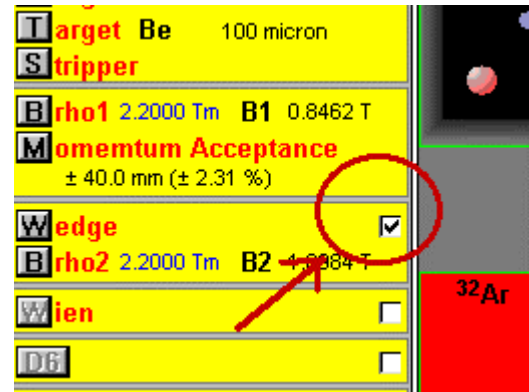
Also the given calculator can be used for estimating the intensity of the primary beam falling on the detector for registration of scattered particles, that very often is applied in physical experiments for monitoring the beam.

In the new version of the program in case of calculations of kinematics of a two-body reaction (menu *Utilities -> Reaction's kinematics /two body/*) the user will receive two additional plots  $\theta_{4\text{LAB}} = f(\theta_{3\text{LAB}})$  and  $\text{Energy}_{\text{LAB}} = f(\theta_{\text{LAB}})$ .

## 24.3. Mass-separator mode - version 4.12

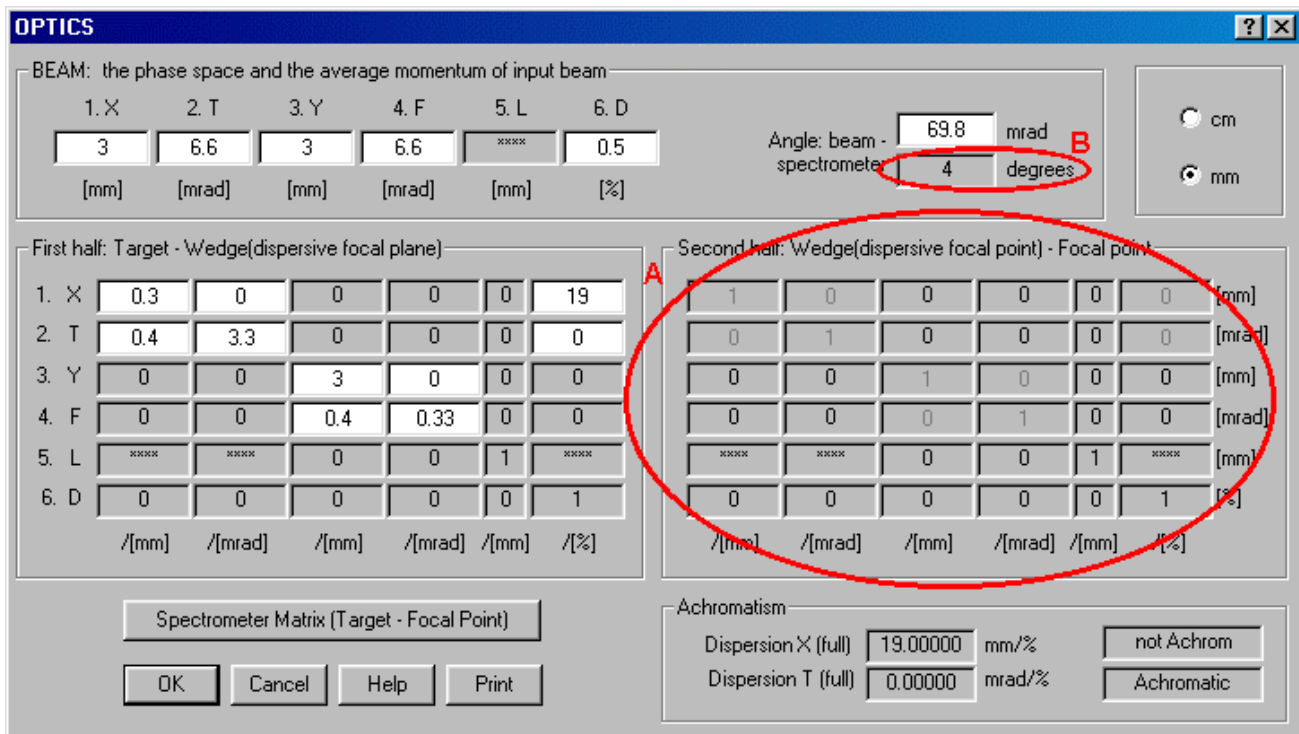
### 24.3.1. Cutout of the second dipole

Initially the program LISE was made for model operation of spectrometers consisting of two dipoles. Further the Wien filter of velocities, and later one dipole behind the filter permitting to yield a classification by A/Q was supplemented as an option. However, during operation with the program was clarified, that more prime configuration of operation in a mode of a mass separator consisting of one of a dipole is not realized, that makes possible to simulate experiments on such installations as SPEG, S800, MSP-144 and so on. Certainly, it was possible to accept an optical matrix of the second part of a spectrometer for single and to increase acceptances of the second part of a spectrometer, and also to increase slots in a final focal plane, so that there were no losses in transmission in the second part of a spectrometer. However, all this causes inconveniences, owing to what by more prime expedient it was embodied in the program. Now the user can switch off (Fig.622) the second dipole (accordingly to exclude from the program all calculations, connected to a wedge).



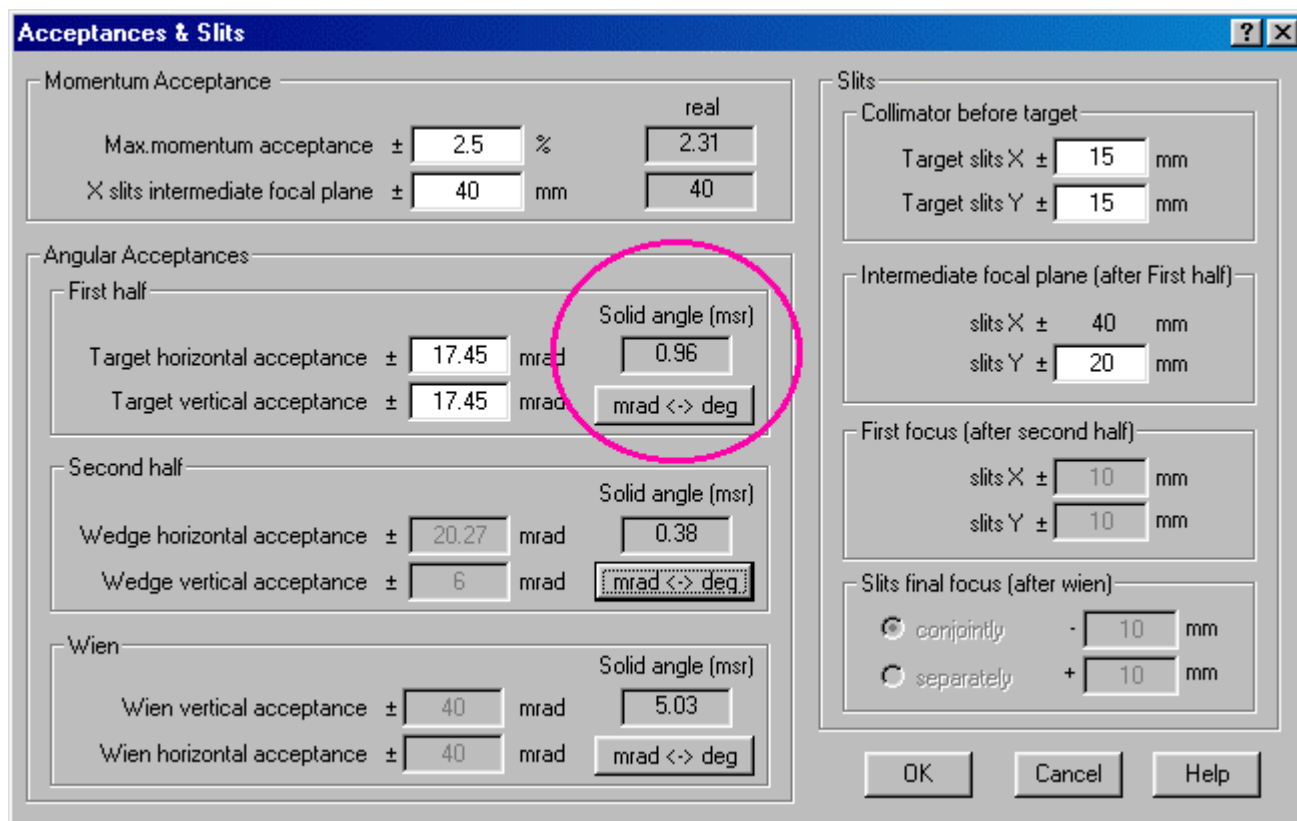
**Fig.622.** The button of insert / lockout of the second part of a spectrometer.

Switching off the second part of the spectrometer reduces the optical matrix of the second part of the spectrometer to identity matrix (see A on Fig.623), and the acceptances of the second part of the spectrometer are disregarded (see Fig.624). After lockout of the second part of the spectrometer, the user is



**Fig.623.** Dialogue "Optics" in the mass-separator mode

notified, that the configuration of the program was automatically changed. At repeated insert of the second part of the spectrometer there is again a message, that the user should tune the second part of the spectrometer by hand or load it from the configuration file.

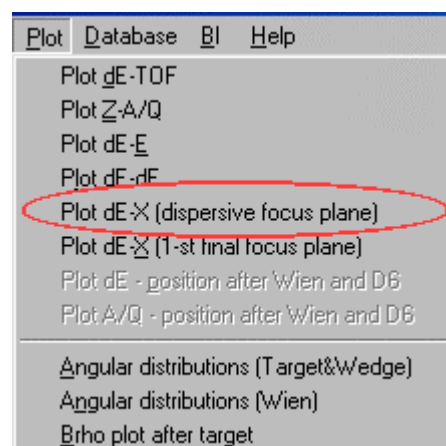


**Fig.624.** Dialogue “Acceptances and Slits” in the mass-separator mode

### 24.3.2. New dE-X plot in the dispersive focal plane

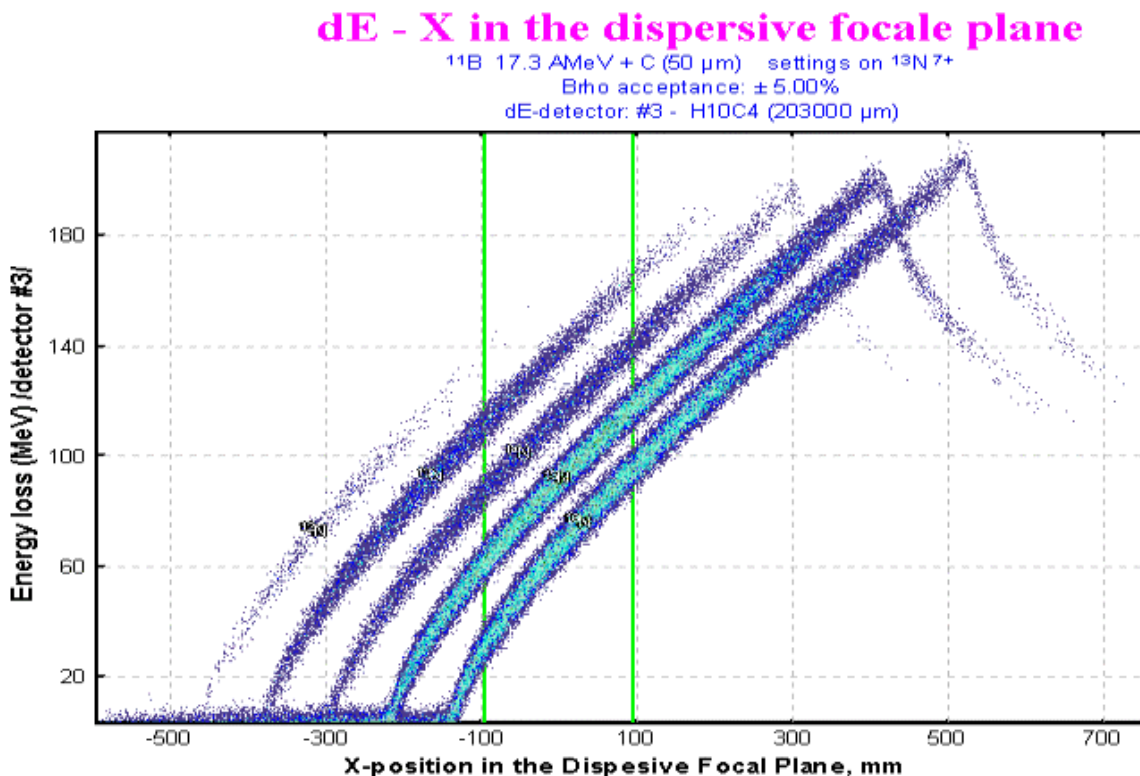
The dE-X plot in the dispersive focal plane is the most important one for experiments on mass separators. For this reason it was created in the new version of the program by adding it to already the existing dE-X plot in the final focal plane. In the program already there was an one-dimensional plot of horizontal distribution of fragments (X-Brho selection plot in IDFP). To obtain the plot of total kinetic energy versus X it is necessary first to enter major enough thickness of the detector for a stopping in him of products of reaction.

In Fig.625 the dependence of energy losses of the isotopes of nitrogen in the third detector on the horizontal position in the focal plane of the magnetic spectrograph MSP-144 [Bel98] in the reaction  $^{12}\text{C}(190\text{MeV}) + \text{B}$  is shown. In this case the focal detector was an the ionization chamber [Bel89] with 4 segmented anodes. The pressure of the gas is selected so that the studied ions are stopped in the third detector. In the figure it is well visible,

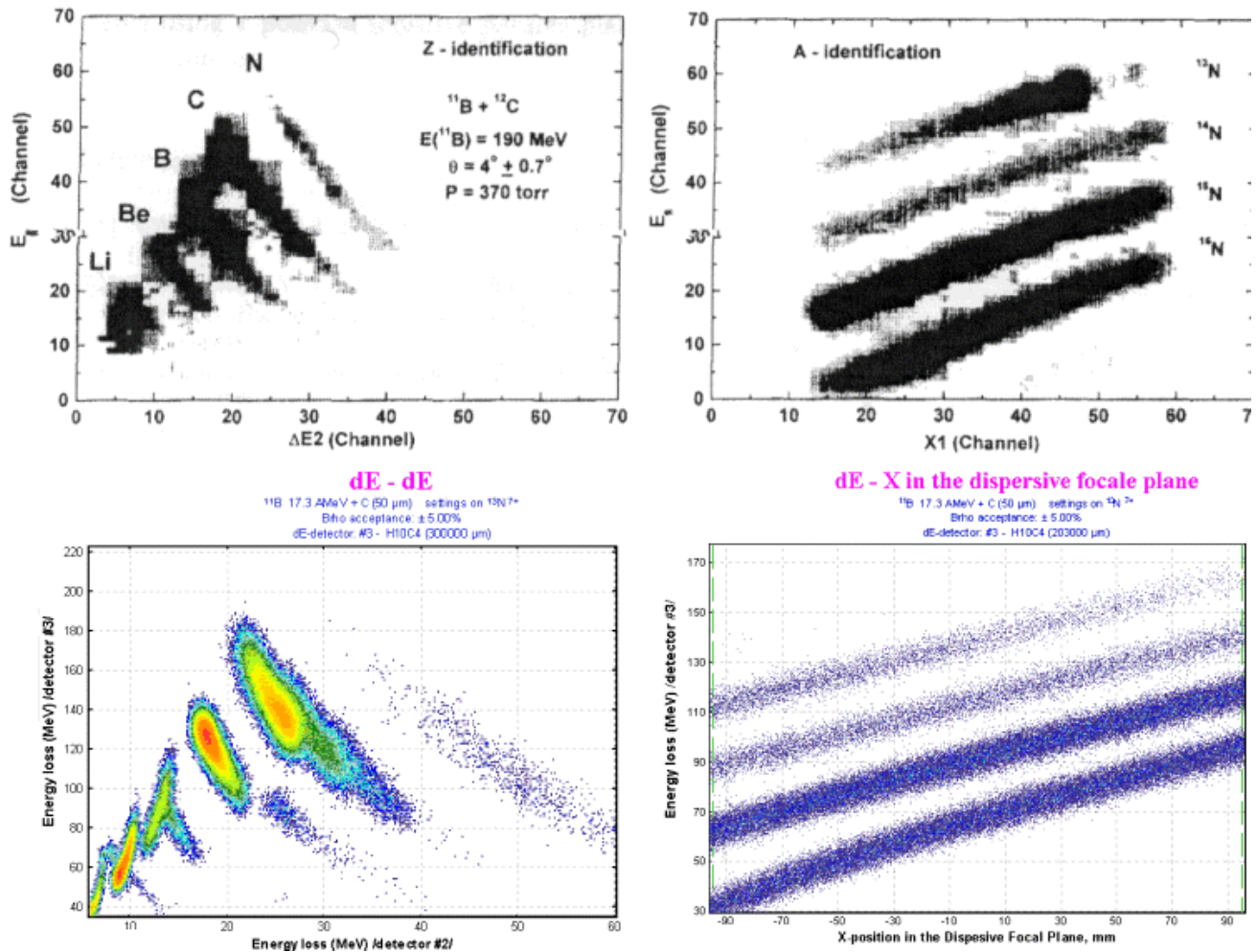


that at small energies the ions of nitrogen do not reach the 3-rd detector and are stopped in the second detector, which corresponds to the left-hand part of the spectrum. At higher energy, that corresponds to the right part of the diagram, the ions fly further than the third detector. Two vertical lines in the figure denote the size of the detector (-95 ÷ 95 mm).

The configuration file of the magnetic spectrograph MSP-144 has been incorporated in the list of LISE's setups.



**Fig.625.** The LISE code simulation: Two-dimensional plot of  $E_R$  vs.  $X$  for the  $^{12}\text{C}(^{11}\text{B}, ^{13}\text{N})^{10}\text{Be}$  reaction at 190 MeV incident energy. For details see the text.



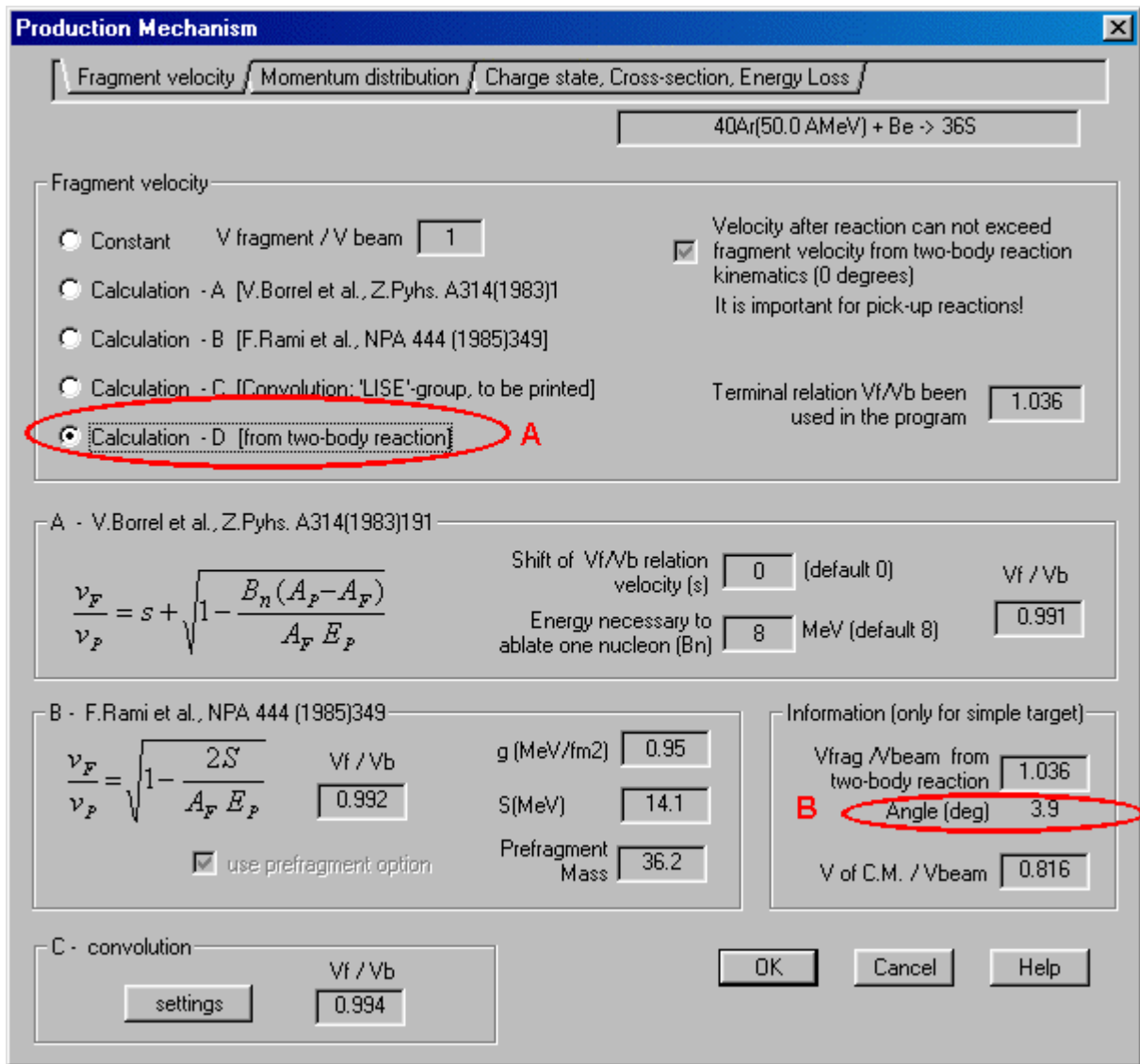
**Fig.626.** Comparison of experimental (upper) and calculated (lower) distributions. See the text for details

In Fig.626 the comparison of experimental distributions [Bel98] with calculated ones by the program LISE for the reaction  $^{12}\text{C}(190\text{MeV}) + \text{B}$  is presented. The upper plots represent experimental spectra  $\Delta E_2$  vs.  $E_R$  and  $E_R$  vs.  $X$ , where  $E_R$  is the rest energy, given by the third detector. On the lower panels the calculations accordingly represented. Inferior two-dimensional plot of  $X$  vs.  $E_R$  there is a fragment of Fig.625 that corresponds to a working band of the focal detector.

### 24.3.3. New opportunity to select the velocity of reaction products

The new version of the program to be used for a mass separator gives the opportunity to select the velocity of the reaction products in the two body relativistic kinematics (Fig.627-A). In the given evaluations the angle (Fig.627-B) of the mass separator with respect to the beam direction is included. This was made so as to be able to simulate results not only for fragmentation reactions, as was included earlier in the program, but also for transfer reactions. It is a first step in the program for this type of reaction, but as shown in chapter 24.3.5. it is still necessary to work in this direction.

In Fig.628 the distributions of velocities of reaction products from mass of an ion and from particle energy represented, where the calculations with evaluation, new to the program, of velocity of reaction products – two-body kinematics already represented.



*Fig.627. Dialogue “Production mechanism – Fragment velocity”*

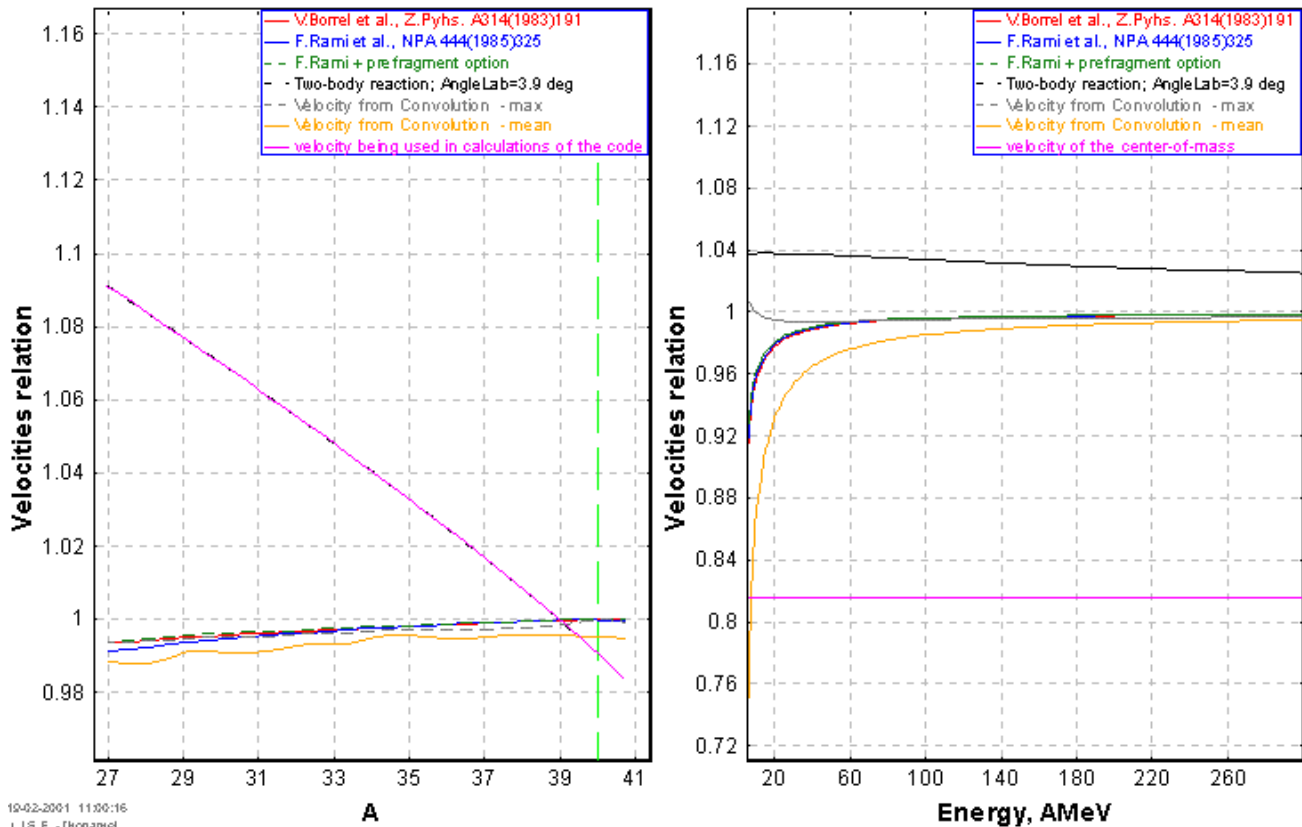


## Velocity of fragments after reaction

LEFT PLOT =>  $^{40}\text{Ar} + ^9\text{Be} \rightarrow Z=16$

RIGHT PLOT =>  $^{40}\text{Ar} + ^9\text{Be} \rightarrow ^{49}\text{S}$  (versus energy)

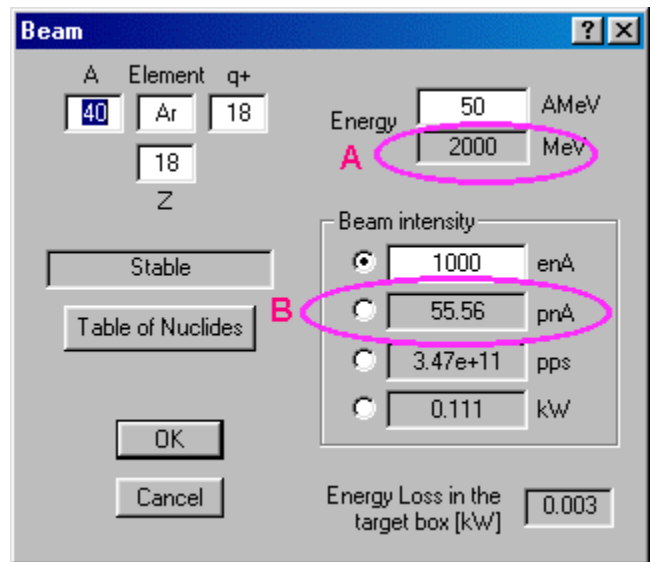
Velocity : from 2-body reaction, Angle (beam-spectrometer) : 3.90 deg



**Fig.628.** The distributions of velocities of reaction products from mass of an ion and from particle energy

### 24.3.4. New image of the dialogue “Beam”

In the version the user can set the beam intensity not only in electrical nanoAmpers (enA), in kilowatts and particles per one second (pps), but also in the well-known format of particles nanoAmpers (pnA) (see Fig.629-B). Also user at input of energy of a beam automatically can supervise its total kinetic energy (Fig.629-A).



**Fig.629.** Dialogue “Beam”

### 24.3.5. It is still necessary to work on:

1. Parameterization of cross-sections of transfer reactions on the basis of Qgg-systematics;
2. Angular distributions of transfer reactions;
3. Width of momentum distributions of transfer reactions;
4. Energy dependence of reaction products on angle for first four choices of velocity;

5. Addition of some more invariance utilities for operation with MSP-144;
6. Parameterization of density of butane from pressure.

#### 24.4. The automatized search of two-dimensional peaks in spectra and definition of their characteristics (BI code) - version 4.11

Definition of the fragment outputs is a rather labour-consuming process: it is necessary to handle tens of matrixes, each carrying the information on several tens of ions. For example, in the experiment on a beam  $^{112}\text{Sn}$  [Lew94] the nuclei with mass number from 8 up to 53 were identified. For each value of the magnetic rigidity there were four matrixes for various charge states of the reaction products, and in everyone more than five hundred ions. After measuring all data are imported to the computer for further analysis. The volume of operation can roughly be estimated:

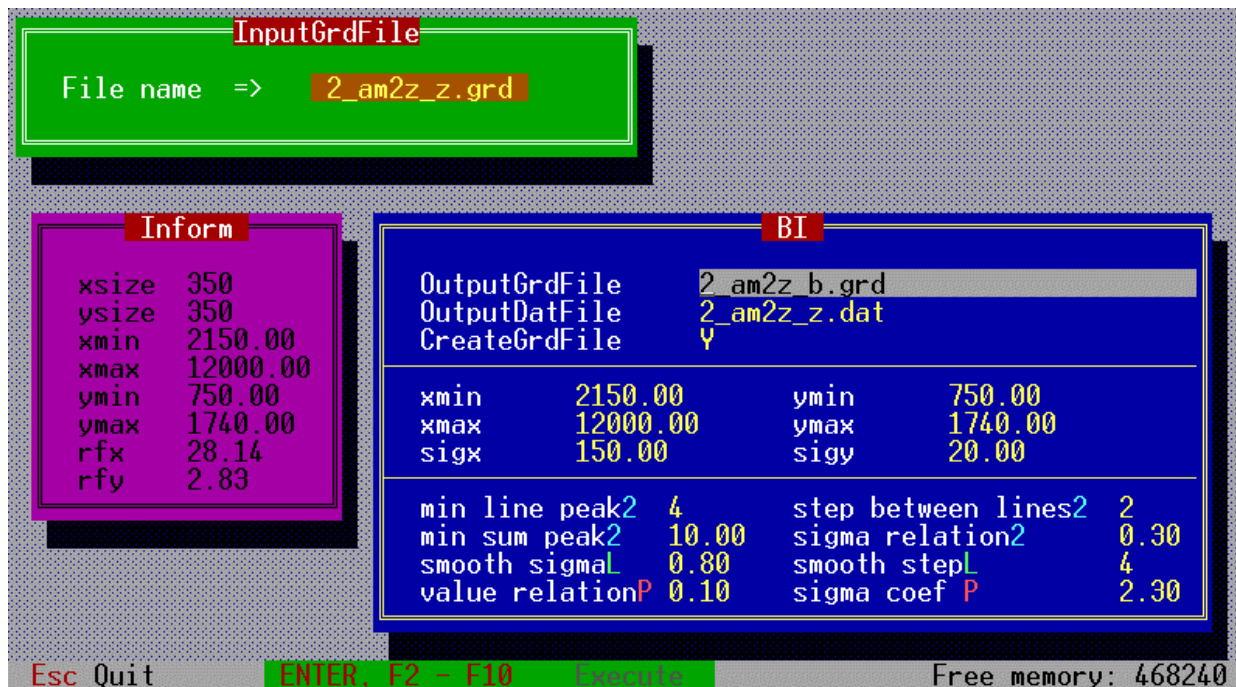


$500 \text{ ions} \times 4 \text{ matrixes for a charge state} \times 10 \text{ values of the magnetic rigidity} = 20\ 000 \text{ values!}$

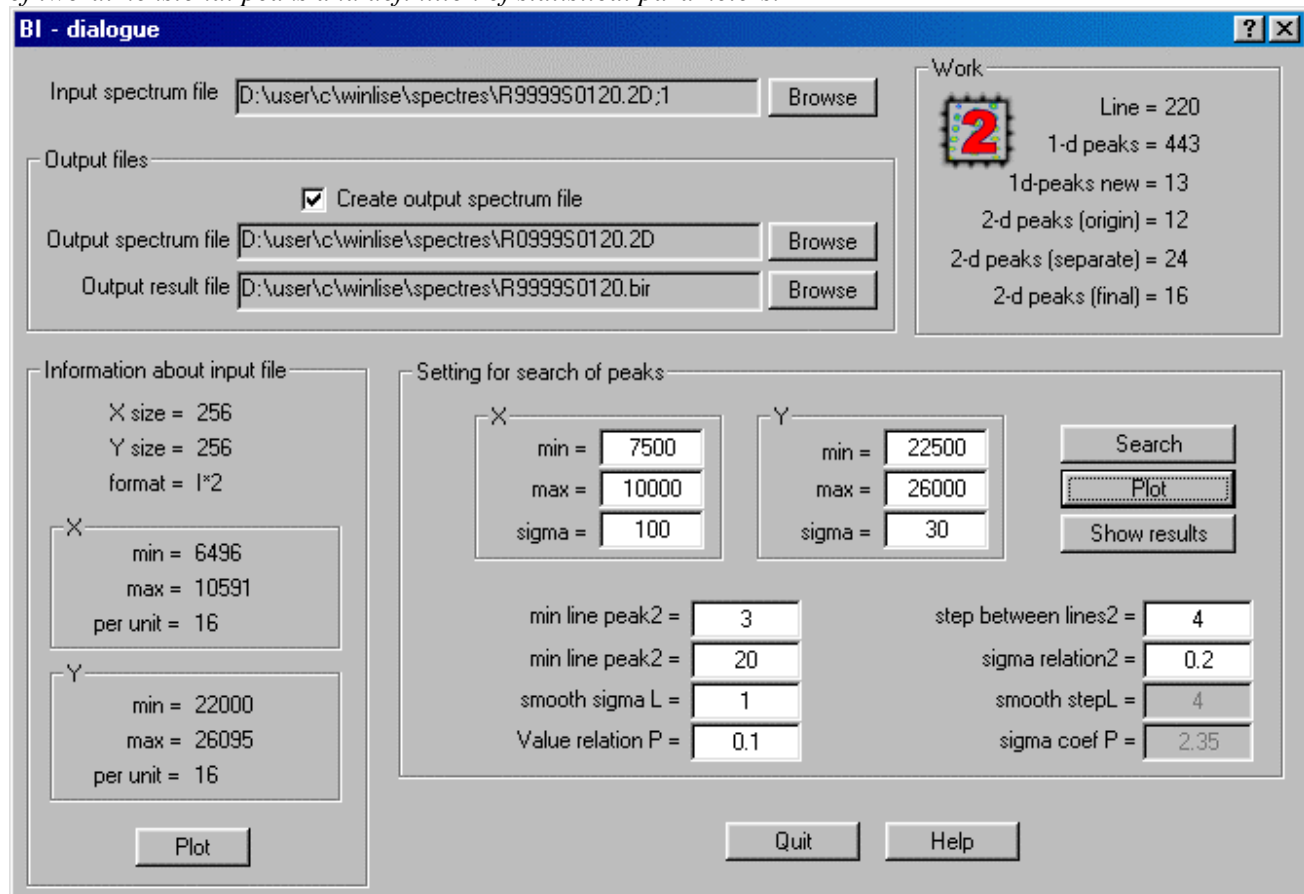
It is necessary also to mark the high probability of subjective errors of the experimenter, connected, both with the analysis of two-dimensional peaks, and with the transport of the information to the computer. In this connection, for the automatized searching of two-dimensional peaks and definition of statistical parameters the “Bi” program was created.

There are three versions of the program:

	Operating system	the programming language	the spectrum format
<b>1</b>	VMS 5.1 and is higher the	Fortran	GANIL Acquisition
<b>2</b> (Fig.630) <a href="ftp://dnr80.jinr.ru/bi">ftp://dnr80.jinr.ru/bi</a>	MS DOS 3.3 and higher	C	the program “Athene” /format “ SURFER /
<b>3</b> (Fig.631) (in-built in LISE code)	Windows 95,98,NT, 2000	C++	SURFER GANIL Acquisition after FTP ASCII files



**Fig.630.** The interface window of the “Bi” program (version under MS DOS), intended for the automatized searching of two-dimensional peaks and definition of statistical parameters.



**Fig.631.** The dialogue “Bi” in LISE code.

The examples of operation of the program are presented in Fig.630,631. All versions produce the results of the analysis (see Fig.632 and Fig.635) in a pictorial view (new spectrum of the same format) and as a table (Fig.633) with all statistical parameters of all the identified peaks. The program can be modified to other spectra formats easily without changing of its basis of a spectrum by adding the relevant subprograms of reading and recording spectra. In order to be able to switch on the new format of a spectrum it is necessary to send a request to the authors of the program with a description of structure of the spectra (desirably a code source), and also as an example an experimental spectrum in this format. It is also planned to make code conversion of spectra of one format in to another.

N	Area	Amp	xmean	ymean	Sigx	Sigy	nb
4	694.8	71.3	8991.1	25016.2	63.19	102.98	20
5	390.9	48.2	8181.7	23488.4	58.30	81.66	17
6	110.1	23.3	8101.1	23965.2	54.84	61.87	9
8	49.0	9.9	8827.6	25934.9	42.45	45.40	8
11	23.5	5.9	8095.3	24495.4	37.53	50.76	5
13	25156.6	2893.4	9430.9	22593.7	65.88	77.28	18
14	20822.8	1298.3	9349.6	23016.3	70.47	113.81	32
15	4763.6	323.7	9257.8	23503.0	73.70	96.69	25
16	5788.4	400.3	9160.8	24017.0	65.70	112.74	32
17	1542.9	109.7	9084.6	24511.7	69.35	108.44	24
18	1868.2	222.2	9984.2	24543.8	21.50	90.86	16
19	2803.6	194.1	9958.5	25016.1	37.67	97.28	27
20	3043.4	210.5	9896.1	25514.4	63.98	117.80	34
22	136.4	32.9	9837.2	25926.8	81.92	21.57	4
23	1347.0	193.4	8322.4	22584.5	67.50	70.32	16
24	1359.6	99.8	8257.3	22992.7	63.06	106.52	30

Fig.633. Window with a text file with the results of searching of two-dimensional peaks in the spectrum represented in Fig.632

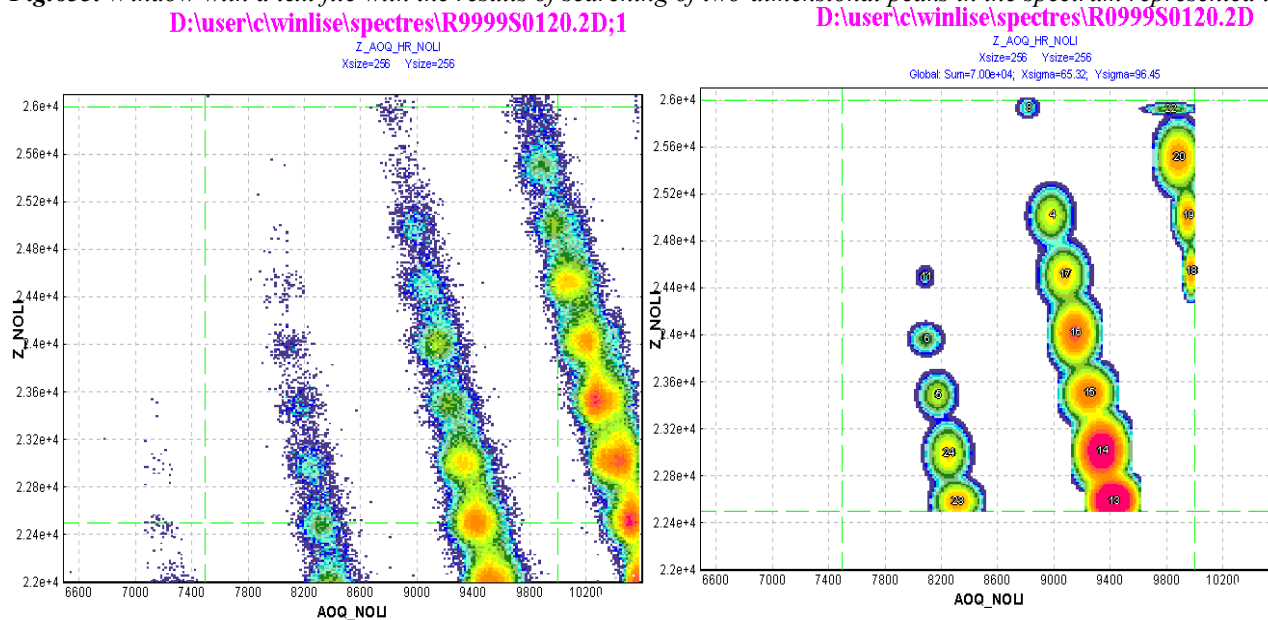


Fig.632. The experimental spectrum is shown in the left figure and in the right figure accordingly the spectrum obtained after searching and definition of parameters of two-dimensional peaks in the selected rectangle by the "Bi" subroutine in "LISE" code.

by the "BI" subroutine in the "LISE" program.

The algorithm of operation of the program of the automatized searching of two-dimensional peaks and definitions of their statistical parameters is presented in a Fig.634. The input of initial model of searching consists in the following:

- Determination of a window of searching  $xmin$ ,  $xmax$ ,  $ymin$ ,  $ymax$  (parameters of a window of an explored spectrum) by default take;
- The important parameters individual for each spectrum  $sigx$  and  $sigy$  are set, which values should be close to average dispersions of explored peaks on horizontal and vertical axes accordingly;
- Depending on quality of a spectrum (background, "diffuseness"<sup>3</sup>, superimposition of peaks) the interior parameters must be modified<sup>4</sup>, which exposition is given below.

The smoothing is carried out with the help of coefficients obtained from a normal distribution. In the beginning for everyone from a point there is a fashion:

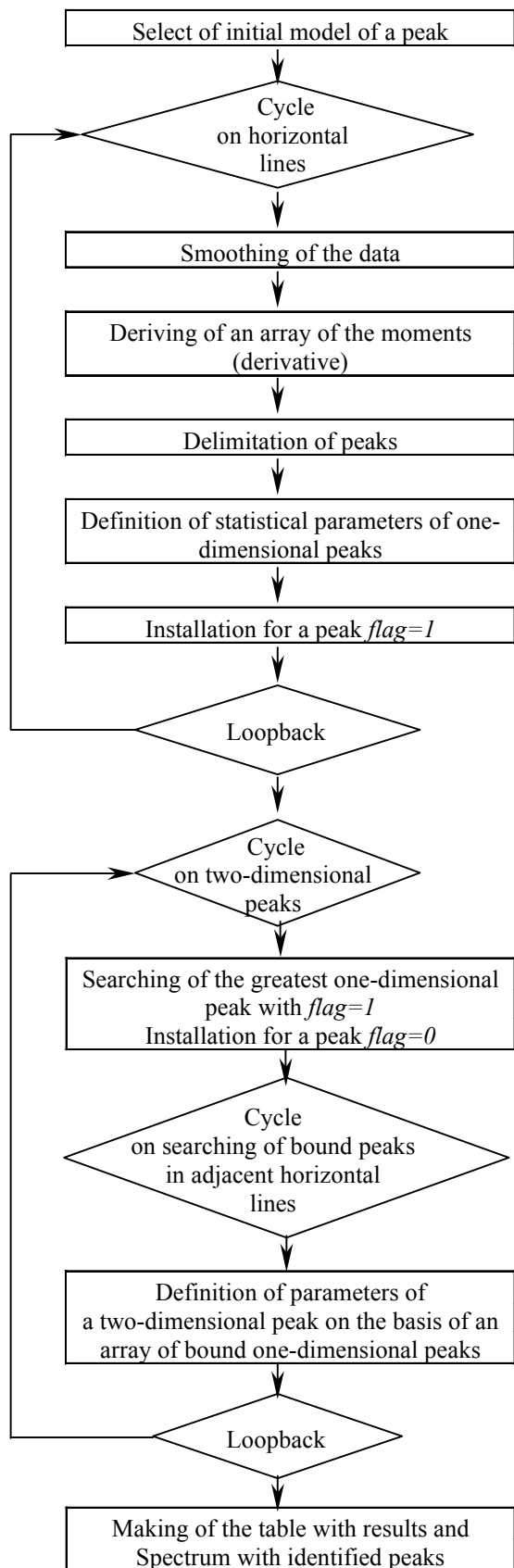
$$T(x_c) = \sum_{i=c-step}^{c+step} f(x_i) \cdot \exp\left[-\frac{(x_i - x_c)^2}{2 \cdot \sigma_{smooth}^2}\right], \quad /57/$$

Where **step** is the number of adjacent points considered in smoothing (according to the menu, represented in Fig.630,631 the given parameter is called "**smooth stepL**" and parameter, defining width of a normal distribution (according to the menu matters by default 4), **smooth** - "**smooth sigmaL**", is by default equal 1). After normalization to maintain the total events in the given horizontal line, we gain rounded value.

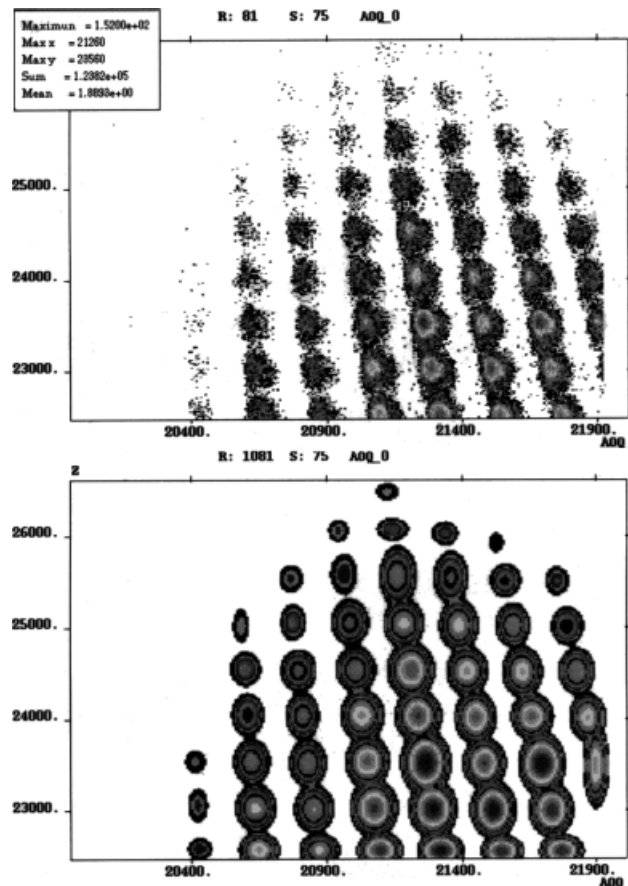
---

3 Low-intensity wide peaks

4 In most cases from experience operation with the program the interior parameters take by default



**Fig.634.** Algorithm of operation of the program of the automatized searching of two-dimensional peaks and definitions of their statistical parameters.



**Fig.635.** In the upper figure the experimental spectrum of yields with  $Z=45-53$  in the reaction  $^{112}\text{Sn}$  (58AMeV)+Ni [Lew94] for completely stripped nuclei ( $Q=Z$ ) at magnetic rigidity  $Br=1.98835$  Tm depending on the mass number  $Z$  and the quantity  $A/Q$ . In the low panel the spectrum obtained after searching and definition of the parameters of two-dimensional peaks by the "Bi" program (VMS-version) is given.

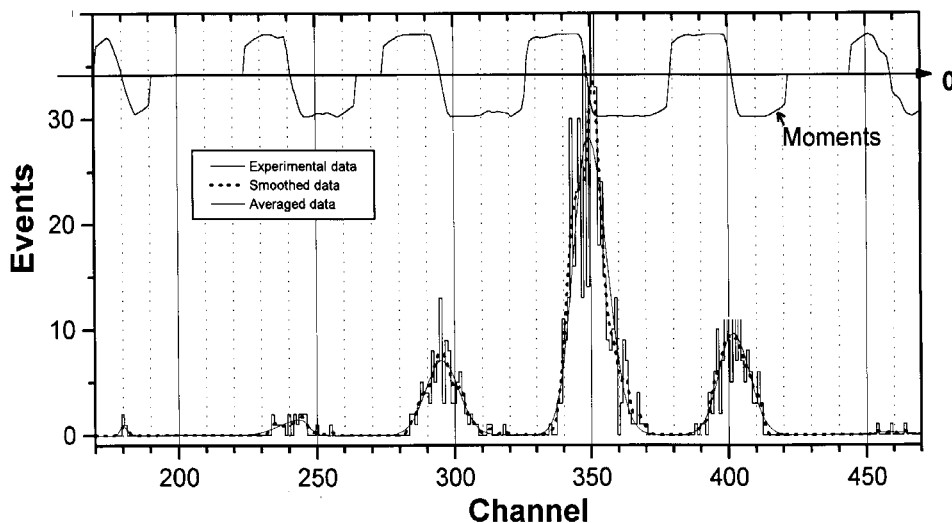
The most important moment of the program is searching an one-dimensional peak and definition of its boundaries, under condition of, that this searching was prompt enough and effective. Originally searching was realized with the help of an evaluation derivative in each point. Radiating from extremes:

$$\begin{aligned} f'(x_c) = 0, f''(x_c) < 0 &\Rightarrow x_c = \min, \\ f'(x_c) = 0, f''(x_c) > 0 &\Rightarrow x_c = \max, \end{aligned} \quad /58/$$

boundaries of peaks (minimums) and sites of maximums of peaks were delimited. To definition by derivative in a point  $x_c$  was applied a fit by a line<sup>5</sup> in an interval  $x_c - step^\# \div x_c + step^\#$ . The value  $step^\#$  is equal to product **sigx** and **sigma\_coef\_P** (see menu in Fig.630,631) and has physical sense of full width on half-height of a peak. Parameter of a declination of the given line was used as derivative. However the fit occupies a lot of time, therefore the simple and effective method was offered on the basis of evaluation of the moment of the first order in a point  $x_c$ :

$$Mom(x_c) = \sum_{x=x_{c-l}}^{x_c+l} f(x) \cdot (x - x_c), \quad /59/$$

where  $l$  is equal to the whole value of the attitude  $step^\#$  to a step of an axis  $\Delta x = x_i - x_{i-1}$ . The example of results of smoothing of experimental data and definition of their "moments" for an one-dimensional spectrum represented in Fig.636. From a figure clearly it is visible, that the crosses of function of the moments with a zero axis and change of signs "+" on "-" correspond to maximums of peaks of experimental data, and with change of signs "-" on "+" according to boundaries of peaks.



**Fig.636.** Results of smoothing of experimental data and definition of their "moments" for an one-dimensional spectrum.

The stayed interior parameters of the program (according to the menu in a Fig. 1) have the following functions:

- **value relationP** - is multiplied on amplitude of a peak (by default 0.1). The obtained quantity is used for definition of a peak boundary, if up to the following of a peak or up to boundary of a spectrum there is a point, the value in which is less than the given quantity. The obtained value is to avoid background events not having attitude to the peak and capable to affect its characteristics;

<sup>5</sup> For fit the subprogram "Minuit" of the "CERNLib" library was used

- **min line peak2** - minimum quantity of one-dimensional horizontal peaks in two-dimensional peak (by default 4). If the quantity of horizontal peaks is less than the given quantity, the peak is eliminated from the list;
- **min sum peak2** - underload area of a two-dimensional peak (by default 10). If the area of a peak is less than the given quantity, the peak is eliminated from the list;
- **step between lines2** - the maximum quantity of horizontal lines, in which happens searching in a determinate direction (upwards or downwards) one-dimensional peaks for a two-dimensional peak (by default 2). If in these lines the one-dimensional peak obeying the given two-dimensional peak was retrieved the searching is prolonged in the same direction, using again same maximum quantity of horizontal lines.

#### 24.5. Prefragment search - version 4.10

For the first time in the program concept the prefragment was input for argument of a discrepancy of experimental values of fragments velocity and formula, calculated with the help formula [Ram85], where it is supposed, that kinetic energy leaves on a difference of surface energies between a fragment at the moment of interaction with a target and its ground state in the guess of the spherical shape. However calculated values were underestimated, that is why it was supposed, that is necessary to calculate velocity of a prefragment, guessing then its equal velocity of a fragment.

In further concept of a prefragment also was entered for calculations of momentum distribution width on [Fri83]. The user in all above-stated cases had the right of a select: to use concept of a prefragment whether or not.

However by more essential usage of calculations of a prefragment was by introduction in the program of a universal parameterization of fragment momentum distribution. Moreover concept of a prefragment underlies this parameterization. In this connection in the new version the dialogue *Prefragment* has appeared Fig.637, where the user can set some methods of searching of a prefragment and see the results of calculations of a prefragment.

	A	B	
Last Prefragment	28Al	28Al	
Previous Prefragment	27Mg	27Mg	
Final prefragment mass	27.7	27.7	
Energy excitation	65.5	65.5	MeV
Probability	4.23e-03	4.23e-03	
Corrected Probability		1.24e-02	
Estimated cross-section	4.59e-02	1.35e-01	mb

Fig.637. Dialogue "Prefragment calculations".



The basic algorithm consists in the following:

- The underload energy necessary for decay of a fragment pays off, accepting, that temperature of the heels will be equal 0. In the program starts by analogy to operation [Gai91] three possible channels: evaporation of proton, neutron or alpha-particle. For a case of charged particles the Coulomb barrier takes in attention. The given underload energy takes to spot an energy window of excitation in which there was a finite product and can not undergo evaporation any more. After that the middle ( $E_R$ ) of an energy window is a start point for calculations.
- Depending on a selected method of searching (about it will be said later) the following nucleus in a chain is determined.
- The energy  $dE$  relieved from this nucleus to daughter nucleus that is toted with the previous energy  $E_R$ . The difference of a surface energy  $E_S$  guessing pays off, what is it there was an initial prefragment. If the difference of a surface energy appears more than  $E_R+dE$ , then the searching of a parent nucleus with the subsequent cycle up to that pore is iterated again while the total of energies bound with a chain of decay will not exceed a difference of a surface energy.
- Final mass of a prefragment used in the program, is approximated from masses of a final prefragment and its daughter nucleus in view of energies.

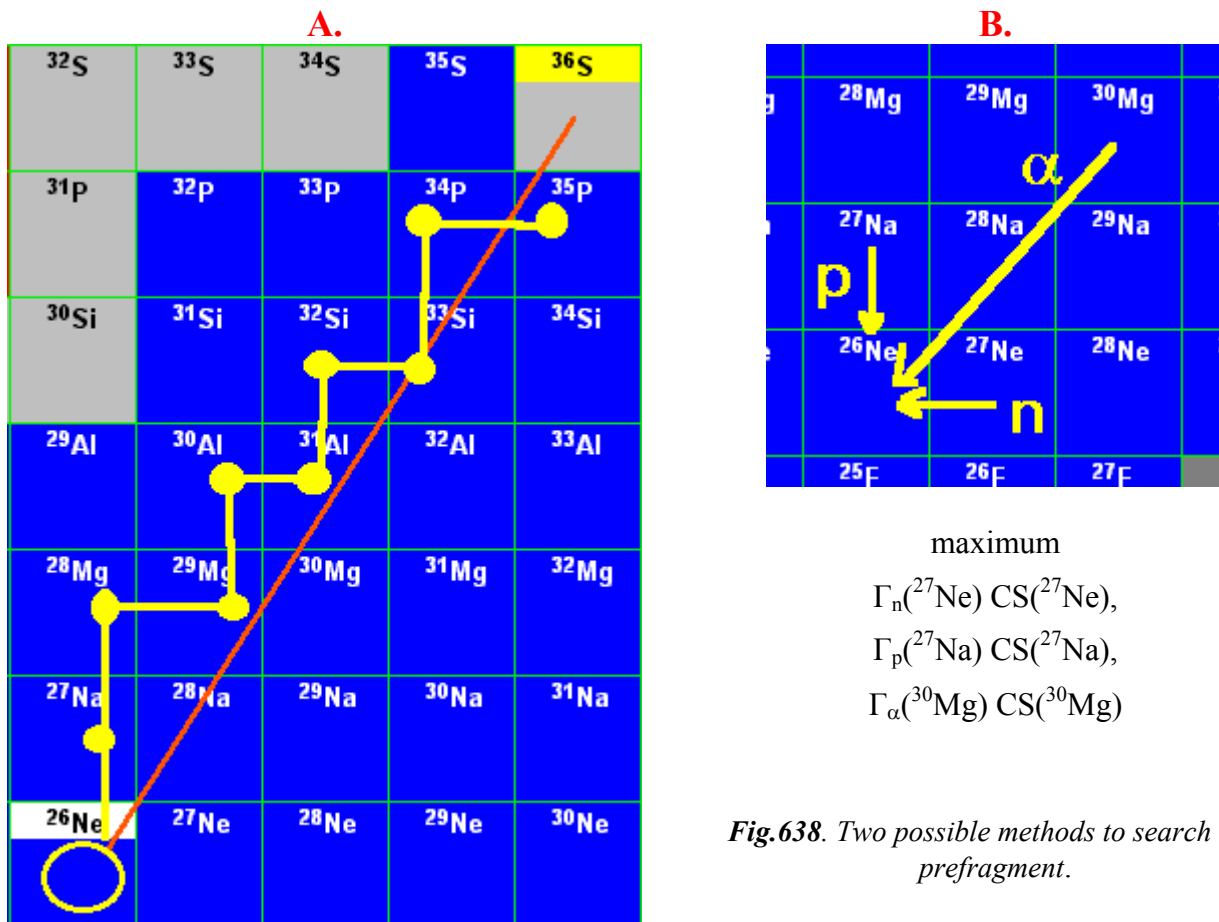
There are two methods for searching a parent nucleus:

1. It is supposed, that the following nucleus is proportional to the relation of neutrons and protons ( $N/Z$ ) of a beam (this method takes by default) (see Fig.638-A);

2. By a principle represented in operation [Gai91] but in the other direction the probabilities of transitions are determined (see Fig.638-B). After that they are multiplied on cross-section of deriving of the given nucleus from the parameterization EPAX. The nucleus is picked preceding what this quantity is more. The given method not up to the end is still worked and has two essential deficiencies:
  - cross-sections take from an experimental parameterization (for this purpose better to enter into the program model abrasion-ablation);
  - such variants are probable, that the failure of two neutrons on an example is less favorable, than one proton but the program will go step by step at first through one neutron, and then and following. In other words it is necessary to switch on in the program also matching with combinations  $2n$  and  $2p$ .

### 24.5.1. Attempt to extrapolate cross-sections of exotic nuclei

The probability of formation of a final fragment from the retrieved fragment automatically pays off by searching a prefragment. Using this quantity and the cross-section of a prefragment production from the parameterization EPAX, it is possible to estimate a production cross-section of a final fragment. It is especially interesting for nuclei far from the stability line. As it was already mentioned, the basic disadvantage is that the experimental cross-sections are used.



*Fig.638. Two possible methods to search of a prefragment.*

In various experiments devoted to the study of the properties of exotic nuclei, it was marked, that the greatest output of reaction products is reached on heavy targets, though the programs, including the given program, predict on the basis of the parameterization EPAX a greater output in the case of light targets. First of all it is possible to explain this by the fact that in the given parameterization the relation between cross-sections for various nuclei is always constant, that does not correspond to the reality. So in experiments on the synthesis of  $^{48}\text{Ni}$  with a beam  $^{58}\text{Ni}$  [Bla00] the advantage of a nickel target compared to a carbon target was supervised, in experiments on study of the stability of  $^{28}\text{O}$  [Tar97] the greatest output for nuclei in region  $N=20$  is shown. So in experiments on the synthesis of  $^{100}\text{Sn}$  [Lew94] the greater output in the case of a Ni-target was explained by the experimenters by the additional contribution from transfer reactions. Also it was marked, that experimental cross-sections for superexotic nuclei are much below the calculated ones.

However, it is possible to explain this by the greater excitation energy of prefragments in the case of light targets, due to the fact that the prefragment has longer chain of daughter nuclei, which leads on to a more stable final nucleus. On the basis of the new model of calculations of a prefragment the attempt was made to estimate cross-sections for the case of proton-rich isotopes of nickel produced with a beam of  $^{58}\text{Ni}$  (see Fig.639). As it was already mentioned, the basic disadvantage is that the cross-sections used for these estimations also are experimental. For the given calculations the searching of a fragment was done by the N/Z method, and the characteristics of nuclei were calculated using the formula, instead of being taken from the database (see Fig.637). From Fig.639 it is visible, that in order to produce the isotope  $^{49}\text{Ni}$  the ratio between the original parameterization EPAX and calculations with prefragment corrections for a Ta-target constitutes 260, whereas for Be-target this value already is more than 4000, which then explains the advantage of heavier targets.

#### 24.5.2. Calculation of isotope characteristics with the semi empirical formula.

In this version of the program the user has got an opportunity to add the data on new isotopes. The insertion of a new record is possible if the user inserts in the dialogue an isotope, which does not

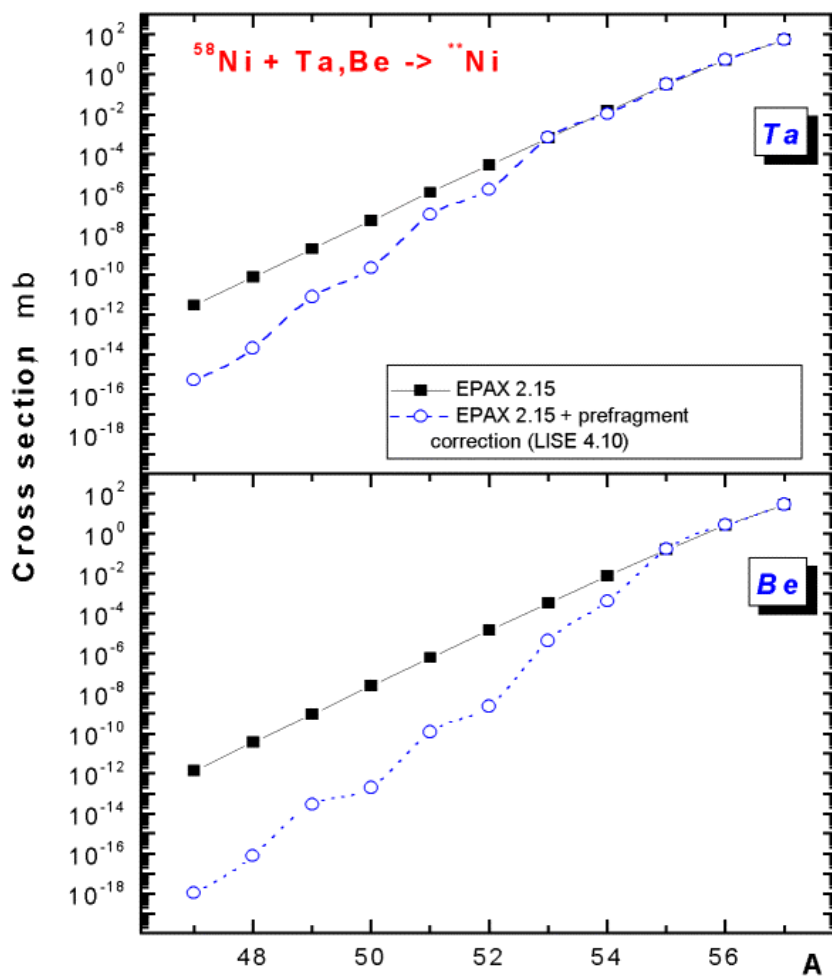
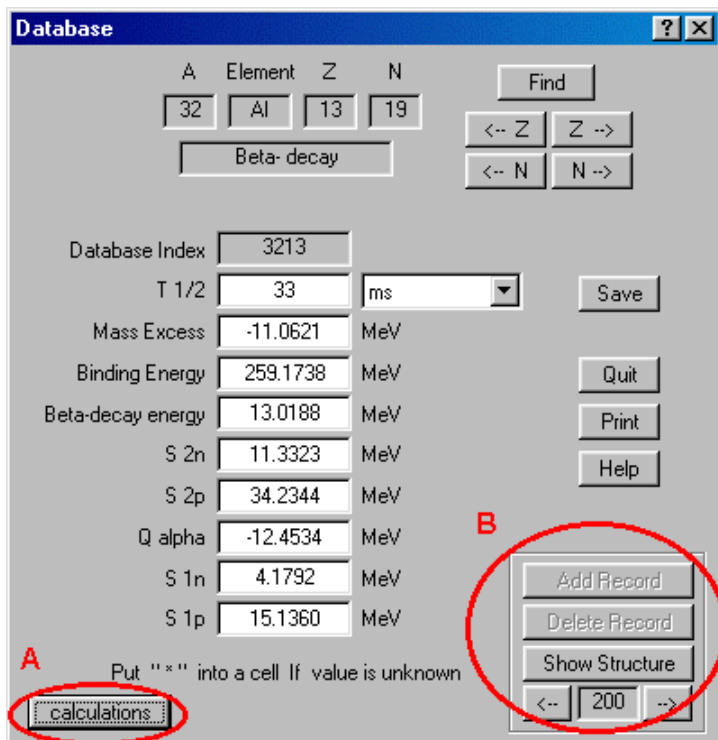
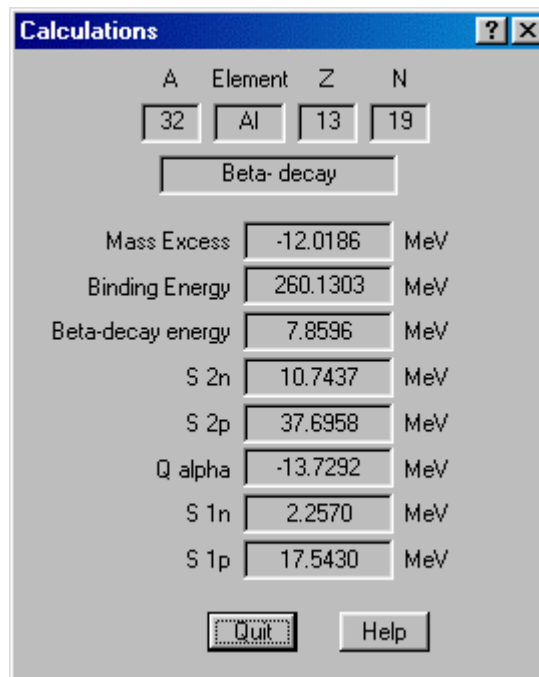


Fig.639. Cross-sections for production of Ni-isotopes with a  $^{58}\text{Ni}$  beam on a Ta-target (upper picture) and a Be-target (bottom picture). Black solid rectangles correspond to cross-sections calculated by EPAX 2.15, open blue circles the previous cross-sections with prefragment corrections.

exist in the database. Pressing on the key “Add record” (Fig.640) the user creates a new record, and the database automatically remakes indexation. Also the user can get calculated values for the given isotope (button “Calculate”) on the basis of the semi empirical formula (Fig.641). For those evaluations, where usage of the characteristics from the database is required, but the data on this isotope is missed in the database, the program calculates them on the basis of the semi empirical formula.



**Fig.640.** Dialogue “Database”.



**Fig.641.** New Dialogue “Calculations of isotope characteristics”.

## 25. Version 4.9

Caen  
25.10.2000

### Momentum distributions of fragments. Universal parametrization

#### 25.1. Introduction

Fragment momentum distributions measured in relativistic heavy ion collisions are typically observed to be Gaussian shaped. Within the framework of the independent particle model, Goldhaber [GOL74] assumed zero net three-momentum in the nucleus and showed that the parabolic dependence of the momentum width of the gaussian curve can be obtained:

$$\sigma_{\parallel} = \sigma_0 \sqrt{\frac{A_f(A_p - A_f)}{A_p - 1}}, \quad /60/$$

where  $\sigma_0 = p_F / \sqrt{5} \approx 90 \text{ MeV} / c$  is the reduced width and  $p_F$  is the Fermi momentum. The fragment velocity is supposed to be equal the projectile velocity. The given model long time was unique in program LISE for calculation of width. However, this model is unable to account for the following:

- a) the differences in widths associated with nuclides of the same mass;
- b) the discrepancy between  $\sigma_0$  and  $p_F / \sqrt{5}$ , where  $p_F$  is obtained from electron scattering experiments;
- c) the observed difference between  $\sigma_{\parallel}$  and  $\sigma_{\perp}$
- d) the apparently anomalously small values of  $\sigma_0$  observed at lower energies;
- e) the isotope yields from the fragmentation process;
- f) the occurrence an exponential tail in momentum distributions in reactions at low energies.
- g) the reduction of the velocity relation of a fragment to projectile at low energies.

Further it was developed different models for an explanation of these phenomena both theoretical, and empirical parametrizations. A part of their these models already were entered earlier in the LISE code, some are entered in the given version.

Certainly, that each of models has the advantages and lacks depending on energy and masse of projectile and so on. In the new version of program LISE the user can choose depending on a task necessary to him models from 3 models of fragment velocities and from 3 models of momentum distribution widths or take advantage of new universal “convolution” model.

The reviews of models of momentum distribution widths, velocities of fragments, systematization of the reduced width from energy are submitted to attention of readers in the following chapters.

Also for the new version the *Universal parametrization* which allows to avoid a significant part of those lacks (a,d,f,g) that were inherent in primary statistical model of A.Goldhaber is developed and adapted in the program.

## 25.2. Longitudinal momentum distribution widths

### 25.2.1. Systematic of momentum distributions from reactions with relativistic ions of D.J.Morrissey

As the practice shows, many physics use for the description given other distributions, in particular take the width from the empirical systematic of Morrissey [MOR89]:

$$\sigma(p_{||}) = \frac{150}{\sqrt{3}} \sqrt{A_p - A_f} \text{ MeV} / c. \quad /61/$$

The opportunity of use of this momentum distribution model in the code LISE has appeared in version 4.7. This parametrization is received on a basis of experimental data and represents a linear dependence on the square root of the mass loss as against the parabolic form assumed by Goldhaber's model.

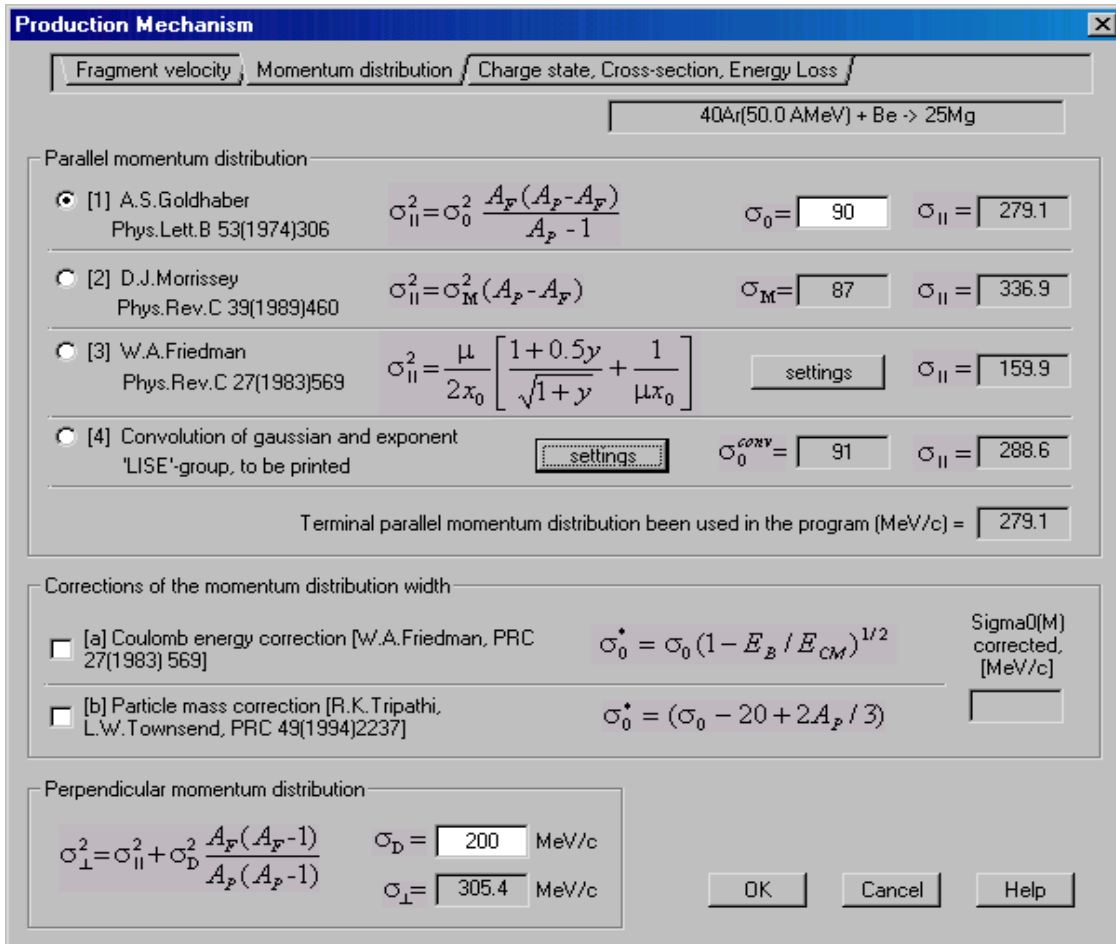


Fig.642. Dialogue "Production mechanism – Momentum distribution"

### 25.2.2. Heavy ion projectile fragmentation: A reexamination by W.A.Friedman

Friedman [Fri83] has shown that a model based on the separation energy of fragments from projectile leads to the same functional form as in Goldhaber's model and a better representation data (at least for light projectiles/O.T./). This model relates the widths of distributions to the separation energies and an absorptive cutoff radius. In this work it is entered a wave function  $\psi_{F-R}(r)$  which describes the relative separation between the observed fragment ( $F$ ) and the removed portion of the projectile ( $R$ ) to calculate only outside of the absorption region:

$$\psi_{F-R}(r) \cong e^{-\mu r} / r, \quad \mu = \sqrt{2m_r E_s} \quad /62/$$

where  $m_r$  is the reduced mass and  $E_s$  is the separation energy. In the calculations he defined after including the lowest order of the Coulomb potential on the bound state wave function tail, that distribution has gaussian form with width:

$$\sigma_{II}^2 = \frac{\mu}{2x_0} \left[ \frac{1+0.5y}{\sqrt{1+y}} + \frac{1}{\mu x_0} \right], \quad y = Z_1 Z_2 / x_0 E_s. \quad /63/$$

The given model has been incorporated in the new version of the code (see Fig.642).

On the other hand, the fragment will be observed if the process leads to any of its particle-stable excited states. This possibility provides a range and upper value for  $E_s$ . The user can choose one of three possible separation energy: energy on a basis cluster separation from projectile, excitation energy to the surface exceed, and their sum (see Fig.643).

However the registered nucleus is consequence of prefragment evaporation of neutrons and light charged particles. Prefragment momentum distribution can differ from a registered fragment considerably. To calculate momentum distribution for prefragment the opportunity of prefragment calculation is entered adjusted for momentum distribution in connection with evaporation.

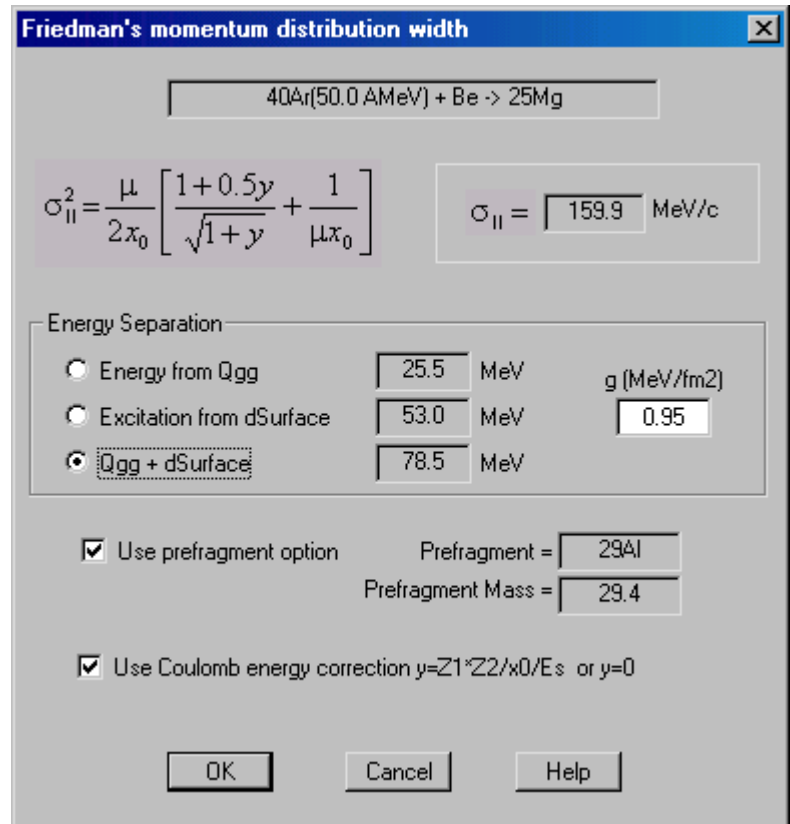


Fig.643. Dialogue "Friedman's momentum distribution width"

### 25.2.2.1. “Coulomb correction” of Friedman

The opportunity of use of the correction for reduced width was added at small energies from distortions due to Coulomb force proposed by W.A.Friedman was incorporated in version 4.7 of the code (see Fig.642):

$$\sigma_0^* = \sigma_0 (1 - E_B / E_{CM})^{1/2} \quad /64/$$

This correction becomes significant only for energies below 20 MeV/u.

### 25.2.3. Simple parametrization of fragment reduced widths in heavy ion collisions (R.H.Tripathi et al.)

A systematic analysis of the observed reduced widths obtained in relativistic heavy ion fragmentation reactions was used to develop a phenomenological parametrization [Tri94a] of these data:

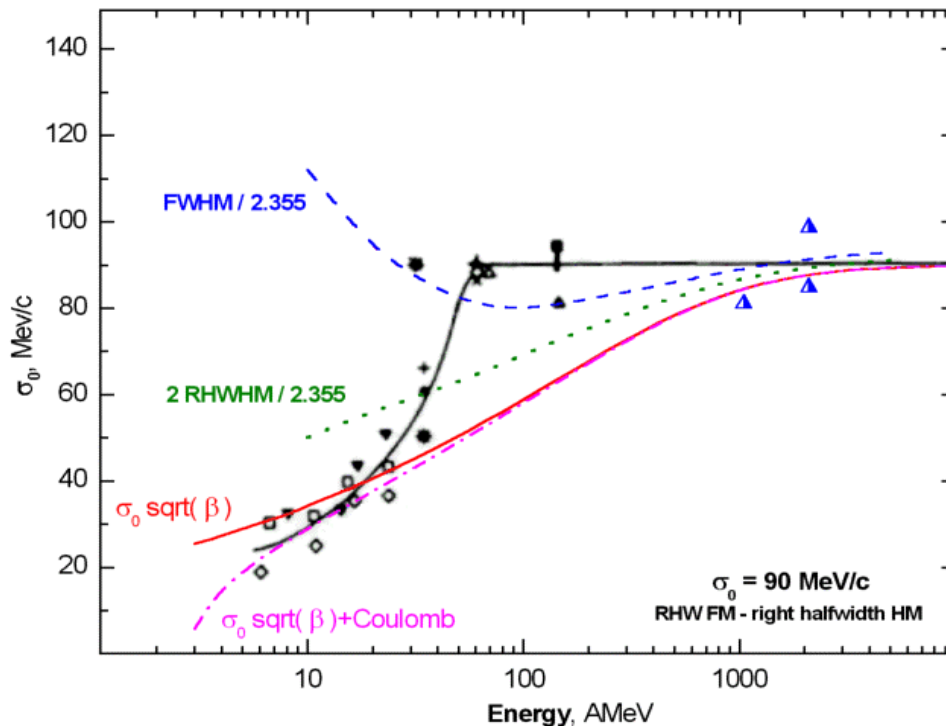
$$\sigma_0^* = (1 + E_c / 4T_{lab})(70 + 2A_p / 3) \quad /65/$$

In new version 4.9 of program LISE this parametrization is entered as the amendment (see Fig.642) to reduced width of other models as.

$$\sigma_0^* = (\sigma_0 - 20 + 2A_p / 3) \quad /66/$$

### 25.2.4. Role of intrinsic width in the fragment momentum distributions in heavy ion –collisions (R.H.Tripathi et al.)

In work [Tri94b] has been demonstrated comparison of intrinsic widths incorporating correlations in conjunction with dynamical effect with intrinsic widths alone without correlations [Gol74]. They suggested the momentum distribution of the observed fragments depends upon the initial (intrinsic) momentum distribution of the projectile nucleus and upon the momentum transferred by the collision (dynamics):



**Fig.644.** Systematic of reduced widths of the linear momentum distributions of fragments measured in various reactions and at different bombarding energies [Ram85]. The points (triangles) from ref. [Gre75] have been corrected. See details in the text.



$$\sigma_{\text{total}}^2 = \sigma_{\text{int}}^2 + \sigma_{\text{dyn}}^2$$

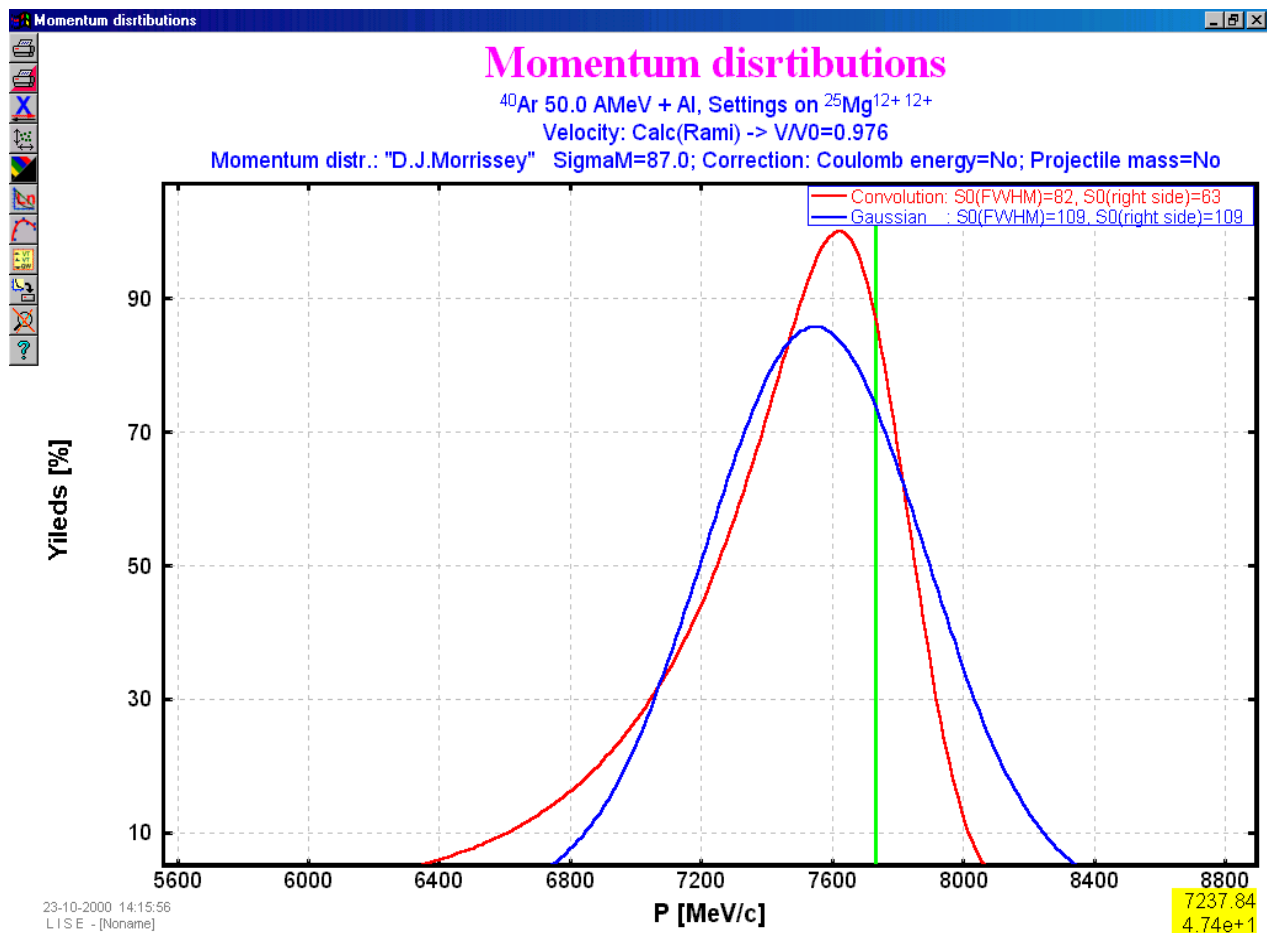
/67/

where  $\sigma_{\text{int}}$  is the intrinsic width due to internal Fermi motion of the nucleons, and  $\sigma_{\text{dyn}}$  is the dynamical distribution. This model is not used in the code.

### 25.2.5. Influence of projectile energy on the reduced width of longitudinal momentum distribution

Systematics of reduced widths for projectile like fragments [Ram85,Bor86] have shown abnormal behavior at small energies. From energy 100 AMeV sharp recession of width (see Fig.644) is observed. Different hypotheses were offered, but any of them can not describe a course of a curve at energy of some tens MeV per nucleon. It spoke as the contribution of other mechanisms of reactions, or influence of Coulomb forces. The concept of the contribution of other mechanisms was entered first of all for an explanation low-energetic exponential tail, accompanying gaussian distribution. Coulomb interaction starts to play a role in area below 20 AMeV.

With input of new universal parametrization on the basis of convolution (it will be in more detail submitted in the following chapters) it is possible to explain experimental results. As a result of work on parametrization it was shown, that the width is proportional to a root of velocity. In the figure the given dependence is shown by a red line. The greater consent is achieved for low energies, when to this depend-



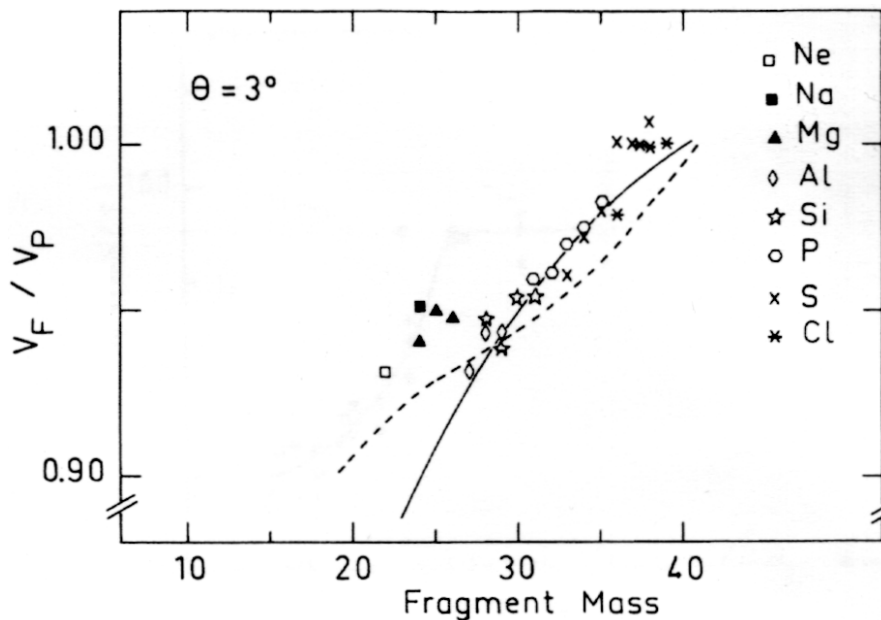
**Fig.645.** Momentum distributions of  $^{25}\text{Mg}$  in reaction  $^{40}\text{Ar}(50\text{AMev})+\text{Al}$  calculated by two methods: new universal convolution method (red curve), Morrissey parametrization for the momentum width and Rami model for relation of velocities (blue curve).

ence the Coulomb amendment is added: magenta dash-dot curve. However, how to explain a strong divergence with the data at energies 60-100 A MeV? The answer consists in a method of measurement of width of momentum distribution. At energy 100 A MeV the momentum distribution under the form is very close to gaussian and accordingly experimenters measure full width on maximal height to extract reduced width: a dark blue line received from new universal parametrization. At lower energies however the contribution exponential tail is more appreciable, that is why physics describe distribution by several others. Roughly it can be presented if to consider the right part of distribution as gaussian and to take right half-width for calculations of the given width: in Fig.644 it is shown by green dotted curve. Two last curves was calculated for reaction  $^{40}\text{Ar} + \text{Al} \rightarrow ^{25}\text{Mg}$ .

Momentum distributions of  $^{25}\text{Mg}$  in reaction  $40\text{Ar}(50\text{A MeV})+\text{Al}$  calculated by two methods are presented on Fig.645, where it is well seen an exponential tail in distribution on the basis of new parametrization. At initial corrected sigma0 is equal to 43 ( $\sigma_0^* = 90 (\beta(1 - E_B / E_{CM}))^{1/2}$ ) as a result of convolution it turns out 82 of full width and 63 of right halfwidth.

### 25.3. Fragment velocity

As it was already mentioned, velocity of fragmentation reaction products is equal to projectile velocity. In initial versions of the program velocity was considered independent of energy, masses of fragments and an ion of beam. The user in manual entered the relation of velocity of a fragment to a beam. At small energies the relation of velocities is experimentally shown decreases (see Fig.646). Many works show change of this relation due to the contribution of other mechanisms of reactions to an output of products, that accordingly changes the form of momentum distribution.



**Fig.646.** Ration of the ejectile to projectile velocities versus the mass of the fragment in the  $^{40}\text{Ar}(26.5\text{A MeV})+^{68}\text{Zn}$  reaction measured at  $\theta_{\text{lab}}=3^\circ$  [RAM85]. The solid and dotted curves correspond to the two types of velocity calculation: suggestion that for each ablated nucleon requires 8 MeV[BOR83] and surface energy exceeds [RAM85].

### ***25.3.1. Fragment velocity: removing 8 MeV per ablated nucleon***

First estimation [BOR83] of velocity issuing from a fragmentation reaction: if one conjectures that in the fragmentation process the nucleons are removed from the projectile to another and that an average of 8 MeV is required for each (this corresponds to the solid curve in Fig.646):

$$\frac{v_F}{v_P} = \sqrt{1 - \frac{B_n(A_P - A_F)}{A_F E_P}} \quad /68/$$

However experimental data show, that the estimation underestimates velocity, in consequence of that began possible to change in the program a quality of energy necessary to ablate one nucleon. The estimation of the velocity relation is inserted into the program (see Fig.647).

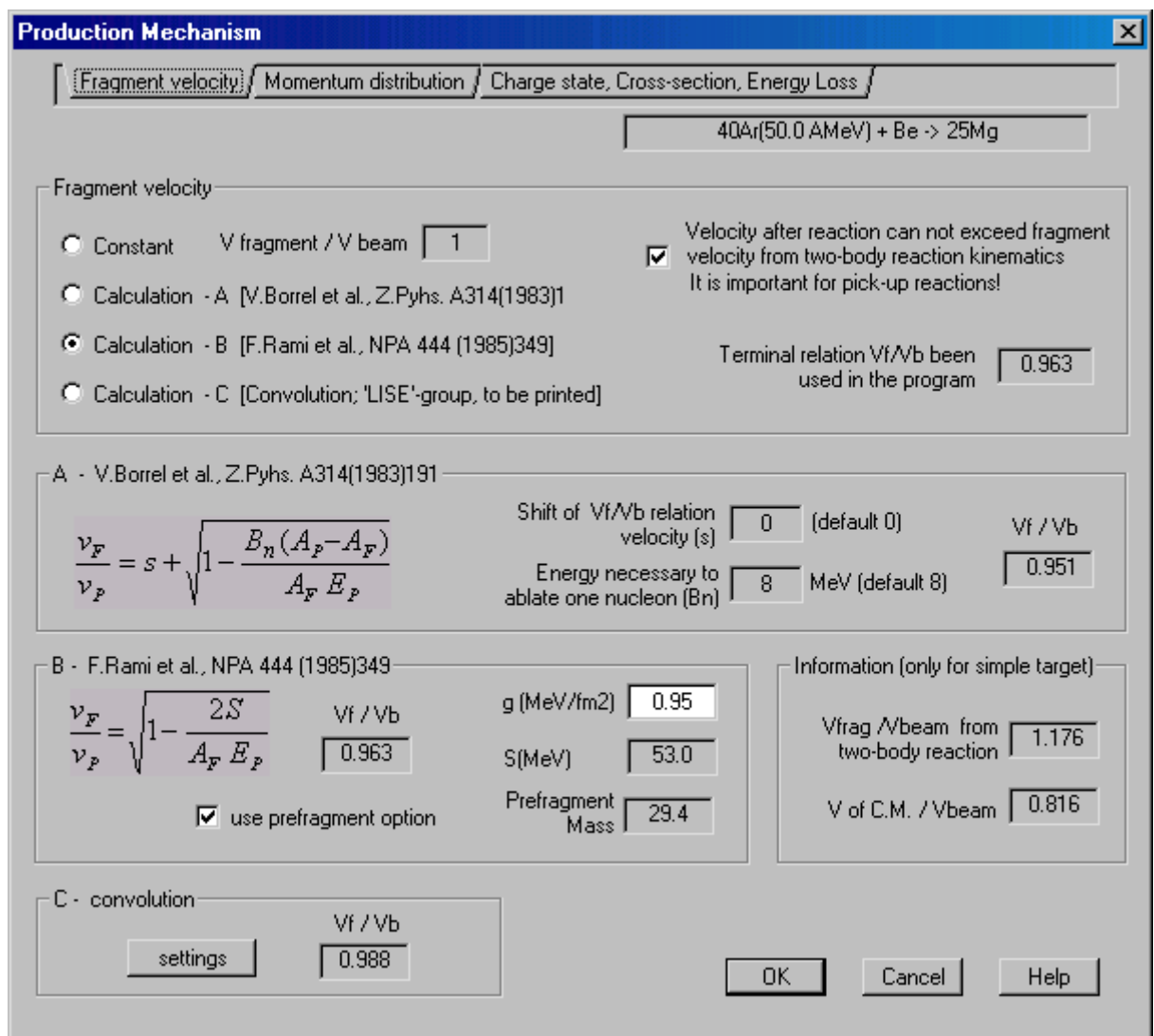
### ***25.3.2. Fragment velocity on the basis of surface energy exceed***

If one assumes that the projectile is sheared in two, then several nucleons bonds have to be broken simultaneously. The number broken can be treated as being proportional to the surface geometry. In the this case [RAM85]:

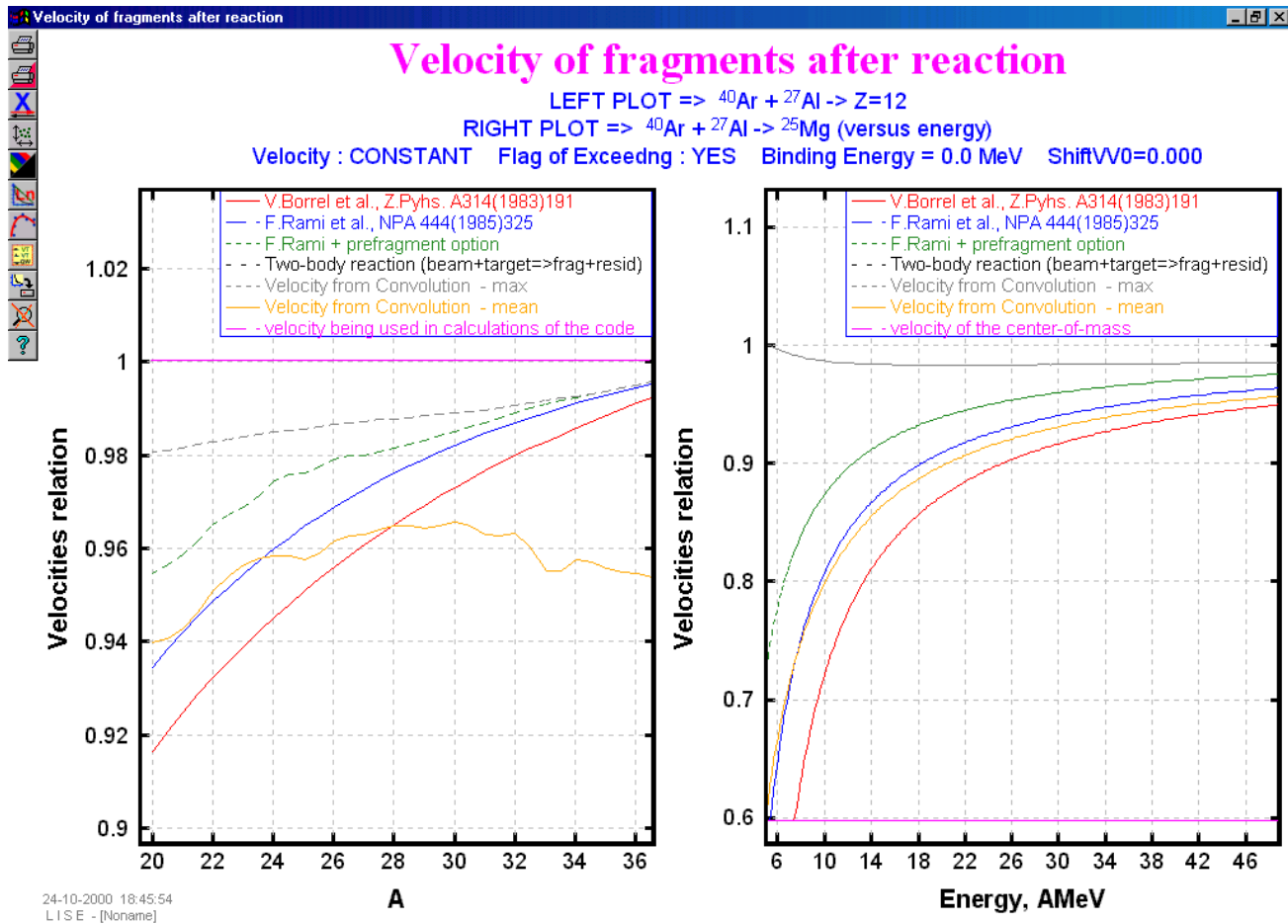
$$\frac{v_F}{v_P} = \sqrt{1 - \frac{2S}{A_F E_P}}, \quad /69/$$

where  $S$  (MeV) is the surface energy of contact and equal to  $2\gamma s$  (this corresponds to the dotted curve in Fig.646).  $\gamma$  is the nuclear surface tension coefficient ( $0.95 \text{ MeV}/\text{fm}^2$ ) and  $s$  the area of the interface between the abraded zone and the remaining fragment.  $s$  is calculated using clean-cut abrasion model of Gosset et al.[GOS77]. The given estimation of the velocity relation is added in the new version of the program (see Fig.647). The option calculation of the prefragment mass for use of this value instead of the fragment mass further for velocity calculation is entered.

Velocities of fragments calculated by different methods in the program LISE for reactions  $^{40}\text{Ar}+\text{Al}\rightarrow^*\text{Mg}$  (setting nucleus is  $^{25}\text{Mg}$ ) are shown in Fig.648.



**Fig.647.** Dialogue “Production mechanism – Fragment velocity”



**Fig.648.** Velocities of fragments calculated by different methods in the program LISE for reactions  $^{40}\text{Ar} + \text{Al} \rightarrow ^*\text{Mg}$ .

#### 25.4. New universal model of momentum distribution on the basis of gaussian and exponent convolution.

Developed in the new version of the program the model of momentum distribution is universal: definition width of distribution depending on beam energy and energy of prefragment excitation, an estimation of the most probable fragment velocity, occurrence a low-energetic exponential tail. Attempt to describe experimental distributions of products of a fragmentation with strongly pronounced gaussian form of beam velocity and with a low-energetic tail at lower energies was undertaken entering convolution between gaussian and exponent. In a basis of model the postulate lays, that energy necessary on division of a projectile on prefragment and participants, and also on prefragment excitation acts **ONLY** from kinetic energy of projectile. The given assumption lays also in a basis of estimations of speed of a fragment that was described in the previous chapters (equations /68,69/). Obtaining of final distribution needs to be divided into two stages:

1. obtaining prefragment momentum distribution in view of kinetic energy loss,
2. evaporation process for prefragment.

Assuming, that one of convolution components is the initial momentum distribution of prefragment according to the equation /60/, it is possible to write both these stages for prefragment and fragment momentum distributions in a general view:

$$\psi(\vec{p}_{pf}) = \int_0^{t_0} \frac{1}{(\sqrt{2\pi}\sigma_{pf}\tau)^3} \exp\left(\frac{-(\vec{p}_{pf} - \Delta\vec{p})^2}{2\sigma_{pf}^2}\right) \cdot \exp(-\Delta\vec{p}/\tau) d^3\Delta p \quad /70/$$

$$f(\vec{p}) \approx \int \psi(\vec{p}_{pf} - \Delta\vec{p}) \exp\left(-\frac{\Delta\vec{p}^2}{2m\tau^*}\right) d^3\Delta p. \quad /71/$$

where  $\tau^*$  is the temperature of prefragment. Solution of the first equation for momentum distribution in the beam direction, assuming  $t_0$  tending to infinity, it is possible to write then as follows:

$$\psi(p_{pf}) = \exp\left(\frac{p_{pf} - p_{0pf} + \frac{\sigma_{pf}^2}{2\tau}}{\tau}\right) \cdot \left[1 - ferr\left(\frac{p_{pf} - p_{pf0} + \frac{\sigma_{pf}^2}{\tau}}{\sqrt{2}\sigma_{pf}}\right)\right], \quad /72/$$

where  $p_{0pf}$  is the more probable momentum of prefragment, which corresponds of the velocity of projectile. Assuming, that the second stage does not carry the big contribution to the form of distribution, and only shifts the distribution from  $p_{0pf}$  to  $p_0$  ( $p_0$  is the more probable momentum of prefragment), it is possible then to write in final view the equation /71/ as result of both stages as follows:

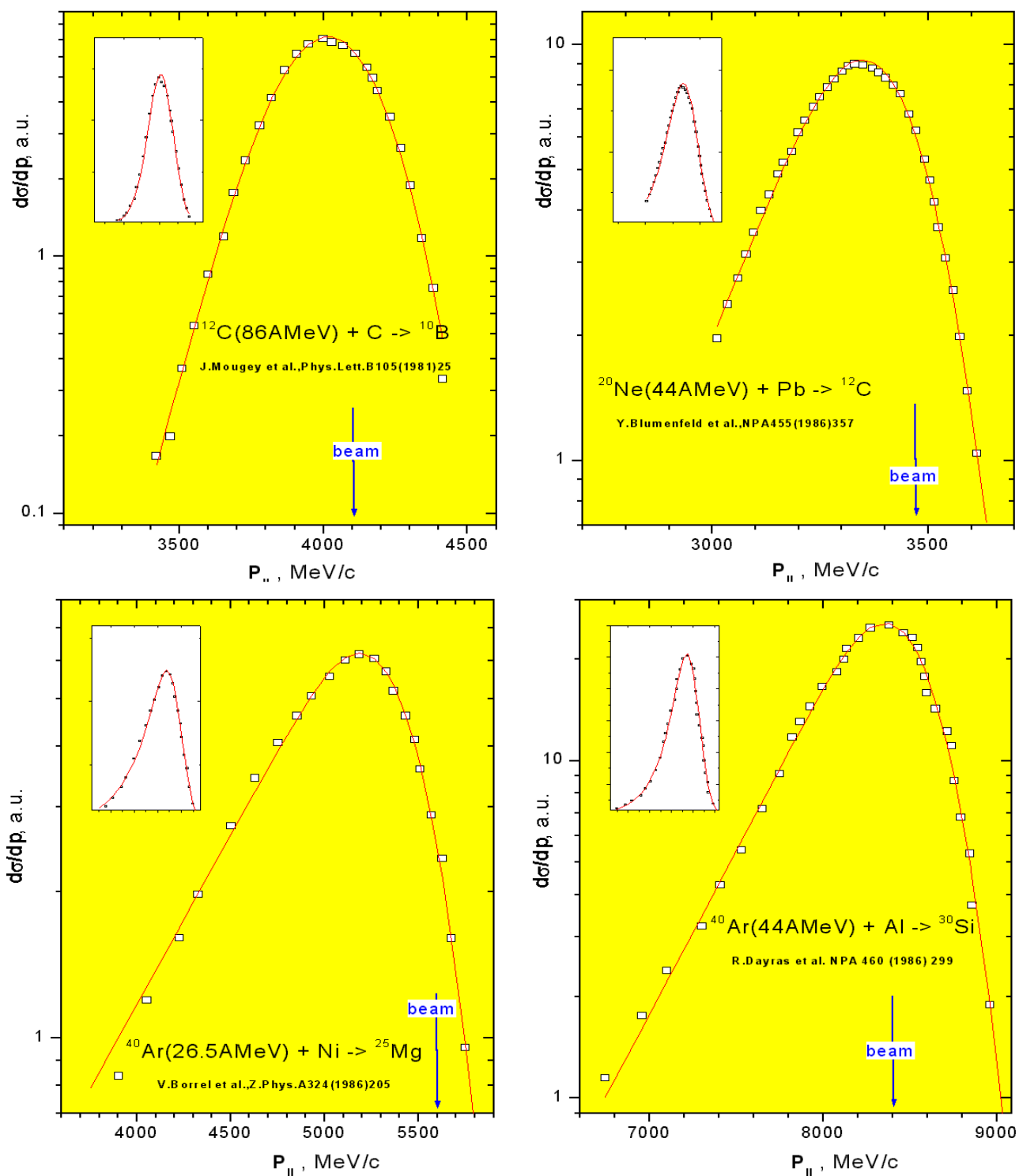
$$f(p) \approx \exp\left(\frac{p}{\tau}\right) \cdot \left[1 - ferr\left(\frac{p - p_0 + \frac{\sigma_{pf}^2}{\tau}}{\sqrt{2}\sigma_{pf}}\right)\right], \quad /73/$$

where addends from the exponent were moved in normalizing coefficient.

For determination of  $\tau$  the evident form was offered:

$$\tau \approx \sqrt{m \cdot E_S}, \quad /74/$$

where  $E_S$  is the energy spent on break of a particle in prefragment and participants, and on prefragment excitation. As mass the following possible values were used: the mass of prefragment, the reduced mass of prefragment and residual, the fragment mass, a difference between mass of the projectile and prefragment. The best approximation was received as mass in the equation /74/ use of prefragment mass. However in result of fit it was found out, that  $\tau$  must be inversely proportional to fragment velocity to explain of an amplitude of exponential tail. Whence at once follows, that  $\sigma_{pf}$  used in the equation /73/ should be proportional to a root of velocity. Thus their final kind with the account Coulomb amendments can be submitted as:



**Fig.649.** Energy spectra and results of their fit by the formula /77/.

$$\tau = \text{coef} \cdot \sqrt{A_{pf} \cdot E_S} / \beta, \quad /75/$$

$$\sigma_{pf}^2 = \beta \sigma_0^2 (1 - E_B / E_{CM}) \frac{A_{PF} (A_P - A_{PF})}{A_P - 1}. \quad /76/$$

In process of the data fit it was noticed, that shift on velocity much more than it was expected, in this connection it was necessary to insert additional the amendment into error function to compensate this shift which is proportional to  $\tau$ :

$$f(p) = \exp\left(\frac{p}{\tau}\right) \cdot \left[ 1 - \text{ferr} \left( \frac{p - p_0 + \frac{\sigma_{pf}^2}{\tau} - s \cdot \tau}{\sqrt{2} \sigma_{pf}} \right) \right]. \quad /77/$$

35 spectra from the following works [Bor86,Blu86,Dar86,Gre75,Mer86,Mou81,Viy79] were used for fit. In works where distributions from energy were presented, spectra were transformed in momentum distribution in view of the appropriate amendments (see the description to the version 4.5 “Transformation of distributions”). From fit it was received, that value of  $\sigma_0$  in expression /76/ is **equal to 91,5**. Energy spectra and results of their fit by the formula /77/ shown in Fig.649.

The experimental data was fitted for three different values of separation energy: energy separation prefragment from projectile, excitation energy of prefragment, and their sum. The best consent was received in a case of “tau” for the second case, for definition of velocity shift the best result was for the third case. All these three opportunities are given in the program (see Fig.650).

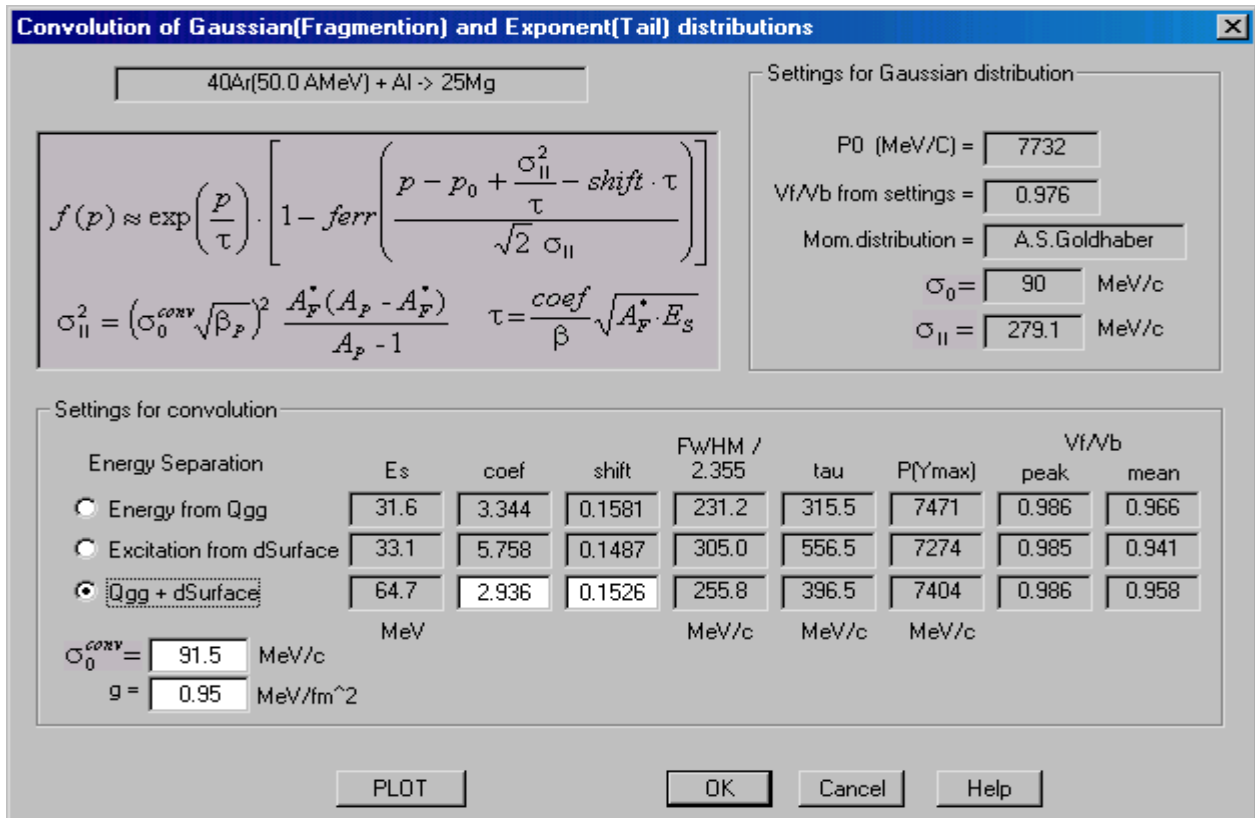


Fig.650. Dialogue “Convolution of Gaussian and exponent” called from dialogue “Production mechanism”.



## 26. Version 4.8

Caen  
20.09.2000

### Secondary reactions in a target (II)

#### 26.1. Reduction of a fragment output due to reactions

In the new version of the program losses from reactions in a target, a stripper and a wedge, and also contributions of secondary reactions to outputs of fragments are more accurately investigated. In the previous versions simple dependence of formation of reactions products that is true in a case only thin targets was assumed:

$$N_F(x) = N_P(0) x \sigma_{P \rightarrow F} , \quad /78/$$

where  $N_F(x)$  is the number of fragments  $F$  produced at thickness  $x$ ,  $N_P(0)$  is the beam intensity which is supposed to be constant,  $x$  is the target thickness,  $\sigma_{P \rightarrow F}$  is the cross section for producing the fragment  $F$  from projectile  $P$ .

So for an example usage of new algorithm of fragments outputs calculation with losses due to responses in a target and in wedge reduce in 4 times a  $^{40}\text{Ti}$  output in reaction  $^{58}\text{Ni}$  (500AMeV) + Be [Liu98] in comparison with the previous version of the program.

##### 26.1.1. Reactions in a target (stripper)

As the target thickness is increased, the probabilities of destroying the fragment of interest and the projectile become significant. These probabilities are governed by the total cross sections of the fragment  $\sigma_F$  and accordingly the projectile  $\sigma_P$ . Taking this into account, the number of fragments  $F$  is determined as:

$$N_F(x) = N_P(0) \sigma_{P \rightarrow F} \frac{(e^{-x\sigma_F} - e^{-x\sigma_P})}{\sigma_P - \sigma_F} . \quad /79/$$

In a case  $F=P$  the equation /79/ assumes the following:

$$N_P(x) = N_P(0) e^{-x\sigma_P} . \quad /80/$$

In the program was entered the new coefficient of transmission to number 22 which shows the ratio of the lost fragments to number derived in target and stripper after target (from equation /78/). Number of lost fragment is defined as the difference between outputs of fragments counted on the Formulas /78/ and /79/. This coefficient is calculated at any modes (options: secondary reactions, charge states etc.) also can be observably also on a plot of transmission at calculation of optimal target thickness. The curve describing the given coefficient is marked on Fig.651 with arrows of red color.

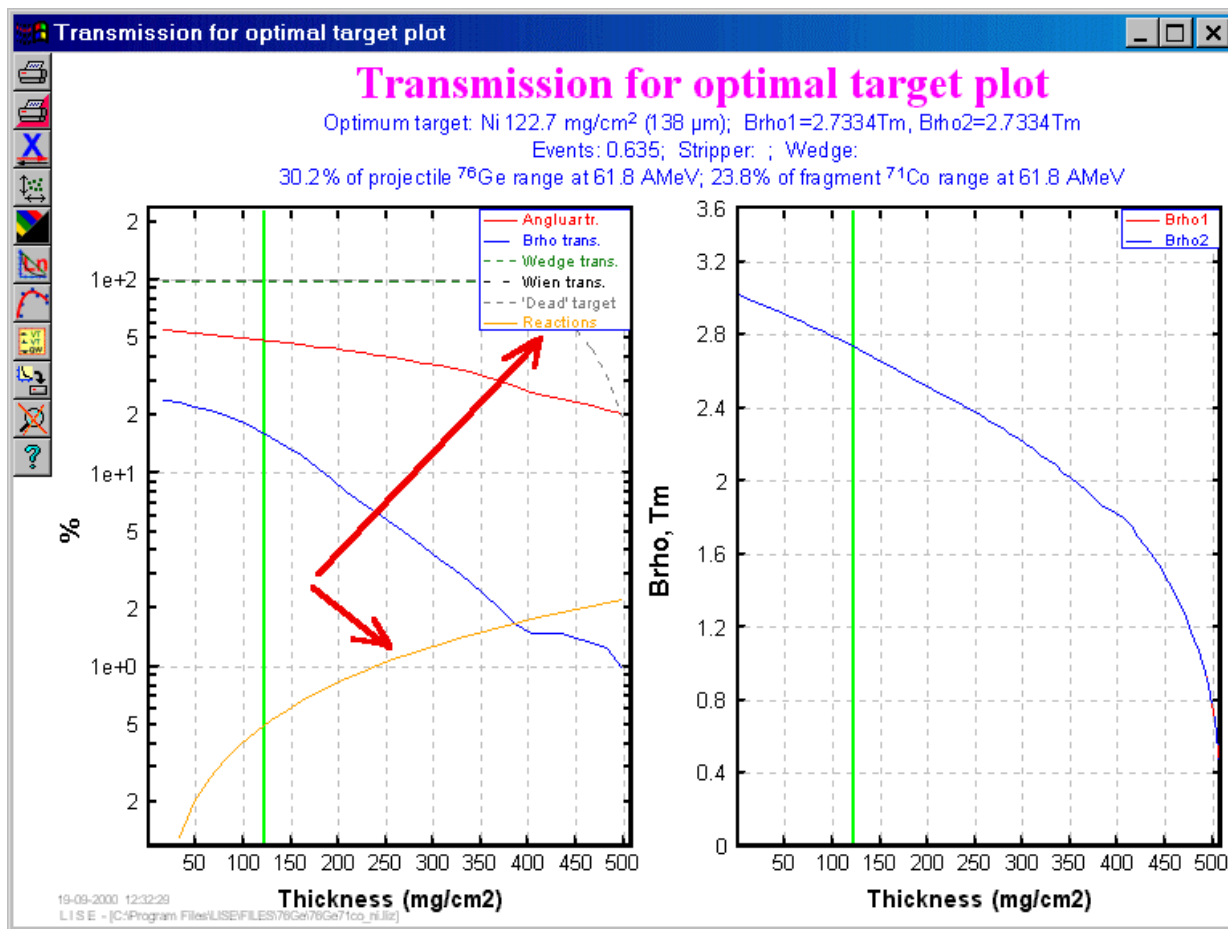


Fig.651.

### 26.1.2. Reactions in a wedge

In the new version of the program losses of number of fragments due to responses in a wedge also are taken into account. The new coefficient 23 showing the ratio of lost fragments to a total number got in a wedge ( $x$  is its thickness) is entered  $coef = 1 - e^{-x\sigma_F}$ .

### 26.1.3. Reactions in materials

The user also can see the considering of reactions in materials in dialogue "GOODIES" which represented on Fig.652. It is possible to observe as loss in the given material (A), and how many percent of fragments has remained from a beginning number got in a telescope.

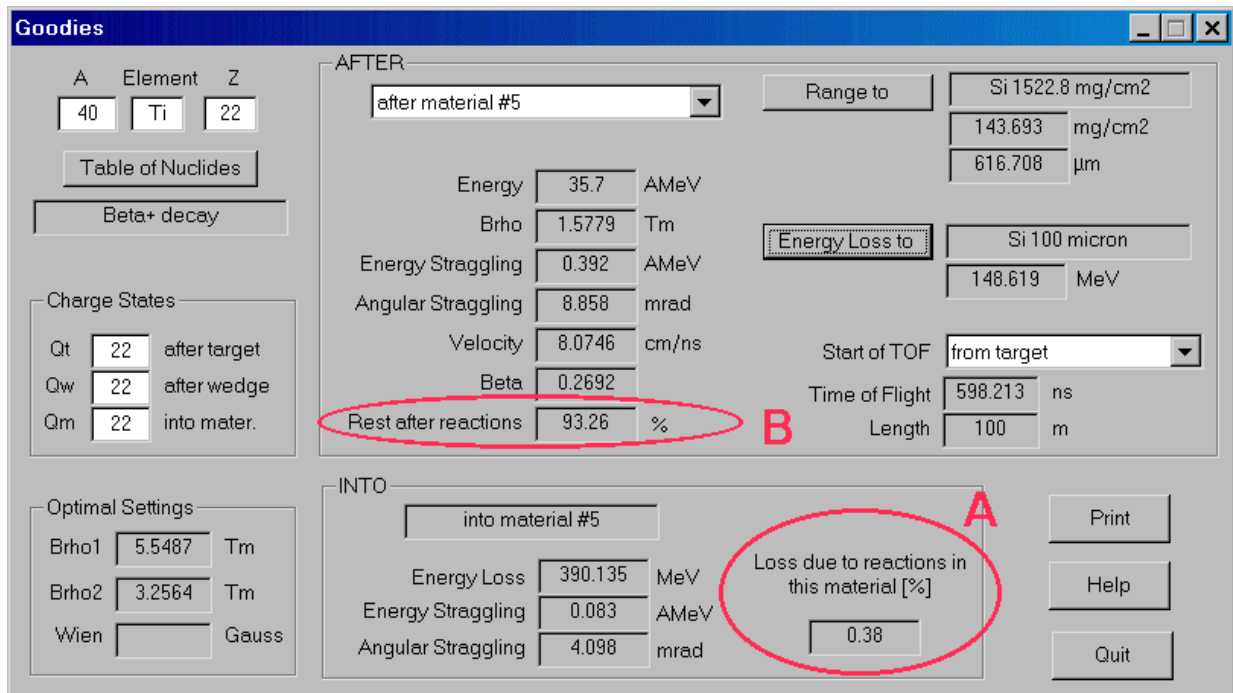


Fig.652. Dialogue "GOODIES": calculation of reactions in materials

## 26.2. Calculation of the secondary reactions contribution in a fragment output

In version 4.7 the user only could make the plot of the contribution of secondary reactions for one fragment. In the new version Possibility to take into account the contribution of secondary reactions for all se-

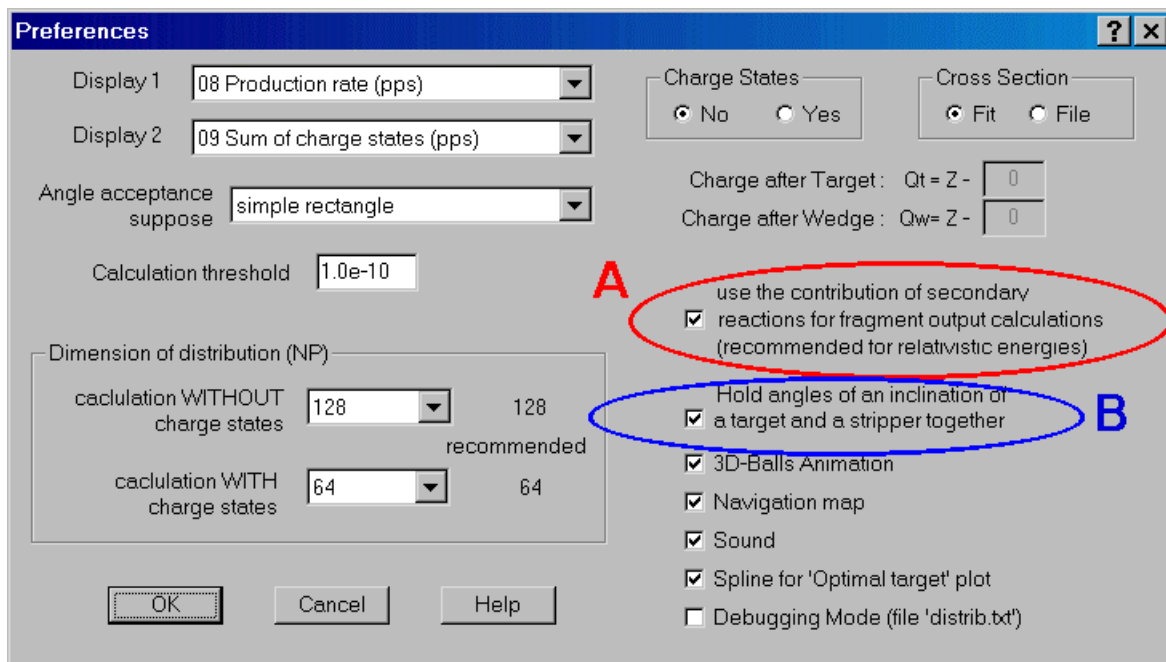


Fig.653. Dialogue "Preferences"

lected products of projectile fragmentation has appeared directly at calculation of transmission. To apply the calculation of secondary responses it is necessary to include an appropriate option (A) in menu PREFERENCES (see Fig.653). In the mode of the

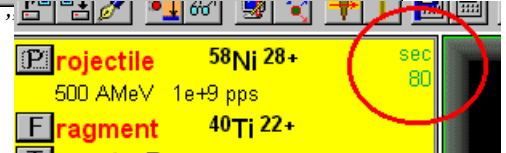


Fig.654. Flag of secondary reaction calculations is set.

calculation of secondary reactions in an upper right corner of SETTINGS window the green flag **SEC** will appear (see Fig.654). The number under this flag designates quantity of fragments involved for calculation of the secondary reaction contribution. Allocations of fragment outputs after a target depending on target thickness are kept in memory. They are deleted, if thickness of a target or has decreased in 5 times, or has increased in 2 times and also if the energy of an initial beam has varied on 10 percents. If new thickness of a target satisfies to the above-stated conditions an output of fragments are interpolated from the saved arrays. When the user sets area of nuclei ( $F_{top,right}$ ,  $F_{bottom,left}$ ) for transmission calculation, the program determines new square for calculation of secondary reactions in view of that the projectile (P) also should enter into this area, and then expands the given square on one unit in all sides:

$$\begin{aligned}
 N_{max} &= \max[N(F_{top,right}), N(P)] + 1 \\
 Z_{max} &= \max[Z(F_{top,right}), Z(P)] + 1 \\
 N_{min} &= \min[N(F_{bottom,left}), N(P)] - 1 \\
 Z_{min} &= \min[Z(F_{bottom,left}), Z(P)] - 1
 \end{aligned}
 \tag{81}$$

where  $N$  and  $Z$  are numbers of neutrons and protons correspondingly. After the given stage the program fills in arrays of outputs depending on thickness of a target for all nuclei of this square and only after that starts to count transmission. If after calculation of transmission of isotopes in the given square the user will decide to count transmission of an isotope outside of this square the program will calculate in addition arrays of outputs to the same principle defining square.

For the registration of the secondary reaction contribution the new coefficient of transmission at number 24 is entered. The algorithm of calculation of the secondary reaction contribution also counts losses of outputs in a target and in a stripper. However and the coefficient 22 (look the previous paragraph) takes into account it. To avoid the repeated registration of losses thanking responses in targets, coefficient 24 it is written as follows:

$$C24 = SecReact / Nsimple / (1 - C22), \tag{82}$$

where  $SecReact$  is number of the interest nucleus calculated by an algorithm which was demonstrated in previous version 4.7,  $Nsimple$  is output without any corrections calculated with equation /78/. Summary coefficient  $K$  is a result of all three coefficients (22-24) which gives in the table of transmission in an output file of results:

$$K = C24 (1 - C22) (1 - C23). \tag{83}$$

If the option “Secondary Reactions” is switched off, coefficient 24 is equal to one.

### 26.2.1. Secondary reactions and Optimal target calculations subroutine

The new version of the program also allows to take into account the contribution of secondary responses at calculation of an optimal target thickness. If the energy of an initial beam is more 200 AMeV or the option “Secondary Reactions” is set, the program will offer automatically to calculate thickness in view of secondary reactions. The user has possibility to disable the given option (see Fig.655). For matching on a graphics outputs of a fragment are shown depending on target thickness as well as in view of secondary responses, and without them (see Fig.656).

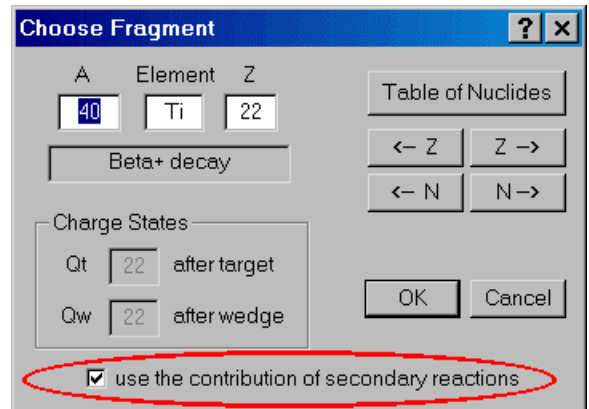


Fig.655.

## 26.3. Other

### 26.3.1. New generator of random numbers

In the new version of the program the generator random numbers was replaced on more advanced. A range of the new generator up to  $2^{32}-1$ , that best allows to feign bidimensional plots in a mode of Monte Carlo acquisition. The reference to generators of random numbers: [http://www.ulib.org/-webRoot/Books/Numerical\\_Recipes/bookcpdf/c7-0.pdf](http://www.ulib.org/-webRoot/Books/Numerical_Recipes/bookcpdf/c7-0.pdf)

### 26.3.2. Creation of a file with results of secondary reactions contribution

Using the plot "Output of products from a target with the contribution of secondary reactions" through the menu "Utilities", the user can get access to a file of results of calculations of fragments outputs in

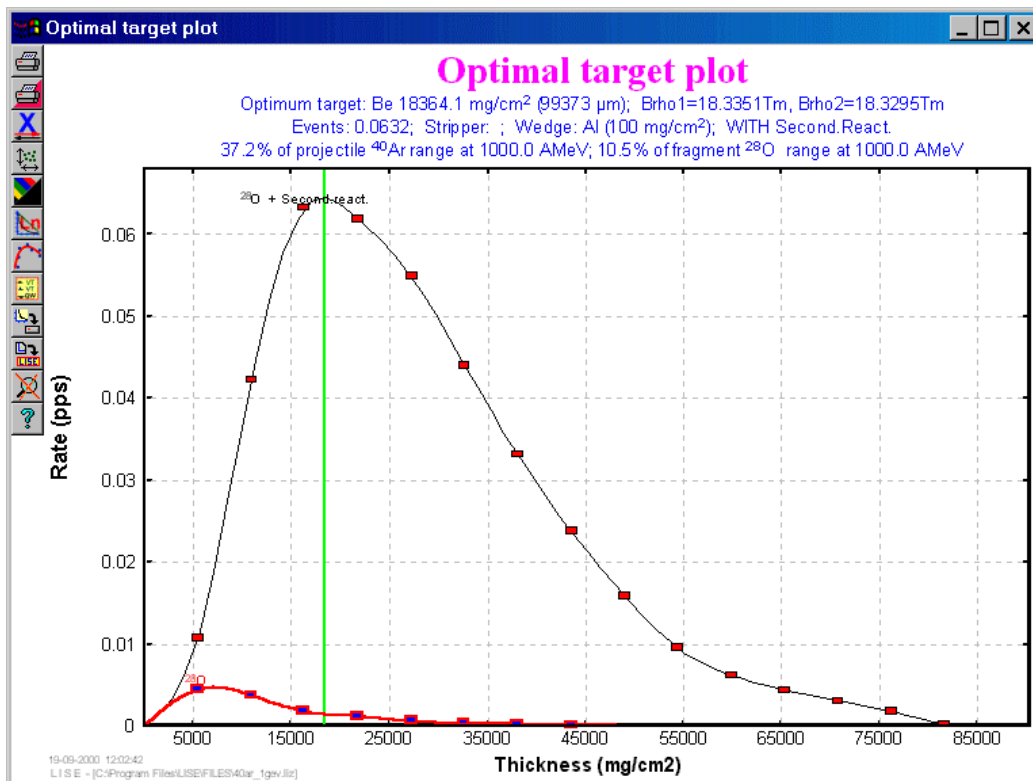


Fig.656. Optimal target plot with contribution of secondary reactions.

view of the contribution of secondary reactions (see Fig.657). The given file is in root directory LISE and called "contribution.txt".

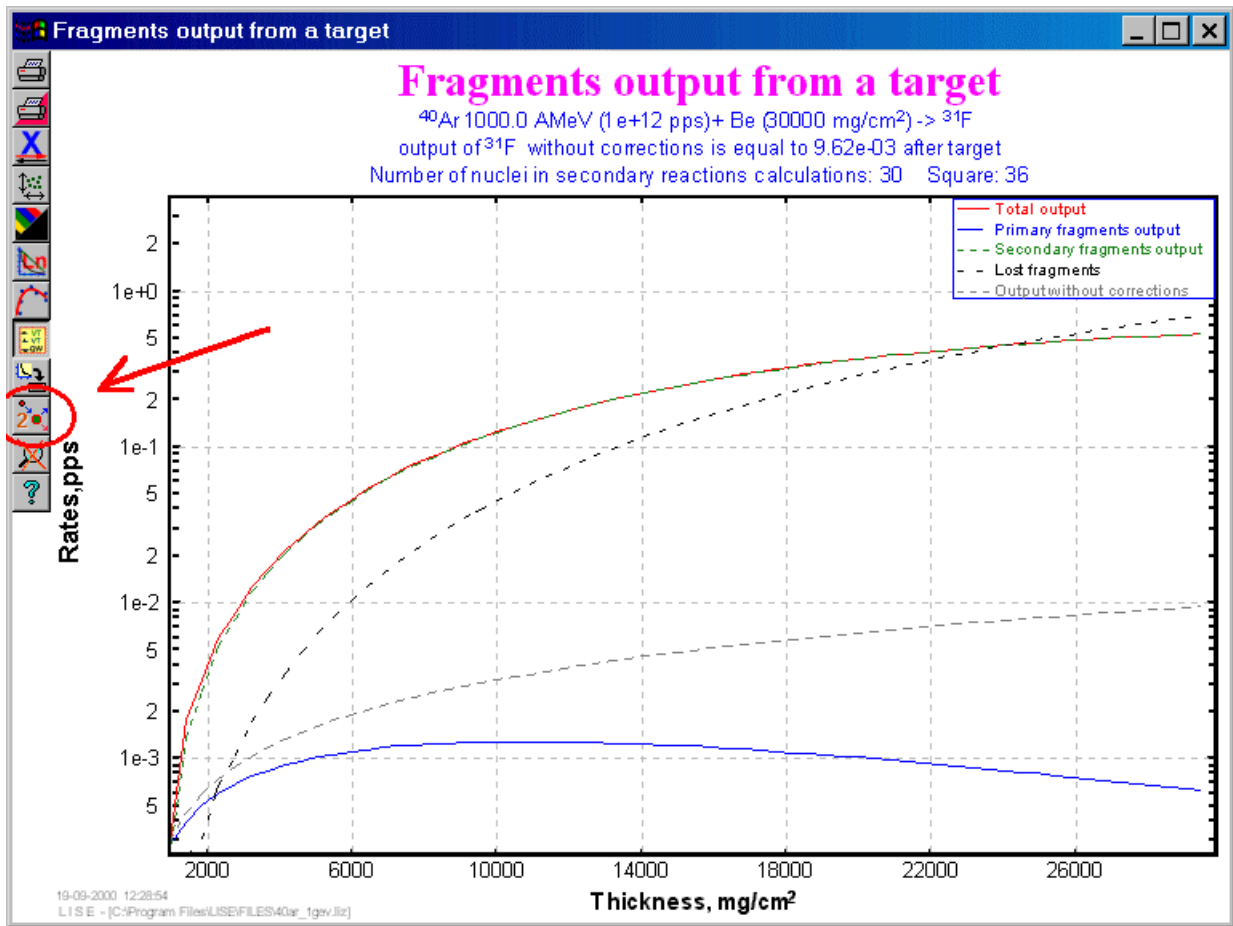


Fig.657. Call of a file of results through plot "Output of products from a target with the contribution of secondary reactions".

The given file allows to see what fragments give the greater contribution through secondary reactions in a fragment of interest and also to analyze a difference between fragments outputs without amendments on the basis of the formula /78/ with outputs in view of secondary reactions. Whence it is possible to draw a conclusion on an example what fragments has advantage at relativistic energies with use of a thick target.

The example of the given file for a fragment  $^{31}\text{F}$  gives below:

```

LISE CALCULATIONS Version 4.8.1
Date : 9/19/2000 Time : 12:28:10
Projectile : 40Ar 18+ at 1000 MeV/u - Intensity : 1e+12 pps
Target : Be Thickness : 30000 mg/cm2 (162338 microns)
Settings calculated on 31F
Methods: Cross Section=4 NP=128

=====
CONTRIBUTION OF SECONDARY REACTIONS in output of 31F
=====

```

A	B	C	B/C	relation		
E	Z	N	contribution	fragment's	fragment's	SECONDARY/

			from fragment into 31F w/out loss	output with secondary reactions	output w/out any correct. (pps)		PRIMARY after target
40Ar	18	22	6.03e-04	5.64e+10	1.00e+12	0.056	0.0014
42K	19	23	4.45e-07	8.59e+07	1.56e+09	0.055	0.1488
41K	19	22	7.73e-08	1.62e+08	2.64e+09	0.061	0.2596
40K	19	21	6.09e-08	5.78e+08	9.81e+09	0.059	0.1898
41Ar	18	23	9.91e-05	5.47e+08	9.81e+09	0.056	0.1356
39Ar	18	21	2.18e-06	8.10e+09	1.40e+11	0.058	0.1413
40Cl	17	23	1.01e-03	1.70e+08	2.64e+09	0.064	0.2797
39Cl	17	22	1.60e-03	2.23e+09	3.78e+10	0.059	0.1577
38Cl	17	21	6.16e-05	4.07e+09	6.35e+10	0.064	0.2356
39S	16	23	3.42e-03	1.97e+07	2.18e+08	0.090	0.7564
38S	16	22	6.98e-03	2.38e+08	3.12e+09	0.076	0.4587
37S	16	21	6.57e-04	7.68e+08	9.93e+09	0.077	0.4553
38P	15	23	7.30e-03	1.61e+06	9.82e+06	0.164	2.1123
37P	15	22	2.57e-02	2.16e+07	2.08e+08	0.104	0.9416
36P	15	21	5.29e-03	1.03e+08	1.10e+09	0.094	0.7220
37Si	14	23	1.39e-02	1.22e+05	3.77e+05	0.323	4.9994
36Si	14	22	7.52e-02	1.70e+06	1.13e+07	0.151	1.7554
35Si	14	21	2.94e-02	1.02e+07	8.44e+07	0.121	1.1659
36Al	13	23	2.09e-02	8.29e+03	1.13e+04	0.737	12.3321
35Al	13	22	1.46e-01	1.12e+05	4.21e+05	0.266	3.7289
34Al	13	21	8.22e-02	7.37e+05	3.95e+06	0.187	2.2621
35Mg	12	23	2.17e-02	4.95e+02	1.92e+02	2.582	44.5410
34Mg	12	22	1.79e-01	6.30e+03	9.49e+03	0.664	10.5002
33Mg	12	21	9.95e-02	4.27e+04	1.18e+05	0.363	5.1821
34Na	11	23	1.47e-02	2.60e+01	2.01e+00	12.901	220.6899
33Na	11	22	1.80e-01	3.16e+02	1.38e+02	2.289	37.6172
32Na	11	21	9.39e-02	2.11e+03	2.36e+03	0.895	13.8098
32Ne	10	22	1.40e-01	1.40e+01	1.39e+00	10.077	164.3482
31Ne	10	21	6.90e-02	9.01e+01	3.20e+01	2.819	44.3615
31F	9	22	4.68e-02	5.39e-01	9.62e-03	56.013	892.3932

Characteristics of fragment output ( 31F ) after target

Total output	5.39e-01
Primary fragments output	6.03e-04
Secondary fragments output	5.38e-01
Lost fragments	7.28e-01
Output without corrections	9.62e-03

### 26.3.3. Call of a web-homepage of the LISE program from dialogue ABOUT

Pressing the left key of a mouse on dialogue About, the user automatically causes a browser and loads the homepage of program LISE located to the address: <http://dnr080.jinr.ru/lise>. In the following versions it is planned to make automatic check on presence of the new version of program LISE on the appropriate servers, and also access through the INTERNET to various bases to the data (on an example on a database изомеров to the address: <http://www.ganil.fr/LISE/isom.html>)

### 26.3.4. Angles of an inclination of a target and a stripper

In the new version the user can establish in the menu "Preferences" (see Fig.653, ellipse B) an option of simultaneous turn of a target and stripper, taking place for a target. If the user has changed an angle of an inclination of a target automatically there will be a change of an inclination of a stripper, and the user will receive the message on it. If this option is established, Optimum thickness of a target from an inclination of a target will be calculated also under condition of a simultaneous inclination of a target with a stripper (see the following paragraph).

### 26.3.5. Calculation of optimal target thickness from an inclination of a target

In the new version the user can calculate an optimum corner of an inclination of a target (simultaneously with a stripper and without it: see above). Through menu “Calculations” (Fig.658) it is possible to call the given utility. For calculation initial thickness of detectors are accepted at an inclination in 0 degrees. This procedure works can work also with options “Secondary reactions” and “Charge states”. The example of calculations is given in Fig.659.

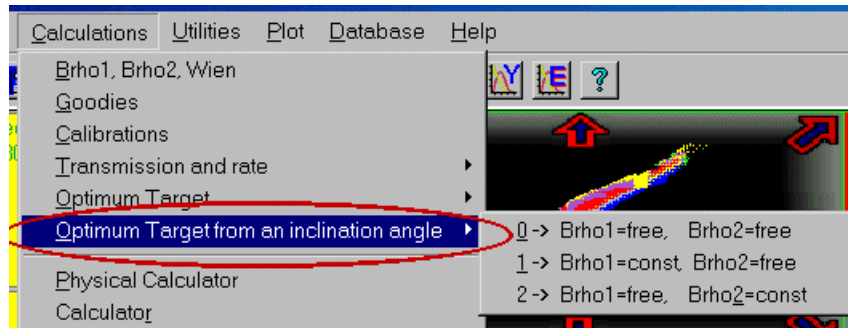


Fig.658.

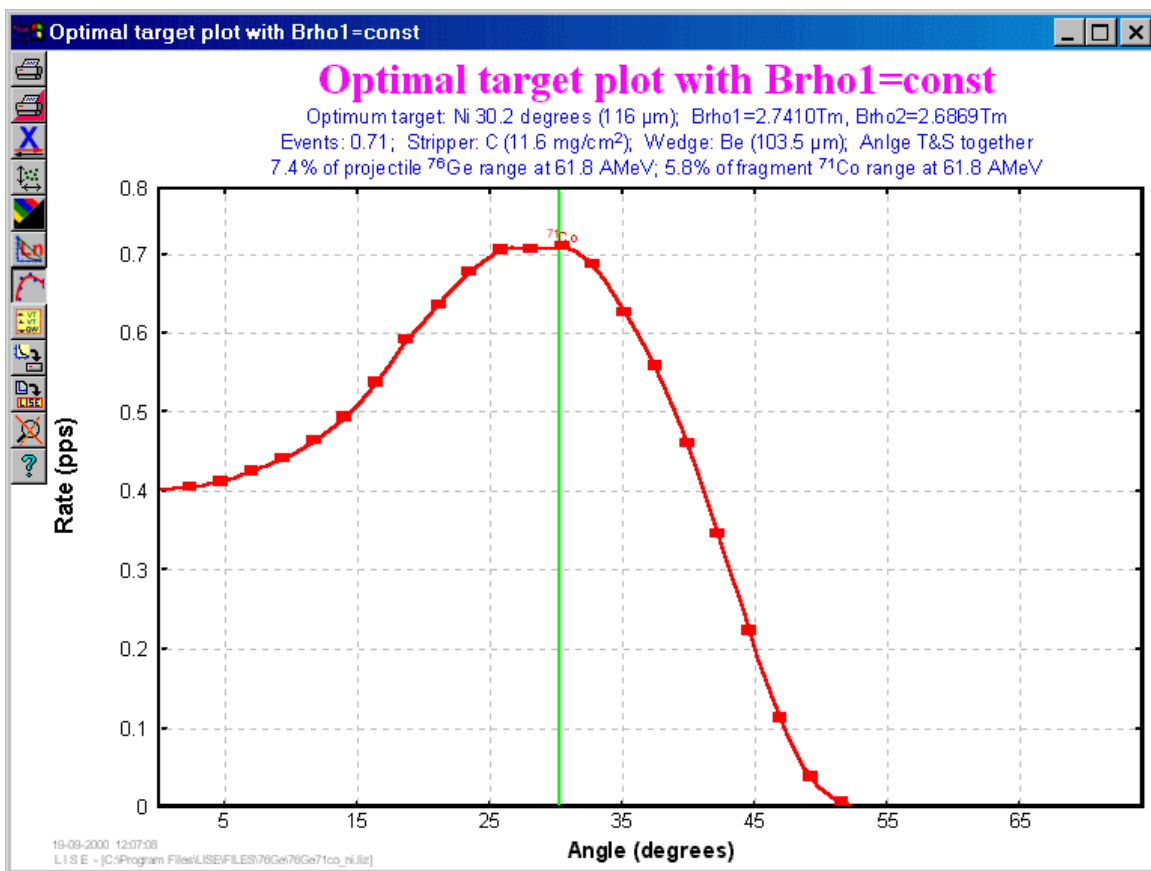


Fig.659. Plot of optimal target thickness from an an inclination of a target.

### 26.3.6. File of transmission calculation results

In a file of transmission calculation results the angles of an inclination of a target (stripper, wedge, materials) and according to their thickness under zero of degrees now are deduced. The factor  $K$  (equation /83/), showing change of an output of fragments due to reactions in a target (stripper, wedge) also is added.



## 27. Version 4.7

Caen  
17.08.2000

### Secondary reactions in a target (II)

#### 27.1. Secondary reactions in a target

The question on the contribution of secondary reactions products in an output of exotic nuclei at relativistic energies is intriguing, as substantial growth of an exotic nucleus output is supposed due to two-step reactions in a thick target. Also it is necessary to apply a correction factor to deduce the production cross section to take into account the losses due to attenuation of the beam inside the target.

In a real case calculation of the contribution of secondary reactions represents system from large (for a case of a heavy ion beam) quantities of the differential equations which is not solved an analytical way. For fast estimations the summarized section is used in view of interaction of the given fragment with a target on basis Kox's predictions as it is made in work [Rej00] where the measured apparent mass distribution was written as:

$$\begin{aligned} \sigma_{app}(A) &= \sigma_0(A) - \sigma_0(A) \cdot P_{loss}(A) + \sigma_m(A), \quad \text{with} \\ \sigma(A) &= \sum_Z \sigma(A, Z) \quad \text{and} \quad /84/ \\ \sigma_m(A) &= \sum_{A_i=A+1}^{A_{proj}-1} \left[ \sigma_{Kox}(A_{proj}) P(A_{proj} \rightarrow A_i) \right] \left[ \sigma_{Kox}(A_i) P(A_i \rightarrow A) \frac{N_t}{2} \right] \end{aligned}$$

In the new version of the program the contribution of secondary reactions is not taken into account in calculations of transmission and outputs of fragments (due to durable calculations), but the User only can make a rating using the menu "Utilities" -> "Output of products from a target with the contribution of secondary reactions". Calculations are carried out step by step on the basis of system from j differential equations with given below start conditions:

$$\begin{aligned} dN_i &= \sum_j \sigma_{j \rightarrow i}^{frag} N_j dt - \sigma_i^{Kox} N_i dt, \\ \text{with start conditions for } t &= 0 \quad /85/ \\ \left\{ \begin{array}{l} N_{i=beam}(0) = Intensity(pps) \\ N_{i \neq beam}(0) = 0 \end{array} \right. \end{aligned}$$

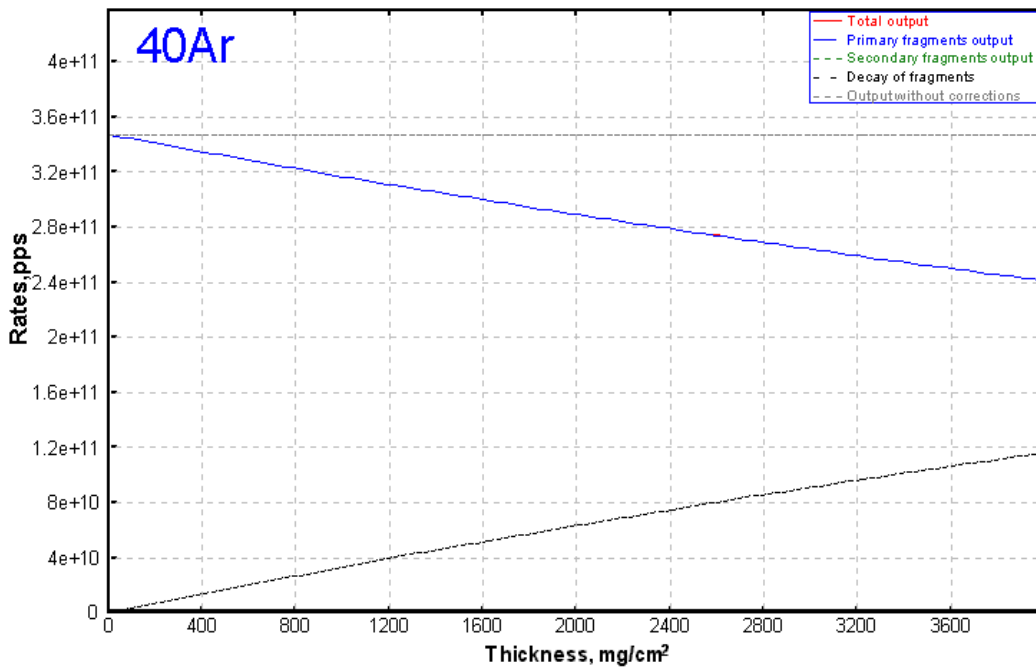
Nuclei settle up only those which are in a rhombus (Nbeam+3, Zbeam+1), (Nbeam-3, Zbeam+1), (Nfrag+3, Zfrag-1), (Nfrag-3, Zfrag-1) to avoid superfluous calculations in the case of the fragment is found very far from the projectile. The given plot represents five distributions depending on thickness of a target, which describe the following:

1. the sum of products (primary and secondary)

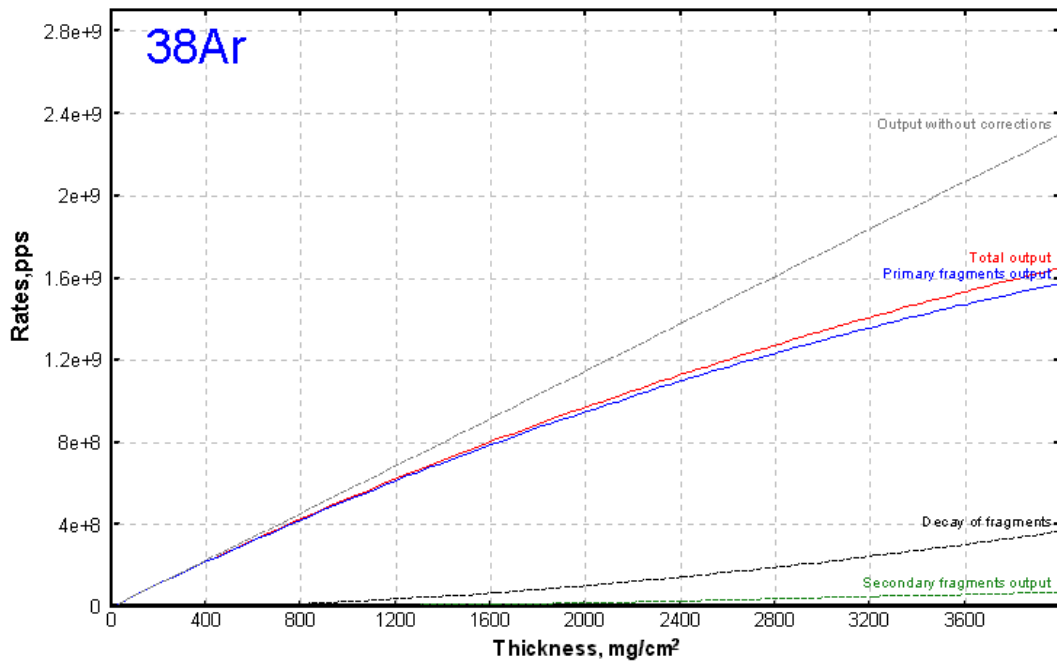
2. products formed from a fragmentation of a primary beam;
3. products formed as a result of secondary reactions
4. the sum of the broken fragments
5. the output of products without secondary reactions (as well as the program generally considers).

It is necessary to notice, that momentum distribution of secondary products should be wider, than primary. It is visible from the system submitted above, that also reduction of a primary beam also is taken into account due to reactions with a target.

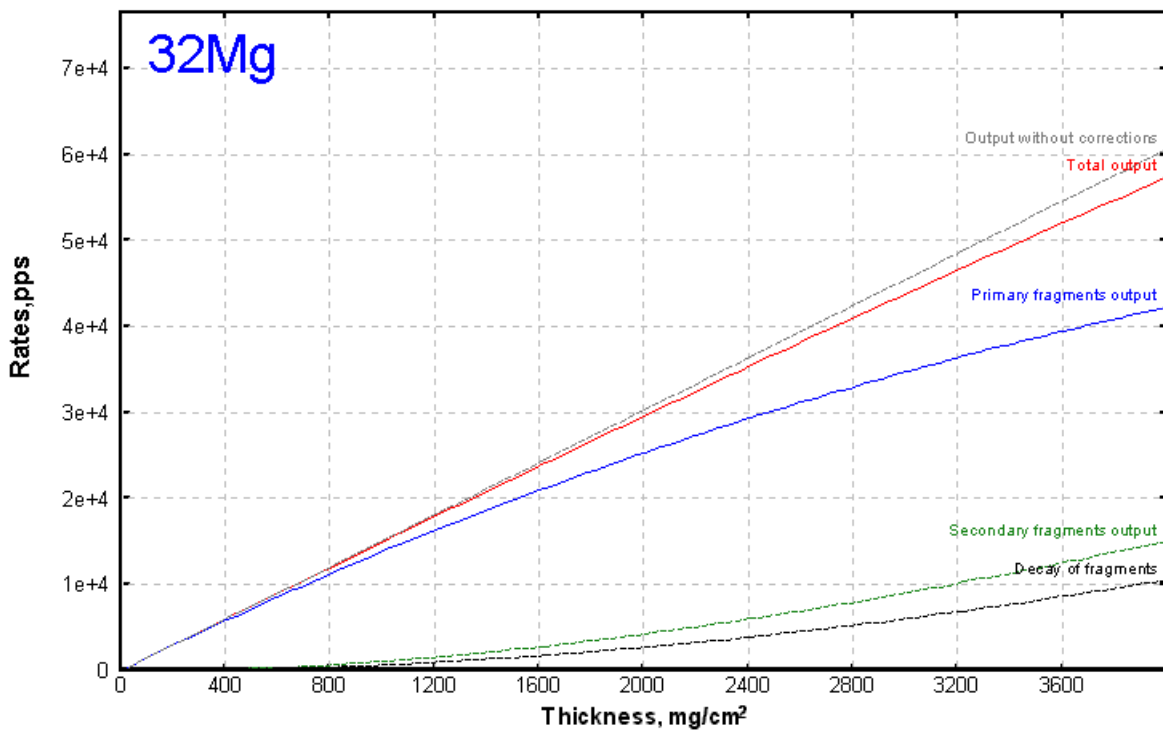
As an example we shall take recent work on studying cross-sections of neutron-rich nuclei from  $^{40}\text{Ar}$  fragmentation at about 1 AGeV [Oza00]. For super neutron-rich isotopes was used in this experiment the Be-target by thickness  $4007 \text{ mg/cm}^2$  (21.7 mm). On figures 660-663 calculations of outputs are presented depending on thickness of a target for this experiment. The first figure shows reduction of intensity of an initial beam. From three following strong influence of secondary reactions for unstable super neutron-rich nucleus  $^{28}\text{O}$  where their contribution exceeds on the order the contribution from initial reactions is visible.



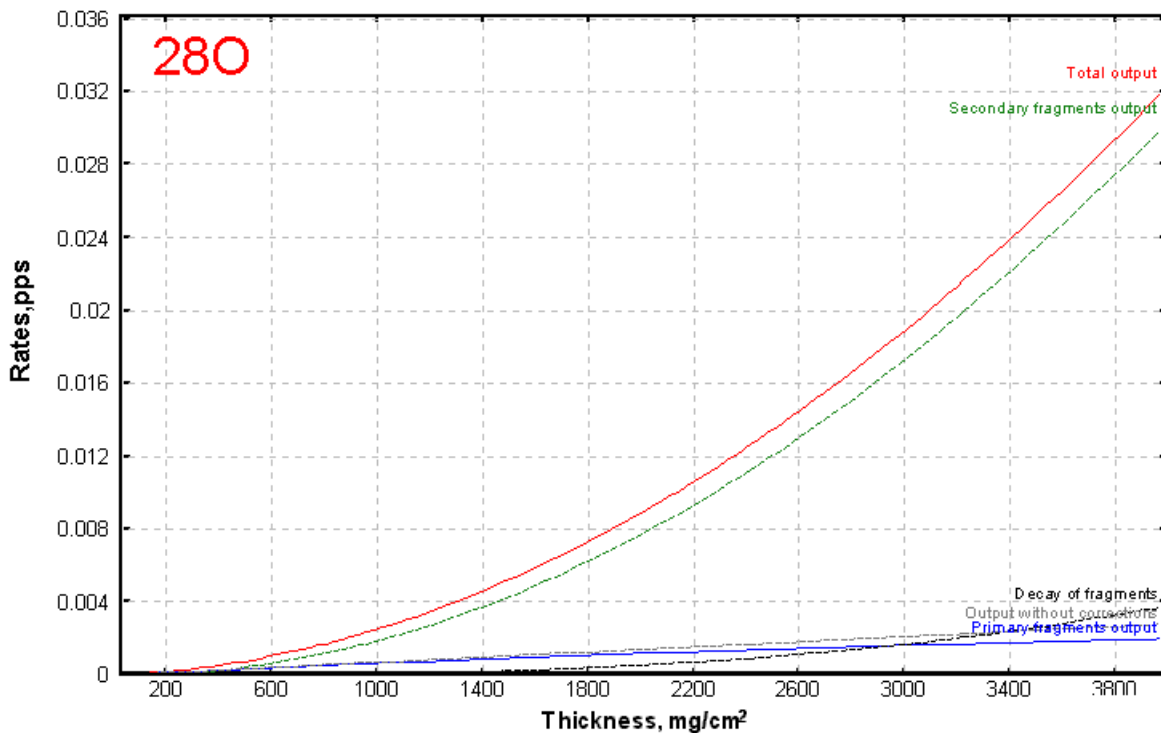
**Fig.660.**  
 $^{40}\text{Ar}$  (beam) outputs  
 in the reaction  
 $^{40}\text{Ar}(1\text{AGeV}) +$   
 $\text{Be}(4007 \text{ mg/cm}^2)$



**Fig.661.**  
 $^{38}\text{Ar}$  outputs in the  
 reaction  
 $^{40}\text{Ar}(1\text{AGeV}) +$   
 $\text{Be}(4007\text{ mg/cm}^2)$



**Fig.662.**  $^{32}\text{Mg}$  outputs in the reaction  $^{40}\text{Ar}(1\text{AGeV}) + \text{Be}(4007\text{ mg/cm}^2)$



**Fig. 663.**  $^{28}\text{O}$  outputs in the reaction  $^{40}\text{Ar}(1\text{AGeV})+\text{Be}(4007\text{ mg/cm}^2)$

Whence it is possible to draw a conclusion on expediency of use of beams at relativistic energies for reception super neutron-rich isotopes. There is a natural question: the same effect for proton-rich isotopes is expected? Calculations give the negative answer to this question. It is possible to show it a simple example. For a case  $^{40}\text{Ar}\rightarrow^{28}\text{O}$  through an intermediate nucleus of  $^{32}\text{Mg}$  product of cross sections is equal to  $3.77\text{e-}7\text{mb}^2$  ( $6.5\text{e-}4 \times 5.8\text{e-}4$ ), whereas for a case  $^{48}\text{Ni}$  ( $^{58}\text{Ni} \rightarrow ^{48}\text{Ni}$ ) through an intermediate nucleus  $^{52}\text{Ni}$  product is equal to  $1.92\text{e-}12\text{mb}^2$  ( $1.6\text{e-}5 \times 1.2\text{e-}7$ )! The difference between these products is 50000 times in consequence of that is not observed the contribution of secondary reactions to an output of  $^{48}\text{Ni}$ . Though for a case  $^{124}\text{Xe}+\text{Be}\rightarrow^{100}\text{Sn}$  the small contribution of secondary reactions is already observed.

## 27.2. Plots

### 27.2.1. Some distributions for cross section distribution plot

On a wish of users in the program was new opportunities for visualization of distributions of cross sections and others are entered: the user can look simultaneously some distributions (for different Z depending on mass and so on). It is possible to make selection of distributions: even Z, odd Z, and all distributions. In a figure on the right it is presented menus of a choice of distributions for the plot.

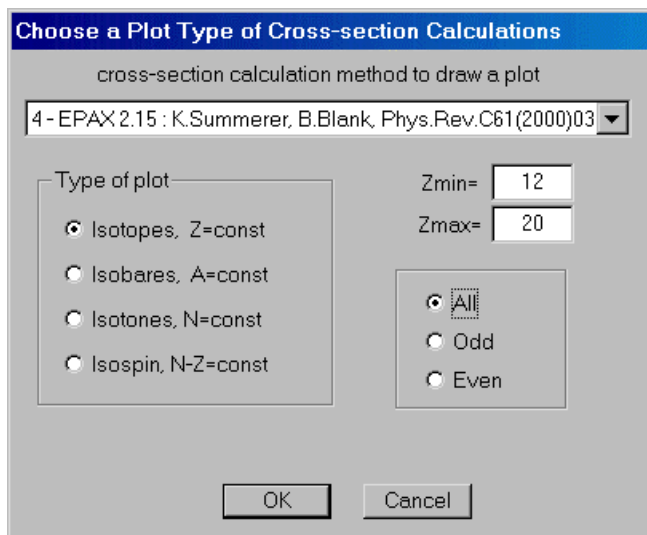


Fig.664.

### 27.2.2. Possibility to plot transmitted fragments with given charge states

As a result of the analysis of the data physicist can select outputs of fragments on charge state conditions. In the previous versions the program deduced all charging conditions on one plot, that not always was convenient.. In the new version the opportunity by analogy to data analysis given has appeared to make selection on plots on charge state conditions. Installation of this option is carried out in the menu the "Plots" -> "Options".

### 27.2.3. Transmission characteristics plot

The opportunity to observe distribution of characteristics of transmissions of fragments to plots has appeared ("Plots"-> "Transmission characteristics") in the new version at users. In other words it is possible to look outputs of fragments, outputs of charging states and to compare angular or spatial transmission of fragments and so on. (look a picture on the right). The example of this new type of the plots, representing an output of fragments with even Z and with a charge state condition equal  $Qt=Z$  is below submitted.

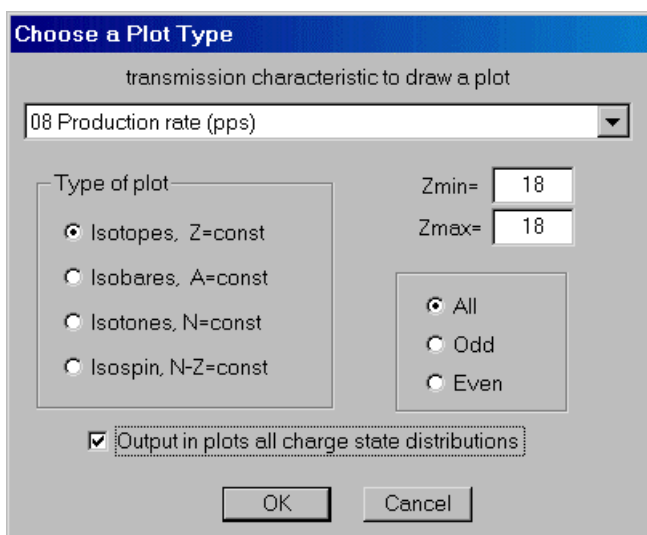


Fig.665.

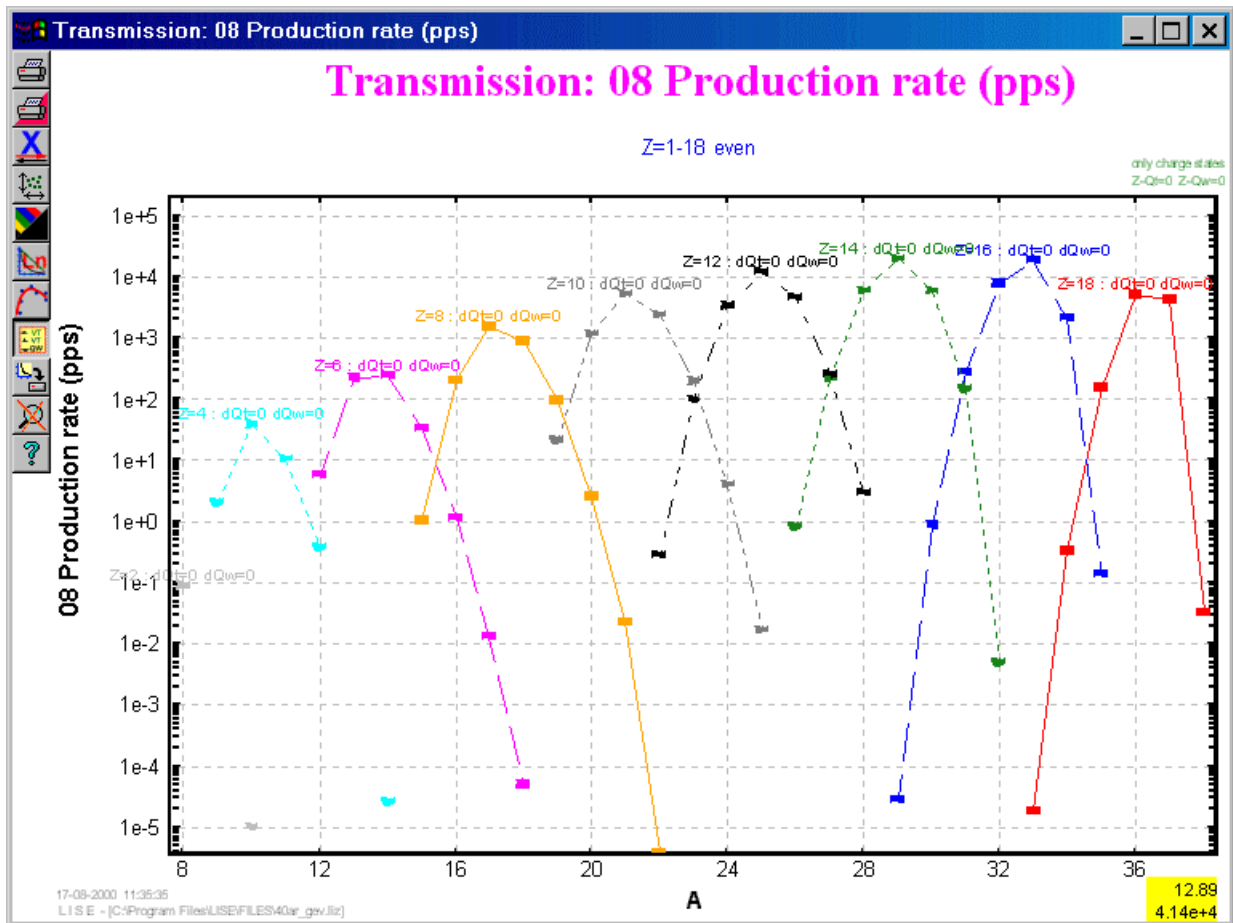


Fig.666.

#### 27.2.4. Manual scale of axis

The program automatically finds optimum values of axes. With the help of zoom the user can increase scale. However to reduce for limits of the established values not it was possible earlier, though there is a necessity at times for comparison with other plots to change values of axes. In the new version the user can in manual change using an icon (see Fig.667).

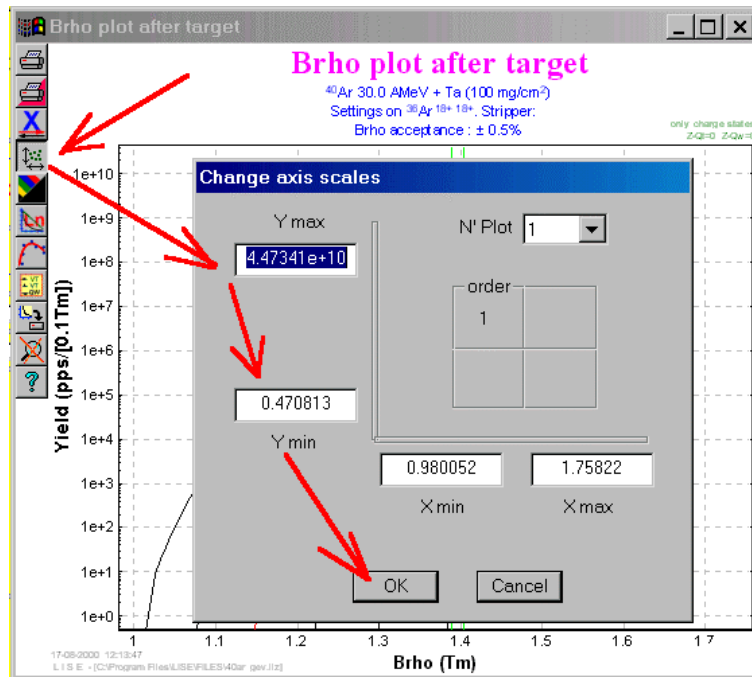


Fig.667.

## 27.3. Mechanism of Reaction

### 27.3.1. Momentum distributions from reactions

The program counts by default Gaussian curves for the momentum distribution with widths from the Goldhaber formula [Gol74]. However as the practice shows, many physics use for the description given other distributions, in particular take the width from the empirical systematic [Mor89]:

$$\sigma(p_{11}) = \frac{150}{\sqrt{3}} \sqrt{A_p - A_f} \text{ MeV} / c. \quad /86/$$

The opportunity of a choice of momentum distribution width is included in the new version of the program (Fig.668). Also the opportunity of use of the correction for reduced width was added at small energies from distortions due to Coulomb force [Bor86].

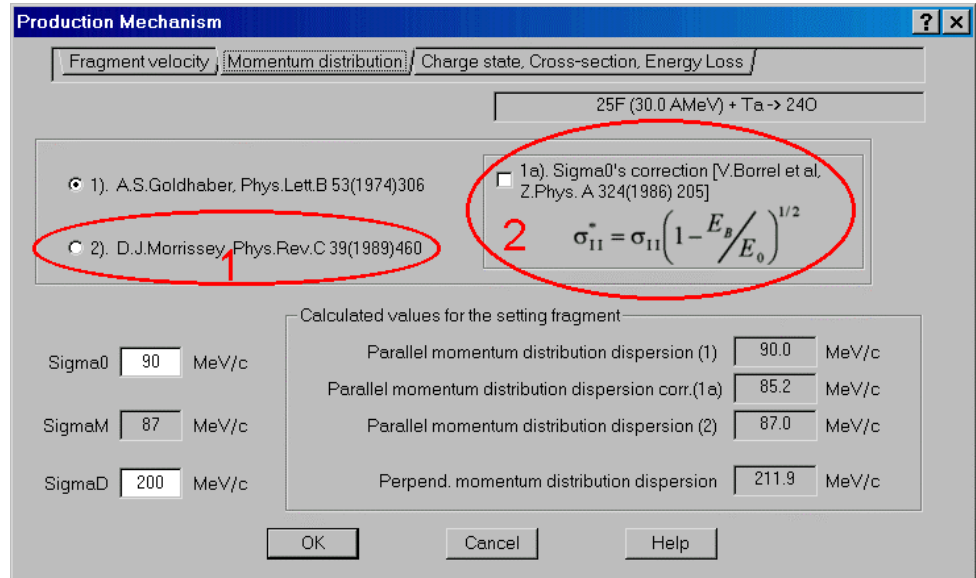


Fig.668.

### 27.3.2. Fragment velocity

For the description of experimental data [Dau00] in the formula [Bor83] of velocity of fragments after reaction were entered two parameters which the user can change (see Fig.669).

The first parameter is connected with energy which are necessary to ablate one nucleon. Default value is equal to 8 MeV. Also it was added a shift of the velocity relation. From comparison of experimental data and the LISE's simulation the shift is close to 0, but the energy to ablate one nucleon is equal to 2 MeV.

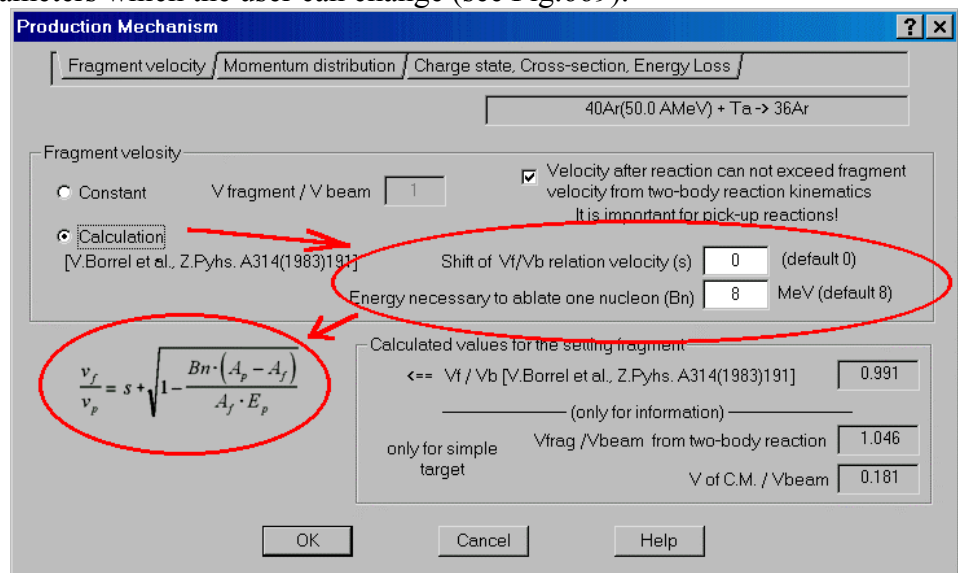


Fig.669.

### 27.3.3. Charge states distribution

For the analysis given the same work that was mentioned earlier, parametrization of charging conditions was modified [Leo98]. There was to correct a width of distributions (the factor 1,14 which is mentioned in the article [Leo98] is entered) and two parameters are added. Values are by default equal 1.

The first parameter **gzt** is entered into the formula ([Leo98]-11) and is responsible for position mean charge at equilibrium:

$$g'(Z_t, v_p / Z_p^{0.477}) = 0.929 + 0.269 \exp(-0.160Z_t) + (0.022 \cdot \mathbf{gzt} - 0.249 \exp(-0.322Z_t)) \frac{v_p}{Z_p^{0.477}} . \quad /87/$$

The second **dn** is accordingly entered into the formula ([Leo98]-13) and allows to change width of distributions:

$$d = \mathbf{dn} \cdot 1.1432 \cdot \sqrt{\bar{Q}(0.07535 + 0.19 \cdot \bar{Q} / Z_p - 0.2654(\bar{Q} / Z_p)^2)} . \quad /88/$$

These parameters were entered only for simulation of experimental data and what physical basis does not carry.

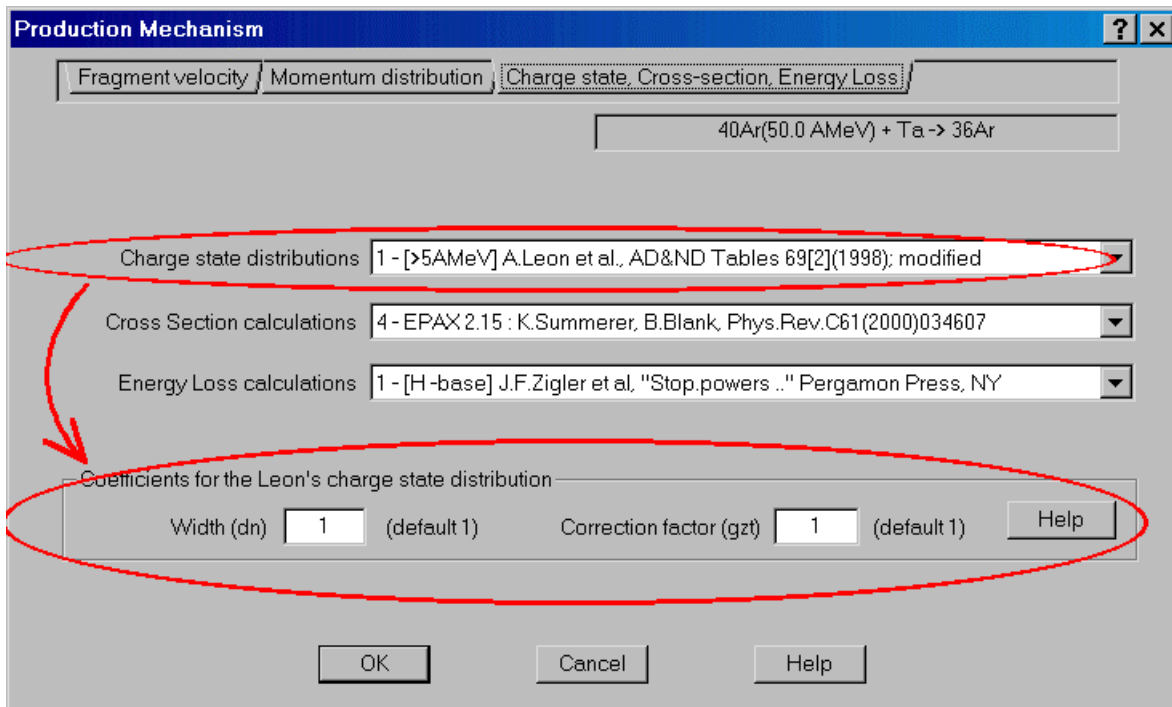


Fig.670.

## 27.4. Other

### 27.4.1. New configuration files

It was added new configuration files for spectrometers RIPS at RIKEN, and A1200 at NSCL MSU. Configurations A1900 with its acceptances and a dispersion also were added, but optical factors (except for a dispersion) are taken equal 1 or 0 (see a file). This configuration was made only for estimations of products outputs on this spectrometer.



### 27.4.2. Total reaction cross section

In the previous version the total cross section of reaction was used only as the help information in the menu of the Utilities -> Reaction's characteristics. In the new version the given section is used for an estimation of a fragments output in the new utility for calculation of the secondary reactions contribution. The total cross section was taken from work [MSL89] where for a basis the Kox's formula [Kox87] takes. Authors have taken linear dependence of parameter  $c$  with from energy that is true only for area energy 30 MeV per nucleon. For application of the given formula at relativistic energies the given parameter on the basis of Kox's work was analytically described in the following kind:

$$\begin{cases} E > 200 \text{ AMeV} \Rightarrow & c = 1.941 \\ E \leq 200 \text{ AMeV} \Rightarrow & c = 1.941 \cdot \exp(-\exp(-0.04798(E - 31.41065))) \end{cases} \quad /89/$$

### 27.4.3. Database half-lives

In previous version the database contained half-lives of nuclei only up to  $Z=74$ . In the new version the database of half-lives was completed on the basis of Nuclear wallet cards - 2000, Jagdish K.Tuli, BNL, PO Box 5000, Uton, NY 11973-5000

### 27.4.4. Corrections

It has been corrected:

- Data output file of plots,
- "Optimal target" calculation subroutine,
- Distribution widths for bidimensional plots.

From analysis of experimental data it is recommended to take as values by default for two-dimensional diagrams the following sizes:

- High frequency resolution      0.2 ns
- Energy resolution of detector    0.2 %
- Time resolution of detector      0.1 ns
- Defect of detector                0.6 %

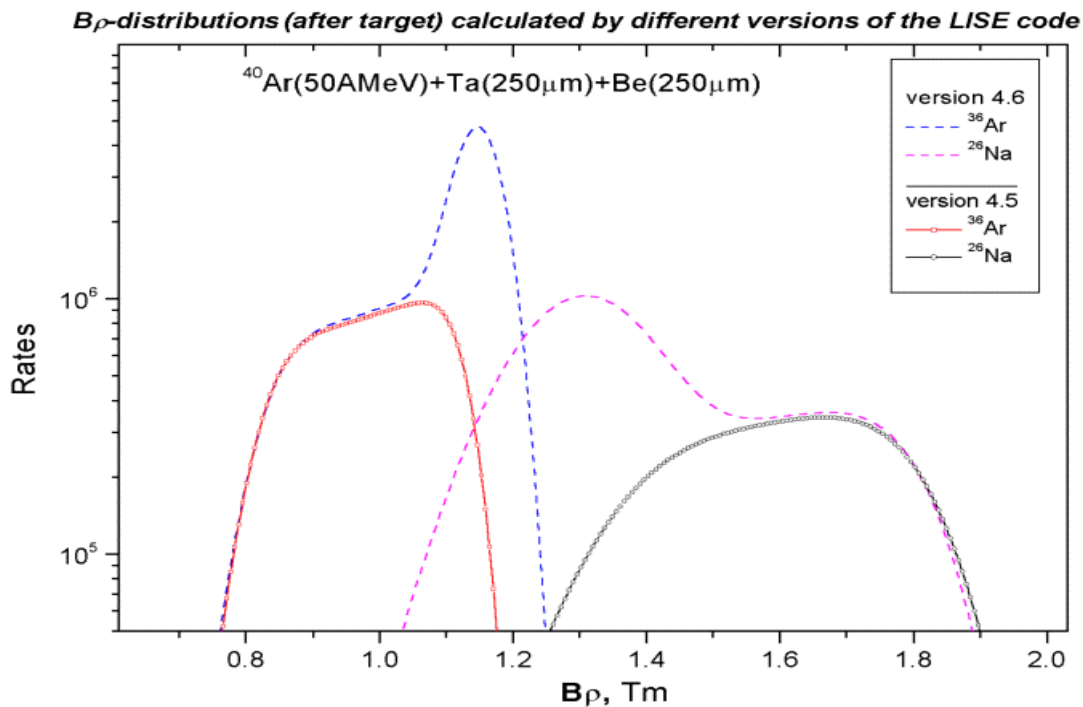
## 28. Version 4.6

Dubna  
15.06.2000

### Stripper after target: contribution in fragment distributions Charge state distribution in transmission calculation

#### 28.1. Degraded after target: contribution in fragment distributions

As a result of comparison of the data received in experiment E243a (GANIL), with results of simulation of the LISE program, the divergence was marked in connection with use of a thick degrader after a target. The degrader after a target is used more strongly to strip ions for what after a target with large nuclear number the foil with small  $Z$  is used. In the previous versions the program did not expect reactions in an absorber. In the new version of the program the contribution of reactions occurring in a degrader also is taken into account (see Fig.671). For this example were used the Ta-target by thickness of 250 micron and the degrader Be by thickness of 250 micron also, that in  $\text{mg}/\text{cm}^2$  accordingly 415 and 46,2. The contribution from reactions in the degrader it is well visible for in the given figure in consequence of that maxima of distributions on magnetic rigidity are displaced to the right for 36-th argon and to the left for 26-th sodium accordingly.



**Fig.671.** Magnetic rigidity distributions of fragments  $^{36}\text{Ar}$  and  $^{26}\text{Na}$  in case of the thick degrader calculated by different versions of the code.

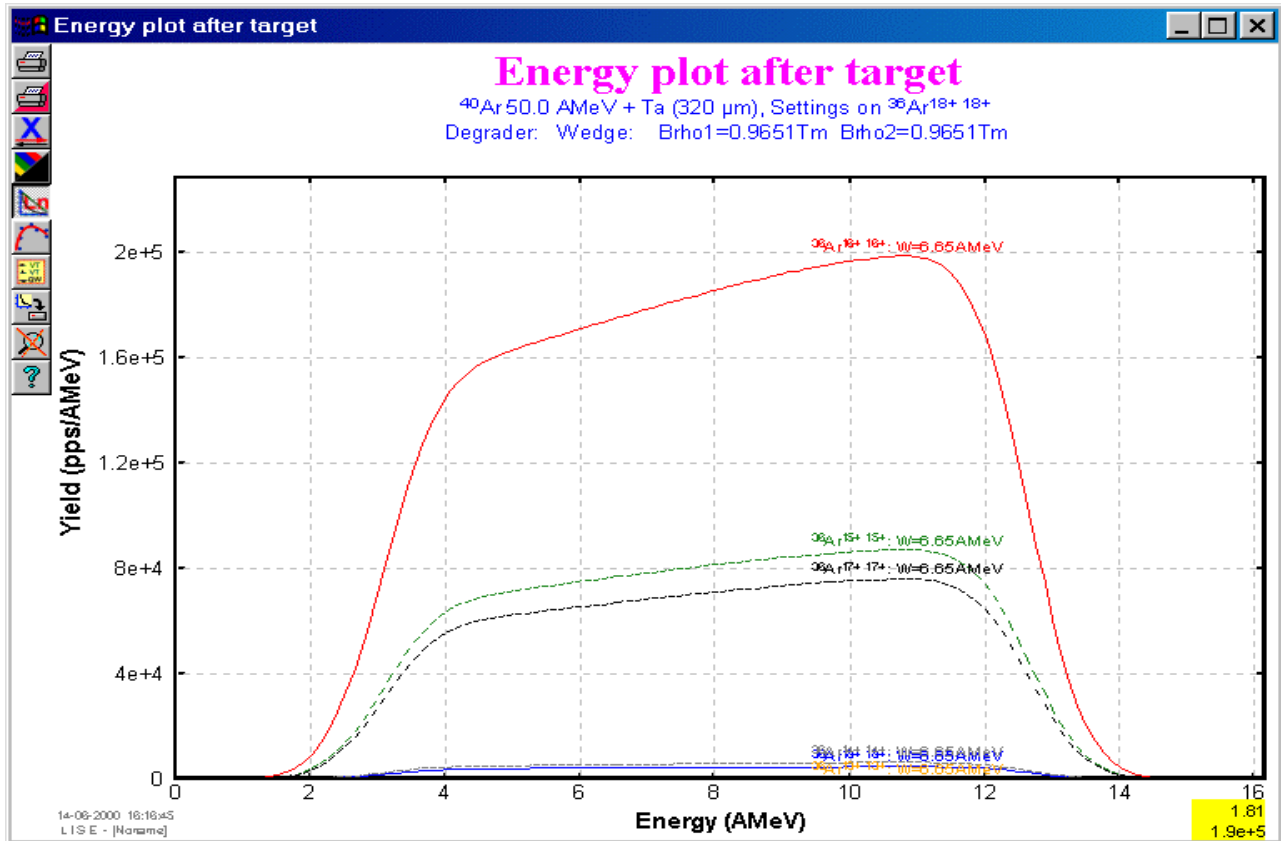


Fig.672. Energy distributions of  $^{36}\text{Ar}$  ions in the reaction  $^{40}\text{Ar}(50\text{AMeV})+\text{Ta}(320\mu\text{m})$  calculated by the *previous* version 4.5 of the code.

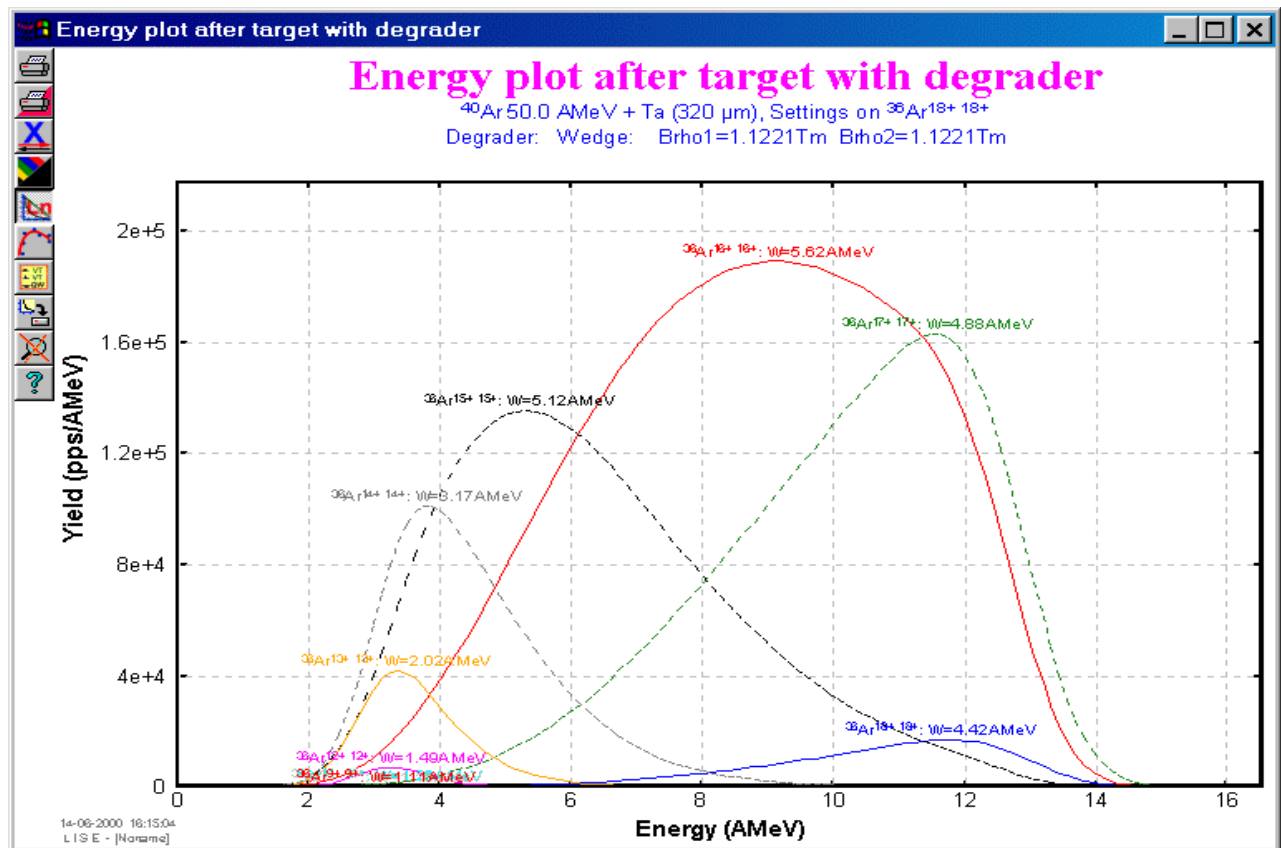


Fig.673. Energy distributions of  $^{36}\text{Ar}$  ions in the reaction  $^{40}\text{Ar}(50\text{AMeV})+\text{Ta}(320\mu\text{m})$  calculated by the *new* version 4.6 of the code.

## 28.2. Charge state distribution in transmission calculation

In the previous versions of the program the relation of charge states calculated twice after a target (or after a degrader after a target if its thickness is not equal to 0) for average value of energy distribution and after a wedge in the intermediate dispersive focal plane. In other words it was assumed that the relation between charging states was identical in any point of energy distribution that certainly is simplified (see Fig.672). The new version of the program calculates charge states in each of points of energy distribution (see Fig.673). The ratio between charge states is determined from the ratio of energy distribution area given charge state to the sum of all areas.

## 28.3. Development

### 28.3.1. M5678-spectrometer's calibration

By analogy to calibrations for the LISE spectrometer the scheme with the buttons was made for the M5678 spectrometer in Dubna, permitting to output dialogues of calibrations of spectrometer dipoles (see Fig.674).

### 28.3.2. Energy Rest in Physical calculator

In the dialogue " Physical calculator" at the request of users possibility to look values of residual energy in MeV is added. Before the energy was output only in MeV per nucleon.

### 28.3.3. TOF shift

During experiment a physicist can change a time delay for parameter time of flight, when start (or stop) time of flight takes from high frequency of the accelerator. It is done that interesting fragments was in the middle of time distributions and was not cut off by the following bunch. Similar simulation can be made in the new version changing parameter " Shift TOF" (see Fig.675).

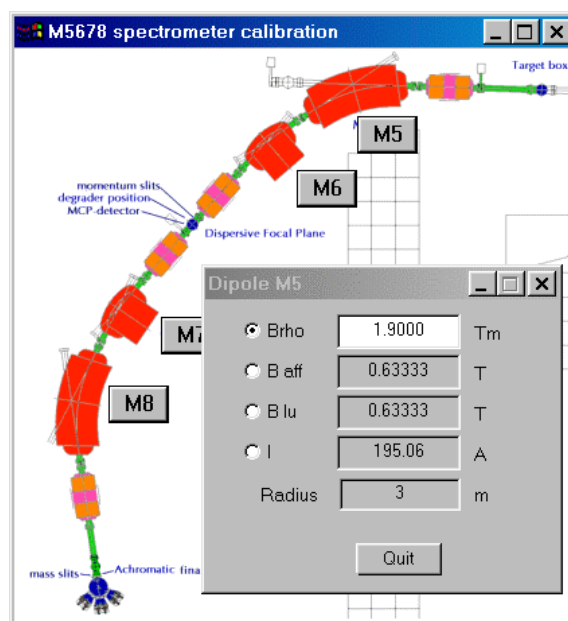


Fig.674. Scheme of the M5678-spectrometer

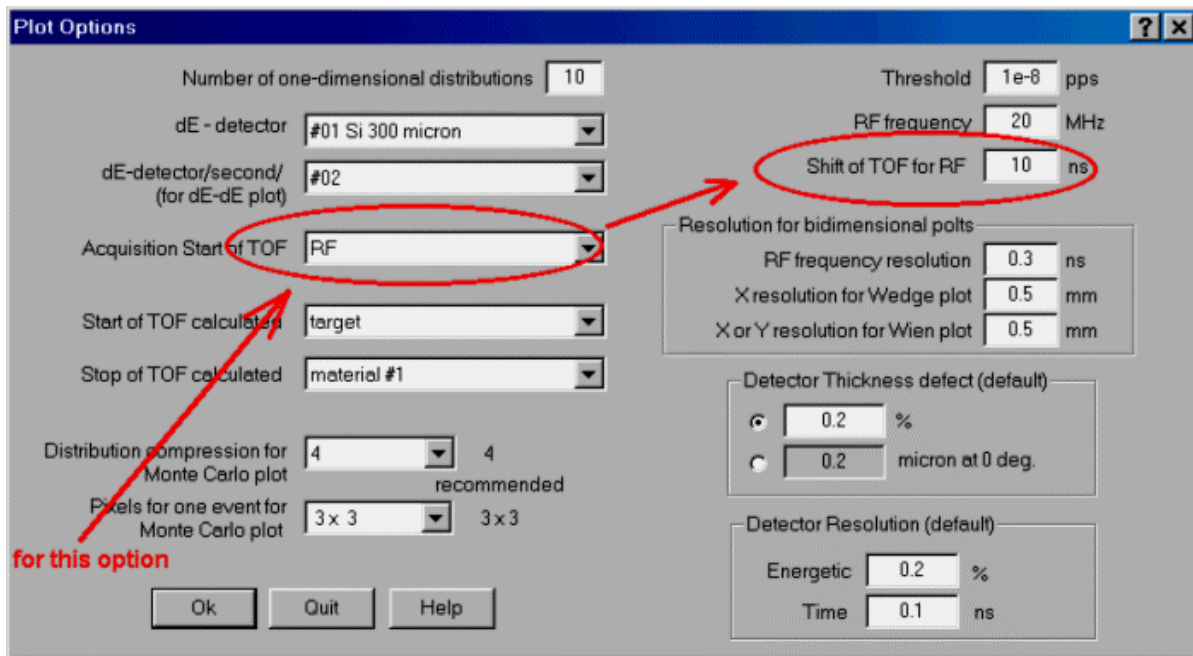


Fig.675. The dialogue "Plot options".

#### 28.3.4. Note of base configuration used for calculations

(see 27.4.1. New configuration files also 29.3.5. Note of base configuration used for calculations)

The user can see a mention of the current configuration right after materials in the window of customizations (see the picture on the right).

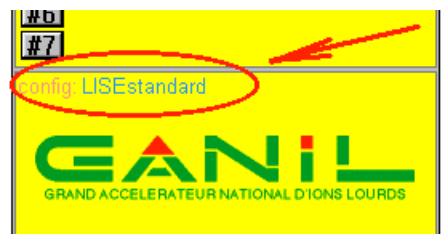


Fig.676

#### 28.3.5. Bug

The bug was retrieved in a memory allocation in the previous version of the program in this connection on *some* computers immediate failure in the program followed.

### 28.4. Brief description of previous version (4.5.5-4.5.8) changes

#### version 4.5.8

During calculations of transmission and in a mode of a acquisitions for Monte Carlo plots the program allowed to process other processes. Now other processes are not analyzed behind exception button ESCAPE and pressing of a mouse a key STOP accordingly, that has considerably allowed to increase speed of calculations. Switch on/switch off the 3D-balls animation window in a mode of a data set for Monte Carlo to estimate acquisition speed. As shows experience for some computers better to not switch off animation.

**The important reminder** - values by default in the menu PLOT OPTIONS for options the energetic resolution of detectors, the time resolution of detectors, thickness defect of detectors will be will be applied

only after the following loading the program!!! If the program is already started, it is necessary to change these values for detectors directly in their menu.

#### version 4.5.7

Negative numbers were not entered into versions 4.5.4 on plots of  $Q_{gg}$ -systematization and the data from base. Now all works normally.

#### version 4.5.6

There are considered pick-up reactions. Amendments to cross-sections which recently B.Blank has given, It was made in own way.

#### version 4.5.5

The tag is entered into the dialogue "Preference", that velocity of a fragment may not exceed its velocity from two-body reaction kinematics. It is very important for pick-up reactions (see the dialogue "Preference" in Fig.677).

The plot of the velocities relation is made. The example is given in Fig.678.

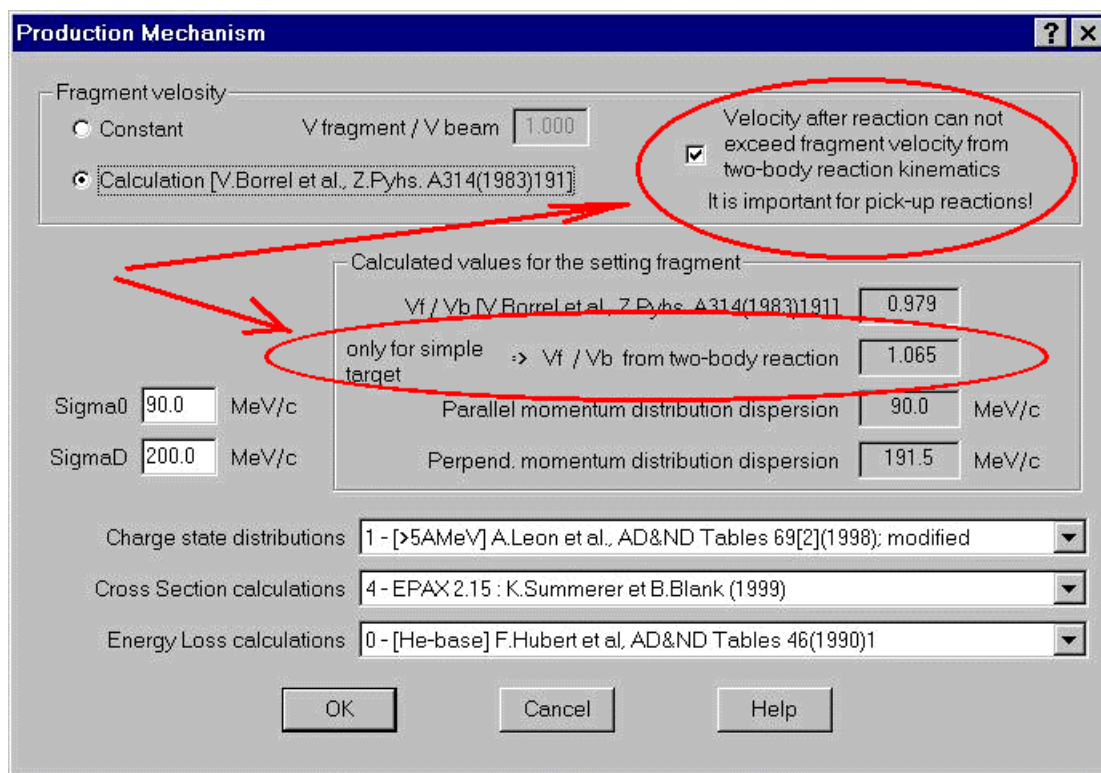


Fig.677. The dialogue "Preferences".

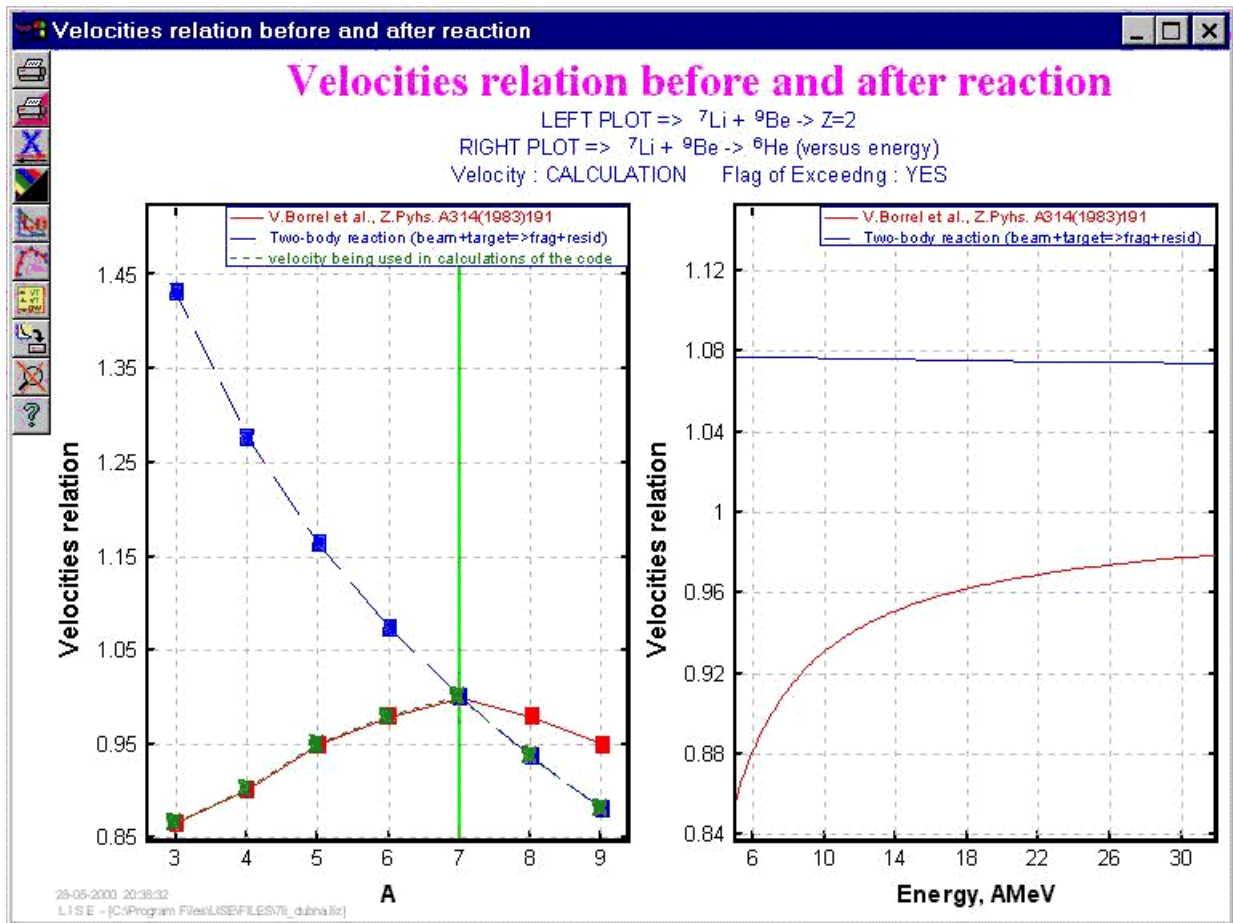
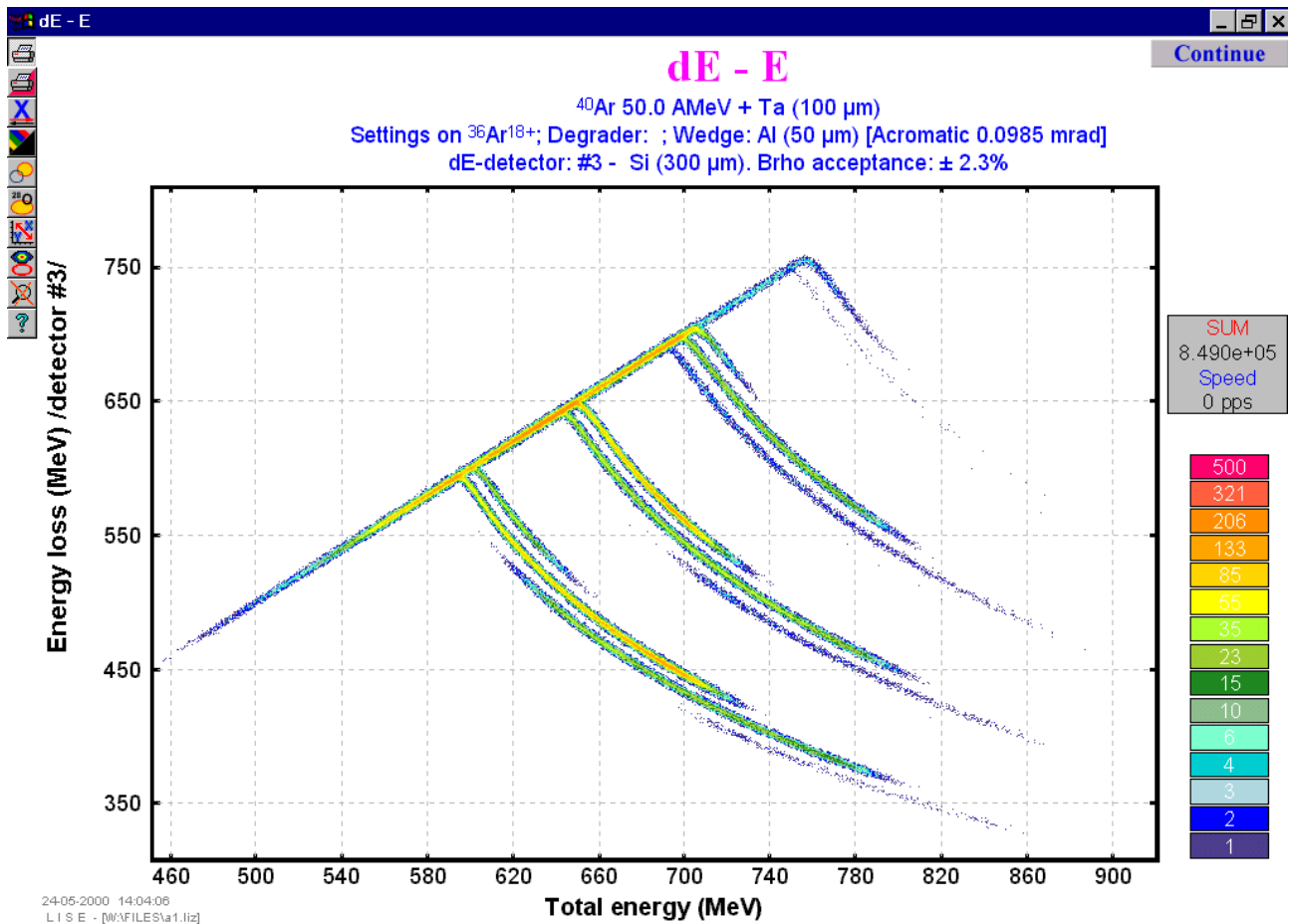


Fig.678. New plot "Velocity relation".

## 29. Versions 4.2.1 - 4.5

Caen  
26.05.2000

### Monte Carlo method for two-dimensional plots

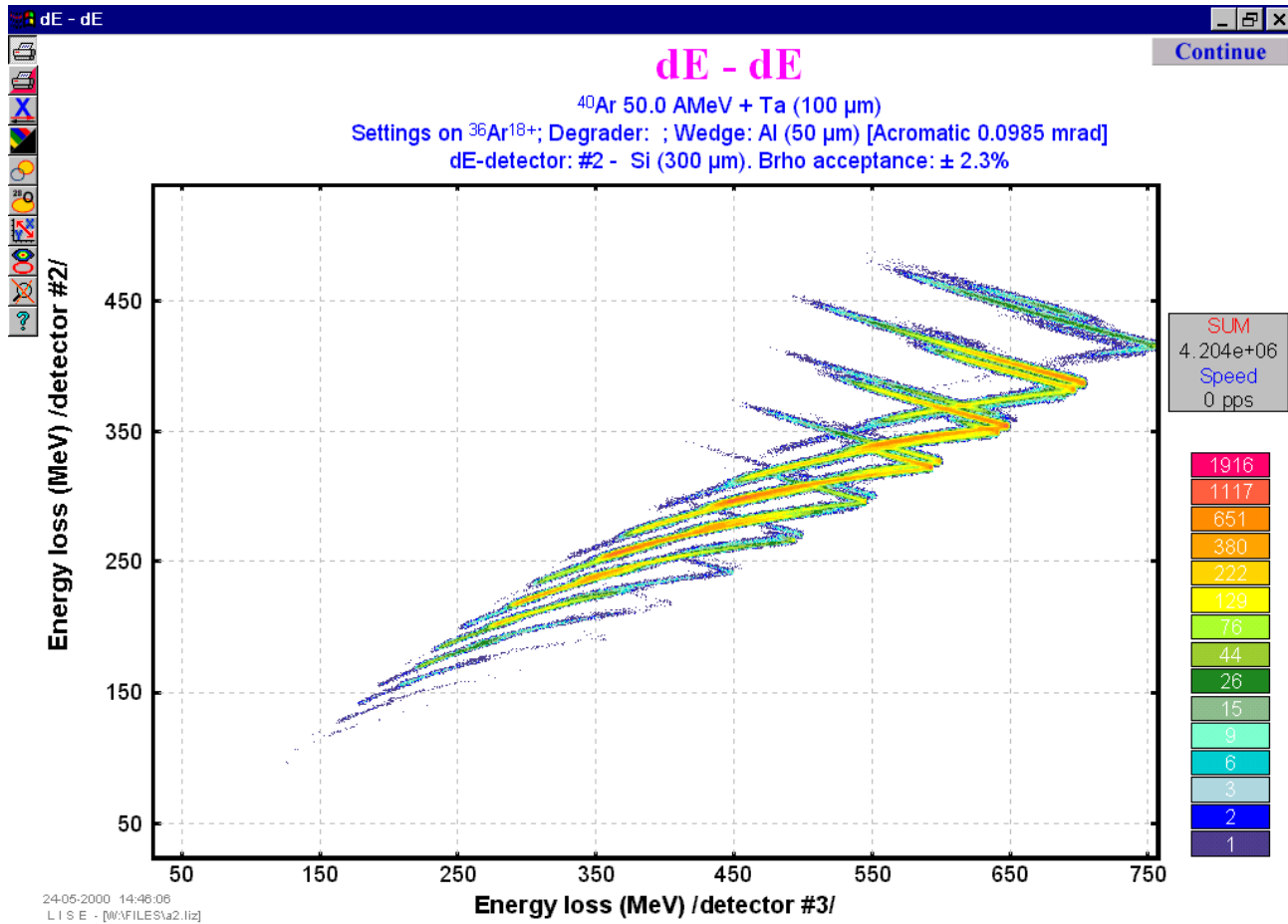


*Fig. 679. The example of application of a method of Monte Carlo for two-dimensional plot when the part of nucleus stops in the third detector, and the others fly by it.*



### 29.1. Monte Carlo method for two-dimensional plots (version 4.5)

Two-dimensional plots are powerful tools to observe expected results of experiments or to compare with experimental results. However previous versions of the code allowed only to draw two-dimensional plots by ellipses on base average values of distribution and their distribution widths. Especially given lack was shown in cases  $dE-E$ ,  $dE-dE$  plots when the particle stops in one of these detectors. It is impossible to reproduce expected tails of these distributions simply ellipses. To help to correct this lack of the program method Monte Carlo (MC) was included. The example of application of a method of Monte Carlo for two-dimensional plot represented in Fig.679,680 when the part of nucleus stops in the third detector, and the others fly by it.



**Fig.680.** The example of application of a method of Monte Carlo for two-dimensional plot when the part of nucleus stops in the third detector, and the others fly by it.

To visualize two-dimensional plots on the base MC method, User has to choose a plot of interest as it was in previous version. After standard two-dimensional plot on the base ellipses drawing is appeared it necessary to click on the button **Monte Carlo** in the left-top corner of the plot window. To stop a acquisition, the user should press the button **STOP** the left key of a mouse. Accordingly to continue an acquisition it is necessary to press the button **Continue**. In an acquisition mode of a set the user may change a direction of the X-axis, swap horizontal and vertical axes, make zoom or on the contrary restore original parameters a graphics, to print out the plot and to place or remove identification of nuclei. The method of

Monte Carlo may be used for all two-dimensional plots which have been built - in the program, such as which example represented in Fig.681

The data represented on a graphics by various color on quantity of events on the given point a graphics. The program automatically calculates a logarithmic scale with normalization for a maximum output. The given logarithmic scale of colors represented the a graphics.

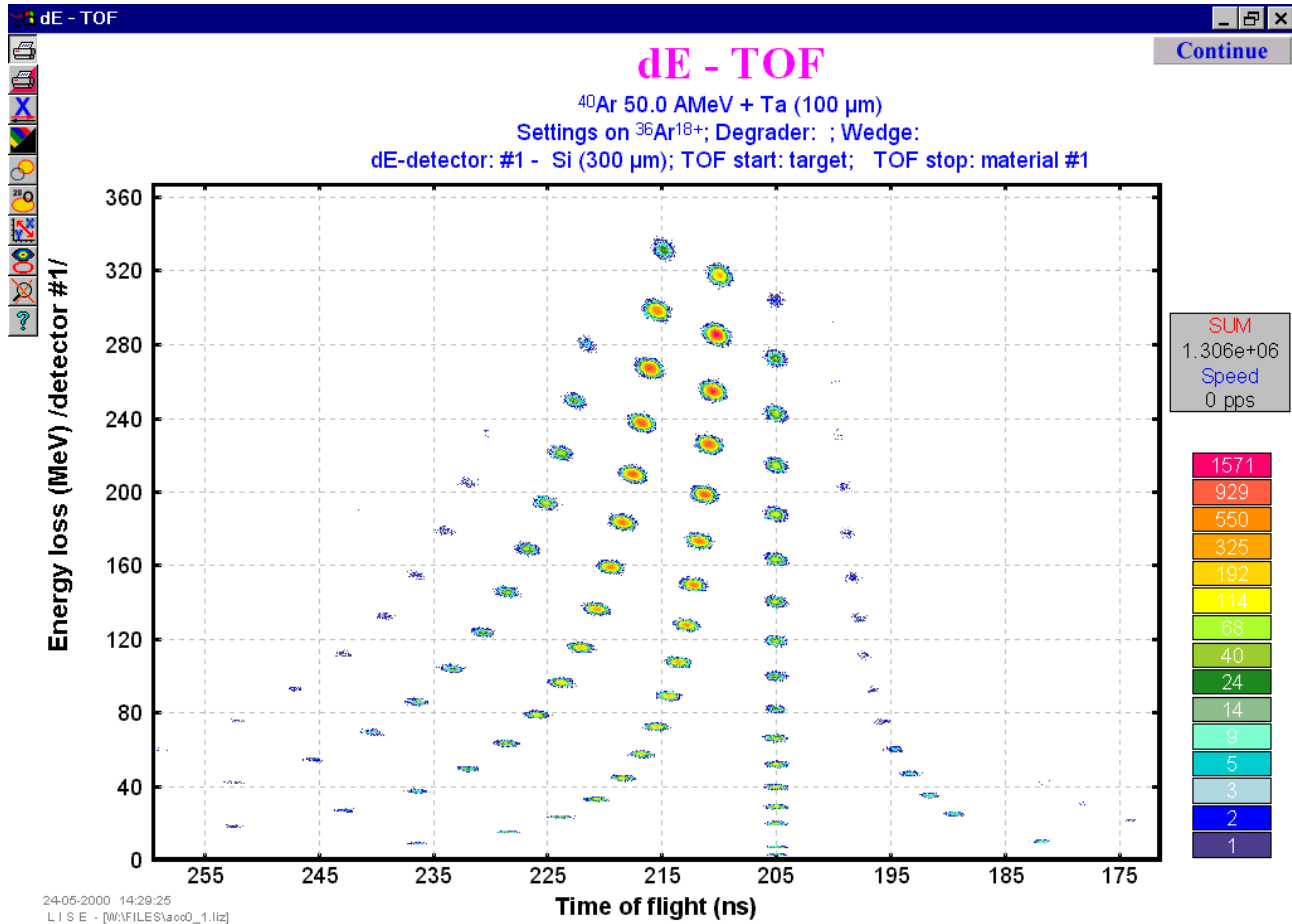
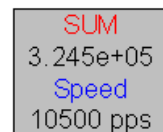


Fig.681. A Monte Carlo method for dE-TOF plot.

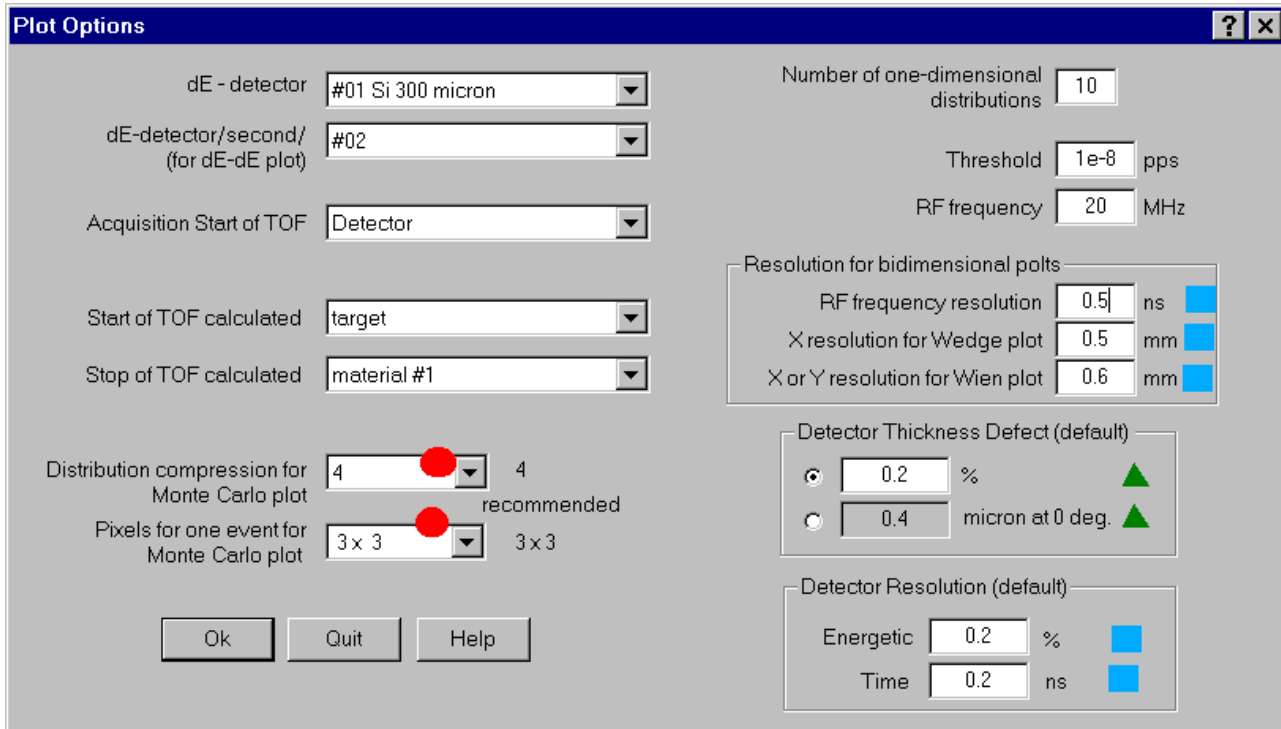
### 29.1.1. Speed of Monte Carlo acquisition

During a MC data acquisition the window occurs in which the sum of the typed events and speed of a set (events per one second) is shown. Speed of an acquisition depends first of all on computer speed, and also from installations by the user for MC-method. So for example, Pentium-II (frequency 233 MHz) at standard installations of a method of Monte Carlo allows to reach speed of an acquisition up to 15 thousand events in one second that is much higher, than sometimes presume to itself of physics during experiment with registration of all events.



### 29.1.2. Settings of Monte Carlo method for two-dimensional plots

The user may make all customizations of MC-method necessary in the dialogue “Plot Options” (see Fig.682). Red circles mark customizations used only for MC-method, blue squares mark items used for all two-dimensional diagrams, and by green triangles accordingly items used by default for all calculations in the program.



**Fig.682.** The user may make all customizations of MC-method necessary in the dialogue “Plot Options”. Red circles mark customizations used only for MC-method, blue squares mark items used for all two-dimensional diagrams, and by green triangles accordingly items used by default for all calculations in the program.

#### 29.1.2.1. Distribution compression for Monte Carlo plot

Distributions used in the program for Monte-Carlo application may be compressed, for this purpose increase speed of calculations and first of all size of occupied RAM. At a plenty of nuclei and at small compression of allocations at shortage of the RAM may even be involved swapping on the disk, that appreciably will slow down operation. However strong compression of allocations worsens quality of simulation. It is necessary to find the compromise as always in similar cases. Value of compression is by default equal to 4.

#### 29.1.2.2. Pixel for one event for Monte Carlo plot

All of a graphics in the program are output in virtual coordinates by dimension 1000×1000. To draw MC-method in colors, it is necessary to save in memory the typed data as the appropriate array who also is used for the subsequent upgrade of the screen and printing of plots. Simple counts show, that at output at permission one pixel on one unit from the array it is necessary to reserve memory hardly less than two megabytes. Certainly decrease of permission does not improve the diagram, however allows to save the RAM seriously. Recommended permission 3×3.

### 29.1.2.3. Resolutions and thickness defects

All resolution settings are used only for two-dimensional plots. Material thickness defect are applied also to calculate energy and range distributions for one-dimensional plots. Default values of thickness defect and energy and time resolution User may input necessary in the dialogue “Plot Options”. For the next start of the code “LISE” these defaults values will be used. For changes of thickness defects of and energetic and time resolutions in calculations the user should use accordingly dialogues of materials. All defaults values are saved in file *lise.ini*.

It is necessary to mark, that defect of width of a material also is applied and in calculations of transmission with degrader (wedge) in the intermediate disperse focal plane where the contribution of it may be rather noticeable in transmission of fragments.

## 29.2. In-built cubic spline procedure (version 4.4)

In the previous versions for definition of a distribution value in a point  $x$  two were used simple interpolation methods: a method of a trapeze on the basis of two next with  $x$  points and a method on the basis of three points. However with introduction in the program of a new class of distributions connected to transformation of one distribution (for example on magnetic rigidity) in the appropriate distribution but already on energy the new method of interpolation cubic spline was One of advantages of a new method is the opportunity of calculation of the first and second derivatives for any point of distribution. We shall remind, that it is connected to a continuity of derivatives as cubic spline is under construction on the basis of equality of the first and second derivatives for known points of distribution:

$$P'_{i-1}(x_i) = P'_i(x_i) \quad \text{and} \quad P''_{i-1}(x_i) = P''_i(x_i) \quad i = 2, \dots, (N - 1). \quad /90/$$

### 29.2.1. Transformation of distributions

In a basis of conversion of one distribution in another (the scheme represented in Fig.683) lays saving of squares between every each  $i-1$  and  $i$  points. In the last versions the given task was solved rather simple way that had an effect for quality of conversions at such small dimension of distributions (NP=128).

The edge effects were especially appeared in distributions of energy, ranges in matter as they may not be negative. We shall assume that the nucleus with the certain distribution passes through substance and the  $i$ -point of distribution stops in matter, and following passes. Then function appropriate between  $i-1$  and  $i$  points for preservation of the area should aspires to infinity. Rather complex mechanism of smoothing was applied. But all the same it is ideal to solve this problem it was not possible!

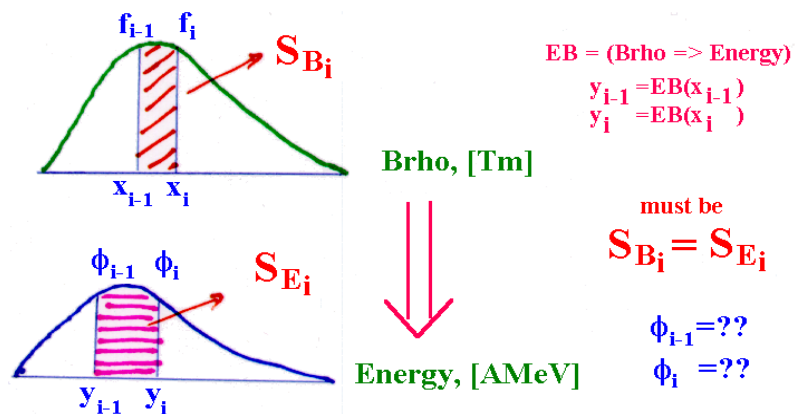


Fig.683. The scheme of conversion of one allocation in another

In the last versions the area between points was determined by the next primitive expression:

$$S_i = \frac{(f_{i-1} + f_i)}{2} \cdot |x_i - x_{i-1}|. \quad /91/$$

We may use now correct calculation of area is next:

$$S_i = \int_{x_{i-1}}^{x_i} f(x) dx, \quad /92/$$

because we have infinite function  $f(x)$  due to introduction of procedure cubic spline.

The condition of equality of the areas in both distributions between in an interval can be presented in the following kind:

$$S_{E_i} = S_{E_i} \Rightarrow \int_{x_{i-1}}^{x_i} f(x) dx = \int_{y_{i-1}}^{y_i} \phi(y) dy. \quad /93/$$

Doing substitution  $y=EB(x)$  it possible to get simple and good solution with application of the first derivative of the function  $f(x)$ :

$$\phi[y(x)] = f(x) \cdot \left( \frac{dEB}{dx} \right)^{-1}. \quad /94/$$

This derivative can be taken with the help of cubic spline procedure having constructed distribution  $x$  from  $y$ . Using further cubic spline procedure for  $\phi(y)$  distribution can be proceeded from complicated distribution with a variable step between points to more simple with a constant step accordingly.

### 29.2.2. Edge's effects

Introduction of new transformation of distributions yet does not solve a problem of edge effects. To resolve the given problem in the program use negative values of energy, magnetic rigidity and range in material was entered. The user certainly as always deals only with positive these sizes. The second, that was made for avoidance of edge effects in case of calculation of range in detectors (as energy loss calculation) - transformation of complicated distribution (with a variable step between points of distribution) to simple (a constant step) with positive values occurs only once for required distribution. All this qualitatively allows to expect in a case the attitude(relation) of fragments stopped in different detectors. The contribution of distribution broadening due to straggling (and also thickness defect of detectors) conducts down to the detector of interest, where already after transformation to simple distribution (with constant step between points) there is a convolution with transformed straggling distribution.

## 29.3. Development

### 29.3.1. Different methods to draw one-dimensional plots

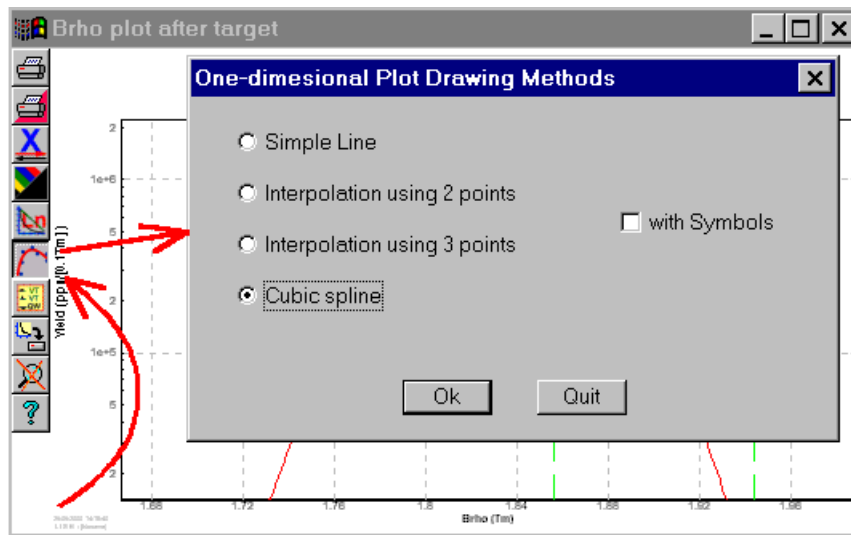


Fig.684. The dialogue "One-dimensional .plot drawing methods"

### 29.3.2. Dimension of distributions

Calculation of fragment transmission is based on an estimation of a part of distribution (spatial, angular, momentum) through given device acceptances. Under operating system DOS in old versions the dimension of distributions was equal to 64. With adaptation of the program under operating system Windows dimension became equal to 128. The increase of dimension conducts to better results, but slows down calculations and demands the greater operative memory. Especially strongly it is shown at calculation of fragments outputs with the established option of charge state condition calculation. At the same time at calculations of optimum thickness of target a step-type behaviour of calculations at small dimension of distributions becomes more appreciable. In the new version of the program the user itself may establish in dialogue "Preferences" (Fig.685) desirable dimension both for calculations without charge state condition, and with charge state condition. By default dimension of distributions is equal 128 for an option of calcu-

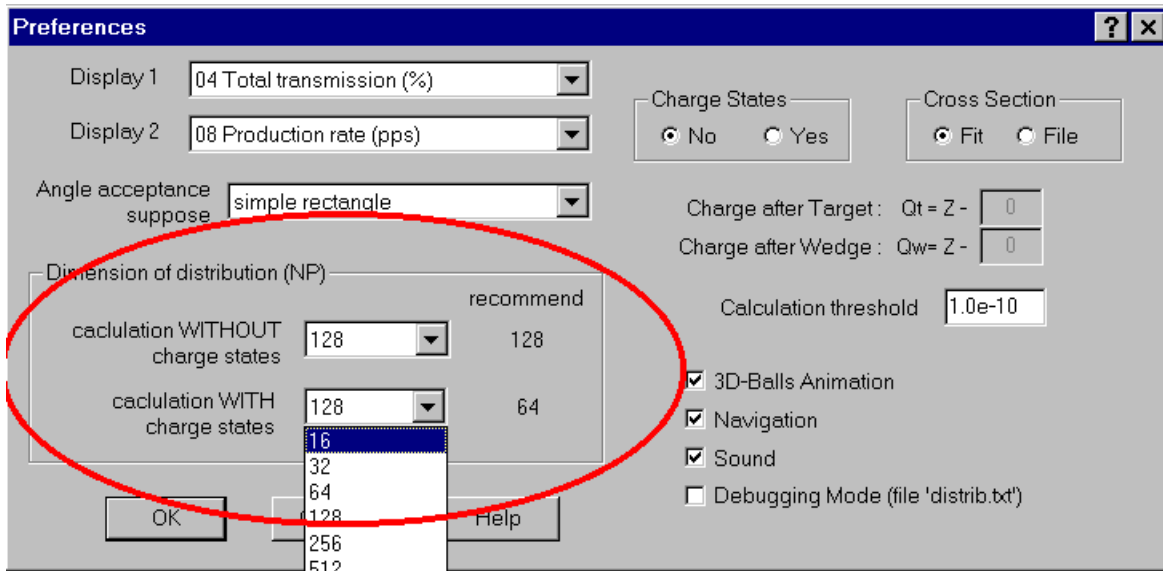


Fig.685. The dialogue "Preferences": setting of distribution dimension.

lation without chargt state condition, and 64 accordingly without charge state condition. In a state line of the program (Fig.686) the user always may observe the current value of dimension of distributions (NP).

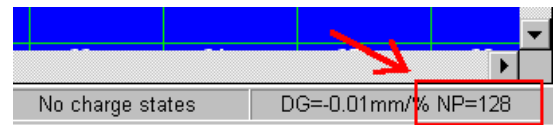
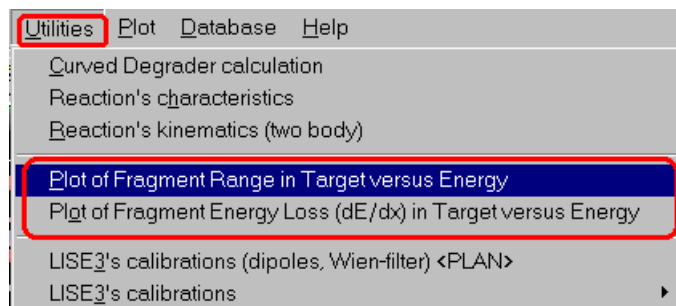


Fig.686. The fragment of the code state line (gadget) where it is possible to observe the current dimension of distributions.

### 29.3.3. New plots

In the new version opportunities to compare different methods of energy loss calculations have appeared, quickly to estimate values of range and energy losses in material (applying ZOOM) on the basis of new plots "Plot of Fragment Range in Target versus Energy" and "Plot of Fragment Energy Loss (dE/dx) in Target versus Energy" which settle down in menu Utilities.



### 29.3.4. Mode “auto” for the Wien filter and D6-dipole calculations

The previous versions automatically calculated adjustments of the Wien filter and the D6-dipole, well as showed experience sometimes it is necessary to have possibility to disable this mode to put any values. In the new version the given possibility has appeared. The user may in appropriate dialogues of adjustment of the filter and the dipole to place or remove an option “automatically”. If this option is placed, the flag will appear in the window of adjustments (see Fig.687). It shows that calculations of parameters of the Wien filter and dipole D6 occurs automatically to changes of the setting fragment and magnetic rigidity of the second dipole.



Fig.687. Window of adjustments: installed flags *AUTO* show, that calculations of parameters of the Wien filter and dipole D6 occurs automatically to changes of the setting fragment and magnetic rigidity of the second dipole.

### 29.3.5. Note of base configuration used for calculations

At start of the program the configuration of the LISE3 spectrometer boots. The user may load other configuration files or create the new configuration file. Fast to find out with what configuration he works (instead of to look at an example optical coefficients) in standard program files with extension “\*.liz” and in files results “\*.res” the name of the base configuration is saved.

### 29.3.6. Bugs

#### 29.3.6.1. Energy loss calculation in thin material

In the previous versions of the program at calculation of the residual energy after passage by a nucleus of a material with thickness close to 0 user may receive, that the residual energy exceeds initial! Calculation was carried out as follows: initial energy  $E_i$  was transformed through tables to range  $R_i$ , then detector thickness  $t$  was subtracted from  $R_i$  and already received value  $R_r$  was taken away was transformed to energy  $E_r$ . In the new version for avoidance of this effect the following amendment is entered: the range  $R_i$  is again translated in energy  $E_i^*$ , and then the difference  $(E_i^* - E_r)$  is subtracted from initial value of energy  $E_i$  to get final residual energy  $E_r^*$ .

#### 29.3.6.2. Calculations with a primary beam in dialogues *TOOLS* and *Physical calculator*

The bug of calculations with a primary beam in dialogues “TOOLS” and “Physical calculator” was found out. It was corrected.

## 29.4. Brief description of previous version (4.2.1-4.3.15) changes

### version 4.3

1. Two possibility to calculate angular transmission (Dialog "Acceptances")

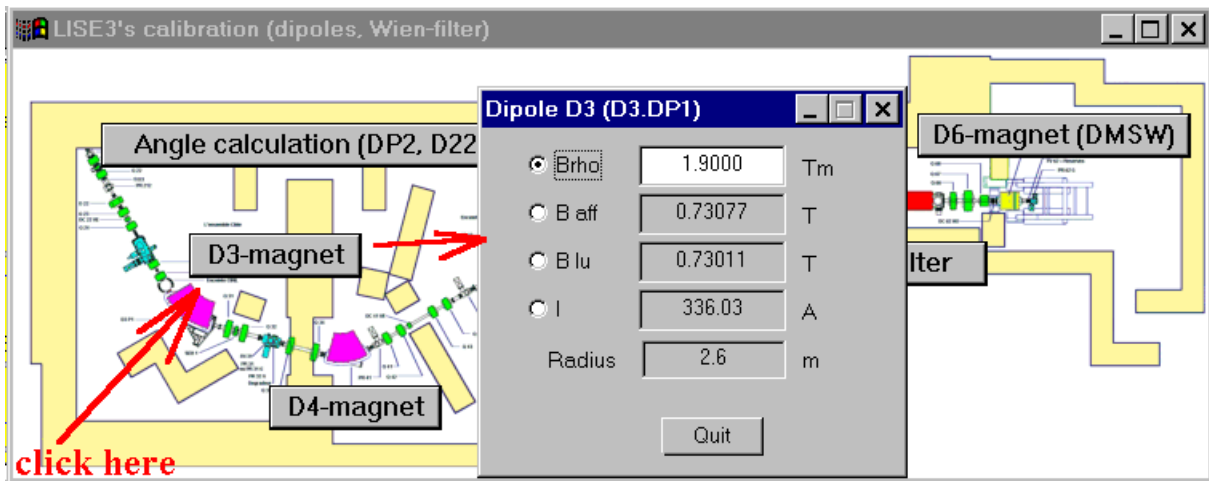
- rectangle acceptance (like it was in DOS-version)



- gaussian acceptance (beginning from v.4.0)

By default the angular acceptance mode is rectangle acceptance. Previous version files will be immediately recalculated.

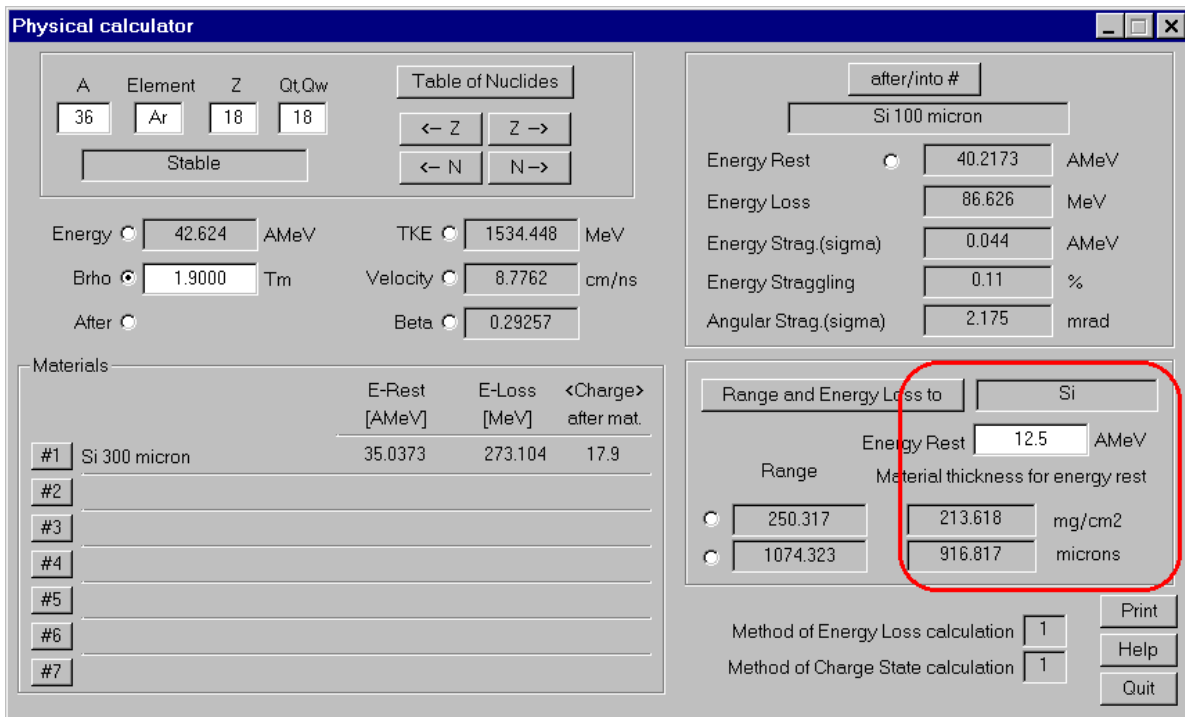
2. The M5678-spectrometer(at Dubna) plot has been added
3. Pictures in the dialogs "Curved degrader" & "Angle on the target" has been corrected.
4. The Bug in the dialog "Beam" (the button "Table of Nuclides" didn't work) has been corrected.
5. Calibrations of all LISE's magnets have been added (see Fig.688).
6. Calibrations of setting of the angle on the LISE's target have been corrected.



*Fig.688. Plan of the LISE spectrometer with buttons of calibrations dialogues of spectrometer elements.*

### *version 4.2.5*

Calculation of material thickness between start energy and energy rest has been added in the Physical Calculator (see Fig.689).



**Fig. 689.** The dialogue “Physical calculator”: new possibility to calculate of material thickness between start energy and energy rest.

#### version 4.2.4

Utilities -> LISE3's calibration (dipoles, Wien-filter): Transformation between values of Brho, B real(affiche), B red(lu), I(Ampere) for the LISE dipoles D3.DP1(D3) and D3.DP2(D4).

#### version 4.2.3

Utilities -> Curved degrader: Calculation (see Fig.690) and plots (see Fig.691) of curved degrader profiles for different operating modes (achromatic, monochromatic, homogeneous).

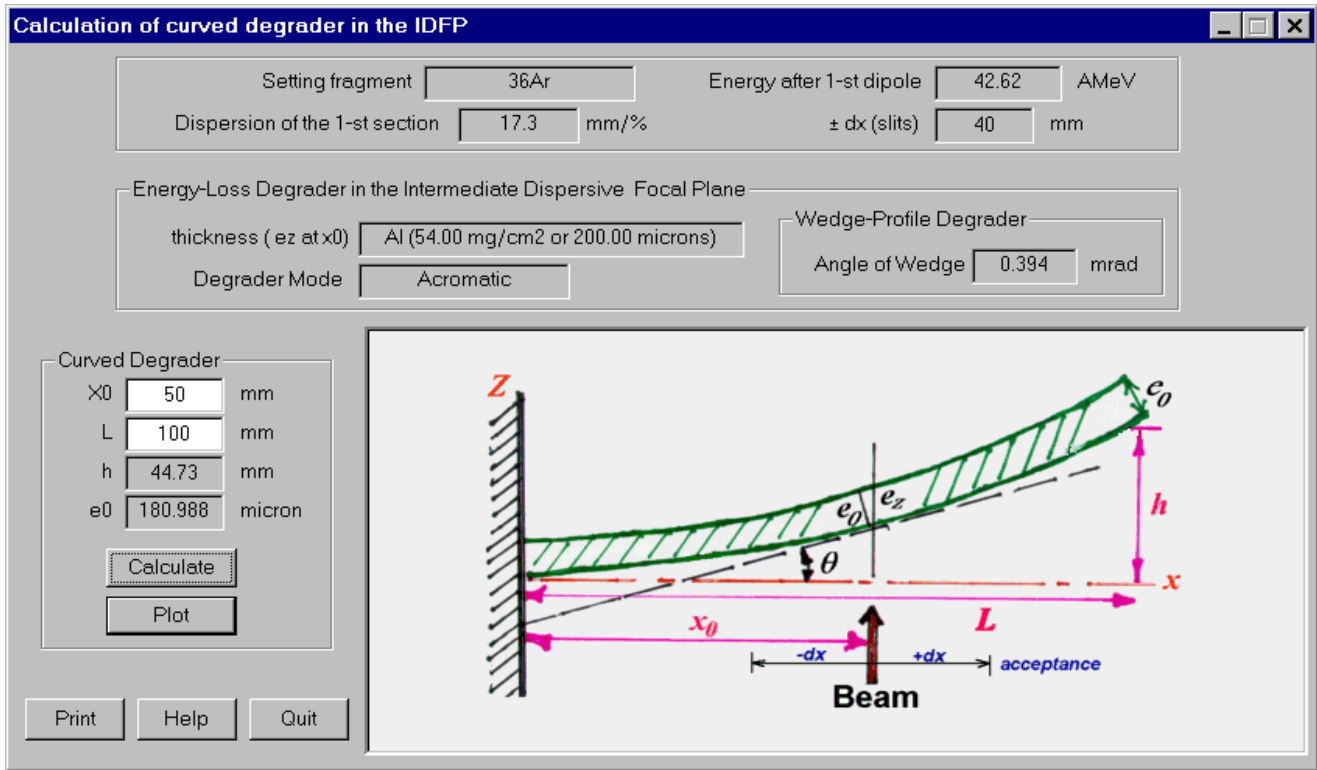


Fig.690. The dialogue "Calculation of curved degrader in the IDPF".

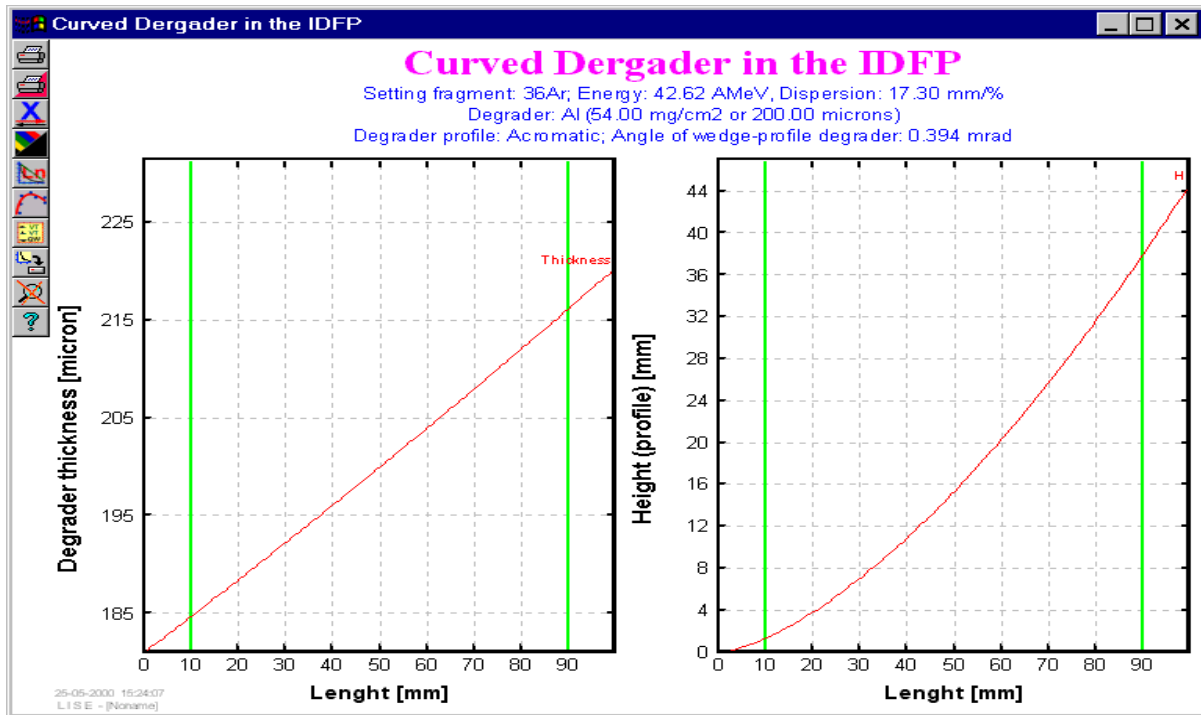
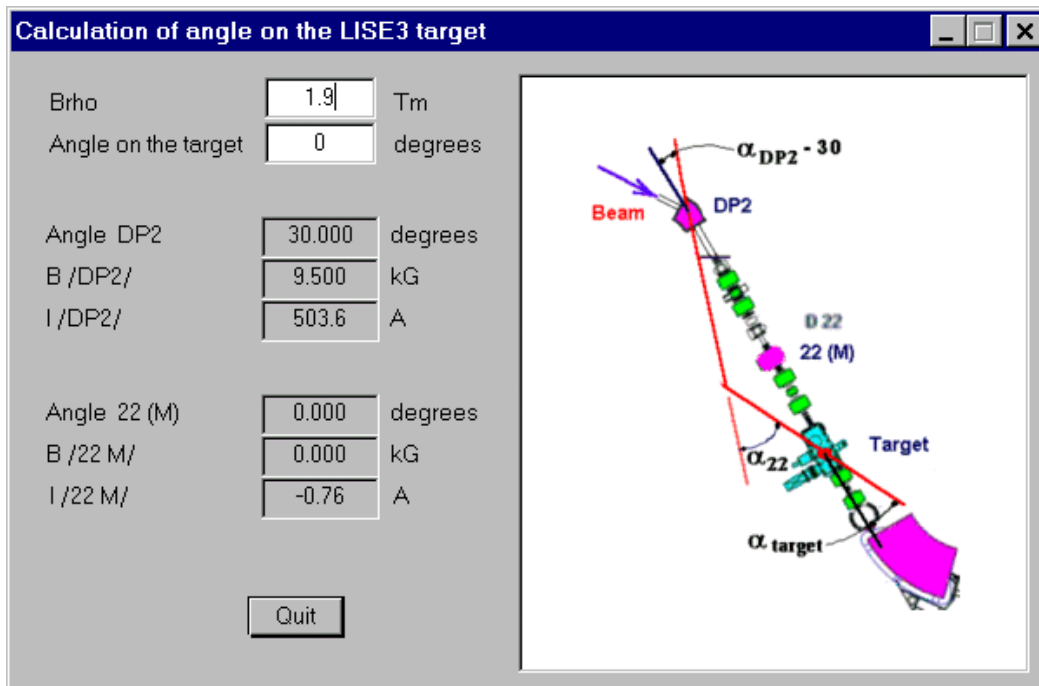


Fig.691. The plot "Curved degrader in the IDPF".

### version 4.2.2

Utilities -> Calculation of angle on the LISE target: calculation magnetic fields (also dipoles currents ) of two dipoles to get the determined angle on the target (see Fig.692).



**Fig.692.** The dialogue “Calculation of angle on the LISE3 target calculation magnetic fields (also dipoles currents ) of two dipoles to get the determined angle on the target.

**version 4.2.1**

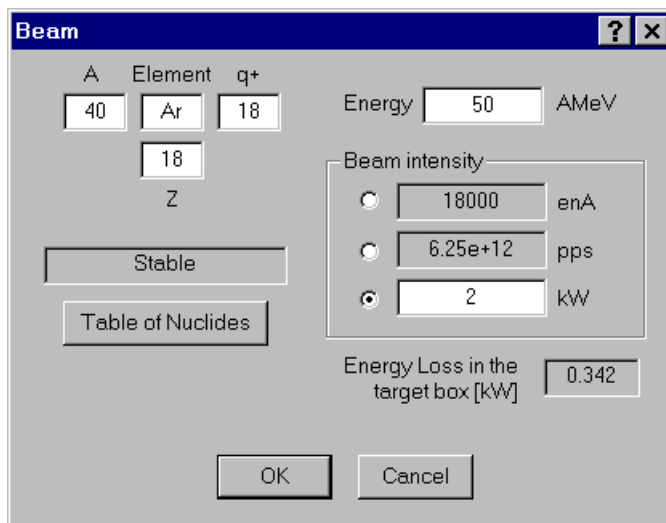
Energy distribution plot after wedge has been corrected.

## 30. Version 4.2

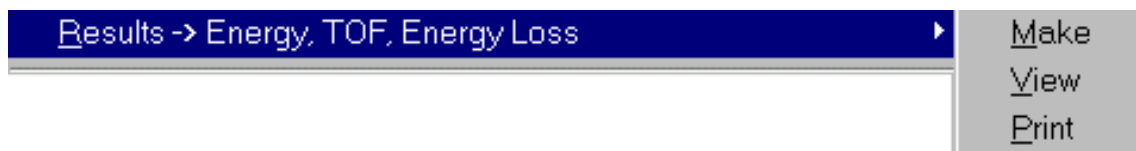
**Dubna, Caen**  
**30.03.2000**

### 30.1. New Dimension “ kW ” to enter an intensity of the primary beam

The new possibility to enter an intensity of the primary beam has been incorporated. The intensity is inputted via the power of beam in kW. User may observe also in the dialog “ Beam ” the separable power beam in the target.



### 30.2. New result file - Energy, TOF, Energy Loss in materials



### 30.3. Configuration files

Some new configurations files have been added , another one have been corrected accurately. Following are the configuration files in the view version :

#### Abbreviation :

<b>SI</b>	SISSI	<b>LD</b>	degrader in the LISE spectrometer
<b>AD</b>	degrader in the Alpha spectrometer	<b>SP</b>	SPEG
<b>po</b>	object point	<b>ci</b>	cible (target)
<b>pf</b>	final point	<b>D*</b>	number of the “D” hall

#### Directory CONFIG

LISE standard.lcf	standard LISE3	<a href="http://www.ganil.fr/LISE">http://www.ganil.fr/LISE</a>
LISE2000bis.lcf	project	GANIL information, N 146, 12.1999
GSI_FRS.lcf	standard (achrom)	NIM B70 (1992) 286
VAMOS.lcf	project	<a href="http://www.ganil.fr/vamos/">http://www.ganil.fr/vamos/</a>

#### Directory CONFIG\SISSI

SI_AD_AA.lcf	SISSI target- degrader in the Alpha spectr. - final point at the Alpha spectr. (Alpha Arete)
SI_AD_D3ci.lcf	SISSI target- degrader in the Alpha spectr. - final point at the LISE target box ( <b>D3</b> )
SI_AD_D5.lcf	SISSI target- degrader in the Alpha spectrometer - final point at the INDRA hall ( <b>D5</b> )

SI\_AD\_D6.lcf            SISSI target- degrader in the Alpha spectr. - final point of the LISE3 spectr. (D6)  
 SI\_LD\_D6.lcf            SISSI target- degrader in the LISE spectr. - final point of the LISE3 spectr. (D6)  
 reference : “ Guide de l'utilisateur de SISSI ”, GANIL R96 05-A, revision 19.03.99  
<http://www.ganil.fr/operation/sissi/sissi.html>

### Directory CONFIG\SPEG

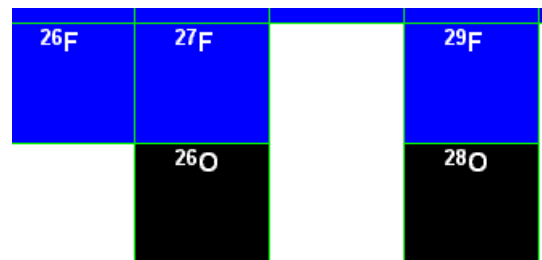
SI\_AD\_SPpf.lcf            SISSI target- degrader in the Alpha spectr. - SPEG final point  
 SI\_AD\_SPci.lcf            SISSI target- degrader in the Alpha spectr. - SPEG target box (cible)  
 SI\_AD\_SPci\_a.lcf        SISSI target- degrader in the Alpha spectr. - SPEG target box (cible) - achromatic model  
 SPpo\_SPci\_SPpf.lcf    standard SPEG -> point object - cible - point final (in french)  
 references :            “ Guide de l'utilisateur de SISSI ”, GANIL R96 05-A, revision 19.03.99 ;  
                           “SPEG : an energy loss spectrometer for GANIL ”, NIM A276 (1986) 509

### Directory CONFIG\FLNR

COMBAS.lcf                NIM A426 (1999) 605-617  
 m34.lcf  
 m5678.lcf                [http://dnr080.jinr.ru/project/spectrometer\\_fobos/tz.htm](http://dnr080.jinr.ru/project/spectrometer_fobos/tz.htm)

### 30.4. “ Unbound ” - new characteristic mode to plot in the nuclide chart

At times it is to perform transmission calculations for unknown nuclei to estimate the possibility to synthesize an isotope (like  $^{26,28}\text{O}$ ). For this aim the isotope of interest was usually marked as beta-decay isotope, because the transmission of unstable nuclei was not calculated by program. The mode “ Unbound ” (black color) has been added to fill up this shortage.



### 30.5. New command - Transmission calculation of nuclei chosen by previous command Area Transmission Calculation.



The code clean previous calculations after any changes of target, beam, wedge and spectrometer's characteristics. User is obliged to repeat a choice of the nuclei area for next calculations. From now, it is possible to repeat previous transmission calculation simply clicking on an icon for the command “ Previous Area Transmission Calculation ”.

**30.6. New plot A/Q - Y (position in the the final focal point after the Wien filter)**

**30.7. Corrections**

*B.Blank's modification of the cross section parametrization - 4 (EPAX 2.15) to treat more correctly pick-up reactions. ()*

*revision of the nuclide table*

*changes MeV/A to AMeV*

*revision of half-lives in the nuclides database*

*correction of the charge distribution 1 (Leon et al. ) for high energy*

*bug in the animation subroutine*

## 30.8. Version 4.1

Dubna  
01.03.2000

### 30.8.1. version 4.0.30 (16-02-00) *Menu "Calculations" -> Reaction's characteristics*

1. Reaction's kinematics (two body) relativistic calculations. User may set excitation energy of outgoing fragments. Plots ("ThetaFragment in CMS & Theta Lab" and "ThetaFragment in CMS & Energy Lab" ) have been added.
2. Reaction's characteristics dialog was created

### 30.8.2. version 4.0.29 (11-02-00) *Ion charge state distribution for low energy*

1. New Ion charge state distribution for low energy has been added. (K.Shima et al., NIM 200 (1982) 605).
2. New plot - "Average charge state plot"
3. In the dialog "Physical calculator" user may observe average charge state of selected ion after materials

### 30.8.3. version 4.0.25 (01-02-00)

1. Some Sound application has been inserted into the code
2. The banner of laboratories has been inserted in the left-bottom window.

### 30.8.4. version 4.0.19 (22-01-00) *Struggle with bugs*

1. If You try to calculate something with version older 4.0.18 using the Energy loss method=1 (Ziegler) You'll get a mistake. Unfortunately, after change  $\text{pow}(x,y) \rightarrow \exp((y)*\log(x))$  due to problems with emulator of Windows on Mac, we have got it.. if  $x=0$ ...  $\text{pow}(0,y)=0$ , but  $\log(0)$  is error! It has been corrected.
2. The LISE code sets "zero" momentum dispersion equal to 0.1. But it was made as  $\text{if}(\text{dispersion} < 0.1)$   $\text{dispersion}=0.1$  But some configurations has negative dispersion, and the program also set their equal to 0.1 Nowadays ,  $\text{if}(\text{fabs}(\text{dispersion}) < 0.1)$   $\text{dispersion}=0.1$  and if the program opens old file with wrong dispersion User immediately receive the message "Dispersion is wrong! Check!"
3. Range distribution plot has been corrected Different profiles of a degrader (wedge) in the intermediate dispersive focal plane.



## 31. Version 4.0.17

Dubna  
20.01.2000

### Different profiles of a degrader (wedge) in the intermediate dispersive focal plane

#### 31.1. Wedge profiles

The code used in previous versions only achromatic profile of wedge. Nowadays, There are 4 possible profile of a degrader (wedge) in the intermediate dispersive focal plane in the new version (see Fig.693):

- achromatic
- monochromatic
- homogeneous
- user-defined

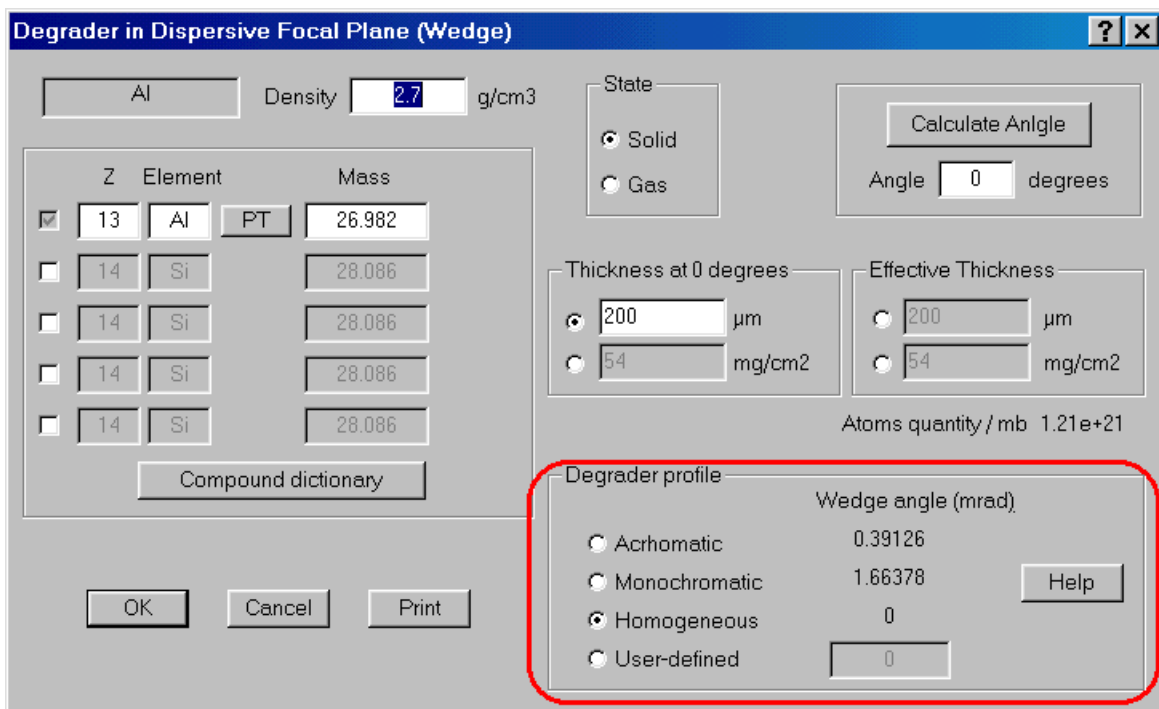
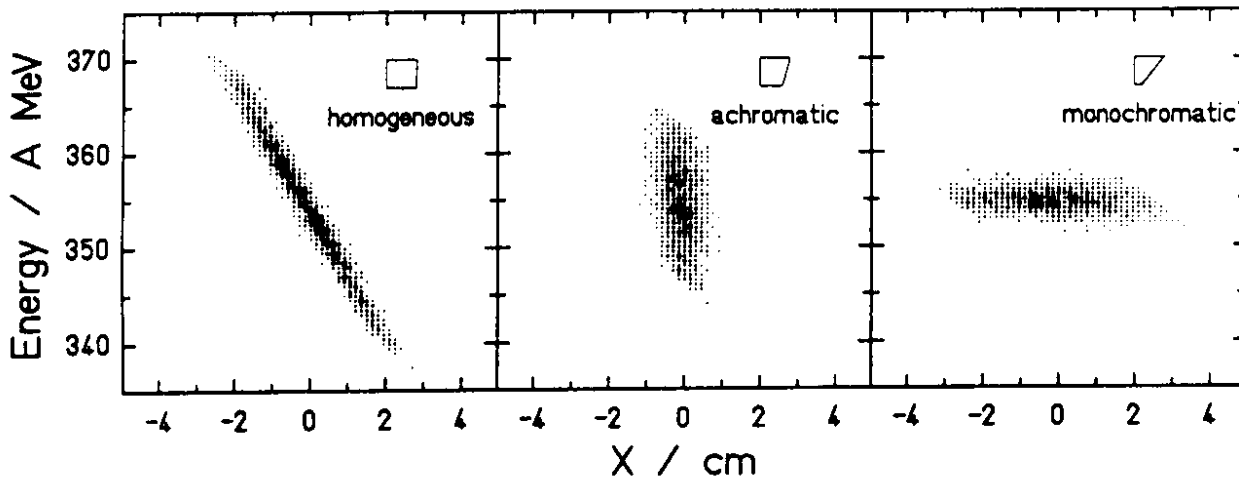


Fig.693. The dialog “Dergader in dispersive focale plane”

All profiles in the code suggest wedge-shape where only an angle of wedge is changed. User may find a negative angle of wedge in the case of negative momentum dispersion of the first path of spectrometer. It means a wedge is turned on 180 degrees.

In the example [Gei95], a fragment beam of  $^{19}\text{Ne}$  with 600 A MeV with a velocity spread of  $\sim 1.5\%$  penetrates through differently shaped degraders all having the same thickness at the optical axis ( $d/r=0.5$ ). In

the left panel of Fig.694, the profiles of the degraders are chosen such that the thickness is constant along the x coordinate (homogenous degrader). In the middle panel, the slope of thickness preserves the achromatism of the ion-optical system (achromatic degrader), and in the right panel, the profile matches the velocity dispersion in the x direction and thus bunches the energy spread as well as range distribution (monoenergetic degrader). The position distributions at the final focus in Fig.694 suggest that the achromatic degrader is superior for spatial isotopic separation because it is shaped so that the image size is independent of the incident momentum spread of the fragments. Interesting applications are suggested by the use of a monoenergetic degrader, especially if a narrow implantation distribution proves to be of importance, e.g. for implantation in thin detectors used in nuclear decay spectroscopy or in biomedical treatments.



**Fig.694.** Phase-space imaging of differently shaped degraders within the achromatic ion-optical system. The results for a homogeneous, an achromatic, and a monoenergetic degrader are given. All degraders have the same thickness on the optical axis ( $d/r=0.5$ ) [Gei95].

### 31.2. Optic and degrader

When introducing an energy degrader in the intermediate dispersive focal plane of dipole  $D_1$  general conditions for double achromatism of the spectrometer change into the following [Ann87]:

$$\begin{pmatrix} x \\ x \end{pmatrix}_B \begin{pmatrix} x \\ \delta \end{pmatrix}_A + F \cdot \begin{pmatrix} x \\ \delta \end{pmatrix}_B = 0, \quad /95/$$

$$\begin{pmatrix} \theta \\ x \end{pmatrix}_B \begin{pmatrix} x \\ \delta \end{pmatrix}_A + \begin{pmatrix} \theta \\ \theta \end{pmatrix}_B \begin{pmatrix} \theta \\ \delta \end{pmatrix}_A + F \cdot \begin{pmatrix} \theta \\ \delta \end{pmatrix}_B = 0, \quad /96/$$

where  $F$  is equal to the ratio  $(\Delta p/p)_B / (\Delta p/p)_A$  of the momentum dispersions at the exit the entrance of the degrader.  $F$  depends on nature, thickness and shape of the degrader. Two cases can be practically considered  $F \neq 1$  and  $F = 1$ .

For  $F \neq 1$ , the two above matching conditions are thus only obtained by optics tuning, especially varying the dispersion coefficient  $(X/\delta)_B$ . It expects to use such a degrader with  $F < 1$  in order to reduce momentum spread (or energy spread) in the second part of the spectrometer and particularly at the final focus point, to minimize range dispersion of selected products stopped in solid state detectors.

In the second case ( $F=1$ ), optic matching conditions remain the same as without using of degrader . The field of all the magnetic elements of the second section has only to be scaled to the proper value  $B_2/B_1$ , calculated for a chosen value  $A^3/Z^2$  of the selected nuclei. One however has to build a special shaped degrader (achromatic degrader) in order to maintain the condition  $F=1$  (i.e. the same relative momentum spread before and after the degrader).

The next problems with degrader [Ann87] was considered in the code:

- Image broadening in a thick degrader.
- Energy straggling in the degrader
- Focal point magnification
- Intrinsic aberration
- Degrader defect (1% default)

### **31.3. Examples of calculation with degrader of different profiles**

For example the default configuration after loading of the code was used only the Al-wedge was installed with the thickness 200 micron. The magnetic rigidity of dipoles was calculated for  $^{36}\text{Ar}$ .

Calculations of transmission was made only for all Ar-isotopes:

<b>Profile of Wedge</b>	<b>Number of Ar-isotopes</b>	<b>Almost events</b>	<b><math>^{36}\text{Ar}</math> events</b>	<b><math>^{36}\text{Ar}/\Sigma</math> <i>k1</i></b>	<b><math>^{36}\text{Ar}/^{36}\text{Ar}</math> w/t wedge <i>k2</i></b>	<b><i>k1*k2</i> optimum</b>
<b>without wedge</b>	<b>6</b>	<b>9.3e+5</b>	<b>3.3e+5</b>	<b>35.5%</b>	<b>100%</b>	<b>35.5%</b>
<b>Achromatic</b>	<b>3</b>	<b>2.9e+5</b>	<b>2.8e+5</b>	<b>96.6%</b>	<b>84.8%</b>	<b>81.9%</b>
<b>Monochromatic</b>	<b>4</b>	<b>5.5e+4</b>	<b>4.2e+4</b>	<b>76.4%</b>	<b>12.7%</b>	<b>9.7%</b>
<b>Homogeneous</b>	<b>5</b>	<b>4.5e+5</b>	<b>1.3e+5</b>	<b>28.9%</b>	<b>39.4%</b>	<b>11.4%</b>

### 31.3.1. Wedge selections plots for different cases of degrader profile

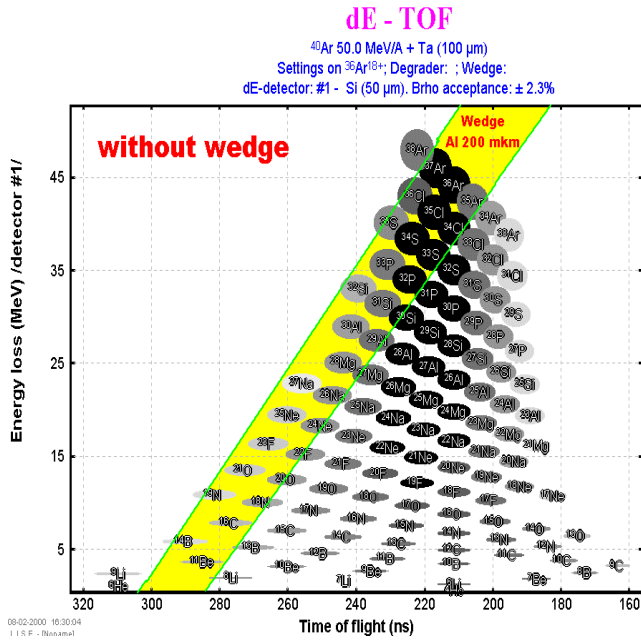


Fig. 695.

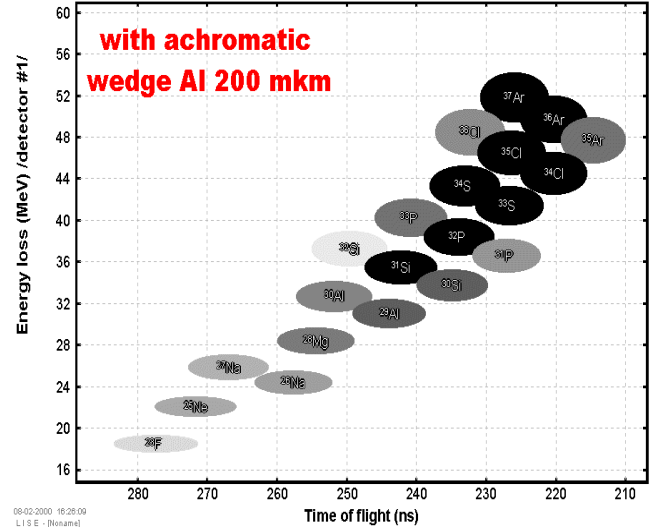
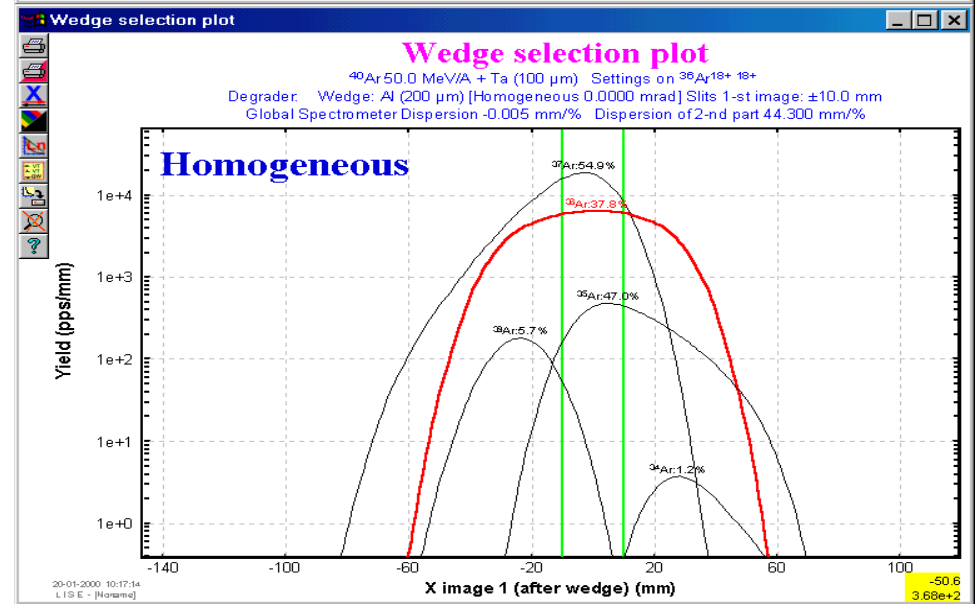
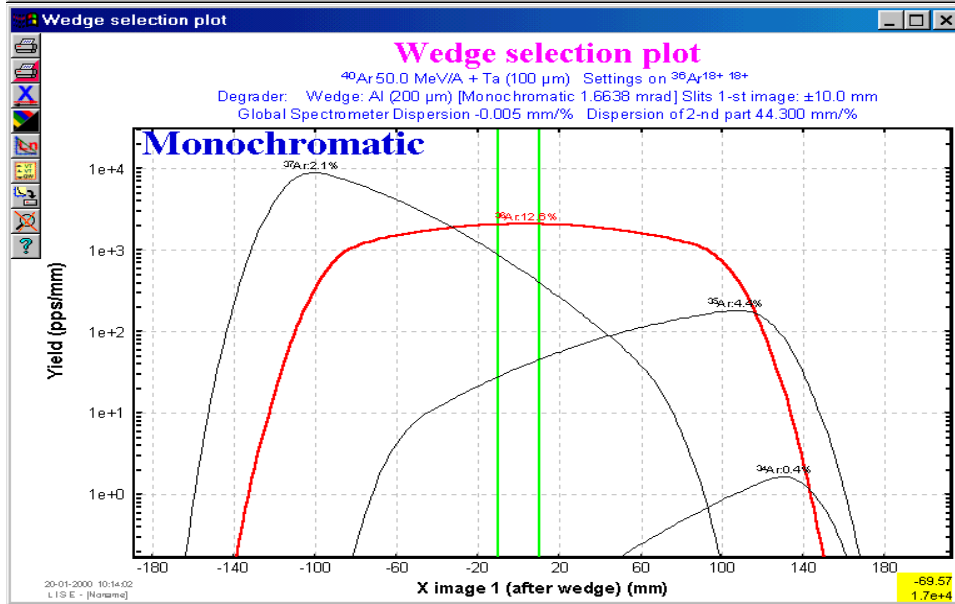
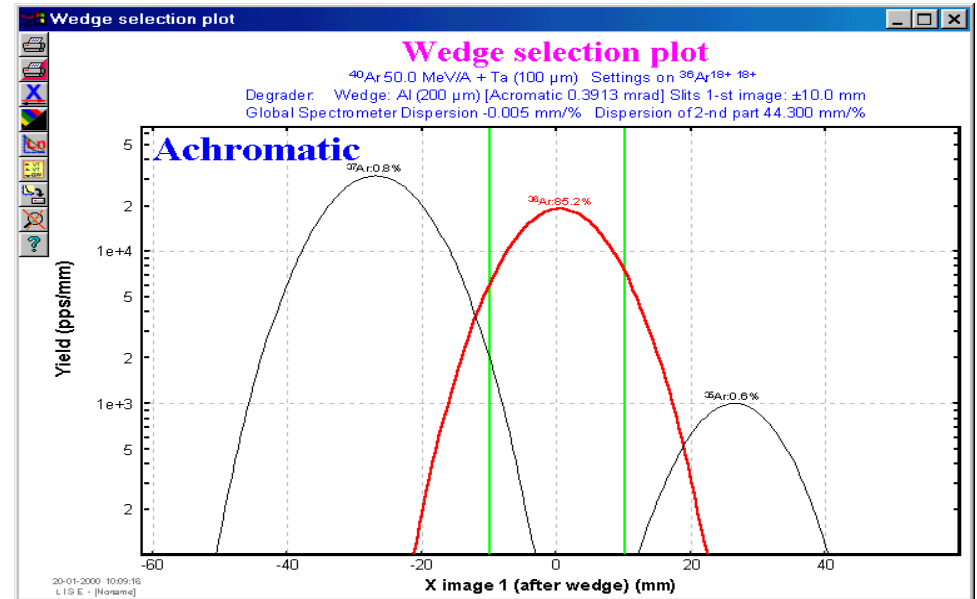
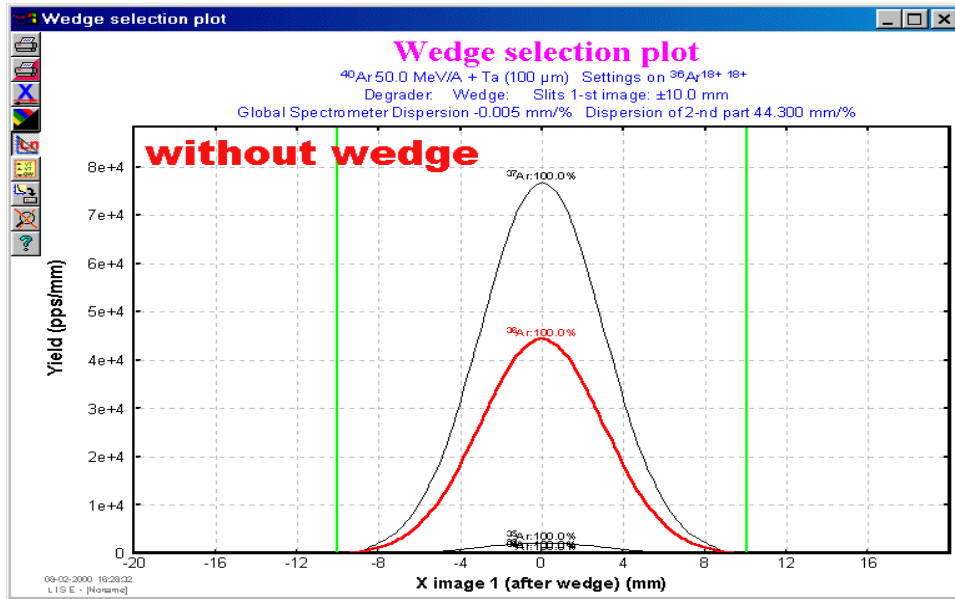


Fig. 696.



Figures 697, 698, 699, 700.

31.3.2. Range distributions in the silicon detector for different cases of degrader profile

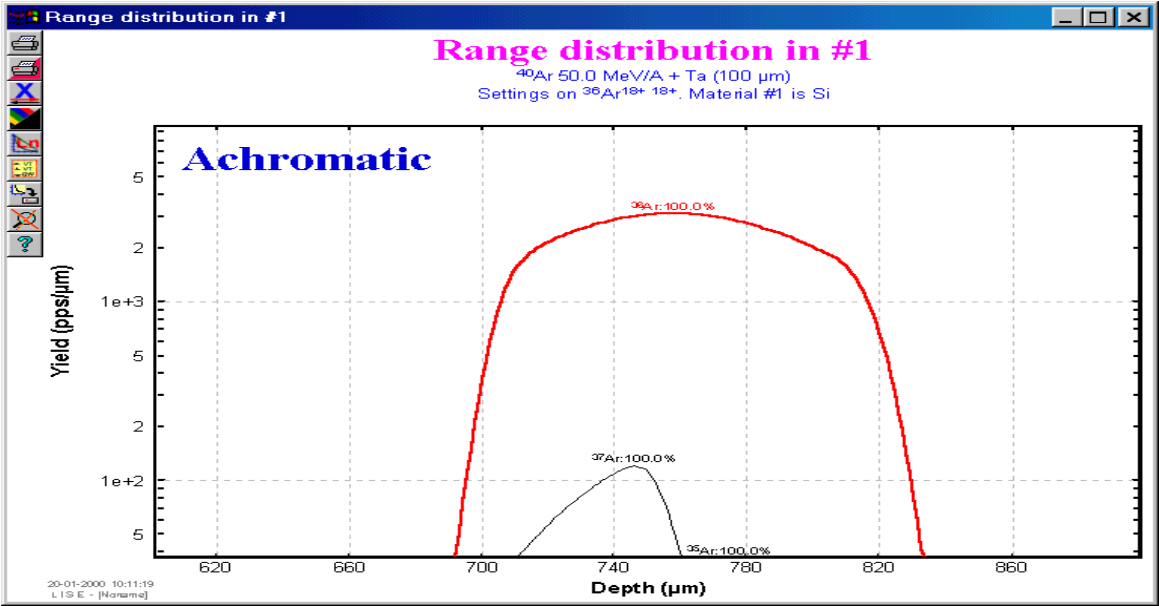


Fig. 701.

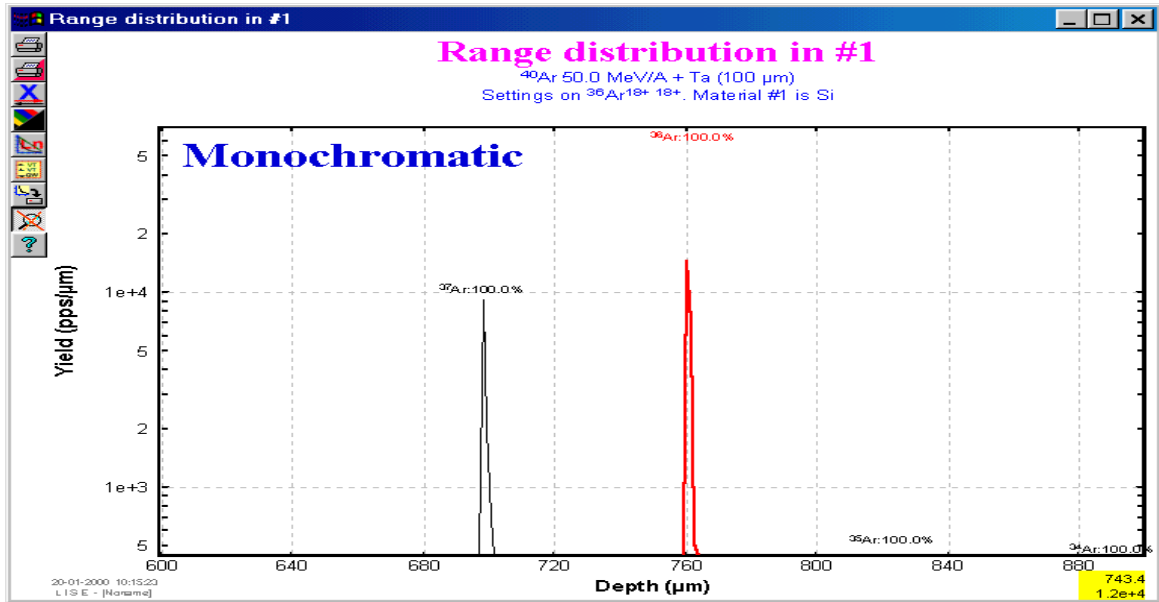


Fig. 702.

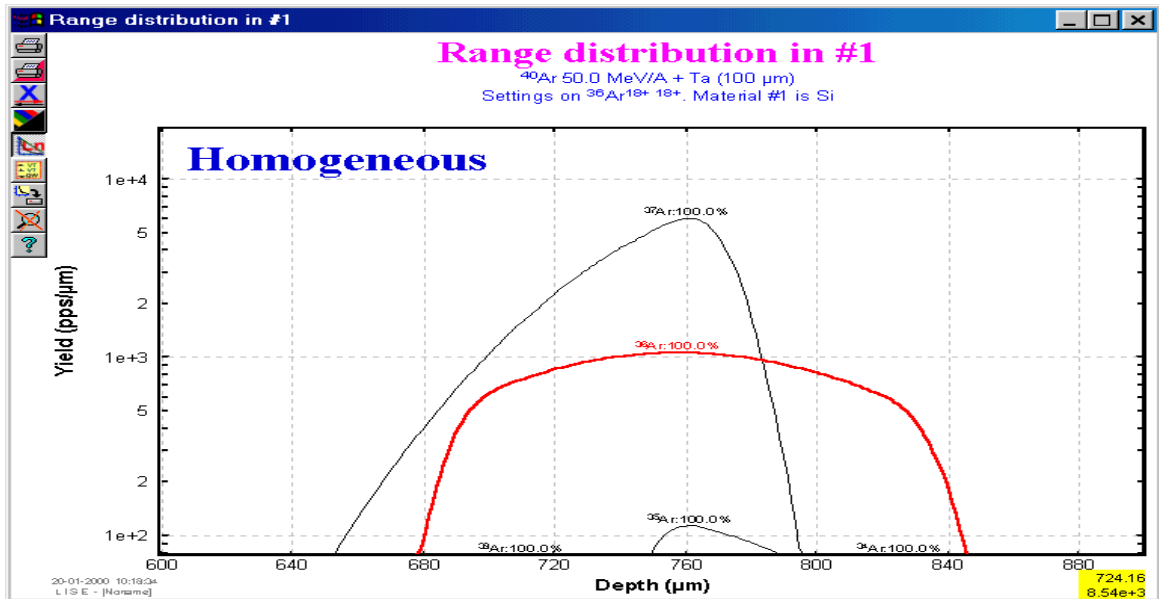


Fig. 703.

# 32. Version 4.0

Caen  
20.12.1999

## COMPOSITE TARGETS and MATERIALS

### 32.1. version 4.0.\*

#### version 4.0.14

1. Possibility to calculate the full spectrometer matrix
2. Calculation of the beam vector in the IDFP and Final Focal Point
3. Input new parameters  $x/\theta$  and  $y/\phi$  in the optical matrices to calculate transmission.

**OPTICS**

BEAM: the phase space and the average momentum of input beam

1. X	2. T	3. Y	4. F	5. L	6. D	Angle: beam - spectrometer	<input type="radio"/> cm
1.5	3.3	1.5	3.3	<input type="text" value=""/>	0.15	0 mrad	<input checked="" type="radio"/> mm
[mm]	[mrad]	[mm]	[mrad]	[mm]	[%]		

First half: Target - Wedge(dispersive focal plane)

1. X	-0.783	0	0	0	0	17.3
2. T	0.267	-1.284	0	0	0	3.51
3. Y	0	0	-4.26	0	0	0
4. F	0	0	-0.858	-0.273	0	0
5. L	<input type="text" value=""/>	<input type="text" value=""/>	0	0	1	<input type="text" value=""/>
6. D	0	0	0	0	0	1
	/[mm]	/[mrad]	/[mm]	/[mrad]	/[mm]	/[%]

Second half: Wedge(dispersive focal point) - Focal point

-2.561	0	0	0	0	44.3	[mm]
0.4	-0.389	0	0	0	-5.56	[mrad]
0	0	-0.432	0	0	0	[mm]
0	0	-0.32	-2.4	0	0	[mrad]
<input type="text" value=""/>	<input type="text" value=""/>	0	0	1	<input type="text" value=""/>	[mm]
0	0	0	0	0	1	[%]
	/[mm]	/[mrad]	/[mm]	/[mrad]	/[mm]	/[%]

Achromatism

Dispersion X (full)	-0.00530	mm/%	Achromatic
Dispersion T (full)	-0.00539	mrad/%	Achromatic

**Spectrometer Matrix (Target - Focal Point)**

OK Cancel Help Print

**Spectrometer Matrix (Target - Focal Point)**

Spectrometer Matrix

1. X	2.0053	0	0	0	0	-0.0053
2. T	-0.4171	0.4995	0	0	0	-0.0054
3. Y	0	0	1.8403	0	0	0
4. F	0	0	3.4224	0.6552	0	0
5. L	<input type="text" value=""/>	<input type="text" value=""/>	0	0	1	<input type="text" value=""/>
6. D	0	0	0	0	0	1
	/[mm]	/[mrad]	/[mm]	/[mrad]	/[mm]	/[%]

Beam

target	wedge	final f.p.	
1.5	1.4205	3.0071	[mm]
3.3	-3.3102	1.0219	[mrad]
1.5	-6.39	2.7605	[mm]
3.3	-2.1879	7.2958	[mrad]
0	0	0	[mm]
0.15	0.15	0.15	[%]

OK Help Print

cm  mm

Fig.704.

### *version 4.0.10*

#### **Global reconstruction of transmission calculation modules**

- I. Reconstruction of two already existed and creation of a new one “ Brho-separation plot ”
  - a. Real Brho distribution plot behind the target
  - b. Horizontal distribution in IDFP in Tm (as was initially)
  - c. Horizontal distribution in IDFP in mm (as was made in October, 1999)
- II. Solution of problem “ large object on the target and global unachromatism (chromatism)
- III. Input Wien angular acceptance
- IV. Creation of an angular distribution before the Wien-filter
- V. Creation “block” structure in the code to calculate transmisson.

Creation of a possibility to choose a X-plane or Y-plane velocity selection.

It has been corrected -The bug of TOF-calculation in the dialog “GOODS” and the plot “dE-TOF”.

### *version 4.0.9*

1. Checking all new subroutines of energy loss calculation for both methods to
  - different energy
  - gaseous and solid media
  - compounds
2. Creation of warning “Save Changes in file” before
  - to exit from the programme
  - to load another file

### *version 4.0.8*

1. Solution of the problem with “**edge’s**” **effect of Range’s plots**.
2. Solution of the problem with the dialog “Calibration” (Dialog change a thickness of setting detectors) and for the Range Plot if User takes a detector set not at 0 degrees.
3. Input of additional energy loss calculation method on the base **H-parameterization**.
4. Input of a possibility to calculate energy loss into **gaseous media**.
5. Creation of additional component of energy loss : **nuclear energy stopping powers**, that it is very important for low-energy particles and for gaseous media.
6. Creation of tables of ranges beginning **from 10 KeV/A** to work with low-energy particles.
7. Creation of a dialog to choose a compound target from the **list of all possible compounds** on the base of Ziegler compound file.



Charge state distributions 1 - Atom.Data & Nucl.Data Tables 69[2](1998); modified

Cross Section calculations 4 - EPAX 2.15 : K.Summerer et B.Blank (1999)

Energy Loss calculations 0-[He-base] F.Hubert et al, At.Data & Nucl.Data Tables 46(1990)1

0-[He-base] F.Hubert et al, At.Data & Nucl.Data Tables 46(1990)1

1-[H-base] J.F.Zigler et al, "Stop.powers ..." Pergamon Press, NY

**Material # 03**

H8C10O4 Density 1.397 g/cm3

State

Solid

Gas

Calculate Angle

Angle 51.1 degrees

Z	Element	Mass	Stoich
<input checked="" type="checkbox"/>	1 H PT	1.008	8
<input checked="" type="checkbox"/>	6 C PT	12.011	10
<input checked="" type="checkbox"/>	8 O PT	15.999	4
<input type="checkbox"/>	14 Si	28.086	
<input type="checkbox"/>	14 Si	28.086	

Thickness at 0 degrees

143.164  $\mu\text{m}$

20 mg/cm2

Effective Thickness

227.981  $\mu\text{m}$

31.849 mg/cm2

Atoms quantity 2.20e+21

Compound dictionary

OK Cancel

**Physical calculator**

A 36 Element Ar Z 18 Qt,Qw 18

Table of Nuclides

Stable

Energy  42.624 MeV/A

TKE  1534.461 MeV

Brho  1.9 Tm

Velocity  8.7762 cm/ns

After  2-nd dipole

Beta  0.29257

after/into #

Si 100 micron

Energy Rest  40.2651 MeV/A

Energy Loss 84.918 MeV

Energy Stragg. 0.044 MeV/A

Energy Stragg. 0.11 %

Angular Stragg. 2.175 mrad

Materials	Rest (AmeV)	Loss (MeV)
#1 Si 300 micron	35.2007	267.235
#2 H19C18O3 201 micron	29.6705	199.087
#3 H8C10O4 20 mg/cm2	26.4757	115.014
#4 Si 200 micron	19.1893	262.311
#5 Si 200 micron	8.9640	368.109
#6 Si 50 micron	5.0969	139.218
#7 Si 10 micron	4.1546	33.919

Range to

Si

255.352 mg/cm2

1095.93  $\mu\text{m}$

Method of Energy Loss calculation 0

Print Help Quit

Fig. 705.

### **version 4.0.7**

creation of an **identification table of mouse position** (Nucleus name, Events, dE,E, TOF) for bidimensional plots like it was in a DOS-version. (*also X,Y -identification for one-dimensional plots*).

### **version 4.0.3**

1. **COMPOSITE TARGETS and MATERIALS.**
2. **new format of LISE-file** due to introduction of new class "compounds" in the code .
  - a. *LISE-files of version 3.\* are readable by the code with version higher than 4.0.3*
  - b. *LISE-files of versions 4.0.0 - 4.0.2 are not readable by the code with version higher than 4.0.3*
3. Increasing the nuclides isotopes **up to Z=130 and N=200.**
4. Approximation of **ranges for Z=104-130** on the base of work F.Hubert et al , AD & NDT 46 (1990) 1.
5. **Ranges for H** on the base of work L.C.Northcliffe and R.F.Schilling, NDT A7 (1970) 233.
6. Correct "old" and input new LISE-configurations files for different setups.

## **32.2. version 3.9.\***

### **version 3.9.5**

**Zoom** for plots (Clear Zoom).

### **version 3.9.4**

1. Correctin of **energy straggling**. (Error in NIM A257!!! )
2. Input of correct **energy straggling in a wedge**.

### **version 3.9.2**

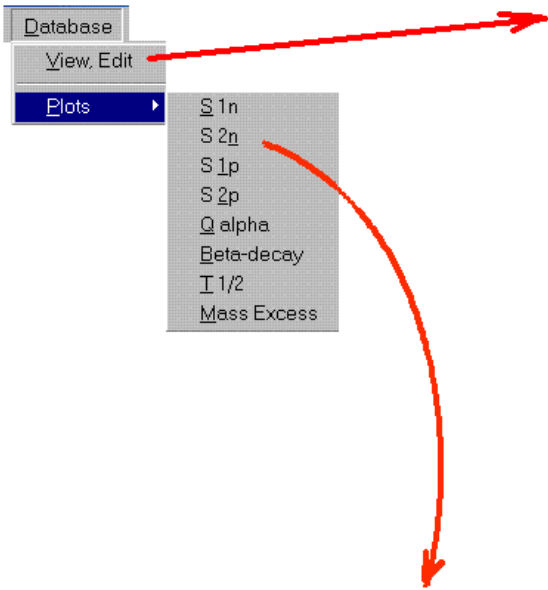
1. Possibility to **view and edit the in-built database**.
2. Input of calculated values in the database for some isotopes of interest ( $^{25-30}\text{O}$ , \*F, \*Ne)

### **version 3.9.1**

**Plots of data (S1n, S2n, S1p, S2p, T1/2, Qalpha, Beta-decay, Mass excess)** from the in-built database for constant Z,N,A,N-Z.

### **version 3.5**

01.07.99 The directories "Range" and "Isotopes" don't exist!!! All tabulated ranges in the new version are written in the binary file "range.bin" which is found in the LISE directory. The file of the nuclide chart "table.iso" is found also in the LISE directory. You may delete the directories "range" and "isotope" using the new version. Default cross section parameterization is 3 - "EPAX 2.13 [Sum00].



### Database

A	Element	Z	N
37	K	19	18

Find

<- Z    Z ->  
<- N    N ->

Beta+ decay

Database Index: 3719

T 1/2: 1.226 sec

Mass Excess: -24.7992 MeV

Binding Energy: 308.5735 MeV

Beta-decay energy: -11.6386 MeV

S 2n: 29.7748 MeV

S 2p: 10.3637 MeV

Q alpha: -6.2206 MeV

S 1n: 15.4455 MeV

S 1p: 1.8578 MeV

Save

Quit

Print

Help

Put "\*" into a cell if value is unknown

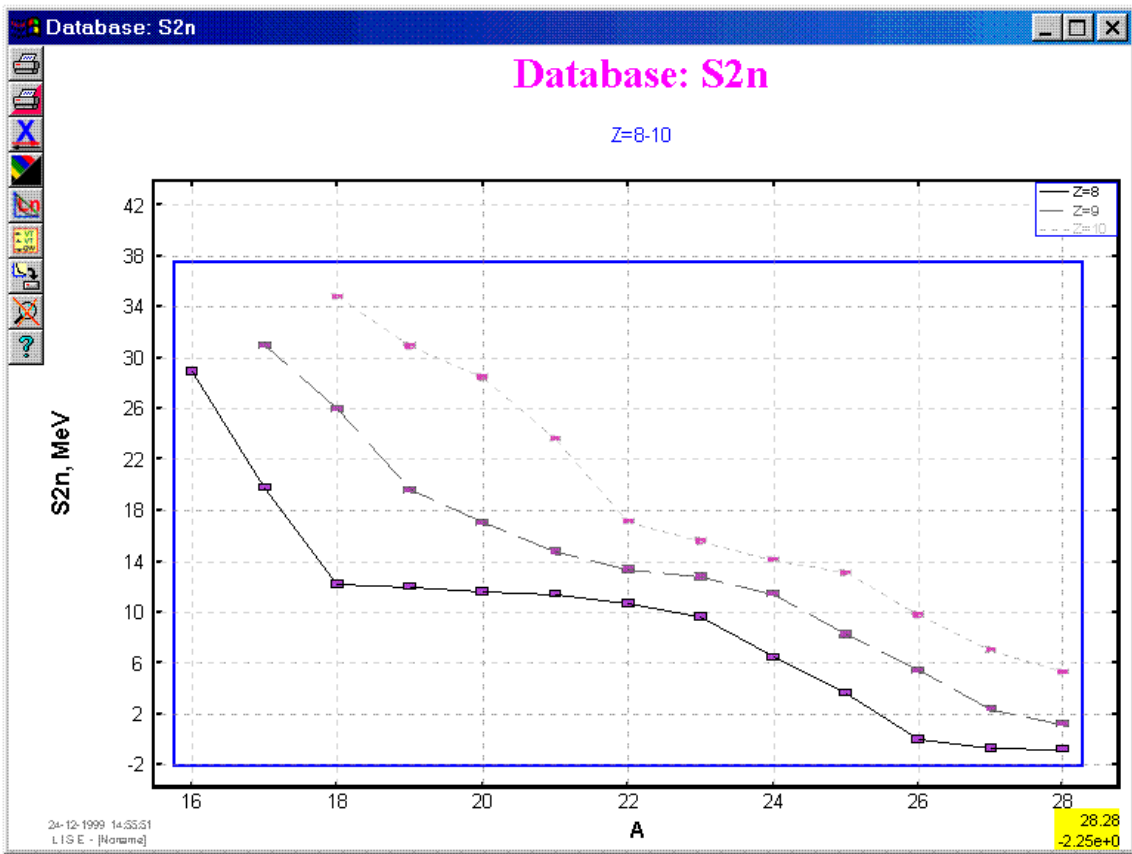


Fig. 706.

## 33. Version 3.4

Caen  
19.05.1999

### Dipole “D6” after the Wien Filter

#### 33.1. Introduction (brief description of previous series)

The program [Baz01] called after the spectrometer “LISE” [Ann87] has been developed in GANIL (Caen, France) to calculate the transmission and yields of fragments produced and collected in an achromatic spectrometer. This code allows to simulate an experiment, beginning from the parameters of the reaction mechanism and finishing with the registration of products selected by a spectrometer. The program allows to quickly optimize the parameters of the spectrometer before or during the experiment. It also makes it possible to estimate and work in conditions of maximum output of studied reaction products and their unambiguous identification.

Wedge and Wien filter selections are also included in the program. In-built Energy loss, Time-of-Flight, Position, Angular, Charge, Cross-Section distribution plots and dE-E, dE-TOF and Z-A/Q two-dimensional plots allow to visualize the results of the program calculations.

An application of transport integral [Baz94] lies in the basis of fast calculations of the program for the estimation of temporary evolution of distributions of phase space.

Recently in the frame of the collaboration Dubna-GANIL the program has undergone a number of serious changes and has been adapted to the environment of "Windows":

- Being adapted to the 32-bit operating system “Windows” the program has received an improved interface with which the user gets all opportunities of the given operating system (work in several windows, drivers of a seal etc.);
- The concept of a “dead” layer of a target has been incorporated (that is very important for work with thick targets producing light exotic nuclei);
- There appeared an opportunity to choose the parameterization of fragmentation cross-sections [Sum90,Sum00,Tar98] and model the charge distributions of ions [Leo98];
- A number of the graphic subroutines have been changed, while some discrepancies have been corrected;
- A number of the utilities for account of optimum sizes (thickness of a target, energy of a beam, magnetic rigidity) are added at the given parameters of spectrometer;
- In-built information support helps the user quickly take possession of the program;
- In-built database of nuclides (Mass excess, Binding energy,  $\beta$ -decay energy,  $S_{2n}$ ,  $S_{2p}$ ,  $Q_{\alpha}$ ,  $S_n$ ,  $S_p$ ,  $T_{1/2}$ ) [Aud95,Nuc] has been added. It is possible to see a transmission of a given isotope, its characteristics and energy after second dipole clicking on an isotope of interest in the table of nuclides by the right button of the mouse;
- The optical parameters of the spectrometer are entered as transport matrices [Bro80] that are more convenient. Initial angular, spatial and energy emittances of beam are used;

- The new dipole after the Wien filter of velocities has been added (see §33.2. Dipole “D6”).

The more detailed description of the program and also all information about changes and new versions of the program can be found using the WWW-reference: <http://dnr080.jinr.ru/LISE.html>.

It is possible to receive this program and the last version for MS-DOS using FTP to the address (user: *anonymous*):

- [192.93.218.174](http://192.93.218.174) (at Caen);
- [159.93.20.89](http://159.93.20.89) (at Dubna).

You can send all your wishes and remarks to the address, indicated in the program.

### 33.2. Dipole “D6” after the Wien Filter

**D6** The dipole “D6”<sup>6</sup> is placed on the turning platform in a vertical plane behind the Wien Filter. The dipole radius is determined as  $R \cong Lm / \theta$ , where  $\theta$  is the angle of platform turning. Angle may be varied from 0 up to 23 degrees. This dipole (denoted as DSMW on the Fig.707) serves for the fourth selection on the mass and the charge of nucleus (A/Q). Selection by this dipole as the Filter Wien is performed in a vertical plane.

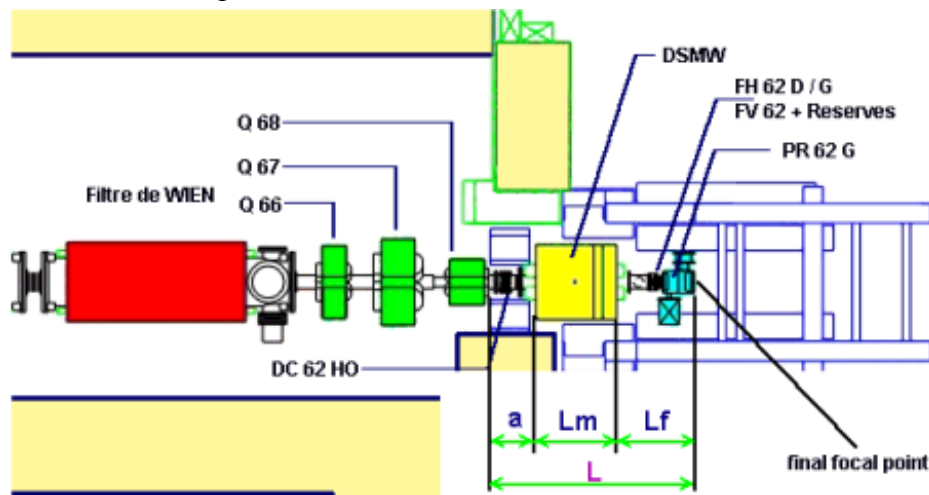


Fig.707

#### 33.2.1. Angle of platform

The angle of platform turning is calculated from the optical conditions and as much as possible to compensate the filter velocity dispersion to get only A/Q dispersion at the focal point after turning dipole. The Wien filter optical structure supposes that six focalization conditions must be fulfilled to have the best matching at the detection location. With addition of the turning dipole D6 these conditions must be saved. To find the angle of turning it is necessary to solve the following equation (given by R.Anne) arising from optical conditions:

$$\begin{aligned} & \cos(\theta) \cdot D_F + R \cdot \sin(\theta) \cdot DS_F - R \cdot (1 - \cos(\theta)) - \\ & Lf \cdot D_F \frac{1}{R} \cdot \sin(\theta) + Lf \cdot \cos(\theta) \cdot DS_F - Lf \cdot \sin(\theta) = 0 \end{aligned} \quad [97]$$

where  $D_F$  is the dispersion [mm/%] from Wien filter calculations,  $DS_F$  is the angular dispersion [mrad/%],  $R$  is the radius of dipole,  $Lf$  is the distance (see Fig.707) from the dipole up to the final fo-

<sup>6</sup> This dipole is called “D6” in the code due to its location in the experimental hall “D6” of the LISE spectrometer.

cus point ( $L = a + Lm + Lf = 2$  meters (default), where  $Lm = 0.8\text{m}$  and  $Lf = 0.8\text{m}$ ). The solution of the equation above supposing negligible contribution of  $DS_F$  is

$$\theta = \frac{-Lm + \sqrt{Lm^2 + \frac{8 \cdot D_F^2 \cdot Lm}{Lm + Lf}}}{2 \cdot D_F} \quad [\text{rad}] . \quad [98]$$

### 33.3. Image shift

The image shift of nuclei in the final focus plane can be roughly determined in the following way:

$$\text{shift}_{FD} = \text{shift}_{\text{filter}} + \text{shift}_{D6}, \quad [99]$$

where

$$\text{shift}_{\text{filter}} = D_{\text{filter}} \cdot \frac{v - v_0}{v_0}, \quad [100]$$

$$\text{shift}_{D6} = D_{D6} \cdot \frac{\Delta B\rho}{B\rho}, \quad [101]$$

$D_{\text{filter}}$  is the filter dispersion [mm/%] and  $D_{D6}$  is the dipole dispersion [mm/%].

Using equation

$$B\rho = c \frac{A}{Q} \frac{\beta}{\sqrt{1 - \beta^2}}, \quad [102]$$

we find that

$$\frac{\Delta B\rho(A/Q, \beta)}{B\rho} = \frac{\frac{\partial B\rho}{\partial(A/Q)} \cdot \Delta(A/Q)}{B\rho} + \frac{\frac{\partial B\rho}{\partial\beta} \cdot \Delta\beta}{B\rho} \quad [103]$$

and then

$$\frac{\Delta B\rho(A/Q, \beta)}{B\rho} = \frac{\Delta(A/Q)}{A/Q} + \frac{\Delta\beta}{\beta \cdot (1 - \beta^2)}. \quad [104]$$

Taking into account that the sum

$$\frac{\Delta\beta_{D6}}{\beta_{D6} \cdot (1 - \beta_{D6}^2)} \cdot D_{D6} + \frac{\Delta\beta_{\text{filter}}}{\beta_{\text{filter}}} \cdot D_{\text{filter}} \quad [105]$$

is close to 0 (in the case of combined work must be  $\beta_{D6} = \beta_{\text{filter}}$ ), one can estimate the image shift as

$$\text{shift}_{FD} \cong \frac{\Delta(A/Q)}{A/Q} \cdot D_{D6} \quad [106]$$

or, in other words, only the  $A/Q$  selection takes place.

Some possible combinations are considered in the program :

1.  $D_{D6} = 0$  (the dipole is absent)
2.  $D_{\text{filter}} = 0$  (the velocity filter is absent)
3.  $D_{D6} \neq 0, D_{\text{filter}} \neq 0, D_{\text{filter}} \neq D_{D6}$  (it means that the angle of platform turning is not correct)
4.  $B\rho_2 \neq B\rho_{D6}$

### 33.3.1. Image size

The image size (distribution) defined in the program LISE is a result of convolution of two distributions  $P_Y$  and  $P_{Y'}$  :

$$P_Y^* = \bar{P}_Y \otimes \bar{P}_{\delta/Y} , \quad [107]$$

where

1.  $P_Y$  - The image in the vertical focal plane before the Wien filter multiplied by the vertical magnification (y/y) of the filter-dipole system;
2.  $P_{\delta/Y}$  - contribution of momentum distribution due to dispersion in the final focus plane which is possible to determine as

$$P_{\delta/Y} = \frac{PM - B\rho_2}{B\rho_2} \cdot D_{FD} , \quad [108]$$

where  $PM$  is a nucleus momentum distribution before the Wien Filter in  $Tm$ ,  $D_{FD}$  is the total dispersion of the filter-dipole system ("fd-system") [mm/%],  $B\rho_2$  is the magnetic rigidity of the second dipole.

Repeating all steps like in the previous section it is possible to conclude that the use of the "fd-system" supposes that  $P_{\delta/Y}$  vanishes because as it was mentioned before the sum (equation 105) is close to 0 and the value  $\Delta(A/Q)$  for an isotope relatively itself is equal 0. It means that the final Y-image will be narrower, thus providing a better resolution than in the simple case of the velocity filter only. Hence the second distribution is taken as the  $\delta$ -function in order to get  $P_Y^* = P_Y$  as a result of convolution.

After this consideration it is possible to compare the "fd-system" with an ordinary velocity filter (see Table 1) : application of the "fd-system" provides better results for smaller object size and wider momentum distribution.

**Table 1.**

Spectrometer	SISSI + degrader in LISE	SISSI + degrader in ALPHA	LISE	LISE2000 <sup>7</sup>
Y-object size, mm	0.2	0.2	1.5	1.5
magnification (Y/Y) 1	15.91	12.18	4.26	3.14
magnification (Y/Y) 2	0.43	3.44	0.43	0.60
magnification (Y/Y) Wien	1	1	1	1
Y-object size final, mm	1.37	8.37	2.76	2.83
Acceptance, %	0.5	0.5	2.5	5
Dispersion W, mm/%	3	3	3	3
Acc*DispW, mm	1.5	1.5	7.5	15
Y-image final, mm	2.0	8.5	8.0	15.3
<b>Y-image / Y-object</b>	<b>1.5</b>	<b>1.0</b>	<b>2.9</b>	<b>5.4</b>

### 33.3.2. Separation with the Dipole D6

<sup>7</sup> Under construction, but this spectrometer is planning without a possibility to conjoint with the Wien filter.

The LISE standard configuration was chosen in order to compare different modes of selection. These experimental settings (beam, target, wedge, slits) are given below.

Projectile : 40Ar 18+ at 50 MeV/u - Intensity : 1000 enA	
Target : Ta Thickness : 100	mg/cm2 (60.241 microns)
Wedge : Al Thickness : 100	mg/cm2 (370.37 microns)
Settings calculated on 36Ar 18+ 18+	
Brho1=1.9467 Tm Brho2=1.7067 Tm (B1=0.7487 T B2=0.8521 T)	
Wien filter : E=3500.0 kV/m B=417.9618 G Disp=3.725 mm/%	Magn=1
D6 : B=0.6069 T Angle=15.87 deg Disp=3.725 mm/%	
Acceptances :	
Maximum momentum acceptance : +/- 2.50 %	
Target : Theta : +/- 17.45 mrad	Phi : +/- 17.45 mrad
Wedge : Theta : +/- 20.27 mrad	Phi : +/- 6.00 mrad
Slits :	
X,Y Slits before target (Collimator) mm +/- :	15 15
X,Y Slits intermediate (Momentum sel.) mm +/- :	45 20
% in Brho +/- : 2.50	
X,Y Slits first focus (Wedge selection) mm +/- :	10 10
Second image slits (Wien selection) mm +/- :	7

Table 2.

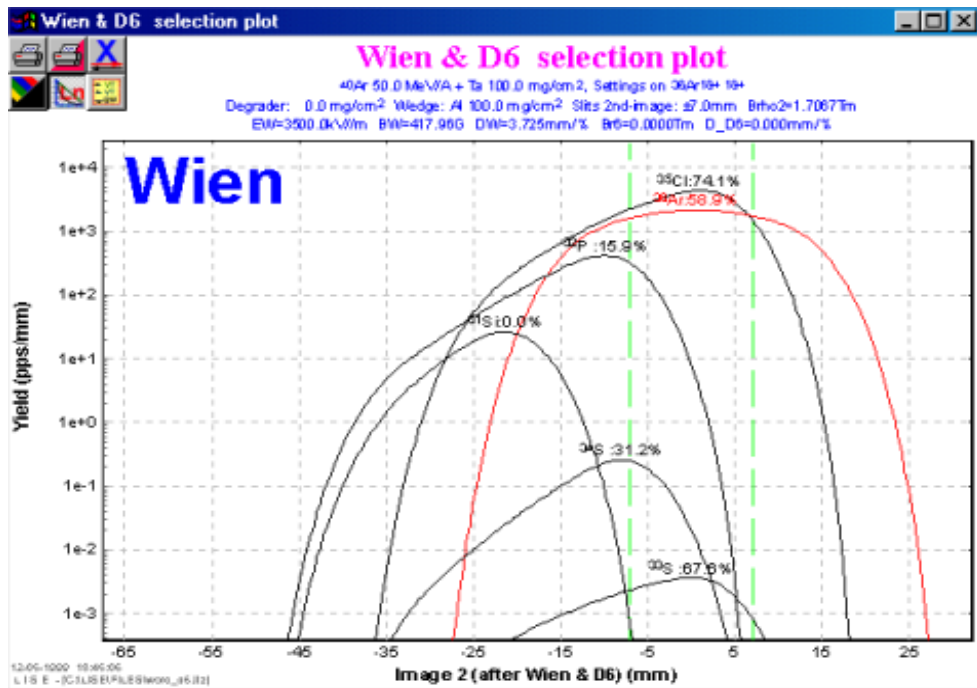


Fig. 708.

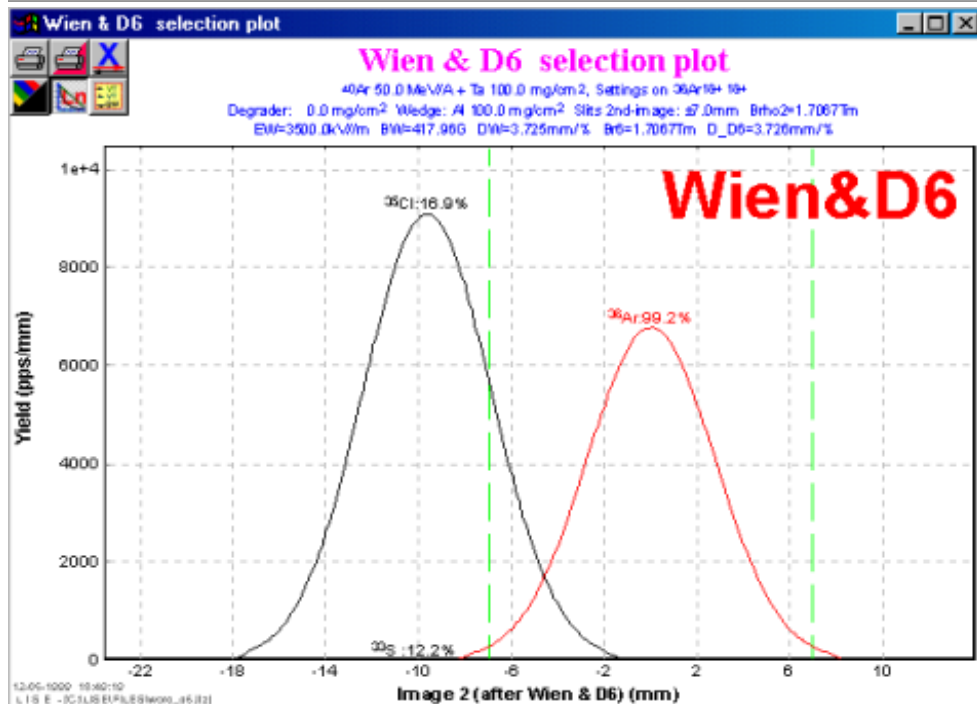


Fig. 709.



	Mode	Selection	N° nuclei	$\Sigma$ , pps	$^{36}\text{Ar}$ rate	$^{36}\text{Ar}$ rate / $\Sigma$
1	First dipole	$v \cdot A/Q$	116	2.4e+6	7.0e+4	2.9%
2	1 + Wedge	$A^{2.5}/Z^{1.5}$	8	1.1e+5	4.6e+4	41.8%
3	2 + Wien Filter	$v$	6	7.5e+4	2.8e+4	37.3%
4	3 + D6-dipole	$A/Q$	3	5.7e+4	4.6e+4	80.7%

The advantage of using all 4 selections follows apparently from Table 2. In this case the purification is 30 times better than after the first selection, but the  $^{36}\text{Ar}$  rate is lower only in 1.5 times. Figures 708 and 709 show vertical space distributions in the focal final plane for selections by the velocity filter and the "fd-system". The contribution of momentum distribution into the vertical image due to existence of non-zero velocity dispersion in the mode only with the velocity filter (Fig.708) makes the image wider as compared to the "fd-system" that was already discussed in "§33.3.1. Image size".

### 33.3.3. The program "LISE" for the new spectrometer VAMOS

VAMOS is a collaboration to build a large acceptance spectrometer [VAMOS] for identifying products of reactions induced by the Systeme de Production d'Ions Radioactifs et d'Acceleration en Ligne (SPIRAL) facility at the Grand Accelérateur National d'Ions Lourds (GANIL).

The QQFD-spectrometer VAMOS has the following main properties and characteristics:

- A very large geometrical acceptance, of the order of 100 msr, that is equivalent to an angular acceptance of  $\pm 160$  mrad ;
- A nominal dispersion of about 2.5 cm/% at the focal plane ;
- A momentum acceptance of the order of  $\pm 5\%$  ;
- A velocity filter function.

The new version of "LISE" may be useful to perform estimations of transmission, to view different plots of space distributions. The spectrometer VAMOS is developed for the energy region from 4 to 20 MeV/A where for example the parameterization of reaction cross-sections does not work. Due to this fact the program unfortunately can not be used with all its possibilities. It is necessary to examine the procedures of reaction mechanisms more accurately. The configuration file<sup>8</sup> allowing to view space distributions in the focal plane of the spectrometer is given below.

```
Version 3.4
[general]
File = C:\LISE\config\VAMOS.lcf
Date = 12-05-1999
Time = 13:41:31
Title = VAMOS

[object]
X Slits before target = 10      (±)mm      ; hor.slit width before target to collimate a beam
Y Slits before target = 10      (±)mm      ; ver.slit width before target to collimate a beam
X Slits intermediate = 100      (±)mm      ; hor.slit width at the dispersive focal plane
Y Slits intermediate = 10      (±)mm      ; ver.slit width at the dispersive focal plane
X Slits first focus = 10        (±)mm      ; hor.slit width at the first focal point /after wedge/
Y Slits first focus = 10        (±)mm      ; ver.slit width at the first focal point /after wedge/
Slits second focus = 10        (±)mm      ; ver.slit width at the second focal point /after Wien/

[acceptances]
Maximal momentum accept = 5     (±)%       ; upper limit for the setting of the slits
Theta target acceptance = 160   (±)mrad    ; angular target horiz.acceptance
Theta wedge acceptance = 200    (±)mrad    ; angular wedge horiz.acceptance
Phi target acceptance = 160     (±)mrad    ; angular target vert.acceptance
Phi wedge acceptance = 200      (±)mrad    ; angular wedge vert.acceptance

[optics]
BX = 1.5      (±)mm      ; one-half the horizontal beam extent (x)
BT = 3.3      (±)mrad    ; one-half the horizontal beam divergence (x')
BY = 1.5      (±)mm      ; one-half the vertical beam extent (y)
```

<sup>8</sup> The definition of a configuration file as one of the new features of the program can be found in §33.4.2. Configuration file.

```


BF = 3.3      (±)mrad      ; one-half the vertical beam divergence (y')
BD = 0.1      (±)%        ; one-half of the momentum spread (dp/p)
Ra1 = 2.6     m           ; Curvature radius of first dipole
Ra2 = 2.003   m           ; Curvature radius of second dipole
L target-wedge = 0       m           ; Object - DispFocPlane
L wedge-detector#1 = 0   m           ; DispFocPlane-AchrFinalPlane
M1X = 1       ; X Magnification target -> wedge
D1X = 10      mm/%       ; X dispersion target -> wedge
M1T = 1       ; theta magnific. target -> wedge
D1T = 0       mrad/%     ; theta dispers. target -> wedge
ThX = 0.1     mrad/mm    ; theta/x coef. target -> wedge
M1Y = 1       ; Y Magnification target -> wedge
PhY = 0.1     mrad/mm    ; fi/y coef. target -> wedge
M1P = 1       ; fi magnificat. target -> wedge
M2X = 1       ; X Magnification wedge -> focal
D2X = -10     mm/%       ; X dispersion wedge -> focal
M2T = 1       ; theta magnific. wedge -> focal
D2T = -1      mrad/%     ; theta dispers. wedge -> focal
T2X = 0.1     mrad/mm    ; theta/x coef. wedge -> focal
M2Y = 1       ; Y Magnification wedge -> focal
P2Y = 0.1     mrad/mm    ; fi/y coef. wedge -> focal
M2P = 1       ; fi magnificat. wedge -> focal
Angle = 0     mrad       ; beam respect to the spectrometer axis

[wien_filter]
Wien filter = Enabled      ; Disabled & Enabled
E_F = 2000                 kV/m      ; electric field
B_F = 478.861416          G         ; magnetic field
DiC = 1.3856e-4           mm/%     ; dispersion coefficient
LenE = 1                  m         ; effective electric length
LenB = 1                  m         ; effective magnetic length
Red = 1                   ; Real/Red field
Mag = 1                   ; Magnification

```

### 33.4. New features of the version 3.4

#### 33.4.1. Physical calculator

 Very often it is necessary for User to perform a fast transformation of one physical value to another while working with the program. The dialog “GOODIES” allows to get calculated correlated value only for a given Bp-value obtained for a setting fragment. However, if User needs to know (for example) a range in some material for energy unconnected with given settings? The new version of the code “LISE” allows to solve this problem. The new dialog “Physical calculator” permits immediately to perform calculations of correlated values independently from calculations for a setting fragment. Clicking on any radiobutton User may choose the respective form to type a physical value in order to get other correlated values. For example, User may input the Bp-value for <sup>36</sup>Ar (see Fig.710) and get all correlated values including the range in the given material and the energy loss for the chosen thickness, or typing the energy rest <sup>22</sup>Al after the material (Si 100 mg/cm<sup>2</sup> in Fig.710), one can recalculate initial energy of a nucleus before the material and other correlated values as shown in Fig.711.

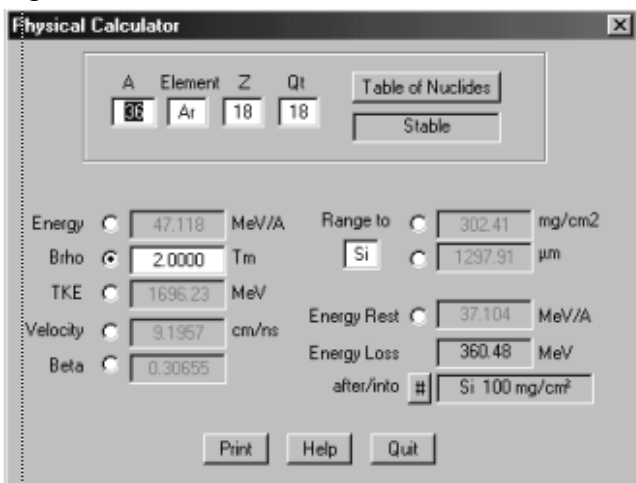


Fig.710

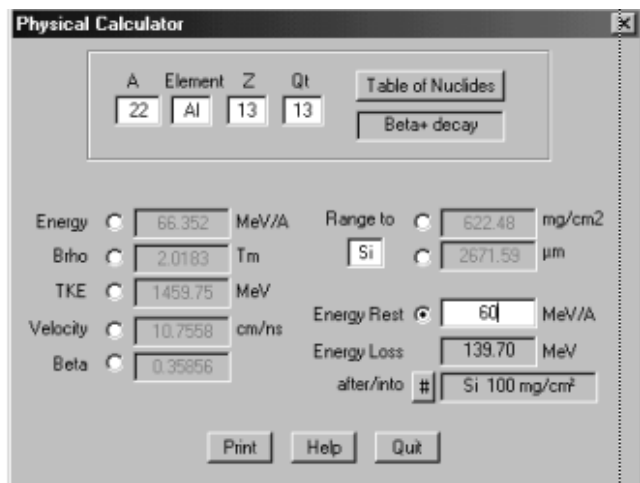


Fig.711

The eight correlated values of a nucleus (which is inputted in the upper part of the dialog) are in-

cluded to “Physical calculator”:

- Energy [MeV per nucleon] ;
- Bp-value [Tm] (for calculations it is taken Qt - the ionic charge) ;
- TKE is the Total Kinetic Energy [MeV] ;
- Velocity [cm/ns] and beta ;
- Range in the specific material chosen by User. The Range may be inputted in mg/cm<sup>2</sup> as well as in micron form.
- Energy rest of a nucleus [MeV per nucleon] after the material defined by User. For convenience the energy loss [MeV] in the material is shown in the static window below.

Correlated values of Time of flight and Wien magnetic field will possibly also be added to Physical calculator. All this makes Physical Calculator a power tool allowing User to quickly obtain a physical value of interest from other correlated values.

### 33.4.2. Configuration file

Two types of files were used in the previous version of the program: LISE-file (extension LIZ) and Result-file (extension RES).

The data settings could be recovered only from LISE-files. If User wanted to repeat old settings for a new file it was necessary first to find the corresponding LISE-file with same setup configuration and then to save it with a new name. In the new version there is an additional possibility to save and to extract settings to/from the new kind of file is called Configuration-file. User has an access to these files via the menu “File -> Configuration”.

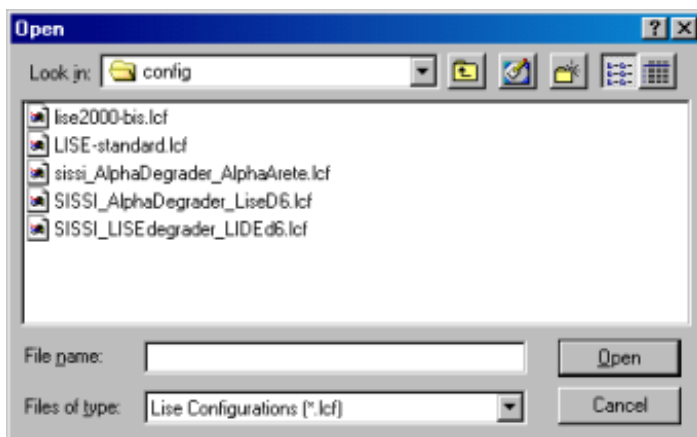


Fig. 712.

file :

- general (date of creating, description);
- object (size of all slits);
- acceptances;
- optics;
- Wien-filter.

Configuration files (file extension “LCF”) are placed default in the directory “CONFIG” which is daughter for the LISE-directory (see Fig.712). The listing of the configuration file “VAMOS.lcf” has been already enclosed to in

the section "33.3.3. The program “LISE” for the new spectrometer VAMOS".

On the base of optical matrices and physical characteristics of setups given in the Ref.[VAMOS,SISSI], different setups for the LISE program were put to configuration files. User may find these configuration files in the distributive version “lise34.zip” :

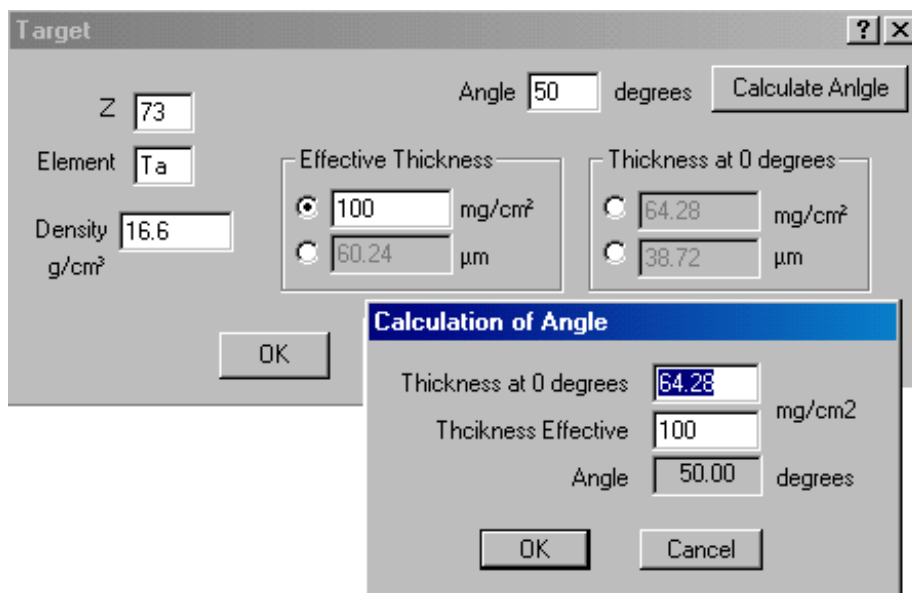
- LISEstandard.lcf - *the standard spectrometer LISE configuration. A target is placed into the LISE target box ;*
- LISE2000-bis.lcf - *the new project of the spectrometer LISE with large angular and momentum acceptances, maximal magnetic rigidity of the second dipole is 4.3 Tm . A target is placed into the LISE target box ;*

- SISSI\_AlphaDegrader\_AlphaArete.lcf - a target is placed into the device **SISSI**, an achromatic degrader in the dispersive focal plane of the spectrometer **Alpha**. The final focus plane is “**ARETE**” (the Alpha spectrometer outlet) ;
- SISSI\_AlphaDegrader\_LISEd6.lcf - a target is placed into the device **SISSI**, an achromatic degrader in the dispersive focal plane of the spectrometer **Alpha**. The final focus plane is the hall “**D6**” of the spectrometer **LISE** ;
- SISSI\_LISEdegrader\_LISEd6.lcf - a target is placed into the device **SISSI**, an achromatic degrader in the dispersive focal plane of the spectrometer **LISE**. The final focus plane is the hall “**D6**” of the spectrometer **LISE**;
- VAMOS.lcf - this configuration has been already discussed in ”§33.3.3. The program “LISE” for the new spectrometer VAMOS“.

Using this new feature User may call these configuration files to estimate which setup is more profitable for given experimental settings (beam, target, degrader, wedge, Bp-values and setting fragments). Experiment parameters will not be changed while acceptances, optics, slits and velocity filter coefficients will be taken from a configuration file.

**F T D W M**

### 33.4.3. Target Angle



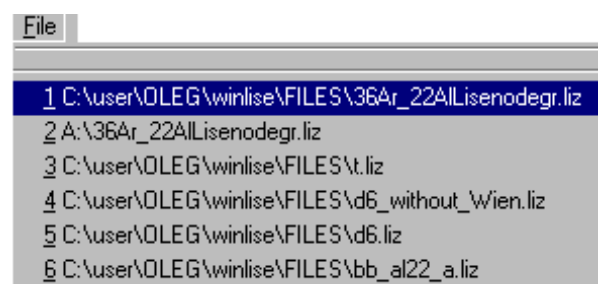
Physicist may vary a target thickness changing an angle of target that is placed into the target box of the SISSI device or the LISE spectrometer. Sometimes it is necessary to calculate and input the value of the angle in the experiment. In the new version of the code User can change the angle of a target (wedge, degrader, materials). There is a possibility to calculate each of three values from the two other known ones: Effective thickness,

Fig.713.

Thickness at 0 degrees or Angle of turning (see Fig.713). For example, if User knows the effective target thickness and the thickness at 0 degrees he can simply click on the button “Calculate Angle” to get the angle value as shown in Fig.713. User may input the material thickness using two dimensions: mg/cm<sup>2</sup> or microns.

### 33.4.4. List of recently used files

To open a document User has used recently, it is necessary to click its name at the bottom of the File menu where the list of recently used documents is placed.



### 33.4.5. Calculation of Q-ground value for binary reaction

In the new version User may see a Q-value of reaction at the bottom of the window “ Statistics ” (this window is appeared when User clicks on an isotope of interest in the table of nuclides by the right button of the mouse). Q-value is calculated from the supposition that the reaction has two nuclei as a result. The first nucleus is the nucleus chosen by User, the second one is calculated as residual from “Projectile + Target - Fragment of Interest”. Therefore Q-value is estimated as :

$$Q = (ME_{\text{projectile}} + ME_{\text{target}}) - (ME_{\text{fragment}} + ME_{\text{residual}}) , \quad [109]$$

where  $ME$  is the Mass Excess from the database in-built into the program. The database uses the recommended values proposed by G.Audi and A.H.Wapstra [Aud95].

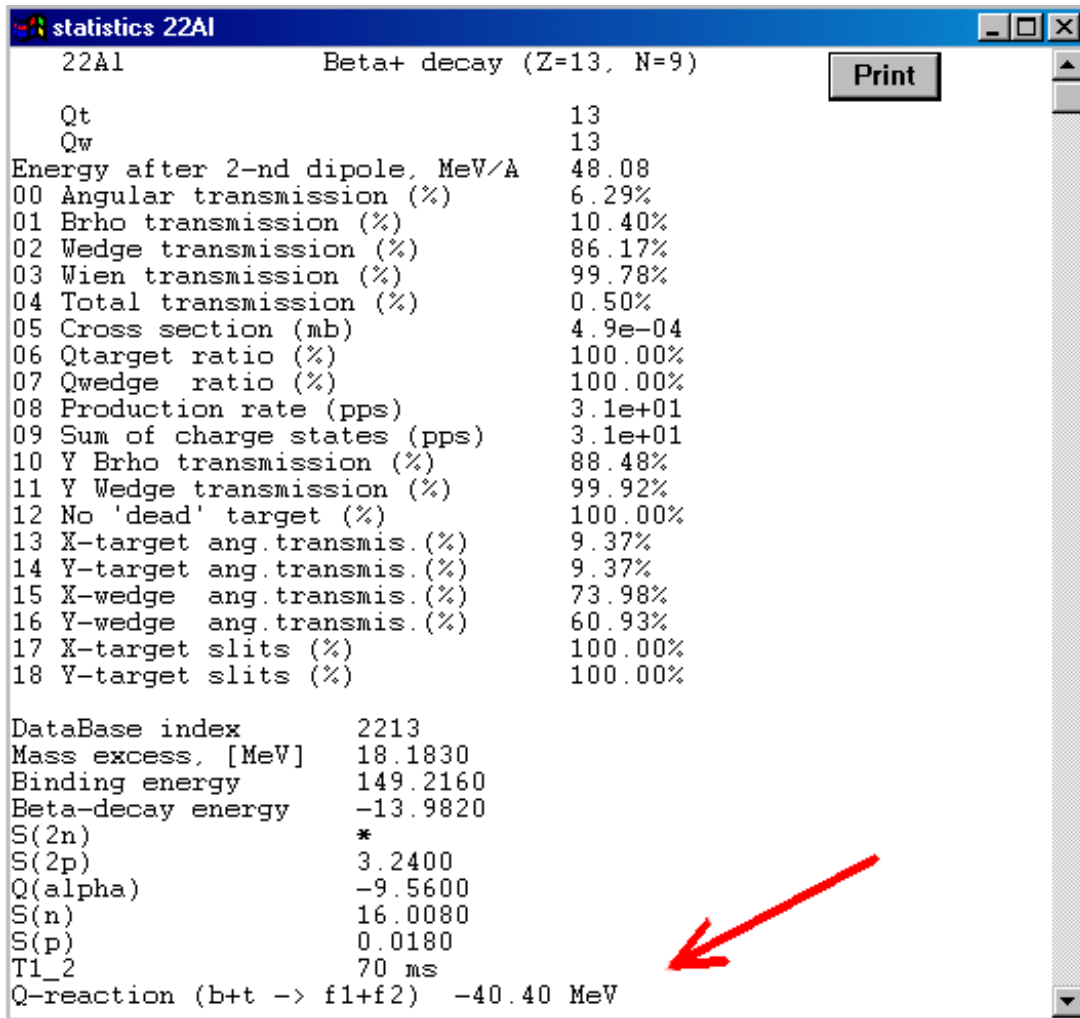


Fig.714.

### 33.4.6. Chromatic mode (Dispersion ≠ 0)

Since its first version, the program has been adapted to operate only in the achromatic mode. The focal plane of the second section being achromatic, there is no momentum dependence of the final horizontal position (as well as vertical). In the new version the admission that the full momentum dispersion is not equal to 0 has been included. User may observe this admission on the Wedge image (X) plot in the First focal plane. This assumption is fulfilled because the selection by the velocity filter and the dipole “D6” takes place in the Y-plane. Using this new mode User may visualize the images and obtain a transmission not only for “ideal” case of an achromatic spectrometer.

The code is calculated full momentum and angular dispersions<sup>9</sup> on the base of inputted in the program the two transport matrices for both parts of the spectrometer as:

$$\left(\frac{x}{\delta}\right)_G = \left(\frac{x}{\delta}\right)_1 \left(\frac{x}{x}\right)_2 + \left(\frac{x}{\delta}\right)_2 \quad [mm/\%] \quad [110]$$

$$\left(\frac{\theta}{\delta}\right)_G = \left(\frac{x}{\delta}\right)_1 \left(\frac{\theta}{x}\right)_2 + \left(\frac{\theta}{\delta}\right)_1 \left(\frac{\theta}{\theta}\right)_2 + \left(\frac{\theta}{\delta}\right)_2 \quad [mrad/\%] \quad [111]$$

The code always accepts the angular achromatism at the second focal point, though User may observe in the dialog “Optics” a nonzero value of the full angular dispersion from Equation 111. User may see the calculated value of the full momentum dispersion in the dialog “Optics” as well as in the StatusBar at the bottom of the code screen.

Figures 715 and 716 demonstrate the new possibility. Three distributions on the Wedge selection plot are presented in Fig.715 for the achromatic case as it was in previous versions. The distributions of the same nuclei as in Fig.715 are shown in Fig.716, but for this case the global momentum

dispersion is equal to 9.7 mm/%. It is apparent clear in the chromatic case the distributions are wider and a transmission is not equal to 100%. Peak shifts in the distributions of <sup>35,37</sup>Ar as well as shapes of these distributions are explained by not optimal Bp-value for these nuclei as demonstrated for <sup>36</sup>Ar isotope (see the Brho Selection plot in Fig.717). The low energy part of the <sup>37</sup>Ar distribution and the high energy part of the <sup>35</sup>Ar distribution have been cut by the momentum slits. Their momentum distributions are similar on a triangle than the <sup>36</sup>Ar distribution presents itself a symmetrical cut gaussian. The convolution of these distributions with the object distributions gives result shown in Fig.716.

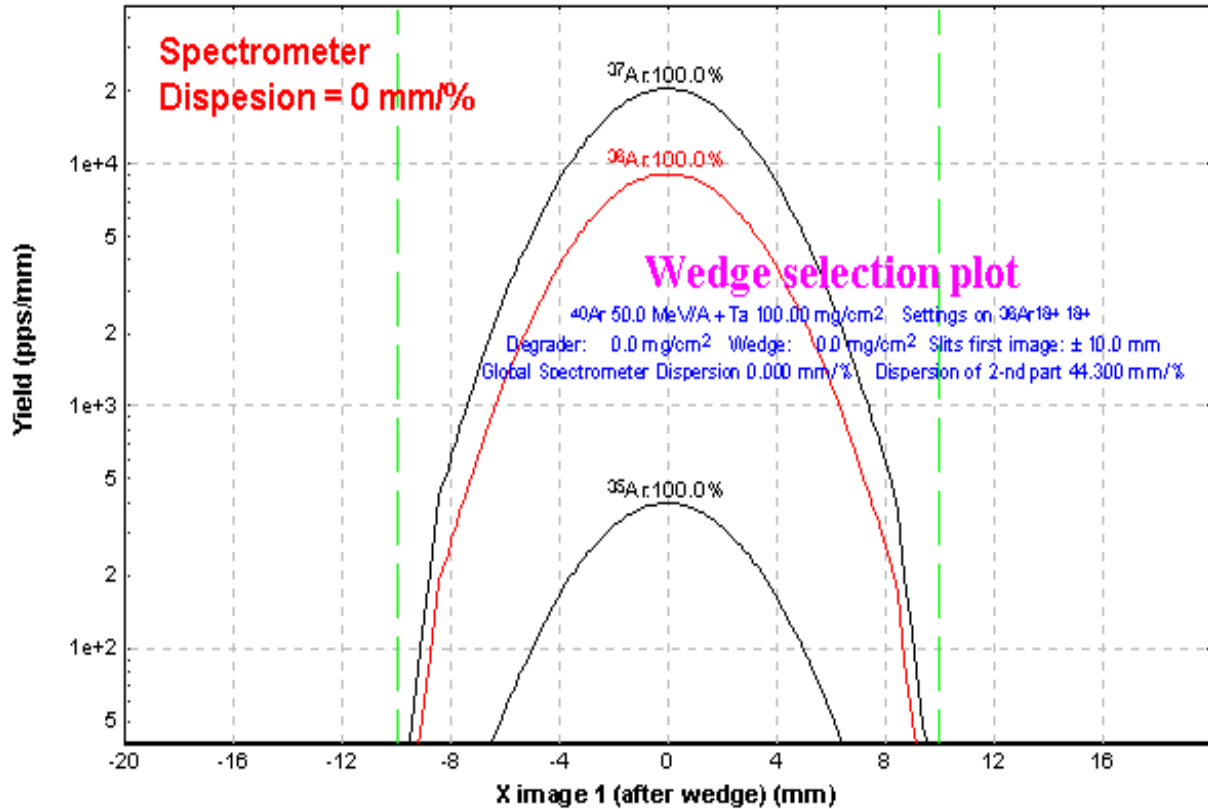
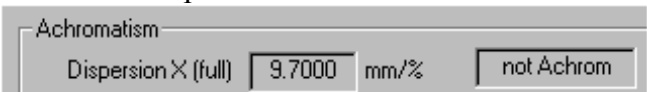


Fig. 715.

<sup>9</sup> Suggesting that the spectrometer has foci  $(x/\theta)_1=(y/\phi)_1=(x/\theta)_2=(y/\phi)_2$

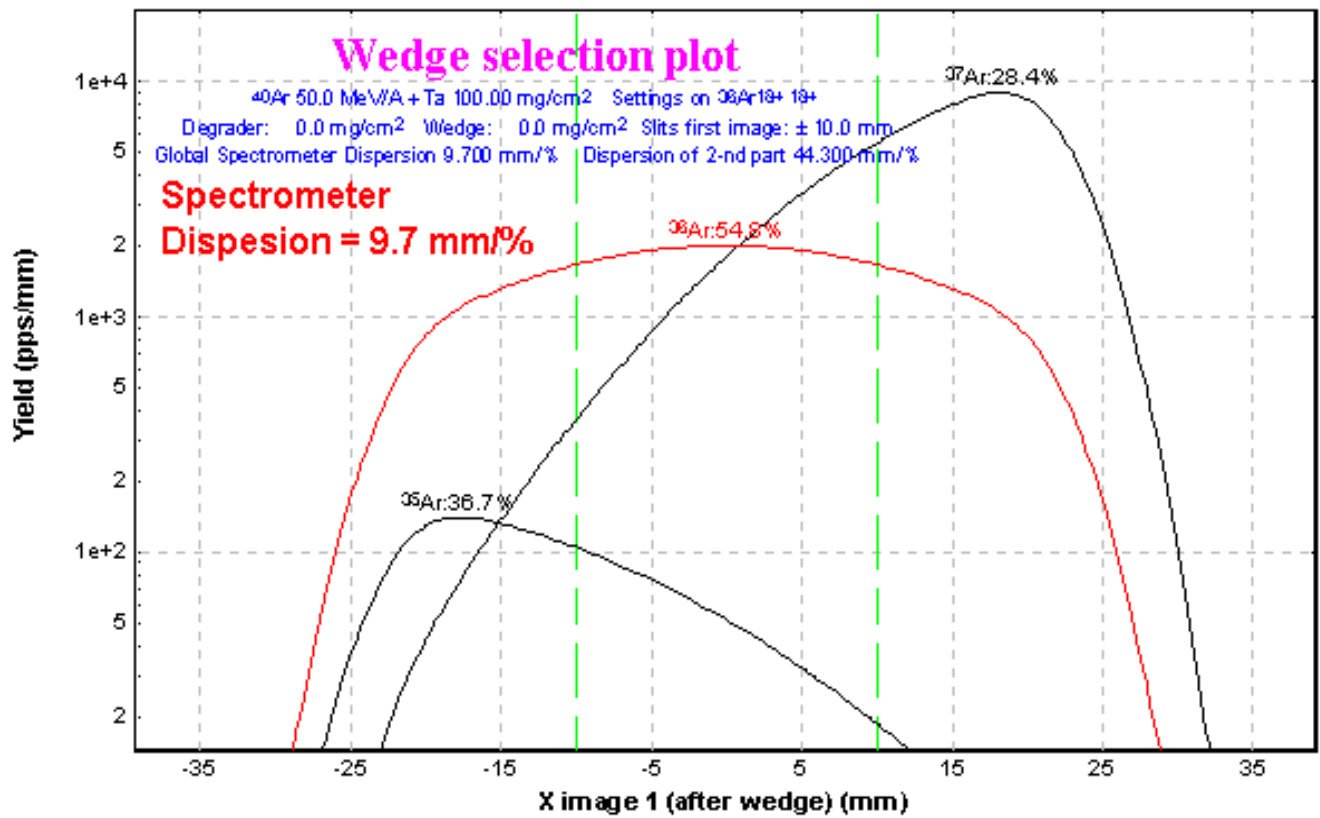


Fig.716.

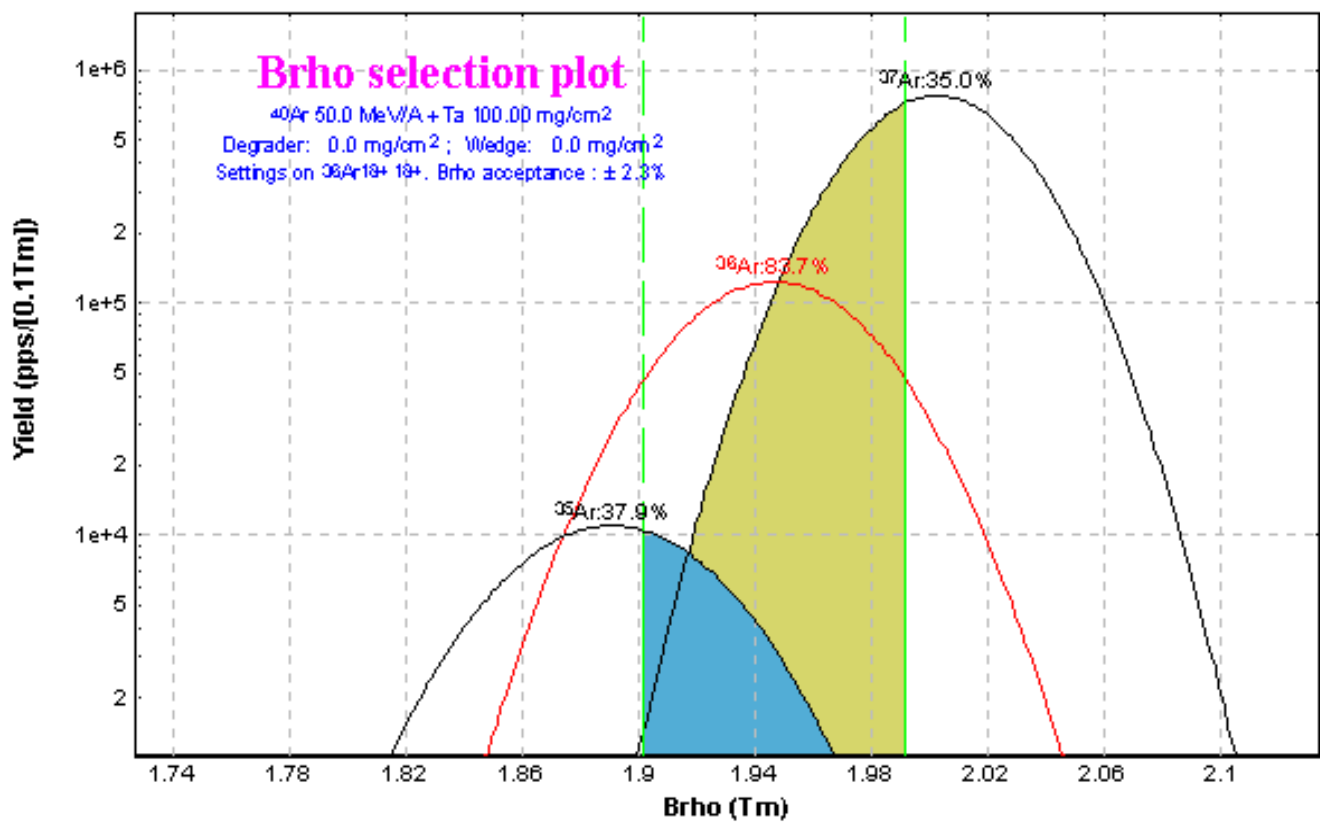


Fig.717.

## 33.5. Development

### 33.5.1. Results file

The Results file has not been changed since its DOS-version 2.5, and consequently in versions 3.0-3.3.05 it does not reflect all parameters needed for User ("D6"-dipole parameters, applied methods of the cross-section parameterization and the ionic charge state distributions, target angle). In the new version the Results file has got more readable form, and all values needed for further work of User with this file have been included.

```

LISE CALCULATIONS      Version 3.4

File : C:\user\OLEG\winlise\FILES\36Ar_22AlLisenodegr.liz
Date : 5/19/1999      Time : 9:13:01
Title : 22Al

      Projectile : 36Ar 18+ at 94.4 MeV/u - Intensity : 1000 enA
      Target      : Be Thickness : 537.95 mg/cm2 (2907.84 microns)
      Wedge       : Be Thickness : 196.47 mg/cm2 (1062 microns)
Material(s) :
#1 : Si Thickness : 69.9 mg/cm2 (300 microns)
#2 : Si Thickness : 69.9 mg/cm2 (300 microns)
#4 : Si Thickness : 116.5 mg/cm2 (500 microns)
#5 : Si Thickness : 116.5 mg/cm2 (500 microns)
#6 : Si Thickness : 1398 mg/cm2 (6000 microns)

Settings calculated on 22Al 13+ 13+
Brhol=1.9530 Tm Brho2=1.7100 Tm (B1=0.7512 T B2=0.8537 T)
Wien filter : E=3500.0 kV/m B=331.8000 G Disp=3.184 mm/% Magn=1
              D6 : B=0.5354 T Angle=13.97 deg Disp=3.185 mm/%

Mechanism: Vopt/Vbeam=1.000 Sigma0=90.0 MeV/c SigmaD=200.0 MeV/c
Methods: Cross Section=0 Charge states=0

Acceptances :
Maximum momentum acceptance : +/- 2.50 %
Target : Theta : +/- 17.45 mrad Phi : +/- 17.45 mrad
Wedge : Theta : +/- 20.26 mrad Phi : +/- 6.00 mrad
Slits :
X,Y Slits before target (Collimator) mm +/- : 15 15
X,Y Slits intermediate (Momentum sel.) mm +/- : 8.6 10
              % in Brho +/- : 0.50
X,Y Slits first focus(Wedge selection) mm +/- : 7 10
Second image slits (Wien selection) mm +/- : 5

Beam emittance (+/-): 1.5 mm 3.3 mrad 1.5 mm 3.3 mrad 0.1 %
Beam angle on target : 0 mrad

OPTICS ([mm],[mrad]):
Target - DispFocalPlane(Wedge)      DispFocalPlane(Wedge)-First image
-0.783 * * * 17.3 -2.5607 * * * 44.3
0.267 -1.284 * * 3.51 0.4 -0.389 * * -5.56
* * -4.26 * * * * -0.432 * * *
* * -0.858 -0.273 * * * * -0.32 -2.4 *

TRANSMISSION AND RATE CALCULATIONS

A Z |Qt |Qw | Ang. | Brho |Wedge |WienD6|Y&C&DT| Total | Cross | Rate | Qt | Qw
| | | |Trans.|Trans.|Trans.|Trans.|Trans.| Trans.|Section| | | |
| | | (%) | (%) | (%) | (%) | (%) | (%) | (mb) | (pps) | (%) | (%)
-----|-----|-----|-----|-----|-----|-----|-----|-----|-----|-----|-----|-----|-----
23Si | | | 6.534 | 4.692 | 85.05 | 2.641 | 88.41 | 0.0061 | 3.3e-06 | 0.0025 | | |
22Al | | | 6.291 | 10.40 | 86.17 | 99.78 | 88.41 | 0.4972 | 0.00049 | 31 | | |
21Mg | | | 6.018 | 4.905 | 84.89 | 0.921 | 88.41 | 0.0020 | 0.029 | 7.5 | | |
=====
ALMOST : 38 pps

```

### 33.5.2. New parameterization

 The code used three in-built parameterizations of cross-sections on the EPAX [Sum90, Sum00]



base. B.Blank and K.Summerer have kindly presented the new parameterization EPAX 2.13 for the new LISE-version. This new approximation shows very good agreement in cross-section estimation for proton rich fragments, while for the super neutron rich isotopes placed far from a beam [Tar97] the discrepancy appears (see Fig.718) as in the previous parameterization but from the other side.

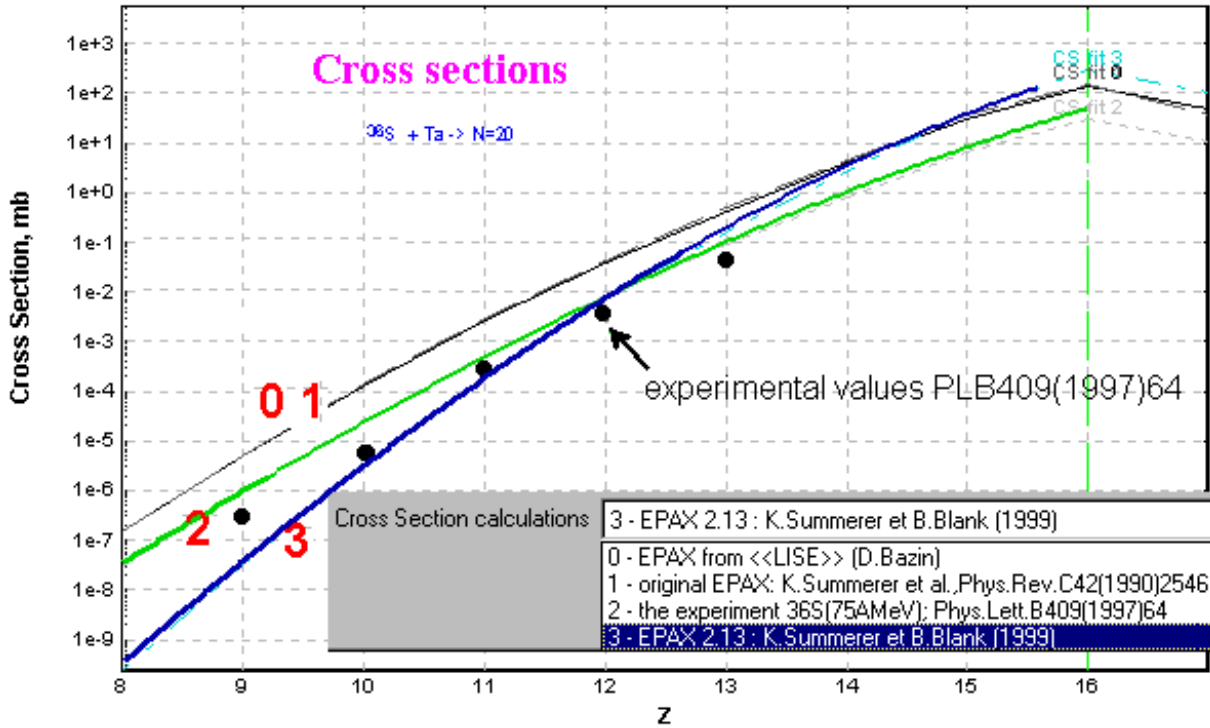



Fig.718.

User may choose the new parameterization to perform calculations via the Menu “Options->Production Mechanism”.

### 33.5.3. Trigonometric function of the in-built calculator

 The trigonometric functions (sin, cos, tan, arcsin, arccos) have been added in the in-built calculator. User has also got an opportunity to choose units (degrees or radian) for trigonometric calculations (see Fig.719).

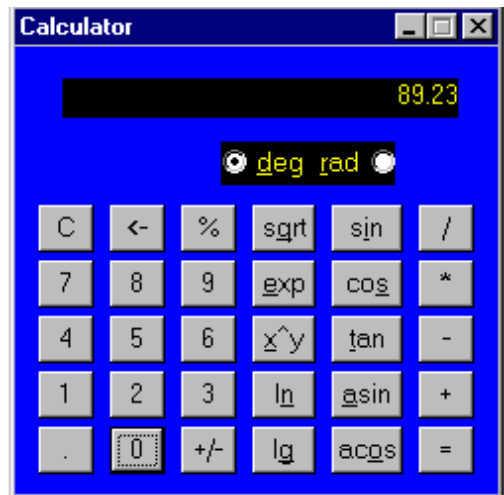


Fig.719.

### 33.5.4. Three points interpolation for the energy loss and range subroutines

In the previous version the energy loss and range subroutines used the linear interpolation to get a result from the tabulated values. The new code version describes the tabulated values by a second order polynomial using three points (see Fig.720). This allows to smooth some distributions (for example the Range distribution in materials).

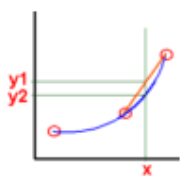


Fig.720.

### 33.6. Plots

#### 33.6.1. Image after Wedge & D6 (one-dimensional plot) and dE - Y image (after wedge & D6)

Plot	Help
Plot dE-TOF	
Plot Z-A/Q	
Plot dE-E	
Plot dE-dE	
Plot dE-X	
Plot dE-Y after Wien and D6	
Angular distributions	
Rho selection plot	
Wedge selection plot	
Wien and D6 selection plot	
Y selection plots	
Range distributions	
Charge distributions	
Cross Section distributions	
Q-ground distributions	
Options	

Two kinds of plots have been created to visualize Y-image distribution in the final focus plane after the velocity filter and the dipole “D6”. The one-dimensional plot (left menu) has been already presented in Fig.708 and 709.

The two-dimensional plot (right menu) dE-Y (Energy Loss versus Y-image) is presented in Fig.721.

Plot	Help
Plot dE-TOF	
Plot Z-A/Q	
Plot dE-E	
Plot dE-dE	
Plot dE-X	
Plot dE-Y after Wien and D6	
Angular distributions	
Rho selection plot	
Wedge selection plot	
Wien and D6 selection plot	
Y selection plots	
Range distributions	
Charge distributions	
Cross Section distributions	
Q-ground distributions	
Options	

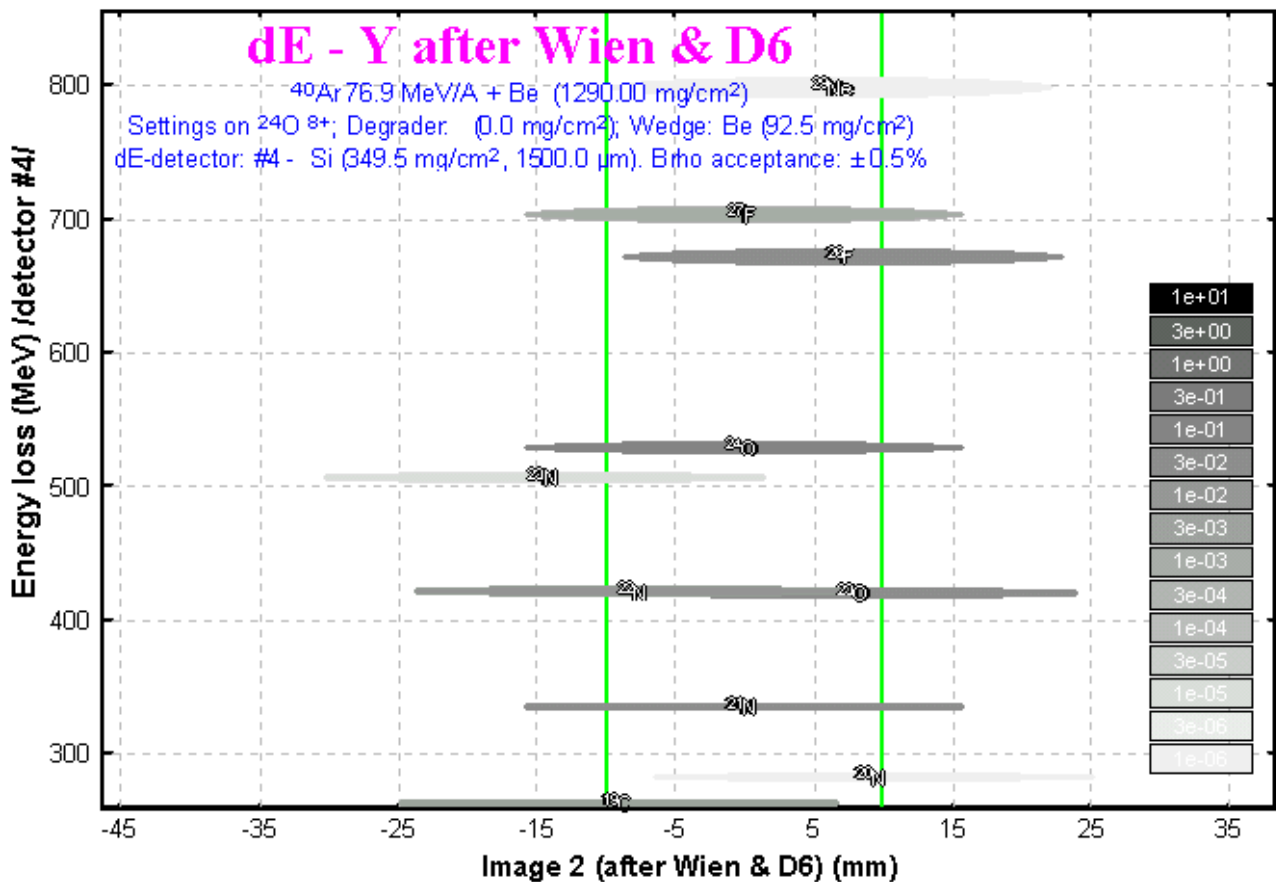


Fig.722.

### 33.6.2. dE-dE plot

Plot	Help
Plot dE-TOF	
Plot Z-A/Q	
Plot dE-E	
<b>Plot dE-dE</b>	
Plot dE-X	
Plot dE-Y after Wien and D6	
Angular distributions	
Brho selection plot	
Wedge selection plot	
Wien and D6 selection plot	
Y selection plots	
Range distributions	
Charge distributions	
Cross Section distributions	
Q-ground distributions	
Options	

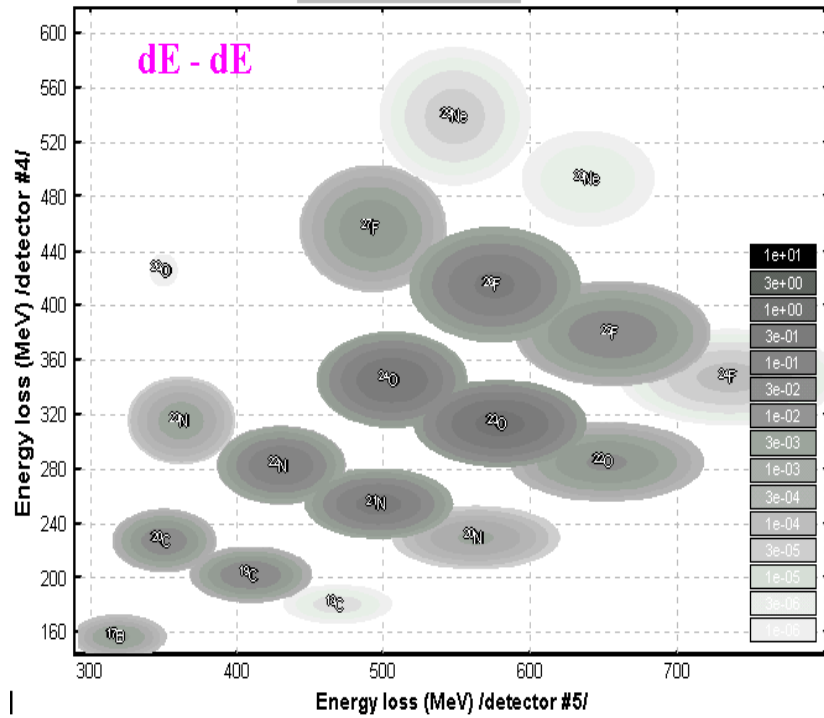


Fig. 723.

### 33.6.3. dE-X plot

Plot	Help
Plot dE-TOF	
Plot Z-A/Q	
Plot dE-E	
Plot dE-dE	
<b>Plot dE-X</b>	
Plot dE-Y after Wien and D6	
Angular distributions	
Brho selection plot	
Wedge selection plot	
Wien and D6 selection plot	
Y selection plots	
Range distributions	
Charge distributions	
Cross Section distributions	
Q-ground distributions	
Options	

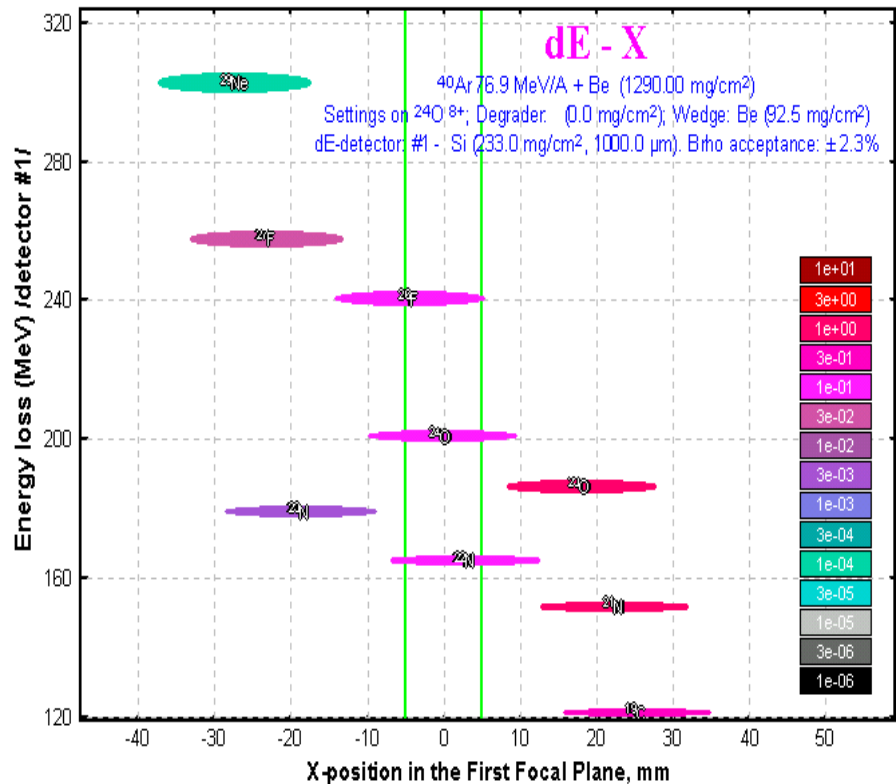


Fig. 724.

### 33.6.4. Realistic image of peaks



Two-dimensional plots in standard mode are drawn only by one color corresponding to their intensity. The width of peak is equal to its distribution FWHM. “Realistic” mode for peak drawing uses some colors depending on a distance between the peak center and given point inside the peak (width  $\pm 2\sigma$ ). Example of the plot drawn in the “realistic” mode is presented in Fig. 723.

### 33.6.5. Plot of Q-ground values

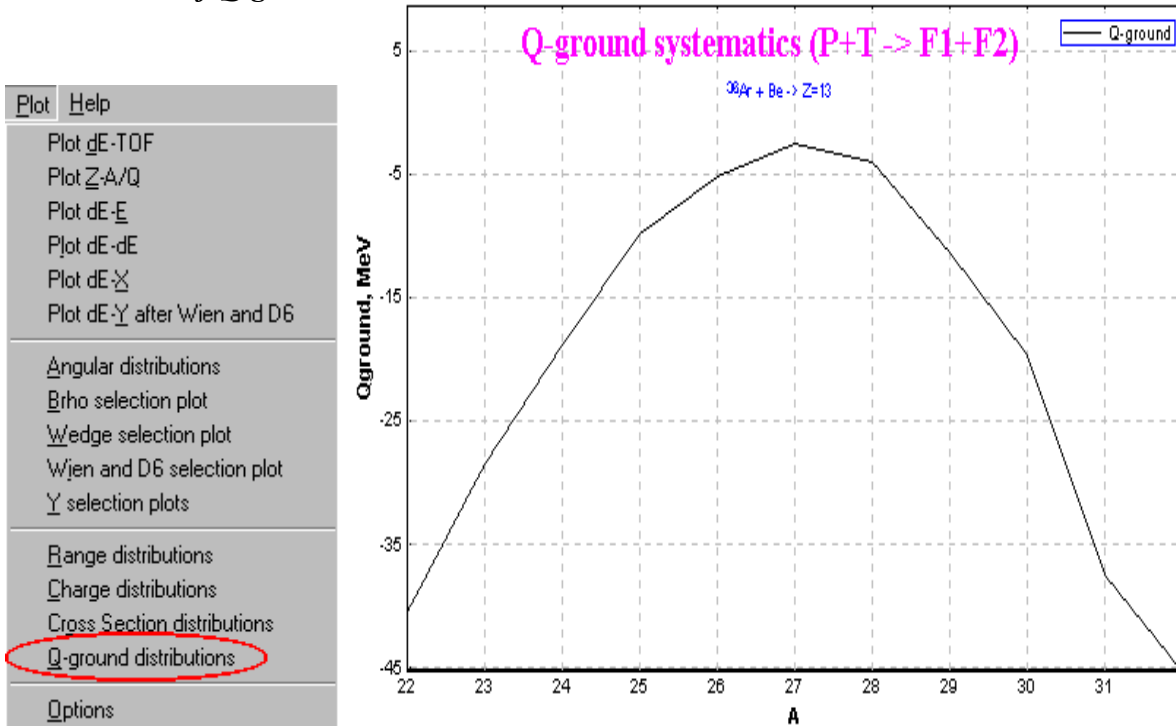


Fig. 725.

### 33.6.6. Gray and Color Palettes for two-dimensional plots

User does not always have a possibility to print two-dimensional plots on color printers. Therefore the button has been added to switch the palettes of plot to reproduce intensity of peak for printing.

### 33.7. Bugs

#### 33.7.1. The thickness dialog - density

Before it was impossible to input a float value into the density window of the thickness dialog. This has been corrected.

#### 33.7.2. The dialog "Calibrations"

After inputting new nucleus in the calibration dialog the range was not recalculated. This has been corrected.

#### 33.7.3. Adaptation the code to the PC emulator on Mac

Cross-section calculations were performed incorrectly on Mac under the PC-emulator due to some discrepancy in the C function "pow(x,y)" between these system platforms (?). The function pow(x,y) has been changed in the code by redefinition #define pow(x,y) exp((y) log(x))

#### 33.7.4. Negative dispersion

The negative momentum dispersion provoked a crash of the program. This has been corrected and User may use the negative momentum dispersion.

#### 33.7.5. After reading of a LISE-file the program did not calculate magnetic field

The conjugate values ( $B_p$  and  $B$ ) are immediately recalculated when User changes the  $B_p$ -values or the  $B$ (magnetic field)-values using the dipoles dialog or when the program calculates these values. When User read a LISE-file, the  $B_p$ -values were inputted into the code without recalculation of the magnetic field. This has been corrected.

#### 33.7.6. Distributions

Some bugs provoking crash of the program have been corrected.

## **34. Version 2.2: LISE (DOS )reference manual**

**Caen  
08.06.1992**

### **34.1. General description**

LISE is a program to calculate the transmission and yield of fragments produced and collected in a zero degree achromatic spectrometer. This method has been used for several years to produce and select radioactive nuclei far from stability, and is now opening a new era in nuclear physics research through the production of radioactive secondary beams. The program is designed to be as user-friendly as possible, and to be used not only before an experiment to forecast the settings, rates and contaminants, but also during the run for the identification of the different nuclei and charge states, and to allow the experimenter to recalculate anything quickly and easily in case some parameter of the experiment has been changed (different selected nucleus, different detector, ...).

### **34.2. List of features**

#### ***34.2.1. Simulation of experimental conditions***

The program adapts to any spectrometer operating in the achromatic mode by adjusting the relevant optical parameters.

Adapts to a Wien filter installed after the spectrometer.

Free adjustment of the geometrical and momentum acceptances as well as slits to determine the selectivity of the whole apparatus.

Stacks of up to 7 different materials at the focal plane of the spectrometer (or Wien filter) in order to simulate the slowing down and/or implantation media for the different transmitted nuclei.

Adjustment of the parameters related to the production mechanism simulated in the program. E.g. a realistic cross section of a different reaction process used in the experiment can be specified.

#### ***34.2.2. Calculations performed***

The  $B\rho$  settings of the spectrometer and electric (or magnetic) field of the Wien filter for the best transmission of a given fragment. The  $B\rho$  of any charge state of any transmitted nucleus (specially useful to keep track of the beam charge states).

The Transmission of any fragment at a given setting of the fields. These numbers are then multiplied by the beam intensity, the target thickness and the cross sections to give an estimate of the rates. Angular and energy straggling are taken into account in the transmission calculations.

The optimal target thickness can be calculated.

The kinetic energy, the energy loss in a given material thickness, the range and both angular and energy straggling at different positions in the spectrometer. The range and energy loss calculations can be performed at any energy (although the valid range is from 2.5 MeV/u to 500 MeV/u) for elements

Li through U into materials Be through U. The program 'remembers' the range tables whenever they are calculated by storing them on disk.

Calibration of either the beam energy or the target thickness using a charge state of the beam and the  $B\rho$  at which the ion is centered on the dispersive focal plane. The same feature for calibrating the wedge thickness using any transmitted nucleus is provided.

The program includes the possibility to calculate the charge state distribution of any fragment and the corresponding transmission.

### ***34.2.3. Display***

The results of the calculations are displayed on a "chart of the nuclides" which can be scrolled in order to see the results obtained for a different region of nuclei (the screen contains  $7\times 7$  nuclei). Two pieces of information per nucleus can be chosen from the list of transmission, charge state distribution, cross section and final rate.

It is possible to add (or remove) any nucleus to the nuclear chart. If a new nucleus has been added, the automatic calculation of rates will take it into account. The chart of nuclides is updated each time the program is terminated.

One of the main features of this program is to produce an identification plot (Energy loss vs Time Of Flight). The parameters of this plot can be adjusted. They include the material in which the particles lose their energy, the flight path length, and other things such as the High Frequency of an accelerator (cyclotron) in case it is used as a time reference (this method usually leads to a wrap around of the identification plot).

Display of Energy loss vs Total Kinetic Energy using the same conditions as for the identification plot.

The distributions calculated for the transmission of the fragments can be displayed together with the acceptances or slits positions in order to visualize the selections and cuts created by the spectrometer. These include the angular distributions after both the target and the wedge, the  $B\rho$  distributions at the dispersive focal plane, the position distributions at the first focal plane (after the wedge) and at the second focal plane (after the Wien filter in case it is used).

The implantation distribution can also be displayed in any of the 7 chosen materials.

### ***34.2.4. Files and results output***

Any set of parameters and calculations can be saved in a file and later recalled.

The results of the calculations can be stored in a separate file. This file is automatically printed when a printer is connected to the computer. Right now, the only way to copy the graphic screens produced by LISE is by using the "Print Scrn" key and hope that the PC has been correctly configured to produce a valid screendump. Postscript files of the graphic screen will be available in the next version.

### ***34.2.5. User-friendly features***

The program uses a pop-up menu structure relying on the mouse to select the commands and functions. Different parameters also appear in these menus and they are constantly updated. They can be

changed by simply selecting the corresponding item and then entering the new value. Once a command has been issued, one can recall the last submenu, or start again from the root.

### **34.3. Calculations**

#### **34.3.1. Reaction mechanism and cross sections**

The production reaction mechanism assumed in this program is the so-called projectile fragmentation, as pictured for example by the abrasion model followed by sequential evaporation by both projectile and target spectators (fragments). Although this picture has been shown to be fairly accurate at high energy (above a few hundred MeV/u), the reaction mechanisms goes over to energy relaxation processes such as deep-inelastic or incomplete fusion in the intermediate energy range (between 30 MeV/u and 200 MeV/u). Therefore the model may produce incorrect cross sections.

In the program the cross sections are calculated according to a global fit to fragmentation [Sum90] with no energy dependence. For the production cross sections of nuclei far from stability, the values provided by this fit are valid only within one to two orders of magnitude: we have observed systematic deviations of the predicted rates coming from the lack of data in the cross section fit for the production of nuclei close to the drip-lines. Therefore the possibility to input directly the cross sections for a given reaction is included, provided these were actually measured or calculated by more sophisticated codes. It is also possible to calculate the transmission and rates for transfer products (i.e. for "fragments" having more protons and/or neutrons than the projectile). In these cases the fit based on target fragmentation only gives a qualitative guess, and a better estimate of the cross section is needed in order to obtain reasonable yield predictions. Once the cross sections are manually input in the program they are automatically saved whenever a set of calculations is saved in a file.

#### **34.3.2. Beam optics**

The spectrometer is assumed to function in the achromatic mode. This statement implies the following:

The spectrometer is composed of two sections : a first part which is dispersive, and a second part in which the fragments are refocused, providing the achromatism.

At the focal plane of the first section (called "intermediate focal plane") the horizontal position (perpendicular to the beam axis) of the fragments only depends on  $B$  ( and their horizontal position at the target. Therefore, the two optical parameters which determine the horizontal distribution at this focal plane are the dispersion ( $x/\delta\rho/\rho$ ) and the magnification ( $x/x$ ).

A wedge can be installed at the intermediate focal plane. This wedge is assumed to be achromatic (i.e., providing the same dispersion after as before). The proper slope can be calculated in the program.

The focal plane of the second section being achromatic, there is no momentum dependence of the final horizontal position (as well as vertical). Consequently, the only optical parameter taken into account in the determination of the final image size is the magnification from the target to the achromatic focal plane(called "image 1").

In addition to the achromatic spectrometer previously described, the program can calculate the selection provided by an additional Wien filter (velocity filter). The velocity dispersion created by this device is assumed to occur in the vertical plane, the resulting image (called "image 2") is determined by

the magnification and the dispersion of the filter (this last parameter is automatically calculated from the physical dimensions as well as the electrical and magnetic fields set on the filter).

### ***34.3.3. Acceptance and transmission calculations***

The selection of the nuclei transmitted through the spectrometer is separated in three steps corresponding to three different criteria:

The first section of the spectrometer provides a B( selection depending on the  $Av/Q$  ratio of each nucleus ( $A$  being the mass,  $v$  the velocity and  $Q$  the ionic charge). The horizontal slits at this first section focal plane ("Slits intermediate focal plane") set the momentum acceptance.

In case an achromatic wedge is used at the dispersive focal plane, different nuclei are refocused at different horizontal positions at the second focal plane, depending on the different amounts of energy they lose in the wedge, and the dispersion of the second section. This provides a second selection criteria which depends also on the horizontal size of the beam spot on target ("Object size"), the magnification, and setting of the horizontal slits at the second section focal plane ("Slits first focus (after wedge)").

Finally, the third selection is the velocity selection provided by the Wien filter (optional). Here again the relevant optical parameter are the magnification and the dispersion. This third selection criteria being different from the two previous ones, allows a further selection of the nuclei after the slits (called "Slits second focus (after Wien)").

The other acceptances taken into account for the calculation of the transmission are the geometrical acceptances after the target and after the wedge. Their values can be set in both the horizontal ( $\theta$ ) and the vertical ( $\phi$ ) planes. The maximum  $B\rho$  acceptance of the device can also be set and is used as an upper limit for the slits of the intermediate focal plane.

In all the calculations mentioned above, both the energy and angular straggling in the target and the wedge are taken into account. The effect of the energy loss in the wedge on the size of the image at the first focus is also included [Duf86]. These effects, in addition to the fixed range of the particles, limit the maximum thickness one can accept before starting to lose particles. The best target and wedge thicknesses result from two compromises. The first is the balance between the rate increase due to a larger number of interacting nuclei in the target, versus the decrease due to the slowing down of the fragments which reduces the actual momentum acceptance, and the angular and energy straggling. The command "Optimal target" calculates the dependence of the fragment yield on the target thickness, and finds the "best" target thickness with the maximum rate. The second compromise concerns the wedge thickness and is a balance between better selectivity - the images of different nuclei are further apart when increasing the wedge thickness - and rate loss due to angular straggling, secondary reactions (which are not taken into account), and image broadening.

### ***34.3.4. Energy loss and range tables***

The energy losses are calculated according to the latest functions provided by [Hub90]. These calculations are valid between 2.5 MeV/u and 500 MeV/u. Whenever an energy loss and range calculation needs to be performed, the program looks for the range table corresponding to the beam-absorber pair on disk. If it doesn't already exist, the program calculates it (a display appears on the screen) and stores it on the disk (files TABZ1Z2.RAN in the sub-directory "\RANGE"). Thus, the tables of range



data are built up over time. These range tables are calculated using Simpson's rule for integration, and the energy losses are deduced by inverted-interpolation on the range.

The starting point for the integration is given by range tables of Northcliffe and Schilling [Nor70] at 2.5 MeV/u (files NORTH\*.RAN in the sub-directory "\RANGE").

Between 0 and 2.5 MeV/u the range is calculated linearly, matching the value at 2.5 MeV/u. Above 500 MeV/u a power function fit is used as an extrapolation from the last points of the table.

### **34.4. Detailed operating description**

#### **34.4.1. Mouse handling in menus**

As soon as the program is started the mouse appears as a small smiling face enclosed in the active area of the menu. Clicking on either of the mouse buttons (they are equivalent) opens the main menu, and the mouse is automatically placed at the top center of this new menu. By scrolling the mouse up and down with the buttons released, one can select an item of the menu, which appears high-lighted on a black background, the smiling face disappearing. Once an item has been selected, clicking will activate the corresponding action. This allows the user to go down in the menu structure. To go up (go back to previous menus), just move the mouse out of any selection to make the smiling face reappear and click.

When a nucleus is required from the chart of nuclides, one has just to point to and to click on the desired nucleus. To scroll the chart in any direction, move the mouse to the side from which the chart has to appear (the face will change into an arrow), and click. If the button is held down, the chart will scroll faster after a fraction of a second. Placing the mouse at any corner of the chart will make it scroll diagonally (hence allowing "isospin" and "isobaric" scrolls).

Once an action has been performed, the program displays again on the top line the choice between "Previous menu" or "Main menu". One can jump back to the depth from which the last action was executed by selecting "Previous menu", or start from the root by selecting "Main menu". Some calculated results are displayed in a window centered on the screen. This window is automatically suppressed when clicking again to ask for another action.

#### **34.4.2. Keyboard entries**

Some information is entered via the keyboard. In every case, one can erase characters using the "delete" key, and terminates the entry by striking either "return" or "enter". This is also true when entering data directly into the menus : the cursor is placed where the entry should occur, and the data is reformatted to fit into the menu (this means that the format in which it appears in the menu might be different from the format in which it has been entered).

#### **34.4.3. Description of each command following the menu structure**

**Previous Menu:** returns to the menu previous depth.

**Main Menu:** goes to the root menu.

**Settings:** calls the settings menu.

**Projectile:** calls the projectile menu.

**Nature, mass and charge:** the program displays the chart of nuclides surrounding the current projectile ( $^{40}\text{Ar}$  by default) and asks to click on the desired new projectile (one can scroll the chart in any direction to access a different area). The new projectile will then flash red on the chart, and the program asks for its ionic charge (this parameter is only used to convert enA into pps). Any previous transmission calculation is cleared by this command. The program then automatically asks for the energy and intensity, assuming these parameters are different for a different projectile.

**Energy:** asks for the energy of the projectile (in MeV/nucleon). Previous calculations are cleared.

**Intensity:** asks for the primary beam intensity. The unit can be enA or pps depending on how the intensity unit option is set (see the Options menu) The default is enA. Previous calculations are cleared.

**Target:** calls the target menu.

**Nature:** selects the periodic table menu to choose the element corresponding to the target. Then automatically asks for the thickness. The mass used corresponds to the natural abundance of the selected element (this holds also for the wedge and material(s)). Clears previous calculations.

**Thickness:** asks for the thickness of the target. The unit can be  $\text{mg}/\text{cm}^2$  or (m depending on how the thickness unit option is set (see the Options menu)). Clears previous calculations.

**Wedge:** calls the wedge menu.

**Nature:** same entry than for the target.

**Thickness:** same entry than for the target. The thickness entered here corresponds to the thickness seen by the particles travelling on the beam axis (i.e. at the middle of the dispersive focal plane).

**Material(s):** calls the material(s) menu.

**Material #1..7:** selects on which material the action will take place.

**Add:** calls the periodic table menu to choose the element of the material. Then asks for its thickness. This command allows to add or insert a new material.

**Remove:** removes the specified material.

**Change:** changes the nature and/or thickness of the material by first calling the periodic table menu and then asking for a new thickness.

**Production mechanism:** calls the production mechanism menu.

$v_{\text{opt}}/v_0$ : sets the ratio of the velocity corresponding to the maximum of the momentum distribution over the beam velocity. The default value is 1.

**Sigma0:** sets the reduced width of the momentum distribution. The final width is calculated according to the Goldhaber formula:  $\sigma^2 = \sigma_0^2 A_F (A_P - A_F) / (A_P - 1)$  where  $A_F$  and  $A_P$  are the fragment and projectile masses respectively. The default value is 90 MeV/c.

**Setting fragment:** allows the user to pick the fragment on which the field calculations will be performed. The program places the chart of nuclides on the previous setting fragment and waits for a new one. Once it has been selected (same entry style as for the projectile), it flashes purple at the center of the screen. Clears previous calculations.

**Spectrometer:** calls the spectrometer menu.

**Slits:** calls the slits menu.

**Object size (2 sigma):** this command asks for the size of the beam spot on the target. The beam spot is assumed to be gaussian in both horizontal and vertical directions with the same width. The number entered is sigma. This parameter plays a very important role in the wedge selection, since it determines the size of the images corresponding to different nuclei at the first focus. The smaller these images are, the better the selection can be by closing the slits. Previous calculations are cleared when issuing this command.

**Slits intermediate focal plane:** sets the slit width at the dispersive focal plane. These slits determine the  $B\rho$  acceptance of the spectrometer, which is automatically calculated and displayed in %. The maximum opening is set by the maximum momentum acceptance parameter (see the Acceptance menu). Previous calculations cleared.

**Slits first focus (after wedge):** sets the slit width at the first focal point. These slits are important when a wedge is used, since the images corresponding to different nuclei are spread out in position. Closing the slits will therefore allow a better selection of the nuclei which are focused at or close to the center. Previous calculations cleared.

**Slits second focus (after Wien):** sets the slit width at the second focal point, which is the focal point of the Wien filter. They therefore set the velocity acceptance of the filter, allowing to select more or less nuclei, depending on the velocity dispersion. Only valid if the Wien filter has been enabled (see the Options menu). Clears previous calculations.

**Dipoles:** calls the dipole menu.

**Brho 1:** this command allows the user to enter the  $B\rho$  of the first section. This is useful when an experimental value has been determined (e.g. by centering a charge state of the beam on the dispersive focal plane), and one wants to calibrate either the beam energy or the target thickness (see the Calibrations menu). The  $B\rho$  of the second section is automatically recalculated for the best transmission of the selected fragment. Clears previous calculations.

**Brho 2:** allows the user to enter the  $B\rho$  of the second section (after the wedge). It can be used to calibrate the wedge thickness when the image of a beam charge state or of an identified nucleus has been experimentally centered at the first focal point (see also the Calibrations menu). Clears previous calculations.

**Radius 1:** radius of the first section dipole(s). Used to display the value of the magnetic field on the screen. The default value is the radius of the GANIL LISE dipoles.

**Radius 2:** radius of the second section dipole(s).

**Wien filter:** calls the Wien filter menu. The following commands are valid only if the Wien filter has been enabled (see the Options menu).

**Electric field:** sets the electric field of the filter in kV/m (the user has to know the gap between the electrodes). Calculates the magnetic field for the best transmission of the selected fragment and the dispersion. All these calculations are then updated on the screen. Clears previous calculations.

**Magnetic field:** sets the magnetic field of the filter in Gauss, calculates the electric field for the best transmission of the selected fragment and the dispersion. Clears previous calculations.

**Dispersion coefficient:** coefficient used to calculate the velocity dispersion in mm/% according to the formula:  $D=KE/(B\rho_2\beta)$  where E is the electric field in kV/m,  $B\rho_2$  the  $B\rho$  of the second section of the

spectrometer in Tm, and  $v$  the velocity of the particle. This coefficient depends on the field set on the quadrupoles used to focus the beam after the filter. Clears previous calculations.

**Magnification:** vertical magnification between the object (target position) and the filter. Clears previous calculations.

**Electric length:** effective electric length of the filter taking into account the fringe fields. Clears previous calculations.

**Magnetic length:** effective magnetic length of the filter taking into account the fringe fields. Clears previous calculations.

**Acceptances:** calls the acceptances menu.

**Maximum momentum acceptance:** This parameter is used as an upper limit for the setting of the slits at the intermediate focal plane.

**Target  $\theta$  acceptance:** horizontal angular acceptance after the target (in degree). Clears previous calculations.

**Target  $\phi$  acceptance:** vertical angular acceptance after the target (in degree). Clears previous calculations.

**Wedge  $\theta$  acceptance:** horizontal angular acceptance after the wedge (in degree). Clears previous calculations.

**Wedge  $\phi$  acceptance:** vertical angular acceptance after the wedge (in degree). Clears previous calculations.

**Optics:** calls the optics menu.

**Dispersion 1:** horizontal dispersion of the first section of the spectrometer in mm/%. Clears previous calculations.

**Dispersion 2:** horizontal dispersion of the second section of the spectrometer in mm/%. Clears previous calculations.

**Magnification 1:** horizontal magnification of the first section of the spectrometer. Clears previous calculations.

**Magnification 2:** horizontal magnification of the second section of the spectrometer. Clears previous calculations.

**$\theta$  magnification:** horizontal angular magnification at the wedge position. This parameter is used in conjunction with the wedge  $\theta$  acceptance to calculate the transmission. Clears previous calculations.

**$\phi$  magnification:** vertical angular magnification at the wedge position used with the  $\phi$  acceptance. Clears previous calculations.

**Angle on target:** Offset of the angular distributions at the target position in the case the beam is tilted with respect to the spectrometer axis. Clears previous calculations.

**Options:** calls the options menu.

**Wien filter:** switch used to enable or disable the calculations for the Wien filter. Clears previous calculations.

**Thickness unit:** toggles between mg/cm<sup>2</sup> and (m for the unit used in all thicknesses entries. The default is mg/cm<sup>2</sup>).

**Intensity unit:** toggles between enA and pps for the beam intensity entry. The default is enA.

**Display 1:** calls the display menu to select the first line of information displayed on the chart of nuclides. The default is the total transmission.

**Angular transmission:** displays the angular transmission (in %) as the first number displayed for each nucleus of the chart for which a calculation has been performed. The angular transmission is the product of the target and the wedge angular transmission, both being calculated as the average between horizontal ( $\theta$ ) and vertical ( $\phi$ ) transmissions.

**Brho transmission:** displays the B $\rho$  or momentum transmission (in %) calculated at the intermediate focal plane.

**Wedge transmission:** displays the transmission (in %) calculated at the first focus (after the wedge).

**Wien transmission:** displays the transmission (in %) calculated at the second focus (after the Wien filter).

**Total transmission:** displays the total transmission (in %) which is the product of the four transmissions cited above.

**Cross section:** displays the cross section (in mb) used in the calculation of the production rate.

**Charge state ratio:** displays the charge state fraction (in %) corresponding to the charge state selected on the chart (see the Charge state displayed option).

**Production rate:** displays the production rate (in pps) estimation based on the transmission, cross section, beam intensity, charge state ratio and target thickness.

**Display 2:** calls the display menu to select the second line of information displayed on the chart of nuclides. The default is the production rate.

**Cross section:** toggles between analytical (cross sections automatically calculated) and file (cross sections entered manually and stored on file) for the cross sections used in the calculations. Clears previous calculations.

**Charge states:** enables or disables the calculation of the charge state distributions and their corresponding transmissions. Clears previous calculations.

**Charge state displayed:** selects the charge state (entered as C in  $Q=Z-C$ ) displayed on the chart of nuclides.

**Calculation threshold:** lower limit of the production rate. The calculations are neither displayed nor stored if the rate is below this threshold.

**Cross sections:** calls the cross section menu.

**Enter a value:** the program waits for the selection of a nucleus from the chart and then prompts for the value of its cross section in mb. This value will only be used if the cross section option is set on "File".

**Read a value:** displays the cross section (analytical value or both analytical and file values if this last has been entered) of the selected nucleus.

**Isotopes:** calls the isotope menu.

**Add a nucleus:** calls the menu used to select the type of nucleus. Once this selection has been made, the program asks the user to click on the position of the new isotope on the chart of nuclides. The chart is automatically stored whenever the program is terminated.

**Stable:** selects a stable isotope (grey).

**$\beta^-$  decay:** selects a  $\beta^-$  emitter (blue).

**$\beta^+$  decay:** selects a  $\beta^+$  emitter (red).

**$\beta^-$  and  $\beta^+$  decay:** selects a  $\beta^-$  and  $\beta^+$  emitter (cyan).

**$\alpha$  decay:** selects an  $\alpha$  emitter (green).

**$\beta$  and  $\beta^+$  decay:** selects an  $\alpha$  and  $\beta^+$  emitter (orange).

**Proton decay:** selects a direct proton emitter (purple).

**Remove a nucleus:** the program asks the user to click on the nucleus which will be removed.

**Read characteristics:** not yet implemented.

**Write characteristics:** not yet implemented.

**Calculations:** calls the calculation menu.

**Brho1, Brho2, Bwien:** calculates the  $B\rho$  of the two sections of the spectrometer and the magnetic field of the Wien filter (if it has been enabled) for the best transmission of the setting fragment. The current settings of the spectrometer are updated to these new values. Clears previous calculations.

**Brho charge state:** calculates the  $B\rho$ s and Wien magnetic field for any charge state of any nucleus. Specially useful calculating the  $B\rho$ s of the beam charge states. Can also be used to set the spectrometer on a charge state different than the fully stripped fragment. Then one has to record the calculated values and enter them manually via the command "Settings→Spectrometer→Dipoles→Brho 1 or 2".

**Transmission and rates:** calls the transmission and rates menu. The results of the calculations are automatically updated on the chart of nuclides, showing the information lines selected in the menu "Options→Display 1 or 2" for each fragment. If nothing appears after a calculation has been done, it means that the rate of this particular nucleus is below the threshold (see also the "Options" menu).

**One nucleus:** the program asks the user to click on the nucleus in the chart for which the calculation will be performed.

**Area of nuclei:** the program asks the user to click on the upper rightmost nucleus first, and then on the lower leftmost nucleus second, in order to define the area of nuclei to calculate.

**All nuclei:** the program automatically starts the calculation for all nuclei displayed in the chart from the projectile down to the lithium isotopes. Be aware that you can't interrupt this command once it has been issued.

**Goodies:** calls the goodies menu.

→: clicking on this arrow will open the menu used to select the spectrometer position for which the following calculations will be performed. The default is after the wedge.

**After target:** this selection means that the calculations will be performed assuming the fragments have a kinetic energy determined by the  $B_0$  of the first section.

**After wedge:** with this selection, the kinetic energy is taken after the energy loss in the wedge, not regarding whether the fragment is actually transmitted by the second section or not. That way, the calculations for the fragments which are not centered at the first focus are more realistic than assuming that their kinetic energy corresponds to the  $B_p$  of second section, which is only true at first approximation within the  $B_p$  acceptance.

**Into material:** in this case, the kinetic energy is taken after the energy losses in the wedge and the 1st to (i-1)th material(s) where i is the number of the selected material. This allows calculation, for instance, of the energy loss in a detector after the fragments have been slowed down by some other material(s).

**After material:** same as "Into material" but the energy loss into the ith material is included to deduce the kinetic energy. Adds more flexibility to the calculational possibilities.

**Energy and  $\beta$ :** asks the user to pick a nucleus of the chart and then calculates its energy and  $\beta$  at the specified position.

**Energy loss:** calls the periodic table menu to pick an element, and then asks for its thickness, and finally the fragment for which the calculation has to be performed. If the position "Into material \#i" is selected, the program only asks to pick a fragment and calculates the energy loss in this material.

**Energy straggling:** displays the energy straggling at the specified position after a fragment has been chosen.

**Angular straggling:** same as for the energy straggling.

**Range:** same as in the energy loss calculation but for the range.

**Optimum target:** asks the user to pick a nucleus from the chart, and then starts to calculate and draw the dependence of the production rate of this nucleus versus the target thickness. For each step of target thickness, the program recalculates the settings for the best transmission. One can clearly see the saturation and then decrease of the production rate as the energy of the fragment decreases and the straggling increase. The result are shown on the graphic screen.

**Wedge slope:** calculates the slope of an achromatic wedge in % of  $\partial B_p/B_p$ .

**Calibrations:** calls the calibrations menu. The precision of the calibrations relies on the absolute energy loss calculation precision which is around 2%.

**Beam energy from  $B_{p1}$  and beam charge state:** calculates the beam energy from  $B_{p1}$ , which has to be input manually, and its corresponding charge state. This command is used during an experiment when one has centered a known charge state of the beam at the intermediate focal plane, and knows precisely the thickness of the target (or doesn't have any target).

**Target thickness from  $B_{p1}$  and beam charge state:** same as above, but this time the beam energy is precisely known, and one wants to measure the thickness of the target.

**Wedge thickness from Bp2 and nucleus:** used to calibrate the thickness of the wedge during an experiment, once a charge state or identified fragment has been centered at the first focus. B(2 is then entered manually, and the program asks the user which nucleus corresponds to this B( (and its charge state if it is the projectile). The calculated thickness is the thickness seen on the beam axis of the spectrometer.

**Material \#i thickness for implantation in \#j:** This command is used to calculate the amount of material \#i needed to implant a given nucleus at a given depth in \#j. \#i and \#j are first specified by selecting 'material' and 'implantation in' respectively, and then the program asks for which nucleus and at which depth the calculation will be performed when selecting 'thickness'. If the nucleus doesn't make it through to the material \#j, the command is ignored. One can check easily the average range by calculating the range after the material \#j-1 using the command "Calculations→Goodies→range".

**Files:** calls the files menu.

**Read:** calls the directory menu and asks the user to select a file to read. If the number of files is greater than 50, a second page of files can be selected by clicking on "Page". Going back to the previous page is just like going back to the previous menu : move the mouse out of any selection and click. Once a file has been selected, the program displays the title and asks for a confirmation. Striking any key but "n" or "N" will be interpreted as yes. The screen and internal parameters are then updated according to the file data.

**Write:** writes the current settings and calculations to a specified file or a new file. If a filename has been selected, the program asks for confirmation to overwrite it. If it is a new file, the program prompts for a filename (the extension ".fic" is automatically added) and a title.

**Remove:** erases the specified file (with confirmation).

**Results:** creates or updates a result file which has the same name as the current setting file, but with the extension ".liz". This file is stored under the directory "\\RESULT" and is automatically sent to the printer manager via the DOS command "Print" whether one is installed or not (if it is not, the DOS will only issue an error message, no big deal !). This file contains the parameters of the spectrometer and the results of the transmission and rate calculations.

**Spawn:** this command is used to copy the program to any other disk or directory. The program asks for the DOS path corresponding to the destination, creates the needed directories, and copies all the necessary files including this manual.

**Plots:** calls the plot menu.

**Table isotopes:** this command is used to browse through the chart of nuclides in order to look at different areas of nuclei.

**Plot (E-TOF:** calls the identification spectrum menu.

**Go !:** used to start the plotting once all parameters are set to their correct values. Only the fragments for which a transmission calculation has been performed will appear on the screen. Once the plot has been completed, the mouse can be moved to any nucleus to read its time of flight and energy loss, as well as the corresponding channels on the actual spectrum if the calibrations have been entered (see the following). The time of flight axis is reversed as in most experiments in which the start detector has a much greater counting rate than the stop detector. Reversing start and stop therefore prevents starting the TAC or TDC without stopping it.



**Detector:** selects which material will be used to calculate the energy loss.

**TOF calibration (ns):** once the identification has been made, one can calculate a calibration of the time of flight. Using this calibration, the program displays the channel number on the horizontal axis.

**(E calibration (MeV):** same as for the energy loss.

**Length start → wedge:** flight base length between start detector (target if the HF of a cyclotron is used) and wedge.

**Length wedge → stop:** flight base length between wedge and stop detector.

**Start of TOF:** toggles between "Detector" (the default) and "RF" for the start of the time of flight measurement. In case "RF" is selected, the plot shows the wrap around due to the periodicity of the cyclotron radiofrequency.

**RF frequency:** used to input the radiofrequency of the cyclotron.

**Identification:** selects whether the identification of the plotted nuclei is directly displayed on the screen or not. This option has to be turned off in case a lot of nuclei are being displayed, in which case all the characters are overlapping and it becomes very difficult to distinguish one isotope from the other. In both cases (identification on or off), the nature of the nuclei is displayed whenever the mouse is moved on them.

**Threshold:** one can set a display threshold corresponding to the rate below which the nuclei are not plotted.

**Plot  $\delta E$ -E:** plots a  $\delta E$ -E spectrum using the parameters set for the  $\delta E$ -TOF spectrum.

**Angular distributions:** displays the angular distributions ( $\theta$  and  $\phi$  after both target and wedge) for the setting fragment and the most intense contaminants. The different angular acceptances as well as the angular transmission for each fragment are shown on the plot. The distributions plotted are  $\partial\sigma/\partial\Omega$  as a function of  $\theta$  (or  $\phi$ ). They can be drawn on a linear or log scale, and their total number is fixed (see the two last selections of the Plot menu).

**B $\rho$  selection plot:** displays the distributions at the intermediate focal plane, where the B $\rho$  selection occurs. The momentum acceptance of the spectrometer is also shown. Same display comments apply as for the angular distributions.

**Wedge selection plot:** displays the distributions at the first focus, where the images corresponding to different nuclei are selected by the slits at this position. Same display possibilities as for the angular distributions.

**Wien selection plot:** displays the distributions at the second focus, which is the dispersive focal plane of the Wien filter. Only valid if the Wien filter has been enabled. Same display possibilities as for the angular distributions.

**Range distributions:** the program asks the user first in which material these distributions should be drawn. Then it displays the range distributions for the fragments which actually stop in this material. These distributions are only drawn on a linear scale.

**Display:** toggles between "lin" and "log" for the display of the distributions. The default is "lin".

**Number of distributions:** selects how many distributions will be drawn on the plots. The program always starts with the distributions of the selected fragment, and then adds the most intense contami-

nants. Only the nuclei for which a transmission and rate calculation has been performed will be displayed.

**End:** terminates the program and returns to DOS. The chart of nuclides is automatically updated.

### **34.5. Tutorial : a sample calculation**

The following lines describe an example of a calculation performed for a  $^{84}\text{Kr}$  beam at 60 MeV/u fragmented on a Be target in order to produce  $^{68}\text{Co}$ . Although it does not explore all the possibilities of the program, this example tries to exhibit most of its different features. The calculations performed in this example are stored in three different files "example1", "example2" and "example3" provided with the diskette. Each correspond to a further cleaning of the  $^{68}\text{Co}$  secondary beam using different selection criteria.

The first step when starting from scratch is to set the projectile, target and the secondary beam.

Start the program by typing "LISE".

Click on either "Previous menu" or "Main menu" to open the main menu.

Select the "Setting" submenu by moving the mouse on it until it is high-lighted, and then click.

Select the "Projectile" submenu.

Select the option "Nature, mass and charge". The program then asks to choose the projectile from the chart of nuclides. The default projectile being  $^{40}\text{Ar}$ , it flashes red at the middle of the screen. Move the mouse to the right side until it changes to an arrow and then click to scroll the chart to the left. Scroll down the chart by moving the mouse to the top and clicking until you see the Krypton isotopes appearing. Once you see  $^{84}\text{Kr}$  on the screen, move the mouse at its position and click to select it. Then the program asks to enter successively the ionic charge, energy and intensity. Enter the numbers 25 for the charge, 60 for the energy and 200 for the intensity using the numeric keypad (it's easier) and "Enter". Once all of this has been done, the information related to the projectile is displayed in red on the right side of the screen, and  $^{84}\text{Kr}$  flashes red on the chart of nuclides. The program displays back the bar "Previous menu?Main menu". Click on "Previous menu" (the default position of the mouse) to recall the projectile submenu.

Since all information related to the projectile has been entered, go back to the setting menu by clicking once the smiling face appears (it automatically appears on top of the submenu when "Previous menu" has been selected).

Select the target submenu.

Select the option "Nature". The program displays the periodic table submenu. Move the mouse to "Be" until it appears high-lighted and click. The target element is then displayed in green on the right side of the screen. Enter the target thickness ( $100 \text{ mg/cm}^2$ ) and go back to the previous submenu depth (select "Previous menu").

To return to the setting submenu, click to go back to the target submenu, then move the mouse out of the "Nature" selection (the smiling face should reappear) and click.

Scroll down to the "Setting fragment" selection and click. As for the choice of the projectile, scroll the chart of nuclides until  $^{68}\text{Co}$  appears, then click on it.

Return to the Setting submenu using "Previous menu", and select the Spectrometer submenu.

Select "Slits" and then "Slits intermediate focal plane". Enter the opening of the slits (enter  $\pm 15$  mm). This value appears on the right side of the screen followed by corresponding momentum acceptance ( $\pm 0.9$  %).

The above actions provide the minimum information required to calculate the settings of the spectrometer and the transmissions. The following lines describe an example of these calculations.

Select the "Calculations" submenu from the main menu.

Select the "Brho1, Brho2, Bwien" option. The program starts to calculate the field settings of the spectrometer. It first calculates the range tables of Krypton and Cobalt in Beryllium (a flashing box appears on the screen for each energy). Once these tables are calculated, they are automatically stored on the disk (see 3.4.). Then the B( of the two sections of the spectrometer as well as the corresponding magnetic fields are displayed on the right side of the screen.

Click on "Previous menu" to return to the calculation submenu.

Select the "Transmission and rate" submenu.

Choose the "One nucleus" option. Select the  $^{68}\text{Co}$  from the chart. The program then calculates and displays two numbers : 11.60 % which is the total transmission (first line of information by default), and  $2.8\text{e}+01$  which is an estimation of the rate in pps (second line of information by default).

The program predicts a production rate of 28  $^{68}\text{Co}$  per second for a beam intensity of 200 enA. It is now possible to determine which other fragments are transmitted with the  $^{68}\text{Co}$ . Let's first set the rate threshold at one count per minute since we are only concerned by the fragments having a larger production rate.

Select "Main menu→Settings→Options".

Select "Calculation thres." in the Options submenu. The cursor appears in the submenu. Enter the number  $1.67\text{e}-2$ . To verify that this value has been effectively taken into account, select "Previous menu" : the value displayed for the calculation threshold is now  $1.7\text{e}-02$ . Only the format of the number has been changed, and the value in memory is still  $1.67\text{e}-2$ .

Go back to the main menu using the smiling face, and select "Calculation→Transmission and rate→All nuclei". The program will calculate the rate for all possible fragments, starting from the projectile with fewer neutrons, down to the Lithium isotopes. During this process, it will calculate and store the range tables of all these elements in Beryllium (except for Cobalt which has already been calculated). All this may take a while (depending on the computer speed) and cannot be interrupted but by a reset of the system, so it's probably time for coffee break !

For each nucleus transmitted at a rate larger than one per minute, the program displays the total transmission in % and the rate in pps. A lot of nuclei are transmitted together with the  $^{68}\text{Co}$  because the only selection used is the Bp selection of the first section of the spectrometer.

Select "Main menu→Settings→Options→Display1→Angular transmission". The first line of information now displays the angular transmission (or geometrical transmission due to the ( and ( acceptances after the target and the wedge positions). It is possible to display any of the informations listed in the Display1 or 2 submenu.

Select "Main menu→Plots→Table isotopes". Browse through the chart of nuclides in order to look at different regions of transmitted nuclei. Click on any nucleus to return to the menu.

Let's now assume that there is a silicon detector at the focal point of the spectrometer. Measuring the energy loss and time of flight of each particle allow to identify them. The plot generated by LISE tries to reproduce the actual bidimensionnal spectrum observed during the experiment. Establishing the correspondance between these two spectra allows to identify the nuclei and get a calibration of both energy loss and time of flight.

Select "Main menu→Settings→Options→Thickness unit". This command toggles the thickness unit to  $\mu\text{m}$ .

Go back to the Settings submenu and select "Material(s) →Material \#1→Add→Si". Then enter the thickness in  $\mu\text{m}$  (enter 100  $\mu\text{m}$ ).

Select "Main menu→Plots→Plot  $\delta\text{E}$ -TOF→Detector". Enter the material number of the detector used to measure the energy loss (this is obviously 1).

Return to the Plot  $\delta\text{E}$ -TOF submenu and toggle the Identification off. This is to prevent having the names of the nuclei plotted on the screen, in the case too many of them are overlapping and therefore impossible to read.

Select "Go !". This will start generating the plot. The screen stays erased until the energy loss calculations are performed. If the range tables of elements Krypton through Lithium into Silicon are not yet calculated, the program will generate them and store them on disk (this might take a little more time). Once the plot is produced, the mouse appears as a cross. The name, transmission and rate of any nucleus appears on the right side of the screen whenever the cross is pointing on it. One can clearly see the isospin lines on the plot (the most obvious one is the  $N=Z$  straight line), as well as the tilted  $Z$  lines which flatten for the lighter elements. To return to the menu, click anywhere and strike any key.

The second step in the purification of the  $^{68}\text{Co}$  beam is performed by the selection of the second section of the spectrometer when an achromatic wedge is inserted at the intermediate dispersive focal plane. Due to their different energy losses in the wedge, different nuclei are focused at different positions at the focal point of the spectrometer, where the opening of the slits determines the transmission.

Select "Main menu→Settings→Options→Thickness unit" to toggle back to  $\text{mg}/\text{cm}^2$ .

Select "Previous menu→go back→Wedge→Nature→Al" and enter the thickness of the wedge (50  $\text{mg}/\text{cm}^2$ ). As soon as this entry is made, the calculations are cleared.

Select "Previous menu→go back→go back→Spectrometer→Slits→Slits image1" and enter  $\pm 2$  mm. This opening determines the selectivity of the second section of the spectrometer when a wedge is used

Select "Main menu→Calculations→Brho1, Brho2, Bwien" to calculate the new settings of the spectrometer corresponding to the best transmission for  $^{68}\text{Co}$ .

Select "Previous menu→go back→Transmission and rate→area of nuclei" and click on  $^{74}\text{Ga}$  first (the upper rightmost nucleus) and then on  $^{63}\text{Cr}$  (the lower leftmost nucleus). This will start the calculation only for the nuclei located in the square defined by  $^{74}\text{Ga}$  and  $^{63}\text{Cr}$ . Since a lot few nuclei are being transmitted, it is not necessary to calculate the transmission for all of them.

The insertion of an achromatic wedge has considerably reduced the amount of nuclei transmitted with the  $^{68}\text{Co}$ . This additional selection can be visualized by looking again at the  $\delta\text{E}$ -TOF plot.

Select "Main menu→Plots→Plot  $\delta\text{E}$ -TOF→Identification' to toggle the identification back on.

Select "Previous menu→Go !" to start the plot. In an actual experiment, one would use the calibration determined from the previous plot to identify the nuclei on the experimental spectrum. If this calibration is entered in the Plot  $\delta E$ -TOF submenu, the numbers labelled "Ch# X" and "Ch# Y" give the channel numbers corresponding to the position of the mouse.

One can also visualize the selection performed by the wedge and the second section of the spectrometer by plotting the position of the images corresponding to different nuclei at the first focal point. Select "Previous menu→go back→Wedge selection plot". The images are spread along the horizontal axis,  $^{68}\text{Co}$  being centered with respect to the slits. It is interesting to notice that the image of  $^{71}\text{Cu}$  is also rather well centered, therefore it is impossible to get rid of it using the wedge technique. Another selection criteria such as the one provided by a Wien filter (velocity filter) has to be used.

Just by looking at the (E-TOF spectrum obtained with the wedge, it is possible to tell what selection a velocity filter will provide. The cut in velocity will correspond to a cut in TOF centered around  $^{68}\text{Co}$ . It will therefore be possible to reduce the amount of  $^{71}\text{Cu}$  contamination using a Wien filter.

Select "Main menu→Settings→Options→Wien filter" to enable its use in the calculations. This command clears the previous calculations.

Select "Previous menu→go back→Spectrometer→Wien filter→Electric field" and enter a value of 3000 kV/m. The magnetic field setting of the Wien filter is then automatically calculated for the best transmission of  $^{68}\text{Co}$ , as well as the dispersion. All these informations appear on the right side of the screen.

Select "Previous menu→go back→Slits→Slits second image" and enter an opening of  $\pm 2$  mm.

Do the calculations of the rates (select "Main menu→Calculations→Transmission and rate→Area of nuclei" and click on  $^{74}\text{Ga}$  then on  $^{63}\text{Cr}$ ). The amount of  $^{71}\text{Cu}$  is greatly reduced and  $^{68}\text{Co}$  is now the main component of the beam. However,  $^{70}\text{Ni}$  is still present at a competitive rate.

Select "Main menu→Plots→Wien selection plot" to plot the distributions at the second focal point. It then becomes obvious that although the Wien filter is efficient to get rid of  $^{71}\text{Cu}$ , it can't do the same for  $^{70}\text{Ni}$  because its velocity is close to that of  $^{68}\text{Co}$ .

Select "Previous menu → Wedge selection plot" to look again at the selection provided by the wedge.  $^{70}\text{Ni}$  appears to be shifted from the slits position. Two solutions are possible to reduce further its contamination of the beam : one can close the slits of the first image further, although this will also decrease the amount of  $^{68}\text{Co}$  transmitted, or one can also increase the thickness of the wedge in order to shift the image of  $^{70}\text{Ni}$  further to the left. This last solution appears to be the best. However it ought to be tested, since a thicker wedge will cause a broadening of the images and an increase the angular scattering, resulting in a loss in the transmission of  $^{68}\text{Co}$ .

### **34.6. Computer considerations**

LISE is a DOS-based software running on any IBM compatible PC. It runs under DOS 3.1 and following versions, and only needs 640 kbytes of memory. The speed of the program depends greatly on the CPU type, speed and configuration. The use of a co-processor is greatly recommended : the program uses FFT (Fast Fourier Transform) algorithms which contain extensive floating-point operations.

The last version has been developed on a 386-SX at 16 MHz with a co-processor which provides a reasonable speed (about 1 second per transmission calculation). Trying the program on a 486-based

system showed a great improvement (it was impossible to measure the time lapse of the same calculation !).

The program uses a mouse driver loaded at the start-up of the computer. This driver has to be Microsoft compatible (most of them are). The graphics interface included with the program (file "EGAVGA.BGI") insures the compatibility with any EGA or VGA compatible graphic card. The program looks automatically for the best resolution the card can provide (although it is limited to the maximum standard VGA resolution 640x480x16 colors). The hardcopy of the graphic screen can be made on a printer provided the command "graphics" is executed at start-up.

The first version of LISE has been written in 1987, using the Borland Turbo C compiler. It is written in C for several reasons : it is one of the few languages that allow piloting the mouse driver directly via software interrupts, in order to create one's own menu system. Also, Turbo C provides an extensive number of graphic routines, and finally recursivity, the ability to manipulate data structures, and the possibility to allocate and deallocate memory dynamically are a major improvement in programming. Today, the C language has evolved even further towards Object Oriented Programming, producing the C++. Following this evolution, the latest parts of LISE are written in C++. Portability is always a critical issue in programming, and C++ is certainly one of the best suited language for this task. However, this software is still tightly bound to MS-DOS, and its transfer to other machines running under different systems would require a non negligible amount of time and has not yet been done.

## References

- [A1903] M.Steiner, A.Stolz, private communications of A1900 group.
- [AME03] G.Audi, A.H.Wapstra and C.Thibault, Nucl. Phys. A **729** (2003) 337.
- [Ann87] R.Anne, D.Bazin, A.C.Mueller, J.C.Jacmart and M.Langevin, **NIM A257**(1987) 215-232; Web-site of the LISE spectrometer: <http://www.ganil.fr/LISE>.
- [Ann88] R.Anne et al, **NIM B34** (1988) 295-308.
- [Aoi02] N.Aoi et al., RIKEN Accel. Prog. Rep. **35** (2002) 75.
- [Arm96] P.Armbruster et al., Z.Phys.**A355** (1996) 191-201.
- [Arm04] P.Armbruster et al., Phys. Rev. Lett. **93** (2004) 212701.
- [Aum95] T.Aumann et al., Z.Phys. **A352** (1995) 163-169.
- [Aud95]
- [A&W95] G.Audi and A.H.Wapstra, Atom.Data and Nucl.Data Tables (1995) 1.
- [Bal98] A.B.Balantekin and N.Takigawa, Rev.Mod.Phys. 70 (1998) 77-99.
- [Bas74] R.Bass, Phys.Rev.Lett. **39** (1977) 265.
- [Baz94] D.Bazin and B.Sherrill, **Phys.Rev. E50**(1994) 4017-4021.
- [Baz01]
- [Baz02] D.Bazin, O.B.Tarasov, M.Lewitowicz, O.Sorlin, [NIM A482 \(2002\) 307-327](#).
- [Bla94] B.Blank et al., Phys.Rev.C 50 (1994) 2398.
- [Bla00] B.Blank et al, Phys.Rev.Lett. **84** (2000) 1116-1119.
- [Bel89] A.V.Belozorov et al., Report P15-89-2255, JINR, Dubna, 1989.
- [Bel98] A.V.Belozorov et al., NIM A 411 (1998) 343-350.
- [Ben98] J.Benlliure et al., Eur.Phys.J. A 2 (1998) 193.
- [Ben98] J.Benlliure et al., Nucl.Phys. **A628** (1998) 458-478.
- [Ben99] J.Benlliure et al., Nucl.Phys.A 660 (1999) 87.
- [Ben01] J.Benlliure et al., Nuclear Physics **A683** (2001) 513-539.
- [Ben02] J.Benlliure et al., NIM **A478** (2002) 493-505.
- [Ber97] M.Bernas et al., Nucl.Phys. **A616** (1997) 352-362, M.Bernas et al., Phys.Lett. **B415** (1997) 111.
- [Ber03] M.Bernas, et al., Nucl.Phys. **A725** (2003) 213
- [Ber88] C.A.Bertulani and G.Baur, Physics Report **163** (1988) 299-408.
- [Bha86] K.H.Bhattm, P.Grange and B.Hiller, Phys.Rev.C **33** (1986) 33.
- [Bis70] C.J.Bishop et al., Nucl.Phys.**A150** (1970) 129-142.
- [Blu86] Y.Blumenfeld et al., Nucl.Phys **A455** (1986) 357.
- [Bla94] B.Blank et all., Phys.Rev.**C50** (1994) 2398.
- [Bla00] B.Blank et all., Phys.Rev.Lett. **84** (2000) 1116.
- [Boh40] N.Bohr and J.A.Wheeler, Phys.Rev. **56** (1939) 426.
- [Bor83] V.Borrel et al., Z.Phys.**A 314** (1983) 191.
- [Bor86] V.Borrel et al., Z.Phys.**A 324** (1986) 205.
- [Bro80] K.L.Brown, D.C.Carey, Ch.Iselin, F.Rothacker. CERN 80-04.
- [Coh63] S.Cohen, W.K.Swiatecki, Ann. Phys. **22** (1963) 406.
- [Coh74] S.Cohen, F.Plasil, W.J.Swiatecki, Ann.Phys. **82** (1974) 557.
- [Dar86] R.Dayras et al., Nucl.Phys. **A460** (1986) 299.
- [Dau00] J.M.Daugas et al., Phys.Lett. **B476**, (2000) 213.
- [De96] J.N.De et al., Phys.Rev.**C53** (1996)
- [Dio89] J.S.Dionisio et al., NIM A282 (1989) 10-21.

- [Duf86] J.P. Dufour et al., Nucl. Instr. and Meth. **A248** (1986) 267-281.
- [Enq99] T. Enqvist et al., Nucl.Phys. **A658** (1999) 47-66.
- [Enq01] T.Enqvist et al., Nucl.Phys. **A686** (2001) 481-524.
- [Enq02] T.Enqvist et al., Nucl.Phys. **A703** (2002) 435-465.
- [Fau02] H.R.Faust, Eur.Phys.J.**A14** (2002) 459-468.
- [Fri83] W.A.Friedman, Phys.Rev. **C27**(1983) 569.
- [Fri03] W.A.Friedman and M.B.Tsang, Phys.Rev.C**67** (2003) 051601.
- [Gai91] J.-J.Gaimard, K.-H.Schmidt, Nucl.Phys. **A531** (1991) 709-745.
- [Gav80] A.Gavron, Phys.Rev. **C21** (1980) 230-236;  
(see [ftp://ftp.nsl.msui.edu/lise/PACE\\_source](ftp://ftp.nsl.msui.edu/lise/PACE_source)).
- [Gei95] H.Geissel, G.Münzenberg, K.Riisager, Annu. Rev. Nucl. Part. Sci. **45** (1995) 163-203.
- [Gre75] D.E.Greiner et al., Prys.Rev.lett. **35** (1975) 152.
- [Gre97] A.Grewe et al., Nucl.Phys.**A614** (1997) 400-414.
- [Gol74] A.S.Goldhaber, Phys.Lett. **B53** (1974) 306.
- [Gos77] J.Gosset et al., Phys.Rev. **C16** (1977) 629.
- [Gol96] F.Goldenbaum et al., Phys.Rev.Lett. **77** (1996) 1230-1233.
- [Gui86] D.Guillemaud-Mueller et al.,IEEE **33**(1986)343.
- [Hau88] Atomic. Data Nucl. Data Tables **39**, 185 (1988); edited by P.E. Haustein.
- [HBF9] M.Samyn, S.Goriely, P.-H.Heenen, J.M.Pearson, F.Tondeur, Nucl.Phys. **A700** (2001) 142;  
S.Goriely, M.Samyn, P.-H.Heenen, J.M.Pearson, F.Tondeur, Phys. Rev. **C66** (2002) 024326;  
M.Samyn, S.Goriely, J.M.Pearson, Nucl. Phys. **A725** (2003) 69;  
S.Goriely, M.Samyn, M.Bender, J.M.Pearson, Phys.Rev. **C68** (2003) 054325;  
M.Samyn, S.Goriely, M.Bender, J.M.Pearson, Phys.Rev. **C70** (2004) 044309;  
S.Goriely, M.Samyn, J.M.Pearson, M.Onsi, Nucl.Phys. **A750** (2005) 425.
- [Hes96] M.Hesse et al., Z. Phys. **A355** (1996) 69-75.
- [Hil53] D.L.Hill and J.A.Wheeler, Phys.Rev. **89** (1953) 1102.
- [Hub90] F. Hubert et al., Atom. Dat. and Nucl. Dat. Tabl. **46** (1990) 1-213.
- [Ign75] A.V.Ignatyuk et al., Yad.Fiz. **21** (1975) 485.
- [Ign95] A.V.Ignatyuk et al., Nucl.Phys.**A593** (1995) 519-534.
- [Ilj92] A.S.Iljjinov et al., Nucl. Phys. **A543** (1992) 517-557.
- [Itk86] M.G.Itkis, S.I.Mulgin, A.Ya.Rusanov, A.N.Okolovich, G.N.Smirenkin, Yad.Fiz. **43** (1986) 1125  
(Sov.J.Nucl.Phys. **43**(1986) 719).
- [Itk88] M.G.Itkis, A.N.Okolovich, A.Ya.Rusanov, G.N.Smirenkin, Fiz.Elem.Chastits At. Yadra **19** (1988)  
701 (Sov.Journal Nucl.Phys. **19** (1988) 301).
- [Jon97] M.de Jong et al., Nucl.Phys.A**613** (1997) 435.
- [Jon98] M.de Jong et al., Nucl.Phys.A**628** (1998) 479.
- [Jur02] B.Jurado, Ph.D. thesis, University Santiago de Compostela, 2002.
- [Jur03] B.Jurado, K.-H.Schmidt, J.Benlliure, Phys.Lett. **B553** (2003) 186-190.
- [Jur04] B.Jurado et al., arXiv nucl-ex / 0403006, submitted to Nucl.Phys.A.
- [Kra40] H.A.Kramers, Physika VII **4** (1940) 284.
- [Kra87] "Introductory nuclear physics", K.S.Kraime, publ. By John Wiles & sons, New York, 1987.
- [Kox87] S.Kox et al., Phys.Rev.C **35**, 1987, p.1678.
- [Lan80] W.Lang et al., Nucl.Phys. **A345** (1980) 34.
- [Leo98] A.Leon et al., Atom.Data and Nucl.Data Tables, v.69, 1998.
- [Lew94] M.Lewitowicz et al., Phys. Lett. B **332** (1994) 20-24.
- [Lin96] J.Lindhard, A.H.Sorensen, Phys.Rev. **A53** (1996) 2443.
- [LISE71] [http://groups.nsl.msui.edu/lise/7\\_1/lise++\\_7\\_1.pdf](http://groups.nsl.msui.edu/lise/7_1/lise++_7_1.pdf)



- [Liu98] W.Liu et al, PRC 58, 1998, 2677
- [Mam98] A.Mamdouh, J.M.Pearson, M.Rayet and F.Tondeur, Nucl. Phys. **A644** (1998) 389.
- [Mam01] A.Mamdouh, J.M.Pearson, M.Rayet and F.Tondeur, Nucl. Phys. **A679** (2001) 337.
- [Mer86] M.C.Mermaz et al., Z.Phys. **A324** (1986) 217.
- [Moc03] M.Mocko et al. to be printed.
- [Mom02] S.Momota et al., Nucl. Phys. **A701** (2002) 150;  
M.Notani, PhD thesis, University of Tokyo (2001).
- [Mor89] D.J.Morrissey, Phys.Rev. **C39** (1989) 460.
- [Mou81] J.Mougey et al., Phys.Lett. **B105** (1981) 25.
- [MSL89] M.G.Saint-Laurent et al. (Z.Phys.A 332, 1989, p.457)
- [Mye66] W.D.Myers and W.J.Swiatecki, Nuclear Physics 81(1966) 1-60.
- [Nor70] L.C. Northcliffe and al., Nucl. Dat. Tabl. A7 (1970) 233.
- [Not01] M.Notani, PhD thesis, University of Tokyo (2001).
- [Not02] M.Notani et al., Phys.Lett. **B542** (2002) 49.
- [Nuc] The code "NUCLEUS" - I.Duflo, G.Audi et al, CSNSM, Orsay
- [Oga98] Yu.Ts.Oganessian, et al. Proceedings of Fourth International Conference on Dynamical Aspects of Nuclear Fission, 19–23 October 1998, Casta-Papiernicka, Slovak Republic, World Scientific, Singapore, 2000, p. 334;
- [Oga03] Yu.Oganessian et al., NIM B 204 (2003) 606-613.
- [Oza00] A.Ozava et al, Nucl.Phys A673 (2000) 411.
- [Par98] Particle Physics Booklet, 1998, pp.184,185; <http://pdg.lbl.gov>; (extracted from the Review of Particle Physics C3 (1998) 1).
- [Pau89] M.Paul et al., NIM A277 (1989) 418-430.
- [Per04] Jorge Pereira Conca, PhD thesis, Universidad de Santiago de Compostela (USC), 2004.
- [Pom93] S.Pommé et al., Nucl.Phys. **A560** (1993) 689-714.
- [PDG00] Particle physics booklet; <http://pdg.lbl.gov>
- [Ram85] F.Rami et al., Nucl.Phys. **A444** (1985) 325.
- [Rei98] J.Reinhold et al., Phys.Rev.C58 (1998) 247.
- [Rej00] F.Rejmund et al., GSI-Preprint 2000-06.
- [Rub03] V.A.Rubchenya and J.Äystö, EURISOL research report, Jyväskylä 2003.
- [Rub96] Th.Rubehn et al., Phys.Rev. **C53** (1996) 3143-3146.
- [Sak97] H.Sakurai et al., Nucl.Phys. **A616** (1997) 311.
- [Sar00] F.Sarazin et al., PRL 84 (2000) 5062.
- [Sch98] C. Scheidenberger, H. Geissel, NIM **B 135** (1998) 25.
- [Sch98] C.Scheidenberger, Th.Stohlker, W.E.Meyerhof, H.Geissel, P.H.Mokler, B. Blank, NIM B 142 (1998) 441-462; <http://www-aix.gsi.de/~scheid/CHARGE.html> & <http://www-aix.gsi.de/~scheid/GLOBAL.html>
- [Sch00] K.-H.Schmidt et al., Nucl.Phys. **A665** (2000) 221-267.
- [Sch00] K.-H.Schmidt, J.Benlliure, P.Armbruster, private communications.
- [Sch01] K.-H.Schmidt et al., Nucl.Phys. **A685** (2001) 60-71.
- [Sch01] K.-H.Schmidt, J.Benlliure, A.R.Junghans, Nucl.Phys. **A693** (2001) 169-189.
- [Sch02] K.-H.Schmidt et al., Nuclear Physics A 710 (2002) 157-179.
- [Sch83] A.S.Schlachter et al., PRA 27 (1983) 3372-3374.
- [Sie86] A.Sierk, Phys. Rev. **C33** (1986) 2039.
- [SISSI] Guide de l'utilisateur de SISSI, M-H.Moscatello et le groupe SISSI, GANIL R96 05 ; WEB-refernce [http://www.ganil.fr/equipements/equip\\_detect.htmlx](http://www.ganil.fr/equipements/equip_detect.htmlx).
- [Sym79] T.J.M.Symons et al., Phys.Rev. C42 (1979) 40.

- [Smi93] G.N.Smirenkin (1993) IAEA-Report INDC(CCP)-359.
- [Sou02] “Improved mass parameterization in reaction models”, S.R.Souza et al. To be published.
- [Sub02] K.Subotic et al., NIM A 481 (2002) 71–80.
- [Sum90] K.Sümmerer et al., **Phys.Rev. C42**(1990)2546-2561.
- [Sum00] K.Summerer, B.Blank, Phys.Rev. **C61**(2000)034607
- [Tai03] J.Taïeb et al, Nucl.Phys. A724 (2003) 413.
- [Tar97] O.B.Tarasov et al., Phys.Lett. **B409** (1997) 64-70.
- [Tar98] O.Tarasov et al., **Nucl.Phys. A629**(1998)605.
- [Tar03] O.Tarasov and D.Bazin, NIM **B204** (2003) 174-178.
- [Thi85] P.Thieberger, H.E.Wegner, J.Alonso, H.Gould, C.Munger, R.Anholt, W.E.Meyerhof, IEEE Trans. Nucl.Sci. 32 (1985) 1767.
- [Tho04] M.Thoennessen, Rep. Prog. Phys. **67** (2004) 1187-1232.
- [Tri89] R.E.Tribble, R.H.Burch, C.A.Gagliardi, NIM A 285 (1989) 441-446.
- [TRI94a] R.K.Tripathi, L.W.Towsend, Phys.Rev. **C49**(1994) 2237.
- [TRI94b] R.K.Tripathi, L.W.Towsend, F.Khan, Phys.Rev. **C49**(1994) R1775.
- [Tsa03] B.Tsang et al., NSCL experiment 1036: intermediate results.
- [VAMOS] VAMOS: WEB-reference <http://www.ganil.fr/vamos/index.html>.
- [VIY79] Y.P.Viyogi et al., Phys.Rev.Lett. **C42** (1979) 33.
- [Web94] M.Weber et al., Nucl. Phys. **A578** (1994) 659.
- [Wei00] H.Weick et al., NIM **B164-165** (2000) 168-179.
- [Wei04] the MOCADI code: <http://www-linux.gsi.de/~weick/mocadi/>
- [Wil76] B.D.Wilkins et al., Phys.Rev.**C14** (1976) 1832.
- [Wil86] B.D.Wilkins et al., Proc.Int.Symposium Nucl.Fission, Heavy Ion Induced Reactions, W.Schroder, ed. Harwood 1986.
- [Wil87] J.W.Wilson, L.W.Towsend, F.F.Badavi, NIM B18 (1987) 225-231.
- [Won73] C.Y.Wong, Phys.Rev.Lett. 31 (1973) 766.
- [Yer94] A.V.Yeremin et al., NIM A350 (1994) 608-617.
- [Zei92] K.Zeitelhack, PhD thesis, Universität München, Physik Department E12, 1992.
- [Zie85] J.F.Ziegler et al, Pergamon Press, NY, 1985;  
SRIM2000 <http://www.research.ibm.com/ionbeams/#SRIM>